Tectonics of the Nanga Parbat Syntaxis and the Western Himalaya

edited by M. A. Khan, P. J. Treloar, M. P. Searle and M. Q. Jan

Geological Society
Special Publication
No. 170

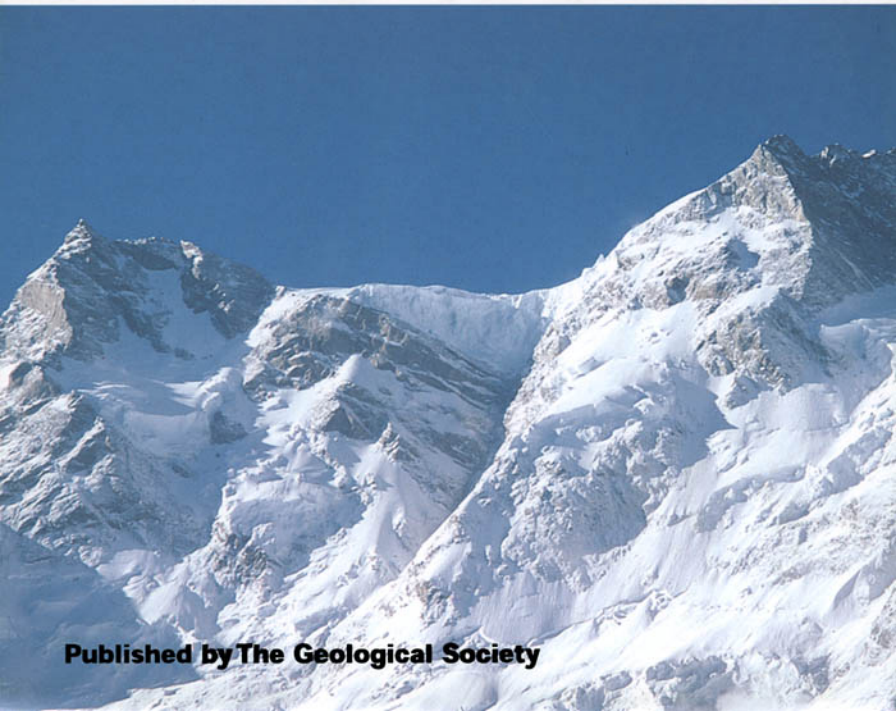

Published by The Geological Society

Tectonics of the Nanga Parbat Syntaxis and the Western Himalaya

Geological Society Special Publications
Series Editors
A. J. HARTLEY
R. E. HOLDSWORTH
A. C. MORTON
M. S. STOKER

Special Publication reviewing procedure

The Society makes every effort to ensure that the scientific and production quality of its books matches that of its journals. Since 1997, all book proposals have been refereed by specialist reviewers as well as by the Society's Publications Committee. If the referees identify weaknesses in the proposal, these must be addressed before the proposal is accepted.

Once the book is accepted, the Society has a team of series editors (listed above) who ensure that the volume editors follow strict guidelines on refereeing and quality control. We insist that individual papers can only be accepted after satisfactory review by two independent referees. The questions on the review forms are similar to those for *Journal of the Geological Society*. The referees' forms and comments must be available to the Society's series editors on request.

Although many of the books result from meetings, the editors are expected to commission papers that were not presented at the meeting to ensure that the book provides a balanced coverage of the subject. Being accepted for presentation at the meeting does not guarantee inclusion in the book.

Geological Society Special Publications are included in the ISI Science Citation Index, but they do not have an impact factor, the latter being applicable only to journals.

More information about submitting a proposal and producing a Special Publication can be found on the Society's web site: www.geolsoc.org.uk

It is recommended that reference to all or part of this book should be made in one of the following ways.

KHAN, M. A., TRELOAR, P. J., SEARLE, M. P. & JAN, M. Q. (eds) 2000. *Tectonics of the Nanga Parbat Syntaxis and the Western Himalaya.* Geological Society, London, Special Publications, **170**.

WHITTINGTON, A., HARRIS, N. B. W., AYRES, M. W. & FOSTER, G. 2000. Tracing the origins of the western Himalaya: an isotopic comparison of the Nanga Parbat Massif and Zanskar Himalaya. *In:* KHAN, M. A., TRELOAR, P. J., SEARLE, M. P. & JAN, M. Q. (eds) *Tectonics of the Nanga Parbat Syntaxis and the Western Himalaya.* Geological Society, London, Special Publications, **170**, 201–218.

GEOLOGICAL SOCIETY SPECIAL PUBLICATION NO. 170

Tectonics of the Nanga Parbat Syntaxis and the Western Himalaya

EDITED BY

M. ASIF KHAN
University of Peshawar, Pakistan

PETER J. TRELOAR
Kingston University, UK

MICHAEL P. SEARLE
Oxford University, UK

and

M. QASIM JAN
University of Peshawar, Pakistan

2000
Published by
The Geological Society
London

THE GEOLOGICAL SOCIETY

The Geological Society of London was founded in 1807 and is the oldest geological society in the world. It received its Royal Charter in 1825 for the purpose of 'investigating the mineral structure of the Earth' and is now Britain's national society for geology.

Both a learned society and a professional body, the Geological Society is recognized by the Department of Trade and Industry (DTI) as the chartering authority for geoscience, able to award Chartered Geologist status upon appropriately qualified Fellows. The Society has a membership of 8600, of whom about 1500 live outside the UK.

Fellowship of the Society is open to persons holding a recognized honours degree in geology or a cognate subject and who have at least two years' relevant postgraduate experience, or not less than six years' relevant experience in geology or a cognate subject. A Fellow with a minimum of five years' relevant postgraduate experience in the practice of geology may apply for chartered status. Successful applicants are entitled to use the designatory postnominal CGeol (Chartered Geologist). Fellows of the Society may use the letters FGS. Other grades of membership are available to members not yet qualifying for Fellowship.

The Society has its own Publishing House based in Bath, UK. It produces the Society's international journals, books and maps, and is the European distributor for publications of the American Association of Petroleum Geologists (AAPG), the Society for Sedimentary Geology (SEPM) and the Geological Society of America (GSA). Members of the Society can buy books at considerable discounts. The Publishing House has an online bookshop (http://bookshop.geolsoc.org.uk).

Further information on Society membership may be obtained from the Membership Services Manager, The Geological Society, Burlington House, Piccadilly, London W1V 0JU (Email: enquiries@geolsoc.org.uk; tel: +44 (0)171 434 9944).

The Society's Web Site can be found at http://www.geolsoc.org.uk/. The Society is a Registered Charity, number 210161.

Published by The Geological Society from:
The Geological Society Publishing House
Unit 7, Brassmill Enterprise Centre
Brassmill Lane
Bath BA1 3JN, UK
Orders: Tel. +44 (0)1225 445046
Fax +44 (0)1225 442836
Online bookshop: http://bookshop.geolsoc.org.uk

First published 2000

British Library Cataloguing in Publication Data

A catalogue record for this book is available from the British Library.

ISBN 1-86239-061-4
ISSN 0305-8719

Typeset by WKS, Westonzoyland, UK

Printed by Hobbs the Printers, Southampton, UK

Distributors

USA
AAPG Bookstore
PO Box 979
Tulsa
OK 74101-0979
USA
Orders: Tel. +1 918 584-2555
Fax +1 918 560-2652
Email bookstore@aapg.org

Australia
Australian Mineral Foundation Bookshop
63 Conyngham Street
Glenside
South Australia 5065
Australia
Orders: Tel. +61 88 379-0444
Fax +61 88 379-4634
Email bookshop@amf.com.au

India
Affiliated East-West Press PVT Ltd
G-1/16 Ansari Road, Daryaganj,
New Delhi 110 002
India
Orders: Tel. +91 11 327-9113
Fax +91 11 326-0538

Japan
Kanda Book Trading Co.
Cityhouse Tama 204
Tsurumaki 1-3-10
Tama-shi
Tokyo 206-0034
Japan
Orders: Tel. +81 (0)423 57-7650
Fax +81 (0)423 57-7651

Contents

Acknowledgements

The papers in this volume arise from the thirteenth Himalaya–Karakoram–Tibet workshop held in the University of Peshawar, Pakistan on 20–22 April 1998. The meeting was convened by M. Asif Khan and M. Qasim Jan. Peter Treloar wishes to express admiration to Pam Nieto for, yet again, permitting her home to be overrun by mountains of Geological Society-related paperwork (see Geological Society of London Special Publications Numbers 74 and 138).

We also express our thanks to Bob Holdsworth and the Tectonic Studies Group for partial funding for the reproduction of the colour fold-out maps for the Hildebrand *et al.* and Corfield & Searle papers in this volume.

The editors wish to acknowledge reviews by the following geoscientists:

R. Anckiewicz
L. Arbaret
T. W. Argles
J.-P. Burg
R. W. H. Butler
P. R. Cobbold
S. J. Cuthbert
S. M. de Bari
P. D. Clift
W. D. Cunningham
G. R. Davies
T. Dempster
E. Derbyshire
J. A. DiPietro
M. A. Edwards
E. Fielding
C. R. L. Friend
M. Gaetani
M. T. George
J. Grocott
D. Haddad
N. B. W. Harris
P. R. Hildebrand
M. S. Hubbard
S. H. Lamb
R. D. Law
R. J. Lisle
K. J. McCaffrey
J. Miller
P. J. O'Brien
A. I. Okay
Y. M. R. Najman
R. R. Parrish
M. G. Petterson
L. Ratschbacher
H. G. Reading
A. Richards
A. H. F. Robertson
H. R. Rollinson
D. Rust
J. W. Shervais
R. A. Strachan
I. M. Villa
J. D. Vitek
D. J. Waters
J. Wheeler
B. F. Windley
A. G. Whittington
H. Yamomoto
A. Zanchi
P. K. Zeitler

This page intentionally left blank

Tectonics of the Nanga Parbat syntaxis and the western Himalaya: an introduction

PETER J. TRELOAR[1], MICHAEL P. SEARLE[2], M. ASIF KHAN[3] & M. QASIM JAN[3]
[1]*Centre for Earth and Environmental Sciences Research, School of Geological Sciences, Kingston University, Kingston-upon-Thames, Surrey KT1 2EE, UK*
[2]*Department of Earth Sciences, Oxford University, Parks Road, Oxford OX2 3PR, UK*
[3]*National Centre of Excellence in Geology, University of Peshawar, Peshawar, NWFP, Pakistan*

Often described as a natural laboratory, the Himalaya are probably the ideal place in which to study ongoing continent–continent collision. This volume focuses on the geology of the northwestern part of the Himalaya which provides the most complete and best-exposed transect across the range. Here, in northern Pakistan and in Ladakh in northwest India, the full profile across the south Asian continental margin, and the north Indian margin is superbly exposed in mountains reaching as high as K2 (8611 m) and Nanga Parbat (8125 m). The south Asian geology is exemplified in the Karakoram and Hindu Kush ranges along the north and northwestern frontiers of Pakistan. The unique Kohistan–Dras island-arc terrane is sandwiched within the Tethyan suture zone between India and Asia. Rocks of the northern margin of the Indian Plate are exposed in both the Zanskar and the Pakistan Himalaya. The northern sedimentary carbonate platform of the Indian Plate, magnificently exposed in the mountains of Zanskar and Ladakh, is largely missing in Pakistan where the Kohistan arc has been obducted southward onto the metamorphosed rocks of the internal crystalline zones of the Indian Plate. The Nanga Parbat syntaxis represents an orogenic bend developed within a convergent zone in the thrust belt where the south-vergent thrusts of the central and eastern Himalaya swing around through 300 degrees.

The history of geological research in the Himalaya extends back to some of the earliest explorers and climbers who visited the region. Two significant problems have affected mapping of the topography and geology of the Himalaya. The first of these is the sheer logistical problem of attaining access to extremely rugged terrain. The second is a political problem. In the NW Himalaya, access to rocks along the disputed border between India and Pakistan is largely forbidden to foreigners. Similarly, easy access northward across the Chinese–Pakistan border has only been possible since the opening of the Khunjerab Pass in 1986. It is arguable that prior to the Russian invasion of Afghanistan in 1980, the geologically best known of the Himalayan nations was Afghanistan, largely through the detailed mapping of Wittekindt & Weipper (1973) and Wolfart & Wittekindt (1980). Since then, advances in understanding of the geology of Afghanistan have been limited to re-interpretations based on satellite imagery or increases in knowledge of the geology of surrounding states such as Pakistan. As a result of these problems, many regions of the Himalayan chain remain poorly mapped or completely unmapped. Containing many new maps, this volume goes part of the way towards addressing this shortfall.

Despite the problems of access, the Himalaya and adjoining mountain ranges continue to be a magnet to earth scientists. The geology of northern Pakistan was largely unknown until about 20 years ago. Until then much of what was known of the region was due to the work of the Geological Survey of India, especially Hayden (1915) and Wadia (1931, 1932). Some aspects of the geology were summarized in volumes that dealt with the geology of the whole of pre-partitioning India (e.g. Wadia 1919). Some geology was carried out by geologists attached to major expeditions to the Karakoram (e.g. Desio 1930; Auden 1938). However, really detailed regional scale work truly commenced only in the 1970s during which R. A. K. Tahirkelli from the University of Peshawar carried out much pioneering work in the northern part of the Indian Plate, the Hindu Kush and

From: KHAN, M. A., TRELOAR, P. J., SEARLE, M. P. & JAN, M. Q. (eds) *Tectonics of the Nanga Parbat Syntaxis and the Western Himalaya*. Geological Society, London, Special Publications, **170**, 1–6. 1-86239-061-4/00/$15.00

Karakoram mountains of the southern part of the Asian Plate and what is now recognized as the Kohistan arc. This work was summarised in 1982 in a superbly illustrated Geological Bulletin of the University of Peshawar (Tahirkelli 1982) as well as in Tahirkelli *et al.* (1979). A then useful summary of the broader effects of the Himalayan orogeny was given in Farah & De Jong (1979). In 1980 the Karakoram Highway (KKH), that stretches from Islamabad in Pakistan through to Kashgar in China, was opened and this stimulated an extraordinary influx of geoscientists into the region. The KKH straddles not just the northern margin of the Indian Plate and the southern margin of the Asian Plate, but also the Cretaceous Kohistan island arc sandwiched between the two. An early synthesis of the geology along the Pakistani section of the KKH was given in the proceedings of an international expedition that traversed the KKH immediately on its completion (Miller 1982). A recent literature audit showed that between 1980 and 1997, over 200 papers had been authored or co-authored on the region traversed by the KKH by British, French and German geoscientists alone. A complete reference list up to 1996 and synthesis of the geology of N. Pakistan is given in Kazmi & Jan (1997). This volume builds upon this recent explosion of geological knowledge.

The essential geological framework of the Pakistan Himalaya is summarized briefly below. The Kohistan–Dras island arc was initiated offshore of Asia during the late Jurassic or early Cretaceous. The arc sutured to the southern margin of the Asian Plate at between 102 Ma, the age of emplacement of the pre-suturing Matum Das pluton (Petterson & Windley 1985) and 85 Ma. The later age is derived from an *c.* 84 Ma U–Pb zircon age (Zeitler *et al.* 1981) for undeformed gabbro-norites of the Chilas complex, which contain xenoliths of Gilgit Formation gneisses that had been deformed during suturing. The age is compatible with a Rb–Sr age of 87 ± 19 Ma (Mikoshiba *et al.* 1999) assuming that their sample 92CH60 is included in the regression. After suturing the arc behaved as an Andean-style volcanic arc. Thickening of the arc accompanied suturing. Most of the deformation and metamorphism in the arc appears to have post-dated suturing, but predated collision with India. Deformation and metamorphism within the southern margin of the Asian plate appears to have been diachronous with tectonothermal events during the late Cretaceous (after suturing with Kohistan) and the Tertiary. A full review of the Cretaceous through to Tertiary history of the Asian Plate in Pakistan is given in Searle *et al.* (1999) and of the Kohistan arc in Treloar *et al.* (1996) and Searle *et al.* (1999). Collision between the arc and continental India followed closure of neo-Tethys. The age of collision is not precisely determined, although on the basis of the sedimentary record is likely to have been at about 55 Ma (see discussions in Garzanti *et al.* 1996, Pivnik & Wells 1996, Rowley 1996 and Treloar 1997). A late Cretaceous to Paleocene ophiolite emplacement event predated final closure of Neotethys (Searle 1986; Beck *et al.* 1995; Searle *et al.* 1997). Since collision the leading edge of the Indian Plate has undergone deformation, burial, metamorphism and exhumation. In contrast to the main Himalayan chain to the east, peak metamorphism in the Pakistan Himalaya was Eocene in age (Treloar & Rex 1990). Exhumation during the early Miocene was by a combination of north-vergent extension (Burg *et al.* 1996; Vince & Treloar 1996) and erosion with sediments deposited in the foreland basins to the south of the topographic high (Burbank *et al.* 1996). Deformation of these sedimentary basins continues to the present day.

The northwest Himalaya differ from the main Himalayan chain for three main reasons. Here the Asian and Indian plates are separated by the Kohistan–Dras island arc, peak metamorphism was Eocene rather than Miocene in age, and the south-vergent thrust systems are deformed by the West Himalayan syntaxes. First recognized by Wadia (1931, 1932), the syntaxes are crustal-scale, north-trending antiformal structures which are essentially half windows. The Hazara syntaxis to the south deforms thrusts of the external zones. Within its core, foreland basin sediments on the footwall of the Main Boundary Thrust have been tectonically uplifted (Bossart *et al.* 1988). The Nanga Parbat syntaxis deforms thrusts of the internal zones. Within its core, crystalline rocks of the Indian plate have been tectonically exhumed from beneath their cover of volcanic rocks of the Kohistan–Ladakh arc sequence that had been thrust onto the Indian Plate early in collision. Present day uplift rates within the Nanga Parbat syntaxis may be as high as 6 mm a^{-1} (Zeitler 1985). Mechanisms of uplift and its deformational effects, timing of uplift, and the magmatic effects of rapid uplift and exhumation have been the focus of exhaustive research within the Nanga Parbat syntaxis during the last ten years. A number of British scientists funded by the Natural Environmental Research Council and the Royal Society have been working in the syntaxis. At the same time, a team from the USA under the leadership of P. K. Zeitler has been working in the area with funding from the National Science Foundation. Papers

from both of these groups are included in this volume.

In setting the regional scene for the volume, **Caporali** describes the gravity field of the Karakoram Mountain Range and surrounding areas. He demonstrates the gravimetric low associated with the Nanga Parbat syntaxis which is a function of the rapid differential uplift within the syntaxis as well as the presence of large negative anomalies between the Karakoram Fault and the Main Karakoram Thrust. The relationship between crustal scale geological features (sutures, thrusts and syntaxes) and gravitational potential is clear when plotted on a regional scale geology map (Caporali, fig. 3).

The next seven papers deal with the Nanga Parbat syntaxis. In the first of these, **Treloar *et al.*** outline the significance of field relationships in defining long term geological histories. Mafic sheets within Indian plate gneisses within the Nanga Parbat syntaxis clearly document a polyphase deformation and metamorphic history. In stressing the importance of recognising complex histories, the authors recall the seminal work of John Sutton and Janet Watson in the Lewisian Complex.

The next papers relate to the structural and topographic evolution of the syntaxis. **Butler** revisits his earlier studies (Butler & Prior 1989*a*, *b*; Butler *et al.* 1989) on the western margin of the syntaxis to refine, in the light of recent field-work, an interpretation of the structures that accommodated bodily uplift of the syntaxis along west-vergent thrust faults. **Edwards *et al.*** describe structures exposed along the south-west of the syntaxis (i.e. to the south of those described by **Butler**). Uplift here was along steep, east-side up shear zones. Whereas **Butler** and **Edwards *et al.*** describe structures that accommodated uplift along the western margin of the syntaxis, **Argles** describes the structural evolution of part of the eastern margin of the syntaxis. **Butler *et al.*** describe a structural section that crosses the syntaxis and incorporate data presented here and elsewhere to derive a model for the structural evolution of the syntaxis as a whole. This model should be viewed in connection with that published by Schneider *et al.* (1999). As geochronological data were first used to hint at the speed of syntaxial growth (Zeitler 1985), it is appropriate that a more profound data set should be used in an attempt to constrain uplift mechanisms. To this end, **Treloar *et al.*** use geochronological data to outline firstly, that peak metamorphism within the syntaxis is Eocene–Oligocene, rather than Miocene, in age, and also to indicate how geochronological data can be used to refine the regional scale features that accommodated uplift within the syntaxis. This set of five papers provide a benchmark on which future structural studies of the syntaxis can be built. The Nanga Parbat massif encompasses greater than 6000 m of relief. This relief is a function of the rapid Neogene uplift and results in rapid erosional unroofing of the crystalline basement complex. **Shroder & Bishop** explore aspects of this unroofing and demonstrate that late Pleistocene processes were sufficiently rigorous to produce the present-day pronounced relief. Whereas elsewhere in the Himalaya, extensional unroofing has played an important part in exhumation, at Nanga Parbat, where exhumation is most rapid, it appears not to have done so, a point also made by **Edwards *et al.***, **Bishop & Shroder** argue that accelerated uplift and erosion are part of a feed-back loop with tectonic uplift. They also use remotely sensed imagery to derive a hierarchical order of topographic complexity that is a function of erosion dynamics. The use of remote sensing is probably the prime way in which the topography of the Himalaya will be mapped in future.

Large crustal-scale structures like the Nanga Parbat syntaxis should encourage debate. Two papers here do just that. In a far-reaching paper **Burg & Podladchikov** model the evolution of the Himalayan syntaxes numerically, (the Nanga Parbat syntaxis and the Namche Barwhe syntaxis at the eastern end of the Himalayan chain). Their numerical modelling indicates that pure shear thickening and symmetric buckling accommodate shortening until, at a certain strain, an asymmetric thrust-like flow pattern occurs on a crustal to lithospheric scale and it is on this that the syntaxes grow. A side-effect of the model is that syntaxial growth is accompanied by the growth of marginal basins, in the case of the Nanga Parbat syntaxis these are the Kashmir and Peshawar basins. That these basins may be the result of syntaxial uplift is in contradiction to previous models which infer them to be piggy-back basins developed above late-stage thrusts such as the Main Boundary Thrust. **Whittington *et al.*** use isotopic data to demonstrate that the crystalline Indian Plate rocks contained within the core of the Nanga Parbat syntaxis are typical of the Lesser Himalaya rather than of the Higher Himalaya. The implications of this are profound as they stress the differences between the Pakistan Himalaya and the Indian and Nepalese Himalaya, and indicate that models that suggest that the syntaxis is developed above the lateral tip of the Main Central Thrust may be incorrect.

The remaining papers in this volume provide a cross section across the Himalayan collision zone from the Asian plate through the Kohistan arc to

the Indian plate. It has long been known that, prior to collision, the southern margin of the Asian plate was a tectonic collage formed of a series of exotic blocks sequentially accreted to the southern margin of continental Asia. The Kohistan–Dras arc was the last of these blocks to be accreted to Asia. **Zanchi *et al.*** describe one of the suture zones that encompassed the southward growth of Asia during the late Mesozoic and show how the Tirich Mir Fault Zone can be described as a suture on the basis of the presence of ophiolitic peridotites. Also on the Asian Plate, **Hildebrand *et al.*** describe the geological evolution of the Hindu Kush in the NW Frontier of Pakistan. They document a major late Mesozoic deformation probably related to suturing of Kohistan to Asia as well as an Oligocene–Miocene metamorphism–deformation event that was likely related to indentation of Kohistan into Asia following collision of Kohistan and India. This paper comes together with an important new geological map of a large part of the Hindu Kush.

Three papers deal with aspects of the Kohistan arc sequence. **Yamamoto & Nakamura** and **Anczkiewicz & Vance** date peak metamorphism within the Kamila amphibolite belt at the structural base of the arc at *c.* 95 Ma with amphibolite-facies retrogression at *c.* 85 Ma (see Treloar *et al.* 1989). **Arbaret *et al.*** describe a variety of SW-vergent structures within the Kamila amphibolite belt that range from magmatic through sub-magmatic to amphibolite facies. This deformation spans the period documented geochronologically by **Yamamoto & Nakamura** and **Anczkiewicz & Vance**. What remains unclear is to what these deformation, magmatic and metamorphic events relate. **Arbaret *et al.*** interpret the magmatism and deformation as having occurred at the base of the arc during ongoing subduction of the Tethyan oceanic lithosphere beneath Kohistan. An alternative solution is that the deformation documents a change in subduction dynamics following on from suturing of Kohistan to Asia.

Three papers deal with the sutures that bound the arc. **Weinburg *et al.*** describe the suture zone between Asia and the Ladakh part of the Kohistan–Ladakh arc sequence and show that closure must have pre-dated 68 ± 1 Ma. **Robertson** and **DiPietro *et al.*** discuss the evolution of the suture between the Mesozoic arc and the Indian Plate. **Robertson** finds the Indus Suture Zone in Ladakh to be a zone of complex multi-stage processes involving deformational features which span the time interval from subduction through emplacement to post-collisional shortening. **DiPietro *et al.*** provide a detailed account of the Main Mantle Thrust (MMT) which separates the Kohistan arc from the Indian Plate and which is the true western continuation of the Indus–Tsangpo Suture Zone. They highlight the fact that the MMT is constituted of a number of strands of various ages. Although clearly a major early Tertiary tectonic feature, the MMT has been transposed many times during the Tertiary.

Three papers detail the geology of the internal zones of the Indian Plate. **Corfield & Searle** describe the geology of the north Indian continental margin in Zanskar. They include an important new map and estimate shortening amounts across the north Indian margin. These estimates incorporate both late Cretaceous to Palaeocene ophiolite emplacement events and subsequent post-collisional shortening. **Lombardo *et al.*** describe the occurrence of glaucophane- and barroisite-bearing eclogites from the Upper Kaghan Valley. **Fontan *et al.*** also describe high-pressure rocks from Indian plate sequences in the Neelum Valley. Although eclogites have previously been described from Indian Plate sequences of north Pakistan (Pognante & Spencer 1991), it is only recently that the high pressure nature of these rocks has been recognized (O'Brien *et al.* 1999). The full significance of these rocks is as yet unclear.

Abassi & Friend explore the significance of exotic conglomerates in the Neogene Siwalik succession and relate them in part to growth of the Nanga Parbat syntaxis. They show the Pliocene-aged Janak conglomerate to be derived from a topographic high, with erosion shedding into the Neogene foreland basin.

Finally, **Badshah *et al.*** provide a detailed map of part of the Pakistan–Afghanistan border. This important map forms a link between those of Jones (1960). Wittekindt & Weippert (1973) and Bender & Raza (1995) and with these documents an important part of the collision zone between the Indian Plate and the Afghanistan Block (see Treloar & Izatt 1993).

References

AUDEN, J. B. 1938. Geological Results. *In*: SHIPTON, E. (ed.) *The Shaksgam Expedition 1938. Geographical Journal*, **91**, 335–336.

BECK, R., BURBANK, D. W., SERCOMBE, W. J., RILEY, G. W., BARNDT, J. K., BERRY, J. R., AFZAL, J., KHAN, A. M., JURGEN, H., METJE, J., CHEEMA, A., SHAFIQUE, N. A., LAWRENCE, R. D. & KHAN, M. A. 1995. Stratigraphic evidence for an early collision between northwest India and Asia. *Nature*, **373**, 55–58.

BENDER, F. K. & RAZA, H. A. 1995. *The geology of Pakistan*. Bietrage zur regionalen geologie der Erde. Band 25.

BOSSART, P., DIETRICH, D., GRECO, A., OTTIGER, R. & RAMSAY, J. G. 1988. The tectonic structure of the Hazara-Kashmir syntaxis, southern Himalayas, Pakistan. *Tectonics*, **7**, 273–297.

BURBANK, D. W., BECK, R. A. & MULDER, T. 1996. The Himalayan Foreland Basin. *In*: YIN, A. & HARRISON, T. M. (eds) *The Tectonic Evolution of Asia*. Cambridge University Press, 149–188.

BURG, J.-P., CHAUDHRY, M. N., GHAZANFAR, M., ANCZKIEWICZ, R. & SPENCER, D. A. 1996. Structural evidence for backsliding of the Kohistan arc in the collisional system of NW Pakistan, *Geology*, **24**, 739–742.

BUTLER, R. W. H. & PRIOR, D. J. 1988*a*. Tectonic controls on the uplift of Nanga Parbat, Pakistan Himalaya. *Nature*, **333**, 247–250.

—— & —— 1988*b*. Anatomy of a continental subduction zone. *Geologische Rundschau*, **77**, 239–255.

——, —— & KNIPE, R. J. 1989. Neotectonics of the Nanga Parbat syntaxis, Pakistan, and crustal stacking in the northwest Himalaya. *Earth and Planetary Science Letters*, **94**, 329–343.

DESIO, A. 1930. Geological work of the Italian expedition to the Karakoram. *Geographical Journal*, **75**, 402–411.

FARAH, A. & DEJONG, K. A. (eds) 1979. *Geodynamics of Pakistan*. Geological Survey of Pakistan, Quetta.

GARZANTI, E., CRITELLI, S. & INGERSOLL, R. V. 1996. Paleogeographic and paleotectonic evolution of the Himalayan Range as reflected by detrital modes of Tertiary sandstones and modern sands (Indus transect, India and Pakistan). *Geological Society of America Bulletin*, **108**, 631–642.

HAYDEN, H. H. 1915. Notes on the geology of Chitral, Gilgit and the Pamir. *Records of the Geological Survey of India*, **45**, 271–326.

JONES, A. G. 1960. *Reconnaissance geology of part of western Pakistan: A Colombo Plan Co-operative Project Report*. Government of Canada.

KAZMI, A. H. & JAN, M. Q. 1997. *Geology and tectonics of Pakistan*. Graphic Publishers, Karachi.

MILLER, K. (ed.) 1982. *Continents in Collision*. Royal Geographical Society International Karakoram project. George Philip & Son, London.

MIKOSHIBA, M. U., TAKAHASHI, Y., KAUSAR, A. B., KHAN, T., KUBO, K. & SHIRAHASE, T. 1999. Rb-Sr isotopic study of the Chilas igneous complex, Kohistan, northern Pakistan. *In*: MACFARLANE, A., SORKHABI, R. B. & QUADE, J. (eds) *Himalaya and Tibet: Mountain roots to mountain tops*. Geological Society American, Special Papers, **328**, 47–57.

O'BRIEN, P. J., ZOTOV, N., LAW, R., KHAN, M. AHMED & JAN, M. Q. 1999. Coesite in eclogite from the Upper Kaghan Valley Pakistan: a first record and implications. *Terra Nostra*, **99**, 109–111.

PETTERSON, M. G. & WINDLEY, B. F. 1985. Rb-Sr dating of the Kohistan arc batholith in the trans-Himalaya of N. Pakistan and its tectonic implications. *Earth and Planetary Science Letters*, **74**, 45–57.

POGNANTE, U. & SPENCER, D. A. 1991. First record of eclogites from the Himalayan belt, Kaghan Valley, Northern Pakistan. *European Journal of Minerology*, **3**, 613–618.

PIVNIK, D. A. & WELLS, N. A. 1996. The transition from Tethys to the Himalaya as recorded in NW Pakistan. *Geological Society of America Bulletin*, **108**, 1295–1313.

ROWLEY, D. B. 1996. Age of initiation of collision between India and Asia: a review of the stratigraphic data. *Earth and Planetary Science Letters*, **145**, 1–13.

SCHNEIDER, D. A., EDWARDS, M. A., KIDD, W. S. F, KHAN, M. A., SEEBER, L. & ZEITLER, P. K. 1999. Tectonics of Nanga Parbat, western Himalaya: synkinematic plutonism within the doubly vergent shear zones of a crustal scale pop-up structure. *Geology*, **27**, 999–1002.

SEARLE, M. P. 1986. Structural evolution and sequence of thrusting in the High Himalaya, Tibetan-Tethys and Indus suture zones of Zanskar and Ladakh, western Himalaya. *Journal of Structural Geology*, **8**, 923–936.

——, CORFIELD, R. M., STEPHENSON, B. & MCCARRON, J. 1997. Structure of the North Indian continental margin in the Ladakh–Zanskar Himalayas: implications for the timing of the Spontang ophiolite, India–Asia collision and deformation events in the Himalaya. *Geological Magazine*, **134**, 297–316.

——, KHAN, M. A., FRASER, J. E., GOUGH, S. J. & JAN, M. Q. 1999. The tectonic evolution of the Kohistan–Karakoram collision belt along the Karakoram Highway transect, north Pakistan. *Tectonics*, **18**, 929–949.

TAHIRKELLI, R. A. K. 1982. Geology of the Himalaya, Karakoram and Hindukush in Pakistan. *University of Peshawar Geological Bulletin*, **15**, 1–31.

——, MATTAUER, M., PROST, F. & TAPPONNIER, P. 1979. The India–Eurasia suture zone in northern Pakistan: synthesis and interpretation of recent data at plate scale. *In*: FARAH, A. & DEJONG, K. A. (eds) *Geodynamics of Pakistan*. Geological Survey of Pakistan, 125–130.

TRELOAR, P. J. 1997. Thermal controls on early-Tertiary, short-lived, rapid regional metamorphism in the NW Himalaya, Pakistan. *Tectonophysics*, **273**, 77–104.

—— & IZATT, C. N. 1993. Tectonics of the Himalayan collision zone between the Indian plate and the Afghan Block: a synthesis. *In*: TRELOAR, P. J. & SEARLE, M. P. (eds) *Himalayan Tectonics*. Geological Society, London, Special Publications, **74**, 69–87.

—— & REX, D. C. 1990. Cooling, uplift and exhumation rates in the crystalline thrust stack of the North Indian Plate, west of the Nanga Parbat syntaxis. *Tectonophysics*, **180**, 323–349.

——, ——, GUISE, P. G., COWARD, M. P., SEARLE, M. P., WINDLEY, B. F., PETTERSON, M. G., JAN, M. Q. & LUFF, I. W. 1989. K-Ar and Ar-Ar geochronology of the Himalayan collision on

NW Pakistan: constraints on the timing of suturing, deformation, metamorphism and uplift. *Tectonics*, **8**, 881–909.

——, PETTERSON, M. G., JAN, M. Q. & SULLIVAN, M. 1996. A re-evaluation of the stratigraphy and evolution of the Kohistan arc sequence, Pakistan Himalaya: implications for magmatic and tectonic arc-building processes. *Journal of the Geological Society, London*, **153**, 677–680.

VINCE, K. J. & TRELOAR, P. J. 1996. Miocene, north-vergent extensional displacements along the Main Mantle Thrust, NW Himalaya, Pakistan. *Journal of the Geological Society, London*, **153**, 677–680.

WADIA, D. N. 1919. *The geology of India*. Macmillan & Co, London.

—— 1931. The syntaxis of the northwest Himalaya; its rocks, tectonics and orogeny. *Records of the Geological Survey of India*, **65**, 189–220.

—— 1932. Note on the geology of Nanga Parbat (Mt Diamar) and adjoining portions of Chilas, Gilgit district, Kashmir. *Records of the Geological Survey of India*, **66**, 212–234.

WITTEKINDT, H. & WEIPPERT, D. 1973. *Geologisches karte von Zentral und Sud-Afghanistan. 1 : 500000*. 4 sheets. Bundesanst fur Bodenforsch. Hannover.

WOLFART, R. & WITTEKINDT, H. 1980. *Geologie von Afghanistan*. Beitrage zur regionalen geolgie der Erde. **14**.

ZEITLER, P. K. 1985. Cooling history of the NW Himalaya. *Tectonics*, **4**, 127–135.

——, TAHIRKHELI, R. A. K., NAESSER, C., JOHNSON, N. & LYONS, J. 1981. Preliminary fission track ages from the Swat Valley, northern Pakistan. *Geological Bulletin of the University of Peshawar*, **13**, 63–65.

The gravity field of the Karakoram Mountain Range and surrounding areas

A. CAPORALI

Dipartimento di Geologia, Paleontologia e Geofisica, Università di Padova, Via Giotto 1, I-35137 Padova, Italy (e-mail: alex@geol.unipd.it)

Abstract: A 'blank on the map' only 60 years ago, the Karakoram Range has been explored and surveyed with greater difficulty than the Himalaya and Tibet due to its rugged terrain and extensive glaciation. In the past ten years we have succeeded in doubling the number of gravity stations. A substantial improvement in coverage and overall quality was obtained by concentrating on previously unsurveyed areas and by validating older data with more accurate measurements. Our data were merged with earlier data, converted to full Bouguer anomalies and gridded. The resulting Bouguer anomaly map defines very precisely the gravimetric low associated with the Nanga Parbat–Haramosh syntaxis, and the huge negative anomalies between the Karakoram Fault and the Main Karakoram Thrust. Large negative values are now visible also in the Ghujerab–Khunjerab areas. Correlation of the topography and Bouguer anomaly shows that a plate of flexural rigidity with $D = 2 \times 10^{24}$ Nm fits the coherence data in the Karakoram at all but two distinct frequency ranges centred at wavelengths of 80 and 300 km. In a rheologically layered lithosphere developing a buckling instability under horizontal compression, the observed spectral features of the topography and Bouguer gravity anomalies constrain the depth of the competent layers to be in the range 13–20 km and 50–75 km respectively.

In a short note presented at the Royal Society, Airy (1855) outlined fundamental ideas on the relationship between gravity anomalies and topography. The work was stimulated by the failure of earlier attempts (Pratt 1855) to explain the exceedingly small change in the observed deflection of the vertical between trigonometric stations of the Great Meridian Arc in India. It gave a physically sound basis to a suggestion of Walker (1879), formerly Surveyor General, that there was an apparent mass deficiency underneath the Himalaya. Nearly ten years later, Stokes (1864) took interest in the idea of root formation as a mechanism of support of topographic relief, and recommended a densification of gravity stations by means of measures of the anomalies in the vertical component of gravity, rather than the horizontal components. The argument was that the former measures could be made at low cost by pendulums, while the latter required the comparison of precisely measured astronomic and geodetic latitudes and longitudes, which was possible only at trigonometric vertexes.

An analysis of gravity anomalies on a global scale (Heiskanen & Vening Meinesz 1958) has provided a solid indication that the crust is, on average, supported by isostasy, in the sense that isostatic anomalies tend to average to zero on a global scale. On a smaller scale, departures from the Airy isostatic model are not rare. Airy himself (1855) emphasized that the crust could not deform under localized loads. Several authors (e.g. Turcotte & Schubert 1982), examining regional situations in different areas, have pointed out that departures from an Airy-type mechanism can be accommodated assuming the existence of a thin, elastic plate somewhere in the region comprising the lower crust and upper mantle. The plate acts as a low-pass filter: roots mirror low frequency topographic loads, whereas loads of shorter wavelengths are supported by the strength of the plate. The amplitude of the crustal thickening decreases as the wavelength of the load decreases.

In the classical theory of cylindrical bending of a thin, elastic plate, the flexural rigidity is the coefficient of the fourth horizontal derivative of the deformation (Landau & Lifshitz 1964): the product of the two is the force which, besides buoyancy and gravity, participates in the balance equation. In the space domain, this equation has been successfully applied to a variety of cases, using more refined versions of the original

From: KHAN, M. A., TRELOAR, P. J., SEARLE, M. P. & JAN, M. Q. (eds) *Tectonics of the Nanga Parbat Syntaxis and the Western Himalaya*. Geological Society, London, Special Publications, **170**, 7–23. 1-86239-061-4/00/$15.00

regional compensation model, along with analytical and numerical solutions: one estimates the flexural rigidity and the abscissa of the end point of the infinite plate by matching, in a least squares sense, the profile of a deformed plate to the density interface which is obtained by inverting the Bouguer anomalies (Parker 1972). This density interface is normally identified as the depth of the neutral fibre of the thin, elastic plate. In the simplest version of this regional compensation model, assuming a value of the crust/mantle density contrast leaves the flexural rigidity D of the plate as the only adjustable parameter (Banks *et al.* 1977). For an acceptable fit, it is necessary to introduce end-conditioning moments and forces at a point in the profile, for example the edge of a broken plate. These boundary conditions are specified by the value of the second and, respectively, third horizontal derivative of the depth of the neutral fibre of the elastic plate at that point, and are interpreted as the result of additional, possibly subsurface, loads. In the frequency domain, the admittance is introduced as the transfer function between topographic load and Bouguer anomaly (Dorman & Lewis 1970). The admittance depends on the flexural rigidity that can be estimated by comparing the theoretical and experimental admittance over a sufficiently wide range of wave numbers. However, in a number of examples (e.g. Lewis & Dorman 1970; McNutt & Parker 1978), inverting the admittance yielded unrealistically low values of the flexural rigidity. Forsyth (1985) has argued that the admittance provides a biased estimate of the flexural rigidity, in the sense that provinces of higher flexural rigidity are down weighted relative to weaker tectonic areas. He suggested the use of the coherence method and, following earlier ideas of McNutt (1983), described a statistical method of treating the subsurface loads. The method has since been used in a number of situations such as, for example, East Africa (Bechtel *et al.* 1987), Australia (Zuber *et al.* 1989) and Tibet (Jin *et al.* 1994). More recently, McKenzie & Fairhead (1997) have shown that the coherence method, in conjunction with Bouguer anomalies, provides at most an upper limit to the flexural rigidity. They proposed to use free air anomalies instead, and showed that the resulting equivalent thickness of the continental lithosphere would decrease and become consistent with the mean depth of the continental crust.

This paper addresses the gravity field of the Karakoram and the way it constrains some basic mechanical properties of the underlying lithosphere. An improved set of gravity data is presented, and the corresponding Bouguer anomalies are shown to constrain the depth of (at least) two density interfaces near 8 and 58 km. The Bouguer anomalies and the topography constrain the equivalent elastic thickness to approximately 61 km, but there are large discrepancies from the purely elastic behaviour at two distinct wavebands. Taking into consideration recent results on the structure of the yield stress envelope of the continental lithosphere, and of the response of a layered lithosphere to horizontal compression, it is concluded that the statistical properties of the gravity and topography data in the Karakoram are interpretable in terms of buckling instability.

Regional tectonic setting

The Karakoram and Hindu Kush (Fig. 1) have been under compression since *c.* 60 Ma, with active continental crust subduction zones converging both from the north (Tarim plate) and south (Indian plate). Seismology studies of the Hindu Kush and Karakoram (Chen & Molnar 1983) show that earthquakes are abundant at depths of 70–100 km and indicate subduction of crustal material from the south and the north. Beneath the Karakoram, the upper mantle is relatively cold (Brandon & Romanowicz 1986), in contrast to the hot upper mantle of Central Tibet (Molnar 1988). Crustal thickening of the west side of the Tibetan plateau is less important than in Central Tibet (Le Pichon *et al.* 1992). The dominant topographic feature of this asymmetry is the Tarim Basin, an old stable mass that has been subsiding from the Carboniferous to the present, and filled by Tertiary sediments (Norin 1946). The Tarim Basin is bordered to the north by the Tien Shan Mountains, with a sharp thrust contact. The low rate of seismic activity in the Tarim supports the hypothesis of the Tarim being underlain by an undeformed lithosphere. Houseman & England (1996) have proposed a 'thin, viscous sheet' model in which the Tarim block acts as a stress guide transmitting stresses to the regions north of the block, and as a secondary indenting block (Molnar & Tapponier 1975; Vilotte *et al.* 1984, 1986; England & Houseman 1985). The predicted region of high strain immediately north of the indenter could be identified within the Tien Shan Range which, according to Roecker *et al.* (1993), has a crustal thickness of 50 km and is one of the most seismically active areas of the collision zone (Molnar & Deng 1984; Avouac *et al.* 1993). Eastwards crustal extrusion of Tibet has been proposed by Molnar & Tapponier (1975) and Armijo *et al.* (1989), on the basis of the large-scale pattern of the sinistral Altyn Tagh strike-

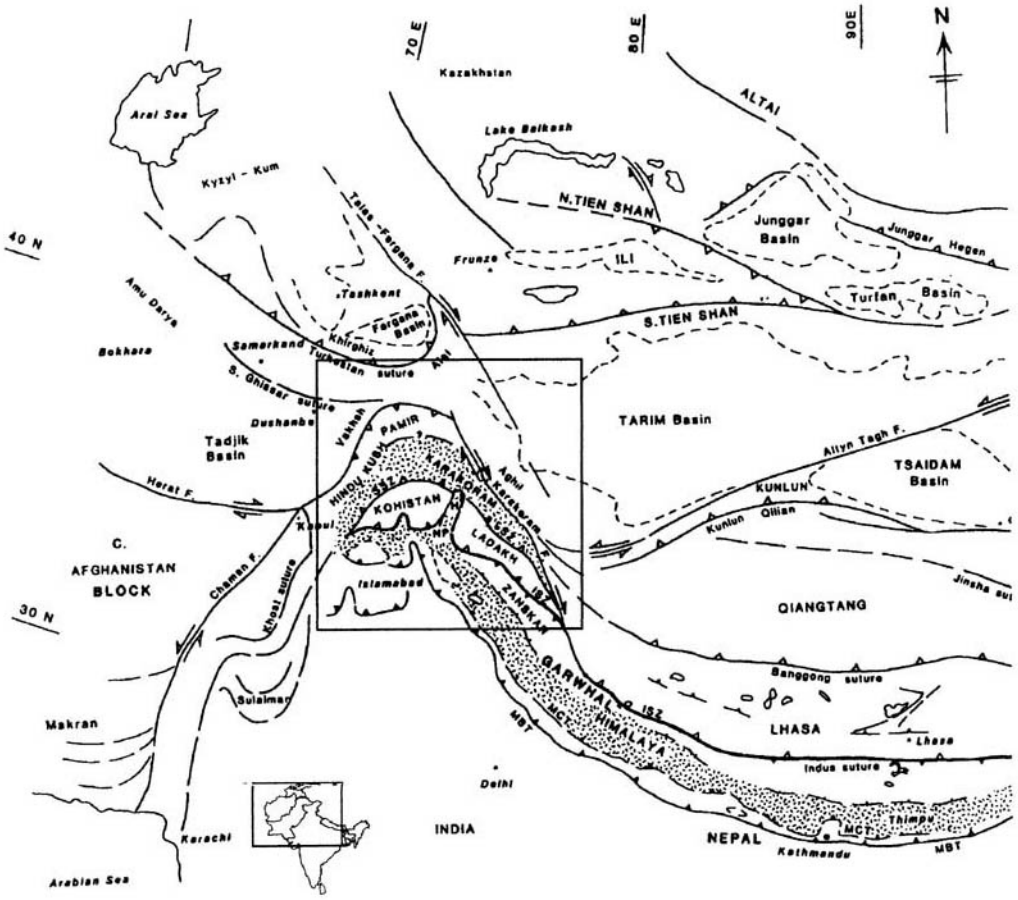

Fig. 1. Major tectonic features of the Karakoram, Tibet and Tien Shan (from Searle 1991). Stippled area indicates outcrop of post-collisional metamorphic rocks. SSZ: Shyok Suture Zone. ISZ: Indus Suture Zone. NP: Nanga Parbat–Haramosh syntaxis. MBT: Main Boundary Thrust. Rectangle indicates the study area.

slip fault to the north and the dextral Karakoram Fault to the south (Avouac & Tapponier 1993).

The Indus Suture Zone is a belt of ophiolites marking the boundary between the Indian and Eurasian plates. In Northern Pakistan the suture bifurcates into the Main Mantle Thrust to the south and the Main Karakoram Thrust/Shyok Suture Zone to the north. The sequence of rocks in between is the Kohistan Ladakh arc terrane. In the Cretaceous, this island arc was squeezed between the colliding Indian and Asian blocks and then thrust onto the Indian plate (Tahirkeli *et al.* 1979; Bard *et al.* 1980). The Kohistan Ladakh arc is cut in two by the Nanga Parbat–Haramosh syntaxis, a domed mass of high grade Indian plate rocks exhumed upwards between the south-moving thrusts of Northern Pakistan and the southwest-moving thrusts of western India (Searle 1991).

Gravity data

Although the first gravity measurements in India date back to the early nineteenth century, systematic pendulum observations started only in 1865 in response to Stokes' argument (1864) that '... pendulum observations may be expected to throw light on the geology of a country'. In the Karakoram, Abetti & Alessio (1929) made the first gravimetric measurements with the Italian expedition to Karakoram and Chinese Turkestan led by F. de Filippi. In 1913 and 1914 they measured 14 stations from Dehra Dun in India to Tashkent in Uzbekistan, via Skardu, Leh and Kashgar, crossing the Karakoram pass. Pendulum observations were made by Glennie and Osmaston of the Survey of India south of Skardu, in the Deosai plains (Tandy 1921). Due to a route accident, no gravimetric observation

was possible during the Italian expedition of the Duke of Spoleto in 1929, when Desio (1936), following earlier accounts by Younghusband (1904), made the first geological reconnaissance of the Karakoram north of K2. From 1929 to 1933 Amboldt (1948), with the Sino-Swedish expedition led by Sven Hedin, measured 42 stations between Urumqi and Leh, some of which coincided with those of de Filippi. A major thrust came from the Desio expedition in 1953–1955 when Marussi (1964) used, for the first time in this zone, the astatic Worden gravimeter to measure 270 gravity stations in Northern Pakistan. Under the leadership of Marussi, a further 72 stations were measured by Ebblin in 1974 and 102 stations by Poretti & Rahim in 1978 (Ebblin *et al.* 1983), covering the Indus valley, Chitral, the Baltoro region and the Hunza valley, to the Khunjerab pass. Under Desio's leadership, from 1988 to 1998 new measurement campaigns were undertaken with the Lacoste Romberg 'G' gravimeter, in the Kun-Lun and Aghil Shaksgam areas (1988), Hispar Biafo glacier system (1990), Chogo Lungma and Haramosh glaciers (1993) (Caporali *et al.* 1991; Caporali 1993, 1995). The Shimshal and Ghujerab valleys were surveyed in 1998. Stations common with previous surveys ensured consistency in the calibration of the gravimeters. Eventually, all the data prior to 1988 were converted from the Potsdam system to the IGSN71 gravity system (Fig. 2). Station coordinates were checked on the maps, which were in turn tested, and sometimes corrected, using coordinates derived from the satellites of the Global Positioning System (GPS) of the US. Terrain corrections were computed for all available data using a modified version of the ETOPO5 Digital Terrain Model (DTM) of the National Oceanic and Atmospheric Administration of the US. To minimize the model deficiencies, the DTM was complemented with the heights of the gravity stations, measured by calibrated aneroids and/or differential GPS, and regridded, thereby minimizing spurious near-field effects. Terrain corrections conventionally assume uniform density of 2670 kg m^{-3}. They were computed with the TC program (Forsberg 1984) of the GRAVSOFT package (Tscherning 1992) up to a distance of 166.7 km from each station using full prism, line mass or point mass models according to the distance. The discrepancy between the heights of the modified model and the observed heights were at most a few metres. The terrain corrections were tested at common stations against the corrections computed manually by Marussi (1964) using the 'quarter inch' maps of the Survey of India and templates based on Hayford zones. The overall uncertainty of the Bouguer anomalies is dominated by the height of the gravity stations. Additional interpolation error comes from the sparse location of the data points. Contouring the Bouguer anomalies with a spacing of 20 mGal (1 mGal = 10^{-5} m s^{-2}) is deemed to be consistent with the overall error budget.

Superposition of the gravity anomaly map with the geological map synthesized by Searle & Khan (1996) (Fig. 3) shows some interesting eatures. The axis of the Karakoram, extending roughly in the SE–NW direction, corresponds to a strip of large negative anomalies (< -500 mGal), suggesting deep root formation. On the NE flank, the anomalies are more negative than on the SW flank, in agreement with the greater average height on the Chinese side than on the Indo-Pakistani side. The comparatively smaller anomalies along the Kohistan arc are consistent with the presence of high-density magmatic rocks to a depth of 7–9 km (Malinconico 1986, 1989). The Nanga Parbat–Haramosh syntaxis represents a major asymmetry in the gravity data. The southernmost (Nanga Parbat) low anomaly area is associated with the Shengus high grade gneisses; in the northernmost area (Haramosh) higher gravity anomalies are associated with the Iskere gneisses. Our data (Fig. 3) indicate that this syntaxial structure of the gravity anomalies is mirrored across the axial Karakoram to the north, in the less well known Shimshal and Ghujerab valleys, which exhibit large negative anomalies. For this gravimetric feature no geological or structural counterpart has, at this time, been reported.

A structural model of the gravity anomalies

Earlier results

Analysing data collected by de Filippi, Amboldt and himself, Marussi (1964) reported important deviations from isostatic equilibrium in the Karakoram. He noticed that the isostatic

Fig. 3. Gravity anomaly map of the Karakoram (subset of Fig. 2). Base geological map is the 1:650000 map of Searle & Khan (1996, with permission). Gravity was measured by Abetti & Alessio (1929), Amboldt (1948), Marussi (1964), Ebblin *et al.* (1983), Caporali *et al.* (1991) and Caporali (1993, 1995). Contour interval is 20 mGal. Location of the gravity stations is indicated by red dots. Terrain corrections are computed using a modified ETOPO5 Digital Terrain Model.

MAP OF THE BOUGUER GRAVITY ANOMA

Contour interval: 20 mGal. Terrain corrections computed up to 166.7

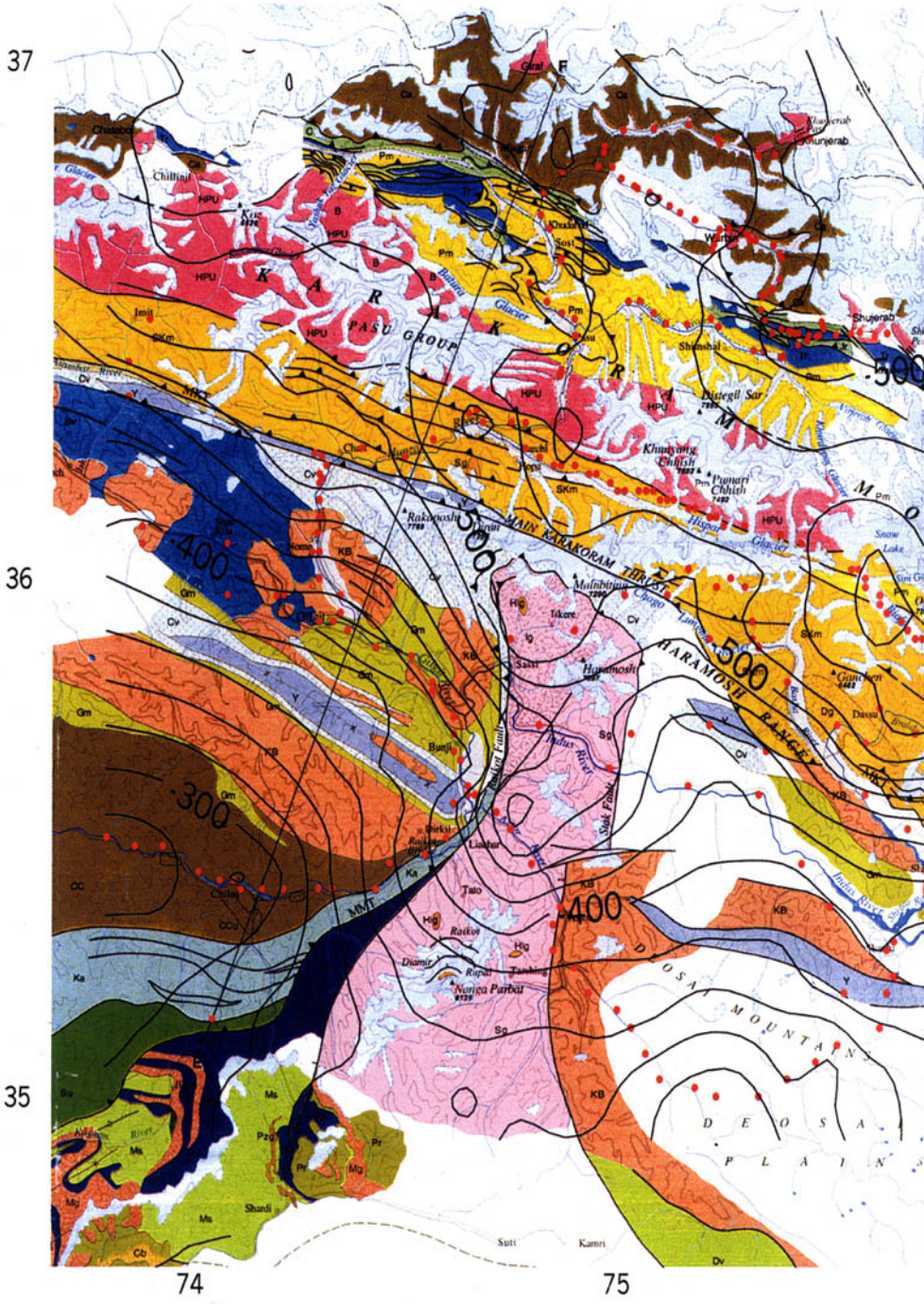

ALIES IN THE KARAKORAM, PAKISTAN

km. ETOPO5 Digital Earth Model and mean density 2670 kg/m^3

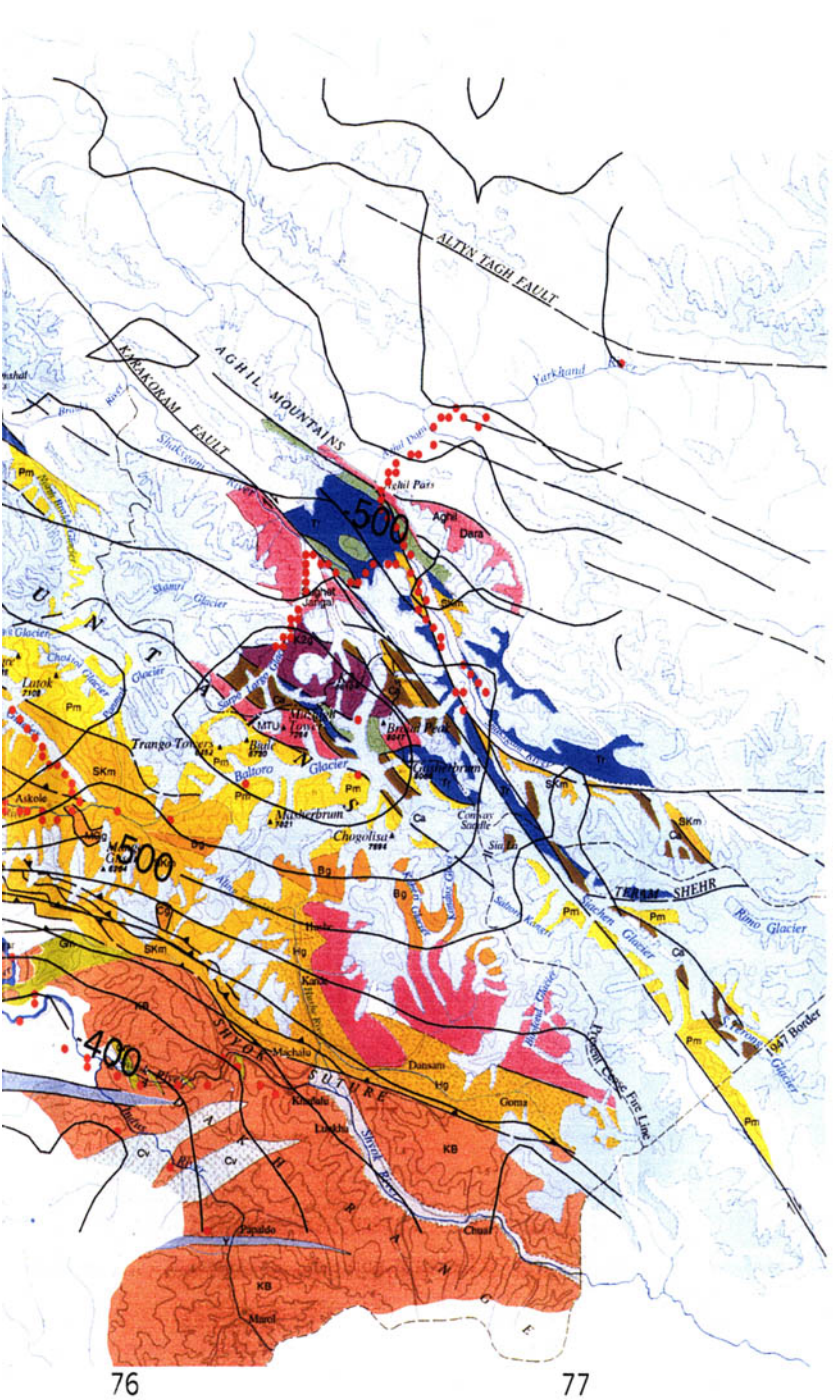

Edited by A. Caporali, University of Padova, Italy

Base Map: Geological Map of North Pakistan. Scale 1:650000. Ed. by M.P. Searle and M.Asif Khan, 1996.

● = gravity station

Surveys:

F. de Filippi (1913-1914): Ladakh, Sin Kiang, Baltistan

S. Hedin (1929-1933): Sin Kiang

A. Marussi (1954-1978): Indus Valley, Chitral, Hunza, Baltoro Glacier, Deosai Plains

A. Caporali (1988-1998): Aghil Mountains, Shaksgam Valley, Biafo-Hispar glaciers, Chogo Lungma · Haramosh glaciers, Shimshal · Ghujerab valleys

Index map:

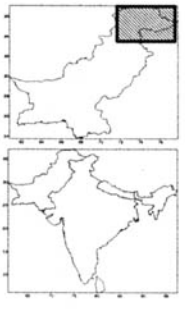

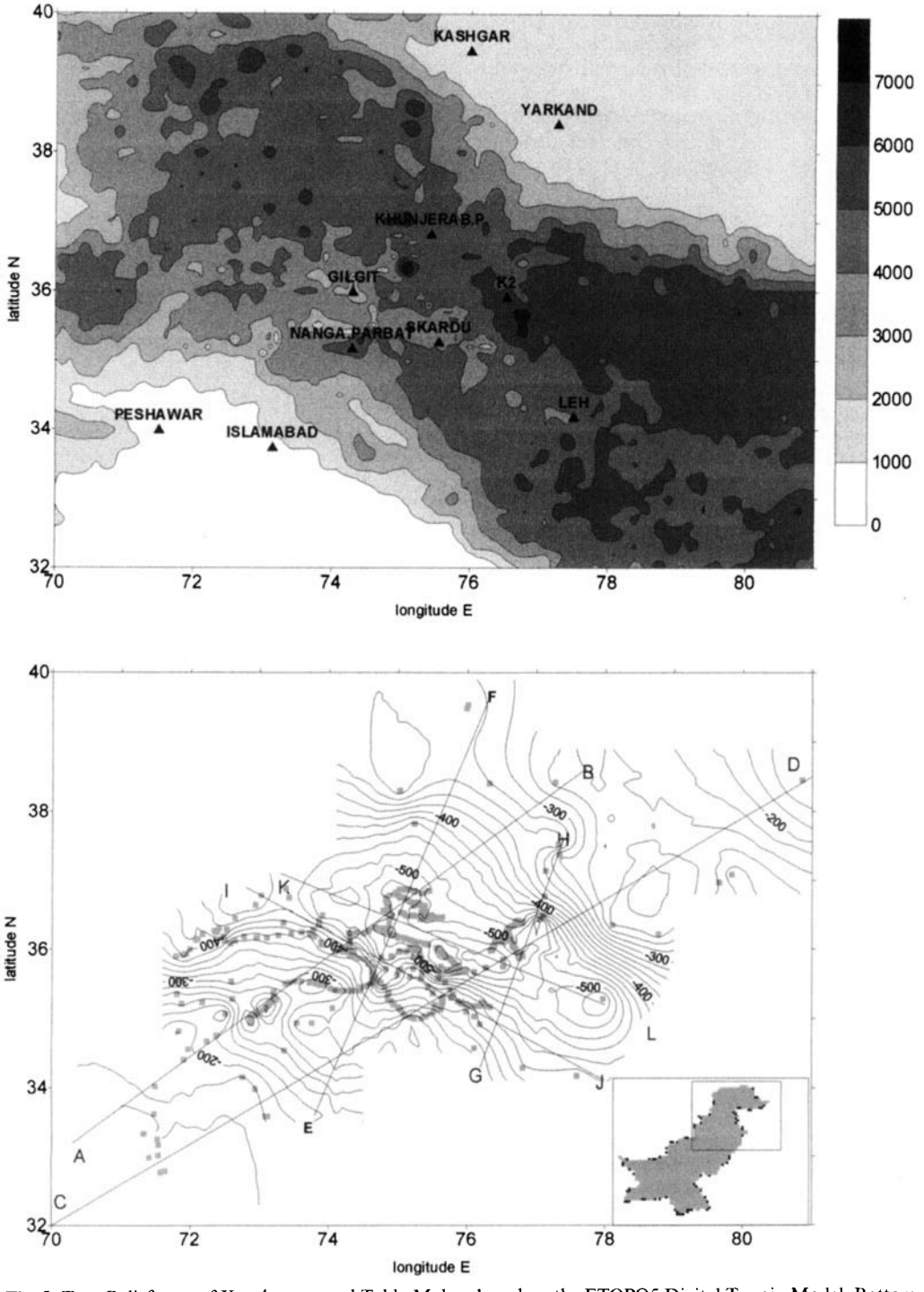

Fig. 2. Top: Relief map of Karakoram, and Takla Makan based on the ETOPO5 Digital Terrain Model. Bottom: Corresponding gravity anomaly map in Northern Pakistan and SW Sin Kiang.

anomalies along a profile extending from India to the Tarim Platform had an oscillatory pattern, with maxima up to 80 mGal and wavelength of 300–350 km. The central minimum was attributed to the thickening of a low density, granite layer. The positive anomaly corresponding to the Hercynian folding of the Kun Lun was attributed to a thinning of the granite layer. The positive anomaly corresponding to the Tethys Himalaya is related to granodioritic and basic occurrences in the Deosai Plains and Pir Panjal. Using seismic and heat flow data, Molnar (1988) proposed an interpretation of Marussi's isostatic anomalies in which negative anomalies caused by an 'oversize' crust would be partially compensated by positive anomalies produced by high density material down-welling into the mantle. The flexural bulge of a rigid lithosphere would have explained the lateral highs. Lyon Caen & Molnar (1984) used Amboldt's gravity data to obtain estimates of the rigidity of the Tarim lithosphere. They concluded in favour of a strong Tarim plate ($D = 5 \times 10^{23}$ Nm) extending between 80 and 120 km beneath the Kun Lun Range. Further north, Burov *et al.* (1990) pointed out that the flexural rigidity in southern Tien Shan should be of the order of 10^{24} Nm. The Tien Shan data were further re-evaluated by Burov & Diament (1992). Extending earlier ideas of McAdoo *et al.* (1985) for the oceanic lithosphere to the case of continental lithosphere, they embodied in their analysis the concept of a three-layer (brittle–elastic–plastic) yield–stress envelope to account for non-uniform mechanical properties of the continental lithosphere (Lyon Caen & Molnar 1983). A flexural rigidity $D = (4 \pm 2) \times 10^{23}$ Nm was found on the Pakistani side by Duroy *et al.* (1989), who numerically integrated the flexural equation along a profile in Northern Pakistan and used the gravity data to constrain the flexural rigidity, vertical shear stress and bending moment. Higher values $(4.6–9) \times 10^{24}$ Nm were obtained by Karner & Watts (1983) along Himalayan profiles adjacent to those considered by Duroy *et al.* (1989). Similar values were obtained by Caporali (1995) who, in addition, revised the estimate of the flexural rigidity of the Tarim plate in the range $(0.9–1.5) \times 10^{25}$ Nm. Thus, estimates of the flexural rigidity can differ by one order of magnitude, and the values tend to be larger if subsurface loads are taken into account. In the Karakoram, both the Indian and Eurasian plates have a non-zero strength, but the estimates of the flexural rigidities are scattered over one order of magnitude. As shown by Macario *et al.* (1995), the estimates of the flexural rigidity may be biased depending on the correlation between surface and subsurface loads, or the length of the profiles.

Analysis of gravity and topography data

To build an isostatic model of the Bouguer anomalies, the extended Bouguer anomaly map and the modified ETOPO5 DTM, with a grid spacing of 0.1 °, are considered (Fig. 2). Because of the non-uniform distribution of the data points, it is preferable to work with profiles which are closest to the actual gravity stations, rather than using the two-dimensional Fourier transform. The profiles have different lengths and a 16-frequencies multiple of the fundamental frequency (the inverse of the length of each profile) will be analysed. This will enable the construction of sufficiently populated, contiguous wavebands suitable for averaging. The six profiles are described in Table 1.

We can expect to work in a range from 0.006 ($=2\pi/1131$) to 0.3 ($=2\pi*16/332$) km^{-1}, which is sufficiently wide to include the most interesting features.

If $B(k)$ and $H(k)$ denote the Fourier transform of the Bouguer anomaly and topographic model respectively, and k (km^{-1}) is the wave number, the coherence function of gravity and topography is defined by the formula (Forsyth 1985):

$$\gamma^2(k) = \frac{\langle B(k)H^*(k)\rangle^2}{\langle B(k)B^*(k)\rangle\langle H(k)H^*(k)\rangle}. \qquad (1)$$

The brackets represent averaging over wavebands, to smooth the high frequency noise. The

Table 1. *Endpoints and length of the profiles in Fig. 2*

Profile	Length (km)	Starts at (longitude, latitude)	Ends at (longitude, latitude)
a–b	873	(70.3, 33.2)	(77.7, 38.6)
c–d	1131	(70.0, 32.0)	(81.0, 38.5)
e–f	622	(73.8, 33.6)	(76.3, 39.6)
g–h	332	(76.2, 34.3)	(77.4, 37.6)
i–j	630	(72.8, 36.9)	(78.0, 34.1)
k–l	550	(73.3, 36.1)	(78.0, 35.2)

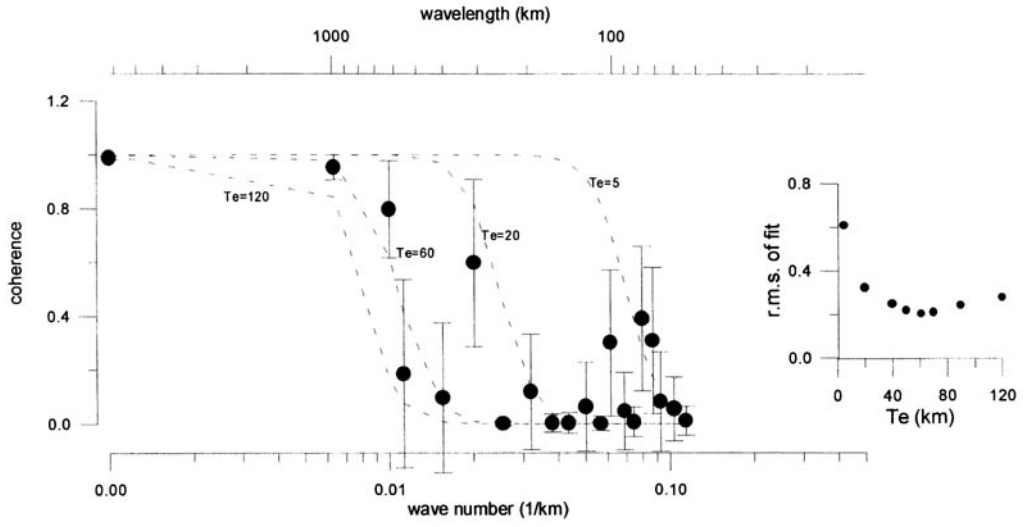

Fig. 4. Theoretical and observed coherence of Bouguer gravity anomaly and topography. Theoretical coherences are computed for equivalent elastic thicknesses ranging from 5 to 120 km. The small plot on the right shows that the minimum root mean square error between observed and computed coherence corresponds to an equivalent elastic thickness of 61 km. The figure suggests that the coherence method is accurate for plates of small thickness and becomes coarser with higher T_e.

asterisk (*) denotes complex conjugation. The plot of the 'observed' coherence is presented in Fig. 4. The coherence is close to one at very low frequency, where isostasy prevails. The coherence is close to zero at high frequency, implying that the loads that belong to this spectral region do not require isostatic equilibrium. In the thin plate approach, it is generally concluded that at high frequencies the inner strength of the plate is the compensating force. Between the two extreme frequencies there exists a transition zone. Its position in the spectrum calibrates the flexural rigidity of the plate. Tests indicate that for an old continental lithosphere the flexural rigidity estimated in this way may be biased towards high values, when using Bouguer anomalies (McKenzie & Fairhead 1997). The equivalent elastic thickness T_e is computed with the equation:

$$D = \frac{ET_e^3}{12(1-\nu^2)}. \qquad (2)$$

$E = 10^{11}\,\mathrm{N\,m^{-2}}$ is Young's modulus and $\nu = 0.25$ is Poisson's ratio, of the lithospheric plate. In the rest of this section it will be shown that a plate of equivalent elastic thickness $T_e = 61$ km best fits the transition from high to low coherence. However, a model of coherence in which surface and subsurface loads are assumed to be statistically independent is unable to reproduce the features of the observed coherence. To enable the model to include such features, the assumption of statistical independence of bottom and top loads must be relaxed at appropriate frequencies.

A relief of amplitude $U(k)$, density contrast $\Delta\rho$ and depth Z produces a Bouguer anomaly (Karner & Watts 1983):

$$B(k) = 2\pi G\Delta\rho U(k)e^{-kZ} \qquad (3)$$

where $G = 6.67 \times 10^{-11}\,\mathrm{m^3\,kg^{-1}\,s^{-2}}$ is the gravity constant. The mean depths of the density discontinuities are estimated from the slope of the logarithm of the power spectrum. In our case, considering all the six profiles, two major discontinuities are found at 58 and 8 km (Fig. 5). Accordingly, two adjacent spectral regions are defined and the corresponding relief is computed with the downward continuation formula (equation 3) applied to the appropriate frequency range (Table 2).

Following Forsyth (1985), Bechtel *et al.* (1987) and Zuber *et al.* (1989), the relief at each of the three interfaces $H(k)$, $V(k)$ and $W(k)$ results from

Table 2. *Depths, spectral range and denomination of the density interfaces*

Depth (Z)	Spectral range	Symbol
58 km	$k < 0.02\ \mathrm{km^{-1}}$ ($\lambda > 311$ km)	$W(k)$
8 km	$k > 0.02\ \mathrm{km^{-1}}$ ($\lambda < 311$ km)	$V(k)$

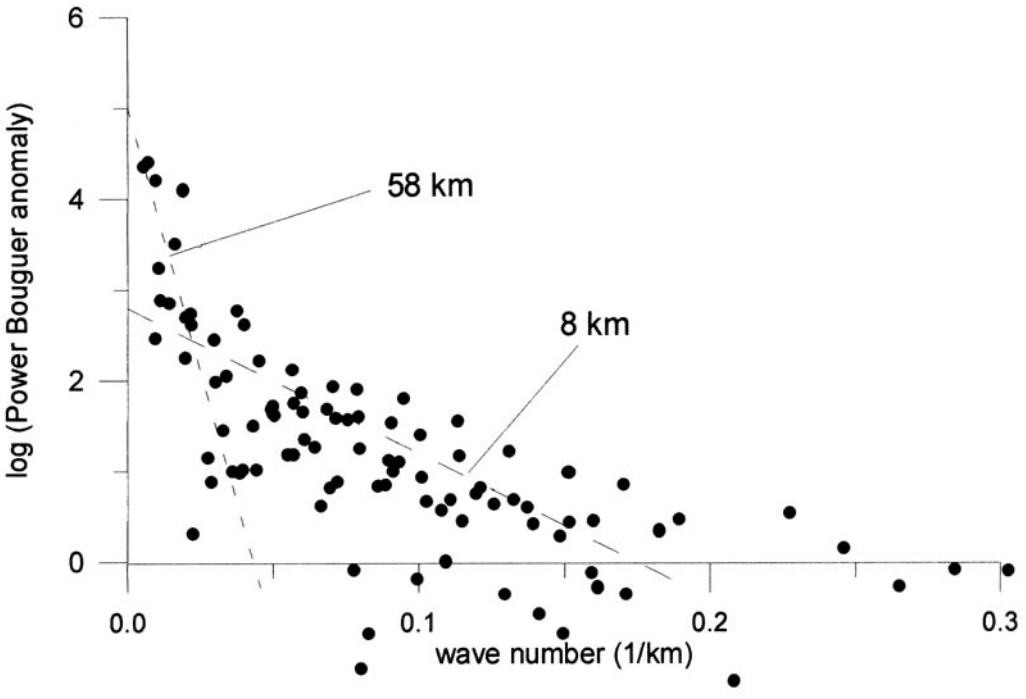

Fig. 5. Power spectrum of the Bouguer anomaly as a function of the wave number, k. The slope of regression lines estimates the mean depth of the density interfaces responsible for the anomaly. Two density interfaces are identified at 58 km and 8 km.

loads at the interface itself and at the other two. Using the labels t, m and b to denote load at the top, intermediate and bottom interface:

$$\begin{aligned} H &= H_t + H_m + H_b \\ V &= V_t + V_m + V_b \\ W &= W_t + W_m + W_b. \end{aligned} \tag{4}$$

The nine complex numbers on the right-hand side of equation 4 are related by six additional algebraic expressions, which follow from the general equation of bending of a thin, elastic plate (McNutt 1983; Forsyth 1985):

$$\begin{aligned} W_t &= V_t \\ W_t &= -\frac{\rho_0 H_t}{\Delta\rho_1 \xi} \\ W_m &= H_m \\ W_m &= -\frac{\Delta\rho_2 V_m}{[(\rho_m - \Delta\rho_2)\psi]} \\ W_b &= -\frac{\rho_c H_b \phi}{\Delta\rho_3} \\ H_b &= V_b. \end{aligned} \tag{5}$$

Table 3. *The assumed density model*

Layer	Symbol	Assumed value (kg m^{-3})
Cover	ρ_0	2670
Crust	ρ_c	2900
Mantle	ρ_m	3200

The densities are defined in Table 3. The density contrasts are:

$$\begin{aligned} \Delta\rho_1 &= \rho_m - \rho_0 \\ \Delta\rho_2 &= \rho_c - \rho_0 \\ \Delta\rho_3 &= \rho_m - \rho_c. \end{aligned} \tag{6}$$

The isostatic kernels are:

$$\begin{aligned} \xi &= 1 + \frac{Dk^4}{\Delta\rho_1 g} \\ \psi &= 1 + \frac{Dk^4}{[(\rho_m - \Delta\rho_2)g]} \\ \phi &= 1 + \frac{Dk^4}{\Delta\rho_c g} \end{aligned} \tag{7}$$

where g is the acceleration of gravity (9.8 m s^{-2}). If D is known, the algebraic system:

$$\begin{bmatrix} 1 & -\dfrac{\Delta\rho_2}{(\rho_m - \Delta\rho_2)\psi} & -\dfrac{\Delta\rho_3}{\rho_c\phi} \\ -\dfrac{\rho_0}{\Delta\rho_1\xi} & 1 & -\dfrac{\Delta\rho_3}{\rho_c\phi} \\ -\dfrac{\rho_0}{\Delta\rho_1\xi} & -\dfrac{\Delta\rho_2}{(\rho_m - \Delta\rho_2)\psi} & 1 \end{bmatrix} \begin{bmatrix} H_t \\ V_m \\ W_b \end{bmatrix} = \begin{bmatrix} H \\ V \\ W \end{bmatrix} \tag{8}$$

can be solved whenever $Dk^4 \neq 0$. If this term is zero, we are in the case of Airy isostasy.

The flexural rigidity D can be estimated by comparing the observed and theoretical coherence. The theoretical coherence is computed by combining expression (1) of γ with the decomposition (4) of H and B and the expression (3) of downward continuation to the intermediate and bottom interfaces. If the loads at the interfaces are statistically independent, in the sense that in each waveband the cross products like $\langle H_t V_m \rangle$, $\langle H_t W_b \rangle$ and similar average to zero, then the predicted coherence is

$$\gamma_c^2 = \frac{\langle (W_t H_t^* + W_m H_m^* + W_b H_b^*)\alpha + (V_t H_t^* + V_m H_m^* + V_b H_b^*)\beta \rangle^2}{\langle H_t H_t^* + H_m H_m^* + H_b H_b^* \rangle \langle (W_t W_t^* + W_m W_m^* + W_b W_b^*)\alpha^2 + (V_t V_t^* + V_m V_m^* + V_b V_b^*)\beta^2 \rangle} \tag{9}$$

where:

$$\alpha = 2\pi\Delta\rho_3 e^{-kZ_m}$$
$$\beta = 2\pi\Delta\rho_2 e^{-kZ_c}. \tag{10}$$

The assumption of statistical independence needs to be introduced a priori but will be verified a posteriori, once a least squares estimate of D has been obtained. In fact it will be seen that this assumption is invalid at some wavebands.

The theoretical coherence (9) has been computed for several values of the flexural rigidity D. The value of D that gave the least root mean square (rms) discrepancy was $D = 2.0 \times 10^{24}$ Nm, which is the flexural rigidity of an ideal, elastic plate of thickness $T_e = 61$ km. The formal uncertainty is of the order of a few kilometres but a more realistic estimate is probably higher. Assuming that the average uncertainty of the coherence data is 5%, a change of T_e of 10–15 km is required to increase the rms. of that amount.

As illustrated in Fig. 4, the coherence of a thin plate with independent loads fails to reproduce the observed coherence in two distinct frequency bands. To investigate the details of these departures, the correlation coefficients between topography and deformation at the intermediate and deep interfaces are considered. Figure 6 shows the plots of the real part of

$$\frac{\langle W_b H_t^* \rangle}{\langle W_b W_b^* \rangle \langle H_t H_t^* \rangle}, \quad \frac{\langle V_m H_t^* \rangle}{\langle V_m V_m^* \rangle \langle H_t H_t^* \rangle}. \tag{11}$$

The negative correlation between top and intermediate loads is evident (Fig. 6) in the high frequency band (wavelengths between 75 and 85 km) and bears a very close resemblance to the corresponding feature of the observed coherence in Fig. 4. In the low frequency band, there are two concurrent correlations: one is negative, between loads on the top and deep interface. The other is positive, somewhat at higher frequencies, between topographic load and load at the intermediate interface. We conclude that in the waveband between 250 and 350 km the spike in the observed coherence may be accounted for by a combination of effects of opposite signs, resulting from the interaction of surface loads with loads placed at the intermediate and deep interfaces. This could explain the oscillations of the isostatic anomalies that were reported by Marussi (1964).

Having established that top and bottom loads do correlate at certain frequencies, the computed coherence can be corrected to match the observed coherence exactly. This is done by adding the necessary cross terms in the two appropriate wavebands, that is by introducing *ad hoc* ratios between the amplitudes of bottom and top loads at those frequencies. It turns out that a ratio of 2 is required in the lowest frequency band.

Discussion of the profiles

On the basis of these constraints, the six profiles in Fig. 2 are analysed in Fig. 7. For each profile we give the geometry of topography, intermediate (mean depth 8 km) and deep (mean depth 58 km) interfaces before (left) and after (right) isostatic equilibrium. Vertical units are metres. However, note that the vertical scale is, in general, different for different profiles.

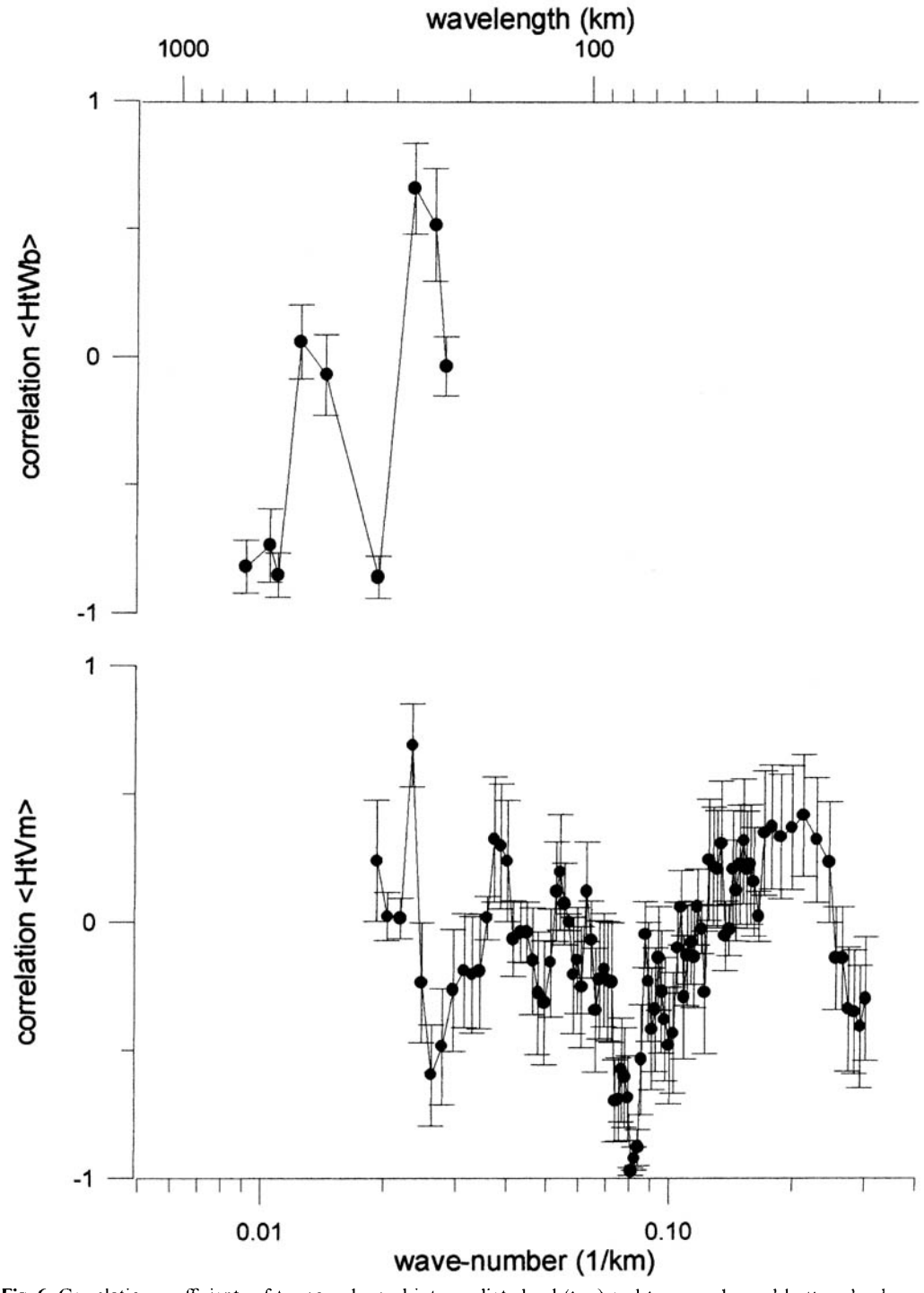

Fig. 6. Correlation coefficients of topography and intermediate load (top) and topography and bottom load (bottom).

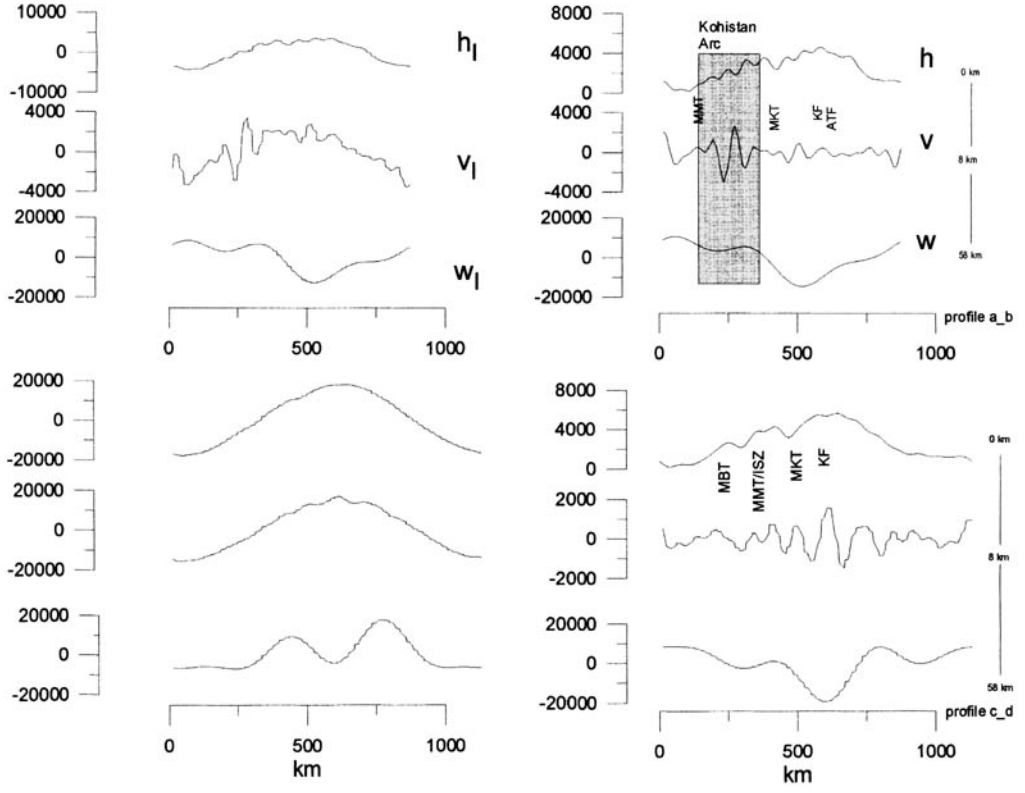

Fig. 7(a).

Profile a–b

This profile starts west of Peshawar, near the Khyber pass. It intercepts the Kohistan arc between the Main Mantle Thrust (MMT) and Main Boundary Thrust (MBT), and ends in the Takla Makan desert, east of Yarkand. Initially, the topographic and intermediate profiles were convex. At equilibrium the intermediate interface loses its convexity and the topography readjusts accordingly. This readjustment, however, leaves unchanged the feature associated with the Kohistan arc. Also the deep interface maintains its geometry during the isostatic readjustment.

Profile c–d

This profile starts in the Potwar Plateau, east of Kalabagh, and ends in the Tarim Depression. The profile intercepts twice the MBT as it crosses the Neelum syntaxis. The Ladakh arc is entered across the Indus Suture Zone (ISZ), an alias of the MMT. Further north, after crossing the MKT, the profile intercepts the Karakoram Fault (KF) and eventually the Altyn Tagh Fault (ATF). The profile differs considerably from a–b. Here the initial topography and intermediate layers are very similar, of considerable amplitude and unrelated to the geometry of the deep interface. After readjustment, the intermediate interface reduces to a noisy and small amplitude waveform, and the isostatic root formation is evident in the anticorrelation between topography and deep interface.

Profile e–f

This profile starts halfway between Rawalpindi and the border with India, and continues north along the west flank of the Nanga Parbat–Haramosh syntaxis to end just east of Kashgar. This profile is parallel to the profile labelled E–G in the geological map of Searle & Khan (1996), but is slightly east of it because of the requirement to overlap with observed gravity stations. The deep interface does not change appreciably in the process of isostatic readjustment. The Kohistan arc, bordered by the MMT and MKT, and the Indus gorge near Chilas are features that were left unaltered by the isostatic compensation, a situation similar to profile a–b. The depth of the deep interface reaches 75 km near the Nanga

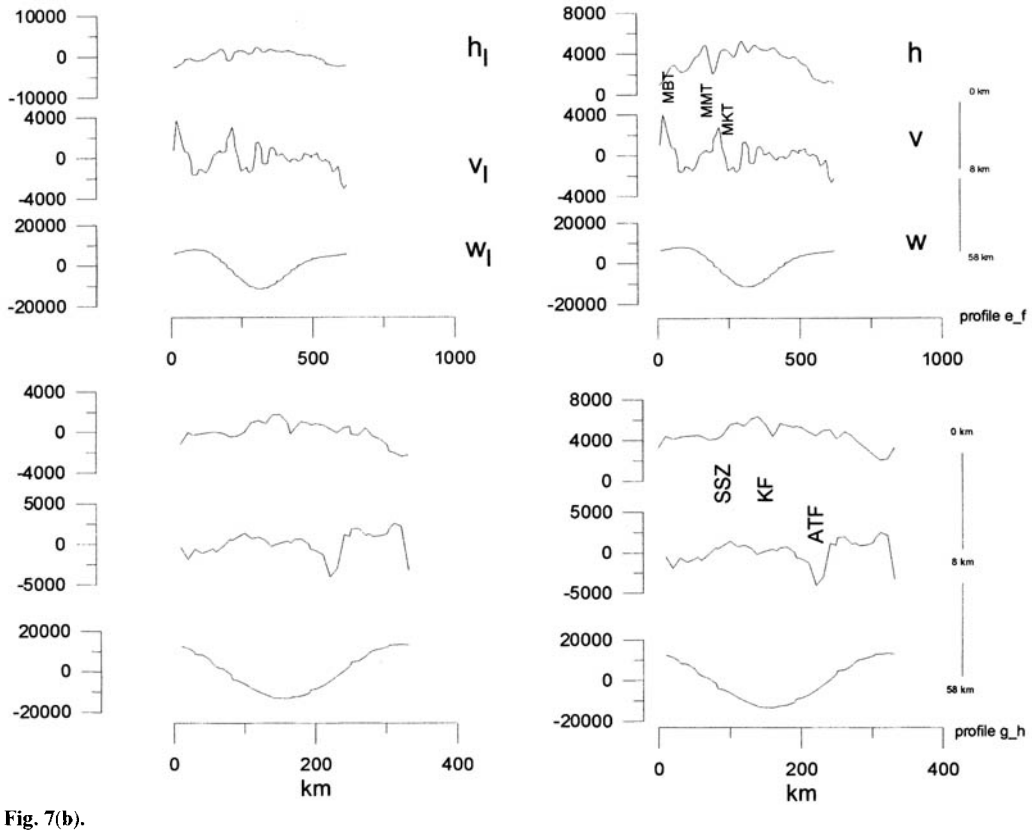

Fig. 7(b).

Parbat–Haramosh massif, in agreement with results from explosion seismology (Kaila *et al.* 1982; Verma & Prasad 1987).

Profile g–h

This profile starts in India, just south of the Deosai Plains, and ends in the Takla Makan, close to Yecheng, after crossing the Ladakh arc and the Kun Lun and Aghil mountains, an area of very steep gradient of the Bouguer anomaly. Again it appears that the isostatic readjustment has hardly changed the geometry of the initial topography and intermediate and deep interfaces. In particular the trough associated with the dextral strike-slip Altyn Tagh Fault apparently existed before compensation, and remained uncompensated.

Profiles i–j and k–l

These profiles are closely aligned to the axis of the Karakoram. Again no appreciable change is visible as a consequence of isostatic readjustment.

It can be concluded that the effects of isostatic readjustment are visible only in the a–b and c–d profiles, i.e. those longer than 800 km. It cannot be excluded that the limited length of some profiles prevents the full reconstruction of the isostatic readjustment.

Discussion and conclusion

There exists no single, elastic plate model with uncorrelated top and bottom loads that fits the coherence data of gravity and topography in the Karakoram. Relaxing the assumption of statistical independence and allowing for correlation at two ranges of wavelengths, 250–350 km and 70–85 km, a model can be built such that the computed coherence matches the observed coherence, and the gravity anomalies and surface topography correlate in a manner similar to the observed correlation. Under horizontal stresses of several hundreds of MPa, comparable to those associated with the early stages of the collision of India and Eurasia, a rheologically stratified lithosphere (Ranalli & Murphy 1987; Ranalli 1995) may develop folding instabilities of the

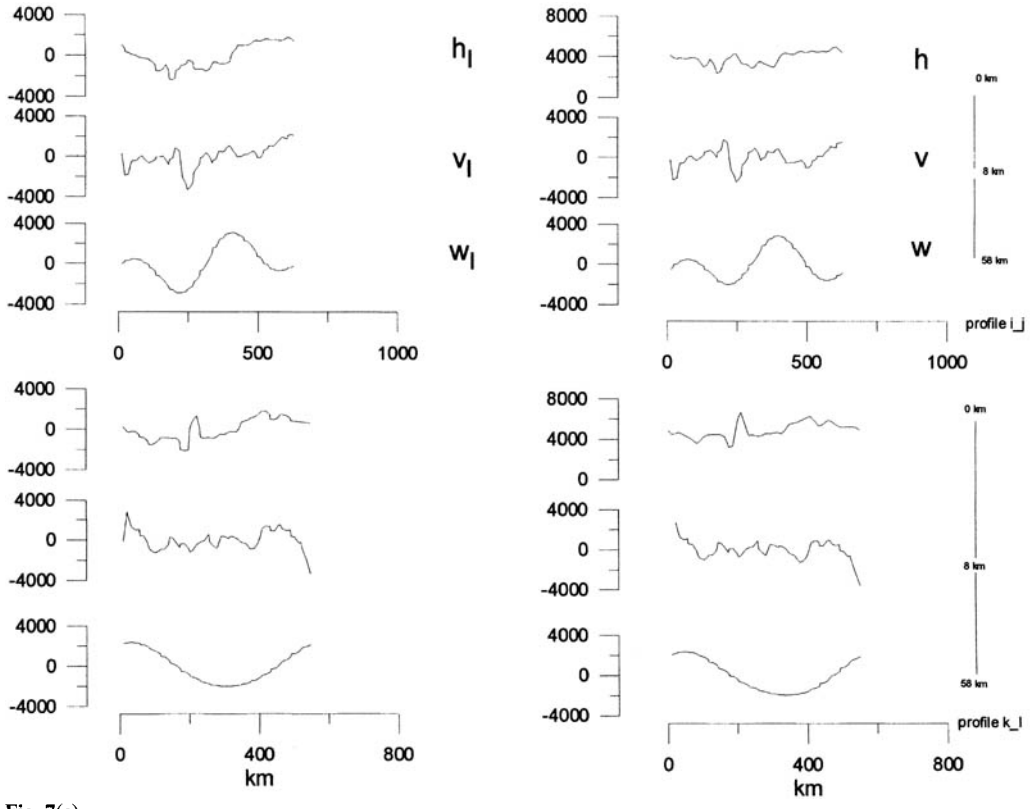

Fig. 7(c).

Fig. 7(a–c). Isostatic model for the profiles in Fig. 2. On the left are plotted the relief h, v, w before isostatic adjustments. On the right the same relief after isostasy has been completed. It is assumed that isostasy is the only process taking place (e.g. no erosion). See text for the definition of the symbols.

strong layers, provided a lower plastic layer exists, i.e. Moho temperatures are below 600–650 °C (Martinod & Davy 1992), and there exists a weak intermediate layer. According to experimental data on the mechanical properties of rocks, the upper crust and mantle are controlled by brittle (plastic) failure associated with seismic activity. For the brittle upper crust with quartz-rich rocks, the yield–stress envelope (YSE) is a linear function of the overburden pressure and is temperature independent (Byerlee 1978). At depths lower than 15–20 km, depending on the strain rate (typically $3 \times 10^{-15}\,s^{-1}$ (Molnar & Tapponier 1981)) the crust becomes increasingly weak and fails by thermally activated, ductile creep flow of diorite or (at greater depths) diabase. The Moho represents a major rheological and density discontinuity. For temperatures below 600–650 °C a new plastic layer exists. Due to the higher strength of olivine, the underlying layer deforms quasi-elastically. Then, depending again on the viscosity and the strain rate, the YSE is controlled by the exponential curve of the ductile creep. Quite independently of its rheology, the intermediate layer acts as a permanent decoupling/detachment zone. The dominant wavelengths of the folding are proportional by a factor of 4 to 6 to the depths of the strong layers (Martinod & Davy 1992; Burov *et al.* 1993; Burg *et al.* 1994). Applying this model to our case (Fig. 8), the thickness of the upper layer would be about 13–20 km (i.e. $\frac{1}{6}$–$\frac{1}{4}$ of 80 km). Similarly, folding at a wavelength between 250 and 350 km implies a total depth to the base of the strong region, in the upper mantle, as high as 80–85 km (i.e. *c.* $\frac{1}{4}$ of 350 km). This is approximately the depth at which most earthquakes in the Karakoram occur. If one accepts that the corresponding temperature should be in the range 600–800 °C (Molnar 1988), the geothermal gradient must be as low as $10\,K\,km^{-1}$ or less, confirming previous

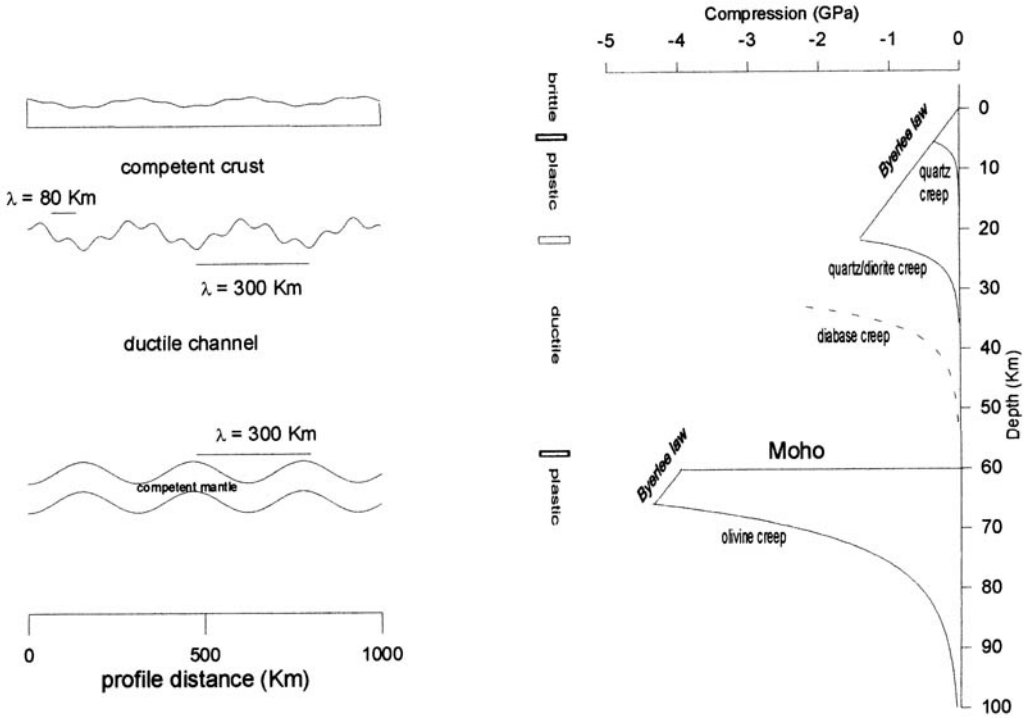

Fig. 8. Yield–stress envelope (right) and structure of the deformation at depth, as constrained by gravity and topography data (left). The brittle/plastic part of the YSE is represented by a linear law with slope -0.66×10^5 Pa km^{-1} in the upper crust and -0.75×10^5 Pa km^{-1} in the upper mantle. The ductile creep law is governed by the relation $\Delta\sigma = \sqrt[n]{\dot{\varepsilon}/A}e^{H/nRT}$, where $\Delta\sigma$ is the deviatoric yield stress, or difference between maximum and minimum principal stress (negative for compression); the strain rate is 10^{-15} s^{-1}, $R = 8.314$ J mol^{-1} K^{-1} and T is the temperature in Kelvin. The remaining numerical values are listed in Table 4. The temperature gradient is 10 °C km^{-1} in the upper crust and 6 °C km^{-1} in the upper mantle. The temperature is then 570 °C at the Moho and 605 °C at the base of the lowermost plastic layer, in the upper mantle. The depths of the bottom of the competent layers on the left are defined by the temperature of thermally activated plastic/ductile creep transition. The depths of the layers are $\frac{1}{4}$ of the buckling wavelength.

Table 4. *The parameters used in the calculation of the yield–stress envelope*

Mineral	Material constant A [Pa^{-n} s^{-1}]	Stress exponent n	Activation enthalpy H [J mol^{-1}]
Quartzite	5×10^{-12}	3	190 000
Quartz/diorite	5×10^{-15}	2.4	212 000
Diabase	6×10^{-20}	3.1	276 000
Olivine/dunite	7×10^{-14}	3	520 000

From Burov & Diament (1995) and Ranalli (1995).

suggestions of a cold mantle underneath the Karakoram.

Similar buckling is reported by Jin *et al.* (1994) for Tibet, and by Burov *et al.* (1993) in Western Gobi, but with some important differences. The first, perhaps most obvious, is that in the Karakoram the topographic folding of the compressed zone, north of MMT, is masked by the rough topography, contrary to the relatively smooth topographic profile of the Tibetan plateau or Western Gobi. Second, the deformation style in the Karakoram seems closer to buckling than to the 'inverse boudinage' proposed for Tibet (Jin *et al.* 1994). Third, our wavelengths are closer to Burov *et al.*'s (1993) (50 and 300 km) than to Jin *et al.*'s (1994), who report deformation developing in two wavebands centred at wavelengths 150 km and 500-700 km,

and the Moho at 60 km depth. One then concludes that the plastic layers in Tibet should be nearly twice as thick as in the Karakoram and Western Tibet. Consequently, as shown in Fig. 8, the Karakoram and Western Gobi should have a quartz/diorite controlled upper crust, whereas in Tibet a competent upper crust extending to depths of 30–35 km implies that quartz/diabase would dominate.

This research was encouraged by Ardito Desio and supported by the Ev-K2-CNR Project and the Italian Space Agency. Special thanks to Francesco Palmieri, who did the gravity measurements in 1988, 1990 and 1993 with instrumentation loaned from Istituto di Ricerche Geotermiche of CNR in Pisa, and to Giovanna Berrino of Osservatorio Vesuviano in Naples for the gravimeter used in 1998. Roberto Cassinis gave rare original historical data from the de Filippi expedition. Giorgio Poretti of the University of Trieste provided the pre-1988 data in digital form. I am very grateful to J. P. Burg, M. McNutt, P. Molnar, G. Ranalli and an anonymous referee for suggesting improvements to the manuscript, and to M. P. Searle, and M. Asif Khan for permission to use their geological map of Northern Pakistan. Maurizio Gallo led the field work in 1990, 1993 and 1998, and Ashraf Amman was responsible for the logistics. The 1998 campaign was supported by a travel grant from the Italian Ministry of Foreign Affairs, in scientific cooperation with the Government of Pakistan.

References

ABETTI, G. & ALESSIO, A. 1929. Geofisica, Gravità e Magnetismo. *In*: *Spedizione Italiana De Filippi nell'Himalaia, Caracorum e Turkestan Cinese (1913–1914)*, ser. 1, Vol. 2, Geodesia e Geofisica-Zanichelli, Bologna.

AIRY, G. B. 1855. On the computation of the effect of the attraction of mountain masses as disturbing the apparent astronomical latitude of stations of geodetic surveys. *Philosophical Transactions of the Royal Society of London*, **145**, 101–104.

AMBOLDT, N. 1948. Relative Schwerkraftbestimmungen mit Pendeln in Zentral Asien. *In*: *Reports from the Scientific Expedition to the NW Provinces of China under the Leadership of Dr Sven Hedin*. The Sino Swedish Expedition; Publication 30, II Geodesy/2, Stockholm.

ARMIJO, R. P., TAPPONIER, P., MERCIER, J. L. & HAN, T. 1989. Quaternary Extensions in Southern Tibet: Field Observations and Tectonic Implications. *Journal of Geophysical Research*, **94**, 2787–2838.

AVOUAC, J. P. & TAPPONIER, P. 1993. Kinematic Model of Active Deformation in Central Asia. *Geophysical Research Letters*, **20**, 895–898.

——, ——, BAI, M., YOU, M. & WANG, G. 1993. Active Thrusting and Faulting Along the Northern Thien Shan and Late Cenozoic Rotation of the Tarim relative to Dzungaria and Kazakhstan. *Journal of Geophysical Research*, **98**, 6755, 6804.

BANKS, R. J., PARKER, R. L. & HUESTIS, S. P. 1977. Isostatic Compensation on a Continental Scale: Local versus Regional Mechanisms. *Geophysical Journal of the Royal Astronomic Society*, **51**, 431–452.

BARD, J. P., MALUSKI, H., MATTE, P. & PROUST, F. 1980. The Kohistan Sequence: Crust and Mantle of an Obducted Island Arc. *Proceedings of the International Commission on Geodynamics*, Group 6, 87–94.

BECHTEL, T. D., FORSYTH, D. W. & SWAIN, C. J. 1987. Mechanism of Isostatic Compensation in the Vicinity of the East African Rift, Kenya. *Geophysical Journal of the Royal Astronomic Society*, **90**, 445–465.

BRANDON, C. & ROMANOWICZ, B. 1986. A "no-lid" Zone in the Central Chang-Tang Platform of Tibet: Evidence from Pure Path Phase Velocity Measurements of Long Period Rayleigh Waves. *Journal of Geophysical Research*, **91**, 6547–6564.

BURG, J. P., DAVY, P. & MARTINOD, J. 1994. Shortening of Analogue Models of the Continental Lithosphere: New Hypothesis for the Formation of the Tibetan Plateau. *Tectonics*, **13**, 475–483.

BUROV, E. B. & DIAMENT, M. 1992. Flexure of the Continental Lithosphere with Multilayered Rheology. *Geophysical Journal International*, **109**, 449–468.

—— & —— 1995. The Effective Elastic Thickness (Te) of Continental Lithosphere: What does it really mean? *Journal of Geophysical Research*, **100**, 3905–3927.

——, LOBKOVSKY, L. I., CLOETINGH, S. & NIKISHIN, A. M. 1993. Continental Lithosphere Folding in Central Asia (Part II): Constraints from Gravity and Topography. *Tectonophysics*, **226**, 73–87.

BUROV, E. V., KOGAN, M. G., LYON CAEN, H. & MOLNAR, P. 1990. Gravity Anomalies, the Deep Structure, and Dynamic Processes beneath the Tien Shan. *Earth and Planetary Science Letters*, **96**, 367–383.

BYERLEE, J. 1978. Friction of Rocks. *Pure and Applied Geophysics*, **73**, 4741–4750.

CAPORALI, A. 1993. Recent Gravity Measurements in the Karakoram. *In*: TRELOAR, P. J. & SEARLE, M. P. (eds) *Himalayan Tectonics*. Geological Society London, Special Publications, **74**, 9–20.

—— 1995. Gravity Anomalies and the Flexure of the Lithosphere in the Karakoram, Pakistan. *Journal of Geophysical Research*, **100**, 15075–15085.

——, MARZARI, F. & PALMIERI, F. 1991. Geodetic and Geophysical Report. *In*: *Geodesy, Geophysics and Geology of the Upper Shaksgam Valley (North East Karakorum) and South Sinkiang*. Scientific Reports of the Italian Expedition to Karakorum 1988, Prof. A. Desio leader, Ev-K2-CNR, Milano.

CHEN, W. P. & MOLNAR, P. 1983. Focal Depths of Intracontinental and Intraplate Earthquakes and their Implications for the Thermal and Mechanical Properties of the Lithosphere. *Journal of Geophysical Research*, **88**, 4183–4214.

DESIO, A. & SAVOIA AOSTA, A. 1936. *La Spedizione Geografica Italiana nel Karakoram*. Arti Grafiche Bertarelli, Milano.

DORMAN, L. M. & LEWIS, B. T. R. 1970. Experimental Isostasy, I, Theory of the Determination of the Earth's Isostatic Response to a Concentrated Load. *Journal of Geophysical Research*, **75**, 3357–3365.

DUROY, Y., FARAH, A. & LILLIE, R. J. 1989. Surface Densities and Lithospheric Flexure of the Himalayan Foreland in Pakistan. *In*: MALINCONICO, L. L. & LILLIE, R. J. (eds) *Tectonics of the Western Himalayas*. Geological Society of America, Special Paper **232**, 217–236.

EBBLIN, C., MARUSSI, A., PORETTI, G. & RICHARDUS, P. 1983. Gravity Measurements in the Karakoram. *Bollettino di Geofisica Teorica e Applicata*, **25**, 303–316.

ENGLAND, P. C. & HOUSEMAN, G. A. 1985. Role of Lithospheric Strength Heterogeneities in the Tectonics of Tibet and Neighbouring Regions. *Nature*, **315**, 297–301.

FORSBERG, R. 1984. *A Study of Terrain Reductions, Density Anomalies and Geophysical Inversion Methods in Gravity Field Modeling*. Reports of the Dep. of Geodetic Science and Surveying, The Ohio State University, Columbus, Ohio.

FORSYTH, D. W. 1985. Subsurface Loading and Estimates of the Flexural Rigidity of Continental Lithosphere. *Journal of Geophysical Research*, **90**, 12623–12632.

HEISKANEN, W. A. & VENING MEINESZ, F. A. 1958. *The Earth and its Gravity Field*. McGraw Hill, New York.

HOUSEMAN, G. & ENGLAND, P. 1996. A Lithospheric-thickening model for the Indo Asian collision. *In*: YN, A. & HARRISON, M. (eds) *The Tectonic Evolution of Asia*. Cambridge University Press, Cambridge, 3–17.

JIN, Y., MCNUTT, M. K. & ZHU, Y. 1994. Evidence from Gravity and Topography Data for Folding Tibet. *Nature*, **371**, 669–674.

KAILA, K. L., ROY CHOUDHURY, K., KHRISHNA, V. G., DIXIT, M. M. & NARAIN, H. 1982. Crustal Structure of Kashmir Himalaya and Inferences about the Asthenosphere Layer from DSS Studies along the International Profile, Qarrakol–Zorkol–Nanga Parbat–Srinagar, Pamir Himalaya. *Bollettino di Geofisica Teorica e Applicata*, **25**, 221–234.

KARNER, J. D. & WATTS, A. B. 1983. Gravity Anomalies and flexure of the Lithosphere at Mountain Ranges. *Journal of Geophysical Research*, **88**, 10449–10477.

LANDAU, L. D. & LIFSHITZ, E. M. 1964. *Theory of Elasticity* (2nd edition). Mir Editor, Moskow.

LE PICHON, X., FOURNIER, M. & JOLIVET, L. 1992. Kinematics, Topography, Shortening and Extrusion in the Indian Eurasian Collision. *Tectonics*, **11**, 1085–1098.

LEWIS, B. T. R. & DORMAN, L. M. 1970. Experimental Isostasy 2: An Isostatic Model for the U.S.A. Derived from Gravity and Topographic Data. *Journal of Geophysical Research*, **75**, 3367–3386.

LYON-CAEN, H. & MOLNAR, P. 1983. Constraints in the Structure of the Himalaya from the Analysis of Gravity Anomalies and Flexural Model of the Lithosphere. *Journal of Geophysical Research*, **88**, 8171–8191.

—— & —— 1984. Gravity Anomalies and the Structure of Western Tibet and the southern Tarim Basin. *Geophysical Research Letters*, **11**, 1251–1254.

MACARIO, A., MALINVERNO, A. & HAXBY, W. F. 1995. On the Robustness of the Elastic Thickness Estimates obtained using the Coherence Method. *Journal of Geophysical Research*, **100**, 15163–15172.

MALINCONICO, L. L. 1986. The Structure of the Kohistan Ladakh Arc Terrane in Northern Pakistan as Inferred from Gravity Data. *Tectonophysics*, **124**, 297–307.

—— 1989. Crustal Thickness Estimates of the Western Himalayas. *In*: MALINCONICO, L. L. & LILLIE, R. J. (eds) *Tectonics of the Western Himalayas*. Geological Society of America, Special Paper **232**, 237–242.

MARTINOD, J. & DAVY, P. 1992. Periodic Instabilities During Compression or Extension of the Lithosphere. 1. Deformation Modes from and Analytical Perturbation Method. *Journal of Geophysical Research*, **97**, 1999–2014.

MARUSSI, A. 1964. *Geophysics of the Karakorum, Italian Expeditions to the Karakorum (K2) and Hindu Kush* (Prof. A. Desio Leader), II-Geophysics, Vol. 1. E. J. Brill, Leiden.

MCADOO, D. C., MARTIN, C. F. & POLOUSE, S. 1985. Seasat Observations of Flexure: Evidence for a Strong Lithosphere. *Tectonophysics*, **116**, 209–222.

MCKENZIE, D. & FAIRHEAD, D. 1997. Estimates of the Effective Elastic Thickness of the Continental Lithosphere from Bouguer and Free Air Gravity Anomalies. *Journal of Geophysical Research*, **102**, 27523–27552.

MCNUTT, M. K. 1983. Influence of Plate Subduction on Isostatic Compensation in Northern California. *Tectonics*, **2**, 399–415.

—— & PARKER, R. L. 1978. Isostasy in Australia and the Evolution of the Compensating Mechanism. *Science*, **199**, 773–775.

MOLNAR, P. 1988. A Review of Geophysical Constraints on the Deep Structure of the Tibetan Plateau, the Himalaya and the Karakoram, and their Tectonic Implications. *Philosophical Transactions of the Royal Society of London A*, **326**, 33–88.

—— & DENG QIDONG 1984. Faulting Associated with Large Earthquakes and the Average Rate of Deformation in Central and Eastern Asia. *Journal of Geophysical Research*, **89**, 6203–6227.

—— & TAPPONIER, P. 1975. Cenozoic Tectonics of Asia: Effects of a Continental Collision. *Science*, **189**, 419–426.

—— & —— 1981. A Possible Dependence of the Tectonic Strength on the Age of the Crust in Asia. *Earth and Planetary Sciences Letters*, **52**, 107–114.

NORIN, E. 1946. Geological Exploration in Western Tibet. *In*: *Report on Sino-Swedish Expedition 1929*. Swedish Aktiebolaget Thule, Stockholm.

PARKER, R. L. 1972. The Rapid Calculation of Potential Anomalies. *Geophysical Journal of the Royal Astronomic Society*, **31**, 447–455.

PRATT, J. H. 1855. On the attraction of the Himalayan Mountains, and of the elevated region beyond them, upon the plumb line in India. *Philosophical Transactions of the Royal Society of London*, **145**, 53–100.

RANALLI, G. 1995. *Rheology of the Earth—Deformation and Flow Processes in Geophysics and Geodynamics* (2nd edition). Chapman & Hall, London.

—— & MURPHY, D. C. 1987. Rheological Stratification of the Lithosphere. *Tectonophysics*, **132**, 281–295.

ROECKER, S. W., SABITOVA, T. M., VINNIK, L. P., BOURMAKOV, Y. A., GOLVANOV, M. I., MAMATKANOVA, R. & MUNIROV, L. 1993. Three dimensional Elastic Wave Velocity Structure of the Western and Central Tien Shan. *Journal of Geophysical Research*, **98**, 15779–15795.

SEARLE, M. P. 1991. *Geology and Tectonics of the Karakoram Mountains*. J. Wiley & Sons.

—— & ASIF KHAN, M. (eds) 1996. *Geological Map of North Pakistan, scale 1:650 000*. Department of Earth Sciences, Oxford University, UK.

STOKES, G. G. 1864. Letter to General Sir Edward Sabine, President of the Royal Society, dated June 22, 1864. Quoted in Marussi, A. 1964. *Geophysics of the Karakorum, Italian Expeditions to the Karakorum (K2) and Hindu Kush* (Prof. A. Desio Leader), II-Geophysics, Vol. 1. E. J. Brill, Leiden, pp. 12–13.

TAHIRKELI, R. A. K., MATTAUER, M., PROUST, F. & TAPPONIER, P. 1979. The India Eurasia suture in North Pakistan: Synthesis and Interpretation of Recent Data at Plate Scale. *In*: FARAH, A. & DEJONG, K. A. (eds) *Geodynamics of Pakistan*. Geological Survey of Pakistan, Rawalpindi, 125–130.

TANDY, E. A. 1921. *Triangulation in India and Adjacent Countries, Sheet 43.M (Skardu)* (International Sheet N I 43 M), Dehra Dun.

TSCHERNING, C. C. 1992. The GRAVSOFT Package for Geoid Determination. *In*: HOLOTA, P. & VERMEER, M. (eds) *Proceedings of the 1st Continental Workshop for the Geoid in Europe*. Research Institute of Geodesy, Cartography and Topography, Czechoslovakia and IAG-Subcommission for the Geoid in Europe, Prague, 327–333.

TURCOTTE, D. L. & SCHUBERT, G. 1982. *Geodynamics: Application of Continuum Physics to Geological Problems*. J. Wiley & Sons, New York.

VERMA, R. K. & PRASAD, K. A. V. 1987. Analysis of Gravity Fields in the Northwestern Himalayas and Kohistan Region Using Deep Seismic Sounding Data. *Geophysical Journal of the Royal Astronomical Society*, 869–889.

VILOTTE, J. P., DAIGNIERES, M., MADARIAGA, R. & ZIENKIEWICZ, X. 1984. The Role of a Heterogeneous Inclusion During Continental Collision. *Physics of Earth and Planetary Interiors*, **36**, 236–259.

——, MADARIAGA, R., DAIGNIERES, M. & ZIENKIEWICZ, X. 1986. Subduction of Asian Lithospheric Mantle beneath Tibet Inferred from Models of Continental Collision. *Nature*, **369**, 642–645.

WALKER, J. T. 1879. Details of the pendulum operations by Captains J. P. Basevi, R.E. & W. J. Heaviside, R.E. and of their reduction. *Account of the Operations of the Great Trigonometrical Survey of India*, vol. V. Dehra Dun and Calcutta.

YOUNGHUSBAND, F. 1904. *The Heart of a Continent* (4th edition), London.

ZUBER, M. T., BECHTEL, T. D. & FORSYTH, D. W. 1989. Effective Elastic Thickness of the Lithosphere and Mechanism of Isostatic Compensation in Australia. *Journal of Geophysical Research*, **94**, B7, 9353–9367.

This page intentionally left blank

Mafic sheets from Indian plate gneisses in the Nanga Parbat syntaxis: their significance in dating crustal growth and metamorphic and deformation events

P. J. TRELOAR[1], M. T. GEORGE[2] & A. G. WHITTINGTON[3]

[1]*Centre for Earth and Environmental Science Research, School of Geological Sciences, Kingston University, Kingston-upon-Thames, Surrey KT1 2EE, UK (e-mail: p.treloar@kingston.ac.uk)*

[2]*Department of Earth Sciences, University of Wales, PO Box 914, Cardiff CF1 3YE, UK*

[3]*Department of Geology, 1301 W Green Street, Urbana, IL 61801, USA*

Abstract: Indian plate, granulite facies, migmatitic basement gneisses exposed within the Nanga Parbat syntaxis host at least two generations of mafic sheets. In the southern part of the syntaxis, concordant sheets yield Palaeo-Proterozoic model ages of 2.2–2.6 Ga, which probably date early stages of continental growth. In the northern part of the syntaxis the sheets include a suite of discordant, silica-saturated or oversaturated sub-alkaline basalts extracted from a slightly depleted sub-continental mantle. Nd model ages and an imprecise Sm–Nd isochron yield an age of emplacement at between 1.6 and 1.8 Ga. That these dykes cross-cut granulite facies migmatitic fabrics implies that peak metamorphism in the Indian plate gneisses was, at latest, Meso-Proterozoic and not Tertiary in age. Zircon and amphibole ages published elsewhere suggest that this metamorphism was probably *c.* 1850 Ma in age. That the basement gneisses were refractory by the Tertiary has implications for the derivation of leucogranite sheets during the Neogene. Although the gneisses experienced a Tertiary-aged metamorphism, it was to lower temperatures than the Meso-Proterozoic metamorphism. Unless the gneisses were rehydrated during the Tertiary, the leucogranites need to have been sourced from more fertile rocks underplating the granulite facies basement complex.

Ever since Sutton & Watson (1951) demonstrated the early history of the Lewisian basement complex of NW Scotland to be divisible into two distinct tectonothermal events, separated by a phase of dyke emplacement, geologists studying basement terrains have been conscious of the need to distinguish between different cycles of deformation in crustal sections that may have passed through more than one orogenic event. In a region such as the Himalaya, where it is tempting to ascribe all deformational and metamorphic features to Tertiary orogenesis, the problems of polycyclic evolution are acute. That not all granites within the Himalayan chain are Tertiary in age has been demonstrated by the recognition, along the length of the chain, of Cambrian-aged granites (Debon *et al.* 1986). There is some debate as to the age of migmatites in the High Himalaya on the hanging wall of the Main Central Thrust. In Zanskar, the migmatites can be traced into Miocene leucogranites (Noble & Searle 1995). By contrast, in Nepal, migmatites differ isotopically from Miocene leucogranites, and thus the former cannot be the source of the latter (Inger & Harris 1993), and need not necessarily be Tertiary in age. In addition, a crustal evolution event at *c.* 1850 Ma, including formation of a penetrative fabric and ending in emplacement of granites that cross-cut the fabric, has been documented from the internal zones of the Himalaya in NW Pakistan (Treloar *et al.* 1989*a*; Zeitler *et al.* 1989; Treloar & Rex 1990; Schneider *et al.* 1999) and India (Bhanot *et al.* 1977; Trivedi *et al.* 1984; Valdiya 1988). These basement gneisses were subsequently deformed during the Himalayan orogeny.

Hence, it is clear that even in the most internal zones of the Himalaya, penetrative gneissic fabrics, migmatites and granite sheets need not be Tertiary in age. Confusion arises because, although some of the migmatites and granites are Tertiary in age, others are not, and because pre-Tertiary magmatic and deformational fabrics may have been transposed during the Tertiary. It

From: KHAN, M. A., TRELOAR, P. J., SEARLE, M. P. & JAN, M. Q. (eds) *Tectonics of the Nanga Parbat Syntaxis and the Western Himalaya*. Geological Society, London, Special Publications, **170**, 25–50. 1-86239-061-4/00/$15.00

is also clear that, if the polycyclic nature of deformation, metamorphism and melting ranging from Precambrian to Neogene in age is not recognized, high strain deformation events and high-grade metamorphic events may all be attributed unquestioningly to the effects of Himalayan orogenesis. If so, our understanding of Tertiary processes will be flawed.

An area where recognition of pre-Tertiary events can significantly affect interpretation of event sequences is within the Indian plate gneisses of the Nanga Parbat syntaxis. Based on a combination of metamorphic textures, post-metamorphic peak ductile deformation and mafic dykes which cross-cut metamorphic fabrics, Treloar *et al.* (1994) and Wheeler *et al.* (1995) argued the main phase, regional granulite facies metamorphism preserved in Indian plate gneisses exposed within the core of the syntaxis to be pre-Tertiary, and probably pre-Permo-Trias in age. In postulating this, they did not dispute that temperatures reached $>700\,^{\circ}C$ during a Tertiary metamorphic overprint, or that local Neogene melting and leucogranite generation occurred as recently as 1–2 Ma ago. Evidence for the latter is given by young zircon and monazite ages (Smith *et al.* 1992; Zeitler *et al.* 1993; Schneider *et al.* 1999), preserved within leucocratic fractions of migmatites from the Fairy Meadows section (Whittington *et al.* 1998, 1999) and from leucogranite dykes and stocks which cross-cut the massif. As an alternative to the polymetamorphic interpretation, Winslow *et al.* (1995) cited P–T paths in garnet cores and the <10 Ma monazite and zircon ages to support a statement that 'no pre-Neogene migmatites and granites are found in the massif' and subsequently argued (Winslow *et al.* 1996) that 'metamorphism in the [syntaxis] is a result of two phases over a period of 50 Ma' and that the initial high pressure metamorphism, attained under an increasing pressure path, 'could have been as recent as 10–12 Ma'. In so doing they failed to recognize that there may be more than two generations of migmatites within the syntaxis—the regionally developed, *c.* 10 kbar, granulite facies migmatites (Wheeler *et al.* 1995) and the more locally developed low- to medium-pressure amphibolite facies migmatites at Fairy Meadows.

That the main metamorphic fabrics in the Indus and Astor gorges may be cut by dykes of pre-Tertiary age (Wheeler *et al.* 1995) suggests that models that constrain timing of high-grade metamorphism and melting within the syntaxis without considering the polycyclic nature of these rocks are over-simplifications. The aim of this study is to explore the relationships between metamorphic events within the syntaxis, and the role that cross-cutting mafic dykes may play in distinguishing between them. We review evidence that peak, granulite facies metamorphism within the syntaxis predated India–Asia collision; provide new data relating to the nature of the mafic sheets which are critical to that view; and, in the light of those data, critically assess the interpretations of Winslow *et al.* (1995, 1996) and of Treloar *et al.* (1994) and Wheeler *et al.* (1995). Throughout we stress that it is essential, in interpreting high-grade terrains, to be conscious of the problems imposed by polycyclic deformation and metamorphism.

Geology of the Nanga Parbat syntaxis

In the NW Himalaya, Tertiary collision was between the Kohistan island arc and the Indian plate, with the arc thrust south onto the leading edge of the Indian plate. The Nanga Parbat syntaxis (Figs 1 and 2) is a north-trending window, within the core of which Indian plate rocks have been tectonically exhumed from beneath the overlying arc. Increasingly rapid Neogene uplift has been accommodated by a combination of NW- to W-vergent thrusting along the western margin of the syntaxis and large wavelength buckle folding within the core of the syntaxis (Coward 1986; Butler & Prior 1988*a*, *b*; Butler *et al.* 1989, 1992; Madin *et al.* 1989; Treloar *et al.* 1991; Winslow *et al.* 1996). The extreme youth of the uplift is shown by extremely young amphibole and mica Ar–Ar and zircon and apatite fission track ages within the syntaxis, that are significantly younger than those in rocks which flank it (Zeitler 1985; Treloar *et al.* 1989*a*, 1991; Zeitler *et al.* 1993; George *et al.* 1995).

Synchronous with uplift was emplacement, within the last 10 Ma, of leucogranites enriched in radiogenic Sr. Granite generation was by decompressive, vapour-absent melting of a continental crustal source involving incongruent muscovite breakdown (Smith *et al.* 1992; George *et al.* 1993; Zeitler *et al.* 1993; Winslow *et al.* 1995; Butler *et al.* 1997; Whittington *et al.* 1999). The youngest leucogranites are *c.* 1 Ma old (Zeitler & Chamberlain 1991; Zeitler *et al.* 1993). U–Pb and Pb–Pb monazite (Smith *et al.* 1992) and zircon data (Zeitler *et al.* 1993) have been interpreted as implying that rocks exposed within the syntaxis experienced a Neogene, high-grade regional metamorphism (Smith *et al.* 1992; Zeitler *et al.* 1993; Winslow *et al.* 1995) and that there is a causal link between Neogene high temperature metamorphism, decompression melting and granite emplacement during regional uplift.

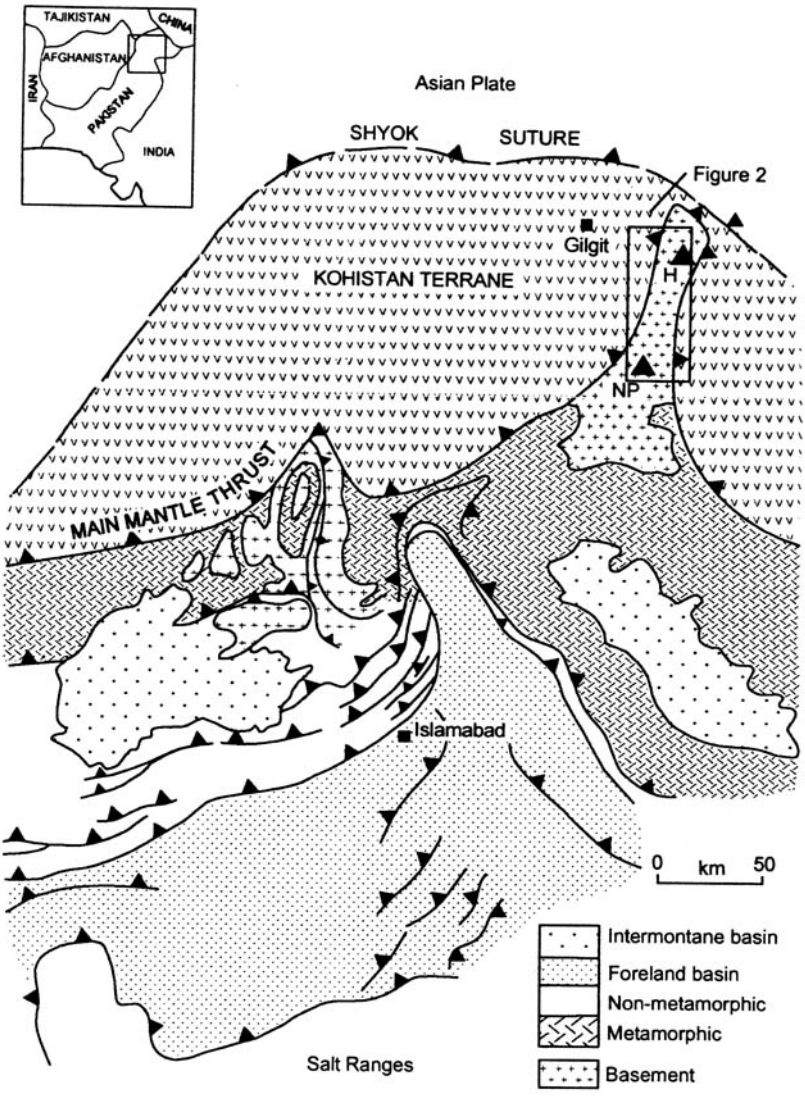

Fig. 1. Schematic map of the NW Himalaya showing the location of the Nanga Parbat syntaxis. NP: Nanga Parbat, H: Haramosh.

Pre-Neogene deformation and metamorphism

The Indian plate rocks exposed within the core of the syntaxis include biotite-rich quartzo-feldspathic basement gneisses (the Iskere gneisses), and meta-sedimentary cover rocks (the Shengus gneisses) (Madin *et al.* 1989). Both sequences are intruded by mafic sheets and Neogene leucogranites and are characterized by variable, and often extensive, migmatization. Within the Shengus paragneisses the main metamorphic paragenesis is quartz–plagioclase–orthoclase–garnet–biotite–kyanite and/or sillimanite–rutile (Wheeler *et al.* 1995). The presence of sillimanite fibres within garnet and of kyanite, sometimes replaced by sillimanite, in the matrix suggests that garnet growth took place during pressure increase. Over much of their outcrop the Shengus gneisses are migmatitic with a stromatic melt phase segregated from the metapelites by *in situ* anatexis. The presence of kyanite and garnet in equilibrium with the orthoclase and melt is consistent with vapour-absent melting, initially of muscovite and latterly of biotite at metamorphic conditions of *c.* 10 kbar and $>850\,^{\circ}C$ (Wheeler *et al.* 1995). The common

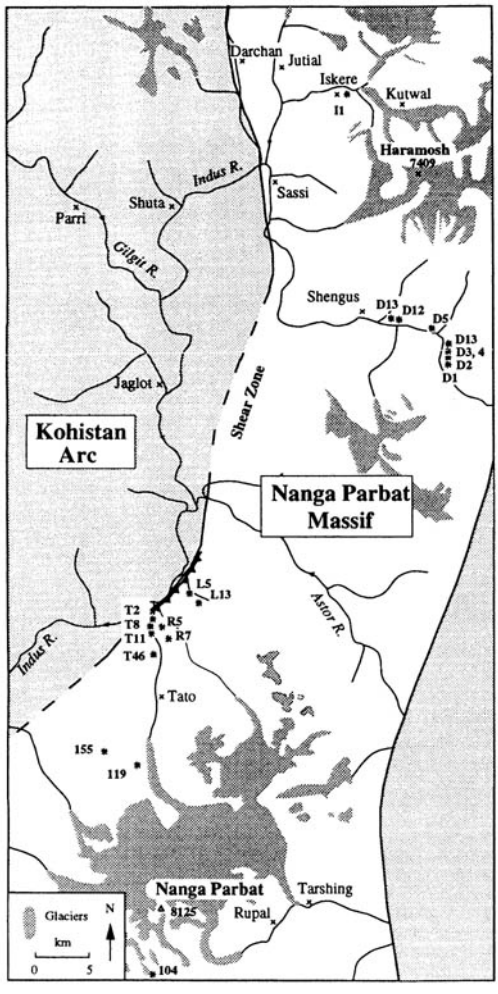

Fig. 2. Schematic geological map of the Nanga Parbat syntaxis showing the location of places mentioned in the text and of the analysed samples.

absence of muscovite implies that it was completely destroyed during melting.

Both the Shengus and Iskere gneisses show evidence for ductile shearing with the development of a mylonitic fabric that postdates peak metamorphism. In outcrop this fabric appears as intense S–, L– and S–L tectonite fabrics. Microstructures within the gneisses include: quartz ribbon fabrics, since annealed, that anastomose around garnet porphyroclasts; mortar texture developed within rounded feldspar porphyroclasts; and cataclasis of kyanite blades with cleavage rhombs stretched along the main fabric (Treloar *et al.* 1994). These features all suggest that ductile shearing postdated the metamorphic peak. The presence of sillimanite bundles, that overprint the main tectonic fabric, indicates that ductile shearing was postdated by a later thermal event.

The planar fabrics are folded by large wavelength, upright, north-trending domal structures (Madin *et al.* 1989; Treloar *et al.* 1991; Butler *et al.* 1992). The simplest interpretation of these is that the L–S fabrics, with N–S trending stretching lineations, represent ductile shearing during south-vergent thrusting of Kohistan onto the leading edge of the Indian plate early in Himalayan collision. The large wavelength folding of the S-surfaces dates from the < 10 Ma old, large-scale buckling that accompanied syntaxis growth. Thus, fabrics that deform, and postdate, the migmatites predate initial stages of syntaxis growth and the main phase migmatization cannot be the result of Neogene decompressive melting. Both the fabrics and the migmatites are cut by < 10 Ma old garnet–tourmaline-bearing leucogranite sheets.

The respective timings of: (a) high pressure granulite facies metamorphism that occurred along a path of increasing pressure culminating in biotite vapour-absent melting; (b) post-peak-metamorphic ductile shearing; and (c) folding of the shear fabrics permit two possible scenarios. Either granulite facies metamorphism is pre-Tertiary and the ductile deformation was associated with early stages of thrusting of Kohistan onto the Indian plate (Treloar *et al.* 1994; Wheeler *et al.* 1995), or both metamorphism and deformation are Tertiary in age (Winslow *et al.* 1995, 1996). In the latter case the high temperatures attained would imply that peak metamorphism and subsequent deformation are relatively late in the history of the India–Kohistan collision. This is the view of Chamberlain *et al.* (1989) and Winslow *et al.* (1995) who argued that prograde P–T paths are late Tertiary in age, and of Smith *et al.* (1992) who interpreted monazite ages within fabric-forming muscovites at < 10 Ma old, as dating the main deformation phase. Such an analysis, though, overlooks the significance of the presence of a swarm of mafic sheets emplaced into the migmatite complex. In the following section we review the geology, mineralogy and geochemistry of these sheets in order to define their likely age and tectonic setting of emplacement and to constrain a relative age of fabric development and high-grade metamorphism.

Mafic sheets within the Indian plate gneisses

The critical field evidence cited by Wheeler *et al.* (1995) that dates the granulite facies metamorphism as pre-Tertiary relates to cross-cutting

relationships between mafic dykes emplaced into the migmatitic gneisses and the fabrics and textures preserved within those gneisses. Three sets of mafic rocks from within the Nanga Parbat syntaxis have been studied: mafic dykes from the northern part of the syntaxis in the Indus and Iskere valleys; metabasites from Fairy Meadows, the Liachar Shear Zone and the Rupal Valley, all in the southern part of the syntaxis; and picrites from the Liachar Shear Zone and the Jalipur Pass, both in the southern part of the syntaxis.

With the exception of samples 104, 119 and 155, which were analysed at the Open University (Whittington 1997) by INAA (REE, Th, U, Ta, Hf) and XRF (major elements and all other trace elements), all major and trace element analyses were carried out in Cardiff using XRF (major elements, Ni, Cr, Zn, V and Cu) and ICP-MS (all other elements) techniques. ICP-MS data were obtained by solution nebulization on a Perkin Elmer Elan 5000. Rock powders were digested in PTFE vials using ultrapure concentrated HF and HNO_3. Due to the presence of zircon, Hf and Zr concentrations were obtained on samples which had been prepared by fusion with Li tetraborate. Quantitative limits for ICP-MS, based on the 10σ variation of 11 repeat measurements of the total procedural blank, are <10 ppb for REE, Y, Th, U and 10–100 ppb for all other elements analysed. In-run analytical precision lies in the range 1–5%. Sm/Nd ratios were analysed separately on the ICP-MS using relatively long replicate times to give the best possible precision (0.3–0.5% relative based on five duplicates/sample). Samples for isotope ratio determination were digested in Cardiff and $^{87}Sr/^{86}Sr$ and $^{143}Nd/^{144}Nd$ ratios were measured on Finnagan MAT261 and 262 mass spectrometers at the Open University. Total procedural blanks were <1 ng Sr and <0.5 ng Nd. During the period of analysis, six measurements of NBS987 gave $^{87}Sr/^{86}Sr = 0.710272 \pm 32$, and seven of the J&M standard gave 0.511774 ± 10 (1σ).

Field relations and petrography of metabasite dykes from the northern part of the syntaxis

Thirteen dykes were sampled from the Indus and Iskere valleys. They occur as 1–3 m wide bodies with exposure lengths of up to a few hundred metres. Contacts are sharp and usually concordant with the foliation in adjacent gneisses. However, in low-strain areas, the dykes cross-cut migmatitic fabrics within the Iskere and Shengus gneisses. Some of the larger dykes contain xenoliths of layered migmatitic gneiss (Fig. 3b) and elsewhere the migmatitic fabric is offset across discordant sheets (Fig. 3a), suggesting that the sheets postdate migmatization. The dykes are occasionally cut by veins (<1 m wide) of pegmatitic tourmaline leucogranite. The dykes vary from undeformed to intensely sheared. Undeformed dykes are fine grained, the thinnest ones extremely so, suggesting emplacement into cold rocks. Most dykes have a penetrative metamorphic foliation which, in places, is strongly mylonitic (i.e. sample D1). Where the dykes carry a penetrative shear fabric, it is parallel to the external fabric, suggesting emplacement before the main stage ductile deformation. Hence the mafic dykes postdate the granulite facies metamorphism, but predate the regionally developed shear fabrics which most likely reflect shearing related to early stages of emplacement of the Kohistan–Ladakh arc onto the Indian plate. The dykes acted as relatively competent units and represent low strain boudins around which shear strains were partitioned (see discussion in Wheeler *et al.* 1995).

The relatively undeformed sheets (D6, D12A, D12C, D12D), contain relicts of ophitic texture, with pyroxenes rimmed by a corona-like development of fine-grained hornblende. The more deformed sheets have been extensively amphibolitized and consist of a fine- to medium-grained assemblage of hornblende, plagioclase and Fe–Ti oxide, sometimes with minor amounts of quartz, biotite and titanite. Garnet (20–25%) is present in samples D11, D4 and D1. Sample D4 is also unusually biotite rich (*c.* 25%). In sample I1, the groundmass biotite has been partially altered to chlorite, but the other samples are unaltered. The amphibolite facies secondary assemblage suggests that, subsequent to their emplacement into cold rocks, the sheets have been through a medium-grade metamorphism.

Geochemistry of mafic sheets from the northern part of the syntaxis

Major and trace element data are presented in Table 1. As expected, there is some evidence that the more mobile elements have been affected to varying degrees by metamorphism and deformation. For example, K, Na, Rb, Ba and Sr show scatter on variation diagrams, whereas the less mobile elements show consistent trends. The following discussion is therefore largely restricted to the relatively immobile elements. The majority of samples are either silica-saturated or silica-oversaturated subalkaline basalts (Le Maitre 1989). Sample D11 is classified as a

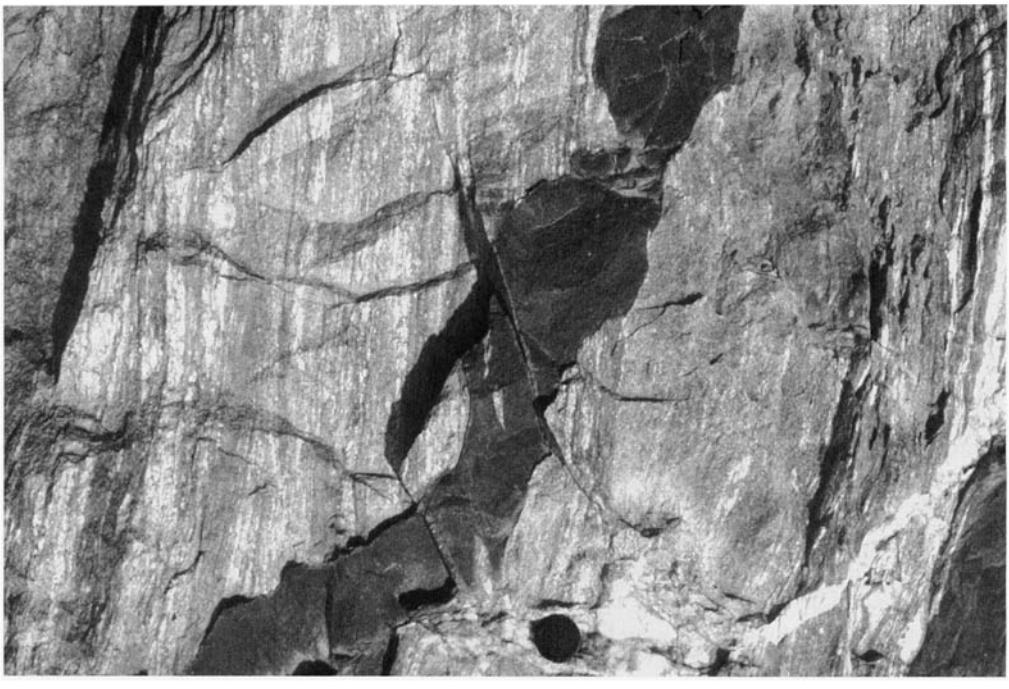

(a)

(b)

Fig. 3. Field photos of relations between basement gneisses and mafic dykes from the Indus Gorge, in the northern part of the Nanga Parbat syntaxis. (**a**) Dyke cross-cutting migmatitic fabrics within basement gneisses; (**b**) xenoliths of migmatitic gneiss contained within a mafic sheet.

Table 1. *Whole rock major and trace element data for metabasite sheets from the northern part of the Nanga Parbat syntaxis*

	D1	D3	D4	D5	D6	D11	D13	D12A	D12B	D12C	D12D	D12E	I1
(wt%)													
SiO_2	46.1	48.5	45.8	48.4	46.9	45.2	47.2	48.3	47.7	47.4	46.2	44.6	49.1
K_2O	0.35	0.56	1.75	0.42	0.49	0.48	0.73	0.65	0.33	0.84	0.41	0.67	1.34
TiO_2	1.51	1.49	3.88	1.66	1.30	1.89	1.53	2.30	1.07	1.21	1.21	1.19	1.36
Al_2O_3	15.8	13.6	13.0	13.6	16.7	14.6	16.0	13.7	16.8	16.8	16.3	16.1	14.9
Fe_2O_3	13.0	13.2	20.6	14.4	11.7	16.0	13.8	14.2	11.6	12.1	12.4	12.5	14.3
MnO	0.19	0.21	0.26	0.21	0.16	0.23	0.19	0.23	0.17	0.16	0.18	0.17	0.20
MgO	8.84	8.02	4.12	7.21	8.59	6.56	7.46	6.41	8.65	7.86	8.31	8.92	8.36
CaO	10.4	11.9	7.6	11.4	10.3	9.9	9.9	10.5	10.7	10.2	10.2	11.0	7.1
Na_2O	1.56	0.37	0.71	0.47	1.21	3.51	0.74	1.54	1.31	1.34	1.30	0.78	0.78
K_2O	0.35	0.56	1.75	0.42	0.49	0.48	0.73	0.65	0.33	0.84	0.41	0.67	1.34
P_2O_5	0.14	0.15	0.44	0.15	0.12	0.23	0.20	0.27	0.12	0.14	0.14	0.13	0.14
LOI	1.06	1.32	0.73	1.31	1.74	0.81	0.16	0.34	0.89	1.25	0.94	0.99	0.99
Total	98.8	99.3	98.9	99.3	99.2	99.4	98.0	98.5	99.4	99.3	97.5	97.1	98.6
Mg No.	47.6	44.8	21.1	40.0	49.5	35.4	41.9	37.5	49.9	46.3	47.1	48.7	43.8
(ppm)													
Zn	73	113	121	79	71	85	83	106	63	94	72	71	82
Cr	137	215	49	78	124	133	125	92	195	131	141	191	42
Ni	109	85	46	62	94	55	99	57	44	67	78	92	46
V	245	359	219	400	232	390	236	352	203	232	228	225	348
Cu	77	34	147	173	50	57	76	61	38	54	98	65	64
Li	6.7	25.4	13.2	10.1	9.1	17.0	21.5	15.9	22.1	28.1	16.7	19.7	n/a
Be	0.73	1.70	2.65	0.92	0.65	0.79	0.91	1.33	0.57	0.92	0.72	0.78	3.73
Sc	46.1	58.0	39.7	44.4	38.4	48.6	34.1	38.0	34.5	32.8	32.5	32.3	45.6
Ga	25.9	23.2	37.0	25.6	24.1	22.3	22.2	23.9	19.0	20.7	19.9	20.4	19.8
Rb	10.4	24.3	81.2	14.3	18.0	9.9	25.6	16.1	10.3	28.8	14.0	19.4	73.4
Sr	257	135	202	174	259	228	206	298	203	203	230	230	36
Y	31.3	41.3	74.0	27.0	27.3	38.3	32.3	36.7	23.3	26.3	25.7	25.2	28.0
Zr	86.7	84.4	330.0	97.8	86.5	131.0	137.5	189.2	64.7	100.8	88.0	86.3	101.8
Nb	6.55	6.19	25.12	6.63	6.58	10.29	11.00	17.44	4.55	7.69	6.34	7.47	11.80
Sn	1.08	2.74	2.25	1.12	0.97	1.12	0.97	2.33	0.69	1.33	0.86	1.20	1.95
Cs	0.18	11.32	1.63	0.35	3.07	0.36	1.45	0.41	1.02	3.84	0.57	0.68	2.41
Ba	125	61	546	91	146	82	225	172	98	175	126	136	38
Hf	1.84	1.82	6.92	2.16	1.88	2.29	2.39	3.36	1.28	1.86	1.65	1.73	2.16
Pb	2.05	6.35	12.64	3.10	3.13	9.29	9.56	9.92	4.60	13.68	5.05	7.52	10.56
Th	0.94	1.74	9.16	1.57	1.41	1.71	3.63	2.72	0.70	1.90	1.24	1.11	1.20
U	0.19	1.03	1.06	0.39	0.15	0.37	0.38	0.63	0.13	0.20	0.29	0.18	0.38
REE													
La	9.1	9.7	46.7	9.2	10.8	13.0	16.6	16.2	6.0	11.6	9.1	8.7	12.2
Ce	20.6	22.6	99.1	22.1	23.4	30.0	35.6	39.3	14.4	25.8	20.4	20.2	28.5
Pr	2.89	3.39	12.57	3.14	3.11	4.18	4.71	5.53	2.06	3.45	2.86	2.81	3.95
Nd	12.5	15.2	49.6	13.9	13.1	18.6	19.5	25.2	9.5	15.0	13.2	13.0	17.0
Sm	3.55	4.60	11.60	4.01	3.46	5.25	5.00	6.78	2.90	4.20	3.70	3.88	4.57
Eu	1.35	1.59	3.10	1.36	1.33	2.03	1.86	2.26	1.34	1.59	1.52	1.56	1.79
Gd	4.04	5.61	12.24	4.57	3.96	6.52	5.89	7.63	3.84	4.86	4.60	4.52	5.40
Tb	0.75	1.03	2.09	0.82	0.71	1.18	1.08	1.30	0.73	0.90	0.84	0.81	0.97
Dy	4.62	6.40	12.58	5.04	4.36	7.55	6.58	7.93	4.66	5.60	5.28	5.33	5.96
Ho	0.95	1.35	2.51	1.03	0.90	1.57	1.37	1.56	0.97	1.12	1.09	1.12	1.23
Er	2.52	3.58	6.77	2.74	2.39	4.47	3.79	4.26	2.83	3.26	3.18	3.19	3.33
Tm	0.38	0.50	0.99	0.41	0.35	0.66	0.56	0.58	0.41	0.48	0.46	0.43	0.50
Yb	2.25	2.91	5.93	2.34	2.11	4.19	3.46	3.46	2.57	2.81	2.91	2.82	3.02
Lu	0.37	0.45	0.93	0.36	0.33	0.65	0.53	0.51	0.39	0.44	0.45	0.44	0.47
Norms													
Q		5.34	5.61	6.32			3.06	3.19					4.45
ne						4.84							
di	12.85	19.75	6.87	18.06	9.34	20.81	7.81	18.09	10.81	10.29	9.99	12.36	1.12
hy	19.95	25.73	28.23	25.84	29.66		30.94	22.59	29.50	26.03	27.47	21.91	37.44
ol	7.97				0.65	18.13			0.52	2.16	2.35	6.78	

nepheline normative alkali basalt due to an anomalously high sodium content, but this may be the result of sub-solidus alteration. Mg numbers, calculated using a Fe^{2+}/Fe^{3+} ratio of 0.25, mostly range from 35 to 50. On variation diagrams Ti, P, Mn, Zr, Nb and Yb (REE) (Fig. 4) display clear fractionation trends, increasing in abundance with decreasing MgO. Fe, U, Th and Hf show similar trends.

On chondrite-normalized spidergrams (Fig. 5), the metabasites show moderate incompatible element enrichment and negative Hf, P, Sr, Nb and Ba anomalies. Sample D4, which has a low Mg number (21), is trace element enriched and displays a large negative Sr anomaly, but the overall shape of the pattern resembles the other spidergrams. The altered sample (I1) contains anomalous concentrations of the mobile elements Ba, Rb, K and Sr. Chondrite-normalized REE patterns (Fig. 6) are moderately fractionated, with $(Ce/Yb)_N$ varying from 1.5 to 4.3 and $(Tb/Yb)_N$ varying from 1.2 to 1.5. Eu/Eu* varies from 0.75 to 1.23 and decreases as total REE content increases (Fig. 7A). The degree of REE fractionation, expressed as $(Ce/Yb)_N$, increases with decreasing Mg number (Fig. 7B).

On a Ti–Zr–Y tectonic discriminant diagram (Fig. 8), the metabasites plot in the fields of mid-ocean ridge and island arc tholeiites rather than the within-plate field. Other occurrences of continental basalts have also been found which do not plot in the within-plate field (Holm 1985). It is probably inappropriate to use a discriminant diagram based on modern basalt compositions to assess the tectonic setting of ancient (probably Precambrian) basalts. Suites of basalts from adjoining regions in the Himalaya, including the Panjal Trap basalts (Honneger *et al.* 1982; Papritz & Rey 1989; Vannay & Spring 1993; Spencer *et al.* 1995), plot in distinct sub-fields, mostly in the field of within-plate basalts (Fig. 8). The Nanga Parbat metabasites overlap the field of the lower Palaeozoic Bafliaz volcanics, which occur 400 km away in northwestern India (Bhat *et al.* 1994).

Radiogenic isotope data are presented in Table 2. The metabasites are characterized by $^{87}Sr/^{86}Sr$ and $^{143}Nd/^{144}Nd$ ratios of 0.7055–0.7140 (excluding I1) and 0.51225 to 0.51267, respectively. On an Sm/Nd isochron diagram (Fig. 9), the data are scattered, although seven out of eight samples plot along an 'errorchron' which gives an age of 1730 ± 211 Ma (MSWD = 24). Five of these samples give a reasonable fit (MSWD = 0.6) and an age of 1636 ± 238 Ma ($^{143}Nd/^{144}Nd_i = 0.51073$). However, there is no clear petrological justification for excluding three of the samples from the age calculation and therefore this age determination should be interpreted with caution. The scatter shown on the Sm–Nd isochron diagram is probably due to the existence of slight variations in $^{143}Nd/^{144}Nd_i$. The average Nd model age, based on a depleted mantle model composition and excluding sample D12A, is 1697 Ma. $\varepsilon_{Nd}(1.7\ Ga)$ values for the same samples lie in the range +2.7 to +4.5 (Table 2).

Interpretation of the northern suite of mafic sheets

The northern suite of metabasic dykes are geochemically coherent with narrow abundance ranges for most trace elements. The REE and spidergram plots for different dykes have broadly similar shapes, due to the absence of significant variations in incompatible element ratios. Due to their relatively low Ni and Cr contents and low Mg numbers, the metabasites are unlikely to represent primary magmas. They are slightly LREE enriched, depleted in Sr, and show correlations between Eu/Eu* and both $(Ce/Yb)_N$ and MgO. These observations, together with major element variation trends, suggest that magma fractionation was controlled by a combination of olivine, clinopyroxene and plagioclase. As Ti and Yb behave as incompatible elements, it is unlikely that Fe–Ti oxide and garnet were important fractionating phases. The most primitive dykes have minor positive Eu anomalies, which may be related to oxygen fugacity in the source, or the presence of a small proportion of cumulus plagioclase.

The dykes are moderately enriched in incompatible trace elements and have negative P and Nb anomalies. These could be a reflection of an unusual mantle source composition, fractionation, crustal assimilation, or a combination of these (Carlson 1991; Jochum *et al.* 1991). Nb/Th and Ti/Zr ratios are low and variable relative to both primitive mantle and modern oceanic basalts, and both ratios decrease with an increasing degree of magma evolution (Fig. 10). The compositional ranges of Nanga Parbat felsic gneiss samples (George 1995) are plotted on Fig. 10 to assess whether the trends could have been generated by mixing between basic magma and upper crustal material. Although some of the variation in La/Sm_N shown in Fig. 10 may be due to clinopyroxene fractionation, this is unlikely to alter the Nb/Th ratio. The trends in Fig. 10 could be taken as an indication that there has been crustal contamination, in which case the isochron (Fig. 9) may be a fictitious mixing

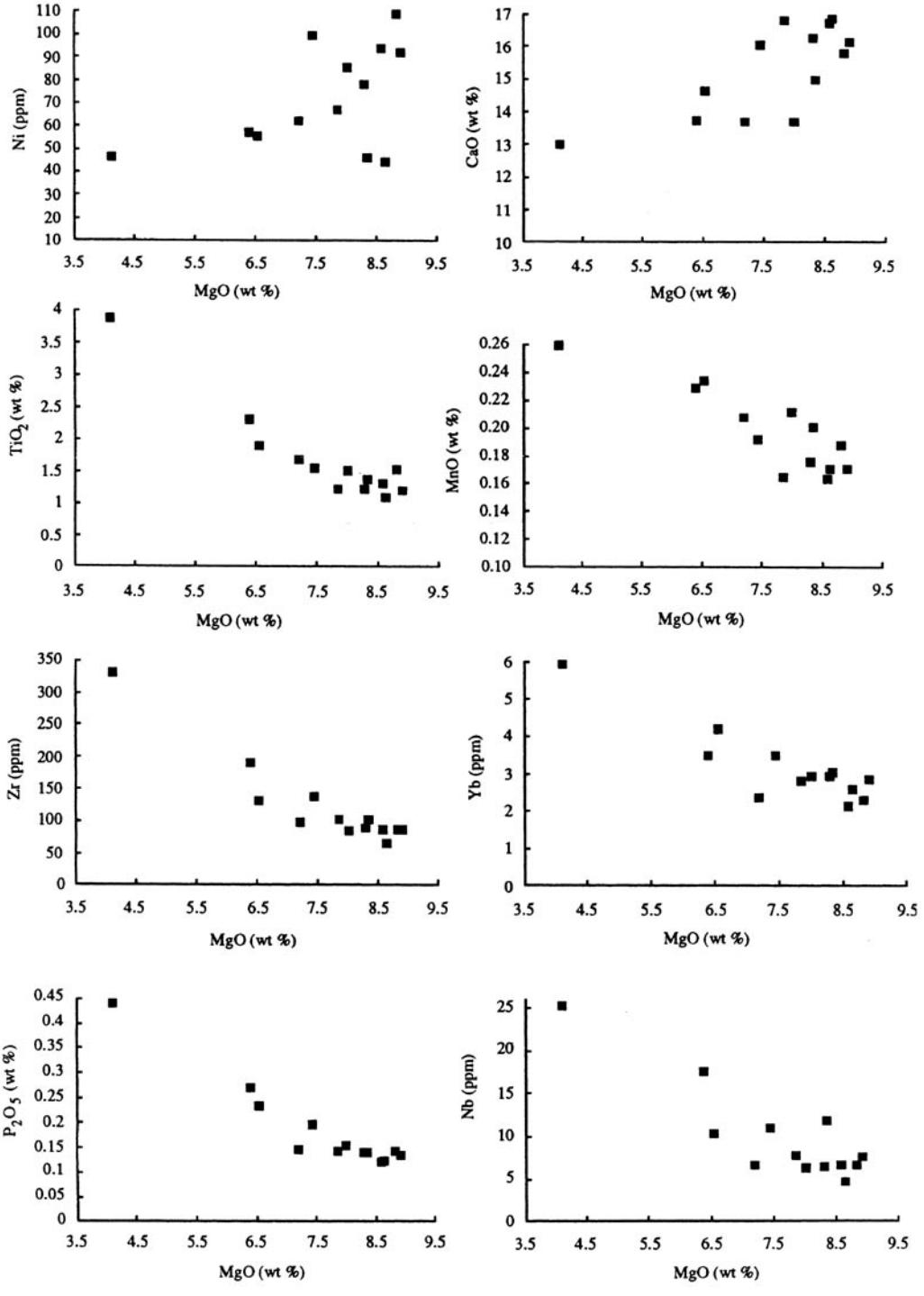

Fig. 4. Variation diagrams for metabasite samples from the northern part of the Nanga Parbat massif.

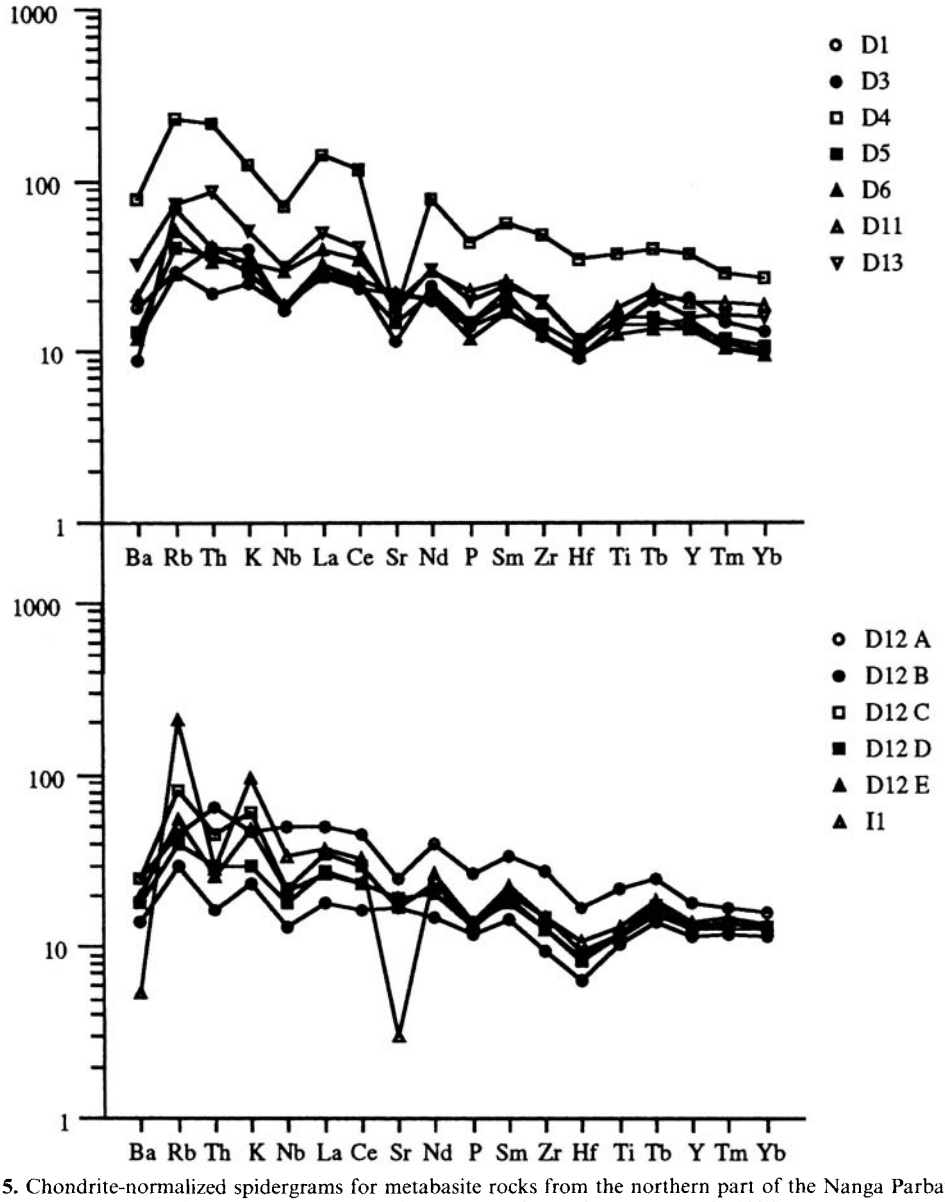

Fig. 5. Chondrite-normalized spidergrams for metabasite rocks from the northern part of the Nanga Parbat syntaxis (two separate plots for clarity). Normalizing values from Thompson *et al.* (1984).

line. The felsic gneisses are characterized by low and variable $^{143}Nd/^{144}Nd$ ratios (George *et al.* 1993), with recalculated Nd model ages (based on recently measured Sm/Nd ratios) in the range 2.4–2.6 Ga. If contamination with such material occurred, the calculated $^{143}Nd/^{144}Nd_i$ ratio will be an underestimate. The calculated age will also be incorrect if the contaminants and host magma were not isotopically homogenized. However, on a plot of $^{147}Sm/^{144}Nd$ v. $^{143}Nd/^{144}Nd_i$ (Fig. 11), the metabasic rocks do not plot on a mixing line between depleted mantle and felsic gneiss and therefore the geochemical trends are not thought to be significantly influenced by crustal contamination. This conclusion is supported by the observation that the $\varepsilon_{Nd}(1.7\,Ga)$ values (Table 2) are geologically reasonable. $^{87}Sr/^{86}Sr_i$ ratios mostly lie in the range 0.700–0.704, with no evidence for involvement of continental crust. Furthermore, although there is a positive

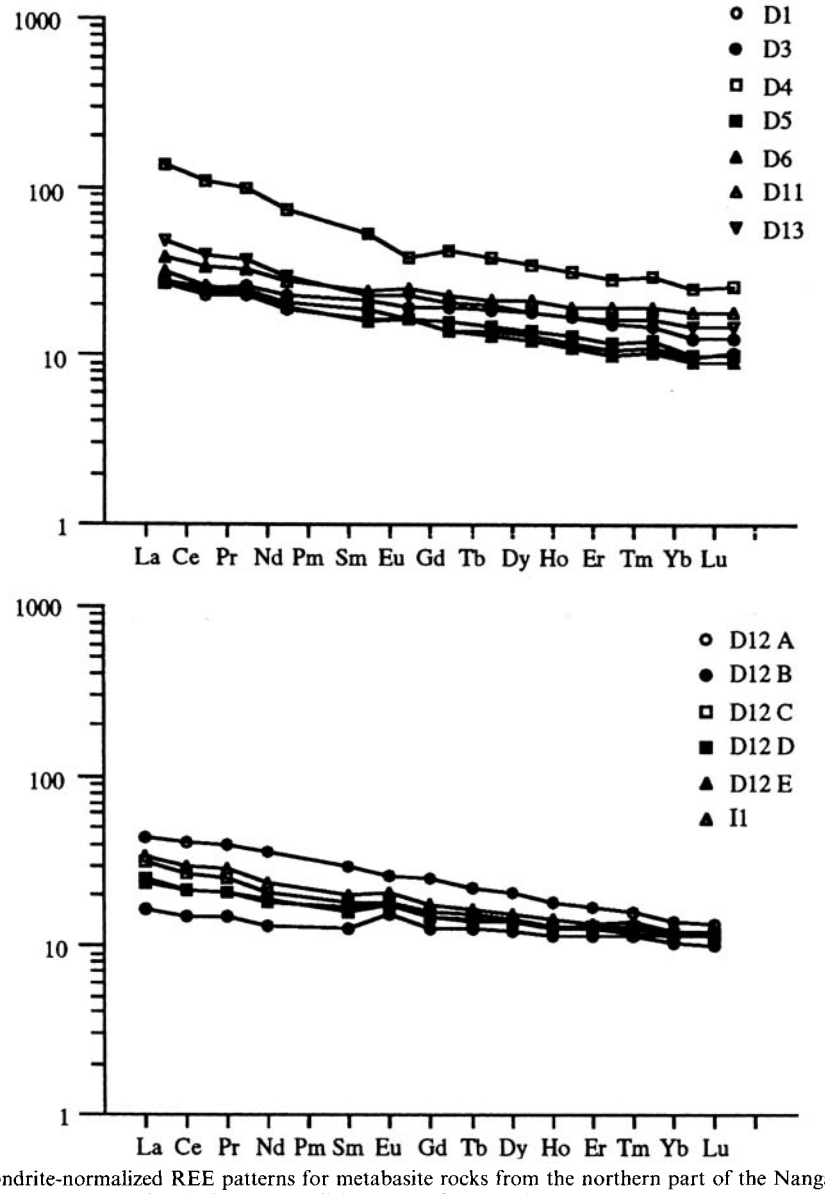

Fig. 6. Chondrite-normalized REE patterns for metabasite rocks from the northern part of the Nanga Parbat massif (two separate plots for clarity). Normalizing values from Taylor & McLennan (1985).

correlation between $^{143}Nd/^{144}Nd$ and Nb/Th and Ti/Zr (Fig. 12), due to the fact that samples enriched in Th and Zr are also LREE enriched and therefore relatively unradiogenic, there is no correlation between any major element and the Nd isotopic composition, which would be expected if the magma had undergone crustal contamination.

Anomalous incompatible element ratios in basic dyke swarms may be a reflection of enriched mantle source regions (Condie *et al.* 1987). However, the $\varepsilon_{Nd}(1.7\ Ga)$ values suggest that the source region was slightly depleted in LREE relative to bulk earth, and such a source would be unlikely to have anomalously low Nb/Th and Ti/Zr ratios. It seems most likely that the Nb/Th and Ti/Zr ratios are controlled by magmatic fractionation. Although it is generally thought that these ratios are not modified by high degrees of partial melting or fractional

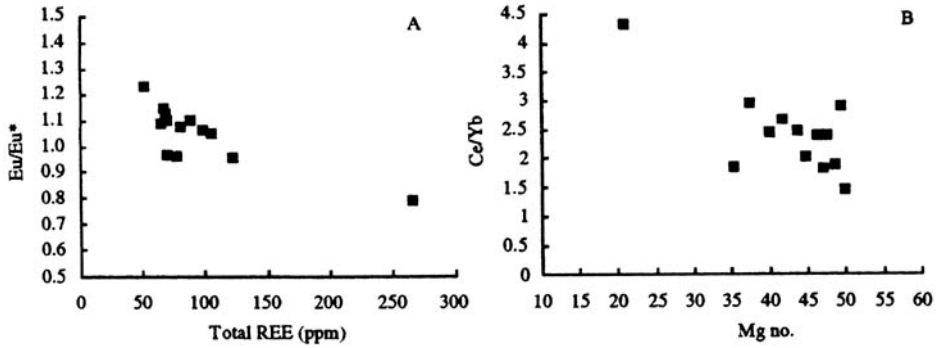

Fig. 7. Bimodal plots showing (**A**) variation in Eu/Eu* ratios with total REE content; (**B**) correlation between the degree of fractionation $(Ce/Yb)_N$ and Mg number for metabasic rocks from the northern part of the Nanga Parbat massif.

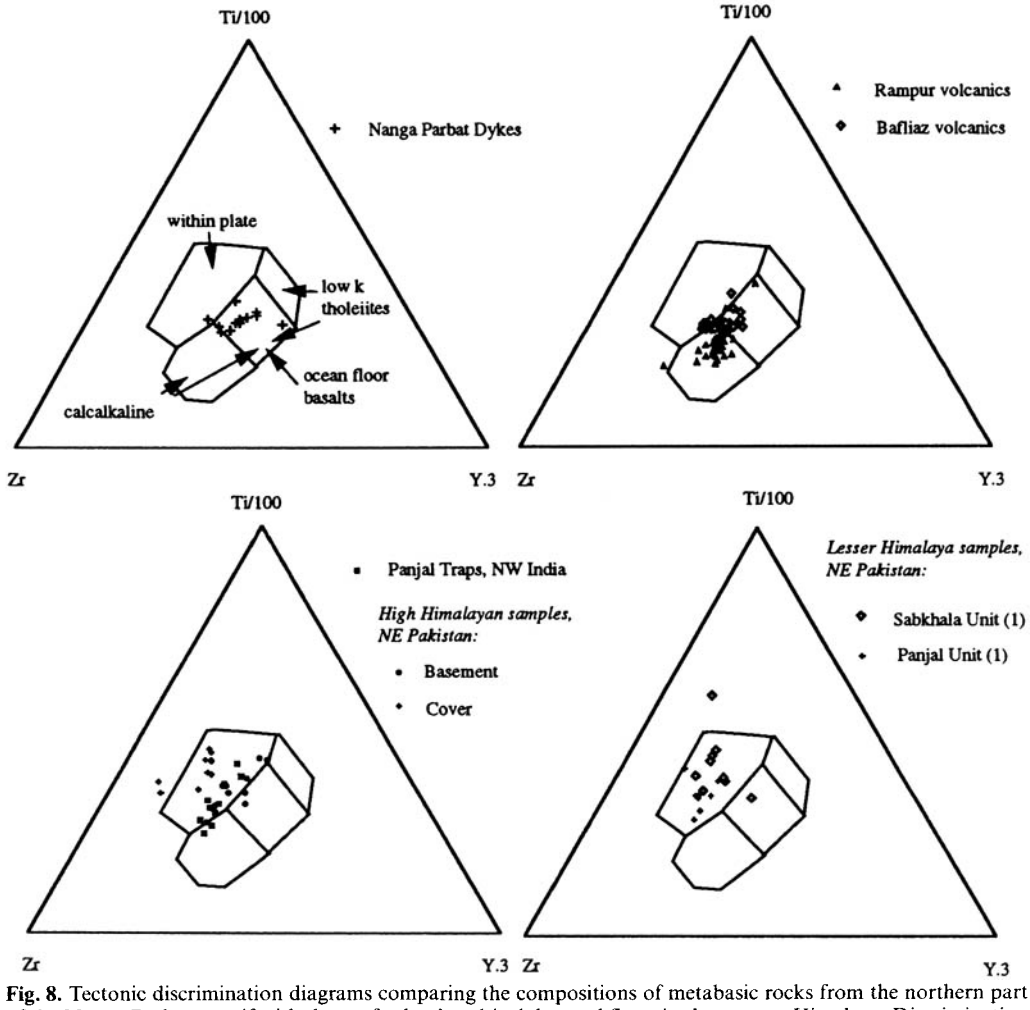

Fig. 8. Tectonic discrimination diagrams comparing the compositions of metabasic rocks from the northern part of the Nanga Parbat massif with those of other basaltic dykes and flows in the western Himalaya. Discrimination fields from Pearce & Cann (1973). Bafliaz volcanics from Bhat *et al.* (1994); Rampur volcanics from Bhat & Le Fort (1992); Panjal Traps from SE Zanskar (Vannay & Spring 1993), Suru (Honneger *et al.* 1982) and NE Pakistan (Papritz & Rey 1989; Spencer *et al.* 1995).

Table 2. *Rb/Sr and Sm/Nd isotope data for metabasite samples from the northern part of the Nanga Parbat syntaxis. Sm/Nd ratios were determined in a separate run by ICP-MS for optimum precision. Errors refer to the last two digits of the isotope ratios*

Sample	Rb	Sr	$^{87}Rb/^{86}Sr$	$^{87}Sr/^{86}Sr$	$\pm1\sigma$	Sm/Nd	$^{147}Sm/^{144}Nd$	$^{143}Nd/^{144}Nd$	$\pm1\sigma$	T_{DM}^{Nd} (Ma)	ε_{Nd} (1.7 Ga)
D4	81.2	202.0	1.162	0.714014	66	0.235	0.1415	0.512251	40	1637	4.5
D6	18.0	258.6	0.201	0.707565	10	0.264	0.1589	0.512439	06	1637	4.3
D11	9.9	227.8	0.126	0.707344	09	0.280	0.1686	0.512463	06	1850	2.7
D13	25.6	206.0	0.360	0.708749	23	0.252	0.1517	0.512288	07	1788	3.0
D12A	16.1	298.3	0.156	0.705554	22	0.266	0.1598	0.512666	06	1131	8.6
D12D	14.0	229.9	0.176	0.706810	06	0.278	0.1674	0.512535	04	1623	4.4
D12E	19.4	230.5	0.243	0.706554	17	0.280	0.1686	0.512535	05	1657	4.1
I1	71.4	34.20	6.036	0.871844	16	0.255	0.1535	0.512356	07	1689	3.9

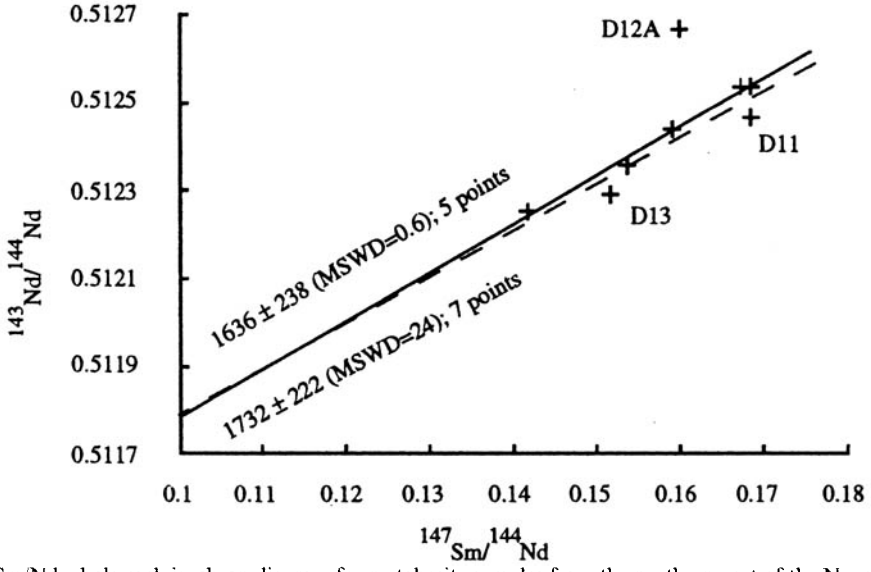

Fig. 9. Sm/Nd whole rock isochron diagram for metabasite samples from the northern part of the Nanga Parbat massif.

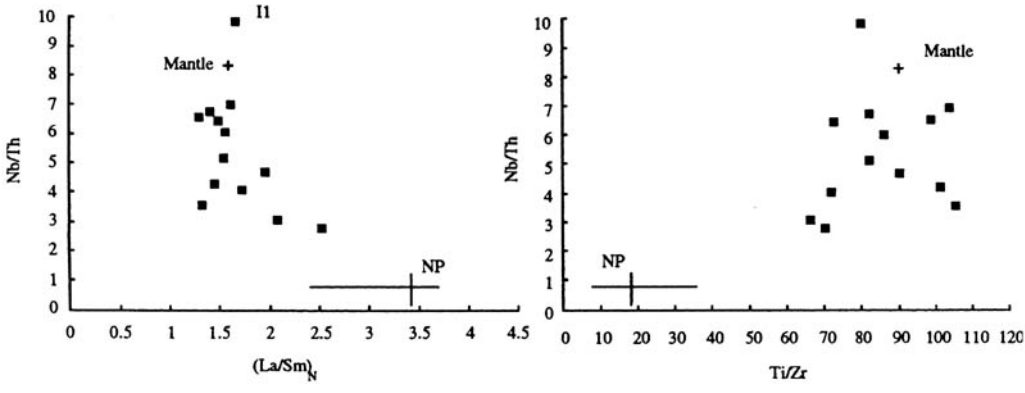

Fig. 10. Diagrams showing variations in incompatible element ratios for the metabasite rocks from the northern part of the Nanga Parbat massif. Mantle composition from Thompson *et al.* (1984). NP: range of compositions from gneisses from the Nanga Parbat massif (cross marks the mean compositions).

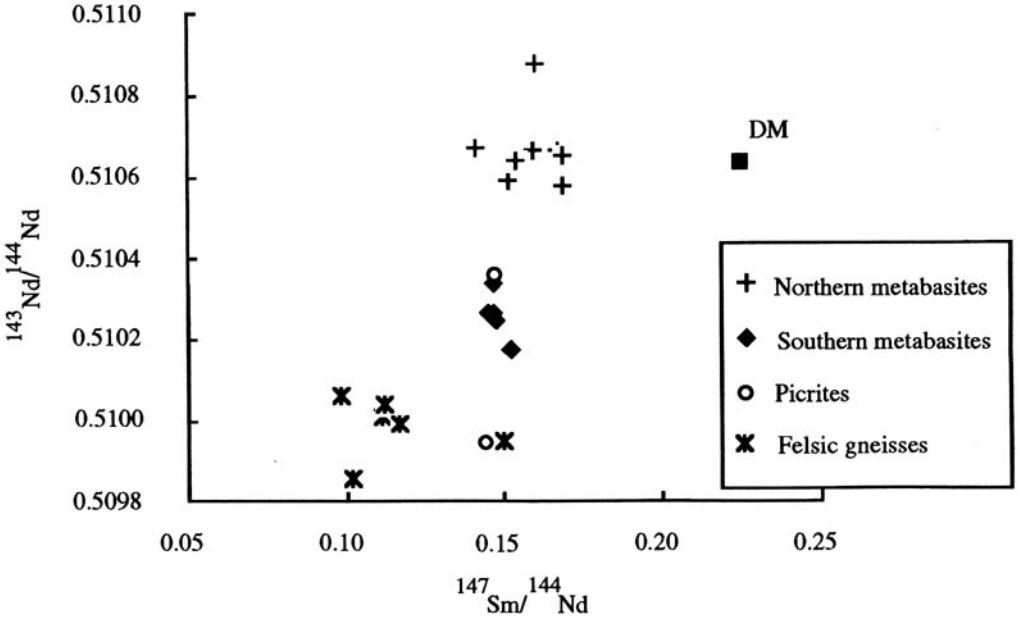

Fig. 11. Diagram comparing the initial (1.7 Ga) Nd isotopic compositions of metabasic rocks, picrites and felsic gneisses from the Nanga Parbat massif. DM = depleted mantle.

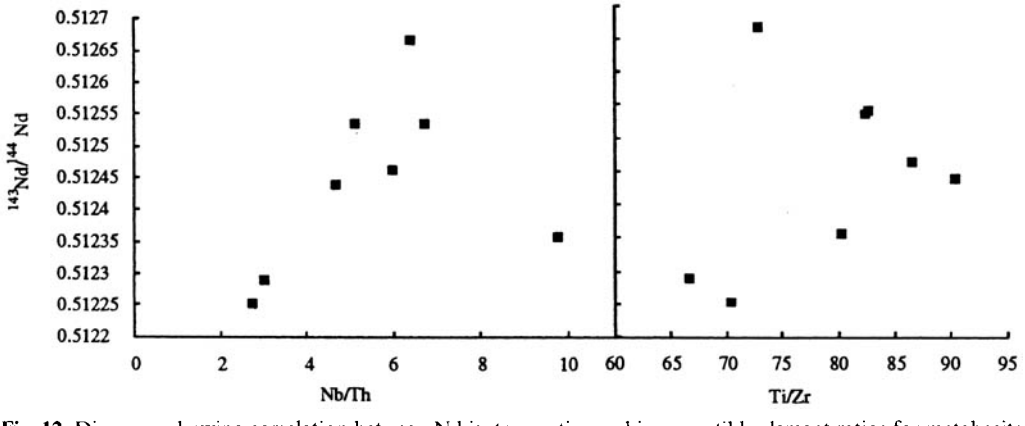

Fig. 12. Diagrams showing correlation between Nd isotope ratios and incompatible element ratios for metabasite samples from the northern part of the Nanga Parbat massif.

crystallization of basic magma, the ratios may be modified by the behaviour of residual accessory phases during low degrees of partial melting. For example, during the formation of the basalts, residual Th- and Zr-rich phases may have become involved in the melt reactions, producing liquids with successively lower Nb/Th and Ti/Zr ratios.

Only one sampled dyke (I1) shows petrographic evidence for secondary alteration. This dyke has positive Rb and K anomalies and a negative Sr anomaly, which is a typical fingerprint of hydrothermal alteration (Holm 1985). The high $^{87}Sr/^{86}Sr$ determined for this dyke falls within the $^{87}Sr/^{86}Sr$ range of metamorphic rocks in the region (George *et al.* 1995), and biotite in the dyke is out of strontium isotopic equilibrium with the whole rock (George *et al.* 1995). This suggests that the dyke experienced localized open system Sr isotope exchange with the country rocks. The Nd isotopic composition has not been affected by this exchange, which is probably a reflection of the relative immobility of the REE during low temperature alteration.

Metabasites and picrites from southern parts of the Nanga Parbat massif

Metabasic rocks were sampled from Fairy Meadows, the Liachar Shear Zone, and the Rupal Valley. Picritic sheets were sampled from the Liachar Shear Zone and from the Jalipur Pass. Metabasites and picrites from the Liachar Shear Zone, and the metabasite collected from Fairy Meadows (119), are structurally concordant and often strongly boudinaged. The concordant metabasites could conceivably be metatuffs or para-amphibolites (originally calcareous shales) rather than intrusive sheets. Although the sampled horizons were not closely associated with metasedimentary lithologies, some caution will be attached to the interpretation of geochemical data from these sheets.

The picrites occur as green coloured sheets up to 15 m thick, containing numerous rounded, brown-weathering grains of olivine. In thin section the picrites are composed of fragmented, 2–3 cm long grains of olivine (<40%) and clinopyroxene (<20%), largely pseudomorphed by iron oxide and tremolite, set in a fine-grained, schistose groundmass of chlorite, tremolite and biotite. One of the picrites (T11) has a mylonitic fabric in which olivines occur as highly fragmented porphyroclasts. Metabasites from the southern areas are petrographically similar to those studied from the northern part of the Nanga Parbat massif.

The major element compositions of the southern suite of metabasites (Table 3) are similar to those from the north, with the exception of the Rupal sheet (104) which is a nepheline normative alkali basalt. Multiple analyses of the Rupal and Fairy Meadows metabasites indicate significant intra-body variation in K, Rb, Cs, Ba, Cu and Pb (>10% RSD). In the Rupal dyke the Sr concentration is also variable. Metabasites from the Liachar Shear Zone (T2, T8 and T46) display scattered abundances of the relatively mobile elements Rb, Ba, Th and K, probably due to sub-solidus alteration during shearing. In general, abundances of Ti, Zr, Nb and P for a given MgO content are lower than in the northern suite of metabasites. Spidergram patterns (Fig. 13A) are significantly more spikey than those of the northern suite (Fig. 5), with deep troughs for P, Sr and Nb and peaks for the LREE. However, the Fairy Meadows sample (119) has a relatively flat pattern which resembles the northern dykes. Total REE contents are lower than for the northern metabasites but the LREE are more fractionated (Fig. 14A), with an average $(La/Sm)_N$ ratio of 2.5 compared with 1.7 for dykes in the north. These observations indicate that the northern and southern dyke suites cannot be related by simple fractional crystallization of a common parental magma. On a plot of La/Yb_N v. La_N (Fig. 15) (Rossy *et al.* 1992), the two basalt suites lie on separate trends which probably indicates that they were generated from two different sources. Horizontal scatter on Fig. 15 is probably due to variable degrees of crystal fractionation of magma with variable proportions of clinopyroxene and plagioclase in the fractionating assemblage. Ti/Zr and Nb/Th ratios are lower than in the northern metabasites, and the Nb/Th ratios overlap those of the Nanga Parbat gneisses (*c.* 1.0). On a trace element discriminant diagram (Fig. 16), most of the dykes from the south plot within the calc-alkaline field, whilst the dyke from Fairy Meadows (119) plots on the edge of the within-plate field. In general, the southern metabasites are characterized by more variable trace element compositions than the northern samples, and they do not comprise such a geochemically coherent suite.

Isotopically the Rupal and Fairy Meadows metabasites are significantly more enriched than the northern suite, with $^{87}Sr/^{86}Sr$ and $^{143}Nd/^{144}Nd$ ratios varying from 0.7502–0.7707 and 0.51181–0.51201, respectively (Table 4). The negative ε_{Nd}(1.7 Ga) values are in marked contrast to the positive values of the northern suite (Table 2). The Nd data do not define an isochron and Nd model ages are variable, in the range 2.2–2.7 Ga. These isotopic differences probably indicate that the southern suite is older than the northern one. Since the Nd model ages overlap those calculated for the felsic gneisses (George 1995), the dykes may have a similar age to the basement. The combined trace element and isotope data suggest that the southern metabasites were generated in a more incompatible element (especially Th, Zr and LREE) enriched source region. However, it is possible that the various geochemical characteristics, including the calculated model ages, are a reflection of crustal contamination, as the southern metabasites lie on a mixing line between depleted mantle and felsic gneiss of the Nanga Parbat massif (Fig. 11). Unfortunately it is not yet possible to evaluate the relative importance of these alternatives, largely due to uncertainty regarding the reliability of Nd model ages for metabasites. However, data from the picrites, described below, which show no major element evidence for crustal contamination, suggests that enriched mantle sources were available at 2.2 Ga.

Table 3. *Whole rock major and trace element data for metabasite sheets from the southern part of the Nanga Parbat syntaxis*

	T2	T8	T46	104A	104B	104C	104D	104E	119A	119B	119C	119D	119E
(wt%)													
SiO_2	51.07	46.95	52.65	46.81	48.45	46.14	46.49	47.08	51.60	51.46	50.96	51.04	53.95
K_2O	1.11	1.72	0.38	1.10	0.85	1.22	1.15	1.02	1.01	0.94	1.04	1.69	2.05
TiO_2	0.93	0.55	0.70	0.69	0.63	0.63	0.67	0.64	1.60	1.58	1.63	1.52	1.42
Al_2O_3	14.50	14.62	15.46	15.23	14.43	14.87	15.15	14.99	14.31	14.47	14.18	13.78	14.90
Fe_2O_3	12.43	11.87	11.04	12.64	11.76	12.03	12.48	12.09	12.78	12.72	12.99	13.68	11.88
MnO	0.17	0.17	0.15	0.18	0.18	0.19	0.18	0.19	0.22	0.22	0.23	0.23	0.18
MgO	6.68	9.46	7.60	8.56	8.61	8.40	8.46	8.60	6.35	6.30	6.41	7.17	6.08
CaO	9.69	9.81	10.47	11.05	10.98	11.62	11.26	10.92	8.85	8.93	8.93	7.98	6.41
Na_2O	1.07	1.01	0.12	2.08	2.31	2.09	2.08	2.25	2.07	2.12	1.92	1.63	1.93
K_2O	1.11	1.72	0.38	1.10	0.85	1.22	1.15	1.02	1.01	0.94	1.04	1.69	2.05
P_2O_5	0.08	0.06	0.07	0.07	0.07	0.07	0.07	0.07	0.14	0.14	0.14	0.14	0.14
LOI	1.52	1.44	0.50	1.22	1.65	2.49	1.68	1.89	1.01	1.08	1.03	1.11	0.59
Total	99.25	97.64	99.13	99.63	99.92	99.75	99.67	99.73	99.93	99.95	99.46	99.96	99.53
Mg No.	41.7	51.5	47.9	47.5	49.4	48.2	47.5	48.7	39.8	39.8	39.7	41.1	40.6
(ppm)													
Zn	115	73	64	94	102	104	94	104	114	113	115	131	265
Cr	59	490	333	462	406	460	477	467	213	209	211	197	162
Ni	38	151	44	157	150	157	155	161	56	57	55	55	44
V	250	206	211	276	255	261	262	266	300	307	306	296	254
Cu	28	n/d	n/d	104	9	130	123	69	80	94	78	63	52
Li	n/d	n/d	n/d	n/a	n/a	n/a	n/a	n/a	n/a	n/a	n/a	n/a	n/a
Be	0.86	1.57	1.72	n/a	n/a	n/a	n/a	n/a	n/a	n/a	n/a	n/a	n/a
Sc	29.7	16.9	12.8	36	36	32	38	37	37	33	32	31	30
Ga	18.42	16.12	17.85	18	17	18	16	17	22	21	23	20	21
Rb	56.17	93.81	4.52	68.3	56.7	91.7	72.7	72.1	47.6	40.4	54.6	143	139.9
Sr	155.8	109.4	78.2	160	154.2	157.6	160.7	158	381.4	391.7	344	225.6	211.8
Y	19.6	18.2	17.4	20.5	19.3	18.2	19.4	18.6	24.2	24.1	25.4	22.1	24.2
Zr	89.84	59.23	73.35	66	64	64	65	62	120	114	125	115	144
Nb	5.00	3.84	4.50	2.4	3.7	2.4	3.1	3.4	7.1	7.4	7.9	6.8	11.9
Sn	5.16	5.33	4.03	n/a	n/a	n/a	n/a	n/a	n/a	n/a	n/a	n/a	n/a
Cs	2.89	9.26	0.12	3.6	7.2	5.9	3.1	8.2	2.1	n/a	n/a	n/a	n/a
Ba	85.9	195.9	27.4	161	132	127	122	162	229	202	230	411	362
Hf	1.887	1.213	1.544	1.81	1.71	1.84	1.79	1.84	3.22	n/a	n/a	n/a	n/a
Pb	10.02	11.58	8.25	15	9	12	15	13	23	24	24	17	36
Th	5.30	3.22	3.31	3.3	3.1	3.2	3.4	3.1	3.2	n/a	n/a	n/a	n/a
U	4.30	0.69	0.91	0.6	0.7	1	0.6	0.5	1.2	n/a	n/a	n/a	n/a
REE													
La	14.6	10.6	12.5	9.9	9.3	10.2	10.3	9.4	15.5	n/a	n/a	n/a	n/a
Ce	30.6	21.7	25.6	19.3	18.5	18.3	19.7	18.3	31.2	n/a	n/a	n/a	n/a
Pr	3.8	2.7	3.2	n/a	n/a	n/a	n/a	n/a	n/a	n/a	n/a	n/a	n/a
Nd	15.3	10.4	12.3	10.3	10.3	10.2	10.9	9.7	17.5	n/a	n/a	n/a	n/a
Sm	3.73	2.54	2.92	2.5	2.47	2.48	2.57	2.44	4.24	n/a	n/a	n/a	n/a
Eu	1.13	0.69	0.88	0.76	0.78	0.76	0.8	0.77	1.41	n/a	n/a	n/a	n/a
Gd	4.23	3.10	3.43	n/a	n/a	n/a	n/a	n/a	n/a	n/a	n/a	n/a	n/a
Tb	0.71	0.54	0.61	0.58	0.56	0.52	0.58	0.54	0.78	n/a	n/a	n/a	n/a
Dy	4.34	3.57	3.82	n/a	n/a	n/a	n/a	n/a	n/a	n/a	n/a	n/a	n/a
Ho	0.88	0.77	0.76	n/a	n/a	n/a	n/a	n/a	n/a	n/a	n/a	n/a	n/a
Er	2.41	2.19	2.14	n/a	n/a	n/a	n/a	n/a	n/a	n/a	n/a	n/a	n/a
Tm	0.33	0.31	0.31	n/a	n/a	n/a	n/a	n/a	n/a	n/a	n/a	n/a	n/a
Yb	2.03	1.95	1.91	1.66	1.59	1.6	1.63	1.6	2.01	n/a	n/a	n/a	n/a
Lu	0.30	0.29	0.29	0.24	0.24	0.23	0.25	0.24	0.29	n/a	n/a	n/a	n/a
Norms													
Q	6.58		12.99						4.41	4.17	4.19	3.22	7.24
ne				0.33		2.32	1.16	0.29					
di	13.30	14.71	9.01	20.85	22.54	24.28	22.00	21.26	13.46	13.45	13.60	11.11	4.16
hy	25.39	18.64	28.33		5.79				23.94	23.77	24.26	28.50	26.89
ol		9.44		19.83	14.29	17.79	19.10	19.28					

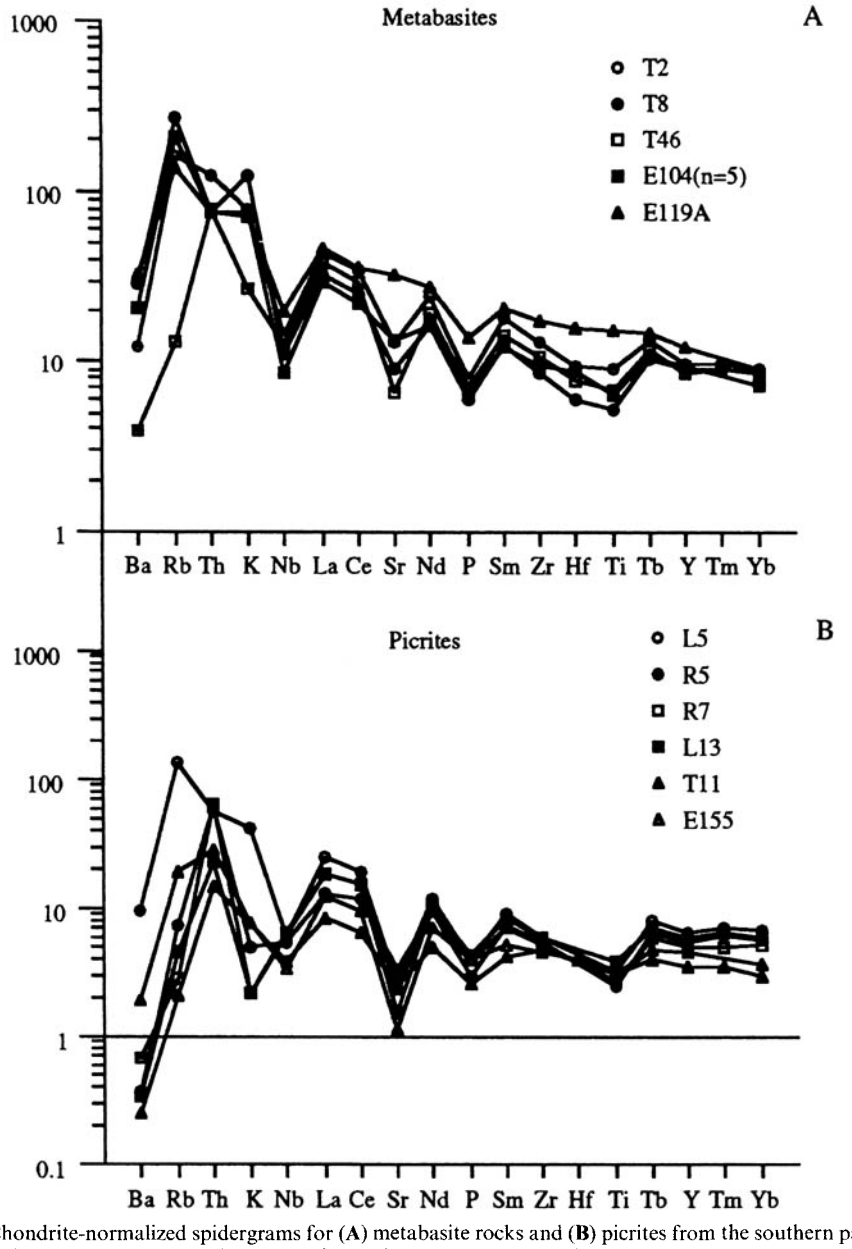

Fig. 13. Chondrite-normalized spidergrams for **(A)** metabasite rocks and **(B)** picrites from the southern part of the Nanga Parbat syntaxis. Normalizing values from Thompson *et al.* (1984).

The picrites are characterized by high Mg numbers (68–77) and high Ni and Cr contents (Table 5), which are also typical characteristics of komatiites (Arndt & Jenner 1986). Loss on ignition (LOI) values are high, reflecting the hydrous secondary mineralogy of the picrites. Compared with the metabasites, the picrites are significantly depleted in incompatible trace elements, although the shapes of the spidergrams are similar (Fig. 13B). Ba, Rb, Th and K concentrations are variable, and one of the picrites (L5) contains anomalously high concentrations of K, Rb, Ba and Cs, which may have been introduced from the adjacent gneisses (cf. Gill & Bridgwater 1979). Absolute REE contents are mostly < 10 times chondrite, and REE profiles (Fig. 11) have slightly concave-up shapes due to LREE enrichment, with $(La/Sm)_N$ in the range

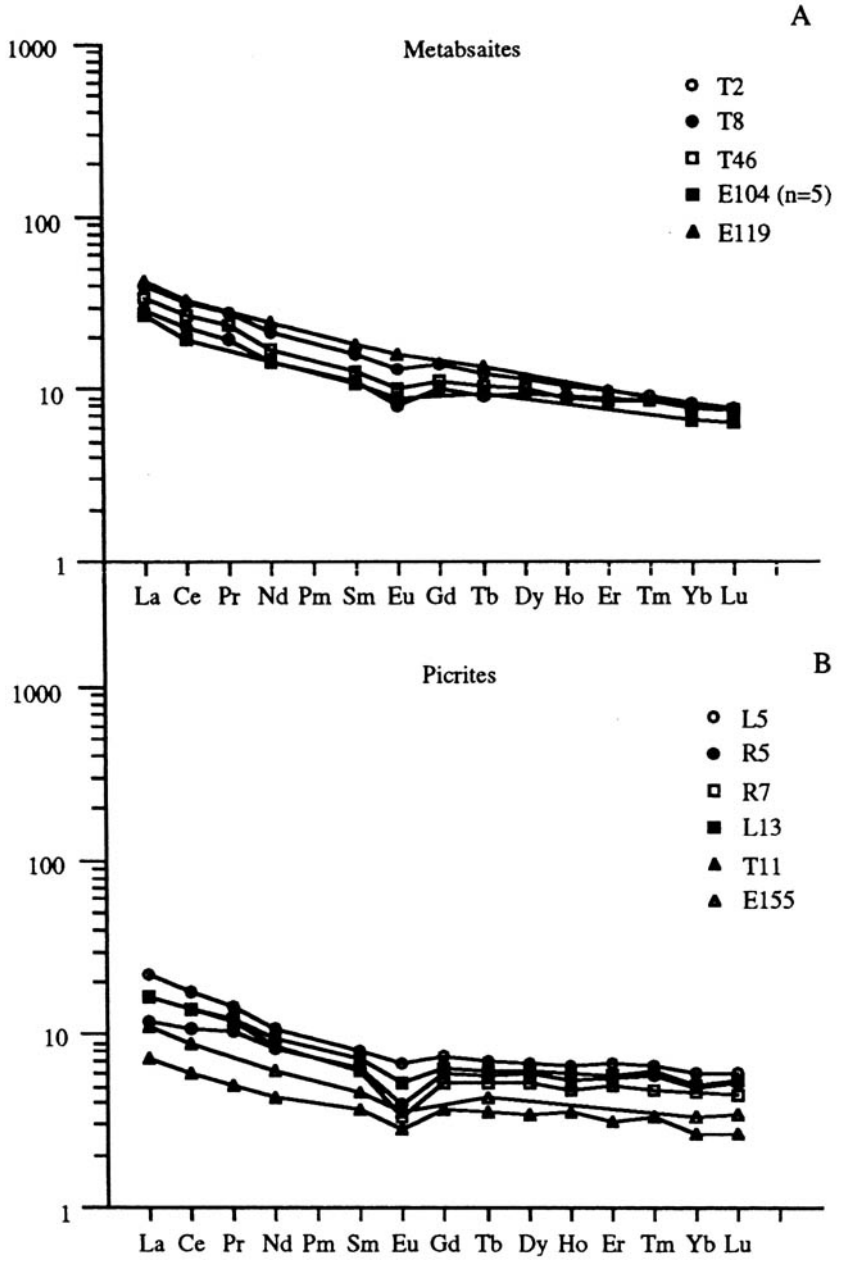

Fig. 14. Chondrite-normalized REE patterns for (**A**) metabasite rocks and (**B**) picrites from the southern part of the Nanga Parbat syntaxis. Normalizing values from Taylor & McLennan (1985).

1.9–2.7 and $(Tb/Yb)_N$ in the range 1.2–1.4. The picrites have minor negative Eu anomalies (Eu/Eu* = 0.58–0.88). There is no correlation between either Eu/Eu* or Ce/Yb and total REE content or Mg number, but there is a clear negative correlation between total REE content and Mg number. Geochemically the Nanga Parbat picrites resemble picritic dykes of the Lewisian complex, although the latter are more enriched in the LILE (Weaver & Tarney 1981).

The presence of olivine accounts for the high Mg, Ni and Cr contents, and the major

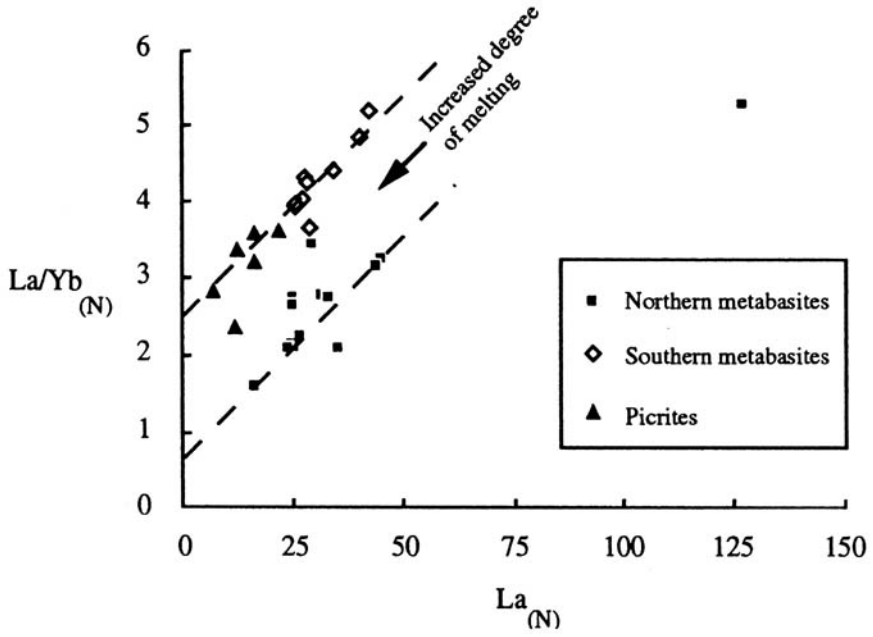

Fig. 15. Plot of La/Yb_N v. La_N for the Nanga Parbat metabasites. Metabasites from the north and south of the Nanga Parbat massif plot along different trends, suggesting that they come from mantle source regions with contrasting La/Yb_N ratios (Rossy *et al.* 1992).

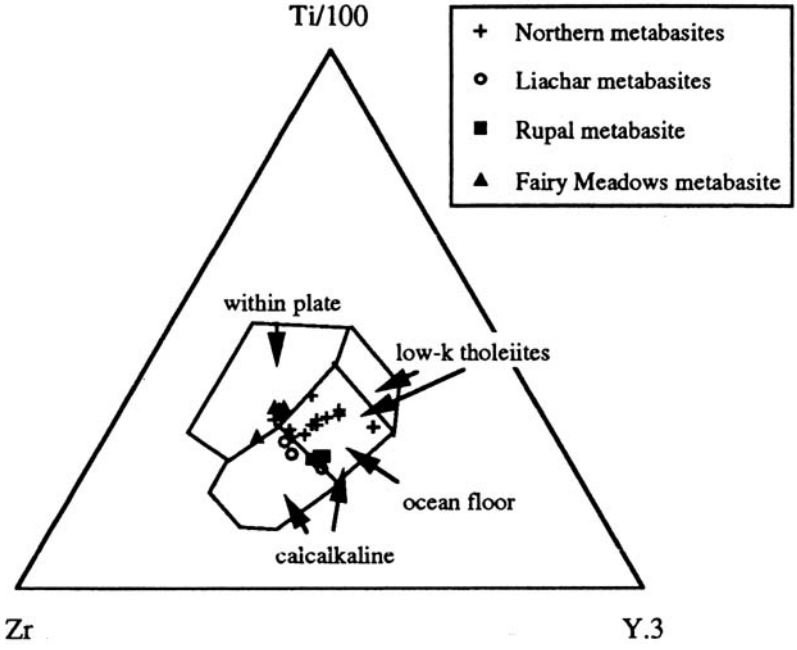

Fig. 16. Tectonic discrimination diagram for metabasic rocks from the south of the Nanga Parbat syntaxis. The composition of metabasite samples from the north of the massif are shown for comparison. Discrimination fields from Pearce & Cann (1973).

Table 4. *Rb/Sr and Sm/Nd isotope data for metabasite sheets and picrites from the southern part of the Nanga Parbat syntaxis. (1) = assumed $^{147}Sm/^{144}Nd$ ratio of 0.1466 used*

	Rb	Sr	$^{87}Rb/^{86}Sr$	$^{87}Sr/^{86}Sr$	Sm/Nd	$^{147}Sm/^{144}Nd$	$^{143}Nd/^{144}Nd$	T_{DM}^{Nd} (Ma)	ε_{Nd} (1.7 Ga)
Metabasite									
E104A	68.3	160.0	1.236	0.749876	0.243	0.1468	0.511907	2411	−3.4
E104B	56.7	154.2	1.065	0.751775	0.240	0.1449	0.511887	2392	−3.4
E104C	91.7	157.6	1.685	0.750259	0.243	0.1471	0.511893	2448	−3.8
E104D	72.7	160.7	1.310	0.752296	0.236	0.1419			
E104E	72.1	158.0	1.322	0.750550	0.252	0.1522	0.511874	2657	−5.3
E119A	47.6	381.4	0.361	0.757660	0.242	0.1466	0.511979	2267	−2.0
E119B	40.4	391.7	0.299	0.757680					
E119C	54.6	344.0	0.460	0.760182		(1)	0.512013	2202	−1.3
E119D	143.0	225.6	1.836	0.761970		(1)	0.511982	2261	−1.9
E119E	139.9	211.8	1.913	0.770687		(1)	0.511810	2591	−5.3
Picrite									
E155	6.80	13.3	1.481	0.736207	0.243	0.1471	0.512002	2237	−1.6
R7	0.98	28.1	0.101	0.765834	0.240	0.1442	0.511555	2990	−9.8

element variation displayed by the picrites is suggestive of olivine fractionation. The picrites are characterized by absolute REE abundances which correlate with Mg number, but there is no correlation between Ce/Yb and Mg number. Both are typical features of olivine fractionation. Cr contents decrease with increasing differentiation, suggesting fractionation of Cr-spinel or possibly clinopyroxene. There is no correlation between CaO/Al_2O_3 ratio and Mg content which, together with the absence of modal plagioclase, argues against plagioclase fractionation. The picrites may have been formed by either *in situ* equilibrium crystallization of primitive ultrabasic magma, or by addition of cumulus olivine to a less primitive parental magma (Cox 1978). The sheets are probably too small to have differentiated significantly *in situ* and, if they have a cumulate origin, must therefore have been intruded as a crystal-rich mush. The major element variations suggest that magma evolution was governed solely by olivine fractionation, whilst both olivine and clinopyroxene are present as modal phases. As discussed by Cox (1978), this suggests that olivine and clinopyroxene crystallized together in the final stage of magma evolution, probably through equilibrium crystallization of a primitive magma rather than addition of cumulus olivine to a less Mg-rich melt.

Since the picrites and the southern metabasites plot along similar trends on Fig. 15, it is tempting to suggest that the metabasites were generated by olivine fractionation of the picritic magmas, with complementary cumulates being formed at depth. However, the picritic sheets display more fractionated LREE profiles than most of the mafic dykes. Assuming that these LREE abundances are not partly the result of crustal contamination, it is unlikely that the picrites and metabasites represent cogenetic magmas, since there is no realistic major phase or phase assemblage which could decrease $(La/Sm)_N$ during magmatic fractionation.

Two picrite samples (155 and R7) are characterized by $^{87}Sr/^{86}Sr$ ratios of 0.7362 and 0.7658 and $^{143}Nd/^{144}Nd$ ratios of 0.5120 and 0.5116, respectively (Table 4). The Jalipur Pass sample yields a Nd model age of 2.2 Ga, which overlaps the model ages of the metabasites from the southern region, whereas the sample from the Liachar Shear Zone (R7) yields an anomalous model age of 3.0 Ga. The isotope systematics of R7 may have been opened during recrystallization and fluid flow associated with shear zone movements and little weight can be attached to this model age.

The picrites are characterized by chondritic Ti/V ratios (Shervais 1982) which would be consistent with formation by high degrees of partial melting. However, there are also some unusual geochemical characteristics, including negative Sr and Eu anomalies (despite lack of other evidence for plagioclase fractionation), fractionated LREE patterns and low Ti/Zr and Nb/Th ratios relative to primitive mantle. These features, which are also displayed by the southern metabasites, may be due to crustal contamination, or to partial melting of an enriched sub-continental mantle source (Kyle 1980; Weaver & Tarney 1981). However, crustal contamination would be inconsistent with the high MgO contents of the picrites, which are sufficiently high for the dykes to be in equilibrium with mantle peridotite. It is difficult to interpret the petrogenesis of the picrites fully

Table 5. *Whole rock major and trace element data for picrites from the southern part of the Nanga Parbat syntaxis*

	L5	R5	R7	L13	T11	155
(wt%)						
SiO_2	42.39	41.44	41.29	42.35	41.53	43.87
K_2O	0.58	0.07	0.03	0.03	n/d	0.11
TiO_2	0.34	0.26	0.28	0.39	0.31	0.32
Al_2O_3	9.33	7.79	7.37	8.27	6.21	6.13
Fe_2O_3	12.88	13.61	14.32	13.49	11.76	14.01
MnO	0.17	0.15	0.19	0.17	0.15	0.19
MgO	20.58	23.12	24.90	22.44	29.13	28.31
CaO	7.47	6.38	5.79	6.35	4.71	5.29
Na_2O	n/d	n/d	n/d	n/d	n/d	0.22
K_2O	0.58	0.07	0.03	0.03	n/d	0.11
P_2O_5	0.04	0.03	0.04	0.04	0.03	0.04
LOI	3.96	4.86	4.28	4.75	4.42	0.34
Total	97.74	97.73	98.49	98.28	98.25	98.84
Mg No.	68.1	69.4	69.9	68.9	76.8	72.9
(ppm)						
Zn	68	78	74	69	55	86
Cr	2370	2993	2841	2539	4719	3969
Ni	789	738	895	780	1259	1589
V	175	149	147	146	118	151
Cu	58	196	95	115	n/d	183
Li	19.23	8.22	8.62	n/d	n/d	n/d
Be	0.63	0.64	0.53	n/d	n/d	n/d
Sc	24.22	17.24	20.42	18.9	17.5	24
Ga	11.43	10.81	9.22	9.17	6.91	9
Rb	47.83	2.55	0.98	1.59	0.74	6.8
Sr	31.52	39.09	28.09	18.5	28.9	13.3
Y	12.96	11.10	10.13	11.8	7.0	9.1
Zr	40	37	36	40	32	31
Nb	2.20	1.93	2.19	2.25	1.36	1.2
Sn	n/a	n/a	n/a	n/a	n/a	n/a
Cs	8.51	0.48	0.18	0.21	0.16	0.8
Ba	66.9	2.5	4.6	2.3	1.7	13
Hf	n/a	n/a	n/a	n/a	n/a	n/a
Pb	2.51	1.50	1.79	1.28	3.21	2
Th	2.43	2.56	2.69	0.95	0.62	1.2
U	2.68	0.35	1.45	1.72	0.48	0.5
REE						
La	8.00	4.35	6.01	6.1	2.7	4.1
Ce	16.72	10.21	13.21	13.3	5.7	8.4
Pr	2.01	1.43	1.64	1.7	0.7	n/a
Nd	7.61	5.95	6.01	6.7	3.1	4.4
Sm	1.84	1.47	1.44	1.67	0.86	1.07
Eu	0.60	0.34	0.29	0.46	0.25	0.31
Gd	2.32	1.83	1.61	1.99	1.13	n/a
Tb	0.41	0.34	0.31	0.36	0.21	0.25
Dy	2.57	2.27	1.98	2.35	1.33	n/a
Ho	0.57	0.47	0.41	0.51	0.30	n/a
Er	1.71	1.39	1.26	1.46	0.78	n/a
Tm	0.24	0.21	0.17	0.22	0.12	n/a
Yb	1.48	1.24	1.13	1.28	0.65	0.82
Lu	0.23	0.20	0.17	0.21	0.10	0.13
Norms						
Q						
ne						
di	10.48	8.34	6.77	7.03	4.98	8.45
hy	23.04	26.13	24.44	31.68	24.23	23.79
ol	28.81	32.61	38.24	27.62	43.78	43.77

because of uncertainty regarding their age and hence initial isotopic composition, but they were probably generated by large degrees of melting of a relatively incompatible element (LREE, Th, Zr) enriched mantle source during early Proterozoic stabilization of the crust.

Discussion

The metabasite rocks studied here can be divided into two suites. The northern suite of dykes locally cross-cut metamorphic fabrics and are geochemically coherent with fractionation trends controlled by pyroxene, plagioclase and olivine. They show moderate enrichments in incompatible trace elements and Nd model ages of 1.6–1.8 Ga (Table 2). A poorly constrained Sm–Nd errorchron gives an age of *c.* 1.7 $\pm$ 0.2 Ga and suggests that basalt genesis occurred in a mantle source region which had experienced long-term LREE depletion relative to bulk earth. The southern suite is usually structurally concordant and geochemically more variable than the northern suite, with lower abundances of most trace elements but more fractionated LREE profiles, and with Nd model ages in the range 2.2–2.6 Ga. Picrites form a distinct suite of Mg-rich compositions generated by high degrees of partial melting and linked by olivine fractionation, with relatively low abundances of incompatible trace elements but slightly fractionated LREE contents. There is no evidence that they are petrogenetically linked to the southern suite of metabasites.

Geochemical data are indirectly used here to refine the age of crustal growth and of granulite facies metamorphism, partly through use of Nd model ages, and partly through comparing mafic sheet chemistries with those of other mafic rocks from the western Himalaya. On the basis of their Palaeo-Proterozoic Nd model ages, the southern suite may have been associated with early stages of continental growth. Both metabasites and picrites are characterized by low Nb/Th and Ti/Zr and enriched Nd and Sr isotope compositions relative to the present mantle. However, there is no evidence from major elements for assimilation of crustal material into the parental magma. The LREE enrichment displayed by the picrites provides the clearest evidence for the existence of an enriched mantle source region, since these bodies were probably generated under relatively high degrees of partial melting. The anomalous incompatible trace element ratios probably reflect either an unusual mantle source composition, or control by accessory mineral behaviour during partial melting.

Despite their imprecise nature, the errorchron age and estimated ε_{Nd} values for the northern suite suggest derivation from a slightly depleted source region with intrusion during a period of Meso-Proterozoic rifting. Field data show that this postdated granulite facies metamorphism and melting. The isotope ratios reflect a long history of *in situ* radiogenic decay rather than crustal contamination or metasomatism. Whether basalt extraction from the mantle was synchronous with metamorphism is uncertain. The metabasites lack relict granulite facies assemblages and cross-cut migmatitic fabrics. Had melting and basalt magmatism been part of the same HT event, dyke emplacement must have occurred at a late stage of it. A tentative correlation between the dykes of the northern suite described here, and the Permo-Triassic Panjal Trap volcanic series (Wheeler *et al.* 1995), appears unlikely on geochemical grounds as the two sets of mafic rocks plot in different fields on a discrimination diagram (Fig. 8). This differentiates the dykes studied here from those described by Pognante *et al.* (1993) from the northeastern part of the Nanga Parbat massif which are chemically indistinguishable from the Panjal Trap basalts and which show granulite facies mineral assemblages. In addition, the isotope data suggest that the dykes were extracted from the mantle during the Meso-Proterozoic. Hence, it is likely that the mafic dykes studied here correlate with Proterozoic dyke swarms in northern India such as the Rampur volcanics (cf. Bhat *et al.* 1994). Given the age of the dyke swarm, it is likely that the age of granulite metamorphism can be dated at about 1.85 Ma. Evidence for this is given by zircon core ages (Zeitler *et al.* 1989, 1993; Schneider *et al.* 1999) from the Nanga Parbat massif, and amphibole cooling ages from the Besham region some 200 km to the SW (Treloar & Rex 1990).

If the northern suite of dykes postdates a granulite facies event associated with melting, it follows that the earliest, and highest-grade, metamorphism that affected rocks of the syntaxis was at latest Meso-Proterozoic in age. This allows a clearer interpretation of the Neogene events. A number of implications pertaining to the Tertiary metamorphic and magmatic history that arise from accepting a polycyclic history of crustal evolution, are highlighted and addressed here.

Based on the presence of sillimanite fibres in garnet cores and of stable kyanite external to the garnets, Wheeler *et al.* (1995) argued that prograde metamorphism within basement gneisses was along a path of increasing pressure. As peak metamorphic fabrics are cross-cut by pre-Tertiary dykes, they argued that this P–T path

was unrelated to India–Kohistan collision. In contrast, on the basis of forward modelling of garnet zonation patterns, Winslow *et al.* (1995) related the increasing pressure path to Tertiary collision, arguing that it was consistent with underthrusting of India beneath Kohistan. Tertiary metamorphism during increasing pressure has been described from Indian plate cover sequences to the west of the Nanga Parbat syntaxis (Treloar *et al.* 1989*a*, 1997; Di Pietro 1991), and it is probable that Tertiary metamorphism in the syntaxis was also along a path of increasing pressure. However, evidence for it will not be reliably retrieved from gneisses that experienced Proterozoic granulite facies metamorphism.

The presence of sillimanite fibres replacing cataclased kyanite crystals led Wheeler *et al.* (1995) to argue that the Tertiary metamorphism that overprinted the Meso-Proterozoic granulite facies metamorphism was to amphibolite facies. Assemblages in basic dykes of Panjal trap composition from the NE part of the syntaxis led Pognante *et al.* (1993) to argue that this metamorphism was, locally at least, to granulite facies. Data from Winslow *et al.* (1995), Butler *et al.* (1997) and Whittington *et al.* (1998) suggest that Tertiary temperatures probably peaked at *c.* 700–750 °C. Peak metamorphic pressures were at >7 kbar (Winslow *et al.* 1995; Whittington *et al.* 1998) and probably >10 kbar (Pognante *et al.* 1993). This would be consistent with studies to the southwest of Nanga Parbat (Treloar *et al.* 1989*b*; Pognante & Spencer 1991; Treloar 1997). Melting occurred during decompression across the muscovite vapour-absent melt curve to pressures of $\leqslant 5$ kbar. These temperatures are significantly lower than those estimated for pre-Tertiary granulite facies metamorphism by Wheeler *et al.* (1995).

That the Shengus and Iskere gneisses had been through a Proterozoic metamorphic event at temperatures (*c.* 900 °C) consistent with vapour-absent melting of biotite has implications for the derivation of Neogene leucogranites. Rocks that have been through a high temperature melting event, involving incongruent breakdown of biotite, will be infertile during later re-metamorphism at 700–750 °C. The Shengus gneisses are characterized by a lack of muscovite, and the Iskere gneisses carry minor amounts of muscovite. Hence, neither set of gneisses, with their history of Proterozoic granulite facies metamorphism, makes sensible parental materials for the Neogene granites, although both dykes and country rocks have elevated $^{87}Sr/^{86}Sr$ ratios and the gneisses high levels of the incompatible elements (George 1995). There are two possible sources for the sheets: first, fertile, previously unmetamorphosed rocks underthrust beneath the basement gneiss; second, the granulite facies gneisses themselves, although only if they had undergone local hydration during the Tertiary, or earlier, and thus been sufficiently refertilized to melt a second time during decompression at amphibolite facies. The presence of muscovite-rich zones within the Shengus and Iskere gneisses and of young monazites within fabric-forming muscovites (Smith *et al.* 1992) suggest that Neogene, and older Tertiary(?), focused fluid flow may have hydrated the Proterozoic gneisses along narrow shear zones, although whether there was sufficient rehydration to generate the

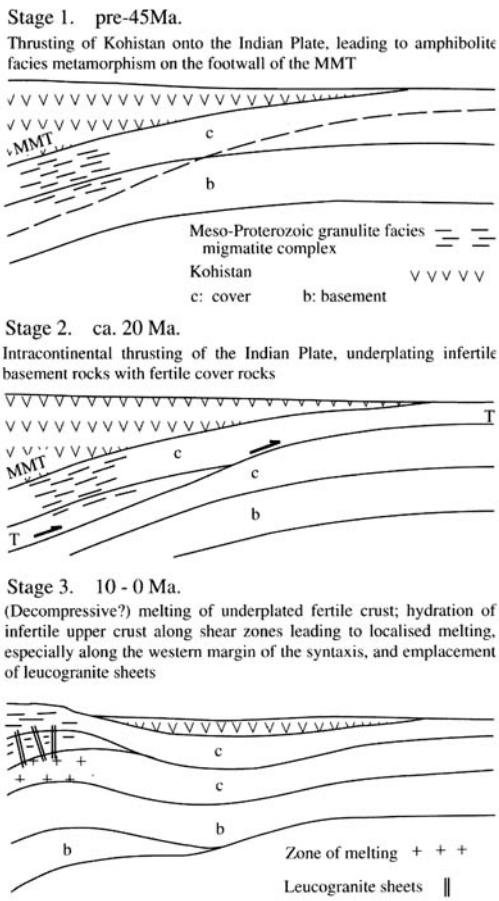

Fig. 17. Schematic diagram showing potential relationships between the underthrusting of fertile Indian plate rocks beneath the Nanga Parbat granulite facies basement complex, decompression and melting of the underthrust rocks, and emplacement of leucogranite sheets into the basement gneisses.

Table 6. *Temporal sequence of events affecting the Indian plate basement gneisses exposed within the core of the Nanga Parbat syntaxis*

6.	Neogene (< 10 Ma) uplift and rapid decompression, localized hydration of basement gneisses along zones of channellized fluid flow permitting local remelting, melting of underplated fertile slab and leucogranite sheet emplacement into basement gneisses.
5.	*c.* 10 Ma. Initiation of uplift of Nanga Parbat syntaxis.
4b.	Eocene–Oligocene upper amphibolite facies (> 700 °C) metamorphism followed by late Oligocene to early Miocene cooling through 500°C.
4a.	Palaeogene early 'Himalayan' thrusting of Kohistan onto the Indian plate causing shearing and mylonitization of Proterozoic migmatitic fabrics.
3.	Mansehra granite emplacement (*c.* 0.52 Ga).
2.	Meso-Proterozoic emplacement of basic sheets that cross-cut migmatitic fabrics (*c.* 1.6 ± 0.1 Ga).
1.	Granulite facies metamorphism and migmatization (P *c.* 10 kbar, T *c.* 850–900 °C; *c.* 1.85 Ga).

full suite of leucogranite sheets is unlikely. Hence, it is more likely that the leucogranites are derived from melting of radiogenically enriched, previously unmelted fertile sediments underthrust beneath the syntaxis. This model is illustrated in Fig. 17, and summarized in Table 6.

Although Neogene migmatites are exposed at surface in some areas of the Nanga Parbat syntaxis, it is apparent, on the basis of cross-cutting relationships involving Meso-Proterozoic mafic dykes, that regional granulite facies metamorphism and melting in Indian plate rocks now exposed within the core of the syntaxis was Proterozoic in age. On this basis we infer: first, that prograde P–T paths that show increasing pressure are as likely to be derived from Proterozoic garnets as from Tertiary ones; second, that models that require metamorphism of Indian plate rocks to be solely of Tertiary age are incorrect; third, that leucogranites emplaced into infertile granulites are sourced not from them but from fertile rocks underthrust beneath them. During the Himalayan orogeny, the basement gneisses were reheated to a temperature sufficient to cause local resetting of isotope systems, growth of high-U zircon rims, replacement of kyanite by sillimanite and, in zones of fluid flow characterized by muscovite growth, the crystallization of monazite.

Field work in the Nanga Parbat region has been supported by the UK Natural Environment Research Council and by the Royal Society. We acknowledge discussions over the years with Rob Butler, Nigel Harris, John Wheeler and Gavin Foster, and critical reviews by Brian Windley and Hugh Rollinson.

References

ARNDT, N. & JENNER, G. 1986. Crustally contaminated komatiites and basalts from Kambalda, western Australia. *Chemical Geology*, **56**, 229–255.

BHANOT, V. B., SINGH, V. P., KANSAL, A. K. & THAKUR, V. C. 1977. Early Proterozoic Rb–Sr whole rock age for the Central Crystalline Gneiss of the Higher Himalayan Kumaun. *Journal of the Geological Society of India*, **18**, 90–91.

BHAT, M. I. & LE FORT, P. 1992. Sm–Nd age and petrogenesis of Rampur metavolcanic rocks, NW Himalaya: late Archaean relics in the Himalayan belt. *Precambrian Research*, **56**, 191–210.

——, —— & AHMAD, T. 1994. Bafliaz volcanics, NW Himalaya; origin of a bimodal, tholeiite and alkali basalt suite. *Chemical Geology*, **114**, 217–234.

BUTLER, R. W. H. & PRIOR, D. J. 1988*a*. Tectonic controls on the uplift of Nanga Parbat, Pakistan Himalaya. *Nature*, **333**, 247–250.

—— & —— 1988*b*. Anatomy of a continental subduction zone. *Geologische Rundschau*, **77**, 239–255.

——, GEORGE, M. T., HARRIS, N. B. W., JONES, C., PRIOR, D. J., TRELOAR, P. J. & WHEELER, J. 1992. Geology of the northern part of the Nanga Parbat massif, northern Pakistan, and its implications for Himalayan tectonics. *Journal of the Geological Society of London*, **149**, 557–567.

——, HARRIS, N. B. W. & WHITTINGTON, A. G. 1997. Interactions between deformation, magmatism and hydrothermal activity during active crustal thickening: a field example from Nanga Parbat, Pakistan Himalayas. *Mineralogical Magazine*, **61**, 37–51.

——, PRIOR, D. J. & KNIPE, R. J. 1989. Neotectonics of the Nanga Parbat syntaxis, Pakistan, and crustal stacking in the northwest Himalaya. *Earth and Planetary Science Letters*, **94**, 329–343.

CARLSON, R. W. 1991. Physical and chemical evidence on the cause and source characteristics of flood basalt volcanism. *Australian Journal of Earth Sciences*, **38**, 525–544.

CHAMBERLAIN, C. P., JAN, M. Q. & ZEITLER, P. K. 1989. A petrological record of the collision between the Kohistan island arc and Indian plate, northwest Himalaya. *In*: MALINCONICO, L. L. & LILLIE, R. J. (eds) *Tectonics of the Western Himalaya*. Geological Society of America Special Papers, **232**, 23–32.

——, ZEITLER, P. K., BARNETT, D., WINSLOW, D. P., POULSON, S., LEAHY, T. & HAMMER, J. 1995. Active hydrothermal systems during the recent uplift of Nanga Parbat, Pakistan Himalaya. *Journal of Geophysical Research*, **89B**, 525–535.

CONDIE, K. C., BOBROW, D. J. & CARD, K. D. 1987. Geochemistry of Precambrian mafic dykes from the southern Superior Province of the Canadian Shield. *In*: HALLS, H. & FAHRIG, W. (eds) *Mafic Dyke Swarms*. Geological Association of Canada Special Paper, **34**, 95–108.

COWARD, M. P. 1986. A section through the Nanga Parbat syntaxis, Indus Valley, Kohistan. *Geological Bulletin of the University of Peshawar*, **18**, 147–152.

COX, K. 1978. Komatiites and other high-magnesia lavas: some problems. *Philosophical Transactions of the Royal Society of London*, **288**, 599–609.

DEBON, F., LE FORT, P., SHEPPARD, S. M. F. & SONET, J. 1986. The four plutonic belts of the Transhimalaya–Himalaya: a chemical, mineralogical, isotopic and chronological synthesis along a Tibet–Nepal section. *Journal of Petrology*, **27**, 219–250.

DIPIETRO, J. A. 1991. Metamorphic pressure–temperature conditions of Indian Plate rocks south of the Main Mantle Thrust, Lower Swat, Pakistan. *Tectonics*, **10**, 742–757.

GEORGE, M. T. 1995. *The magmatic, thermal and exhumation history of the Nanga Parbat-Haramosh massif, Western Himalaya*. PhD thesis, Open University, UK.

——, BUTLER, R. W. H. & HARRIS, N. W. B. 1993. The tectonic implications of contrasting granite magmatism between the Kohistan island arc and the Nanga Parbat–Haramosh massif. *In*: TRELOAR, P. J. & SEARLE, M. P. (eds) *Himalayan Tectonics*. Geological Society, London, Special Publications, **74**, 173–191.

——, REDDY, S. M. & HARRIS, N. B. W. 1995. Isotopic constraints on the cooling history of the Nanga Parbat–Haramosh massif and Kohistan arc, western Himalaya. *Tectonics*, **14**, 237–252.

GILL, R. C. O. & BRIDGWATER, D. 1979. Early Archaean basic magmatism in west Greenland, the geochemistry of the Ameralik dykes. *Journal of Petrology*, **20**, 695–726.

HOLM, P. 1985. The geochemical fingerprints of different tectonomagmatic environments using hygromagmatophile element abundances of tholeiitic basalts and basaltic andesites. *Chemical Geology*, **51**, 303–323.

HONNEGER, K., DIETRICH, D., FRANK, W., GANSSER, A., THONI, M. & TROMMSDORFF, V. 1982. Magmatism and metamorphism in the Ladakh Himalaya (the Indus–Tsango Po suture Zone). *Earth and Planetary Science Letters*, **60**, 252–292.

INGER, S. & HARRIS, N. B. W. 1993. Geochemical constraints on leucogranite magmatism in the Langtang Valley, Nepal Himalaya. *Journal of Petrology*, **34**, 345–369.

JOCHUM, K. P., ARNDT, N. T. & HOFFMAN, A. W. 1991. Nb–Th–La in komatiites and basalts: constraints on komatiite petrogenesis and mantle evolution. *Earth and Planetary Science Letters*, **107**, 272–289.

KYLE, P. 1980. Development of heterogeneities in the sub-continental mantle: evidence from the Ferrar Group, Antarctica. *Contributions to Mineralogy and Petrology*, **73**, 89–104.

LE MAITRE, R. 1989. *A classification of igneous rocks and glossary of terms*. Blackwells, Oxford.

MADIN, I. P., LAWRENCE, R. D. & UR-RAHMAN, S. 1989. The North-western Nanga Parbat–Haramosh massif: evidence for crustal uplift at the north-western corner of the Indian craton. *In*: MALINCONICO, L. L. & LILLIE, R. J. (eds) *Tectonics of the Western Himalaya*. Geological Society of America Special Papers, **232**, 169–182.

NOBLE, S. R. & SEARLE, M. P. 1995. Age of crustal melting and leucogranite formation from U–Pb zircon and monazite in the western Himalaya, Zanskar, India. *Geology*, **23**, 1135–1138.

PAPRITZ, K. & REY, R. 1989. Evidence for the occurrence of Permian Pamela Trap basalts in the Lesser- and Higher Himalayas of the western syntaxis area, NE Pakistan. *Eclogae geologicae Helvetiae*, **82**, 603–627.

PEARCE, J. A. & CANN, J. R. 1973. Tectonic setting of basic volcanic rocks determined using trace element analyses. *Earth and Planetary Science Letters*, **19**, 290–300.

POGNANTE, U. & SPENCER, D. A. 1991. First report of eclogites from the Himalayan belt, Kaghan Valley, northern Pakistan. *European Journal of Mineralogy*, **3**, 613–618.

——, BENNA, P. & LE FORT, P. 1993. High-pressure metamorphism in the High Himalayan crystallines of the Stak valley, northeastern Nanga Parbat–Haramosh syntaxis, Pakistan Himalaya. *In*: TRELOAR, P. J. & SEARLE, M. P. (eds) *Himalayan Tectonics*. Geological Society, London, Special Publications, **74**, 161–172.

ROSSY, M., AZAMBRE, B. & ALBARADE, F. 1992. REE and Sr–Nd isotopic geochemistry of the alkaline magmatism from the Cretaceous North Pyrenean Rift Zone (France–Spain). *Chemical Geology*, **97**, 33–46.

SCHNEIDER, D. A., EDWARDS, M. A. & ZEITLER, P. K. 1999. Mazemo Pass pluton and Jutial pluton, Pakistan Himalaya: age and implications for entrapment mechanisms of two granites in the Himalaya. *Contributions to Mineralogy and Petrology*, **136**, 273–284.

SHERVAIS, J. W. 1982. Ti–V plots and the petrogenesis of modern and ophiolitic lavas. *Earth and Planetary Science Letters*, **59**, 101–118.

SMITH, H. A., CHAMBERLAIN, C. P. & ZEITLER, P. K. 1992. Documentation of Neogene regional metamorphism in the Himalayas of Pakistan using

U–Pb in monazite. *Earth and Planetary Science Letters*, **113**, 93–106.

SPENCER, D. A., TONARINI, S. & POGNANTE, U. 1995. Geochemical and Sr–Nd isotope characterisation of Higher Himalayan eclogites (and associated metabasalts). *European Journal of Mineralogy*, **7**, 89–102.

SUTTON, J. & WATSON, J. V. 1951. The pre-Torridonian metamorphic history of the Loch Torridon and Scourie areas in the north-west Highlands and its bearing on the chronological classification of the Lewisian. *Quarterly Journal of the Geological Society of London*, **106**, 241–296.

TAYLOR, S. R. & MCLENNAN, S. M. 1985. *The continental crust: its composition and evolution*. Blackwells, Oxford.

THOMPSON, R. A., MORRISON, M. A., HENDRY, G. L. & PARRY, S. J. 1984. An assessment of the relative roles of crust and mantle in magma genesis: an elemental approach. *Philosophical transactions of the Royal Society of London*, **A310**, 549–590.

TRELOAR, P. J. 1997. Thermal controls on early-Tertiary, short-lived, rapid regional metamorphism in the NW Himalaya, Pakistan. *Tectonophysics*, **273**, 77–104.

—— & REX, D. C. 1990. Cooling and uplift histories of the crystalline thrust stack of the Indian Plate internal zones west of Nanga Parbat, Pakistan Himalaya. *Tectonophysics*, **180**, 323–349.

——, ——, GUISE, P. G., COWARD, M. P., SEARLE, M. P., WINDLEY, B. F., PETTERSON, M. G., JAN, M. Q. & LUFF, I. W. 1989*a*. K–Ar and Ar–Ar geochronology of the Himalayan collision in NW Pakistan: constraints on the timing of collision, deformation, metamorphism and uplift. *Tectonics*, **8**, 881–909.

——, COWARD, M. P., WILLIAMS, M. P. & KHAN, M. A. 1989*b*. Basement-cover imbrication south of the Main Mantle Thrust, North Pakistan. *In*: MACFARLANE, A., SORKHABI, R. B. & QUADE, J. (eds) *Himalaya and Tibet: Mountain roots to mountain tops*. Geological Society of America Special Papers, **232**, 137–152.

——, POTTS, G. J., WHEELER, J. & REX, D. C. 1991. Structural evolution and asymmetric uplift of the Nanga Parbat syntaxis, Pakistan Himalaya. *Geologisches Rundschau*, **80**, 411–428.

——, WHEELER, J. & POTTS, G. J. 1994. Metamorphism and melting within the Nanga Parbat syntaxis, Pakistan Himalaya. *Mineralogical Magazine*, **58A**, 910–911.

TRIVEDI, J. R., GOPALAN, K. & VALDIYA, K. S. 1984. Rb–Sr ages of granitic rocks within the Lesser Himalayan nappes, Kumaun Himalaya. *Journal of the Geological Society of India*, **25**, 641–654.

VALDIYA, K. S. 1988. Tectonics and evolution of the central sector of the Himalaya. *Philosophical Transactions of the Royal Society of London*, **326A**, 151–175.

VANNAY, J. & SPRING, L. 1993. The geochemistry of the continental basalts within the Tethyan Himalaya of Lahul-Spiti and S.E. Zanskar, northwest India. *In*: TRELOAR, P. J. & SEARLE, M. P. (eds) *Himalayan Tectonics*. Geological Society, London, Special Publications, **74**, 237–249.

WEAVER, B. L. & TARNEY, J. 1981. The Scourie dyke suite: petrogenesis and geochemical nature of the Proterozoic sub-continental mantle. *Contributions to Mineralogy and Petrology*, **78**, 175–188.

WHEELER, J., TRELOAR, P. J. & POTTS, G. J. 1995. Structural and metamorphic evolution of the Nanga Parbat syntaxis, Pakistan Himalayas on the Indus Gorge transect: the importance of early events. *Geological Journal*, **30**, 349–371.

WHITTINGTON, A. G. 1996. Exhumation overrated at Nanga Parbat, northern Pakistan. *Tectonophysics*, **260**, 215–226.

—— 1997. *The thermal, metamorphic and magmatic evolution of a rapidly exhuming terrane: the Nanga Parbat massif, northern Pakistan*. PhD thesis. Open University, Milton Keynes.

——, HARRIS, N. B. W. & BAKER, J. 1998. Low pressure crustal anatexis: the significance of spinel and cordierite from metapelitic assemblages at Nanga Parbat, northern Pakistan. *In*: TRELOAR, P. J. & O'BRIEN, P. (eds) *What Drives Metamorphism and Metamorphic Reactions?* Geological Society, London, Special Publications, **134**, 183–198.

——, —— & BUTLER, R. W. H. 1999. Contrasting anatectic styles at Nanga Parbat, northern Pakistan. *In*: MACFARLANE, A., SORKHABI, R. B. & QUADE, J. (eds) *Himalaya and Tibet: Mountain roots to mountain tops*. Geological Society of America, Special Papers, **328**, 129–144.

WINSLOW, D. M., CHAMBERLAIN, C. P. & ZEITLER, P. K. 1995. Metamorphism and melting of the lithosphere due to rapid denudation, Pakistan Himalaya. *Journal of Geology*, **103**, 395–408.

——, ZEITLER, P. K., CHAMBERLAIN, C. P. & WILLIAMS, I. S. 1996. Geochronological constraints on syntaxial development in the Nanga Parbat region, Pakistan. *Tectonics*, **15**, 1292–1308.

ZEITLER, P. K. 1985. Cooling history of the NW Himalaya. *Tectonics*, **4**, 127–135.

—— & CHAMBERLAIN, C. P. 1991. Petrogenetic and tectonic significance of young leucogranites from the northwest Himalaya. *Tectonics*, **10**, 729–741.

——, —— & SMITH, H. A. 1993. Synchronous anatexis, metamorphism and rapid denudation at Nanga Parbat (Pakistan Himalaya). *Geology*, **22**, 347–350.

——, SUTTER, J. F., WILLIAMS, I. S., ZARTMAN, R. & TAHIRKELLI, R. A. K. 1989. Geochronology and temperature history of the Nanga Parbat–Haramosh massif, Pakistan. *In*: MALINCONICO, L. L. & LILLIE, R. J. (eds) *Tectonics of the Western Himalaya*. Geological Society of America Special Papers, **232**, 1–22.

Structural evolution of the western margin of the Nanga Parbat massif, Pakistan Himalaya: insights from the Raikhot–Liachar area

R. W. H. BUTLER
School of Earth Sciences, The University of Leeds, Leeds LS2 9JT, UK

Abstract: There are several competing interpretations of the structure of the margins of the Nanga Parbat massif: that the massif is bounded by the original suture between the Indian continent and the Kohistan–Ladakh island arc—the Main Mantle Thrust; that the massif is entirely bounded by neotectonic faults; that it is bounded by a combination of early and late faults and shear zones. If the marginal structures of the massif are to be related to local and regional geo-tectonic evolution then their correct characterization is critical. The Raikhot Bridge area on the western margin of the massif is useful in this regard, as it provides accessible and near-continuous outcrops. This contact, sometimes called the Raikhot Fault, is composite. Sheared metagabbros of the Kohistan arc are juxtaposed tectonically against metasediments and orthogneisses of the Nanga Parbat massif along an early ductile shear contact, developed under amphibolite facies conditions. In this regard it may be a preserved segment of the Main Mantle Thrust. However, this ductile shear zone has been strongly modified, flattened and rotated, and is cut by younger shears and faults. The original kinematics of the shear zone have been largely overprinted by these subsequent deformations. The younger structures include NE–SW striking, dextral strike-slip faults and a major top-to-NW thrust and shear zone. A sequence of metamorphism, deformation and igneous emplacement may be used to study the history of structural evolution within the massif. The use of a single name (e.g. Raikhot Fault) for the present-day map contact between the Nanga Parbat massif and neighbouring Kohistan is misleading. The early contact (termed here the Phuparash Shear Zone, possibly the northeastern continuity of the Main Mantle Thrust) is modified by the Buldar Fault Zone (dextral strike-slip) and the Liachar Thrust Zone (top-to NW carriage of the Nanga Parbat massif across the Phuparash Shear Zone and onto Kohistan). The activity of the Buldar Fault and Liachar Thrust Zone continued during exhumation of the massif, through amphibolite facies to the Earth's surface. The interaction between these structures is at present unknown. However, establishing these and similar interactions within the Nanga Parbat area remain central to establishing the role of regional NE–SW dextral transpression in the modern structure of the massif.

The Nanga Parbat massif represents the NW termination of the main Himalayan arc (Fig. 1a) and opens a structural half-window into otherwise buried units of the Indian continental crust that have been overridden by the Kohistan–Ladakh island arc complex. Understanding the tectonics by which the massif has become exposed at the Earth's surface has a direct bearing on the origin, evolution and role of syntaxes in orogenic construction. In this regard the kinematics and timing of deformation structures are of critical importance.

Over the past 20 years research has generally established that active or recently active structures associated with the uplift and exhumation of the massif are concentrated along its western margin (Butler & Prior 1988*a*; Butler *et al.* 1989; Madin *et al.* 1989). In contrast, its northern (Butler *et al.* 1992) and eastern margins (Treloar *et al.* 1991; Wheeler *et al.* 1995; Argles this volume) preserve early ductile shear contacts that are interpreted as the original juxtaposition structure of the Indian continental crust with the Kohistan–Ladakh arc sequence (Fig. 1b). The early contact thus shows broadly top-to-the-south overshear (Kohistan–Ladakh onto Indian continental crust) under broadly amphibolite facies conditions (e.g. Butler & Prior 1988*b*). This relationship can be readily explained in terms of the original tectonic contact by which the arc sequence was emplaced onto the Indian continent. However, there is some dispute about the kinematics and continuity of the younger structures on the western flank of the massif. This is perhaps unsurprising. The early reports on the neotectonic character of the western

From: KHAN, M. A., TRELOAR, P. J., SEARLE, M. P. & JAN, M. Q. (eds) *Tectonics of the Nanga Parbat Syntaxis and the Western Himalaya*. Geological Society, London, Special Publications, **170**, 51–75. 1-86239-061-4/00/$15.00

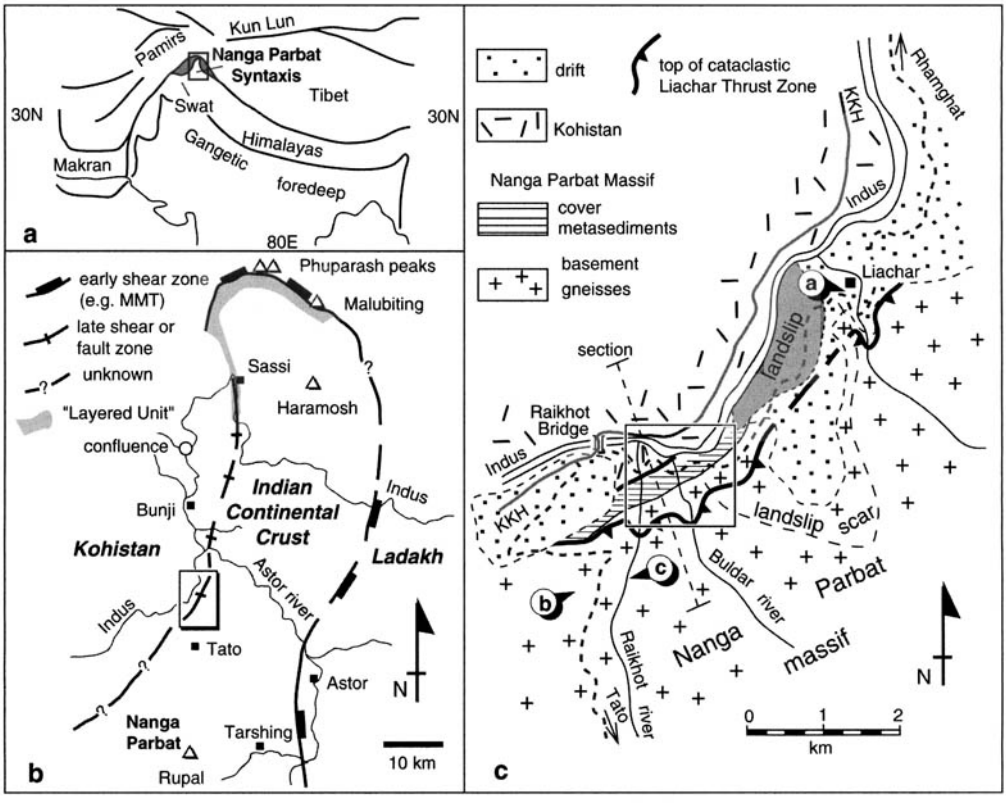

Fig. 1. (**a**) Location map for the Nanga Parbat area in the NW Himalaya. The shaded area denotes the Kohistan–Ladakh island arc (boxed area—location of (b)). (**b**) Simplified map of the Nanga Parbat syntaxis, cored by the Nanga Parbat massif and rimmed by the Kohistan–Ladakh island arc series. The nature of the contact between these two tectonic units is distinguished by ornament (after Butler *et al.* 1992; Butler *et al.* 2000; boxed area—location of (c)). (**c**) Simplified geological sketch map of the Raikhot Bridge study area. Various detailed locations are indicated (a—viewpoint for Fig. 2a; b—viewpoint for Fig. 9a, b; c—viewpoint for Fig. 12a; the boxed area locates Fig. 4a; the section line is for Fig. 15).

margin (Lawrence & Ghauri 1983; Madin *et al.* 1989) contain no kinematic data pertaining to this problem. The subsequent reports (Butler & Prior 1988*a*; Butler *et al.* 1989) were too brief for detailed kinematic data to be presented. Consequently some recent regional analyses (e.g. Seeber & Pêcher 1998) have reopened debate on the kinematics of the neotectonic structures on the western margin of the massif. This contribution provides a range of field descriptions and data for a particularly well-exposed and readily accessible segment of the margin of the massif at Raikhot Bridge, the Indus crossing of the Karakoram Highway closest to the summit of Nanga Parbat (Fig. 1c). The aims are to clarify both the structural nomenclature and the data required for larger-scale models of the NW syntaxis and to provide a framework for investigating strain localization during syntaxis growth.

Background

Since the work of Wadia (1933) and Misch (1949), there has been general recognition that the margins of the Nanga Parbat massif define a broadly antiformal structure, rimmed by rocks that are now known to be part of the Kohistan–Ladakh island arc complex (e.g. Tahirkheli & Jan 1979). Consequently, attempts to place the massif in its regional context have used this antiformal structure to infer the presence of a crustal-scale thrust tip that is the lateral pin to the arcuate system of Himalayan thrusts (e.g. Coward *et al.* 1986, 1988). These studies assumed that the edge of the Nanga Parbat massif was the original suture between the Indian continent and the Kohistan–Ladakh island arc complex. By correlation with its better-known occurrence in the Swat and Hazara areas (Fig. 1a), the contact

was thus labelled as a segment of the Main Mantle Thrust (MMT; Tahirkheli & Jan 1979; Coward *et al.* 1982, 1986).

On the basis of faulted contacts of the massif against Indus river gravels, Lawrence & Ghauri (1983) proposed that the western margin of the massif was marked by a neotectonic feature which they named the Raikhot Fault. This terminology was followed in the more extensive studies of Madin *et al.* (1989) and Shroder *et al.* (1989), who further proposed that virtually the entire margin of the massif, together with many of the internal contacts between different lithologies, was controlled by young faults.

The tacit assumption that the western margin of the massif is defined entirely by a neotectonic structure is at variance with other studies. In many exposures, early shear zone contacts between Kohistan and the massif have been exhumed from syntectonic amphibolite facies conditions. In the Sassi location (Fig. 1b), Butler & Prior (1988*b*) interpreted these as segments of the old MMT, interpretations supported by later studies in the northern part of the massif (Butler *et al.* 1992). However, this interpretation has significant problems on regional grounds because of its timing.

If the MMT represents the original suture between the Kohistan–Ladakh arc complex and the Indian continent, then it should date from about 50 Ma ($\pm$ 10 Ma), the timing of collision (perhaps as old as 57 Ma, Beck *et al.* 1995). Peak metamorphism dates at about 47 Ma in Kaghan (Smith *et al.* 1994) with post-burial cooling of the Indian continental crust in the Hazara Hills (East of Swat on Fig. 1a) dated from about 39 Ma (e.g. Treloar & Rex 1990). Yet on the NW margin of the Nanga Parbat massif, the earliest ductile contact between the massif and Kohistan (as described by Butler & Prior 1988*b*) deforms a suite of granite sheets that are as young as 26 Ma (George *et al.* 1993). Furthermore, the chemistry of these granites precludes underthrusting of Indian continent beneath this part of Kohistan until after their formation.

Notwithstanding the nature of the early ductile contact between Kohistan and Nanga Parbat, there is little consistency in the descriptions of younger structures along the western margin of the massif. Butler *et al.* (1989) briefly report on the basis of sparse kinematic datasets, top-to-the-NW thrusting (the Liachar Thrust of Butler & Prior 1988*a*) acting in tandem with dextral N–S orientated strike-slip along the western margin of the massif. Building on these descriptions, the composite structure, which includes segments of the early ductile contact between Kohistan and Nanga Parbat, was termed the Raikhot–Sassi Fault Zone by Treloar *et al.* (1991). Seeber & Pêcher (1998) also stress the composite nature of the margin but suggest, without corroborating data, that reverse dip-slip, dextral and sinistral strike-slip components are active. In contrast, Chamberlain *et al.* (1995, fig. 2) show the western margin to be represented solely by the Raikhot Fault, interpreted without supporting structural data as a sinistral strike-slip fault. To date there are no published interpretations of this margin as an extensional fault but otherwise all kinematic scenarios have been proposed.

Absolute and relative chronologies

The history of deformation and metamorphism within the Indian continental crust of the Nanga Parbat massif is controversial. Many of the salient points are reviewed elsewhere (e.g. Treloar *et al.* this volume). These issues are particularly critical in understanding the high temperature metamorphic history of the massif and in correctly assigning coeval structures to the Himalayan or an earlier orogeny (Butler *et al.* this volume). For the purpose of this study, the critical markers within Nanga Parbat massif are the suites of, generally pegmatitic, peraluminous leucogranite veins and sheets. These may be related through their trace element and Sr isotopic chemistry to larger leucogranite bodies. The larger intrusions yield Rb–Sr ages of less than 10 Ma (George *et al.* 1993; Butler *et al.* 1997). In the Raikhot valley they also contain zircons that yield similar ion microprobe U–Pb ages (Smith *et al.* 1992). These leucogranites are petrogenetically linked to the uplift and erosion of the massif in that their trace element geochemistry is most plausibly explained by decompression melting of muscovite under low-vapour conditions (Butler *et al.* 1997; Whittington *et al.* 1999). Thus structures which deform these leucogranites may be related directly to uplift and erosion of the massif and the structural evolution of the NW Himalayan syntaxis.

The rocks of the massif were cooled and exhumed rapidly (Zeitler 1985; Whittington 1996). Consequently, individual rock volumes pass systematically through the evolving thermal structure and are likely to have only experienced cooling through time over the past *c.* 5 Ma (e.g. Whittington 1996; Butler *et al.* 1997). This simple deduction has an important corollary: fault zones may be placed in a relative sequence on the basis of their inferred depth or temperature of activity. Consequently fault zones with similar characteristics (e.g. some ultracataclasites) must be broadly coeval if they occur within the same

rock volume, provided they and others within the rock volume have relatively low displacements. Although qualitative, this deduction permits a temporal correlation between closely spaced faults which can aid understanding of kinematic interactions. All structures that postdate peak metamorphic fabrics must be related directly to syntaxis formation and the denudation history of the Nanga Parbat massif. These late structures include arrays of localized cataclastic–mylonitic shears and gouge zones, some of which are the focus for hydrothermal activity (Butler & Prior 1988*a*). Field data are now presented for a collection of sub-areas around Raikhot Bridge (Fig. 1).

The Liachar area

The faulted contact between gneisses of the Nanga Parbat massif and poorly consolidated river gravels of the Indus valley was first described from the Liachar area by Lawrence & Ghauri (1983). They coined the name 'Raikhot Fault' for this structure. However, their type outcrop lies within the area of a large landslip (Butler *et al.* 1988; Owen 1989) and is not in place. The *in situ* fault contact was described by Butler & Prior (1988*a*) from the Indus valley wall east of the village of Liachar (Fig. 2a). The foot of the hillside contains poorly consolidated Indus valley sediments. These are dipping at 80° towards the valley and young in that direction. They are overlain with a faulted contact by a band of highly shattered augen gneisses, local metasediments and leucogranite sheets (Fig. 2b, c).

The fault surface between gneisses and young sediments is exposed in several locations (although it commonly requires some excavation; Fig. 2d). The fault zone is marked by a band of cataclasites derived from the gneisses. Subsidiary slip surfaces generally dip to the SE and have SE-plunging striations upon them (Fig. 3a). Offset of markers across these fault zones shows a widespread top-NW slip. There are also well-developed Riedel shear geometries evident within individual fault zones.

The gneissic banding within the intensely fractured hanging wall to this lower thrust zone is steeply orientated. However, there is another low-angle fault break that separates the steeply banded gneisses from the moderately dipping gneisses above (Fig. 2). This upper fault zone is marked by the same types of brittle mesostructures as the lower thrust segment and has a well-preserved 5–10 cm fault gouge along it. As before, the subsidiary fault surfaces dip synthetically with respect to the main fault break and these have SE-plunging striations upon them. However, there are also sparse strike-slip striations here (Fig. 3b). The panels of fractured gneisses between the main, moderate-angle faults are themselves cut by low-angle shears and faults on a variety of scales. These have the geometry of Riedel shears and also imply a bulk shear sense of top-to-the-NW.

The cataclastic deformation described above is strongly localized in the lower 100 m of the valley side at Liachar. Above this, however, are intensely deformed gneisses derived from the Nanga Parbat massif. These include leucogranite sheets which show various deformation states. Many, although concordant with the gneissic banding in the adjacent gneisses, retain pegmatitic textures. These bodies were emplaced as gently dipping sheets. However, other leucogranite sheets have moderate to intense crystal plastic grain shape fabrics and associated tectonic banding—the products of substantial solid state ductile strain.

The conclusions to be drawn from the Liachar site are that the Nanga Parbat massif is bounded, locally at least, by a zone of faulting. The geometry and kinematics of subsidiary faults within the zone show that it acted as a thrust. Although discrete through-going faults are evident, collectively this zone of cataclasis represents the youngest exposed, shallow level displacements. Butler & Prior (1988*a*) termed this structure the Liachar Thrust. It has been active in the past few tens of thousand years so that gneisses of the massif have been uplifted and emplaced onto poorly consolidated sediments of the Indus valley. However, these displacements were preceded by ductile deformation. Regrettably, at the Liachar site it is difficult to gain evidence on the kinematics of the ductile deformation. Additionally, the Indus valley sediments mask the structural relationships between rocks of the Nanga Parbat massif and Kohistan. Fortunately, clear exposures of each setting, above and below the cataclastic Liachar Thrust, are preserved elsewhere.

The Indus shore: Buldar–Raikhot Bridge

Much of the low ground of the Indus valley is covered by active slope deposits and abandoned fluvial-glacial deposits. However, there are some accessible platforms *c.* 50 m above the river, which were stripped of their late Pleistocene fluvial-glacial and debris flow deposits by catastrophic floods (e.g. 1841; Butler *et al.* 1988; Shroder *et al.* 1989). In addition there are a series of low outcrops in the river bed which are exposed during the low winter flows on the

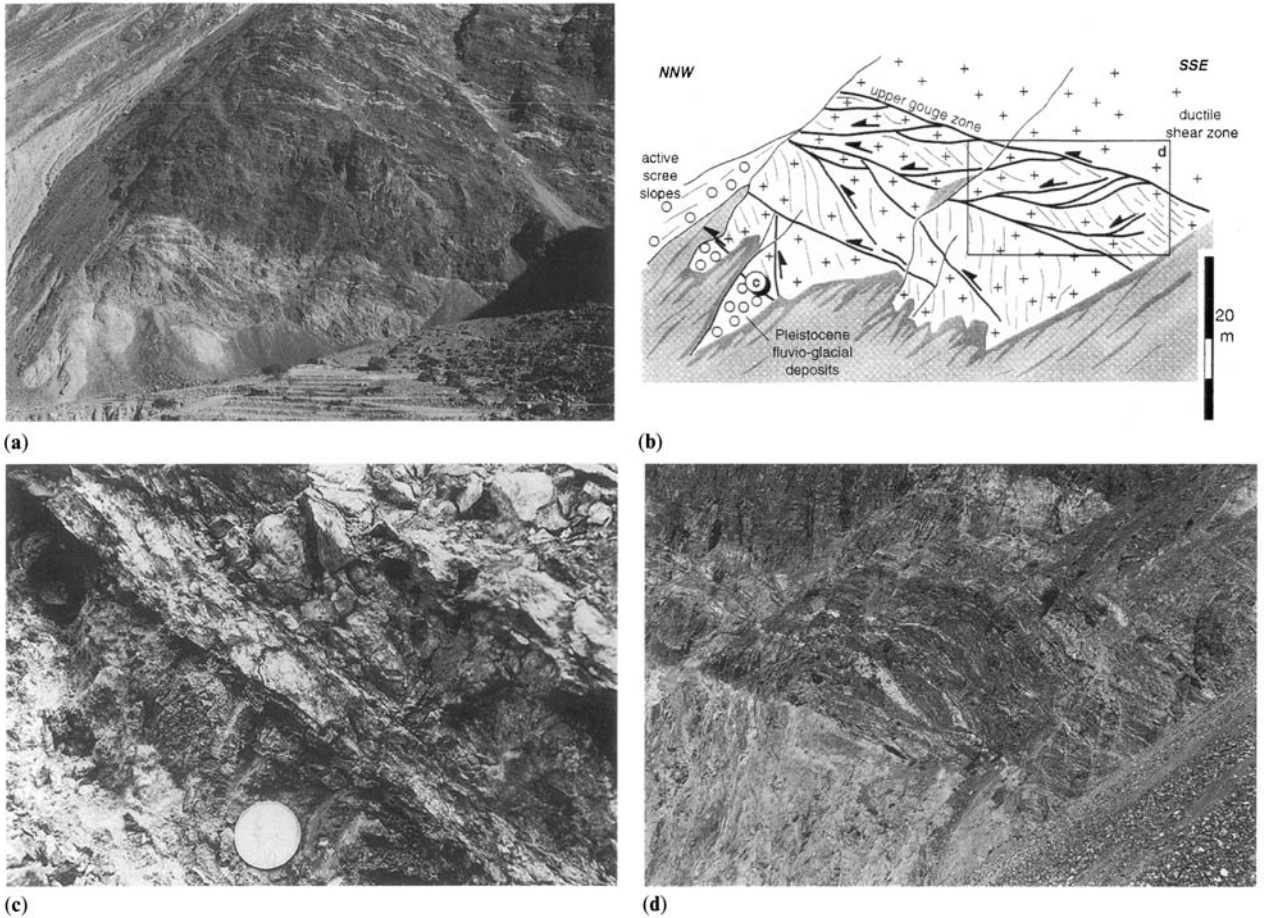

Fig. 2. Field relationships at the neotectonic contact of the Nanga Parbat massif at Liachar (Fig. 2). This is the type locality for the Liachar Thrust. (**a**) View onto the cliff section (from a on Fig. 1c); (**b**) sketch of the fault zone; (**c**) detail of the excavated basal fault contact (c on Fig. 2b), looking NE. The coin (2 cm) lies on fractured and disaggregated Indus valley sediments. The fault contact separates these from fractured gneisses above. (**d**) Low-angle fault contacts offset banded gneisses and white leucogranite sheets (see b).

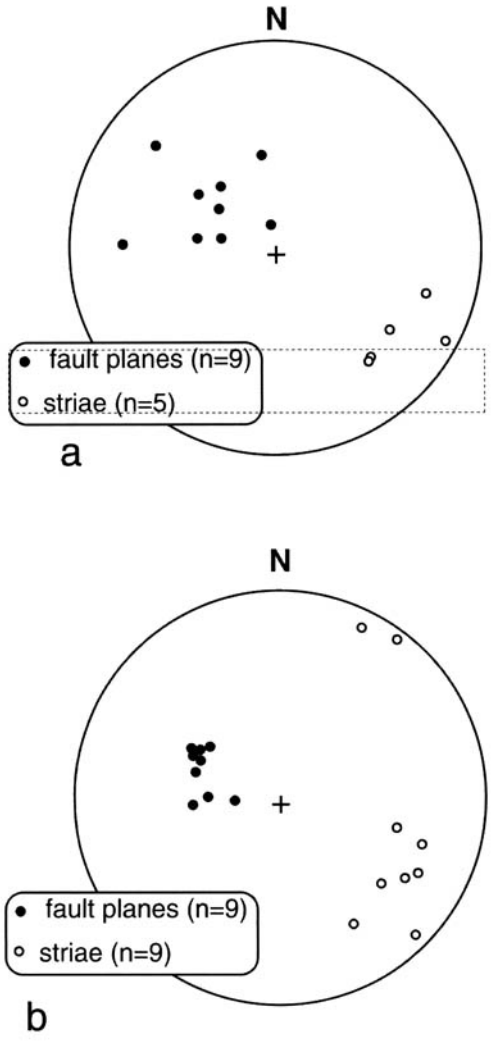

Fig. 3. Lower hemisphere stereoplots of fault data from the Liachar Thrust Zone: (**a**) shows data from the lower fault zone, where shattered gneisses (with generally steep banding) are carried onto poorly consolidated Indus valley sediments (c on Fig. 2b); (**b**) more complex fault kinematics from the central fault break (between steeply dipping and moderately dipping gneisses).

Indus. These outcrops were reported by Butler & Prior (1988*b*) although more detail was provided of an equivalent succession at Sassi (Fig. 1), further north along the margin of the massif. Northeast of Raikhot Bridge there is a complex tract of rock types and structures (Fig. 4). Metaigneous rocks of the Kohistan arc terrane crop out on the NW side of the Indus valley. The SE side of the valley includes augen gneisses of the Nanga Parbat massif. Between there is a tract of dominantly metasedimentary rocks. Regionally there are several distinct metasedimentary successions, including those associated with the Kohistan arc (the Jaglot Group of Treloar *et al.* 1996) together with those associated with the Indian continent (e.g. DiPietro *et al.* 1993), both of Late Palaeozoic–Mesozoic (cover) and Early Palaeozoic–Proterozoic (basement) age. Assigning the Raikhot metasediments to their correct tectonostratigraphic affinities clearly is critical for any structural model of the Nanga Parbat massif. Consequently, it is pertinent to discuss rock types and structures in turn.

Rock types

Between the confluences of the Indus with the Buldar and Raikhot rivers there are continuous sections of basic gneisses. In many locations within this area the metabasic rocks preserve crude gabbroic textures. However, the cleanest outcrops are found north of the Buldar–Indus confluence within the Indus river. These exposures are accessible only in winter months when water levels are low. Here (e on Fig. 4a) there is a distinctly banded sequence of basic gneisses. Banding is defined by the relative proportions of amphibole and plagioclase although there is subordinate garnet (Fig. 5a). At one locality there is a streaked 3 cm grain of chromite (Fig. 5b) and elsewhere chromite occurs in millimetre wide seams. This observation, together with the general aspect of the rocks, strongly suggests that the banded basic gneisses were derived by shearing of a layered metagabbro. Above the river, particularly near Raikhot Bridge, these rock-types are continuous with those of the NW bank of the Indus. Consequently, these rocks are considered to represent part of the Kohistan arc complex.

To the SE of the banded basic gneisses lies a succession of metasediments with thin amphibolites. Although highly variable in detail, broad compositional units are laterally continuous and amenable to mapping. These units trend parallel to the contact with the banded basic gneisses. Much of the succession consists of interlayered psammites and pelites (e.g. Fig. 5c) containing flattened feldspathic porphyroblasts. Lithological banding is generally between 10 cm and 1 m thick although these thicknesses relate to strongly deformed rocks. They also include thin (*c.* 50 cm) bands of amphibolite. These amphibolites may be distinguished from the banded basic gneisses of Kohistan affinity described above in that they are thin with very little plagioclase, although minor concentrations of garnet are present. They lack internal banding.

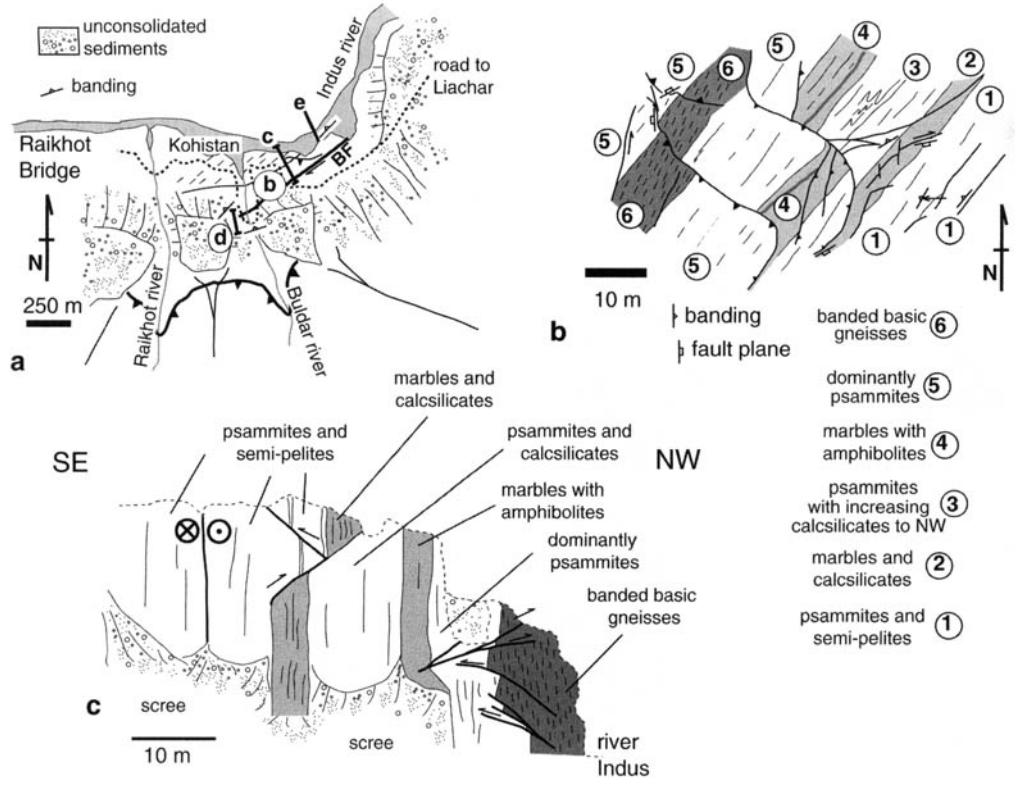

Fig. 4. Field relationships in the Buldar–Raikhot outfall area. (**a**) Location map. BF—Buldar Fault. Other diagrams in this figure are also located (b–c). d—location of photograph (Fig. 5e); e—location of photographs (Fig. 5a, b, f). (**b**) Outcrop platform showing rock succession into the banded basic gneisses (presumed deformed metagabbro of Kohistan). (**c**) equivalent vertical section seen in vertical river cliff (accessible at low-flow conditions on the Indus).

Presumably they represent minor basic intrusions within the protolith to the metasediments.

At several levels within the metasediments there are distinctive 1 m marble layers together with thicker mixed sequences of calc-silicates, psammites and thin amphibolites (e.g. Fig. 5d). The calcareous metasediments (carbonate + garnet + feldspar + biotite + white mica + kyanite) define thin (*c.* 20 cm) layers. Pods composed of aggregates of garnet are present within these layers, although this material can also form continuous layers within some marbles.

In detail the passage of basic gneisses into metagabbro is not continuous. Panels of metasediments are tectonically interleaved with the gneisses. On the transect shown in Fig. 4c, a package of psammites separates the outcrops of banded basic gneisses from the main section of Kohistan arc rocks. Interleaving between Kohistan metabasic units and metasediments is common elsewhere along the western and northern margin of the Nanga Parbat massif. At the mountains of Phuparash and Malubiting (Fig. 1b), the interleaving occurs in a zone over 1 km across where it constitutes the 'Layered Unit' of Butler *et al.* (1992). However, at Raikhot interleaving is limited to a zone about 50 m wide.

Given the intimate relationship between metagabbro and metasediments, it is tempting to relate all units to the Kohistan arc. The nearest possible correlatives are the metasediments of the Jaglot Group (Treloar *et al.* 1996). The protolith to these strata are greywackes with intercalated basalts and volcaniclastic sediments. However, the Raikhot strata described here have substantial calcareous members, including pure marbles and calcschists, which have no direct equivalents in local Kohistan geology. Consequently, correlation with Kohistan for these metasediments looks poor. Lithologically the calcareous metasediments and thin metabasic sheets are similar to the Alpurai Group (Kashala Formation) of inferred late Palaeozoic age described by DiPietro *et al.* (1993) from Swat (Fig. 1a).

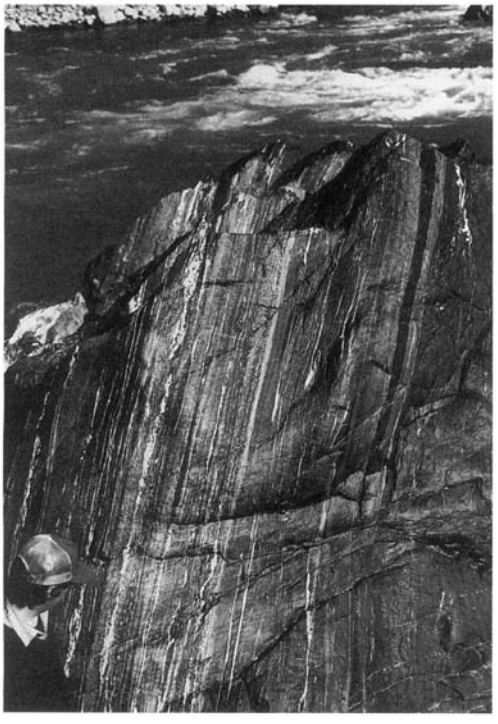

(a)

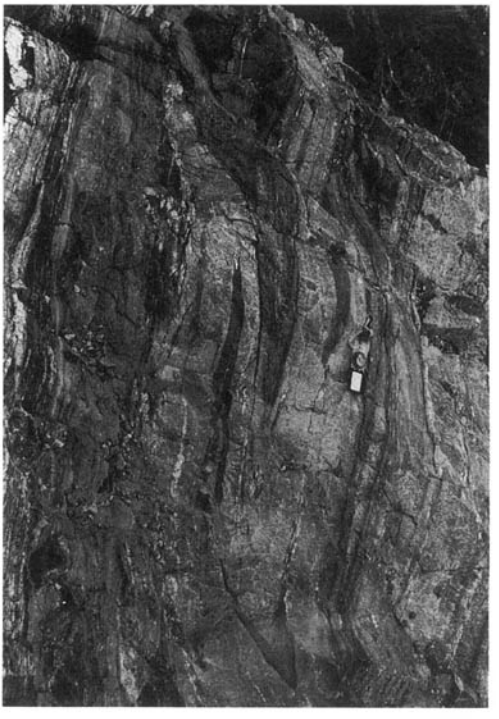

(c)

(d)

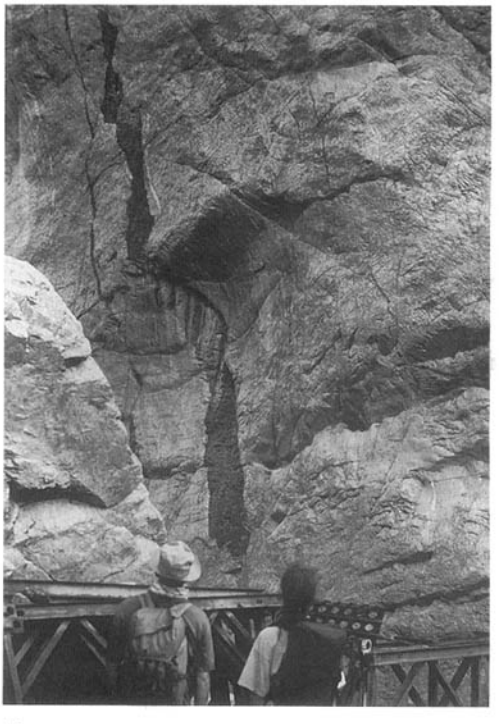

(e)

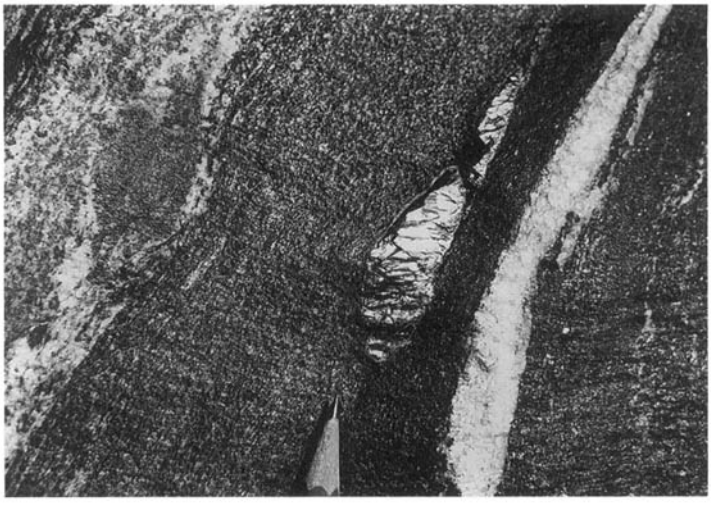

(b)

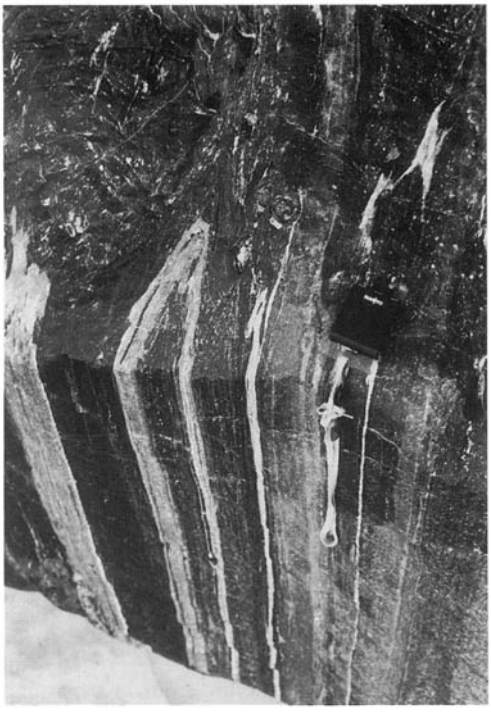

(f)

Fig. 5. Field photographs for the Buldar–Indus confluence area. **(a)** Banded basic gneiss unit (located at e on Fig. 4a), looking along strike (NE). **(b)** Sheared chromite embedded within hornblende–plagioclase gneisses. On left of view the light band is chiefly composed of plagioclase and garnet. This is a detail from **(a)**. **(c)** Tight, steeply-plunging folds in psammites and semipelites (unit 1 on Fig. 4b). **(d)** Mixed sequence (unit 3 on Fig. 4b) of layered calc-silicates, garnetiferous amphibolites and garnetites. Looking SSW along strike (general banding strikes 228, dips 83°). Vertical ductile extension is evidenced by the layer boudinage (chiefly of the amphibolites within pale calcareous layers). The late fault (120–56SW) is marked by gouges and veins of chlorite + epidote. **(e)** Subvertical amphibolite sheet emplaced within the orthogneiss. Note the shear offsets in the sheet (looking towards a bearing of 210; outcrop located at d on Fig. 4a). **(f)** Block top and side of intrafolial folds within banded basic gneisses. The folds plunge parallel to the local mineral lineation, at about 60° towards the viewer (SW). These units are interpreted as derived from metagabbro of Kohistan (location e on Fig. 4a). **(g)** Conjugate array of cataclastic faults (with subsidiary veins of chlorite + epidote), developed in interlayered psammites with minor garnetiferous amphibolites (unit 5 on Fig. 4b), looking SW. **(h)** Ultracataclastic fault (032–64S) with associated bend-in developed in augen orthogneiss. This fault shows top-NW shearing and passes up and down dip into intense foliation within the host gneisses. The steep fabric (248–83N) defined by aligned feldspar augen together with thin banding is typical of these outcrops at the foot of the Buldar gorge (looking NE).

These strata are part of the Indian continental crust. Consequently, the metasediments at Raikhot are assigned to the Nanga Parbat massif. The contact between these units and the metagabbro is considered to be exclusively tectonic—the early ductile shear zone between Kohistan and the massif. Presumably interleaving occurred as either folding or imbrication

(g)

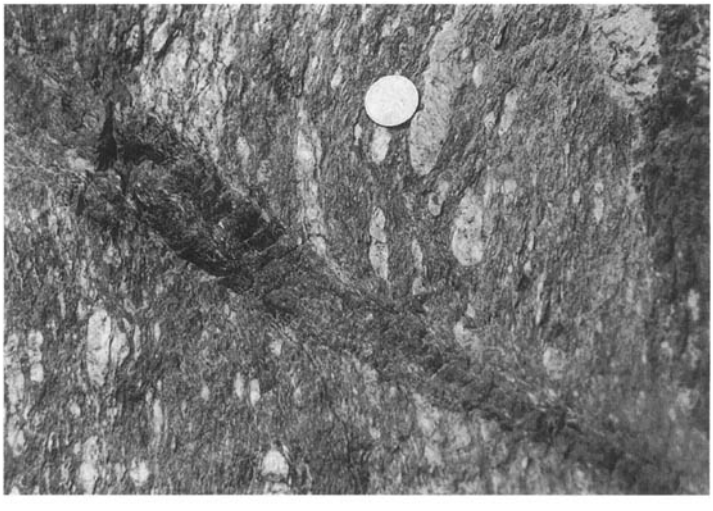

(h)

during the shearing process, a common feature of many large-displacement shear zones.

The cliff sections which overlook and bound the Buldar outcrops to the SE are composed of feldspathic biotite augen gneiss. This orthogneiss is the classical dominant lithology of the Nanga Parbat massif (e.g. Wadia 1933). In general this unit is homogeneous on a > 10 m scale. However, it contains thin subvertical metabasic sheets (Fig. 5e) which display intrusive relationships.

The relationships between the augen orthogneisses and the metasediments are commonly obscured by active slope deposits and a broad zone of cataclastic faulting. However, in both the Buldar and Raikhot valleys the augen gneiss lies adjacent to a mixed sequence of porphyroblastic psammites and pelites. The lithological contacts are broadly concordant with banding within the metasediments and to the penetrative shape fabric within both the augen gneiss and the metasediments.

On a larger scale, the augen orthogneiss and metasediments are interleaved. Alternations of conformable metasediments (including thin marbles and calc-silicate layers) and orthogneiss are exposed to the SE, upstream in the Buldar and Raikhot valleys. Metabasic sheets, presumed intrusives, are found within the metasediments and the orthogneisses. Thus these units share a

common geological history, at least for those events that may be discerned in the field. This in part corroborates the interpretation above that the metasediments are exclusively part of the massif.

Structures

Within the Buldar–Raikhot section, the earliest preserved contacts between all main rock types are concordant and parallel to the penetrative shape fabrics. In general this is steeply dipping with a NE–SW strike (Fig. 6a). Most outcrops contain a prominent mineral lineation upon the foliation surface. Generally these lineations plunge moderately SW. However, within the augen gneiss the mineral stretching lineation plunges more steeply, essentially down the dip of the foliation. The following comments apply to rock units to the NW of the augen orthogneiss.

Intrafolial folds are found in metasediments (Fig. 5c) and the various metabasic units (Fig. 5f). These plunge moderate-to-steeply SW, parallel to local mineral alignment lineations (Fig. 6). Boudinage is also evident—in the amphibolites embedded in calcareous metasediments and on a 20 m scale of entire banded units. Boudin axes also plunge to the SW (Fig. 6b). Thus generally all linear structures are subparallel. All these structures developed under peak metamorphic, amphibolite facies, conditions. They are concentrated at or near the contact between metasediments (Nanga Parbat) and the banded basic gneisses (Kohistan), indicative of large values of ductile strain.

Apart from intense penetrative ductile strain fabrics, the area contains localized deformation zones marked by centimetre to metre-wide mylonites and abundant cataclastic faults (Fig. 5g). In general the fault surfaces and mylonitic seams strike NE–SW and are moderate-to-steeply dipping (Fig. 7). However, striations upon these surfaces indicate a spectrum of kinematics, from ideal reverse dip-slip, through oblique-slip to dextral strike-slip senses (Fig. 7b). A range of fault rock types exist throughout the fault population. The highest temperature localized shears are characterized by recrystallized biotite and bend-in fabrics defined by feldspar porphyroblasts (Fig. 5h). These features suggest deformation initiating at temperatures in excess of 450 °C. However, other faults include epidote–chlorite seams, weakly consolidated gouges and open fault breccias. Thus faulting occurred under a range of different temperatures and confining pressures, from >450 °C to the Earth's surface.

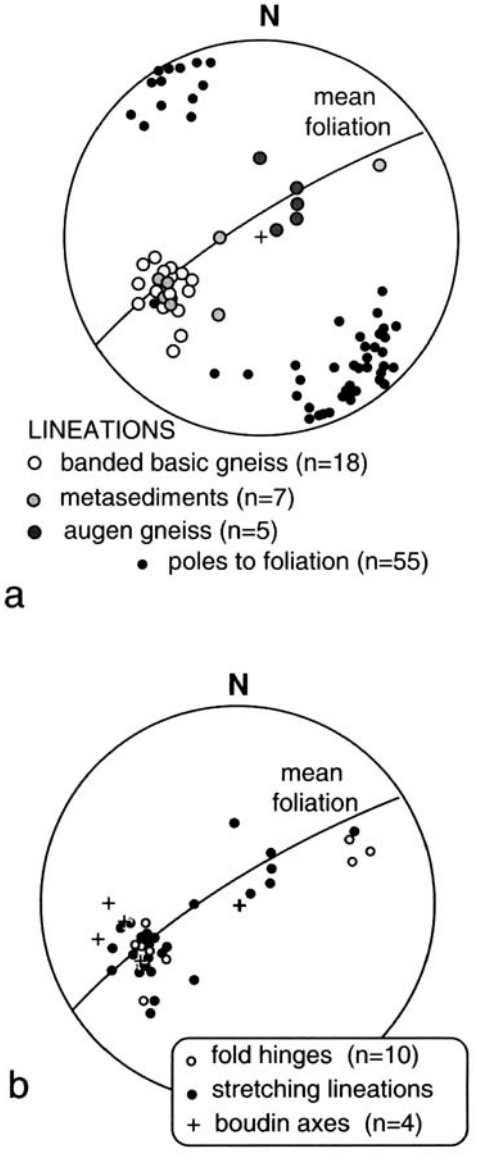

Fig. 6. Lower hemisphere stereoplots of ductile planar and linear structures from the Buldar–Raikhot area at the Indus. **(a)** Illustrates the relationship between mineral lineations in the main rock units, which are spread along the calculated mean foliation plane (237–82). The SW-plunging cluster reflects linear fabrics at or adjacent to the early ductile contact between Kohistan and Nanga Parbat rocks. The sparse data from the augen gneiss are steeply plunging, chiefly indicating vertical stretching in this unit. **(b)** Illustrates the relationship between fold hinge lines (intrafolial folds) and boudin axes with the stretching lineations (not distinguished by rock-type, stretching lineations are the same dataset as in Fig. 8a). These data are concentrated along and adjacent to the ductile contact between Kohistan and Nanga Parbat rocks.

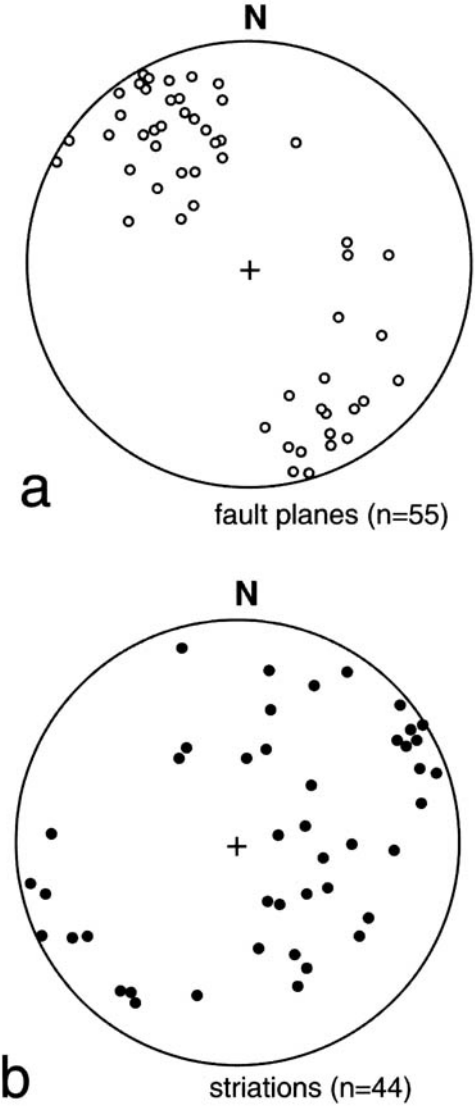

Fig. 7. Lower hemisphere stereoplots of (**a**) poles to fault planes and (**b**) striations for the discrete ultramylonitic zones and cataclasites found in the Buldar–Raikhot area.

The most prominent of the higher temperature faults is a 1–5 m zone (vertical—SW–NW trending) of fabric intensification and ultramylonites (Fig. 8) that crops out at the bridge over the Buldar river. Consequently, this structure is named the Buldar Fault. In general the fault and its subsidiary strands are steeply dipping, with broadly NE–SW strikes. Striations and aligned mineral aggregates plunge towards the NE quadrant but with a variety of pitches upon the fault surfaces (Fig. 8b). Bend-in and S–C fabrics in biotite-rich seams record dextral shear (Fig. 8c). Taken collectively, the kinematic data suggest that the Buldar Fault accommodated dextral transpressive strike-slip.

The immediate vicinity of the Buldar Fault is composed principally of augen orthogneisses. However, these are intensely fractured and sheared adjacent and NW of the fault. Early descriptions of this zone (e.g. Butler *et al.* 1989) focused on examples where the inclined reverse faults are cut by the steeper strike-slip fault zones. However, it is clear that many of the inclined and steep fault zones merge together and have similar deformation fabrics. These record dominantly dip-slip motion and are inclined both to the SE and NW. Macroscopically the geometry of dip-slip faults spawning from the vertical strike-slip fault is that of a flower structure that accommodated NE–SW dextral transpression. Some of these faults initiated under the same general metamorphic conditions as the dominant fabric within the local orthogneisses—there is no sign of retrogression along them. Some, however, are associated with retrogression to epidote–chlorite assemblages and others are seamed with clay minerals.

To the NW of the ultramylonitic fault zone and striking generally parallel to it are zones of fracturing within the metasediments. Fracturing is associated with deep weathering and alteration: consequently it is not well exposed. It is clearly a significant fault zone, presumably one that operated under lower temperatures and confining pressures to the ultramylonitic one. Veining and alteration around these faults suggest that this deformation was accompanied by fluid ingress and the growth of chlorite + epidote assemblages. Other such faults exist throughout the metasediments, commonly with <1 m offsets but with complex dip-slip and oblique-slip kinematics (e.g. Fig. 5g). Collectively the dip-slip faults extend the steeply dipping layering. However, the fault population as a whole shows strike-slip, oblique and dip-slip (Fig. 7) and presumably therefore accommodated similar bulk kinematics as the Buldar Fault Zone, namely NE–SW dextral transpression.

Summary

The Buldar area shows complex polyphase deformation of both a syn-metamorphic shearing under amphibolite-facies conditions and much shallower-level faulting with alteration under greenschist facies. The poorly-consolidated gouges imply that at least the later periods of faulting in the site occurred under very low

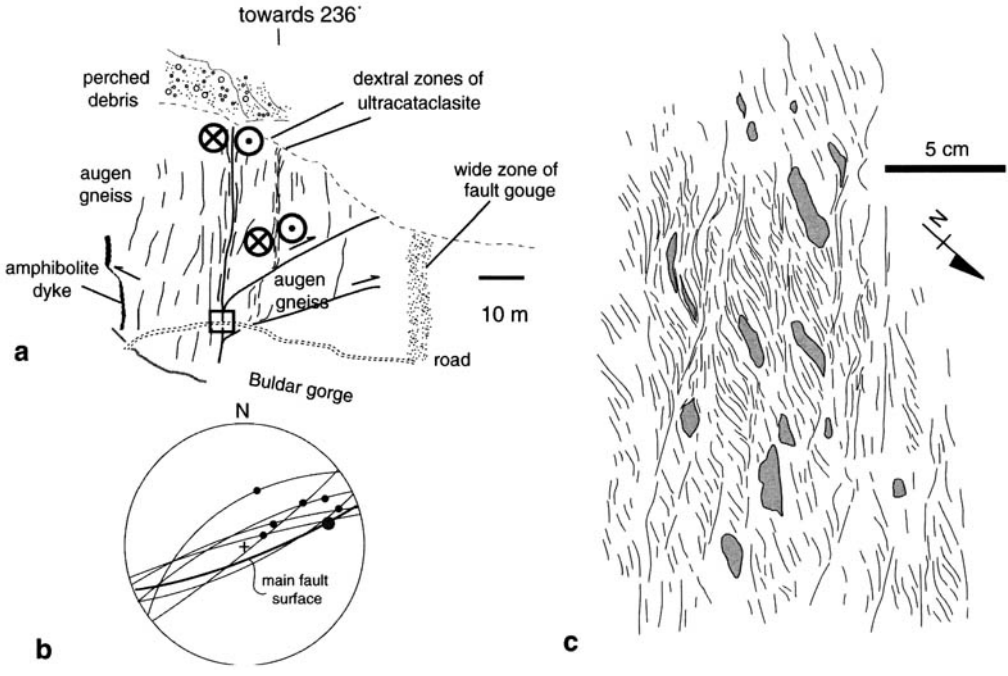

Fig. 8. Structural data from the Buldar Fault. **(a)** Field view of the fault in its type area. The senses of fault slip indicated were interpreted from observed kinematic indicators. The boxed area denotes the site of more detailed observations. **(b)** Fault data from this boxed area ($n = 7$) for anastamosing slip surfaces decorated with black ultracataclasite. **(c)** Foliation trends in plan view (shaded objects are larger feldspar porphyroblasts) indicative of dextral shear senses.

confining pressures. The earliest recognized structures here affect both Kohistan-derived and Nanga Parbat rocks. They may be associated with the emplacement of Kohistan, as proposed by Butler & Prior (1988*a*). In detail this early contact is complex, consisting of interleaved Kohistan-derived metagabbroic gneisses and metasediments belonging to the Nanga Parbat massif. However, simple untilting of the now-steep lineation found in these units by rotation about the modern NE–SW strike does not restore the linear deformation fabrics into the expected regional alignment. Rather than trend NNE–SSW, as at Sassi (Fig. 1; Butler & Prior 1988*b*), they trend ENE–WSW. Consequently, deformation of this early contact may have involved more than simple rotation. Flattening of an early NNE-plunging lineation during rotation could generate steeply WNW-plunging linear fabrics. To achieve the present orientation from the inferred original NNE trend requires more complex strain paths and perhaps variations in regional plunge. Conversely the modified earlier structures maybe had some other orientation. Further discussion is hypothetical in the absence of additional structural data from outside the Raikhot study area.

Later deformation affects all units within the Buldar site. It consists of important dextral strike-slip zones, striking broadly parallel to layering and the local margin of the massif (i.e. NE–SW), together with conjugate, thrust-sense shears and faults. This deformation is markedly heterogeneous and occurred from amphibolite facies up to the Earth's surface. The timing of this deformation postdates the juxtaposition of the Nanga Parbat and Kohistan units. The lower age range may be established since the structures continued to be developed up to the Earth's surface. The youngest faults must therefore have formed over the past few tens of thousands of years. The kinematics and orientations of the very youngest faults are essentially indistinguishable from those of the ultramylonitic and ultracataclasite zones that formed at depth. Therefore, all of these localized displacement features are likely to have developed after the penetrative ductile shear fabrics were in their current, steep attitude. Critically it appears that dextral strike-slip and NW–SE compression on

(a)

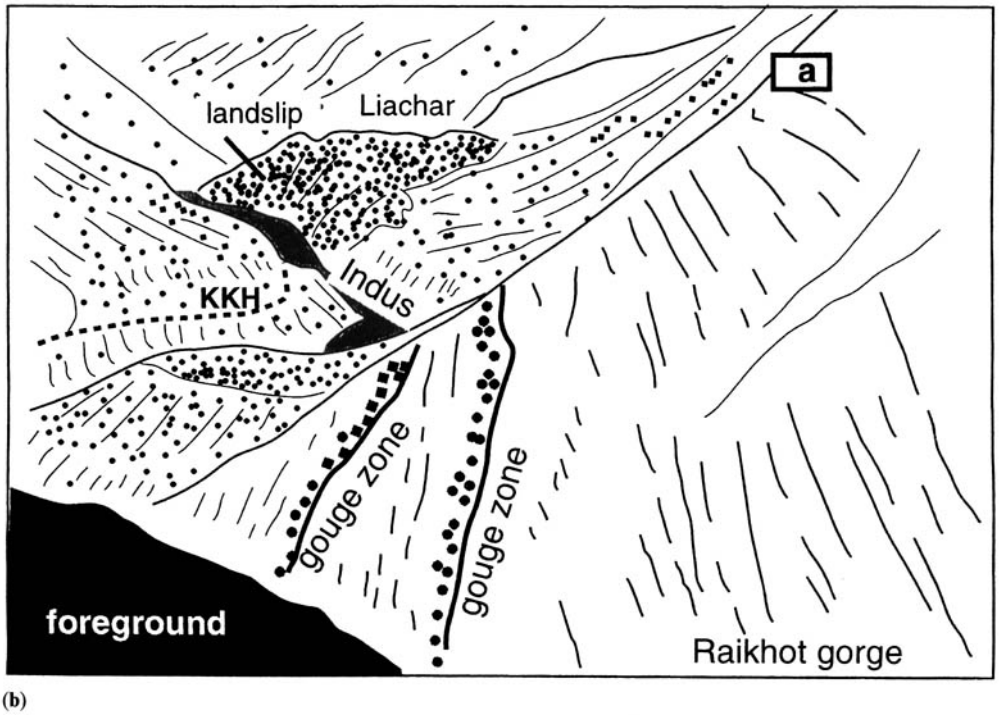
a
landslip
Liachar
Indus
KKH
gouge zone
gouge zone
foreground
Raikhot gorge

(b)

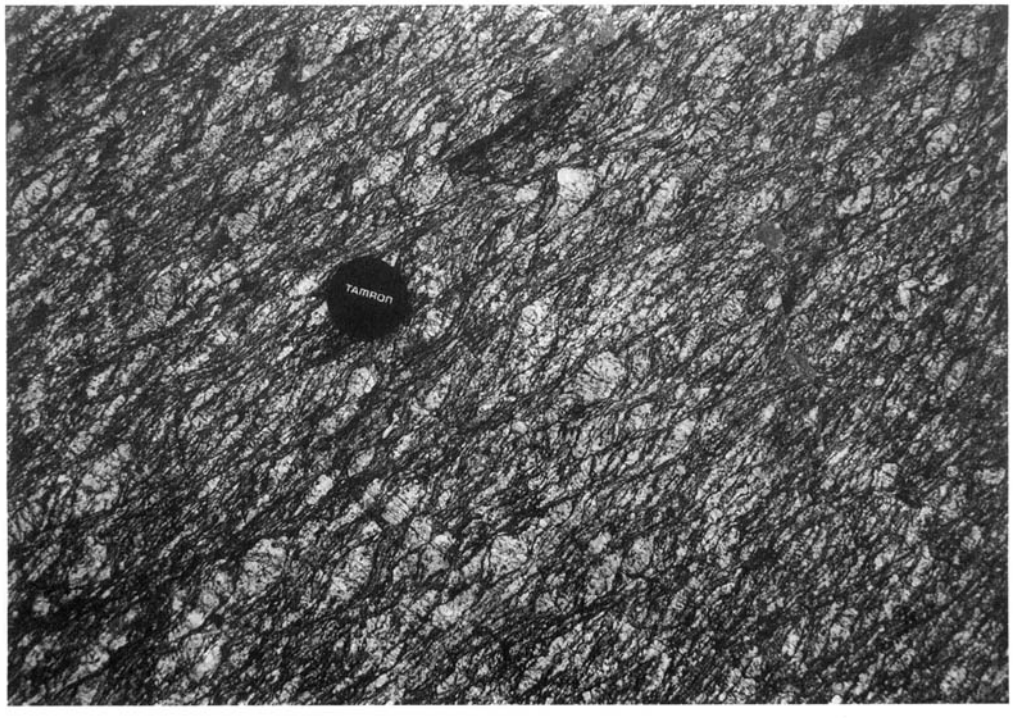

(c)

Fig. 9. (**a**) View and (**b**) sketch looking NE across the lower Raikhot gorge (from b on Fig. 1c). The sheared orthogneisses above (SE of) the gouge zones show intensely asymmetric overshear (see Fig. 9, located on Fig. 9b). The gouge zones are correlated with the Liachar Thrust, which lies about 4 km along strike. They have similar fault rock characteristics and kinematics. (**c**) Sheared augen gneisses from an elevation of about 1900 m on the east ridge of the Raikhot valley (a on Fig. 9b). Looking SW onto a vertical face. The S–C fabrics imply penetrative top-NW overshear.

steeply-dipping reverse faults were coeval but heterogeneously distributed in space and time. Collectively these structures represent NE–SW dextral transpression which operated from temperatures in excess of 450 °C to those pertaining to the Earth's surface.

The Raikhot-Buldar ridge

The preceding discussion has highlighted that near the Indus the foliation and banding in all units is steep. However, higher on the hillsides on the SE side of the Indus, deformation foliations and banding dip moderately towards the SE (Fig. 9a, b; Butler & Prior 1988*a*). Much of the rock here is augen orthogniess with panels of metasediments. All contain intense stretching lineations on the shape foliation which plunge essentially down dip implying dip-slip shearing (Fig. 10). The sense of shear may be established unambiguously from ubiquitous asymmetric shear indicators (e.g. Fig. 9c). These imply top-to-the-NW overshear. The deformation fabrics affect thin seams of leucogranite, indicating that at least some of this strain has accumulated in the past few million years.

Previous descriptions of this zone based on reconnaissance work (Butler & Prior 1988*a*) suggested that the change between the two dip domains (steeply dipping foliation to those with moderate dips) occurred across a single discrete zone of faulting—the Liachar Thrust. However, in detail these relationships are more complex (Fig. 11). Transects provided by a visible 700 m vertical section in the Buldar and Raikhot gorges reveal a series of discrete thrusts that dip moderately to the SE, cutting and offsetting the steep banding of augen orthogneisses and metasediments. Three have been identified that cut and offset rock units for the entire visible section, implying individual displacements of at least 1 km. The upper of these marks the transition between the two dip domains in the gneisses. It is marked by a zone of cataclasis, up

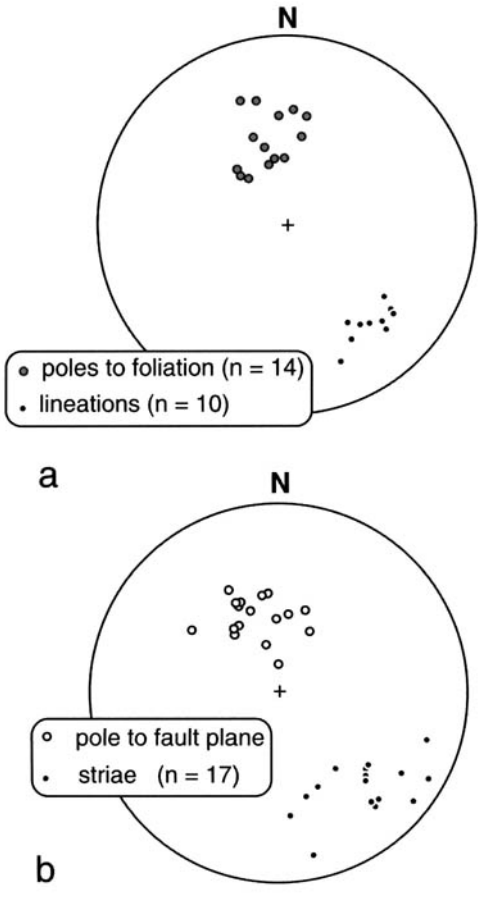

Fig. 10. Lower hemisphere stereoplots of structural data from the ridge section between the Buldar and Raikhot rivers (se Fig. 9). (**a**) Ductile strain fabrics. (**b**) Localized fault structures from the same area.

to 10 m wide. This fault represents, at this locality, the uppermost part of the Liachar Thrust Zone. Although there are moderately dipping faults that are broadly parallel to foliation in the moderately dipping gneisses, these are marked by little wall-rock damage and are generally just a few centimetres wide. The inference is that most of the cataclastic displacement in the Liachar Thrust Zone was accommodated on the through-going faults, the upper one carrying a ductile shear zone with little further modification.

The concept of a single discrete fault break marking the Liachar Thrust at Raikhot is misleading. Rather, cataclastic displacement is distributed in a zone of discrete thrust faults, with a collective width in excess of 500 m. This structure is also evident at the outcrops near Liachar village. Individual fault breaks may be traced, discontinuously on the Indus valley wall, between the two sites.

The cataclasitic faults on the Raikhot–Buldar ridge have similar kinematics to the ductile strain fabrics (Fig. 10b). Thus it is tempting to suggest that the localized, brittle faults represent merely the latest, highest level part of the thrusting process that is more fully represented by the ductile shears (Butler & Prior 1988*a*). However, on the ridge section it is difficult to establish outcrop continuity into the ductile shear zone. Above an elevation of about 2000 m above sea-level (*c.* 800 m above the Indus river) the foliation within the orthogneisses steepens and defines an antiformal fold closure. The folded foliation is cross-cut by leucogranite sheets but some sheets are also deformed by the fabric. Consequently, it is deduced that folding occurred during the broad period of leucogranite generation and emplacement, over the past few million years. The folding is thus broadly contemporaneous with top-to-NW overshear at lower structural levels on this transect. Consequently, the fold may be related to a deformation gradient in the hanging wall to the Liachar Thrust.

The west side of the lower Raikhot gorge

The east side of the Raikhot valley provides an excellent vantage point for examining the large-scale structure of the shear zone in the hanging wall to the cataclastic Liachar Thrust. Unfortunately the cataclastic thrust zones are largely obscured by active slope deposits above Raikhot Bridge. However, the overlying shear zone is dramatically and continuously exposed (Fig. 12a, b). The section contains both augen orthogneisses and metasediments, as on the opposite side of the valley. The foliation and lithological banding dip moderately into the massif. These too show unambiguous top-to-the-NW shear senses (Fig. 12c). Mineral lineations throughout the section plunge broadly downdip, towards the SE (Fig. 13).

The orthogneisses contain several amphibolite sheets, now orientated conformably to the host foliation and banding. The sheets are internally foliated. In more sheared examples the deformation is accompanied by metasomatic alteration to biotite schists, commonly with included quartz veins (Fig. 12e). These layers show excellent asymmetric shear criteria, parallel to the shear sense in the orthogneisses. Subsidiary shears, also with intense biotite fabrics, link through the surrounding orthogneisses onto the biotite schists. Thus the metabasic intrusions act as weak horizons within the shear zone once they

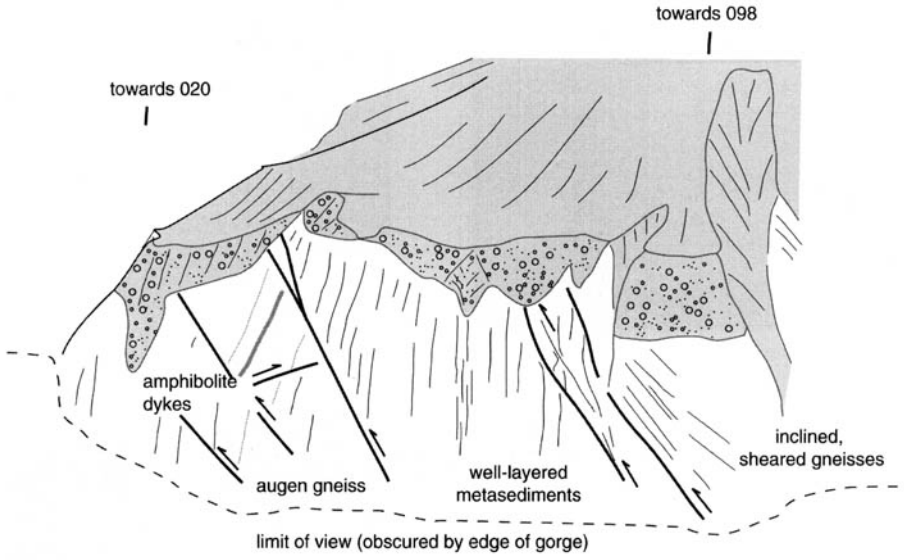

Fig 11. Field sketch of the NE wall of the lower Buldar gorge showing the relationship between through-going thrust surfaces (sense of offset inferred from remote observation of minor fabric deflections in the wall rocks) and the banding in the host gneisses. The shaded material represents modern slope and glacial deposits. Visible height of the valley wall is approximately 400 m.

have evolved to biotite schists, presumably at a late stage in the exhumation of the massif. While the sheets remain as amphibolites they show boudinage structures when embedded within the augen orthogneisses. Presumably at this stage in the exhumation the amphibolites were more competent than the host gneisses.

The west side transect of the Raikhot gorge differs from that on the east in that there is more metasedimentary material, particularly further into the massif. These are dominated by psammites and pelites with rare marbles and calc-silicate layers. Lithologically the successions of metasediments are similar to those by the Indus near the Buldar river confluence (see above), although the amount of carbonate is less. However, the main distinction is that pelites contain local leucosomal layers and *lit-par-lit* migmatitic textures. Locally these textures are cross-cut by amphibolite sheets, suggesting that they formed relatively early and presumably predate the shear structures described here. However, as the entire section is affected by the top-to-the-NW kinematics and shearing experienced by the augen gneisses, it is difficult to establish the original structural relationships between these units here.

Leucogranite sheets

The west side of the Raikhot valley, in common with the east, contains significant numbers of leucogranite sheets. The easier access on this side allows direct study of these sheets and consequently permits investigation of emplacement mechanism, texture and subsequent deformation histories. The sheets range in width from several metres to about 10 cm, although most are between 50 cm and 2 m across. Most of the sheets are coarsely pegmatitic with a framework of feldspars, although many are deformed. Existing geochemical studies (George *et al.* 1993; Butler *et al.* 1997) show that the leucogranites were generated by small batch-melting through vapour-absent muscovite breakdown. Although the leucogranites in the lower Raikhot section described here lie within migmatitic metasediments and augen orthogneisses, it is difficult to relate individual leucogranite bodies to a local source on textural grounds.

The majority of sheets are concordant with the SE-dipping deformation fabric in the surrounding gneisses. Several are folded—with axial surfaces roughly parallel to the banding and deformation fabrics in the host gneisses. In addition, the host gneisses contain concordant leucosome layers. Some of these may be traced into discordant pegmatitic leucogranite sheets. These examples represent highly attenuated limbs to folds of leucogranite. However, the majority of the 5–10 cm wide leucosomal layers are discontinuous and locally are cross-cut by leucogranite. Perhaps these leucosomes are merely an earlier

(a)

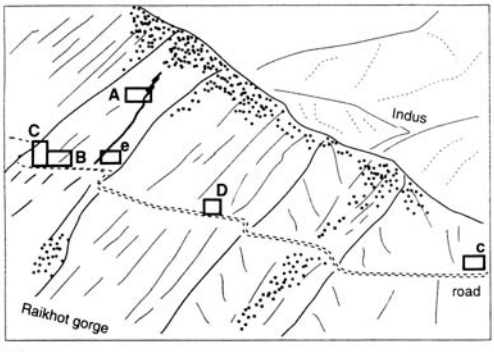

(b)

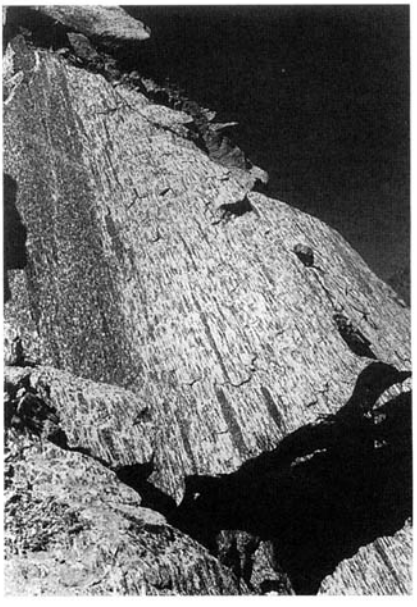

(d)

(c)

(e)

Fig. 12. (**a**) Photograph of the west side of the lower Raikhot valley, looking SW (from c on Fig. 2). This provides a spectacular continuous profile through the shear zone in the hanging wall to the cataclastic Liachar Thrust Zone. The sketch (**b**) shows locations of detailed photographs related to structural kinematics (c, e; d lies just to the left of view). A–D relate to locations for photographs of granite field relationships (Fig. 14). (**c**) Asymmetrically sheared augen fabrics in orthogneisses, looking SW. Field of view *c.* 50 cm. (**d**) Looking onto foliation surface in sheared augen gneiss on the road section. The melanocratic pods plunge down dip, into the massif (SE). (**e**) Asymmetrically sheared biotite schist (presumed derived from amphibolite sheets emplaced within the augen orthogneiss). Looking SW, these outcrops show top-NW shear sense.

part of the process of leucogranite emplacement that has been fully transposed by high strains. Alternatively, they may represent an entirely separate episode of differentiation that perhaps long predated the Himalayan orogeny.

If syn-tectonic melting within the shear zone had occurred it might be expected that strain would be localized transiently onto melt patches. Yet the concordant leucosomes within the migmatites are generally boudinaged, indicating

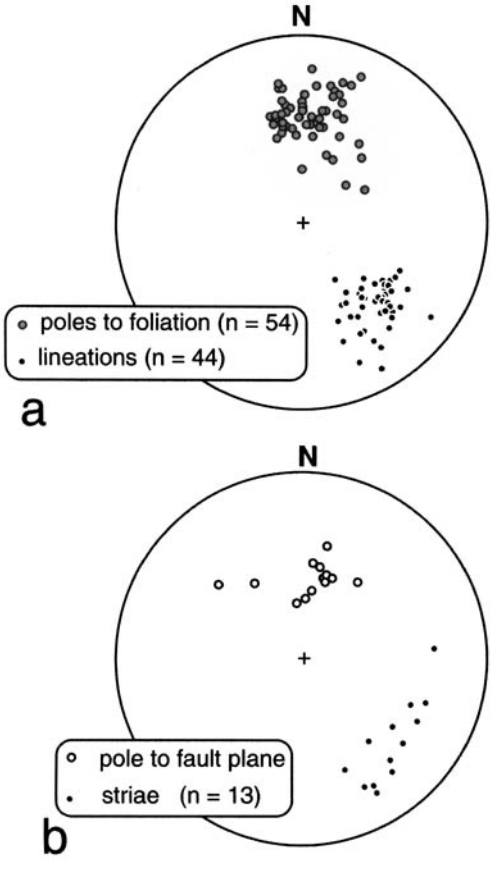

Fig. 13. Lower hemisphere stereoplot of structural data from the road section in the lower Raikhot valley: (**a**) ductile strain fabrics; (**b**) fault structures.

that they were more competent than the surrounding biotite-rich gneisses. Available field evidence apparently suggests that the migmatites deformed under dominantly solid-state conditions, and therefore that migmatization predated deformation. The corollary is that the leucogranites—which show both solid-state and pre-full crystallization textures were emplaced into the active shear zone. The influence of deformation upon fractional crystallization and segregation within the leucogranites is the subject of continuing research.

A local structural chronology may be established within the section. The principal migmatite and augen textures in the gneisses predate the metabasic sheets which, in turn, predate the deformation and shearing discussed here. However, at present it is not possible to rule out the possibility that some local remelting of the migmatites has occurred within the shear zone to provide a local source for some of the leucogranites. The metasomatic reaction of amphibolites to biotite schists presumably requires the ingress of K-bearing aqueous fluids during part of the history of the shear zone. At higher temperatures such fluids may have triggered local anatexis within the gneisses. At present there have been no suitable geochemical studies of a range of leucogranites from the shear zone to test this speculation. Nevertheless, the majority of leucogranite sheets have migrated within the shear zone. Consequently, the interpretation of emplacement modes for the leucogranite sheets must incorporate an ascent mechanism for the magma from an anatectic source, presumably at depth within the massif.

Although the later leucogranite sheets within the shear zone contain internal pegmatitic textures, other sheets experienced distributed crystal-plastic strains after full crystallization. Some sheets show both types of texture. This may be demonstrated where deformation fabrics in the host gneisses pass into the leucogranite sheets (Fig. 14c). In many of these cases, parts of the leucogranite contact are locally discordant, albeit at low angle, to the external foliation. The preferred interpretation is that these sheets were emplaced into gneisses that had already been partially deformed and that the subsequent shear strains were distributed heterogeneously. This type of polyphase history can be deduced from other outcrops in the shear zone (Fig. 14d). A sequence of deformation and leucogranite emplacement is demonstrated by concordant, highly sheared leucogranitic seams—now leucocratic gneisses, cross-cut by less strongly deformed sheets.

Discordant leucogranites (Fig. 14a) link between zones which have experienced later increments of shearing. They commonly terminate abruptly up and down into crystal-plastic shear fabrics with entrained portions of leucogranite. Macroscopically the entrained, concordant parts of these sheets appear to have experienced substantial shear strains post-crystallization. However, direct observation of these concordant zones suggests otherwise (Fig. 14b). Although these segments show macroscopic boudinage shapes, the internal form of the 'boudins' retains a coarse pegmatitic texture with no obvious crystal-plastic strains. In addition, there is fractionation between quartz and feldspar between the neck and body of the 'boudins' respectively. Consequently, it may be concluded that these concordant sheet remnants were disrupted before complete crystallization.

Other examples of leucogranite crystallization being affected by deformation can be found in

(a)

(b)

(c)

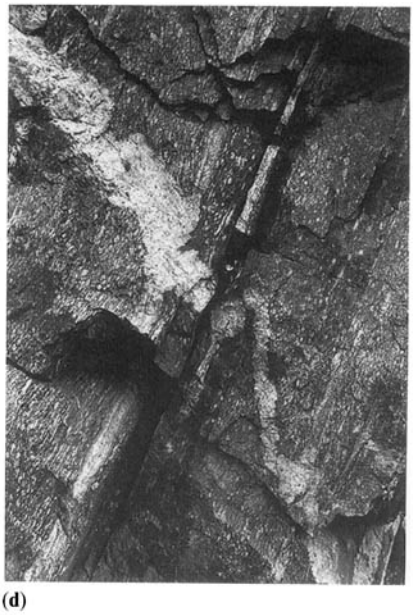

(d)

Fig. 14. Leucogranite emplacement in the hanging wall to the Liachar Thrust (sites A–D shown on Fig. 12b), all viewed looking SW. **(a)** Discordant pod of leucogranite cross-cutting deformed augen gneisses, visible outcrop height *c.* 25 m. **(b)** Pods of leucogranite—apparently boudinaged but with no internal deformation fabric. **(c)** Relationship between deformation fabrics within a sheared leucogranite and the host augen gneisses. Both show S–C fabrics with asymmetry indicative of top-to-NW overshear. **(d)** Field evidence for multiple generation of leucogranites within the shear zone. The view shows thin, highly sheared leucogranite seams, concordant to the foliation within the host augen gneisses, together with a weakly foliated and folded, generally discordant sheet.

hinge areas for those sheets that are folded. These commonly display a crude compositional banding, defined by coarse feldspars together with aligned muscovite and tourmaline. The feldspars are fractured along the length of the banding with intergrowths of quartz. This banding is generally concordant with that in the external gneisses and approximately axial planar to the fold. The conclusion reached is that deformation accompanied crystallization, with axial plane-parallel extension.

The emplacement of magma into an overthrust shear zone has been discussed by Hutton (1988; Hutton & Ingram 1992). He argues that magma may ascend within a thrust zone provided the magma body forces exceed those of the local

tectonics. In this context the magma pressure presumably must exceed the deviatoric stress in the shear zone. In this way, foliation-parallel feeders may open to allow ascent in sheets. Clearly these magmatic sheets will only be able to support very low shear stresses and thus might be expected to localize displacement within the shear zone while still below their critical melt fraction (i.e. 20–30% melt present, Hutton 1988). However, crystallization below the critical melt fraction will generate a much stronger material than the surrounding gneisses by virtue of the coarse-grained, feldspar-supported framework within these pegmatites. Geometric emplacement sites can be generated in downward steps in the shear zone, as strain localizes onto discrete shears, in essence creating tension gashes. However, the shapes of these tension gashes are likely to be complex because of the additional role of magma pressure.

The expectations of leucogranite emplacement processes and geometry discussed above can be tested against observations made in the shear zone. In this context a model is proposed, whereby much of the magma has been drained from an inclined sheet, presumably as magma pressure waned during the later stages of transport. At a late stage the existing feldspar frameworks acted as semi-rigid pods, with later crystallization of the residual quartz in the relative dilation sites of the boudin necks. Therefore, the pegmatitic textures and late-stage crystallization history of these leucogranite bodies were controlled by deformation processes.

In summary, leucogranite sheets within the shear zone represent a multiple history of small batch magma emplacement. These record a protracted history of emplacement during shearing. The detailed crystallization history of individual sheets can be strongly influenced by the concurrent deformation. The leucogranites themselves show that shear strain increments were accumulated in a spatially heterogeneous pattern within the shear zone.

Discussion

This study of field relationships in the vicinity of Raikhot Bridge demonstrates that this part of the margin of the Nanga Parbat massif is a composite structure (Fig. 15). Along the Indus valley there are preserved segments of an early tectonic contact between metabasic gneisses of the Kohistan arc and metasediments of the Nanga Parbat massif. Both of these units have a common array of linear and planar deformation fabrics. Shearing along this margin occurred under amphibolite facies conditions. However, although intense ductile strains are indicated by the parallelism between the hinge lines of intrafolial folds and mineral lineations within these rocks, there are no recognizably asymmetric shear sense indicators preserved. This may suggest significant transpositional strains, also under amphibolite facies conditions, developed during the early stages of syntaxis formation. Certainly this early contact is steeply dipping and the preserved linear fabrics plunge towards the SW, an atypical direction for the Pakistan Himalaya (e.g. Coward *et al.* 1988).

The modern structure of the study area is dominated by the Liachar Thrust Zone. The kinematics of this zone are simple—top-to-the-NW overthrusting, carrying the heart of the Nanga Parbat massif up relative to Kohistan. The thrust zone is marked by a band of cataclastic faults which carry a ductile shear zone in their collective hanging wall. Thus the Liachar Thrust Zone displays a similar structural evolution, as recorded by its hanging wall, as other neotectonic thrusts, such as the Alpine Fault in New Zealand (e.g. Sibson *et al.* 1979).

The datasets for mineral stretching lineations, which record deformation under conditions necessary for biotite stability (>450 °C), and fault striations (up to the Earth's surface) are remarkably consistent. These data support the original interpretation of Butler & Prior (1988*a*). However, in detail the localization of strain within the Liachar Thrust Zone is complex. The cataclastic deformation is not localized onto a single thrust break, as inferred by Butler & Prior (1988*a*). Rather, it is distributed onto several through-going faults which have individual displacements in excess of 1 km. Additional parts of the fault population include minor thrusts with displacements of metres and centimetres. This damage is apparently concentrated in rocks where the ductile deformation fabrics are steeply dipping. While there are faults within the domain of moderately dipping foliation at structurally higher levels, these structures appear to be less strongly developed. In part this may reflect difficulties in recognizing faults which are concordant to banding, but the individual fault zones that are recognized are generally much narrower than those seen in the steeply banded rocks. The asymmetric distribution of minor faults across the cataclastic Liachar Thrust Zone may reflect variations in the propensity for brittle fault localization, itself a possible consequence of asymmetric thermal structure. Certainly the hanging wall emplaces gneisses of the Nanga Parbat massif that have been hotter more recently than those to the NW (e.g. Zeitler 1985). The asymmetric distribution of cataclastic

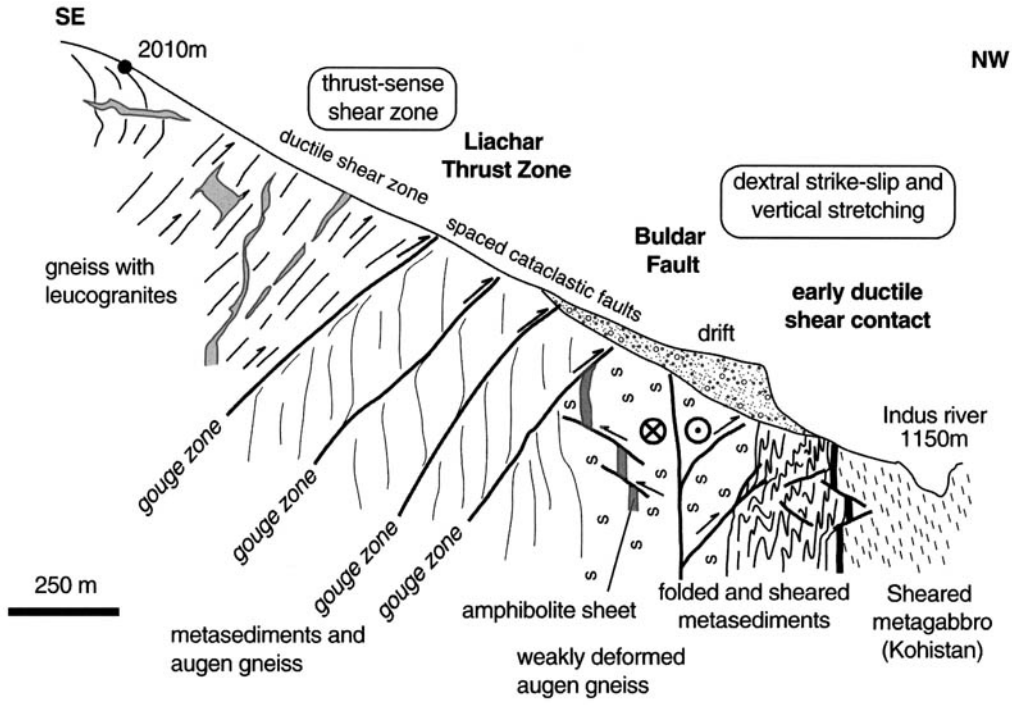

Fig. 15. Simplified cross-section through the margin of the Nanga Parbat massif at Raikhot Bridge (located on Fig. 1c). Note that localized fault displacements occur on a series of subparallel structures that collectively define the cataclastic Liachar Thrust Zone. Precursor ductile shear structures occur in the hanging wall to this zone. This brittle–ductile thrust zone overrides an early ductile shear contact between Nanga Parbat and Kohistan (termed here the Phuparash Shear Zone, a possible correlative of the Main Mantle Thrust) together with a complex dextral transpressive fault and shear population (including the dextral Buldar Fault).

faults across the structure may have a profound bearing on the network of fluid pathways within the massif, particularly for channelling the well-documented hydrothermal systems (e.g. Chamberlain *et al.* 1995).

A striking feature of the fault population below the main cataclastic breaks on the Liachar Thrust is its kinematic complexity. Minor thrusts dip both towards the NW and SE and collectively accommodate vertical stretching rather than an asymmetric overshear. In addition, there are important dextral strike-slip faults. The most prominent of these is termed the Buldar Fault. Comparative fault rock studies indicate that thrust and strike-slip faults were active contemporaneously. This conclusion is at odds with that of Butler *et al.* (1989) who proposed that the strike-slip faulting propagated into rock volumes that were previously involved in thrusting. Thus the bulk strain is of dextral transpression.

Dextral transpression is predicted by some models of syntaxis evolution in the NW Himalaya (e.g. Butler *et al.* 1989; Treloar *et al.* 1991; Seeber & Pêcher 1998). Critical to these models is the relative importance of NW–SE crustal shortening and strike-slip displacements. Both are difficult to quantify. However, qualitatively there are more dip-slip faults than strike-slip ones within the preliminary fault population presented here. There are no identifiable steep strike-slip faults within the moderately dipping shear zone above the cataclastic Liachar Thrust Zone. This composite thrust seems to be far more important than the Buldar Fault and related structures when assessed for fault zone width. Of course such proxies for displacement are very dangerous when applied to high strain zones.

The picture from the distributed ductile structures presents a kinematically clearer picture. There is little evidence for strike-slip or significant oblique-slip shear within any structures moving away from Kohistan. The kinematics are simply of dip-slip shear in both the steeply dipping augen orthogneisses and in the moderately dipping gneisses above. On the scale of the syntaxis, however, strike-slip displacements may have been partitioned into other

rock volumes. Critically this may include levels now exposed in Kohistan, to the NW of the Raikhot Bridge study area. Within the Nanga Parbat massif, many of the gneisses display near strike-parallel mineral lineations, for example along the Astor gorge (Fig. 1; Butler *et al.* 2000). The age of these structures is difficult to establish and consequently an extensive review of structure, kinematics and correlations within the massif lies beyond the scope of this contribution.

Leucogranites were emplaced into the active ductile shear zone of the Liachar Thrust. These sheets show a range of deformation states and internal fabrics. In general these intrusives were emplaced into tectonically controlled sites, in essence tension gashes, so that they record the asymmetric top-to-the-NW kinematics of the host shear zone. The majority, if not all, of these leucogranites have migrated in the shear zone. Collapsed feeder conduits may be identified, generally parallel to the main banding and shear fabrics. The fluctuations in magma pressure required to generate these features, together with possible tectonic controls of fractional crystallization and differentiation of granitic fluids, are the subject of ongoing study. It remains unknown how tectonics may have influenced the emplacement of granite sheets in other parts of the massif. These intrusives offer great potential for tracking strain increments during syntaxis construction.

The final comments are concerned with nomenclature and structural correlation away from the Raikhot Bridge study area. The principal conclusion is that the edge of the Nanga Parbat massif is a composite structure. There are two types of approach to these problems of structure and nomenclature. One is to give the structure a single name and imply a long and complex kinematic history on the fault. In this context, the tectonic break that separates Kohistan from Nanga Parbat along the western margin of the massif could be named as the Main Mantle Thrust (e.g. Tahirkheli & Jan 1979), the Raikhot Fault (Madin *et al.* 1989; Seeber & Pêcher 1998) or a composite name (e.g. the Raikhot–Sassi Fault Zone of Treloar *et al.* 1991). However, this simple approach obscures the true nature of this contact and its composite history. Furthermore, the individual components of the marginal structure, namely the early ductile shear zone and the various later structures, have different orientations and consequently will not coincide at other structural levels. It is inappropriate to describe these structural relationships as reactivation or to infer longevity of structure at this site. Spatial coincidence between structures at an individual site or in a single two-dimensional projection (e.g. a map) can equally be explained by structural truncation—reactivation is a three-dimensional phenomenon. Consequently, the approach adopted here is to isolate and characterize the different structures that define the western margin, giving each a distinct name.

The early ductile contact between Kohistan and rocks of the Nanga Parbat massif, exposed near the Indus river at Raikhot Bridge, has been explicitly named as part of the Main Mantle Thrust by Butler & Prior (1988*b*). However, they point out that the structure cannot be the original suture between the terrains because the lower part of the Kohistan arc was cut out. Furthermore, the shear zone involves and deforms a suite of granites in the Kohistan arc. These Parri and Confluence sheets (George *et al.* 1993) are dated at *c.* 25 Ma, so the shear zone was active at or after this time. In contrast, the Main Mantle Thrust in its type area near Swat (Fig. 1) must have been active much earlier, given the peak metamorphic and cooling ages in its footwall (Treloar & Rex 1990; Smith *et al.* 1994). Consequently, the local term 'Phuparash Shear Zone' (named after the best exposed section through an early contact between Kohistan and Nanga Parbat rocks; Butler *et al.* 1992) is suggested here to denote the high strain, amphibolite facies, ductile shear contact between Kohistan and Indian continental crust at the Nanga Parbat massif. This correlates with the 'MMT' of Butler & Prior (1988a) and a similar structure on the eastern margin of the massif (Argles, this volume; Butler *et al.* this volume). The correlation of this with other ductile shear contacts, including that at the type area for the Main Mantle Thrust remains to be established.

The composite nature of structural evolution at Raikhot Bridge raises general problems for tectonic investigation. The different structures record distinct kinematics at different times and strain appears partitioned, particularly during the later stages. Consequently, great care is needed when using local kinematic studies to test large-scale models of crustal deformation in the Himalayas.

Fieldwork at Nanga Parbat over the past twelve years has been funded by grants from the Royal Society and NERC. During this time I have benefited from discussions, in and out of the field with the following: Andy Barnicoat, Mike Coward, Mark George, Nigel Harris, Rob Knipe, Dave Prior, Peter Treloar, John Wheeler and Alan Whittington. All are thanked, together with Peter Treloar and Tom Argles for vigorous reviews, although the views expressed in this paper are those of the author.

References

ARGLES, T. W. 2000. The evolution of the Main Mantle Thrust in the western syntaxis, N. Pakistan. *This volume*.

BECK, R. A., BURBANK, D. W., SERCOMBE, W. J., RILEY, G. W., BARNDT, J. K. *et al.* 1995. Stratigraphic evidence for an early collision between northwest India and Asia. *Nature*, **373**, 55–58.

BUTLER, R. W. H. & PRIOR, D. J. 1988a. Tectonic controls on the uplift of Nanga Parbat, Pakistan Himalayas. *Nature*, **333**, 247–250.

—— & —— 1988*b*. Anatomy of a continental subduction zone: the Main Mantle Thrust in northern Pakistan. *Geologisches Rundschau*, **77**, 239–255.

——, —— & OWEN, L. A. 1988. Flashfloods, earthquakes and uplift in the Pakistan Himalayas. *Geology Today*, **4**, 197–201.

——, —— & KNIPE, R. J. 1989. Neotectonics of the Nanga Parbat syntaxis, Pakistan, and crustal stacking in the northwest Himalayas. *Earth and Planetary Science Letters*, **94**, 329–343.

——, GEORGE, M., HARRIS, N. B. W., JONES, C., PRIOR, D. J., TRELOAR, P. J. & WHEELER, J. 1992. Geology of the northern part of the Nanga Parbat massif, northern Pakistan, and its implications for Himalayan tectonics. *Journal of the Geological Society, London*, **149**, 557–567.

——, HARRIS, N. B. W. & WHITTINGTON, A. G. 1997. Interactions between deformation, magmatism and hydrothermal activity during active crustal thickening: a field example from Nanga Parbat, Pakistan Himalayas. *Mineralogical Magazine*, **61**, 37–52.

——, WHEELER, J., TRELOAR, P. J. & JONES, C. 2000. Geological structure of the southern part of the Nanga Parbat massif, Pakistan Himalaya, and its tectonic implications. *This volume*.

CHAMBERLAIN, C. P., ZEITLER, P. K., BARNETT, D. E., WINSLOW, D., POULSON, S. R., LEAHY, T. & HAMMER, J. E. 1995. Active hydrothermal systems during the recent uplift of Nanga Parbat, Pakistan Himalaya. *Journal of Geophysical Research*, **100**, 439–453.

COWARD, M. P., JAN, M. Q., REX, D. C., TARNEY, J., THIRWALL, M. & WINDLEY, B. F. 1982. Structural evolution of a crustal section in the western Himalayas. *Nature*, **295**, 22–24.

——, BUTLER, R. W. H., CHAMBERS, A. F., GRAHAM, R. H., IZATT, C. N. *et al.* 1988. Folding and imbrication of the Indian crust during Himalayan collision. *Philosophical Transactions of the Royal Society, London*, **A326**, 89–116.

——, WINDLEY, B. F., BROUGHTON, R. D., LUFF, I. W., PETTERSON, M. G. *et al.* 1986. Collision tectonics in the NW Himalayas. *In*: COWARD, M. P. & RIES, A. C. (eds) *Collision Tectonics*. Geological Society, London, Special Publications, **19**, 203–219.

DIPIETRO, J. A., POGUE, K. R., LAWRENCE, R. D., BAIG, M. S., HUSSAIN, A. & AHMAD, I. 1993. Stratigraphy south of the Main Mantle Thrust, Lower Swat, Pakistan. *In*: TRELOAR, P. J. & SEARLE, M. P. (eds) *Himalayan Tectonics*. Geological Society, London, Special Publications, **74**, 207–220.

GEORGE, M. T., HARRIS, N. B. W. & BUTLER, R. W. H. 1993. The tectonic implications of contrasting granite magmatism between the Kohistan island arc and the Nanga Parbat-Haramosh Massif, Pakistan Himalaya. *In*: TRELOAR, P. J. & SEARLE, M. P. (eds) *Himalayan Tectonics*. Geological Society, London, Special Publications, **74**, 173–191.

HUTTON, D. H. W. 1988. Granite emplacement mechanisms and tectonic controls: inferences from deformation studies. *Transactions of the Royal Society of Edinburgh, Earth Sciences*, **79**, 615–631.

—— & INGRAM, G. M. 1992. The Great Tonalite Sill of southeastern Alaska and British Columbia: emplacement into an active contractional high angle reverse shear zone. *Transactions of the Royal Society of Edinburgh, Earth Sciences*, **83**, 383–386.

LAWRENCE, R. D. & GHAURI, A. A. K. 1983. Evidence for active faulting in Chilas District, N. Pakistan. *University of Peshawar Geological Bulletin*, **10**, 185–186.

MADIN, I. P., LAWRENCE, R. D. & UR-REHMAN, S. 1989. The northwest Nanga Parbat–Haramosh massif: evidence for crustal uplift at the northwestern corner of the Indian craton. *In*: MALINCONICO, L. L. & LILLIE, R. J. (eds) *Tectonics of the Western Himalaya*. Geological Society of America Special Paper, **232**, 169–182.

MISCH, P. 1949. Metasomatic granitisation of batholithic dimensions. *American Journal of Science*, **247**, 209–249.

OWEN, L. A. 1989. Neotectonics and glacial deformation in the Karakoram Mountains and Nanga Parbat Himalaya. *Tectonophysics*, **163**, 227–265.

SEEBER, L. & PĒCHER, A. 1998. Strain partitioning along the Himalayan arc and the Nanga Parbat antiform. *Geology*, **26**, 791–794.

SHRODER, J. F., KHAN, A. S., LAWRENCE, R. D., MADIN, I. P. & HIGGINS, S. M. 1989. Quaternary glacial chronology and neotectonics in the Himalaya of north Pakistan. *In*: Geological Society of America Special Paper, **232**, 275–294.

SIBSON, R. H., WHITE, S. H. & ATKINSON, B. K. 1979. Fault rock distribution within the Alpine Fault Zone: a preliminary account. *Bulletin of the Royal Society of New Zealand*, **18**, 55–65.

SMITH, H. A., CHAMBERLAIN, C. P. & ZEITLER, P. K. 1992. Documentation of Neogene regional metamorphism in the Himalayas of Pakistan using U–Pb in monazite. *Earth and Planetary Science Letters*, **113**, 93–105.

——, —— & —— 1994. Timing and duration of Himalayan metamorphism within the Indian plate, northwest Himalaya, Pakistan. *Journal of Geology*, **102**, 493–508.

TAHIRKHELI, R. A. K. & JAN, M. Q. 1979. Geology of Kohistan, Karakoram Himalaya, northern Pakistan. *University of Peshawar Geological Bulletin Special Issue*, **13**, 1–187.

TRELOAR, P. J. & REX, D. C. 1990. Post-metamorphic cooling history of the Indian plate crystalline

thrust stack, Pakistan Himalaya. *Journal of the Geological Society, London*, **147**, 735–738.

——, PETTERSON, M. G., JAN, M. Q. & SULLIVAN, M. A. 1996. A re-evaluation of the stratigraphy and evolution of the Kohistan arc sequence, Pakistan Himalaya: implications for magmatic and tectonic arc-building processes. *Journal of the Geological Society, London*, **153**, 681–693.

——, POTTS, G. J., WHEELER, J. & REX, D. C. 1991. Structural evolution and asymmetric uplift of the Nanga Parbat syntaxis, Pakistan Himalayas. *Geologisches Rundschau*, **80**, 411–428.

——, GEORGE, M. T. & WHITTINGTON, A. G. 2000. Mafic sheets from Indian plate gneisses in the Nanga Parbat syntaxis: their significance in dating crustal growth and metamorphic and deformation events. *This volume*.

WADIA, D. N. 1933. Note on the geology of Nanga Parbat (Mt. Diamir) and adjoining portions of Chilas, Gilgit District, Kashmir. *Records of the Geological Survey of India*, **66**, 212–234 (and enclosed maps and sections).

WHEELER, J., TRELOAR, P. J. & POTTS, G. J. 1995. Structural and metamorphic exolution of the Nanga Parbat syntaxis, Pakistan Himalayas, on the Indus gorge transect: the importance of early events. *Geological Journal*, **30**, 349–371.

WHITTINGTON, A. 1996. Exhumation overrated at Nanga Parbat, northern Pakistan. *Tectonophysics*, **260**, 215–226.

——, HARRIS, N. B. W. & BUTLER, R. W. H. 1999. Contrasting anatectic styles at Nanga Parbat, northern Pakistan. *In*: MACFARLANE, A., SORKHABI, R. & QUADE, J. (eds) *Himalaya and Tibet: Mountain roots to mountain tops*. Geological Society of America Special Paper, **328**, 129–144.

ZEITLER, P. K. 1985. Cooling history of the NW Himalaya, Pakistan. *Tectonics*, **4**, 127–151.

This page intentionally left blank

Tectonics of the SW margin of the Nanga Parbat–Haramosh massif

M. A. EDWARDS[1,2,5], W. S. F. KIDD[1], M. A. KHAN[3] & D. A. SCHNEIDER[4]

[1]*Department of Earth & Atmospheric Sciences, State University of New York at Albany, 1400 Washington Avenue, Albany, NY 12222, USA*

[2]*Institut für Geologie, Universität Würzburg, Pleicherwall 1, D-97070 Würzburg, Germany*

[3]*National Centre for Excellence in Geology, University of Peshawar, Peshawar, Pakistan*

[4]*Department of Earth and Environmental Sciences, Lehigh University, 31 Williams Drive, Bethlehem, PA 18015, USA*

[5]*Present address: Asian Tectonics Research Unit, Institut für Geologie, TU-Bergakademie Freiburg, Bernhard v-Cotta Strasse 2, D-09596 Freiburg, Germany (e-mail: edwards@geo.tu.freiburg.de)*

Abstract: We present an analysis of the tectonic evolution of the southwestern portions of the Nanga Parbat massif, Pakistan Himalaya, based upon detailed mapping and structural analyses from the Bunar, Biji, Diamir, Airl, Niat and SW Rupal valleys. Mainly metasedimentary cover rocks of the Indian plate are divided into upper and lower cover. There is a marked structural thinning of the cover in the main Bunar valley from south to north, and this is attributed to a major frontal ramp in the original Main Mantle Thrust (MMT). A hitherto unmapped shear zone, the Diamir Shear Zone, is identified, that is associated with a syn-kinematically intruded belt of granitic rocks, the Jalhari Granite. The shear zone is a several kilometre thick, generally W-vergent, ductile to brittle shear zone that is associated with local overturning of the entire MMT section, typified by the Gashit Fold. $^{40}Ar/^{39}Ar$ cooling ages from across the area indicate a steep cooling age gradient across the Diamir Shear Zone from >40 to <5 Ma. The Diamir Shear Zone is mechanically linked to part of the Raikhot Fault System and, together, they are seen to be a crustal-scale reverse fault that has allowed relative uplift and overthrusting of the core of Nanga Parbat.

The Nanga Parbat–Haramosh massif (NPHM) is of considerable interest in the investigation of the India–Asia collision, and collisional tectonics at large. There are a number of salient features of the NPHM worth noting.

(1) It coincides with the NW terminus of the >2500 km Himalayan arc—the western 'syntaxis' of Wadia (1931, 1932).
(2) It forms an anomalous spur (Fig. 1) of Himalayan rock that has resulted from high-grade Indian plate basement gneisses being exhumed from beneath the structurally overlying cover rocks of the upper Indian plate, that are in turn juxtaposed beneath the fossil island arc Kohistan–Ladakh series (KLS), by the Main Mantle Thrust (MMT—Tahirkheli & Jan 1979; Bard *et al.* 1980; Tahirkheli 1982; Bard 1983).
(3) This exhumation is due to crustal-scale antiformal folding (Gansser 1964; Coward 1985) that occurs in the form of both NNE-trending axes of folding recognized within the generally W–E trending Indus Gorge (Madin 1986; Madin *et al.* 1989; Treloar *et al.* 1991; Butler *et al.* 1992; Wheeler *et al.* 1995), and as a pair of antiformal folds in the Astor River Gorge—the Burdish Ridge and Dichil antiforms, in the west and east, respectively (Edwards 1998; Schneider *et al.* 1999*a*).
(4) It is composed of Indian plate crystalline rock that seems to be reworked Proterozoic crust (Chamberlain *et al.* 1989; Smith *et al.* 1992; Schneider *et al.* 1997, 1999*b*; Zeitler *et al.* 1989), a feature presently unreported from studies of the Himalayan crystalline slab outside of the NW Himalaya.
(5) It represents an area of exceedingly young (*c.* 0.9 to >9.0 Ma) plutonism, metamorphism and cooling (Zeitler *et al.* 1982, 1989,

From: KHAN, M. A., TRELOAR, P. J., SEARLE, M. P. & JAN, M. Q. (eds) *Tectonics of the Nanga Parbat Syntaxis and the Western Himalaya*. Geological Society, London, Special Publications, **170**, 77–100. 1-86239-061-4/00/$15.00

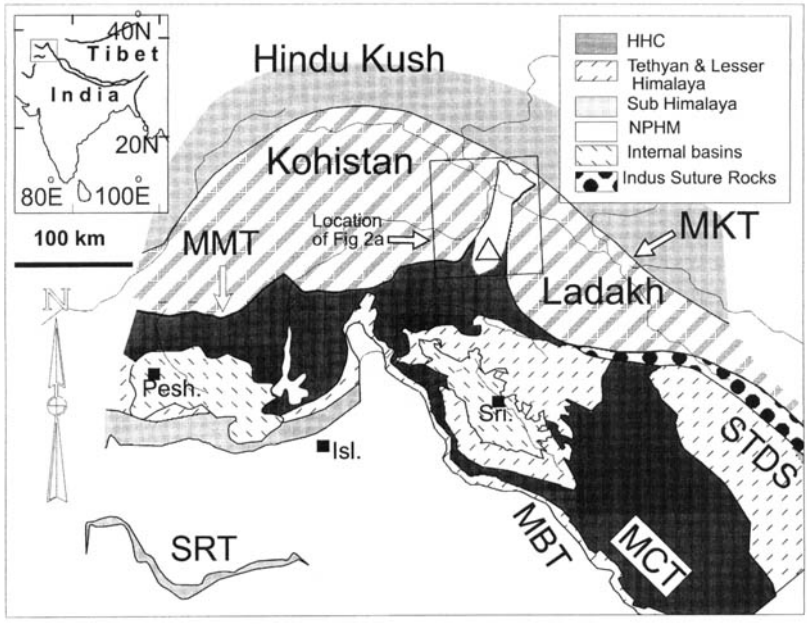

Fig. 1. Regional map of the northwest Himalaya. MKT, Main Karakoram Thrust; MMT, Main Mantle Thrust; SRT, Salt Range Thrust; STDS, Southern Tibet Detachment System (section shown is Zanskar Shear Zone); MCT, Main Central Thrust; MBT, Main Boundary Thrust; NPHM, Nanga Parbat–Haramosh massif (western Himalayan syntaxis); Pesh, Peshawar; Isl, Islamabad; Sri, Srinigar. Regional location of area is identified by box in northwestern part of 'India–Tibet' map shown in inset. Compiled from our own published and unpublished observations and Gansser 1964; Coward *et al.* 1988; Greco & Spencer 1993.

1993; Zeitler 1985; Chamberlain *et al.* 1989; Treloar *et al.* 1991; Zeitler & Chamberlain 1991; Smith *et al.* 1992; George *et al.* 1993, 1995; Winslow *et al.* 1994, 1995, 1996; George & Bartlett 1996; Whittington 1996; Schneider *et al.* 1997, 1999*a*, *b*).

(6) These young events seem to require exhumation of up to 5–10 mm a^{-1} (Craw *et al.* 1994), and hence require tens of kilometres of rock to have been removed from the NPHM in the last few million years.

Identification of the geological structures that are associated with this extremely young exhumation/unroofing and uplift of the NPHM was undertaken by us as part of the multi-disciplinary Nanga Parbat Continental Dynamics project. In addition to lithological and structural mapping and general structural analyses, one of our key objectives was to examine which major structures have accommodated large displacements of rock related to (1) differential exhumation between the inner and outer portions of the massif, and (2) tectonic exhumation of the massif by low-angle normal fault/detachment-type mechanisms. This contribution presents results for the southwestern portion of the NPHM.

Geological background of the SW region of the NPHM

The principal hitherto-recognized feature that is relevant to tectonic investigation in the SW region of the NPHM is the Raikhot Fault. The Raikhot Fault (Madin 1986; Butler & Prior 1988; Madin *et al.* 1989; Butler *et al.* 1989) is a zone of shear structures that forms much of the western margin (KLS–NPHM contact) of the northern and central portions of the NPHM. A portion of the Raikhot Fault Zone cuts away the Main Mantle Thrust at the large bend in the Indus River near Raikhot Bridge (Fig. 2). In this area, the significant displacement sense associated with the fault zone (a strong SE-plunging lineation) is consistent with the NPHM moving upwards with respect to Kohistan, and much of the original linear fabric related to the MMT appears to have been reworked or obliterated. Because the hanging wall is dominated by high-grade rocks that are common to the core of the NPHM and cooling gradients across the Raikhot are extremely steep (Zeitler 1985; George *et al.* 1995), it is generally agreed that the Raikhot Fault is locally the focus for a large portion of the displacement of the NPHM summit region that has continued

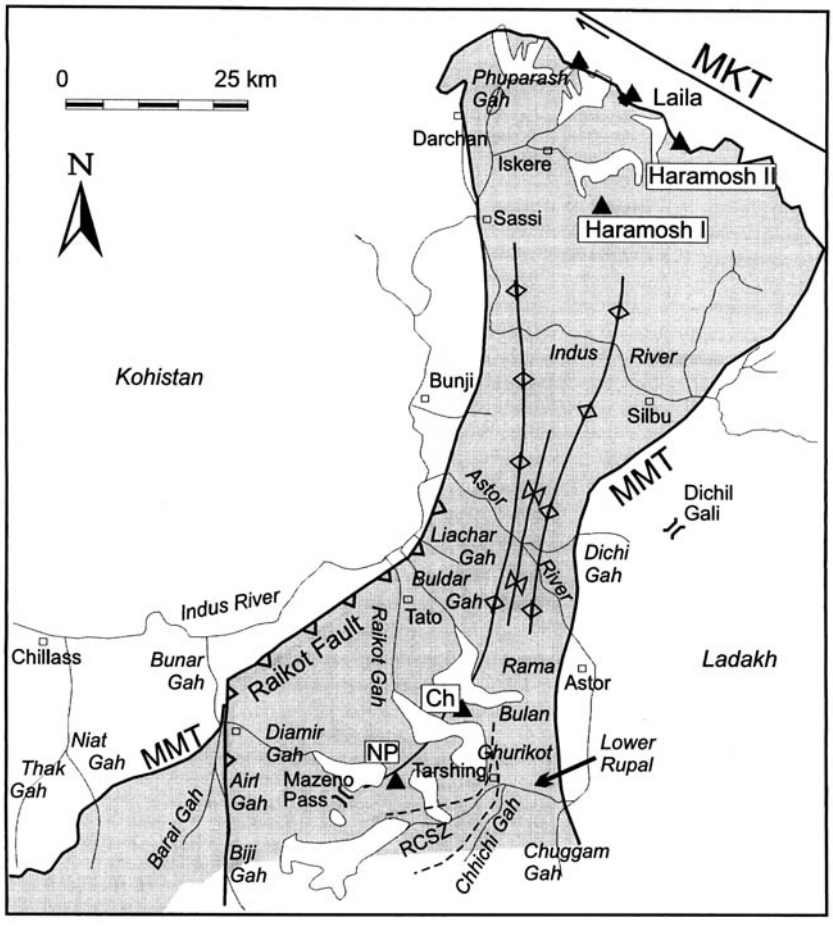

Fig. 2. Overview map of the NPHM. selected valleys and towns shown. Grey, undifferentiated Indian rocks; white, undifferentiated KLS rocks or (north of MKT) undifferentiated Karakoram Terrane. Names in white boxes beside black triangles are major peaks: NP, Nanga Parbat; Ch, Chongra Northern Peak; MKT, Main Karakoram Thrust. MMT, Main Mantle Thrust. RCSZ, Rupal–Chichi Shear Zone (dashed lines are approximate margin locations). Names of valleys/rivers are in italics. Heavy lines with barbs are reverse faults; paired barbs represent (W–E) Burdish Ridge Antiform, Dashkin Synform and Dichil Antiform, respectively. Open squares and villages. Map sources: Kidd, Edwards, Asif Khan, unpublished data; Madin 1986; Madin *et al.* 1989; Treloar *et al.* 1991; Lemmenicier *et al.* 1996; Pêcher & Le Fort 1998.

for the last few Ma until the present day. The nature, if any, of the Raikhot Fault to the south and southwest is not clear as very little of the area west of Raikhot Bridge has been described. Within and west of Bunar Gah, the MMT is present, in its common form, as the KLS/Indian plate contact (Ahmed & Chaudhry 1976; Ghazanfar *et al.* 1991; Khan *et al.* 1998; this study) and it is not removed, nor is the fabric extensively transposed, by the Raikhot Fault, or any other fault. Between Bunar Gah and Raikhot Bridge, therefore, the Raikhot Fault, or some mechanical equivalent that is associated with large cooling age gradients between the inner and outer portion of the massif, must cut structurally downward into the Indian plate, and the surface trace must accordingly fork off from the Kohistan margin towards the SSW. The MMT west of the NPHM is described in general by Ahmed & Chaudhry (1976), Ghazanfar *et al.* (1991), Khan *et al.* (1998), and DiPietro *et al.* (2000), as part of the general descriptions of the Kohistan terrane in the area. However, the only information hitherto available for the rocks of the Indian plate immediately southwest of the summit regions of the NPHM are from Hubbard *et al.* (1995), some of whose descriptions and interpretations have been questioned by Burg

et al. (1996). We incorporate local portions of, and where necessary re-interpret, the data presented in Hubbard *et al.* (1995) in light of our new mapping.

General geological observations

Our investigations southwest of Nanga Parbat were conducted (Figs 3 & 4) in two areas: (1) the N–S trending Bunar Gah, and Biji Gah (the direct southern continuation of Bunar Gah), and the eastern tributaries of Jalhari Gah (forking off at the village of Phailobat), Diamir Gah (WNW–ESE trending), and Airl Gah (*c.* W–E trending), as well as the lower (eastern) portion of Nashkin Gah (a W–E trending tributary to Barai Gah); and (2) the Niat valley. The Diamir Gah and the Nashkin and Airl Gah valleys all provide excellent sections that cut through at a high angle to foliation.

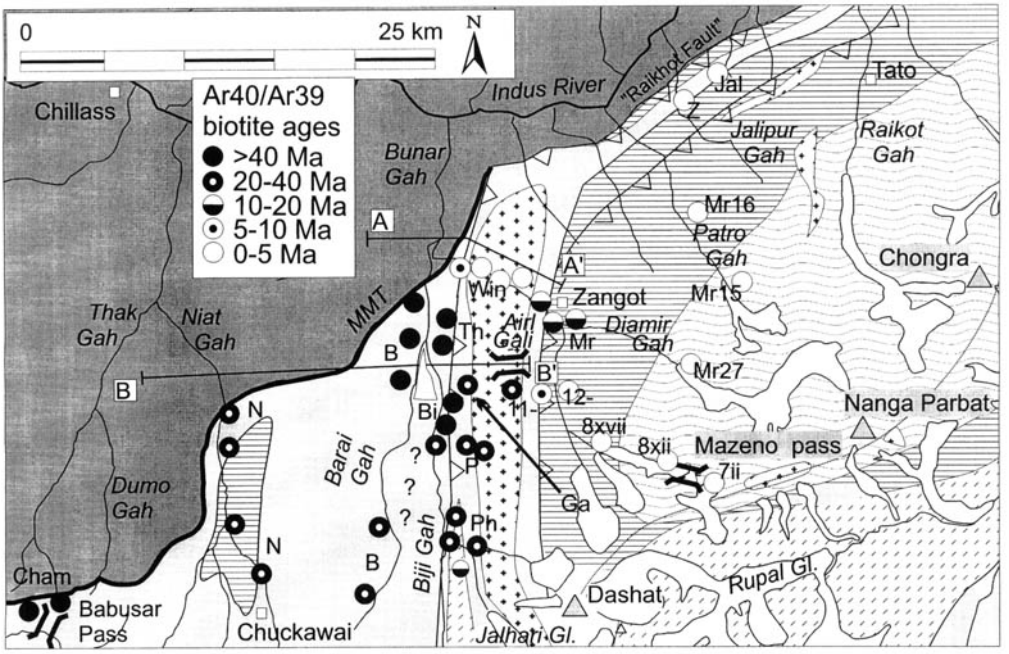

(a)

Fig. 3. (**a**) Geological and thermochronological map of SW NPHM. Dark grey, undifferentiated Karakoram Terrane; light grey, undifferentiated Indian cover rocks; horizontal line ornament, undifferentiated Indian basement rocks; undulating parallel line ornament in NP summit region, approximate location of basement in which cordierite is present (NE boundary from Chamberlain, unpublished data); white with oblique dash, undifferentiated augen gneiss; plus pattern, granite or deformed granite. A–A', B–B', locations of the Diamir and Niat–Nashkin–Airl, respectively, composite cross-sections presented in (b). Barbed black lines are general margins of large brittle and ductile shear zones with reverse sense displacement (Diamir Shear Zone is marked by Jalhari Granite). Thick black line is the Main Mantle Thrust. Grey triangles are high peaks (labelled); white squares are villages/towns. Names of valleys, glaciers (Gl.) and rivers are in italics; sites are in normal script. Variably shaded dots are sample localities for Ar/Ar analyses, divided into five age brackets (see legend). Adjacent normal script single letter or pairs identify individual or groups of dots fully corresponding to those detailed in Table 1 (except: '11' is 11-vii in Table 1; group '12-' is 12-i and 12-iv in Table 1; group 'Win' is group of four bt Ar/Ar [from W to E 5.7, 2.9, 2.0, 1.4 Ma] reported in Winslow *et al.* 1996; group 'Cham' is 22–25 Ma Ar/Ar from Indian rocks near Babusar Pass reported in Chamberlain *et al.* 1991). Area of white at Biji/Barai confluence is Manogoush gneiss, question marks to the south hint at uncertainty of extent of Manogoush gneiss (see Fig. 4 and text for discussion). (**b**) Cross-sections along the Diamir section [A–A'] and the Niat–Nashkin–Airl composite section [B–B']. Horizontal scale in kilometres, vertical scale in feet. No vertical exaggeration. Shading/ornament as employed in (a). Plus/dot symbols in circles respectively represent 'tail' and 'head' of arrow, indicating that, on the MMT, the hanging wall ('Kohistan') has moved outward (with respect to the plane of view) while the footwall ('India') has moved inward. Note overturning of metasedimentary cover rocks in MMT footwall in response to NPHM uplift-related west-vergent overthrusting. The Diamir Shear Zone (DSZ) is primarily located in the Jalhari Granite, emplaced syn-kinematically. Area of white in valley ridge (Manogoush Ridge) is outcrop of Manogoush gneiss, question mark below hints at uncertainty of extent of gneiss (see Fig. 4 and text for discussion).

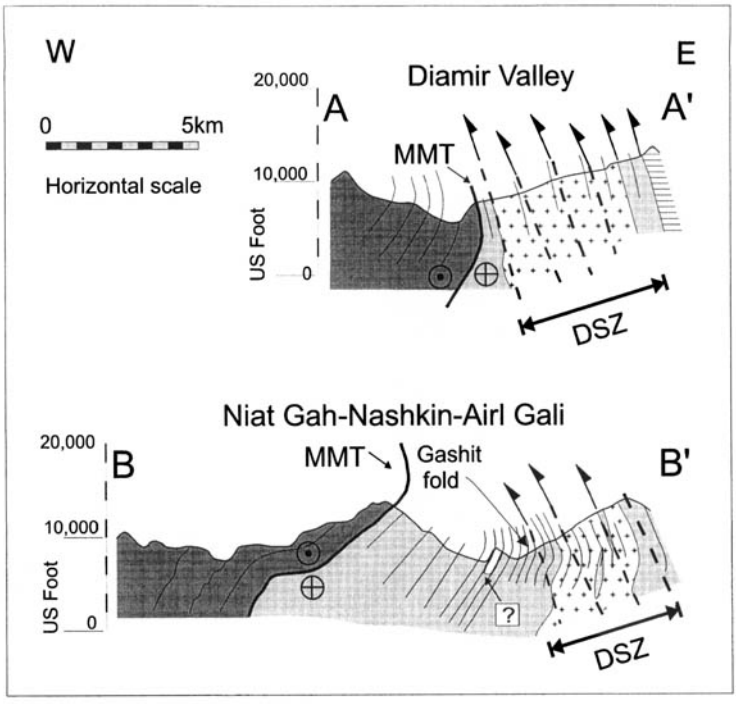

(b)

In addition to reports from the two main drainage areas of Bunar and Niat, we present a summary of observations from the westernmost Rupal valley, in an examination of regional continuity of the observed structural and lithological trends. As will be seen, the geology and structures of the uppermost Rupal valley become fundamental for accurate characterization of the geology of the SW region of the NPHM.

Main Mantle Thrust hanging wall rocks

In Bunar Gah and in Niat Gah (Fig. 4), we have clearly identified and mapped the MMT. Throughout both areas, the contact between the dark mafic rocks of the KLS and the paler Indian plate rocks is clear and highly recognizable (Fig. 4). The MMT in Bunar Gah outcrops near the confluence of Diamir Gah where the contact is clearly visible on each side of the valley, and can be followed all the way to the >4000 m ridge above the western wall of Bunar/Barai Gah (Fig. 5). In Niat Gah we again visited the MMT in outcrop. A strong contrast in spectral character on Thematic Mapper (TM) satellite imagery allows us to interpolate confidently the surface trace of the MMT over ridge tops between the areas where we have mapped it in the valleys.

Rocks of the Kohistan arc are well exposed in the northern portions of the Bunar and Niat/Thak valleys, and include both the Chilas Complex and the Niat Amphibolite. The two units are easily distinguishable; the Chilas Complex comprises medium to coarse-grained gabbronorites, anorthosites, dunites and peridotites (in order of decreasing abundance), while the Niat Amphibolites (which outcrop to the south of the Chilas Complex) are fine-grained, foliated and banded metabasalts. Rocks of the ultramafic–mafic–anorthosite association of the Chilas Complex (Khan *et al.* 1998), characterized by common graded layering and cross-layering, crop out at the mouth of Bunar Gah valley. Immediately south, these are replaced by homogeneous gabbronorites similar to those forming the bulk of the Chilas Complex elsewhere. Foliation of these rocks in both Bunar Gah and Niat Gah is orientated *c.* E–W, and dips moderately north. Further south, the gabbronorites are deformed, forming foliated but lithologically homogeneous amphibolites which are often garnetiferous. These strongly foliated amphibolites are occasionally mylonitic in appearance, with fabrics that dip moderately north in Thak–Niat but steeply to the SE in Bunar Gah. The foliated amphibolites have a sharp tectonic contact with the underlying Niat Amphibolites.

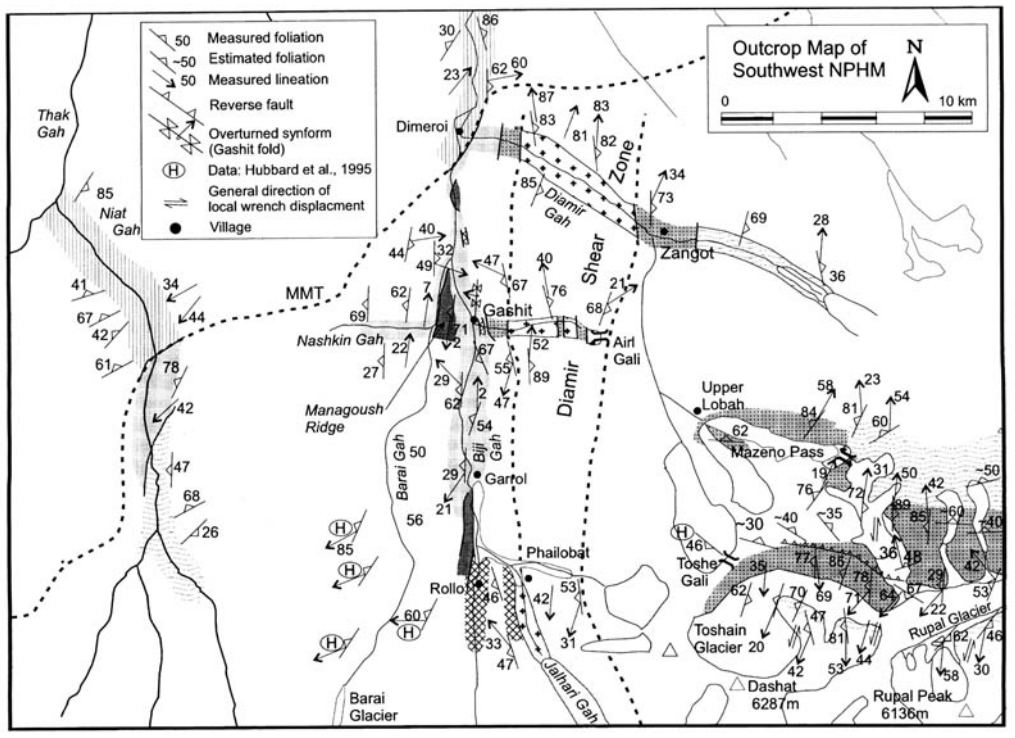

Fig. 4. Outcrop map of SW NPHM showing outcrops that were visited and examined. Dark grey, lath unit; basket-hatch ornament, porphyroclastic orthogneiss; light grey, upper cover; horizontal line ornament, undifferentiated Indian basement rocks; plus pattern, granite or deformed granite; dots with grey background, lower cover; white, glacial moraine (or glaciers where at river heads). Heavy dashed black lines are remote field and TM interpolation of field-constrained boundaries. Belt of Jalhari Granite runs from Diamir Gah to Jalhari Gah; DSZ coincides approximately with margins of Jalhari belt. Note trends in foliation and lineation are highly consistent from western Rupal valley across Toshe Gali (anomalous measurement marked with H is from Hubbard *et al.* 1995; location and orientation of all the Hubbard *et al.* (1995) measurements has only been estimable through visual inspection. Higher in the massif region on the northern side of Rupal valley, however, there is a notable variation (see full discussion in text).

Khan *et al.* (1998) described a 50–60 m wide shear zone marking this contact in Niat–Thak, and in Thor Gah, a valley further to the west. The Niat Amphibolites are fine to medium grained and metabasaltic, and frequently foliated to massive and have a banded appearance due to (1) small-scale feldspathic bands, that probably mimic original volcaniclastic–lava banding and/or are a product of metamorphic segregation, and (2) common veins and dykes of granitic and trondhjemitic composition. The Niat Amphibolites record epidote–amphibolite facies with rare garnet. Garnet is common in the leucogranite–trondhjemite veins and dykes, is primary, and together with common muscovite, identifies their peraluminous nature. Khan *et al.* (1998) suggest that at least some of these trondhjemites are the product of partial melting of the Kohistan terrane basal crust.

For the Niat Amphibolites there is also a significant difference in orientation of foliation between Niat Gah and Bunar Gah. The principal (stretching) lineation in Niat Gah generally plunges subhorizontally to moderately towards the SSW. The main layering is steeply NW dipping (Niat–Nashkin–Airl composite section [B–B′] in Fig. 3b), and is observed to be only locally overturned (on a scale of tens of metres) to become steeply SE dipping. (NB we use the term overturned with respect to the tectonostratigraphic section that forms the MMT foot- and hanging walls, where the original regional orientation of the MMT and the main fabric is NNW dipping.) About midway between the confluence of Thak Gah and Niat Gah, and the MMT, over a few km structural thickness, there is a decrease in the foliation dip. In Bunar Gah, however, the main layering dips steeply ESE, and

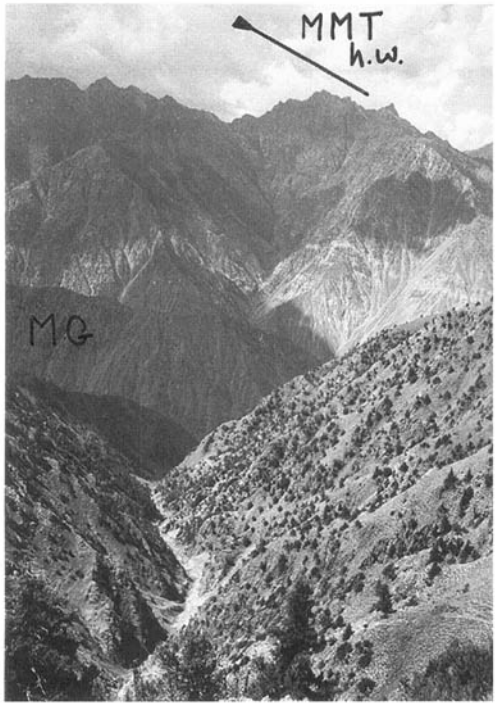

Fig. 5. Looking west from Airl Gali pass. Included in field of view is: (1) Airl Gah valley (foreground) where >5 km of structural thickness of Jalhari Granite is represented (Gashit Fold [Fig. 7] at foot of gully outcrops immediately beyond where gully turns out of field of view), (2) Manogoush Ridge (labelled: 'MG') where a belt of porphyroclastic gneiss is present, (3) Nashkin valley, where *c.* 2600 m of vertical relief, and >8 km of cover sequence is exposed, and (4) dark rocks of Kamila amphibolite that mark the MMT hanging wall at very top of furthest ridge.

the lineation is steeply S to SE plunging. There is thus a change in orientation of the main foliation of the KLS rocks throughout Bunar Gah; dips steepen to become vertical and then are overturned on a large (kilometres) scale, illustrated on the Diamir section [A–A′] of Fig. 3b (also Figs 4, 5 & 6). The overturning in Bunar Gah includes the MMT and much of the footwall Indian plate rocks discussed below. Nowhere are the Niat Amphibolites structurally overturned on a large scale and, hence, neither is the MMT in this area.

Indian plate cover rocks

Indian plate lithologies are exposed south of the MMT (Fig. 4). In Niat Gah, Indian plate rocks are exposed along much of the valley, although glacial till and remaining soil from the recently discontinued forest covers some of the hillsides. In the Diamir–Bunar/Barai/Biji area, exposure is excellent throughout, where the Indian plate cover rock sequences are up to >6 km thick. The continuous exposure between, for example, Nashkin and Airl Gali (Fig. 3, cross-section [B–B′]) allows the lithologies to be mapped in detail, and we are able to divide the cover rocks into an upper and a lower cover. Further afield, constraints are from correlation with (1) 'remote observation' (e.g. clear variety of colours distinguishing foliation on west wall of Bunar Gah in Figs 5 and 7), and (2) TM imagery at 1 : 50 000.

Lithological description of the upper cover rocks

The upper cover has over 50% of meta-carbonate; in decreasing order of abundance, marbles, calc-pelitic schists, calc-silicates, pelitic schists and amphibolites. Marbles are both pure and mixed with calc-silicates and calc-pelites. They are commonly medium to coarse grained and contain grossular garnet, diopside, phlogopite, apatite and graphite in a calcite-rich matrix. In calc-pelites, bands rich in calcite alternate with those rich in feldspar, quartz, muscovite and chlorite. The latter contain prismatic grains of zoisites which are poikiloblastic and contain trails of graphite. Like zoisites, large (at places >1 cm in size) garnets are poikiloblastic and overprinted on the fabric (in one instance the graphite trails containing zoisite are microscopically folded and included in garnet). The calc-silicates comprise a creamy white matrix comprising quartz, plagioclase, calcite, sphene and apatite with garnet porphyroblasts. The latter are rich in quartz inclusions. The pelitic rocks in the upper cover sequence are represented by bluish-grey paragneisses with large garnets that also show internal rotation patterns. These rocks comprise quartz, garnet, kyanite, biotite, muscovite, k-feldspar, rutile and graphite. Garnet and kyanite porphyroblasts incorporate a pre-existing fabric in the form of quartz and graphite trails. The matrix is ductilely deformed with anastamosing bands of mica and quartzofeldspathic layers. Some overgrowth of the micaceous foliation by garnets with inclusion spirals in the innermost grain may indicate more than one generation of deformation-induced garnet growth.

The thick upper cover rocks are identical, in terms of constituent lithologies and kyanite-grade of metamorphism, to rocks of this nature found in the SE portion of the NPHM, where they form a thin part of the section in the Dichil (north and south fork), E. Astor, Rama, Bulan,

Ghurikot (north, middle & south fork) and Lower Rupal valleys (Edwards & Kidd 1997; Edwards 1998). Several km of thickness are also present in Chichi Nullah (Edwards and Kidd 1997; Edwards 1998), Chuggam Gah and Rattu area (Edwards & Kidd 1997; Edwards 1998; Argles this volume). The upper cover is also similar to rocks described in Kaghan (Greco *et al.* 1989; Greco & Spencer 1993) and Swat (Treloar *et al.* 1989; DiPietro *et al.* 1993). These rocks are probably a metamorphosed product of the Permian 'Panjal Traps'—basic igneous rocks repeatedly intruded as sills or extruded as flows during carbonate platform development on the NW passive margin of India, that resulted in a widespread sequence that is typified by interlayered marbles and amphibolites that define part of the recognized cover rocks in the NW Himalaya (Wadia 1931; Honegger *et al.* 1982; Papritz & Rey 1989; Greco *et al.* 1989).

Lithological description of the lower cover rocks

The lower cover lithology is primarily composed of a garnet–two mica schist which contains minor chlorite, tourmaline and zoisite. In most cases the garnet fabric is parallel to the principal fabric in the schists but frequently also incorporates spiral patterns, implying rotation and suggesting that growth is both pre- and syn-kinematic. Meta-psammites are also present in the lower cover. These are massive but foliated and contain muscovite, biotite, tourmaline, garnet, epidote, graphite and rutile. Muscovite and biotite define the fabric while garnet is pre- to syn-kinematic. Local calc-silicates in the inner cover contain quartz, garnet, zoisite, biotite, muscovite in a calcite–siderite matrix. Kyanite, which is common in the upper cover sequence, is not observed in the lower cover sequence.

Two different types of granitic rocks were observed to be present in between the upper and lower cover in continuous outcrop sections (e.g. Diamir section [A–A'] and Nashkin–Airl section [B–B']), and nowhere did we see the upper and lower cover in contact with one another. The two granitic suites were also observed elsewhere within the lower cover section, together with a third granitic suite—the Jalhari Granite plutonic belt (discussed below).

Structural description of the Indian plate cover

In the Diamir–Bunar/Barai/Biji drainage area, Indian plate cover rocks are exposed *c.* 2 km south of the Diamir Gah confluence with the Bunar valley near Dimeroi, where they comprise a few hundred metres of garnetiferous metapelite (lower cover), and *c.* 100 m of marbles and amphibolite (upper cover), sandwiched between the MMT and the western margin of the Jalhari Granite plutonic sequence. Local foliation is moderately to steeply ESE-dipping, with a general stretching lineation plunging moderately to steeply northwards, although occasionally south plunging (Fig. 6). The main foliation is parallel with the structurally overlying MMT hanging wall, and it is clear that here the regionally NW-dipping cover sequences and MMT hanging wall are locally overturned to become ESE-dipping. The overturned section extends north of Dimeroi in Bunar Gah for at least 3 km (where mostly KLS rocks are exposed), and south for 8 km to the Gashit Fold (a recumbent open fold at the confluence of Airl Gah with Bunar/Biji, by the village of Gashit—Fig. 4), where the eastward dipping cover rocks form the upper, overturned, E-dipping limb (Fig. 7). This fold hinge therefore marks a point of regional overturning of several kilometres of MMT foot- and hanging wall sequences. South and west of the village of Gashit, layering is again the 'right way up', and is predominantly W-dipping. The hinge line of the Gashit Fold plunges *c.* 20°N. The general stretching lineation in the region plunges moderately to steeply toward the north, although locally there are a few occurrences of moderately SE plunging stretching lineation.

The Nashkin–Airl section (Fig. 3b, B–B'), crosses the Gashit Fold, while the Diamir section (Fig. 3b, A–A') crosses the Diamir Gah/Bunar valley confluence. It is clear from the sections and map that between the two areas there is a massive northward thinning of the cover rocks; a few hundred metres at Dimeroi compared with >6 km to the south of Nashkin Gah. This is reflected by the map trace of the MMT orientated *c.* NE, while the local strike of foliation between the Nashkin–Airl and the Diamir section remains *c.* N–S. This northward thinning of the cover rocks is probably too large to be an original depositional variation and is discussed below.

Throughout the southern portions of the Bunar/Biji area, foliation consistently dips moderately to the west. There is local (centimetre to metre scale) tight asymmetric 'parasitic' folding, but this is not significant on a large scale. Stretching lineations plunge moderately to steeply towards the NW or SW. Layering observed in the field can be clearly recognized on suitably processed TM scenes for this area

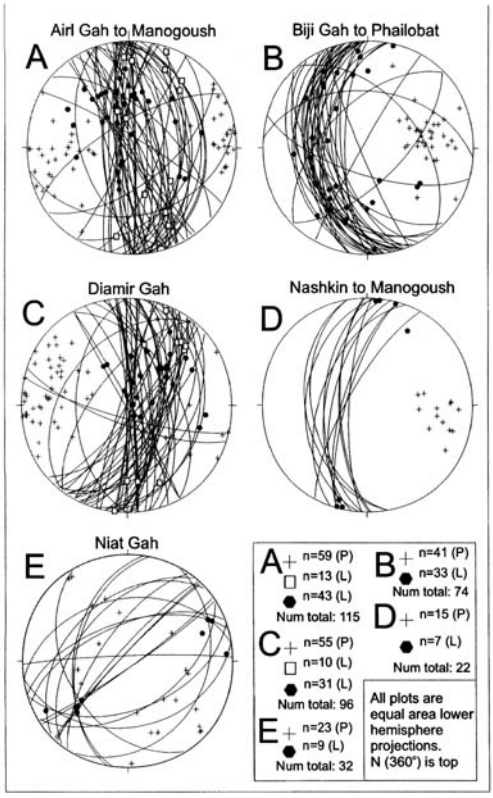

Fig. 6. Lower hemisphere equal-area projections of foliation and lineation measurements in SW NPHM. Lineations in B, D & E represent lineations in the upper and lower cover. Lineations in A and C are divided into Jalhari Granite (black dots) and Indian plate cover rocks (white boxes). Note that Jalhari Granite lineations are generally steep and NE to E-plunging; they are associated with the E over W deformation in the Diamir Shear Zone (see text).

and, in the case of Barai Gah, the thick section of upper cover rock that was mapped in Nashkin can be confidently traced up the valley. Lithological descriptions from Barai Gah by Hubbard *et al.* (1995) are consistent with this interpretation, indicating a general widespread presence of the 'cover'. On Fig. 4, therefore, we reproduce their four foliation and lineation data points from southern Barai Gah (fig. 1c of Hubbard *et al.* 1995). These structural data are consistent with ours, indicating an overall NW dipping foliation and SW plunging lineation. We note that the attention they drew to an absence in the SW region of the NPHM of a NW-plunging MMT footwall convergence-related lineation, that is reported elsewhere by other workers (e.g. Treloar *et al.* 1989), does not appear to hold true for any significant areal coverage (Figs 4 & 6).

The Indian plate sequences in Niat Gah include a short section of upper cover rocks that consist of marbles, amphibolites and a significantly greater presence of metapelite than in the Bunar Gah section to the east. The thickness of the cover is small, occurring structurally above a local section of basement that outcrops to the south. We did not observe the lower cover in this area. The main foliation in Niat Gah dips moderately WNW (locally steeper, and also locally flattening to dip gently ESE in places in the upper portions of the valley). Lineation development is not widespread but, where measured, lineations plunge moderately to the SW, and are accompanied by a top-to-SW displacement sense.

Granitic rocks

The porphyroclastic orthogneiss and the lath unit

The first of three plutonic rocks that we recognize is a grey orthogneiss with 1–3 cm porphyroclast-rich and (locally) porphyroclast-poor horizons. This is found cropping out in four areas: *c.* 2 km south of Dimeroi, near Gashit, near Garol, and in southern Biji Gah south of Rollo (Fig. 4). This is a granitic gneiss with coarse (< 2 cm) feldspar augen. It has a platy, predominantly biotite-rich matrix. Large thicknesses of this orthogneiss south of Rollo are indicated by extensive outcrop on both walls of the valley.

The second of the three plutonic units is a gneiss containing 1–>4 cm laths of feldspar set in a garnetiferous, pink biotite quartzofeldspathic matrix (Fig. 8). The feldspar laths are characteristic of this rock, and are frequently deformed into augen or other shapes resulting from high strain. This rock is present (Fig. 4) *c.* 1 km south of Diameroi, within the Manogoush Ridge (Fig. 5), and on the western wall between Garol and Rollo. An identical rock to this is present in the SE region of the NPHM, where it has been termed the 'lath unit' (Edwards 1998) and we use the term here.

The Manogoush Ridge site was selected for petrologic sampling of the lath unit where the extensive exposure allowed a sampling of a representative portion (Fig. 8). The lath unit is deformed into varying porphyroclastic laminated high strain fabrics, possibly more extensively developed at the margins of the unit. At Manogoush, the rock mostly retains the characteristic feldspar laths, preferentially orientated parallel to the high strain fabric that defines the matrix. Garnet is common in the matrix as well

Fig. 7. Looking NNW to an outcrop of the Gashit Fold, on the right bank of the foreground (near mouth of Airl Gah valley). In this outcrop, the fold is within metasedimentary cover, *c.* 1.5 km west of the edge of the Jalhari Granite. The fold accommodates regional overturning (eastward dip) of MMT footwall, and is inferred to be due to the W-verging, E-dipping Airl-Gah/Diamir Shear Zone. North and east of this point, layering is predominantly E-dipping. South and west of this point, layering is predominantly W-dipping (note W-dipping cover rocks in background on far (west) side of Bunar Gah). Hinge line plunges *c.* 20°N. Trees are a few metres in height.

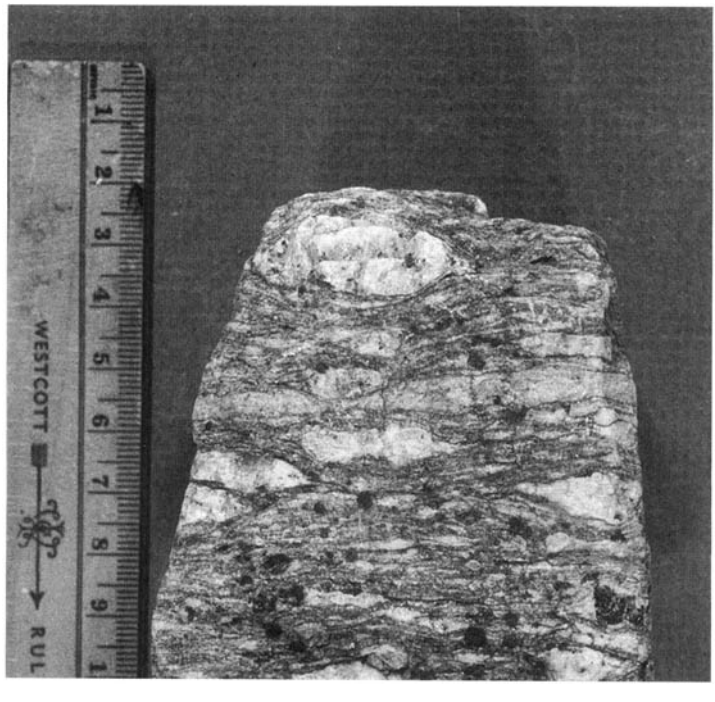

Fig. 8. Sample of lath unit sampled between Garol and Rollo. Note presence of rusty garnets, deformed and lesser deformed feldspar 'laths' (in cases extending across length of sample), local development of asymmetrical ('sense of shear') fabric. U–Th–Pb age for equivalent outcrop of this unit in Manogoush Ridge is *c.* 480 Ma (see text for discussion).

as forming porphyroclasts surrounded by an aggregate of quartz grains. The matrix is rich in muscovite with subordinate biotite, both orientated preferentially together with ribbon quartz to define the high strain fabric. Muscovite flakes are commonly rimmed by biotite at grain boundaries and cleavages. Fine to medium-grained prismatic crystals of kyanite are abundantly disseminated in the matrix within the preferred orientation of fabric. Bent crystal structure in some grains and preferential growth of others in the fabric plane suggests that kyanite is pre- to syn-kinematic. In comparison, garnet is mostly lenticular in shape, apparently grown in the preferred orientation of the fabric, and inferred to be syn-kinematic. Some, however, are skeletal and are overprinted on the fabric, suggesting a syn- to post-kinematic origin. Some larger garnet grains are zoned in terms of inclusions; they contain fibrous sillimanite in the cores and kyanite in their rims. The pink, garnet–muscovite–kyanite-rich matrix allows the lath unit gneiss to be distinguished from those C/S augen gneisses derived from, or those in the vicinity of, the Jalhari Granite. Preliminary ion microprobe data (Schneider *et al.* 2000), for the lath unit sampled at Manogoush Ridge yield concordant zircon U–Pb ages of *c.* 480 Ma.

The outcrop extent of the lath unit at Manogoush Ridge is not constrained. It is present as a tapering thin sheet at the northern tip of the ridge, but how far it persists to the south is unclear (hence the use of question marks on Figs 3a & b). Hubbard *et al.* (1995) discriminated an augen gneiss from their Indian cover rock/basement rock classification scheme. They show the augen gneiss on their Fig. 1c as extending from southern Barai to the central portions of the Manogoush Ridge. Unfortunately they do not describe the augen gneiss; there is only a photomicrograph of a quartzo-feldspathic portion of a thin section, and a report of old sillimanite being found as an inclusion in K-feldspar. Sillimanite is present both in the portion of the lath unit that we identify at the northern end of Manogoush Ridge, and in the porphyroclastic orthogneiss at Rollo, and there is no way to identify which of the two units is the augen gneiss of Hubbard *et al.* (1995). It is possible that the entire length of the Manogoush Ridge is composed of the lath unit. Alternatively, there may simply be only discontinuous scattered outcrops.

The Jalhari Granite

The third of the three plutonic suites that we recognize is the Jalhari Granite. It is named from its occurrence in Jalhari Gah, south of the village of Phailobat. It was also mapped in the Airl Gah and Diamir valleys and we recognize the Jalhari Granite as a N–S trending continuous belt several kilometres wide and tens of kilometres long (Figs 3a & 4). It is a biotite granite/granodiorite that is intrusive into the pelitic–siliceous lower cover. The western margin of the belt is in contact with metapelite *c.* 2 km from Dimeroi, while the eastern contact is a pervasively retrogressed, highly chloritized, metapelite, about 1 km west of the confluence of Zangot. The granite is more commonly deformed than not and, throughout the belt, the deformed portions of the granite have a varying intensity of foliation that is everywhere N–S striking, dipping moderately to steeply to either the west or east. In Jalhari Gah, the deformed granite frequently takes on an augen gneiss appearance marked by a local, very coarse crenulation of biotite layers about the quartz and feldspar grains. The intersection of this coarse crenulation causes spectacular parallel ridges on the main (W-dipping) foliation surfaces of the granite that can be seen from some distance (Fig. 9). In Jalhari Gah, this lineation is SSW plunging on moderately W-dipping surfaces.

The Diamir and Airl Gah valleys both offer almost continuous outcrop sections through the Jalhari belt. In these valleys, the granite is a course- to medium-grained, biotite granite that grades into granitic and porphyroclastic gneiss. Figure 10a illustrates the degree of variability of the Jalhari Granite across the belt as a whole. Note the variation in the amount of felsic component and the porphyroclast preservation. Sections through the granite in Diamir Gah and Airl Gah show that narrow horizons or screens of pelitic and calc-silicate schists and paragneisses, belonging to the lower cover, persist between hundreds of metres wide bodies of Jalhari Granite. Metasedimentary screens, frequently retrograde and highly chloritized, are typically a few tens of metres wide. A few are wider, up to several hundred metres, particularly at the eastern margin of the granite in Diamir Gah. Rare pelitic and granite xenoliths (Fig. 10b) are widely scattered in the granite sections. Throughout the area are internally undeformed portions of the granite that preserve magmatic textures and mineral assemblages. These were selected as characteristic sites for both geochronologic and petrologic sampling.

The Jalhari Granite is characterized by black biotite that occurs either in clusters between the large feldspar grains or forms large equant poikilitic crystals, often in excess of a centimetre in size, enclosing feldspar and quartz grains, and in some samples, hypersthene. These textures are

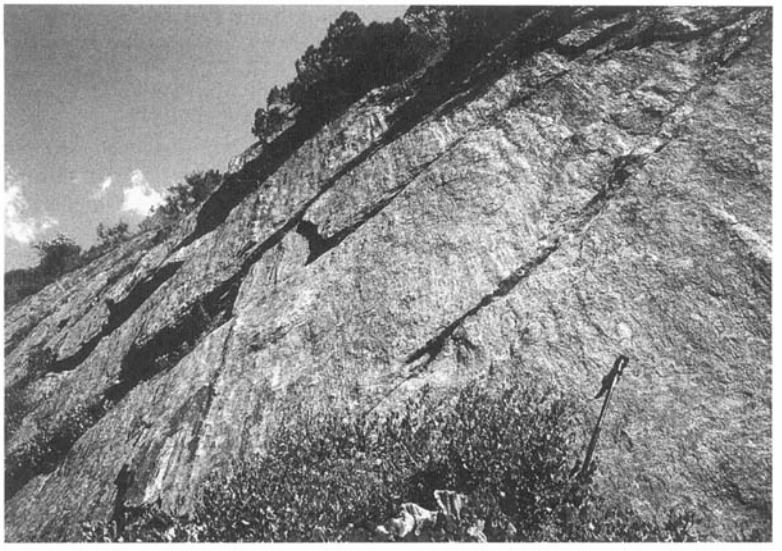

Fig. 9. Deformed augen gneiss-rich portion of Jalhari Granite outcropping on east wall of Jalhari Gah. In this instance, Jalhari Granite has a strong foliation striking N–S and dipping moderately to the W. Lineation is SSW plunging. Intersection on the main foliation surfaces of coarse crenulation of biotite layers about <0.5 cm quartz and feldspar grains causes spectacular parallel ridges of the granite that are seen in photo. Ski stick for scale.

apparently due to late-magmatic, post-cumulus, crystallization from liquids trapped in interstices between cumulus feldspar crystals. The predominant mineral is feldspar, including both orthoclase and albite–oligoclase, with the former dominant. Quartz, biotite, hypersthene and opaque minerals, in decreasing order of abundance, make up the assemblages in most of the fresh rocks sampled from the least deformed portions of the granite in Diamir Gah, although many fresh samples do not show hypersthene. Poikilitic biotite encloses all other minerals, quartz grains include feldspar and hypersthene, while feldspars include only hypersthene. These textural relations suggest earliest crystallization of hypersthene, successively followed by feldspar, quartz and biotite. A reaction relationship is noted between hypersthene and feldspar; the two are rarely in direct contact, and are commonly separated by fresh quartz and biotite. Minor interstitial muscovite is typically present in all samples, except for those from undeformed portions in Diamir Gah. Hypersthene relicts have been noted in two samples collected from near Jalhari village.

For microstructural analyses of the Jalhari Granite we examined 22 petrographic sections from the Diamir valley, Airl Gah and Jalhari Gah. The microstructure of the granite varies with the degree of deformation, although the principal foliation is everywhere defined by preferred grain orientation of biotite and quartz aggregates. In lesser deformed samples, feldspar grains frequently retain their original shapes, but fining of quartz grains, through grain recrystallization and through cataclasis, and alteration to fine-grained disseminated muscovites, is common. Figures 11a & b show optical photomicrographs of thin sections cut from portions of the Jalhari Granite sampled in Airl Gah that are representative of the variability of microstructure. Figure 11a is a finer-grained augen gneiss that displays a strong macroscopic non-coaxial fabric (porphyroclast augen asymmetry and C/S fabric) and has an N-plunging stretching lineation. Based upon the partial development of polymineralic ribbons, the extensive quartz and mica domains recrystallized in preferred orientation, and lack of intracrystalline plasticity in the large feldspar grains, we suggest that deformation temperatures in this rock may have reached *c.* 500°C (Tullis & Yund 1985, 1991; Dell Angelo & Tullis 1989). This assumes that hypersolidus deformation did not create a strong anisotropy or a pre-existing fabric through, for instance, generating a strong biotite alignment that caused the subsequent growth of quartzofeldspathic grains to mimic ribbons that form through deformation. A dextral sense of shear in the figure is indicated by S and C surfaces defined by the biotite and recrystallized quartz grains, and coarser recrystallized quartz grains that mark a strain shadow in the lower left edge of the large feldspar grain. The microstructure is

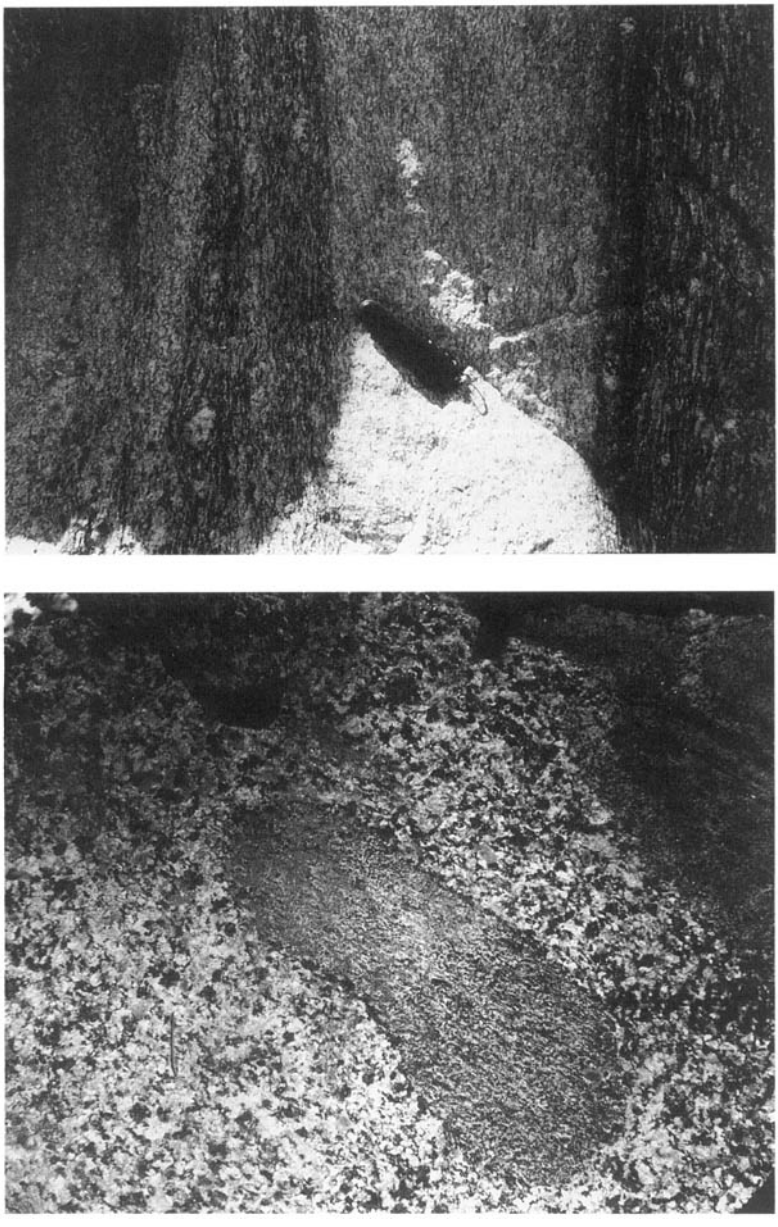

Fig. 10. Degrees of variation in granite rock observed in the Diamir Shear Zone. (**a**) Strained portion of Jalhari Granite within the Diamir Shear Zone, Diamir Gah: Note large variety of granitic gneiss locally housed. Although the large changes across the small area preserved here are atypical of the Jalhari Granite in the Diamir Shear Zone, the sample is nevertheless highly representative of the degree of variation that can be found along a transect through the Jalhari Granite as a whole. Swiss knife for scale. (**b**) Xenolith of finer-grained granite rock that is feldspar poor relative to host—a typical occurrence of Jalhari Granite in Airl Gah. Xenolith is *c.* 30 cm in length.

typical of the entire thin section, and because the thin section is cut parallel to the N-plunging stretching lineation, it represents a west-vergent reverse and dextral displacement. This direction of displacement is typical for a determined sense of shear in all the Jahari Granite thin sections where microstructure shows non-coaxial strain. In addition to the sense of shear indicators seen

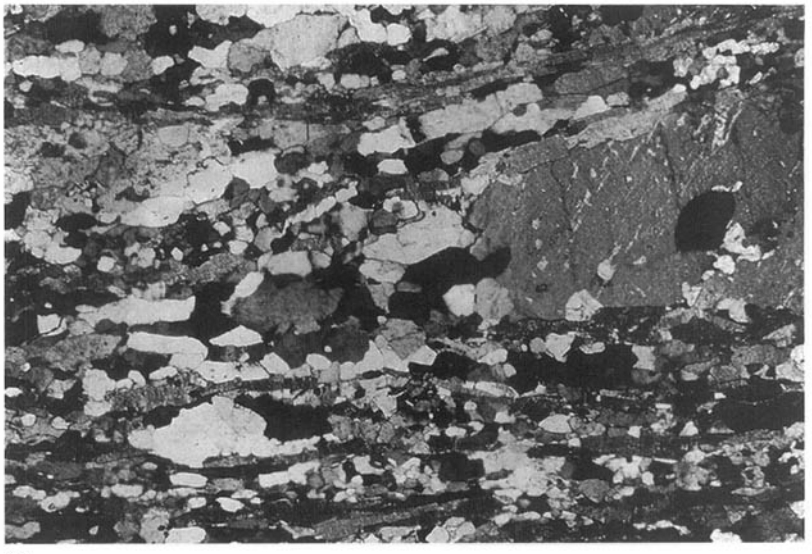

(a)

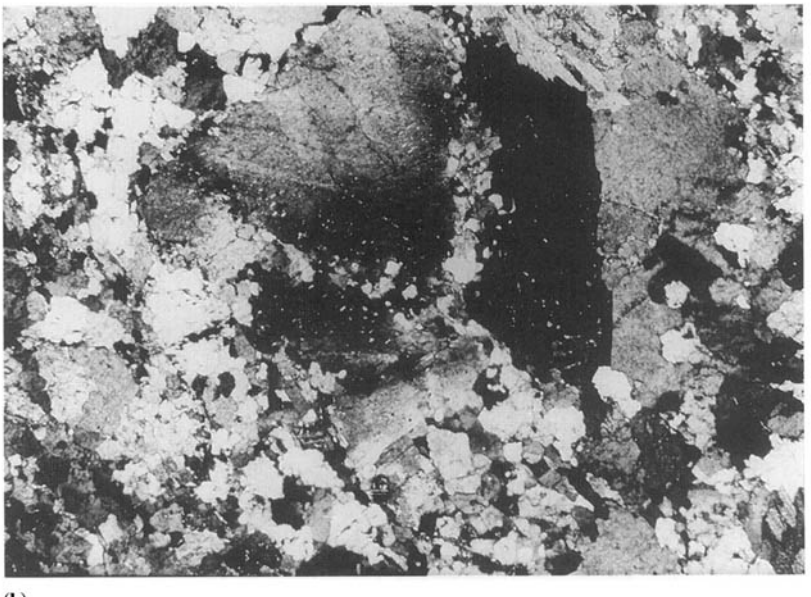

(b)

Fig. 11. Optical photomicrographs of thin sections of Jalhari Granite from Airl Gah. (**a**) Augen gneiss portion with strong C/S fabric and stretching lineation (here plunging 50° towards 350°). Note the partial development of polymineralic ribbons (see text for discussion). The photo shows the characteristic microstructure of deformed granite in the Diamir Shear Zone. Grain size is relatively fine (biotites <300 μm, quartzofeldspathic grains <400 μm). The biotite picks out nicely the S and C surfaces. Sense of shear in this case is clearly dextral and W-vergent. Cut parallel to lineation and perpendicular to foliation (170°/89°E). South is to the left, west is to the top of the image. Base of image is 5.5 mm and parallel to main fabric. (**b**) Flattened portion of granite without C/S fabric development. Note deformed feldspar grains with some sutured internal grain boundaries, and extensive suturing and new grain growth at margins of larger grains, indicating that grain boundary migration and wholesale grain size reduction have operated extensively (both in field of view and elsewhere in thin section) as indicated by very fine (50–100 μm) grain size of surrounding quartzofeldspathic component. Base of image is 5.5 mm. Crossed polars.

in Fig. 11a, other frequently observed microstructures that were used to determine sense of shear include throughgoing fabrics and oblique objects (Means 1981; Lister & Snoke 1984; Passchier & Trouw 1996); C′-surfaces (Berthé *et al.* 1979); *Mica 'fish'* (Eisbacher 1970); porphyroclasts and stiff objects produce strain shadows, 'tails' (trails) and 'wings' that form delta, sigma and quarter structures (Hanmer 1984; Passchier & Simpson 1986; Hooper & Hatcher 1988). These features were consistently observed in a variety of widely distributed samples of deformed portions of the Jalhari Granite from the Diamir and Airl valleys.

Figure 11b is a typical example of the microstructure preserved in the Jalhari Granite in Diamir, where there is no significant C/S fabric or other obvious non-coaxial fabric preserved in hand specimens. Sutured internal grain boundaries of feldspar grains, and extensive suturing and new grain growth at margins of larger grains, indicate significant grain boundary migration and wholesale grain size reduction and suggest conditions of deformation of $>500°C$ (Dell Angelo & Tullis 1989; Tullis & Yund 1991).

In addition to microstructure, deformed portions of the Jalhari Granite show a range of outcrop-scale structures that we used to identify sense of shear. Throughout the Diamir Shear Zone, in both the Airl Gah and Diamir Gah valleys, lenses of the Jalhari Granite, tens to hundreds of metres thick, that show little to no sub-solidus deformation, are separated by, or frequently grade into, tens to hundreds of metres thick layers of augen gneiss with significant sub-solidus strain. Ductile fabric that is associated with microstructures includes spectacular C/S relationships, C′ shears a few millimetres to few centimetres in length, and asymmetry of porphyroclasts up to a few centimetres in size. These non-coaxial strain features are associated with a well-developed mineral stretching lineation in the Jalhari Granite belt that plunges moderately to steeply N or NE (Fig. 6a & c), and consistently indicates a W-vergent reverse displacement with a portion of, typically dextral, wrench motion. In addition to ductile fabrics, brittle and transitional structures include:

(1) narrow zones, tens of centimetres wide where hydrothermal flux has developed thick biotite accumulations (probably late ductile strain features), where well-developed asymmetric folding (centimetre-wavelength) of the biotite layers frequently indicates east side up and over west;
(2) well-developed suites of a few metres long, a few centimetres wide, west-vergent shear bands;
(3) sets of tens of metres long, 5–20 cm wide, local fault gouge horizons that often develop preferentially in areas where brittle deformation involved a broader zone of cataclasis as opposed to a single fracture plane; and
(4) planar, steep, faults that cut all fabrics whose W-vergent reverse displacement is recognized by drag folding of fabric or marker offsets (a few tens of metres).

On the large scale, the E over W sense of displacement is readily identifiable from both the brittle and ductile fabric that define regions of low and high strain; Fig. 12 illustrates higher strain layers of the Jahari Granite anastamosing around the lesser/undeformed granite lenses, marking reverse faults that are seen to 'climb' to the west.

In both Diamir Gah and Airl Gah, the entire thickness of the Jalhari belt has experienced west-vergent reverse faulting with local wrench motion that is constrained by the micro- and outcrop structures. The dextral wrench component is stronger in Airl Gah (compare lineations of Fig. 6a with 6c), although the principal state of strain in the two valleys is similar. The overall deformation is indicative of a major N–S striking steep shear zone. In view of the absence outside the Jalhari belt of any significant development of structures indicative of west-vergent reverse faulting, we regard the width of the shear zone to approximate to that of the main body of the Jalhari belt (4–6 km). We term this the Diamir Shear Zone. We did not conduct a traverse across the southern part of the Jalhari belt, although the outcrop at the margin (Fig. 4) and glacial boulders from Philobat North fork glacier indicate a consistent style of deformation of this part of the granite, and we infer that the Diamir Shear Zone continues south at least to here.

Basement rocks

The basement in Diamir Gah extends from *c.* 500 m west of Zangot to the interior of the NPHM. Several hundred metre structural thickness of quartzofeldspathic gneisses with centimetre to tens of centimetre scale compositional layering due to, for example, differing Fe-weathering and biotite content. These are characteristic of the southern region of the NPHM basement gneisses (Edwards 1998). Foliation is moderately to steeply E-dipping and lineation plunges moderately north. These rocks are replaced by a monotonous granitic orthogneisses sequence that

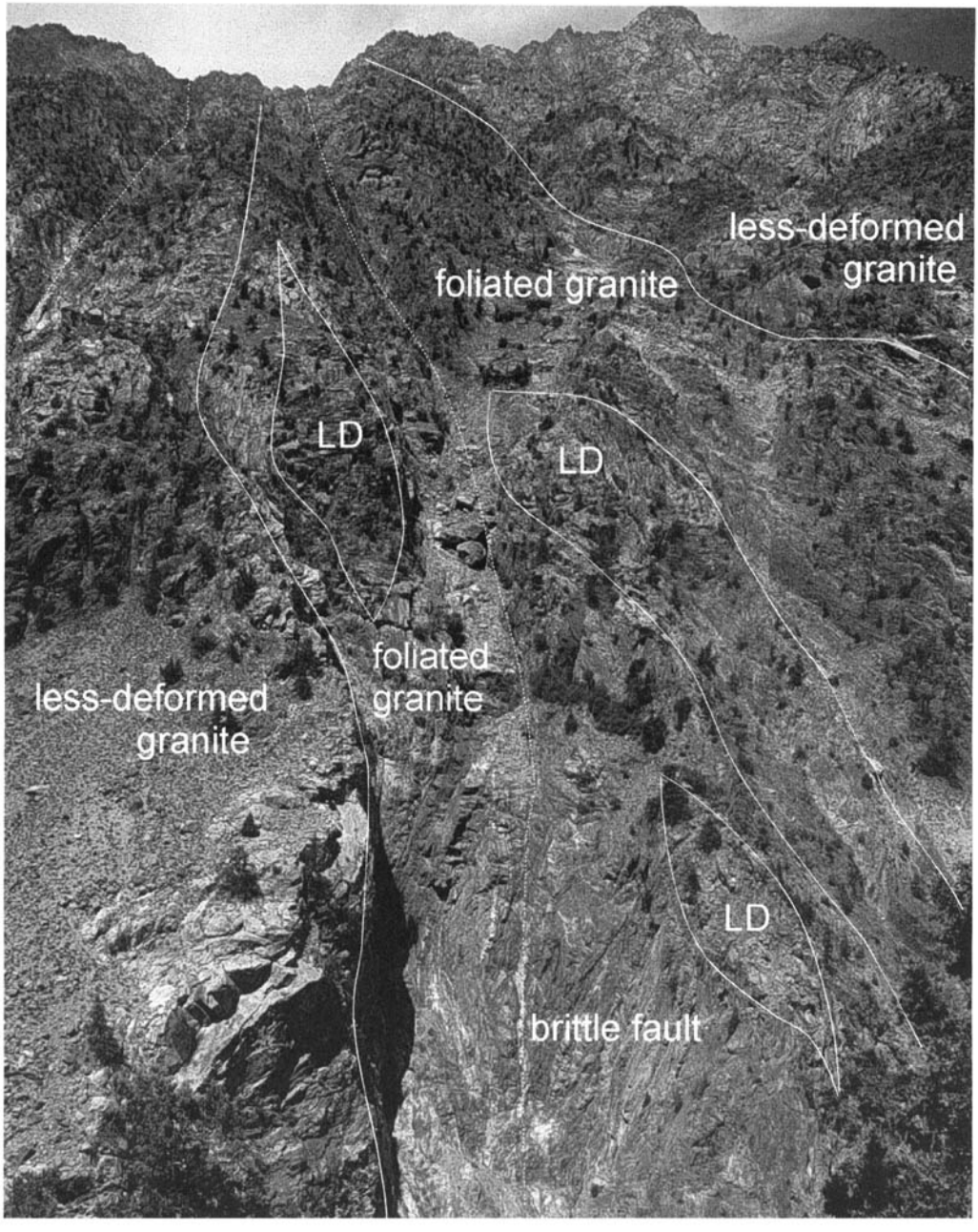

Fig. 12. Right bank view of Diamir Gah looking to the north of right bank of Diamir Valley, showing > 2 km high valley wall made up of Jalhari Granite, which is deformed by the W-vergent, reverse sense Airl–Gah/Diamir shear Zone. LD is less-deformed granite. Observations are based upon remote observation with field glasses and correlation with identical styles on left bank (where viewer stands). Note much ductile strain is localized into gneissic layers (tens to hundreds of metres) that anastamose around lenses of lesser- and undeformed granite.

continues for at least several kilometres towards the central portions of the NPHM. Foliation is N–S trending and moderately E-dipping, with north plunging lineations. A few sense of shear structures were observed but were found to be inconsistent across the area.

The basement in Niat Gah is marked by a prominent grey (occasionally porphyroclastic)

quartzofeldspathic gneiss, and a much larger amount of amphibolite than in the basement section east of Zangot. The main foliation in Niat Gah dips moderately NW or SE. We note that the map of Hubbard *et al.* (1995, Fig. 1c) seems to group a portion of the basement in the cover, possibly under the assumption that significant volumes of amphibolite are characteristic only of the Indian plate cover rocks. We disagree with this in view of the fact that there is no evidence elsewhere that amphibolite is rare within basement rocks in this region, and, moreover, the rocks in question are mostly quartzofeldspathic and are devoid of pelites, and are therefore consistent with basement rocks mapped in Diamir, and in the SE region of the NPHM (Edwards 1998). The section of basement in Niat Gah is structurally very 'high' and is bounded by cover rocks to the north and to the south. We interpret this as the product of kilometre-scale imbrication associated with a possible duplexing, and discuss this below. We disagree with the tens of kilometres-scale nappe that is proposed by Hubbard *et al.* (1995) in the SW region of the NPHM to account for this section of basement. This model requires extrapolation of the footwall anticline in Niat Gah from the <3 km observed half-wavelength (Fig. 3b) to >27 km (cf. fig. 1d of Hubbard *et al.* 1995). Our new observations in the SW region of the NPHM provide no evidence to support this.

Western Rupal valley

Figure 4 presents data from the westernmost Rupal valley, and enables examination of the regional continuity of the structural and lithological trends. There is a contrast between the inner/upper regions of the left bank, the 'summit region' of Nanga Parbat, and SW Rupal, which includes the lowermost portion of the Toshain Glacier left bank and the right bank of the Toshain and Rupal glaciers up to Shaggin' Glacier to the east of the map area.

In the SW region of the Rupal valley, lineations everywhere plunge SSW, and the main foliation is N or NE striking, dipping steeply to the west. Lineation and foliation are therefore similar to the southern portions of the Bunar and Niat/Thak valley systems. On highly strained foliation planes (dipping moderately to WNW) a consistent sense of shear is recognized across all of the Toshain Glacier right bank. Sense of shear is also demonstrated by microstructures which, in most cases, indicate that recorded, stable, deformation largely proceeded at temperature of $<400\,^{\circ}C$. Displacement sense is sinistral with top down to the south-southwest, and an accompanying sinistral wrench component (Fig. 4). This displacement sense is consistent with reports from Hubbard *et al.* (1995) and Burg *et al.* (1996) from Bunar, Niat/Thak, and other areas further to the west.

There is a minor lithological contrast in the SW region of the Rupal valley between the left and right bank of the Toshain Glacier. On the right bank, a sequence of L-tectonite orthogneiss forms mega-lenses and boudins, tens of metres in diameter that are discordantly intruded into a more weakly lineated finer-grained grey gneiss. The original intrusive relationship is preserved in spite of subsequent deformation that has affected both. Stretching lineations in the L-orthogneiss and the grey gneiss are parallel and steeply S to SW plunging.

The principal foliation in the summit region of Nanga Parbat is very steep and N to NE to E striking (Fig. 4). Lineations plunge moderately to steeply to the north. The switch in trends of lineation and foliation between the inner/upper regions of the left bank of SW Rupal is marked by a series of brittle and ductile faults (shown schematically on Fig. 4), whose net offset is not known but is thought to be in the order of several kilometres (Edwards 1998). The N-plunging lineation is an expression of the south-southeast vergence of the summit region over the footwall rocks in the central Rupal valley. This is a part of the general displacement on the Rupal Chichi Shear Zone—a major NE-striking shear zone that represents several kilometres of deep crustal displacement (Edwards 1998; Schneider *et al.* 1999*a*) that is marked by a clear summit-ward younging of biotite cooling and leucogranite ages (Schneider *et al.* 1999*b*, *c*). The eastward change in strike of foliation from NE to E is regarded as part of a gradual swing in foliation that is a product of the Rupal Chichi Shear Zone.

The brittle and ductile faults of the left bank of the Toshain Glacier also mark a lithological contrast. The dominant lithologies in the uppermost Nanga Parbat summit region are basement gneisses including compositionally layered gneisses and monotonous granitic orthogneiss; it is not clear what is the maximum metamorphic grade attained. Immediately SE of Mazeno Pass, green pinnitized cordierite in coarse (pegmatitic) granitoid float was seen in scree debris but not in outcrop. At the pass, a leucogranite pluton (Fig. 4) intrudes the compositionally layered gneisses. Schneider *et al.* (1999*a*) obtained a U–(Th)–Pb monazite and zircon emplacement age of 1.4 ± 0.4 Ma for the Mazeno Pass Pluton. In the eastern part of the left bank, there is a lithological change whereby pelitic metasedimentary (apparently cover) rocks are frequently

interlayered with the granitic orthogneiss. This is regarded as part of the general imbrication that is associated with major reverse faulting on the Rupal Chichi Shear Zone.

Thermochronology of the SW region of the NPHM

In order to constrain some of the cooling history of these rocks, we performed multigrain laser total fusion $^{40}Ar/^{39}Ar$ analyses on biotites from samples from throughout the SW region of the NPHM area. Fusing of samples and flux monitors was performed at Lehigh University via CO_2 laser under visual observation. Results are compiled in Table 1 and displayed in Fig. 3. Cooling ages east of the Diamir Shear Zone, in the hanging wall where Nanga Parbat has been displaced upwards, are generally young (< 5 Ma), typical for Nanga Parbat (Winslow *et al.* 1956; Schneider *et al.* 1997). However, a marked age increase occurs west across the shear zone into the Indian cover metasediments; biotite cooling ages there are > 20 Ma. Our Early Miocene and older cooling ages are consistent with cooling ages in the Babusar area (Chamberlain *et al.* 1991) and cooling ages

Table 1. *Multigrain laser total fusion $^{40}Ar/^{39}Ar$ biotite ages*

Sample	40/39	37/39	36/39	%Ar^{40}*	Age (Ma)	s.e.	LU#
B-3	58.95	−0.0187	0.0291	85.36	28.66	0.19	802
B-9	120.8	0.0490	0.1321	67.68	49.19	0.56	674
B-5	47.73	0.0246	0.0119	92.57	26.74	0.28	675
B-10	194.1	−0.0011	0.0285	95.65	103.41	0.55	804
B-15	130.7	−0.0716	0.1236	72.03	53.07	0.41	807
BI-2	96.26	−0.1020	0.0138	95.73	52.82	0.35	794
BI-3	100.9	−0.2524	0.0133	96.04	55.37	0.40	795
BI-4	67.92	−0.0384	0.0496	78.36	30.58	0.35	796
GA-4	50.08	0.0382	0.0140	91.68	26.37	0.22	797
JAL	6.177	0.0096	0.0114	44.97	1.60	0.02	798
MR-15	6.437	0.0038	0.0157	27.38	1.05	0.02	788
MR-16	7.332	0.0016	0.0142	42.43	1.84	0.02	789
MR-23	26.72	0.0058	0.0296	67.21	10.61	0.05	790
MR-24	25.88	0.0150	0.0181	79.20	11.77	0.07	799
MR-27a	10.26	−0.0150	0.0199	42.41	2.57	0.03	791
MR-32	24.12	0.0101	0.0215	73.59	10.35	0.06	793
N-1	52.76	0.0471	0.0310	82.60	26.38	0.29	676
N-2	50.19	0.0442	0.0542	68.07	20.71	0.23	677
N-3	52.67	0.0336	0.0300	83.13	29.69	0.33	678
N-7	120.6	0.0630	0.2919	28.43	20.78	0.57	679
P-1	58.93	0.0065	0.0335	83.18	27.64	0.29	731
P-2	45.90	0.0032	0.0117	92.42	23.95	0.24	732
PH-1	64.78	−0.0049	0.0147	93.24	34.23	0.27	808
PH-2	53.46	0.0217	0.0181	89.96	27.31	0.21	809
PH-3	23.64	0.0043	0.0129	83.77	11.29	0.06	810
PH-4	37.29	−0.0126	0.0093	92.59	19.65	0.20	811
TH-1	193.3	0.0733	0.0186	97.15	104.87	0.56	800
TH-4	88.40	0.0595	0.0142	95.22	47.72	0.26	801
Z-1	12.07	0.0258	0.0313	23.22	1.84	0.06	668
7-II	5.718	0.0057	0.0098	48.82	1.70	0.03	687
8-XII	6.172	0.0087	0.0041	79.96	2.98	0.03	686
8-XVII	7.554	0.0071	0.0181	28.99	1.39	0.14	685
11-VII	59.51	0.0021	0.0109	94.53	33.78	0.36	684
12-I	17.15	0.0269	0.0118	79.56	8.26	0.12	682
12-IV	10.74	0.0187	0.0157	56.72	3.70	0.05	683

Table represents isotopic results of $^{40}Ar/^{39}Ar$ analyses on multigrain biotite separates from the southwestern valleys of NPHM indicated by scheme of dot symbols detailed in Fig. 3a. Total fusing of samples and flux monitors was performed via CO_2 laser under visual observation. For complete discussion, see Schneider *et al.* (2000).

Sample nomenclature: B = Barai; BI = Biji; GA = Gasht; JAL = Jalipur; MR = Main Massif Region (upper Diamir and Patro valleys); N = Niat; P = Picora; PH = Phailobat; TH = Thamrus; Z = Zangol; Roman numerals = transect from Mazeno to Airl Gali (these samples appeared as e.g. 95/7-ii, cf. Edwards 1998, p. 272).

farther to the southwest in Indian plate rocks of the Hazara syntaxis (Smith *et al.* 1994). Thus, the older ages obtained in this study are probably initial Himalayan cooling dates and not the result of a widespread excess radiogenic argon that is restricted to the Indian cover rocks. The cooling age profile across the Diamir Shear Zone is similar to the cooling age profiles across the Raikhot–Liachar fault system (Zeitler 1985; George *et al.* 1995) in the northern sections of the NPHM and probably similarly represents large displacement of the shear zone. Cooling ages within the shear zone reflect varying degrees of 'resetting' most likely the result of deformation and fluids.

Discussion

Diamir Shear Zone/Jalhari Granite

We define the Diamir Shear Zone (DSZ) as the 4–6 km thick N–S trending shear zone with extensively developed non-coaxial ductile and brittle strain that is associated with steep NE-plunging stretching lineation within the Jalhari Granite belt. The DSZ coincides with almost the entire thickness of the belt. The $^{40}Ar/^{39}Ar$ cooling age gradient that accompanies the shear zone indicates several kilometres of E over W relative displacement across the zone, and, in view of the width of the belt, we infer that the shear zone continues for several kilometres below the surface. Between the exposed Gashit Fold and a few kilometres north of Dimeroi is the surface exposure of the overturned MMT and its immediate foot- and hanging wall. We regard this overturning as a mechanical response of the E over W vergence that has developed adjacent to the DSZ; it is clear that the Diamir Shear Zone and the overturning play key roles in accommodating relative uplift of the central parts of Nanga Parbat with respect to the outer portions of the massif. A similar overturning is recognized in the SE region of the NPHM (Edwards 1998).

Strain in the Jalhari Granite is apparently partitioned into zones of high strain that anastamose around lesser deformed regions (e.g. Fig. 12). Although this may be a true strain partitioning (i.e. regions that experience differing parts of the instantaneously straining area), it is also possible that the lesser deformed regions have been intruded during the ongoing strain, and have therefore experienced only a (later) part of the finite deformation; during continued displacement on the shear zone, some of the lesser- or undeformed portions of the Jalhari Granite many have been intruded as discrete plutons. Preliminary geochronologic investigations on the crystallization age of deformed and undeformed portions of the Jalhari Granite indicate Th–Pb monazite ages that range from *c.* 12 Ma to 3–2 Ma (Schneider *et al.* 2000). Although work is in progress, it appears the granite is young or has recently undergone sufficient reworking during this time to incur Pb loss. Based upon this, we suggest that there has been syn-kinematic magmatism; protracted plutonism has partly overlapped with ongoing deformation between 12 ad 2 Ma.

The portions of Raikhot Fault Zone in the area of Raikhot Bridge (Fig. 2) represent a W to NW-vergent, reverse sense major shear zone that is associated with steep cooling age gradients (Zeitler 1985; Madin 1986; Butler & Prior 1988; Madin *et al.* 1989; Butler *et al.* 1992; George *et al.* 1995). On the large scale, the DSZ is therefore comparable to this section of the Raikhot Fault Zone. We propose that, on a first order basis, the DSZ forms the mechanical continuation of the main Raikhot Fault; noting, however, that the latter is much narrower (<2 km) and represents more focused strain.

Thinning of cover rocks

An abrupt northward thinning of cover sequences in the southwest region of the NPHM is evident from the change in the upper cover structural thickness from a few hundred metres near Dimeroi to *c.* 12 km at Nashkin Gah. Even very steep palaeotopography of the original depositional surface is unlikely to result in such a large variation in original thickness and there must therefore be some type of tectonic excision, with >5 km thickness of material removed. The same thinning of the Indian cover is also clearly displayed along the southeast and eastern margin of the NPHM (Fig. 2), where there is no younger, NPHM-age, modification or truncation of the Himalayan and MMT fabrics. There are three possibilities; an MMT frontal ramp, post-thrusting MMT normal displacement, or lateral ramps in the Indian basement/cover or MMT (Fig. 13).

Our favoured interpretation (Fig. 13A) involves a large frontal ramp in the MMT which results in a duplex structure with extensive imbricated slices of Indian cover and basement. This hypothesis provides a plausible explanation for the occurrences of basement 'high' in the thick Indian cover in Niat and also for larger examples of basement highs found to the S and SE of the NPHM. In addition it is consistent with structural interpretations further west along and to the south of the MMT (Coward *et al.* 1988; Treloar *et al.* 1989). Our frontal ramp

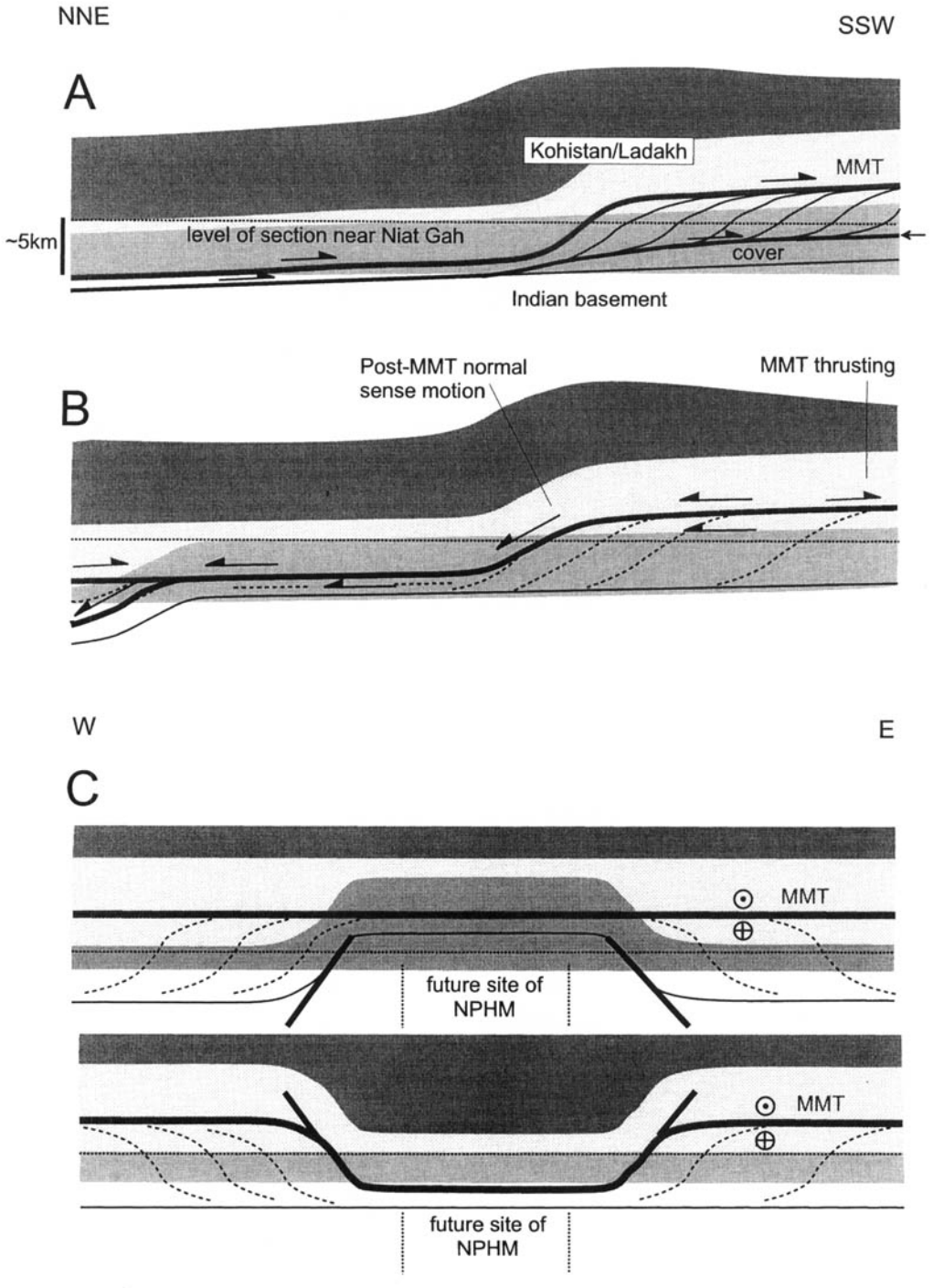

Fig. 13. Cartoon structural sections depicting three possible scenarios prior to Nanga Parbat exhumation and uplift. Weight of shading labelled in A is used throughout. See discussion in text.

model is additionally consistent with the dominant thrust motion seen on the MMT around the north end and along the eastern side of the NPHM (Edwards 1998), and can also explain the presence of the lath unit. In addition to the various outcrops of the lath unit in the SW region of the NPHM, it has been recognized extensively throughout the SE region of the NPHM (Edwards 1998) and is correlated with a typically high strain pink matrix gneiss that is present along the eastern margin of the NPHM in the Indus Gorge (Madin 1989; Wheeler *et al.* 1995). In many cases the lath unit, or an equivalent high strain pink gneiss, is structurally sandwiched between two contrasting suites of rocks (e.g. the upper and lower cover) whose juxtaposition is probably the result of displacement accommodated in part by deformation within the lath unit. We therefore suggest that the lath unit is a site for localization of the floor thrust that accompanies our inferred duplex in the Indian cover that developed from a ramp in the MMT. The very deformed portions of the lath unit, including the high strain pink gneiss found in the northern regions of the NPHM, represent large amounts of floor thrust displacement while the relatively lower strain parts of the lath unit (e.g. Fig. 8) are inferred to have been imbricated into the duplex and preserved after experiencing a smaller amount of floor thrust displacement.

Edwards (1998) has documented spectacular strain variation in the lath unit and its intrusive origin is clear. In addition to the *c.* 480 Ma U–Pb zircon microprobe age for the lath unit from Manogoush (Schneider *et al.* 2000), Foster *et al.* (1999) have obtained *c.* 500 Ma monazite SHRIMP ages from the cores of garnets within the lath unit from the SE region of the NPHM, and Zeitler *et al.* (1989) obtained a 500 Ma inheritance age from a NE NPHM Shengus gneiss sample. It is clear that the lath unit represents the deformed product of, or a suite of, widespread Cambro-Ordovician granitoids bodies intruded into the basement-cover contact, or upper cover–lower cover contact.

We do not think that the abrupt northward thinning of cover sequences in the SW region of the NPHM is due to post-thrusting MMT normal displacement, or lateral ramps within the Indian plate. Although post-thrusting MMT normal displacement (Fig. 13B) explains the thinning of Indian plate cover between Raikhot and Bunar, it does not explain the occurrences of basement at Niat and other areas in the southern portions of the NPHM, nor is it consistent with the absence of evidence for significant normal motion on the MMT. Large pre-thrusting lateral fault ramp(s) in the Indian cover/basement contact (Fig. 13C, upper) or on the MMT (Fig. 13C, lower) could explain some of the thickness variation in the Indian cover, but cannot provide an explanation for the direction of shear sense along the MMT subparallel with the length of the NPHM, the distribution of basement within the cover, or the presence of high strain rocks, including the lath unit, located near the base of the cover sequence on both sides of the NPHM.

Stretching lineations

SW of the NPHM, Burg *et al.* (1996) and Hubbard *et al.* (1995) report regionally distributed SW-directed shear fabric that is accompanied by a *c.* SW plunging lineation on W to NW dipping foliation. We have observed lineation trends with a corresponding plunge in the southern portions of the Bunar and Niat/Thak valley systems, and in the SW region of Rupal valley. South of the portion where lineation is related to the northward dip of the main Rupal Chichi Shear Zone in SW Rupal, the *c.* SW plunging lineation is accompanied by clear SW-vergence (top to the SW); an apparently extensional motion that is consistent with that observed by Hubbard *et al.* (1995). Hubbard *et al.* (1995) proposed a tens of kilometres wide extensional shear zone based upon this apparently extensional motion and a simple assessment of metamorphic grade and deformation from which they concluded that lower grade rocks pass structurally downwards into medium and higher grade rocks. Burg *et al.* (1996) argued that the extensional fabric described by Hubbard *et al.* (1995) was actually a misinterpreted SW-directed shear fabric that was generated early in the history of India underthrusting the Kohistan island arc. We concur with Burg *et al.* (1996), applying their interpretation to much of our mapping outside the DSZ. In, for example, the SW Rupal valley, the extensive occurrence of a SW-plunging lineation coinciding with steep *c.* W-dipping foliation can be easily restored to a NE plunge if the foliation is rotated to become N-dipping, as part of a retrodeformation to a time that predates NPHM relative uplift. In this, we assume that the relative uplift of the centre of the massif has caused all the foliation on the western flank of the syntaxis to be rotated to steep W-dipping or locally overturned. This assumption is consistent with the observed E over W thrusting and overturning that is part of, or associated with, the Diamir Shear Zone.

In the southern portions of the Bunar and Niat/Thak valley systems, and in the lower cover of the Diamir and Airl Gah sections, we

additionally observe N- or NE-plunging lineations (Fig. 6). We suggest that these are part of the regional, non-overturned, MMT-related NW-plunging stretching lineation (Greco *et al.* 1989; Treloar *et al.* 1989); this lineation plunge would rotate to SW where original foliation has been overturned.

In the southwestern region of the NPHM, therefore, and indeed across the remainder of the massif (Edwards 1998; Schneider *et al.* 1999*a*), we have found no evidence for any major extensional structure (such as an STDS-type low angle detachment) that has allowed the very young unroofing and exhumation of the massif.

Conclusions

The Diamir Shear Zone is an E over W displacement structure with a minor wrench component that represents a crustal-scale reverse fault, together with the Raikhot Bridge portion of the Raikhot Fault System. It has resulted in overturning of the local MMT section in association with the Gashit Fold, as a response to the relative uplift/overthrusting, or 'bulging out', of the NPHM. NPHM-related rotation of pre-existing fabric is recognized throughout the Biji/Bunar and SW Rupal valleys. The $^{40}Ar/^{39}Ar$ cooling data show a steep age gradient that coincides with the Diamir Shear Zone, and indicates that it has accommodated very young relative uplift of the central portions of the Nanga Parbat massif.

The Indian plate cover rocks are thinned by >5 km due to variation in imbrication in the MMT footwall. The thick sequences that continue south from Nashkin–Airl are most likely the product of a frontal ramp in the MMT footwall, and they neither show evidence for any extensional thinning/exhumation, nor a tens of kilometre-scale nappe structure.

Research supported by USA National Science Foundation grants EAR 9418730 to W. S. F. Kidd and EAR 9418849 to P. K. Zeitler. We thank Aslam Mohammad (deceased), Sarbuland Khan, Akhtar Karim (deceased), Anton Seimon and Mitchel Wemple for logistic support, and A. Pêcher, L. Seeber and P. K. Zeitler for discussion. We thank R. W. H. Butler and P. J. Treloar for comments that helped us to improve the manuscript.

References

AHMED, Z. & CHAUDHRY, M. N. 1976. Petrology of the Babusar area, Diamir District, Gilgit, Pakistan. *Geological Bulletin, Punjab University*, **12**, 67–78.

ARGLES, T. W. 2000. The evolution of the Main Mantle Thrust in the western syntaxis, N. Pakistan. *This volume.*

BARD, J.-P. 1983. Metamorphism of an obducted island arc: an example of the Kohistan sequence (Pakistan) in the Himalayan collided range. *Earth and Planetary Science Letters*, **65**, 133–144.

——, MALUSKI, H., MATTE, P. & PROUST, F. 1980. The Kohistan sequence: crust and mantle of an obducted island arc. *Geological Bulletin of the University of Peshawar Special Issue*, **13**, 87–94.

BERTHÉ, D., CHOUKROUNE, P. & JEGOUZO, P. 1979. Orthogneiss, mylonite and non-coaxial deformation of granites: the example of the south Armorican shear zone. *Journal of Structural Geology*, **1**, 31–42.

BURG, J.-P., CHAUDHRY, M. N., GHAZANFAR, M., ANCZKIEWICZ, R. & SPENCER, D. 1996. Structural evidence for back sliding of the Kohistan arc in the collisional system of northwest Pakistan. *Geology*, **24**, 739–742.

BUTLER, R. W. H. & PRIOR, D. J. 1988. Tectonic controls on the uplift of the Nanga Parbat Massif, Pakistan Himalayas. *Nature*, **333**, 247–250.

——, —— & KNIPE, R. J. 1989. Neotectonics of the Nanga Parbat syntaxis, Pakistan, and crustal stacking in the northwest Himalayas. *Earth and Planetary Science Letters*, **94**, 329–343.

——, GEORGE, M. T., HARRIS, N. B. W., JONES, C., PRIOR, D. J., TRELOAR, P. J. & WHEELER, J. 1992. Geology of the northern part of the Nanga Parbat massif, northern Pakistan, and its implications for Himalayan tectonics. *Journal of the Geological Society, London*, **149**, 557–567.

CHAMBERLAIN, C. P., ZEITLER, P. K. & ERICKSON, E. 1991. Constraints on the tectonic evolution of the northwestern Himalaya from geochronologic and petrologic studies of Babusar Pass, Pakistan. *Journal of Geology*, **99**, 829–849.

——, —— & JAN, M. Q. 1989. The dynamics of a crustal suture in the Pakistan Himalaya. *Journal of Metamorphic Geology*, **7**, 135–149.

COWARD, M. P. 1985. A section through the Nanga Parbat syntaxis, Indus valley, Kohistan. *Geological Bulletin of the University of Peshawar*, **18**, 147–152.

—— & nine others. 1988. Folding and imbrication of the Indian crust during Himalayan collision. *Philosophical Transactions of the Royal Society of London*, **A326**, 89–116.

CRAW, D., KOONS, P. O., WINSLOW, D. M., CHAMBERLAIN, C. P. & ZEITLER, P. K. 1994. Boiling fluids in a region of rapid uplift, Nanga Parbat massif, Pakistan. *Earth and Planetary Science Letters*, **128**, 169–182.

DELL'ANGELO, L. N. & TULLIS, J. 1989. Fabric development in experimentally sheared quartzites. *Tectonophysics*, **169**, 1–21.

DIPIETRO, J. A., HUSSAIN, A., AHMED, I. & ASIF KHAN, M. 2000. The Main Mantle Thrust in Pakistan: its character and extent. *This volume.*

——, POGUE, K. R., LAWRENCE, R. D., BAIG, M. S., HUSSAIN, A. & AHMED, I. 1993. Stratigraphy of the Main Mantle thrust, Lower Swat, Pakistan.

In: TRELOAR, P. J. & SEARLE, M. P. (eds) *Himalayan Tectonics*. Geological Society, London, Special Publications, **74**, 207–220.

EDWARDS, M. A. 1998. *Examples of tectonic mechanisms for local contraction and exhumation of the leading edge of India. Southern Tibet (28–29°N; 89–91°E) and Nanga Parbat, Pakistan*. PhD thesis, State University of New York at Albany.

—— & KIDD, W. S. F. 1997. Structural investigations around southern and eastern Nanga Parbat. *In*: ANGIOLINI, L. *et al.* (eds) *Abstract Volume, 12th Himalaya–Karakoram–Tibet Workshop*. Accademia Nazionale dei Lincei, 29–30.

EISBACHER, G. H. 1970. Deformation mechanics of mylonitic rocks and fractured granites in Cobequid Mountains, Novia Scotia. *Canadian Bulletin of the Geological Society of America*, **81**, 2009–2020.

FOSTER, G., KINNY, P., VANCE, D., HARRIS, N., ARGLES, T. & WHITTINGTON, A. 1999. The pre-Tertiary metamorphic history of the Nanga Parbat Haramosh Massif, Pakistan, Himalaya. *In*: SOBEL, E. *et al.* (eds) *Abstract Volume, 14th Annual Himalayan–Karakorum–Tibetan Workshop*. Germany, 44–45.

GANSSER, A. 1964. *Geology of the Himalayas*. Wiley, London.

GEORGE, M. T. & BARTLETT, J. M. 1996. Rejuvenation of Rb–Sr mica ages during shearing on the northwestern margin of Nanga Parbat–Haramosh Massif. *Tectonophysics*, **260**, 167–185.

——, HARRIS, N. B. W. & BUTLER, R. W. H. 1993. The tectonic implications of contrasting granite magmatism between the Kohistan island arc and the Nanga Parbat—Haramosh Massif, Pakistan Himalaya. *In*: TRELOAR, P. J. & SEARLE, M. P. (eds) *Himalayan Tectonics*. Geological Society, London, Special Publications, **74**, 173–191.

——, REDDY, S. & HARRIS, N. 1995. Isotopic constraints on the cooling history of the Nanga Parbat—Haramosh Massif and Kohistan arc, western Himalaya. *Tectonics*, **14**, 237–252.

GHAZANFAR, M., CHAUDHRY, M. N. & HUSSAIN, M. S. 1991. Geology and petrotectonics of southeast Kohistan, northwest Himalaya. *Pakistan Kashmir Journal of Geology*, **8/9**, 67–97.

GRECO, A. & SPENCER, D. A. 1993. Geology of Kaghan Valley. *In*: TRELOAR, P. J. & SEARLE, M. P. (eds) *Himalayan Tectonics*. Geological Society, London, Special Publications, **74**, 221–236.

——, MARTINOTTI, G., PAPRITZ, K., RAMSEY, J. G. & REY, R. 1989. The Himalayan crystalline nappes of the Kaghan Valley (NE Pakistan). *Eclogicae Geologicae Helveticae*, **82**, 692–653.

HANMER, S. 1984. The potential use of planar and elliptical structures as indicators of strain regime and kinematics of tectonic flow. *Geological Survey of Canada Paper*, **84**, 133–142.

HONEGGER, K., DIETRICH, V., FRANK, W., GANSSER, A., THÖNI, M. & TROMMSDORFF, V. 1982. Magmatism and metamorphism in the Ladakh Himalayas (the Indus-Tsangpo suture zone). *Earth and Planetary Science Letters*, **60**, 253–292.

HOOPER, R. J. & HATCHER, R. D. 1988. Mylonites from the Towaliga fault zone, central Georgia: products of heterogeneous non-coaxial deformation. *Tectonophysics*, **152**, 1–17.

HUBBARD, M. S., SPENCER, D. A. & WEST, D. P. 1995. Tectonic exhumation of the Nanga Parbat Massif, northern Pakistan. *Earth and Planetary Science Letters*, **133**, 213–227.

KHAN, M. A., TRELOAR, P. J., KHAN, M. A., KHAN, T., QAZI, M. S. & JAN, Q. 1998. Geology of the Chalt–Babusar transect, Kohistan Terrane, N. Pakistan: implications for the constitution and thickening of island arc crust. *Journal of Asian Earth Sciences*, **16**, 253–268.

LE FORT, P. 1988. Crustal melting and granite genesis during the Himalayan collision orogenesis. *Transactions of the Royal Society of Edinburgh*, **79**, 183–195.

LEMMENICIER, Y., LE FORT, P., LOMBARDO, B., PÊCHER, A. & ROLFO, F. 1996. Tectonometamorphic evolution of the Central Karakoram (Baltistan, northern Pakistan). *Tectonophysics*, **260**, 119–143.

LISTER, G. S. & SNOKE, A. W. 1984. S–C Mylonites. *Journal of Structural Geology*, **6**, 617–638.

MADIN, I. P. 1986. *Structure and neotectonics of the northwestern Nanga Parbat–Harramosh massif*. MSc thesis, Oregon State University, Oregon.

——, LAWRENCE, R. D. & UR-REHMAN, S. 1989. The northwestern Nanga Parbat Haramosh Massif; Evidence for crustal uplift at the northwestern corner of the Indian craton. *In*: MALINCONICO, L. L. & LILLIE, R. J. (eds) *Tectonics of the Western Himalayas*. Geological Society of America Special Paper, **232**, 169–182.

MEANS, W. D. 1981. The concept of steady-state foliation. *Tectonophysics*, **78**, 179–199.

PAPRITZ, K. & REY, R. 1989. Evidence for the occurrence of Permian Panjal Trap basalts in the Lesser- and Higher-Himalayas of the Western Syntaxis area, NE Pakistan. *Eclogicae Geologicae Helveticae*, **82**, 603–625.

PASSCHIER, C. W. & SIMPSON, C. 1986. Porphyroclast systems as kinematic indicators. *Journal of Structural Geology*, **8**, 831–843.

PASSCHIER, C. W. & TROUW, R. A. J. 1996. *Microtectonics*. Springer-Verlag, Berlin & Heidelberg.

SCHNEIDER, D. A., ZEITLER, P. K., EDWARDS, M. A. & KIDD, W. S. F. 1997. Geochronological constraints on the geometry and timing of anatexis and exhumation at Nanga Parbat: A progress report. *Eos Transactions of AGU*, **78**, Spring Meeting Supplement, **17**, 111.

—— & eight others. 1999*a*. Synkinematic plutonism within the doubly-vergent shear zones of a crustal-scale pop-up structure. Active tectonics of Nanga Parbat, western Himalaya. *Geology* (in press).

——, EDWARDS, M. A., ZEITLER, P. K. & COATH, C. 1999*b*. Mazeno Pass Pluton and Jutial Granite, Pakistan Himalaya: Age and implications for entrapment mechanisms of two granites in the Himalaya. *Contributions to Mineralogy and Petrology*, **136**, 273–284.

——, ——, KIDD, W. S. F., ZEITLER, P. K. & COATH, C. 1999*c*. Early Miocene anatexis identified in the western syntaxis, Pakistan Himalaya. *Earth & Planetary Science Letters*, **167**, 121–129.

——, ZEITLER, P. K., EDWARDS, M. A., KIDD, W. S. F. & COATH, C. 2000. Evolution of a Himalayan gneiss done at Nanga Parbat, northern Pakistan. *Tectonics*, in press.

SMITH, H. A., CHAMBERLAIN, C. P. & ZEITLER, P. K. 1992. Documentation of Neogene regional metamorphism in the Himalayas of Pakistan using U–Pb in monazite. *Earth & Planetary Science Letters*, **113**, 93–105.

——, —— & —— 1994. Timing and denudation of Himalayan metamorphism with the Indian plate, NW Himalaya, Pakistan. *Journal of Geology*, **103**, 493–508.

TAHIRKHELI, R. A. K. 1982. Geology of the Himalaya, Karakoram, and Hindu Kush, Pakistan. *University of Peshawar Geological Bulletin*, **15**, 1–50.

——, & JAN, M. Q. 1979. Geology of Kohistan, Karakoram Himalaya, northern Pakistan. *University of Peshawar Geological Bulletin* Special Issue, **11**, 189 pp.

TRELOAR, P. J., BROUGHTON, R. D., WILLIAMS, M. P., COWARD, M. P. & WINDLEY, B. F. 1989. Deformation, metamorphism and imbrication of the Indian plate, south of the Main Mantle Thrust, north Pakistan. *Journal of Metamorphic Geology*, **7**, 111–127.

——, POTTS, G. J., WHEELER, J. & REX, D. C. 1991. Structural evolution and asymmetric uplift of the Nanga Parbat syntaxis, Pakistan Himalaya. *Geologische. Rundschau*, **80**, 411–428.

TULLIS, J. & YUND, R. A. 1985. Dynamic recrystallisation of feldspar: a mechanism for ductile shear zone formation. *Geology*, **13**, 238–241.

—— & —— 1991. Diffusion creep in feldspar aggregates: experimental evidence. *Journal of Structural Geology*, **13**, 987–1000.

WADIA, D. N. 1931. The syntaxis of the northwest Himalaya, tectonics and orogeny. *Records of the Geological Survey of India*, **65**, 189–220.

——, 1932. Note on the geology of Nanga Parbat (Mt. Diamir), and adjoining portions of Chilas, Gilgit district, Kashmir. *Records of the Geological Survey of India*, **66**, 212–234.

WHEELER, J., TRELOAR, P. & POTTS, G. 1995. Structural and metamorphic evolution of the Nanga Parbat syntaxis, Pakistan Himalayas, on the Indus gorge transect: the importance of early events. *Geological Journal*, **30**, 349–371.

WHITTINGTON, A. G. 1996. Exhumation overrated at Nanga Parbat, northern Pakistan. *In*: BURG, J.-P. (ed.) Uplift and exhumation of metamorphic rocks. The Himalayan Tibet region. *Tectonophysics*, **260**, 215–226.

WINSLOW, D. M., ZEITLER, P. K., CHAMBERLAIN, C. P. & HOLLISTER, L. S. 1994. Direct evidence for a steep geotherm under conditions of rapid denudation, western Himalaya, Pakistan. *Geology*, **22**, 1075–1078.

——, ——, —— & WILLIAMS, I. S. 1996. Geochronologic constraints on syntaxial development in the Nanga Parbat region, Pakistan. *Tectonics*, **15**, 1292–1308.

——, CHAMBERLAIN, C. P. & ZEITLER, P. K. 1995. Metamorphism and melting of the lithosphere due to rapid denudation in the northwest Himalaya. *Journal of Geology*, **103**, 395–409.

ZEITLER, P. K. 1985. Cooling history of the northwest Himalaya, Pakistan. *Tectonics*, **4**, 127–151.

—— & CHAMBERLAIN, C. P. 1991. Petrogenetic and tectonic significance of young leucogranites from the northwestern Himalaya, Pakistan. *Tectonics*, **10**, 729–741.

——, —— & SMITH, H. A. 1993. Synchronous anatexis, metamorphism, and rapid denudation at Nanga Parbat, Pakistan Himalaya. *Geology*, **21**, 347–350.

——, JOHNSON, N. M., NAESER, C. W. & TAHIRKHELI, R. A. K. 1982. Fission-track evidence for the Quaternary uplift of the Nanga Parbat region, Pakistan. *Nature*, **298**, 255–257.

——, SUTTER, J. F., WILLIAMS, I., ZARTMAN, R. E. & TAHIRKHELI, R. A. K. 1989. Geochronology and temperature history of the Nanga Parbat–Haramosh Massif, Pakistan, *In*: MALINCONICO, L. L. & LILLIE, R. J. (eds) *Tectonics of the Western Himalayas*. Geological Society of America Special Paper, **232**, 1–22.

The evolution of the Main Mantle Thrust in the Western Syntaxis, Northern Pakistan

T. W. ARGLES

Department of Earth Sciences, The Open University, Walton Hall, Milton Keynes MK7 6AA, UK (e-mail: t.w.argles@open.ac.uk)

Abstract: Neogene events in the Nanga Parbat–Haramosh massif have obscured much of its earlier evolution. However, structural mapping of the eastern margin reveals a ductile contact zone preserving many features of the original Main Mantle Thrust that emplaced the Ladakh island arc over the Indian margin in the late Cretaceous. The sequence of ductile deformation was controlled both by the contrasting rheologies of the Ladakh island arc and the Main Mantle Thrust footwall, and the changing thermal regime during subduction, collision and burial. Preliminary P–T estimates indicate conditions during southward thrusting on the Main Mantle Thrust of *c.* 650 °C and 9.5 kbar, with later deformation (post-dating garnet growth) in some units at *c.* 500 °C and 7.4 kbar. The concordant fabrics and lithological boundaries on either side of the contact are only disrupted by a NW-vergent, brittle thrust south of the village of Subsar (Indus gorge) which cross-cuts the steepened Main Mantle Thrust Zone. This thrust is related to the neotectonic Liachar Thrust on the western margin of the massif, and is an expression of the regional tectonics at the western termination of the Himalayan arc. This late thrusting followed formation of the syntaxial antiform in Neogene times.

Studies in orogenesis have always provided a wealth of data on the latter stages of the evolution of mountain belts (e.g. Zeitler 1985; Dewey *et al.* 1988; Platt & Vissers 1989; Hodges *et al.* 1992; Smith *et al.* 1992; Searle 1996; Andersen 1998), while the earlier stages of their evolution often remain obscure. In particular, the proliferation of isotopic methods for characterizing orogenic processes, and their dependence on closure temperatures for data, means that results are weighted towards the end of any mountain-building episode. Techniques such as U–Pb and Sm–Nd dating can reveal information on orogenic processes further in the past (Cliff 1981; Vance & O'Nions 1992; Vavra *et al.* 1994), but in isolation these data have limited value in deciphering the processes occurring early in an orogenic episode, or in previous orogenies. An integrated approach is required to provide a context for these data and interpret the partial record of these earlier processes, particularly when studying major structural lineaments with long and commonly polyphase histories.

Himalayan research throughout its history has focused on the major contacts separating the terranes which make up the mountain belt (see Le Fort 1996, and references therein). These contacts, from south to north, are the Main Frontal Thrust, the Main Boundary Thrust, the Main Central Thrust, the South Tibet Detachment System, and the Indus–Tsangpo Suture Zone (or Main Mantle Thrust in the west). These separate the Indo-Gangetic plain in the south from the Sub-Himalaya (Neogene molasse), the Lesser Himalaya (low-medium grade metamorphic rocks), the Higher Himalaya (high-grade metamorphic rocks and leucogranites), the Tethyan Himalaya (sedimentary cover) and Tibet (including the Transhimalayan batholith). These components of the orogen were defined by Gansser (1964), except for the South Tibet Detachment System, whose significance was only recognized later (Burg *et al.* 1984; Burchfiel & Royden 1985). The terranes and contacts show remarkable arc-parallel continuity, with the exception of the Main Frontal Thrust and the South Tibet Detachment System, although even the latter has been mapped in southern Tibet, Nepal and western India (Herren 1987; Burchfiel *et al.* 1992). However, the position of the Main Central Thrust in Pakistan is controversial, and neither the Main Central Thrust nor the South Tibet Detachment System can be traced into the Nanga Parbat–Haramosh massif. In many cases, the 'contacts' are high-strain zones up to several kilometres wide (e.g. Le Fort 1996), particularly

From: KHAN, M. A., TRELOAR, P. J., SEARLE, M. P. & JAN, M. Q. (eds) *Tectonics of the Nanga Parbat Syntaxis and the Western Himalaya*. Geological Society, London, Special Publications, **170**, 101–122. 1-86239-061-4/00/$15.00

in the metamorphic core of the orogen, as might be expected for such major lineaments. As a result, it may be impossible to define a single thrust surface within the zone; the Main Central Thrust is obscure along much of its length, and there is considerable tectonic interleaving within the Main Mantle Thrust Zone in Northern Pakistan (e.g. Butler *et al.* 1992).

The situation in Northern Pakistan is complicated by the Kohistan–Ladakh island arc, which is sandwiched between the Indian and Eurasian plates (Fig. 1, inset); it is bounded to the north and south by the Main Karakoram Thrust and the Main Mantle Thrust respectively. This study follows Butler & Prior (1988*a*) and Butler *et al.* (1992) in defining the 'Main Mantle Thrust' as the ductile contact between the Kohistan–Ladakh island arc and the Indian plate which shows top-to-the-south shear sense, post-dating arc magmatism. The excision of lower arc rocks at the contact implies that the thrust does not equate to the original subduction zone, although fabrics in both footwall and hanging wall are parallel (Butler & Prior 1988*a*).

The aim of this study is to provide a preliminary framework for further study of the lesser-known eastern margin of the Nanga Parbat–Haramosh massif, by characterizing the structural and metamorphic evolution of the Main Mantle Thrust Zone. Unlike much of the western contact, the eastern margin contains a wealth of information on the earlier parts of the Himalayan orogenic episode, and also pre-Himalayan events. It is hoped that field relationships documented here will enable ongoing geochemical and isotopic studies to be focused efficiently, and aid in the interpretation of their data, particularly with respect to age determinations.

Geological context

The Himalayan arc terminates abruptly at both extremities in pronounced antiformal re-entrants of the main thrust systems, enclosing the most northerly exposures of Indian plate rocks in the orogen. These syntaxes (Namche Barwa to the east and Nanga Parbat to the west) contain rocks from deep structural levels exposed by some of the most rapid recent exhumation in the mountain belt (e.g. Zeitler *et al.* 1993). Much of the established anatomy of the central Himalayas is distorted or absent in the vicinity of the syntaxes; the Nanga Parbat–Haramosh massif (Fig. 1) lacks recognizable analogues of the Main Central Thrust or the South Tibet Detachment System, and even the affinities of the gneisses which form the bulk of the massif are debatable (Whittington *et al.* 1999, 2000). Other structural features were re-orientated N–S during syntaxis formation, including the Main Mantle Thrust, which separates the Indian plate rocks from the Ladakh and Kohistan island arc associations (Tahirkheli *et al.* 1979; Coward 1985), and originally dipped gently north. There are varying degrees of tectonic and metamorphic overprinting in the massif; hence the western margin of the syntaxis is modified by strike-slip (Shahbatot Fault) and top-to-the-NW thrust faulting (Liachar Thrust) (Butler & Prior 1988*b*; Butler *et al.* 1989), while in the core of the massif, anatectic leucogranites have been dated at 1 to 7 Ma (Zeitler & Chamberlain 1991; Zeitler *et al.* 1993). The relative contributions of Neogene, Himalayan and earlier (generally Precambrian) processes to the present aspect of the rocks within the syntaxis is much debated (e.g. Butler *et al.* 1992; Wheeler *et al.* 1995; Chamberlain & Zeitler 1996); but since the degree of reworking varies with both lithology and locality (Butler *et al.* 1992, 1997; Wheeler *et al.* 1995), generalization is impossible.

Eastern margin of the Nanga Parbat–Haramosh massif

The eastern flank of the Nanga Parbat–Haramosh massif (Fig. 2) has received less attention than the western because the latter is readily accessible from the Karakoram Highway and the Indus valley, while the former cuts more isolated mountainous terrain. To the south, study is further restricted near the border with occupied Kashmir. The most accessible section is at Stak Nala on the Gilgit–Skardu road, but this turns out to be atypical of the contact, a fact which may have been exploited by the down-cutting Indus River through the syntaxis. Elsewhere, the eastern margin of the syntaxis differs markedly from the western contact. Although there is some brittle faulting along the contact (e.g. the 'Stak Fault': see Verplanck 1986; Pognante *et al.* 1993; Le Fort *et al.* 1997), later workers have de-emphasized the extent of brittle deformation, viewing the eastern contact essentially as a major ductile contact variably steepened during syntaxis formation (Butler *et al.* 1992), preserving top-to-the-south shear (Wheeler *et al.* 1995). Figure 1 shows some faulting in the Indus gorge, but also a late thrust just to the south that cuts and offsets the eastern contact, of similar style and possibly related to the 'Stak Fault' to the north. The presence of both a large amphibolite body with arc affinities west of these faults (Wheeler *et al.* 1995) and minor occurrences of mélange containing ultramafic lenses (Le Fort

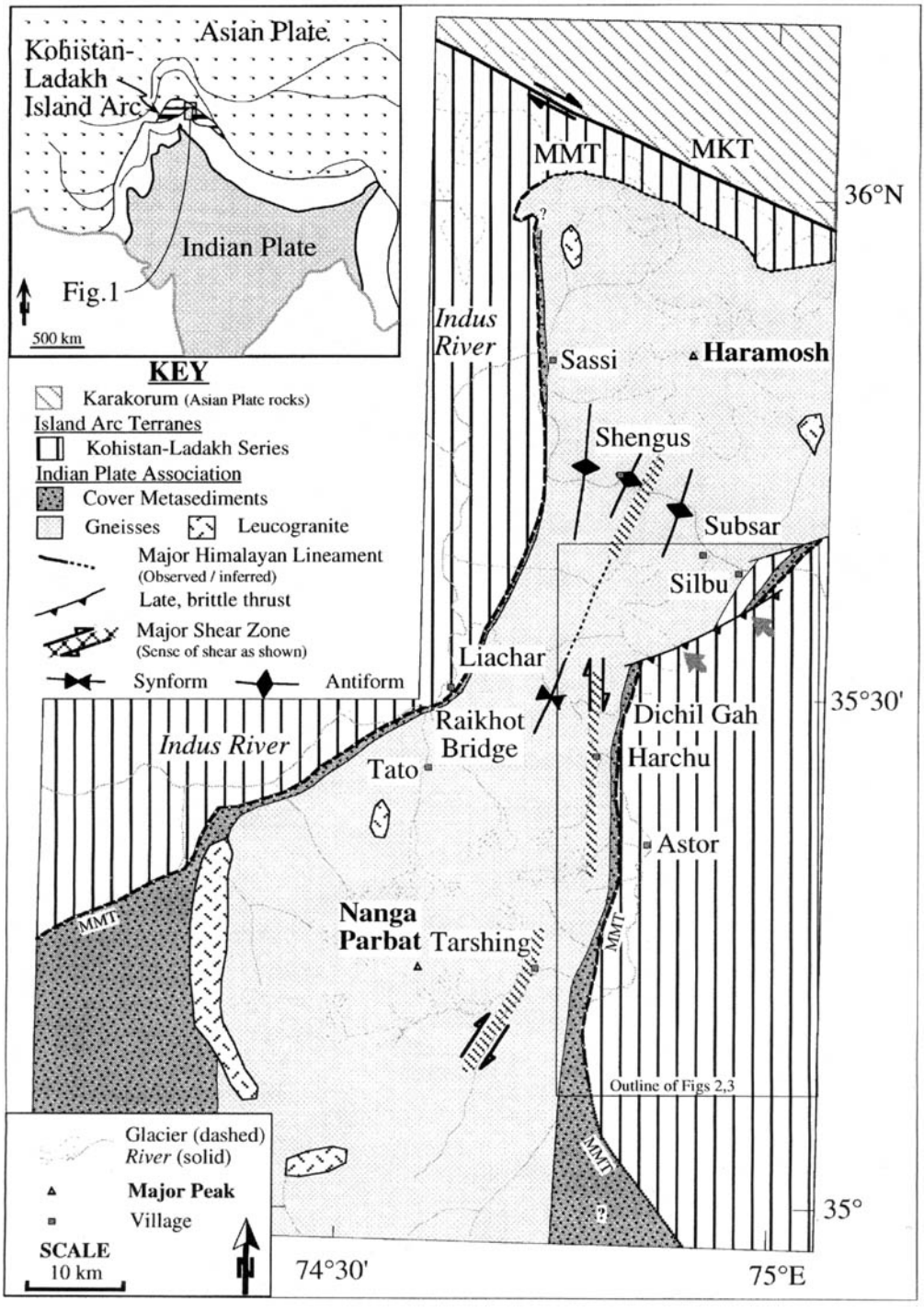

Fig. 1. Location of the Nanga Parbat–Haramosh massif and study area. Inset shows location of western syntaxis in the context of the India–Asia collision zone. The Indian plate is shown in grey, the Asian is stippled; the Himalaya are unornamented. Major structural features of the syntaxis are also shown. MMT, Main Mantle Thrust; MKT, Main Karakoram Thrust.

et al. 1997) suggests a degree of tectonic interleaving at the contact. The ultramafic lenses confirm the correlation of this contact with the Indus suture to the east, and the Main Mantle Thrust to the west in Pakistan (e.g. Desio & Shams 1980; Jan 1985). There has been considerable uncertainty on the nature of the contact between the Indus and Astor valleys (e.g. Searle *et al.* 1996; Le Fort *et al.* 1997), which this paper hopes to address by presenting maps of the contact from the village of Subsar (Fig. 1) on the Gilgit–Skardu road to the village of Rattu to the south (Figs 2, 3), along with a number of detailed traverses across the contact zone (Fig. 4).

Description of the eastern margin

Lithological units

The Nanga Parbat–Haramosh massif has been divided broadly into 'cover' and 'basement' rocks (e.g. Butler & Prior 1988*a*), the former occurring as thin sections along the margins of the massif, rarely more than a few hundred metres thick, except in the south. The basement has been subdivided into Iskere and Shengus gneiss (Chamberlain *et al.* 1989; Madin *et al.* 1989), which although possibly applicable in the northern part of the massif is less tenable elsewhere; in the vicinity of Nanga Parbat Sm–Nd model ages indicate that the basement rocks are a single, coherent Proterozoic complex of orthogneisses and paragneisses with a distinct signature typical of Lesser Himalayan units elsewhere in the orogen (Whittington *et al.* 1999, 2000). The cover has an entirely different isotopic character, usually indicating High Himalayan affinities (Whittington *et al.* 1999, 2000).

A variety of leucocratic rocks, from concordant layers to discordant dykes, occur throughout the massif (e.g. Wheeler *et al.* 1995); some larger leucogranite bodies with dates ranging from 24 to <1 Ma are also present (Zeitler & Chamberlain 1991), and a number of mafic dykes (e.g. Butler *et al.* 1992; Pognante *et al.* 1993; Whittington 1997; Treloar *et al.* this volume) which in some cases cross-cut the basement gneissic banding (Butler *et al.* 1992; Wheeler *et al.* 1995). In the core of the massif, one- or two-mica orthogneisses, often augen gneisses, dominate, with subsidiary leucogranite and rare mafic dykes; the proportion of paragneisses increases towards the eastern margin, with pelites and calcareous semi-pelites dominant. Other rock types include garnet-bearing amphibolites, calc-silicate and thin marble layers, and leucogranites (commonly peraluminous, garnet–tourmaline leucogranites, some with Al-silicate).

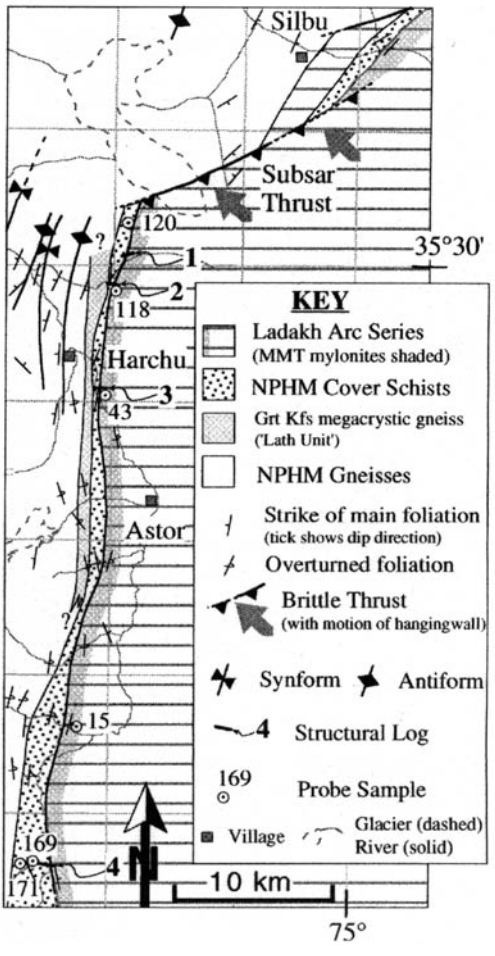

Fig. 2. Summary map of the eastern margin of the Nanga Parbat–Haramosh massif, showing major lithological divisions and structural features. Foliation data are a representative selection to avoid congestion; note the extensive zone of overturned rocks adjacent to the Main Mantle Thrust from Harchu southwards, and the anomalous strikes in the NE part of the map, near Silbu. The locations of the four structural traverses (Fig. 4) are marked in bold. Also marked are the locations of samples used for thermobarometry. Note the overall co-parallelism of lithological and structural boundaries, fold axes and foliation strikes, indicating the coherent ductile nature of the contact, with the exception of the cross-cutting thrust south of Silbu. NPHM, Nanga Parbat–Haramosh massif. MMT, Main Mantle Thrust.

The cover rocks are a similar association, but at lower grade; true pelites are more common and marble layers thicker and more abundant, particularly west of Rattu where the cover section thickens appreciably and includes pure quartzites intercalated with the marbles.

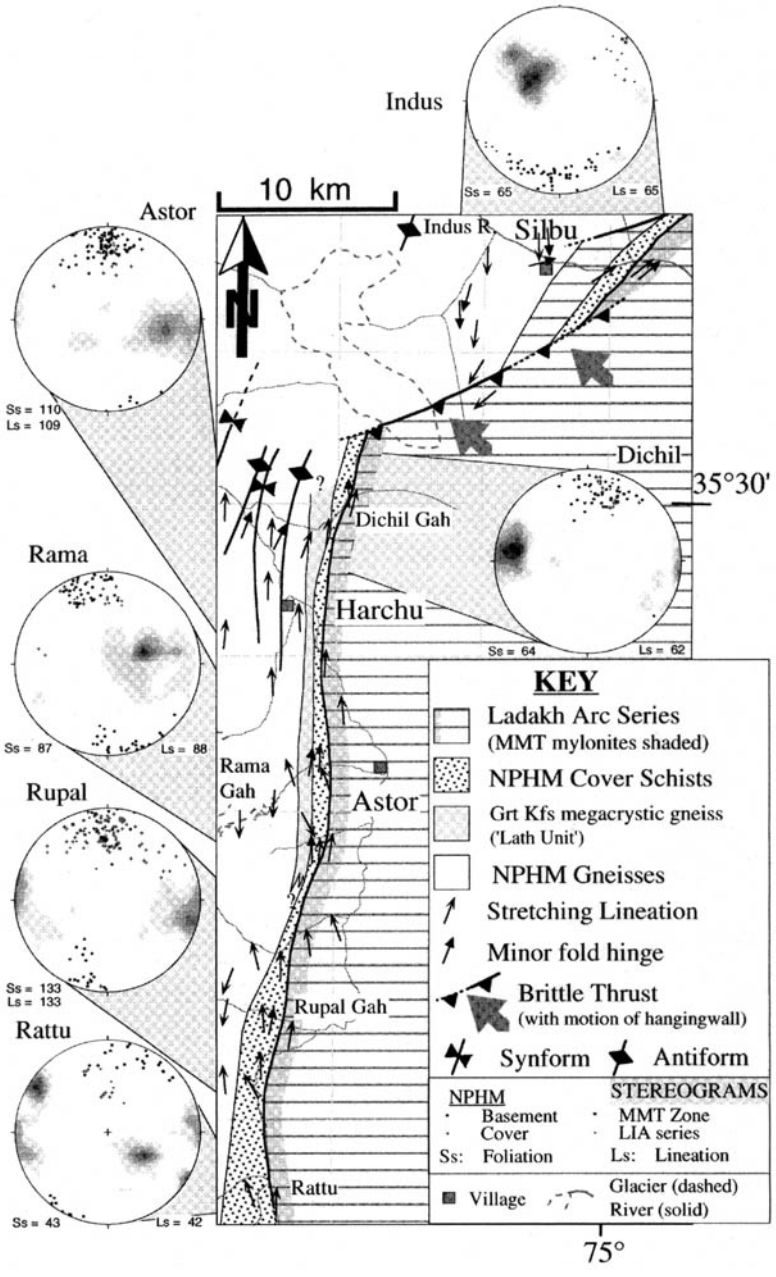

Fig. 3. Orientation of stretching lineations along the eastern margin of the Nanga Parbat–Haramosh massif. As in Fig. 2, data symbols are a representative sample to avoid overcrowding. Stereograms show full datasets for the valleys indicated approximately by the shading. Rattu and Dichil include data for Rattu and Dichil Gah alone respectively; Rupal includes data from Rupal, Chhugam and Gurikot valleys; Rama includes Rama and Bulan valley data; Astor includes data from Harchu and Mamocha valleys as well as the main Astor valley; Indus includes data from Subsar Gah and the Indus gorge. In all cases, data are only included from localities included within the map area as shown. Stereograms combine 1% area contoured poles to foliations with scatter plots of lineations. Most foliations are steep, while lineations trend broadly N–S, mostly plunging N. Notable features are the scatter of cover lineations, particularly in the Rupal area, reflecting the less regular deformation style of the cover sequence, and the swing to the NE of lineations within the Indus area. Abbreviations as Fig. 2, except LIA, Ladakh island arc.

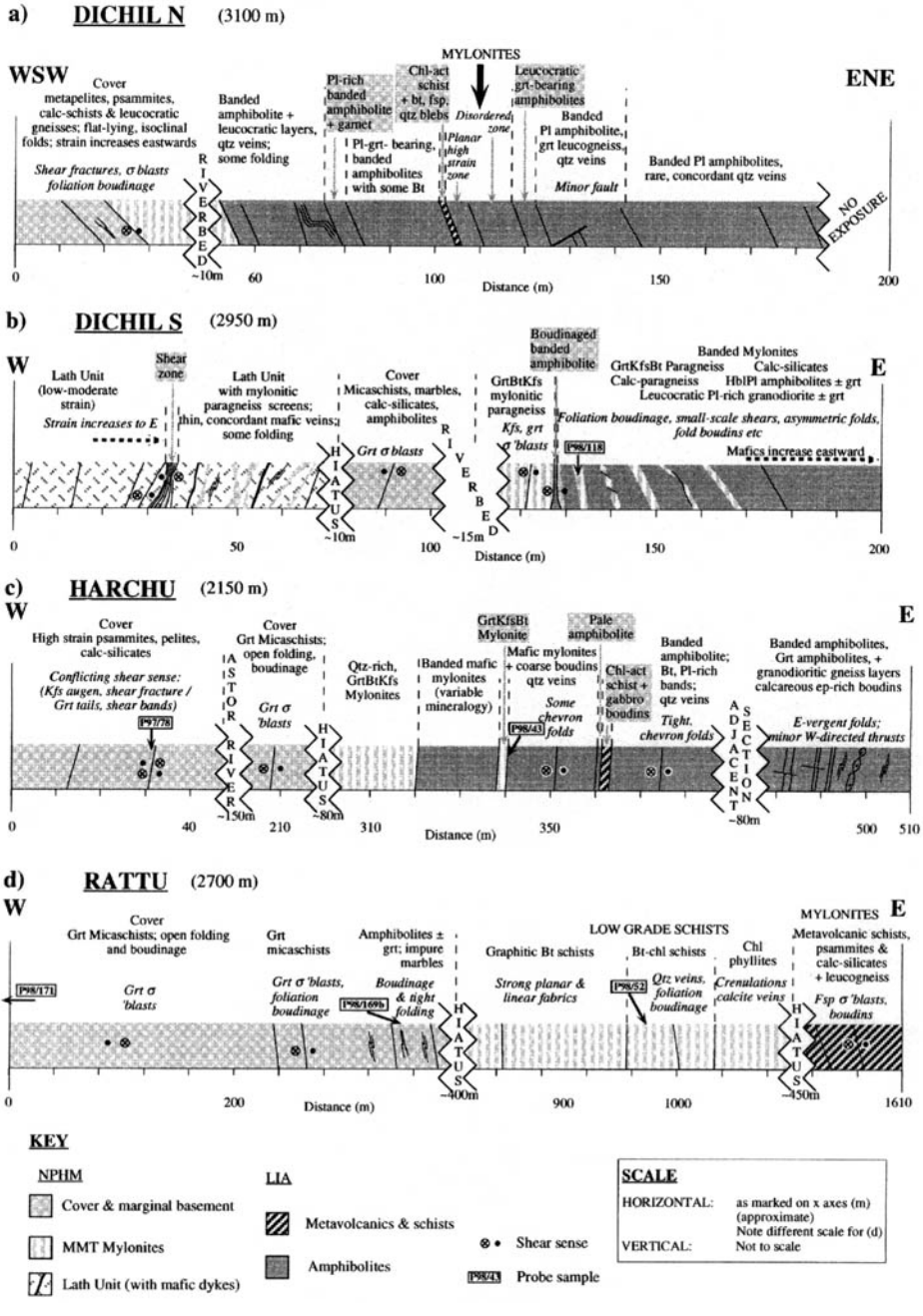

Fig. 4. Four schematic traverses across the Main Mantle Thrust Zone from Dichil Gah in the north to Rattu Gah in the south (see Fig. 2 for locations). The attitude of the foliation and boundaries is schematic, but with actual structural data employed, and since foliations invariably strike perpendicular to the traverses the representation is quite faithful. Lithologies and other features in plain type; structural features in italics. Sense of shear is shown where unequivocally determined. Some probe samples are marked (in boxes). Note the overturned nature of the Dichil S and Harchu sections, while Dichil N is clearly on the eastern limb of the syntaxis antiform; the most attenuated cover sequence also occurs in Dichil S, caught between the Lath Unit and the Main Mantle Thrust mylonites. The variation in tectonic interleaving of Ladakh island arc and Nanga Parbat–Haramosh massif rocks is illustrated clearly, as well as the lithological variation along the contact (see text).

Adjacent to the margin in some sections there are lower-grade biotite–chlorite schists lacking garnet; these also thicken southwards, reaching a thickness of some 250–300 m at Rattu (Fig. 5a). Whichever rock type is adjacent to the eastern contact with the arc rocks possesses an intense ductile fabric grading into the mylonites of the contact zone (Fig. 5b).

Between Dichil Gah and Gurikot Gah there is another lithological component to the eastern margin, occurring in the basement/cover contact zone. This is a striking K-feldspar–megacrystic augen gneiss (the 'Lath Unit'), distinctly different to the orthogneisses in the massif interior, with 1–4 cm Carlsbad-twinned K-feldspars and garnets up to 5 mm. The unit is at most a few hundred metres thick, exhibiting strong strain at its margins but in some cases only weakly deformed in the interior. Its margins include thin, concordant screens of mylonitic paragneiss, which may be tectonically interleaved but most probably reflect sheeting of the original intrusion into the country rock. Outcrops in Dichil Gah in the strain shadow of a large body of mafic rock suggest the Lath Unit intruded (or possibly mingled with) the mafic material, and therefore presumably also intruded the host paragneisses. The Lath Unit is difficult to trace south of Gurikot Gah, which may be the limit of the original intrusion; however, this difficulty extends to other units, making detailed north–south correlation suspect. This may reflect a number of factors, including tectonic excision of units, plunge of syntaxial structures and variation in ductile strain both across and along strike. The rocks in the Main Mantle Thrust contact zone on the Gilgit–Skardu road are very different to those described above.

Basement paragneisses similar to those in the south of the Nanga Parbat–Haramosh massif, with strongly boudinaged calc-silicate layers and mafic dykes (e.g. at Subsar), give way around the village of Silbu to amphibolites with garnet and plagioclase identical to rocks from the Ladakh island arc series (Wheeler *et al.* 1995), intercalated with granodioritic and granitic gneisses. The contact between the two is not exposed in the Indus gorge, but the rapid change in structural orientations suggests a discontinuous, brittle contact. Faults in identical lithologies occur on the jeep road north into the Stak valley to the east, and between the two is a prominent col on the ridge to the west of the Stak river, suggesting a through-going fault zone as shown in Figs 1–3. The section along the Indus gorge to the eastern contact is composed largely of arc amphibolites and granitoids, but includes low-grade micaschists, calc-silicates, and ultramafic pods in a mélange-type association. The schists probably represent the groundmass of a mélange whereby ultramafic material was brought up from depth along the Main Mantle Thrust (Le Fort *et al.* 1997). Ten kilometres to the south, in the valley running south of Subsar, a major thrust (the Subsar Thrust) juxtaposes calcareous, hornblende-bearing gneisses, amphibolites and some pelites in its footwall with typical Ladakh arc amphibolites, metagabbros and pyroxenites. The absence of cover rocks is probably due to excision by the thrust cross-cutting the steep Main Mantle Thrust, but the footwall gneisses are largely uncharacteristic of the Nanga Parbat–Haramosh massif to the south, and further attest to the presence of anomalous structure in the area.

The Ladakh arc series rocks at the contact are dominantly high-strain amphibolite mylonites, with garnet–hornblende-bearing leucocratic veins and pods in less strained outcrops. In rare cases, individual layers up to a metre thick with chlorite–ferro-tschermakite assemblages occur in the mylonite zone. Coarser lithologies in scree, moraines and riverbed deposits include metagabbros, pyroxenites (including chrome diopside–rich layers), and granodiorites. From Astor village south there are occurrences of chlorite–amphibole–epidote schists adjacent to the Main Mantle Thrust Zone, of highly variable thickness (usually less than 100 m wide), which represent fragments of the supra-arc volcanogenic sediments (Pudsey 1986; Searle 1991).

Structure of the Ladakh/Nanga Parbat contact

Ductile

The eastern margin of the Nanga Parbat–Haramosh massif is, for much of its length, a steep, ductile zone of high strain dominated by structures associated with the southward emplacement of the Kohistan–Ladakh island arc over the Indian plate. The zone dips eastward from the Stak valley to Dichil Gah, but to the south it is either vertical or overturned, along with the adjacent Indian plate rocks (Fig. 2). This oversteepening is likely related to the recent uplift history of the massif. Despite these minor variations in the attitude of the Main Mantle Thrust Zone, linear fabrics in adjacent rock units conform to the pattern of the whole massif and trend N–S, plunging gently north in most cases. South-plunging stretching lineations characterize the Rupal valley from Churit to Tarshing, upper

(a)

(b)

Fig. 5. (**a**) High-strain, biotite grade schists *c.* 350 m west of the Main Mantle Thrust, Rattu Gah. Stretching lineation plunges north on subvertical foliation. Note fold in calcareous layer below lens cap (6 cm diameter). (**b**) Boudinage and asymmetric shears in banded mylonites, locality P98/118, Dichil Gah, looking south. Dark amphibolites interleaved with brown metapelites and pale calc-silicates. Hammer, lower left quadrant, for scale. (**c**) Looking ENE at fracture with stepped quartz slickenfibres in Subsar Gah. Fracture dips 22° to 244°; motion is top-to-the-NW. Interpreted as a subsidiary footwall fault to the Subsar Thrust. Hammer, centre, for scale. (**d**) Thrust and fault propagation fold in banded calc-silicates and amphibolites, Subsar Gah, looking south and down at inclined surface. Thrust runs left to right just below lens cap (note truncation of layers centre left), with top-to-the-west motion. Lens cap 6 cm across.

Rama Gah, and rocks in the vicinity of Silbu on the Indus. The latter are largely due to the slightly anomalous strikes of the main foliation round Silbu, but the occurrences further south are more problematic. They may be related to discrete high-strain zones such as the Rupal–Chhichi Nala Shear Zone (well exposed south from Tarshing along Chhichi Nala), or a similar zone at Harchu, which trend roughly N–S through the massif (Fig. 1). North–south correlation of these zones is difficult, but the Harchu Shear Zone runs south from the east limb of a tight antiform (Figs 2, 3), and this may be part of the change in style from the open folds of the

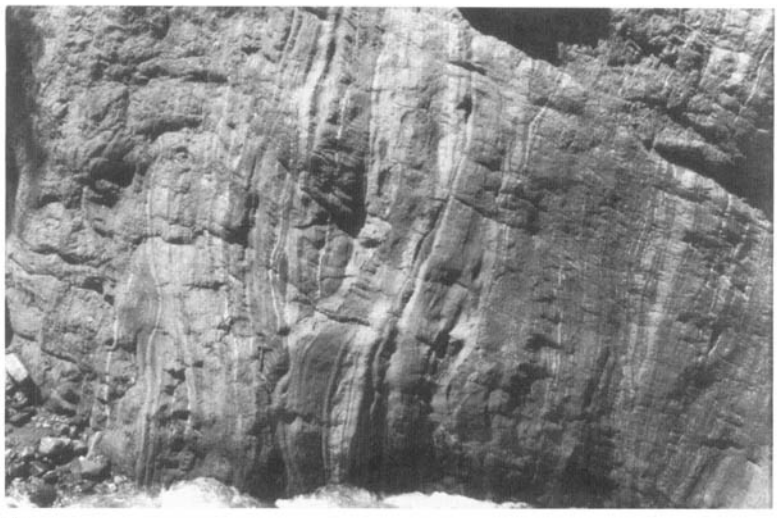

(c)

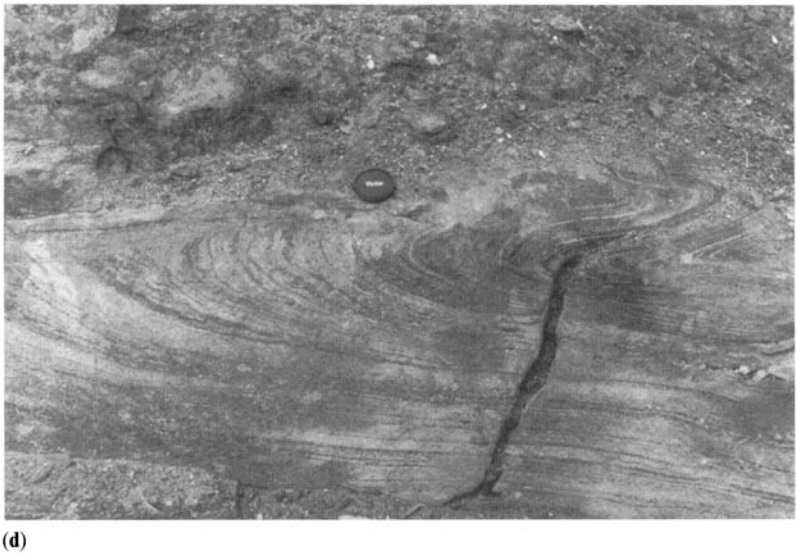

(d)

Indus gorge to the apparently unfolded, variably strained sections to the south. Even in the Indus section, the two major antiforms are separated not by a synform but a mylonite zone (e.g. Wheeler *et al.* 1995), and this is characteristic of the large-scale configuration of the main foliation within the massif. The anomalous orientations of fabrics round Silbu (and further north) may be due to a change in general trend of the contact from N–S to NE–SW. Southwest of Silbu, N–S lineations swing in to trend NE near the contact, and lineations in the Ladakh island arc amphibolite sheet within the massif at Silbu all have this trend (Fig. 3); brittle deformation may have accentuated these anomalies subsequently.

The N–S lineations reflect the steep, N–S-striking foliation along the eastern margin, but are also interpreted as recording the original southward emplacement of the Kohistan–Ladakh island arc over the Indian plate margin early in the Himalayan orogeny (e.g. Butler *et al.* 1992). Both planar and linear fabrics are formed by amphibolite-grade minerals in all rock types, and there is surprisingly little evidence for retrograde shearing. Garnets in the metapelitic cover schists are prograde-zoned and contain included fabrics (commonly graphite) oblique to the external foliation; some are demonstrably syn-kinematic, with sigmoidal inclusion trails. These garnets have been dated at between 40 and

45 Ma using the Sm–Nd method (Foster *et al.* 1998), in excellent agreement with eclogites from the Kaghan valley in Northern Pakistan (49 Ma; Tonarini *et al.* 1993). This confirms that the main foliation is related to Himalayan collision. In the basement gneisses, this foliation is axial-planar to tight or rootless folds in the gneissic banding, and also affects the mafic dykes which cross-cut gneissic banding; a few incompletely transposed examples trend oblique to the foliation (Wheeler *et al.* 1995). Further evidence for the Himalayan age of the foliation is in its parallelism to tectonically interleaved sheets of Ladakh island arc and Nanga Parbat–Haramosh massif material within the Main Mantle Thrust Zone along the eastern margin (e.g. Wheeler *et al.* 1995 and Fig. 4).

Shear sense in the high-strain Main Mantle Thrust Zone is generally dextral, i.e. indicative of original southward thrusting of the arc over the Indian margin. Kinematic indicators are few and far between, the intensity of the strain resulting in a strong parallelism of fabric elements. In addition, the mylonites' relatively coarse matrix grain size indicates a degree of metamorphic annealing, which may have erased non-coaxial indicators. This is particularly true of the Ladakh amphibolite mylonites, which generally lack porphyroblast phases and form very coherent mylonites. Structural style is strongly controlled by rheology in the Main Mantle Thrust Zone; quartz-rich mylonites along the Main Mantle Thrust are also coherent, but the varied cover sequence shows abundant evidence of strain partitioning with the result that structure is less consistent (Fig. 3). Coherent amphibolites and calc-silicates are boudinaged (Fig. 5b), while pelitic schists develop anastomosing fabrics, with shear band structures in places. Strain is strongly partitioned along both margins of the Lath Unit, while its interior, like much of the massif core, is much less deformed. This strain variation so near the contact suggests that the fabrics deep in the interior of the massif might not be directly related to motion on the Main Mantle Thrust. The narrow zone between the easternmost paragneisses and the Main Mantle Thrust is characterized by further strain partitioning and evidence for a complex kinematic evolution; work is in progress to constrain the details and implications of the history of this zone.

Brittle

The eastern margin of the Nanga Parbat–Haramosh massif is a dominantly ductile structure from Dichil Gah southwards to Rupal Gah. South of here, the contact zone is poorly exposed in the main river valley, and this may be due to exploitation of brittle faults. However, another cause may be the susceptible rock types on both sides of the contact here (Fig. 4). In several excellent sections across the contact (four of which are shown in Fig. 4), few brittle features are found. Mylonites of all compositions contain uncommon, minor shear fractures of centimetre scale. Most of these are associated with boudinage structures in competent layers such as amphibolites or calc-silicates, and may therefore have formed while the less competent mylonites were deforming plastically. Entirely brittle faults are hardly observed at all (e.g. Fig. 4a, c), and are unsystematic, isolated occurrences. Veining in some localities indicates hydraulic fracturing associated with the contact (e.g. at Rattu, Fig. 4d), but many veins have been subsequently rotated into parallelism with the ductile fabrics and must be due to high fluid pressure during ductile deformation.

One part of the margin (from Stak Nala to just north of Dichil Gah) is characterized by more abundant brittle features (Verplanck 1986; Pognante *et al.* 1993; Le Fort *et al.* 1997). A major top-to-the-NW thrust fault (Fig. 6) has been mapped in the valley running south from the village of Subsar, along with subsidiary brittle features within the footwall whose kinematics are identical to those of the main fault (Fig. 5c, d). The main fault dips 23–30° SE, with almost entirely down-dip lineations. Abundant, systematic, west-dipping fractures in the massive leucogneisses in the immediate footwall exhibit beautifully exposed, polished slickenfibres of quartz and other minerals. Measured lineations plunge W or NW (some surfaces contain overlain sets of fibres), but the shear sense on all surfaces is top-to-the-W or NW. These fractures are interpreted as Riedel fractures associated with motion on the main thrust. Where two sets of lineations occur, NW-plunging fibres overlay and cross-cut W-plunging fibres.

Four other localities up to 5 km north of the exposed thrust plane provide further evidence for extensive, NW-directed brittle thrusting in footwall gneisses. Most show a number of lineated fault surfaces either parallel to the main thrust or to the Riedel fractures (Fig. 5c), with the same shear sense. At three localities, irregular folds are associated closely with the fractures; one case represents a clear pre-frontal fold related to a metre-scale thrust in banded amphibolites (Fig. 5d). Retrograde assemblages (chlorite–actinolite–pyrite) are prevalent in parts of the faulted outcrops.

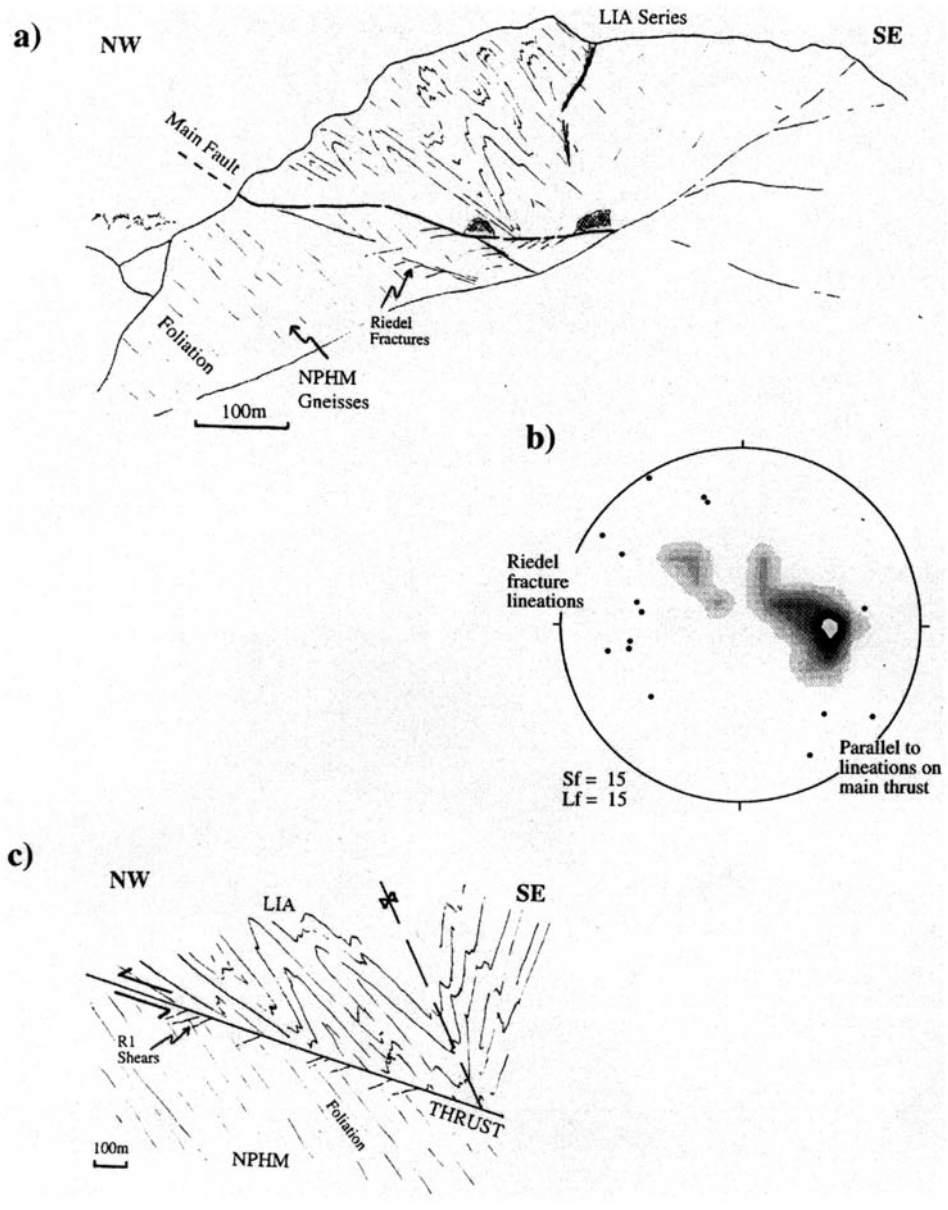

Fig. 6. (**a**) Field sketch (redrawn from notebook) of the Subsar Thrust exposed on the eastern side of the valley running south from Subsar (Fig. 1). Riedel fractures are clearly visible just beneath the main thrust surface in low, mainly accessible crags above steep slopes down to the valley. Intense folding characterizes the Ladakh island arc rocks in the subvertical cliffs above two caves developed along the thrust. Structural data for this locality were taken from the vicinity of the left-hand cave and in the underlying crags. (**b**) Structural data from the above locality and four others in the footwall to the north. Poles to fracture surfaces (Sf) are shown as 1% area contours, with related slickenside fibre and groove lineations shown as single points. Two of the three lineations plunging SE were taken from the main thrust surface at the above locality. NW- and W-plunging lineations were taken from NW- and W-dipping suspected Riedel fractures. All locations showed consistent top-to-the-NW motion sense, interpreted as the major fault movement. (**c**) Sketch showing interpretation of thrust from field evidence in Subsar Gah. Tight folding at other localities in the valley appears genetically related to brittle fractures with the same kinematics as the main fault, so the thrust may have either caused or exploited the folds in the hanging wall.

Conditions of deformation

The variety of rock types condensed into such a narrow zone as the Main Mantle Thrust Zone presents both a challenge and an opportunity for thermobarometry, particularly when most exhibit a polyphase history, stretching back to the Proterozoic in the case of the Nanga Parbat–Haramosh massif basement (e.g. Zeitler *et al.* 1989; Wheeler *et al.* 1995). This section presents the results of preliminary petrographic and thermobarometric studies on a very restricted portion of the Nanga Parbat–Haramosh massif adjacent to the eastern margin in an attempt both to better constrain the evolution of the Main Mantle Thrust Zone, and to augment the existing dataset for the syntaxis. More detailed work is in progress to place these preliminary data in the context of the Nanga Parbat–Haramosh massif as a whole.

Samples and methodology

Table 1 lists the samples employed for thermobarometry; these were selected from a much larger dataset of rocks investigated petrographically, as being the most suitable for P–T determinations and comparisons. The locations of the samples are given in Fig. 2, and four of the six are indicated on the traverses in Fig. 4. Four samples (43b, 15a, 118b and 120b) are from the immediate vicinity of the contact, within the mylonite zone. Samples 169b and 171b are some distance west of the contact, but within the cover rocks, in Rattu Gah. Both samples 43b and 169b are mafic, allowing some comparison across the contact (sample 43b is from the Ladakh island arc series). The others are metapelites, except sample 15a, a metavolcanic schist of the Ladakh island arc.

Following petrographic investigation of standard thin sections of a range of samples from the eastern margin of the Nanga Parbat–Haramosh massif, polished thin sections of the six samples in Tables 1 and 2 were analysed on the Cameca SX261 Electron Microprobe at the Open University, UK. Operating conditions were as follows: 20 kV accelerating voltage, 20 nA beam current, and a 10 μm diameter fixed electron beam. Where appropriate, inclusions of phases in garnet were analysed, and line profiles of the largest garnets in each section were also acquired to determine zonation patterns. X-ray maps of garnets in some samples were also acquired as an aid to identifying 2D zonation. Line profiles of other porphyroblast phases were performed to verify the general absence of zoning

Table 1. *Analysed samples*

Sample	Description	Assemblage
P98/43b	Mylonitic amphibolite	Qtz–Pl–Amph–Bt–Dol–Ttn
P97/15a	Metavolcanic calc-schist	Qtz–Pl–Amph–Grt–Bt–Wm–Ep–Chl–Ilm–Rt
P98/118b	Mylonitic metapelite	Qtz–Pl–Kfs–Grt–Ky–Bt–Wm–Ep–Rt–Tur–Gr
P98/120b	Metapelitic schist	Qtz–Pl–Grt–Ky–Bt–Wm–Scp–Ep–Ap–Gr–Py
P98/169b	Garnet amphibolite	Qtz–Pl–Amph–Grt–Ep–Ilm–CO_3
P98/171b	Metapelitic schist	Qtz–Pl–Grt–Bt–Wm–Ep–Scp–Rt–Gr

Samples selected for thermobarometry. All major phases present are listed and do not necessarily represent equilibrium assemblages for the individual samples. Mineral abbreviations after Kretz (1983), except Amph (amphibole); CO_3 (undifferentiated carbonate mineral).

Table 2. *P–T estimates*

Sample	Km from MMT	T (°C)	Thermometer	P (kbar)	Barometer
P98/43b	—	662 ± 40	HblPl	—	—
P97/15a	−0.3	524 ± 20	GrtBt	8.3 ± 1.4	R5,R6,GRIPS*
P98/118b	—	759 ± 35	GrtBt	12.14 ± 1.9	GASP,R5,R6
P98/120b	0.2	581 ± 25	GrtBt	9.6 ± 1.5	GASP,R5,R6
P98/169b	1.3	632 ± 40	HblPl	9.66 ± 1.5	GPHQ
P98/171b	2.1	505 ± 20	GrtBt	7.43 ± 1.3	R5,R6,GRIPS*

* a(ilm) assumed unity.

Pressure and temperature estimates for samples along the eastern margin of the Nanga Parbat–Haramosh massif. Quoted errors are reduced significantly when comparing estimates from a single thermometer or barometer. Calibrations as follows: Hornblende–Plagioclase (Edenite–Tremolite) (Holland & Blundy 1994); Garnet–Biotite (Bhattacharya *et al.* 1992); pyp + grs + ms = 3an + phl (R5) and alm + grs + ms = 3an + ann (R6) (table 6 in Hoisch 1990); the garnet–rutile–ilmenite–plagioclase–quartz (GRIPS) (Bohlen & Liotta 1986); garnet–aluminosilicate–quartz–plagioclase (GASP) (Holland & Powell 1990); garnet–plagioclase–hornblende–quartz (GPHQ) (Kohn & Spear 1990).

in minerals other than garnet. Cations were calculated by the Cameca software, and the resulting analyses collated and checked. Means were taken for different petrographic populations of each mineral—generally from 10 analyses or more—and the analysis closest to the mean was employed for thermobarometry. In this preliminary study, individual thermometers and barometers were used for ease of comparison amongst samples (Table 2); careful petrographic choice of phases was designed to minimize disequilibrium problems. For instance, extreme garnet rims were avoided since there was generally evidence for down-T diffusive re-equilibration and, where possible, phases included in the near-rim regions of garnets were used instead of matrix phases, again to eliminate retrograde diffusive effects. Due to a lack of inclusions in garnet cores, the P–T estimates obtained relate to the latter stages of the samples' history. The use of garnet cores for thermobarometry was not considered reliable, since many garnets contained evidence of complex growth histories (e.g. included fabric generations and rim overgrowths highlighted by X-ray mapping), implying pronounced disequilibrium between cores and matrix.

Petrography and results

Samples 43b and 169b are amphibolites on opposite sides of the eastern contact. Sample 43b (Fig. 4c) is a mafic mylonite from the immediate hanging wall of the Main Mantle Thrust, on the ductile margin of a 2 m metapelitic band. Sample 169b is a garnet-bearing amphibolite from a mafic and calcareous section within the cover sequence (Fig. 4d). Both have well-developed linear and planar fabrics defined by amphibole, with all phases apparently in equilibrium. Sample 43b exhibits higher strain, with locally developed, ductile, high-T shear bands defined by biotite identical to that in the main foliation. The main foliation in sample 169b wraps millimetre-sized garnets, with a consistent asymmetry indicating dextral (S-directed) shear. Shear bands and other field indicators at locality 43 indicate the same shear sense; hence a direct comparison of the thrust-related assemblages within the two samples can be made. As can be seen from Table 2, the temperatures obtained on matrix amphibole and plagioclase using the hornblende–plagioclase (edenite–richterite) thermometer (Holland & Blundy 1994) agree within error. For 169b, a pressure estimate of 9.66 ± 1.5 kbar was also obtained using the garnet–plagioclase–hornblende–quartz barometer (Kohn & Spear 1990) on near-rim garnet and matrix plagioclase and amphibole, iterating with the thermometer to achieve the best solution. The absence of garnet from sample 43b precluded barometry, and a pressure of 9.5 kbar was chosen for temperature determination from a collation of nearby pressure estimates. An additional upper limit of 10.9 kbar from the garnet–rutile–ilmenite–plagioclase–quartz barometer (Bohlen & Liotta 1986) was calculated for the rutile-absent assemblage in sample 169b. Garnet profiles from sample 169b show moderate prograde zonation (core-rim decrease) in Mn, with minor rimward increase in Mg, Fe and X(Mg) (X(Mg) = (Mg/Mg + Fe)), indicating preservation of growth chemistry at temperatures just below Yardley's (1977) postulated 'homogenization temperature' of 670 °C. Although the temperatures agree within error, the presence of epidote as inclusions in garnet and in the matrix in sample 169b suggests this sample equilibrated at a slightly lower temperature (and/or higher pressure) than sample 43b, which lacks epidote. The lack of epidote in sample 43b could be a compositional effect, but it should be noted that the amphibole and plagioclase compositions in both rocks are almost identical.

A similar pressure estimate was obtained from sample 120b, a calc-pelite from cover rocks adjacent to the eastern contact. Averaging of three barometers, garnet–aluminosilicate–quartz–plagioclase (Holland & Powell 1990), pyp + grs + ms = 3an + phl (R5) and alm + grs + ms = 3an + ann (R6) (table 6 in Hoisch 1990) gave a figure of 9.6 kbar, using garnet near-rim with matrix phases (including unzoned plagioclase), at a temperature of 581 ± 12 °C from the garnet–biotite Fe–Mg exchange thermometer (Bhattacharya *et al.* 1992) (Table 2). Garnets contain a fine, graphitic fabric at high angles to the external foliation, which is defined by coarse muscovite and biotite wrapping garnet, kyanite and scapolite porphyroblasts. Garnet zonation shows complex Fe and Mg patterns, possibly reflecting extensive diffusional re-equilibration at rims and along cracks; at the same time Ca and Mn profiles are almost flat. Flat Mn profiles are generally indicative of homogenization, which may have occurred during an earlier stage of the sample's evolution at higher temperatures than are recorded here by the Fe–Mg isotopic system.

Another calc-pelite, sample 171b, is located approximately 2.1 km west of the eastern contact in Rattu Gah (Fig. 1). P–T conditions for this sample are lower than the other samples in the Main Mantle Thrust Zone (505 ± 11 °C, 7.43 kbar; Table 2), but typical for the metapelites in the cover section of the Nanga Parbat–Haramosh massif (i.e. 500–600 °C, 7–8 kbar) (e.g. Winslow *et al.* 1995). Petrography is similar to sample 120b, except that kyanite is absent from the assemblage and clinozoisite is present

both in garnet and matrix; garnet inclusion trails are weakly sigmoidal, indicating syn-kinematic growth. Weak growth zoning is evident in the garnets, with some diffusional re-equilibration at the rims. These figures seem to record conditions at higher crustal levels than the mafic assemblages, possibly a later phase of deformation in the immediate footwall of the Main Mantle Thrust. Work to constrain the kinematics of this episode is in progress.

P–T estimates for sample 15a, approximately 300 m east of the contact in the lower Rupal valley, fall between those for the cover section and the mafic rocks of the Main Mantle Thrust Zone (524 ± 12 °C, 8.3 kbar), using the same calibrations as sample 171b (Table 2). Garnets have Mn growth zoning and weakly curved inclusion trails at a high angle to the external foliation, where relic microfold hinges attest to its origin as a crenulation cleavage. Amphibole porphyroblasts overgrow the external foliation with minor deflections, indicating late syn-kinematic growth. These features suggest that the *P–T* conditions relate to a fabric-forming event, probably at increasing pressure and/or temperature in order to grow substantial garnet, and as kinematic indicators at this locality indicate S-directed motion, thrusting on the Main Mantle Thrust is the most likely candidate. However, another factor is the composition of the rock as a whole, which means that mineral compositions may not fall within the ideal ranges for the thermobarometric calibrations. Although garnets are not calcic or Mn-rich in this case, components such as Ti in biotite could exert a moderate effect on the *P–T* values.

Sample 118b is a pelitic mylonite in the heart of the Main Mantle Thrust Zone, where significant tectonic interleaving has taken place (Fig. 4b). *P–T* estimates from this sample are strikingly different from others obtained from the Main Mantle Thrust Zone (Table 2). The mylonitic foliation is defined by fine-grained quartz and biotite, which have both suffered grain size reduction. The trails strongly wrap garnet, plagioclase, K-feldspar and kyanite porphyroblasts, but quartz ribbons show signs of annealing and recrystallization to form medium-grained, granular aggregates. Plagioclase crystals have experienced ductile strain, forming curved strain twins with undulose extinction and developing mantles of recrystallized feldspar. This suggests a combination of high strain and temperatures of *c.* 600–700 °C (e.g. Tullis & Yund 1987). Garnets show weak Mn growth zonation, with asymmetric profiles for other elements. The Mn zonation is centred on sigmoidal inclusion trails indicating syn-kinematic growth for the garnet core. The high temperature (759 ± 14 °C) derived from the garnet–biotite Fe–Mg exchange thermometer (Bhattacharya *et al.* 1992) could be regarded as suspect (and would therefore contribute to a high pressure estimate). However, the presence of abundant K-feldspar (and corresponding scarcity of muscovite), the relatively calcic plagioclase (An_{47}), high-Ti biotite (3.3 wt% TiO_2), and rather pyropic garnet compared to other Nanga Parbat–Haramosh massif cover rocks all suggest increased temperature in this sample. Rutile occurs in garnet and the matrix, in rare cases replacing titanite; hence a pressure of 8.7 kbar from the garnet–rutile–ilmenite–plagioclase–quartz barometer (Bohlen & Liotta 1986) represents a minimum value only. Pressures of 10–12 kbar have been recorded in the Nanga Parbat–Haramosh massif (Winslow *et al.* 1995; Le Fort *et al.* 1997; Foster & Argles unpublished data), but not generally from the Main Mantle Thrust mylonite zone, suggesting that these rocks were re-set at higher levels in the crust than the deepest metamorphism. The possibility remains that sample 118b records that high-*P* event, and garnet zonation, despite its subsequent reworking at high metamorphic grades. Alternatively, an erroneously high temperature would result in an overestimate of the pressure. Recalculation of the pressure with the same calibrations and analyses for lower temperatures does lower the pressure (11.29 kbar at 662 °C; 8.89 kbar at 524 °C). A final problem is the cause of the elevated temperature, however high the absolute value. This problem is addressed in the discussion.

The brittle deformation associated with the Subsar Thrust clearly took place at significantly lower temperatures and pressures than the ductile deformation within the Main Mantle Thrust Zone. All mineralization and alteration related to NW-directed thrusting is retrograde in nature, and the style of deformation confirms that motion on the Subsar Thrust occurred at high levels in the crust. Brittle deformation in the bulk of the massif is rather sparse, perhaps reflecting the elevated geotherms (and brittle–ductile transition) associated with rapid Neogene exhumation during syntaxis formation.

Discussion

This study confirms the view of other workers (Butler *et al.* 1992; Wheeler *et al.* 1995) that the eastern margin of the Nanga Parbat–Haramosh massif is essentially the ductile Main Mantle Thrust steepened passively on the limb of the antiformal Neogene syntaxis. Concordance of

planar and linear fabrics as well as lithological boundaries with the main contact suggest that these features are associated with the evolution of the Main Mantle Thrust, and not syntaxial development, and this is confirmed by thermobarometry and petrographic studies. The corollary is that where this pattern is interrupted, later brittle deformation can be demonstrated to have cross-cut the ductile structures. The affinities of the rocks within the Nanga Parbat–Haramosh massif are currently under debate (Whittington *et al.* 1999, 2000), so the divisions of 'cover' and 'basement' in the massif may not be as simple as it appears; Sm–Nd model ages suggest a major discontinuity has to exist between the two units. The pronounced southward thickening of the cover section, despite the northward plunge of the syntaxis antiform, may result in part from excision across such a discontinuity. If the isotopic evidence is correct, this attenuated zone would have included the Main Central Thrust, or its equivalent tectonic boundary (Whittington *et al.* 1999, 2000). No structural evidence remains in this extensively reworked zone for such a theory, but the coincidence of the Lath Unit, a peraluminous orthogneiss apparently pre-dating Neogene deformation, with the basement/cover contact suggesting it to be more than a simple unconformity.

P–T conditions for the thrusting of Kohistan southwards over the Indian plate are difficult to determine, since the present contact throughout much of Northern Pakistan is a composite zone reflecting a complex evolution up to and including neotectonic activity (e.g. Butler & Prior 1988*a*, *b*; Madin *et al.* 1989; Burg *et al.* 1996; Vince & Treloar 1996; Treloar 1997; DiPietro *et al.* this volume). The preservation of an unmodified ductile Main Mantle Thrust Zone with S-directed thrusting shear sense indicators allows direct estimation of the conditions of deformation. Whereas on the western margin near Liachar, there is a significant Neogene metamorphic overprint (Zeitler & Chamberlain 1991; Winslow *et al.* 1995), the eastern margin appears only weakly affected, with lower temperatures and garnet prograde zoning preserved in cover schists. Hence *P–T* estimates on amphibolites in the Main Mantle Thrust Zone can record conditions during thrusting faithfully, for a number of reasons. First, the isotopic systems used in thermobarometry for mafic rocks are not susceptible to retrograde diffusional effects, since cation diffusion in plagioclase is slow (Grove *et al.* 1984), so the *P–T* conditions relate to the equilibration of the assemblage during crystallization. Second, mafic rocks are rheologically strong, and less liable to recrystallize under strain at lower temperatures or higher crustal levels. Finally, the thermal consequences of thrusting would be initial cooling of the base of the arc (e.g. Treloar 1997), tending to 'freeze in' the mylonitic structures developed there ('subduction refrigeration'; Peacock 1987). Strain hardening and the strong mylonitic fabric combined with the inherent strength of the amphibolites would partition subsequent strain into the Main Mantle Thrust. Field evidence confirms this, as the few observations of N-directed shear in the arc rocks are invariably of brittle or semi-brittle features.

These considerations further highlight the anomalous *P–T* conditions of sample 118b. There is ample qualitative evidence for high temperature in this sample; the absolute value is less important. Shear heating (Peacock 1987; Molnar & England 1990; England & Molnar 1993) was invoked by Treloar (1997) in a thorough discussion of the inverted metamorphic gradient developed in the Main Mantle Thrust footwall to the west of the Nanga Parbat–Haramosh massif. His conclusion was that dissipative shear heating cannot have played a significant role in the inverted gradient since the predominately quartz-rich rocks of the Main Mantle Thrust footwall were too weak to support the stresses involved (50–100 Mpa; Treloar 1997). However, the likelihood is that the present configuration of the footwall represents an extensively modified shear zone, in which significant excision may have occurred, destroying vital evidence. What remains is an extensive mylonite zone in mafic rocks of the Ladakh island arc which would have been capable of generating significant heat during shearing before deformation was partitioned into the footwall. Sample 118b may, at least to some extent, record this episode of transient heating, albeit not to such extreme temperatures. Another possible explanation for this high-T sample is fluid activity—for which there is ample evidence in the Main Mantle Thrust Zone—which may have resulted in heat advection, or chemical modification affecting the *P–T* estimates. Alternatively, the sample itself may be an 'out of sequence' tectonic slice, originating from deeper levels. A point to note is that the similarity of *P–T* conditions derived from mafic rocks either side of the Main Mantle Thrust Zone suggests that only minor amounts of excision occurred between those two points (169b and 43b). Clearly this is conditional on barometric errors, and the along-strike separation of the two samples, but it implies relatively low strain since these *P–T* conditions were recorded, and thus reduces the potential

effects of shear heating within the Main Mantle Thrust zone.

A narrow zone on the eastern margin, roughly coincident with the band of cover rocks, shows complex fabric and kinematic relationships suggesting more than simple S-directed thrusting in the Main Mantle Thrust footwall. The lower P–T conditions derived for rocks in this zone may owe something to retrograde diffusional re-setting, but also reflect the reworking of fabrics and recrystallization during this subsequent ductile phase. The foliations wrap garnets with included fabrics and prograde growth zoning dated at 40 to 45 Ma (Foster *et al.* 1998). Since garnet growth was related to burial metamorphism following collision, this subsequent deformation phase must post-date this, but at the same time probably pre-dates a period of rapid cooling in Northern Pakistan from 25 to 16 Ma interpreted as northward extension of the crust (Treloar *et al.* 1989; Chamberlain *et al.* 1991), since deformation in the cover is demonstrably ductile and at conditions near to those attained during thrusting. Alternatively, the deformation may have been coeval with this cooling phase but at deeper crustal levels, and without causing significant exhumation in the region of the syntaxis, since there is no evidence for brittle extensional faulting subparallel to the Main Mantle Thrust. Some exhumation may have occurred, as evidenced by the lower pressures (and temperatures) recorded by the cover rocks that experienced this deformation.

The recognition of a NW-directed thrust cutting the eastern margin of the Nanga Parbat–Haramosh massif (the Subsar Thrust) has further implications for the Neogene tectonics of the massif. The thrust has a similar trend to the continuation of the Liachar Thrust SW from Raikhot Bridge (Fig. 1), a particularly active segment of the boundary (Butler & Prior 1988*b*; Madin *et al.* 1989), though no hydrothermal activity was observed south of Subsar. This is presumably due to the distance from Nanga Parbat itself, whose rapid uplift on the Liachar Thrust system has resulted in a vigorous hydrothermal circulation at depth beneath the summit region and along the Liachar Fault (Butler *et al.* 1997). The two thrust segments are in fact almost aligned across the massif (Fig. 1), and it is tempting to suggest a relay between them, but this is not borne out by available field evidence (e.g. Winslow *et al.* 1995; Treloar & Wheeler, unpublished data). It appears that the Subsar Thrust is independent of the western margin faults, though clearly related via the regional kinematics. Whatever its cause, the fault may have exploited the rheological contrast between the Ladakh island arc and the Nanga Parbat–Haramosh massif on the eastern margin in a similar way to the Liachar Thrust in the west, as part of the overall NW-vergent antiformal syntaxis (Butler & Prior 1988*b*; Butler *et al.* 1989; Seeber & Pêcher 1998). The intense folding in Ladakh island arc amphibolites in the hanging wall of the Subsar Thrust (Fig. 6a, c) is certainly related to the thrust, and may represent fault-propagation folds; also notable is the local concentration of NNE-trending fold axes north of Harchu (Fig. 2), just west of the termination of the Subsar Thrust, which may be associated with it too. In the context of Seeber & Pêcher's (1998) model for the western syntaxis, the Subsar Thrust is a further expression of arc-parallel shortening at the termination of the arc, but the fact that it is not now the locus of motion, and that the main antiform lies to the west of it, suggests that the Subsar Thrust was a subsidiary to the Liachar Fault, or possibly even a 'failed' precursor. Since the thrust surface cuts an already-steepened Main Mantle Thrust Zone, the former seems the most likely. In broader tectonic terms, the fault is part of the shortening regime developed at the extremes of the orogen by the extension of Tibet (e.g. England and Houseman 1989). The presence of a second NW-vergent thrust in the Nanga Parbat–Haramosh massif cross-cutting a previously steepened marginal mylonite zone begs the question of that initial steepening. One possibility is that the syntaxial antiform is entirely due to uplift on the Liachar Fault (and its continuation at depth; e.g. Butler *et al.* 1997; Seeber & Pêcher 1998), but the occurrence throughout the northern part of the massif of broad antiforms separated by tight, pinch synclines or even simply mylonite zones (Wheeler *et al.* 1995) suggests that syntaxis formation was initiated by motion on shear zones analogous to the Subsar and Liachar Faults, but at greater depth. A date of *c.* 8 Ma on biotites from shear zones on the western margin near the village of Sassi (Reddy *et al.* 1997) may give a minimum age for this phase of deformation. During the latter stages of syntaxis formation, these shear zones would have been passively steepened as the syntaxis tightened, resulting in the present configuration.

Conclusions

The eastern margin of the Nanga Parbat–Haramosh massif from the Indus valley to the village of Rattu is characterized by ductile deformation related to S-directed thrusting on the Main Mantle Thrust, centred on an intense

mylonite zone marking the contact of the Ladakh island arc with the Indian plate rocks. The structure of concordant units on both sides of the contact is dominated by fabrics developed during southward emplacement of the Kohistan–Ladakh island arc over the Indian margin in the late Cretaceous. Preliminary *P–T* determinations on mylonites within the Main Mantle Thrust Zone, and other samples from the Main Mantle Thrust footwall, suggest conditions of thrusting of *c.* 650 °C and 9.5 kbar. One sample in the zone where tectonic interleaving of Ladakh island arc and Nanga Parbat–Haramosh massif rocks is intense shows features which appear to indicate elevated temperatures along the thrust, though further work is needed to confirm whether this is due to shear heating, displacement from deeper structural levels, or fluid activity.

Lower pressures and temperatures (*c.* 500 °C and 7.4 kbar) from metapelitic schists of the cover sequence along the eastern margin indicate equilibration at slightly higher levels in the crust (and probably a degree of retrograde diffusional re-setting of isotopic systems). These data coincide with a zone of complex kinematic overprinting in the footwall of the Main Mantle, post-dating prograde garnet growth dated at 40–45 Ma (Foster *et al.* 1998). To the west of this zone, the intensity of Main Mantle Thrust-related deformation peaks at the margins of a K-feldspar megacrystic orthogneiss (the 'Lath Unit'), before waning in the basement gneisses forming the interior of the Nanga Parbat–Haramosh massif.

A shallow, SE-dipping thrust south of the village of Subsar on the Indus River juxtaposes folded Ladakh island arc amphibolites in its hanging wall with Nanga Parbat–Haramosh massif gneisses of intermediate composition in its footwall. The thrust and related features indicate NW-directed motion of the Ladakh island arc over the Indian plate rocks, cutting the steep, ductile Main Mantle Thrust Zone. Kinematically similar to the Liachar Thrust, the Subsar Thrust implies that the western syntaxis was generated by the impingement of orogen-scale tectonic forces on the termination of the Himalayan arc, and is still subject to their influence today.

The author thanks Asif Khan, Qasim Jan and Mubarik Ali for hospitality in Pakistan, and G. Foster for insights in the field. This paper has benefited from discussions with, among others, N. B. W. Harris and M. A. Edwards, as well as thoughtful reviews from R. W. H. Butler and J. Wheeler, but any errors or omissions are the authors's. A. Tindle is acknowledged for assistance with microprobe analysis. This study was undertaken while the author was in receipt of an NERC Research Fellowship.

Appendix: Mineral analyses

Sample	P9843b	P9843b	P9815a	P9815a	P9815a	P9815a	P98118b	P98118b	P98118b	P98118b	P98120
No	DB	DV	CD3	AD	BA	BW	EK5	DQ	AE	DW	CY5
Mineral	Hbl	Pl	Grt	Bt	Wm	Pl	Grt	Bt	Wm	Pl	Grt
Description	core	core	nr rim	core	core	core	nr rim	core	core	core	nr rim
SiO_2	42.86	62.53	36.79	36.64	46.59	62.62	38.76	37.35	46.98	56.28	37.77
TiO_2	0.59	na	0.06	1.66	0.29	na	0.05	3.30	1.87	na	0.09
Al_2O_3	15.33	23.37	21.08	17.16	33.52	22.81	22.08	18.02	32.68	27.44	21.41
FeO^T	14.94	0.05	30.90	20.31	2.33	0.02	22.26	13.77	1.17	0.01	26.24
MnO	0.27	na	2.92	0.09	0.01	na	0.57	0.07	0.00	na	0.96
MgO	10.30	bd	1.81	10.28	0.98	na	5.82	13.03	1.45	bd	2.43
CaO	11.18	4.67	6.31	0.01	0.00	4.25	11.22	0.00	bd	9.55	11.70
Na_2O	1.47	9.04	na	0.12	0.79	9.15	na	0.04	0.26	5.97	na
K_2O	0.55	0.07	na	9.25	10.02	0.09	na	9.85	10.88	0.28	na
Total	97.49	99.73	99.86	95.53	94.52	98.93	100.76	95.42	95.28	99.53	100.60
Oxygens	23	8	12	22	22	8	12	22	22	8	12
Si	6.34	2.78	2.97	5.58	6.27	2.80	2.97	5.52	6.27	2.54	2.97
Ti	0.06	—	0.00	0.19	0.03	—	0.00	0.37	0.19	—	0.01
Al	2.67	1.22	2.00	3.08	5.32	1.20	2.00	3.14	5.14	1.46	1.99
Fe	1.85	0.00	2.09	2.59	0.26	bd	1.43	1.70	0.13	bd	1.73
Mn	0.03	—	0.20	0.01	bd	—	0.04	0.01	bd	—	0.06
Mg	2.27	bd	0.22	2.33	0.20	—	0.67	2.87	0.29	bd	0.29
Ca	1.77	0.22	0.55	bd	bd	0.20	0.92	bd	bd	0.46	0.99
Na	0.42	0.78	—	0.03	0.20	0.79	—	0.01	0.07	0.52	—
K	0.10	0.00	—	1.80	1.72	0.00	—	1.86	1.85	0.02	—
Total	15.52	5.00	8.03	15.61	14.00	5.00	8.03	15.48	13.93	5.00	8.03

Appendix: Continued

Sample	P98120	P98120	P98120	P98169	P98169	P98169	P98171b	P98171b	P98171b	P98171b
No	CD	BZ	BA20	AX1	AF	AV	BL57	CW	CU	At
Mineral	Bt	Wm	Pl	Grt	Hbl	Pl	Grt	Bt	Wm	Pl
Description	cores	cores	core	rim	core	core	nr rim	incl nr rim	incl nr rim	core
SiO_2	36.96	47.13	57.91	37.41	44.10	62.93	37.10	37.64	47.61	57.52
TiO_2	3.11	1.21	na	0.04	0.43	na	0.10	2.11	1.36	na
Al_2O_3	17.51	32.30	26.22	21.28	12.95	23.39	20.94	18.39	32.94	26.71
FeO^T	15.94	1.67	0.02	28.39	17.37	0.04	28.51	15.40	1.33	0.03
MnO	0.06	bd	na	2.98	0.14	na	0.72	0.07	0.00	na
MgO	11.74	1.60	bd	1.74	9.01	bd	1.87	12.66	1.54	bd
CaO	0.03	0.01	8.12	8.53	11.00	4.57	10.36	0.02	0.03	8.60
Na_2O	0.08	0.21	6.96	na	1.37	9.17	na	0.18	0.54	6.70
K_2O	9.74	11.16	0.25	na	0.40	0.04	na	9.19	10.55	0.07
Total	95.19	95.28	99.46	100.36	96.78	100.13	99.60	95.65	95.90	99.62
Oxygens	22	22	8	12	23	8	12	22	22	8
Si	5.54	6.31	2.61	2.98	6.62	2.78	2.97	5.57	6.30	2.58
Ti	0.35	0.12	—	0.00	0.05	—	0.01	0.24	0.14	bd
Al	3.09	5.10	1.39	2.00	2.29	1.22	1.98	3.21	5.14	1.41
Fe	2.00	0.19	bd	1.89	2.18	0.00	1.91	1.90	0.15	0.00
Mn	0.01	bd	—	0.20	0.02	—	0.05	0.01	bd	—
Mg	2.62	0.32	bd	0.21	2.02	—	0.23	2.79	0.30	bd
Ca	0.01	bd	0.39	0.73	1.77	0.22	0.89	0.01	0.01	0.41
Na	0.02	0.06	0.61	—	0.40	0.79	—	0.05	0.14	0.58
K	1.86	1.91	0.01	—	0.07	0.00	—	1.73	1.78	0.00
Total	15.49	14.00	5.01	8.02	15.42	5.00	8.03	15.49	13.95	5.00

FeO^T, all Fe ($Fe^2 + Fe^3$); na, not analysed; bd, below detection.

References

ANDERSEN, T. 1998. Extensional tectonics in the Caledonides of southern Norway, an overview. *Tectonophysics*, **285**, 333–351.

BHATTACHARYA, A., MOHANTY, L., MAJI, A., SEN, S. K. & RAITH, M. 1992. Non-ideal mixing in the phlogopite–annite boundary: constraints from experimental data on Fe–Mg partitioning and a reformulation of the biotite–garnet geothermometer. *Contributions to Mineralogy and Petrology*, **111**, 87–93.

BOHLEN, S. R. & LIOTTA, J. J. 1986. A barometer for Garnet Amphibolites and garnet Granulites. *Journal of Petrology*, **27**(5), 1025–1034.

BURCHFIEL, B. C. & ROYDEN, L. H. 1985. North–South extension within the convergent Himalayan region. *Geology*, **13**, 679–682.

——, CHEN, Z., HODGES, K. V., LIU, Y., ROYDEN, L. H., DENG, C. & XU, J. (eds) 1992. *The South Tibetan detachment system, Himalayan orogen: Extension contemporaneous with and parallel to shortening in a collisional mountain belt*. Geological Society of America Special Paper, **269**.

BURG, J. P., BRUNEL, M., GAPAIS, D., CHEN, G. M. & LIU, G. H. 1984. Deformation of the leucogranites of the crystalline main central sheet in southern Tibet. *Journal of Structural Geology*, **6**, 532–542.

——, CHAUDRY, M. N., GHAZANFAR, M., ANCZKIEWICZ, R. & SPENCER, D. 1996. Structural evidence for back sliding of the Kohistan arc in the collisional system of northwest Pakistan. *Geology*, **24**(8), 739–742.

BUTLER, R. W. H. & PRIOR, D. J. 1988*a*. Anatomy of a continental subduction zone: the main mantle thrust in Northern Pakistan. *Geologische Rundschau*, **77**(1), 239–255.

—— & —— 1988*b*. Tectonic controls on the uplift of the Nanga Parbat massif, Pakistan Himalayas. *Nature*, **333**, 247–250.

——, GEORGE, M., HARRIS, N. B. W., JONES, C., PRIOR, D. J., TRELOAR, P. J. & WHEELER, J. 1992. Geology of the northern part of the Nanga Parbat massif, northern Pakistan, and its implications for Himalayan tectonics. *Journal of the Geological Society, London*, **149**, 557–567.

——, HARRIS, N. W. B. & WHITTINGTON, A. G. 1997. Interactions between deformation, magmatism and hydrothermal activity during active crustal thickening: a field example from Nanga Parbat, Pakistan Himalayas. *Mineralogical Magazine*, **61**, 37–52.

——, PRIOR, D. J. & KNIPE, R. J. 1989. Neotectonics of the Nanga Parbat Syntaxis, Pakistan, and crustal stacking in the northwest Himalayas. *Earth and Planetary Science Letters*, **94**, 329–343.

CHAMBERLAIN, P. C. & ZEITLER, P. K. 1996. Assembly of the crystalline terranes of the northwestern Himalaya and Karakoram, northwestern Pakistan. *In*: YIN, A. & HARRISON, M. (eds) *The Tectonic Evolution of Asia*. Cambridge University Press, Cambridge, 138–148.

——, —— & JAN, M. Q. 1989. The dynamics of the suture between the Kohistan island arc and the Indian plate in the Himalaya of Pakistan. *Journal of Metamorphic Geology*, **7**, 135–149.

CLIFF, R. A. 1981. Pre-Alpine history of the Pennine Zone in the Tauern Window: U–Pb and Rb–Sr geochronology. *Contributions to Mineralogy and Petrology*, **77**, 262–266.

COWARD, M. P. 1985. A section through the Nanga Parbat syntaxis, Indus valley, Kohistan. *Geological Bulletin of the University of Peshawar*, **18**, 147–152.

DESIO, A. & SHAMS, F. A. 1980. The age of blueschists and the Indus Kohistan suture line, NW Pakistan. *Proceedings of the Italian Academy of Sciences*, **68**, 74–79.

DEWEY, J. F., SHACKLETON, R. M., CHENGFA, C. & YIYIN, S. 1988. The tectonic evolution of the Tibetan plateau. *Royal Society of London Philosophical Transactions*. **A327**, 379–413.

DIPIETRO, J. A., HUSSAIN, A., AHMED, I & KHAN, M. A. 2000. The Main Mantle Thrust in Pakistan: its character and extent. *This volume*.

ENGLAND, P. C. & HOUSEMAN, G. A. 1989. Extension during continental convergence, with application to the Tibetan Plateau. *Journal of Geophysical Research*, **94**, 17561–17579.

—— & MOLNAR, P. 1993. The interpretation of inverted metamorphic isograds using simple physical calculations. *Tectonophysics*, **12**, 145–157.

FOSTER, G. L., VANCE, D. & HARRIS, N. B. W. 1998. The prograde thermal history of the Nanga Parbat Haramosh Massif, Pakistan. *In*: HAMIDULLAH, S., LAWRENCE, R. D. & JAN, M. Q. (eds) 13th Himalayan–Karakoram–Tibet International Workshop Abstract Volume. *Geological Bulletin of University of Peshawar*, **31**, 64–65.

GANSSER, A. 1964. *The Geology of the Himalayas*. Interscience Publishers, New York.

GROVE, T. L., BAKER, M. B. & KINZLER, R. J. 1984. Coupled CaAl–NaSi diffusion in plagioclase feldspar: Experiments and applications to cooling rate speedometry. *Geochimica et Cosmochimica Acta*, **48**, 2113–2121.

HERREN, E. 1987. Zanskar shear zone: Northeast–southwest extension within the Higher Himalayas (Ladakh, India). *Geology*, **15**, 409–413.

HODGES, K. V., PARRISH, R., HOUSH, T., LUX, D., BURCHFIEL, B. C., ROYDEN, L. & CHEN, Z. 1992. Simultaneous Miocene extension and shortening in the Himalayan orogen. *Science*, **258**, 1466–1470.

HOISCH, T. D. 1990. Empirical calibration of six geobarometers for the mineral assemblage quartz + muscovite + biotite + plagioclase + garnet. *Contributions to Mineralogy and Petrology*, **104**, 225–234.

HOLLAND, T. J. B. & BLUNDY, J. 1994. Non-ideal interactions in calcic amphiboles and their bearing on amphibole–plagioclase thermometry. *Contributions to Mineralogy and Petrology*, **116**, 433–447.

—— & POWELL, R. 1990. An enlarged and updated internally consistent thermodynamic dataset with uncertainties and correlations: the system K_2O–Na_2O–CaO–MgO–MnO–FeO–Fe_2O_3–Al_2O_3–TiO_2–SiO_2–C–H_2–O_2. *Journal of Metamorphic Geology*, **8**, 89–124.

JAN, M. Q. 1985. High-P rocks along the suture zones around the Indo-Pakistan plate and phase chemistry of blueschists from eastern Ladakh. *Geological Bulletin of the University of Peshawar*, **18**, 1–40.

KOHN, M. J. & SPEAR, F. S. 1990. Two new geobarometers for garnet amphibolites, with applications to southeastern Vermont. *American Mineralogist*, **75**, 89–96.

KRETZ, P. 1983. Symbols for rock-forming minerals. *American Mineralogist*, **68**, 277–279.

LE FORT, P. 1996. Evolution of the Himalaya. *In*: YIN, A. & HARRISON, M. (eds) *The Tectonic Evolution of Asia*. Cambridge University Press, Cambridge, 95–109.

——, GUILLOT, S. & PECHER, A. 1997. HP metamorphic belt along the Indus suture zone of NW Himalaya: new discoveries and significance. *Comptes Rendus de l'Academie des Sciences*, **325**, 773–778.

MADIN, I. P., LAWRENCE, R. D. & UR-REHMAN, S. 1989. The northwest Nanga Parbat–Haramosh Massif; evidence for crustal uplift at the northwestern corner of the Indian craton. *In*: MALINCONICO, L. L. & LILLIE, R. J. (eds) *Tectonics of the Western Himalayas*. Geological Society of America Special Paper, **232**, 169–182.

MOLNAR, P. & ENGLAND, P. C. 1990. Temperatures, heat flux and frictional stress near major thrust faults. *Journal of Geophysical Research*, **95**, 4833–4856.

PEACOCK, S. M. 1987. Creation and preservation of subduction-related inverted metamorphic gradients. *Journal of Geophysical Research*, **92**, 12763–12781.

PLATT, J. P. & VISSERS, R. L. M. 1989. Extensional collapse of thickened continental lithosphere: a working hypothesis for the Alboran Sea and the Gibraltar arc. *Geology*, **17**, 540–543.

POGNANTE, U., BENNA, P. & LE FORT, P. 1993. High-pressure metamorphism in the High Himalayan Crystallines of the Stak valley, north-eastern Nanga Parbat–Haramosh syntaxis, Pakistan Himalaya. *In*: TRELOAR, P. J. & SEARLE, M. P. (eds) *Himalayan Tectonics*. Geological Society, London, Special Publications, **74**, 161–172.

PUDSEY, C. J. 1986. The Northern Suture in Pakistan; margin of a Cretaceous Island Arc. *Geological Magazine*, **123**, 405–423.

REDDY, S. M., KELLEY, S. P. & MAGENNIS, L. 1997. A Microstructural and Argon Laserprobe Study of Shear Zone Development at the Western Margin of the Nanga Parbat–Haramosh Massif, Western Himalaya. *Contributions to Mineralogy and Petrology*, **128**, 16–29.

SEARLE, M. P. 1991. Geological Map of the Central Karakoram Mountains, Scale 1:250,000. *In*: SEARLE, M. P. (ed.) *Geology and Tectonics of the Karakoram Mountains*. J. Wiley & Sons, Chichester, 358.

—— 1996. Cooling history, erosion, exhumation, and kinematics of the Himalaya–Karakoram–Tibet orogenic belt. *In*: YIN, A. & HARRISON, M. (eds) *The Tectonic Evolution of Asia*. Cambridge University Press, Cambridge, 110–137.

——, KHAN, M. A., JAN, M. Q., DIPIETRO, J. A., POGUE K. R. *et al.* 1996. *Geological Map of North Pakistan*. Department of Earth Sciences, Oxford University.

SEEBER, L. & PÊCHER, A. 1998. Strain partitioning along the Himalayan arc and the Nanga Parbat antiform. *Geology*, **26**(9), 791–794.

SMITH, H. A., CHAMBERLAIN, C. P. & ZEITLER, P. K. 1992. Documentation of Neogene regional metamorphism in the Himalayas of Pakistan using U–Pb in Monazite. *Earth and Planetary Science Letters*, **113**, 93–105.

TAHIRKHELI, R. A., MATTAUER, M., PROUST, F. & TAPPONNIER, P. 1979. The India–Eurasia suture zone in Northern Pakistan; synthesis and interpretation of recent data at plate scale. *In*: FARAH, A. & DEJONG, K. A. (eds) *Geodynamics of Pakistan*. Geological Survey of Pakistan, 125–130.

TONARINI, S., VILLA, I., OBERLI, F., MEIER, M., SPENCER, D. A., POGNANTE, U. & RAMSAY, J. G. 1993. Eocene age of eclogite metamorphism in Pakistan Himalaya: implications for India–Asia collision. *Terra Nova*, **5**, 13–20.

TRELOAR, P. J. 1997. Thermal controls on early-Tertiary, short-lived, rapid regional metamorphism in the NW Himalaya, Pakistan. *Tectonophysics*, **273**, 77–104.

——, BROUGHTON, R. D., WILLIAMS, M. P., COWARD, M. P. & WINDLEY, B. F. 1989. Deformation, metamorphism and imbrication of the Indian plate, south of the Main Mantle Thrust, north Pakistan. *Journal of Metamorphic Geology*, **7**, 111–125.

——, GEORGE, M. & WHITTINGTON, A. G. (2000). Cross-cutting mafic sheets from Indian plate gneisses in the Nanga Parbat syntaxis: their significance in dating metamorphic and deformation events. *This volume*.

TULLIS, J. & YUND, R. A. 1987. Transition from cataclastic flow to dislocation creep of feldspar: mechanisms and microstructures. *Geology*, **15**, 606–609.

VANCE, D. & O'NIONS, R. K. 1992. Prograde and retrograde thermal histories from the central Swiss Alps. *Earth and Planetary Science Letters*, **114**, 113–129.

VAVRA, G., GEBAUER, D. & SCHMID, R. 1994. The thermal history of the lower crust recorded by zircon growth and recrystallisation: an ion microprobe (SHRIMP) study from the Ivrea zone (Southern Alps). *Mineralogical Magazine*, **58A**, 936–937.

VERPLANCK, P. L. 1986. *A field and geochemical study of the boundary between the Nanga Parbat–Haramosh massif and the Ladakh arc terrane, northern Pakistan*. MSc, Oregon State University.

VINCE, K. J. & TRELOAR, P. J. 1996. Miocene, north-vergent extensional displacements along the Main Mantle Thrust, NW Himalaya, Pakistan. *Journal of the Geological Society, London*, **153**, 677–680.

WHEELER, J., TRELOAR, P. J. & POTTS, G. J. 1995. Structural and metamorphic evolution of the Nanga Parbat syntaxis, Pakistan Himalayas, on the Indus gorge transect: the importance of early events. *Geological Journal*, **30**, 349–371.

WHITTINGTON, A. G. 1997. *The thermal, metamorphic and magmatic evolution of a rapidly exhuming terrane: the Nanga Parbat Massif, northern Pakistan.* PhD thesis, Open University, Milton Keynes, UK.

——, FOSTER, G. L., HARRIS, N. B. W. & AYRES, M. W. 1999. Lithostratigraphic correlations in the western Himalaya—an isotopic approach. *Geology*, **7**, 585–588.

——, HARRIS, N. B. W., AYRES, M. W. & FOSTER, G. L. 2000. Tracing the origins of the western Himalaya—an isotopic comparison of the Nanga Parbat massif and Zanskar Himalaya. *This volume.*

WINSLOW, D. M., CHAMBERLAIN, C. P. & ZEITLER, P. K. 1995. Metamorphism and Melting of the Lithosphere Due to Rapid Denudation, Nanga Parbat Massif Himalaya. *Journal of Geology*, **103**, 395–409.

YARDLEY, B. W. D. 1977. An empirical study of diffusion in garnet. *American Mineralogist*, **62**, 793–800.

ZEITLER, P. K. 1985. Cooling history of the NW Himalaya, Pakistan. *Tectonics*, **4**, 127–151.

—— & CHAMBERLAIN, C. P. 1991. Petrogenetic and tectonic significance of young leucogranites from the northwestern Himalaya, Pakistan. *Tectonics*, **10**, 729–741.

——, —— & SMITH, H. A. 1993. Synchronous anatexis, metamorphism, and rapid denudation at Nanga Parbat (Pakistan Himalaya). *Geology*, **21**, 347–350.

——, SUTTER, J. F., WILLIAMS, I. S., ZARTMAN, R. & TAHIRKHELI, R. A. K. 1989. Geochronology and temperature history of the Nanga Parbat–Haramosh Massif, Pakistan. *In*: MALINCONICO, L. L. & LILLIE, R. J. (eds) *Tectonics of the Western Himalayas*. Geological Society of America Special Paper, **232**, 1–22.

Geological structure of the southern part of the Nanga Parbat massif, Pakistan Himalaya, and its tectonic implications

R. W. H. BUTLER[1], J. WHEELER[2], P. J. TRELOAR[3] & C. JONES[4]

[1]*School of Earth Sciences, The University of Leeds, Leeds LS2 9JT, UK*

[2]*Department of Earth Sciences, The University of Liverpool, Liverpool L69 3BX, UK*

[3]*School of Geological Sciences, Kingston University, Penrhyn Road, Kingston-upon-Thames, UK*

[4]*Formerly of the Department of Geological Sciences, Durham University, South Road, Durham DH1 3LE, UK*

Abstract: The Nanga Parbat massif lies in the core of the major north–south trending, broadly upright antiform that marks the NW syntaxis of the Himalayan arc. However, this antiformal structure is not evident in the trend of foliation and banding within the central and southern parts of the massif. Reconnaissance field studies in this region (Astor, Rama and Rupal areas) have delineated an important shear zone with top-to-the-south overthrust kinematics. This Rupal Shear Zone carries the migmatitic core of the massif onto non-migmatitic metasediments locally termed the Tarshing Group. The shear zone traces north into a broad high strain zone of steep foliation with gently plunging mineral elongation lineations with no consistent sense of shear. A tentative model is proposed whereby top-to-the-south overshear in the Rupal area passes northwards into a steep belt of apparently constrictional N–S elongation. This type of large-scale transpression may record the early growth of the syntaxis. However, relating these structures to Himalayan orogenesis and the amplification of the NW syntaxis is problematic. The Nanga Parbat massif displays a long and complex history of polyphase deformation, metamorphism and magmatism, as might be expected of a terrane derived from the basement of the Indian sub-continent. Although at least the later part of the constrictional steep belt developed with syn-kinematic leucogranite intrusions (< 10 Ma), the old age limit on the Rupal Shear Zone remains unconstrained.

As the northernmost outcrop of continental crust derived from the Indian plate within the Himalayan collision (Fig. 1), the Nanga Parbat massif has long held a position of considerable importance for regional tectonic and geological models (Gansser 1964; Desio 1976). The massif represents an uplifted and exhumed half-window of Indian continental basement rocks framed by the structurally overlying Kohistan–Ladakh island arc terrane. As a consequence of this large-scale map-pattern, the structure of the massif is commonly summarized as an upright antiform with a broadly north–south hinge line (Wadia 1933; Coward *et al.* 1988; Seeber & Pêcher 1998). This was consistent with the notion that the eastern and western margins of the Nanga Parbat massif represented segments of the same tectonic contact—the Main Mantle Thrust (e.g. Tahirkheli & Jan 1979). Various workers have tested this geometric model over the past 15 years. Coward (1985) recognized a broadly antiformal structure in the late folds of gneissic banding, a synthesis broadly followed by Madin *et al.* (1989), Treloar *et al.* (1991), Butler *et al.* (1992) and Wheeler *et al.* (1995). All of these studies focused on the northern part of the massif, especially that part transected by the Indus gorge, and recorded several antiformal closures in the gneissic banding. The aim of this contribution is to examine whether the antiformal structure is present further south in the massif, particularly along the Astor gorge and the Rupal valley on the south side of the peak of Nanga Parbat. The research described here was carried out on two reconnaissance expeditions (1988, 1990). However, structural studies in polydeformed basement terrains such as the deformed continental crust of Nanga Parbat can be meaningless without appropriate stratigraphic control (as emphasized by Wheeler *et al.* 1995). As a consequence of research over the intervening years it is now appropriate to present

From: KHAN, M. A., TRELOAR, P. J., SEARLE, M. P. & JAN, M. Q. (eds) *Tectonics of the Nanga Parbat Syntaxis and the Western Himalaya.* Geological Society, London, Special Publications, **170**, 123–136. 1-86239-061-4/00/$15.00

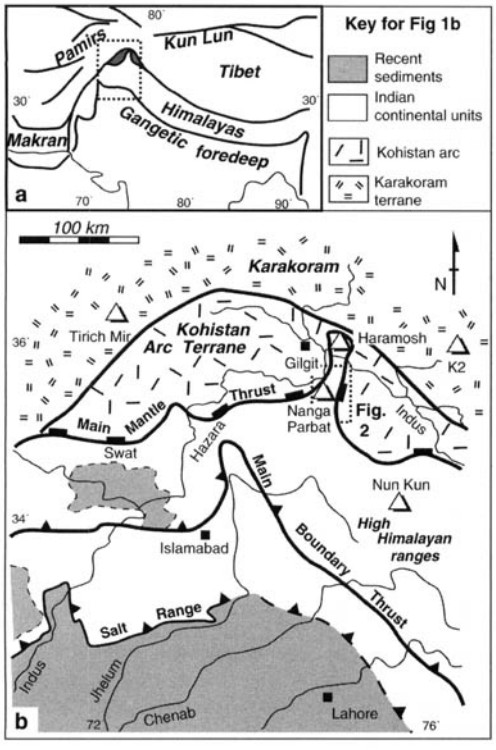

Fig. 1. Location maps for the Nanga Parbat massif: (**a**) the setting of the NW Himalayan syntaxis (boxed area, location of (b), shaded area, Kohistan island arc terrane); (**b**) simplified geological map of NW Himalaya and location of Fig. 2.

our geological findings. However, we first discuss the geological and, particularly, chronological framework of the Nanga Parbat massif.

Nanga Parbat basement: towards a stratigraphic framework

The Nanga Parbat massif chiefly comprises a suite of metasedimentary paragneisses together with a tract of augen orthogneiss, collectively termed the Nanga Parbat Gneisses by early workers (Misch 1949; Wadia 1961; Desio 1976). In the northern part of the massif, Madin *et al.* (1989) divided these into three units with distinct structural positions. From highest to lowest these were termed the Haramosh Schist, Iskere Gneiss and Shengus Gneiss. These units, with boundaries conformable to gneissic banding, were used by Madin *et al.* (1989) to map out broad antiformal structures, chiefly in the transition between Iskere and Shengus Gneiss units. However, these two units may have had the same protolith, except that the Iskere Gneiss includes broad tracts of rather homogeneous augen orthogneiss. Butler & Prior (1988) interpreted the augen gneiss as being a deformed and metamorphosed tonalite which had been intruded into the metasediments before Himalayan orogenesis. Treloar *et al.* (1991) tentatively consider the Shengus and Iskere gneisses to be a cover and basement series respectively. They certainly record different histories.

Detailed structural and petrographic work by Wheeler *et al.* (1995) has established that paragneisses within both the Shengus and the Iskere gneisses are migmatitic. However, the differences are interpreted as reflecting the different degrees of melt segregation, extraction and back reaction during migmatization. The Shengus Gneiss is interpreted as having lost a significant melt fraction, although sufficient volumes remained to drive back-reaction and regrowth of biotite. The Iskere Gneiss experienced segregation within the migmatite and melt extraction. These histories, the resultant principal compositional banding and migmatitic textures in these rocks, pre-date a suite of amphibolite dykes (Butler & Prior 1988; Butler *et al.* 1992; Wheeler *et al.* 1995). These dykes cross-cut all the above units (for photographs see Wheeler *et al.* 1995; Butler *et al.* 1997; Treloar *et al.* this volume), together with a coarsely porphyritic suite of granitoids and granodiorites (locally termed the Lath Unit by Edwards *et al.* this volume).

Structurally, the youngest suite of rocks within Nanga Parbat are an extensive swarm of leucogranite pegmatite veins and at least 4 kilometre-sized granitic plutons. Leucogranites are found along much of the length of the Himalayan chain where they are dated at 24–18 Ma (e.g. Noble & Searle 1995 and references therein). In common with other leucogranites in the Himalayas (e.g. Harris *et al.* 1993), Nd and Sr isotopic studies have shown that the Nanga Parbat leucogranites are derived from small batch-melting of old continental crust (Butler *et al.* 1992, 1997; George *et al.* 1993). However, in contrast to the main Himalayan suite of leucogranites, Rb–Sr geochronology shows those within the Nanga Parbat massif to be younger than 10 Ma (George *et al.* 1993). Petrogenetic studies (reported by George *et al.* 1993 and Butler *et al.* 1997) strongly indicate that the leucogranites are sourced from muscovite breakdown under low vapour concentrations through rapid decompression. This result, coupled with the young ages, indicate that leucogranite formation is a direct result of rapid exhumation of the Nanga Parbat massif. South of the massif, however, there are recent reports of early Miocene U–(Th)–Pb ages (monazite

and zircon) for a leucogranite (Schneider *et al.* 1999*a*). No geochemical results pertaining to the petrogenesis of this leucogranite are available. Consequently, we cannot place this body unambiguously into a basement stratigraphy.

Apart from the status of the leucogranites other aspects of the basement stratigraphy remain highly controversial. For Chamberlain *et al.* (1995), the dominant structural fabric, represented by a well-developed gneissic banding, and therefore the structures that deform this banding, have formed in the past 10 Ma. As a consequence they link the migmatites found within the Tato area of the massif (Fig. 2) to the generation of leucogranites. A test of this relationship might be provided by additional radiometric dating. In this regard, the U–Pb studies of accessory phases (chiefly monazite) within both the migmatitic gneisses and the leucogranites are especially pertinent. Although Zeitler *et al.* (1989) report U–Pb SHRIMP ages from the cores of monazites as old as 1850 Ma, the rims to monazites from the central part of the massif (Tato area, Fig. 1) have yielded ages younger than 10 Ma (Smith *et al.*

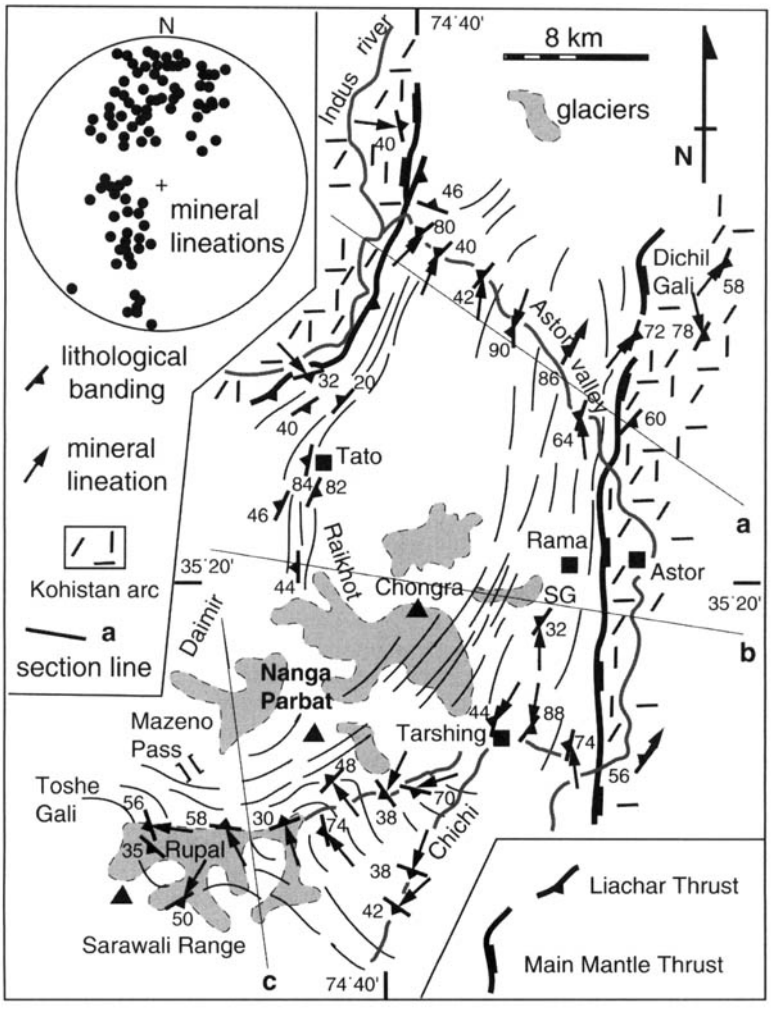

Fig. 2. Form-surface map of the south-central part of the Nanga Parbat massif (location on Fig. 1b), showing the regional orientations of planar and linear deformation fabrics (all quantified data were measured *in situ*), together with a stereoplot of mineral lineation data from this area ($n = 116$). In this and other figures in this paper the stereoplot is a lower-hemisphere, equal-area projection. SG, Siachen glacier. Note that this map does not show the different rock types because the boundaries between units cannot be located with certainty by distant inspection.

1992). Clearly then, the Nanga Parbat massif experienced high temperatures during the late Cenozoic.

Although the raw isotopic data remain undisputed, the interpretation of these as dates of specific geological 'events' is far from certain. For Chamberlain *et al.* (1995) it is the rim ages for monazites that date the main fabrics and structures of the massif. Presumably then the core ages are relict and do not correlate with events recorded in the surrounding gneisses. As noted above (also Butler *et al.* 1992; Wheeler *et al.* 1995; Treloar *et al.* this volume), the main migmatitic fabric within the massif predates a suite of basic dykes. For the monazite ages to date the formation of migmatitic banding these dykes must be of late Tertiary age, essentially coeval with the leucogranites. However, the Sr isotope chemistry of the leucogranites is not compatible with co-existing basaltic magma (George *et al.* 1993). Since these intrusives show granulite facies mineral assemblages (Pognante *et al.* 1993), they must have been emplaced prior to 'peak' Himalayan metamorphism. It is probable that they are very much older than this; consequently, the results of on-going isotopic studies of these critical units are awaited with interest.

Even without definite published ages on the metabasic intrusions (but see Treloar *et al.* this volume), the basement stratigraphy described above presents severe problems to chronologies for the Nanga Parbat basement based on accessory phase dating (e.g. Smith *et al.* 1992; Edwards *et al.* this volume). It is probable, although not unambiguously demonstrated, that the rocks of the Nanga Parbat massif have experienced high temperatures and have cooled rapidly over the past 10 Ma or less (Zeitler 1985; Whittington 1996). These are estimated at about 720 ± 50 °C and 5 ± 1 kbar (Whittington *et al.* 1998). However, we suspect that monazites and the rims of zircons have grown under sub-solidus conditions, perhaps due to heterogeneous hydrothermal fluid flow during exhumation (as shown elsewhere by Teufel & Heinrich 1997). Consequently, it is the core ages of these phases (*c.* 1850 Ma for zircons, Zeitler *et al.* 1989) that we believe date the main migmatization, formation of gneissic banding and, presumably, the emplacement of the porphyritic granitoids and metatonalites ('Lath Unit' of Edwards *et al.* this volume) that are locally cross-cut by the metabasic sheets. Although precise isotopic dating is possible, the geological significance of the ages from accessory phases is difficult to assess without micro- and meso-structural context.

The combined geochronology, as discussed and interpreted above, confirms the view derived from structural studies that the Nanga Parbat massif has had a long history of metamorphism, deformation and magmatism. Only the most recent parts of this are related to Himalayan orogenesis and to the exhumation tectonics of the massif. It is only those structures that deform the leucogranites that may unambiguously be related to exhumation tectonics and therefore be younger than about 10 Ma. Note that this chronology may not be taken away from the Nanga Parbat area for the leucogranite petrogenesis reflects the specific conditions within and acting upon the massif.

Geology of the southern and central part of the massif

In comparison to the ground directly accessible from the Indus valley, the south side of Nanga Parbat has seen very little attention in recent years. Original mapping by Wadia (1933) showed that the rocks of the SE quarter of the massif are at upper greenschist to lower amphibolite facies and show no sign of migmatization. In this respect they may be similar to the Haramosh schists of Madin *et al.* (1989). Given the relatively low metamorphic grade, it is tempting to view these metasediments as constituting a cover sequence to the migmatitic high-grade rocks of the massif. We do not follow this interpretation since the Himalaya show many different types of basement (contrast the Lesser Himalaya with the Higher Himalayan crystallines; e.g. Le Fort 1989).

The geology described in this contribution was studied in three general areas: the Rupal valley on the southern side of the mountain of Nanga Parbat, the Rama valley to the east of the mountain and the Astor gorge which cuts through the entire massif from east to west (Fig. 2). These different locations are described in turn. Note that some of these locations are described in the independent studies of Edwards *et al.* (this volume) and Argles (this volume) to which readers are directed for comparison. Additional studies are provided by Schneider *et al.* (1999*a*) for the Chichi valley (Fig. 2), although it is unclear how the rock types and field relationships correlate with those described here.

The principal aim of our studies was to investigate the general structure of the massif, as defined by the primary layering and lithological banding, placing these into the stratigraphic context described earlier where possible. The orientations of linear and planar structures were measured directly where accessible. However, this was possible in only some localities, access being limited by the rather rugged terrain. There are,

however, compensating advantages as the 6 km of vertical relief within our study area coupled with generally continuous outcrop, allow the main foliations to be mapped efficiently once 'ground-truthed' at accessible outcrops. These observations were supplemented by measured kinematic data, essentially the orientations of the principal mineral stretching lineation and, where evident, the sense of shear along the linear fabric. The general results are displayed on a form-surface map (Fig. 2) and an array of cross-sections (Fig. 3). The chief planar rock fabric is gneissic banding. This contains a locally strong linear mineral alignment which has a variable orientation within our study area (Fig. 2). The bulk of the lineations plunge northward, although a significant proportion fall on a north–south trending great circle.

Rupal area

The Rupal valley lies at the foot of the awesome southern face of the mountain of Nanga Parbat. It is accessible from the roadhead at the village of Tarshing, at an elevation of about 2500 m, and becomes glaciated above Shaigiri meadows at about 3800 m. However, the upper glacier basin offers relatively easy access south of the Mazeno pass and up to below Toshe Gali and the southern satellite peaks of the Nanga Parbat massif (Sarawali range, Fig. 2). A sketch map in Schneider *et al.* (1999*b*) illustrates this area.

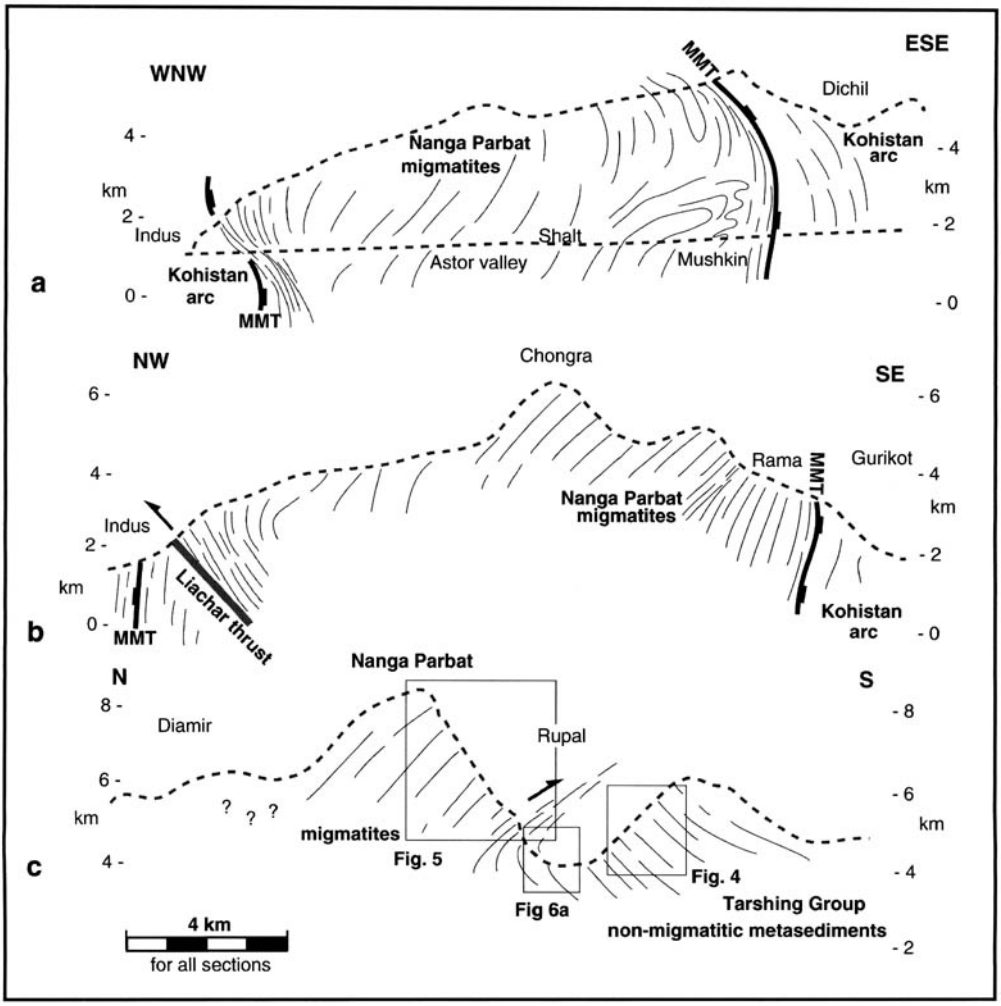

Fig. 3. Simplified structural sections across the Nanga Parbat massif: (**a**) Indus to the Dichil pass (based on the Astor valley section); (**b**) the Chongra section; (**c**) the Rupal Nanga Parbat section.

Below Tarshing village, the principal rock types are a suite of metasediments at relatively low grade (upper greenschist to lower amphibolite facies). In contrast with much of the massif further north and west, these metasediments show no signs of migmatization. The metasediments consist of psammites, pelites and subordinate calcschists. For Misch (1949), these rocks formed the low-grade outer rim of the massif. Other workers (e.g. Wadia 1933) correlate these sediments with the so-called 'Salkhala Group' of rocks which crop out in the Lesser Himalaya of the Hazara Hills, 300 km to the SW (Fig. 1). If the correlation with the Salkhala is correct, these units are Late Proterozoic in age. Alternatively these strata might correlate with the lithologically similar Permo-Triassic Alpurai Group of Lower Swat (DiPietro *et al.* 1993), an area that lies to the SE in the Pakistan Himalaya (Fig. 1). Alternatively, these could be much older strata, perhaps the lower grade protolith to the Proterozoic metasediments of the Shengus and Iskere gneisses. As none of these correlations are secure we refer to these strata as the Tarshing Group.

Tarshing Group metasediments crop out on the southern flank of the Rupal valley where they display a thickness in excess of 3000 m, dipping moderately southwards (Fig. 4). These are spectacularly exposed in profile on the sides of the un-named southern side-glaciers of the Rupal–Toshain glacier system (Fig. 2). However, the northern side of the valley, including the south face of Nanga Parbat, is dominantly composed of augen gneiss, high-grade metasediments and local leucogranite bodies of various dimensions (up to *c.* 1 km across, as estimated via binocular observation of the cliffs). Schneider *et al.* (1999*b*) describe one such leucogranite body in the Mazeno pass area.

The summit region of Nanga Parbat together with its southwestern ridge (the Mazeno peaks) appear to be composed of the same units, with the principal foliation dipping to the NW (Fig. 5). This is confirmed by accessible outcrops along the foot of the steep side valleys to the Rupal and on the approaches to the Mazeno pass (the 'interlayed gneisses and schists' of Schneider *et al.* 1999*b*). This facies assemblage of the Nanga Parbat gneisses is generally that of the Iskere type of Madin *et al.* (1989) and is principally represented by augen orthogneisses.

The upper part of the Rupal glacier basin (Fig. 6a) contains important outcrops which show the relationship between metasedimentary and metaigneous protoliths within the Iskere-type gneisses. Where undeformed, the augen gneiss shows primary igneous textures, it is a coarse-grained tonalitic rock (presumed to be equivalent to the 'Lath Unit' of Edwards *et al.* this volume). It contains autoliths of medium-grained granodiorite and xenoliths of psammitic metasediments (Fig. 6b). On the south side of the valley these igneous bodies clearly intrude the

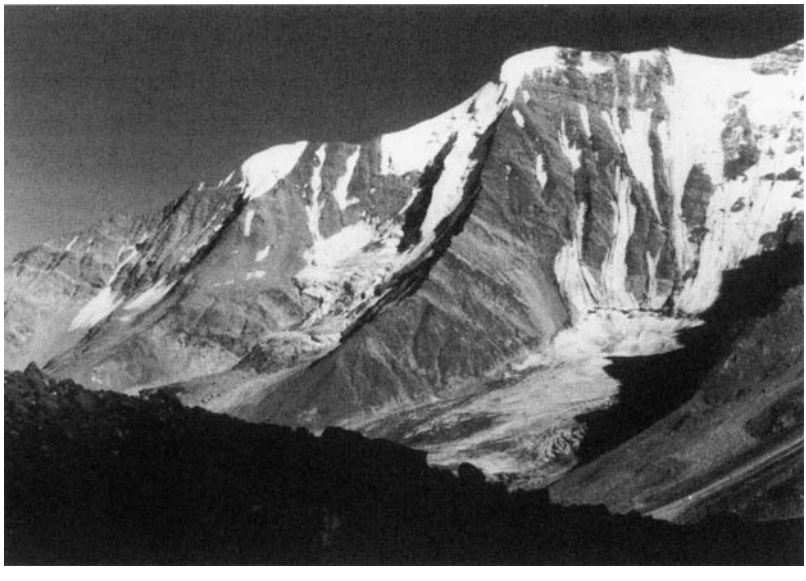

Fig. 4. Photograph of the south side of Rupal valley opposite Nanga Parbat, viewed to the east, across the lower Rupal glacier. The hillside is approximately 2000 m high. This view was taken from near the foot of the Mazeno pass.

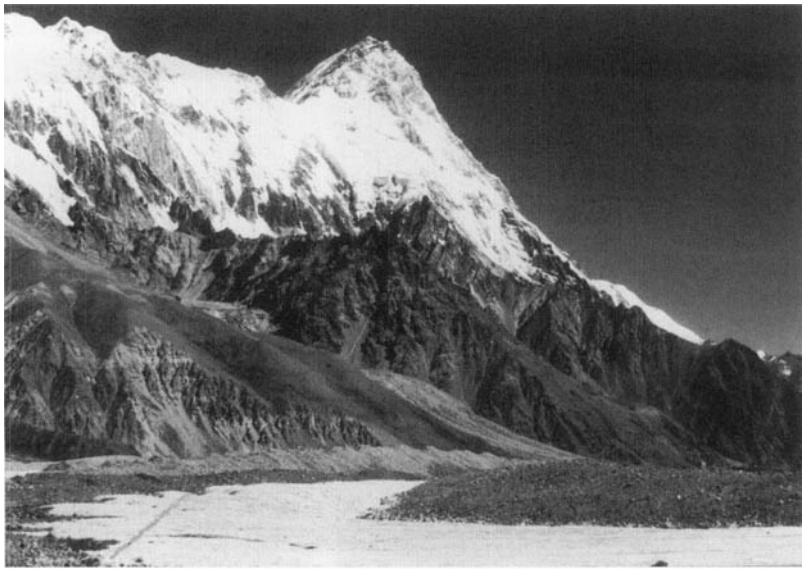

Fig. 5. Rupal face of Nanga Parbat, viewed from the upper Rupal glacier. Approximately 4000 m of topography is visible, looking NE. The upper slopes of the mountain contain prominent foliation dipping NW, presumed (from drift samples) to consist of augen gneisses. This banding is cross-cut by biotite–tourmaline-bearing leucogranites. The foreground is S-dipping Tarshing Group metasediments (see also Fig. 4).

metasediments of the Tarshing Group, forming bodies a few hundred metres across (Fig. 6c). On the north side these intrusions tend to be conformable with layering in the metasediments. There is feldspar porphyroblast growth in both the igneous and sedimentary rocks—a feature that undoubtedly led to Misch's (1949) interpretation of metasomatic granitization.

The principal banding within the Rupal area defines a southward-gaping synform (Fig. 6a), with the NW-dipping Iskere-type gneisses on the north side of the valley, and the south-dipping Tarshing Group on the south representing the two fold limbs (Fig. 3). Clearly the upper limb contains rocks at a higher metamorphic grade than the lower limb. It is also apparently more deformed, with a moderate shape fabric developed in the augen gneiss with local S–C fabrics. The stretching lineation generally plunges towards the NW (Fig. 3). The asymmetric augen and S–C fabrics imply a shear sense of top-to-south.

The fold structure of the Rupal area may be investigated in parallel with a consideration of the pattern of mineral lineations. Collectively these lineations fall on a west-dipping great circle (Fig. 7a). A subset of these data, collected on a broad transect across the upper Rupal valley, are displayed in Fig. 7b. We interpret the lineation pattern as lying on a deformation gradient. The low strain area is represented by the southern limb of the Rupal Fold, with lineations plunging moderately to steeply southward. This population becomes progressively re-orientated into the northern fold limb. We regard the north-dipping, northern limb of this fold to be a major shear zone, directed top-to-south.

The presence of deformation fabrics, including stretching lineations in the southern limb, is important. The principal foliation and lithological banding appear to be cut by the tonalitic intrusions. However, the augen gneisses derived from these intrusions are strongly sheared on the northern limb of the fold. Therefore, the linear fabrics within the metasediments are presumably composite in nature. We consider the principal foliation and lineations within the metasedimentary gneisses of the northern limb of the fold to be transposed structures. This raises a difficulty for deformation studies at the outcrop scale in the massif. Early fabrics and late fabrics can have similar field aspects and clear overprinting relationships are rarely evident. We can present no direct evidence that any of the structures we have described from the Rupal valley are of Himalayan age, rather than earlier. Although leucogranites are visible cross-cutting deformation fabrics and banding on the Rupal face of Nanga Parbat (see also Schneider *et al.* 1999*b*), our reconnaissance studies failed to unearth leucogranite bodies that had been penetratively sheared in this area.

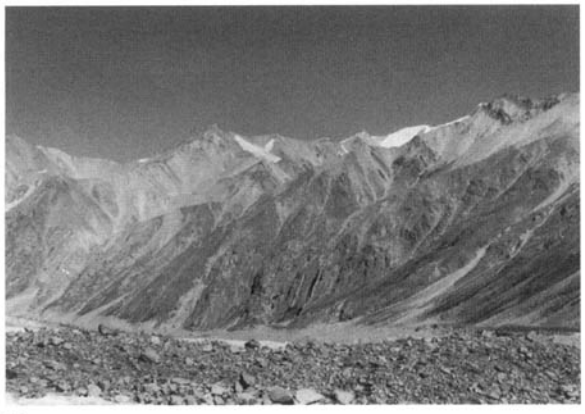

(a)

(b)

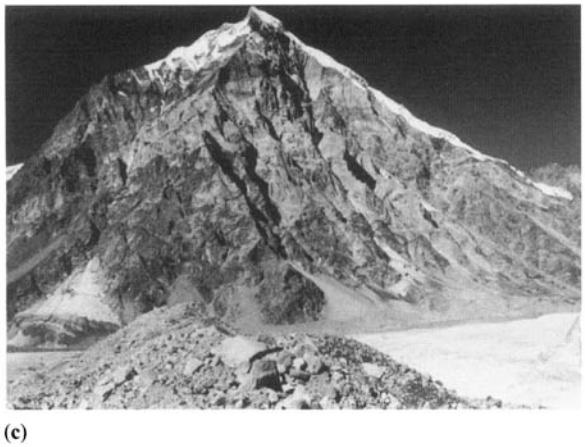

(c)

Fig. 6. (**a**) Field geology in the upper Rupal valley. Looking west to Toshe Gali across the upper Rupal glacier. This view is obliquely across the fold closure. Height of visible topography is approximately 2000 m. The outcrops with vertical layering in central foreground are migmatitic psammites with conformable biotite granite. (**b**) Field geology in the upper Rupal valley. Detail of the rock type shown in (a) (pencil for scale). This outcrop photograph comes from the low cliffs in the centre of (a), with the prominent subvertical banding. On a larger scale these granites cross-cut lithological banding within the metasediments, as seen on the south side of the upper Rupal glacier basin. (**c**) Field geology in the upper Rupal valley. This view, towards SW, cliff height about 2500 m, shows S-dipping layering (e.g. bottom left of view) with cross-cutting biotite granite bodies. The country rocks consist of well-differentiated metasediments (the Tarshing Group; cf. Schneider *et al.* 1999*b*).

Rama–Siachen glacier area

The Rama valley, running west from the town of Astor (Fig. 2) climbs up to the east face of the mountain Chongra. The 2 km high headwall to the valley was inaccessible to us. However, the southern side, overlooking the snout of the Siachen glacier, is readily accessible. It is from this area that we provide some basic field data. A more extensive study is provided by Argles (this volume). In our Rama study area the chief rock type is a suite of pink migmatitic gneisses (Fig. 8) which have the field aspect of Madin *et al.*'s (1989, see also Wheeler *et al.* 1995) Shengus Gneiss. The migmatites are folded by tight upright structures with gently NNE-plunging hinge-lines. There is a prominent mineral alignment lineation within these outcrops (Fig. 9) which broadly plunges northwards. Thus the fold hinges and stretching lineations are subparallel.

Distant observation of cliff sections south from the Siachen glacier (Bulan peak and the hillsides north of Tarshing) suggest that there is broad continuity of the principal foliation within the Nanga Parbat gneisses, linking onto the north side of the Rupal valley. However, there is not an equivalent synformal structure that gapes away from the heart of the massif as there is in

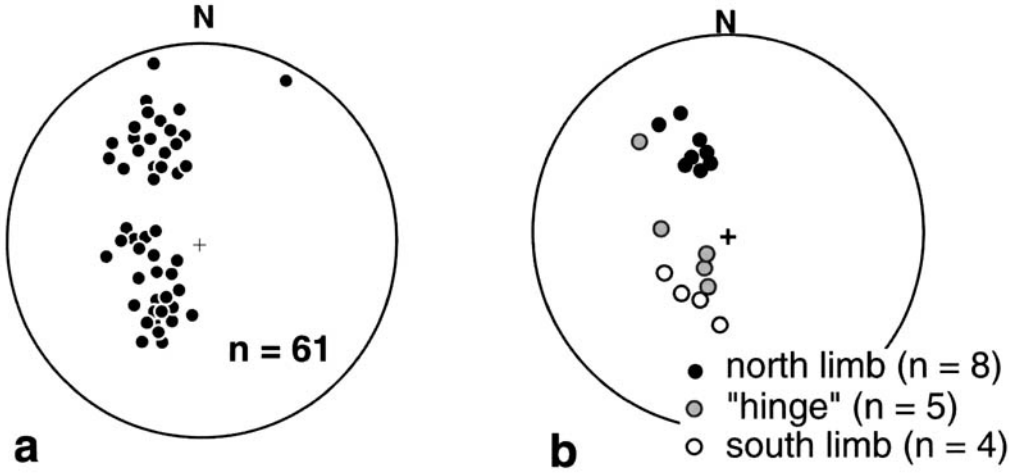

Fig. 7. Stereoplots (lower hemisphere) of mineral lineation data for the Rupal–Tarshing area, southern Nanga Parbat massif: (**a**) all lineations, falling broadly on a great circle; (**b**) sub-set of the data, from the upper Rupal glacier basin, correlated with position on the major fold structure.

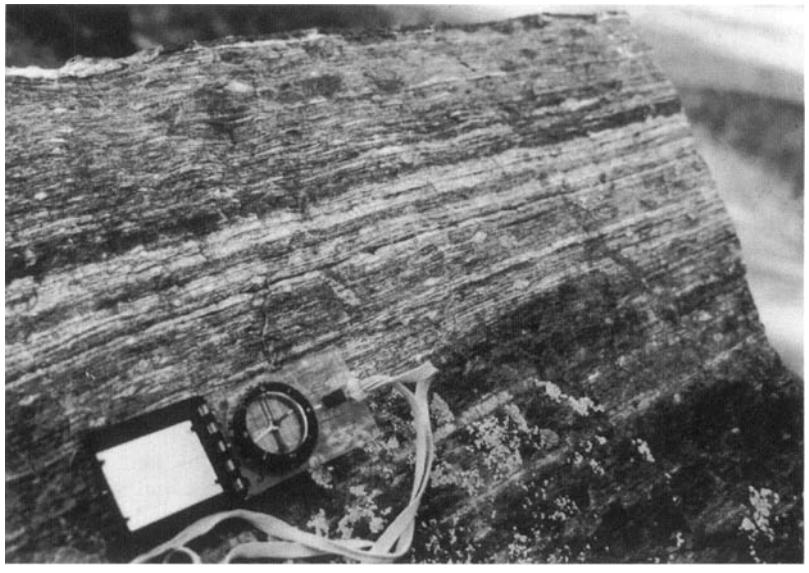

Fig. 8. Field aspect of the migmatitic gneisses (Shengus facies of Madin *et al.* 1989) seen in outcrop above and south of the snout of the Siachen glacier (*c.* 4100 m).

the south (Fig. 3). It is possible that this structure has been severely tightened or sheared out on the Rama section.

The Rama section may be linked across the watershed into the Raikhot drainage, on the western flanks of Chongra peak. Distant observation of the headwall of the Siachen glacier suggest that the principal foliations in the gneisses dip moderately towards the WNW. These orientations are broadly consistent with the orientation of banding in the Raikhot valley (see also Chamberlain *et al.* 1995). The general westward dip of banding is maintained until about 2 km structurally above the recent Liachar Thrust which locally defines the western margin of the massif (e.g. Butler *et al.* 1989; Figs 2 and 3b). However, the critical central part of this transect lies at high altitude and much of it is heavily glaciated. Consequently, the structure may include further complexities under the ice.

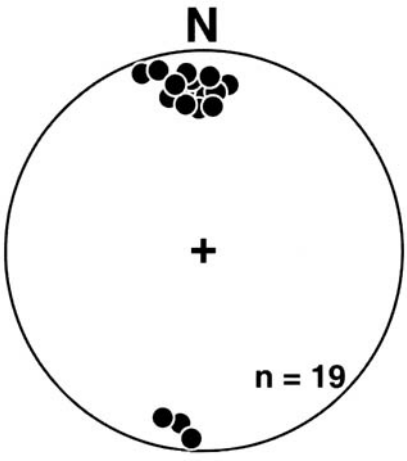

Fig. 9. Stereoplot (lower hemisphere) of mineral lineation data for the site near Rama (Fig. 2), just south of the snout of the Siachen glacier ($n = 19$).

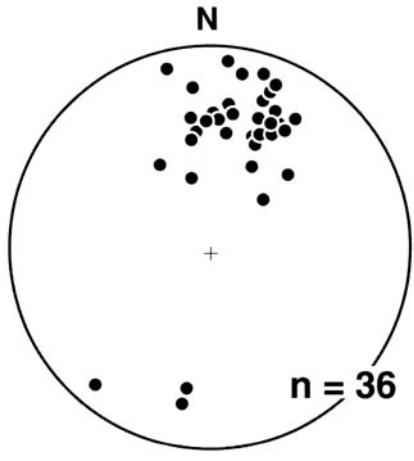

Fig. 10. Stereoplot (lower hemisphere) of mineral lineation data for the Astor valley transect (Fig. 2).

Astor gorge

The Astor gorge runs across the entire massif, the only valley to do so apart from the Indus. It is presumably antecedent to the modern structure of the massif. Like the Indus gorge, it provides an excellent transect through the massif. Our cross-section was defined over several days of combined outcrop studies supplemented by distant views, particularly onto the precipitous north wall of the Astor gorge.

The structure shown by the Astor transect is remarkably different from that shown in the Indus gorge. While the Indus displays several broad antiforms with prominent fold closures, the Astor gorge is dominated by steeply westward-dipping lithological banding and foliation. There are no broad fold closures (Fig. 3). There are tight-to-isoclinal, essentially intrafolial folds on different scales. For example, near the village of Mushkin close to the eastern margin of the massif (Fig. 3), one of these structures achieves an amplitude in excess of *c.* 2000 m, as evident in the gorge wall. It is conceivable that this closure links northwards to be continuous with one of the eastern antiforms on the Indus gorge section (e.g. Wheeler *et al.* 1995). However, it is much tighter than these more northern structures. At present the intervening ground across the Astor–Indus watershed has not been mapped away from the Dichil Gali. One of us studied this high ground on the eastern margin of the massif (CJ) but more detail is provided by Argles (this volume).

Given its position close to the eastern edge, it is unlikely that the antiform at Mushkin has the regional significance of being the chief antiformal closure of the Nanga Parbat massif. Thus the Astor gorge section shows little sign of the bulk antiformal structure inferred for the massif since the studies of Wadia (1933) and Misch (1949). Additionally, there is no broad repetition of lithology as might be expected for a fold. The antiform at Mushkin separates dominantly augen gneiss units (Iskere facies of Madin *et al.* 1989) in the west from well-differentiated migmatitic gneisses (Shengus facies of Madin *et al.* 1989) in the east.

Although there are no recognizable major fold structures defined by gneissic banding along the Astor gorge, the Nanga Parbat gneisses do contain locally prominent mineral alignment lineations. In general these are weakly northward-plunging (Fig. 10) and parallel small-scale intrafolial-style fold hinges. This parallelism between hinge lines and stretching lineation is also described for the Indus transect to the north (Wheeler *et al.* 1995). However, there are no consistent shear senses associated with this lineation and in many locations the rock fabric is lineation-dominated, which may be consistent with dominantly constrictional finite strains.

The Astor valley is important for our study because it provides a rare chance to relate deformation directly to Himalayan, rather than an earlier episode of tectonics. Sheets and veins of leucogranite, which elsewhere in the massif are younger than 10 Ma (George *et al.* 1993; Zeitler *et al.* 1993), are both deformed and cross-cut the deformation structures described above. Therefore, we conclude that at least some of the deformation occurred in the past 10 Ma.

Summary

The south-central segment of the Nanga Parbat massif yields some surprises. Misch's (1949) core of the massif, dominated by augen gneisses, appears to have been carried southward on a major shear zone, which we here refer to as the Rupal Shear Zone. Schneider *et al.* (1999*a*) infer the shear zone to be broad, essentially straddling the Rupal–Chichi drainage divide. For us, the shear zone is represented by the upper limb for the south-gaping synform in the Rupal valley (Fig. 3c). This structure carries the gneisses onto a footwall that includes non-migmatitic metasediments (our Tarshing Group). In this context the Rupal Shear Zone acts as a thrust. The shear zone has reworked earlier banding and so we have tacitly assumed that it is Himalayan (i.e. Tertiary) but there is no corroborating evidence, save the kinematics of generally top-to-the-south overshear. Local portions of this shear zone are cut by leucogranites which have yielded <2 Ma U–(Th)–Pb ages on zircon rims and monazites (Schneider *et al.* 1999*b*) so at least parts of the shear zone are older than this. Clearly dating undeformed young leucogranites alone does not aid in discriminating between pre-Himalayan and younger structures.

Foliation associated with the Rupal Shear Zone steepens up as it swings north from its type area on the lower part of the eponymous face of Nanga Parbat. Mineral alignment lineations associated with the gneissic banding generally plunge gently northwards, or gently south, indicating that this is the principal shearing direction. In the Astor valley transect at least, some of this strain postdates leucogranite sheets and therefore is younger than about 10 Ma. However, further north the structure changes. There is little evidence in our opinion, for the broad antiformal structure assumed by most previous workers—at least as defined by fabrics within the Nanga Parbat gneisses.

Structural model

The range of structural geometries evident on profiles across the Nanga Parbat massif demand a three-dimensional solution for the deformation. Our task here is to provide a preliminary model for the deformation, linking the Rupal Shear Zone to the more upright fabrics of the Astor valley section and then, in turn, to the Indus section with its folds and the more complex structures of the western margin (Butler *et al.* 1989). In building this model we are aware that the age of deformation is poorly constrained, particularly within the Rupal Shear Zone. We have not discovered leucogranites deformed within the shear zone. However, existing petrogenetic studies strongly suggest that the leucogranites within the Nanga Parbat massif formed during decompression, in essence during the neotectonic formation of the massif. So if the Rupal Shear Zone formed prior to active denudation of the massif, or even early in this process, it would not be expected to deform decompression-related products.

We present our model in terms of a block diagram of foliation within the massif (Fig. 11). The Rupal Shear Zone is considered to pass laterally, north and east, into a zone of dominantly transcurrent shearing, presumably with a broadly left-lateral sense of displacement. However, this zone broadens to include the width of the Astor valley transect. If the deformation kinematics of the Rupal Shear Zone is overthrust shear, the fabrics within the Astor section are more consistent with N–S orientated constrictional elongation. We relate this zone to the Indus section further north. We tentatively propose that the Indus folds are tightened and transposed into the Astor valley section. Thus the deformation in the massif varies from top-to-the south overshear in the south to N–S constrictional elongation in the north. If we are correct in this kinematic model, which remains tentative in the absence of sound measurements of finite strain or estimates of the strain path, it at least has some virtue for this regional structural setting. Constrictional elongation might be expected at the lateral tips of shear zones (Coward & Potts 1983). The NW Himalayan syntaxes, including the Nanga Parbat massif, have been interpreted as the lateral tips to Himalayan crustal thrusts (Coward *et al.* 1988). However, in this context the wrench shear component should be right-lateral. Presumably the Rupal Shear Zone predates, perhaps entirely, structures such as the Liachar Thrust and its related shear zone (e.g. Butler *et al.* 1989) that were responsible for the modern structure of the massif. Critical structural relationships should lie in the Diamir area, on the north and west of the pass of Toshe Gali (Fig. 2)—an area discussed by Edwards *et al.* (this volume).

Discussion

The recognition that both the Tarshing Group and Iskere-type gneisses share a common history of intermediate-composition igneous intrusions is important. The units do not appear to represent a basement and cover sequence. Rather they were assembled and experienced different degrees of metamorphism and igneous activity,

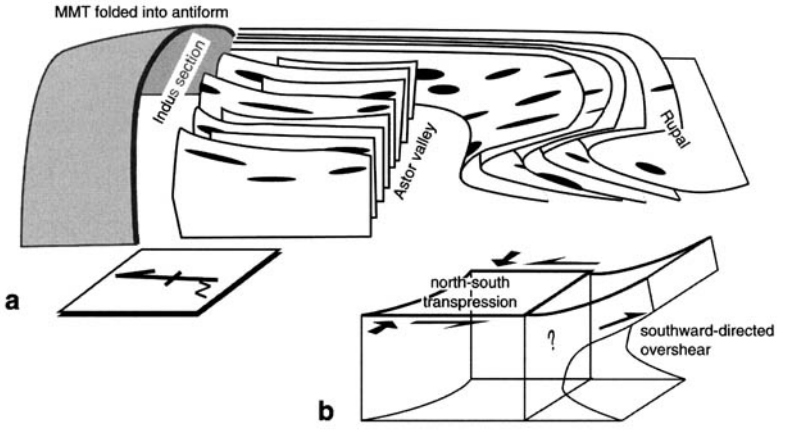

Fig. 11. A schematic structural model for southern-central part of the Nanga Parbat massif. (**a**) Illustrates the orientation of foliation and stretching lineation, together with the form of the Main Mantle Thrust which is considered to envelope the internal structure of the massif. Unscaled—so use Fig. 2 for locations. Note that the elliptical markers indicate the inferred geometry of linear fabrics and do not represent measured strain values. (**b**) Hypothetical kinematic distribution within the area of the massif.

presumably prior to Himalayan orogenesis. The intermediate-composition plutons are the local protolith to at least some of the gneisses with feldspathic augen within the massif. Elsewhere in the massif (Butler *et al.* 1992; Wheeler *et al.* 1995), these gneisses are cross-cut by metabasic sheets which are assumed to long predate Himalayan orogenesis (e.g. Treloar *et al.* this volume). Thus the Nanga Parbat basement has a long history of deformation and metamorphism, only part of which is associated with Tertiary mountain building. Using field data, it is only those structures that deform leucogranite sheets that can be inferred directly to be Tertiary in age. However, as leucogranites formed only during the late, exhumation-related history of the Nanga Parbat massif (George *et al.* 1993; Butler *et al.* 1997), some structures that postdate the basic dykes yet predate the leucogranites may be of Tertiary age. Although many of these points have been made before for the massif as a whole, they are supported by our studies in its southern districts.

Given the polyphase deformation history, it is difficult to present a coherent structural history for the massif away from the Main Mantle Thrust. However, the finite structure is relatively clear. Foliation and banding within the massif does not define a simple, upright antiform with a north–south trending hinge line. The central part of the massif does not appear to show broad fold structures. Those structures that have been identified by us (also Edwards *et al.* and Argles this volume) are essentially large-scale intrafolial folds with generally gently plunging hinge lines. Tight-to-isoclinal folds are also described by Coward (1985) in the Indus transect where they are folded by the main upright antiforms. Correlating these structures between the Indus and Astor gorges is difficult. However, the general north–south, gently plunging mineral elongation lineation is common to both the Astor gorge (this study) and the Indus transect (Wheeler *et al.* 1995).

The rodding lineation typical of the Astor transect may reflect constrictional finite strains. This type of finite deformation may occur as a consequence of distributed transpression (reviewed, for example, by Fossen & Tikoff 1998). This type of deformation was proposed for our study area on the basis of fault kinematic studies along the western margin of the Nanga Parbat massif (Butler *et al.* 1989) and on regional grounds (Seeber & Pêcher 1998). However, until now this has not been considered for the ductile strain history within the massif itself. So it is possible that N–S constrictional elongation may be the finite result of distributed dextral shear and east–west compression acting through the present volume of the massif.

In the Rupal area the migmatitic core of the massif, represented by the summit of Nanga Parbat and its northern (Raikhot) slopes, has been carried southwards by the Rupal Shear Zone, over lower-grade metasediments of the Tarshing Group. The age of this shearing is unclear. However, the Rupal Shear Zone appears to pass laterally—or be deformed into—part of the north–south transcurrent shear zone. This strain zone, marked by apparently constrictional

strain, is at least partially of late Tertiary age in that it deforms leucogranites. These structural relationships are unexpected for the broadly antiformal structure of the massif, as sketched by other workers, is not evident in the internal structure of the massif. For example, along the Astor valley section, the foliation and gneissic banding consistently dips moderately to steeply westwards with no sign of a major antiformal closure. The antiforms evident in the Indus valley, just 10–15 km to the north, are unrecognizable here. Perhaps the folds have been transposed by the intense L–S tectonite fabric in the Astor gorge where they are represented by the rare intrafolial closures within the gneissic banding. However, it is probable that the Main Mantle Thrust defines an antiform (e.g. Butler *et al.* 1992). Consequently, information on the structural relationships between the internal fabric orientations and deformation unambiguously associated with the Main Mantle Thrust is needed.

The fieldwork was completed in 1988 and 1990. The earlier trip was funded partially by Durham University. The second trip was supported by the Natural Environment Research Council. Our results were first presented at the Himalaya–Karakoram–Tibet workshop at Auris-en-Oisans in 1991. We thank the participants at this workshop for stimulating discussion, together with other members of our field expeditions, particularly Nigel Harris and Dave Prior. We thank the editors of this volume for prodding us into submitting this paper after its exceptional gestation period, to the present collection. Vigorous reviews were provided by M. Edwards and J. P. Burg—although the opinions expressed in this paper remain the responsibility of the authors alone.

References

ARGLES, T. W. 2000. The evolution of the Main Mantle Thrust in the Western Syntaxis, Northern Pakistan. *This volume.*

BUTLER, R. W. H. & PRIOR, D. J. 1988. Anatomy of a continental subduction zone: the Main Mantle Thrust in northern Pakistan. *Geologisches Rundschau*, **77**, 239–255.

——, —— & KNIPE, R. J. 1989. Neotectonics of the Nanga Parbat syntaxis, Pakistan, and crustal stacking in the northwest Himalayas. *Earth and Planetary Science Letters*, **94**, 329–343.

——, HARRIS, N. B. W. & WHITTINGTON, A. G. 1997. Interactions between deformation, magmatism and hydrothermal activity during active crustal thickening: a field example from Nanga Parbat, Pakistan Himalayas. *Mineralogical Magazine*, **61**, 37–52.

——, GEORGE, M., HARRIS, N. B. W., JONES, C., PRIOR, D. J., TRELOAR, P. J. & WHEELER, J. 1992. Geology of the northern part of the Nanga Parbat massif, northern Pakistan, and its implications for Himalayan tectonics. *Journal of the Geological Society, London*, **149**, 557–567.

CHAMBERLAIN, C. P., ZEITLER, P. K., BARNETT, D. E., WINSLOW, D., POULSON, S. R., LEAHY, T. & HAMMER, J. E. 1995. Active hydrothermal systems during the recent uplift of Nanga Parbat, Pakistan Himalaya. *Journal of Geophysical Research*, **100**, 439–453.

COWARD, M. P. 1985. A section through the Nanga Parbat syntaxis, Indus valley, Kohistan. *Geological Bulletin of the University of Peshawar*, **18**, 147–152.

—— & POTTS, G. J. 1983. Complex strain patterns developed at the frontal and lateral tips to shear zones and thrust zones. *Journal of Structural Geology*, **5**, 383–399.

——, BUTLER, R. W. H., CHAMBERS, A. F., GRAHAM, R. H., IZATT, C. N. *et al.* 1988. Folding and imbrication of the Indian crust during Himalayan collision. *Philosophical Transactions of the Royal Society, London*, **A326**, 89–116.

DESIO, A. 1976. Geotettonica delle zone orogeniche del Kashmir Himalaya, Karakorum–Hindu Kush–Pamir. *Atti dei Convegni Lincei*, **21**, 115–129.

DIPIETRO, J. A., POGUE, K. R., LAWRENCE, R. D., BAIG, M. S., HUSSAIN, A. & AHMAD, I. 1993. Stratigraphy south of the Main Mantle Thrust, Lower Swat, Pakistan. *In*: TRELOAR, P. J. & SEARLE, M. P. (eds) *Himalayan Tectonics*. Geological Society, London, Special Publications, **74**, 207–220.

EDWARDS, M. A., KIDD, W. S. F., KHAN, M. A. & SCHNEIDER, D. A. 2000. Tectonics of the SW margin of the Nanga Parbat–Haramosh massif. *This volume.*

FOSSEN, H. & TIKOFF, B. 1998. Extended models of transpression and transtension, and application to tectonic settings. *In*: HOLDSWORTH, R. E., STRACHAN, R. A. & DEWEY, J. F. (eds) *Continental Transpressional and Transtensional Tectonics*. Geological Society, London, Special Publications, **135**, 15–33.

GANSSER, A. 1964. *The Geology of the Himalayas*. John Wiley, London.

GEORGE, M. T., HARRIS, N. B. W. & BUTLER, R. W. H. 1993. The tectonic implications of contrasting granite magmatism between the Kohistan island arc and the Nanga Parbat–Haramosh Massif, Pakistan Himalaya. *In*: TRELOAR, P. J. & SEARLE, M. P. (eds) *Himalayan Tectonics*. Geological Society, London, Special Publications, **74**, 173–191.

HARRIS, N. B. W., INGER, S. & MASSEY, J. A. 1993. The role of fluids in the formation of High Himalayan leucogranites. *In*: TRELOAR, P. J. & SEARLE, M. P. (eds) *Himalayan Tectonics*. Geological Society, London, Special Publications, **74**, 391–400.

LE FORT, P. 1989. The Himalayan orogenic segment. *In*: SENGOR, A. M. C. (ed.) *Tectonic evolution of the Tethyan Region*. Kluwer Academic Publishers, Dordrecht, 289–286.

MADIN, I. P., LAWRENCE, R. D. & UR-REHMAN, S. 1989. The northwest Nanga Parbat–Haramosh massif: evidence for crustal uplift at the northwestern

corner of the Indian craton. *In*: MALINCONICO, L. L. & LILLIE, R. J. (eds) *Tectonics of the Western Himalayas*. Geological Society of America Special Paper, **232**, 169–182.

MISCH, P. 1949. Metasomatic granitisation of batholithic dimensions. *American Journal of Science*, **247**, 209–249.

NOBLE, S. R. & SEARLE, M. P. 1995. Age of crustal melting and leucogranite formation from U–Pb zircon and monazite dating in the western Himalaya, Zanskar, India. *Geology*, **23**, 1135–1138.

POGNANTE, U., BENNA, P. & LE FORT, P. 1993. High-pressure metamorphism in the High Himalayan Crystallines of the stak valley, north-eastern Nanga Parbat–Haramosh syntaxis, Pakistan Himalaya. *In*: TRELOAR, P. J. & SEARLE, M. P. (eds) *Himalayan Tectonics*. Geological Society, London, Special Publications, **74**, 161–172.

SCHNEIDER, D. A., EDWARDS, M. A., KIDD, W. S. F., ZEITLER, P. K. & COATH, C. D. 1999*a*. Early Miocene anatexis identified in the western syntaxis, Pakistan Himalaya. *Earth and Planetary Science Letters*, **167**, 121–129.

——, ——, ZEITLER, P. K. & COATH, C. D. 1999*b*. Mazeno Pass Pluton and Jutial Pluton, Pakistan Himalaya: age and implications for entrapment mechanisms of two granites in the Himalaya. *Contributions to Mineralogy and Petrology*, **136**, 273–284.

SEEBER, L. & PÊCHER, A. 1998. Strain partitioning along the Himalayan arc and the Nanga Parbat antiform. *Geology*, **26**, 791–794.

SMITH, H. A., CHAMBERLAIN, C. P. & ZEITLER, P. K. 1992. Documentation of Neogene regional metamorphism in the Himalayas of Pakistan using U–Pb in monazite. *Earth and Planetary Science Letters*, **113**, 93–105.

TAHIRKHELI, R. A. & JAN, M. Q. (eds) 1979. *Geology of Kohistan, Karakoram Himalaya, northern Pakistan*. Geological Bulletin of the University of Peshawar (Special Issue), **11**, 187 (with map).

TEUFEL, S. & HEINRICH, W. 1997. Partial resetting of the U–Pb isotope system in monazite through hydrothermal experiments: an SEM and U–Pb isotope study. *Chemical Geology*, **137**, 273–281.

TRELOAR, P. J., POTTS, G. J., WHEELER, J. & REX, D. C. 1991. Structural evolution and asymmetric uplift of the Nanga Parbat syntaxis, Pakistan Himalayas. *Geologisches Rundschau*, **80**, 411–428.

——, GEORGE, M. T. & WHITTINGTON, A. G. 2000. Mafic sheets from Indian plate gneisses in the Nanga Parbat syntaxis: their significance in dating crustal growth and metamorphic and deformation events. *This volume*.

WADIA, D. N. 1933. Note on the geology of Nanga Parbat (Mt. Diamir) and adjoining portions of Chilas, Gilgit District, Kashmir. *Records of the Geological Survey of India*, **66**, 212–234 (and enclosed maps and sections).

—— 1961. *The geology of India*. MacMillan, New York.

WHEELER, J., TRELOAR, P. J. & POTTS, G. J. 1995. Structural and metamorphic exolution of the Nanga Parbat syntaxis, Pakistan Himalayas, on the Indus gorge transect: the importance of early events. *Geological Journal*, **30**, 349–371.

WHITTINGTON, A. 1996. Exhumation overrated at Nanga Parbat, northern Pakistan. *Tectonophysics*, **260**, 215–226.

——, HARRIS, N. & BAKER, J. 1998. Low-pressure crustal anatexis: the significance of spinel and cordierite from metapelitic assemblages at Nanga Parbat, northern Pakistan. *In*: TRELOAR, P. J. & O'BRIEN, P. J. (eds) *What Drives Metamorphism and Metamorphic Reactions?* Geological Society, London, Special Publications, **138**, 183–198.

ZEITLER, P. K. 1985. Cooling history of the NW Himalaya, Pakistan. *Tectonics*, **4**, 127–151.

——, SUTTER, J. F., WILLIAMS, I. S., ZARTMAN, R. & TAHIRKHELI, R. A. K. 1989. Geochronology and temperature history of the Nanga Parbat–Haramosh Massif, Pakistan. *In*: MALINCONICO, L. L. & LILLIE, R. J. (eds) *Tectonics of the Western Himalayas*. Geological Society of America Special Paper, **232**, 1–22.

——, CHAMBERLAIN, C. P. & SMITH, H. A. 1993. Synchronous anatexis, metamorphism, and rapid denudation at Nanga Parbat (Pakistan Himalayas). *Geology*, **21**, 347–350.

Geochronological constraints on the evolution of the Nanga Parbat syntaxis, Pakistan Himalaya

P. J. TRELOAR[1], D. C. REX[2], P. G. GUISE[2], J. WHEELER[3], A. J. HURFORD[4] & A. CARTER[4]

[1]*CEESR, School of Geological Sciences, Kingston University, Kingston-upon-Thames KT1 2EE, UK (e-mail: p.treloar@kingston.ac.uk)*

[2]*Department of Earth Sciences, Leeds University, Leeds LS2 9JT, UK*

[3]*Department of Earth Sciences, Liverpool University, Brownlow Street, Liverpool L69 3BX, UK*

[4]*Research School of Geological Sciences, Birkbeck College and University College London, Gower Street, London WC1E 6BT, UK*

Abstract: New amphibole, muscovite and biotite Ar–Ar and K–Ar data and zircon and apatite fission track data are presented from the western margin of the Nanga Parbat syntaxis as well as from the Indus and Astor valley sections which cross the syntaxis. Amphibole data date a regional cooling through 500 °C at 25 ± 5 Ma and are inconsistent with earlier suggestions that the peak of regional metamorphism was Neogene in age, although there is no doubt that some rocks were still at upper amphibolite facies temperatures as recently as 5 Ma. The data can be used to constrain structural models for syntaxial uplift. After an initial phase of crustal-scale buckling, bodily uplift of the syntaxis was along subvertical shear zones developed along its margins, although with a significantly higher time-averaged strain rate for shears developed along the western margin than along the eastern margin. The latter may be antithetic to the former. These shears were operative from 10 to < 1 Ma. In the southwestern part of the syntaxis, this subvertical uplift was superseded, since 6 Ma, by uplift along moderately SE-dipping NW-vergent shears on the hanging wall of which are located Neogene-aged migmatites.

The Nanga Parbat syntaxis, located in the NW Himalaya (Fig. 1), is a N-trending structural half window within which Indian plate rocks have been uplifted from beneath a tectonic cover of volcanic and plutonic rocks of the Kohistan–Ladakh island arc (Fig. 2). Recognition that the syntaxis is a region of continuing, rapid uplift was based on differences between young amphibole and mica Ar–Ar and zircon and apatite fission track ages within the syntaxis and significantly older equivalent ages outside it (Zeitler 1985). These data indicate substantial, and increasingly rapid, cooling throughout the late Neogene (Treloar *et al.* 1989*b*, 1991; Zeitler *et al.* 1989; George *et al.* 1995; Winslow *et al.* 1996). Zeitler (1985) suggested present-day exhumation rates to be as great as 7 mm a^{-1}, although Whittington (1996) argues this to be an overestimate. Uplift has been accommodated by a combination of large wavelength and amplitude folding within the syntaxis core (Madin *et al.* 1989; Treloar *et al.* 1991; Butler *et al.* 1992, 2000; Wheeler *et al.* 1995) and NW-directed thrusting along its western margin (Butler & Prior 1988*a*, *b*; Butler *et al.* 1989; Butler this volume; Edwards *et al.* this volume).

Uplift and related exhumation has been accompanied by melting and leucogranite generation and emplacement (Zeitler & Chamberlain 1991; Zeitler *et al.* 1993; Winslow *et al.* 1995, 1996; Butler *et al.* 1997) which has continued since 10 Ma (Zeitler & Chamberlain 1991; Zeitler *et al.* 1993; Schneider *et al.* 1999*a*). Leucogranites, derived through vapour-absent incongruent dissolution of muscovite at $T \geqslant 720$ °C (Winslow *et al.* 1995; Butler *et al.* 1997), were emplaced into upper crustal rocks at $T \leqslant 400$ °C (George *et al.* 1995). Cooling histories of rocks now exposed at surface, and the derivation of leucogranites from rocks underlying them at temperatures > 700 °C, imply that amphibolite facies temperatures persist at mid-crustal levels.

From: KHAN, M. A., TRELOAR, P. J., SEARLE, M. P. & JAN, M. Q. (eds) *Tectonics of the Nanga Parbat Syntaxis and the Western Himalaya*. Geological Society, London, Special Publications, **170**, 137–162. 1-86239-061-4/00/$15.00

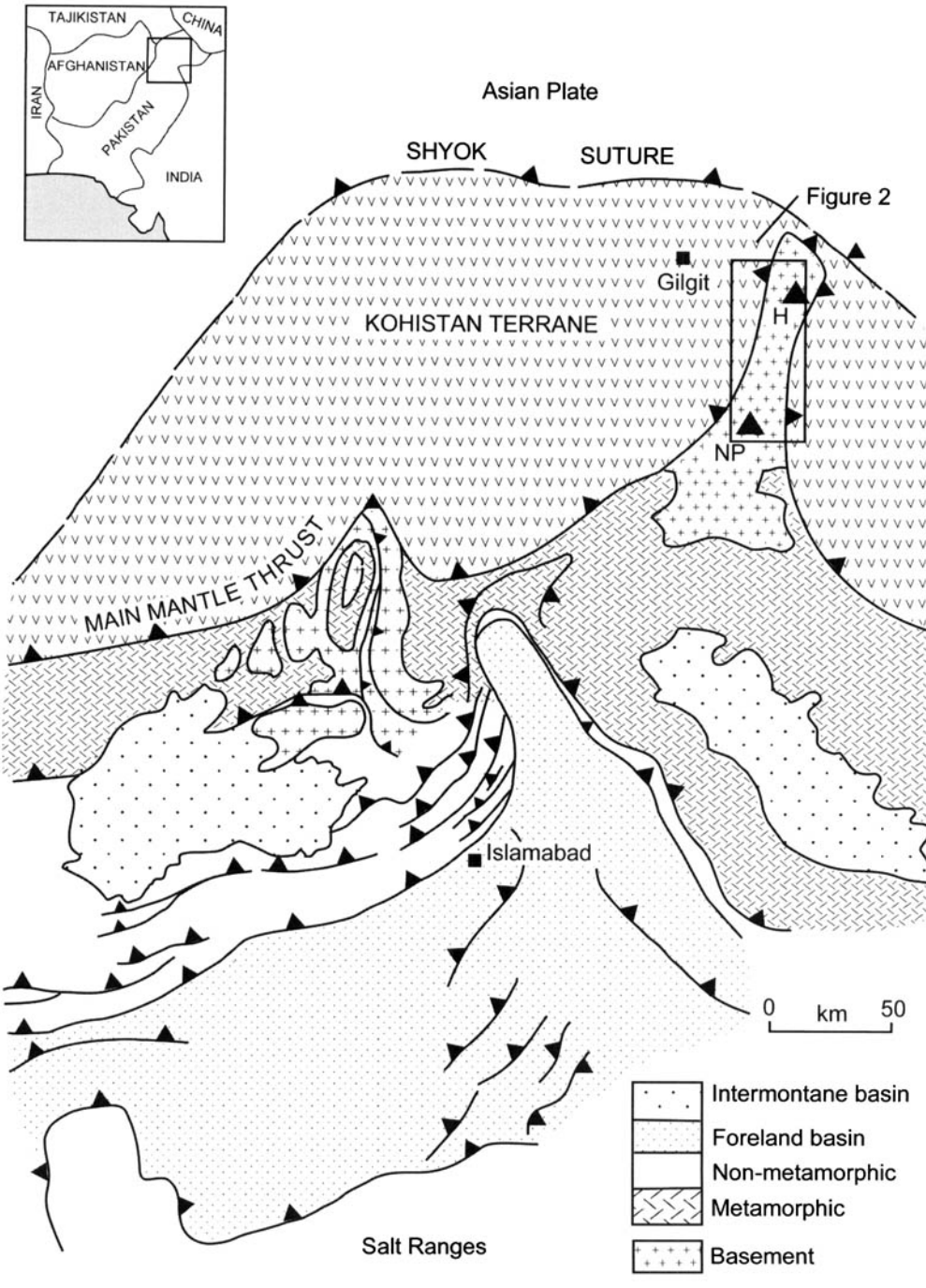

Fig. 1. Regional geology map showing the location of the Nanga Parbat syntaxis and of Fig. 2.

Zeitler *et al.* (1993) and Smith *et al.* (1992) used U–Pb data from zircon rims and monazites to date 'peak metamorphism' in rocks exposed throughout the syntaxis as Neogene in age. However, hornblende cooling ages of about 25 Ma (Zeitler *et al.* 1989; Treloar *et al.* 1991; Winslow *et al.* 1996) do not fit well with this assertion.

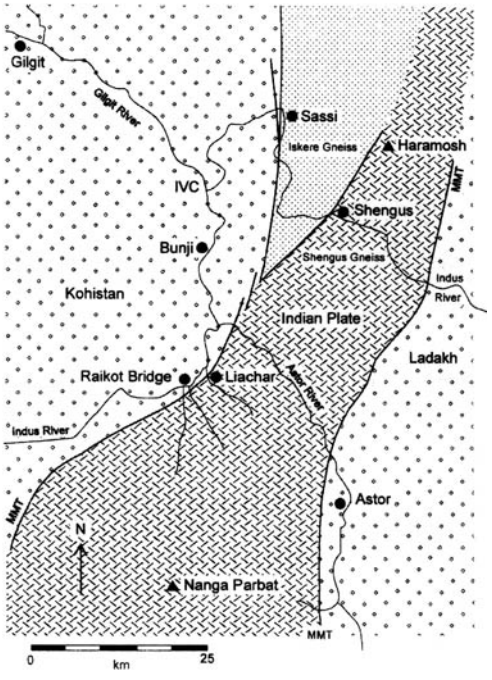

Fig. 2. Map of the Nanga Parbat syntaxis showing the main lithologies present and the location of the Indus and Astor valley sections.

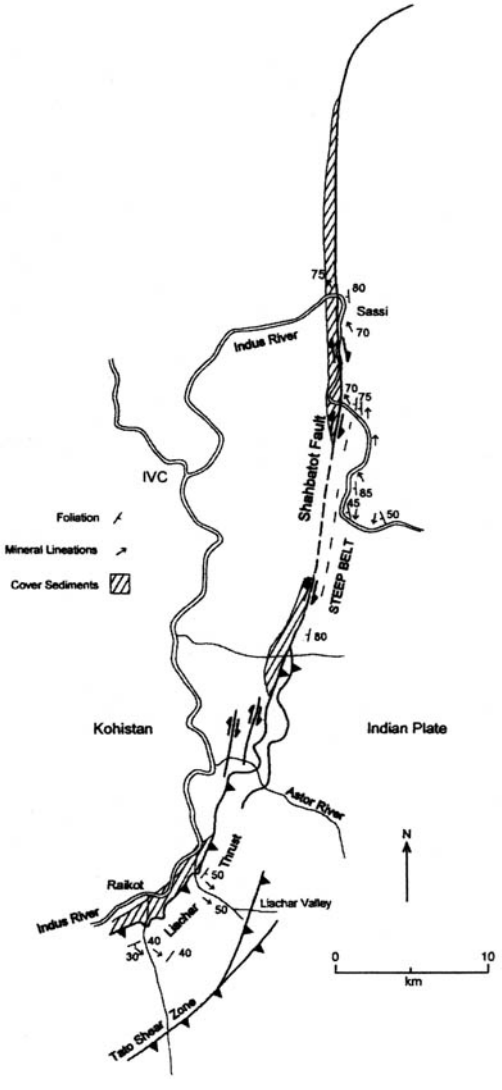

Fig. 3. Simplified structural map of the western margin of the syntaxis derived from data in Madin *et al.* (1989), Butler & Prior (1988*a*, *b*), Butler *et al.* (1989, 1992) and George & Bartlett (1996).

Despite the increasing wealth of geochronological data from the Nanga Parbat massif, it has not yet proved possible to correlate geochronological evidence for uplift with structures that accommodate uplift. Treloar *et al.* (1991) attempted this for the Indus valley section, which is one of the better dated sections through the syntaxis (Fig. 2). Due to the antecedent nature of the river, exhumation rates along the section should equal uplift rates and, in the apparent absence of extensional faulting, exhumation must be the result of erosion consequent on tectonic uplift. Treloar *et al.* (1991) hypothesized that younger ages within the eastern rather than the western part of the syntaxis implied sequential growth of two large antiformal structures. By contrast, Winslow *et al.* (1996), for the Astor River section, found no evidence for an asymmetry in cooling ages, and suggested that exhumation history was a function of the growth of a single, large antiformal structure. Near the western margin of the syntaxis, Smith *et al.* (1992) and Winslow *et al.* (1996) have shown that the NW-vergent Tato Shear Zone (Fig. 3) places rocks with a younger cooling history onto rocks with an older cooling history.

Here, new geochronological data are summarized from the western margin of the syntaxis and from the Indus and Astor valley sections. When combined with previously published geochronological, structural and metamorphic history data, these may be used to address the following questions. What constraints can the distribution of measured ages within the syntaxis place upon its metamorphic evolution? To what extent can geochronology constrain mechanisms of syntaxis growth?

Sample preparation and analytical techniques for K–Ar and Ar–Ar analysis are given in Treloar & Rex (1990) and for fission track

analysis in Johnson *et al.* (1997). Despite the recent questioning by Villa (1998) of the concept that temperature, albeit affected by crystal size and diffusion kinetics (Dodson 1973), is the prime rate-controlling factor in determining the closure of isotopic systems, this paper adheres to the primacy of temperature in determining when isotopic systems close. Closure temperatures used in this paper (hornblende Ar–Ar: *c.* 500 °C; muscovite Rb–Sr: *c.* 500 °C, Ar–Ar: *c.* 400 °C, biotite Rb–Sr and Ar–Ar: *c.* 300 °C, and zircon and apatite fission track annealing temperatures: *c.* 200 and *c.* 140 °C respectively) are discussed in Treloar & Rex (1990).

The presence of excess Ar as a problem in interpreting Ar–Ar data has been previously identified in the Nanga Parbat syntaxis (Zeitler *et al.* 1989; Treloar *et al.* 1991; Smith *et al.* 1992; George *et al.* 1993; George & Bartlett 1996; Winslow *et al.* 1996). The incorporation of excess ^{40}Ar into minerals in metamorphic rocks is thought to be due to a high partial pressure of ^{40}Ar in the fluid phase (Roddick *et al.* 1980), probably due to the degassing of older and/or deeper rocks into a circulating fluid phase. A large proportion of the excess ^{40}Ar may be harboured within inclusions or alteration phases rich in excess ^{40}Ar, but containing little or no radiogenic argon (Wartho *et al.* 1996). In order to identify whether or not phases have been affected by excess Ar, correlation plots are presented here as well as the standard incremental heating plots. Data for isotope correlation plots were reduced using Isoplot (Ludwig 1990). Best fit lines and intercepts were calculated using Yorkfit 1 and errors taken from the 95% confidence level values. For most minerals, regression lines on a $^{39}Ar/^{40}Ar$ v. $^{36}Ar/^{40}Ar$ correlation plot will only pass through atmospheric argon (40/36 = 295) on the $^{36}Ar/^{40}Ar$ axis when there is no excess Ar present. The presence of excess Ar will deflect the correlation plot to increasingly high 40/36 values. Although true for muscovite and hornblende, this appears not to be so for biotite. Because of its crystal chemistry properties, biotite incorporates excess Ar more easily than muscovite (Dahl 1996) and often yields ages anomalously older than those derived from associated muscovites (Brewer 1969; Foland 1983; Gaber *et al.* 1988). For reasons which remain unclear, biotites that have excess argon, and hence anomalously old ages, yield flat plateaux and have correlation plots on which regression lines pass through atmospheric argon on the $^{36}Ar/^{40}Ar$ axis. In these phases, both radiogenic and excess argon appear to be completely homogenized throughout the mineral, due to either irradiation damage in the reactor (Pankhurst *et al.* 1973) or to structural breakdown during *in vacuo* heating (Foland 1983; Gaber *et al.* 1988). Whatever the cause, in this paper we interpret biotite ages that are older than muscovites from the same, or nearby, samples to be the result of excess argon and interpret them accordingly. In addition, points that fall off well defined regression lines, which pass through atmospheric argon on the $^{36}Ar/^{40}Ar$ axis, frequently have Ca/K ratios higher than the other points. These, normally high temperature, points are interpreted as reflecting degassing of a phase, maybe an inclusion, other than that being analysed.

The western margin of the Nanga Parbat syntaxis

Along the western margin of the syntaxis (Fig. 3), an array of thrusts and strike-slip faults developed within the Raikot–Sassi Fault Zone (Treloar *et al.* 1991) separate mafic rocks of the Kohistan arc to the west from Indian plate gneisses to the east, and deform the Main Mantle Thrust (MMT) along which Kohistan was thrust south onto the Indian plate. East-side-up, dip-slip faults, including both steep and moderately SW-dipping ductile thrust zones and brittle reverse faults, outcrop along the length of the fault zone. At Sassi (Treloar *et al.* 1991) and Darchan (George & Bartlett 1996), steeply dipping ductile shear fabrics with east-side-up displacement senses (Fig. 4a) are cut by brittle shear fabrics with an east-side-up sense of displacement (Fig. 4b). Imposed on these structures are steep, dextral oblique to strike-slip faults that postdate early phases of dip-slip thrusting and that propagated southward (Butler *et al.* 1989). Two major SW-dipping shear zones crop out at the south end of the fault zone (Fig. 3). The Liachar (LSZ) and Tato (TSZ) shear zones are developed in Indian plate gneisses, have down-dip stretching lineations and S–C fabrics indicating NW-directed transport of Indian plate gneisses onto Kohistan. Stability of biotite and muscovite and crystal plastic deformation of quartz and plagioclase suggest that ductile deformation was at upper greenschist to lower amphibolite conditions. In the LSZ a transition from ductile to brittle faulting is identified (Butler *et al.* 1989, 2000). NW-vergent thrusting continues to the present with brittle thrusts exposed at the surface reworking ductile shear fabrics. At Liachar Gar, the LSZ places strongly sheared Indian plate gneisses directly onto < 100 ka Indus valley alluvial sediments. That early ductile fabrics are

transposed by present-day brittle faults suggests that thrusting can be modelled as a continuum during which rocks were exhumed from significant crustal depths.

At Raikot, a strip of cover metasediments is exposed on the footwall of the Liachar Thrust. They are similar in lithology, appearance and metamorphic grade to the Permo-Triassic

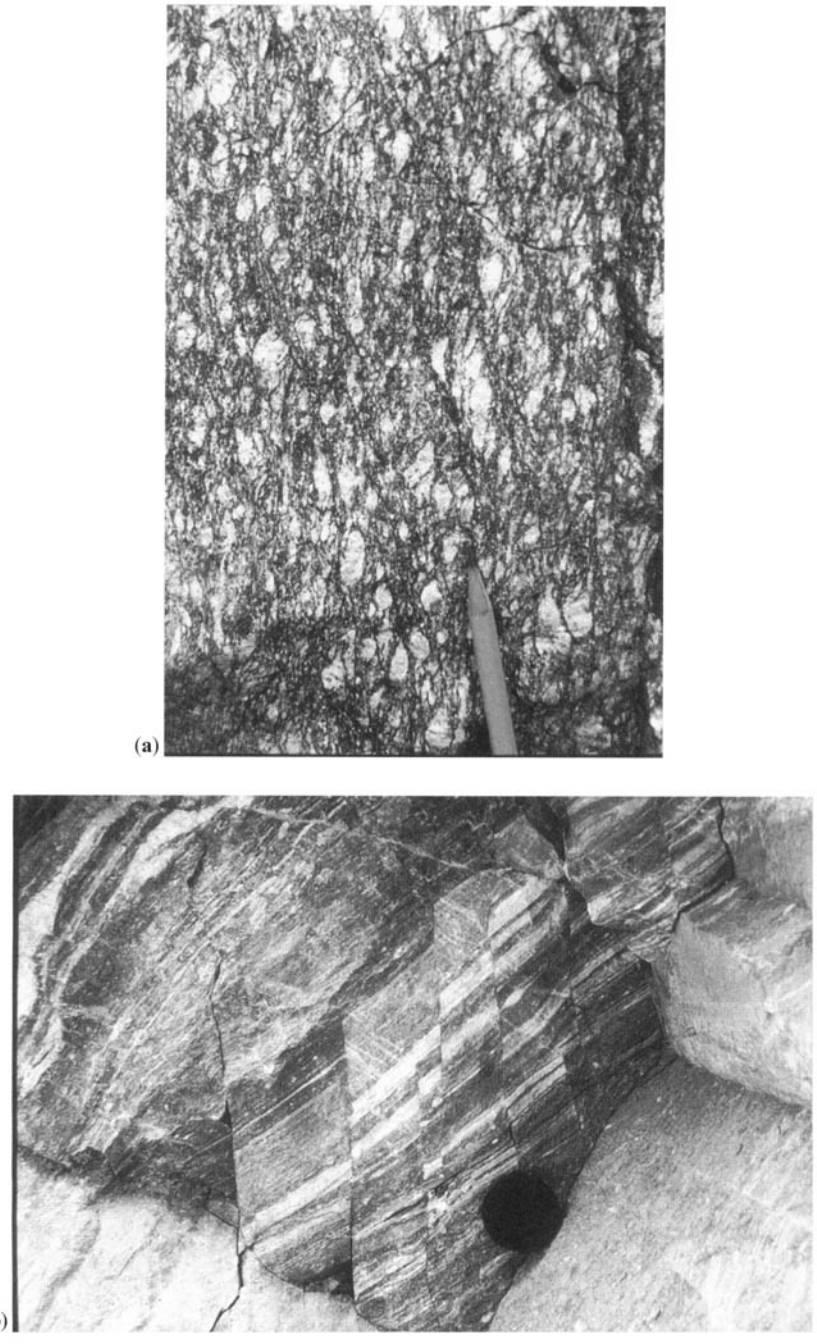

Fig. 4. Field photos from the Sassi section: (**a**) ductile, east-side-up C′ shear bands dip steeply down to the right (east); (**b**) brittle east-side-up microfaults dip steeply down to the right (east). Both views look northward.

sequences of the Swat region (Treloar *et al.* 1989*b*; DiPietro 1991; DiPietro & Lawrence 1991) and the Upper Kaghan Valley (Chaudhry & Ghazanfar 1990) and have been interpreted (Butler & Prior 1988*a*, *b*; Butler *et al.* 1989; Treloar *et al.* 1991) as cover to the Indian plate gneisses. They include qtz–pl–or–ky–grt–bt–ms–cal–rt-bearing calc-pelites, interlayered with amphibolites and marbles. They are separated from volcanic rocks of the island arc by the MMT, locally steeply dipping due to rotation on the LSZ footwall (Butler *et al.* 1989; Treloar *et al.* 1991).

Geochronology of the western margin of the syntaxis

In this section data are summarized in order to synthesize the evolution of the fault zone developed along the western margin of the syntaxis, and to comment on its role in the evolution and uplift of the Nanga Parbat syntaxis.

The Kohistan arc. Hornblende, muscovite and biotite Ar–Ar and K–Ar data and zircon and apatite fission track data from eastern Kohistan within 10 km of the western margin of the syntaxis, have been published by Zeitler (1985), Coward *et al.* (1986), Treloar *et al.* (1989*b*), Zeitler *et al.* (1989) and George *et al.* (1993). The data show cooling through the hornblende blocking temperature at *c.* 34 ± 4 Ma, the muscovite and biotite blocking temperatures at *c.* 19 ± 2 Ma, and the zircon and apatite annealing temperatures at *c.* 10.5 ± 1 and 4 ± 1 Ma respectively. Similarity between muscovite and biotite ages may be the result of excess Ar yielding unrealistically old biotite ages. These ages are younger than those obtained elsewhere in Kohistan and have been attributed (cf. Zeitler 1985; Treloar *et al.* 1989) to greater amounts of Neogene uplift near to the Nanga Parbat syntaxis, or to heating during emplacement of the Indus Confluence and Parri granitic sheets (Petterson & Windley 1985).

The Raikot cover metasediments. Hornblendes have been analysed from four amphibolites (DR84, DR85, DR86 and DR87), muscovites from three calc-pelites (PJT732, PJT737 and PJT741), and a biotite from PJT741. All the hornblende separates are affected by excess Ar with K–Ar ages of $> 155 \pm 6$ Ma. The youngest, sample DR87, has a $^{40}Ar/^{39}Ar$ plateau at 97 ± 4 Ma defined by 73.5% of the gas. For this sample, the intercept on an Ar correlation plot with a 40/36 ratio of 1175 indicates Ar mobility, and no significance is attached to this age. These data, as well as other K–Ar, Ar–Ar and fission-track data used in this study, can be obtained from the Society Library or the British Library Document Supply Centre, Boston Spa, Wetherby, West Yorkshire LS23 7BQ, UK as Supplementary Publication No. SUP 18141 (11 pages) or from the first author.

Muscovites from PJT737 have a broad U-shaped Ar–Ar spectrum in which 90% of the gas gives a plateau with an age of 15.00 ± 0.20 Ma (Fig. 5a). On a correlation plot, all steps plot on a regression line which passes through air ($^{40}Ar/^{36}Ar = 295$), with an intercept age of 14.2 ± 1.2 Ma (Fig. 5b). This age is similar to muscovite K–Ar ages from samples PJT732 and PJT737 (available as a Supplementary Publication, see above). Biotites from the same samples contain large amounts of excess radiogenic argon. A. G. Whittington (pers. comm.) report Ar laser ages of 12.7 and 11.9 Ma for fine-grained muscovites in mylonites from the Raikot section that might date movement on the LSZ.

Rb–Sr analyses of plagioclase, muscovite and biotite from sample PJT741 yield ages of 20.3 ± 3.0 Ma for muscovite and 9.6 ± 1.0 Ma for biotite. An Rb–Sr age of 8.2 ± 1.0 Ma for biotite is derived from sample DR87 by analysis of hornblende and biotite (Rb–Sr data are available as a Supplementary Publication, see above).

The Sassi section. At Sassi, arc rocks are separated from Indian plate gneisses by a metasedimentary sequence similar to that at Raikot. Biotites from sample HS9 have a K–Ar age of 9.4 ± 0.4 Ma (available as a Supplementary Publication, see above). For biotites from a sheared biotite-amphibolite, Reddy *et al.* (1997) derived a laserprobe Ar–Ar age of *c.* 8 Ma. George & Bartlett (1996) document two sets of muscovite Rb–Sr ages for rocks within the shear zone. The older of these, at 17–21 Ma, they attribute to cooling through 500 °C; the younger, at 8–12 Ma, to resetting during shearing at temperatures below that of the muscovite closure temperature. Mylonites from the Sassi section are cut by a leucogranite sheet dated at 6.5 Ma (Kidd *et al.* 1998).

The Liachar section. Ductile shear fabrics within the LSZ are cut by bt–ms–tur-bearing leucogranite sheets. These show incipient ductile shearing and are interpreted as having been emplaced during shearing (Butler *et al.* 1989; Butler this volume). Muscovites, that occur in large isolated books, have been separated from three

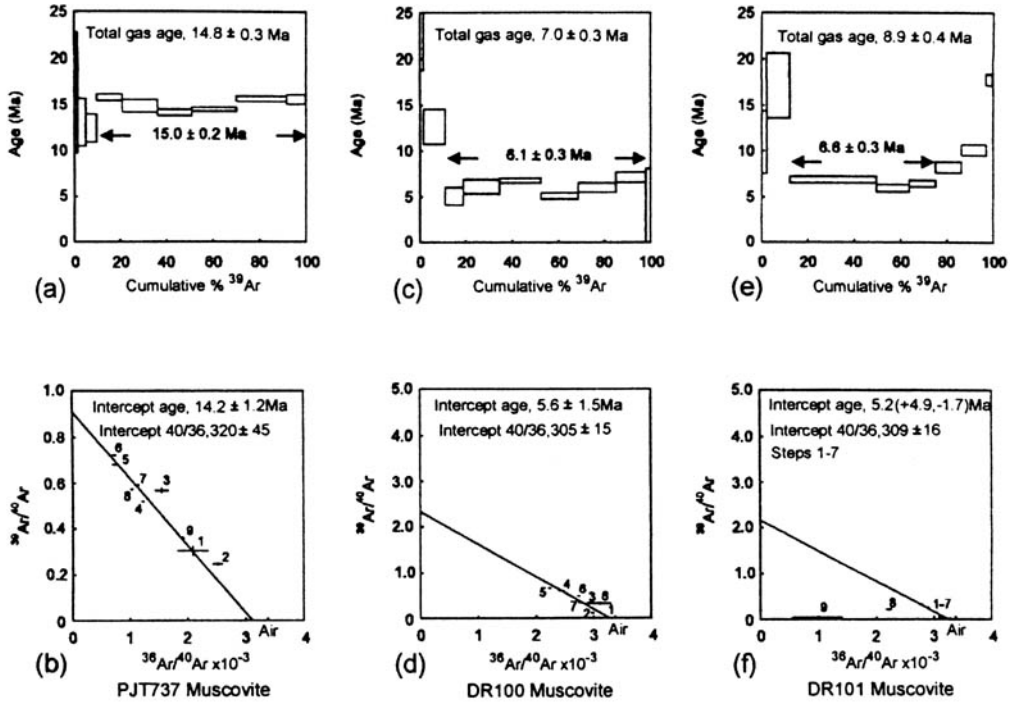

Fig. 5. Ar–Ar data from muscovites from the Raikot and Liachar Thrust sections. PJT737, muscovite: (**a**) age spectrum, (**b**) correlation plot; DR100 muscovite: (**c**) age spectrum, (**d**) correlation plot; DR101 muscovite: (**e**) age spectrum, (**f**) correlation plot. K–Ar and Ar–Ar analytical and isotopic data for these and other samples are listed in the Supplementary Publication (see p. 142).

pegmatitic leucogranite sheets that cross-cut the gneissic fabrics. K–Ar and Ar–Ar data are available as a Supplementary Publication, see p. 142. Muscovites from sample DR100 have a flat, saddle-shaped spectrum, with 87% of the gas defining an age of 6.1 ± 0.3 Ma (Fig. 5c). On a correlation plot, all steps fall on a regression line with an intercept near air on the $^{36}Ar/^{40}Ar$ axis, and an intercept age of 5.6 ± 1.5 Ma (Fig. 5d). Muscovites from sample DR101, have a U-shaped spectrum with a plateau, defined by 80% of the gas, at 6.6 ± 0.3 Ma (Fig. 5e). Steps 8 and 9 have very different Ca/K ratios from the other steps. On a correlation plot, steps 1 to 7 cluster closely around a regression line with an intercept near air on the $^{36}Ar/^{40}Ar$ axis and an intercept age of 5.2 +4.9/ − 1.7 Ma (Fig. 5f). The muscovite age from sample DR101 either dates emplacement of leucogranite sheets at *c.* 6 Ma into rocks undergoing shearing within the LSZ at *c.* 350 to 400 °C, or their subsequent cooling through that temperature.

Biotites from sample RC2, a biotite gneiss, have a spectrum with an irregular plateau defined by 95% of the gas and an integrated age of 2.6 ± 0.3 Ma (available as a Supplementary Publication, see p. 142). On a correlation plot, the sample has a poorly defined regression line passing through air on the $^{36}Ar/^{40}Ar$ axis, albeit with large errors. Given the irregular plateau, the poorly defined regression line and the excess Ar problems affecting biotites to be discussed below, this age has to be disregarded. A. G. Whittington (pers. comm.) report a muscovite age of 3.1 Ma and a biotite age of 1.5 Ma, and George & Bartlett (1996) an Rb–Sr muscovite age of 3.5 ± 0.1 Ma from the Liachar area.

Data from the Liachar section should be interpreted with caution. Cliff *et al.* (1991) described a sample from here in which muscovite yielded a U-shaped spectrum with a minimum at *c.* 2.3 Ma defined by 47.5% of the gas, but with a correlation plot on which data points are scattered indicating complete Ar disequilibrium. This sample also showed resetting of isotope systematics in the Rb–Sr, U–Pb and Nd–Sm systems. If the isotope systematics in some samples have been completely reset by fluid mobility, there must remain some doubt about the interpretation of data derived from other samples, even if calculated regression lines on correlation plots pass through atmospheric argon.

The Tato Road section. The LSZ is the structurally lowest of the two major NW-vergent shear zones that outcrop at the south end of the Raikot–Sassi Fault Zone. Its hanging wall fabrics pass upward into those of the structurally higher TSZ, on the hanging wall of which outcrop the Fairy Meadow migmatites (Zeitler *et al.* 1993). Lineations and shear criteria have a consistent top-to-NW thrust sense. Cooling ages from the TSZ hanging wall (Winslow *et al.* 1996) suggest cooling through the amphibole closure temperature significantly later than the footwall, implying displacement at <3 Ma. For this study, micas were separated from biotite gneisses and biotite-rich enclaves from the lower part of the TSZ. K–Ar and Ar–Ar data for these are available as a Supplementary Publication, see p. 142. Biotite K–Ar ages are from 1.8–4.8 Ma. Two muscovite K–Ar ages are at 1.8 and 3.1 Ma.

Muscovites from PJT748 have a spectrum with a plateau defined by 91% of the gas at 0.8 ± 0.1 Ma (Fig. 6a). On a correlation plot, a regression line passes through air on the $^{36}Ar/^{40}Ar$ axis with an intercept age of 0.7 ± 0.15 Ma (Fig. 6b). Step 8, the highest temperature step, falls off the regression line. The gas released for this step has a higher Ca/K ratio than that for the other steps. Muscovites from DR93 have a saddle-shaped spectrum containing a plateau with 64% of the gas with an age of 1.40 ± 0.20 Ma (Fig. 6c). On a correlation plot, all steps except the highest temperature one, which has a significantly different Ca/K ratio from the rest, fall on a regression line with an intercept age of 1.3 ± 0.3 Ma (Fig. 6d).

Biotites from DR97 have a plateau defined by 100% of the gas at 2.4 ± 0.3 Ma (Fig. 6e). On a correlation plot, all steps fall on a regression line that passes through air on the $^{36}Ar/^{40}Ar$ axis (Fig. 6f). Biotites from DR89 have an irregular plateau defined by 89% of the gas at 1.5 ± 0.3 Ma (Fig. 6g). Step 4, with a lower age than the others, is interpreted as an experimental artefact. Steps 1 to 6, point 7 having a high Ca/K ratio, fall on a straight line on a correlation plot with an intercept near air on the $^{36}Ar/^{40}Ar$ axis and an age of 1.3 ± 1.3 Ma (Fig. 6h). Biotites from Rex1 have a U-shaped spectrum, although with a plateau defined by 93% of the gas at 2.1 ± 0.1 Ma (Fig. 6i). On a correlation plot, all steps except step 6 fall on a regression line with an intercept near air on the $^{36}Ar/^{40}Ar$ axis (Fig. 6j). Step 6 has a similar Ca/K ratio to the other steps, indicating that this sample has been affected by excess Ar.

Hornblendes from sample DR95 have a U-shaped Ar–Ar spectrum with a minimum at about 18.2 ± 1.2 Ma (Fig. 6k) defined by the two youngest steps which contain 47% of the gas. This is a maximum age for this sample. The correlation plot shows a straight line on which all points fall with an intercept age of 18 ± 2.5 Ma, although the intercept on the $^{36}Ar/^{40}Ar$ axis at 416 ± 25 indicates the presence of excess radiogenic argon (Fig. 6l).

Although biotite K–Ar and Ar–Ar ages from the TSZ are similar to each other, muscovite Ar–Ar ages are younger than their K–Ar equivalents (available as a Supplementary Publication, see p. 142). On correlation plots regression lines for both muscovites and biotites pass through atmosphere on the $^{36}Ar/^{40}Ar$ axis. However, as muscovite ages are younger than biotite ages, we view the latter, at least, as unreliable. A number of thin biotite mats, <0.5 cm thick, contained within the shear zone probably reflect passage of hydrothermal fluids through it during shearing, and it is this fluid which may be the source of the excess Ar within the biotite crystals. Within the Raikot–Sassi Fault Zone, George *et al.* (1993) described element mobility and isotope resetting, which they attributed to fluid movement through the shear zone. The muscovite ages suggest shearing along the TSZ at *c.* 2.0 Ma.

Summary

Data from the western margin of the syntaxis are interpreted as follows. Indian plate Permo-Triassic cover sediments, located on the west side of the major shears that define the western margin of the syntaxis, cooled through *c.* 500 °C (the muscovite Rb–Sr age) at *c.* 20 Ma; through *c.* 400 °C (the muscovite Ar–Ar age) at *c.* 14 ± 1 Ma, and through *c.* 300 °C (biotite Rb–Sr and Ar–Ar ages) at 8–10 Ma. These ages are younger than those for the Kohistan arc and older than those from internal parts of the syntaxis. The older ages are dominantly a function of uplift-related exhumation, probably during a crustal-scale folding event that defined early stages of syntaxis growth. The *c.* 8 Ma biotite ages from Sassi, including those of Reddy *et al.* (1997), date east-side-up shearing that was accompanied by resetting of Sr isotopes in the shear zone (George & Bartlett 1996). NW-verging shear zones developed within Indian plate basement rocks, active at a later stage than this, accommodated significant uplift for rocks on their hanging wall. The LSZ was probably active in the ductile region at *c.* 6 Ma and the TSZ at *c.* 2 Ma, an age consistent with data in Winslow *et al.* (1996).

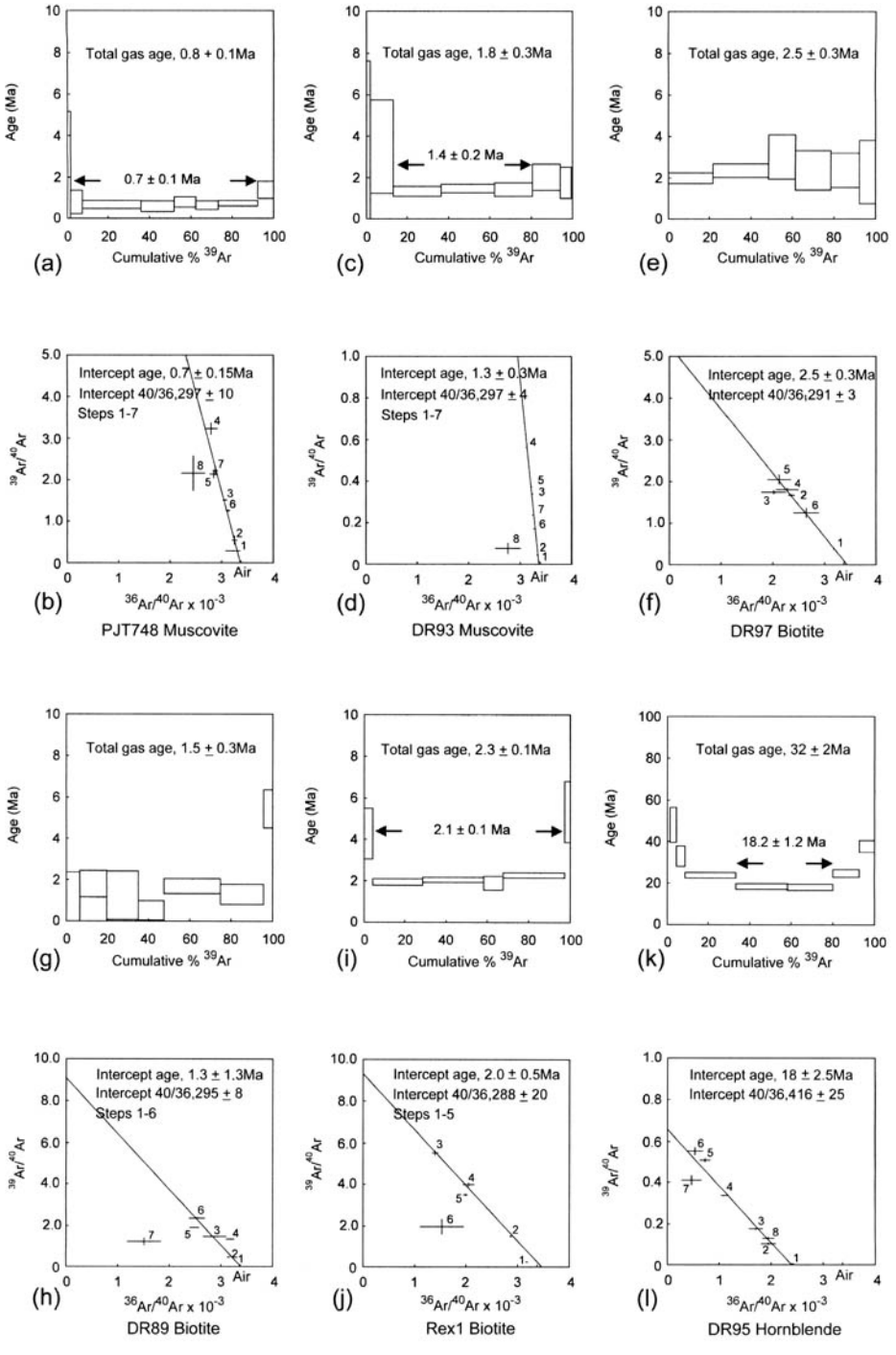

Fig. 6. Ar–Ar data from mica and amphibole separates from the Tato Road section. PJT748, muscovite: (**a**) age spectrum, (**b**) correlation plot; DR93 muscovite: (**c**) age spectrum, (**d**) correlation plot; DR97 biotite: (**e**) age spectrum, (**f**) correlation plot; DR89 biotite: (**g**) age spectrum, (**h**) correlation plot; Rex1 biotite: (**i**) age spectrum, (**j**) correlation plot; DR95 hornblende: (**k**) age spectrum, (**l**) correlation plot. K–Ar and Ar–Ar analytical and isotopic data for these and other samples are listed in the Supplementary Publication (see p. 142).

The Indus valley section

The Indus River flows west across the Nanga Parbat syntaxis (Fig. 2). Along the line of section planar fabrics describe an antiformal shape, although divided into two smaller S-plunging antiforms (Coward 1986; Madin *et al.* 1989; Treloar *et al.* 1991) flanked to the west by the Raikot–Sassi Fault Zone. On the basis of a preliminary geochronological dataset, Treloar *et al.* (1991) suggested that, of the two antiforms, the more easterly formed first. K–Ar, Ar–Ar and fission track data from this section have been published by Zeitler (1985), Zeitler *et al.* (1989), Treloar *et al.* (1991) and George *et al.* (1993). Smith *et al.* (1992) and Zeitler *et al.* (1993) have published U–Pb zircon and monazite data. Here these data are amplified by presenting new hornblende, muscovite and biotite Ar–Ar and K–Ar data and zircon and apatite fission track data. Sample locations and summary data are shown in Fig. 7. New analytical data and derived ages are presented in Figs 8 and 9 and, together with those published by other workers, summarized in Table 1 and Fig. 10.

The analytical strategy was to analyse a range of samples for K–Ar dating and from these to select samples for irradiation and further Ar–Ar analysis. The rationale for this was: K–Ar analysis is cheap and fast and a comprehensive dataset can be rapidly obtained; K–Ar analysis enables the ready identification of samples affected by excess Ar which are not worth analysing further; and, in an area in which excess Ar is a problem, trends shown by the K–Ar data can be validated by the less numerous Ar–Ar data. Some of the Ar–Ar data are from samples for which only K–Ar data were then available (Treloar *et al.* 1991).

Three samples are from arc rocks to the east of the syntaxis. Hornblendes from a biotite–hornblende pegmatite (sample 121, located *c.* 5 km to the east of Fig. 7) show a plateau defined by 95% of the gas (Fig. 8a). The plateau age of 27.6 ± 0.6 Ma, is consistent with an intercept age on a correlation plot of

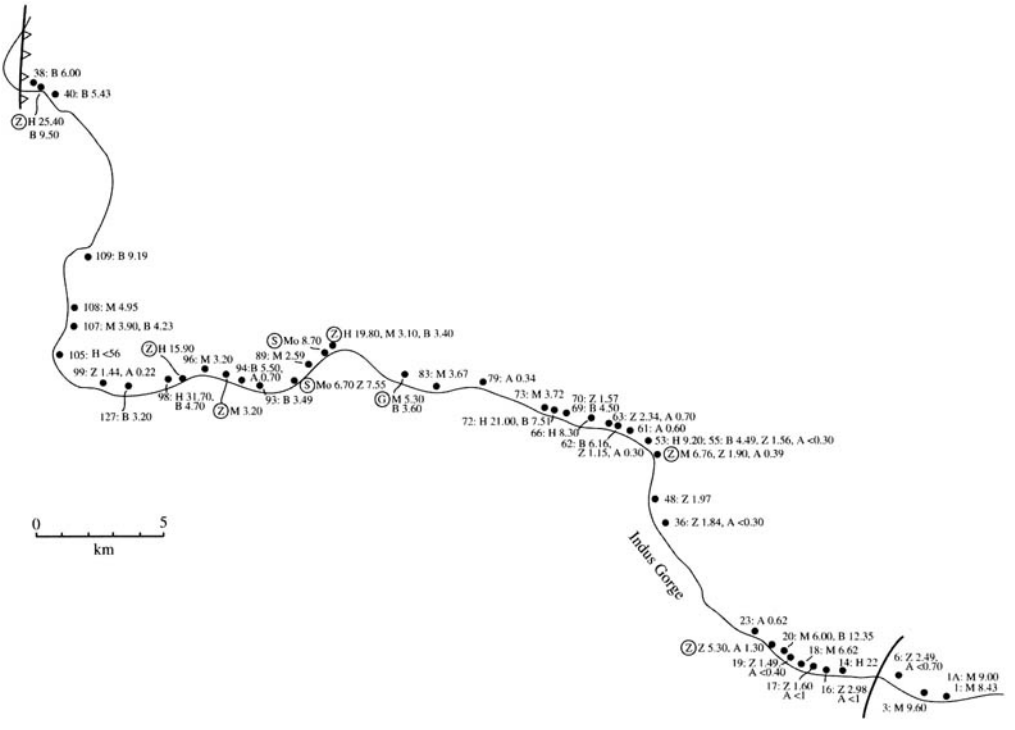

Fig. 7. Map of the Indus Gorge section across the syntaxis showing location of the analysed samples, together with their derived ages. The data include those presented elsewhere. A, apatite; Z, zircon; B, biotite; M, muscovite; H, hornblende. Encircled letters indicate data from: Z, Zeitler (1985) and Zeitler *et al.* (1989, 1993); G, George *et al.* (1995); S, Smith *et al.* (1992). Raw analytical data and Ar–Ar age spectra and correlation plots for biotites from the Indus Gorge section are available as a Supplementary Publication (see p. 142).

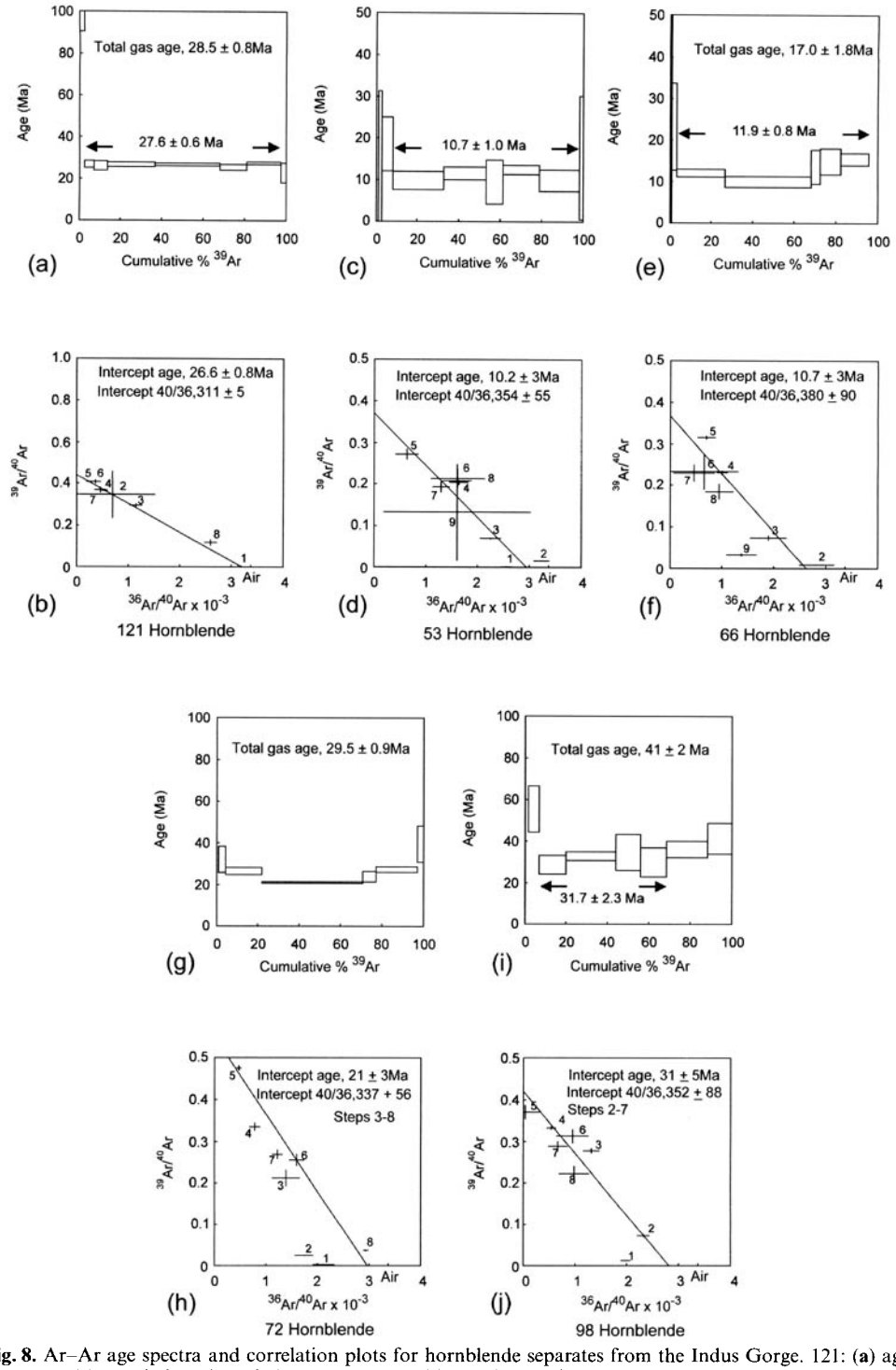

Fig. 8. Ar–Ar age spectra and correlation plots for hornblende separates from the Indus Gorge. 121: (**a**) age spectrum, (**b**) correlation plot; 53: (**c**) age spectrum, (**d**) correlation plot; 66: (**e**) age spectrum, (**f**) correlation plot; 72: (**g**) age spectrum, (**h**) correlation plot; 98: (**i**) age spectrum, (**j**) correlation plot. K–Ar and Ar–Ar analytical and isotopic data for these and other samples are listed in the Supplementary Publication (see p. 142).

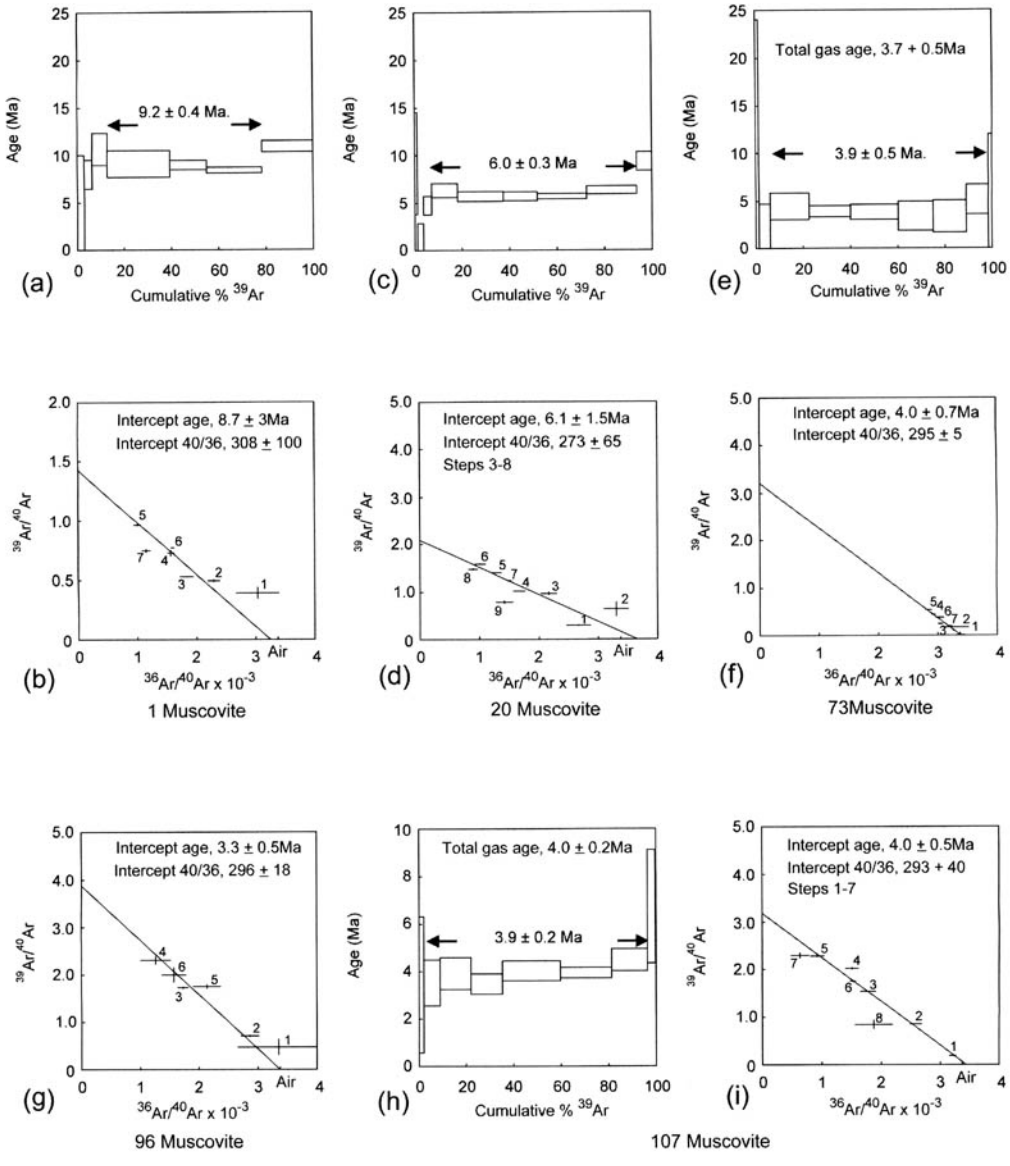

Fig. 9. Ar–Ar age spectra and correlation plots for muscovite separates from the Indus Gorge. 1: (**a**) age spectrum, (**b**) correlation plot; 20: (**c**) age spectrum, (**d**) correlation plot; 73: (**e**) age spectrum, (**f**) correlation plot; 96: (**g**) correlation plot; 107: (**h**) age spectrum, (**i**) correlation plot. K–Ar and Ar–Ar analytical and isotopic data for these and other samples are listed in the Supplementary Publication (see p. 142).

26.6 ± 0.8 Ma in which all steps plot close to a regression line intersects the $^{36}Ar/^{40}Ar$ axis close to air (Fig. 8b). Muscovite flakes from a pegmatite in the arc (sample 1) have a plateau at 9.20 ± 0.4 Ma defined by 86% of the gas (Fig. 9a). On a correlation plot a regression line intersects the $^{36}Ar/^{40}Ar$ axis close to air (Fig. 9b). Biotite from another nearby pegmatite (sample 3) has an irregular plateau defined by 94% of the gas, yielding an age of *c.* 13.2 ± 0.4 Ma. On a correlation plot, all points except 5 and 8, which have high Ca/K ratios, fall on a regression line that passes through air on the $^{36}Ar/^{40}Ar$ axis with a similar age. Older than muscovites from adjacent samples, the irregular nature of the steps defining the plateau imply this age to be an artefact of excess argon.

Table 1. *Summary table showing all the available age data from the Indus valley section across the syntaxis from this and earlier studies*

Sample	Hbl	Ms	Bt	Zn	Ap
120	27 ± 1				
121	**26.60 ± 0.60**		15.2 ± 0.6		
122				4.87 ± 0.43	2.08 ± 0.28
123		10.40 ± 0.4	9.95 ± 0.4		
1		**9.20 ± 0.40**			
1A		**9.00 ± 0.4**			
3			**13.20 ± 0.46**		
3A		9.60			
6				2.49 ± 0.41	< 0.4
14	**22 ± 10**				
16				2.98 ± 0.27	< 1
17				1.60 ± 0.26	< 1
18A		6.62 ± 0.27			
19				1.49 ± 0.17	< 0.4
20		**6.00 ± 0.30**	**12.33 ± 0.60**		
23					0.68 ± 0.2
811-1 (Zeitler 1985)				5.30	1.30
36				1.84 ± 0.18	< 0.3
48				1.97 ± 0.18	
NPG (Zeitler 1985)		6.76		1.90	0.39
53	**10.7 ± 1.0**				
55			4.49	1.56 ± 0.19	< 0.3
61					0.6 ± 0.23
62			6.16	1.15 ± 0.16	0.3 ± 0.08
63				2.34 ± 0.3	0.7 ± 0.1
66	**11.9 ± 0.8**				
69			4.45 ± 0.31		
70				1.57 ± 0.16	
72	**21.06 ± 0.39**		***7.51 ± 0.2***		
73		**3.90 ± 0.5**			
79					0.34 ± 0.09
83		3.67 ± 0.15			
S92		**5.3**	**3.6**		(George *et al.* 1995)
83-56	**19.8**				(Zeitler *et al.* 1989)
83-84		**3.1**	**3.4**		(Zeitler *et al.* 1989)
PK20	Monazite	9.8			(Smith *et al.* 1992)
89		2.59 ± 0.10	3.90 ± 0.16		
PK19	Monazite	8.7			(Smith *et al.* 1992)
	Zircon rim	> 5.5			(Zeitler *et al.* 1993)
93			3.49		
83-85		**3.2**	3.50 ± 0.10		(Zeitler *et al.* 1989)
94			***5.55 ± 0.5***		0.27 ± 0.07
96		**3.20 ± 0.30**	3.33 ± 0.14		
83-69	**15.9**				(Zeitler *et al.* 1989)
83-86			3.27 ± 0.09		(Zeitler *et al.* 1989)
98	**31.7 ± 2.3**		**4.70 ± 0.70**		
99				1.44 ± 0.14	0.22 ± 0.06
127			3.20 ± 0.13		
?				1.70	(Zeitler 1985)
105	< 56				
83-97			4.69 ± 0.09		(Zeitler *et al.* 1989)
107		**3.9 ± 0.2**	4.23 ± 0.17		
108		4.95			
109			9.19 ± 0.37		
40			5.43		
83-71	25.4		9.5		(Zeitler *et al.* 1989)
38			6.00		
HS9			9.4 ± 0.4		
?				2.0	(Zeitler 1985)

The data are ordered from east (top of table) to west (base of table) and include data presented here (Figs 8 and 9), as well as from the Supplementary Publication (see p. 142) and Zeitler (1985), Zeitler *et al.* (1989, 1993), Smith *et al.* (1992) and George *et al.* (1995). Monazite and zircon growth ages are given in the column headed 'Hbl'.

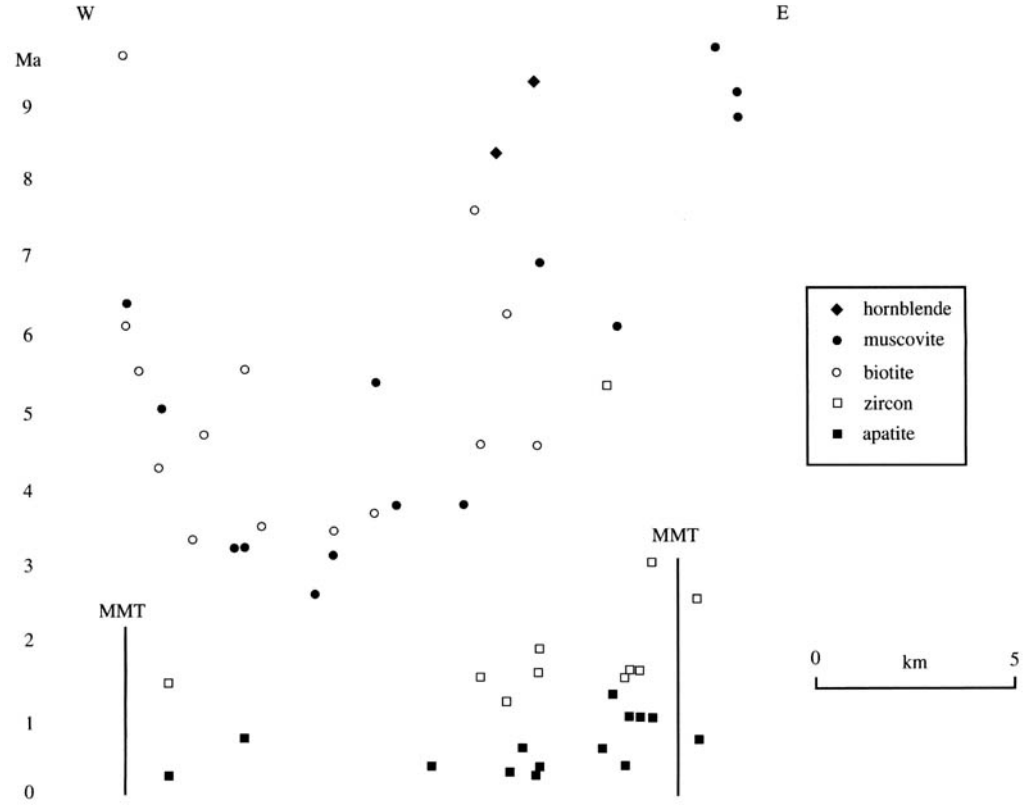

Fig. 10. Distance v. age plot of data from the Indus valley section.

Sample 20 (a two-mica pegmatite) yields both muscovite and biotite ages. The biotite K–Ar age is older than that of the muscovite. For the muscovite, 86% of the gas defines a plateau age at 6.0 ± 0.3 Ma (Fig. 9b) identical to an intercept age, defined on a correlation plot by a regression line that passes near to air on the $^{36}Ar/^{40}Ar$ axis (Fig. 9d). By contrast, the biotite has an irregular spectrum, although on a correlation plot a well-defined regression line intersects the $^{36}Ar/^{40}Ar$ axis with a 40/36 ratio less than air and an apparent age of 12.4 ± 0.6 Ma (K–Ar and Ar–Ar data are available as a Supplementary Publication, see p. 142). This latter age is clearly erroneous, being constrained by a poor spectrum and an age older than that of the accompanying muscovite, and is disregarded.

Hornblendes from Indian plate amphibolites (samples 53 and 66) provide young cooling ages. Both are affected by excess Ar, each with a regression line on the correlation plot intersecting the $^{36}Ar/^{40}Ar$ axis with a 40/36 ratio greater than air. Sample 53 has a slightly saddle-shaped spectrum with >95% of the gas defining an age of 10.7 ± 1.0 Ma (Fig. 8c). A poorly defined regression line has an intercept age of 10.2 ± 3.0 Ma (Fig. 8d). Sample 66 has a broad U-shaped spectrum with a plateau at 11.9 ± 0.8 Ma defined by >90% of the gas (Fig. 8e). On a correlation plot a regression line has an intercept age of 10.7 ± 3 Ma (Fig. 8g). If point 9, which has a high Ca/K ratio, is omitted from the correlation plot, the corrected line intersects the $^{36}Ar/^{40}Ar$ axis closer to air with an intercept age of 8.3 ± 2 Ma. The plateau ages for both samples are likely to be minimum ages and are consistent with cooling through 500 °C near to 10 Ma, although the presence of excess argon allows no firmer interpretation.

Two other hornblendes yield Mio-Oligocene cooling ages. Hornblende from sample 72 has a shallow U-shaped Ar spectrum with a minimum of 21 Ma defined by a plateau with 49% of the gas (Fig. 8g). On a correlation plot, utilizing all points except 1 and 2, which show clear signs of excess Ar, a regression line has an intersect on the $^{36}Ar/^{40}Ar$ axis slightly greater than air and an intercept age of 21.0 ± 3.0 Ma (Fig. 8h). Hornblende from sample 98 has a broad U-shaped

spectrum with a plateau defined by 61% of the gas at 31.7 ± 2.3 Ma (Fig. 8i). On a correlation plot, all points except 1 and 8, which have high Ca/K ratios, define a regression line which intersects the $^{36}Ar/^{40}Ar$ axis close to air with an age of 31 ± 5 Ma (Fig. 8j).

Biotites from samples 72 (garnet amphibolite), 94 (migmatitic biotite gneiss) and 98 (amphibolite) and muscovites from samples 73 (muscovite pegmatite), 96 (two mica pegmatite) and 107 (mica schist) are from the western part of the syntaxis. All have plateaux defined by >90% of the gas (Fig. 9e, h). For each sample, all points on a correlation plot fall close to a regression line that intersects the $^{36}Ar/^{40}Ar$ axis near air with an intercept age close to that of the plateau age (Fig. 9f, g, i). The muscovite ages are younger than the biotite ages. The latter are interpreted as being too old due to the effect of excess argon, even though this is not apparent from the correlation plots.

Zircon and apatite fission track data collected from the Indus River traverse are presented in Table 7. Although zircon crystals yield many spontaneous tracks, the extreme youth of cooling through the apatite annealing temperature means that only those apatites with a high radiogenic production of fission tracks yielded useful age determinations. The paucity of spontaneous tracks in the apatites meant that confined tracks were neither observed nor measured.

The Astor valley section

The Astor River section is dominated by N- to NE-striking fabrics with steep to moderate westerly dips. Fold axes and mineral stretching lineations plunge consistently towards the N or NNW at shallow to moderate angles (Butler *et al.* this volume), in contrast to the Indus Gorge where the dominant plunge direction is southward (Treloar *et al.* 1991). Along the length of the section, an antiforming direction, derived from facing directions on small-scale folds, is consistently towards the west with no evidence for antiformal folds as in the Indus Gorge (Butler *et al.* this volume). From this it is clear that the apparent symmetry seen in the major structures within the Indus Gorge is not replicated along the length of the syntaxis, and that the plunge directions of the major folds are not constant along the length of the syntaxis.

Geochronology

A limited number of geochronological data are already available from the Astor River section (Zeitler 1985; Smith *et al.* 1993; George & Bartlett 1996; Winslow *et al.* 1996). Here, new K–Ar and Ar–Ar ages from muscovites and biotites, Ar–Ar ages from hornblendes, and fission track ages from zircons and apatites are presented. The analytical strategy was as outlined above. Sample locations and summary data are shown in Fig. 11. New analytical data and derived ages are presented in Figs 12 and 13 and, together with those published by other workers, summarized in Table 2 and Fig. 14.

Sample 205 is an amphibolite collected <1 km east of the steeply dipping MMT. As the MMT is not transposed here to the same extent as it is on the western margin, this sample should show similar ages to those from Indian plate rocks within the syntaxis. A hornblende K–Ar age is 27 ± 1 Ma. Ar–Ar data yield a broadly U-shaped spectrum with a minimum, defined by 54% of the gas, at 30.1 Ma (Fig. 12a). The correlation plot yields an intercept on the $^{36}Ar/^{40}Ar$ axis close to air with an age of 29 ± 2 Ma (Fig. 12b).

Two micas were analysed from sample 207, an Indian plate paragneiss close to the MMT. On Ar–Ar plots (Fig. 13a, b) both have a plateau defined by most of the gas (97% for muscovite and 93% for biotite), and correlation plots on which all points fall on a regression line passing through air on the $^{36}Ar/^{40}Ar$ axis and an intercept age identical to that of the plateau age (muscovite 8.70 ± 0.10 Ma; biotite 7.70 ± 0.10 Ma). The similarity between K–Ar and Ar–Ar ages, as well as muscovite ages being older than biotite ages, suggest these ages to be reliable.

Hornblendes were analysed from four Indian plate samples along the Astor River section. Hornblende from sample 210 has a broad, shallow U-shaped spectrum in which 92% of the gas defines an age of 28.0 ± 0.7 Ma (Fig. 12c). Steps 3 to 7 define a regression line on a correlation plot with a near air intercept and an age of 27.2 ± 0.7 Ma (Fig. 12d). Hornblende from sample 213 has an Ar–Ar spectrum at 22.0 ± 6 Ma defined by a plateau, including 99% of the gas (Fig. 12e). For this sample a correlation plot yields a regression line which intersects the $^{36}Ar/^{40}Ar$ axis near to air (Fig. 12f) with an intercept age of 21.5 ± 1.4 Ma. The other two samples (220, Fig. 12g, h; 234, Fig. 12i, j) have been affected by excess argon. Given the amount of gas (71%) that defines the plateau for the latter, it is unlikely that its true age is much younger than 22 Ma.

Muscovites from sample 260 have a saddle-shaped spectrum with 70% of the gas defining a plateau with an age of 7.8 ± 0.1 Ma (Fig. 13c). On a correlation plot all points fall on a regression line which passes through air on the

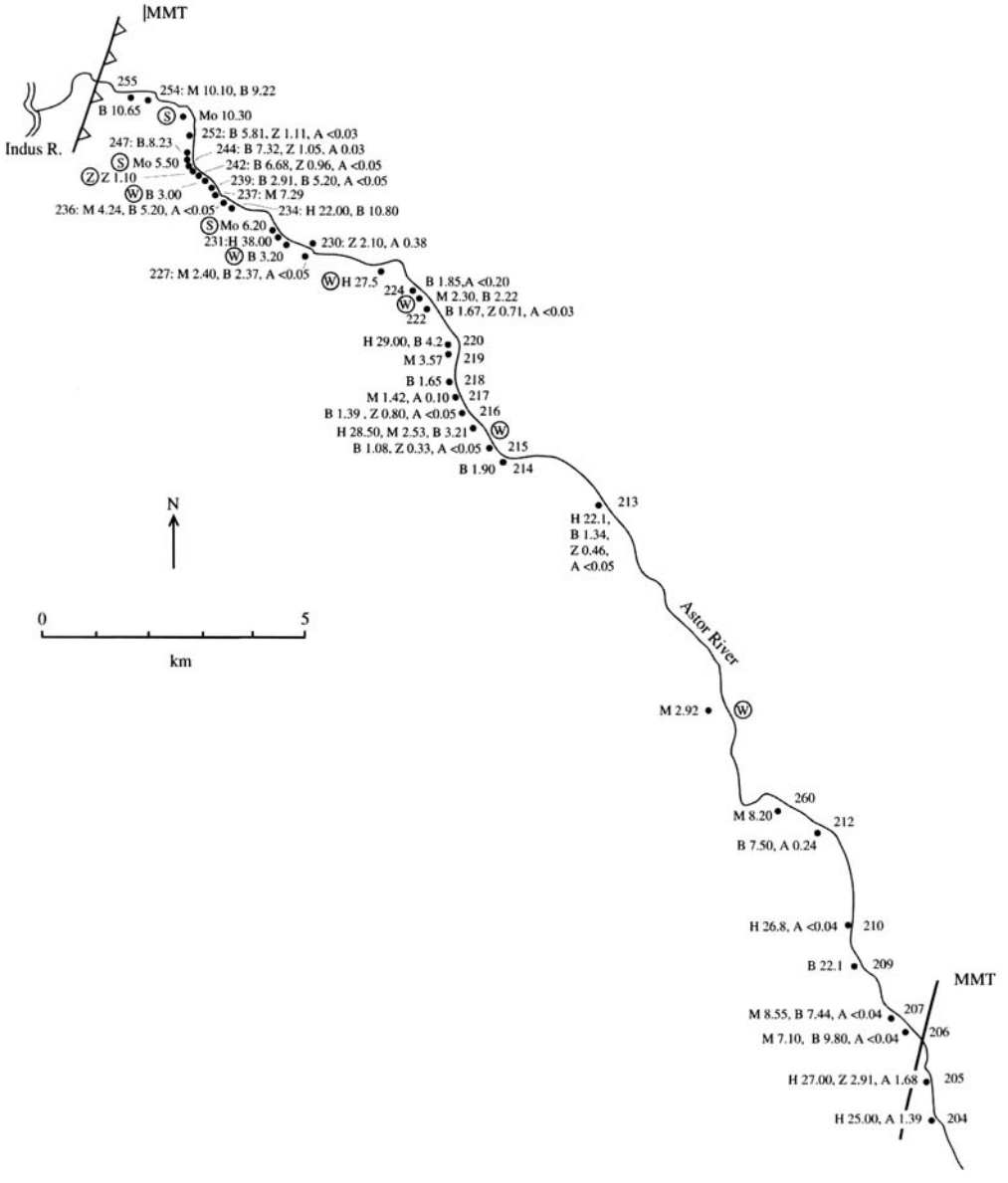

Fig. 11. Map of the Astor valley section across the syntaxis showing location of the analysed samples, together with their derived ages. The data include those presented elsewhere. Symbols as in Fig. 7, with the addition of encircled letter W indicating data from Winslow *et al.* (1996). Raw analytical data and Ar–Ar age spectra and correlation plots for biotites from the Astor Valley section are available as a Supplementary Publication (see p. 142).

$^{36}Ar/^{40}Ar$ axis with an age of 7.8 ± 0.1 Ma (Fig. 13d). In contrast, biotite has a broad U-shaped spectrum with a minimum at about 25 Ma indicative of excess argon. Muscovite from sample 236 has an Ar–Ar age of 4.3 ± 0.10 Ma defined by a plateau with 98% of the gas (Fig. 13e). On a correlation plot, a regression line, utilizing steps 1 to 7, passes near air on the $^{36}Ar/^{40}Ar$ axis, defining an age of 4.2 ± 0.3 Ma (Fig. 13f). Point 8, which falls off this line, is characterized by a high Ca/K ratio.

Biotites have been analysed from samples 213, 216, 222, 232, 236 and 255. All samples have regression lines on correlation plots defined by all points, which pass through air on the $^{36}Ar/^{40}Ar$ axis with intercept ages within error of the

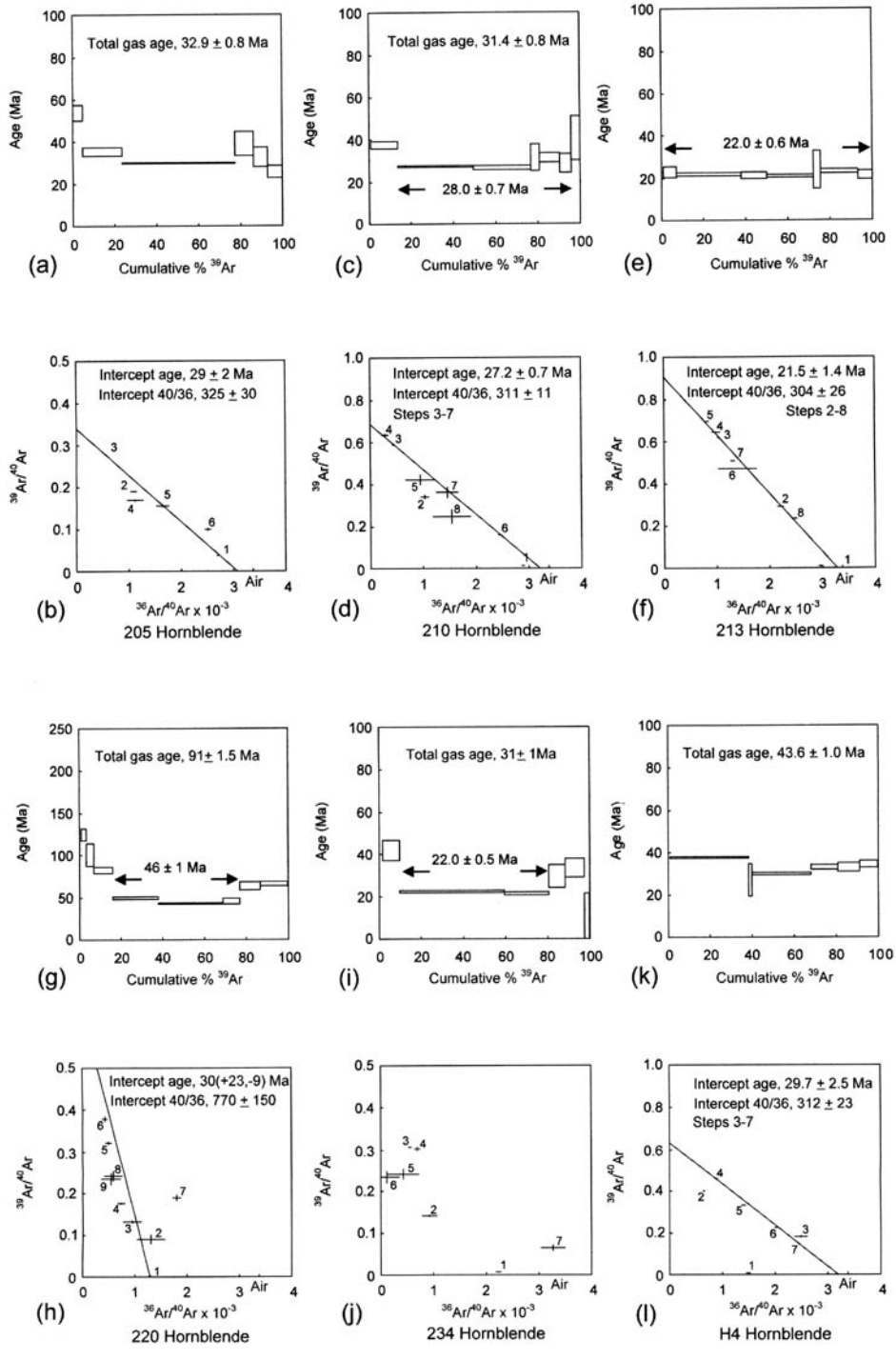

Fig. 12. Ar–Ar age spectra and correlation plots for hornblende separates from the Astor valley and Mazemo Pass. 205: (**a**) age spectrum, (**b**) correlation plot; 210: (**c**) age spectrum, (**d**) correlation plot; 213: (**e**) age spectrum, (**f**) correlation plot; 220: (**g**) age spectrum, (**h**) correlation plot; 234: (**i**) age spectrum, (**j**) correlation plot; H4: (**k**) age spectrum, (**l**) correlation plot. K–Ar and Ar–Ar analytical and isotopic data for these and other samples are listed in the Supplementary Publication (see p. 142).

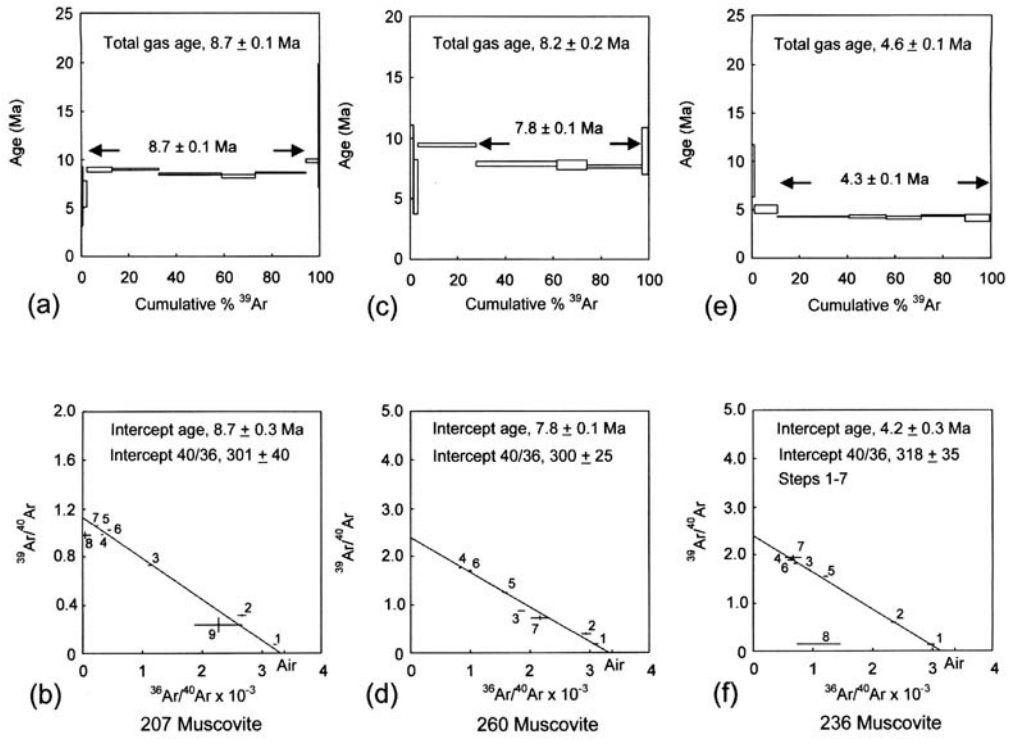

Fig. 13. Ar–Ar age spectra and correlation plots for muscovite separates from the Astor valley. 207: (**a**) age spectrum, (**b**) correlation plot; 260: (**c**) age spectrum, (**d**) correlation plot; 236: (**e**) age spectrum, (**f**) correlation plot. K–Ar and Ar–Ar analytical and isotopic data for these and other samples are listed in the Supplementary Publication (see p. 142).

plateau ages. Other than sample 213, which has a broad, if erratic plateau defined by 79% of the gas, all the plateaux are defined by >90% of the gas. Biotite from sample 236 has a plateau age of 5.20 ± 0.2 Ma defined by 99% of the gas, which is older than the age from the muscovite from the same sample (Fig. 13e).

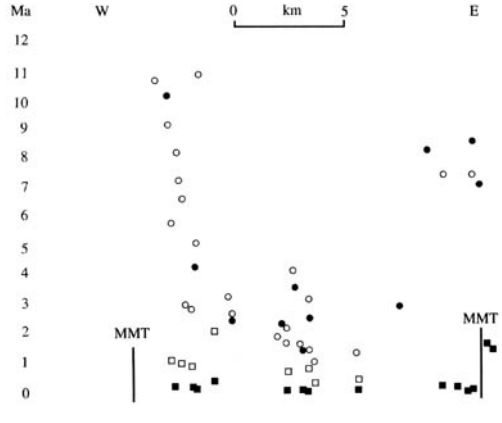

Fig. 14. Distance v. age plot of data from the Astor valley section.

Zircon and apatite fission track data from the Astor River traverse are available as a Supplementary Publication, see p. 142. As in the Indus section, zircon fission track ages are older on both margins of the syntaxis than within the core. Interpretation of the apatite data is hampered by their extreme youth, meaning that few samples yield well-defined ages. However, apatite ages from the eastern margin are older than those from within the core which are, within error, constant along the section length. Again, no confined tracks were found within the apatites.

Discussion

Many new K–Ar, Ar–Ar and fission track data are presented here from the Nanga Parbat syntaxis which significantly expand the existing geochronological database. One problem affecting the interpretation of these data is that many of the samples have been affected by excess argon. That isotopic resetting and mobility is a

Table 2. *Summary table showing all available age data from the Astor valley section across the syntaxis from this and earlier studies*

Sample	Hbl	Ms	Bt	Zn	Ap
204	25 ± 1				1.39 ± 0.26
205	**30.1 ± 0.3**			2.91 ± 0.16	1.68 ± 0.13
206		7.10 ± 0.55	*9.8 ± 0.80*		< 0.04
207		**8.70 ± 0.10**	**7.70 ± 0.10**		< 0.04
209			**22.0 ± 1.0**		
210	**28.0 ± 0.7**				< 0.04
212			**7.50 ± 0.20**		0.24 ± 0.09
260		**7.80 ± 0.10**	**29.3 ± 0.6**		
Pk/R-7–92		**2.92 ± 0.02**		Winslow *et al.* (1996)	
213	**22.0 ± 0.6**		**1.90 ± 0.30**	0.46 ± 0.09	< 0.05
214			1.90 ± 0.20		
215			1.08 ± 0.04	0.33 ± 0.04	< 0.05
Pk/A-11-94	**28.5 ± 0.03**	**2.58 + 0.01**	3.21	Winslow *et al.* (1996)	
216			**1.50 ± 0.10**	0.85 ± 0.13	< 0.05
217		1.42 ± 0.06			0.10 ± 0.06
218			1.65 ± 0.05		< 0.06
219		3.57 ± 0.29			
220	**46 ± 1**		4.52 ± 0.20		
222			**1.67 ± 0.07**	0.71 ± 0.10	< 0.03
Pk/A-8-94		**2.30 ± 0.01**	2.22	Winslow *et al.* (1996)	
224			1.85 ± 0.07		< 0.2
Pk/A-6-94	**27.5** (model age)			Winslow *et al.* (1996)	
227		2.40 ± 0.07	2.37 ± 0.07		< 0.05
228			1.64 ± 0.07		
230			2.10 ± 0.08		0.38 ± 0.07
?			**3.2**	Winslow *et al.* (1996)	
231	***38***				
PK7	6.20 (Monazite)			Smith *et al.* (1992)	
232			**3.00 ± 0.10**		
234	**22.0 ± 5**		*10.8 ± 0.4*		
236		**4.30 ± 0.10**	**5.20 ± 0.20**		< 0.05
237		7.29 ± 0.29			
239			2.91 ± 0.27		0.14 ± 0.04
?			**3.0**	Winslow *et al.* (1996)	
241			2.41 ± 0.18	0.96 ± 0.09	< 0.05
242			6.68 ± 0.27		
PK8	5.50 (Monazite)			Smith *et al.* (1992)	
	1.1 (Zircon rim)			Zeitler *et al.* (1993)	
244			7.32 ± 0.29	1.05 ± 0.09	0.03 ± 0.02
247			8.23 ± 0.33		< 0.02
248	**115**		**28.1 ± 0.6**		
250			5.81 + 0.17	1.11 ± 0.09	< 0.03
PK9	10.3 (Monazite)			Smith *et al.* (1992)	
252				1.70 ± 0.29	< 0.02
254		10.1 + 0.4	9.22 ± 0.37		< 0.03
255			**10.40 ± 0.20**		< 0.03

The data are ordered from east (top of table) to west (base of table) and include data presented here (Figs 12 and 13), as well as in the Supplementary Publication (see p. 142) and from Zeitler *et al.* (1993), Smith *et al.* (1992) and Winslow *et al.* (1996). Monazite and zircon growth ages are given in the column headed 'Hbl'.

problem within the syntaxis is well known (Cliff *et al.* 1991; George *et al.* 1993; George & Bartlett 1996). Smith *et al.* (1992) inferred the difference between their monazite ages of < 10 Ma and the older Ar–Ar hornblende ages, described by Zeitler *et al.* (1989) to be the result of excess Ar within the amphiboles. Numerous data collected for this study, not all of which are described here, show a scattering of points on Ar correlation plots, or have regression lines on such plots that do not pass through atmospheric argon. Biotite K–Ar and Ar–Ar ages are frequently older than muscovite ages from the same sample (i.e. 20, 89, 107, 206, 236, 260) or adjacent samples (i.e. 72

and 73; 94 and 96), indicating that excess argon has affected these samples even though the biotite Ar–Ar data yield good plateaux and regression lines which pass through atmospheric argon on correlation plots. Possible reasons for this were discussed earlier. In light of this, there must be a doubt about the accuracy of any biotite Ar–Ar age from within the syntaxis. Both muscovite and biotite Ar ages display reasonably smooth profiles on distance v. age plots (Figs 10 and 14), and this, together with the extreme youth of the measured biotite ages, suggests that excess Ar may have affected biotite closure ages by only a small amount. That many muscovite and hornblende separates yield regression lines on correlation plots that intersect the $^{36}Ar/^{40}Ar$ axis at, or near to, atmospheric argon suggests that Ar mobility was not pervasive and that Ar data can provide robust age constraints on the timing of metamorphism and cooling within the syntaxis.

The K–Ar, Ar–Ar and fission track data from the Indus and Astor valley sections demonstrate the following.

1. Within both the Indus and Astor sections, mica Ar–Ar and K–Ar ages get older from the core of the syntaxis outward towards its margins (Figs 10 and 14). Data from the Indus section confirm the interpretation of Treloar *et al.* (1991) that mica ages are younger within the western half of the section than the eastern half. Muscovite ages in the eastern part of the syntaxis are at 4–6 Ma. Those in the western half are at 3–4 Ma. By contrast, within the Astor valley section, both muscovite and biotite ages show an approximately symmetrical distribution of ages, getting older outward, consistent with data presented by Winslow *et al.* (1996, fig. 13).
2. In both sections, muscovite and biotite ages show a trend from younger to older approaching the western margin. Over a distance of *c.* 3 km, muscovite ages increase by *c.* 8 Ma in the Astor valley and *c.* 3 Ma in the Indus Gorge and biotite ages by *c.* 9 Ma in the Astor valley and *c.* 3 Ma in the Indus Gorge. Although the trends could reflect the effect of excess argon and isotope resetting, particularly in biotite, due to fluid movement within the marginal shear zones (cf. George *et al.* 1993; George & Bartlett 1996), they are probably the result of differential uplift and associated rapid cooling across this zone. Trends shown by the biotite ages parallel the more robust muscovite ages. Both ductile and brittle fabrics in the Indus Gorge (Fig. 4) show consistent steep east-side-up displacements that span the ductile to brittle transition. The structural and age data suggest that this zone can be modelled as a simple shear zone with the locus of uplift, and related cooling, migrating eastward.
3. With the exception of samples 53 and 66, hornblende ages are significantly older than the monazite and zircon rim ages reported by Smith *et al.* (1992) and Zeitler *et al.* (1993). Hornblende ages reported here from samples 14, 72, 28 and 121 in the Indus Gorge and samples 205, 210, 213 and 234 in the Astor valley are in the range of 21–28 Ma (Figs 8 and 12). These are consistent with a hornblende age of 25.4 from the Indus Gorge (Table 1; Zeitler *et al.* 1989), hornblende ages of 28.5 ± 0.3 and 27.5 (model age) in the Astor valley section (Winslow *et al.* 1996; table 2) and a muscovite Rb–Sr age from Raikot (K–Ar and Ar–Ar data are available as a Supplementary Publication, see p. 142).
4. Zircon and apatite fission track ages are also younger within the core of the syntaxis than at the margins. This is well defined by the zircon data for which ages are older on the margins than within the core where they are, within error, constant. It is less clear from the apatite data, for which there is a paucity from the margins. For the Indus section, an age from the western margin is older than those from within the core. For the Astor section, an age from the eastern margin is older than those from the core. This leads to a conclusion that the differential uplift indicated by the mica data continued until < 1 Ma ago.

The analytical data may be used to address two major questions. What was the age of the peak Himalayan metamorphism within the syntaxis, and what constraints can be placed on models of structural evolution of the syntaxis?

Age of peak Himalayan metamorphism

Smith *et al.* (1992) and Zeitler *et al.* (1993) used monazite and zircon U–Pb data to suggest that peak metamorphism within the syntaxis was Neogene in age. Although most of the zircon data, at < 4 Ma (Zeitler *et al.* 1993), are from leucogranite sheets, one sample is from a migmatite from Fairy Meadows (Fig. 3). Some of these zircons have high U rims (Zeitler *et al.* 1989) and this suggests that they might date a hydrothermal, rather than a metamorphic, event. Monazite ages, ranging from 4 to 11 Ma, are all

from gneisses (Smith *et al.* 1992), mainly from the Indus and Astor valleys. Although migmatites now exposed at Fairy Meadows (Whittington *et al.* 1998*a*) were at $>700\,^{\circ}C$ at <5 Ma, we argue below that not all rocks exposed within the syntaxis were this hot so recently.

First, the majority of the robust hornblende ages presented here are at 20–30 Ma. Data from samples 121, 98, 205, 210 and 213 (Figs 8 and 12) satisfy the normally accepted criteria for hornblende Ar–Ar data with a plateau defined by much, or most, of the gas and a regression line on a correlation plot that passes through, or near, to atmosphere on the $^{36}Ar/^{40}Ar$ axis. These are similar to hornblende ages from the Indus Gorge (Zeitler *et al.* 1989) and the Astor valley (Winslow *et al.* 1996). In addition to samples described above, hornblendes from sample H4 from Mazemo Pass, south of Nanga Parbat, have an Ar release spectrum with a shallow U-shaped profile and *c.* 50% of the gas defining an age of 32 ± 2 Ma (Fig. 12k). Points 3 to 7 yield a regression line on a correlation plot which intersects the $^{36}Ar/^{40}Ar$ axis close to air with an age of 29.7 ± 2.5 Ma (Fig. 12l), consistent with the base of the U-shaped profile on the gas release spectrum. Winslow *et al.* (1996) document a hornblende from here with an age of *c.* 30 Ma. The consistency and general robustness of the hornblende data are taken here to indicate regional cooling of the Indian plate gneisses now exposed within the syntaxis through $500\,^{\circ}C$ at 25 ± 5 Ma. Although other hornblendes analysed during this study, but not presented here, have been affected by fluid mobility and excess argon, the more robust data suggest that Neogene argon mobility was not pervasive, and that amphibole data can be used to date regional cooling through $500\,^{\circ}C$. Smith *et al.* (1992) argued that hornblende ages of >20 Ma (cf. Zeitler *et al.* 1989) are older than the monazite ages, and thus reflect argon mobility and are to be mistrusted. We contend this to be a false argument that ignores the robust nature of the hornblende ages, and relies too heavily on an interpretation of rocks exposed at Fairy Meadows as well as on too simple an interpretation of what the monazite ages mean.

Second, leucogranites dated at <10 Ma (Zeitler *et al.* 1993), were emplaced into rocks already at $<400\,^{\circ}C$ (George *et al.* 1995). The Chichi leucogranite in the southern part of the massif was emplaced into cold rocks at *c.* 20 Ma (Schneider *et al.* 1999*b*). Hence, it is clear that rocks exposed today reflect a wide range in age of cooling through $500\,^{\circ}C$. It is possible that only those rocks in the extreme core of the massif, as at Fairy Meadows, were at amphibolite facies late in the Neogene.

Third, Smith *et al.* (1992) interpreted their monazite ages as dating peak, high temperature metamorphic conditions. However, Teufel & Heinrich (1997) have shown that interactions with hydrothermal fluids will result in lead loss well below the closure temperature of monazite through a dissolution–precipitation process. In addition, monazites also grow at temperatures well below the monazite closure temperature (Finger *et al.* 1998). Largely stripped of muscovite during pre-Tertiary granulite facies metamorphism and melting, some of the basement gneisses contain mats of late-stage muscovite, the growth of which was probably linked to hydration in zones of focused fluid flow. Although the exact textural location of monazites dated by Smith *et al.* (1992) is unclear, BSE micrographs suggest that some, at least, are hosted by muscovites. This would be consistent with monazite-growth in late-stage hydrous shear zones during cooling, rather than at peak metamorphic conditions. Clearly, zircon ages from leucogranites date neither peak metamorphism nor post-metamorphic cooling of rocks now exposed at surface, as they document melting at lower structural levels. Only those from migmatites at Fairy Meadows can date, *in situ*, a Neogene metamorphic event.

What are the significance of the younger (*c.* 10 Ma) hornblende ages reported here? Wheeler *et al.* (1995) and Treloar *et al.* (2000) have shown that the Tertiary metamorphism recorded within basement gneisses exposed within the syntaxis overprints a pre-Tertiary granulite-facies metamorphism. Sillimanite bundles that replace kyanite and overgrow the main Tertiary S-, L–S- and L-fabrics, themselves folded by antiformal structures developed during syntaxis growth, show that Tertiary metamorphism postdates shearing related to obduction of Kohistan onto the Indian plate. This metamorphism should predate the 20 Ma muscovite Rb–Sr cooling age from the cover sediments at Raikot which did not experience any pre-Tertiary metamorphic event, and was probably synchronous with the pre-40 Ma metamorphism documented elsewhere in the Indian plate of Northern Pakistan (Treloar & Rex 1990; Zeitler & Chamberlain 1991; Smith *et al.* 1992). As such, it is unlikely that the <10 Ma ages date peak metamorphism but instead date events that occurred during exhumation. One cause for this could be emplacement of leucogranite sheets and dykes which commenced as early as 10 Ma. Some of these bodies, such as the *c.* 6 Ma Jutial leucogranite (George *et al.* 1993), are large and it

is likely that local, anomalously low, ages reflect heat advection into cool rocks through granite emplacement.

The preferred interpretation of the data presented here is that many of the rocks exposed within the syntaxis had cooled through 500 °C by 20 Ma. This is consistent with the more robust hornblende data, the muscovite data from Raikot and the slightly older ages from the overlying rocks of the arc. Hence the peak of Tertiary metamorphism within the syntaxis is not Neogene in age, as suggested by Smith *et al.* (1992) and Zeitler *et al.* (1993), but predates 25 ± 5 Ma, and may be as old as *c.* 40 Ma. It is likely that cooling, probably related to exhumation, continued slowly until about 10 Ma when exhumation rates began to increase, decompression melting started and early leucogranite sheets were emplaced.

Structural evolution of the syntaxis

This, and earlier, studies have shown that: first, ages within the syntaxis are younger than in the arc rocks that flank it; second, along the Indus and Astor valley sections, ages within the syntaxis get older from the syntaxis core outward; and, third, ages within the strip of metasediments, originally cover to the Indian plate basement, that outcrop along the western margin of the syntaxis are older than within the basement gneisses that now structurally overlie them. Although the hornblende ages probably date cooling after the metamorphic peak, the mica ages constrain syntaxis growth. The distribution of mica cooling ages along the two sections provides an approximate symmetry, albeit with a steeper age v. distance gradient toward the western side of the syntaxis than the eastern side (Figs 10 and 14).

Both Treloar *et al.* (1991) and Winslow *et al.* (1996) argue that the distribution of mica cooling ages result from crustal-scale folding, and subsequent unroofing. A contoured map of biotite ages from the northern half of the syntaxis (Winslow *et al.* 1996, fig. 13) shows a symmetrical distribution extending from south of the Astor valley to north of the Indus Gorge, although with ages decreasing overall to the south. This distribution could be interpreted as the result of cooling following the growth, between 2 and 5 Ma, of a single, large N-plunging fold that essentially defines the syntaxial shape. This interpretation is probably an oversimplification. Although two antiformal folds are present in the Indus Gorge, they plunge south (Treloar *et al.* 1991; Wheeler *et al.* 1995), whereas in the Astor valley fold axes plunge north. In contrast to the Indus section, no clear late-stage fold is present within the Astor section (Butler *et al.* 2000). This suggests that, rather than there being a single fold, the core of the syntaxis is comprised of a number of N-trending domes which postdate and deform the early Himalayan fabrics.

That the core of the syntaxis is composed of a series of smaller domes rather than a single, large antiformal fold suggests that, although folds may control uplift on a local scale, they are unlikely to be solely responsible for total uplift of the syntaxis core. Rather than large wavelength folding playing the dominant role in syntaxial uplift (cf. Butler *et al.* 1992; Wheeler *et al.* 1995), it is as likely that the major controls on uplift in the northern part of the syntaxis are the steeply dipping shear zones located along its margins. The ductile through to brittle structures which accommodate this uplift are clear, especially in the western margin shear zones (Fig. 4). The sharp increase in age westward across these shear zones in both the studied sections (Figs 10 and 14) is consistent with a model in which the ductile through to brittle shears define an east-side-up simple shear zone within which the locus of deformation shifted progressively eastward with time, and within which rocks were uplifted and cooled through the brittle–ductile transition. Treloar *et al.* (1991), Wheeler *et al.* (1995) and Butler *et al.* (2000) have shown how strains increase markedly into the marginal zones. Initial stages of uplift may have been the result of crustal-scale buckling, but once the gneissic layering had rotated beyond a critical point, stress was increasingly accommodated by dip-slip shearing as fold limbs became more and more attenuated.

How much uplift did the western margin shear zone accommodate? It is not possible to use a steady state geothermal gradient to calculate uplift rates as, for a constant exhumation rate, cooling rates will increase through time as isotherms become telescoped near the surface (Whittington 1996; Mancktelow & Grasemann 1997). To provide a conservative estimate of uplift it is necessary to consider the depth at which rocks cooled through 500 °C, and that at which they cooled through 300 °C. Winslow *et al.* (1995) estimate peak, Tertiary metamorphic conditions away from the Fairy Meadow migmatites at *c.* 700 °C and 10 kbar, consistent with estimates of Pognante *et al.* (1993). Had cooling been along an adiabatic gradient, cooling through 500 °C would have been at *c.* 7 kbar. Given the evidence for short-lived Eocene metamorphism followed by rapid cooling in the Indian plate (Treloar 1997), and of rapid cooling events within Kohistan (Krol *et al.* 1994), this pressure

estimate is probably an over-estimate. Conservatively, we would estimate pressure of cooling through 500 °C at *c.* 5 kbar, or 17 km depth. Craw *et al.* (1994), Winslow *et al.* (1994) and Whittington *et al.* (1996) estimate that during rapid uplift the 300 °C isotherm, which equates to the biotite cooling temperature, was at *c.* 6 km depth.

The thin strip of metasediments exposed between Sassi and Raikot has cooling ages intermediate between those of the Kohistan arc and the Indian plate basement gneisses, implying that these rocks experienced some uplift relative to Kohistan prior to the main phase of subvertical east-side-up shearing which probably started at *c.* 9 Ma (Reddy *et al.* 1997). Muscovite Ar–Ar data show that rocks along the western margin cooled through 400 °C at *c.* 10 Ma. Hence we assume that rocks now exposed within the Indus and Astor sections were at *c.* 450 °C at a depth of *c.* 17 km prior to syntaxial uplift beginning to accelerate at *c.* 10 Ma. The total uplift accommodated by the western margin shear zones, prior to cooling through the biotite closure temperature, will thus be the difference in depth of cooling through 450 °C for rocks within the shear zone, and that of cooling through 300 °C for rocks within the core of the syntaxis. On this basis it can be inferred that the 3 km wide shear zone, located along the western margin of the syntaxis in the Indus Gorge, accommodated *c.* 10 (17 to 6) km of differential uplift over 3 (6 to 3) Ma (Fig. 10), giving a total accumulated shear strain of $\gamma = 3$–4. Within the Astor River section, a similar total strain was accumulated but over a longer time scale of *c.* 7 (10 to 3 Ma) Ma. As zircon and apatite fission track ages are younger within the centre of the syntaxis than at the western margin implies that differential uplift across the zone continued after 3 Ma, and that the total differential uplift and distributed shear strain is higher still. That shear strains were less, and probably distributed more homogeneously, along the eastern margin is indicated by the shallower age gradient and by the observation that primary structures, such as the Main Mantle Thrust, are preserved along the eastern margin, although steepened toward the vertical.

Our preferred model for the northern part of the syntaxis involves growth through a combination of folding and shearing along the margins. Early, regional-scale, buckling, is indicated by cooling ages from the metamorphosed cover sediments, exposed along the western margin and from the fabric shapes present along the Indus Gorge section (Wheeler *et al.* 1995) and to the north (Butler *et al.* 1992). Initial uplift was probably accommodated by these folds. The distribution of ages along the Indus Gorge section suggests that the easternmost fold, with slightly older muscovite ages, may have developed before the more westerly one (Treloar *et al.* 1991). However, once the fold limbs had become sufficiently steep, with rotation of the gneissic banding to the subvertical, uplift was thereafter accommodated by subvertical dip-slip displacements along the marginal shear zones. Thus, syntaxial growth, at least within and to the north of the Astor valley, is largely the result of distributed ductile through to brittle subvertical shearing concentrated within the marginal shear zones that accommodated vertical uplift of the whole structure. Muscovite and biotite ages within the western marginal shear zone suggest that the locus of shearing migrated eastward within the shear zone. Zircon and apatite ages suggest that shearing continued until < 1 Ma. A synchronous antithetic, but lower strain, shear zone controlled uplift along the eastern margin of the syntaxis. Both steeply dipping shears uplifted basement gneisses with respect to the metamorphosed cover sediments which flank them. This uplift is essentially analogous to a 'toothpaste-extrusion' model (Thompson *et al.* 1997) in which hot, ductile rocks are squeezed upwards along a narrow failure zone. This solution is compatible with that of Schneider *et al.* (1999).

South of the Astor valley the simple 'toothpaste' model break downs. Major, moderately SW-dipping, NW-vergent shear systems began to develop at about 5 Ma. A simple thrust chronology suggests a sequence in which the latest shears are the structurally higher ones. The earliest shears are the steep, east-side-up shears, that crop out at the western end of the Indus and Astor sections, and which operated as early as 9 Ma. In the south, subvertical shearing was superseded, first, by shearing within the Liachar Shear Zone, operative as a ductile shear at *c.* 6 Ma (this study), and then by the Tato Shear Zone, operative at *c.* 2 Ma (Winslow *et al.* 1996; this study). The implication is that after 6 Ma, uplift along the southwestern margin of the syntaxis, south of the Astor valley, was by NW-vergent moderately dipping shear systems rather than by the steeply dipping east-side-up shear systems active to the north of the Astor valley. This change is important as it ultimately explains the presence at surface level of the *c.* 5 Ma old migmatites exposed in the Fairy Meadows.

Three phases of uplift are indicated by the geochronological and structural data: (a) early doming that predated 9 Ma; (b) uplift along steeply dipping antithetic shears developed along

the syntaxis margins during the period of 9 to < 1 Ma; and (c) uplift along the moderately SW-dipping Liachar and Tato ductile to brittle shears between 6 and 2 Ma. The last stage was responsible for rapid, late-stage exhumation of the Fairy Meadows migmatites. It is likely that exhumation of these migmatites on the hanging wall of moderately dipping thrusts involved extensional collapse, although this remains unrecognized. What accommodated the change in uplift style from the second to third stage is uncertain, but it highlights a major outstanding problem. Although the regional structural framework within which the syntaxis evolved is now well understood (Treloar *et al.* 1991; Seeber & Pêcher 1998), the relationships between the structures which accommodated uplift still remains uncertain.

Fieldwork was supported by the Natural Environment Research Council (NERC) Grant (GR3/6113 to M. P. Coward) and by the Royal Society. Fission track analyses were funded through an NERC Grant (GR3/7068) to A. J. Hurford. We acknowledge discussions with R. W. H. Butler, J.-A. Wartho, P. K. Zeitler and G. Foster, and critical reviews by A. G. Whittington and a reviewer who wishes to remain anonymous. S. M. Bignold drew the diagrams.

References

BREWER, M. S. 1969. Excess radiogenic argon in metamorphic micas from the Eastern Alps, Austria. *Earth and Planetary Science Letters*, **6**, 321–331.

BUTLER, R. W. H. 2000. Structural evolution of the western margin of the Nanga Parbat massif, Pakistan Himalaya: insights from the Raikot–Liachar area. *This volume.*

—— & PRIOR, D. J. 1988*a*. Tectonic controls on the uplift of Nanga Parbat, Pakistan Himalaya. *Nature*, **333**, 247–250.

—— & —— 1988*b*. Anatomy of a continental subduction zone. *Geologische Rundschau*, **77**, 239–255.

——, GEORGE, M. T., HARRIS, N. B. W., JONES, C., PRIOR, D. J., TRELOAR, P. J. & WHEELER, J. 1992. Geology of the northern part of the Nanga Parbat massif, northern Pakistan, and its implications for Himalayan tectonics. *Journal of the Geological Society, London*, **149**, 557–567.

——, HARRIS, N. B. W. & WHITTINGTON, A. G. 1997. Interactions between deformation, magmatism and hydrothermal activity during active crustal thickening: a field example from Nanga Parbat, Pakistan Himalayas. *Mineralogical Magazine*, **61**, 37–51.

——, PRIOR, D. J. & KNIPE, R. J. 1989. Neotectonics of the Nanga Parbat syntaxis, Pakistan, and crustal stacking in the northwest Himalaya. *Earth and Planetary Science Letters*, **94**, 329–343.

——, WHEELER, J., TRELOAR, P. J. & JONES, C. 2000. Geological structure of the southern part of the Nanga Parbat massif, Pakistan Himalaya, and its tectonic implications. *This volume.*

CHAMBERLAIN, C. P., JAN, M. Q. & ZEITLER, P. K. 1989. A petrological record of the collision between the Kohistan island arc and Indian Plate, northwest Himalaya. *In*: MALINCONICO, L. L. & LILLIE, R. J. (eds) *Tectonics of the Western Himalaya*. Geological Society of America Special Papers, **232**, 23–32.

CHAUDHRY, N. & GHAZANFAR, M. 1990. Position of the Main Central Thrust in the tectonic framework of the western Himalaya. *Tectonophysics*, **174**, 321–329.

CLIFF, R. A., BARNICOAT, A. C. & TRELOAR, P. J. 1991. Generation and migration of isotopically extreme partial melts in active fault zones. EUG VI, Strasbourg. *Terra Abstracts*, **3**, 489.

COWARD, M. P. 1986. A section through the Nanga Parbat syntaxis, Indus Valley, Kohistan. *Geological Bulletin of the University of Peshawar*, **18**, 147–152.

——, WINDLEY, B. F., BROUGHTON, R. D., LUFF, I. W., PETTERSON, M. G., PUDSEY, C. J., REX, D. C. & KHAN, M. A. 1986. Collision tectonics in the NW Himalayas. *In*: COWARD, M. P. & RIES, A. C. (eds) *Collision Tectonics*. Geological Society, London, Special Publication, **19**, 205–221.

CRAW, D. P. O., KOONS, D., WINSLOW, D. P., CHAMBERLAIN, C. P. & ZEITLER, P. K. 1994. Boiling fluids in a region of rapid uplift: Nanga Parbat massif, Pakistan. *Earth and Planetary Science Letters*, **128**, 169–182.

DAHL, P. S. 1996. The crystal chemical basis for Ar retention in micas: inferences from interlayer partitions and implications for geochronology. *Contributions to Mineralogy and Petrology*, **123**, 22–39.

DIPIETRO, J. A. 1991. Metamorphic pressure–temperature conditions of Indian Plate rocks south of the Main Mantle Thrust, Lower Swat, Pakistan. *Tectonics*, **10**, 742–757.

—— & LAWRENCE, R. D. 1991. Himalayan structure and metamorphism south of the Main Mantle Thrust, Lower Swat, Pakistan. *Journal of Metamorphic Geology*, **9**, 481–495.

DODSON, M. H. 1973. Closure temperature in cooling geochronological and petrological systems. *Contributions to Mineralogy and Petrology*, **40**, 259–274.

EDWARDS, M. A., KIDD, W. S. F., KHAN, M. A. & SCHNEIDER, D. A. 2000. Tectonics in the SW margin of the Nanga Parbat–Haramosh massif. *This volume.*

FINGER, F., BROSKA, A., ROBERTS, M. P. & SCHERMAIER, A. 1998. Replacement of primary monazite by apatite-allanite-epidote coronas in an amphibolite facies granite gneiss from the eastern Alps. *American Mineralogist*, **83**, 248–258.

FOLAND, K. A. 1983. $^{40}Ar/^{39}Ar$ incremental heating plateaux for biotites with excess argon. *Chemical Geology*, **41**, 3–21.

GABER, L. J., FOLAND, K. A. & CORBATOR, C. E. 1988. On the significance of argon release from biotite and amphibole during $^{40}Ar/^{39}Ar$ vacuum heating. *Geochimica et Cosmochimica Acta*, **52**, 2457–2465.

GEORGE, M. T. & BARTLETT, J. M. 1996. Rejuvenation of Rb–Sr mica ages during shearing on the northwestern margin of the Nanga Parbat–Haramosh massif. *Tectonophysics*, **260**, 167–185.

——, BUTLER, R. W. H. & HARRIS, N. W. B. 1993. The tectonic implications of contrasting granite magmatism between the Kohistan island arc and the Nanga Parbat–Haramosh massif. *In*: TRELOAR, P. J. & SEARLE, M. P. (eds) *Himalayan Tectonics*. Geological Society, London, Special Publications, **74**, 173–191.

——, REDDY, S. M. & HARRIS, N. B. W. 1995. Isotopic constraints on the cooling history of the Nanga Parbat–Haramosh massif and Kohistan arc, western Himalaya. *Tectonics*, **14**, 237–252.

JOHNSON, C., HARBURY, N. & HURFORD, A. J. 1997. The role of extension in the Miocene denudation of the Nevado-Filabride complex, Betic Cordillera (SE Spain). *Tectonics*, **16**, 189–204.

KIDD, W. S., EDWARDS, M. A., KHAN, M. A., SCHNEIDER, D. A., ZEITLER, P. K. *et al.* 1998. Structure and chronology of Nanga Parbat Haramosh massif. *1998 Fall meeting, EOS*, **79**(45), suppl., F909.

KROL, M. A., ZEITLER, P. K. & COPELAND, P. 1996. Episodic unroofing of the Kohistan batholith, Pakistan: implications from K-feldspar thermochronology, *Journal of Geophysical Research*, **101**, 28 149–28 164

LUDWIG, K. R. 1990. *A plotting and regression program for radiogenic-isotope data, for IBM-PC compatible computers*. USGS Open-File Report 88-557.

MADIN, I. P., LAWRENCE, R. D. & UR-RAHMAN, S. 1989. The North-western Nanga Parbat–Haramosh massif: evidence for crustal uplift at the northwestern corner of the Indian craton. *In*: MALINCONICO, L. L. & LILLIE, R. J. (eds) *Tectonics of the Western Himalaya*. Geological Society of America Special Papers, **232**, 169–182.

MANCKTELOW, N. S. & GRASEMANN, B. 1997. Time dependant effects of heat advection and topography on cooling histories during erosion. *Tectonophysics*, **270**, 167–195.

PANKHURST, R. J., MOORBATH, S., REX, D. C. & TURNER, G. 1973. Mineral age patterns in ca. 3700 my old rocks from West Greenland. *Earth and Planetary Science Letters*, **20**, 157–170.

PETTERSON, M. G. & WINDLEY, B. F. 1985. Rb–Sr dating of the Kohistan arc batholith in the Trans-Himalaya of N. Pakistan and tectonic implications. *Earth and Planetary Science Letters*, **74**, 54–75.

POGNANTE, U., BENNA, P. & LE FORT, P. 1993. High pressure metamorphism in the High Himalayan Crystallines of the Stak Valley, northeastern Nanga Parbat-Haramosh syntaxis, Pakistan Himalaya. *In*: TRELOAR, P. J. & SEARLE, M. P. (eds) *Himalayan Tectonics*. Geological Society, London, Special Publications, **74**, 161–172.

REDDY, S. M., KELLEY, S. P. & MAGENNIS, L. 1997. A microstructural and argon laserprobe study of shear zone development at the western margin of the Nanga Parbat–Haramosh massif, western Himalaya. *Contributions to Mineralogy and Petrology*, **128**, 16–29.

RODDICK, J. C., CLIFF, R. A. & REX, D. C. 1980. The evolution of excess argon in alpine biotites. *Earth and Planetary Science Letters*, **45**, 185–208.

SCHNEIDER, D. A., EDWARDS, M. A. & ZEITLER, P. K. 1999*a*. Mazemo Pass pluton and Jutial pluton, Pakistan Himalaya: age and implications for entrapment mechanisms of two granites in the Himalaya. *Contributions to Mineralogy and Petrology*, **136**, 273–284.

——, ——, KIDD, W. S. F., ZEITLER, P. K. & COATH, C. D. 1999*b*. Early Miocene anatexis identified in the western syntaxis, Pakistan Himalaya. *Earth and Planetary Science Letters*, **167**, 121–129.

——, EDWARDS, M. A., KIDD, W. S. F., KHAN, M. A., SEEBER, L. & ZEITLER, P. K. 1999c. Tectonics of Nanga Parbat, western Himalaya: synkinematic plutonism within the doubly vergent shear zones of a crustal-scale pop-up structure. *Geology*, **27**, 999–1002.

SEEBER, L. & PÊCHER, A. 1998. Strain partitioning along the Himalayan arc and the Nanga Parbat antiform. *Geology*, **26**, 769–864.

SMITH, H. A., CHAMBERLAIN, C. P. & ZEITLER, P. K. 1992. Documentation of Neogene regional metamorphism in the Himalayas of Pakistan using U–Pb in monazite. *Earth and Planetary Science Letters*, **113**, 93–106.

TEUFEL, S. & HEINRICH, W. 1997. Partial resetting of the U–Pb isotope system in monazite through hydrothermal experiments. *Chemical Geology*, **137**, 273–281.

THOMPSON, A. B., SCHULMANN, K. & JEZEK, J. 1997. Soft orogenic deformation and metamorphism in convergent to transpressive regimes. EUG9, Strasbourg. *Terra Nova*, **9**, abstract suppl. 1, 84.

TRELOAR, P. J. 1997. Thermal controls on early-Tertiary, short-lived, rapid regional metamorphism in the NW Himalaya, Pakistan. *Tectonophysics*, **273**, 77–104.

—— & REX, D. C. 1990. Cooling, uplift and exhumation rates in the crystalline thrust stack of the North Indian Plate, west of the Nanga Parbat syntaxis. *Tectonophysics*, **180**, 323–349.

——, GEORGE, M. T. & WHITTINGTON, A. G. 2000. Mafic sheets from Indian plate gneisses in the Nanga Parbat syntaxis: their significance in dating crustal growth and metamorphic and deformation events. *This volume*.

——, POTTS, G. J., WHEELER, J. & REX, D. C. 1991. Structural evolution and asymmetric uplift of the Nanga Parbat syntaxis, Pakistan Himalaya. *Geologisches Rundschau*, **80**, 411–428.

——, REX, D. C., GUISE, P. G., COWARD, M. P., SEARLE, M. P. *et al.* 1989*b*. K–Ar and Ar–Ar geochronology of the Himalayan collision in NW Pakistan: constraints on the timing of collision, deformation, metamorphism and uplift. *Tectonics*, **8**, 881–909.

VILLA, I. 1998. Isotopic closure. *Terra Nova*, **10**, 42–47.

WARTHO, J.-A., REX, D. C. & GUISE, P. G. 1996. Excess argon in amphiboles linked to greenschist facies metamorphism in the Kamila amphibolite belt, Kohistan island arc system, northern Pakistan: insights from $^{40}Ar/^{39}Ar$ step-heating and acid leaching experiments. *Geological Magazine*, **133**, 595–609.

WHEELER, J., TRELOAR, P. J. & POTTS, G. J. 1995. Structural and metamorphic evolution of the Nanga Parbat syntaxis, Pakistan Himalayas on the Indus Gorge transect: the importance of early events. *Geological Journal*, **30**, 349–371.

WHITTINGTON, A. G. 1996. Exhumation overrated at Nanga Parbat, northern Pakistan. *Tectonophysics*, **260**, 215–226.

——, HARRIS, N. B. W. & BAKER, J. 1998. Low pressure crustal anatexis: the significance of spinel and cordierite from metapelitic assemblages at Nanga Parbat, northern Pakistan. *In*: TRELOAR, P. J. & O'BRIEN, P. (eds) Geological Society of London, Special Publication, **134**, 183–198.

WINSLOW, D. M., CHAMBERLAIN, C. P. & ZEITLER, P. K. 1995. Metamorphism and melting of the lithosphere due to rapid denudation, Pakistan Himalaya. *Journal of Geology*, **103**, 395–408.

——, ZEITLER, P. K. & CHAMBERLAIN, C. P. 1994. Direct evidence for a steep geotherm under conditions of rapid denudation, western Himalaya, Pakistan. *Geology*, **22**, 1075–1078.

——, ——, —— & WILLIAMS, I. S. 1996. Geochronological constraints on syntaxial development in the Nanga Parbat region, Pakistan. *Tectonics*, **15**, 1292–1308.

ZEITLER, P. K. 1985. Cooling history of the NW Himalaya. *Tectonics*, **4**, 127–135.

—— & CHAMBERLAIN, C. P. 1991. Petrogenetic and tectonic significance of young leucogranites from the northwest Himalaya. *Tectonics*, **10**, 729–741.

——, —— & SMITH, H. A. 1993. Synchronous anatexis, metamorphism and rapid denudation at Nanga Parbat (Pakistan Himalaya). *Geology*, **21**, 347–350.

——, SUTTER, J. F., WILLIAMS, I. S., ZARTMAN, R. & TAHIRKELLI, R. A. K. 1989. Geochronology and temperature history of the Nanga Parbat–Haramosh massif, Pakistan. *In*: MALINCONICO, L. L. & LILLIE, R. J. (eds) *Tectonics of the Western Himalaya*. Geological Society of America Special Papers, **232**, 1–22.

Unroofing of the Nanga Parbat Himalaya

J. F. SHRODER, JR. & M. P. BISHOP
Department of Geography and Geology, University of Nebraska at Omaha, Omaha, NE 68182, USA (e-mail: john_shroder@unomaha.edu)

Abstract: The rapid erosional unroofing of the Nanga Parbat Himalaya in late Cenozoic time is thought to have been initiated when the Indus River, initially flowing somewhat north and well to the west of its present location, was captured and diverted south close to the massif of today by extensional structures and downfaulted topography across the Kohistan–Ladakh island arc terrane. It is hypothesized that the Nanga Parbat pop-up structure was initiated at *c.* 12–10 Ma, as a tectonic aneurysm caused by rapid incision by the Indus River and other surface processes. Because of this subsequent rapid unroofing of the region, however, the oldest sediments to record erosion in the immediate region of Nanga Parbat are <200 ka old: most sediments and our cosmogenic and ISRL exposure dates are more than five times younger. Diverse field measurements of rates of local incision and areal denudation for mass movement, glacial, river and catastrophic floods for the past *c.* 55 ka are highly differential but internally replicative and externally consistent with research indicating long-term, severe denudation. Averaged rates of maximum incision at more than 15 points around the massif are 22 mm $\pm$ 11 mm a^{-1}. Late Pleistocene surface processes at Nanga Parbat were capable of erosional unroofing of the massif sufficiently vigorous to produce the pronounced relief of today.

The Nanga Parbat Himalaya (Fig. 1) has been recognized as an unusual portion of the crust that has areas of exceptionally young metamorphic and igneous rocks uplifted rapidly to the surface of the ninth highest mountain in the world (Zeitler 1985; Treloar *et al.* 1989; Searle 1991; Zeitler *et al.* 1993). The Nanga Parbat massif is known to be a structural half window of largely Proterozoic-aged, Indian-plate basement rocks, flanked on the north by the rocks of the Asian plate and to the east and west by rocks of the Ladakh–Kohistan island arc that once overlaid the rocks of the massif (Edwards 1998; Schneider *et al.* 1999). The core of the massif has young metamorphic mineral assemblages showing granulite-facies metamorphism coincident with the highest topography, and decreasing across tight concentric isograds to the active margins of the Nanga Parbat syntaxis (Smith *et al.* 1994; C. P. Chamberlain, pers. comm. 1998), along which the antiformal pop-up structure is being uplifted (Schneider *et al.* 1999). Young leucogranite dykes, close to shear zones, suggest that anatectic episodes at Nanga Parbat were strain induced, with deformation-enhanced, melt migration focusing the melt into the shear zones, which was possibly further enhanced by fluid infiltration (Schneider *et al.* 1999).

The overall model of the generation of the Nanga Parbat structure as presently conceived involves strain-partitioning wherein radial convergence along the arcuate Himalayan front is coupled with arc-parallel extension in the hanging wall and arc-parallel shortening in the arc termini (Seeber & Pêcher 1998). This is manifested at Nanga Parbat as a compressional transpression structure where northwestward transport of the antiform may be more than half the rate of convergence in the central Himalaya, or as much as 12 mm a^{-1}. The rapid uplift of the massif is accounted for in this model by thrust-related folding as a kind of tectonic aneurysm in which the upward movement of the mountain in a spatially restricted area was caused by rapid unroofing of the surface in late Cenozoic time. The nature and timing of this unroofing is, therefore, of paramount importance to understand the overall tectonics of the Nanga Parbat massif.

Searle & Khan (1995) showed three north-dipping normal faults near the head of the Raikot valley on the north face of Nanga Parbat. M. Searle (pers. comm. 1995) noted the likelihood of detachment faulting on the huge relief (7 vertical km in 21 km horizontal), although he was uncertain about the overall nature of this hypothesized tectonic unroofing high on the

From: KHAN, M. A., TRELOAR, P. J., SEARLE, M. P. & JAN, M. Q. (eds) *Tectonics of the Nanga Parbat Syntaxis and the Western Himalaya*. Geological Society, London, Special Publications, **170**, 163–179. 1-86239-061-4/00/$15.00

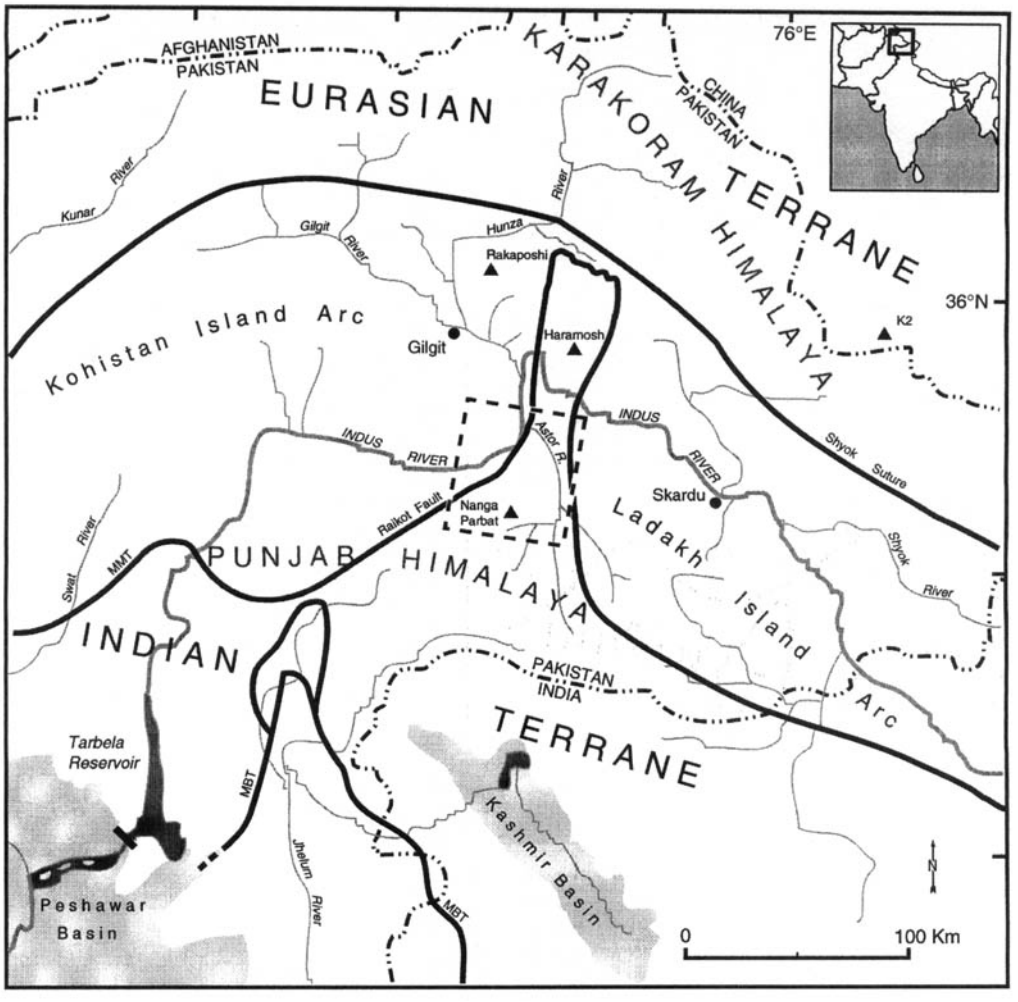

Fig. 1. Location map of Nanga Parbat study area (dashed rectangle shows satellite imagery coverage used for study area). MMT, Main Mantle Thrust; MBT, Main Boundary Thrust.

unclimbed face. P. Koons (pers. comm. 1998) did observe faults on the Raikot face but noted the sense of motion was not determined. Seeber & Pêcher (1998) interpreted seismogenic normal faulting on the northwest part of the mountain as gravity-driven collapse of the eastern wall of the Indus Gorge by bookshelf-like block rotation about horizontal axes, and also as flexural slip in the overturned northwestern limb of the Nanga Parbat anticline. Similarly, Edwards (1998) noted that brittle normal faulting occurring throughout the southern side of the mountain indicates that it, too, is in a state of gravitational collapse. On the other hand, structures below *c.* 5500 m mapped by Schneider *et al.* (1999) throughout the massif demonstrate that the high rates of exhumation, suggested by the thermobarometry and geochronology, are not from orogen-scale extensional exhumation, and that, instead, sustained high rates of surficial erosion unroofed the massif.

The study reported here is a part of the Nanga Parbat Continental Dynamics Project in which *c.* 5000 km^2 of the central Nanga Parbat massif was studied intensively. Analyses of the massif in this project involved a comprehensive assessment of petrology, geochronology, seismology, magnetotellurics, structural geology, neotectonics, geochemistry, dynamic modelling, remote sensing and geomorphology. We used field measurement and computer modelling of mass movement, glaciation, rivers and catastrophic flooding to characterize modern rates of geomorphic processes. In addition, we also mapped

overall geomorphology and Quaternary stratigraphy, dated with cosmogenic nuclides and infra-red stimulated luminescence (W. Phillips and H. Rendell, pers. comm. 1998), to elucidate past rates of processes. Rates of incision at points and cross-sections were calculated, along with rates of denudation for areas of glacier and river basins. Remote sensing and a geographical information system were used to characterize the topography and map landscape features. Linkages between terrain and tectonic character, topographic complexity and process geomorphology were obtained with multiple datasets (Bishop *et al.* 1998*b*).

Capture of the Indus River

Tectonic exhumation of the area to the southwest of the main Nanga Parbat massif has been mapped and described by Hubbard *et al.* (1995) as completed by *c.* 20 Ma (Table 1). During this tectonic exhumation, the rocks of the Kohistan sequence and the cover sequence of the Indian plate moved WSW relative to the rocks of the Indian plate basement, including the Nanga Parbat gneiss. W. S. F. Kidd (pers. comm. 1998) has noted that these data can also be explained by strike-slip motion on the Main Mantle Thrust (MMT). Similarly, Treloar *et al.* (1991) reported that the originally south-verging MMT later underwent down-to-the-north extension that was complete after *c.* 20 Ma. Further deformation on the hanging wall of the Main Boundary Thrust (MBT) developed from 15–8 Ma (Treloar *et al.* 1991).

The extensional collapse of the Himalayan orogen from the southwest to the north of Nanga Parbat and obliquely transverse across the mafic-rich rocks of the Kohistan–Ladakh arc are likely to have produced surficial depressions along which a potentially pirate drainage to the south and into the foreland basins would have developed over time.

Marine fossils specific to monsoonal precipitation first appeared in the northern Indian Ocean 11–10 Ma ago (Quade *et al.* 1989), and terrigenous sediment also increased on the Indus submarine fan *c.* 10 Ma ago (Ruddiman *et al.* 1997). Intensification of the reversing monsoon is marked by a strong ecological shift in the latest Miocene (*c.* 8–7 Ma) of Pakistan (Quade *et al.* 1989, 1997; Retallack 1991). Increase in high run-off events associated with the initiation of the monsoon would enhance erosional feedbacks such as valley incision (Prell & Kutzbach 1997). Thus, the stronger monsoonal precipitation that developed on southwestern Himalayan slopes in the middle and late Miocene (Derry & France-Lanord 1997) could have further contributed to the formation and evolution of the pirate stream that captured the Indus River.

In any case, the first blue-green hornblende grains from the unroofing of the Kohistan terrane arrived in the foreland Siwalik basin at *c.* 11 Ma ago (Cerveny *et al.* 1989), perhaps as the originally west-flowing ancestral Indus (Brookfield 1998) was captured and entrained south close to where it resides today. The fluvial stratigraphy of the Nagri Formation of the Siwaliks is compatible with the shifting of a far larger, Indus-like drainage southeast through the fore-

Table 1. *Model of evolutionary development of Indus River system and its association to the Nanga Parbat Himalaya*

Event		Time (Ma)
NW–W flowing ancestral Indus from Kailas in Tibet deposits Indus molasse in Ladakh and Neogene sedimentary basin fills in Afghanistan (Brookfield 1998).		*c.* < 40
Ancestral Indus superposed on Ladakh arc rocks northeast of Nanga Parbat (Andrews-Speed & Brookfield 1982).		*c.* 20
Structurally controlled development of pirate drainage between MMT & MBT.	Tectonic exhumation SW Nanga Parbat complete (Hubbard *et al.* 1995).	*c.* 20
	Down-to-N extension of MMT complete (Treloar *et al.* 1991).	*c.* 20
Incipient capture of Indus.	Deformation hanging wall MBT (Treloar *et al.* 1991).	15–8
Blue–green hornblende in Nagri Fm. of Siwalik Group in Pakistan from first unroofing of Kohistan arc rocks (Cerveny *et al.* 1989; Zaleha 1997*b*). Indus River diverted south and fully erosive through arc rocks.		*c.* 11
Initiation of Nanga Parbat pop-up structure by abrupt increase of strong erosion (Schneider *et al.* 1999).		12–10

land at that time (K. Behrensmeyer, pers. comm. 1999). Discharges of the largest Nagri rivers appear larger or equivalent (Zahela 1997*a*, *b*) to discharges of the modern Indus (Jorgensen *et al.* 1993). Thus, this may mark the beginning of the severe surficial denudation in the western Himalaya that ultimately led to exhumation of the Nanga Parbat massif (Table 1). The capture of the Indus into an extensional depression across Kohistan seems to have initiated the Nanga Parbat pop-up structure at *c.* 10–12 Ma, which Schneider *et al.* (in press) believed was consistent with the Himalayan arc-parallel extension, the beginning of which is dated as not younger than 8–11 Ma (Harrison *et al.* 1995).

Older ideas concerning palaeo-positions of the ancestral Indus River (Shroder 1993) are partly supplanted in this new model of the evolution of the drainage system (Table 1). Evidence of the older river positions and flow directions throughout the foreland basins in central and southern Pakistan were most likely caused by the many other rivers of the Punjab that also drain the western Himalaya.

The hypothesized capture and diversion of the Indus River southwest across Kohistan *c.* 11 Ma ago seems to have initiated the surficial erosion of the Nanga Parbat massif, but the post-capture record of unroofing from late Miocene to middle Pleistocene seems, not surprisingly, to be generally missing from the area. Only in the late Pleistocene and Holocene are sufficient records of erosional and depositional events preserved that record rates of unroofing by surficial processes. Prior to this time no recognizable records of unroofing processes exist, but the sands of the Indus River do contain a distinctive population of young (1–5 Ma) zircons derived from the Nanga Parbat area that suggest a similarity of process through time. Furthermore, on a broad scale the Himalayan landscape has been a relatively steady-state feature for the past *c.* 18 Ma (Cerveny *et al.* 1988), so we may presume that the evidence of surficial processes of the late Pleistocene–Holocene is reasonably representative of the greater time span of the hiatus.

Mass movement

A wide variety of slope failures initiated the major part of the denudation cascade in the Himalaya (Shroder & Bishop 1998). Such mass movement is commonly high frequency and can be exceptionally high magnitude (Goudie *et al.* 1984; Hewitt 1998; Shroder 1998). At Nanga Parbat the gravitational collapse of the massif, noted by Edwards (1998) and Seeber & Pêcher (1998), contributes to the pervasive and scale-dependent instability, passing downward into the crust as seismogenic normal faults, or outward onto slopes as mass movement (Shroder 1998; Shroder & Bishop 1998).

The largest (>1 km^2) rockfalls and rockslides on Nanga Parbat occur on all sides of the mountain in the Diamir, Rupal, Astor and Indus valleys and are associated with the peripheral faults. Smaller failures are widespread on the steep slopes. All types of mass movement are the main source of the thick debris cover on the glaciers radiating from the massif. The main slope failures studied for this project are in the Rupal, Astor and Raikot River valleys that drain from the massif, and in the main Indus Gorge at the base of the north side of the mountain.

Tap rockfall and rockslide

The Tap failure is a *c.* 1×10^5 m^3 mass of 10–30 m sized boulders that represents collapse of the right-side (SW) buttress of the Tap cirque that fell from an altitude of 4900–4500 m on the steep Rupal face of Nanga Parbat. The failure represents collapse *c.* 4000 years ago (^{10}Be date; W. Phillips, pers. comm. 1998) of the scarp along the Rupal Chichi Shear Zone (Edwards 1998), directly following deglaciation of the Rupal valley and the monsoon-enhanced ice advance in early to middle Holocene (^{10}Be exposure dates W. Phillips; IRSL dates, H. Rendell; pers. comms. 1998) that undercut the mountain wall of the scarp. Similar large rockfall masses abound throughout the valleys in the massif.

Doian and Mushkin rockslides

At the mouth of the Astor River, where it crosses the Raikot Fault Zone, two slow moving rockslides are known to have been pouring rock down secondary foliation planes (W. S. R. Kidd, pers. comm. 1998) into the river for well over a century of historical records (Shroder 1998), and undoubtedly for thousands of years previously, following deglaciation in the mid-Holocene. Collectively along 7.2 km of the river, *c.* 17×10^9 m^3 of rock has moved downslope and into the river. Here, the debris has been efficiently removed because of the increase in river gradient and velocity caused by the narrowing and obstruction of the river outflow past the partial barrier. The volume of rock removed from the area of the Mushkin basin since deglaciation equates to a rate of denudation of *c.* 16–38 mm a^{-1}.

Liachar–Indus landslides, 1841 and antiquity

In the winter of 1840–1, an earthquake caused the Liachar spur of bedrock gneiss faulted over till to fail and slide into the Indus Gorge. The famous landslide blocked the river for several months and produced a catastrophic breakout flood that carried a huge load of debris of *c.* 2×10^6 m^3 away with it in a short time (Shroder 1998; Shroder *et al.* 1998). The volume of the sediment eroded, coupled with several prior slope failures of similar magnitude at the site and environs within an estimated past 500 to 1000 years, allowed calculation of a rate of denudation at this location of *c.* 120–260 mm a^{-1}.

Raikot–Biale debris avalanches

Profuse light-coloured scars between *c.* 3000 and 5500 m altitude in the upper Raikot valley show the pervasive influence of slope failures produced by torrential rains and rapid snow melt. Such debris avalanches and rapid, wet debris flows generally mobilize only the upper few metres of frost-shattered rock and thin overlying sediments, but the moderate to high frequency on Nanga Parbat has caused significant denudation of small alpine basins. Two such basins on the east-facing slopes of the Jalipur Kamm ridge above Biale village experienced debris avalanches that corraded trees with a return period of 67 years.

Rupal alpine basins and debris fans

Thirty-three debris fans and five small alpine basins in the upper Rupal valley were assessed in order to determine how much the alpine processes of snow avalanches, debris avalanches and rapid, wet, debris flows were responsible for denudation of the massif (Shroder *et al.* 1999). Volumetric estimates of fans and basins, constrained by mid-Holocene dates since deglaciation, indicate that average denudation rates in these areas have been *c.* 2 mm a^{-1} over about the past 5 millennia.

Hewitt (1989, 1993) discussed the many depositional processes alongside glaciers in the Himalaya and showed that the overwhelming preponderance of debris brought to, and accumulated along, glacier margins in the Himalaya is from mass movement. All of the glaciers on Nanga Parbat are thickly debris-covered (Bishop *et al.* 1998*b*) from mass movement by high-altitude avalanches of snow and ice, and lower down by failure of undercut steep slopes. In addition to erosion, glaciers provide an efficient transporting mechanism for the plentiful material that arrives on the surface from the mass movement. The result is a pervasive erosion and transportation system that delivers massive quantities of sediment to glacier termini for redistribution downstream by fluvial processes (Shroder 1998).

Glaciers

Nanga Parbat is extensively glacierized in its upper reaches by 69 separate glaciers that cover an area of 302 km^2 and have an estimated volume of 25 km^3 (Kick 1980) (Fig. 2). The mean elevation of the glaciers is 5140 m on the north side of the mountain and 4720 m on the south side, with the lowest ice reaching down to 3000 m. The mountain is strongly influenced by orographic precipitation because it is the first major topographic barrier to monsoon winds that travel north from the Indian Ocean and Arabian Sea. Summer monsoon rain below *c.* 5000 m turns to snow above. Westerly winter storms also strongly impact the mountain. Precipitation is less than 120 mm a^{-1} at altitudes below 2500 m, but rises to more than 8000 mm a^{-1} at elevations above 4500 m (Kick 1980).

Glaciers in the western Himalaya have high debris-load variability (Bishop *et al.* 1995, 1998*a*, *b*), and those on Nanga Parbat are no exception. Furthermore, they have varying efficiencies of sediment transfer from the termini to other transport pathways, such as rivers (Shroder *et al.* 2000). In general, the glaciers on Nanga Parbat are highly efficient in sediment transfer.

Measurements of the velocity of ice, debris-load content and thickness and ice thickness were made to calculate modern rates of glacier denudation on the massif. Rates of glacier denudation were known to be *c.* 5 mm a^{-1} in the Raikot valley in the 1980s (Gardner & Jones 1993), but had declined when we repeated similar measurements, probably as a result of recent velocity reductions and debris removal by catastrophic breakout floods (Bishop *et al.* 1998*b*; Shroder *et al.* 1998). The mean rate of denudation of the Bazhin Glacier catchment at present is *c.* 2 mm a^{-1} (L. Copland, pers. comm. 1998).

Most preliminary measured rates of glacier denudation at Nanga Parbat, thus, are thought to be < 10 mm a^{-1}, but are still sufficient to remove a great deal of rock from the massif, even in the diminished state during the late Holocene warming trends of the present. During the expanded glacial periods of the Quaternary, glacier erosion is likely to have been far greater.

Quaternary glaciation

The record of ice advance in the western Himalaya during the Quaternary (Table 2) is

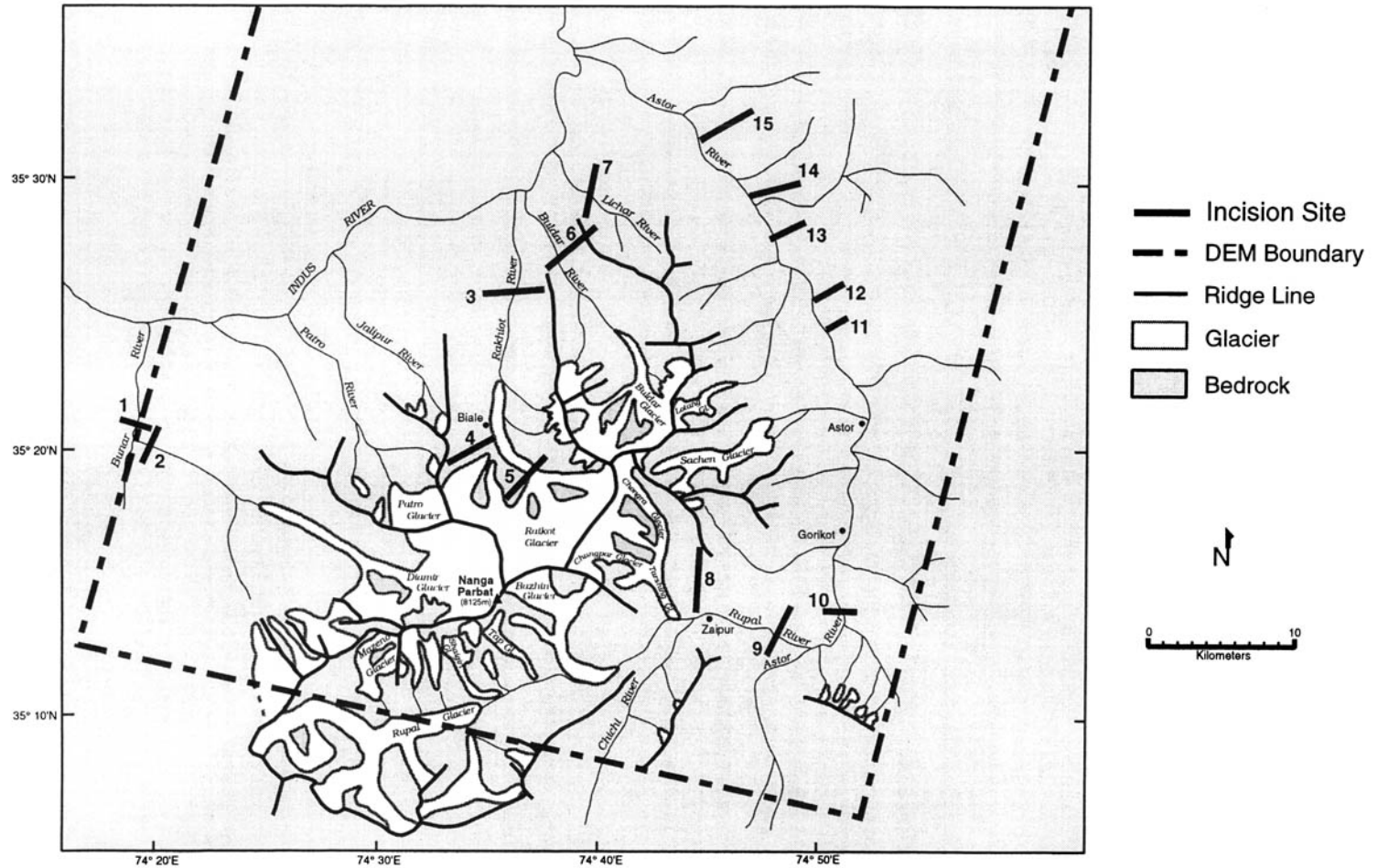

Fig. 2. Location map of glaciers and rivers discussed in text, together with location of glacial terraces and sites of measurement of incision at Nanga Parbat (Table 4).

Table 2. *Tentative glacial chronology during the Quaternary in the western Himalaya and Nanga Parbat*

Western Himalaya (Hunza, Indus)	Nanga Parbat	Time	Dating method
Holocene			
Pasu II	Modern	Twentieth century	WS, D, G
Pasu I	Little Ice Age	Several centuries ago to late nineteenth century	WS, D, G, ^{14}C
Batura	Neoglacial	Early–Middle Holocene	G, WS, ^{14}C, ^{10}Be, IRSL
Pleistocene			
Ghulkin II (Last Glaciation)	?Drang	34–38 ka	^{10}Be
Ghulkin I (Last Glaciation)	?High Moraine?	47 ka	G, TL
Borit Jheel (earliest Last Glaciation) (Late Middle Glaciation)	High Moraine	50–65 ka	G, TL, ^{3}He
Yunz	(Gorikot?)	139 ka	TL
(Early Middle Glaciation)	(Jalipur?)	*c.* 250 ka?	S
Shanoz–Bunthang (Early Glaciation)		1.1–1.25 Ma	G, S, PM

Dating methods: D, dendrochronology; G, geomorphic position; IRSL, infrared stimulated luminescence; PM, palaeomagnetic estimate; S, stratigraphic position; TL, thermoluminescence dating; WS, weathering and soil development; ^{14}C, radiocarbon dating; ^{10}Be & ^{3}He, cosmogenic nuclide dating.
Chronology terminology in the western Himalaya and Nanga Parbat is after Derbyshire *et al.* (1984), Shroder *et al.* (1993) and Derbyshire (1996). Chronology terminology for Nanga Parbat includes informal field terminology as well.

complex and ambiguous (Derbyshire *et al.* 1984; Shroder *et al.* 1989, 1993; Derbyshire 1996), but is known to be largely asynchronous to the standard chronologies of the Northern Hemisphere (Gillespie and Molnar 1995). Near Nanga Parbat, the Jalipur Formation deep in the Indus Gorge is a glacial tillite of mafic-rich rocks derived from the Kohistan volcanic island arc rocks that were stripped from the rising mountain (Shroder *et al.* 1989), perhaps 250 ka ago. The ongoing problem of the age of the Jalipur Formation (Shroder *et al.* 1993; E. Derbyshire, pers. comm. 1999) is compounded by evidence of considerable age, as well as alternate interpretations of youth. On the one hand, the unit occurs in disconformable contact beneath apparent Yunz-age tills at the mouth of Bunar Gah, is subject to severe tectonic deformation, and is lithified to tillite, sandstone and conglomerate. On the other hand, the unit has purported glaciotectonic deformation (Shroder *et al.* 1993) and has young luminescence dates (E. Derbyshire, pers. comm. 1999). Part of this controversy may be the result of mismapping or miscorrelation of Jalipur for much younger material, and part may be related to misidentification of tectonic v. lodgement pressures. Only thorough remapping and dating of deposits of clear Jalipur affinity are likely to solve this problem.

The Yunz glaciation at *c.* 150–140 ka brought major ice from Hunza to join with ice from Nanga Parbat to pass down the Indus Gorge to its furthest advance. The Gorikot glacial deposits (Fig. 3) in the Astor valley may correlate with the Yunz, although they could be equivalent to the High Moraine of Borit Jheel age (Table 2).

A strong and asynchronous, monsoon-driven glaciation 57–34 ka ago at Nanga Parbat (W. Phillips, pers. comm. 1998) was as much as eight times wider in the Raikot valley and much thicker than the ice of the present day. The north face of the mountain was ice covered up to an altitude of *c.* 5000 m, and an ice fall filled the gorge of the Indus River at the mountain foot to a depth of at least 3 km (Figs 4 & 5). This must have blocked the Indus River for a time, and has been noted as the most likely source of the Punjab erratics, carried from the mountain by icebergs in catastrophic breakout floods (Shroder *et al.* 1989). Ice from the Rupal and Astor rivers was similarly massive and the source of floods as well (Fig. 6). During the last glacial maximum of the standard Northern Hemisphere chronology, the glaciers of Nanga Parbat were also developed but were precipitation limited and so could not advance greatly. As the southwest Asian monsoon intensified, and became warmer and wetter in the lower altitudes, enhanced snowfall in the higher elevations on the mountain caused glaciers to advance between 8.4 and 5 ka ago in the early to middle Holocene (W. Phillips, pers. comm. 1998; Fig. 6).

The major glaciations, in concert with the associated processes of mass movement and running water on the mountain in the late Quaternary, eroded large masses of rock from the massif and caused major alteration of the landscape. Geomorphometric analysis has

Fig. 3. View looking south in the Gorikot region of the middle Astor valley, with intermediate-level, lithified Gorikot till in the left foreground and central middle ground. Five arrows left to right: (1) middle-level kame terrace has ablation valley lake deposits dated at 34.17 ± 4.74 IRSL ka (H. Rendell, pers. comm. 1998); (2) lower level kame terrace has lake deposits dated at 6.64 ± 0.86 IRSL ka (H. Rendell, pers. comm. 1998); (3) modern Astor River trench which has been diverted east and incised downward from its palaeovalley directly to the west; (4) right valley wall of palaeo-Astor valley; and (5) high-level, till infilling of palaeo-Astor valley that is of either Yunz or Borit Jheel equivalency (Table 2).

Fig. 4. High glacial terrace of Bezar Gali on the west side of the lower Raikot valley (Location #3, Table 4). The terrace bottom lies between 4000 and 3700 m altitude and the glacially eroded side wall extends up to *c.* 4225 m. This terrace is matched by another at *c.* 3800 m on the east side of Raikot valley on the ridge above both sides of the adjacent Buldar valley (Fig. 5).

Fig. 5. Foreshortened telephoto view of glacial rock-cut and depositional moraine terraces on the east side of Raikot valley (right arrow) and Buldar valley (centre arrow). These terraces correlate in altitude on the opposite side of the Raikot valley, with the Bezar Gali terrace, dated at *c.* 55 ka. Astor valley occurs in the background.

Fig. 6. View to the west up the middle Rupal valley on the right and the Chhichi valley on the left from atop the Rupal Kamm ridge between them. This ridge was entirely overtopped by confluent glaciers from both valleys, probably at *c.* 55 ka. The dark, vegetated terraces in the Rupal valley to the right are till and outwash of Early to Middle Holocene age. Arrow indicates ice portal of Rupal River that has been periodically blocked by the Bazhin glacier above it to produce catastrophic floods downstream. Light-coloured sand deposits occurring in the Rupal valley on the lower right are deltas that were caused in the 1850s by several damming events of the Chungpar glacier out of the picture to the right.

demonstrated removal of significant mass from the mountain and confirms ideas of complex erosion dynamics, leading to differential denudation of the massif (Bishop & Shroder 2000).

Rivers

Brookfield (1998) has discussed river capture in the fault-bounded syntaxial bends at the east and west ends of the Himalayan chain, and has noted that the development of the Indus is related to the river capture of deformed, originally westward-flowing streams whose truncated remnants now lie in Afghanistan. In this model of topographic evolution at Nanga Parbat, the pronounced change in direction of the Indus River across the massif (Fig. 1) is an elbow of capture reflecting stream piracy by an ancestral drainage that allowed the Indus to divert south across the Kohistan–Ladakh island arc and thereby force the uplift of the massif because of rapid surficial unloading (Table 1).

The Rupal–Astor River system flows across the entire Nanga Parbat massif to be tributary to the Indus master drainage of the area. The Rupal and Indus rivers are essentially parallel to the northeastward-trending antiform of the mountain, and together with the massif-crossing Astor River, seem to reflect the original superposition of drainage down upon the rising massif from the overlying cover of the Kohistan–Ladakh island arc rocks. In terms of temporal evolution, the combination of past superimposition of drainage through cover rocks onto buried structures, together with present-day antecedence of drainage upon actively rising structures, forms the main drainages thought to be causative of the active tectonics (Zeitler *et al.* 1993; Schneider *et al.* 1999). The other smaller valleys of the massif are generally transverse to the antiform of the massif and formed the main axes of later glacial and fluvial erosion and transport.

Fluvial transport of sediment at Nanga Parbat was significant in the glacier meltwater streams that were measured and analysed by K. Cornwell, R. Marston and D. Norsby (pers. comms. 1998, 1999). Annual export of solid fluvial sediment and storage (total valley fill and storage in the active floodplain) was calculated for the Rupal drainage on the south side of the massif and the Buldar and Raikot drainages on the north (Table 3). Field assessment of 23 sites included measurements of channel and valley cross-sections, pebble counts, velocity measurements, suspended sediment load and morphometric measures. Data were analysed using software for steep, high-elevation streams, and flow duration and sediment data rating curves were compiled.

Rates of denudation in the Indus River basin are known to be exceptionally high at *c.* 1 mm a^{-1} (Hewitt 1972). Similarly, the rate of denudation for the large Hunza River basin in the western Himalaya is *c.* 1.8 mm a^{-1} (Ferguson 1984), but the values of mean annual fluvial sediment discharge or denudation equivalent at Nanga Parbat exceed those previously reported. For example, the mean rate of denudation that was calculated for the Rupal River was 25 mm a^{-1} and 7 mm a^{-1} for both the Buldar and Raikot Rivers (Table 3). Nevertheless, these rates must be recognized as highly variable spatially and temporally because of sample bias caused by: (1) remobilization of stored sediment; (2) high-discharge summer meltwater measurements; (3) low frequency flood flushing, and other factors. In comparison, Burbank *et al.* (1996) used three rock exposure dates to assess incision of bedrock by the Indus River across the Nanga Parbat massif at 2–12 mm a^{-1}. Nevertheless, in spite of some measurement variance, the overall

Table 3. *Fluvial data collected at Nanga Parbat in summer 1996 and 1997 and analysed using US Corps of Engineers WinXSPRO program (M. Teal, West Consultants) for high altitude, steep mountain streams*

	Rupal River	Raikot River	Buldar River
Drainage basin area (km^2)	315	299	212
Stream length from glacier terminus to outlet (km)	27.8	13.2	11.9
Mean annual sediment discharge at river outlet ($m^3\ a^{-1}$)	8×10^6	2.07×10^6	1.47×10^6
Total valley fill between glacier terminus and basin outlet (m^3)	n/a	2.17×10^6	1.57×10^6
Total floodplain sediment storage (m^3)	2.52×10^6	8.18×10^5	7.39×10^5
Mean residence time of floodplain-stored sediment (hours)	5	0.5	1
Mean denudation rate (mm a^{-1})	25	7	7

rates of fluvial erosion of the massif appear exceptionally high.

Catastrophic floods

The capacity of floods to transport sediment is large compared to all other processes. Costa (1983) has noted that a consequence of large floods in small basins is enormous channel erosion of as much as 1000–3000 times average annual sediment yield. Sediment concentrations of *c.* 20–40% by weight were estimated by Lord & Kehew (1987) as typical of hyperconcentrated sediment flows bursting out of ice-dammed lakes. The formation and failure of natural dams produced by ice, slope failures and moraines is now well known (Baker 1973; Costa & Schuster 1988), and records of such events in the Himalaya are profuse (Hewitt 1968; Shroder *et al.* 1998). The mobilization of sediment under such conditions where glaciers and landslides so commonly block rivers is exceptionally large because of the built-in feedback mechanism in which the larger the blockage, the larger is the resulting flood. Hewitt (1968), Shroder (1998) and Cornwell (1998) summarized the work by others on the massive volumes of catastrophic flood sediment from breaking of dams in the upper Indus watershed, and concluded that the process accounts for a considerable portion of the denudation of the western Himalaya in Quaternary time.

At Nanga Parbat, evidence for catastrophic flood flushing of sediment occurs throughout the massif (Shroder *et al.* 1998). Floods from within glaciers include the 1995 Shaigiri glacier event, the 1994 Raikot glacier flood, and the Sachen glacier flood of the 1920s. Floods known from cross-valley glacier dams occurred at Tarshing 1850–1 and 1856, the multiple Bazhin glacier floods in antiquity (Fig. 6), and the past and present-day blockages by the Tap glacier moraine. Slope failure dam-induced floods include the huge 1840–1 event on the Indus, as well as the Biale debris-avalanche floods in the Raikot valley, and the high flows at the mouth of the Astor River that have removed much of the Doian and Mushkin slope failures.

Glacial terraces

Numerous erosional (rock-cut) glacial terraces covered by thin deposits occur on all sides of Nanga Parbat, between about 4000 and 5000 m altitude. These have been dated or correlated to depositional surfaces for this project (Table 2). The terraces have gone largely unnoticed before because they only occur away from the main ice-covered massif, and are at altitudes high enough to be missed by travellers in the vigorously eroding, lower valleys. The terraces represent former valley bottoms and sides, the oldest of which we dated at *c.* 55 ka, thus probably representing glaciations of Borit Jheel and Ghulkin I age (Table 2). During these times, most of the north face of Nanga Parbat (the Patro, Raikot, Buldar and Liachar areas) was completely glacier covered, with a huge icefall that cascaded down into the Indus valley below, leaving moraines in Gor on the opposite wall of the Indus Gorge (Shroder *et al.* 1989). Similarly, the Rupal–Astor valley was almost completely buried in ice, as was the Diamir valley down into the Bunar Gah drainage.

These major glaciations were most probably driven mainly by increased summer monsoon precipitation (Benn & Owen 1998), and not by temperature decrease. The result was that the higher-altitude zone of cold-based, relatively non-erosive ice presumably would not have been established at significantly lower altitudes on the massif, with the result that warm-based, erosive ice would have produced most of the terraces. Subsequent profuse deglacial meltwaters, coupled with the several reglacial events, dissected the mountain to such an extent that the high-terrace remnants are scattered widely. Nevertheless, enough terraces exist to allow reconstruction of the past high glaciations and the valley-floor gradients below.

Rates of incision

Incision and denudation are not only the result of temporally sustained, high frequency erosion processes, but are also the result of lower frequency episodic events. Magnitudes and spatial distributions of processes are also highly variable. The spatial and temporal variation of processes means that an understanding of the erosion of Nanga Parbat must take into account the initial erosional mobilization of debris, its temporary storage along valleys, and its remobilization thereafter. Only in aggregate does a reasonable view emerge of the processes of incision and denudation. The overall denudation of the Nanga Parbat massif is a spatially and temporally complex mosaic of topography produced by tectonics overprinted with the surficial processes of mass movement, glaciers, rivers and catastrophic floods, all operating at different rates, through time.

The high terraces produced by the Borit Jheel and Ghulkin I glaciations were dissected by running water and subsequent glaciations into a variety of forms (Figs 3, 4, 5 & 7). We used these

Fig. 7. High glacial terrace in sunlight at *c.* 4250 m altitude in Rupal valley between Tarshing and Bazhin glaciers. The lower portions of the snow-covered spur of Nanga Parbat (Raikot Peak, 6955 m) are visible in the upper background. The shadowed area directly below is hummocky moraine. The valley floor at *c.* 3000 m at the bottom of the photograph is moraine and outwash of Middle Holocene age.

high terraces to categorize the types of incision that they represent (Figs 9 & 10). We also dated the terraces directly with, or correlated them to, cosmogenic nuclide measurements of rock exposure, to calculate maximum rates of local valley incision at more than 15 points around the massif (Table 4). The average of these measurements is 22 ± 11 mm a^{-1}. With these rates as maximum values commonly sited near valley mouths, a rate of areal denudation calculated back upstream to the top of the watershed would obviously be less, perhaps half as much. Nevertheless, the past denudation at Nanga Parbat has been extremely rapid.

Conclusion

The unroofing of the Nanga Parbat Himalaya is now understood to be a product of surfical geomorphic processes in late Quaternary time with complex feedbacks to deep lithospheric processes (Bishop *et al.* 1998*b*; Bishop & Shroder this volume; Schneider *et al.* 1999). Reasonable convergence between our independent datasets (mass movement, glacial, fluvial, hypsometry, incision, etc.) has led to results that are internally adequate, externally consistent and not unlike the independent work of others on surface processes and bedrock character. These results and other work (Zeitler *et al.* 1993) indicate that denudation at Nanga Parbat is not overrated (Whittington 1996), because surface processes efficiently erode and transport sediment away from the massif. Nevertheless, when we consider the unroofing of the Nanga Parbat Himalaya, we must especially note the extremely differential nature of incision and denudation. An unfortunate tendency of some workers unfamiliar with the highly variable nature of erosion is to assume that our measurements of modern process rates are sustainable over periods of 10^5 a. Furthermore, the evidence indicates that Nanga Parbat is a pre-steady-state mountain massif (Hovius *et al.* 1998) in which the fluctuating and differential, micro- and meso-scale dynamics of erosion that we report here are not necessarily in balance spatially or temporally with the macro-scale tectonic mass flux.

The overall differential incision and denudation that we report was largely responsible for the huge, knife-edged massif of Nanga Parbat, with the steepest relief on the planet. The formation of this great mountain was a complex of surface processes of unusual sequence and character. The initiation of mountain uplift began once the ancestral Indus, which originally flowed north of the Kohistan–Ladakh island arc in the mid-Tertiary, was captured and diverted into a steeper south-southwest tectonic depression caused by extensional delamination of the crust due to erosion during enhanced monsoonal conditions. Thereafter, the Indus and its Rupal–Astor tributary breached the island arc terrane and began to cut down rapidly, eventually becoming deep superposed-antecedent trenches across the massif. The profound local erosion initiated the spatially restricted uplift that, once begun, was further reinforced in a positive feedback. Once uplift had carried tectonic- and frost-shattered rock high enough into the permafrost zone (>5000 m today), denudation by mass-movement would have decreased because rock strength increased through freezing of joints and protection by covering, cold-based ice, frozen to its bed. Where incision was most concentrated in the lower altitude areas of erosion by warm-based glaciers, rivers and catastrophic floods, the valleys grew ever deeper as the mountain rose higher. Ridges tended to increase in steepness and relief as the

Fig. 8. View to the south of the Raikot glacier terminus in July 1997. The steep terminus was the result of renewed advance, apparently begun in 1994 when the subglacial drainage was blocked and finally burst out of four new portals that removed considerable morainal debris along the front and west side. The absence of significant moraine at the terminus is a reflection of the high transfer efficiency of sediment from this glacier to its meltwater. The dashed line in the background shows the most likely configuration of the valley bottom of *c.* 55 ka. Rock-cut terraces and valley sidewalls on either side, together with the central bedrock remnant of the 'Grosse Moraine' define the pre-existing valley that was subsequently incised. The Fairy Meadow moraine in right foreground is Early to Middle Holocene in age.

Fig. 9. High glacial terraces (arrows) on the east side of the Astor River valley. From right to left the terraces are Gare North #12, Dichil South #13, and Salibur #14 (Table 4 and Fig. 6). These terraces are respectively, *c.* 770 m, *c.* 1250 m and *c.* 1750 m above the valley floor. The photo was taken from the left (NW) flank of the Mushkin slope failure, looking upstream.

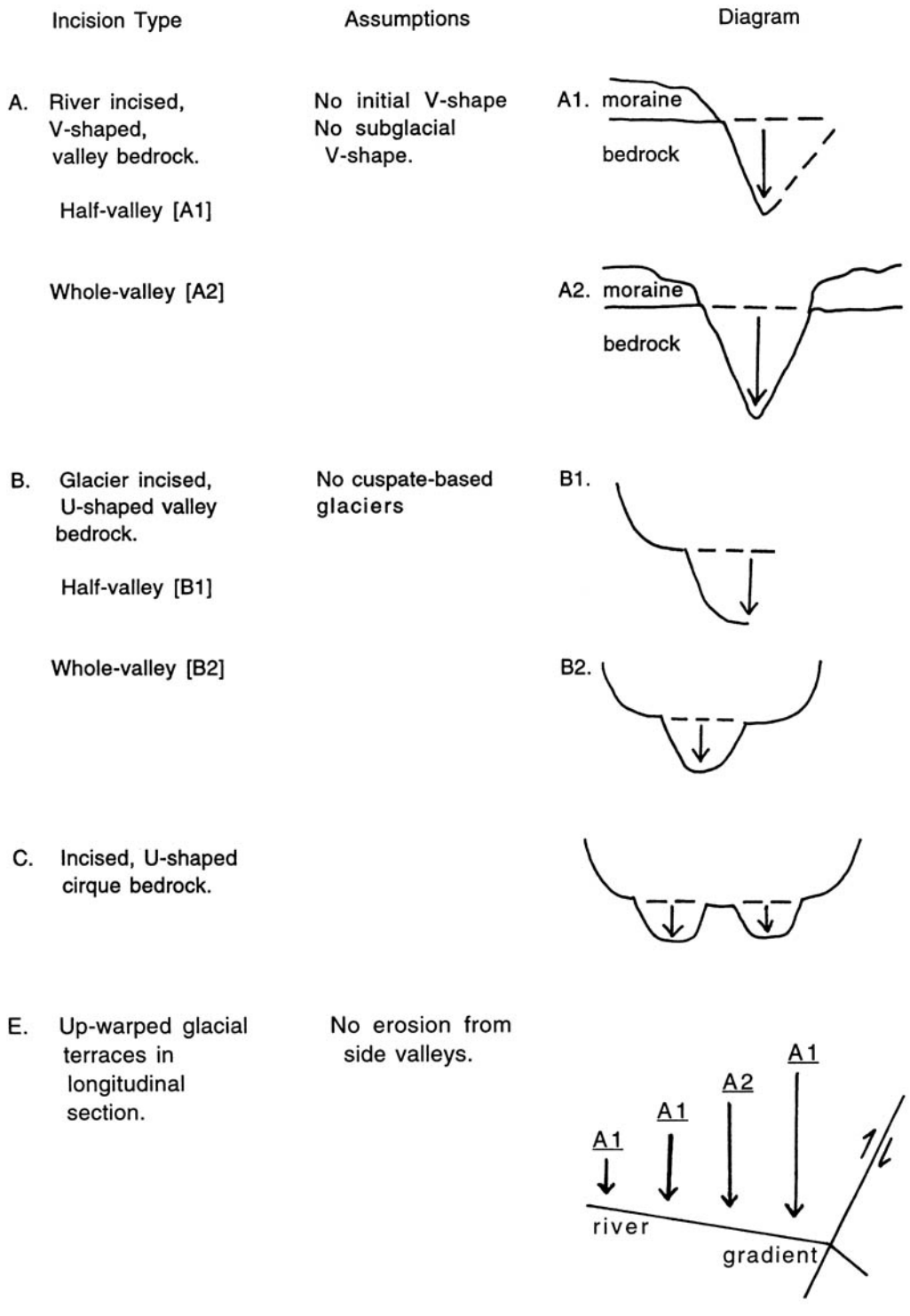

Fig. 10. Types of incision at Nanga Parbat used to calculate the rates of incision listed in Table 4.

Table 4. *Rates of incision at Nanga Parbat calculated from glaciated terraces (Fig. 10) and dated with cosmogenic nuclides or correlated by geomorphic position*

Location	Incision type	Period measured (ka)	Rate (mm a^{-1})
1. Bunar–Diamir	A1	8.5	24
2. Lower Diamir	A2	55	16
3. Bezar Gali	A2	46.5	20
4. Ganalo Ridge	B1	55	14
5. Great 'moraine'	C	55	16
6. Buldar	A2	55	20
7. Liachar	A2	55	15
8. Tarshing	B2	55	21
9. Lower Rupal	B2	55	7
10. Bulashbar Astor	A1	38	15
11. Gare (S) Astor	A1	55	13
12. Gare (N) Astor	A1	55	23
13. Dichil (S) Astor	A1	55	32
14. Salibur Astor	A1	55	39
15. Burdish Astor	A1	55	52
			22 ± 11

Location numbers are plotted in Fig. 2.

valleys deepened between them (Derbyshire 1996). The highly differential, spatial and temporal denudation by surface processes has, thus, been responsible for the unroofing of the Nanga Parbat Himalaya, while at the same time producing the spectacular relief. Prior findings of relations between tectonics and denudation that were suggested by the rock record (Zeitler 1985; Zeitler *et al.* 1993) are supported by the work described here.

Sincere thanks are extended to the large number of people who contributed directly or indirectly to this project. This paper was reviewed by Edward Derbyshire and John Vitek, whom we greatly thank, but the authors are solely responsible for the data and conclusions expressed here. Researchers who provided valuable data and insights are J. Blum, K. Cornwell, J. Harbor, P. Koons, R. Marston, H. Rendell, L. Seeber, J. Poths, J. Quade and P. Zeitler. Students who contributed to a greater or lesser extent are L. Copland, A. Elmore, M. Jacobs, A. Jacobson, P. Nieland, D. Norsby, W. Phillips, R. Scheppy, A. Schmidt and V. Sloan. Karim and Shakheel of Hunza were our most superb guides and general camp commanders, Dalheeb assisted, and Ali provided his always excellent food. This research was a product of funding from the US National Science Foundation grant EAR-9418839.

References

ANDREWS-SPEED, C. P. & BROOKFIELD, M. E. 1982. Middle Palaeozoic to Cenozoic geology and tectonic evolution of the northwestern Himalaya. *Tectonophysics*, **82**, 253–275.

BAKER, V. R. 1973. *Paleohydrology and sedimentology of Lake Missoula flooding in eastern Washington*. Geological Society America Special Papers, **144**.

BENN, D. I. & OWEN, L. A. 1998. The role of the Indian summer monsoon and the mid-latitude westerlies in Himalayan glaciation: review and speculative discussion. *Journal of the Geological Society, London*, **155**, 353–363.

BISHOP, M. P. & SHRODER, J. F. JR. 2000. Remote sensing and geomorphometric assessment of topographic complexity and erosion dynamics in the Nanga Parbat massif. *This volume*.

——, —— & WARD, J. L. 1995. SPOT multispectral analysis for producing supraglacial debris-load estimates for Batura Glacier. *Geocarto International*, **10**, 81–90.

——, ——, HICKMAN, B. L. & COPLAND, L. 1998*a*. Scale-dependent analysis of satellite imagery for characterization of glacier surfaces in the Karakoram Himalaya. *Geomorphology*, **21**, 217–232.

——, ——, SLOAN, V. F., COPLAND, L. & COLBY, J. D. 1998*b*. Remote sensing and GIS technology for studying lithospheric processes in a mountain environment. *Geocarto International*, **13**, 75–87.

BROOKFIELD, M. E. 1998. The evolution of the great river systems of southern Asia during the Cenozoic India–Asia collision: rivers draining southwards. *Geomorphology*, **22**, 285–312.

BURBANK, D. W., LELAND, J., FIELDING, E., ANDERSON, R. S., BROZOVIC, N. *et al.* 1996. Bedrock incision, rock uplift and threshold hillslopes in the northwestern Himalayas. *Nature*, **379**, 505–510.

CERVENY, P. F., NAESER, N. D., ZEITLER, P. K., NAESER, C. W. & JOHNSON, N. M. 1988. History of uplift and relief of the Himalaya during the past 18 million years: Evidence from fission-track ages of detrital zircons from sandstones of the Siwalik Group. *In*: KLEINSPEHN, K. L. & PAOLA,

C. (eds) *New Perspectives in Basin Analysis*. Springer-Verlag, Berlin, 43–61.

——, JOHNSON, N. M., TAHIRKHELI, R. A. K. & BONIS, N. R. 1989. Tectonic and geomorphic implications of Siwalik Group heavy minerals, Potwar Plateau, Pakistan. *In*: MALINCONICO, L. L. & LILLIE, R. J. (eds) *Tectonics of the Western Himalayas*. Geological Society of America Special Papers, **232**, 129–136.

CORNWELL, K. 1998. Quaternary break-out flood sediments in the Peshawar basin of northern Pakistan. *Geomorphology*, **25**, 225–248.

COSTA, J. E. 1983. Paleohydraulic reconstruction of flash-flood peaks from boulder deposits in the Colorado front range. *Geological Society of America Bulletin*, **94**, 986–1004.

—— & SCHUSTER, R. L. 1988. The formation and failure of natural dams. *Geological Society of America Bulletin*, **94**, 986–1004.

DERBYSHIRE, E. 1996. Quaternary glacial sediments, glaciation style, climate and uplift in the Karakoram and northwest Himalaya: review and speculations. *Palaeogeography, Palaeoclimatology, Palaeoecology*, **120**, 147–157.

——, LI, J., PERROTT, F. A., XU, S. & WATERS, R. S. 1984. Quaternary glacial history of the Hunza Valley, Karakoram mountains, Pakistan. *In*: MILLER, K. J. (ed.) *The International Karakoram Project*, **2**, 456–495.

DERRY, A. & FRANCE-LANORD, C. 1997. Himalayan weathering and erosion fluxes: Climate and tectonic controls. *In*: RUDDIMAN, W. F. (ed.) *Tectonic Uplift and Climate Change*. Plenum Press, 290–313.

EDWARDS, M. A. 1998. *Examples of tectonic mechanisms for local contraction and exhumation at the leading edge of India, southern Tibet and Nanga Parbat, Pakistan*. PhD dissertation, State University of New York at Albany.

FERGUSON, R. I. 1984. Sediment load of the Hunza river. *In*: MILLER, K. J. (ed.) *The International Karakoram Project*, **2**, 581–598.

GARDNER, J. S. & JONES, N. K. 1993. Sediment transport and yield at the Raikot Glacier, Nanga Parbat, Punjab Himalaya. *In*: SHRODER, J. F. JR. (ed.) *Himalaya to the Sea. Geology, Geomorphology, and the Quaternary*. Routledge, 184–197.

GILLESPIE, A. & MOLNAR, P. 1995. Asynchronous maximum advances of mountain and continental glaciers. *Reviews of Geophysics*, **33**, 311–364.

GOUDIE, A., BRUNSDEN, D., COLLINS, D. N., DERBYSHIRE, E., FERGUSON, R. I. *et al.* 1984. The geomorphology of the Hunza Valley, Karakoram mountains, Pakistan. *In*: MILLER, K. J. (ed.) *The International Karakoram Project*, **2**, 359–410.

HARRISON, T. M., COPELAND, P., KIDD, W. S. F. & LOVERA, O. M. 1995. Activation of the Nyainquentanghla shear zone: Implications for uplift of the southern Tibetan Plateau. *Tectonics*, **14**, 658–676.

HEWITT, K. 1968. Records of natural damming and related events in the upper Indus basin. *Indus*, **10**, 11–19.

—— 1972. The mountain environment and gepmorphic processes. *In*: SLAYMAKER, H. O. & MCPHERSON, H. J. (eds) *Mountain Geomorphology: Geomorphological Processes in the Canadian Cordillera*. Tantalus Research, Vancouver.

—— 1989. The altitudinal organization of Karakoram geomorphic processes and depositional environments. *Zeitschrift für Geomorphologie, Supplementeband*, **76**, 9–32.

—— 1993. Altitudinal organization of Karakoram geomorphic processes and depositional environments. *In*: SHRODER, J. F. JR. (ed.) *Himalaya to the Sea: Geology, Geomorphology, and the Quaternary*. Routledge, 159–183.

—— 1998. Catastrophic landslides and their effects on the Upper Indus streams, Karakoram Himalaya, northern Pakistan. *Geomorphology*, **26**, 47–80.

HOVIUS, N., STARK, C. P., TUTTON, M. A. & ABBOT, L. D. 1998. Landslide-driven drainage network evolution in a pre-steady-state mountain belt: Finisterre Mountains, Papua, New Guinea. *Geology*, **26**, 1071–1074.

HUBBARD, M. S., SPENCER, D. A. & WEST, D. P. 1995. Tectonic exhumation of the Nanga Parbat massif, northern Pakistan. *Earth and Planetary Science Letters*, **133**, 213–225.

JORGENSEN, D. W., HARVEY, M. D., SCHUMM, S. A. & FLAMM, L. 1993. Morphology and dynamics of the Indus River: implications for the Mohen Jo Daro site. *In*: SHRODER, J. F. JR. (ed.) *Himalaya to the Sea: Geology, Geomorphology, and the Quaternary*. Routledge, 288–326.

KICK, W. 1980. Material for a glacier inventory of the Indus drainage basin—the Nanga Parbat massif. World Glacier Inventory, Proceedings of the Reideralp Workshop, *International Association of Hydrological Sciences, Publication*, **126**, 105–109.

LORD, M. L. & KEHEW, A. E. 1987. Sedimentology and paleohydrology of glacial-lake outburst deposits in southeastern Saskatchewan and northwestern North Dakota. *Geological Society of America Bulletin*, **99**, 663–673.

PRELL, W. L. & KUTZBACH, J. E. 1997. The impact of Tibet–Himalayan elevation on the sensitivity of the monsoon climate system to changes in solar radiation. *In*: RUDDIMAN, W. F. (ed.) *Tectonic Uplift and Climate Change*. Plenum Press, 172–203.

QUADE, J., CERLING, T. E. & BOWMAN, J. R. 1989. Development of Asian monsoon revealed by marked ecological shift during the latest Miocene in northern Pakistan. *Nature*, **342**, 163–166.

QUADE, J., ROE, L., DECELLES, P. G. & OJHA, T. P. 1997. The Late Neogene $^{87}Sr/^{86}Sr$ record of lowland Himalayan rivers. *Science*, **276**, 1828–1831.

RETALLACK, G. J. 1991. *Miocene Paleosols and Ape Habitats of Pakistan and Kenya*. Oxford.

RUDDIMAN, W. F., RAYMO, M. E., PRELL, W. L. & KUTZBACH, J. E. 1997. The uplift–climate connection. *In*: RUDDIMAN, W. F. (ed.) *Tectonic Uplift and Climate Change*. Plenum Press, 471–515.

SCHNEIDER, D. A., EDWARDS, M. A., KIDD, W. S. F., KHAN, M. A., SEEBER, L. & ZEITLER, P. K. 1999. Tectonics of Nanga Parbat, western Himalaya: synkinematic plutonism within the doubly-vergent shear zones of a crustal-scale pop-up structure. *Geology*.

SEARLE, M. P. 1991. *Geology and Tectonics of the Karakoram Mountains*. Wiley.

SEARLE, M. P. & KHAN, M. A. 1995. *Geological map of north Pakistan*, Department of Earth Sciences, Oxford University.

SEEBER, L. & PÊCHER, A. 1998. Strain partitioning along the Himalayan arc and the Nanga Parbat antiform. *Geology*, **26**, 791–794.

SHRODER, J. F. JR. 1993. Himalaya to the sea: geomorphology and the Quaternary of Pakistan in the regional context. *In*: SHRODER, J. F. JR. (ed.) *Himalaya to the Sea: Geology, Geomorphology, and the Quarternary*. Routledge, London, 1–42.

—— 1998. Slope failure and denudation in the western Himalaya. *Geomorphology*, **246**, 81–105.

—— & BISHOP, M. P. 1998. Mass movement in the Himalaya: new insights and research directions. *Geomorphology*, **246**, 13–35.

——, KHAN, M. S., LAWRENCE, R. D., MADIN, I. P. & HIGGINS, S. E. 1989. Quaternary glacier chronology and neotectonics in the Himalaya of northern Pakistan. *In*: MALINCONICO, L. L. & LILLIE, R. J. (eds) *Tectonics of the Western Himalaya*. Geological Society of America Special Paper, **232**, 275–294.

——, OWEN, L. & DERBYSHIRE, E. 1993. Quaternary glaciation of the Karakoram Mountains and Nanga Parbat Himalaya. *In*: SHRODER, J. F. JR. (ed.) *Himalaya to the Sea: Geology, Geomorphology, and the Quaternary*. Routledge, London, 132–158.

——, BISHOP, M. P. & SCHEPPY, R. 1998. Catastrophic flood flushing of sediment, western Himalaya, Pakistan. *In*: KALVODA, J. & ROSENFELD, C. L. (eds) *Geomorphological Hazards in High Mountain Areas*. Kluwer Academic Publishers, 27–48.

——, SCHEPPY, R. & BISHOP, M. P. 1999. Denudation of small alpine basins, Nanga Parbat Himalaya. *Arctic, Antarctic and Alpine Research*, **31**, 99–105.

——, BISHOP, M. P., SLOAN, V. & COPLAND, L. 2000. Debris-covered glaciers and rock glaciers in the Nanga Parbat Himalaya. *Geografiska Annaler*, in press.

SMITH, H. A., CHAMBERLAIN, C. P. & ZEITLER, P. K. 1994. Timing and duration of Himalayan metamorphism within the Indian Plate, Northwest Himalaya, Pakistan. *Journal of Geology*, **102**, 493–508.

TRELOAR, P. J., REX, D. C., GUISE, P. G., COWARD, M. P., SEARLE, M. P. *et al.* 1989. K–Ar and Ar–Ar geochronology of the Himalayan collision in NW Pakistan: constraints on the timing of suturing, deformation, metamorphism and uplift. *Tectonics*, **8**, 881–909.

——, —— & WILLIAMS, M. P. 1991. The role of erosion and extension in unroofing the Indian plate thrust stack, Pakistan Himalaya. *Geological Magazine*, **128**, 465–478.

WHITTINGTON, A. G. 1996. Exhumation overrated at Nanga Parbat, northern Pakistan. *Tectonophysics*, **206**, 215–226.

ZALEHA, M. J. 1997*a*. Fluvial and lacustrine palaeoenvironments of the Miocene Siwalik Group, Khaur area, northern Pakistan. *Sedimentology*, **44**, 349–368.

—— 1997*b*. Intra- and extra-basinal controls on fluvial deposition in the Miocene Indo-Gangetic foreland basin, northern Pakistan. *Sedimentology*, **44**, 369–390.

ZEITLER, P. K. 1985. Cooling history of the NW Himalaya Pakistan. *Tectonics*, **4**, 127–151.

——, CHAMBERLAIN, C. P. & SMITH, H. A. 1993. Synchronous anatexis, metamorphism, and rapid denudation at Nanga Parbat (Pakistan Himalaya). *Geology*, **21**, 347–350.

This page intentionally left blank

Remote sensing and geomorphometric assessment of topographic complexity and erosion dynamics in the Nanga Parbat massif

M. P. BISHOP & J. F. SHRODER JR

Department of Geography and Geology, University of Nebraska at Omaha, Omaha, NE 68182, USA (e-mail: bishop@data.unomaha.edu)

Abstract: The dynamic mountains of the western Himalaya are the result of complex interactions involving tectonic, structural, lithological, climatic and surface processes. The multi-scale dynamics of surface processes in this region are largely unknown. This paper assesses the spatial complexities of the topography at Nanga Parbat, as we seek to understand erosion dynamics, differential denudation and the geodynamics of uplift and denudation. Spatial analysis of a high resolution digital elevation model and three-dimensional terrain simulations using satellite imagery indicate that the topographic complexity of Nanga Parbat is highly scale-dependent and exhibits a hierarchical order that is reflective of erosion dynamics. Observations and analyses reinforce prior understandings of rapid rates of uplift and high rates of surficial denudation. Results indicate that climate controls the topographic complexity of the massif, although a tectonic influence is present and is largely masked by the overprinting of surface processes with time. Consequently, Nanga Parbat is seen to owe its origin to erosionally induced tectonic uplift and rapid surficial denudation. Rapid uplift altered erosion dynamics and further accelerated erosion resulting in extreme relief. Nonetheless, the differential denudation resulting from erosion dynamics does not appear to be in spatial balance with the regional scale tectonic mass flux. Systematic integration of dynamic models that account for the scale-dependencies of subsurface and surface processes are required to study the nature of this complex system and explain topographic evolution.

The morphology and hypsometry (frequency distribution of altitude) of mountain environments is the result of complex interactions between tectonic, climatic and erosional processes (Masek *et al.* 1994; Avouac & Burov 1996; Pinter & Brandon 1997). Identifying and characterizing the influences of these factors on landscape evolution has been the focus of much research. Empirical and deterministic investigations provide a theoretical framework for understanding the dynamic interactions of climate and tectonics, and evidence for the significance of surface processes in affecting tectonic processes (Molnar & England 1990; Raymo & Ruddiman 1992; Montgomery 1994; Pinter & Brandon 1997; Schneider *et al.* 1999). The multi-scale coupling of tectonic processes and surface processes can produce topographic variation that reflects the geodynamics of landscape evolution (Chase 1992; Koons 1995; Gao & Xia 1996). Theoretical modelling and field investigations have demonstrated that topographic parameters are related to rates of denudation at various scales (Ahnert 1987; Milliman & Syvitski 1992; Summerfield & Hulton 1994), while others have demonstrated limits to correlations between topography and denudation (Burbank *et al.* 1996). These results may reflect the multi-scale dynamics of mountain building and topographic evolution.

Remote sensing and geomorphometric analysis of digital elevation models (DEM) can be used to investigate the complexities of mountain geomorphology and topography, and assess the multi-scale dynamics of the coupling of tectonic and surface processes on landscape evolution (Chase 1992; Lifton & Chase 1992; Koons 1995; McDermid & Franklin 1995; Bishop *et al.* 1988*a*, 1998*b*, 1999). Consequently, investigators have attempted to link geological processes with topographic form to explain topographic complexity and mountain evolution (Montgomery 1994; Schmidt & Montgomery 1995; Burbank *et al.* 1996; Fielding 1996; Brozovik *et al.* 1997). This approach can be complicated by the fact that landform-generating processes operate over a wide range of spatial and temporal scales (Molnar & England 1990; Raymo & Ruddiman 1992), and that topographic and landscape characteristics may not

From: KHAN, M. A., TRELOAR, P. J., SEARLE, M. P. & JAN, M. Q. (eds) *Tectonics of the Nanga Parbat Syntaxis and the Western Himalaya*. Geological Society, London, Special Publications, **170**, 181–200. 1-86239-061-4/00/$15.00

be diagnostic of a particular process (Shroder & Bishop 1998). Research has demonstrated, however, that functional relationships between topography and erosion do exist that are compatible with physical processes and modelling efforts (Koons 1995).

In the western Himalaya, few quantitative remote sensing and geomorphometric studies have been designed to examine and quantify erosion dynamics and the spatial complexity of the landscape (Bishop *et al.* 1995, 1998*a*). Currently, little is known about the scale-dependent nature of erosion dynamics (Shroder & Bishop 1998), and spatial analysis and modelling using DEM and satellite multispectral imagery is required (Bishop *et al.* 1998*b*, 1999).

The Nanga Parbat massif in Pakistan represents an excellent location to study the geodynamics of mountain building, where rapid uplift and denudation produce extreme relief (Burbank *et al.* 1996; Shroder & Bishop this volume; Schneider *et al.* 1999). Different ideas about topographic complexity and evolution have emerged regarding dominant surface processes (Burbank *et al.* 1996; Brozovic *et al.* 1997; Shroder *et al.* 1998), tectonic denudation (Searle 1991; Searle & Khan 1995), magnitude and significance of denudation (Whittington 1996), and rates of erosion and uplift (Harbor & Warburton 1992, 1993; Gilchrist *et al.* 1994; Harrison 1994). Furthermore, the spatial variability of erosion processes are fundamental to understanding the influence of climate on uplift (Montgomery 1994), although this information is notoriously difficult to obtain. Obviously, the multi-scale geodynamics of this system require further investigation. For example, erosion dynamics at Nanga Parbat have not been adequately characterized and associated with topographic parameters so that the anisotropic nature of the topography can be understood. Furthermore, denudation and uplift coupling could be related such that the highest erosion rates are spatially correlated to high rates of uplift. Therefore, investigations involving scale-dependent analysis of topography may provide new insights and a conceptual framework to link physical models in studying the geodynamics at Nanga Parbat.

The purpose of this paper is to report on our initial assessment of the topographic complexities of Nanga Parbat, as we seek to understand differential denudation and the dynamic relationships between uplift and denudation. Specifically, our objectives are to identify the complex spatial nature of erosional processes, and relate topographic characteristics to erosion dynamics. This is necessary in order that functional relationships can be established between physical processes and relief characteristics for modelling purposes.

Background

Scientists have been interested in the western Himalaya because of its extreme topography, complex tectonics and active geological processes. Nanga Parbat mountain (Fig. 1) has been recognized as unusual in terms of extreme relief and modern surficial denudation rates, and in terms of long-term denudation rates based upon radiometric cooling ages, rock ages and metamorphic and structural characteristics (Zeitler & Chamberlain 1991; Gardner & Jones 1993; Zeitler *et al.* 1993; Burbank *et al.* 1996; Bishop *et al.* 1998*b*; Park & Mackie 1998; Seeber & Pecher 1998; Shroder & Bishop 1998; Schneider *et al.* 1999). These observations suggest complex feedback dynamics between denudational unloading, metamorphism and surface uplift (Schneider *et al.* 1999). Consequently, scientists are developing a comprehensive geophysical and geological database to characterize and model the geodynamics of the system to better understand the relationships between tectonics and erosion.

Zeitler (1985) first described extremely young fission tracks and $^{40}Ar/^{39}Ar$ cooling ages from the rocks of Nanga Parbat that indicated rapid rates of exhumation. Gardner & Jones (1993) calculated rates of glacial denudation of 4–6 mm a^{-1} for the Raikot glacier on the north side of Nanga Parbat. Burbank *et al.* (1996) used exposure-age dating of strath terraces with cosmogenic ^{10}Be and ^{26}Al to calculate incision rates for the Indus River where it cuts across the Nanga Parbat massif to be 2–12 mm a^{-1}. Other studies identified the dominant surface processes and estimated the magnitude of incision and denudation for selected areas (Shroder 1998; Shroder *et al.* 1998, 1999, 2000). These contributions, and much other work uncited here, have documented the active geological processes at Nanga Parbat. This work has enabled the development of a simplistic conceptual model of the dominant surface processes which includes river incision and slope failure, glaciation, fluvial transport of sediment and catastrophic flooding. Erosion dynamics, however, have not been adequately characterized or linked to the topography of the massif (Bishop *et al.* 1998*b*).

The topographic complexity of the Nanga Parbat massif contains information about erosion dynamics and the geodynamics of the system. Burbank *et al.* (1996) and Brozovic *et al.* (1997) conducted the first significant

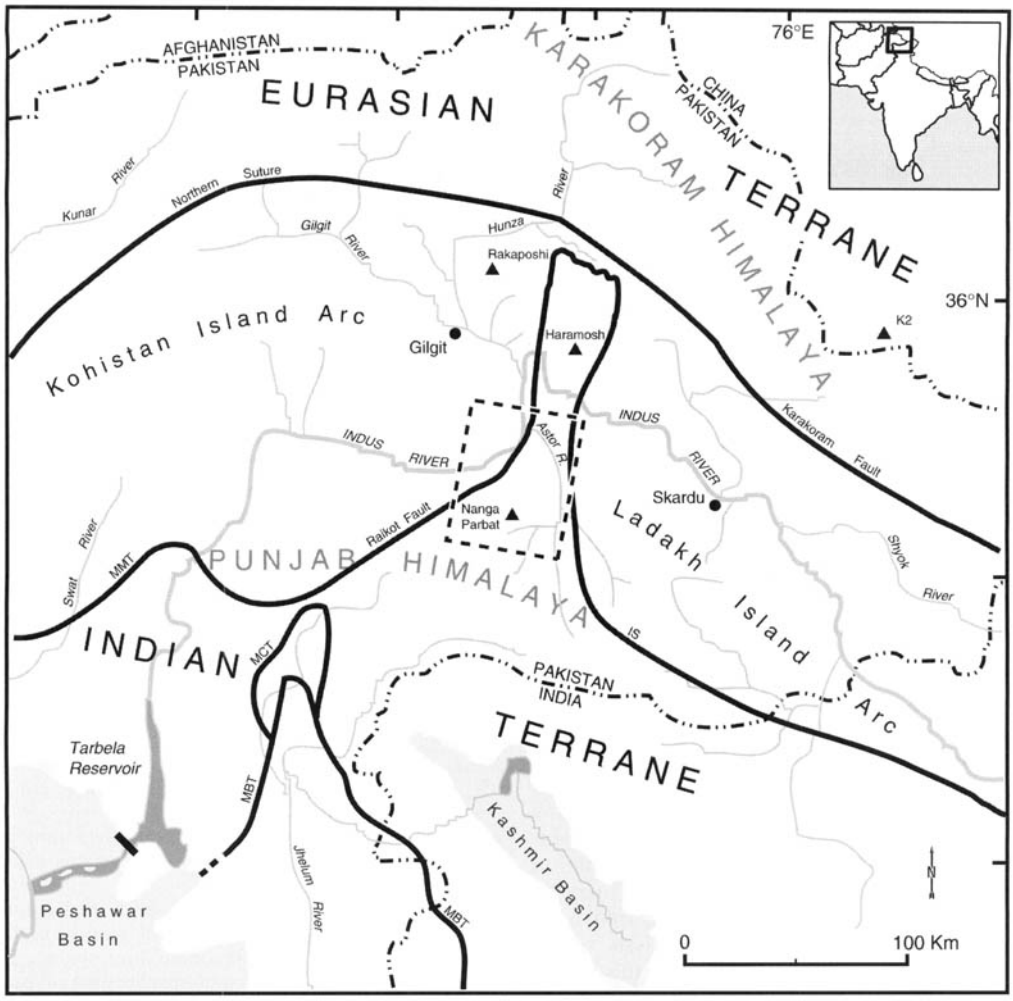

Fig. 1. Location map of Nanga Parbat in Pakistan. The dashed rectangle shows satellite imagery and digital elevation model coverage. MMT, Main Mantle Thrust; MBT, Main Boundary Thrust.

geomorphometric analyses of Nanga Parbat using a DEM with 3 arcsecond (*c.* 90 m) grid spacing. Burbank *et al.* (1996) used slope analysis to determine if slope angles were correlated to rates of denudation along the Indus River. They concluded that there was not a hillslope response to accelerated denudation above a high threshold and that landsliding is the dominant denudational process. Furthermore, they indicated that topographic characteristics are largely independent of denudation variations in the landscape. Brozovic *et al.* (1997) found a correlation between slope angles and the extent of glaciation. They concluded that glacial and periglacial processes place an upper limit on altitude, relief and the development of topography, regardless of the rate of tectonic processes operating. This work provided new insight into the erosion dynamics at Nanga Parbat and resulted in the development of conceptual models of topographic evolution. With the advent of new satellite sensors specifically designed to obtain imagery for DEM generation, scientists should be able to test these models at a variety of scales and further characterize the topography. It is important to note that the scale of characterizing topographic parameters, type of geomorphometric analysis and spatial-analysis design will determine what information can be extracted from a DEM (Shroder & Bishop 1998).

Field work, laboratory results and traditional geomorphometric analyses have led to the

development of numerous conceptual models regarding erosion dynamics and topography, and the topographic evolution of the massif, beyond the work of Burbank *et al.* (1996) and Brozovic *et al.* (1997). We now know that the Nanga Parbat massif is a northeast striking antiform which is the structural and topographic expression of arc-parallel Himalayan shortening (Seeber & Pêcher 1998). The great relief is associated with high unroofing rates (*c.* 5 mm a^{-1}) as documented at several timescales by geomorphic, petrological and fluid inclusion investigations (Schneider *et al.* in press). Geophysical and petrological data indicate that there is rapid advection of material into the centre of the massif (Schneider *et al.* in press). There is little evidence of tectonic denudation (Shroder & Bishop this volume), and the magnitude of surface processes has been found to be among the highest in the world (Burbank *et al.* 1996; Shroder & Bishop this volume). Therefore, surface denudation is capable of removing significant mass from the massif. It is not yet clear what effect the spatial-erosion dynamics have had on the rapid advection of material into the massif or upon the uplift velocity vectors. As expected, our preliminary geomorphometric analyses indicate that strong relationships occur between topographic variability and surface processes. Furthermore, there appears to be a structural fabric in the topography that is anisotropic. It is possible that differential uplift could be related to the erosion dynamics and differential denudation, such that the highest erosion rates may be spatially correlated with the most rapid uplift rates. Scale-dependent spatial analysis of the topography is required to investigate this possibility and identify and characterize the anisotropic nature of the topography. This represents a first step towards understanding topographic complexity resulting from the coupling of tectonics and surface processes. Analysis of scale dependency may also provide new insights and a conceptual framework for effective linkage of process models for studying the geodynamics of topographic evolution and mountain building.

Methods

SPOT panchromatic and multispectral imagery were acquired on 9 June 1996. A SPOT panchromatic stereo-pair was acquired on 27 and 28 October 1996. A DEM was generated using the imagery and the stereo-autocorrelation method (Bishop *et al.* 1998*b*). Spectral saturation was not a problem and good correlations were obtained at high altitudes. Topographic map coverage was used to construct the topography at the summit of Nanga Parbat where spectral saturation did occur. This area was extremely small and represents an insignificant area with respect to mapping and analysis. A large sample of global and local control points from topographic maps of the region were used to ensure quality control. Separate control points were used to determine accuracy. The resolution is 20 m with an absolute vertical accuracy of ± 8–12 m. The DEM covers a radius of *c.* 30 km centred over Chongra Peak on the Nanga Parbat massif (Fig. 1).

We conducted a variety of geomorphometric analyses using the DEM. Swath profile analysis was performed using the entire DEM to characterize the regional relief conditions, whereas basin hypsometric analysis provided information about the distribution of land mass volume. Slope angles, slope aspect and slope curvature were also analysed to determine if unique terrain characteristics were associated with erosion dynamics and rapid denudation. In an attempt to further characterize topographic complexity with erosion dynamics, we conducted semivariogram and fractal analysis using the methodology of Bishop *et al.* (1998*a*). Specifically, semivariogram functions were produced and subsequent fractal analysis was used to demonstrate the differences in topographic variability related to erosion dynamics. The transect sampling method was used to generate the semivariogram as follows:

$$\bar{S}^2(h) = \frac{1}{2} m \sum_{i=1}^{m} (\beta_i - \beta_{i+h})^2. \quad (1)$$

$\bar{S}^2$ is an unbiased estimate of the average semivariance $\gamma(h)$ (Curran, 1988), where β is a topographic parameter (i.e. slope angle), h represents the sampling lag distance, and m is the number of sampled pairs per lag.

Satellite imagery was radiometrically calibrated and various ratio images generated to reduce beam irradiance variations (i.e. shadows) over the scene. Original spectral band and ratio images were draped over the DEM to produce several three-dimensional perspectives of the Nanga Parbat massif. A Silicon Graphics Inc. ONYX 2 multiprocessor system with an infinite reality graphics engine and virtual reality capabilities enabled us to simulate flying through the landscape to study it from different perspectives. This allowed us to examine areas that we could not go to in the field and relate satellite information to our field data and ground photography. This was extremely valuable, as we discovered elevated lake beds, flood deposits and accordant summit ridges on the landscape. This information was related to geomorphometric parameters and characteristics of the topography.

The significance of this methodology is that satellite information and topographic parameters can be viewed in three dimensions and at various scales. Such terrain simulations provide valuable information that cannot be easily obtained from the field. Specifically, spatial and contextual information about the topography and landscape can be derived to study the spatial variability of erosion dynamics in lithologically and structurally complex mountains.

Nanga Parbat morphology

Satellite imagery (Fig. 2) and virtual reality 'flyby' simulations around Nanga Parbat provide unique perspectives of the morphology and topographic complexity of the massif. Figure 3 includes four different azimuth view directions of the massif that highlight geomorphic features at various scales. The most significant features of the landscape in terms of topographic evolution are the major river systems that transport significant amounts of sediment (Indus, Astor and Rupal rivers). The Rupal River, on the south side, flows into the Astor which cuts through the massif to the north and empties into the Indus (Fig. 3a). The Indus River flows along the north and west sides of Nanga Parbat and is responsible for ultimately removing large quantities of sediment from lower-order rivers and streams (Fig. 3b). Burbank *et al.* (1996) estimated Indus incision rates just north of Nanga Parbat to be 2–12 mm a^{-1}. Glacier- and river-dominated valleys of Nanga Parbat, yield average rates of incision of 22 ± 1.1 mm a^{-1} (Shroder & Bishop 2000). Consequently, rapid river incision, coupled with rapid uplift (Schneider *et al.* 1999) produced extreme regional relief.

Hypsometric analysis of Nanga Parbat proper (bounded by the Indus, Astor and Rupal rivers) reveals that *c.* 69% of the landscape lies within the 3000–6000 m range (Table 1). Cumulatively, 96% of the landscape is below 6000 m and an extremely small percentage (4%) of land is at high altitude. The average elevation is *c.* 3600 m and the altitude distribution statistics reflect the dominance of a glacial landscape and the knife-edged ridge of the massif at high altitude (Fig. 3). In general, these results are similar to Brozovic *et al.* (1997), although statistics may vary as a result of DEM resolution differences, spatial sampling variations and region of analysis.

Swath profile analysis across the entire DEM provides greater insight into the regional/local variability of river incision and relief characteristics (Figs 4, 5). In general, local relief (max–min) is highly correlated with maximum elevations because minimum elevations are controlled by river incision. The maximum relief on the north side of Nanga Parbat is 7 km, *c.* 6 km on the eastern side, and *c.* 5 km on the south side. Minimum elevations represent maximum river incision depths across the massif. The steep gradient of the minimum elevation plot in Fig. 4 represents active river incision along the north/northwestern-facing scarp of the Indus River valley. Here the Nanga Parbat antiform is cut by the nearly vertical Raikot Fault. Active uplift along this zone has caused rapid river incision which triggers slope failure and the development of steep slopes and V-shaped valleys.

Terrain-curvature analysis of the massif was used to better define the spatial distribution of extreme concavity associated with river incision and V-shaped valleys. Based upon morphometric analysis and field work, active river incision occurs along both sides of the Indus valley and especially over the active Raikot Fault Zone, where rapid river incision has produced steep gorges in the lower Buldar, Raikot and Diamir valleys. A prominent gorge also occurs in the lower Astor valley, and elevated strath terraces are located on the eastern valley wall (Fig. 6). The upper Astor and Rupal rivers are not actively down-cutting through bedrock as they are adjusting to middle Holocene deglaciation and transport a considerable amount of sediment. Hydrologic modelling of the average rate of denudation for the Rupal River is estimated to be 25 mm a^{-1} based upon cross-section data, velocity measurements and sediment yield estimates (Shroder & Bishop this volume).

Virtual reality simulations and slope analysis of the massif provided additional insight into the spatial variability of geomorphic processes which control the topography. Shallow slope angles generally occur in broad flat valley floors (e.g. Indus and Rupal valleys), in glacially eroded valleys, whereas steeper slope angles are associated with the knife-edged ridge of the mountain, areas of rapid incision and slopes that are dominated by mass-movement processes (Fig. 3). Slope distributions were examined by calculating histograms from a slope map that was generated with a window size of 40 × 40 m (Fig. 7). Histograms were calculated for Nanga Parbat (bounded by the Indus, Astor and Rupal rivers) and numerous basins (Fig. 8). The mean slope angle over Nanga Parbat proper is *c.* 32° (mode *c.* 37.0°). A similar mean slope angle estimate was calculated by Burbank *et al.* (1996). This is a minimum estimate as our analysis also includes

Table 1. *Altitude distribution of the landscape at Nanga Parbat*

Altitude (m)	Frequency (%)	Cumulative (%)
1000–1999.9	8.9	8.9
2000–2999.9	18.6	27.5
3000–3999.9	30.8	58.3
4000–4999.9	29.3	87.6
5000–5999.9	8.4	96.0
6000–6999.9	2.9	98.9
7000–7999.9	0.83	99.7
8000–8125.0	0.004	100.0

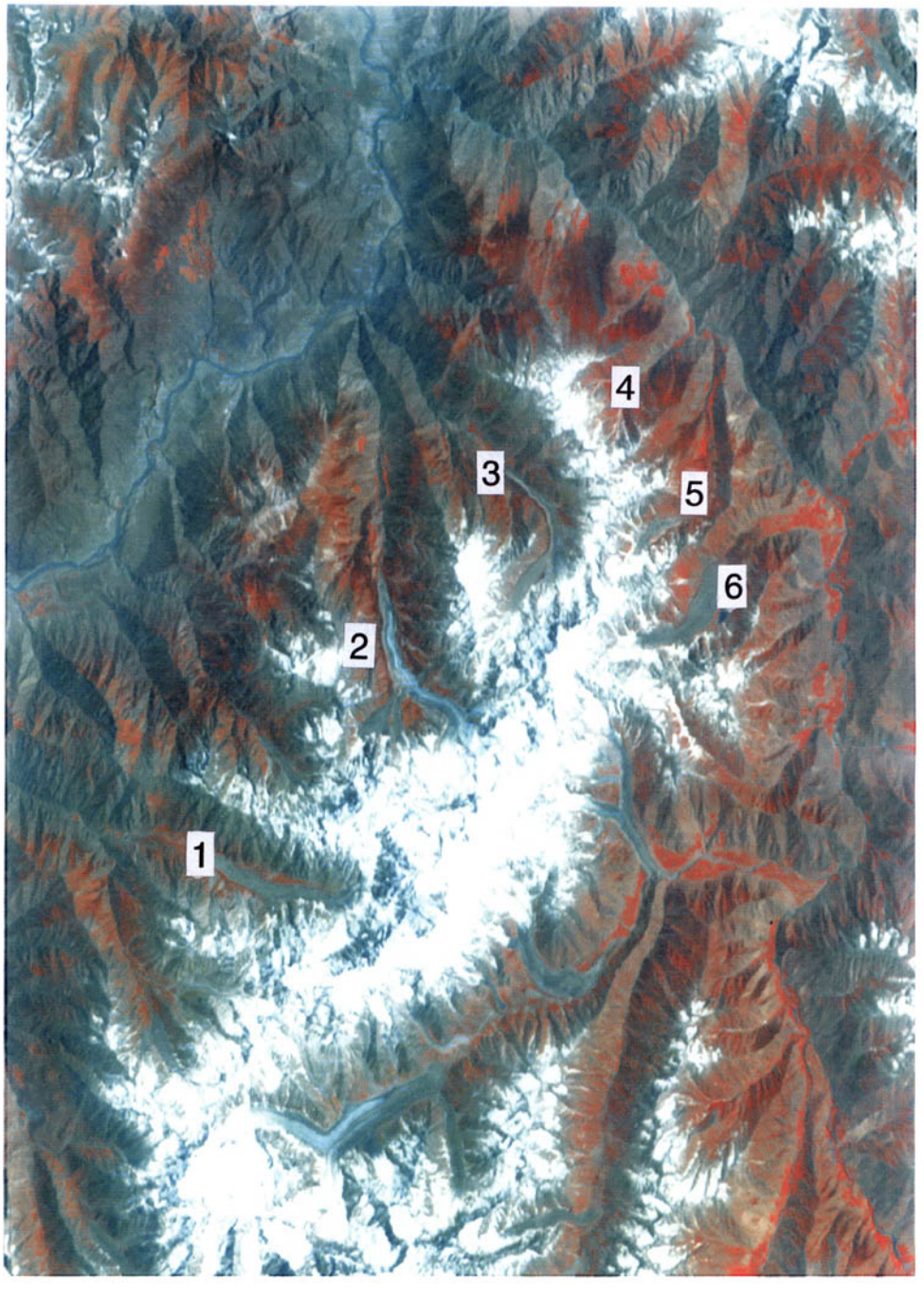

Fig. 2. LANDSAT MSS false colour composite of Nanga Parbat. False colour composite was generated using MSS band 6 (red), MSS band 5 (green) and MSS band 4 (blue). Image width represents *c.* 60 km. In general, snow appears white, bare glacial ice appears light blue, bare bed rock and rock detritus appear brown and dark blue, and vegetated surfaces appear in shades of red. The Indus River and valley are located in the upper left portion of the image. The Astor River and valley are located on the east side of Nanga Parbat. Alpine glaciers are found in most basins surrounding the mountain. Drainage basins used for geomorphometric analyses are enumerated and include: (1) Diamir, (2) Raikot, (3) Buldar, (4) Mamocha, (5) Lotang and (6) Sachen.

(a)

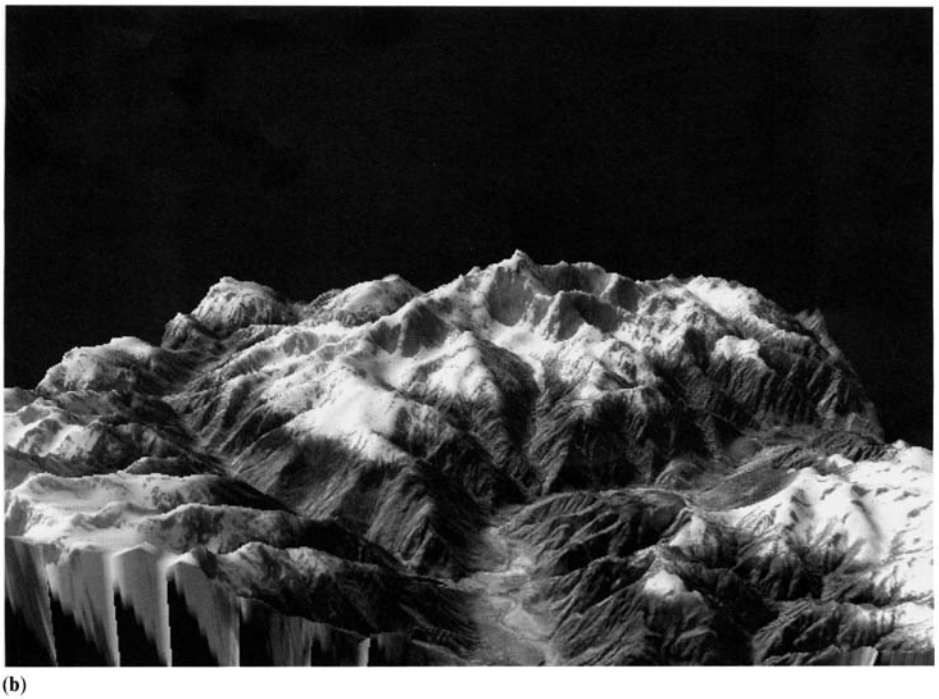

(b)

Fig. 3. Satellite image three-dimensional perspectives of the Nanga Parbat massif (vertical exaggeration 2×). Ortho-rectified SPOT panchromatic imagery (10 m resolution) was draped over a high resolution (20 m) digital elevation model. The azimuth view directions are as follows: **(a)** upper left image-view from south; **(b)** upper right image-view from north; **(c)** lower left image-view from west; **(d)** lower right image-view from east.

(c)

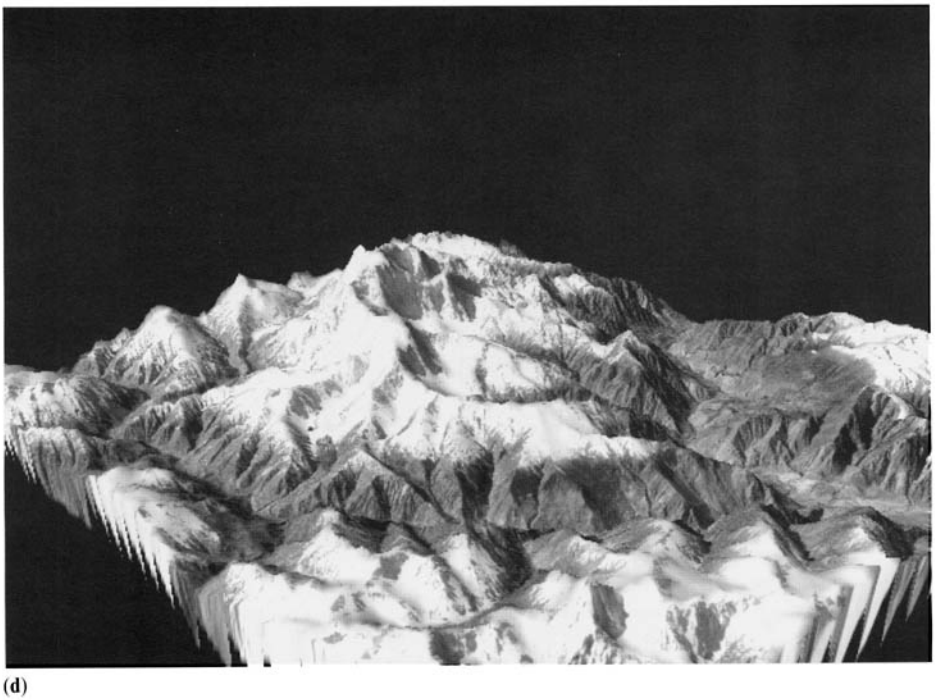

(d)

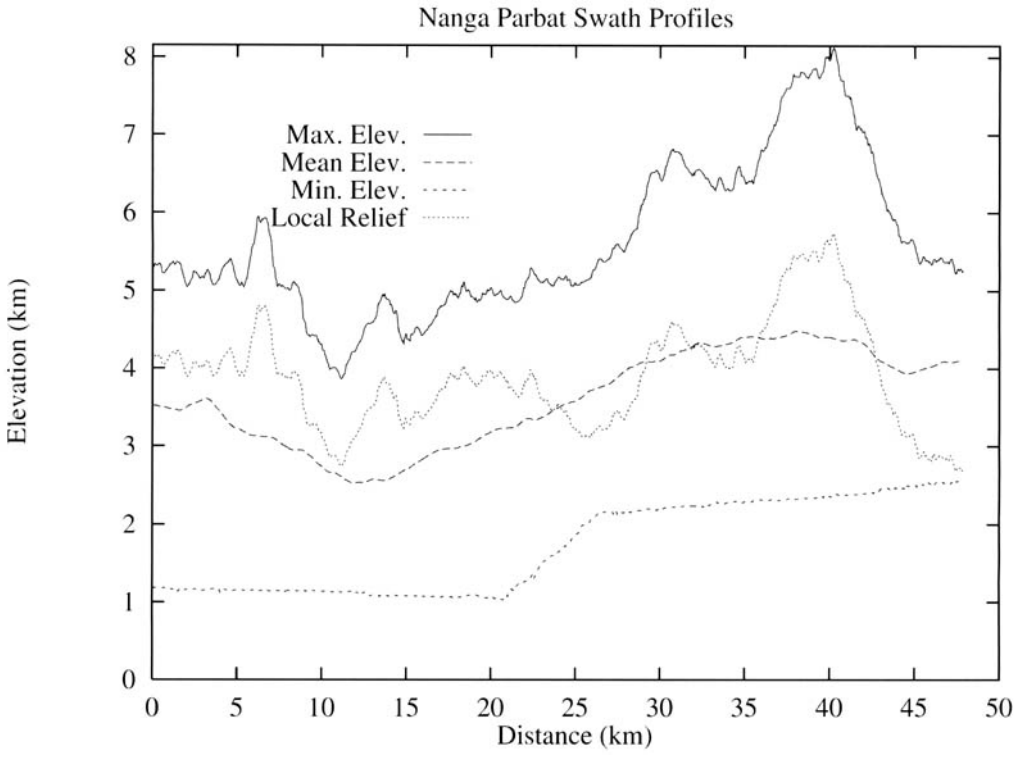

Fig. 4. North–south topographic profile across the Nanga Parbat massif. Relief statistics were calculated from the DEM using a swath width of *c.* 40 km.

shallow slope angles at lower altitudes. Slope distributions indicate that steep slopes occur throughout the massif and that many variations in the relative frequency of slope angles reflect basin erosion dynamics acting on structure and lithology. For example, the secondary peak of frequencies at *c.* 8° represents the influence of glaciation on the landscape. Glaciation is responsible for redistributing sediment and shallow slope angles reflect moraine and glacial outwash deposits, and glacier surfaces themselves. Basins that have not been directly influenced by glaciation may not exhibit a significant distribution of shallow slope angles, depending upon the geomorphic history of the basin (i.e. spatial and temporal erosion dynamics).

Visual examination of satellite imagery (Fig. 2), a slope angle map (Fig. 7), and plots of slope angle versus altitude derived from the DEM (Fig. 9) reveal that glaciation has had a significant influence on the topographic evolution and complexity of the massif. Shallow slope angles are highly correlated with the spatial extent of glaciation. The maximum slope angles are consistently high over all altitudes, and the relationship between slope angle and altitude is not linear. At lower elevations in basins above the Indus valley, mean slope angles rise dramatically to a maximum of *c.* 45° from *c.* 1500–2000 m. This terrain includes the Raikot Fault Zone and the steep slopes at this altitude are the result of active river incision and associated slope failure. With altitude, the dominance of these processes decreases, and other surface processes are responsible for active erosion and deposition. With increasing altitude, mean slope angles systematically decrease and then gradually increase. From 3000–5000 m, the typical elevation of glacial valleys, shallower slope angles represent the influence of glaciation on the landscape. No evidence of uplifted pre-existing erosion surfaces exists on Nanga Parbat, unlike other nearby preserved surfaces. Shallow slope angles characterize the moraine deposits that were controlled by changing equilibrium line altitudes caused by shifting monsoonal precipitation gradients. At higher elevations, the average slope angles increase due to a decrease in temperature (freeze–thaw action) and the dominance of mass movement. We collected samples of boulders

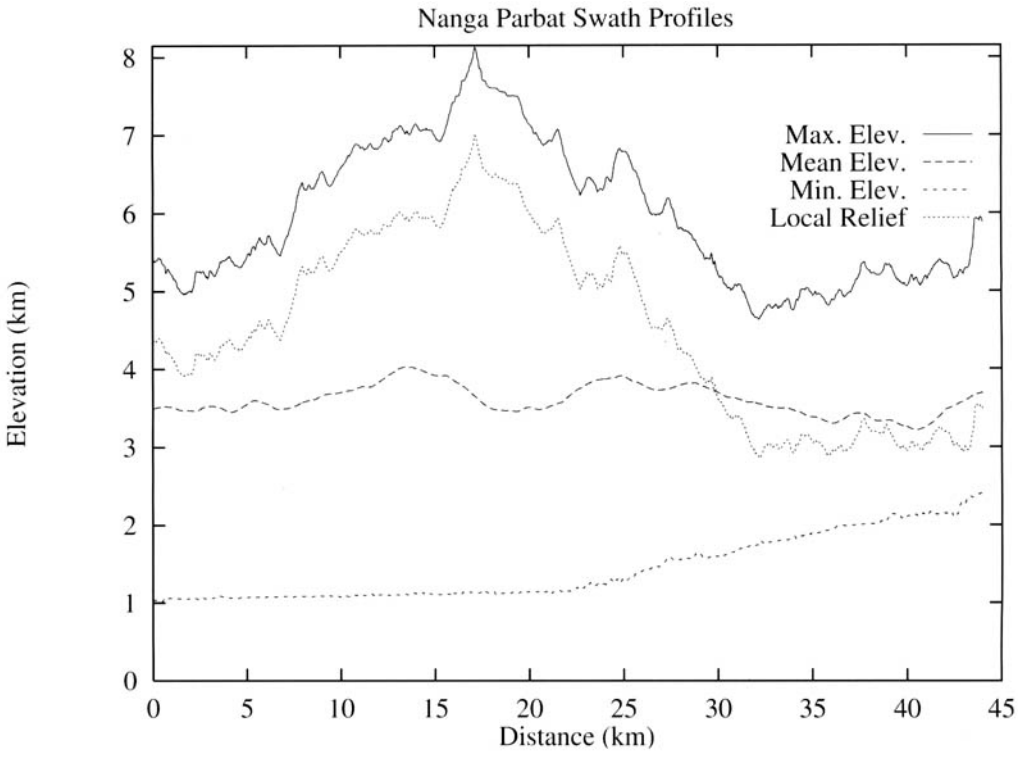

Fig. 5. West–east topographic profile across the Nanga Parbat massif. Relief statistics were calculated from the DEM using a swath width of *c.* 40 km.

Fig. 6. Ground photograph of rock-cut strath terraces on the eastern wall of the lower Astor River valley. These terraces represent former channel bottoms and demonstrate that the Astor valley at this location has undergone active vertical incision. Increased stream power is controlled collectively by the stream gradient and the narrowing of the channel due to the Mushkin rock-slide on the left.

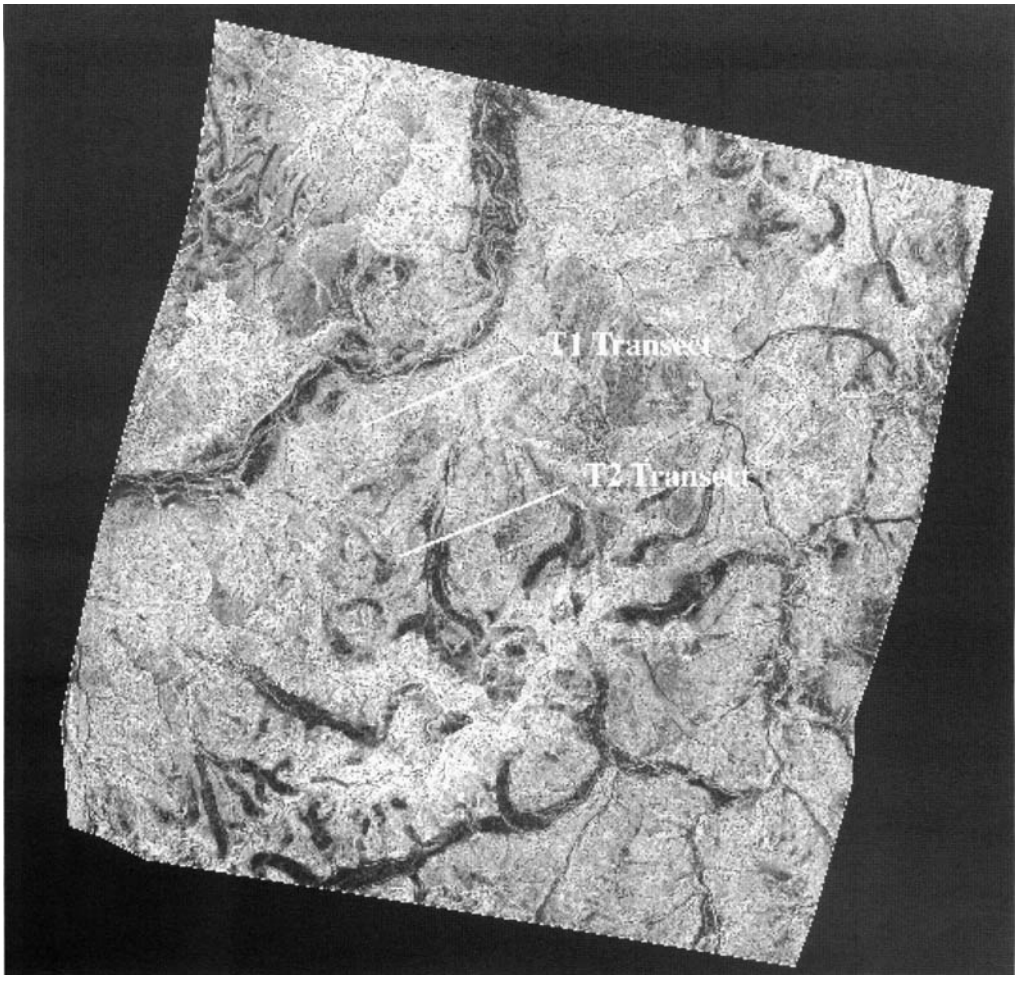

Fig. 7. Slope angle map of the Nanga Parbat massif. Average slope angles were derived from the DEM over a 40 × 40 m area using least squares regression analysis. Transect locations represent data sampled for semivariogram analysis. This is a greyscale image in which grey tones reflect low slope angle and light tones reflect high slope angle.

exposed on the moraine surfaces at various altitudes, in order to determine rock-exposure ages using cosmogenic-nuclide dating.

Moraines indicating a major glaciation occur at over 4000 m, but many others *c.* 3000 m lower show the great extent of ice formerly emanating from the mountain. Geomorphological mapping and dating by cosmogenic isotope exposure ages provide temporal control indicating that, although several glacial advances > 100 ka are known from tills and glacio-lacustrine sediments, much of the modern landscape is dominated by a glacial heritage from late Pleistocene and early Holocene (Shroder & Bishop 2000) that is asynchronous to continental glaciers elsewhere (Gillespie & Molnar 1995). Glacial advances occurred during periods of heightened monsoon activity (57–34 ka; 8.4–5 ka), but were precipitation limited during the global last full glacial (*c.* 18 ka) when monsoon intensity was low and conditions more arid (Shroder & Bishop 2000). These results indicate that glaciation at Nanga Parbat was far more extensive in the past and played a significant role in the mass flux of sediment.

Modern-day glaciation at Nanga Parbat represents a significant process responsible for removing sediment (Shroder *et al.* 2000). One of our field and remote sensing investigations has focused on characterizing glacier surfaces and the highly variable patterns of supraglacial debris (Bishop *et al.* 1995, 1999). Our preliminary

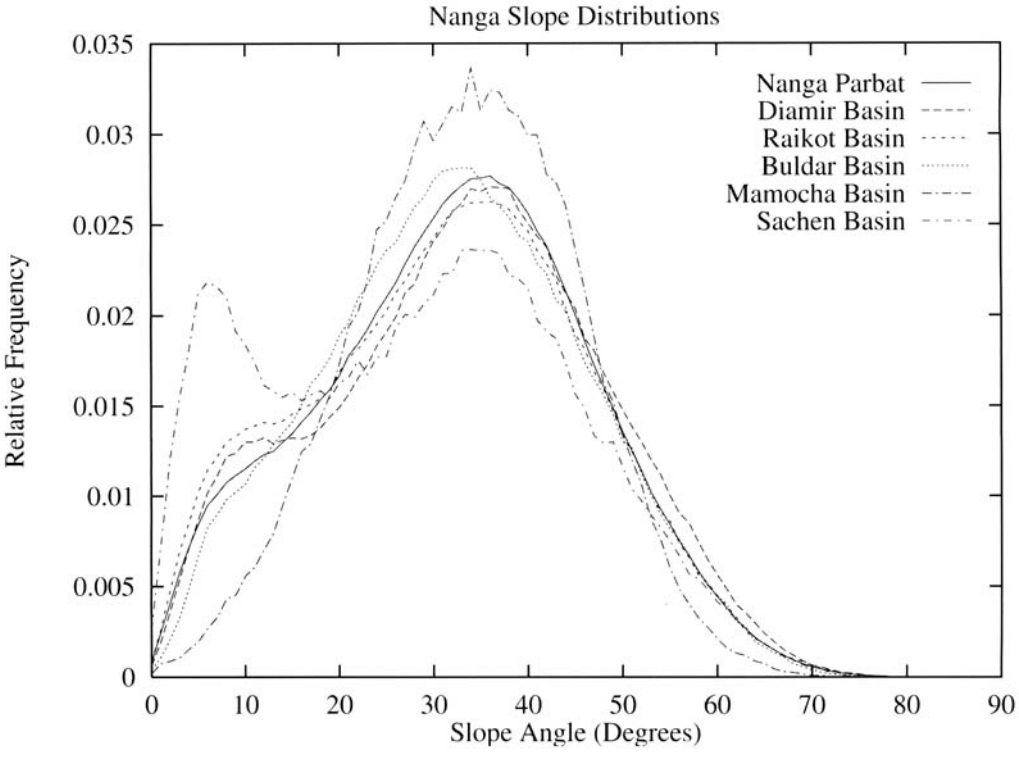

Fig. 8. Slope distributions for Nanga Parbat and various basins around the mountain. The modal slope angles are *c.* 37°. The secondary peak of frequencies at *c.* 8° represents the influence of glaciation on the landscape.

calculations and the work of Gardner & Jones (1993) indicate that modern-day glacial rates of denudation can be high, although they fluctuate significantly with time. For example, we have discovered that glaciers at Nanga Parbat periodically produce outburst floods at various locations which represent an additional process responsible for removing debris (Shroder *et al.* 1998). One event in 1996 was responsible for removing *c.* 2–3 m of supraglacial debris from the lower terminus of the Raikot glacier. Various sediment transport efficiencies have been documented in numerous basins; however, glaciation coupled with other surface processes have collectively removed significant mass from the massif (Fig. 10). For example, sediment transfer and removal in the Sachen basin on the east side of Nanga Parbat is less efficient than sediment transport and removal in the Raikot basin on the north side. The Sachen glacier moves on a low gradient, has lower ice velocities, produces limited meltwater, and has no efficient system of debris removal. Consequently, it has huge moraines in its forefield and a pronounced digitate terminus showing multiple directions of prior movement. Conversely, Raikot glacier has a rather high and uniform ice velocity distribution that decreases abruptly at the margins. The glacier also produces abundant meltwater and it is now known that blockage and release of subglacial drainage (outburst floods) effectively transports and removes debris from the basin. For more details regarding sediment transport efficiencies at Nanga Parbat, see Shroder *et al.* (2000).

Virtual reality simulations at lower viewing elevation angles also reveal the presence of well defined accordant summit ridges (gipfelflur) on the north side of the massif (Fig. 3c, d). This phenomenon is common to many mountains and thought to be either the remains of a planar erosion surface or the result of quasi-equal spacing of stream incision. These accordant summit ridges are gently sloping and interrupted, however, by a number of upstanding peaks, including the main peak of Nanga Parbat, which forms the southern termination of the gipfelflur. In general, these ridges range from

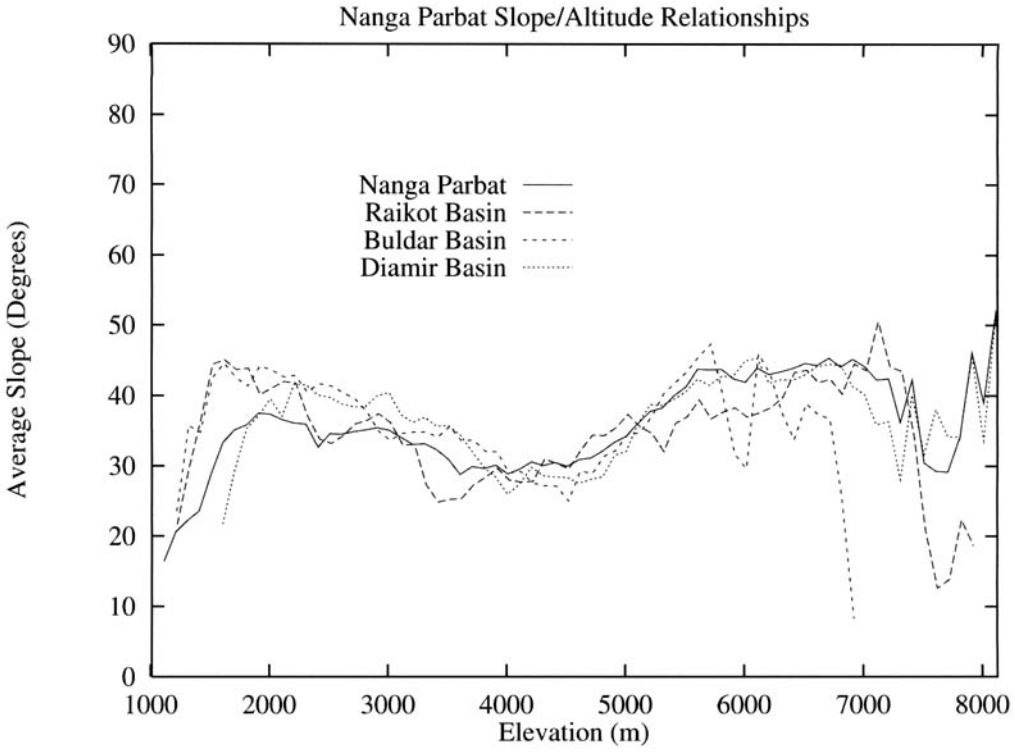

Fig. 9. Slope–altitude relationships for Nanga Parbat and several basins. Average slope angles were calculated over an elevation range of 100 m. The relationship between slopes and altitude is not linear. Steep slopes can be found at all altitudes. Average slope angles decrease to a minimum from 3000–5000 m due to the influence of glaciation.

c. 6000 m altitude close to the main peak, down to *c.* 4000 m above the gorge of the Indus River below.

Landscape dynamics

The Nanga Parbat antiform is a unique topographic, lithologic and structural feature (Zeitler & Chamberlain 1991; Seeber & Pêcher 1998). A high correlation exists between the axis of the antiform and the topography, as the knife-edged ridge of the mountain is aligned relatively parallel to the Indus River and Rupal River valleys. This distinctive topographic signal reflects the tectonic influence on the landscape, and represents the first-order topographic relief. The uplift is thought to have been initiated at *c.* 12–10 Ma, resulting from isostatic rebound due to denudation caused by the Indus River and associated surface processes (Shroder & Bishop this volume). The dominant erosion agent was most likely rapid river incision coupled with pervasive slope failure (Shroder 1998). Late Cenozoic climate change and the Indian monsoon augmentation of glaciation could have accelerated denudational unloading (Molnar & England 1990; Shroder & Bishop 2000). This resulted in first-order landscape dissection and rock uplift.

The first-order topography and climate change clearly controlled the surface processes that were responsible for further erosion and transportation of rock and debris, such that the modern-day landscape exhibits drainage basin alignment predominantly transverse to the massif. This second-order topographic relief is dominated by the smaller glacial and fluvial valleys that radiate from the mountain. Surface uplift and an influx of moisture would have increased glacier accumulation areas and ice flux, resulting in increased erosion rates and further denudational unloading of the massif. The topographic characteristics at Nanga Parbat support this idea, although the topography can only be used to characterize landscape dynamics over the last *c.* 100 ka due to rapid denudation. Examination

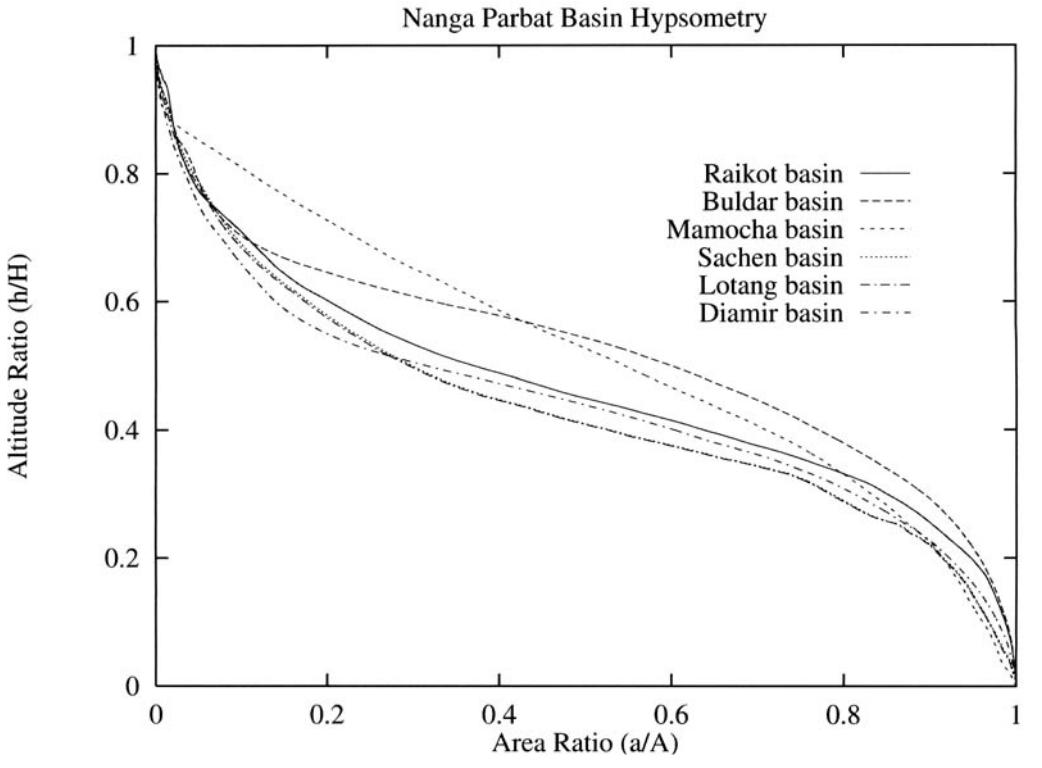

Fig. 10. Hypsometric curves for the major basins on Nanga Parbat. Relatively low hypsometric integrals (*c.* 0.4) are associated with Raikot, Sachen, Lotang and Diamir basins. Raikot and Diamir basins exhibit rapid river incision and have large, efficient glaciers. Sachen and Lotang basins have smaller glaciers that are inefficient now, but large moraines show that they were large and efficient in the past. Mamocha basin has limited glaciation in the past or present. The magnitude of denudation is relatively high in major basins because glaciation, coupled with mass movement inputs and fluvial-process outputs, have removed significant rock and sediment mass.

of the modern-day topography reveals that glaciation is ultimately responsible for the production of the second-order topographic relief.

Topographic evolution and the production of steep slopes at various scales have enabled mass-movement processes to contribute significantly to denudational unloading. The modern-day landscape exhibits third-order topographic relief that can be characterized by the dominance of mass-movement and periglacial processes, resulting in small alpine basins, debris chutes and topographic variation that is controlled by second-order features and slope characteristics. This hierarchy of topographic complexity can be seen in slope azimuth (ϕ_T) images of the terrain that show the directionality of slopes in a north–south and east–west orientation (Figs 11, 12). Examination of these images clearly reveal spatial patterns in the topography that appear to be scale-dependent.

In an attempt to characterize some of this complexity, semivariogram analysis was conducted on the slope-angle map (Fig. 7). We calculated a semivariogram function from a transect (T1) located along the Raikot Fault Zone, where the slope angle variability is the result of the dominance of river incision-slope failure processes (D1). A second transect (T2) was located (parallel with the first and higher on the massif), where the slope angle variability is the result of the dominance of glacial-polygenetic slope formation processes (D2). Both transects were located on the north side of Nanga Parbat and were approximately 5 km in length (Fig. 7).

The results indicate that $\sqrt{\bar{S}^2}$ values are greater for D1 than D2 at scales $<c.$ 0.7 km (Fig. 13). Conversely, $\sqrt{\bar{S}^2}$ values are greater for D2 than D1 at scales $>c.$ 0.7 km. This indicates that topographic complexity (i.e. slope variability) over the massif in this direction significantly varies as a function of scale depending upon erosion dynamics. It should be noted that high-frequency periodicity (fluctuations in $\sqrt{\bar{S}^2}$ values over short distances) is present in the D1

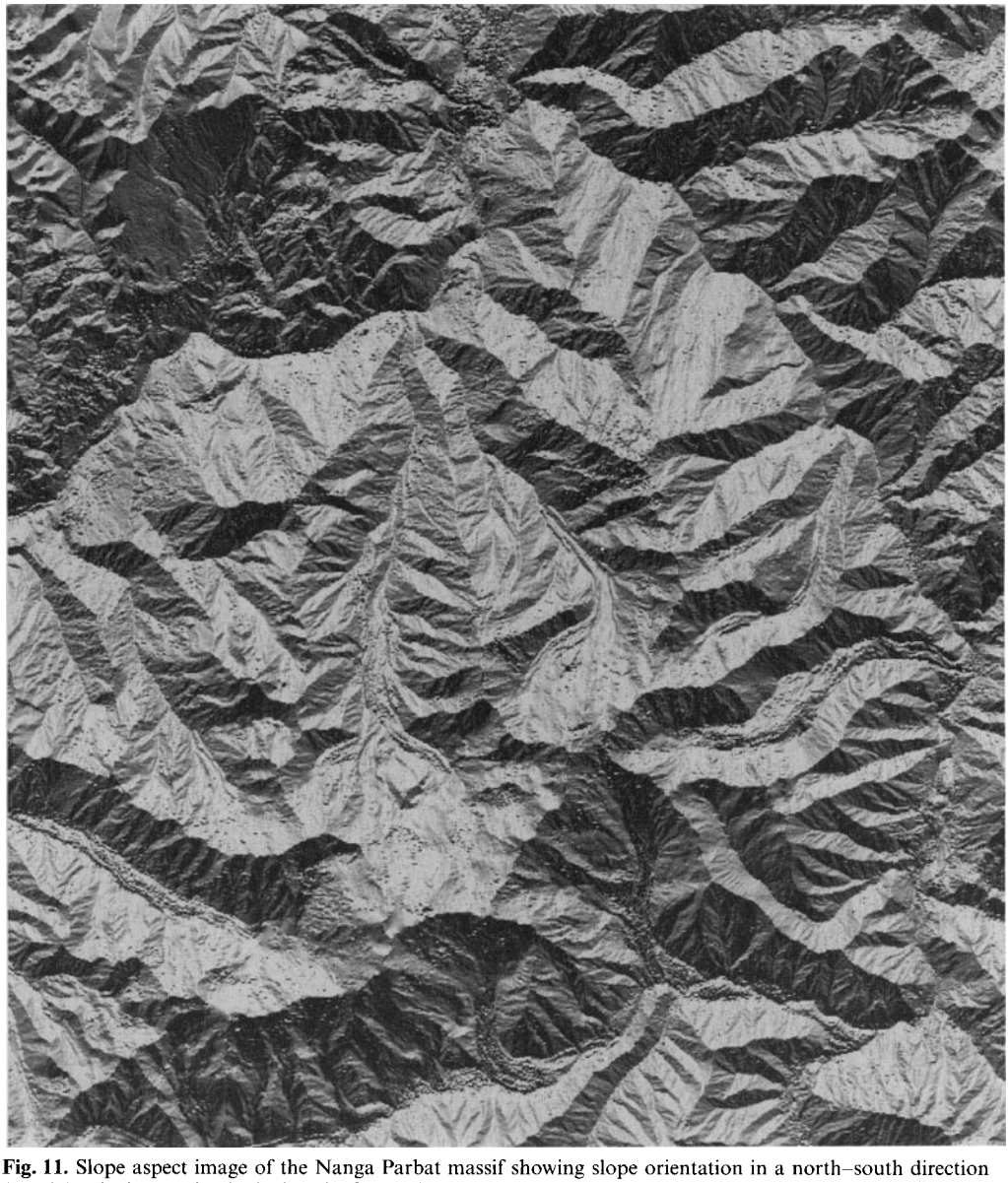

Fig. 11. Slope aspect image of the Nanga Parbat massif showing slope orientation in a north–south direction ($\cos \phi_T$). The image clearly depicts the first-order topography and the orientation of the massif in a northeasterly direction. The massif is highlighted by north-facing slopes resulting from the influence of the Indus River. Third-order topography is also highlighted in many basins on the north side of Nanga Parbat.

semivariogram. Field evidence suggests that the periodicity has geological significance. The semivariogram characterizes the relatively uniform steep slope angles throughout the T1 region that are generated as a result of active uplift, rapid river incision and associated slope failure (i.e. rock slides and rock falls). The high spatial frequency of slope variability is controlled by the lithology and structure (i.e. alternating basement rocks and metasediments, and the presence of foliation; W. Kidd, pers. comm. 1998), such that erosion dynamics produce variations in slope angles at distances of 200–500 m. More research is required to determine the sensitivity of semivariogram analysis to lithology and structure variations at Nanga Parbat.

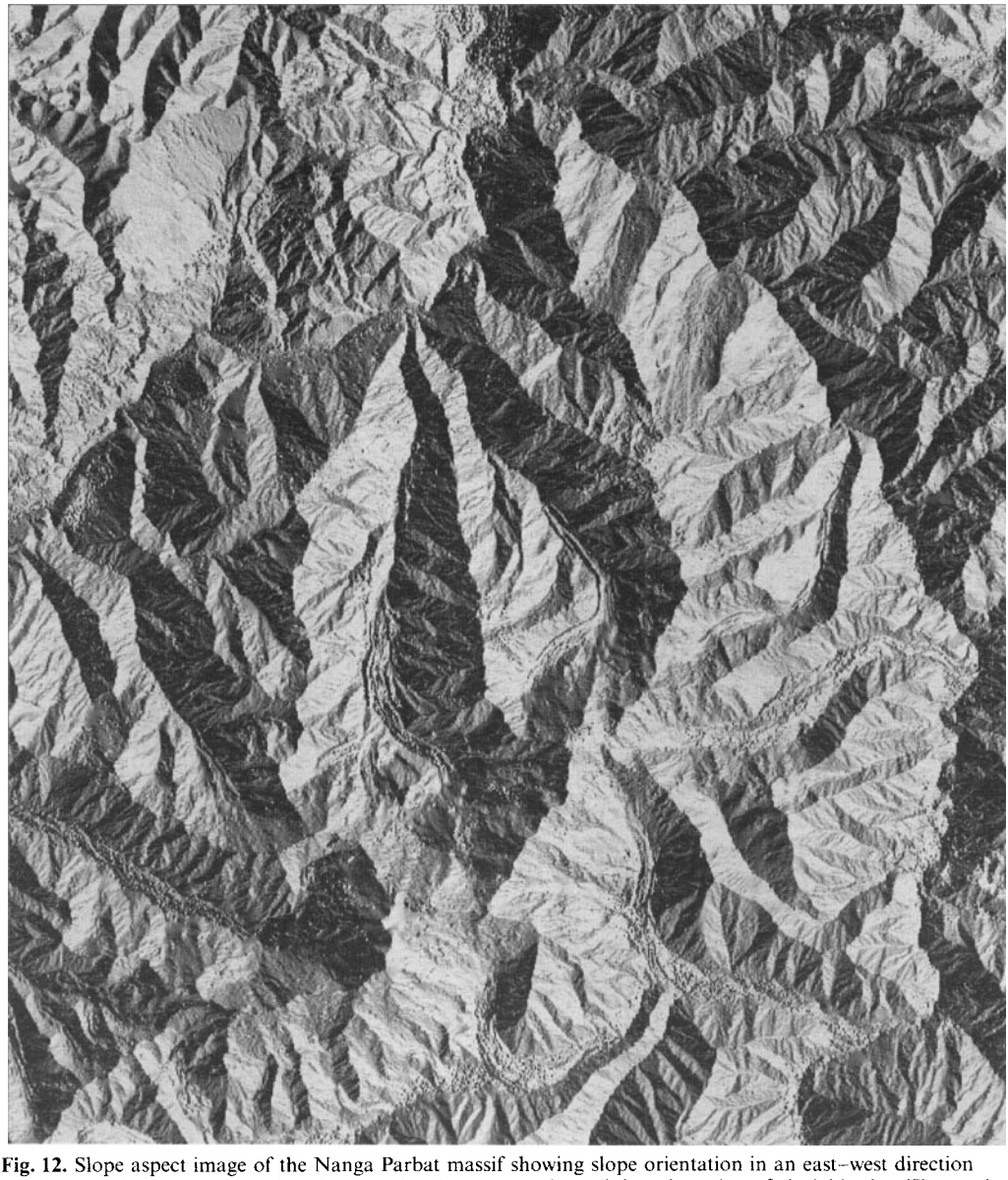

Fig. 12. Slope aspect image of the Nanga Parbat massif showing slope orientation in an east–west direction ($\sin \phi_1$). The image clearly depicts the second-order topography and the orientation of glacial basins. The north–northwest side of the massif exhibits the largest glaciers and third-order topography is highlighted in some basins.

Glaciation is known to produce longer wavelength topographic variation, and shallow to moderate slope angles are highly correlated with past and modern-day glaciation at Nanga Parbat. This process is responsible for spatial autocorrelation of slope angles which accounts for the systematic increase in $\sqrt{\bar{S}^2}$ values for D2 as a function of scale (Fig. 13). Periodicity of $\sqrt{\bar{S}^2}$ values in the semivariogram function for D2 is present and represents the influence of polygenetic slope-forming processes such as debris flows, wet-snow avalanches, nonglacial fluvial action, and glacial meltwater outwash. Increased precipitation at this elevation (Gardner 1986) influences the topographic complexity as redistribution of sediment caused by fluvial processes and debris flows produce less variability at shorter wavelengths. Conversely, mass

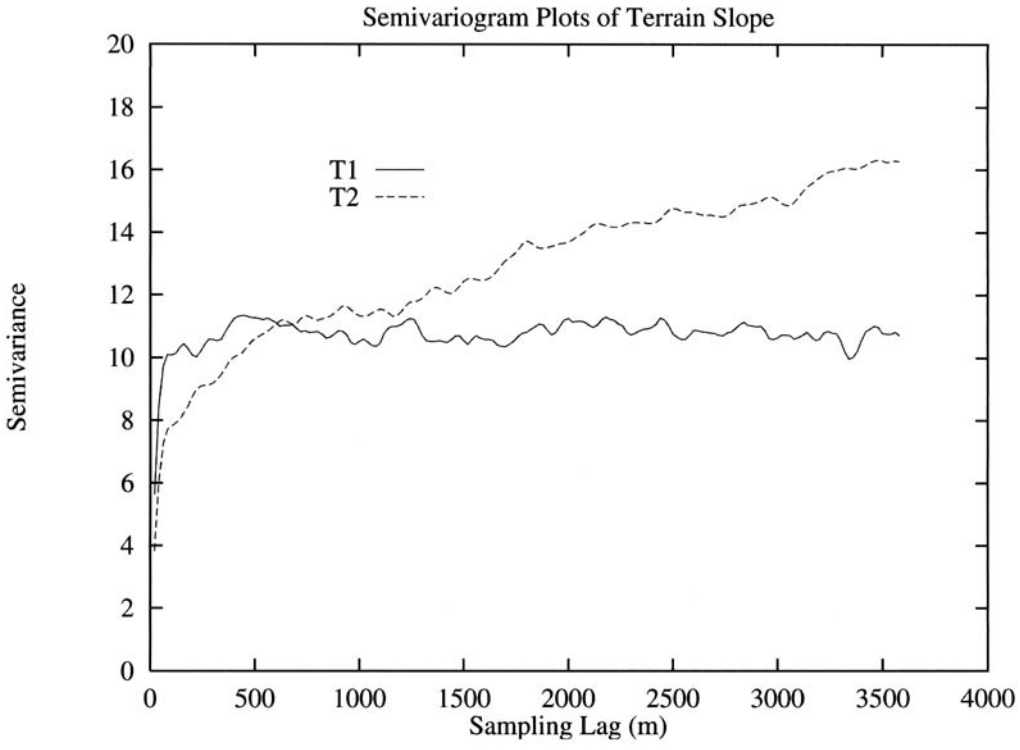

Fig. 13. Semivariograms of two different erosion dynamics over the Nanga Parbat massif. Transect 1 represents river incision-slope failure processes and Transect 2 represents glacial-polygenetic slope formation processes. Slope variability is highly scale-dependent and semivariogram functions can be used to characterize the topography resulting from different erosion dynamics.

movement processes dominate along the T1 transect which samples terrain from an arid climate. Consequently, fluvial processes do not effectively modify the topography and topographic variability is greater at shorter wavelengths.

Visual examination of the log-transformed semivariogram functions reveal differences in the slope of various segments of the D1 and D2 log–log plots. This reveals the fractal nature of the topography at Nanga Parbat and indicates that the topographic complexity (i.e. fractal dimension) is different for D1 and D2. The fractal dimension provides important information about the roughness of the topography and also contains information on the underlying geodynamics of erosional and tectonic coupling (Koons 1995). We do not report numerical analysis results, as the objective was not to characterize the multi-fractal nature of the topography, but to provide insight into the scale-dependent nature of erosion dynamics and topography. This simple analysis demonstrates that the topographic complexity at Nanga Parbat can be characterized and that more rigorous scale-dependent analysis may provide additional information regarding erosion dynamics.

Erosion dynamics have been documented by Shroder & Bishop (this volume). Sufficient geological evidence concerning uplift/exhumation rates indicates that surface processes are of first-order importance in controlling the topographic and structural evolution of the massif at a suborogen scale (Zeitler *et al.* 1993; Schneider *et al.* 1999; Shroder & Bishop this volume). Decoupling the geodynamic topographic signals that may be present at various scales is extremely difficult because of the temporal overprinting of surface processes. We have, however, demonstrated that a high-spatial-frequency lithologic signature is present in the slope distribution over the Raikot Fault Zone. Our analysis indicates that climate fluctuations and glaciation have decreased topographic complexity at a local scale while increasing relief and slope variability at intermediate scales. Furthermore, high-spatial-frequency relief variation is the result of

the dominance of localized mass movement and periglacial processes over the landscape. Although surface processes appear ultimately to control the topographic complexity, we speculate that additional topographic signals are present and represent the localized coupling of tectonics and surface processes. More spatial-analysis research utilizing DEM and satellite imagery is required to further characterize this aspect of the topography.

Discussion

Remote sensing and geomorphometric analysis of Nanga Parbat have produced a tremendous volume of new spatial data which, when coupled with field measurements, have enabled us to investigate the erosional dynamics of the massif. This information, integrated with petrologic, thermochronologic and geophysical information, provides new insight into this complex dynamic system and explains much of the topographic complexity of the massif.

Active seismicity is associated with the highest topography, youngest metamorphic and igneous ages and active fluid flow, which suggests that fundamental processes link these factors (Schneider *et al.* 1999). Furthermore, much of the observed shallow seismicity is from a set of normal faults on the northeast that strike roughly parallel to the main massif and dip south to southeast, back towards the summit. At *c.* 7 km depth beneath the mountain a cut-off in seismicity suggests a shallow brittle–ductile transition. The spatial distribution of microseismicity also indicates rapid upward advection of rock material within the core of the massif (Schneider *et al.* 1999). Rapid river incision and these observations explain the first-order geometry and relief at Nanga Parbat (Shroder & Bishop this volume).

The second-order topographic relief can be explained by complex erosion dynamics that have changed with time. Analysis of the topography provides insight into the spatial complexity of erosion, because surface processes operating at various spatial scales have produced scale-dependent topographic variation as a function of lithology and structure. Our work indicates that the modern landscape is dominated by a glacial heritage from the late Pleistocene and early Holocene (Shroder & Bishop this volume). These results are quite significant as these time periods are associated with monsoon-enhanced glacial activity and indicate that glaciation was much more extensive in the past, playing an expected significant role in mass flux of sediment, and the production of second-order topography. Fluvial processes are also responsible for the long-term removal of significant mass, as the largest basins on the north side of Nanga Parbat exhibit mean fluvial rates of denudation of *c.* 7 mm a^{-1} and the Rupal River on the south side *c.* 25 mm a^{-1} (Shroder & Bishop this volume). These are the highest reported rates for the western Himalaya.

High-frequency topographic variations at Nanga Parbat are the result of spatially varying erosion interactions. For example, numerous alpine basins exhibit small glaciers that contribute to basin development. Other basins are dominated by debris flows that erode and transport material. Consequently, the polygenetic slope-forming processes control the development of third-order topography. Analysis of these processes in alpine basins was conducted by Shroder *et al.* (1999), and rates of denudation were found to be highly variable, although average rates of denudation are estimated to be *c.* 2 mm a^{-1}. Alpine basins with glaciers exhibit topographic variability at longer wavelengths than basins dominated by debris flows. At lower altitudes, even higher-frequency relief and slope variations are associated with lithology and slope failure (D1).

At the centre of the massif, a concentric pattern of young igneous and metamorphic rock ages has been documented (Schneider *et al.* 1999). A similar pattern of shallow slope angles, excluding the knife-edged ridges, appears to be spatially correlated to the distribution of the relatively young rock ages. This suggests that the magnitude of denudational unloading at the spatial centre of the massif has been exceptionally high and caused by glacier denudation. Thermochronological data and long-term rates of denudation show that the accordant summits on the north side of Nanga Parbat have undergone significant erosion, so that the crests do not represent the remnants of some initial plateau surface, but reflect the erosion dynamics and denudational unloading. More analysis and modelling is required to verify this, although supportive evidence exists in the Karakoram Himalaya at K2 (Foster *et al.* 1994).

A scale-dependent perspective of tectonics, erosion dynamics and topographic complexity will provide new insights about the denudational unloading and extreme relief at Nanga Parbat. Various workers have examined and/or discussed the relative contributions of erosional and tectonic processes in the formation of topography; however, numerical characterizations of the spatial geodynamics have generally been lacking (Koons 1995). Our preliminary results indicate that the topographic complexity at

Nanga Parbat is highly variable at a variety of spatial scales, which reflects the erosion dynamics and possibly even the geodynamics of the system (i.e. structure, lithology and tectonics). The use of remote sensing and geomorphometry has greatly assisted us in identifying the key geomorphic domains, erosion dynamics and the complex anisotropic nature of the topography. Fractal characterization of the spatial and anisotropic characteristics of Nanga Parbat topography is required to better understand the dynamic behaviour of this complex system, and the role of lithology, structure and tectonics.

Finally, erosion rates are very difficult to quantify, and landscape information could provide an index of erosion rates, provided that calibration is feasible (Howard 1996). We have found strong relationships between the topography and erosion dynamics, which suggest that scale-dependent analysis may provide a foundation for linking topographic complexity to the magnitude of denudation. Our initial working model has focused on the major surface processes responsible for rapid denudation, and we have documented that denudation at Nanga Parbat is highly variable in space and time. Further development and testing of erosion models should provide new insights into topographic evolution at Nanga Parbat.

Conclusions

Satellite imagery and a high-resolution DEM were used to study the topographic complexity of the Nanga Parbat massif. Virtual reality simulations and geomorphometric analyses reveal hierarchical topographic organization and extreme relief that is the result of tectonic uplift, ferocious denudation, spatial-erosion dynamics and lithology/structure. Topographic characterization and spatial analyses indicate that topographic complexity is highly scale-dependent and the result of the coupling of surface uplift and erosion dynamics. Strong relationships were found between erosion dynamics and denudation such that topographic signals were found at various scales. Additional characterization of topographic complexity is required in order to further study the relationship between surface processes and uplift.

Our results provide evidence that surface processes are capable of eroding and transporting critical amounts of rock and sediment away from the massif. Furthermore, we speculate that modern-day differential denudation associated with localized surface processes would not be likely to be in spatial balance with the regional tectonic mass flux. It is important to identify the fundamental scale (or scale range) at which denudation influences uplift in order to characterize the localized coupling between the two. Surface erosion models need to account for spatial erosion dynamics and be linked with mechanical tectonic models in order to further study the geodynamics between erosion and uplift.

Sincere thanks are extended to L. Copland, K. Cornwell, M. Edwards, W. Kidd, P. Koons, V. Sloan, W. Phillips and P. Zeitler. This work was funded in part by the University Committee on Research at the University of Nebraska at Omaha, University of Nebraska Foundation and the US National Science Foundation (Grant No. EAR-9418839 and Grant No. EPS-9720643). We also thank John Flocken and Jeff Olsenholler for their contributions.

References

AHNERT, F. 1987. Process-response models of denudation at different spatial scales. *Catena Suppl.*, **10**, 31–50.

AVOUAC, J. P. & BUROV, E. B. 1996. Erosion as a driving mechanism of intracontinental mountain growth. *Journal of Geophysical Research*, **101**, 747–769.

BISHOP, M. P., HICKMAN, B. L. & SHRODER JR., J. F. 1999. High resolution satellite imagery and neural networks for information extraction in a complex mountain environment. *Geocarto International*, **14**, 1–15.

——, SHRODER JR., J. F., HICKMAN, B. L. & COPLAND, L. 1998*a*. Scale dependent analysis of satellite imagery for characterization of glacier surfaces in the Karakoram Himalaya. *Geomorphology*, **21**, 217–232.

——, ——, SLOAN, V. F., COPLAND, L. & COLBY, J. 1998*b*. Remote sensing and GIS technology for studying lithospheric processes in a mountain environment. *Geocarto International*, **13**, 75–87.

——, —— & WARD, J. L. 1995. SPOT multispectral analysis for producing supraglacial debris-load estimates for Batura Glacier, Pakistan. *Geocarto International*, **10**, 81–90.

BROZOVIK, N., BURBANK, D. & MEIGS, A. J. 1997. Climatic limits on landscape development in the northwestern Himalaya. *Science*, **276**, 571–574.

BURBANK, D., LELAND, J., FIELDING, E., ANDERSON, R. S., BROZOVIK, N., REID, M. R. & DUNCAN, C. 1996. Bedrock incision, rock uplift and threshold hillslopes in the northwestern Himalayas. *Nature*, **379**, 505–510.

CHASE, C. G. 1992. Fluvial landsculpting and the fractal dimension of topography. *Geomorphology*, **5**, 39–57.

CURRAN, P. J. 1988. The semivariogram in remote sensing. *Remote Sensing of Environment*, **24**, 493–507.

FIELDING, E. J. 1996. Tibet uplift and erosion. *Tectonophysics*, **260**, 55–84.

FOSTER, D. A., GLEADOW, A. J. W. & MORTIMER, G. 1994. Rapid Pliocene exhumation in the

Karakoram (Pakistan), revealed by fission-track thermochronology of the K2 gneiss. *Geology*, **22**, 19–22.

GAO, J. & XIA, Z. 1996. Fractals in physical geography. *Progress in Physical Geography*, **20**, 178–191.

GARDNER, J. S. 1986. Recent fluctuations of Rakhiot Glacier, Nanga Parbat, Punjab Himalaya, Pakistan. *Journal of Glaciology*, **32**, 527–529.

—— & JONES, N. K. 1993. Sediment transport and yield at the Raikot Glacier, Nanga Parbat, Punjab Himalaya. *In*: SHRODER JR., J. F. (ed.) *Himalaya to the Sea. Geology, geomorphology and the Quaternary*. Routledge, London, 184–197.

GILCHRIST, A. R., SUMMERFIELD, M. A. & COCKBURN, H. A. P. 1994. Landscape dissection, isostatic uplift, and the morphologic development of orogens. *Geology*, **22**, 963–966.

GILLESPIE, A. & MOLNAR, P. 1995. Asynchronous maximum advances of mountain and continental glaciers. *Reviews of Geophysics*, **33**, 311–364.

HARBOR, J. & WARBURTON, J. 1992. Glaciation and denudation rates. *Nature*, **356**, 751.

—— & —— 1993. Relative rates of glacial and nonglacial erosion in alpine environments. *Arctic and Alpine Research*, **25**, 1–7.

HARRISON, C. G. 1994. Rates of continental erosion and mountain building. *Geologisches Rundschau*, **83**, 431–447.

HOWARD, A. 1996. The ephemeral mountains. *Science*, **379**, 488–489.

KOONS, P. O. 1995. Modeling the topographic evolution of collisional belts. *Annual Review of Earth and Planetary Sciences*, **23**, 375–408.

LIFTON, N. A. & CHASE, C. G. 1992. Tectonic, climatic and lithologic influences on landscape fractal dimension and hypsometry: implications for landscape evolution in the San Gabriel Mountains, California. *Geomorphology*, **5**, 77–114.

MASEK, J. G., ISACKS, B. L., GUBBELS, T. L. & FIELDING, E. J. 1994. Erosion and tectonics at the margins of continental plateaus. *Journal of Geophysical Research*, **99**, 941–13,956.

MCDERMID, G. J. & FRANKLIN, S. E. 1995. Remote sensing and geomorphometric discrimination of slope processes. *Zeitschrift fur Geomorphologie N.F.*, **101**, 165–185.

MILLIMAN, J. D. & SYVITSKI, J. P. 1992. Geomorphic/tectonic control of sediment discharge to the ocean: the importance of small mountain rivers. *Journal of Geology*, **100**, 525–544.

MOLNAR, P. & ENGLAND, P. 1990. Late Cenozoic uplift of mountain ranges and global climate change: chicken or egg? *Nature*, **346**, 29–34.

MONTGOMERY, D. R. 1994. Valley incision and the uplift of mountain peaks. *Journal of Geophysical Research*, **99**, 913–13,921.

PARK, S. K. & MACKIE, R. L. 1998. Crustal structure at Nanga Parbat, northern Pakistan, from magnetotelluric soundings. *Geophysical Research Letters*, **24**, 2415–2418.

PINTER, N. & BRANDON, M. T. 1997. How erosion builds mountains. *Scientific American*, April, 74–79.

RAYMO, R. E. & RUDDIMAN, W. F. 1992. Tectonic forcing of late Cenozoic climate. *Nature*, **359**, 117–122.

SCHMIDT, K. M. & MONTGOMERY, D. R. 1995. Limits to relief. *Science*, **270**, 617–620.

SCHNEIDER, D. A., EDWARDS, M. A., KIDD, W., KHAN, A., SEEBER, L. & ZEITLER, P. K. 1999. Tectonics of Nanga Parbat, western Himalaya: Synkinematic plutonism within the doubly-vergent shear zones of a crustal-scale pop-up structure. *Geology*, **27**, 999–1002.

SEARLE, M. P. 1991. *Geology and tectonics of the Karakoram Mountains*. Wiley.

—— & KHAN, M. A. 1995. *Geological Map of North Pakistan*.

SEEBER, L. & PÊCHER, A. 1998. Strain partitioning along the Himalayan Arc and the Nanga Parbat antiform. *Geology*, **26**, 791–794.

SHRODER JR., J. F. 1998. Slope failure and denudation in the western Himalaya. *Geomorphology*, **26**, 81–105.

—— & BISHOP, M. P. 1998. Mass movement in the Himalaya: new insights and research directions. *Geomorphology*, **26**, 13–35.

—— & —— 2000. Unroofing of the Nanga Parbat Himalaya. *This volume*.

——, ——, COPLAND, L. & SLOAN, V. 2000. Debris-covered glaciers and rock glaciers in the Nanga Parbat Himalaya. *Geografiska Annaler*, in press.

——, —— & SCHEPPY, R. 1998. Catastrophic flood flushing of sediment, western Himalaya, Pakistan. *In*: KALVODA, J. & ROSENFELD, C. L. (eds) *Geomorphological Hazards in High Mountain Areas*. Kluwer Academic Publishers, Dordrecht, 27–48.

——, SCHEPPY, R. & BISHOP, M. P. 1999. Denudation of small alpine basins, Nanga Parbat Himalaya. *Arctic, Antarctic, and Alpine Research*, **31**, 121–127.

SUMMERFIELD, M. A. & HULTON, N. J. 1994. Natural controls on fluvial denudation rates in major world drainage basins. *Journal of Geophysical Research*, **99**, 871–884.

WHITTINGTON, A. G. 1996. Exhumation overrated. *Tectonophysics*, **206**, 215–226.

ZEITLER, P. K. 1985. Cooling history of the northwest Himalaya. *Tectonics*, **4**, 127–151.

—— & CHAMBERLAIN, C. P. 1991. Petrogenetic and tectonic significance of young leucogranites from the northwestern Himalaya, Pakistan. *Tectonics*, **10**, 729–741.

——, —— & SMITH, H. A. 1993. Synchronous anatexis, metamorphism, and rapid denudation at Nanga Parbat (Pakistan Himalaya). *Geology*, **21**, 347–350.

Tracing the origins of the western Himalaya: an isotopic comparison of the Nanga Parbat massif and Zanskar Himalaya

A. WHITTINGTON[1,2], N. B. W. HARRIS[1], M. W. AYRES[1] & G. FOSTER[1]

[1]*Department of Earth Sciences, Open University, Walton Hall, Milton Keynes MK7 6AA, UK*

[2]*Present address: Department of Geology, 1310 W. Green Street, Urbana, IL 61801, USA (e-mail: awhittin@uiuc.edu)*

Abstract: New Sr and Nd isotope data for basement gneisses and leucogranites are presented from two contrasting areas of the western Himalaya; the Nanga Parbat–Haramosh massif (NPHM) and Zanskar. Sr-isotope systematics of metapelites and anatectic migmatites from the Zanskar Himalaya are characterized by ε_{Sr} of 515–930, typical of the High Himalayan Crystalline unit as exposed for more than 2000 km along strike. Moreover, Zanskar leucogranites are typical of the belt of Early Miocene granites intruding the High Himalayan Crystallines across the orogen (mean $\varepsilon_{Sr} = 834$). In contrast, the NPHM leucogranites show an elevated average ε_{Sr} of 2400, and basement samples show a wide range in ε_{Sr} from 1850 to 8150. Errorchrons for the metasedimentary gneisses indicate isotopic homogenization of the basement at *c.* 500 Ma for the Zanskar samples compared with *c.* 1800 Ma from the NPHM, confirming that the two terrains have experienced contrasting pre-Himalayan histories.

Nd isotopic data from the NPHM indicate model ages from 2300 to 2800 Ma, indicating the mean crustal formation ages of the protoliths from which the sediments were derived. A compilation of published Nd data from the Himalaya indicates average protolith formation ages of 2640 ± 220 Ma for the Lesser Himalaya lithologies, compared with 1940 ± 270 Ma for the High Himalaya unit.

Gneissic lithologies from Zanskar and the NPHM have previously been correlated with the High Himalayan Crystalline Series, since both display high-grade Himalayan metamorphism and are intruded by syn- to post-tectonic tourmaline-bearing leucogranites. Isotopic systematics in the Zanskar region confirm this correlation. In contrast, the NPHM basement rocks are better correlated with Lesser Himalayan lithologies, exposed south of the Main Central Thrust. We conclude that the NPHM represents either a lower structural level of the Lesser Himalaya Series, or its protolith.

Along most of its 2500 km length, the Himalayan orogen presents a generally uniform series of parallel tectonic units bounded by major faults. At either end of the main orogenic belt are syntaxial loops, which show a pronounced deviation from the usual pattern in structural orientation, timing and intensity of metamorphism. Both syntaxes are conspicuous by the anomalously high elevation achieved by their peaks, Namche Barwa in the east and Nanga Parbat in the west, which is accompanied by anomalously high exhumation rates of several mm a^{-1}, and intense neotectonic activity (Zeitler *et al.* 1982; Zeitler 1985; Butler & Prior 1988*a*; Owen 1989; Whittington 1996; Winslow *et al.* 1994; Burg *et al.* 1997). While Namche Barwa marks the eastern limit of Indian plate rocks, to the west of Nanga Parbat Indian plate rocks continue to crop out in Northern Pakistan. An outstanding problem in the geology of the western Himalayas has been to map the westward continuation of the main tectonostratigraphic units, which crop out regularly across the main orogen.

One crucial aspect of this is the correlation of rocks of the Nanga Parbat–Haramosh massif (NPHM) with those found in the main orogen. Two possible equivalents are the High Himalayan Crystalline Series (HHCS) and the Lesser Himalayan Series (LHS), both composed mainly of thick sequences of pelites, metagreywackes, carbonates and crystalline bodies, and which crop out uninterrupted for over 2000 km along the length of the main orogen. The HHCS crop out in the hanging wall of the south-vergent Main Central Thrust (MCT), and the LHS lie in

From: KHAN, M. A., TRELOAR, P. J., SEARLE, M. P. & JAN, M. Q. (eds) *Tectonics of the Nanga Parbat Syntaxis and the Western Himalaya*. Geological Society, London, Special Publications, **170**, 201–218. 1-86239-061-4/00/$15.00

the footwall, separated from Tertiary molasse deposits to the south by the Main Boundary Thrust (Fig. 1). Different criteria have been used to map the MCT by different authors and in different regions of the Himalaya. It is usually described as a high-strain zone, often with a zone of inverted metamorphic isograds (Searle *et al.* 1988, 1992; Hubbard 1989; Stäubli 1989), or a sharp metamorphic discontinuity (Macfarlane *et al.* 1992). The MCT is also marked by a change in model ages between the LHS and the HHCS (Parrish & Hodges 1996).

An investigation of Nd model ages from these two sequences in the central Himalaya indicate T_{DM} of 2300 to 2530 Ma (ε_{Nd} −23 to −26) for the LHS and 1860 to 2040 Ma (ε_{Nd} −14 to −19) for the HHCS (Parrish & Hodges 1996). Detrital zircon ages from the two units are similarly bimodal, at about 1860 to 2660 Ma for the Lesser Himalaya and about 800 to 1000 Ma for the High Himalaya (Parrish & Hodges 1996). These authors also presented a multigrain zircon Pb–Pb age of 1993 Ma from the HHCS, documenting the presence of an Early Proterozoic component.

Despite the clear difference between the sample populations, the interpretation of the relations between the LHS and HHCS remains contentious. The zircon and model age data of Parrish & Hodges (1996) led those authors to interpret the HHCS as a Late Proterozoic–Cambrian succession, stratigraphically equivalent to the upper part of the LHS. This contrasts strongly with the view of most previous workers who interpreted the High Himalaya as being basement to the Lesser Himalaya, which was regarded as a cover sequence and thought to have been deposited between the mid-Proterozoic and the Early Cambrian on the basis of stromatolites and small shelly fauna (Valdiya 1995). Much of the LHS is non-fossiliferous, and the syn-sedimentary Rampur volcanics within the Kulu–Rampur tectonic window, which exposes the LHS, have been dated by an Sm–Nd isochron at 2.5 Ga (Bhat & Le Fort 1992). The Lesser Himalaya and HHC were tentatively

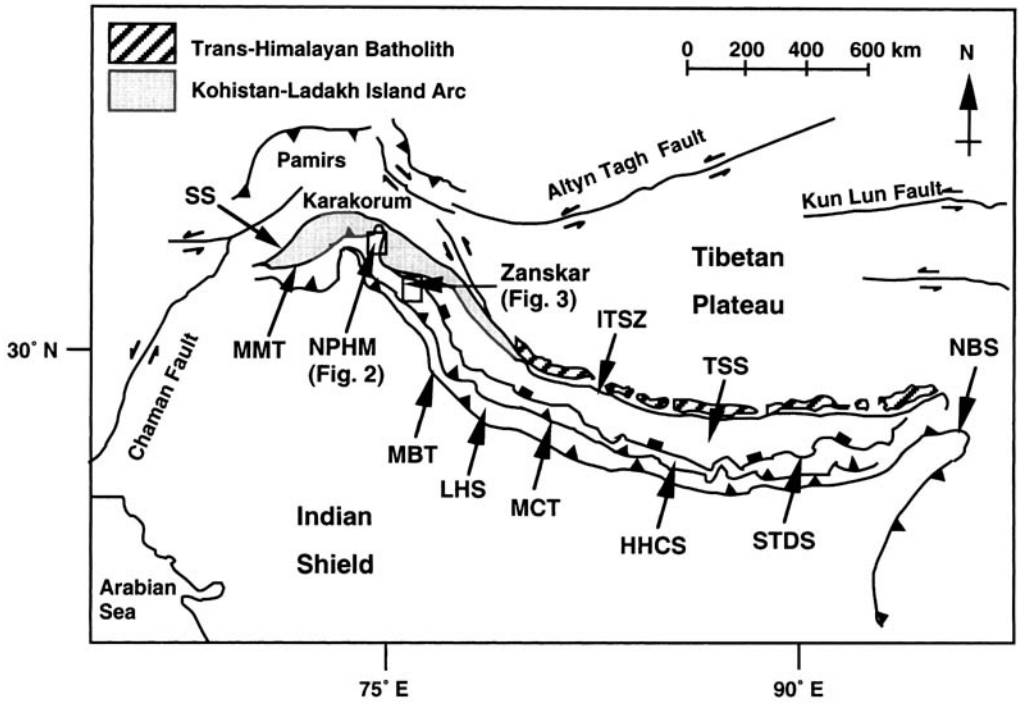

Fig. 1. Tectonic sketch map of the Himalayan orogen, showing the succession of units from north to south across the main orogen, divided by the main Himalayan faults. In Northern Pakistan, this sequence is complicated by the Kohistan–Ladakh island arc terrain (shaded), through which the Nanga Parbat–Haramosh massif has been exhumed in the last 10 Ma. SS, Shyok Suture; MMT, Main Mantle Thrust; NPHM, Nanga Parbat–Haramosh massif; ITSZ, Indus–Tsangpo Suture Zone; TSS, Tethyan sedimentary series; STDS, South Tibet Detachment System; HHCS, High Himalayan Crystalline Series; MCT, Main Central Thrust; LHS, Lesser Himalayan Series; MBT, Main Boundary Thrust; NBS, Namche Barwa Syntaxis.

correlated with the Lower and Upper parts of the Vindhayan Supergroup of the Indian plate by Chanda & Bhattacharyya (1982), while Draganits *et al.* (1998) found that dominant sedimentary transport directions are to the south for the HHCS but to the north for the LHS, and concluded that the LHS and HHCS were probably deposited in the same basin but from different source regions.

While the sedimentary and possible early metamorphic histories of the two sequences are somewhat unclear, the Tertiary history of the orogen is much better constrained. The HHCS have attained upper amphibolite grade during the Himalayan orogeny (Hodges *et al.* 1988; Hubbard 1989; Searle *et al.* 1992; Massey *et al.* 1994). In addition to anatectic migmatites, the HHCS contains both a suite of micaceous Palaeozoic leucogranites (Le Fort *et al.* 1986), and a suite of Miocene leucogranites, which are often deformed. Simultaneous with reverse movement on the MCT in the early Miocene, the extensional South Tibet Detachment System (STDS) carried the Tethyan Sedimentary Series (TSS) at least 35 km northwards (Burg *et al.* 1984; Herren 1987; Burchfiel *et al.* 1992; Hodges *et al.* 1992), leading to rapid decompression, allowing vapour-absent muscovite breakdown and anatexis in the underlying HHCS (Harris *et al.* 1993; Harris & Massey 1994). The resulting High Himalayan leucogranites (HHL) were emplaced between 24 and 18 Ma (Schärer 1984; Schärer *et al.* 1986; Copeland *et al.* 1988; Noble & Searle, 1995; Harrison *et al.* 1997).

The Lesser Himalaya, by contrast, have been metamorphosed at sub-garnet grade and exhibit no evidence of Tertiary igneous activity. There is widespread evidence for intrusion of granites at 1900 ± 100 Ma in nappes which were subsequently emplaced south of the MCT (Le Fort 1989), although these nappes are of debated origin (Upreti & Le Fort 1999). Other deformed granites have been dated as Cambro-Ordovician, for example the Almora Nappe has yielded an Rb–Sr age of 560 ± 20 Ma (Trivedi *et al.* 1984). While this nappe is also of uncertain provenance, it matches the LHS isotopically (Ahmad *et al.* 1999), and has been correlated with the Munsiari nappe (Trivedi *et al.* 1984) which was assigned to the LHS by Valdiya (1980).

Of the two main tectonostratigraphic units, the NPHM has always been considered to be correlated with the HHCS rather than the Lesser Himalaya (e.g. Valdiya 1995; Blum *et al.* 1998), in part because of its similarly high metamorphic grade, and in part because the NPHM hosts tourmaline-bearing leucogranite bodies of Miocene age or younger (Zeitler & Chamberlain 1991; Zeitler *et al.* 1993; Schneider *et al.* 1999). Although geochemically very similar in many respects to High Himalayan leucogranites, and resulting from a similar 'decompression melting' reaction, the NPHM leucogranites have been noted for their unusually radiogenic isotopic characteristics (Zeitler & Chamberlain 1991; George *et al.* 1993; Butler *et al.* 1997; Whittington *et al.* 1999).

Another reason for the NPHM to be considered an extension of the HHCS is that it lies to the north of the generally accepted continuation of the MCT in Northern Pakistan (Chaudhry & Ghazanfar 1990). There is no single thrust which shows the typical features of the MCT and, while which of the many thrusts in Pakistan is the nearest equivalent to the MCT is still debated, most candidate faults lie very close to the MBT in this area.

While the signatures of Himalayan orogenesis are fairly similar at Nanga Parbat and in the main orogen, the question remains as to whether the two terrains have different pre-Himalayan origins. Isotope systematics may be a useful terrain discriminant where rocks of two different terrains are indistinguishable in the field (e.g. Dickin & McNutt 1989; Guo & Dickin 1996). The nearest outcrop of HHCS to the NPHM occurs in the Zanskar region of northwest India, and an isotopic comparison of the two areas has been conducted to address this problem.

The Nanga Parbat–Haramosh massif (NPHM)

The NPHM is bounded to the north by the Main Mantle Thrust (MMT), locally overprinted by more recent strike-slip and reverse faults that separate the NPHM from the Kohistan–Ladakh island arc terrain (Fig. 2). The NPHM is composed of pelitic and carbonaceous paragneisses, and tonalitic to granitic orthogneisses, and the presence of metabasic sheets cross-cutting the earliest gneissic fabrics indicates a long and polymetamorphic history for the terrain (Wheeler *et al.* 1995). Pelitic lithologies occur at staurolite–kyanite grade on the margins of the massif, but have reached cordierite–sillimanite grade in the core of the massif around Fairy Meadow (Misch 1949). The highest grade assemblages contain rare cordierite–spinel intergrowths which indicate P–T conditions of 710 ± 60 °C and 5.0 ± 1.1 kbar (Whittington *et al.* 1998).

The NPHM was divided into the predominantly orthogneissic Iskere gneiss and predominantly metasedimentary Shengus gneiss by Madin

et al. (1989). One possible relation between the two units is that the Shengus gneiss was the supracrustal cover to the structurally higher Iskere gneiss, the latter tectonically emplaced on a reverse shear zone (Treloar *et al.* 1991), although a subsequent study concluded that this zone of apparent high strain was in fact due to the contrasting rheological behaviour of the two units (Wheeler *et al.* 1995). U–Pb studies on the cores of zircons have revealed ages of about 1850 Ma for the Iskere gneiss and about 400 to 500 Ma for the Shengus gneiss (Zeitler *et al.* 1989, 1993), with some zircons from the Shengus gneiss defining a discordia trend between 400 to 500 Ma and 2500 Ma, and two concordant analyses at about 2500 Ma (Zeitler *et al.* 1989).

Gneissic basement samples collected for this study come from the Shengus gneiss in the southern NPHM around Nanga Parbat itself, and are pelitic to semipelitic in composition. A range of grades is represented, from muscovite–biotite in the Rupal valley to biotite–cordierite–sillimanite at Fairy Meadow, covering a north–south traverse over a distance of some 30 km (Fig. 2).

Leucogranite plutons and associated feeder dykes, pegmatites and aplites outcrop throughout the NPHM. In the southern part of the massif, the well-exposed Tato pluton and several leucogranite sheets have been sampled. Post-collisional leucogranites are one of the most distinctive features of the Himalayan orogen, and the Nanga Parbat leucogranites share many petrographic and geochemical features with those from Zanskar and other areas of the main orogen (Whittington *et al.* 1999). The Tato pluton is apparently both compositionally homogeneous and undeformed throughout its outcrop, both horizontally over at least 2 km, and vertically throughout 500 m.

There are also numerous leucogranitic sheets and dykes associated with the pluton, rarely more than 1 m in width. In the core of the massif, both on the Fairy Meadows and Rupal sides of Nanga Parbat itself, undeformed sheets are usually subhorizontal in orientation, consistent with vertical extension during unroofing of the massif. Several sheets show textures indicative of multiple episodes of magma injection. On the western margin of the massif, leucogranitic dykes are often coarser-grained and pegmatitic, and have been deformed in the Liachar Shear Zone. Boudinaged dykes show pre-full crystallization deformation fabrics, indicating syn-tectonic emplacement (Butler *et al.* 1997). Some sheets are almost entirely quartzofeldspathic, while others contain small euhedral clean garnets, and pegmatites usually contain tourmaline and biotite

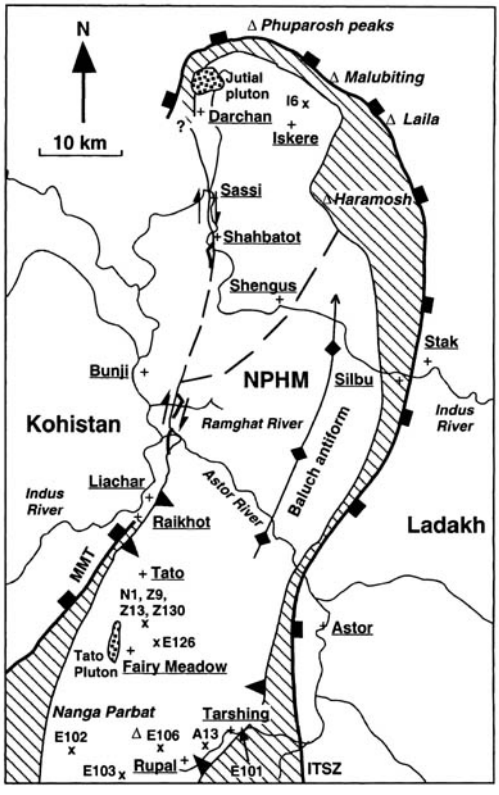

Fig. 2. Tectonic sketch map of the Nanga Parbat–Haramosh massif, showing major tectonic structures and lithological boundaries. Jutial and Tato plutons are stippled; kyanite grade 'cover' sediments are striped. X marks sample locations including A13 and I6 of George *et al.* (1993). All samples are from the Shengus paragneiss (no ornament) except for I6 from the Iskere gneiss. Geology compiled from Butler & Prior (1988*b*), Madin *et al.* (1989), Butler *et al.* (1992), George (1993), Edwards *et al.* (1997) and unpublished mapping by the authors.

megacrysts. Occasional late cross-cutting aplites can be found, apparently undeformed by the Liachar Shear Zone, suggesting their emplacement was very recent. Several undeformed feeder dykes and one deformed sheet from the Liachar Shear Zone (E81) were sampled.

The Zanskar valley

In the Zanskar region the HHC is separated from folded and weakly metamorphosed Tethyan sediments to the north by the extensional Zanskar Normal Fault (ZNF) (Herren 1987), the local equivalent of the STDS, and from the low grade Lesser Himalaya to the south by the

MCT. The MCT zone is characterized by a zone of inverted metamorphic isograds (Searle & Rex 1989; Stäubli 1989), with the highest grade rocks (sillimanite-zone anatectic migmatites) exposed in the core of the HHCS (Pognante & Lombardo 1989; Searle & Rex 1989; Pognante *et al.* 1990; Searle *et al.* 1992), and lower grade rocks found towards the upper structural levels near the ZNF (Fuchs 1982; Searle 1986). Zanskar differs in this respect from other regions of the Himalaya where the highest grade rocks are found at the highest structural levels (e.g. Nepal, Searle *et al.* 1997). Temperatures of up to 750 °C are obtained for the HHC in Zanskar (Searle *et al.* 1992), and pressure–temperature estimates of 690–720 °C at 8–10 kbar and 695–730 °C at 10–12 kbar were obtained by Ayres & Vance (1997). In this region, the Lesser Himalaya crop out in the thrust-bounded klippe of the Kishtwar window (Fig. 3), which may owe its existence to a ramp in the MCT (Searle *et al.* 1992).

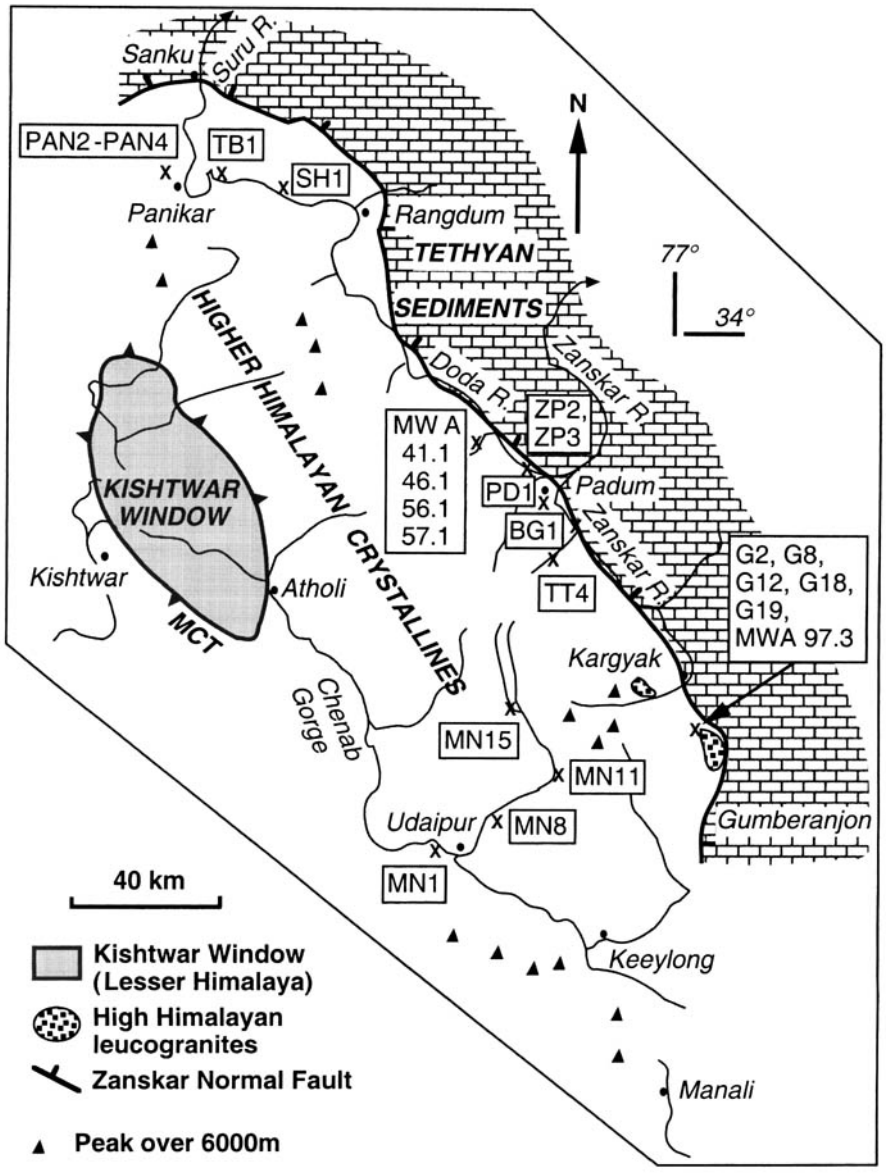

Fig. 3. Tectonic sketch map of the Zanskar Himalaya, showing sample locations (x), major tectonic structures and lithological boundaries. Geology modified after Searle (1986), Searle *et al.* (1988) and Honegger *et al.* (1982).

Table 1. *Rb–Sr isotopic data from the Zanskar region*

Sample	Type*	Rb (ppm)	Sr (ppm)	$^{87}Rb/^{86}Sr$	$^{87}Sr/^{86}Sr$	ε_{Sr}	T_{BE} (Ma)
G2	undef bt lcg	253	110	6.65	0.76243	819	617
G8	undef bt lcg	257	140	5.31	0.75118	660	624
G18	undef tur lcg	290	68	12.33	0.75775	753	304
G19	undef tur lcg	293	72	11.76	0.75724	746	316
PD1	undef tur lcg	315	12	75.89	0.76779	895	59
MWA 97.3	undef tur lcg	248	76	9.43	0.76475	852	451
PAN4	def 2 mica gr	242	119	5.88	0.75385	697	595
MN8	def 2 mica gr	307	86	10.32	0.79313	1255	606
SH1	def 2 mica gr	220	73	8.71	0.76674	880	505
ZP2	def tur lcg	335	27	35.87	0.77259	963	133
ZP3	def tur lcg	314	42	21.61	0.76056	793	182
BG1	def tur lcg	283	55	14.88	0.75349	692	232
G10	HHC metsed	150	123	3.53	0.75375	696	997
PAN2	HHC metsed	188	89	6.11	0.76478	853	699
PAN3	HHC metsed	173	113	4.43	0.76207	814	925
TB1	HHC metsed	162	74	6.33	0.75643	734	581
MN1	HHC metsed	173	77	6.50	0.77000	927	714
MN11	HHC metsed	133	106	3.63	0.74101	515	718
MWA41.1	HHC metsed	197	125	4.56	0.75123	660	729
MWA46.1	HHC metsed	353	192	5.32	0.76491	854	806
MN15BR2	migmatite	206	119	5.00	0.74906	629	632
TT4BR2	migmatite	222	96	6.69	0.78635	1159	866
56.1aBR1	migmatite	209	108	5.59	0.76540	861	772

*Abbreviations are as follows: undef, undeformed; def, deformed; bt, biotite; tur, tourmaline; 2 mica gr, biotite + muscovite leucogranite; lcg, leucogranite; metsed, metasedimentary gneiss.

Samples presented in this study were collected from the HHC near to the ZNF (Fig. 3), and include both metapelitic and migmatitic gneisses. Two suites of Miocene leucogranites have been recognized in the Himalaya; an earlier two-mica phase and a later tourmaline–muscovite phase (Reddy *et al.* 1993; Guillot & Le Fort 1995), and samples of each facies have been collected (Table 1).

Analytical techniques

Standard sample preparation and isotopic analytical techniques are described in Cohen *et al.* (1988) and Whittington (1997). Strontium was loaded in phosphoric acid on single Ta filaments, and the measured $^{87}Sr/^{86}Sr$ ratios were exponentially fraction corrected within each run to $^{87}Sr/^{88}Sr = 0.1194$. Machine standard NBS 987 was run with each batch of samples, and reported analyses have been corrected to a value of NBS 987 of 0.710220. Thirteen measurements of NBS 987 gave an average $^{87}Sr/^{86}Sr$ ratio of 0.710223 ± 17 (1 sigma), and the rock standard NBS 607 gave an $^{87}Sr/^{86}Sr$ ratio of 1.200872 ± 16 (1 sigma). Total procedural Sr blanks were less than 3 ng.

Neodymium was loaded on Ta filaments (a Re ionization filament was used) and run as metal ions. $^{143}Nd/^{144}Nd$ ratios were exponentially fraction corrected to $^{146}Nd/^{144}Nd = 0.72190$. Eight analyses of an internal J&M Nd standard over the period of analysis had a mean value of 0.511753 ± 10 (1 sigma), and reported ratios have been corrected to a value for J&M of 0.511836, corresponding to a value for BCR-1 of 0.512638. Total procedural Nd blanks were less than 1 ng.

$^{87}Rb/^{86}Sr$ and $^{147}Sm/^{144}Nd$ ratios were calculated for each sample from the elemental ratios measured by XRF and INAA. Errors on the Sm/Nd ratio calculated from the data are less than 5% based on multiple analyses of the Whin Sill internal rock standard (Sm = 8.8 ± 0.2 ppm, Nd = 33.0 ± 0.9 ppm, $n = 8$). Present-day ratios are compared to CHUR using the epsilon notation of DePaolo & Wasserburg (1976), taking present-day CHUR values of $^{143}Nd/^{144}Nd = 0.512638$, and $^{147}Sm/^{144}Nd = 0.1967$. Model ages were calculated applying the quadratic equation of DePaolo (1981) for $^{143}Nd/^{144}Nd$ in the depleted mantle as a function of CHUR through time. Errors on the model age propagated from the Sm/Nd ratio determination are typically less than 0.2 Ga and always less than 0.3 Ga.

For granites an average upper crustal $^{147}Sm/^{144}Nd$ ratio of 0.115 was assumed prior to crystallization at 5 Ma for the NPHM and 20 Ma for the HHL. This procedure is followed because Sm/Nd ratios are controlled by the behaviour of accessory phases such as monazite and apatite, and may be changed during anatexis or fractional crystallization (Hawkesworth *et al.* 1981; Vidal *et al.* 1982; Deniel *et al.* 1987; Montel 1993; Ayres & Harris 1997). Erroneous model ages will

therefore be calculated if the Sm/Nd ratio of the granite is used for the pre-anatectic isotopic evolution of the bulk rock.

Isotopic results

The NPHM

On an Rb–Sr isotope errorchron diagram, the majority of NPHM basement lithologies display a poorly defined trend corresponding to an age of between 1800 and 2250 Ma (Fig. 4). George & Bartlett (1996) reported an 1850 Ma trend for samples from the Sassi–Darchan Shear Zone, also plotted for comparison in Fig. 4. Samples from the southern NPHM are characterized in general by higher Rb/Sr ratios, and the combination of the two datasets suggests a minimum errorchron age of about 1800 Ma.

Leucogranites from the NPHM are scattered about a horizontal trend, with elevated Rb/Sr ratios. The 11 samples of the Tato pluton have an average $^{87}Sr/^{86}Sr$ ratio of 0.874 ± 0.009 and ε_{Sr} of 2398 ± 122, similar to ratios of 0.875 to 0.892 reported by George *et al.* (1993) for the Jutial pluton in the northern NPHM. The Tato pluton is characterized by higher Rb/Sr ratios than the Jutial pluton, possibly reflecting slightly different source chemistry (Fig. 4). The degree of scatter indicates some isotopic disequilibrium, which is much more pronounced in the analyses from leucogranite sheets. This may reflect the involvement of non-magmatic fluids during deformation, which were preferentially focused along the shear zones that deform many of the sheets (Butler *et al.* 1997).

Eight basement samples were also analysed for Nd isotopes, and are characterized by very low present-day $^{143}Nd/^{144}Nd$ ratios with ε_{Nd} between -18 and -29 (Table 2). The samples are somewhat scattered, the eight samples presented here yielding a meaningless errorchron of 3675 ± 376 Ma (MSWD = 15.0). If samples Z9/i and Z13/i are not included, the remaining six give an age of 2376 ± 283 Ma (MSWD = 1.64), although there is no *a priori* justification for elimination of these two samples from the dataset. Model ages relative to depleted mantle are between 2.3 and 2.8 Ga (Fig. 5). Note that while these model ages are calculated applying the quadratic equation for $^{143}Nd/^{144}Nd$ in the depleted mantle as a function of CHUR through time, calculations assuming a linear evolution for depleted mantle yield ages on average only 0.1 Ga younger. The coincidence (within the scatter of the data) of errorchron age, model age and some zircon core ages suggests that this age may represent a crust-forming event. The only

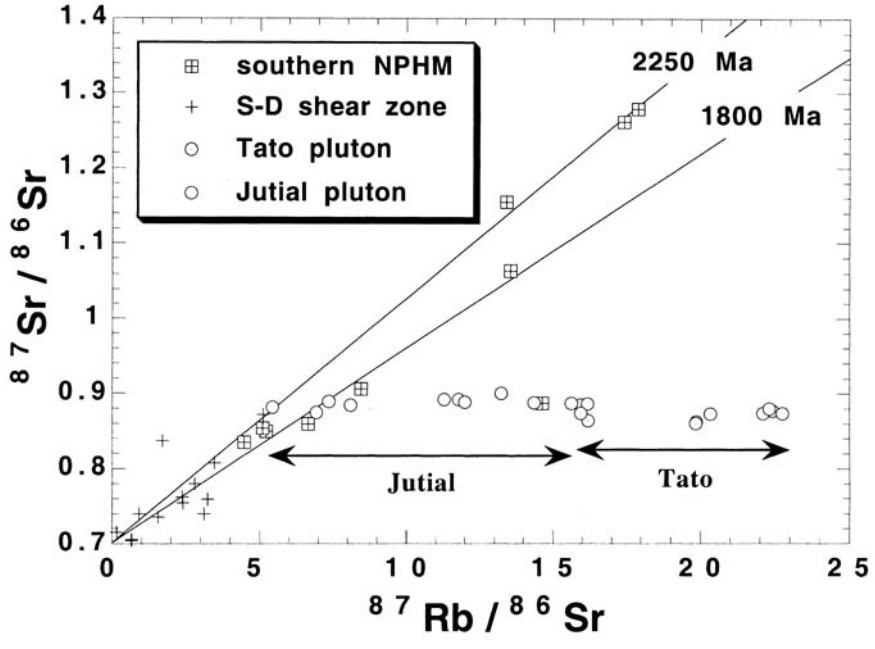

Fig. 4. Rb–Sr errorchron diagram for samples from the NPHM. Samples from the southern NPHM and Tato pluton from Table 3, samples from the Sassi–Darchan Shear Zone and Jutial pluton are from George & Bartlett (1996). Reference lines corresponding to ages of 1800 Ma and 2500 Ma are shown for comparison.

Table 2. *Sm–Nd data for the Nanga Parbat–Haramosh massif*

Sample	Sm (ppm)	Nd (ppm)	$^{147}Sm/^{144}Nd$*	$^{143}Nd/^{144}Nd$	$\pm 2\sigma$	ε_{Nd}†	T_{DM} (Ga)‡
Gneisses							
N1	7.03	41.2	0.103	0.511147	16	−29	2.66
Z9/i	4.44	22.8	0.118	0.511607	16	−20	2.31
Z13/i	5.09	24.2	0.127	0.511704	6	−18	2.40
E101	11.5	62.9	0.111	0.511230	15	−27	2.73
E102	12.4	67.7	0.111	0.511277	15	−27	2.66
E106	8.71	45.0	0.117	0.511353	6	−25	2.72
Z130a/ii	10.2	47.9	0.129	0.511521	14	−22	2.81
Z130b/ii	9.45	46.0	0.124	0.511492	14	−22	2.70
Tato pluton							
E5A/i	3.47	21.7	0.097	0.511402	16	−24	2.56§
E5A/ii	3.47	20.7	0.102	0.511442	14	−23	2.50§
E5B	3.37	21.9	0.093	0.511461	10	−23	2.51§
Z66A	3.93	21.5	0.111	0.511428	14	−24	2.52§
E70A	3.72	24.4	0.092	0.511418	14	−24	2.53§
E70B	4.02	23.9	0.102	0.511451	10	−23	2.48§
E70C	3.65	23.8	0.093	0.511429	10	−24	2.51§
E111	3.30	20.6	0.097	0.511459	12	−23	2.47§
E112	3.33	20.7	0.097	0.511489	8	−22	2.42§
Z140	3.45	21.8	0.096	0.511476	12	−23	2.44§
Z141	3.20	21.4	0.091	0.511466	12	−23	2.45§
Z142	n/d	n/d	n/d	0.511444	8	−23	2.49§
Leucogranite dykes							
E64	3.12	17.4	0.109	0.511449	58	−23	2.49§
E81	0.92	5.1	0.109	0.511277	14	−27	2.77§
Z105	2.45	13.5	0.110	0.511391	16	−24	2.58§
E107	1.30	10.4	0.076	0.511428	16	−24	2.51§
E109	n/d	n/d	n/d	0.511429	16	−24	2.51§
E114	3.42	20.4	0.101	0.511480	10	−23	2.43§
E128	n/d	n/d	n/d	0.511448	12	−23	2.49§
E133	n/d	n/d	n/d	0.511457	16	−23	2.47§

* $^{147}Sm/^{144}Nd$ calculated using natural abundances.
† ε_{Nd} calculated relative to CHUR using present day values.
‡ T_{DM} calculated using the quadratic solution for DM evolution of DePaolo (1981).
§ Assuming average upper crustal $^{147}Sm/^{144}Nd$ of 0.115, prior to crystallization at 5 Ma.

available analysis of Iskere orthogneiss, I6 of George *et al.* (1993), lies on the 2750 Ma reference line and continues the general trend of the other samples which are all from the Shengus paragneiss unit (Fig. 5).

Twelve leucogranites show similarly low ε_{Nd} between −22 and −24, with one sheet at −27. Calculated model ages using present-day $^{147}Sm/^{144}Nd$ ratios are between 1.8 and 2.6 Ma, averaging 2.1 Ga. As explained above, these ages are subject to considerable uncertainty due to the strong possibility of Sm/Nd fractionation during anatexis. Calculated model ages assuming an average upper crustal $^{147}Sm/^{144}Nd$ ratio of 0.115 prior to crystallization at 5 Ma are between 2.4 and 2.8 Ga (Table 2). The granites show much greater homogeneity in ε_{Nd} than the basement gneisses, which may represent preferential sourcing from one particular lithological horizon. The unusually high ε_{Sr} and low ε_{Nd} values for the leucogranites suggest that the source was old crustal material, probably the deeper equivalents of currently exposed basement metapelites which cover the required ranges for both isotopic systems.

Zanskar

Eight metasediments and three migmatites from the Zanskar region show moderately elevated $^{87}Sr/^{86}Sr$ ratios, with ε_{Sr} between 515 and 925 (Table 1). Leucogranite samples indicate significant disequilibrium between different granite samples ($^{87}Sr/^{86}Sr = 0.763 \pm 0.11$ for all 12 samples). The average of the six undeformed samples, including both two-mica and tourmaline facies, is 0.760 ± 0.006. In the High Himalaya, these two facies show slightly different ratios, which were attributed to the signatures of different protoliths by Guillot & Le Fort (1995).

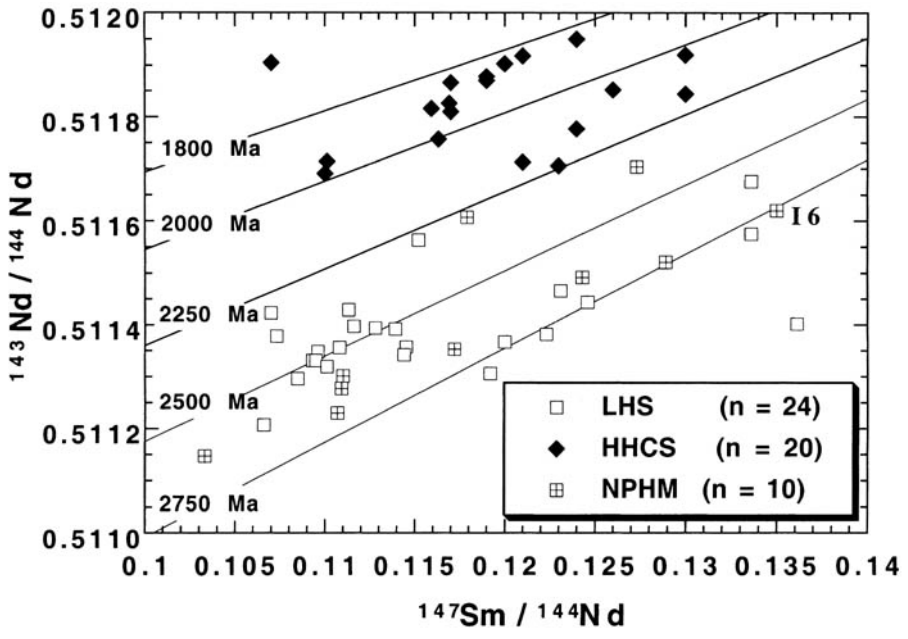

Fig. 5. Sm–Nd errorchron diagram for samples from the NPHM. Filled triangles are NPHM Shengus gneiss samples from Table 2, and sample A13 from George *et al.* (1993). Label 'I6' denotes Iskere gneiss sample from George *et al.* (1993). Open circles are Lesser Himalayan samples, from France-Lanord & Le Fort (1988), Parrish & Hodges (1996) and Ahmad *et al.* (1999). Squares are High Himalayan samples from Deniel *et al.* (1986, 1987), Inger & Harris (1993), Massey (1994) and Parrish & Hodges (1996). Reference lines are calculated to have an initial $^{143}Nd/^{144}Nd$ ratio identical to the depleted mantle at the indicated age, hence samples lying along the same reference lines will have the same model age and errorchron age.

Deformational recrystallization and fluid interaction may have affected $^{87}Sr/^{86}Sr$ ratios in the deformed samples. Variations of a similar magnitude may also be caused by disequilibrium melting, although this is not thought to be a significant feature of the High Himalayan leucogranites (Harris & Ayres 1998). Initial $^{87}Sr/^{86}Sr$ ratios of leucogranites from both Zanskar and the NPHM clearly reflect the isotopic characteristics of the different source rocks from which they were derived.

Terrain correlations

The isotope systematics of the NPHM and Zanskar regions are clearly different. In order to correlate the typical Himalayan lithologies with those in Northern Pakistan therefore, we must compare the NPHM to the LHS. For the purposes of discriminating between terrains, a histogram of ε_{Sr} has been compiled from new and previously published data (Fig. 6).

The first point to note is that the range of Zanskar rocks lies well within the range defined by the HHCS series, and so there is no possibility of a significant change in isotopic characteristics within the HHCS along strike (the HHCS data are compiled from areas as far apart as western India and Bhutan). Second, while no HHCS sample has ε_{Sr} greater than 3000, both NPHM and LHS samples show ε_{Sr} values greater than 8000. While more data would be desirable for the NPHM, it is clear that the range of values far exceeds that of the HHCS but falls within that exhibited by the LHS. Third, while the range of ε_{Sr} values found in the Sassi–Darchan Shear Zone (George & Bartlett 1996) lies within that of the HHCS, the trends indicated on isochron diagrams are quite distinct. For each histogram there is a mixture of orthogneiss and metapelitic lithologies, each of which covers a similar range within each terrain, so that the observed distribution is not due to unrepresentative sampling of specific lithologies.

The different isotopic characteristics of the source terrains are also clearly discernible in the leucogranites (Fig. 7). The highest ε_{Sr} for any High Himalayan leucogranite is less than 1500, while the lowest ε_{Sr} for Nanga Parbat leucogranites is over 2000. The range of ε_{Sr} within each terrain is much more limited than the corresponding range for basement lithologies, perhaps

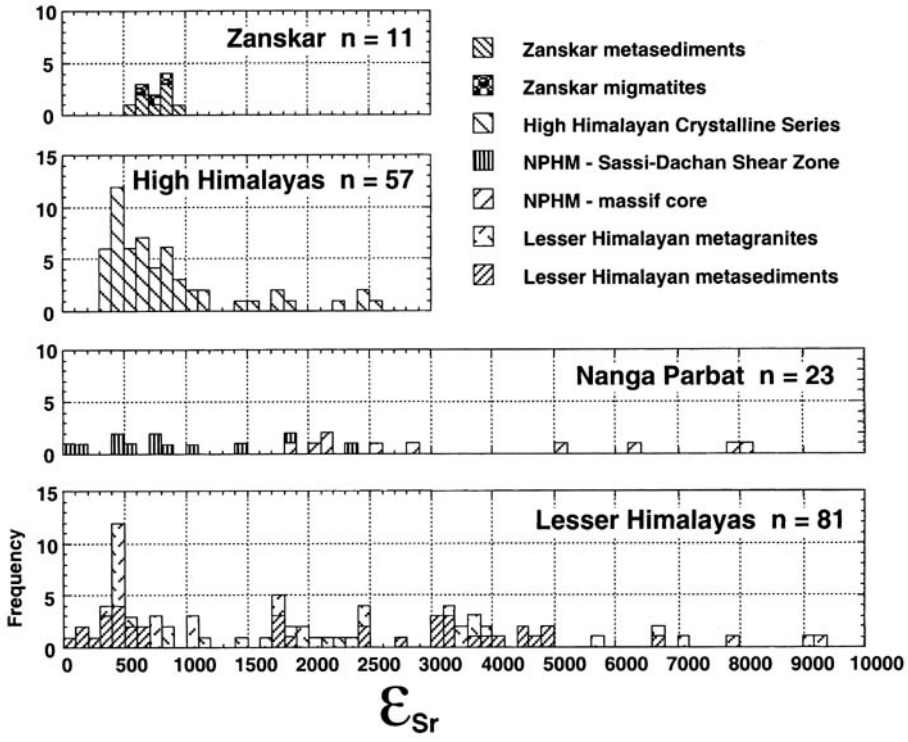

Fig. 6. Histogram of present-day ε_{Sr} for basement rocks of the Himalayan orogen. Data for Zanskar Himalaya from Table 1. Data for the High Himalayan Crystalline Series from Vidal *et al.* (1982), Ferrara *et al.* (1983), Searle & Fryer (1986), Deniel *et al.* (1987), Inger & Harris (1993), and Massey (1994). Data for the southern Nanga Parbat–Haramosh massif from Table 3, and for the Sassi-Darchan Shear Zone from George & Bartlett (1996). Data for the Lesser Himalayan Series from Trivedi *et al.* (1984) for metagranitic lithologies, and from France-Lanord *et al.* (1988, 1993), Sharma *et al.* (1992), Massey (1994), and Ahmad *et al.* (1999) for metasedimentary lithologies. Note the change in scale above ε_{Sr} values of 3000.

reflecting melt formation from a restricted range of fertile lithologies, or mixing between magma batches derived from a range of metasedimentary sources (Harris & Ayres 1998). It is interesting to note that the NPHM leucogranites and HHL are nearly identical in major and trace element geochemistry, because leucogranites from both terrains were generated by the same vapour-undersaturated muscovite breakdown reaction, at similar temperatures of 700 to 750 °C (Harris *et al.* 1995; Whittington *et al.* 1999). Even if some isotopic disequilibrium between melt and source is preserved by a combination of rapid heating and melt extraction, this will shift leucogranite $^{87}Sr/^{86}Sr$ ratios by less than 0.01 (Harris & Ayres 1998), a relatively small difference compared to the range in basement $^{87}Sr/^{86}Sr$ ratios exhibited by the two terrains.

A limited set of Sm–Nd data has also been compiled (Table 2). Whilst less extensive, these data make even clearer the differences between the terrains. A geographically wide-ranging set of 20 samples from the HHCS shows model ages between about 1.6 and 2.25 Ga, clustering between 1.8 and 2.0 Ga. A similar collection of 24 samples from the LHS has model ages between 2.3 and 2.8 Ga, with one outlier at 3.3 Ga. Ten analyses from the core of the NPHM also range between 2.3 and 2.8 Ga, with a median value of 2.6 Ga.

Leucogranite Sm–Nd systematics also show a similar pattern to that for the Rb–Sr system, with two quite distinct populations of ε_{Nd} (Fig. 8). Again, the range of ε_{Nd} exhibited by the NPHM granites is more restricted than that of the NPHM gneisses. The Sm/Nd ratios of leucogranites are controlled by accessory phase dissolution, which is likely to be slow compared to equilibration between the major phases which host Rb and Sr (Ayres *et al.* 1997). While significant variation is observed in the Rb–Sr data for leucogranite dykes from the NPHM (Table 3), this is not the case for the Sm–Nd system. Hence the variability of $^{87}Sr/^{86}Sr$ ratios obtained from the dykes is

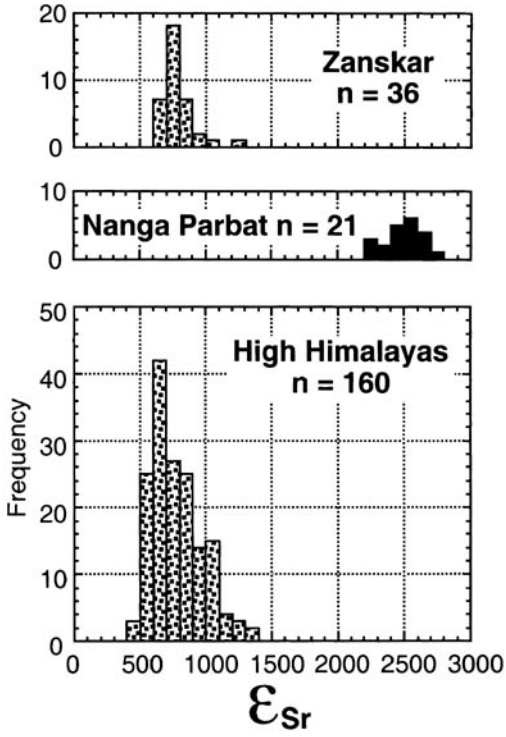

Fig. 7. Histogram of present-day ε_{Sr} for Tertiary granitic rocks of the Himalayan orogen. Data for Zanskar leucogranites from Searle & Fryer (1986), Ferrara *et al.* (1991) and Table 2. Data for other High Himalayan leucogranites from Dietrich & Gansser (1981), Kai (1981), Vidal *et al.* (1982), Ferrara *et al.* (1983, 1991), Deniel *et al.* (1986, 1987), Stern *et al.* (1989), Scaillet *et al.* (1990), Inger & Harris (1993), Massey (1994), and Searle *et al.* (1997). Data for Nanga Parbat leucogranites from Table 3 and George *et al.* (1993).

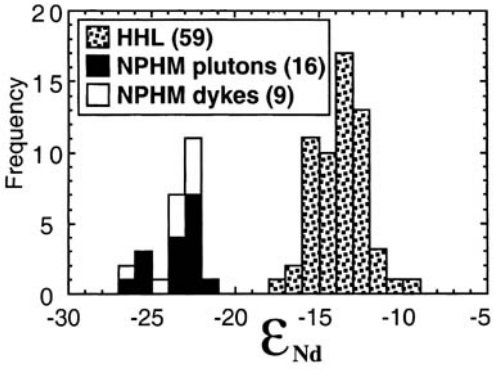

Fig. 8. Histogram of present-day ε_{Nd} for Tertiary granitic rocks of the Himalayan orogen. Data for High Himalayan leucogranites from Allègre & Ben Othman (1980), Vidal *et al.* (1984), Deniel *et al.* (1986, 1987), Stern *et al.* (1989), Ferrara *et al.* (1991), Inger & Harris (1993) and Searle *et al.* (1997). Data for Nanga Parbat leucogranite plutons and dykes from Table 2 and George *et al.* (1993). Number in brackets denotes number of analyses.

attributed to a combination of fluid interaction and possible re-equilibration during deformational recrystallization, rather than to disequilibrium melting.

Hence we conclude that the NPHM terrain shows marked isotopic similarities with the LHS, but not with Zanskar or any other part of the HHCS. This conclusion has potentially important implications, which depend on whether the NPHM is interpreted to be the western equivalent of the LHS, or its protolith.

Discussion

As mentioned above, the Nanga Parbat massif is generally assumed to be correlated with the High Himalaya rather than the Lesser Himalaya due to its similarly high metamorphic grade and the presence of mid-late Tertiary tourmaline leucogranites, both of which are lacking in the Lesser Himalaya. However, this correlation is based on Tertiary features. Although presently at

Table 3. *Rb–Sr isotopic data from the southern Nanga Parbat–Haramosh massif*

Sample	Rb (ppm)	Sr (ppm)	$^{87}Rb/^{86}Sr$*	$^{87}Sr/^{86}Sr$	ε_{Sr}†	T_{BE} (Ma)‡
Gneisses						
N1	233	46.0	14.64	0.88700	2587	876
Z9/i	355	58.9	17.42	1.26178	7905	2227
Z13/i	365	59.0	17.89	1.27876	8146	2235
E101	240	155.0	4.48	0.83493	1848	2058
E102	334	72.0	13.41	1.15483	6387	2339
E103	320	68.3	13.54	1.06308	5086	1850
E106	336	114.9	8.45	0.90613	2858	1676
E126	269	116.7	6.65	0.85901	2190	1635
Z130a/ii	258	142.8	5.22	0.84948	2055	1957
Z130b/ii	273	155.2	5.09	0.85313	2106	2060
Tato pluton						
E5A/i	453	58.5	22.39	0.87733	2450	543
E5A/ii	458	60.0	22.07	0.87382	2400	540
E5B	471	59.9	22.73	0.87411	2404	525
Z66A	444	57.6	22.28	0.88023	2491	555
E70A	395	71.7	15.93	0.88543	2565	799
E70B	397	71.1	16.14	0.88591	2571	790
E70C	395	71.7	15.93	0.87411	2404	749
E111	474	67.5	20.30	0.87300	2388	584
Z140	436	78.0	16.16	0.86356	2254	693
Z141	468	70.1	19.30	0.86057	2212	569
Z142	472	68.8	19.83	0.86287	2245	562
Leucogranite dykes						
E64	497	35.7	40.25	0.89826	2747	339
E81	267	46.5	16.60	0.83809	1893	566
Z105	506	21.5	68.04	0.86245	2239	163
E107	214	16.6	37.27	0.95376	3534	470
E109	396	56.0	20.44	0.88846	2608	633
E114	470	37.1	36.64	0.88701	2587	350
E128	545	20.5	76.86	0.88100	2502	162
E133	500	33.0	43.80	0.89182	2655	301
Late pegmatite						
Z58B	314	45.5	19.95	1.33100	8887	2186

* $^{87}Rb/^{86}Sr$ calculated assuming natural abundances.
† ε_{Sr} calculated using present day values, $^{87}Sr/^{86}Sr_{CHUR} = 0.7047$.
‡ T_{BE} calculated with $^{87}Rb/^{86}Sr_{CHUR} = 0.0847$.

different metamorphic grades, all three sequences are a similar mixture of predominantly pelitic metasediments with greywacke and carbonate horizons, containing extensive granitic orthogneiss bodies. The Himalayan orogeny has masked but not completely erased evidence of the pre-Himalayan history of these terrains, which is the primary focus of this study.

Further insight into the origin of the two terrains can be gained by a comparison of the timing of events recorded by different isotopic systems (Fig. 9). The oldest available age data include Sm–Nd whole-rock model ages from both the Nanga Parbat massif and Lesser Himalaya, each of which indicates an age of 2.3 to 2.8 Ga. This brackets the age of the oldest zircon cores known from the Shengus gneiss of the NPHM at about 2500 Ma (Zeitler *et al.* 1989). Detrital zircons in the Lesser Himalaya cover a range from 1870 to 2600 Ma (Parrish & Hodges 1996). This lower limit of detrital zircon ages in the LHS coincides with zircon core ages from the Iskere orthogneiss of the NPHM (Zeitler *et al.* 1989), and with Rb–Sr errorchron ages from the NPHM (Fig. 4; see also George & Bartlett 1996). The *c.* 1850 Ma age is the earliest recorded event in the HHCS, recorded by Nd model ages (Fig. 5; see also Parrish & Hodges 1996) and Rb–Sr isochrons for orthogneissic bodies (Bhanot *et al.* 1977).

Following this mid-Proterozoic event there is a gap of some 1300 Ma in the isotopic record, marked only by detrital zircon components of 800–1000 Ma from the HHCS (Parrish &

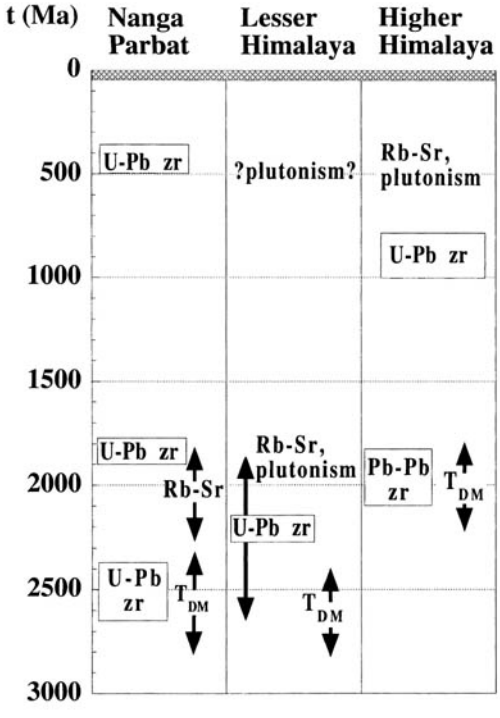

Fig. 9. Summary of available Nd model ages, Rb–Sr whole-rock errorchrons, and U–Pb zircon core age data from the Himalayan orogen. The range of ages recorded from the same technique on the different terrains can be used to rule out a correlation between the Nanga Parbat–Haramosh massif and the High Himalaya, although the nature of the relationship between the Nanga Parbat–Haramosh massif and the Lesser Himalaya remains uncertain. For comparison, the crosshatched bar from 50 to 0 Ma spans the present duration of the Tertiary Himalayan orogeny. Note that Nd model ages from the literature have been recalculated using the same model as the new data presented here. See text for references.

Hodges 1996). The widespread intrusion of granitic bodies in the HHCS at 500 Ma (Le Fort *et al.* 1983, 1986; Schärer & Allègre 1983) was coeval with the resetting of the Rb–Sr system in the HHCS from the Central Himalaya (Inger & Harris 1993). This event may also explain the presence of 500 Ma ages in some zircon cores from the Shengus gneiss of the NPHM, but clearly did not result in isotopic homogenization on a bulk-rock scale. This event has no definite equivalent in the LHS, although a 560 Ma Rb–Sr whole-rock age from the Almora nappe (Trivedi *et al.* 1984) may be one example.

The NPHM and Lesser Himalaya terrains clearly have their origins in an event at least as old as 2500 Ma, but this constrains only the protolith age, not the depositional age. Since fossils are unknown in the NPHM and HHCS, and are very rare in the LHS, palaeontological study is of restricted use. A maximum limit on depositional age is imposed by the ages of the youngest detrital zircons. Conversely, zircons found in metagranitic bodies intruding metasediments constrain the minimum depositional age. However, since there is considerable evidence that both the HHCS and LHS were deposited over a long period of time between the mid-Proterozoic and Cambrian (Valdiya 1995), it is important that comparisons be made between similar structural/stratigraphic levels where possible.

At this point an important difference between the NPHM and Lesser Himalaya should be noted. The NPHM has been intruded by metabasic dykes, which are observed to cut across the oldest gneissic fabrics (Butler *et al.* 1992, 1997; Pognante *et al.* 1993; Wheeler *et al.* 1995; Treloar *et al.* 2000). Geochemical investigation of several mafic bodies suggests the occurrence of several different episodes of basaltic magmatism in the NPHM (Treloar *et al.* 2000), as indeed recorded throughout the Himalaya (Bhat 1987). Age determinations range from a 2500 Ma Sm–Nd whole-rock isochron for the Rampur volcanics (Bhat & Le Fort 1992) through mid-Proterozoic and Palaeozoic suites to the Carboniferous to Permian Panjal Traps (Bhat *et al.* 1981; Honegger *et al.* 1982; Vannay & Spring 1993). Lower Triassic alkaline volcanics have been described from exotic blocks along ophiolitic mélange zones of the Peri-Indian suture zone, intercalated in the Lamayuru unit of Ladakh (Honegger *et al.* 1982), but are not known *in situ*. No younger basic magmatism is known within the Himalaya, and it is concluded that both the metabasic dykes in the NPHM and the gneissic fabrics which they cut across are pre-Himalayan (Wheeler *et al.* 1995).

The NPHM may be a deeper structural level of the Lesser Himalayan unit, exposed due to the exceptional exhumation experienced by the NPHM over the past 10 Ma, or it may be a protolith from which at least a part of the LHS was derived. Either interpretation would explain the similarity between model ages for the two terrains, while the latter would also explain why the LHS contains a range of zircon ages, whereas the NPHM apparently contains two distinct populations, although the relatively small number of samples analysed must be borne in mind.

In the second scenario, the crust currently exposed in the NPHM was probably formed at about 2500 Ma, possibly over an interval from 2800 to 2300 Ma. Erosion and sedimentation may have initiated relatively quickly, on a

timescale not currently resolvable, so that the oldest Lesser Himalayan sediments may indeed have been deposited at about 2500 Ma, coeval with the Rampur metavolcanics which may be related to the crust-forming event. Sedimentation continued throughout the Proterozoic, with a second orogeny and crust-forming event at about 1850 Ma, which resulted in the emplacement of granitic bodies within both the NPHM and LHS terrains. Examples of these bodies may include the Iskere orthogneiss of the NPHM and the Bomdila orthogneiss in the Arunachal Lesser Himalaya (Rao 1998), although in neither case do the field relations between the orthogneiss and metasedimentary sequences exclude the possibility of subsequent tectonic juxtaposition rather than a true intrusive contact.

The presence of a 500 Ma component in zircons from the NPHM may indicate that leucogneiss bodies found within the Shengus gneiss are equivalents of the 500 Ma granitoids found within the HHCS. That both the HHCS and NPHM terrains show evidence for a 500 Ma plutonic event that is apparently absent from the LHS, at least where currently exposed, again argues for the NPHM being the protolith of the LHS rather than its western continuation. The apparent absence of 500 Ma ages from the LHS suggests a model whereby sedimentation of the HHCS was predominantly to the north of the LHS (Parrish & Hodges 1996), consistent with further subsequent southward transport of the HHCS on the MCT. This is supported by palaeocurrent directions, which show predominantly southward transport for the HHCS and predominantly northward transport for the LHS (Draganits *et al.* 1998). The NPHM terrain was therefore probably not the substrate on which the HHCS was deposited, unless its area was large enough that it could provide the protolith for the LHS from the south at the same time. Otherwise, the basement to the HHCS is still an unknown entity.

Alternatively, if orthogneiss bodies of 500 Ma were to be confirmed in the Lesser Himalaya, then it would be more probable that the NPHM represents a deeper structural level of the LHS, metamorphosed at higher grades during pre-Himalayan orogeny. In this case, at least part of the HHCS could have been deposited on the NPHM terrain or its unexposed continuation.

In conclusion, the exceptional uplift and erosion rates of the NPHM during the past 10 Ma have exposed either a deeper level of the LHS, or its protolith. In either case this lithological package is not recognized elsewhere in the Himalaya and is probably the lowest structural horizon exposed in the orogen. The resolution of these two alternatives can be achieved only by the acquisition of more data, particularly searching for conclusive 500 Ma bodies within the LHS and obtaining a more representative sampling of zircon populations from all three sequences.

We thank P. W. C. van Calsteren and M. Gilmour for assistance with isotopic analyses, P. Le Fort and T. Argles for stimulating discussions, and R. Parrish and G. Davies for thoughtful reviews. A. Whittington gratefully acknowledges a Royal Society Conference Grant to enable attendance at the 13th Himalaya–Karakoram–Tibet Workshop in Peshawar. G. Foster was supported by an NERC studentship.

References

AHMAD, T., HARRIS, N., BICKLE, M., CHAPMAN, H., BUNBURY, J. & PRINCE, C. 1999. Isotopic constraints on the structural relationships between the Lesser Himalayan Series and the High Himalayan Crystalline Series, Garhwal Himalaya. *Geological Society of America, Bulletin*, in press.

ALLÈGRE, C. J. & BEN OTHMAN, D. 1980. Nd–Sr isotopic relationship in granitoid rocks and continental crust development: a chemical approach to orogenesis. *Nature*, **290**, 335–342.

AYRES, M. W. 1997. *Trace-element behaviour during high-grade metamorphism and anatexis of the Himalayas*. PhD thesis, Open University, UK.

—— & HARRIS, N. B. W. 1997. REE fractionation and Nd-isotope disequilibrium during crustal anatexis: constraints from Himalayan leucogranites. *Chemical Geology*, **139**, 247–267.

—— & VANCE, D. 1997. A comparative study of diffusion profiles in Himalayan and Dalradian garnets: constraints on diffusion data and the relative duration of metamorphic events. *Contributions to Mineralogy and Petrology*, **128**, 66–80.

——, HARRIS, N. B. W. & VANCE, D. 1997. Possible constraints on anatectic melt residence times from accessory mineral dissolution rates: An example from Himalayan leucogranites. *Mineralogical Magazine*, **61**, 29–36.

BHANOT, V. B., SINGH, V. P., HANSAL, A. K. & THAKUR, V. C. 1977. Early Proterozoic Rb–Sr whole rock age for Central Crystalline gneiss higher Himalaya, Kumaun. *Journal of the Geological Society of India*, **18**, 90–91.

BHAT, M. I. 1987. Spasmodic rift reactivation and its role in the pre-orogenic evolution of the Himalayan region. *Tectonophysics*, **134**, 103–127.

—— & LE FORT, P. 1992. Sm–Nd age and petrogenesis of Rampur metavolcanic rocks, NW Himalayas: Late Archean relics in the Himalaya belt. *Precambrian Research*, **56**, 191–210.

——, ZAINUDDIN, S. M. & RAIS, A. 1981. Panjal Trap chemistry and birth of Tethys. *Geological Magazine*, **118**, 367–375.

BLUM, J. D., GAZIS, C. A., JACOBSEN, A. D. & CHAMBERMAIN, C. P. 1998. Carbonate versus silicate weathering in the Raikhot watershed

within the High Himalayan crystalline series. *Geology*, **26**, 411–414.

BURCHFIEL, B. C., ZHILIANG, C., HODGES, K. V., YUPING, L., ROYDEN, L. H., CHANGRONG, D. & JIENE, X. (eds) 1992. *The South Tibetan Detachment System, Himalayan Orogen: Extension contemporaneous with and parallel to shortening in a collisional mountain belt*. Geological Society of America Special Paper, **269**.

BURG, J.-P., DAVY, P., NIEVERGELT, P., OBERLI, F., SEWARD, D., ZHIZHONG DIAO & MEIER, M. 1997. Exhumation during crustal folding in the Namche Barwa syntaxis. *Terra Nova*, **9**, 53–56.

BUTLER, R. W. H. & PRIOR, D. J. 1988*a*. Tectonic controls on the uplift of the Nanga Parbat Massif, Pakistan Himalayas. *Nature*, **333**, 247–250.

—— & —— 1988*b*. Anatomy of a continental subduction zone: the Main Mantle Thrust in Northern Pakistan. *Geologische Rundschau*, **77**, 239–255.

——, GEORGE, M. T., HARRIS, N. B. W., JONES, C., PRIOR, D. J., TRELOAR, P. J. & WHEELER, J. 1992. Geology of the northern part of the Nanga Parbat massif, northern Pakistan, and its implications for Himalayan tectonics. *Journal of the Geological Society, London*, **149**, 557–567.

——, HARRIS, N. B. W. & WHITTINGTON, A. G. 1997. Interactions between deformation, magmatism and hydrothermal activity during active crustal thickening: a field example from Nanga Parbat, Pakistan Himalayas. *Mineralogical Magazine*, **61**, 37–51.

CHANDA, S. K. & BHATTACHARYYA, A. 1982. Vindhyan sedimentation and paleogeography. *In*: VALDIYA, K. S., BHATIA, S. B. & GAUR, V. K. (eds) *Geology of Vindhyanchal*. Hindustan Publishing Company, New Dehli, 88–101.

CHAUDHRY, M. N. & GHAZANFAR, M. 1990. Position of the Main Central Thrust in the tectonic framework of Western Himalaya. *Tectonophysics*, **174**, 321–329.

COHEN, A. S., O'NIONS, R. K., SIEGENTHALER, R. & GRIFFIN, W. L. 1988. Chronology of the pressure–temperature history recorded by a granulite terrain. *Contributions to Mineralogy and Petrology*, **98**, 303–311.

COPELAND, P., PARRISH, R. R. & HARRISON, T. M. 1988. Identification of inherited radiogenic Pb in monazite and its implications for U–Pb systematics. *Nature*, **333**, 760–763.

DENIEL, C., VIDAL, P. & LE FORT, P. 1986. Les leucogranites himalayens et leur région source probable: les gneiss de la 'Dalle du Tibet'. *Comptes Rendus de l'Academie des Sciences de Paris*, **303**, série 2, 57–62.

——, ——, FERNANDEZ, A., LE FORT, P. & PEUCAT, J.-J. 1987. Isotopic study of the Manaslu granite (Himalaya, Nepal): inferences on the age and source of Himalayan leucogranites. *Contributions to Mineralogy and Petrology*, **96**, 78–92.

DEPAOLO, D. J. 1981. Neodymium isotopes in the Colorado Front Range and crust–mantle evolution in the Proterozoic. *Nature*, **291**, 193–196.

—— & WASSERBURG, G. J. 1976. Nd isotopic variations and petrogenetic models. *Geophysical Research Letters*, **3**, 249–252.

DICKIN, A. P. & MCNUTT, R. H. 1989. Nd model age mapping of the southeast margin of the Archean foreland in the Grenville Province of Ontario. *Geology*, **17**, 299–302.

DIETRICH, V. & GANSSER, A. 1981. The leucogranites of the Bhutan Himalaya (crustal anatexis vs. mantle melting). *Schweize Mineralogie und Petrographie Mitterlung*, **61**, 177–202.

DRAGANITS, E., GRASEMANN, B., FRANK, W., MILLER, CH. & WIESMAYR, G. 1998. The sedimentary protoliths of the HHC in the Chamba–Lahaul area, NW-Himalayas, India. *In*: HAMIDULLAH, S., LAWRENCE, R. D. & JAN, M. Q. (eds) *Special Issue of the Geological Bulletin, University of Peshawar*, **31**, 58–60.

EDWARDS, M. A., KIDD, W. S. F., ASIF KHAN, M., SCHNEIDER, D. A., ZEITLER, P. K. & ANASTASIO, D. 1997. Structural geology of the southwestern margin of Nanga Parbat. *EOS, Transactions of the American Geophysical Union*, **78**, F651.

FERRARA, G., LOMBARDO, B. & TONARINI, S. 1983. Rb/Sr geochronology of granites and gneisses from the Mount Everest region, Nepal Himalaya. *Geologisches Rundschau*, **72**, 119–136.

——, ——, —— & TURI, B. 1991. Sr, Nd and O isotopic characterisation of the Gophu La and Gumberanjun leucogranites (High Himalaya). *Schweize Mineralogie und Petrographische Mitterlungen*, **71**, 35–51.

FRANCE-LANORD, C. & LE FORT, P. 1988. Crustal melting and granite genesis during the Himalayan collision orogenesis. *Transactions of the Royal Society of Edinburgh: Earth Sciences*, **79**, 183–195.

——, DERRY, L. & MICHARD, A. 1993. Evolution of the Himalaya since Miocene time: isotopic and sedimentological evidence from the Bengal Fan. *In*: TRELOAR, P. J. & SEARLE, M. P. (eds) *Himalayan Tectonics*. Geological Society, London, Special Publications, **74**, 603–621.

——, SHEPPARD, S. M. F. & LE FORT, P. 1988. Hydrogen and oxygen isotopic variations in the High Himalaya peraluminous Manaslu leucogranite: evidence for heterogeneous sedimentary sources. *Geochimica et Cosmochimica Acta*, **52**, 513–526.

FUCHS, G. 1982. The geology of western Zanskar. *Geologisches Jahrbuch*, **125**, 513–540.

GEORGE, M. T. 1993. *The magmatic, thermal and exhumation history of the Nanga Parbat–Haramosh Massif, western Himalaya*. PhD thesis, Open University, UK.

—— & BARTLETT, J. M. 1996. Rejuvenation of Rb–Sr mica ages during shearing on the northwestern margin of the Nanga Parbat–Haramosh Massif. *Tectonophysics*, **260**, 167–187.

——, HARRIS, N. B. W. & BUTLER, R. W. H. 1993. The tectonic implications of contrasting granite magmatism between the Kohistan island arc and the Nanga Parbat–Haramosh Massif, Pakistan Himalaya. *In*: TRELOAR, P. J. & SEARLE, M. P.

(eds) *Himalayan Tectonics*. Geological Society, London, Special Publications, **74**, 173–192.

GUILLOT, S. & LE FORT, P. 1995. Geochemical constraints on the bimodal origin of High Himalayan leucogranites. *Lithos*, **35**, 221–234.

GUO, A. & DICKIN, A. P. 1996. The southern limit of Archean crust and significance of rocks with Paleoproterozoic model ages: Nd model age mapping in the Grenville Province of western Quebec. *Precambrian Research*, **77**, 231–241.

HARRIS, N. B. W. & AYRES, M. W. 1998. The implications of Sr-isotope disequilibrium for rates of prograde metamorphism and melt extraction in anatectic terrains. *In*: TRELOAR, P. J. & O'BRIEN, P. (eds) *What drives metamorphism and metamorphic reactions?* Geological Society, London, Special Publications, **138**, 171–182.

——, & MASSEY, J. A. 1994. Decompression and anatexis of Himalayan metapelites. *Tectonics*, **13**, 1537–1546.

——, AYRES, M. W. & MASSEY, J. 1995. Geochemistry of granitic melts produced during the incongruent melting of muscovite; implications for the extraction of Himalayan leucogranite magmas. *Journal of Geophysical Research*, **100**, 15767–15777.

——, INGER, S. & MASSEY, J. A. 1993. The role of fluids in the formation of High Himalayan leucogranites. *In*: TRELOAR, P. J. & SEARLE, M. P. (eds) *Himalayan Tectonics*. Geological Society, London, Special Publications, **74**, 391–400.

HARRISON, T. M., LOVERA, O. M. & GROVE, M. 1997. New insights into the origin of two contrasting Himalayan granite belts. *Geology*, **25**, 899–902.

HAWKESWORTH, C. J., KRAMERS, J. D. & MILLER, R. M. 1981. Old model Nd ages in Namibian Pan-African rocks. *Nature*, **289**, 278–282.

HERREN, E. 1987. Zanskar shear zone: Northeast–southwest extension within the Himalayas (Ladakh, India). *Geology*, **15**, 409–413.

HODGES, K. V., LE FORT, P. & PÊCHER, A. 1988. Possible thermal buffering by crustal anatexis in collisional orogens: Thermobarometric evidence from the Nepalese Himalaya. *Geology*, **16**, 707–710.

——, PARRISH, R. R., HOUSH, T. B., LUX, D. R., BURCHFIEL, B. C., ROYDEN, L. H. & CHEN, Z. 1992. Simuiltaneous Miocene extension and shortening in the Himalayan orogen. *Science*, **258**, 6–10.

HONEGGER, K., DIETRICH, V., FRANK, W., GANSSER, A., THÖNI, M. & TROMMSDORFF, V. 1982. Magmatism and metamorphism in the Ladakh Himalayas (the Indus–Tsangpo suture zone). *Earth and Planetary Science Letters*, **60**, 253–292.

HUBBARD, M. S. 1989. Thermobarometric constraints on the thermal history of the Main Central Thrust zone and Tibetan slab, eastern Nepal Himalaya. *Journal of Metamorphic Geology*, **7**, 19–30.

INGER, S. & HARRIS, N. B. W. 1993. Geochemical constraints on leucogranite magmatism in the Langtang Valley, Nepal Himalaya. *Journal of Petrology*, **34**, 345–368.

KAI, K. 1981. Rb–Sr geochronology of the rocks of the Himalayas, Eastern Nepal. Part I: The metamorphic age of the Himalayan gneiss. *Memoirs of the Faculty of Science, Kyoto University, Series of Geology and Mineralogy*, **47**, 135–157.

LE FORT, P. 1989. The Himalayan orogenic segment. *In*: SENGOR, A. M. C. (ed.) *Tectonic evolution of the Tethyan region*. NATO ASI series C, **259**, Kluwer Academic Publishers, Dordrecht, 289–386.

——, DEBON, F. & SONET, J. 1983. The lower Palaeozoic 'Lesser Himalayan' granitic belt: emphasis on the Simchar pluton of central Nepal. *In*: SHAMS, F. A. (ed.) *Granites of the Himalayas, Karakorum and Hindu Kush*. Punjab University, Lahore, Pakistan, 235–255.

——, ——, PÊCHER, A., SONET, J. & VIDAL, P. 1986. The 500 Ma magmatic event in Alpine southern Asia, a thermal episode at Gondwana scale. *Sciences de la Terre Mémoires*, **47**, 191–209.

MACFARLANE, A. M., HODGES, K. V. & LUX, D. 1992. A structural analysis of the Main Central Thrust Zone, Langtang National Park, central Nepal Himalaya. *Geological Society of America Bulletin*, **104**, 1389–1402.

MADIN, I. P., LAWRENCE, R. D. & UR-REHMAN, S. 1989. The northwestern Nanga Parbat–Haramosh Massif; evidence for crustal uplift of the northwestern corner of the Indian craton. *In*: MALINCONICO, L. L. & LILLIE, R. J. (eds) *Tectonics of the Western Himalayas*. Geological Society of America Special Paper, **232**, 169–182.

MASSEY, J. A. 1994. *Metamorphism, melting and fluids in the High Himalayan Crystallines, Langtang Valley, Nepal*. PhD thesis, Open University, UK.

——, REDDY, S. M., HARRIS, N. B. W. & HARMON, R. S. 1994. Correlation between melting, deformation and fluid interaction in the continental crust of the High Himalayas, Langtang Valley, Nepal. *Terra Research*, **6**, 229–237.

MISCH, P. 1949. Metasomatic granitisation of batholithic dimensions. *American Journal of Science*, **247**, 209–245.

MONTEL, J.-M. 1993. A model for monazite/melt equilibrium and application to the generation of granitic magmas. *Chemical Geology*, **110**, 127–146.

NOBLE, S. R. & SEARLE, M. P. 1995. Age of crustal melting and leucogranite formation from U–Pb zircon and monazite dating in the western Himalaya, Zanskar, India. *Geology*, **23**, 1135–1138.

OWEN, L. A. 1989. Neotectonics and glacial deformation in the Karakorum mountains and Nanga Parbat Himalaya. *Tectonophysics*, **163**, 227–265.

PARRISH, R. & HODGES, K. V. 1996. Isotopic constraints on the age and provenance of the Lesser and Greater Himalayan sequences, Nepalese Himalaya. *Geological Society of America Bulletin*, **108**, 904–911.

POGNANTE, U. & LOMBARDO, B. 1989. Metamorphic evolution of the High Himalayan Crystallines in SE Zanskar, India. *Journal of Metamorphic Geology*, **7**, 9–17.

——, BENNA, P. & LE FORT, P. 1993. High-pressure metamorphism in the High Himalayan

Crystallines of the Stak valley, northeastern Nanga Parbat–Haramosh syntaxis, Pakistan Himalaya. *In*: TRELOAR, P. J. & SEARLE, M. P. (eds) *Himalayan Tectonics*. Geological Society, London, Special Publications, **74**, 161–172.

——, CASTELLI, D., BENNA, P., GENOVESE, G., OBERLI, F., MEIER, M. & TONARINI, S. 1990. The crystalline units of the High Himalayas in the Lahul–Zanskar region (northwest India): metamorphic-tectonic history and geochronology of the collided and imbricated Indian plate. *Geological Magazine*, **127**, 101–116.

RAO, P. S. 1998. Kameng orogeny (1.8–1.9 Ga) from the isotopic evidence on the Bomdila orthogneisses, Kameng sector (NEFA), India. *In*: HAMIDULLAH, S., LAWRENCE, R. D. & JAN, M. Q. (eds) *Special Issue of the Geological Bulletin, University of Peshawar*, **31**, 159–162.

REDDY, S. M., SEARLE, M. P. & MASSEY, J. A. 1993. Structural evolution of the High Himalayan Gneiss sequence, Langtang Valley, Nepal. *In*: TRELOAR, P. J. & SEARLE, M. P. (eds) *Himalayan Tectonics*. Geological Society, London, Special Publications, **74**, 375–389.

SCAILLET, B., FRANCE-LANORD, C. & LE FORT, P. 1990. Badrinath–Gangotri plutons (Garwhal, India): petrological and geochemical evidence for fractionation processes in a High Himalayan leucogranite. *Journal of Volcanological and Geothermal Research*, **44**, 163–188.

SCHÄRER, U. 1984. The effect of initial ^{230}Th disequilibrium on young U–Pb ages: the Makalu case, Himalaya. *Earth and Planetary Science Letters*, **67**, 191–204.

—— & ALLÈGRE, C. J. 1983. The Palung granite (Himalaya): high-resolution U–Pb systematics in zircon and monazite. *Earth and Planetary Science Letters*, **63**, 423–432.

——, XU, R. H. & ALLÈGRE, C. J. 1986. U–(Th)–Pb systematics and ages of Himalayan leucogranites, south Tibet. *Earth and Planetary Science Letters*, **77**, 35–48.

SCHNEIDER, D. A., EDWARDS, M. A., KIDD, W. S. F., ZEITLER, P. K. & COATH, C. D. 1999. Early Miocene anatexis identified in the western syntaxis, Pakistan Himalaya. *Earth and Planetary Science Letters*, **167**, 121–129.

SEARLE, M. P. 1986. Structural evolution and sequence of thrusting in the High Himalayan, Tibetan–Tethys and Indus suture zones of Zanskar and Ladakh, western Himalaya. *Journal of Structural Geology*, **167**, 923–936.

—— & FRYER, B. J. 1986. Garnet, tourmaline and muscovite-bearing leucogranites, gneisses and migmatites of the Higher Himalaya from Zanskar, Kulu, Lahoul and Kashmir. *In*: COWARD, M. P. & RIES, A. C. (eds) *Collision Tectonics*. Geological Society, London, Special Publications, **19**, 185–201.

—— & REX, A. J. 1989. Thermal model for the Zanskar Himalaya. *Journal of Metamorphic Geology*, **7**, 127–134.

——, COOPER, D. J. W. & REX, A. J. 1988. Collision tectonics of the Ladakh–Zanskar Himalaya. *Philosophical Transactions of the Royal Society of London*, **A326**, 117–150.

——, PARRISH, R. R., HODGES, K. V., HURFORD, A., AYRES, M. W. & WHITEHOUSE, M. J. 1997. Shisha Pangma leucogranite, South Tibetan Himalaya: Field relations, geochemistry, age, origin, and emplacement. *Journal of Geology*, **105**, 295–317.

——, WATERS, D. C., REX, D. C. & WILSON, R. N. 1992. Pressure, temperature and time constraints on Himalayan metamorphism from eastern Kashmir and western Zanskar. *Journal of the Geological Society, London*, **149**, 753–773.

SHARMA, K. K., RAMESHWAR RAO, D., AZMI, R. J., GOPALAN, K. & PANTULU, G. V. C. 1992. Precambrian–Cambrian boundary in the Tal Formation of Garwhal Lesser Himalaya: Rb–Sr age evidence from black shales underlying phosphorites. *Current Science*, **62**, 528–530.

STÄUBLI, A. 1989. Polyphase metamorphism and the development of the Main Central Thrust. *Journal of Metamorphic Geology*, **7**, 73–93.

STERN, C. R., KLIGFIELD, R., SCHELLING, D., VIRDI, N. S., FUTA, K., PETERMAN, Z. E. & AMINI, H. 1989. The Bhagirathi leucogranite of the High Himalaya (Garwhal, India); age, petrogenesis and tectonic implications. *In*: MALINCONICO, L. L. & LILLIE, R. J. (eds) *Tectonics of the western Himalayas*. Geological Society of America Special Paper, **232**, 33–45.

TRELOAR, P. J., GEORGE, M. T. & WHITTINGTON, A. G. 2000. Mafic sheets from Indian plate gneisses in the Nanga Parbat syntaxis: their significance in dating crustal growth and metamorphic and deformation events. *This volume*.

——, POTTS, G. J., WHEELER, J. & REX, D. C. 1991. Structural evolution and asymmetric uplift of the Nanga Parbat syntaxis, Pakistan Himalaya. *Geologische Rundschau*, **80**, 411–428.

TRIVEDI, J. R., GOPALAN, K. & VALDIYA, K. S. 1984. Rb–Sr ages of granitic rocks within the Lesser Himalayan nappes, Kumaun, India. *Journal of the Geological Society of India*, **25**, 641–654.

UPRETI, B. N. & LE FORT, P. 1999. Lesser Himalayan crystalline nappes of Nepal: Problems of their origin. *In*: MACFARLANE, A., SORKHABI, R. & QUADE, J. (eds) Himalaya and Tibet: Mountain roots to mountain tops. Geological Society of America Special Paper, **328**, 225–238.

VALDIYA, K. S. 1980. *Geology of the Kumaun Lesser Himalaya*. Wadia Institute of Himalayan Geology, Dehra Dun, India.

—— 1995. Proterozoic sedimentation and Pan-African geodynamic development in the Himalaya. *Precambrian Research*, **74**, 35–55.

VANCE, D., PRINCE, C. I., ANCKIEWICZ, R. & HARRIS, N. 1997. The timing and rate of prograde metamorphism in the Himalayan orogen. *Terra Nova*, **9**, 64.

VANNAY, J. C. & SPRING, L. 1993. Geochemistry of the continental basalts within the Tethyan Himalaya of Lahul–Spiti and SE Zanskar, northwest India. *In*: TRELOAR, P. J. & SEARLE, M. P. (eds) *Himalayan Tectonics*. Geological Society, London, Special Publications, **74**, 237–249.

VIDAL, P., BERNARD-GRIFFITHS, J., COCHERIE, A., LE FORT, P., PEUCAT, J. J. & SHEPPARD, S. M. F. 1984. Geochemical comparison between Himalayan and Hercynian leucogranites. *Physics of the Earth and Planetary Interiors*, **35**, 179–190.

——, COCHERIE, A. & LE FORT, P. 1982. Geochemical investigations of the origin of the Manaslu leucogranite (Himalaya, Nepal). *Geochimica et Cosmochimica Acta*, **46**, 2279–2292.

WHEELER, J., TRELOAR, P. J. & POTTS, G. J. 1995. Structural and metamorphic evolution of the Nanga Parbat syntaxis, Pakistan Himalayas, on the Indus gorge transect: the importance of early events. *Geological Journal*, **30**, 349–371.

WHITTINGTON, A. G. 1996. Exhumation overrated at Nanga Parbat, northern Pakistan. *Tectonophysics*, **260**, 215–226.

—— 1997. *The thermal, metamorphic and magmatic evolution of a rapidly exhuming terrane: the Nanga Parbat Massif, northern Pakistan.* PhD thesis, Open University, UK.

——, HARRIS, N. B. W. & BAKER, J. 1998. Low-pressure crustal anatexis: the significance of spinel and cordierite from metapelitic assemblages at Nanga Parbat, northern Pakistan. *In*: TRELOAR, P. J. & O'BRIEN, P. (eds) *What drives metamorphism and metamorphic reactions?* Geological Society, London, Special Publications, **134**, 183–198.

——, —— & BUTLER, R. W. H. 1999. Contrasting anatectic styles at Nanga Parbat, northern Pakistan. *In*: MACFARLANE, A., SORKHABI, R. & QUADE, J. (eds) *Himalaya and Tibet: Mountain roots to mountain tops.* Geological Society of America Special Paper, **328**, 129–144.

WINSLOW, D. M., ZEITLER, P. K., CHAMBERLAIN, C. P. & HOLLISTER, L. S. 1994. Direct evidence for a steep geotherm under conditions of rapid denudation, western Himalaya, Pakistan. *Geology*, **22**, 1075–1078.

ZEITLER, P. K. 1985. Cooling history of the NW Himalaya, Pakistan. *Tectonics*, **4**, 127–151.

—— & CHAMBERLAIN, C. P. 1991. Petrogenetic and tectonic significance of young leucogranites from the northwestern Himalaya, Pakistan. *Tectonics*, **10**, 729–741.

——, —— & SMITH, H. A. 1993. Synchronous anatexis, metamorphism, and rapid denudation at Nanga Parbat (Pakistan Himalaya). *Geology*, **21**, 347–350.

——, SUTTER, J. F., WILLIAMS, I. S., ZARTMAN, R. & TAHIRKHELI, R. A. K. 1989. Geochronology and temperature history of the Nanga Parbat–Haramosh Massif, Pakistan. *In*: MALINCONICO, L. L. & LILLIE, R. J. (eds) *Tectonics of the western Himalayas.* Geological Society of America Special Paper, **232**, 1–22.

——, TAHIRKHELI, R. A. K., NAESER, C. W. & JOHNSON, N. M. 1982. Unroofing history of a suture zone in the Himalaya of Pakistan by means of fission-track annealing ages. *Earth and Planetary Science Letters*, **57**, 227–240.

From buckling to asymmetric folding of the continental lithosphere: numerical modelling and application to the Himalayan syntaxes

J.-P. BURG & Y. PODLADCHIKOV

Geologisches Institut, ETH-Zentrum, Sonneggstrasse 5, CH 8092 Zurich, Switzerland

(e-mail: jpb@erdw.ethz.ch)

Abstract: The eastern and western Himalayan syntaxes are large-scale, coeval antiforms developed late in the history of India–Asia collision. We use two-dimensional finite element models of lithospheric folding to develop a mechanically plausible structural interpretation. The models mimic the coeval development of adjacent synformal basins, analogous to the Peshawar and Kashmir basins on either side of and adjacent to the western syntaxis. Pure-shear thickening and symmetric buckling accommodate shortening until, at a certain strain, an asymmetric thrust-like flow pattern occurs on a crustal to lithospheric scale. Similarities between geological data and calculated models suggest that lithospheric buckling is a basic response to large-scale continental shortening. To generalize these results, we suggest that a typical shortening history would include: (1) locking of an early thrust system in hinterland regions, followed by (2) pure shear shortening and symmetric buckling of the shortened lithosphere, and (3) loss of symmetry leading to the formation of an asymmetric fold in which a new thrust system will nucleate.

This study aims to advocate large-scale folding as a plausible mechanism of continental shortening and to examine the first-order structural consequences of that process. Buckling instabilities are responses to layer parallel shortening that have been thoroughly investigated (Turcotte & Schubert 1982). Classical theories (Biot 1961; Ramberg 1964; Johnson & Fletcher 1994) have been commonly applied to outcrop- and kilometre-scale folds, in which gravity can be ignored. However, gravity, non-linear elasto-plastic and thermally activated creep rheologies play a fundamental role at a larger scale, which means that other methods are required to model the folding of the oceanic (McAdoo & Sandwell 1985; Martinod & Davy 1992) and continental (Cobbold & Davy 1988; Cobbold *et al.* 1993; Burov & Diament 1995) lithospheres.

Two-dimensional finite element modelling (FEM) is used here with a wide range of non-linear rheologies thought to have a considerable influence on the deformational behaviour of the lithosphere (Johnson & Fletcher 1994). The two-dimensional FEM method is technically more difficult to implement than kinematic modelling (Henry *et al.* 1997) or 'thin sheet' approximations (Vilotte & Daignières 1982; England & McKenzie 1983; England & Houseman 1986; Houseman & England 1986; Sonder *et al.* 1987; Houseman & England 1993; Burov & Diament 1995). However, the numerical code can be verified independently of the geological application. Thus, two-dimensional FEM is a reliable technique for simulating geodynamic histories of areas in which kinematic information is lacking.

This paper begins with a brief description of the western and eastern Himalayan syntaxes. These are antiformal structures, thousands of kilometres apart, that have formed in geodynamically similar environments and evolved metamorphically over the same interval (Burg *et al.* 1997, 1998). We then present the main concepts of our numerical methods and the model parameters chosen to simulate the Indian continental lithosphere. Because many parameters control folding style, we do not attempt a systematic study. We restrict this work to a particular example of continental shortening, namely the development of the West and East Himalayan 'syntaxes', and we report results, including a spontaneous transition from buckling to asymmetric folding. Similarities between the geology of the West and East Himalayan syntaxes and the FEM models are emphasized. We conclude that lithospheric buckling is a basic, mountain-building response to regional shortening.

From: KHAN, M. A., TRELOAR, P. J., SEARLE, M. P. & JAN, M. Q. (eds) *Tectonics of the Nanga Parbat Syntaxis and the Western Himalaya*. Geological Society, London, Special Publications, **170**, 219–236. 1-86239-061-4/00/$15.00

Himalayan 'syntaxes'

The Himalayan range terminates at both ends in nearly transverse syntaxes (Wadia 1931), i.e. areas where orogenic trends turn sharply about a vertical axis (Fig. 1). The syntaxes are named after the highest peaks that core them: Namche Barwa in the east and Nanga Parbat in the west (Wadia 1931; Gansser 1991). In both syntaxes, Himalayan metamorphism and Pliocene–Pleistocene high-grade metamorphism and anatexis overprint basement rocks. The syntaxes are crustal antiforms where the Paleogene Tethyan suture is folded around half-windows of Indian crust (Wadia 1957; Gansser 1966; Treloar *et al.* 1991; Burg *et al.* 1997). Deformation in both syntaxes straddles the same Neogene time span. The areas of the syntaxes have undergone rapid denudation during growth, lasting some 4 Ma (Zeitler *et al.* 1989, 1993; Burg *et al.* 1998).

In Pakistan, the Hazara–Kashmir syntaxis (Bossart *et al.* 1988) is the southern continuation of the Nanga Parbat syntaxis. Similarly, in the Arunachal (eastern) Himalaya, the Siang antiform (Singh 1993) is the southwestern continuation of the Namche Barwa syntaxis. Crustal-scale folding appears to have produced these orogenic structures. A rise of the Moho is recorded under Nanga Parbat (Farah *et al.* 1984). No information on Moho depth is available beneath Namche Barwa. Both western and eastern antiforms result from compression nearly orthogonal to their axial traces (see Butler *et al.* (1988) for Nanga Parbat; Burg *et al.* (1998) for Namche Barwa; Bossart *et al.* (1988) for Hazara–Kashmir). This orientation of compression is also indicated by present-day focal mechanisms in Pakistan (Verma *et al.* 1980) and in the eastern Himalaya (Holt *et al.* 1991). The orogen-parallel compression involved is probably a regional effect of strain concentration and interference at the tips of the arcuate Himalayan thrusts (Treloar *et al.* 1991; Seeber & Pêcher 1998). The purpose of our numerical modelling is to test the plausibility of crustal-scale buckle antiforms arising from compression nearly perpendicular to their axial traces. Furthermore, we aim to explain the outward thrust direction on the steep limbs of the Himalayan syntaxes: the Liachar Thrust, on the northwestern limb of Nanga Parbat (Butler *et al.* 1988) and unnamed northwest-vergent thrusts in the Namche Barwa region (Chang *et al.* 1992).

Numerical modelling

Method

We use a two-dimensional finite element code that couples plane strain mechanical and thermal

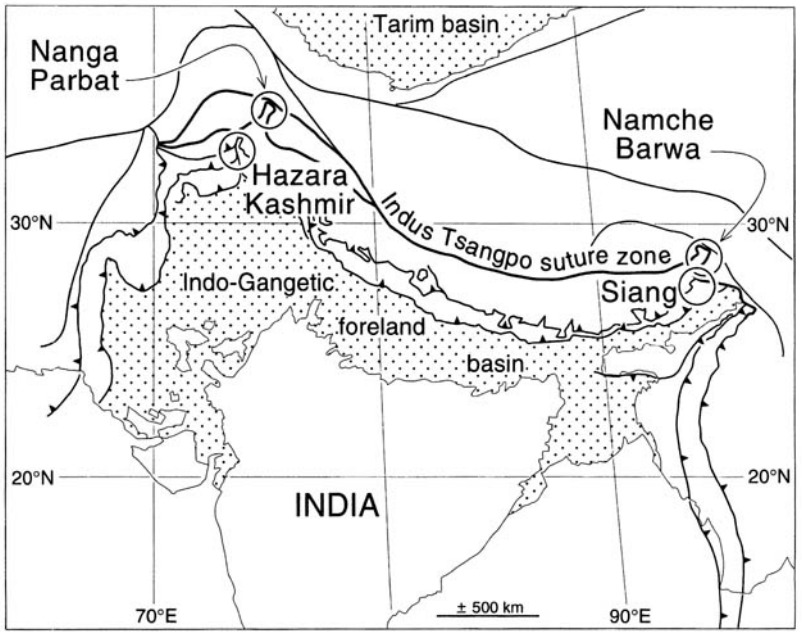

Fig. 1. Location of the Namche Barwa + Siang (eastern) and Nanga Parbat + Hazara–Kashmir (western) Himalayan syntaxes in the India–Asia collisional system.

calculations. The mathematical description is summarized in the Appendix. Finite elements are seven-node quadratic triangles (Poliakov & Podladchikov 1992; Podladchikov *et al.* 1993). Rheology ranges from elasticity to Mohr–Coulomb plasticity (Mandl 1988) or thermally activated power-law creep (Carter & Tsenn 1987), depending upon a yield strength criterion (Poliakov *et al.* 1996). Effects of gravity and thermal and compositional buoyancy, along with viscosity variations, have been included. The number of the finite-element nodes was 901×101.

Model and boundary conditions

We assume a stratified lithosphere (Fig. 2, Table 1) with three compositional layers: (1) an upper granitic crust, 25 km thick, (2) lower mafic crust (10 km of diabase) and (3) sub-crustal olivine lithosphere (85–120 km). Deformation results from horizontal movement at constant velocity, applied at the lateral boundaries. The basal boundary is fixed in the vertical direction and free to slip in the horizontal direction. The lateral boundaries converge at constant velocity and are free to slip in the vertical direction. The upper boundary is a free surface. At each time step, the vertical position of the entire model box is adjusted (i.e. shifted downwards) to keep the far-field surface elevation at sea-level. The technique is justified because the lithosphere distant from the Himalaya is not deforming and, therefore, does not produce topographic elevation. Our approach allows us to adopt a kinematic (vertically fixed) basal boundary condition as opposed to a more complex, though strictly valid, isostatic condition of vanishing differential stresses at some compensation level. In our experience the isostatic lower boundary condition requires smaller time steps but produces similar results. The starting configuration has a relaxed stress state with gravitational load and a non-linear, steady temperature

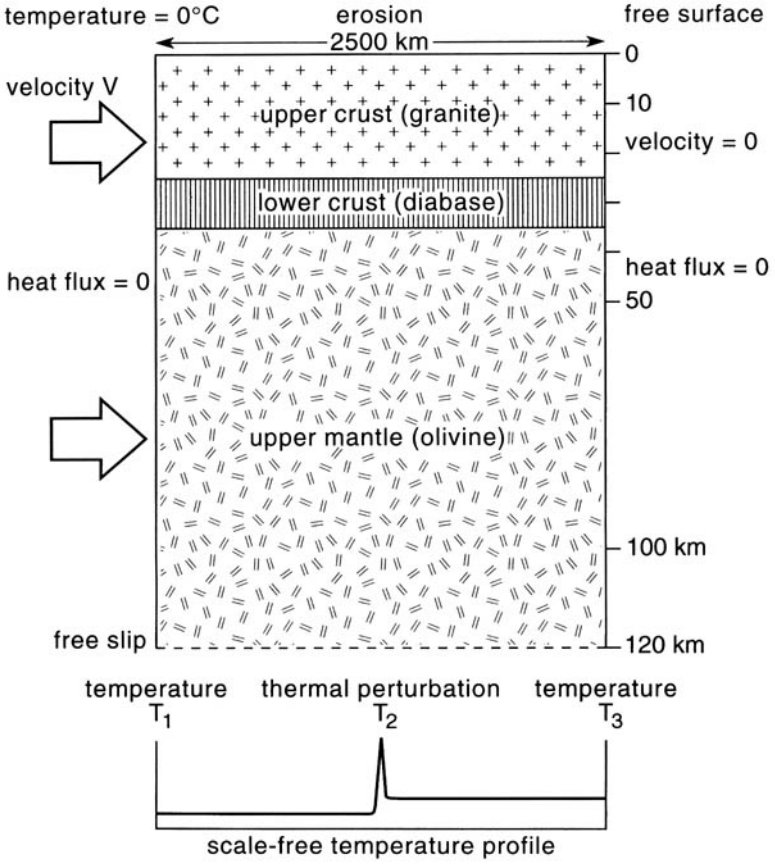

Fig. 2. Lithosphere model used for numerical experiments.

Table 1. *Model parameters (for all runs)*

Box characteristics	
Length of model	2500 km
Depth of model (base of lithosphere)	120 km
Granitic layer thickness (upper crust)	25 km
Diabase layer thickness (lower crust)	10 km
Olivine layer thickness (upper mantle)	85 km
Convergence rate	2×10^{-10} m s^{-1}
Properties common for all rocks	
Bulk modulus	1×10^{10} Pa
Shear modulus	1×10^{10} Pa
Conductivity	2.6 W m^{-1} °C^{-1}
Specific heat	1050 m^2 s^{-2} °C^{-1}
Thermal expansion coefficient	10^{-5} °C^{-1}
Dry granite properties	
Density ($T = 0$ °C)	2700 kg m^{-3}
Power law exponent	3.3
A coefficient	3.16×10^{-26} Pa^{-n} s^{-1}
Activation energy	1.9×10^5 J mol^{-1}
Heat production	10^{-6} W m^{-3}
Wet granite properties	
Density ($T = 0$ °C)	2700 kg m^{-3}
Power law exponent	1.9
A coefficient	7.94×10^{-16} Pa^{-n} s^{-1}
Activation energy	1.4×10^5 J mol^{-1}
Heat production	10^{-6} W m^{-3}
Diabase properties	
Density ($T = 0$ °C)	2900 kg m^{-3}
Power law exponent	3
A coefficient	3.2×10^{-20} Pa^{-n} s^{-1}
Activation energy	2.76×10^5 J mol^{-1}
Heat production	0 W m^{-3}
Olivine properties	
Density ($T = 0$ °C)	3300 kg m^{-3}
Power law exponent	3
A coefficient	7×10^{-14} Pa^{-n} s^{-1}
Activation energy	$5 \times 1 \times 10^5$ J mol^{-1}
Heat production	0 W m^{-3}

distribution. Thermal boundary conditions are 0 °C at the surface and fixed basal temperatures, which are $T(x) = T_1$ beneath the left part of the model; a thermal perturbation with a maximum temperature T_2 exponentially decaying from the centre, and $T(x) = T_3$ beneath the right part of the model (Fig. 2, Table 2). The thermal perturbation T_2 is employed to localize deformation at the centre of the model. There is no lateral heat flux through the sides. Erosion is modelled according to a linear diffusion equation (Appendix, Podladchikov *et al.* 1993). The Himalayan syntaxes are simultaneously undergoing both north–south and east–west compressions. The local, orogen-parallel east–west compression may be caused by the lack of accommodation space, which prohibits lateral escape from the deforming areas (Treloar *et al.* 1991; Seeber & Pêcher 1998). This situation is in contrast to the central parts of the Himalaya, where a significant amount of north–south, tectonic shortening can be easily absorbed by east–west lateral escape. Moreover, topographic loads, which are especially large after long lasting convergence, foster east–west escape from the middle part of the orogen (Armijo *et al.* 1986), thus generating additional orogen-parallel compression at the extremities, in the syntaxis areas. Accordingly, we speculate that orogenic shortening is laterally constrained by simultaneous, orthogonal compressions in the syntaxis areas where orogen-parallel, lateral constraints dominate. Our decision was therefore to model the growth of the crustal antiforms in their middle sections, 100km away from their closure, where two-dimensional plane strain models parallel to the dominant compression are a first, acceptable approximation.

In contrast with other two-dimensional numerical models, we do not prescribe any deformation mode (e.g. homogeneous pure shear or heterogeneous simple shear at a forcing point). In particular, strain localization is not pre-ordained by introducing special 'slippery'

Table 2. *Temperatures used at the base of model lithospheres*

Model name	T_1 °C	$T_2 - T_1$	$T_3 - T_1$	Upper crust	Erosion
COLD	900	150	30	Dry	No
INTERMEDIATE	1000	150	30	Dry	No
INTERMEDIATEW	1000	150	30	Wet	No
WARM	1200	150	30	Dry	No
HOT	1300	50	10	Dry	No
WARME	1200	150	30	Dry	$K_e = 10^{-7}$ m^2 s^{-1}

nodes or employing singular points with abrupt velocity changes as boundary conditions. Instead, deformation is localized by the long wavelength variation of the basal temperature. Inherent shorter wavelength, i.e. more localized, structures develop with growing bulk strain and are controlled by the instantaneous rheological configuration of the lithosphere. Boundary loading is due to the constant-velocity convergence of the sides; in other words, the far-field deformation mode is restricted to rigid plate motions. The asymmetry in the model reflects an inherent physical process triggered by differences in basal temperatures.

In contrast with analogue modelling, the position of the brittle–ductile transition for each compositional layer is not prescribed by the choice of different materials (Davy & Cobbold 1991; Willett *et al.* 1993; Beaumont *et al.* 1996) and it may evolve through time. An internally consistent result of stress modelling is that the three-layer models presented here would be equivalent to a six-layer analogue model. For proper comparison, the analogue model should involve adjustment of the thickness of both the brittle and ductile material layers, because after each strain increment the stress–strength field must be evaluated, brittle material beyond its yield condition replaced by ductile material, and vice versa. This is an incremental exercise where numerical modelling reveals its advantages.

The geometrical parameters and physical constants we have adopted are based on geophysical information available for the structure and properties of the Indian plate (Henry *et al.* 1997). Rheological laws for dry granite, diabase and olivine result from laboratory measurements extrapolated to tectonic timescales (Carter & Tsenn 1987; Ranalli 1995). The parameter values (Table 1) are typical of those adopted for lithospheric-scale modelling. A critical uncertainty is the Indian plate geotherm, which was therefore systematically varied. Numerical runs with different upper crustal thicknesses are not presented here because this parameter is crudely constrained geophysically and has a relatively minor influence on the results. Conversely, we will show that dry v. wet rheology of the upper crust has a major impact on the style of crustal deformation through localization of crustal decoupling.

Results

We restrict this study to a particular example of continental shortening inferred to be active in the West and East Himalayan 'syntaxes'. For all runs $T_2 > T_3 > T_1$, i.e. the left part of the model represents the cold portion of the Indian plate newly involved in collision and the right part represents that portion of the plate heated during its previous orogenic history. Table 2 gives the values of T_1, T_2 and T_3 used in the six numerical models presented here.

A warm lithosphere (WARM, Table 2) is our preferred model because it yields amplitudes and wavelengths comparable with those of both Himalayan syntaxes. Figure 3 focuses on the central part to emphasize a few points.

(1) Buckling is observable only after significant (295 km > 10%) homogeneous, distributed shortening of the lithospheric plate.

(2) The decay in amplitude of the main buckle began at slightly more than 400 km (*c.* 20%) shortening (Fig. 5). This corresponds to low amplification rates with respect to the adjacent hinges, which indicates that the main fold has become locked and that deformation is being transferred to adjacent hinges (Figs 3 and 4). Therefore, the amplitude of the main buckle fold is achieved in the bulk strain range of 10–25%.

(3) Crustal and sub-crustal levels are coupled during symmetrical lithospheric buckling until loss of symmetry at the locking stage (i.e. 411 km shortening, Fig. 3). At this point, decoupling of the granitic and diabase layers is expressed by shearing along their boundary.

(4) Asymmetric folding faces the hot (i.e., orogenically affected) parts of the lithosphere.

(5) The topographic evolution features coeval subsidence of small-amplitude synforms on both sides of the growing antiforms (Figs 3, 4 and 5).

The velocity fields of the COLD model (Fig. 6) and HOT model (Fig. 7) represent two experimental end-members (coldest and hottest lithospheres, respectively). They show remarkable similarities in terms of deformational response to applied shortening. (1) In both cases, as for WARM, ultimately unstable homogeneous thickening (up to 10 to 15%) leads to buckling. (2) Symmetrical buckling terminates at *c.* 20% shortening, crustal decoupling and subsequent asymmetry being triggered by small differences in the lithospheric basal temperature (Table 2). The end-member COLD and HOT experiments differ in three ways: (1) buckle wavelength (200 km in Fig. 6 v. *c.* 100 km in Fig. 7) and amplitude (*c.* 25 v. *c* 5 km, Fig. 5) are larger for the cold lithosphere; (2) lateral propagation of buckling is more manifest in cold than in hot lithosphere (Fig. 6 v. Fig. 7); (3) intercalated basins on cold lithosphere subside less than they do on hot lithosphere (Figs 4 and 5). In particular, subsidence is short lived, and starts to invert on the cold lithosphere (Fig. 5, COLD), whereas subsidence accelerates with time on a hot

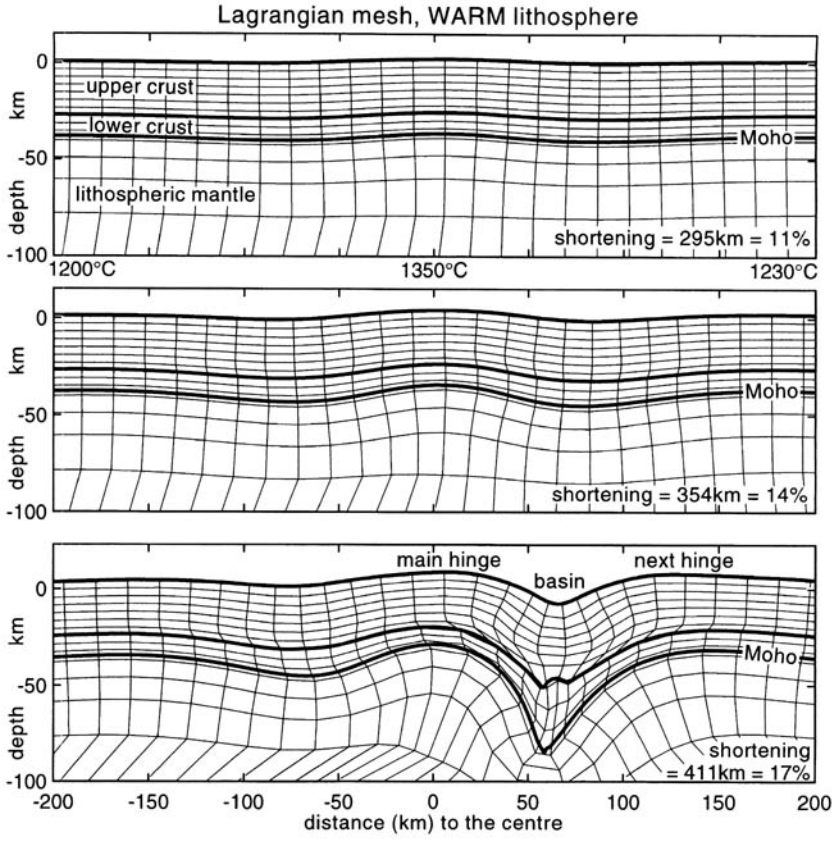

Fig. 3. Central part of model WARM lithosphere. Note that buckling is noticeable only after 295 km (>10%) of homogeneous shortening and quickly amplifies within the next 10–15% shortening. Asymmetry at 411 km shortening faces towards the hot (i.e. orogenically affected) side of the lithosphere ('back-thrusting' effect).

lithosphere, for the duration of these experiments. The INTERMEDIATE model illustrates a situation between those of the cold and hot models (Figs 4, 5 and 8). The four models, all with no erosion, reproduce the fast and rapidly growing differential topography suggested from the geological record in both Himalayan syntaxes. However, the final altitudes of the cold models are obviously too high. We attribute this shortcoming to the unrealistic condition of no erosion. Variations of the erosion coefficient have the obvious effect of reducing topographic elevation.

The velocity fields instantaneously display the appearance of the asymmetric mode (Figs 6–8), whereas the switch from symmetric to asymmetric deformation is not immediately apparent on a Lagrangian mesh (e.g. Fig. 3) that displays the accumulated strain pattern. The COLD end-member (Fig. 6) shows that symmetrical buckling may persist up to significant amounts of shortening (beyond 516 km, i.e. >20%). By comparison, the INTERMEDIATE model (Fig. 8) shows a dramatic loss in symmetry after about 414 km of shortening (i.e. *c.* 15%). Of particular interest to us is that the velocity field then shows the growth of a lithospheric thrust system. The HOT model (Fig. 7) illustrates a peculiar style of asymmetry: subvertical velocity vectors (between markers 50 and 100 km, Fig. 7) show delamination of sub-crustal lithosphere. In contrast, the thrust system is less steeply dipping in the intermediate model (Fig. 8). Above it is a coeval compressional basin on the surface. Finally, all models show various degrees of crustal detachment, which is manifested as an inversion of the velocity field to the right of the developing thrust system, around the 150 km markers (Figs 6, 7 and 8).

Figure 9 displays the effect of a different upper-crustal rheology (wet instead of dry granite) on symmetry. In the early stages, the symmetry

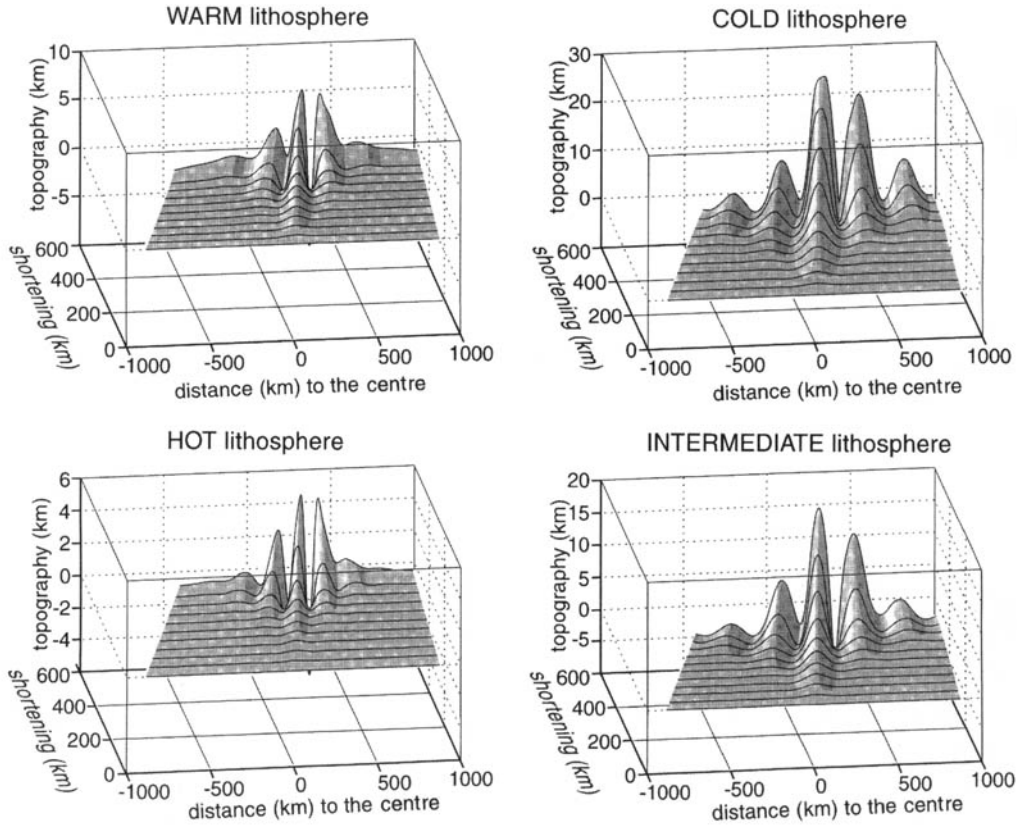

Fig. 4. Perspective view of developing topographic profiles during shortening, in the absence of erosion.

developed in the same manner as in the corresponding INTERMEDIATE dry case (Fig. 8). The fundamental difference is the occurrence of a mid-crustal, channel-like flow in the wet middle crust. In addition, a secondary circulation pattern developed to the right of the thrust system (Fig. 9). This may be a mechanism for exhumation of ultra high-pressure rocks that may have been involved in such kinematic loops. Models run for both hot and cold lithospheres with a wet upper-crustal rheology have shown remarkable similarities to the intermediate case. This implies that the lithospheric basal temperatures do not control symmetry loss and secondary cell formation when the crust is wet.

To enlarge upon our comparison between models and geological information we have avoided the problem of excessively high topography by tuning the erosion coefficient to $10^{-7}\,m^2\,s^{-1}$, which matches the magnitude of the actual topography. Smaller erosion coefficients result in too high topographies, equivalent to those of non-erosion runs; higher erosion coefficients yield too low relief. Figure 10 displays the topography and exhumation histories of the main hinge zone of our preferred model, WARM, with erosion (WARME, Table 2). Topography due to buckling is 5–10 km. The amount of exhumation is limited by fold locking and is typically *c.* 20 km. At the fold locking stage (approaching 400 km of shortening) both uplift and denudation rates start to decrease. Subsidence in the basins adjacent to the main hinge zone is under-compensated because the sedimentation rate (*c.* 5 mm a^{-1}) is slower than basement subsidence (Fig. 10). At the fold locking stage, the sedimentation rate keeps accelerating, whereas the subsidence rate slows down.

Relevance of modelling results to the Himalayan syntaxes: associated synformal basins

The simultaneous subsidence of synformal basins on either side of a lithospheric antiform

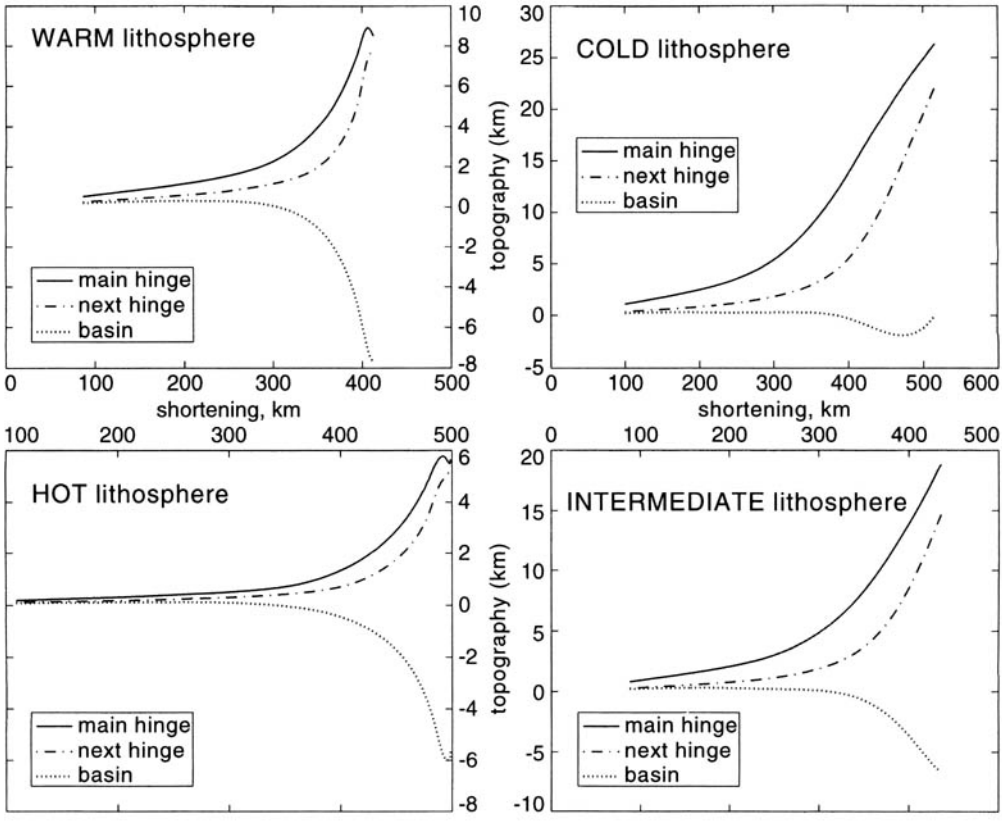

Fig. 5. Vertical motion of the antiformal hinge and the intercalated synformal basin during shortening of model WARM (Fig. 3). No erosion is permitted. Boundary conditions in Table 2.

in the numerical models is an important result. We argue that this pattern is documented in Pakistan where the synclinal Peshawar Basin to the west is readily recognized on geological maps as the structural analogue to the synclinal Kashmir Basin to the east of the Hazara–Kashmir syntaxis (Fig. 11). The lithological and stratigraphical correlations between these two synformal depressions were noted by Yeats & Lawrence (1984). Their formation was coeval with the growth of the Nanga Parbat syntaxis.

The Kashmir Basin includes Palaeozoic and Mesozoic sediments overlying a metamorphosed basement sequence (Wadia 1931). The Mesozoic is, in turn, overlain by a >1300 m thick cover of late Cenozoic to Quaternary fluvio-lacustrine sediments that continue to accumulate in a few lakes today (Burbank & Johnson 1982). Volcanic ashes in the lower levels of the late Cenozoic cover show that sedimentation began *c.* 4 Ma ago. Centripetal drainage dominated the period between 1.7–0.4 Ma, while sediment accumulation rates from 32 to 16 cm ka^{-1} were maintained (Burbank & Johnson 1982; Burbank *et al.* 1986).

The Peshawar Basin comprises a sequence of Cambrian to Jurassic rocks resting on a Precambrian basement (Pogue *et al.* 1992). As in Kashmir, the Peshawar Basin has a thick Plio-Pleistocene to Holocene fill of alluvial sediments that began accumulating at least 2.8 Ma ago (Burbank 1983; Burbank & Khan Tahirkheli 1985). Sediments have accumulated at an average rate of 15 cm ka^{-1} (Burbank & Khan Tahirkheli 1985).

The acceleration and deceleration of sedimentation rates in these basins are reproduced by our calculations (Fig. 10). Thus, we infer that the symmetrically located Peshawar and Kashmir basins are synformal depressions on both sides of, and directly related to, the Nanga Parbat–Hazara–Kashmir syntaxis. Our interpretation explains a first-order feature, namely their location. The syntaxes are traditionally interpreted as the surface expression of low-angle detachment faults that ramp upward further

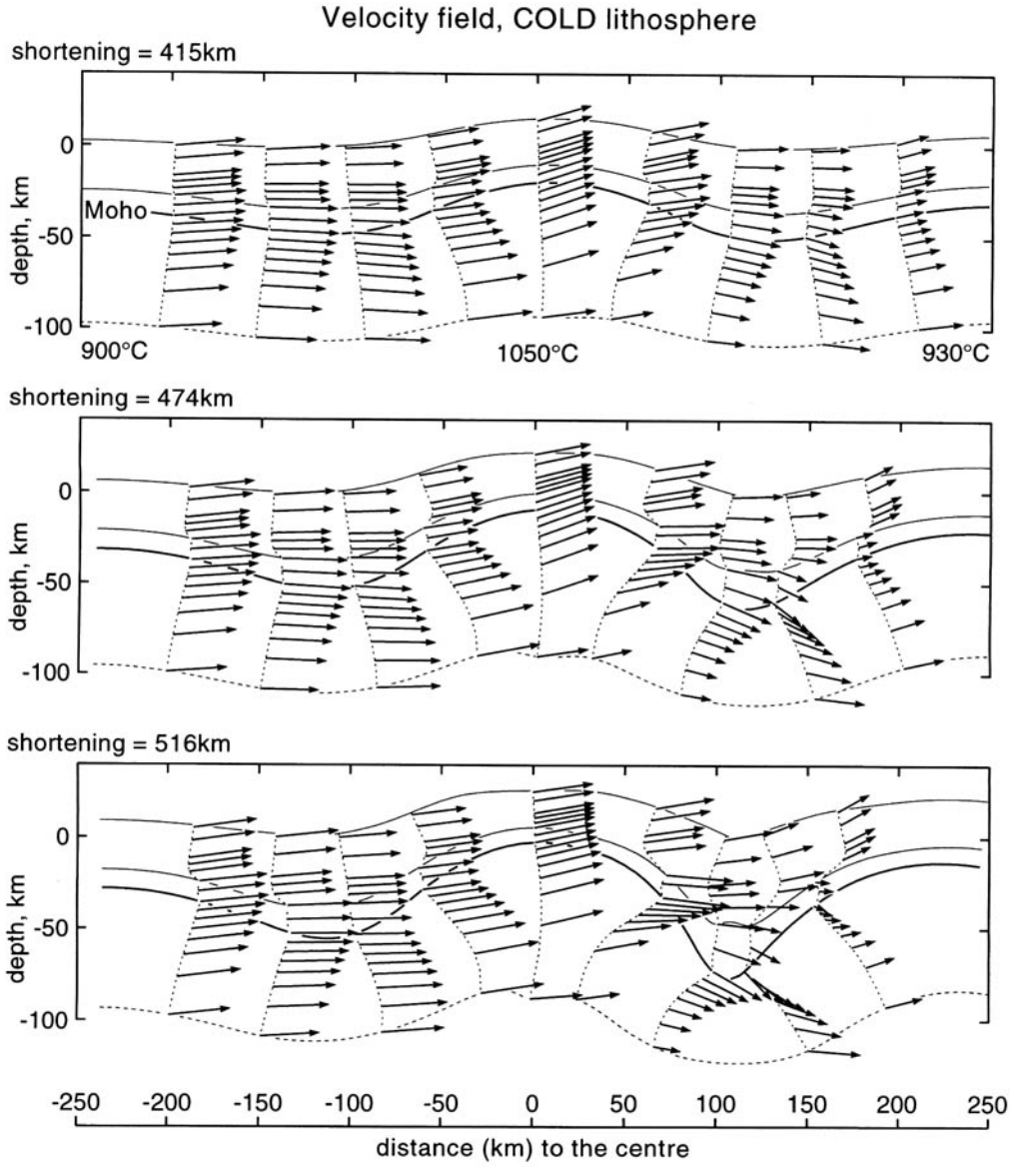

Fig. 6. Shortening experiment with developing velocity field in the central part of the 'COLD' lithosphere. No erosion is permitted. Boundary conditions in Table 2.

south (Burbank & Johnson 1982). However, both basins began receiving sediments in Pliocene time; both are coeval with the syntaxis and lacustrine sedimentation, although their overall history is that of surface uplift (Burbank & Johnson 1982). Burbank & Tahirkheli (1985) emphasize that this lacustrine sedimentation contrasts with the fluvial sedimentation that is predominant in adjacent areas. Differences in basin history, recognized by the latter authors, can be explained by the development of the westward-verging syntaxis, a geometrical character that we have emphasized. This geometrical asymmetry would account for a 1 Ma younger onset of sedimentation in the Peshawar Basin, where Plio-Pleistocene sediments are not as thick as in the Kashmir Basin. Indeed, an important feature of the models is their spontaneous large-scale asymmetry, once initially symmetric buckling is replaced by a thrusting mode. The dip

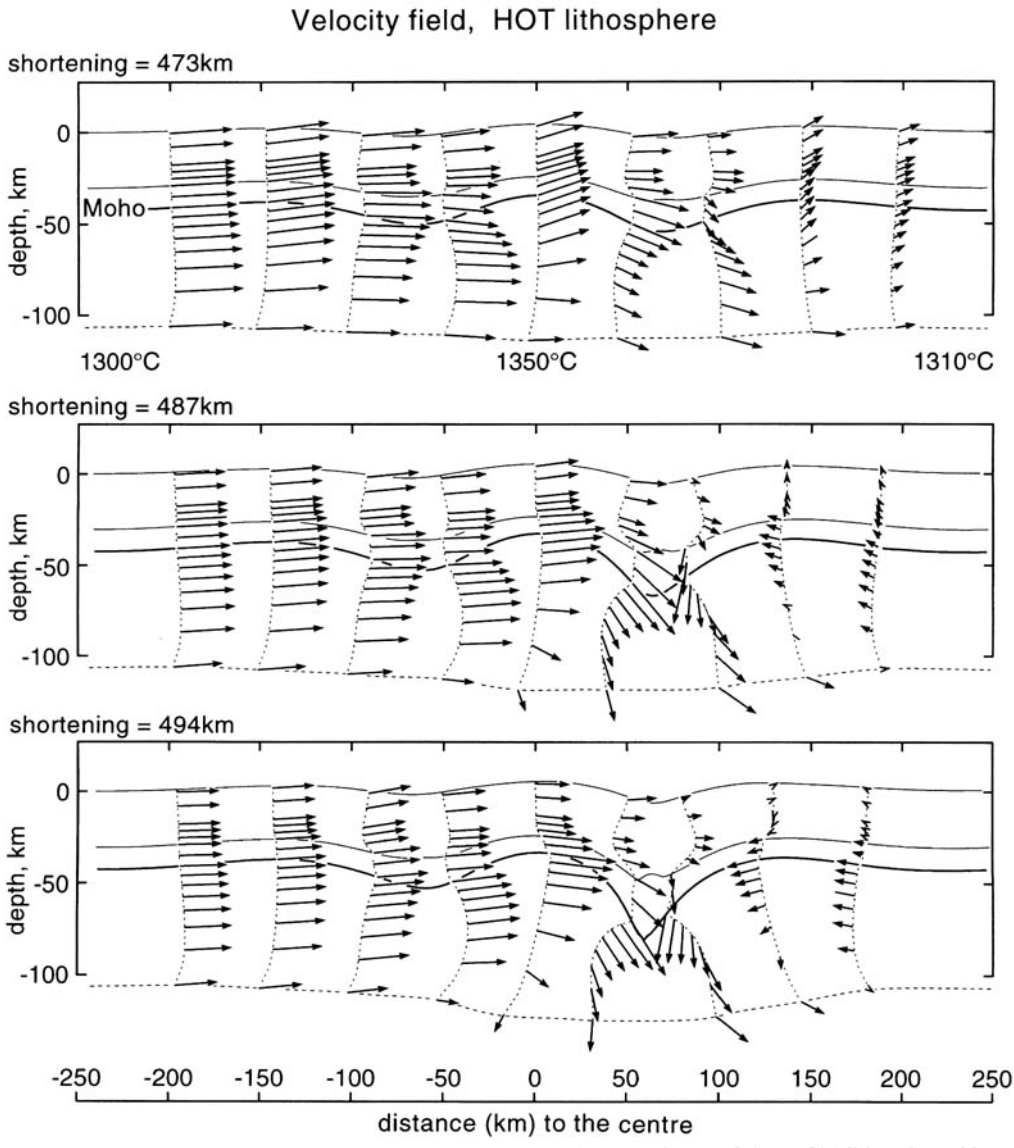

Fig. 7. Shortening experiment with developing velocity field in the central part of the 'HOT' lithosphere. No erosion is permitted. Boundary conditions in Table 2.

direction is controlled by the small difference in bottom temperatures of the colliding plates. This asymmetry is relevant to the vergence of the Himalayan syntaxes, both exaggerated by thrusting on their steeper limbs (see Butler *et al.* (1988) for Nanga Parbat; Chang *et al.* (1992) for Namche Barwa).

Discussion

Early modelling of the India–Asia collision belt was based upon thin sheet approximations (Vilotte & Daignières 1982; England & McKenzie 1983; England & Houseman 1986; Houseman & England 1986; Houseman & England 1993) that allow consideration of the three-dimensional geometry of convergent zones and treat first-order questions such as the relative amounts of lateral extrusion and homogeneous thickening. However, thin sheet models kinematically exclude folding as a response to compression, which is unfortunate, because the stresses necessary to engender folding are smaller than those for homogeneous thickening. This implies that

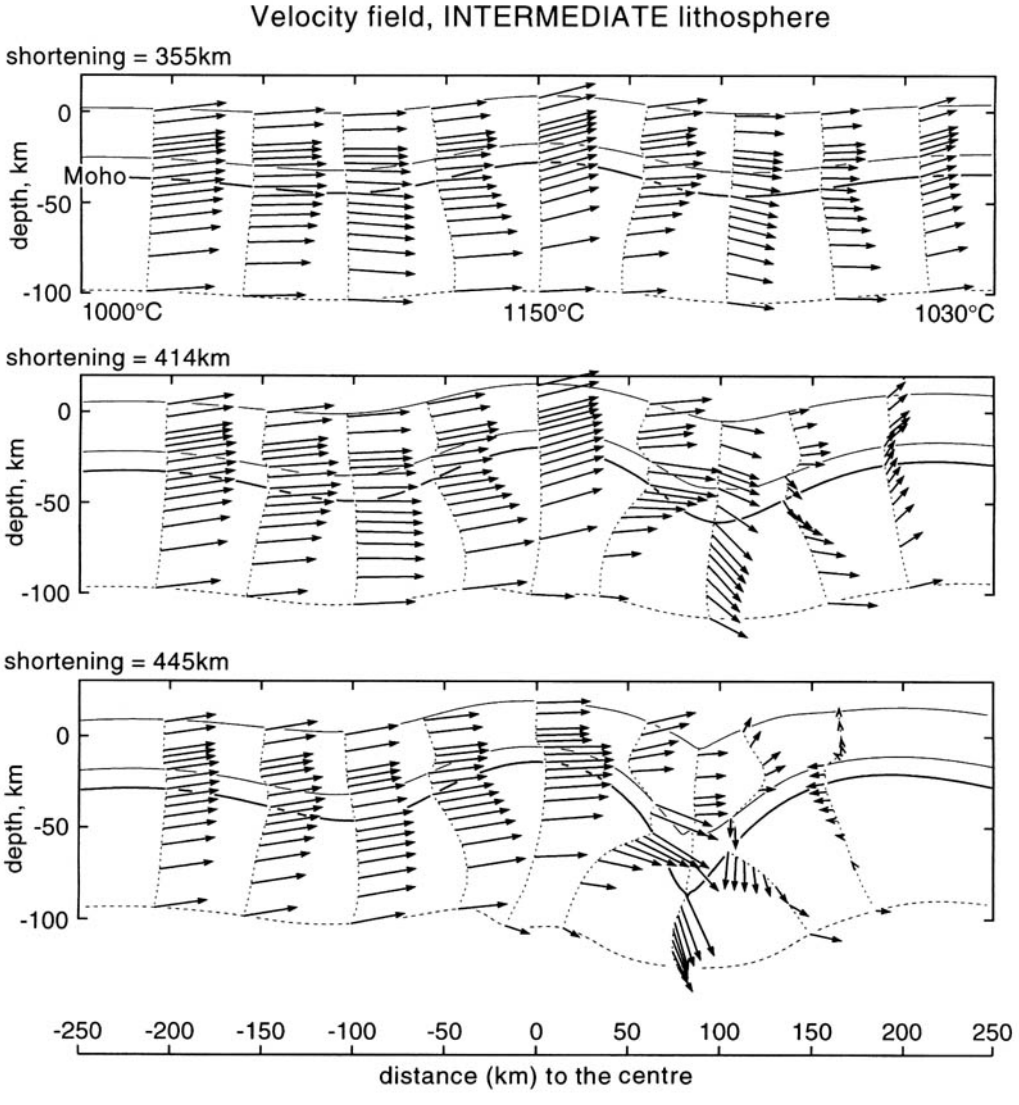

Fig. 8. Shortening experiment with developing velocity field in the central part of the 'INTERMEDIATE' lithosphere. No erosion is permitted. Boundary conditions in Table 2.

homogeneous thickening is dynamically unstable. Therefore, the amount of intraplate shortening v. other modes of localized deformations (strike-slip, thrusting) is intrinsically underestimated by dynamic thin sheet modelling. Although folding can be modelled by extended thin sheet approximations (Medvedev & Podladchikov 1999*a*, *b*), the prediction of three-dimensional distribution of stresses and shortening directions is out of the scope of this work. Indeed, the profiles we consider run across the middle parts of antiforms several hundreds of kilometres long, which allows us to model cross-sections in close to plane strain conditions. The major emphasis is prediction (v. prescription) of the internal deformation mode of a lithosphere responding to far-field shortening. To make the problem tractable we chose to pre-describe the far-field loading as a kinematic squeezing by two rigid plates.

Our finite element modelling yields exhumation rates and amounts similar to those recognized in the eastern and western Himalayan syntaxes. In the models, we delimit only the bulk shortening, whereas exhumation and antiform formation are dynamic responses to shortening.

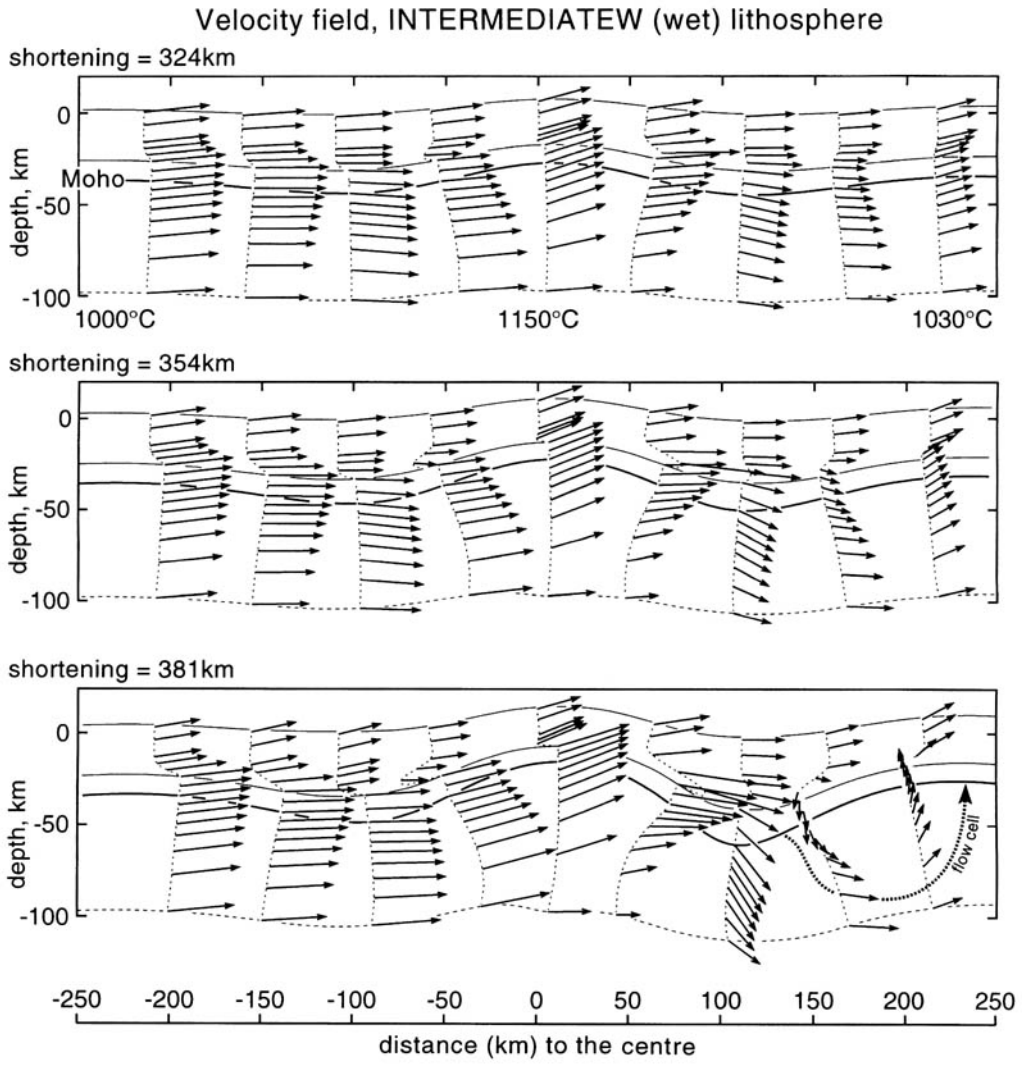

Fig. 9. Shortening experiment with developing velocity field in the central part of the 'INTERMEDIATEW' (wet) lithosphere. No erosion is permitted. Boundary conditions in Table 2. Note the secondary circulation pattern to the right of the thrust system (thick, dotted stream line = flow cell), suggesting a mechanism for burial and exhumation of crustal rocks to and from mantle depth in the early orogenic stages.

Our thermo-mechanical modelling ensures force balance in addition to heat and mass balance, which are satisfied in the thermo-kinematic models. Therefore, our results support the plausibility of crustal folding as envisioned for the syntaxes by the kinematic model of Burg *et al.* (1997). In addition, our calculations also predict the formation of adjacent basins, developed next to the West Himalayan syntaxis. Tuning of the coefficient of erosion and selecting a 'preferred' thermal model successfully and simultaneously reproduced the sedimentation rate, the exhumation rate and the magnitude of the differential relief.

The Himalayan syntaxes provide evidence for lithospheric buckling as a basic response to shortening, a mechanism complementary to the conventionally accepted subduction and accretion. We emphasize that the dominant geological and physiographic features of Northern Pakistan formed during the last 4 Ma have been controlled by the growth of the Nanga Parbat syntaxis. This is also true for the less well known eastern Himalayan syntaxis.

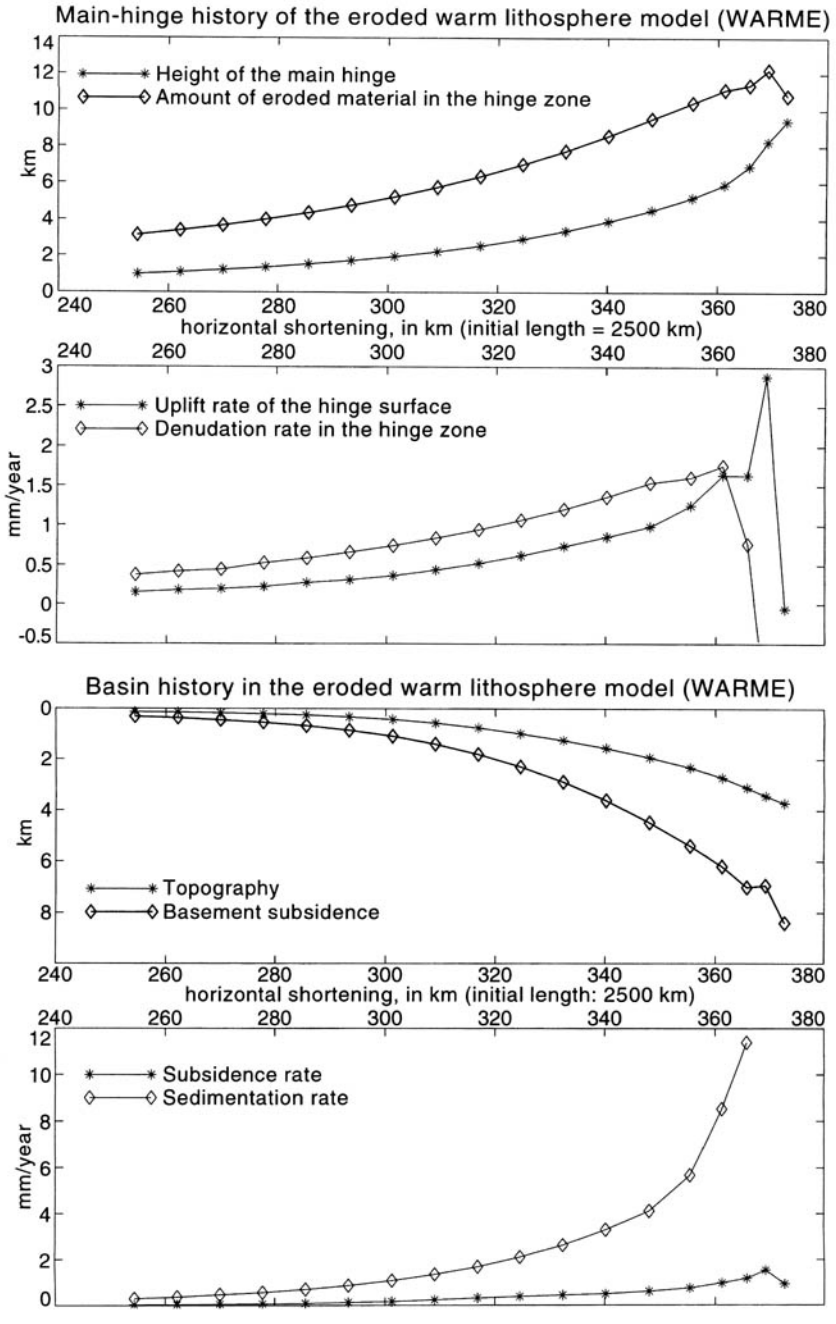

Fig. 10. Topography and exhumation histories of the main hinge zone (top) and topography and basement subsidence of basins next to the main antiformal hinge (bottom) in our preferred model WARM with erosion (WARME, Table 2). Topography due to buckling is up to 5–10 km. Exhumation is limited to *c.* 20 km by fold locking.

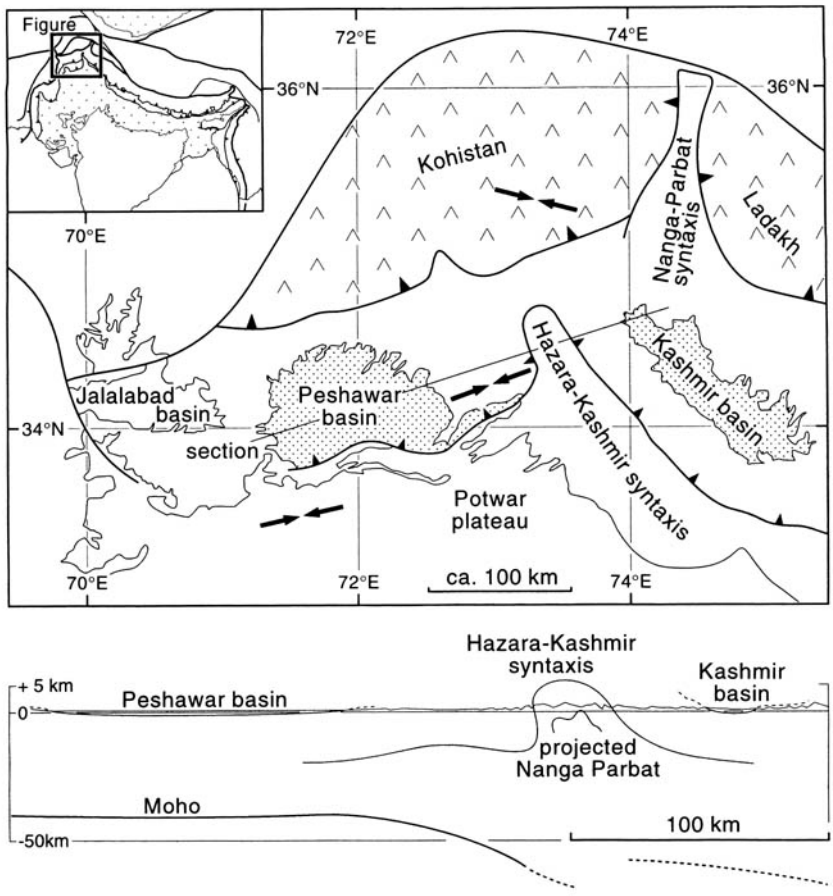

Fig. 11. Tectonic sketch map and simplified cross-section of the Nanga Parbat–Hazara–Kashmir syntaxes showing the synclinal Peshawar Basin to the west as a structural analogue of the synclinal Kashmir Basin to the east. Location in the Himalayan system in inset. Facing black arrows are compression directions from focal mechanism solutions (Verma *et al.*, 1980). Moho projected from Ni *et al.* (1991) and Kaila *et al.* (1983).

The next question to address is whether there is a link between the tectonic location of syntaxes and the dominance of lithosphere-scale folding as a shortening mechanism. We have argued above that the Himalayan syntaxes were likely compressed simultaneously from both north–south and east–west directions, a constrictional environment caused by the lack of accommodation space at the extremities of the Himalayan orogen (see also Treloar *et al.* 1991; Seeber & Pêcher 1998). Lateral constraints imposed by the system enforce close to plane strain conditions and are essential for the fast development of the buckling instability. Indeed, out-of-plane (lateral) extensional strain decreases the growth rate of the folding instability, which minimizes the magnitude of fold hinge magnification achieved at given amounts of shortening. Therefore, constrained areas are expected to be preferred sites of large-scale buckling, instead of vertical thickening. Late convergence stages (because topographic loads need accumulated strain to develop) and syntaxes (due to lack of accommodation space at the corners of the indentor) would favour the buckling mode of shortening. Generalizing these results, we suggest that the regional history of the Himalayan syntaxes included three main stages (Fig. 12): (1) locking of a previously active thrust system to the north of the syntaxes (in the hinterland regions), which triggered regional, intracontinental compression; (2) shortening and symmetric buckling of the colliding Indian lithosphere, which produced the transverse syntaxial antiforms at the extremities of the Himalayan range; and (3) loss of symmetry and the formation of new thrusts in the overturned limbs of the antiforms. This history may be a general element in the evolution of continental shortening.

Conclusion

Our two-dimensional-finite element numerical experiments systematically reproduce deformation features, independently recognized by lithospheric-scale analogue modelling (Cobbold *et al.* 1993; Burg *et al.* 1994; Martinod & Davy 1994).

1. Numerical and analogue models initially undergo homogeneous shortening and coeval thickening before they become unstable and buckle. Hot lithospheres undergo more distributed shortening than cold ones. Regardless of thermal regime, buckling is a basic response of stratified lithospheres to applied, far-field compression.
2. Lithospheric folding is mechanically preferable to homogeneous thickening and can drive mountain building and exhumation of deep-seated rocks. The coefficient of erosion controls the amount of exhumation possible in the core of crustal antiforms and the maximum altitude achieved during shortening.
3. Buckle amplification is limited by fold locking. A cold (strong) lithosphere tends to exhibit higher amplitude folding with a longer wavelength (*c.* 200 km) than a hot lithosphere. Kilometre-scale amplification is achieved in the strain range of 10–25%.
4. With shortening beyond the locking condition, buckling propagates laterally and adjacent crustal folds develop. Propagation is less pronounced in hot than in cold lithospheres.
5. Folding of both crustal and sub-crustal levels indicates coupling of all lithospheric layers during this deformation mode.
6. Synformal, small amplitude basins develop on both sides of the growing antiforms.
7. In all cases, asymmetry grows gradually and becomes dominant after *c.* 25% shortening, giving way to a 'thrusting' mode whose dip is controlled by the bottom temperature distribution.

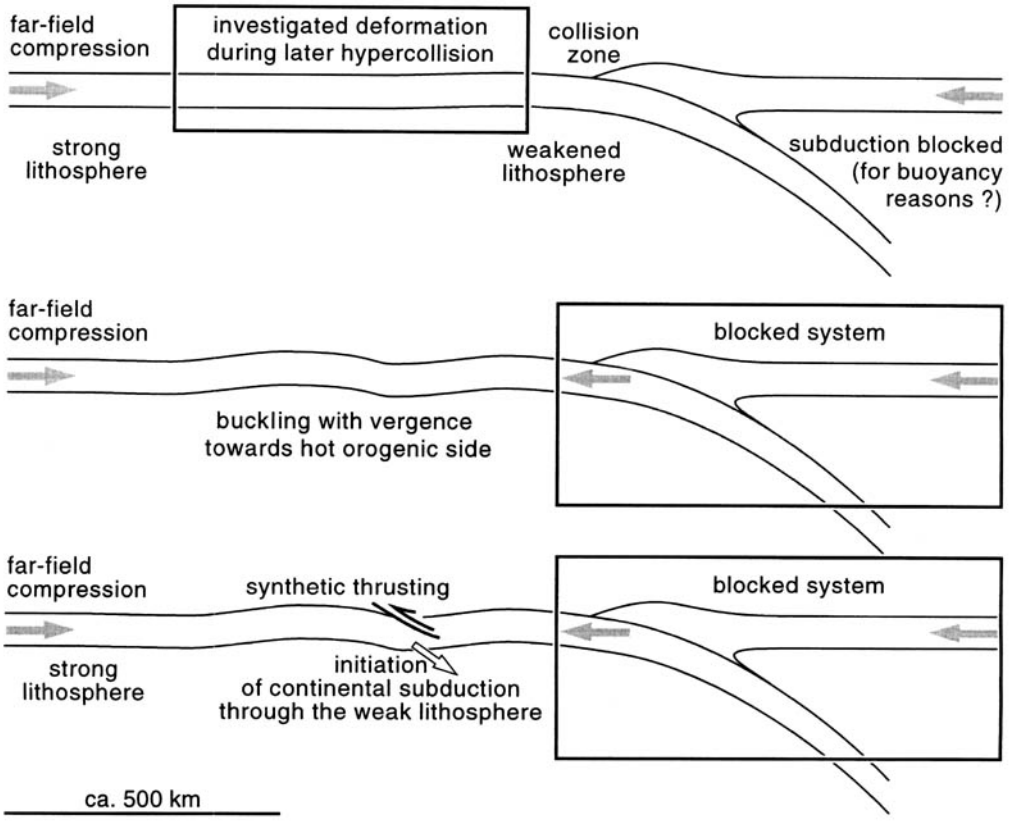

Fig. 12. Sketch of the buckling to thrusting 'tectonic cycle' envisaged in continental lithospheres under compression in the light of the numerical experiments presented here.

The Himalayan syntaxes are preferential sites of large-scale folding. This deformation has been quantified by two-dimensional FEM modelling that couples plane strain mechanical and thermal calculations with non-linear lithospheric rheologies. Both syntaxes have grown within the last 4 Ma, and were accompanied by the formation of fast subsiding synformal basins. Geological data and modelling indicate that these structures have reached their locking stages. Vertical movements should decelerate and buckling of the Indian lithosphere is expected to propagate laterally.

These results have been obtained thanks to the support of the Swiss National Science Foundation (projekts 21-39080.93 and 20-49372.96) and the ETH (projekt 1-20-888-94). J. Connolly and S. Miller improved a first draft of the manuscript. K. McCaffrey, P. Cobbold, K. Burke and P. Treloar have made very useful reviews and editorial remarks that helped us to clarify this work.

Appendix: mathematical model

We use a set of equations for stress and heat balance, coupled with visco-elasto-plastic rheological relationships in incremental form. Stress balance system of the equation used is

$$\begin{aligned} -\frac{\partial P}{\partial x}+\frac{\partial \tau_{xx}}{\partial x}+\frac{\partial \tau_{xy}}{\partial y}&=0\\ -\frac{\partial P}{\partial y}+\frac{\partial \tau_{xy}}{\partial x}+\frac{\partial \tau_{yy}}{\partial y}-\rho(1+\alpha T)g&=0 \end{aligned} \tag{A1}$$

where P is the pressure (negative of the mean part of the stress tensor), τ_{xx}, τ_{xy} and τ_{yy} are the deviator components of the stress tensor, g is the gravity acceleration, ρ is the density, T is the temperature, α is the thermal expansion coefficient, y axis is directed upwards. Heat balance is used in the form:

$$c\rho\left(\frac{\partial T}{\partial t}+V_x\frac{\partial T}{\partial x}+V_y\frac{\partial T}{\partial y}\right) = k\left(\frac{\partial^2 T}{\partial x^2}+\frac{\partial^2 T}{\partial y^2}\right)+Q \tag{A2}$$

where V_x and V_y are the components of the velocity vector, t is time, c is the specific heat, k is the thermal conductivity and Q is the heat production. Q is set to 10^{-6} W m^{-3} for crustal rocks and to zero for the mantle. Incremental form of Maxwell visco-elastic rheology for deviator components of the stress tensor, τ_{ij}, and deviator components of strain rate tensor, e_{ij}, is

$$e_{ij}=\frac{1}{2G}\frac{D\tau_{ij}}{Dt}+\frac{\tau_{ij}}{2\mu} \tag{A3}$$

where D/Dt stands for the Jauman (corrotational) objective derivative (e.g. Biot, 1965), G is the shear elastic modulus and μ is the viscosity coefficient chosen to comply with a uniaxial form of power law relationship:

$$e=Ae^{-E/RT}\sigma^n \tag{A4}$$

where A, E and n are given in Table 1 for each material, R is the universal gas constant, e and σ are axial strain rate and differential stress respectively. Bulk rheology is modelled as purely elastic:

$$\frac{\partial V_x}{\partial x}+\frac{\partial V_y}{\partial y}=-\frac{1}{K}\frac{\mathrm{d}P}{\mathrm{d}t} \tag{A5}$$

where K is the bulk elastic modulus. The treatment of yielding follows non-associated Mohr–Coulomb plasticity (Vermeer & de Borst, 1984). At each loading increment the failure criterion is checked and an instantaneous volume preserving (the dilation angle is set to zero) plastic deformation is added to maintain the stresses within the failure envelope. The friction angle is 30° for all rock types to comply with the Byerlee law.

The above system of equations is solved using a two-dimensional finite element code FEMREV (Podladchikov, 1999) that couples plain strain mechanical and thermal calculations. An implicit Euler time marching scheme is used to discretize all time derivatives. At each time step, spatial derivatives (not related to advection terms) are discretized using a finite element method. Finite elements are enriched seven-node quadratic triangles (for details see Poliakov & Podladchikov, 1992; Podladchikov *et al.*, 1993). The number of the finite element nodes was 901×101. Lagrangian motion of the finite element grid models advection. Iterations are used to resolve the non-linearity of rheology and implicit Lagrangian motion of the finite element grid. At each iteration, a System of Linear Algebraic Equations (SLAE) is solved by a direct (profile) method. Static condensation of the seventh node on the element level is used to reduce the profile of the SLAE matrix. Iterative refinements are used to improve the accuracy of the SLAE solution, to satisfy better the nearly incompressible bulk rheology condition and to control 'off balance' of the current stresses. The corrections of the stresses due to plastic yielding are identical to those employed in the explicit FLAC algorithm (Cundall & Board, 1988) and were performed within the iterative refinements as well. All iterative refinements do not require additional factorization of the SLAE matrix because they only affect the right-hand side of

the SLAE. At each time step, the upper surface is first moved by the velocity field in a Lagrangian manner and then corrected for erosion. Alteration of the upper surface by erosion, $h(t, x)$, is modelled by solving a linear diffusion equation (Podladchikov *et al.*, 1993):

$$\text{e.g.} \qquad \frac{\partial h}{\partial t} = K_e \frac{\partial^2 h}{\partial x^2} \qquad \text{(A6)}$$

where K_e is the coefficient of erosion.

References

ARMIJO, R., TAPPONNIER, P., MERCIER, J. L. & HAN, T.-L. 1986. Quaternary extension in Southern Tibet: Field observations and tectonic implications. *Journal of Geophysical Research*, **91**, 13803–13872.

BEAUMONT, C., ELLIS, S., HAMILTON, J. & FULLSACK, P. 1996. Mechanical model for subduction–collision tectonics of Alpine-type compressional orogens. *Geology*, **24**, 675–678.

BIOT, M. A. 1961. Theory of folding of stratified viscoelastic media and its implications in tectonics and orogenesis. *Geological Society of America Bulletin*, **72**, 1595–1620.

—— 1965. *Mechanics of incremental deformation*. John Wiley and Sons, New York.

BOSSART, P., DIETRICH, D., GRECO, A., OTTIGER, R. & RAMSAY, J. G. 1988. The tectonic structure of the Hazara–Kashmir Syntaxis, Southern Himalayas, Pakistan. *Tectonics*, **7**, 273–297.

BURBANK, D. W. 1983. The chronology of intermontane-basin development in the northwestern Himalaya and the evolution of the northwest syntaxis. *Earth and Planetary Science Letters*, **64**, 77–92.

—— & JOHNSON, G. D. 1982. Intermontane-basin development in the past 4 Myr in the north-west Himalaya. *Nature*, **298**, 432–436.

—— & TAHIRKHELI, R. A. K. 1985. The magnetostratigraphy, fission-track dating, and stratigraphic evolution of the Peshawar intermontane basin, northern Pakistan. *Geological Society of America Bulletin*, **96**, 539–552.

——, RAYNOLDS, R. G. H. & JOHNSON, G. D. 1986. Late Cenozoic tectonics and sedimentation in the north-western Himalayan foredeep: II. Eastern limb of the Northwest Syntaxis and regional synthesis. *In*: ALLEN, P. A. & HOMEWOOD, P. (eds) *Foreland Basins*. Special Publication of the International Association of Sedimentologists, **8**, 293–306.

BURG, J.-P., DAVY, P. & MARTINOD, J. 1994. Shortening of analogue models of the continental lithosphere: New hypothesis for the formation of the Tibetan plateau. *Tectonics*, **13**, 475–483.

——, ——, NIEVERGELT, P., OBERLI, F., SEWARD, D., DIAO, Z. & MEIER, M. 1997. Exhumation during crustal folding in the Namche–Barwa syntaxis. *Terra Nova*, **9**, 53–56.

——, NIEVERGELT, P., OBERLI, F., SEWARD, D., DAVY, P. *et al.* 1998. The Namche Barwa syntaxis: evidence for exhumation related to compressional crustal folding. *Journal of Asian Earth Sciences*, **16**, 239–252.

BUROV, E. B. & DIAMENT, M. 1995. The effective elastic thickness (Te) of continental lithosphere: What does it really mean? *Journal of Geophysical Research*, **100**, 3905–3927.

BUTLER, R. W. H., OWEN, L. & PRIOR, D. J. 1988. Flashfloods, earthquakes and uplift in the Pakistan Himalayas. *Geology Today*, **4**, 197–201.

CARTER, N. L. & TSENN, M. C. 1987. Flow properties of continental lithosphere. *Tectonophysics*, **136**, 27–63.

CHANG, C. G., LIO, H. H., WANG, T. W., YANG, H. X. & HU, B. Z. 1992. *Geology of the Namche Barwa region*. Academia Sinica.

COBBOLD, P. R. & DAVY, P. 1988. Indentation tectonics in nature and experiment. 2. Central Asia. *Bulletin Geological Institute, University of Uppsala, NS*, **14**, 143–162.

——, ——, GAPAIS, D., ROSSELLO, E. A., SADYBAKASOV, E. *et al.* 1993. Sedimentary basins and crustal thickening. *Sedimentary Geology*, **86**, 77–89.

CUNDALL, P. A. & BOARD, M. 1988. L F A microcomputer program for modelling large-strain plasticity problems. *In*: SWOBODA, G. (ed.) *Numerical methods in geomechanics*. Balkema, Rotterdam, 2101–2108.

DAVY, P. & COBBOLD, P. R. 1991. Experiments on shortening of a 4-layer model of the continental lithosphere. *Tectonophysics*, **188**, 1–25.

ENGLAND, P. C. & HOUSEMAN, G. A. 1986. Finite strain calculations of continental deformation 2. Comparison with the India-Asia collision zone. *Journal of Geophysical Research*, **91**, 3664–3676.

—— & MCKENZIE, D. P. 1983. Correction to: A thin viscous sheet model for continental deformation. *Geophysical Journal of the Royal Astronomical Society*, **73**, 523–532.

FARAH, A., LAWRENCE, R. D. & DE JONG, K. A. 1984. An overview of the tectonics of Pakistan. *In*: BILAL, U. H. & MILLIMAN, J. D. (eds) *Marine geology and oceanography of Arabian Sea and Coastal Pakistan*. Van Nostrand Reinhold, New York, 161–176.

GANSSER, A. 1966. The Indian Ocean and the Himalayas. A geological interpretation. *Eclogae Geologicae Helvetiae*, **59**, 831–848.

—— 1991. Facts and theories on the Himalayas. *Eclogae Geologicae Helvetiae*, **84**, 33–59.

HENRY, P., LE PICHON, X. & GOFFÉ, B. 1997. Kinematic, thermal and petrological model of the Himalayas: constraints related to metamorphism within the underthrust Indian crust and topographic elevation. *Tectonophysics*, **273**, 31–56.

HOLT, W. E., NI, J. F., WALLACE, T. C. & HAINES, A. J. 1991. The active tectonics of the Eastern Himalayan Syntaxis and surrounding regions. *Journal of Geophysical Research*, **96**, 14595–14632.

HOUSEMAN, G. A. & ENGLAND, P. C. 1986. Finite strain calculations of continental deformation 1.

Method and general results for convergent zones. *Journal of Geophysical Research*, **91**, 3651–3663.

—— & —— 1993. Crustal thickening versus lateral expulsion in the Indian–Asian continental collision. *Journal of Geophysical Research*, **98**, 12233–121249.

JOHNSON, A. M. & FLETCHER, R. C. 1994. *Folding of viscous layers*. Columbia University Press.

KAILA, K. L., ROY CHOWDHURY, K., KRISHNA, V. G., DIXIT, M. M. & NARAIN, H. 1983. Crustal structure of the Kashmir Himalaya and inferences about the asthenospheric layer from DSS studies along the international profile Qarrakol (Karakul) Zorkol–Nanga Parbat–Srinagar. *Bolletino di Geofisica Teorica ed Applicata*, **25**, 221–234.

MANDL, G. 1988. *Mechanics of tectonic faulting*. Elsevier Science Publishers B.V.

MARTINOD, J. & DAVY, P. 1992. Periodic instabilities during compression or extension of the lithosphere 1. Deformation modes from an analytical perturbation method. *Journal of Geophysical Research*, **97**, 1999–2014.

—— & —— 1994. Periodic instabilities during compression of the lithosphere 2. Analogue experiments. *Journal of Geophysical Research*, **99**, 12057–12069.

MCADOO, D. C. & SANDWELL, D. T. 1985. Folding of oceanic lithosphere. *Journal of Geophysical Research*, **90**, 8563–8569.

MEDVEDEV, S. E. & PODLADCHIKOV, Y. Y. 1999*a*. New extended thin-sheet approximation for geodynamic applications—I. Model formulation. *Geophysical Journal International*, **136**, 567–585.

—— & —— 1999*b*. New extended thin-sheet approximation for geodynamic applications—II. Two-dimensional examples. *Geophysical Journal International*, **136**, 586–608.

NI, J. F., IBENBRAHIM, A. & ROECKER, S. W. 1991. Three-dimensional velocity structure and hypocenters of earthquakes beneath the Hazara Arc, Pakistan: Geometry of the underthrusting Indian plate. *Journal of Geophysical Research*, **96**, 19865–19877.

PODLADCHIKOV, Y. Y. 1999. *FEMREV: a code for modeling of lithospheric deformation*. Unpublished code, ETH-Zürich, accessible on request.

——, TALBOT, C. & POLIAKOV, A. N. B. 1993. Numerical models of complex diapirs. *Tectonophysics*, **228**, 189–198.

POGUE, K. R., WARDLAW, B. R., HARRIS, A. G. & HUSSAIN, A. 1992. Paleozoic and Mesozoic stratigraphy of the Peshawar basin, Pakistan: Correlations and implications. *Geological Society of America Bulletin*, **104**, 915–927.

POLIAKOV, A. & PODLADCHIKOV, Y. Y. 1992. Diapirism and topography. *Geophysical Journal International*, **109**, 553–564.

——, ——, DAWSON, E. & TALBOT, C. J. 1996. Salt diapirism with simultaneous brittle faulting and viscous flow. *In*: ALSOP, I., BLUNDELL, D. & DAVISON, I. (eds) *Salt Tectonics*. Geological Society, London, Special Publications, **100**, 291–302.

RAMBERG, H. 1964. Selective buckling of composite layers with contrasted rheological properties, a theory for simultaneous formation of several orders of folds. *Tectonophysics*, **1**, 307–341.

RANALLI, G. 1995. *Rheology of the Earth*. Chapman & Hall, London.

SEEBER, L. & PÊCHER, A. 1998. Strain partitioning along the Himalayan arc and the Nanga Parbat antiform. *Geology*, **26**, 791–794.

SINGH, S. 1993. Geology and tectonics of the Eastern Syntaxial Bend, Arunachal Himalaya. *Journal of Himalayan Geology*, **4**, 149–163.

SONDER, L. J., ENGLAND, P. C., WERNICKE, B. P. & CHRISTIANSEN, R. L. 1987. A physical model for Cenozoic extension of western North America. *In*: COWARD, M. P., DEWEY, J. F. & HANCOCK, P. L. (eds) *Continental Extensional Tectonics*. Geological Society, London, Special Publications, **28**, 187–201.

TRELOAR, P. J., POTTS, G. J., WHEELER, J. & REX, D. C. 1991. Structural evolution and asymmetric uplift of the Nanga Parbat syntaxis, Pakistan Himalaya. *Geologische Rundschau*, **80**, 411–428.

TURCOTTE, D. L. & SCHUBERT, G. 1982. *Geodynamics: applications of continuum physics to geological problems*. John Wiley & Sons.

VERMA, R. K., MUKHOPADHYAY, M. & BHANJA, A. K. 1980. Seismotectonics of the Hindukush and Baluchistan Arc. *Tectonophysics*, **66**, 301–322.

VERMEER, P. A. & DE BORST, R. 1984. Non-associated plasticity for soils, concrete and rock. *Heron*, **29**, 1–64.

VILOTTE, J. P. & DAIGNIÈRES, M. 1982. Numerical modeling in intraplate deformation: simple mechanical models of continental collision. *Journal of Geophysical Research*, **87**, 10709–10728.

WADIA, D. N. 1931. The syntaxis of the northwest Himalaya: its rocks, tectonics and orogeny. *Records of the Geological Survey of India*, **65**, 189–220.

—— 1957. *Geology of India*. Macmillan Co.

WILLETT, S., BEAUMONT, C. & FULLSACK, P. 1993. Mechanical model for the tectonics of doubly vergent compressional orogens. *Geology*, **21**, 371–374.

YEATS, R. S. & LAWRENCE, R. D. 1984. Tectonics of the Himalayan Thrust Belt in Northern Pakistan. *In*: BILAL, U. H. & MILLIMAN, J. D. (eds) *Marine geology and oceanography of Arabian Sea and Coastal Pakistan*. Van Nostrand Reinhold, New York, 177–198.

ZEITLER, P. K., CHAMBERLAIN, C. P. & SMITH, H. A. 1993. Synchronous anatexis, metamorphism, and rapid denudation at Nanga Parbat (Pakistan Himalaya). *Geology*, **21**, 347–350.

——, SUTTER, J. F., WILLIAMS, I. S., ZARTMAN, R. & TAHIRKHELI, R. A. K. 1989. Geochronology and temperature history of the Nanga Parbat–Haramosh Massif, Pakistan. *In*: MALINCONICO, L. L. & LILLIE, R. J. (eds) *Tectonics of the Western Himalayas*. Geological Society of America Special Paper, **232**, 1–22.

Mantle exhumation along the Tirich Mir Fault Zone, NW Pakistan: pre-mid-Cretaceous accretion of the Karakoram terrane to the Asian margin

A. ZANCHI[1], S. POLI[2], P. FUMAGALLI[2] & M. GAETANI[2]

[1]*Dipartimento di Scienze dell'Ambiente e del Territorio, Università degli Studi di Milano—Bicocca, Piazza della Scienza 1, 20126 Milano, Italy*

(e-mail: zanchi@disat.unimib.it)

[2]*Dipartimento di Scienze della Terra, Università degli Studi di Milano, Via Mangiagalli 34 20134 Milano, Italy*

Abstract: The left-lateral strike-slip Tirich Mir Fault, Chitral, NW Pakistan, is associated with a belt of peridotites, metagabbros and gneisses named the Tirich Boundary Zone (TBZ), separating the Late Palaeozoic–Mesozoic units of the East Hindu Kush from the Palaeozoic successions of the Karakoram block. These rocks were metamorphosed up to upper amphibolite facies conditions, followed by a greenschist facies overprinting, and then thrust on to very low grade metasediments; they were finally intruded at shallow levels by the mid-Cretaceous Tirich Mir pluton. Ultramafic rocks along the fault zone include well-preserved spinel lherzolites and harzburgites (Tirich Gol, Barum valley, Arkari Gol), whereas schistose serpentinites occur in the Rich Gol. Whole-rock analyses and mineral chemistry of olivine, clinopyroxene, orthopyroxene and spinel from these peridotites show a depleted signature. Microstructural and petrological features suggest a mantle origin for these ultramafic bodies, which equilibrated at temperatures ranging from 1000–1100 °C. Peridotites are faulted against partially metamorphosed igneous bodies including hornblende-gabbros, hornblende cumulates and quartz-diorites. Metamorphic rocks of the TBZ, which lay south of the ultramafic–mafic complex, include quartzites, amphibolites, garnet–sillimanite ($\pm$ kyanite $\pm$ K-feldspar)–biotite gneisses and mica schists, locally displaying migmatitic textures.

A sub-continental character of the peridotites indicated by low temperatures of equilibration and by the presence of a deep crustal sequence. These characters along with the absence of an ophiolitic sequence may suggest that the TBZ represents a fragmented crust–mantle boundary developed along a zone of attenuated continental crust. The TBZ is interpreted as a sheared lithospheric section of a Jurassic–Early Cretaceous orogenic complex, formed as a consequence of the accretion of the Karakoram terrane to the southern side of the Pamir belts, which were progressively accreted to the Asian margin.

Mesozoic progressive accretion of Perigondwana terranes along the southern margin of Eurasia, before the docking of the Indian plate, has been recognized by several authors, although the structural relationships, number, identity and evolution of these blocks are still poorly known. In Pakistan, the Main Mantle Thrust (Tahirkeli *et al.* 1979) represents the boundary between India and the Mesozoic Kohistan arc. The Shyok Suture separates Kohistan (Pudsey 1986) from the Karakoram (Fig. 1), which was located along the southern margin of the Mega Lhasa (Gaetani 1997), a composite terrane in the sense of Coney (1989). The distinction among the different sub-terranes forming the Mega Lhasa, and now lying between Karakoram and North Pamir (Fig. 1), is still tentative and based on general stratigraphic and tectonic considerations, due to the lack of ophiolitic sutures and to the severe post-accretion shortening of the region. Continuous ophiolitic belts occur about 200 km north of the Karakoram along the Wanch–Ak Baital Suture, which bounds the North Pamir and testifies to Late Palaeozoic accretion of continental fragments to Eurasia (Burtman & Molnar 1993). Nevertheless, in China and Afghanistan, where shortening was less severe, ophiolitic suture

From: KHAN, M. A., TRELOAR, P. J., SEARLE, M. P. & JAN, M. Q. (eds) *Tectonics of the Nanga Parbat Syntaxis and the Western Himalaya*. Geological Society, London, Special Publications, **170**, 237–252. 1-86239-061-4/00/$15.00

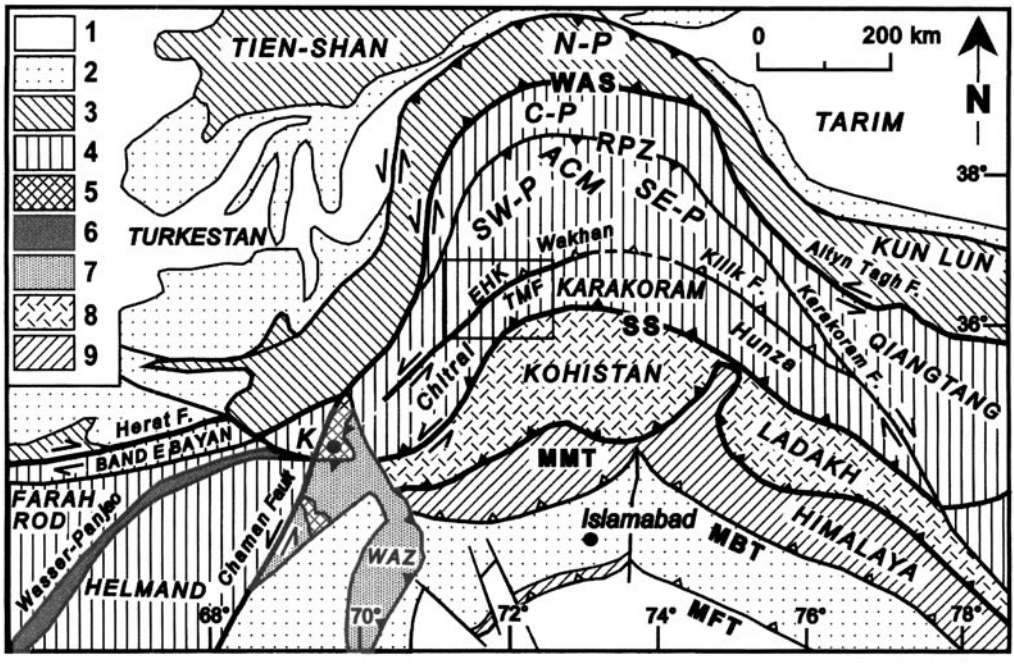

Fig. 1. Tectonic map of Northern Pakistan and surrounding regions. Modified from Gaetani *et al.* (1996) and Boulin (1988). MFT, Main Frontal Thrust; MBT, Main Boundary Thrust; MMT, Main Mantle Thrust; SS, Shyok Suture; TMF, Tirich Mir Fault Zone; EHK, East Hindu Kush; ACM, Alitchur mountains; RPZ, Rushan–Pshart Zone; WAS, Wanch–Ak Baital Suture; N-P, North Pamir; C-P, Central Pamir; SE-P, SE-Pamir; SW-P, SW-Pamir; WAZ, Waziristan; K, Kabul. 1, Quaternary; 2, Tertiary foredeeps; 3, Palaeozoic belts; 4, Terranes of Gondwanan affinity; 5, Kabul Block; 6, Wasser–Panjao Suture; 7, Waziristan ophiolitic complex; 8, Kohistan–Ladakh arc terranes; 9, Himalaya. Heavy lines represent main sutures.

zones, e.g. the Wasser–Panjao (Tapponier *et al.* 1981; Boulin 1988) and the Bangong, testify to the existence of oceanic crust between some of the microplates which represent the lateral continuation of the Pamir and Karakoram blocks.

Ultramafic bodies, along with mélanges or syn-tectonic sediments, have so far been used largely as a marker of sutures or major fault zones between the different terranes, although well documented mantle peridotites are rare. Serpentinitic blocks within the Swat mélanges and the Jijal ultramafic complex occur along the Main Mantle Thrust (Jan & Howie 1981). An olistostromal mélange, including small blocks of serpentinized ultramafics, defines the Shyok Suture (Pudsey 1986). Lenses and boudins of harzburgites, lherzolites and serpentinites within the central–eastern portion of the Karakoram metamorphic complex, the Panmah Unit, were interpreted as an intra-Karakoram fragmented suture (Searle *et al.* 1989).

Our recent discovery of a narrow belt of mantle peridotites, deformed gabbros, amphibolites and gneisses sandwiched between the East Hindu Kush and Karakoram terranes (Zanchi *et al.* 1997) along the Tirich Mir Fault, Chitral, NW Pakistan (Figs 1 and 2), provides a strong argument for the location of the northwestern boundary of Karakoram. The mid-Cretaceous Tirich Mir pluton (Desio *et al.* 1964) intrudes this belt, clearly postdating magmatism, metamorphism and deformation of the unit, which may be related to the early accretion of the Karakoram terrane to the southern section of the Pamir belts. Late Triassic to Jurassic orogenic events have so far been documented in the Pamir belts, as well as in the sedimentary cover of the Karakoram, where Lower Jurassic lithic sandstones suggest erosion of a nearby collisional belt (Pashkov & Budanov 1990; Gaetani *et al.* 1993).

The aim of this paper is to describe the general features of the ultramafic rocks and the metamorphic complexes exposed along the Tirich Mir Fault and to discuss their possible meaning in the light of Mesozoic accretionary processes occurring along the Eurasian margin.

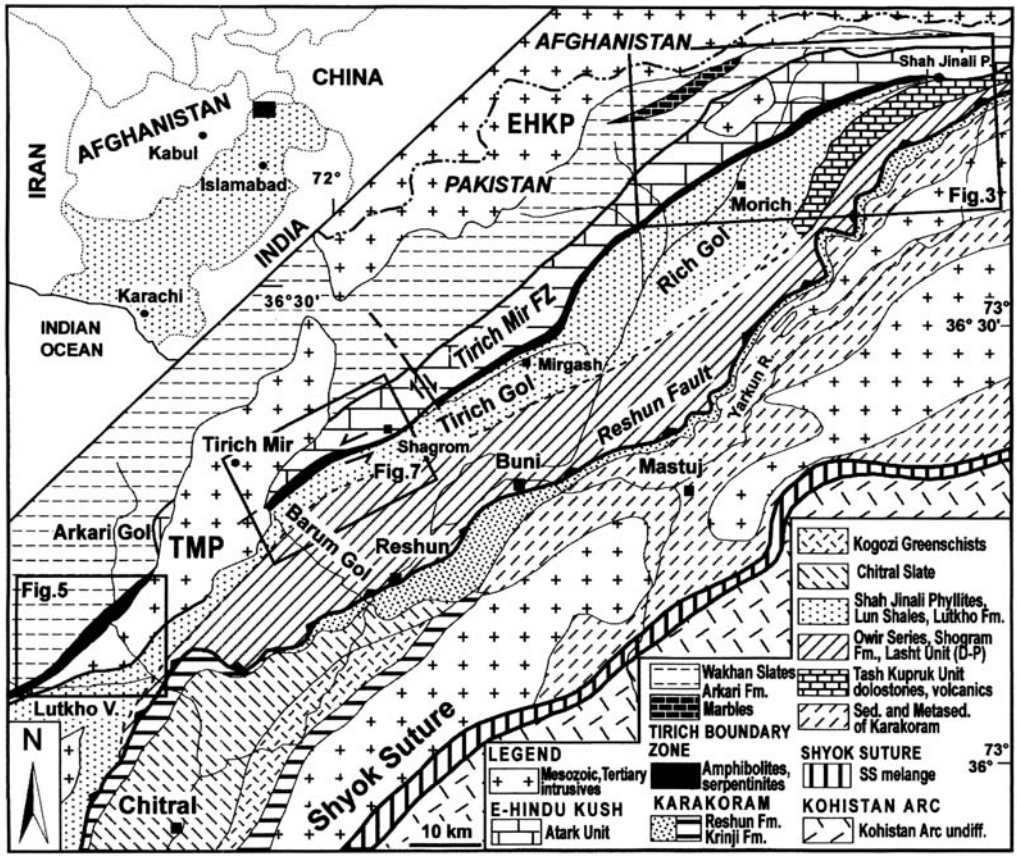

Fig. 2. Simplified structural map of NW Pakistan. Modified from Zanchi *et al.* (1997). EHKP, East Hindu Kush plutonic belt; TMP, Tirich Mir pluton.

Geological setting and Palaeozoic–Mesozoic evolution

Two main blocks crop out in Chitral north of the Kohistan arc: the western part of the Karakoram block between the Shyok Suture and the Tirich Mir Fault and the East Hindu Kush block northwest of the Tirich Mir Fault (Fig. 2).

The Shyok Suture consists of a strongly sheared and cleaved olistostromal unit (Pudsey *et al.* 1985) containing small blocks of serpentinites; this mélange has been related to the Late Cretaceous closure of a back-arc basin formed between the Karakoram and the Kohistan arc.

The Tirich Mir Fault (TMF), mentioned by Buchroithner (1980) and by Leake *et al.* (1989, fig.4: from Austromineral 1978) as the Tirich Fault, has been redefined by Gaetani & Leven (1993) along the Tirich Gol, where the fault stacks the Permo-Mesozoic Atark Unit above the Lun Shales.

We have found that the TMF, a complex NE–SW trending left-lateral strike-slip fault, is associated with a belt of peridotites, metagabbros, amphibolites and gneisses. This complex is here named the Tirich Boundary Zone (TBZ), and extends from the Shah Jinali Pass to the Barum valley and might represent the remnant of a suture zone (Zanchi *et al.* 1997). West of the Tirich Mir the TBZ is still recognizable from the Sunitz valley up to Afghanistan across the Arkari and Lutkho valley (Figs 2 and 5).

Karakoram block

The Karakoram block, of Gondwanan affinity (Gaetani 1997), includes a metamorphic basement intruded by pre-Ordovician granitoids (Le Fort *et al.* 1994). Its sedimentary succession, spanning Ordovician to Cretaceous time, records opening of the Neotethys during the Carboniferous–mid Permian, and the consequent

northward drifting of the block away from Gondwana during the Late Permian–Triassic. The passive margin succession is covered by Liassic orogenic sandstones with clasts of serpentinites, radiolarites, basalts and paragneiss, suggesting the erosion of a nearby, newly formed orogenic wedge (Gaetani *et al.* 1993). Further evidence comes from the Hushe gneiss of the Karakoram metamorphic complex lying south of the Karakoram batholith (Searle *et al.* 1989), which suggests a Jurassic low pressure–high temperature metamorphism associated with hornblende/biotite granodiorites with ages spanning 208–160 Ma. During the Cretaceous, the Karakoram suffered severe deformation combined with intensive plutonic activity. Intrusions are mid-Cretaceous in age and have been related to northward subduction of the Neotethys oceanic crust below the Karakoram (Debon *et al.* 1987*a*). Folds and thrust sheets are sealed by mid-Cretaceous molasse conglomerates (Tupop Fm., Reshun Fm.) and by the Campanian marine Darband Formation (Gaetani *et al.* 1993). This event, coeval with the closure of the Shyok Suture, records the final accretion of Kohistan to the Karakoram.

The western portion of the Karakoram (Gaetani *et al.* 1996) is separated into two major units by the Reshun Fault (Fig. 2), a SE-vergent thrust stacking Palaeozoic rocks on Palaeozoic–Mesozoic metasediments unconformably covered in the east by the Reshun Formation (Hayden 1915; Desio 1963, 1966; Pudsey *et al.* 1985). Cretaceous deformed granitoids occur east of the Reshun Fault (Le Fort & Gaetani 1998).

North of the Reshun Fault, in the western part of the area, Devonian sedimentary rocks include the Lun Shales, the Shogram Fm. (Desio 1963; Talent *et al.* 1981), and Permo-Triassic limestones. South of Tirich Mir around the Owir Pass, Buchroithner & Gamerith (1986) describe slates and phyllites with Devonian limestones, quartzites, volcanics and volcaniclastics, named the Owir Series, in part correlable with the Lun Shales. Along the Arkari valley, in the westernmost part of the study area, Leake *et al.* (1989) define the Sewakht Formation north of the Cretaceous Krinji Limestone (Desio 1966). The formation includes greenschists, limestones, dolomitic carbonates and sandstones and may correlate with the western continuation of the Devonian Owir Series. The same authors introduced the term Lutkho Formation for the monotonous greenish phyllites cropping out between the Sewakt Formation and the Tirich Mir pluton. These rocks have been previously related by Pudsey *et al.* (1985) to the Lun Shales. The same authors have recognized two main deformational events with an increase of deformation and metamorphic grade toward the Tirich Mir pluton.

East of the Shah Jinali Pass the hanging wall of the Reshun Fault consists of the Lasht Unit (Gaetani *et al.* 1996), which also includes several thrust sheets with Devonian and Permian rocks (Fig. 3). The Lasht Unit is bounded to the north by the Tash Kupruk (Kafarskyi & Abdullah 1976; Gaetani *et al.* 1996) between the top of the Rich Gol and the Yarkhun valley. The unit includes Late Devonian to Early Carboniferous yellowish dolostones and basaltic volcanics, which form a continuous belt extending into Afghanistan north of Kan Khun and the Baroghil Pass. The unit suffered polyphase deformation, accompanied by a low greenschist facies metamorphism. The Tash Kupruk Unit, which generally trends E–W (Fig. 4a) from the Yarkhun valley to the Shah Jinali Pass, has been rotated to a NE–SW direction along the mountain divide between the Shah Jinali valley and the Siru Gol, where it is tectonically eliminated east of Morich (Fig. 3). NE–SW left-lateral strike-slip faults occur along its eastern boundary (Fig. 4b).

The Shah Jinali Phyllites include a monotonous succession of greenschist facies quartzite-bearing metapelites cropping out north of the Tash Kupruk Unit. The unit includes garnet–chlorite and chloritoid–chlorite phyllites with muscovite and quartz. At least two deformational events are recognizable in the unit. A previous foliation, defined by muscovite, chlorite and quartz layers with garnet and chloritoid porphyroblasts, has been successively deformed by kink bands and tight folds with NE–SW trending subhorizontal axes (Fig. 4c). A vertical crenulation cleavage defined by stilpnomelane needles, associated with rotation and boudinage of chloritoid and retrogression of garnet, is characteristic of this event. Small sinistral strike-slip faults with chlorite fibres cutting the crenulation cleavage occur in the upper part of the Shah Jinali valley around Shah Gharil (Fig. 4d). The Shah Jinali Phyllites may correlate with the Lun Shales and/or Lutkho Fm. of the western part of the area.

East Hindu Kush block

The East Hindu Kush block is the western continuation of the Wakhan block (Figs 1, 2). The Palaeozoic and Triassic successions of the East Hindu Kush and the Wakhan may represent an area of extended crust, separating the

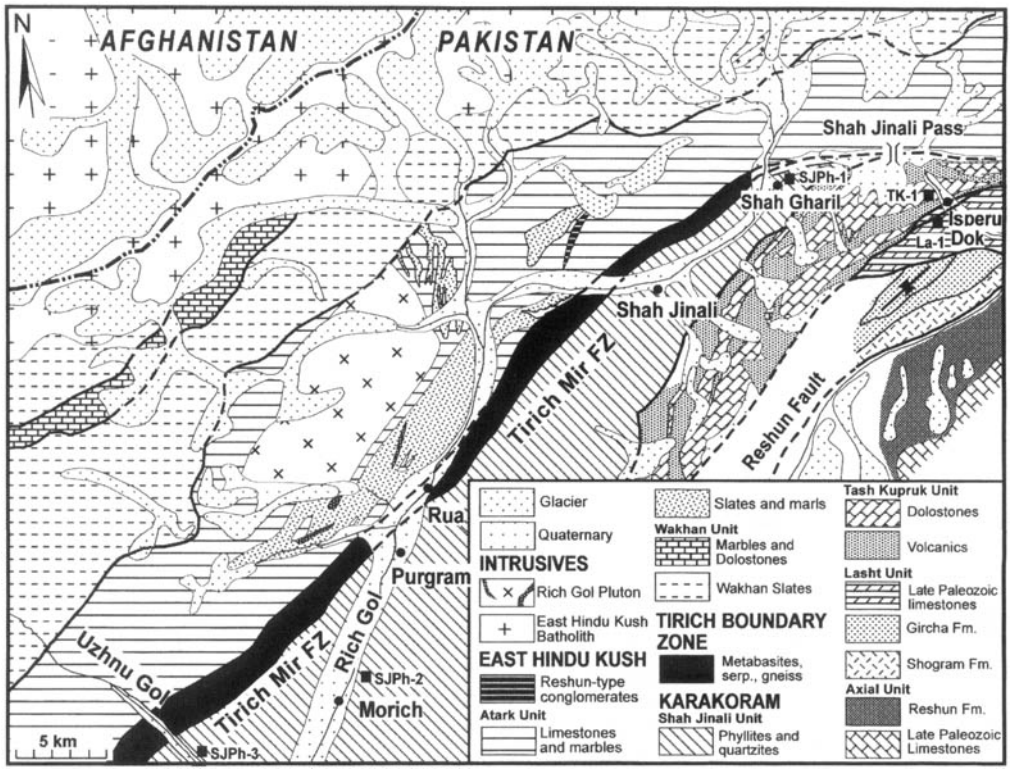

Fig. 3. Geological map of the upper Rich Gol (modified from Zanchi *et al.* 1997).

Karakoram from the South Pamir (Gaetani 1997).

The oldest rocks include deformed granitoids, possibly Cambrian in age (Debon *et al.* 1987*b*), the Qal'a-e Ust Gneiss (Buchroithner 1980), which are always in tectonic contact with the Palaeozoic–Mesozoic metasedimentary successions. Most of the belt consists of the Palaeozoic Wakhan Slates, which record accumulation of thick terrigenous sediments coming from the Gondwana supercontinent in rapidly subsiding rift basins (Gaetani 1997). In Chitral the very thick and monotonous succession delivered only bryozoans and brachiopods of Palaeozoic affinity (Gaetani & Leven 1993), although Triassic conodonts may occur at the top of the unit in Afghanistan (Kafarsky & Abdullah 1976; Buchroithner 1980). Large tectonic slices of carbonate with Late Palaeozoic fusulinids occur close to the Afghan border in the upper Khan Kun Gol within the Wakhan Slates, forming a widespread thrust sheet extending to the north of the Baroghil Pass.

A Permo-Triassic shallow water carbonatic terrigenous succession, the Atark Unit, possibly deposited on the rift shoulders (Gaetani & Leven 1993), occurs between the TBZ and the Wakhan Slates. The unit records the evolution from a continental/marine terrigenous plain to a carbonate ramp with fusulinids in the Early Permian, followed by a wide carbonate platform in the Upper Triassic. In the upper part of the Atark valley from the intrusive contact with the Tirich Mir pluton down to the village of Shagrom, we observed very low grade metabasites, mainly including lava flows interbedded within the terrigenous successions of the unit; this layer is *c.* 100–150 m thick. The Atark Unit is locally sealed with a conglomerate similar to the unconformable Cretaceous conglomerates of the Karakoram (Zanchi *et al.* 1997).

Important tectonic repetitions due to thrust stacking and superposed folds can be observed everywhere in the Atark Unit. Large NNE–SSW to NE–SW trending recumbent folds often related to SE-vergent thrusts and reverse faults suggest dramatic shortening of the unit. Overprinting relationships suggest the presence of earlier folds. Concentric folds deforming the thrust plane stacking the Wakhan Slates above the Atark Unit are also evident along the northern flank of the Tirich Gol. The Atark

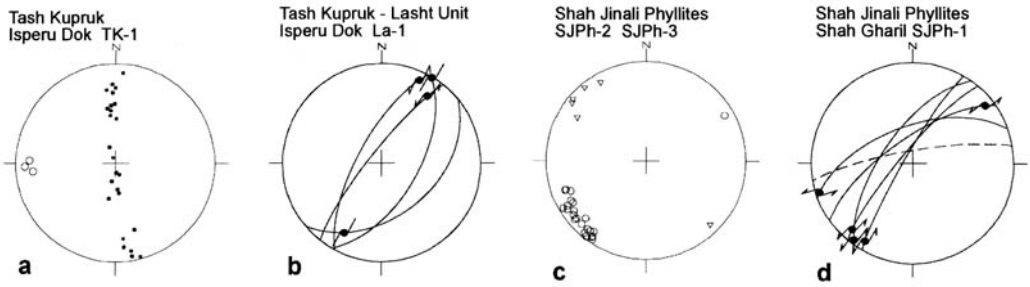

Fig. 4. Mesoscopic structures measured around the Shah Jinali Pass and in the Rich and Uzhnu Gol valleys; Schmidt's projection of lower hemisphere. Faults are shown as thin lines, slickenside lineations as dots with arrows indicating the sense of motion, fold axes as circles, poles to crenulation cleavage as triangles, poles to bedding as black dots; hatched line is cleavage. Location of sites is in Fig. 3. (**a**) F1 (?) folds in bedded limestones of the Tash Kupruk unit; (**b**) large left-lateral strike-slip faults measured in massive limestones (Permian ?) of the Lasht Unit close to the tectonic contact with the Tash Kupruk Unit; (**c**) fold axes and crenulation cleavage in the Shah Jinali Phyllites; (**d**) small strike-slip faults in the Shah Jinali Phyllites at Shah Gharil close to the TBZ.

Unit is still present in the Arkari Gol close to the Tirich Mir pluton, where bioclastic limestones with strongly recrystallized fusulinids have been recognized at the top of the Dir Gol within a steeply dipping succession of very low-grade metapelites very similar to the Wakhan Slates. In this area the Wakhan Slates pass into a composite metamorphic succession reaching medium-grade conditions, named the Arkari Formation by Leake *et al.* (1989). The formation includes mica schists, phyllites, marbles, quartzites and feldspathic gneisses, which may derive from the Palaeozoic Wakhan Slates. A few Belemnite remains found 75 years ago near Besti (Tipper *in* Pascoe 1924) may suggest a Mesozoic age for at least part of the protolith of the metamorphic complex.

Two main deformational events have been recognized within this unit in the Garham Chasma area (Leake *et al.* 1989). A more detailed map and structural analysis is presented by Hildebrand *et al.* (2000) in the same area. The last important metamorphic event seems to have been coeval with the emplacement of leucogranites in the area, occurring during the Miocene (Hildebrand *et al.* 1998).

East Hindu Kush plutonic belt

Jurassic to mid-Cretaceous granitoids intrude the East Hindu Kush units (Debon *et al.* 1987*b*; Gaetani *et al.* 1996). The Shushar pluton, cropping out just north of the studied area between Lasht and Khan Khun along the eastern flank of the Yarkhun valley, has a K–Ar age of 144 Ma (Gaetani *et al.* 1996). An undeformed granodioritic pluton intruded into the Atark Unit occurs in the Rich Gol, north of Rua.

The Tirich Mir pluton, possibly related to the SW continuation of this belt, consists of porphyritic granites with a biotite Rb–Sr age of 115 ± 4 Ma (Desio *et al.* 1964). The pluton intruded both the East Hindu Kush and Karakoram belts, as well as the TBZ. Stoping, moderate effects on host rocks and absence of internal–external foliation indicate a shallow level of emplacement. Spectacular intrusive relationships and dyke swarms occur all around the Tirich Mir pluton except along its southern margin, where the granite is partially deformed showing augen textures and mylonitic shear zones (Momi gneiss in Buchroithner & Gamerith 1986). Here the pluton has been thrust above the Karakoram metasediments of the Lutkho Formation (Fig. 2). Kinematic indicators along a steep NE–SW discontinuous mylonitic foliation observed in the Arkari valley around the village of Momi (Fig. 5) and along the Lutkho valley close to the western tip of the pluton suggest a right-handed shearing of the southern margin of the pluton (Fig. 6a). Metamorphic conditions along the shear zone increase westward toward the Gharam Chasma area. In the Arkari valley the contact between the pluton and the Tirich Boundary Zone is represented by a left-lateral extensional shear zone developed in greenschist facies conditions. Recent plutonic activity in the area is recorded by the emplacement of the two-mica Gharam Chasma pluton SW of the Tirich Mir during the Miocene (Hildebrand *et al.* 1998, this volume), which was also accompanied by medium-grade metamorphism.

The Tirich Boundary Zone (TBZ)

During two field expeditions in 1996 and 1997, we found a narrow belt of amphibolites,

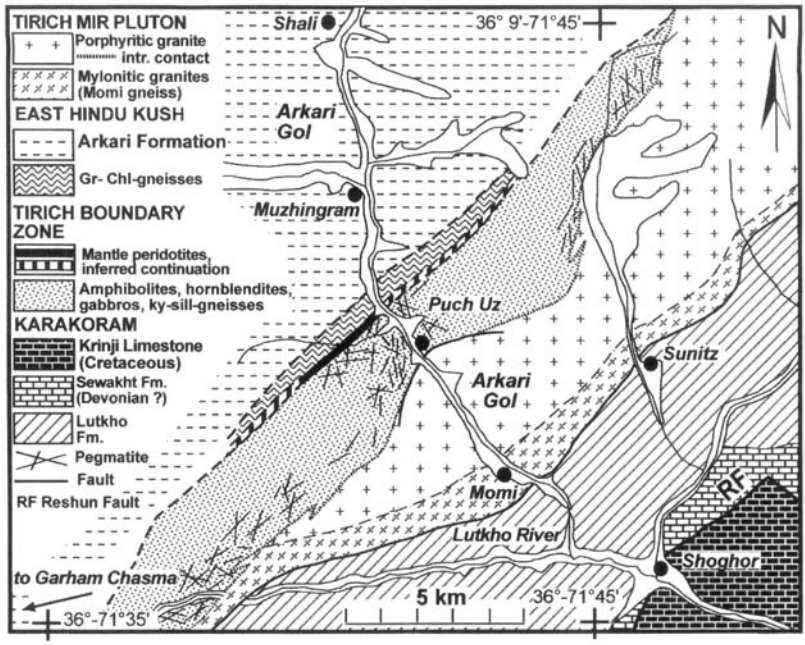

Fig. 5. Simplified geological map of the lower Arkari Gol.

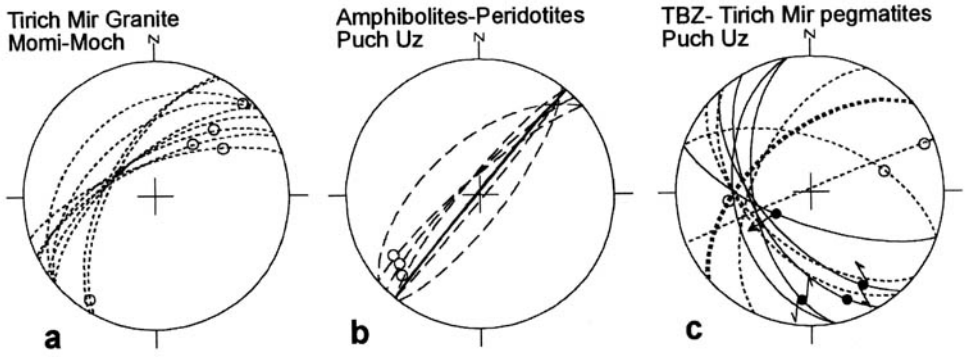

Fig. 6. Structural observations in the Arkari Gol. Thin hatched lines show mylonitic foliation; mineralogical lineation is shown as dots. (**a**) Mylonitic foliations and small faults observed along the southern border of the Tirich Mir pluton at Momi in the Arkari valley and in the Lutkho valley in front of Moch; (**b**) foliations and lineations within the amphibolites of the TBZ in front of Puch Uz; the thick line is the contact between serpentinites and amphibolites; (**c**) extensional shear zones and normal faults crossing the pegmatite dyke swarms around Puch Uz; the thick dashed line is the contact between the TBZ and the Tirich Mir pluton.

metagabbros, peridotites, gneisses and quartzites, named the Tirich Boundary Zone (TBZ), extending from the Shah Jinali Pass to the Barum valley across the Tirich Gol (Fig. 2). The easternmost part of this belt, described as the Rich Gol Metamorphic Complex (Zanchi *et al.* 1997), is now included within the TBZ. East of the Shah Jinali Pass, the TBZ and the Shah Jinali Phyllites end, and the Atark and the Tash Kupruk units are in direct tectonic contact along the Tirich Mir Fault (Fig. 3). The fault extends northward along the western flank of the Yarkhun valley, merging into a complex system of NE–SW trending sinistral strike-slip faults and south-vergent thrusts forming the northwestern boundary of the Karakoram. West of the Tirich Mir pluton, the same rocks occur in the Sunitz, Arkari and Lutkho valleys. From the Lutkho valley (Fig. 5) the belt may extend westward into the poorly known mountains of Nuristan, Afghanistan.

The occurrence of these rocks was briefly mentioned by Calkins *et al.* (1981), Buchroithner & Gamerith (1986) and by Leake *et al.* (1989), who observed amphibolites, metagabbros, hornblendites and serpentinites in the Arkari valley. They also suggested a possible extent of this belt east of the Tirich Mir, where they mapped discontinuous lenses of amphibolites and ultramafic rocks near the mouth of the Tirich Gol and between the Uzhnu Gol and the Shah Jinali Pass (Buchroithner & Gamerith 1978; Gamerith 1982).

Some of the most important outcrops of the TBZ occur between the upper part of the Barum and Tirich Gol valleys (Fig. 7). Due to its remoteness, we were unable to explore the region between the Lun Gol, a tributary valley at the mouth of the Tirich Gol and the Uzhnu Gol. The continuity of the TBZ is inferred on the basis of long-distance observations.

Mantle peridotites and serpentinites

Field relationships. The TBZ unit forms a rather continuous belt for more than 150 km, with the peridotites and serpentinites occurring as isolated bodies tectonically emplaced along the northern margin of the TBZ. Peridotites have been preserved especially in the area close to the rigid mass of the Tirich Mir pluton which, at least in part, preserved the complex from subsequent deformation. The thickness of the ultramafic lenses is limited to a few hundred metres in the Arkari Gol near Puch-Uz (Fig. 5) and in the Barum valley (Fig. 7). In the lower part of the Tirich Gol they are represented only by a few metres of strongly sheared serpentinites cropping out above the village of Mirgash (Fig. 2). Serpentinites have been found in loose blocks at the base of an inaccessible rock wall a few kilometres north of Rua (Fig. 3).

In the Arkari Gol we have observed one of the most important contacts along the eastern flank of the valley in front of Puch Uz. The peridotites are faulted against garnet–chlorite schists of the Arkari Formation to the north; the sharp vertical NE–SW fault separating the two units has been successively affected by metamorphism, indicated by overgrowth of post-kinematic biotite, chlorite and tourmaline. To the south, the ultramafic rocks are faulted against strongly lineated amphibolites (Fig. 6b). The Tirich Mir pluton and swarms of large pegmatite dykes, possibly associated with the intrusion, cross the contact. Extensional shear zones locally cross the contact as well as the pegmatites (Fig. 6c). In the Arkari valley, dykes always end at the northern boundary of the TBZ against the fault, which separates the complex from the metapelites of East Hindu Kush. Faulted serpentinites, characterized by long antigorite fibres indicating left-lateral strike-slip motions, occur along the tectonic boundary between the ultramafic rocks and the metapelites of the Atark Unit at the top of the Tirich Gol and in the Barum valley (Fig. 8a, b and d). Intense

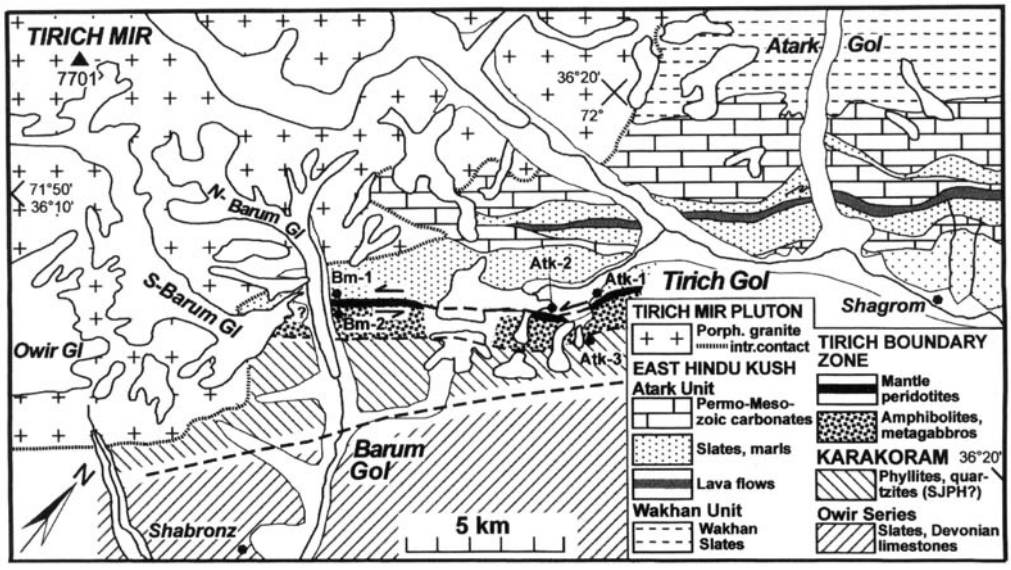

Fig. 7. Simplified geological map of the Tirich Gol and Barum valley.

metasomatic phenomena in ultramafic rocks, leading to ophicarbonates and talc-siderite schists occur close to the northern tectonic contact. The peridotites are also faulted against deformed metagabbros, which display a wide range of mylonitic shear zones (Fig. 8e). The serpentinites found above Mirgash (Fig. 2) form small isolated lenses cropping out within mylonitic quartzites and metapelites, here associated with the TBZ. Strong tectonic disturbances, related to thrusting and strike-slip faulting along the TMF at the base of the Atark Unit, characterize this sector of the Tirich Gol.

Petrology. Well-preserved lherzolites and harzburgites (olivine, orthopyroxene, clinopyroxene and spinel) have been found in the Tirich Gol, in the Barum valley and in the Arkari Gol, whereas schistose serpentinites with olivine and clinopyroxene relicts predominate in the Rich Gol. The modal amount of clinopyroxene is always low, commonly between 3% and 8% (Table 1) and spinel is rarely preserved. Microstructural analysis strongly supports a mantle origin for the TBZ peridotites (Mercier & Nicolas 1975; Boudier & Nicolas 1995): both mylonitic and tectonitic peridotites (Hoogerduijn *et al.* 1993) have been recognized. Tectonites, found in the upper Tirich Gol (Fig. 7), display olivine porphyroclasts, both with undulatory extinction induced by deformation and with tabular shape (Fig. 9a, b), associated with holly-leaf shaped red-brown spinel (Fig. 9c) and pyroxene porphyroclasts. Mylonitic textures, found in the Arkari Gol (Fig. 5), show coarse-grained elongated porphyroclasts of olivine and pyroxene in a fine-grained matrix of recrystallized olivine (OLII). Spinel is not preserved here and chlorite + magnetite pseudomorphs have developed. Talc + antigorite overgrowths on orthopyroxene, antigorite veinlets and diopside indicate a partial greenschist facies recrystallization.

Representative whole-rock analyses (Table 1) show relatively low loss on ignition (LOI) contents, confirming good preservation of primary high-temperature assemblages. High MgO contents, coupled to low CaO, Al_2O_3, Na_2O and TiO_2 concentrations (Fig. 10) indicate a depleted signature for the TBZ peridotites. Major element contents for the TBZ peridotites closely approach the residue of mantle melting, as

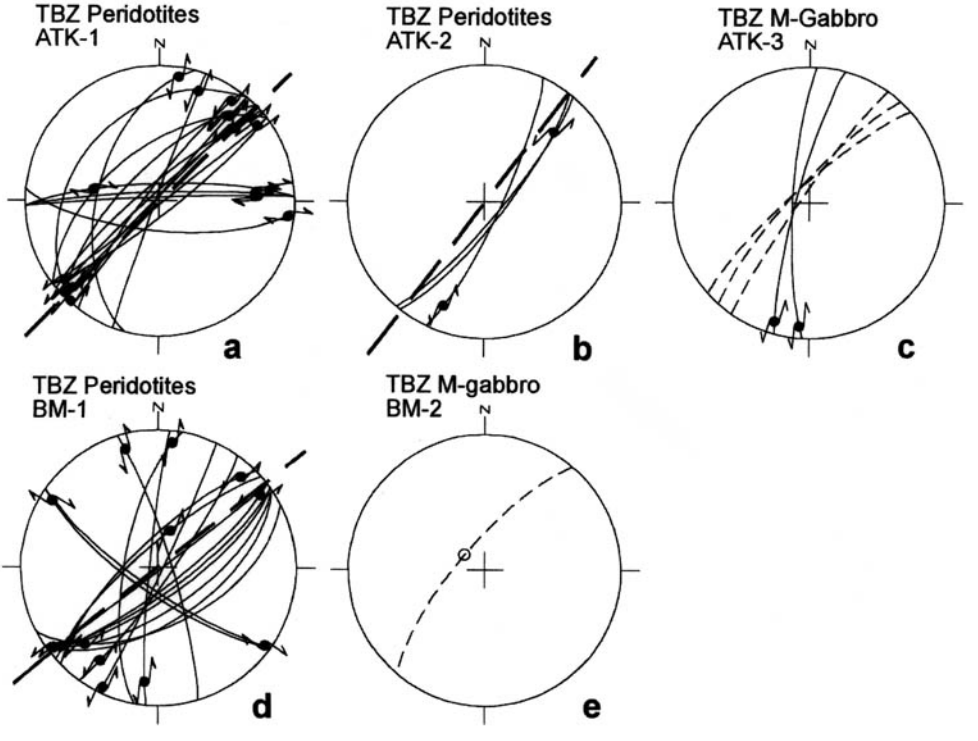

Fig. 8. Structural observations in the upper Tirich Gol and Barum valleys along the Tirich Mir Fault Zone. Thick hatched lines show the trend of the main fault zone. Location of sites is in Fig. 7.

Table 1. *Whole-rock analyses and modal abundance of TBZ peridotites*

	p73	p74
SiO_2	41.17	41.87
Al_2O_3	0.68	1.95
Fe_2O_3	8.79	8.75
MnO	0.11	0.12
MgO	46.68	42.34
CaO	0.86	1.96
Na_2O	0.06	0.04
K_2O	0.01	0.02
TiO_2	0.05	0.05
P_2O_5	0.01	0.01
H_2O^+	1.31	3.07
Total	99.73	100.18
Olivine	87.2	74.4
Orthopyroxene	8.5	14.8
Clinopyroxene	3.3	8.1
Spinel	1.0	2.7

computed by Niu (1997), and plot within the differentiation trend of abyssal peridotites. The depleted character is further confirmed by the mineral chemistry (Table 2). Relatively high X_{Mg} of olivine ($X_{Mg} = 0.895$–0.920, $X_{Mg} = Mg/(Mg + Fe^{2+})$) are consistent with high Mg and Cr contents of clinopyroxene ($X_{Mg} = 0.91$–0.92; $Cr = 0.035$–0.045 apfu) and, conversely, with low Al and Ti concentrations (Fig. 11). The composition of spinel (Fig. 12) is characterized by $Al_2O_3 = 24$–30 wt% and $X_{Cr} = 0.463$, where $X_{Cr} = Cr/(Cr + Al)$. Again, these values fall within the range of compositions from depleted peridotites of ophiolitic terrains and of abyssal peridotites. Low Ti contents in spinel (Table 2) further support an origin from the mantle rather than from an igneous cumulate, where the ulvöspinel component is usually much higher. Temperatures of equilibration ranging from 1000 °C to 1100 °C (at a pressure in the order of *c.* 10 kbar) have been obtained from two-pyroxene thermometry, single orthopyroxene thermometry, and alumina net-transfer thermometry (Carroll Webb & Wood 1986; Brey & Koehler 1990).

Igneous complex and its derivatives

The igneous complex is always faulted against the ultramafic series. It includes a whole range of rocks from hornblende gabbros, hornblendites, to quartz–diorites. The complex suffered an amphibolite to greenschist facies re-equilibration, as observed in the adjoining metamorphic complex, at a variable degree of deformation, leading

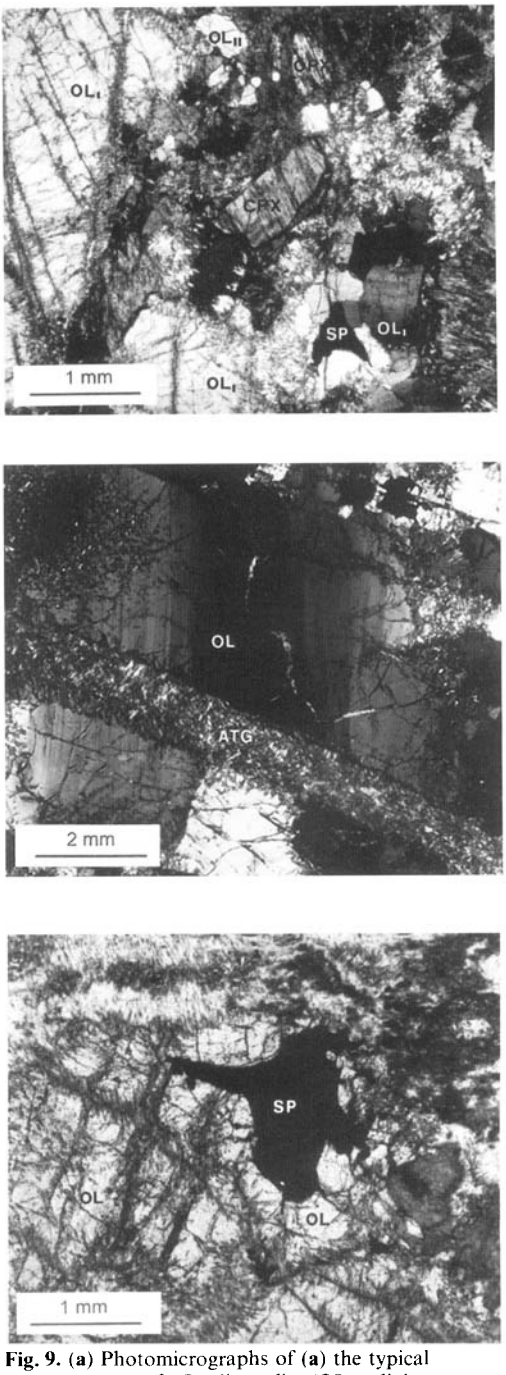

Fig. 9. (**a**) Photomicrographs of (**a**) the typical microstructure of TBZ lherzolite (OL_I, olivine porphyroclasts; OL_{II}, recrystallized olivine; CPX, clinopyroxene; SP, spinel); (**b**) microstructure of TBZ peridotites showing olivine porphyroclasts both with undulatory and tabular extinction (ATG, antigorite); (**c**) microstructure of TBZ peridotites with holly-leaf spinel; see text for further comments.

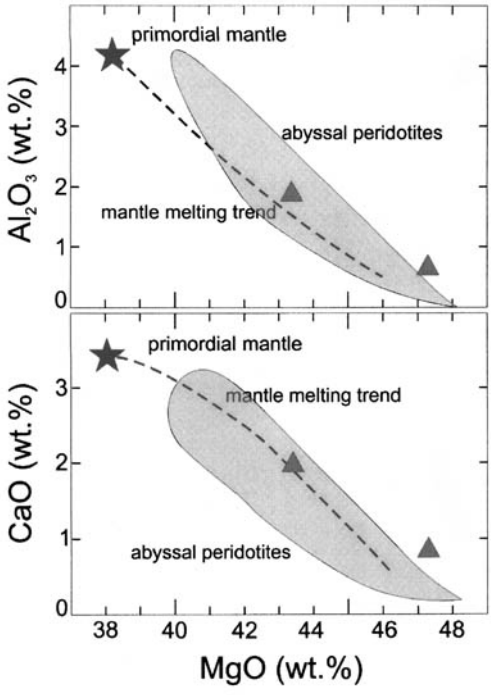

Fig. 10. Whole-rock abundance of CaO and Al_2O_3 v. MgO (all data on anhydrous basis in wt%). The star represents the primordial mantle estimate and the dashed line is the trend of mantle residues after batch partial melting and the shaded field stands for the compositions of abyssal peridotites (Niu 1997).

to flaser gabbros, and to deeply foliated and lineated amphibolites followed by intrusion of garnet-bearing pegmatites possibly associated with the Tirich Mir pluton. Undeformed gabbros and diorites crop out in the upper Tirich Gol and Barum valley (Fig. 7) to the south of the ultramafic bodies. In the upper Tirich Gol they are directly in tectonic contact with the low-grade metapelites of the Karakoram (Fig. 8c). Magmatic texture is still preserved, showing subhedral zoned polysynthetic plagioclase (An 58%), interstitial quartz, magmatic biotite and relicts of clinopyroxene and orthopyroxene with secondary amphibole rim. Ti-rich hornblende cumulates (2.3–5.0 wt% TiO_2) were also found.

Large pods of hornblende cumulates have been recognized in the Arkari Gol at Puch Uz (Fig. 5), within flaser gabbros, and foliated to lineated amphibolites (Figs 6b and 8e). The ubiquitous relict igneous assemblage is represented by the assemblage: amphibole + clinopyroxene + plagioclase + biotite + quartz. The textures of the hornblendites range from adcumulates to orthocumulates of pargasitic hornblende in a plagioclase intercumulus. Metagabbros and amphibolites show variable textures, ranging from coarse-grained pyroxene–amphibolites with symplectites of pyroxene and amphibole, to fine-grained amphibolites mainly consisting of hornblende, plagioclase and quartz which show a variable extent of foliation and greenschist-facies retrogression, indicated by tremolite/actinolite, chlorite and epidote aggregates.

Metamorphic complex

Metamorphic rocks occurring within the TBZ show variable facies assemblages. We also include in this unit mafic schists, which are not clearly related to igneous bodies. Metamorphic rocks south of the ultramafic–mafic complex mainly consist of amphibolites and quartzites, with subordinate gneisses and mica schists. In the Arkari Gol, undeformed garnet pegmatites from the Tirich Mir granite pluton cross-cut the igneous and metamorphic associations. In contrast, in the Lutkho valley the whole metamorphic complex, as well as the pegmatite swarms, have been subsequently refolded. Amphibolites mostly show a granoblastic texture composed of subhedral amphibole, plagioclase and quartz, with interstitial magnetite and titanite and minor greenschist-facies re-equilibration. Mafic rocks with peculiar zoning of amphibole up to 'blue-green' amphibole, possibly of barroisitic composition, have been sampled in the Rich Gol area. Sillimanite gneisses occur in the Lutkho valley. They are composed of garnet, biotite, fibrolitic sillimanite grown on muscovite relicts, zoned plagioclase, muscovite, quartz and accessory tourmaline. In the Shah Jinali Gol, in front of the summer settlement of Shah Jinali (Fig. 3), the occurrence of microscopic segregations of perthitic K-feldspar and the development of both fibrolitic and prismatic sillimanite on relicts of red-brown biotite indicate higher temperature and possibly attainment of partial melting. Kyanite gneisses crop out in the Sunitz valley. They consist of coarse-grained kyanite, biotite, muscovite, plagioclase and accessory tourmaline. They are associated with fine-grained amphibolites, which mainly differ from those previously described by the occurrence of epidote in layers.

Higher temperatures in the crustal sequence are currently constrained by the breakdown of biotite to K-feldspar + sillimanite + garnet (± liquid) in metapelites, i.e. *c.* 800–900 °C (Vielzeuf & Montel 1994). The occurrence of

Table 2. *Crystal chemistry of lherzolites and harzburgites from the Tirich Gol*

	Olivine			Clinopyroxene			Spinel	
	P73	P74	Orthopyroxene	P73	P74	P46	P73	P52
SiO_2	40.73	41.84	57.48	52.42	52.44	52.51	0.01	0.00
TiO_2	0.00	0.00	0.14	0.30	0.19	0.56	0.26	0.04
Al_2O_3	0.00	0.00	2.62	3.75	3.75	4.28	29.59	24.94
Cr_2O_3	0.00	0.02	0.00	1.42	1.26	1.57	38.01	45.04
Fe_2O_3	0.00	0.00	0.00	0.00	0.00	0.00	2.85	0.72
FeO	7.80	8.89	5.48	2.43	2.53	2.70	14.03	15.02
MnO	0.13	0.13	0.26	0.14	0.09	0.07	0.25	0.22
NiO	0.37	0.35	0.00	0.01	0.02	0.04	0.17	0.02
MgO	50.55	50.00	32.97	16.81	17.01	16.83	14.67	13.44
CaO	0.08	0.05	1.42	21.01	22.46	22.40	0.00	0.03
Na_2O	0.00	0.00	0.00	0.98	0.35	0.63	0.00	0.00
Total	99.66	101.34	100.27	99.28	101.10	101.59	99.84	99.47
Si	0.993	1.009	1.969	1.914	1.904	1.883	0.000	0.000
Ti	0.000	0.000	0.004	0.008	0.005	0.015	0.006	0.001
Al	0.000	0.000	0.106	0.161	0.160	0.181	1.034	0.896
Cr	0.000	0.004	0.000	0.041	0.036	0.044	0.891	1.086
Fe^{3+}	0.000	0.000	0.000	0.000	0.000	0.000	0.063	0.016
Fe^{2+}	0.159	0.179	0.157	0.074	0.077	0.081	0.348	0.383
Mn	0.003	0.027	0.005	0.004	0.003	0.002	0.006	0.006
Ni	0.007	0.068	0.000	0.000	0.000	0.001	0.004	0.001
Mg	1.836	1.800	1.683	0.915	0.920	0.899	0.648	0.611
Ca	0.002	0.001	0.052	0.822	0.874	0.860	0.000	0.001
Na	0.000	0.000	0.000	0.069	0.025	0.044	0.000	0.000
$Mg/(Mg + Fe^{2+})$	0.920	0.909	0.915	0.925	0.923	0.917	0.650	0.615
$Cr/(Cr + Al)$							0.463	0.548

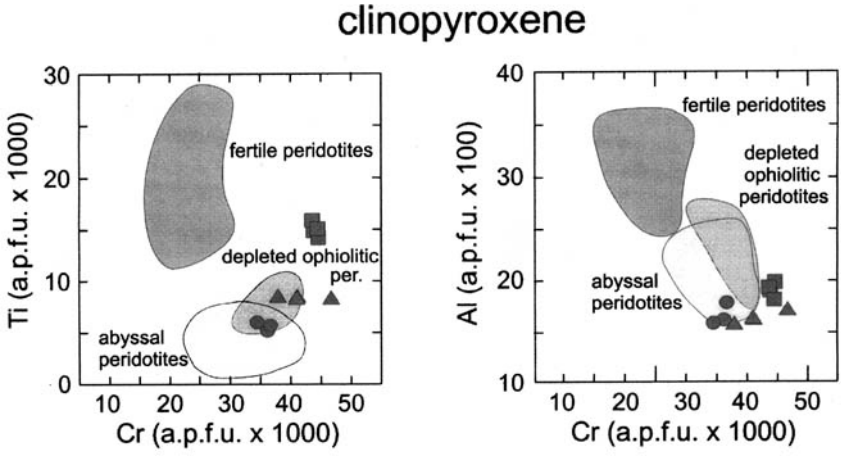

Fig. 11. Variation of Ti and Al v. Cr for clinopyroxenes from the TBZ peridotites. Fields for fertile peridotites, abyssal peridotites and depleted peridotites in ophiolitic terrains are from Rampone *et al.* (1996). Squares, sample P46; circles, P74; triangles, P73.

kyanite and sillimanite schists, as well as epidote-bearing and epidote-free amphibolites records a variable onset of the exhumation of the sequence. North of the mafic–ultramafic complex, and in tectonic contact with it, a slice of garnet–chlorite schists composed of a garnet + chlorite + biotite + muscovite + quartz assemblage crops out in the Arkari Gol (Fig. 5). Pegmatites found here stop at the contact and never cross-cut the garnet–chlorite schists.

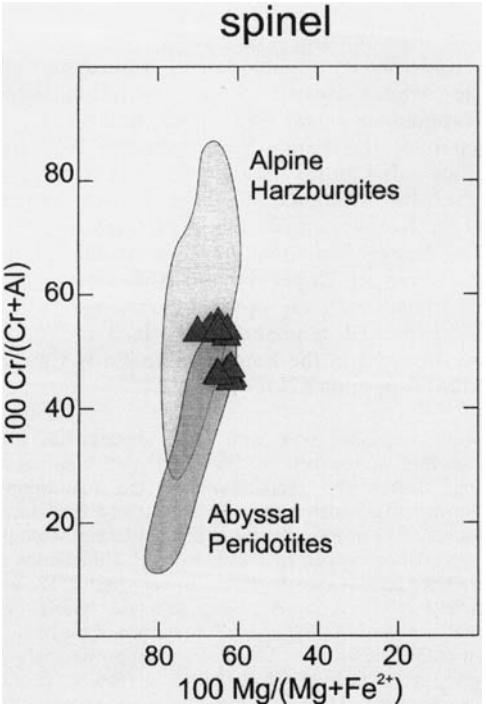

Fig. 12. Cr/(Cr + Al) v. Mg/(Mg + Fe^{2+}) (atoms per 4 oxygens) for spinels from the TBZ peridotites.

Discussion and conclusions

The Tirich Mir Fault Zone

Several hypotheses have been advanced on the location of the boundary between the Karakoram and the East Hindu Kush blocks (Searle 1991; Gaetani & Leven 1993; Gaetani *et al.* 1996; Searle & Khan 1996; Gaetani 1997; Zanchi *et al.* 1997; Hildebrand *et al.* 1998). However, although most of these authors agree to locate the boundary along the Tirich Mir Fault, the region crossed by this fault zone is one of the remotest areas of NW Pakistan, and there is very little information available. The occurrence along the fault of a 150 km long belt of ultramafic rocks of mantle origin, coupled with mafic intrusives and high grade gneisses, suggests that it can be interpreted as a terrane boundary zone (Coney 1989), which defines the NW margin of the Karakoram block. In this sense the term 'Tirich Mir Fault Zone' (TMFZ) seems to be more appropriate for the tectonic contacts bounding the TBZ. The TMFZ is then an important Mesozoic structure, where left-lateral strike-slip faulting represents its most recent brittle reactivation. North of the Shah Jinali Pass, the TBZ has been completely eliminated by south-vergent thrust stacking and left-lateral strike-slip motions related to the post-Cretaceous evolution of the belt. The continuation of the TMFZ can be tentatively traced to the north of the Afghan border along the tectonic contact between the Wakhan Slates and the Karakoram sedimentary units. The fault, after crossing Wakhan, may join the Kilik Fault to the east (Gaetani 1997) in the Hunza valley, separating the Misgar Slates (Zanchi & Gritti 1996), a lateral equivalent of the Wakhan Slates, from the Permo-Mesozoic sediments of the Sost Unit belonging to the Central–Eastern Karakoram.

The mid-Cretaceous Tirich Mir pluton and related pegmatite dyke swarms cross-cut the TBZ, indicating that metamorphism, cooling and imbrication of mafic–ultramafic rocks along with metasedimentary material over very low grade metasediments predates the intrusion, suggesting a pre-mid-Cretaceous docking between the Karakoram and East Hindu Kush. East of Tirich Mir, the TBZ is interrupted against the intrusive boundary of the pluton close to the junction between the North and South Barum glaciers. West of the pluton, the same belt crops out at the top of the Sunitz valley and can be followed up to the Lutkho valley, where it still separates different metapelitic complexes respectively belonging to the Karakoram and East Hindu Kush blocks. Also in this area, the Tirich Mir Fault Zone should then be located along the boundaries of the TBZ.

Accretion of the Karakoram to the Pamir belts

The TBZ indicates a sharp variation in temperature and pressure, with respect to the surrounding units, which never exceeded greenschist facies conditions. Because the geochemically depleted signature of TBZ peridotites cannot be unequivocally ascribed to a specific tectonic setting, other information is needed to unravel the geodynamic meaning of this fossil mantle record. Absence of an ophiolitic sequence *sensu stricto*, relatively low temperatures of equilibration for lherzolites and harzburgites, and close association with a deep crustal sequence might suggest a sub-continental character for the peridotites. Therefore, this belt may have originated from a lower crust–upper mantle sequence, developed either on a passive continental margin or along a zone of attenuated continental crust.

We therefore suggest that the TBZ can fit the evolution of the 'Mega Lhasa superterrane', from its rifting from Gondwana during the Late Palaeozoic to the Mesozoic collisions with the Asian margin (Dercourt *et al.* 1993). As a

consequence of the opening of Neo-Tethys, the terranes that form 'Mega Lhasa' (Karakoram, East Hindu Kush, Helmand, Central and South Pamir) started their movement towards the Asian margin. These blocks collided first with the Iranian Spur in the Late Triassic (Boulin 1988). Most of the docking against Asia occurred in the latest Triassic or Early Jurassic, younging eastwards (Dronov *et al.* 1982; Gaetani 1997). During this accretion, the short-lived oceans or deep-sea ways with thinned crust existing within the blocks of 'Mega Lhasa' closed. Late Triassic intra-'Mega Lhasa' collision is documented in the Alitchur mountains (Pashkov & Budanov 1990) between SE and SW Pamir, which were located just north of the Karakoram and East Hindu Kush (Fig. 1). Emplacement of the ophiolitic Gumbezkol nappe, which includes a gabbro-harzburgite complex, possibly originating from the closure of the Rushan–Pshart Zone between Central and South Pamir, together with flysch deposition in the Alitchur mountains, were related to this event (Shvol'man 1980). The whole South Pamir emerged and was deformed at the end of the Triassic and later transgressed by shallow marine sediments during the Middle Jurassic (Dronov *et al.* 1982). This event is also testified to by the composition of the Liassic orogenic sandstones of the North Karakoram, whose composition points to the erosion of an ophiolite-bearing orogenic complex.

The Tirich Boundary Zone may then represent a remnant of an intra-'Mega Lhasa' orogenic belt related to the Triassic–Early Jurassic convergence and assemblage of the Karakoram against the southern section of the Pamir belts. Even though there is no evidence of an ophiolitic sequence *sensu strictu* in the area, the deposition of the Late Palaeozoic Wakhan Slates suggests the presence of a rifted basin with thinned crust (Gaetani 1997) between the Karakoram and the South Pamir, where the peridotites of the TBZ were originated.

Welding of the southern part of the Pamir belts and the Western Karakoram may have been completed by the Early Jurassic. The first granodioritic stocks were emplaced in the East Hindu Kush at this time, as suggested by the K–Ar age obtained for the Shushar Pluton of the East Hindu Kush Batholith (Gaetani *et al.* 1996). Renewed convergence and crustal shortening during the Neo-Cimmerian event, partly predating the Tirich Mir pluton emplacement, may be responsible for the final fragmentation and emplacement of the belt among the low grade and anchimetamorphic successions of the Karakoram and East Hindu Kush.

A different interpretation of the geodynamic meaning of the TBZ could be suggested considering its possible lateral connection with the Wasser–Panjao Suture in Afghanistan (Tapponnier *et al.* 1981). This suture (Fig. 1) separates the Farah Rud from the Helmand block of Central Afghanistan, a microplate which has strong affinities with the western part of the Karakoram (Boulin 1988, Gaetani 1997). The Wasser–Panjao Suture Zone includes a huge flysch fan of Upper Triassic and Jurassic age associated with an ophiolitic mélange, which represent the remnants of a back-arc basin overthrusted in the Late Jurassic–Early Cretaceous (Tapponnier *et al.* 1981).

Lucia Angiolini was with A.Z. during the first discovery of the belt in 1996 and gave continuous help during the preparation of the manuscript. Constructive criticism from P. Treloar and L. Ratschbacher of a previous version of the manuscript strongly improved our paper; final reviews by P. Hildebrand, J. Shervais and M. Searle were also very useful. We are deeply indebted to A. Gregnanin for whole-rock analyses and to E. Rampone for revision of the section on mantle peridotites. Electronic microprobe analyses were performed at CNR-Centro di Studio per la Geodinamica Alpina e Quaternaria in Milano. We are grateful to the Government of Pakistan and especially to Mr S. Hasan Gahuar, Director General of the Geological Survey of Pakistan for assistance and encouragement. Our Hunza guides Khadir, Fakiri and Fida Jan of Pakistan Adventures are warmly thanked.

References

AUSTROMINERAL 1978. *Mineral exploration and mine development, Chitral District*. Report for Sarhad Development Authority, Peshawar.

BOUDIER, F. & NICOLAS, A. 1995. Nature of the Moho transition zone in the Oman ophiolite. *Journal of Petrology*, **36**, 776–796.

BOULIN, J. 1988. Hercynian and Eocimmerian events in Afghanistan and adjoining regions. *Tectonophysics*, **148**, 253–278.

BREY, G. & KOEHLER, T. 1990. Geothermobarometry in four-phase lherzolites II. New thermobarometers, and practical assessment of existing thermobarometers. *Journal of Petrology*, **31**, 1353–1378.

BUCHROITHNER, M. F. 1980. An outline of the Geology of the Afghan Pamirs. *Tectonophysics*, **62**, 13–35.

—— & GAMERITH, H. 1978. Geological Map of Pamir-e-Wakhan, 1:250.000. *In*: DE GRANCHY, R. S. & KOSTKA, R. (eds) *Enclosure. Graz*. Akad. Druck- und Verlagsanstalt.

—— & —— 1986. On the geology of the Tirich Mir area, Central Hindu Kush (Pakistan). *Jahrbuchtur Geologie B.-A.*, **128**, 367–381.

BURTMAN, V. S. & MOLNAR, P. 1993. *Geological and Geophysical Evidence for Deep Subduction of Continental Crust Beneath the Pamir*. Geological Society of America, Special Paper, **281**.

CALKINS, J. A., JAMILUDDIN, S., BHUYAN, K. & HUSSAIN, A. 1981. *Geology and mineral resources of the Chitral–Partsan area, Hindu Kush Range, Northern Pakistan.* United States Geological Survey Professional Paper, **716-G**.

CARROLL WEBB, S. A. & WOOD, B. J. 1986. Spinel–pyroxene–garnet relationships and their dependence on Cr/Al ratio. *Contributions to Mineralogy Petrology*, **92**, 471–480.

CONEY, P. J. 1989. Structural aspects of suspect terranes and accretionary tectonics in western North America. *Journal of Structural Geology*, **11**, 107–125.

DEBON, F., LE FORT, P., DAUTEL, D., SONET, J. & ZIMMERMANN, J. L. 1987*a*. Granites of Western Karakoram and Northern Kohistan (Pakistan): a composite Mid-Cretaceous to Upper Cenozoic magmatism. *Lithos*, **20**, 19–40.

——, AFZALI, H., LE FORT, P. & SONET, J. 1987*b*. Major intrusive stages in Afghanistan: typology, age and geodynamic setting. *Geologische Rundschau*, **76**, 245–264.

DERCOURT, J., RICOU, L. E. & VRIELINK, B. 1993. *Atlas Tethys Palaeoenvironmental Maps.* Explanatory notes: Ed. BEICIP, Paris.

DESIO, A. 1963. Review of the geological 'formations' of the western Karakoram (central Asia). *Rivista Italiana di Paleontologia e Stratigrafia*, **69**, 475–501.

—— 1966. The Devonian sequence in Mastuj valley (Chitral, N.W. Pakistan). *Rivista Italiana di Paleontologia e Stratigrafia*, **72**, 293–320.

——, TONGIORGI, E. & FERRARA, G. 1964. *On the Geological Age of Some Granites of the Karakorum, Hindu Kush and Badakhshan (Central Asia).* Proceedings of 22nd International Geological Congress, Delhi, 479–496.

DRONOV, V. I., GAZDZICKI, A. & MELNIKOVA, G. K. 1982. Die Triadische Riffe in südöstlicher Pamir. *Facies*, **6**, 107–128.

GAETANI, M. 1997. The Karakorum Block in Central Asia, from Ordovician to Cretaceous. *Sedimentary Geology*, **109**, 339–359.

—— & LEVEN, H. 1993. Permian stratigraphy and fusulinids from Rosh Gol (Chitral, E Hindu Kush). *Rivista Italiana di Paleontologia e Stratigrafia*, **99**, 307–326.

——, JADOUL, F. & GARZANTI, E. 1993. Jurassic and Cretaceous orogenic events in the N Karakorum: age constraints from sedimentary rocks. *In*: TRELOAR, P. J. & SEARLE, M. P. (eds) *Himalayan Tectonics*. Geological Society, London, Special Publications, **74**, 39–52.

——, LE FORT, P., TANOLI, S., ANGIOLINI, L., NICORA, A., SCHUNNACH, D. & KHAN, A. 1996. Reconnaissance geology in Upper Chitral, Baroghil and Karambar districts (northern Karakorum, Pakistan). *Geologische Rundschau*, **85**, 683–704.

GAMERITH, H. 1982. *Geologische Karte von Gilgit/Chitral/Whakhan (North Pakistan und Ost Afghanistan)* 1.250.000. Private Edition, Graz.

HAYDEN, H. H. 1915. Notes on the Geology of Chitral, Gilgit and the Pamirs. *Records of the Geological Survey of Pakistan*, 8, **2**, 1–28.

HILDEBRAND, P. R., NOBLE, S. R., SEARLE, M. P., PARRISH, R. R. & SHAKIRULLAH, 1998. Tectonic significance of 24 Ma crustal melting in the eastern Hindu Kush, Pakistan. *Geology*, **26**, 871–874.

——, SEARLE, M. P., SHAKIRULLAH, KHAN, Z. & VAN HIEJST, H. J. 2000. Geological evolution of the Hindu Kush, NW Frontier, Pakistan: active margin to continent–continent collision. *This volume.*

HOOGERDUIJN STRATING, E. H., RAMPONE, E., PICCARDO, G. B., DRURY, M. R. & VISSERS, R. L. M. 1993. Subsolidus emplacement of mantle peridotites during incipient oceanic rifting and opening of the Mesozoic Tethys (Voltri Massif, NW Italy). *Journal of Petrology*, **34**, 901–927.

JAN, M. Q. & HOWIE, R. A. 1981. The mineralogy and geochemistry of the metamorphosed basic and ultrabasic rocks of the Jijal complex, NW Pakistan. *Journal of Petrology*, **22**, 85–126.

KAFARSKYI, Kh. A. & ABDULLAH, J. 1976. Tectonics of north-east Afghanistan (Badakhshan, Wakhan, Nurestan) and relationship with the adjacent territories. *Atti Convegni Lincei*, **21**, 87–113.

LEAKE, R. C., FLETCHER, H. W., HASLAM, H. W., KHAN, B. & SHAKIRULLAH, T. 1989. Origin and tectonic setting of stratabound tungsten mineralization within the Hindu Kush of Pakistan. *Journal of the Geological Society, London*, **146**, 1003–1016.

LE FORT, P., TONGIORGI, M. & GAETANI, M. 1994. Discovery of a crystalline basement and Early Ordovician transgression in the Karakorum mountain range, northern Pakistan. *Geology*, **22**, 941–944.

—— & GAETANI, M. 1998. Introduction to the Geological Map of Western Central Karakorum, North Pakistan Hindu Raj, Ghamubar and Darkot Areas 1:250,000 scale. *Geologica* (Geoscience Laboratory Project, Islamabad, Pakistan), **3**, 1–68.

MERCIER, J.-C. C. & NICOLAS, A. 1975. Textures and fabrics of upper-mantle peridotites as illustrated by xenoliths from basalts. *Journal of Petrology*, **16**, 454–487.

NIU, Y. 1997. Mantle melting and melt extraction processes beneath ocean ridges: evidence from abyssal peridotites. *Journal of Petrology*, **38**, 1047–1074.

PASCOE, E. H. 1924. General report of the Geological Survey of India for the year 1923. *India Geological Survey records*, **55** part 1.

PASHKOV, B. R. & BUDANOV, V. I. 1990. The tectonics of the zone of intersection between the Southeastern and Southwestern Pamir (in Russian). *Geotektonika*, **3**, 42–57.

PUDSEY, C. J. 1986. The Shyok Suture, Pakistan: margin of a Cretaceous island arc. *Geological Magazine*, **123**, 405–423.

——, COWARD, M. P., LUFF, I. W., SHACKLETON, B. F., WINDLEY, B. F. & JAN, M. Q. 1985. Collision zone between the Kohistan arc and the Asian plate in NW Pakistan. *Transactions of the Royal Society of Edinburgh*, **76**, 463–479.

RAMPONE, E., HOFMANN, A. W., PICCARDO, G. B., VANNUCCI, R., BOTTAZZI, P. & OTTOLINI, L. 1996. Trace element and isotope geochemistry of depleted peridotites from a N-MORB type ophiolite (Internal Liguride, N. Italy). *Contributions to Mineralogy and Petrology*, **123**, 61–76.

SEARLE, M. P. 1991. *Geology and Tectonics of the Karakoram Mountains*. John Wiley and Sons, Chichester.

—— & KHAN, A. (eds) 1996. *Geological map of North Pakistan, 1:650.000*. University Department of Earth Sciences, Oxford.

——, REX, A. J., TIRRUL, R., REX, D. C. & BARNICOAT, A. 1989. Metamorphic, magmatic, and tectonic evolution in the Central Karakoram in the Biafo–Baltoro–Hushe regions of N-Pakistan. *In*: MALINCONICO, L. L. & LILLIE, R. J. (eds) *Tectonics of the Western Himalaya*. Geological Society of America Special Paper, **232**, 47–74.

SHVOL'MAN, V. A. 1980. The Mesozoic ophiolite complex in the Pamir. *Geotectonics*, **14/6**, 465–470.

TAHIRKHELI, R. A. K., MATTAUER, M., PROUST, F. & TAPPONNIER, P. 1979. The India–Eurasia Suture Zone in Northern Pakistan; synthesis and interpretation of recent data at plate scale. *In*: FARAH, A. & DE JONG, K. A. (eds) *Geodynamics of Pakistan*. Geological Survey of Pakistan, Quetta, 125–130.

TALENT, J. A., CONAGHAN, P. J., MAWSON, R., MOLLOY, P. D. & PICKETT, J. W. 1981. Intricacy of tectonics in Chitral (Hindu Kush). Faunal evidence and some regional implications. *Himalayan Seminar (1976), section IIA*. Geological Survey of India, Miscellaneous Publication, **41**, 77–101.

TAPPONNIER, P., MATTAUER, M., PROUST, F. & CASSAIGNEAU, C. 1981. Mesozoic ophiolites, sutures and large-scale tectonic movements in Afghanistan. *Earth and Planetary Science Letters*, **52**, 355–371.

VIELZEUF, D. & MONTEL, J. M. 1994. Partial melting of metagreywackes. Part I. Fluid-absent experiments and phase relationships. *Contributions to Mineralogy and Petrology*, **117**, 375–393.

ZANCHI, A. & GRITTI, D. 1996. Multistage structural evolution of Northern Karakorum (Hunza region, Pakistan). *Tectonophysics*, **260**, 145–165.

——, GAETANI, M. & POLI, S. 1997. The Rich Gol Metamorphic Complex: evidence of separation between Hindu Kush and Karakorum (Pakistan). *Comptes Rendus de l'Academie des Sciences Paris, Sciences de la terre et des planètes*, **325**, 877–882.

New field, structural and geochronological data from the Shyok and Nubra valleys, northern Ladakh: linking Kohistan to Tibet

R. F. WEINBERG[1,2], W. J. DUNLAP[1] & M. WHITEHOUSE[3]

[1]*Research School of Earth Sciences, The Australian National University, ACT 0200, Australia*

[2]*Present address: Department of Earth Sciences, Oxford University, Oxford OX1 3PR, UK*

[3]*Museum of Natural History, Stockholm, Sweden*

Abstract: The Nubra–Shyok confluence in northern Ladakh is a key area for understanding the tectonic evolution of NW Himalaya and provides the basis for linking the geology of Pakistan to that of Tibet. The geology of the confluence area has been the subject of much speculation centred mainly on the existence of ophiolites and their regional significance. These ophiolites are thought to represent the eastward extension of the Shyok Suture Zone (SSZ), which separates the Dras island arc from the southern margin of Eurasia, and which was overprinted by movement along the Khalsar Thrust (often thought to represent the eastern continuation of the Main Karakoram Thrust). The geology of the area is relatively complex and the little information available has hampered regional geological correlations.

The Khalsar Thrust (KT) and the dextral Karakoram Fault (KF), two regional tectonic features of NW Himalaya, merge at the confluence defining a triple point and three blocks: the Ladakh block to the south, the Saltoro block to the northwest, and the Karakoram block to the northeast. Close to the triple point, the KF changes strike and movement direction. Movement vector analysis of the triple point indicates that the KT and the two parts of the KF could have moved contemporaneously, and allows prediction of the movement vectors across the faults. The KT and KF shear preferentially volcano-sedimentary rocks of the Shyok and Nubra formations, respectively. Contrary to previous interpretations, these sheared rocks do not represent disrupted ophiolites. Regional tectonic reconstructions, however, require suturing between the Ladakh block and Eurasia and the strike of the SSZ in Baltistan suggests that the suture zone might crop out north of the KT, either along the southern slopes of the Saltoro Range or further north along the Saltoro valley. In the few outcrops of the Saltoro block we were able to visit, we found no evidence of ophiolitic rocks. Instead we found outcrops of the calc-alkaline Tirit batholith. Although our observations do not confirm the presence of the suture-related rocks in the southern Saltoro block, this possibility cannot be ruled out. Zircons from a sample of Tirit granite (U–Pb ion-microprobe age) yielded an age centred at 68 ± 1 Ma. The similar range of modal composition and age of the Tirit and Ladakh batholiths suggest that they are part of the same magmatic event. This result and a number of other observations indicate that the post-75 Ma geology of the Ladakh and Saltoro blocks is similar. Thus, if there is a suture zone in the southern Saltoro block, suturing must have occurred before 75 Ma, as concluded by others along the same tectonic boundary to the west in Pakistan.

The KF represents a much younger terrane boundary, juxtaposing rocks of the Ladakh and Saltoro blocks to those of the Karakoram terrane. Rocks related to suturing of continents were not found along the KF. Karakoram leucogranites cropping out in the southern part of Karakoram terrane yielded a U–Pb zircon age centred at 15.0 ± 0.4 Ma (2σ). Because these leucogranites were not found south of the KF, this fault must have initiated after leucogranite intrusion and must therefore be younger than 15 Ma old. At the confluence the KF cuts across the regional rock sequence than can be followed from Kohistan into Baltistan and into the confluence area. Movement on the fault displaces the sequence by approximately 150 km to southeastern Tibet where the regional rock sequence can be regained.

Correlating the geology of Northern Pakistan to that of western Tibet has been hampered by a relative lack of information in the intervening area in northern Ladakh (India). Northern Ladakh is particularly important for regional correlation because here the regional rock sequence is cut across and displaced by the right-lateral Karakoram Fault (KF), one of the

From: KHAN, M. A., TRELOAR, P. J., SEARLE, M. P. & JAN, M. Q. (eds) *Tectonics of the Nanga Parbat Syntaxis and the Western Himalaya.* Geological Society, London, Special Publications, **170**, 253–275. 1-86239-061-4/00/$15.00

faults controlling the lateral extrusion of Tibet (e.g. Molnar & Tapponnier 1975). Border conflicts have prevented intensive work in the Nubra–Shyok confluence area (from now on referred to as 'the confluence'), which has remained poorly known. In this area the KF intersects (merges with?) the Khalsar Thrust (KT of Srimal *et al.* 1987), which is presumed to have reworked the older Shyok Suture Zone (SSZ). The SSZ separates the Dras island arc to the south, from the Karakoram terrane to the north (Fig. 1; e.g. Coward *et al.* 1986) and is thought to run parallel to the Shyok River in Ladakh (Srimal 1986*a*, *b*). The KT in Ladakh has often been referred to as the eastern continuation of the Main Karakoram Thrust (MKT). West of

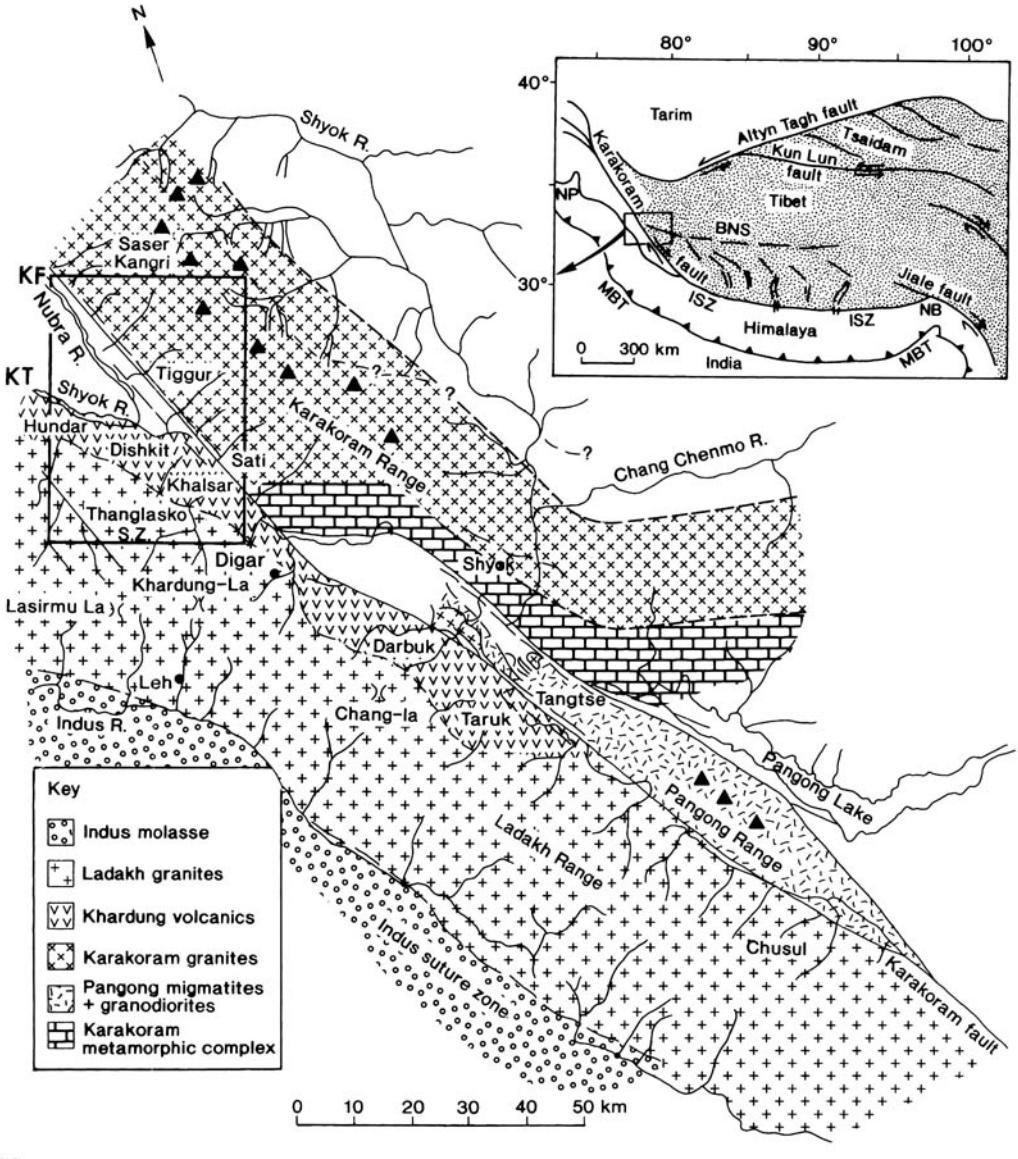

(a)

Fig. 1. (**a**) Regional geological map (after Searle *et al.* 1998). Boxed area marks the Nubra–Shyok confluence area detailed in (b). (**b**) Geological map of the confluence area. Location of samples 711, 021, 95–481 and 95–411 are indicated (95–481 and 95–411 are indicated by numbers 481 and 411, respectively). Inset box shows main tectonic features east and west of the map of the confluence. Legend overleaf.

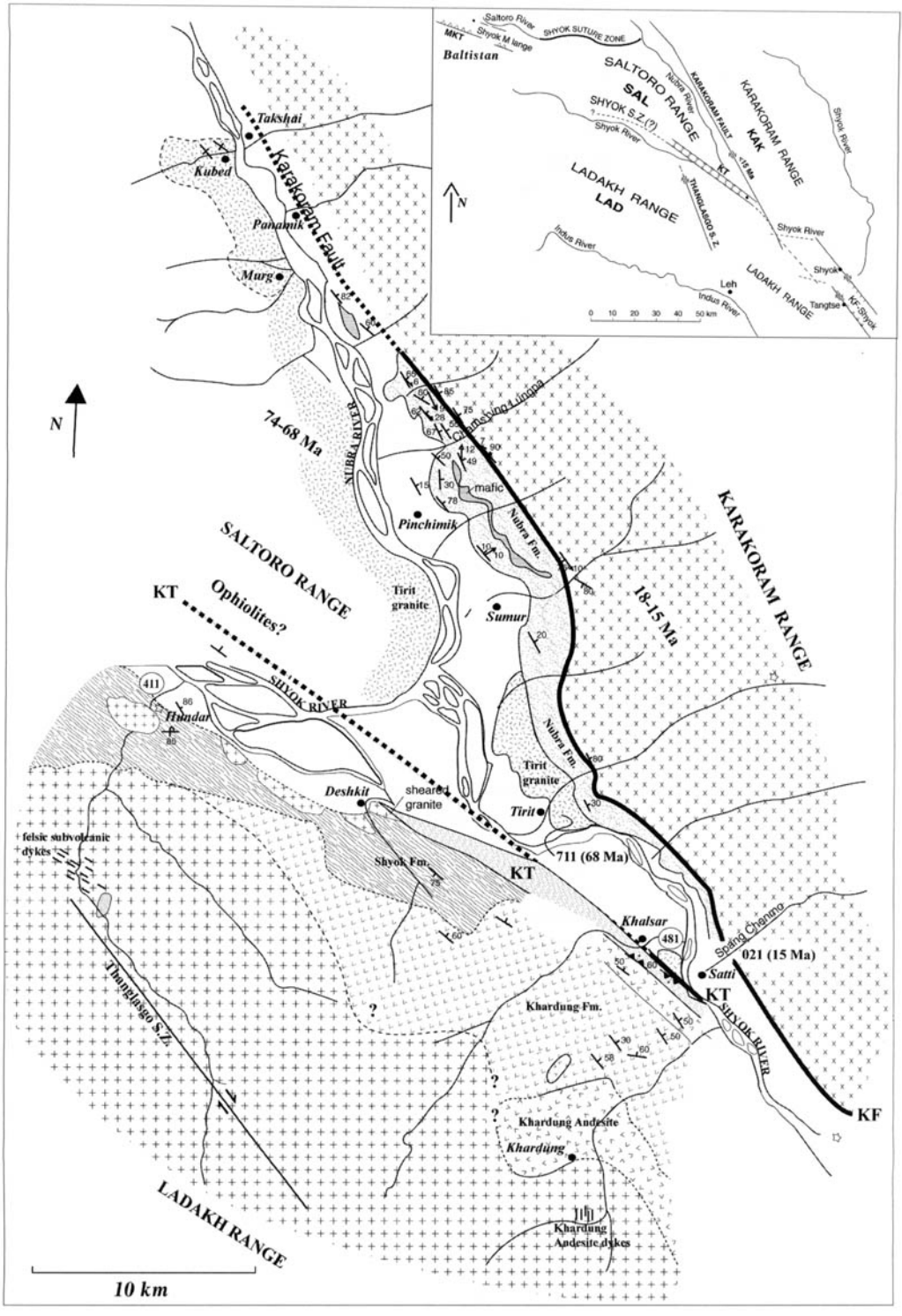
Saltoro River
MKT
Shyok M lange
SHYOK SUTURE ZONE
Baltistan
SALTORO RANGE
SAL
Nubra River
KARAKORAM FAULT
KARAKORAM RANGE
KAK
Shyok River
SHYOK S.Z.(?)
KT
~15 Ma
LADAKH RANGE
LAD
THANGLASGO S.Z.
Indus River
Leh
Tangtse
KF-Shyok
0 10 20 30 40 50 km
N
Takshai
Kubed
Karakoram Fault
Panamik
Murg
74-68 Ma
NUBRA RIVER
Chamshung Lingpa
mafic
Pinchimik
Nubra Fm.
SALTORO RANGE
KT
Ophiolites?
Tirit granite
Sumur
18-15 Ma
KARAKORAM RANGE
411
SHYOK RIVER
Hundar
Deshkit
shear
granite
Tirit
felsic subvolcanic dykes
Shyok Fm.
711 (68 Ma)
KT
Khalsar
481
Spang Chanmo
021 (15 Ma)
Satti
KT
Khardung Fm.
SHYOK RIVER
KF
Khardung Andesite
Khardung
Khardung Andesite dykes
LADAKH RANGE
10 km

(b)

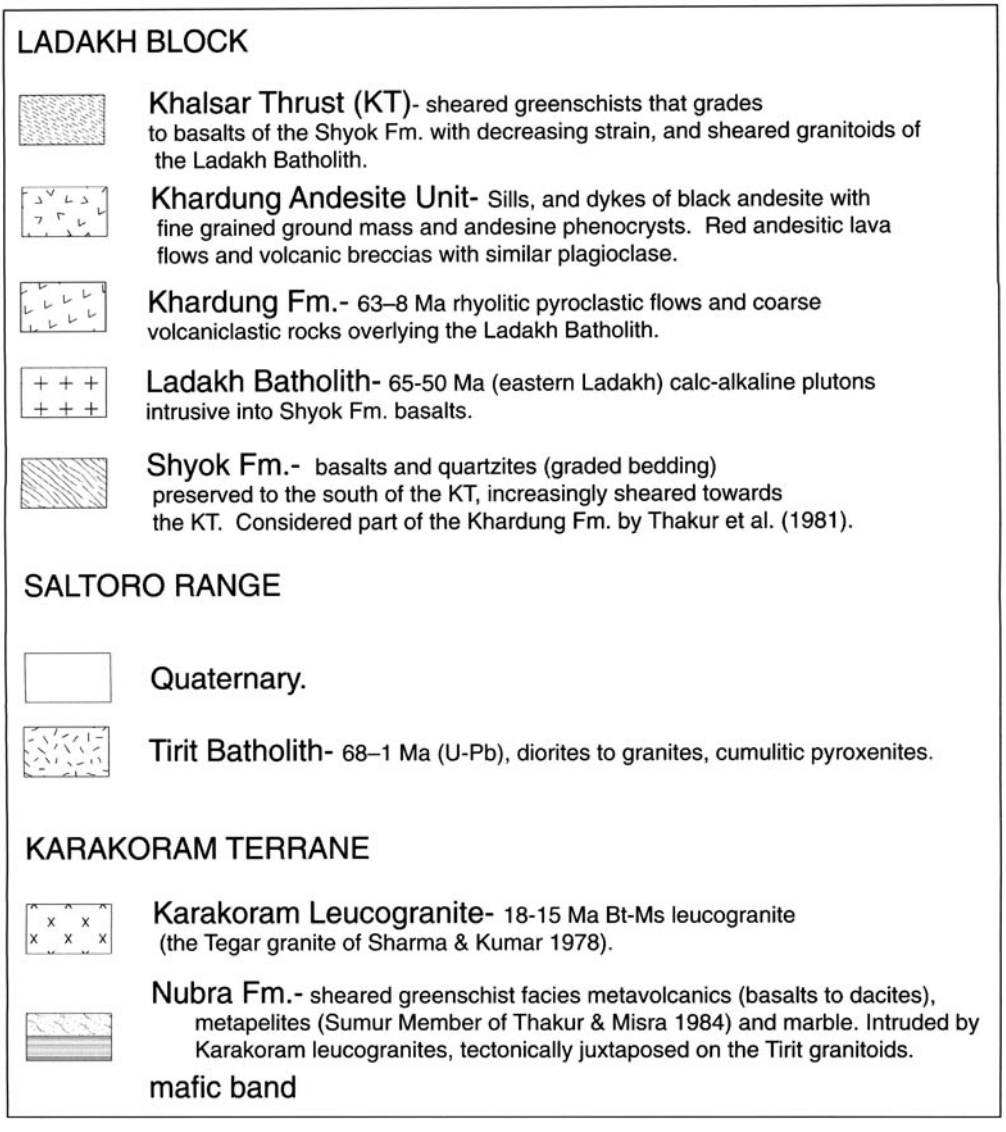

Fig. 1(b) Cont.

Ladakh the MKT reworks the SSZ and follows it along the northern boundary of the Dras island arc, continues west undeflected by the Nanga Parbat–Haramosh spur, and onward to Kohistan where it defines the northern boundary of the Kohistan arc (where it was previously known as the Northern Suture Zone). The Ladakh and Kohistan blocks are bounded to the south by the Indus Suture Zone, and it has been suggested that these two arcs represented a single island arc which collided with the southern margin of Eurasia before India collided with the system (Petterson & Windley 1985; Coward *et al.* 1986; Pudsey 1986; Searle 1991). Despite some doubts raised by Raz & Honegger (1989) on whether the Ladakh batholith developed within a pure island arc (Dras) or a transition between continental and island arc, we prefer the interpretation that Ladakh was an island arc. This is because, unlike the Lhasa block to the east where a Precambrian basement and Mesozoic cover has been found (Allègre *et al.* 1984), no evidence has been found of an older continental basement (see Honegger *et al.* 1982; Weinberg & Dunlap in press and references therein).

Published descriptions and maps of the Nubra–Shyok confluence differ widely and are often contradictory (e.g. Sharma & Kumar 1978; Thakur *et al.* 1981; Rai 1982; Thakur & Misra 1984; Srimal 1986*a*, *b*; Srimal *et al.* 1987). A clear picture of the geological evolution of the confluence has therefore not yet emerged. Despite its obvious importance, the Shyok–Nubra confluence remains relatively poorly known. Several explorers studied the geology of the confluence area and the Pangong lake area late last century and early this century (Hedin 1907; de Terra 1932; Dainelli 1933–1934). After 1939 and later partition between India and Pakistan, very few workers covered this area until the 1970s, when a number of Indian workers started to explore the confluence area. It was only in early 1994 when the Shyok and Nubra valleys were reopened to foreigners. Access remains limited to certain areas along the Nubra and Shyok valleys (excluding the entire Saltoro Range) and to visits not exceeding one week. This work is a result of our observations during six short trips to the area, over three field seasons. We aimed at understanding the relationship between the suture zone and the KT and KF, which merge at the confluence, and to link the geology of the confluence to that of Baltistan (area immediately west of Ladakh in Pakistan); and Kohistan and to that of western Tibet, across the KF. Here, we describe our field observations as well as new U/Pb zircon ages and Ar/Ar cooling ages of key samples. After describing the regional geology we describe our observations on the geology of the confluence in three parts, corresponding to three main geological blocks defined by the KT and KF. We then describe our geochronological results, followed by structural analysis.

Regional geology

The Shyok Suture Zone (SSZ) north of the Ladakh batholith was first described by Gansser (1980) and later by others (Tahirkheli *et al.* 1979; Brookfield & Reynolds 1981; Rai 1982; Thakur & Misra 1984; Srimal 1986*a*, *b*; Hanson 1989; Brookfield & Reynolds 1990; Allen & Chamberlain 1991; Lemennicier *et al.* 1996). Based on the little available information, the main trace of the suture zone has been placed either north of the Saltoro Range along the Saltoro River (Gansser 1980), or more commonly along the Shyok River, south of the Saltoro Range (Fig. 1b insert; e.g. Srimal 1986*a*, *b*). In Kohistan, the SSZ represents the remains of a small back-arc basin that separated the Kohistan–Dras island arc and Asia (Pudsey 1986), which closed in the early late Cretaceous (100–85 Ma e.g. Treloar *et al.* 1989, 1996). Hanson (1989) described in detail the SSZ in the Shigar valley, Baltistan, where it is defined by a simple fault and a few pods of serpentinite of ultramafic origin, separating Paleozoic sedimentary rocks of the Eurasian plate from Cretaceous rocks of the Dras island arc. The presence in Shigar of marine sediments of Cretaceous age suggests a small ocean basin between the two terranes. Brookfield & Reynolds (1990) described in detail the SSZ near the confluence of the Hushe and Saltoro rivers, 100 km west of the Nubra–Shyok confluence area (insert on Fig. 1b). They mapped a tectonic mélange, defining a flower structure, separating Asian rocks from Ladakhi rocks, which may contain ophiolitic units (Coward *et al.* 1986). The geology of the intervening 100 km between the Hushe–Saltoro and the Nubra–Shyok confluences is virtually unknown.

In Baltistan, the Main Karakoram Thrust (MKT) runs approximately N60W along the Shyok valley, and has reworked the SSZ and thrusted Karakoram terrane onto Ladakh terrane (Tahirkheli *et al.* 1979; Coward *et al.* 1986; Searle *et al.* 1989; Allen & Chamberlain 1991). The eastward continuation of the MKT into Ladakh remains unknown. The 700 km long dextral Karakoram Fault (KF) runs through the Nubra and upper (eastern) Shyok valleys, striking N30W to N45W. East of the Nubra–Shyok confluence it separates rocks of the Ladakh terrane from those of the Karakoram terrane (Searle *et al.* 1998). It has been suggested that the KF marks the southern boundary of the Tibetan block, and that together with the sinistral Altyn Tagh Fault, it has accommodated 1000 km of eastward extrusion of the Tibetan Plateau (e.g. Peltzer & Tapponnier 1988). Searle *et al.* (1998), however, determined that the fault is a relatively young structure (<18 Ma) with a maximum dextral displacement of less than 150 km. Rocks southeast of the Pangong Lake in western Tibet define a suture zone, on the east side of the KF, which can be traced all the way to Amdo, 1200 km to the east, defining the Pangong–Nujiang Suture Zone, separating the Changtang and Lhasa blocks (e.g. Allègre *et al.* 1984; Ratschbacher *et al.* 1994). This suture zone has been tentatively related to the SSZ (Searle 1996).

The Ladakh and Karakoram batholiths underlie the two main mountain ranges near the confluence (Fig. 1a). The Ladakh batholith and its extrusive equivalents—the Khardung Fm. (e.g. Srimal 1986*a* and Srimal *et al.* 1987)—are part of the 2500 km long Trans-Himalayan igneous belt, a pre-collisional calc-alkaline belt (e.g. Honegger *et al.* 1982). The batholith was active between 102 ± 2 Ma and 50 ± 1 Ma

(Honegger *et al.* 1982; Schärer *et al.* 1984; Weinberg & Dunlap in press). Three rocks dated close to the confluence area yielded U–Pb zircon crystallization ages between 65 and 50 Ma (Weinberg & Dunlap in press). The Karakoram batholith is a 700 km long arcuate body, composed of older, mid-Cretaceous and Palaeocene–Eocene calc-alkaline plutons, and a distinctive Miocene peraluminous leucogranite suite which originated from widespread crustal anatexis during continental collision (Searle *et al.* 1992). The post-collisional Baltoro Plutonic Unit is the main component of the Karakoram Range in Pakistan. It has U–Pb zircon ages of 21.0 ± 0.5 Ma (Parrish & Tirrul 1989) and monazite ages of $25.5^{+0.3}_{-0.6}$ Ma (biotite leucogranite) and $21.4^{+0.3}_{-0.8}$ Ma (two-mica garnet leucogranite; Schärer *et al.* 1990). These ages are somewhat older than the 18.0 ± 0.6 Ma Karakoram (Tangtse) leucogranite, cropping out some 120 km SE of the confluence (Searle *et al.* 1998).

In between the Ladakh and Karakoram batholiths, volcano-sedimentary rocks have localized deformation. These rocks were divided by Thakur & Misra (1984) into the Shyok and Nubra groups. According to these authors, the Shyok Group consists of dismembered fragments of an ophiolite sequence comprising basic and intermediate volcanic rocks, together with chert, gabbro, peridotite and serpentinite interbedded with phyllite, slate, limestone and quartzite. Their Nubra Group, cropping out along the Nubra River, consists of sandstone, conglomerates and shale interbedded with basic volcanic, serpentinite, pyroxenite and garnet–mica schist. Srimal (1986*b*) and Srimal *et al.* (1987) mapped the Saltoro Range, between the Nubra and Shyok valleys. They found two ophiolitic sequences, one to the south which they called the Biagdang ophiolite, cropping out on both sides of the Shyok River, and the other on the northeastern slopes of the Saltoro Range, which they called the Saltoro ophiolite. Several maps of the confluence area indicate the presence of granites between the KT and the KF close to Tirit and in the Saltoro Range (Tirit batholith; e.g. Thakur & Misra 1984; Srimal *et al.* 1987). We have found no evidence of peridodites, nor of any sheared or deformed ultramafic rocks, and our observations and interpretations broadly disagree with those of previous authors.

Geology of the Shyok–Nubra confluence

The main geological and tectonic features of the confluence area, and the known ages are summarized in Figs 1 and 2. Our observations extend from Khardung in the south to Panamik and Kubed in the north, and from Hundar in the west to SE of Satti. The Khalsar Thrust (KT) and the Karakoram Fault (KF), define a triple point at their intersection at the confluence and separate three blocks: the Ladakh (LAD), the Saltoro (SAL) and the Karakoram (KAK) blocks (insert on Fig. 1b).

Ladakh block and Khalsar Thrust (KT)

The Ladakh block lies south of the KT and KF. It is characterized by granitoids belonging to the Ladakh batholith intruding an older sequence of basalts and quartzites—the Shyok Formation—and overlain by pyroclastic flows of the Khardung Formation. The Shyok Fm. is well preserved near Hundar where it consists of folded basaltic flows interlayered with narrow (0.5–1 m) bands of sandstone. The presence of graded-bedded sandstone suggests that the basalts are not part of an ophiolitic sequence, but more likely part of the Dras island arc. Thakur *et al.* (1981) mention a Lower Cretaceous age for the Shyok Fm.

The Ladakh batholith has been described in a number of papers (e.g. Honegger *et al.* 1982; Weinberg & Dunlap in press) and will not be further described here. The 63 ± 8 Ma (Srimal *et al.* 1987) calc-alkaline Khardung Fm. are the extrusive equivalent of the Ladakh batholith. It is a thick sequence of felsic pyroclastic flows with angular blocks of various volcanic, plutonic and sedimentary rock types, interlayered with coarse volcaniclastic rocks. Its thickness varies considerably along strike (*c.* 5 km at Khardung) from Hundar in the west to Chushul 200 km east. These flows now generally dip 30–60° NE, suggesting post-depositional tilting. The original contact between the Shyok Fm. and the younger Khardung Fm. is obscured by deformation and thrusting along the KT, but it was most likely an unconformity. The contact between the Khardung Fm. and Ladakh granitoids at Khardung is intruded by a large andesite sill which is linked to dykes intruding the underlying granitoids and the overlying Khardung Fm., where they feed smaller sills. This andesite extruded on top of the Khardung Fm., giving rise to a red andesite lava flow. The main sill at Khardung is 2 km wide, and its contact with the underlying granite dips roughly 40–50° NE. These andesitic rocks—which we called the **Khardung Andesite Unit**—are clearly younger and more mafic than the Khardung Fm.

Between Hundar and Deshkit, basalts of the Shyok Fm. and intrusive Ladakh granitoids become increasingly sheared and retrograded to

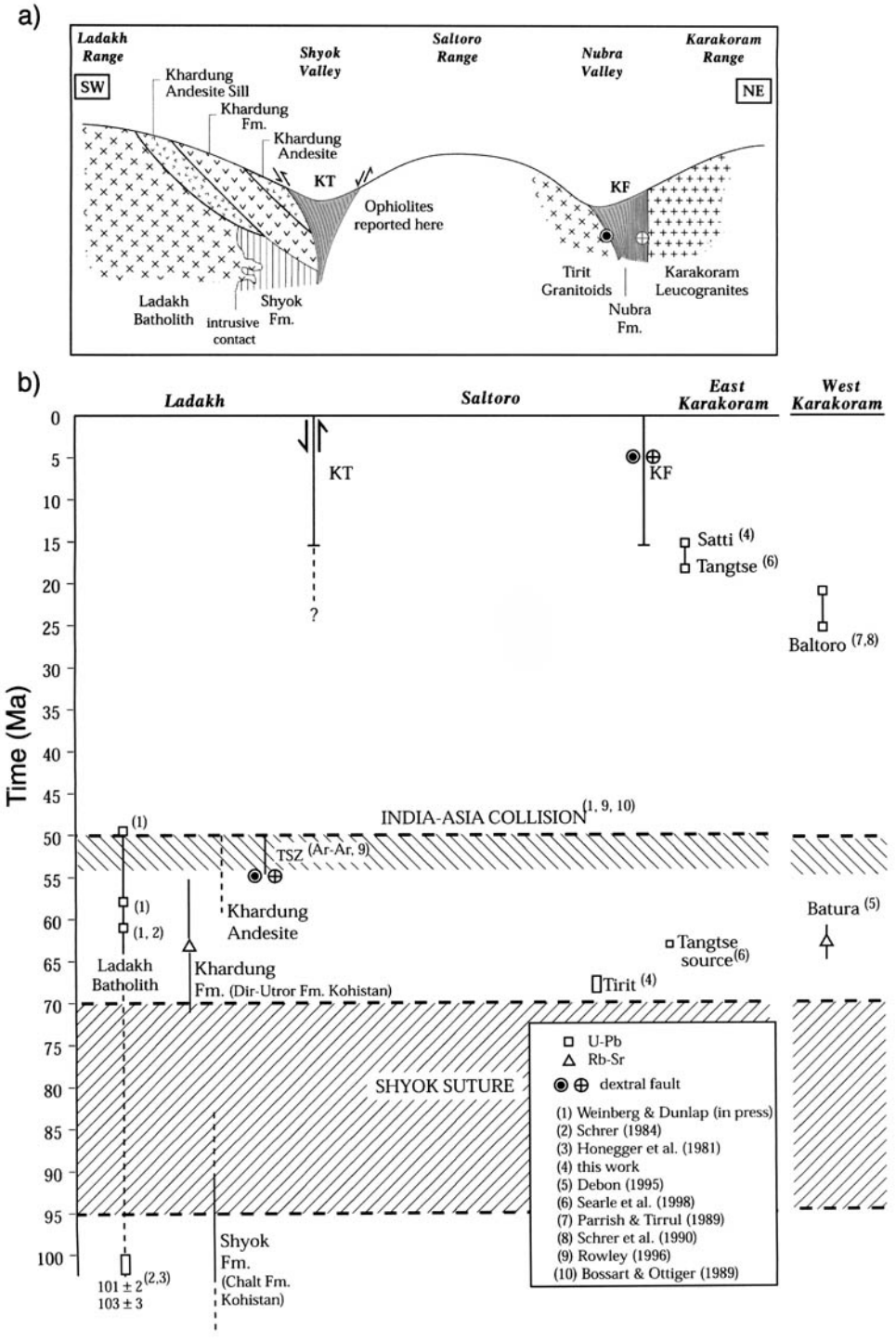

Fig. 2. (**a**) Schematic geological profile across the northern Ladakh Range, the Saltoro Range and the southern Karakoram Range, summarizing our observations. (**b**) Summary of measured and estimated ages of rocks and structures in northern Ladakh, and the Karakoram Range. The Nubra Fm. is not shown and has an estimated Permian age.

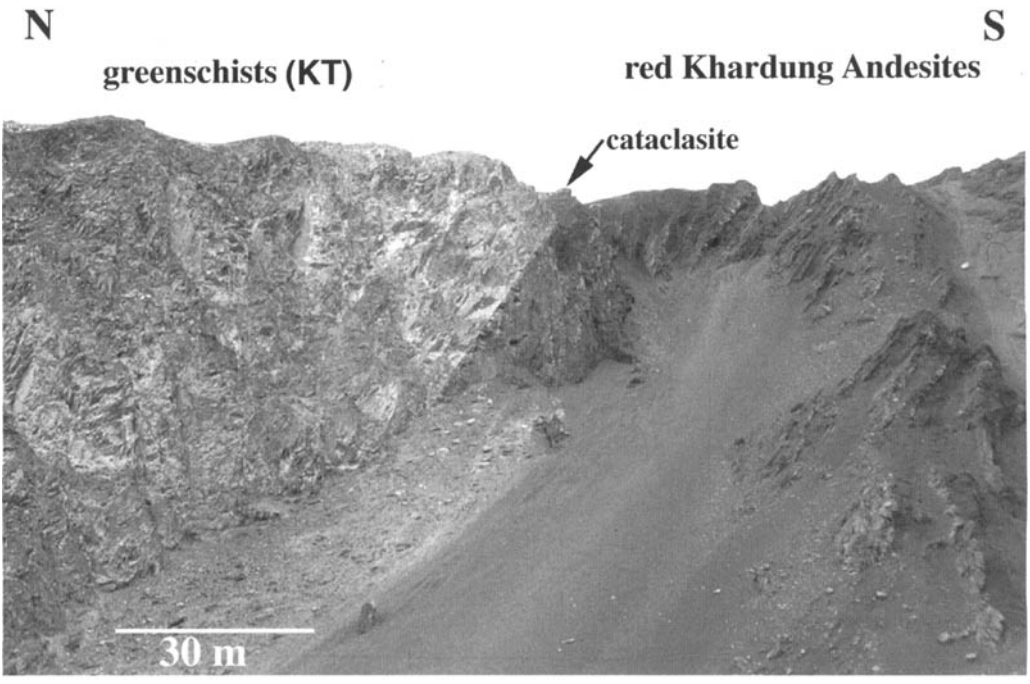

Fig. 3. The Khalsar Thrust (KT) at Khalsar.

greenschist facies as a result of shearing along the KT (Fig. 1). The KT is best exposed between the villages of Deshkit and Khalsar. It is a zone several hundred metres wide and exposures at Khalsar indicate south-directed thrusting (Fig. 3) in accordance with down-dip lineation and kinematic indicators (see the 'Structural analysis' section). Thakur *et al.* (1981) divided the geology into groups based on the deformation state of the rocks. Thus, they joined undeformed or weakly deformed rocks, basalts and quartzites of the Shyok Fm., and younger pyroclastic flows of the Khardung Fm. under the term 'Khardung volcanics'. Sheared greenschists of the Shyok Fm. were separated from preserved basalts of the same formation, and were called the 'Khalsar Member'.

Saltoro block

The Saltoro block forms a wedge north of the KT and west of the KF (Fig. 1b). The most detailed work in the Saltoro Range was that by Srimal (1986*a*, *b*), who described a 7.5 km thick ophiolitic sequence of basic rocks on the south Saltoro Range (the Biagdang ophiolite). These rocks are intruded by granitoids, just as the Shyok Fm., and metamorphosed mainly at greenschist facies (Srimal 1986*a*). Most of the Saltoro block is out of bounds for travellers, but we were nevertheless able to study outcrops of this block in three localities, all of which were located immediately south of the KF and exposed plutonic rocks, collectively referred to as the Tirit batholith (Fig. 1b; Thakur *et al.* 1981).

Rocks of the Tirit batholith are exposed immediately north of the KT, near Khalsar. It is represented by a medium-grained, weakly deformed hornblende diorite, with labradorite and minor biotite (Ar–Ar sample 95–481, below). The Tirit batholith also crops out near Tirit village, directly underlying the mylonitic sedimentary rocks of the Nubra Fm. Here, granitoids are altered and fractured, and two thin sections of augite–hornblende tonalites and one of felsic granite showed rocks intensely fractured but with no signs of plastic deformation, suggesting cold deformation ($T < 300$–250 °C). This contrasts with ductile mylonites of Karakoram leucogranite found within the KF, only a few hundred metres across strike. Sheared Tirit batholith rocks crop out in the Saltoro mountains close to the village of Kubed. We inspected an estimated 4 km across strike, and found sheared plutonic rocks retrogressed in greenschist facies conditions but locally preserving intrusive relationships. In thin sections these rocks are recrystallized and composed mostly of metamorphic minerals. The Nubra valley trends at a small angle to the strike of the foliation in these rocks (N40–60W), and sheared granitoids

crop out along the lower slopes of the Saltoro Range, all the way south to the confluence at Tirit (see Srimal 1986*a*). Morainic and alluvial blocks carried down the Kubed valley are of plutonic rocks (no sedimentary blocks found), mostly unaltered, undeformed gabbros and diorites, coarse cumulitic pyroxenites, and granites and granodiorites, and only a few gneisses. All blocks observed were typical of calc-alkaline sequences, such as the Ladakh batholith, and not related to an ophiolite, as interpreted by Srimal (1986*a*, *b*, 1987; their Saltoro ophiolite).

Karakoram block and Karakoram Fault (KF)

Three rock sequences crop out in the Karakoram Range: the Nubra Fm. (Thakur & Misra 1984), the Karakoram leucogranite batholith (the Baltoro Plutonic Unit in Pakistan) and an older I-type granitoid belt (Srimal *et al.* 1987). The I-type belt crops out in the most remote part of the batholith and was not covered by this work. The Nubra Fm. is a rock sequence *c.* 1–2 km wide cropping out along the foot of the Karakoram Range, between the Tirit batholith and Karakoram leucogranite. It is comprised of metavolcanic and metapelitic rocks metamorphosed to green, grey and black schists and sheared by movement on the KF. Primary structures are preserved locally such as in an outcrop of porphyritic andesite lava breccia (isolated outcrop south of Panamik; Fig. 1b). Metadacites, now metamorphosed to greyschists, preserve primary plagioclase and quartz phenocrysts in a felsic matrix. Common greenschists are composed of actinolite–chlorite–epidote–carbonate–plagioclase–quartz and were most likely originated from metamorphism of basic rocks. Some of these greenschists also have dark green tourmaline aggregates or single crystals up to 5 mm long. Grey and black Bt–Ms–Chl schists with fine felsic and mafic bands were interpreted as metapelites. In one metapelite sample we found sericitized pseudomorphs of cordierite, 1 cm in diameter, which suggests that the Nubra Fm. attained hornblende hornfels facies (Cd + Bt + Ms paragenesis) before greenschist facies retrogression. We report also marble occurrences, in the Sumur Gorge (muddy and sheared carbonates), near Satti and Rongdu (brown folded marble layers).

The presence in the Nubra Fm. of mylonitic leucogranite layers up to tens of metres wide and locally cross-cutting the foliation, particularly

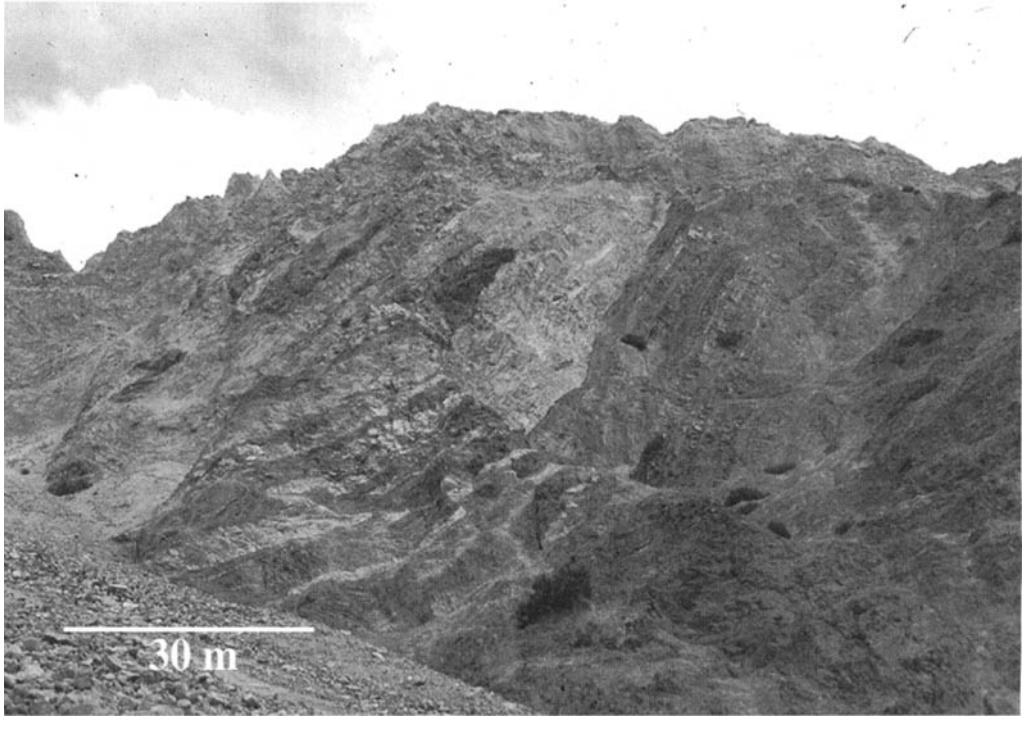

Fig. 4. Intrusive contact between the Karakoram leucogranite (left-hand side) and the Nubra Fm. (right-hand side) near Pinchimik. Note intrusive dykes folded within the Nubra Fm.

close to the contact with the Karakoram leucogranite (Fig. 4), suggest that the Nubra Fm. was the wall rock of the Karakoram batholith and therefore part of the Karakoram terrane. The Nubra Fm. has taken up most of the strain due to movement on the KF. Strain intensity varies across the sequence but generally increases gradually towards the contact between the Nubra Fm. and Karakoram leucogranite where it is characterized by a band of mylonites of *c.* 200–400 m shearing both sides of the contact (see the 'Structural analysis' section). North of the contact mylonites, the Karakoram batholith is composed mainly of Bt–Ms leucogranite with minor Ms leucogranite (the Tegar granite of Sharma & Kumar 1978). We explored 10 km up the Spang Chenmo valley, north of Satti, and up the Rongdu valley to the east, where the batholith is very homogeneous, comprised of massive Bt–Ms leucogranite, with some sedimentary xenoliths but no mafic enclaves. Quartz has been deformed plastically and feldspar grains are fractured. Igneous muscovite comprises up to 2–3% (modal) of the rock. We noted a variety of blocks in the scree coming down from the Karakoram Range, including sheared dolomitic breccia, white marble, black andalusite schist and granodiorite with mafic enclaves (probably part of the older I-type granitoids described by Srimal *et al.* 1987).

In summary, the Nubra Fm. is a sequence of multicoloured schists resulting from greenschist facies metamorphism of basalts, andesites, dacites, pelitic rocks and marble, later intruded by Karakoram leucogranite. The Karakoram Fault shears most of the Nubra Fm., but shearing is concentrated to a 200–400 m wide band of mylonites along the contact with the Karakoram leucogranite.

Geochronology

In order to further constrain the geological history of the confluence area we determined the crystallization age of zircons from two granite samples (Tables 1 and 2) and the Ar–Ar cooling histories of two other samples (Tables 3 and 4).

Tirit batholith—U–Pb and Ar–Ar

We carried out U–Pb dating of zircons from a tonalite sample collected at Tirit (sample 96–711) and Ar–Ar analysis of hornblende grains of sample 95–481. Sample 96–711 has no signs of plastic deformation, but was altered and fractured, with plagioclase partly altered to sericite and calcite, undeformed quartz, green to transparent amphibole, and transparent pyroxene, as well as opaque grains, chlorite and epidote. U–Th–Pb analyses were performed using a Cameca ims1270 ion-microprobe at the Swedish Museum of Natural History, Stockholm (Nordsim facility) following analytical methods described by Whitehouse *et al.* (1997) and Zeck & Whitehouse (in press). U/Pb and Th/Pb ratios are calibrated relative to the 1065 Ma Geostandards zircon 91500 (Wiedenbeck *et al.* 1995). The accuracy of $^{206}Pb/^{238}U$ ages from young zircons

Table 1. *Ion-microprobe (Cameca ims 1270) U–Th–Pb data for zircons from 96–711 (Tirit granite)*

Spot	Date	U (ppm)	Th (ppm)	%co ^{206}Pb	$^{207}Pb/^{206}Pb$	$^{232}Th/^{208}Pb$	$^{238}U/^{206}Pb$	$^{208}Pb/^{232}Th$ age (Ma)	$^{206}Pb/^{238}U$ age (Ma)
5a	1	238	299	1.30	0.0501 ± 27	335 ± 25	93.6 ± 0.8	60.3 ± 4.9	68.5 ± 0.6
4a	1	357	317	0.65	0.0497 ± 19	331 ± 25	93.4 ± 0.8	61 ± 5	68.6 ± 0.6
8a	1	686	1226	0.65	0.0469 ± 13	316 ± 23	93.4 ± 0.8	63.8 ± 5	68.7 ± 0.6
7a	1	511	775	0.14	0.0461 ± 16	333 ± 25	94.7 ± 0.8	60.6 ± 4.9	67.7 ± 0.6
6a	1	321	304	0.57	0.0492 ± 20	328 ± 25	93.6 ± 0.8	61.5 ± 5.1	68.5 ± 0.6
1a	1	127	109	0.83	0.0456 ± 31	309 ± 25	91.2 ± 1.5	65.2 ± 5.7	70.3 ± 1.2
2a	1	117	100	0.46	0.0449 ± 39	298 ± 24	93.6 ± 1.5	67.7 ± 5.9	68.5 ± 1.1
3a	1	161	111	1.34	0.0502 ± 31	324 ± 26	95.9 ± 1.5	62.3 ± 5.4	66.9 ± 1.0
99a	1	416	468	0.38	0.0467 ± 19	319 ± 24	90.7 ± 1.1	63.2 ± 5.1	70.7 ± 0.8
10a	2	138	82	9.13	0.0961 ± 59	393 ± 42	95.3 ± 2.8	51.4 ± 6.1	67.3 ± 2.0
10b	2	135	105	0.23	0.0501 ± 21	284 ± 18	95.9 ± 2.9	71 ± 4.8	66.8 ± 2.0
12a	2	95	79	3.80	0.0497 ± 32	543 ± 53	112.6 ± 4.9	37.2 ± 4	57.0 ± 2.5
11a	2	493	909	2.32	0.0614 ± 20	324 ± 18	101.4 ± 2.7	62.3 ± 3.7	63.2 ± 1.7
13a	2	204	213	0.97	0.0508 ± 17	331 ± 19	98.4 ± 2.4	61 ± 3.7	65.2 ± 1.6
14a	2	200	225	6.95	0.0546 ± 22	567 ± 42	114.5 ± 4.1	35.6 ± 2.8	56.1 ± 2.0
5b	2	176	204	4.07	0.0568 ± 21	359 ± 27	102.7 ± 3.2	56.3 ± 4.6	62.5 ± 2.0
9a	1	113	104	0.00	0.0523 ± 34	317 ± 25	93.2 ± 1.6	63.8 ± 5.4	68.8 ± 1.2

Season date: 1 04/02/98
2 08/02/98

based upon this calibration has been tested by analysis of zircons from a volcanic tuff at Possagno, Italy: conventional measurements of these zircons have yielded 35.5 ± 0.1 Ma (Fischer *et al.* 1989; F. Oberli, pers. comm.), and ion probe measurements yielded 35.1 ± 2.2 Ma (2σ; S. Nicolescu, pers. comm.). The zircons in this study are too young to yield reliable $^{207}Pb/^{206}Pb$ ages because of the large errors associated with measuring very small ^{207}Pb peaks. Th/Pb ages are similarly affected by possible systematic errors in centring of a very small ^{208}Pb peak and are consistently lower than $^{206}Pb/^{238}U$ ages. Common Pb corrections, based upon present-day (Stacey & Kramers 1975) terrestrial Pb are generally *c.* 1% of ^{206}Pb or less (see Table 1).

The results are shown in Fig. 5 and Table 1. Fourteen analyses yielded a group of $^{206}Pb/^{238}U$ with a weighted mean average of 68 ± 1 Ma (2σ). A chi square test resulted in over 99% likelihood that the results belong to the same age group ($\chi^2 = 2.99$ for 13 degrees of freedom). Four points were excluded from the final data analyses (spots 10a, 12a, 14a and 5b) because they had $^{206}Pb/^{238}U$ ages different from the main group, very large common lead corrections (of over 3%,

Table 2. *Zircon U–Pb SHRIMP II analyses of Sample 021 (Satti leucogranite)*

Spot	Date	Core 1 rim 2	U (ppm)	Th (ppm)	%co ^{206}Pb	%co ^{208}Pb	$^{207}Pb/^{206}Pb$	$^{238}U/^{206}Pb$	$^{208}UPb/^{232}Th$ age (Ma)	$^{206}Pb/^{238}U$ age (Ma)
2.1	1	2	2969	140	1.15	57.4	0.0571 ± 23	435.9 ± 17	21 ± 11	14.6 ± 0.6
4.1	1	2	2698	649	1.83	35.4	0.0634 ± 28	412.1 ± 16.2	17.1 ± 5.3	15.3 ± 0.6
5.1	1	1	450	250	9.21	57	0.132 ± 166	406.9 ± 23.5	15 ± 7.7	14.4 ± 0.8
6.1*	1	1	211	77	20.47	66.1	0.2379 ± 94	60.9 ± 2.8	204 ± 66	83.7 ± 3.8
6.2	1	2	882	149	10.91	74.2	0.1479 ± 82	397.3 ± 19.8	27.8 ± 14	14.4 ± 0.7
7.1	1	1	1566	78	2.11	83.6	0.0659 ± 28	398.4 ± 15.7	9.9 ± 8.5	15.8 ± 0.6
8.1	1	1	689	47	3.83	509.9	0.0951 ± 21	9.9 ± 0.4	0 ± 0	599 ± 23
8.2	1	2	2560	760	1.61	28.2	0.0613 ± 19	411.8 ± 16	14.8 ± 3.9	15.4 ± 0.6
9.1	2	1	168	95	0.53	6.2	0.0681 ± 16	8.5 ± 0.1	739 ± 22	717 ± 8.7
10.1	2	1	205	103	0.27	3.9	0.0755 ± 9	5.8 ± 0.1	986 ± 22	1016 ± 9.2
11.1	2	1	239	334	4.49	19.5	0.0881 ± 94	411.9 ± 24.3	14.6 ± 1.3	14.9 ± 0.9
12.1	2	1	312	109	3.48	37.8	0.0787 ± 64	533.8 ± 30.3	14 ± 2.2	11.6 ± 0.7
13.1	2	1	236	104	0	0	0.091 ± 24	4 ± 0.1	1515 ± 106	1437 ± 33
14.1	2	1	138	137	0.16	1.2	0.0655 ± 13	8.2 ± 0.1	738 ± 12	743 ± 6.2
15.1	2	1	542	129	1.15	30.6	0.0575 ± 24	155.8 ± 2.3	31.8 ± 3.7	40.8 ± 0.6

Session date: 1 27/05/96
2 18/06/96
*Spot 6.1 results affected by inclusion.

Table 3. *Ar–Ar age spectrum data for sample 95–481 hornblende (Tinit batholith)*

Temp (°C)	^{36}Ar (mol)	^{37}Ar (mol)	^{39}Ar (mol)	^{40}Ar (mol)	% radiog.	$^{*40}Ar/^{39}K$	Cumulative release	Age (Ma)	Error	Ca/K
700	6.32E-16	5.83E-16	1.38E-16	1.94E-13	3.6	50.61	0.63	70.26	45.52	8.08
900	2.26E-16	3.67E-15	4.12E-16	8.30E-14	20.0	40.44	2.51	56.36	3.18	17.00
1000	1.06E-16	2.31E-15	4.88E-16	5.06E-14	38.4	39.96	4.74	55.70	1.56	9.03
1060	1.38E-16	9.34E-15	6.91E-16	7.49E-14	46.7	50.97	7.88	70.75	1.93	25.90
1100	2.51E-16	2.66E-14	1.94E-15	1.80E-13	60.4	56.40	16.72	78.12	0.60	26.20
1140	3.22E-16	5.20E-14	5.02E-15	3.50E-13	74.3	52.05	39.61	72.22	0.24	19.80
1160	1.80E-16	2.42E-14	2.50E-15	1.81E-13	71.9	52.12	51.03	72.32	0.55	18.50
1170	1.23E-16	1.35E-14	1.38E-15	1.07E-13	67.2	52.43	57.30	72.73	0.63	18.70
1190	1.21E-16	1.36E-14	1.41E-15	1.07E-13	67.8	51.63	63.72	71.64	0.71	18.40
1220	1.37E-16	2.29E-14	2.23E-15	1.55E-13	75.5	52.87	73.88	73.34	0.34	19.60
1240	1.08E-16	1.24E-14	1.14E-15	9.37E-14	67.2	55.84	79.05	77.37	0.67	20.90
1265	1.27E-16	1.23E-14	1.14E-15	1.00E-13	63.8	56.28	84.25	77.96	0.88	20.60
1290	1.40E-16	1.34E-14	1.28E-15	1.12E-13	64.1	56.25	90.10	77.92	0.60	20.00
1330	1.71E-16	1.16E-14	1.08E-15	1.10E-13	55.1	56.42	95.03	78.15	0.98	20.50
1450	4.55E-16	1.32E-14	1.09E-15	1.94E-13	31.3	56.09	100.00	77.70	2.57	23.10
Total	3.24E-15	2.32E-13	2.19E-14	2.09E-12	53.07		73.6 ± 1.02			

Lambda K40 = 5.54E-10 J = 7.85E-04

Table 4. *Ar–Ar age spectrum data for sample 95–411 K-feldspar (Ladakh batholith)*

Temp (°C)	^{36}Ar (mol)	^{37}Ar (mol)	^{39}Ar (mol)	^{40}Ar (mol)	% radiog.	^{*40}Ar/^{39}K	Cumulative release	Age (Ma)	Error	Ca/K
450	2.87E-16	1.13E-16	4.18E-16	1.25E-13	32.3	96.738	0.16	264.24	9.63	0.513
450	8.58E-17	8.32E-16	2.26E-16	2.72E-14	7.1	8.598	0.25	25.12	4.02	7.030
500	1.07E-16	2.74E-16	6.80E-16	8.46E-14	62.5	77.692	0.52	215.18	2.65	0.765
500	3.84E-17	5.96E-17	5.11E-16	1.48E-14	23.0	6.628	0.72	19.39	1.13	0.222
550	1.40E-16	7.23E-16	2.16E-15	1.54E-13	73.2	52.296	1.58	147.63	0.5	0.636
550	2.94E-17	6.68E-17	1.32E-15	1.68E-14	48.1	6.112	2.1	17.89	0.35	0.096
600	9.26E-17	1.99E-16	2.62E-15	9.88E-14	72.3	27.284	3.13	78.53	0.53	0.144
600	2.04E-17	6.69E-17	1.52E-15	1.53E-14	60.5	6.104	3.73	17.87	0.21	0.084
650	6.35E-17	6.70E-17	2.43E-15	6.63E-14	71.6	19.594	4.69	56.74	0.3	0.052
650	1.63E-17	6.70E-17	1.55E-15	1.50E-14	67.7	6.541	5.3	19.14	0.22	0.082
700	4.69E-17	6.71E-17	2.22E-15	4.59E-14	69.7	14.411	6.18	41.9	0.23	0.057
700	9.37E-18	6.71E-17	1.66E-15	1.34E-14	79.1	6.351	6.84	18.59	0.22	0.077
750	2.28E-17	7.92E-16	1.89E-15	2.41E-14	72.1	9.185	7.58	26.82	0.35	0.796
750	6.72E-18	6.72E-17	1.80E-15	1.33E-14	84.8	6.256	8.3	18.31	0.15	0.071
800	1.38E-17	1.03E-16	1.75E-15	1.61E-14	74.6	6.892	8.99	20.16	0.31	0.112
800	7.48E-18	1.49E-15	1.94E-15	1.40E-14	85.1	6.147	9.75	17.99	0.21	1.460
850	1.79E-17	6.74E-17	1.74E-15	1.70E-14	68.6	6.702	10.44	19.61	0.21	0.074
850	1.25E-17	9.28E-16	2.00E-15	1.60E-14	77.3	6.220	11.23	18.2	0.18	0.884
900	3.60E-17	8.39E-18	1.80E-15	2.32E-14	54.0	6.979	11.94	20.41	0.27	0.009
900	2.82E-17	2.80E-16	2.10E-15	2.32E-14	64.0	7.060	12.76	20.65	0.23	0.253
950	7.03E-17	6.76E-17	2.18E-15	3.84E-14	45.8	8.063	13.63	23.56	0.42	0.059
950	6.88E-17	7.65E-16	2.94E-15	4.57E-14	55.5	8.613	14.79	25.16	0.31	0.494
950	1.16E-16	1.18E-16	4.38E-15	7.73E-14	55.4	9.782	16.52	28.55	0.26	0.051
1000	1.21E-16	9.46E-16	3.50E-15	7.62E-14	53.3	11.609	17.9	33.83	0.18	0.513
1000	1.19E-16	7.07E-17	5.30E-15	9.45E-14	62.8	11.185	20	32.6	0.16	0.025
1050	1.76E-16	3.79E-17	7.47E-15	1.44E-13	63.9	12.344	22.95	35.95	0.19	0.010
1050	1.59E-16	1.61E-15	1.01E-14	1.69E-13	72.1	12.010	26.94	34.99	0.14	0.301
1050	1.80E-16	3.61E-15	1.36E-14	2.20E-13	75.9	12.329	32.3	35.91	0.22	0.506
1100	1.25E-16	2.08E-15	8.15E-15	1.49E-13	75.1	13.691	35.52	39.83	0.34	0.484
1100	1.17E-16	2.49E-16	1.05E-14	1.73E-13	80.0	13.181	39.67	38.36	0.11	0.045
1100	1.34E-16	1.56E-15	1.41E-14	2.31E-13	82.8	13.530	45.24	39.37	0.13	0.210
1100	1.51E-16	2.06E-15	1.60E-14	2.66E-13	83.2	13.798	51.57	40.14	0.11	0.244
1100	1.56E-16	1.45E-15	1.59E-14	2.71E-13	83.0	14.138	57.85	41.12	0.13	0.173
1100	1.78E-16	1.29E-15	1.63E-14	2.86E-13	81.5	14.304	64.3	41.59	0.13	0.150
1100	1.91E-16	3.43E-15	1.52E-14	2.77E-13	79.7	14.480	70.32	42.1	0.16	0.428
1100	2.81E-16	2.68E-15	1.85E-14	3.51E-13	76.3	14.493	77.62	42.14	0.15	0.275
1200	1.12E-16	1.24E-16	1.16E-14	1.99E-13	83.1	14.198	82.21	41.29	0.11	0.020
1230	1.63E-16	1.24E-16	1.69E-14	2.86E-13	83.1	14.048	88.89	40.86	0.11	0.014
1260	1.51E-16	1.24E-16	1.52E-14	2.56E-13	82.5	13.906	94.88	40.45	0.12	0.016
1290	9.75E-17	2.15E-15	8.54E-15	1.45E-13	80.1	13.579	98.25	39.51	0.22	0.479
1320	4.92E-17	1.82E-15	3.05E-15	5.59E-14	74.2	13.612	99.45	39.61	0.28	1.140
1350	2.80E-17	1.24E-16	8.93E-16	1.99E-14	58.3	12.957	99.81	37.72	1.06	0.265
1450	4.07E-17	2.05E-16	4.88E-16	1.84E-14	34.6	13.052	100	37.99	1.91	0.800
Total	4.07E-15	3.30E-14	2.53E-13	4.67E-12	13.7	39.86 ± 0.21 Ma				

Lambda K40 = 5.54E-10 J = 1.63E-03

whereas all other data points required less than 2%) and very different $^{206}Pb/^{238}U$, $^{207}Pb/^{235}U$ and $^{208}Pb/^{206}Pb$ ages. The youngest age in the remaining group (11a) required a relatively high common lead correction and the spot that yielded the oldest point (99a) has overlapped with a small inclusion, and these analyses may not have yielded the correct crystallization age of the zircons.

Hornblende diorite 95–481 is composed mainly of plagioclase and hornblende. There are books of chlorite adjacent to concentrations of hornblende, but the amphiboles themselves are fresh looking and do not contain visible chlorite. A pure separate of the hornblende was obtained by conventional separation methods and a $^{40}Ar/^{39}Ar$ step heating analysis was undertaken on a several milligram aliquot. The results (Table 3) are presented as an age spectrum diagram in Fig. 6. The age spectrum is relatively flat for the majority of gas release, such that a plateau age calculated for the middle portion of

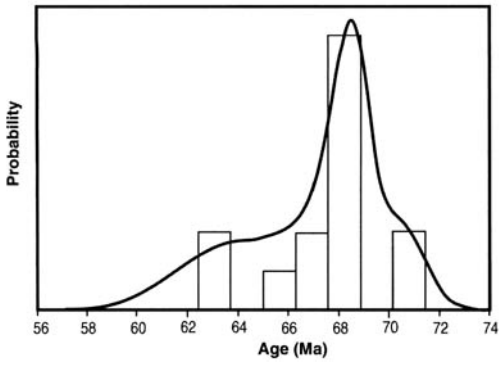

Fig. 5. Histogram of $^{238}U/^{206}Pb$ ages obtained from ion-microprobe analyses of zircons from a Tirit tonalite (sample 96–711; Table 1; location in Fig. 1b). The smooth curve indicates the relative probability plot of the data, constructed by assigning an equal-area Gaussian distribution to each analysis and assuming these over the entire age range.

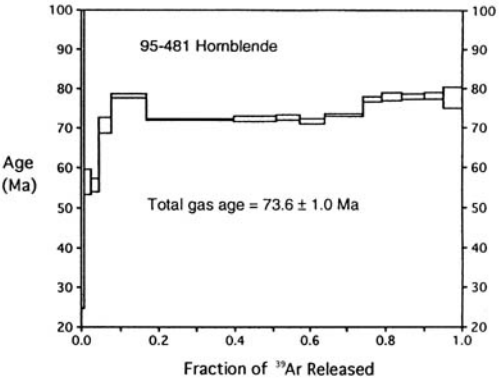

Fig. 6. Age spectrum diagram for hornblende 95–481.

gas release would not be very different from the integrated total gas age of 73.6 ± 1.0 Ma (1σ). A K/Ca for over 90% of gas release is below about 0.06, which indicates no significant contamination of the separate. An isochron plot of all of the data points is in agreement with the age spectrum results, yielding an age of 73.1 ± 1.1 Ma (1σ with MSWD), and the data do not show any clear evidence for excess argon contamination. Thus, we prefer the age of 73.6 ± 1.0 Ma, which we interpret as being very close to the age of crystallization of the diorite, similar to the U–Pb zircon crystallization age determined for the granite at Tirit. This limited dataset suggests that the Tirit batholith intrusion is between 74 Ma to 68 Ma.

Karakoram leucogranite—U–Pb

We carried out U–Pb SHRIMP dating of zircons from a typical leucogranite sample collected north of Satti (sample 021, location in Fig. 1b). Cathodeluminescence images of the zircons revealed idiomorphic zircons with cores truncated by the later growth of rims with fine zonation (Fig. 7a). The position of spots for analysis were chosen according to internal zoning of zircons as revealed by cathodeluminescence. Dating methodology was described in Weinberg & Dunlap (in press). The SHRIMP II at the Australian National University was used and the primary ion beam was focused to spots approximately 30 μm in diameter. The standard used was SL13 (Claoué-Long *et al.* 1995) and two standards were analysed for every four analyses of unknown zircons. Results were corrected for common lead by assuming the isotopic composition of lead from Broken Hill, Australia (the composition of Pb impurities found in exhaust fans at the ANU laboratory). For each analysis, seven cycles were carried out, each cycle measuring the secondary ion yields of Zr_2O^+, the four lead isotopes (^{208}Pb, ^{207}Pb, ^{206}Pb, ^{204}Pb), U^+ and UO^+, Th^+ and ThO^+. Because neither $^{207}Pb/^{206}Pb$ nor $^{207}Pb/^{235}U$ chronology by SHRIMP provide a fine age resolution for the Phanerozoic, we relied entirely on the $^{206}Pb/^{238}U$ and $^{208}Pb/^{232}Th$ geochronometers.

Seven analyses of well-developed zircon rims defined a single young group centred at 15.0 ± 0.4 Ma (2σ) which we interpret as the age of crystallization of the granite (Table 2 and Fig. 7b). One spot was excluded because it yielded a much younger age (11 Ma spot number 12.1) which we considered to be an outlier. Zircon cores yielded a wide spread in ages indicating zircon inheritance. The two U–Pb zircon age determinations for the eastern Karakoram leucogranites now available (15.0 ± 0.4 Ma and 18 ± 0.6 Ma; here and Searle *et al.* 1998, respectively) suggest leucogranites east of the KF are younger than those to the west (20–25 Ma; Parrish & Tirrul 1989; Schärer *et al.* 1990; Fig. 2b).

Thermal history of the Ladakh granite adjacent to the KT

In this section we present thermal modelling, effectively an interpretation, of the results of $^{40}Ar/^{39}Ar$ step heating of a K-feldspar concentrate from Ladakh granite 95–411, which intruded the base of the Shyok Fm. near the bridge at Hundar (Table 4). It is clear from recent U–Pb ion microprobe work that the bulk of the Ladakh batholith crystallized about 60 Ma

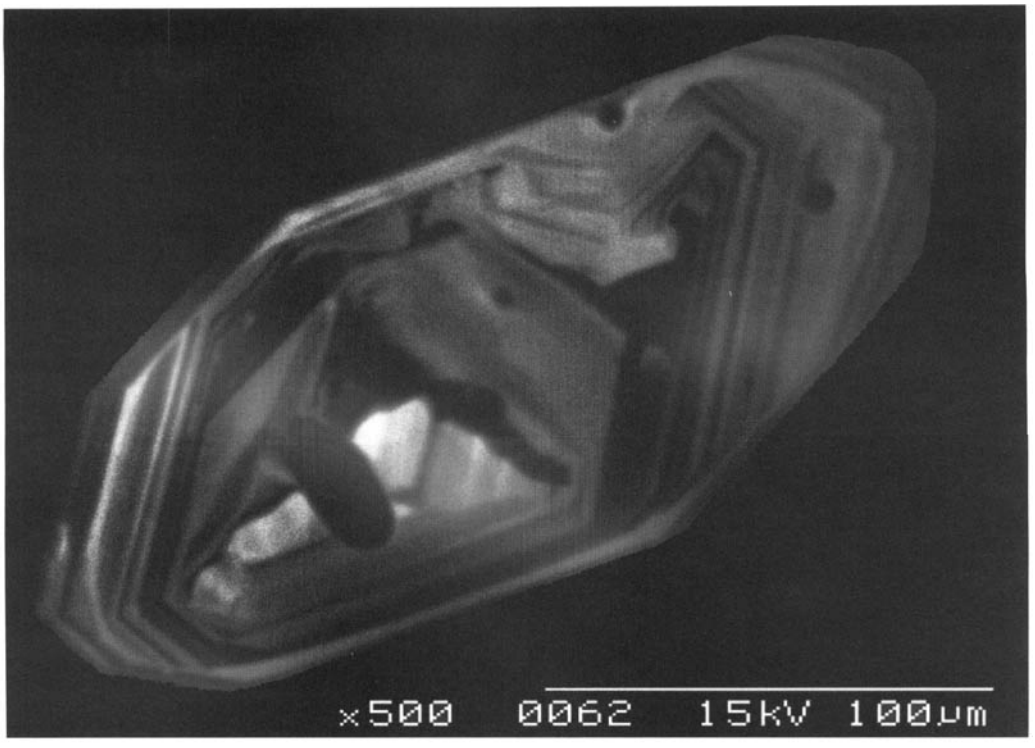

(a)

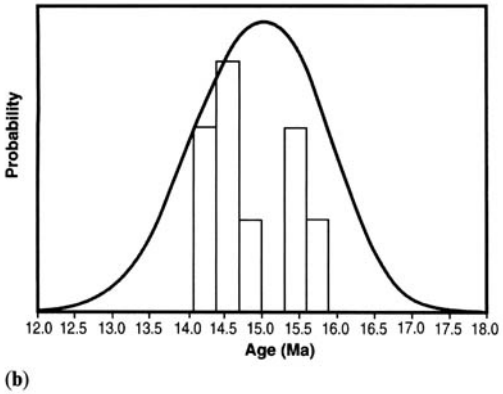

(b)

Fig. 7. (**a**) Cathodeluminescence image of a zircon from sample 021 from N of Satti (Karakoram leucogranite see Fig. 1 for location). (**b**) Histogram of $^{238}U/^{206}Pb$ ages obtained from ion-microprobe analyses of zircons from sample 021; Table 2. The smooth curve indicates the relative probability plot of the data, constructed by assigning an equal-area Gaussian distribution to each analysis and assuming these over the entire age range.

(Weinberg & Dunlap in press), and we use this information as a control point for the thermal modelling.

We assume that the degassing of argon from the sample in the laboratory and that the closure to argon loss during natural cooling is governed by Fickian diffusion, and that the process is effectively reversible. The modelling provides a non-unique continuous cooling path, discussed below. Although non-unique, it will be seen from the solution that the true thermal path experienced by the sample must fall within narrow limits if the assumption of Fickian diffusion is valid. We interpret the results in terms of cooling through a closure temperature range of about 350–150 °C, the typical closure temperature window accessed by K-feldspar (e.g. Lovera *et al.* 1997). The justification for this procedure, outlined in detail by Lovera *et al.* (1997), is that K-feldspars commonly contain pronounced age gradients which cannot be produced by diffusive loss of argon from a single domain. The analytical procedures were essentially the same as those cited by Weinberg

& Dunlap (in press). The step heating results for 95–411 K-feldspar have been inverted into a time–temperature history following the method of Lovera *et al.* (1989). A multi-diffusion domain solution comprising eight domains, all with activation energies of 54.0 kcal mol^{-1}, has been calculated using the time, temperature and fraction of ^{39}Ar released during the course of the degassing experiment. Using this distribution of model diffusion length scales, and the volume fractions of each length scale, thermal paths were calculated by inputting trial thermal histories and minimizing the differences between the measured and modelled age spectra by manual iteration.

The age spectrum derived from detailed step heating of 95–411 K-feldspar, shown in Fig. 8, shows that the sample was not able to finally close to loss of argon until about 18 Ma. Subsequent to cooling from magmatic temperatures at 60 Ma the sample must have cooled to below *c.* 310 °C by about 40 Ma, indicating a cooling rate of at least 20–30 °C Ma^{-1}. Without this initial rapid cooling good model fits are not possible. For a monotonically declining temperature history, one where there is never reheating between the time of intrusion and about 18 Ma, the sample could have experienced 310 °C as a maximum sustainable temperature for this entire period (thermal history shown in Fig. 8). Significant excursions in temperature from the curve shown in Fig. 8b are permissible. However, for temperature spikes with a duration of *c.* 5 Ma a peak temperature of no more than *c.* 340 °C can be sustained and still allow good model fits. From these simple model calculations it is clear that the sample never experienced temperatures greater than greenschist facies conditions (*c.* 250–450 °C) subsequent to cooling rapidly from magmatic temperatures. Age resolution is lost at 18 Ma, but the subsequent thermal history still has an effect of the model age spectrum. To obtain good model fits we have maintained model temperatures in the greenschist facies range until well after 18 Ma.

It is consistent with our geological observations that these rocks experienced greenschist facies temperatures for long periods. Although alternative models involving reheating are equally as likely to have been responsible for the age gradient preserved in K-feldspar 95–411, reheating for any significant time span (> 5 Ma) is limited to temperatures not exceeding *c.* 340 °C. The contact relationships between the Shyok Fm. and the Ladakh granites suggest that the granites were intruded into a volcano-sedimentary section that was already folded. Regardless of the exact form of the postmagmatic thermal history, it is clear that after cooling to below about 310 °C shortly after intrusion, greenschist facies temperatures were maintained for an extended period between 60 and 18 Ma, and perhaps throughout this whole time span. These results suggest that the greenschist facies assemblages preserved in rocks deformed by the KT, cropping out one or two kilometres to the north, are indicative of the conditions prevailing during most of the deformation.

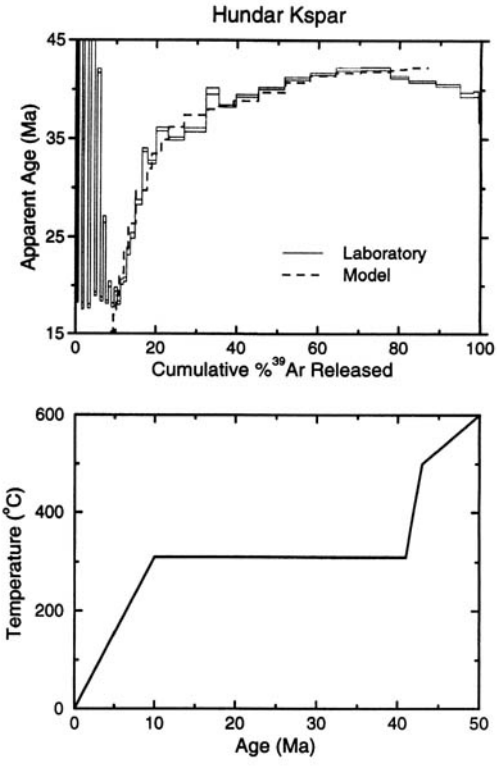

Fig. 8. Age spectrum and thermal history diagrams for K-feldspar sample 95–411. (**a**) Laboratory derived and model age spectra. Note the close fit of the model age spectrum to the laboratory result. (**b**) Thermal history used as input to the modelling program. The calculated domain distribution is combined with the thermal history to produce the theoretical age spectrum model in (a).

Structural analysis

In this section we analyse the structures measured on the Khalsar Thrust (KT) and Karakoram Fault (KF) and derive their possible kinematic relationship. The N60W-striking KT merge with the N30W-striking KF immediately east of the confluence. East of this point the main

strike of the KF changes to N40–45W (Fig. 1b insert) and lineation steepens. We divide the study of the faults into three parts: the KT, the KF west of the confluence (KF–Nubra) and the KF east of the confluence (KF–Shyok). Because the KF–Shyok close to the confluence is mostly covered by Quaternary sediments of the Shyok River, our study of this part concentrates on the area between the Shyok, Darbuk and Tangtse (Fig. 1a), 60 km east of the confluence.

Mineral lineation (chlorite, epidote and quartz) on the KT is generally steep but somewhat shallower than down dip (Fig. 9a), indicating a small dextral component. Thrusting, as observed near Khalsar (Fig. 3), is confirmed by S–C fabric in the greenschists and lineation plunge. A cataclastic rock closest to the thrust contact suggests brittle reactivation. The KT strikes N55–60W/55–60 NE, roughly parallel to penetrative foliation. An outcrop marking the northern limit of the fault zone is characterized by an epidote-rich rock (hydrothermal alteration), where S–C fabric (C = N45W/45SW and S = N45W/65SW) indicates south-side upthrust, parallel to down-dip lineation (Fig. 10). The geometry and sense of shear determined at the north and south margins of the KT (Fig. 10) suggest a flower structure, where rocks within the shear zone have been squeezed upwards.

The N30W KF–Nubra has displaced regional markers dextrally (e.g. Searle *et al.* 1998). Most foliations within the fault zone strike between N30W and N50W, in accordance with dextral shearing. The dip of the foliation within the Nubra Fm. gradually steepens towards the contact with the Karakoram leucogranite, where it is nearly vertical (shown schematically in Fig. 2a). Mineral and stretching lineations as well as crenulation axis are generally 10° from the horizontal (Fig. 9b), and kinematic indicators confirm dextral shearing. The sheared plutonic rocks at Kubed define the Kubed Shear Zone, within which strain varies considerably, and form a band 200–300 m wide of mylonites and where foliation is generally subvertical striking N40–60W. We interpret the Kubed Shear Zone as a splay of the main KF.

The KF–Shyok's main strike is intermediate between that of the KF–Nubra and the KT, at N45W (Fig. 9c). Near Darbuk and Tangtse the shear zone is up to 10 km wide and represents a sharp boundary between rocks of the Ladakh block (Khardung Fm. and Ladakh granitoids) from rocks of the Karakoram terrane. Foliation generally strikes N40–50W but dips vary from 70 SW to subvertical near Shyok village, on the northern part of the shear zone, to 60–70 NE at Tangtse, on the southern edge of the zone (Fig. 9c). Lineation plunges between 50° N and 25° N (more commonly 40–45° N), and over 30 observations of kinematic indicators in the Darbuk and Tangtse gorges, suggest dextral north-side-up sense of shear (including the mylonites limiting the shear zone north and south). Brittle faults in the Darbuk Gorge suggest similar kinematics during brittle deformation. Thus, the KF–Shyok combines elements of both the KT and the KF–Nubra, striking at an intermediate angle and combining roughly equal components of thrusting and dextral strike-slip movement.

Vector analysis

Oblique dextral movement on the KF–Shyok may be interpreted as being partitioned, west of the confluence, into thrusting on the KT and dextral strike-slip on the KF-Nubra (Fig. 9). Whereas the two sections of the KF seem to be kinematically linked and presently active, we have no evidence on the timing of motion on the KT. Thus the KT could either be (a) older and unrelated to the KF, or (b) contemporaneous and kinematically linked to the KF. In order to test whether the faults may all be kinematically linked, we carried out vector analysis of the relative horizontal motion between the three blocks (Fig. 11). We assume that the measured lineations are true measures of the relative motion of blocks at the triple junction, and assume no relative rotation of blocks. At the outset we note that the data for the KF–Shyok define a range of possible horizontal movement directions between the Ladakh (LAD) and Karakoram (KAK) blocks varying from N20W to N60W (Fig. 11b), suggesting internal deformation of the shear zone. Similarly, lineation plunges on the KT (Fig. 9) define a range of possible movement directions, most likely between N30E (down dip) and N15E (thrust with a small dextral component).

For the case of an older KT, relative movement between LAD and the Saltoro Block (SAL) is zero during slip on the KF. In this case the N30W strike-slip motion on the KF–Nubra is maintained along the KF–Shyok and the movement vector SAL–KAK is equal to LAD–KAK (Fig. 11c). Vector analysis indicates that contemporaneous movement on the KT and KF is consistent with the structural data and allows further constraints of their relative motion (we stress, however, that consistency is not proof of their contemporaneity). Structural data from the KT define a NNE-trending vector of undefined length between LAD–SAL. This vector direction constrains the broad range of

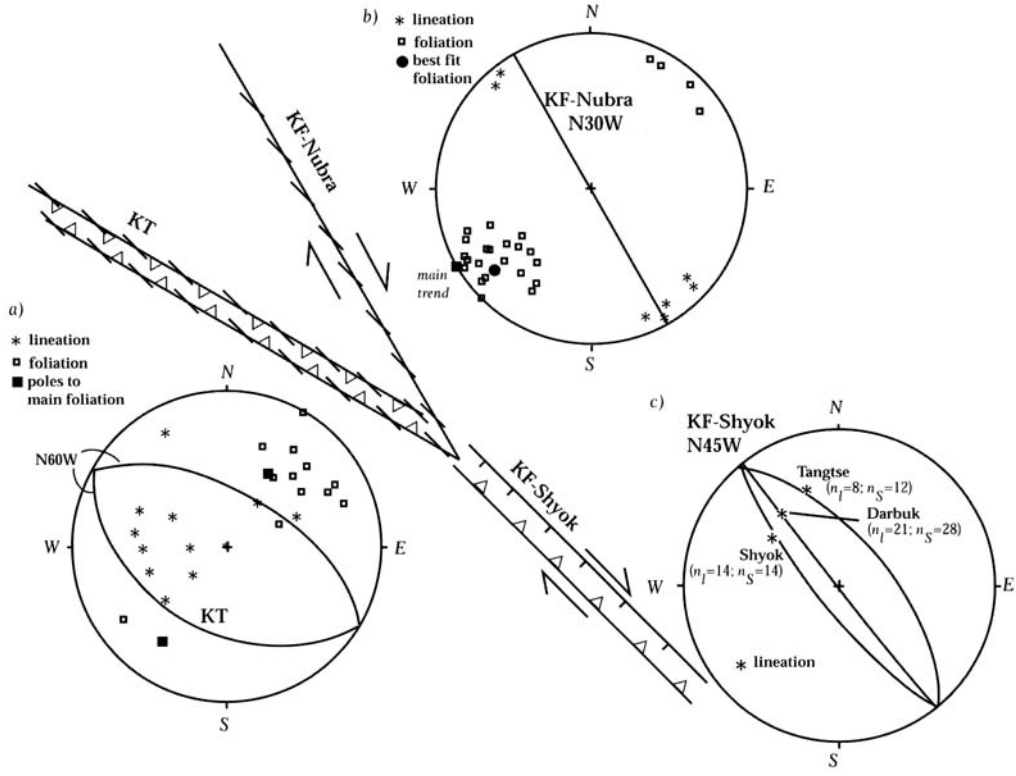

Fig. 9. Summary of the main structural observations in the Nubra–Shyok confluence and lower hemisphere, equal-area stereonet projections of the structural data collected in the three different structural domains. (**a**) Khalsar Thrust between the villages of Khalsar and Deshkit. Poles to foliation tend to plot along a small clockwise angle from the main trend of the thrust zone (solid black square is the pole to one of the two great circles indicating main trend of the KT). Lineation tends to plunge slightly NW of down dip, suggesting a small dextral component on this fault. In (a) lineation plunges close to down dip predominate over shallower plunges, although this is not clear in the figure, because each of these down-dip plunges represents the typical value of long outcrop surfaces, whereas each of the shallower plunges are more anomalous, single measures. (**b**) KF–Nubra between Panamik and Sumur–Tirit. Poles to foliation tend to plot at a small anticlockwise angle from the main trend of the fault zone marked by the great circle. The strike of the foliation in both the KT and KF–Nubra are nearly parallel to each other (*c.* N45W) and are parallel to the main trend of the KF–Shyok (marked in the figure). Each measurement in (b) is the typical value for individual outcrops. (**c**) KF–Shyok between the villages of Shyok–Darbuk–Tangtse and along the Tangtse Gorge (see inset on Fig. 1b for location). This area was divided into three geographical domains, corresponding to the northern margin of the shear zone (Shyok), the core of the zone (Darbuk), and to a 2 km wide band on the southern margin of the zone (Tangtse), and the mean lineation and foliation for each area are plotted. Lineation plunges *c.* 40–45° NNW, and the strike of the foliation is nearly constant at N40W but dips vary systematically from steep SW at the north to moderate NE at the south. Kinematic indicators in all three areas define a dextral, north-side-up movement. Each great circle or lineation is the average value for the data collected in each particular subdivision.

possible movement direction between LAD–KAK to values between N30W and N20W. For increasingly important horizontal movement rates across the KT (longer LAD–SAL vector), the more the relative motion between LAD–KAK is forced towards N20W (more northerly directions are inconsistent with lineation directions in KF–Shyok). These relations allow prediction of the relative motions between the three blocks (Fig. 11c), which may be tested by determining present-day horizontal movement rates across two out of the three faults.

Discussion

Nubra Fm. and Karakoram Fault

Nubra Fm. rocks have been dated as Permian by Thakur *et al.* (1981) and Thakur & Misra (1984), based on fossil fauna recovered from limestones.

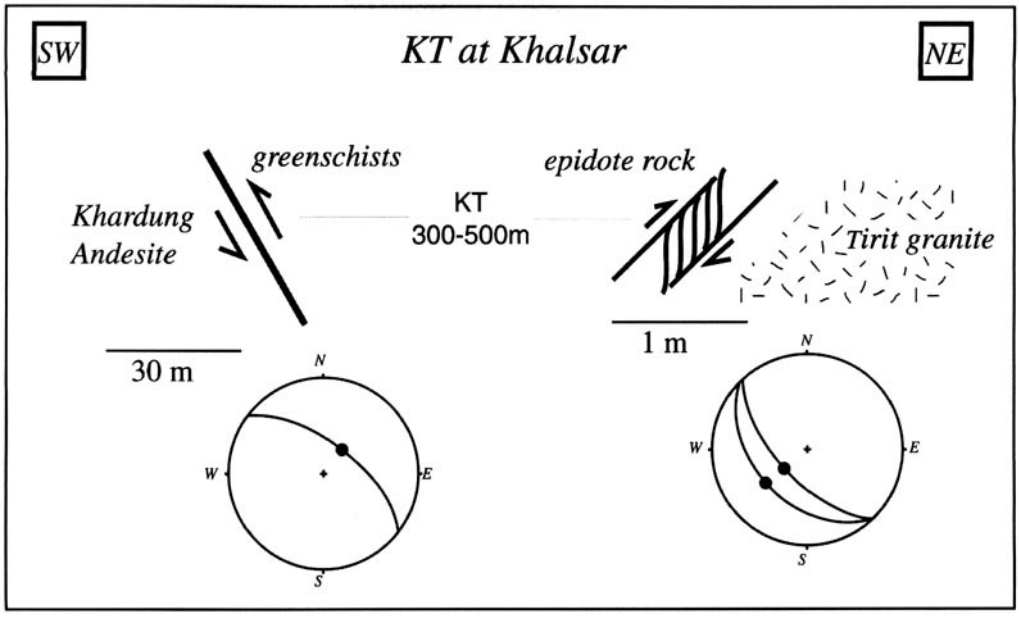

Fig. 10. Schematic summary of the observations defining the flower structure near Khalsar. Contact between the northern margin of the shear zone and Tirit batholith was not observed, but those granitoids crop out tens of metres north of the epidote-rich fault rock.

Rocks of Permian age have also been found within the Shyok Suture Zone (Pudsey 1986) and north of the MKT in Pakistan (Gaetani *et al.* 1990). We have found only minor occurrences of fully recrystallized limestone, which would have lost any evidence of fossils. The Nubra Fm. represents a (disrupted?) volcano-sedimentary sequence intruded by Karakoram leucogranites, neither of which have been found south of the KF. The lack of ultramafic rocks and chert argue against it being a disrupted ophiolite sequence. The intrusive contacts between the Karakoram leucogranite and Nubra Fm., and the apparent absence of Karakoram leucogranites in the northern Saltoro Range, suggest that the Nubra Fm. belongs to the Karakoram terrane and that this terrane was tectonically placed in contact with rocks of the Saltoro Range, which record a different geological history. If this interpretation is correct, there must be another fault, possibly brittle, between the Nubra Fm. and the Tirit batholith to the west. In Searle *et al.* (1998), we used the lack of Karakoram granites south of the KF to argue that faulting should have started after intrusion of the 18 Ma leucogranite (age of the Karakoram leucogranite at Tangtse). The 15 Ma age of the Satti (Karakoram) leucogranite suggests an even later initiation of the KF.

KF–Shyok—sense of shear

In Searle *et al.* (1998), we have suggested that the high-grade rocks of the Pangong Range represent deeper crustal rocks exhumed through transpression between the two strands of the KF at Tangtse. These high-grade rocks are in tectonic contact with medium-grade limestone and shales (with staurolite and garnet), to the north of the fault, and weakly metamorphosed rocks of the Ladakh block to the south. The north-side-up and dextral sense of movement determined here throughout the width of the KF–Shyok is similar to that interpreted from one fault escarpment, caused by Quaternary earthquake on the north (Pangong) strand of the KF (Brown & Molnar pers. comm.). These observations imply that rocks north of the fault should be deeper and hotter than those within the KF–Shyok and not medium-grade rocks. This contradiction needs to be further investigated. A more complex faulting history is suggested by de Terra's (1932) observation that the medium-grade rocks north of the KF–Shyok form only a narrow band, followed northwards by high-grade rocks intruded by Karakoram leucogranites.

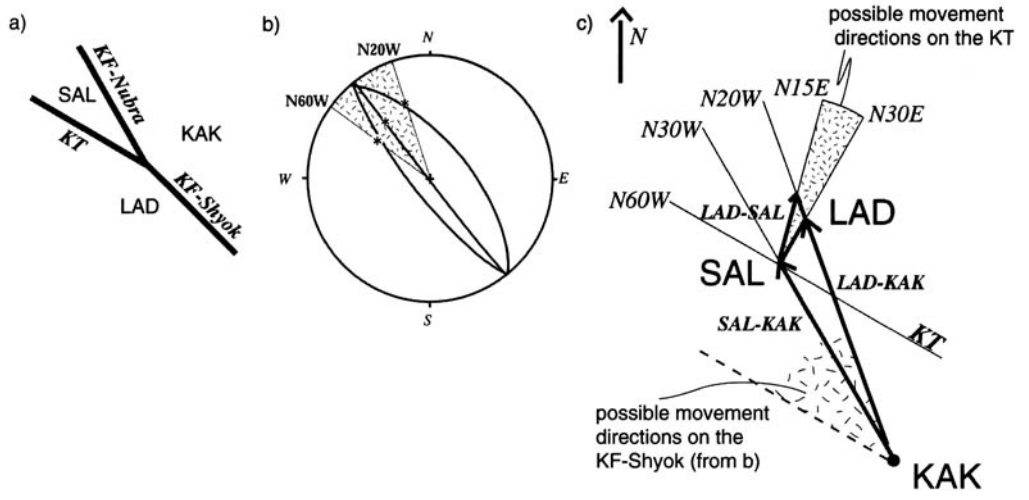

Fig. 11. (**a**) Three blocks and triple point defined by the intersection between the KT, KF–Nubra and KF–Shyok. (**b**) Horizontal projection of the average lineation of the three structural domains of the KF–Shyok, constraining the possible range of horizontal movement direction between LAD and KAK to between N20W and N60W (dashed region; also indicated in c). (**c**) Vector analysis of the triple junction. The dimensions of the vectors between the blocks are unknown, thus the analysis can only yield vector orientation and relative length of these vectors assuming the KAK–SAL vector is unity. For inactive KT during KF slip, the vector LAD–SAL is zero, and the horizontal displacement rate between LAD–KAK is equal to that between the SAL–KAK. For an active KT, LAD–SAL vector trends between N15E and N30E (as constrained by lineation; stippled area) and constrains the movement vector direction LAD–KAK to N30W–N20W. The two small arrows between SAL and LAD indicate a range of possible LAD–SAL vector lengths, from zero (KT inactive), to a maximum length of 0.22 to 0.31 (depending on whether we take the N30E or N15E orientation limits, respectively). The vector LAD–KAK varies from being unity (equal to the SAL–KAK vector, no thrusting on the KT) to a maximum of 1.24 (24% faster than SAL–KAK).

Suture zone and terrane boundary

Although all suture zones are terrane boundaries, not all terrane boundaries are suture zones. Northern Ladakh is an excellent example of this difference. A suture zone defines the region where two continents collided. Suture zones are generally characterized by the presence of heavily sheared and tectonically disaggregated marine sediments and oceanic crust separating terranes of entirely different histories. However, what defines a suture zone is not the presence of marine/oceanic rocks, but the fact that it represents the actual collision site. Thus, whereas the SSZ described in Baltistan represents a suture zone, the sharp terrane boundary between the Ladakh and Karakoram blocks across the KF–Shyok is not the site of suturing, but a boundary caused by post-suturing strike-slip.

Several authors suggested the presence of the Shyok Suture Zone near the confluence area. We were unable to find such rocks. Neither the Nubra Fm. nor the Shyok Fm. and its sheared equivalents within the KT define the suture zone. This suggests that the SSZ runs north of the KT. Srimal (1986*a*, *b*) described the Biagdang ophiolite immediately north of the KT, on the southern slopes of the Saltoro Range. This ophiolite is an obvious candidate for the suture zone, but although we have not been able to reach that area, we are not entirely satisfied that the rocks he described are from an ophiolite. This is partly because Srimal, and most other workers that described these rocks, have presented little data to support their interpretations, partly because authors very often contradict one another, and partly because our few observations on the Saltoro Range contradict Srimal's observations. For example, the map of Rai (1982) shows flysch and molasse where Srimal (1986*a*, *b*) mapped the ophiolite. In Kubed on the northeastern slopes of the Saltoro, where Srimal described the Saltoro ophiolite, we found a sequence of sheared granitoids, diorites and gabbros and cumulitic pyroxenite, all apparently related to Tirit magmatism and not to an ophiolitic sequence.

Descriptions of the geology of the Saltoro Range suggest that its post-75 Ma evolution is similar to that of the northern Ladakh Range. Within the Saltoro Range, Rai (1982) describes a reddish-brown volcanic rock forming dykes and volcanic layers, characterized by random

distribution of euhedral plagioclase phenocrysts in fine ground mass, similar to our Khardung Andesite Unit. Furthermore, Srimal (1986*a*, p. I–10) describes rocks similar to the Khardung Fm. on the Saltoro Range, as well as granitoids (Tirit?) intruding the basic–ultrabasic sequence of the south Saltoro Range. More importantly, the 68 ± 1 Ma crystallization age of our Tirit sample coincides with the age range of Ladakh granitoids, and field relations suggest that the Ladakh and Tirit batholiths may be part of the same magmatic event. We conclude that, if the basic–ultrabasic rocks of the Saltoro Range represent a suture zone, suturing must have occurred before *c.* 75 Ma, confirming conclusions from Baltistan and Kohistan (collision estimates ranging between 85 and 100 Ma, e.g. Petterson & Windley 1985, 1992; Pudsey 1986; Hanson 1989; Treloar *et al.* 1989, 1996; Brookfield & Reynolds 1981). In fact, similar granitoid ages have also been found in the Karakoram Range in Pakistan (Rb–Sr isochron age of 63 ± 2 Ma, Debon 1995) and inferred from igneous zircon core ages from the Tangtse leucogranite (cores of 63.0 ± 0.8 Ma (2σ), Fig. 2b and Searle *et al.* 1998). The geology of the Ladakh and Saltoro blocks is in stark contrast to the geology of the Karakoram terrane. The absence of the 18–15 Ma Karakoram leucogranites, south of the KF, suggests that the Karakoram block was far removed from the Ladakh–Saltoro blocks during leucogranite intrusion.

Regional correlations

The MKT was originally defined in Pakistan as the late Tertiary fault that places Karakoram metamorphic rocks (Eurasian rocks) south over the SSZ or Ladakh–Kohistan batholiths (Dras–Kohistan arcs). In Ladakh most previous authors have referred to the Khalsar Thrust as the MKT. However, there is at present insufficient evidence to enable correlation between the KT and the MKT in Baltistan. Neither its age nor the geology of the two blocks across the fault are sufficiently well-known to be able to establish the correlation. From our observations and literature survey, we concluded that at least the post-75 Ma geology of the Ladakh and Saltoro blocks are the same. Furthermore, we found no evidence that could support the presence of ophiolites in the southern Saltoro.

The rock sequence described above may be correlated to those of Baltistan and Kohistan. The Cretaceous Shyok Fm. corresponds to the tholeiitic, Cretaceous Chalt volcanic group (Treloar *et al.* 1996; also named the Hunza Valley volcanic group by Petterson *et al.* 1990) which crops out south of the MKT in Pakistan. The Ladakh batholith is part of the long calc-alkaline igneous belt that to the west is represented by the Kohistan batholith of similar age and composition (Petterson & Windley 1985, 1991). The Khardung Fm, extruded on top of the Ladakh batholith, corresponds in age and composition to the Eocene Dir–Utror Gp of Kohistan (e.g. Tahirkheli *et al.* 1979; Petterson & Windley 1985, 1991; Sullivan *et al.* 1993). The SSZ lies immediately north of the MKT in Kohistan and Baltistan and most likely follows east towards the KF and crops out somewhere within the Saltoro Range. The less competent volcanic and sedimentary rocks lying in between the Ladakh and Karakoram batholiths were intensely deformed and disrupted by the KF. At the confluence the two batholiths are separated only by the narrow strip of sheared rocks of the Nubra Fm., as opposed to a *c.* 30 km wide band of a range of rock types in Baltistan.

Correlation between Ladakh and southwestern Tibet is somewhat complicated by faulting and shearing as well as sparse data. The Ladakh batholith continues east across the KF into Tibet as a broad arc known as the Transhimalaya (Gangdese) batholith. The Ladakh batholith is cut by the KF, which displaces its original arc by approximately 150 km (Searle 1996). The Karakoram leucogranite, trending at a high angle to the KF in Pakistan, turns to become parallel to the KF in the Nubra valley. It follows the north side of the fault for approximately 150 km and then deviates from it to follow the more westerly regional trend, south of the Chang Chenmo River and north of the Pangong Lake (see Fig. 1a). Its easternmost limit is unknown at present. It is important to notice that both the Ladakh batholith and Karakoram leucogranite become parallel to the KF, the former running on its southern side and the latter on its northern side.

We have found no ophiolite remnants within the narrow deformation corridor separating the Ladakh and Karakoram batholiths, suggesting that the KF cuts across the suture zone. The Shyok Suture Zone counterpart in Tibet is the Pangong (Bangong)–Nujiang Suture Zone (Searle 1996). It crops out immediately south of the eastern Pangong Lake (e.g. Ratschbacher *et al.* 1994; Matte *et al.* 1996) and forms a long belt which can be followed to Amdo, 1200 km to the east. This suture zone is the first suture zone north of the Indus Suture Zone and separates the Changtang and Lhasa blocks. Near Amdo, fossil dating in the sediments transgressing the suture zone suggests that suturing occurred in the late Jurassic–early Cretaceous age (Girardeau *et al.*

1984), considerably earlier than the estimated suturing time in Kohistan (100–80 Ma). In Searle *et al.* (1998), we estimated that dextral movement on the KF was approximately 150 km by determining the southernmost outcrop of Karakoram leucogranites on the NE side of the fault and matching it to the southernmost outcrop of leucogranite on the SW side. Roughly the same value is found for the displacement of the Ladakh batholith. However, the fact that the two batholiths deviate from their regional trend to run parallel to the KF must imply that they were deformed internally, and not simply cut across by the fault. Interestingly, moving the fault back by 150 km, the Pangong–Nujiang Suture Zone becomes juxtaposed to the Saltoro Range, the expected location of the SSZ. Future work should concentrate on mapping the Saltoro Range, and the internal deformation of these two granite belts.

Conclusion

Regional tectonic reconstructions require a suture zone between the Kohistan–Dras arcs and the southern margin of Eurasia. We have not found evidence of this suture zone in the confluence area. Neither the Shyok Fm. nor the Nubra Fm., previously described as dismembered ophiolitic sequences, bear any evidence of including ophiolites. The former, with its graded-bedded sandstones interlayered with basalts, is probably part of the Dras island arc, whereas the metavolcanic rocks (including dacites) and metapelites of the latter represent the disrupted country rock of the Karakoram batholith and not a dismembered ophiolite sequence. The Khalsar Thrust shears rocks that can be directly linked in the field with the Shyok Fm. and Ladakh granitoids. North of the KT, in the southern slopes of the Saltoro Range, Srimal (1986*b*) and Srimal *et al.* (1987) described the Biagdang ophiolitic sequence. We have presented some observations that cast some doubt on that interpretation. An alternative location for the SSZ is the northern part of the Saltoro Range or along the Saltoro River. The presence of 60 ± 10 Ma granitoids north and south of the KT and KF suggests that the Dras–Kohistan island arc was already accreted to Eurasia by that time. The KF initiated after intrusion of the Karakoram leucogranite at 18–15 Ma. Movement on this young fault has juxtaposed the Ladakh and Saltoro blocks to the Karakoram terrane and thus the KF marks a terrane boundary. Vector analysis, using structural data from the KT and the two domains of the KF (KF–Nubra and –Shyok), suggests that these faults may be contemporaneous and kinematically linked. If this is so, oblique movement recorded by the N40–50W KF–Shyok is partitioned to thrusting along the N60W-striking KT and dextral strike-slip along the N30W-striking KF–Nubra. By removing 150 km of dextral displacement accumulated on the KF, the main trend of the Karakoram leucogranite and Ladakh (Transhimalaya) batholith become continuous across the fault, and the Pangong (Bangong)–Nujiang Suture Zone is moved roughly to the expected location of the Shyok Suture Zone.

We would like to thank the support provided by Profs D. Green and I. McDougall and Dr R. Griffiths. We would like to thank Simon Lamb for discussions on vector analysis and Mike Searle and Peter Molnar for discussion on the Karakoram Fault and field assistance. We would also like to thank careful and enlightened reviews of the paper by Mike Petterson and Asif Khan. RFW would also like to acknowledge the financial support of a European Community grant ERBFMBICT960583.

References

ALLÈGRE, C. J., CORTILLOT, V., TAPPONIER, P. & 31 OTHERS. 1984. Structure and evolution of the Himalaya–Tibet orogenic belt. *Nature*, **307**, 17–22.

ALLEN, T. & CHAMBERLAIN, P. C. 1991. Petrologic constraints on the tectonic history of the northern Shyok suture and the main Karakorum Thrust, Baltistan, Northern Pakistan. *Journal of Metamorphic Geology*, **9**, 403–418.

BECK, R. A., BURBANK, D. W., SERCOMBE, W. J. & 11 OTHERS. 1995. Stratigraphic evidence for an early collision between northwest India and Asia. *Nature*, **373**, 55–58.

BOSSART, P. & OTTIGER, R. 1989. Rocks of the Muree formation in northern Pakistan: indicators of a descending foreland basin of late Paleocene to middle Eocene age. *Eclogae Geologicae Helvetiae*, **82**, 133–165.

BROOKFIELD, M. E. & REYNOLDS, P. H. 1981. Late Cretaceous emplacement of the Indus suture zone ophiolitic melange and an Eocene–Oligocene magmatic arc on the northern edge of the Indian plate. *Earth and Planetary Science Letters*, **55**, 157–162.

—— & REYNOLDS, P. H. 1990. Miocene 40Ar/39Ar ages from the Karakoram Batholith and Shyok Mélange, northern Pakistan, indicate late Tertiary uplift and southward displacement. *Tectonophysics*, **172**, 155–167.

CLAOUÉ-LONG, J. C., COMPSTON, W., ROBERTS, J. & FANNING, C. M. 1995. Two Carboniferous ages: a comparison of SHRIMP zircon dating with conventional zircon ages and 40Ar/39Ar analysis. *In:* BERGGREN, W. A., KENT, D. V., AUBRY, M.-P. & HARDENBOL, J. (eds) *Geochronology Time*

Scales and Global Stratigraphic Correlation. Society for Sedimentary Geology, Special Publications, 3–21.

COWARD, M. P., BROUGHTON, R. D., LUFF, I. W., PETTERSON, M. G., PUDSEY, C. J., REX, D. C. & KHAN, M. A. 1986. Collision tectonics in the NW Himalayas. *In*: COWARD, M. P. & RIES, A. C. (eds) *Collision Tectonics*. Geological Society, London, Special Publications, **19**, 203–219.

DAINELLI, G. 1933–1934. *La Serei dei Terreni, Spedizione Italiana De Filippi 1913–1914, Ser. II, Vol. 2, Parte I, II.*

DE TERRA, H. 1932. *Geologische forschungen im westlichen K'un-Lun und Karakorum-Himalaya*, in *Wissenschaftliche ergebnisse der Dr Trinkler schen Zentralasien-expedition*. Dietricht Reimer.

DEBON, F. 1995. Incipient India–Eurasia collision and plutonism: the Lower Cenozoic Batura granites (Hunza Karakorum, North Pakistan). *Journal of the Geological Society, London*, **152**, 785–795.

FISCHER, F., OBERLI, F. & MEIER, M. 1989. Zircon dating of Oligocene and Miocene bentonites by the U–Pb method. *EUG V Abstracts Volume*, 419.

GAETANI, M., GARZANTI, E., JADOUIL, F., NICORA, A., TINTORI, A., PASINI, M. & KHAN, K. S. A. 1990. The north Karakorum side of the Central Asia geopuzzle. *Geological Society of America, Bulletin*, **102**, 54–62.

GANSSER, A. 1980. The division between Himalaya and Karakorum. *Geological Bulletin, University of Peshawar, Special Issue*, **13**, 9–22.

GIRARDEAU, J., MARCOUX, J., ALLEGRE, C. J., BASSOULLET, J. P., YOUKING, T., *et al.* 1984. Tectonic environment and geodynamic significance of the Neo-Cimmerian Donqiao ophiolite, Bangong–Nujiang suture zone, Tibet. *Nature*, **307**, 27–31.

HANSON, C. R. 1989. The northern suture in the Shigar valley, Baltistan, northern Pakistan. *In*: MALINCONICO, L. L. & LILLIE, R. J. (eds) *Tectonics of the Western Himalaya*. Geological Society of America, Special Paper, **232**, 203–215.

HEDIN, S. 1907. *Scientific results of a journey in Central Asia 1899–1902, Vol. VI–2 Geology*, Lithographic Institute of the General Staff of the Swedish Army, Stockholm.

HONEGGER, K., DIETRICH, V., FRANK, W., GANSSER, A., THÖNI, M. & TROMMSDORFF, V. 1982. Magmatism and metamorphism in the Ladakh Himalayas (the Indus–Tsangpo suture zone). *Earth and Planetary Science Letters*, **60**, 253–292.

LEMENNICIER, Y., LE FORT, P., LOMBARDO, B., PÊCHER, A. & ROLFO, F. 1996. Tectonometamorphic evolution of the central Karakorum (Baltistan, northern Pakistan). *Tectonophysics*, **260**, 119–143.

LOVERA, O. M. R., GROVE, M., HARRISON, T. M. & MAHON, K. I. 1997. Systematic analysis of K-feldspar $^{40}Ar/^{39}Ar$ step heating results. I. Significance of activation energy determination. *Geochimica et Cosmochimica Acta*, **61**, 3171–3192.

——, RICHTER, F. M. & HARRISON, T. M. 1989. $^{40}Ar/^{39}Ar$ thermochronology for slowly cooled samples having a distribution of diffusion domain sizes. *Journal of Geophysical Research*, **94**, 17917–17936.

MATTE, P., TAPPONNIER, P., ARNAUD, N., BOURJOT, L., AVOUAC, J. P. *et al.* 1996. Tectonics of Western Tibet, between Tarim and the Indus. *Earth and Planetary Science Letters*, **142**, 311–330.

MOLNAR, P. & TAPPONNIER, P. 1975. Cenozoic tectonics of Asia, effects of a continental collision. *Science*, **189**, 419–426.

PARRISH, R. R. & TIRRUL, R. 1989. U–Pb age of the Baltoro granite, northwest Himalaya, and implications for monazite U–Pb systematics. *Geology*, **17**, 1076–1079.

PELTZER, G. & TAPPONNIER, P. 1988. Formation and evolution of strike-slip faults, rifts, and basins during the India–Asia collision: an experimental approach. *Journal of Geophysical Research*, **93**, 15085–15117.

PETTERSON, M. G. & WINDLEY, B. F. 1985. Rb–Sr dating of the Kohistan arc-batholith in the Trans-Himalaya of north Pakistan, and tectonic implications. *Earth and Planetary Science Letters*, **74**, 45–57.

—— & —— 1991. Changing source regions of magmas and crustal growth in the Trans-Himalayas: evidence from the Chalt volcanics and Kohistan batholith, Kohistan, northern Pakistan. *Earth and Planetary Science Letters*, **102**, 326–341.

—— & —— 1992. The field relationships, geochemistry and petrogenesis of the Cretaceous basalt Jutal dyke suite, Kohistan, N. Pakistan. *Journal of the Geological Society, London*, **149**, 107–114.

——, —— & LUFF, I. W. 1990. The Chalt volcanics, Kohistan, Pakistan, high-Mg tholeiitic and low-Mg calc-alkaline volcanism in a Cretaceous island arc. *Physics and Chemistry of the Earth*, **17**, 19–30.

PUDSEY, C. J. 1986. The Northern Suture, Pakistan: margin of a Cretaceous island arc. *Geological Magazine*, **123**, 405–423.

RAI, H. 1982. Geological evidence against the Shyok palaeo-suture, Ladakh Himalaya. *Nature*, **297**, 142–144.

RATSCHBACHER, L., FRISCH, W., LIU, G. & CHEN, C. 1994. Distributed deformation in southern and western Tibet during and after the India–Asia collision. *Journal of Geophysical Research*, **99**, 19917–19945.

RAZ, U. & HONEGGER, K. 1989. Magmatic and tectonic evolution of the Ladakh Block from field studies. *Tectonophysics*, **161**, 107–118.

ROWLEY, D. B. 1996. Age of initiation of collision between India and Asia: a review of stratigraphic data. *Earth and Planetary Science Letters*, **145**, 1–13.

SCHÄRER, U., COPELAND, P., HARRISON, T. M. & SEARLE, M. P. 1990. Age, cooling history and origin of post-collisional leucogranites in the Karakoram batholith: A multi system isotope study of north Pakistan. *Journal of Geology*, **98**, 233–251.

——, HAMET, J. & ALLÈGRE, C. J. 1984. The Transhimalaya (Gangdese) plutonism in the Ladakh region: U–Pb and Rb–Sr study. *Earth and Planetary Science Letters*, **67**, 327–339.

SEARLE, M. P. 1991. *Geology and tectonics of the Karakoram mountains*. John Wiley & Sons, Chichester.

—— 1996. Geological evidence against large-scale pre-Holocene offsets along the Karakoram Fault: Implications for the limited extrusion of the Tibetan plateau. *Tectonics*, **15**, 171–186.

——, CRAWFORD, M. B. & REX, A. J. 1992. Field relations, geochemistry, origin and emplacement of the Baltoro granite, Central Karakoram. *Transactions of the Royal Society of Edinburgh: Earth Sciences*, **83**, 519–538.

——, REX, A. J., TIRRUL, R., REX, D. C. & BARNICOAT, A. 1989. Metamorphic, magmatic and tectonic evolution of the Central Karakoram in the Biafo–Baltoro–Hushe regions of N. Pakistan. *In*: MALINCONICO, L. L. & LILLIE, R. J. (eds) *Tectonics of the Western Himalayas*. Geological Society of America, Special Paper, **232**, 47–74.

——, WEINBERG, R. F. & DUNLAP, W. J. 1998. Transpressional tectonics along the Karakoram Fault Zone, northern Ladakh. *In*: HOLDSWORTH, R. E. & STRACHAN, R. A. (eds) *Continental Transpressional and Transtensional Tectonics*. Geological Society, London, Special Publications, **135**, 307–326.

SHARMA, K. K. & KUMAR, S. 1978. Contribution to the geology of Ladakh, north western Himalaya. *Himalayan Geology*, **8**, 252–287.

SRIMAL, N. 1986*a*. *Geology and oxygen and $^{40}Ar/^{39}Ar$ isotopic study of India–Asia collision in the Ladakh and Karakoram Himalaya, NW India*. PhD thesis, University of Rochester.

—— 1986*b*. India–Asia collision: implications from the geology of the eastern Karakoram. *Geology*, **14**, 523–527.

——, BASU, A. R. & KYSER, T. K. 1987. Tectonic inferences from oxygen isotopes in volcano-plutonic complexes of the India–Asia collision zone, NW India. *Tectonics*, **6**, 261–273.

STACEY, J. S. & KRAMERS, J. D. 1975. Approximation of terrestrial lead isotope evolution by a two-stage model. *Earth and Planetary Science Letters*, **26**, 207–221.

SULLIVAN, M. A., WINDLEY, B. F., SAUNDERS, A. D., HAYNES, J. R. & REX, D. C. 1993. A palaeogeographic reconstruction of the Dir Group: Evidence for magmatic arc migration within Kohistan, N. Pakistan. *In*: TRELOAR, P. J. & SEARLE, M. P. (eds) *Himalayan Tectonics*. Geological Society, London, Special Publications, **74**, 139–160.

TAHIRKHELI, R. A. K., MATTAUER, M., PROUST, F. & TAPPONNIER, P. 1979. The India–Eurasia suture zone in northern Pakistan, some new data for an interpretation of plate scale. *In*: FARAH, A. & DEJONG, K. A. (eds) *Geodynamics of Pakistan*. Geological Survey of Pakistan, Quetta, 125–130.

THAKUR, V. C. & MISRA, D. K. 1984. Tectonic framework of the Indus and Shyok suture zones in eastern Ladakh, northwest Himalaya. *Tectonophysics*, **101**, 207–220.

——, VIRDI, N. S., RAI, H. & GUPTA, K. R. 1981. A note on the geology of Nubra–Shyok area of Ladakh, Kashmir, Himalaya. *Journal of the Geological Society of India*, **22**, 46–50.

TRELOAR, P. J., GUISE, P. G., COWARD, M. P., SEARLE, M. P., WINDLEY, B. F. *et al.* 1989. K–Ar and Ar–Ar geochronology of the Himalayan collision in NW Pakistan: constraints on the timing of suturing, deformation, metamorphism and uplift. *Tectonics*, **8**, 881–909.

——, PETTERSON, M. G., JAN, M. Q. & SULLIVAN, M. A. 1996. A re-evaluation of the stratigraphy and evolution of the Kohistan arc sequence, Pakistan Himalaya: implications for magmatic and tectonic arc-building processes. *Journal of the Geological Society, London*, **153**, 681–693.

WEINBERG, R. F. 1997. The disruption of a diorite magma pool by intruding granite: the Sobu body, Ladakh Batholith, Indian Himalayas. *Journal of Geology*, **105**, 87–98.

—— & DUNLAP, W. J. in press. Growth and deformation of the Ladakh Batholith, NW Himalayas: implications for timing of continental collision and origin of calc-alkaline batholiths. *Journal of Geology*.

WHITEHOUSE, M. J., CLAESSON, S., SUNDE, T. & VESTIN, J. 1997. Ion-microprobe U–Pb zircon geochronology and correlation of Archaean gneisses from the Lewisian Complex of Gruinard Bay, northwest Scotland. *Geochimica et Cosmochimica Acta*, **61**, 4429–4438.

WIEDENBECK, M., ALLÉ, P., CORFU, F., GRIFFIN, W. L., MEIER, M. *et al.* 1995. Three natural zircon standards for U–Th–Pb, Lu–Hf, trace element and REE analysis. *Geostandards Newsletter*, **19**, 1–23.

ZECK, H. P. & WHITEHOUSE, M. J. in press. Hercynian, Pan-African, Proterozoic and Archean ion-microprobe zircon ages for a Betic–Rift core complex, Alpine belt, W. Mediterranean-consequences for its P–T–t path. *Contributions to Mineralogy and Petrology*.

This page intentionally left blank

Geological evolution of the Hindu Kush, NW Frontier Pakistan: active margin to continent–continent collision zone

P. R. HILDEBRAND[1], M. P. SEARLE[1], SHAKIRULLAH[2], ZAFARALI KHAN[2] & H. J. VAN HEIJST[1]

[1]*Department of Earth Sciences, Oxford University, Parks Rd, Oxford OX1 3PR, UK*

[2]*Sarhad Development Authority Mineral Exploration, Chitral, Northwest Frontier Province, Pakistan*

Abstract: A geological map of the eastern Hindu Kush, northwest of Chitral, Northern Pakistan, is presented. The lithologies are placed into two main categories, divided by the Tirich Mir Fault Zone. To the northwest, the units of the eastern Hindu Kush are dominated by monotonous sequences of graphite-rich pelitic rocks. Southeast of the fault, the phyllites and diamictites are thought to be lateral equivalents of the Northern Sedimentary Belt of the Karakoram. A structural analysis of the area studied identifies a major, early deformation phase which is usually characterized by tight to isoclinal folding with a well developed axial-planar schistosity. This deformation is thought to have been related to the northward-directed subduction and accretion beneath the southern margin of Asia during the Mesozoic, and may have taken place over a considerable period of time. A major phase of crustal melting at *c.* 24 Ma generated migmatites and biotite + muscovite ± garnet ± tourmaline leucogranites (including dykes and the Gharam Chasma pluton). This age is comparable to that of the Baltoro pluton in the Karakoram to the east, confirming the regional importance of crustal melting along the southern margin of the Asian plate during the earliest Miocene. The crustal melting was associated with thrusting and folding of the earlier schistosity. Subhorizontal stretching lineations indicate a phase of strike-slip deformation that is thought to have been associated with anticlockwise rotation of the regional foliation strike from E to NE and N after the emplacement of the Gharam Chasma pluton at *c.* 24 Ma. This deformation and rotation was probably a direct result of the northward-moving Indian plate forcing Kohistan to indent into Asia, resulting in a left-lateral transpressional tectonic environment which remains today. The anomalous height of the Tirich Mir massif, relative to other peaks in the Hindu Kush and the nearby Hindu Raj, may be accounted for by the onset of this transpression.

Intensely active seismicity to depths of 300 km beneath the Hindu Kush is associated with seismic shear wave velocities that are significantly faster than those beneath Tibet, where earthquake occurrence is restricted to the upper crust, and previous geophysical studies indicate elevated thermal conditions and possible crustal melts. U–Pb ages suggest that post-India–Asia collision crustal melting beneath the Hindu Kush is restricted to *c.* 24 Ma, whereas in the Karakoram, the record is both more voluminous and more continuous from *c.* 37 to *c.* 9 Ma. These observations reflect major differences in the thermal histories of these regions, where the relatively cooler conditions beneath the Hindu Kush are associated with continental subduction-related seismicity.

The eastern Hindu Kush mountain range runs from northeastern Afghanistan to northwestern Pakistan (inset in Fig. 1), linking up with the Hindu Raj Range and then the Karakoram Range to the east. From the Jurassic, the site of these mountain ranges and the Lhasa block of south Tibet was the southern margin of Asia (Searle 1991). Northward-directed subduction took place along this margin, leading to the accretion of the Kohistan–Ladakh island arc along the Shyok Suture Zone (also called the Northern suture) in the early Late Cretaceous (e.g. Pudsey 1986) and of India along the Indus–Tsangpo Suture Zone at *c.* 54–50 Ma (e.g. Searle *et al.* 1987; Beck *et al.* 1995). The eastern Hindu Kush, part of the Asian plate, lies between the northwestern edge of the indenting Indian plate and the southwestern edge of the Pamir orogenic arc. Continued northward drift of India resulted in the underthrusting and subduction of Indian

From: KHAN, M. A., TRELOAR, P. J., SEARLE, M. P. & JAN, M. Q. (eds) *Tectonics of the Nanga Parbat Syntaxis and the Western Himalaya*. Geological Society, London, Special Publications, **170**, 277–293. 1-86239-061-4/00/$15.00

plate lithosphere beneath the Hindu Kush and Pamir, causing the most seismically active zone of intracontinental, intermediate-depth earthquakes known on Earth today (e.g. Billington *et al.* 1977; Burtman and Molnar 1993).

Whilst there is a great deal of information about how the northern margin of India has evolved as a result of the India–Asia collision, much less is known about how the southern margin of the Asian plate has responded. Part of the reason for this is that a large proportion of middle and lower crust of the southern margin of Asia lies buried beneath the sediments and volcanics of south Tibet (the Lhasa block). Consequently, only the along-strike Hindu Kush and the Karakoram at the western end of the collision zone provide suitable exposure to address this problem.

The only significant work carried out in the Gharam Chasma region, northwest of Chitral, has been to examine the economic potential of tungsten and other mineralization (Austromineral 1978; Calkins *et al.* 1981; Leake *et al.* 1989). These workers identified small bodies of unfoliated and foliated leucogranite intruded into medium-grade metasediments. Leake *et al.* (1989) reported two mica ± garnet ± tourmaline mineralogies, similar to the High Himalayan leucogranites, and presumed the metamorphism and the leucogranite formation to be related to crustal thickening following the India–Asia collision. U–Pb ages on monazite, xenotime and uraninite from undeformed samples of the Gharam Chasma leucogranite pluton and a leucogranite dyke that cross-cuts the migmatites indicate that crustal melting occurred at *c.* 24 Ma (Hildebrand *et al.* 1998), synchronous with the Baltoro melting event in the Karakoram to the east (Parrish & Tirrul 1989; Schärer *et al.* 1990).

This paper presents the results of geological mapping carried out in the Gharam Chasma and surrounding areas of the eastern Hindu Kush in 1995 and 1996 (Fig. 1). The geological evolution is discussed with a view to understanding the response of the active margin Asian plate to the India–Kohistan–Asia collisional events.

Lithology

A geological map of the Gharam Chasma and surrounding areas of the eastern Hindu Kush is attached (Fig. 1). The stratigraphy of this area is best considered within the framework provided by Gaetani *et al.* (1996) and Zanchi *et al.* (1997), who distinguish two zones: the units of the eastern Hindu Kush, which lie to the northwest of the Tirich Mir Fault Zone; and the units that are the along-strike equivalent of the Northern Sedimentary Belt of the Karakoram which occur between the Tirich Mir Fault Zone and the Reshun Fault (Fig. 2). The rocks to the east of the Reshun Fault have not been investigated in this study, but have been described by Pudsey *et al.* (1985).

Units northwest of the Tirich Mir Fault Zone

Amphibolite unit. Within the Tirich Mir Fault Zone is a unit composed of amphibolites that outcrops in the Arkari valley, and is not more than a kilometre wide. A similar, but much thinner unit, outcrops in the Lutkho valley, which may or may not be laterally continuous with the Arkari valley unit. These amphibolites are strongly deformed and show evidence of migmatization in places. They consist of hornblende, biotite, plagioclase and sometimes clinopyroxene. Sphene and clinozoisite are common accessories, and late stage carbonate veining is sometimes present in the Arkari valley outcrop. This unit may well be a southwestward extension of the mafic and ultramafic rocks observed in the Rich Gol area to the northwest (e.g. Zanchi *et al.* 1997).

Metapelite unit. The majority of the rocks between the Tirich Mir Fault Zone and the Afghanistan border are metapelites which are often highly graphitic. They are interlayered with occasional quartz-rich lenses, calc-silicates (Fig. 3) and amphibolites. Deformation is moderate in northern and northeastern areas, to intense with isoclinal folding, schistosity development and even migmatization (Fig. 4) in the southwest. Metamorphic grade varies from low, sub-biotite grade black slates, through garnet–staurolite schists to sillimanite and occasionally K-feldspar grade migmatites. No fossils were found in this unit, although there is an unconfirmed report of belemnite remains from near Besti, suggesting a Jurassic age (Tipper, in Pascoe 1924). These lithologies are probably the southwestward continuation of the Wakhan slates, which have yielded Palaeozoic fossils (Hayden 1915; Desio 1963; Kafarskyi & Abdullah 1976; Buchroithner 1980; Gaetani & Leven 1993).

Calc-silicate units. Calc-silicate lenses and units are fairly common, and are part of the black slate–metapelite sequence. One of these units has

Fig. 1. Geological map of the eastern Hindu Kush.

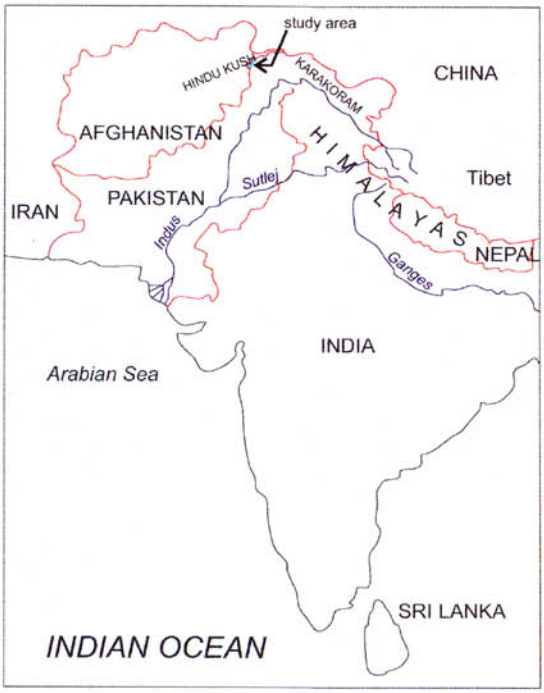

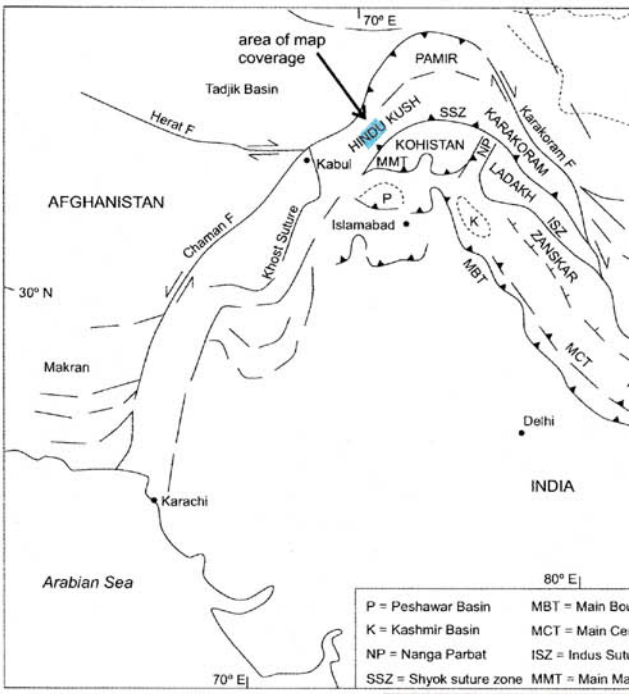

KEY

UNITS OF THE KARAKORAM SOUTHERN METAMORPHIC BELT
(according to Gaetani et al., 1996)

Chitral slates. Monotonous, fairly soft, dark grey slates without bedding. Quartz, illite, chlorite ± albite. Fine, grey sandstone common. Occasional thin ash bed. Very complexly deformed. (Pudsey et al., 1985).

Krinj limestone. Massive to very well banded, grey to cream to white, micritic to finely recrystallised limestone, sometimes with rudist bivalve fragments. It is occasionally brecciated and is locally dolomitic along the western margin. (Pudsey et al., 1985). Probably Early Cretaceous as it contains *Orbitolinas* and rudists (Desio, 1959; Pudsey et al., 1985).

RESHUN FAULT

UNITS OF THE KARAKORAM NORTHERN SEDIMENTARY BELT
(according to Gaetani et al., 1996)

Carbonate rich lithologies with some phyllites, cherts and breccias. The large unit to the immediate NW of the Reshun fault has been called the Sewakht Formation (Leake et al., 1989), and may correlate with the Devonian Shogram Formation to the east (Desio, 1966).

Phyllites. Brown to dark grey fine grained phyllites consisting of quartz, muscovite ± plagioclase ± stilpnomelane ± chlorite ± carbonate ± graphite ± clinozoisite. Strong cleavage and usually highly strained. Sometimes very highly graphitic rocks, particularly adjacent to the Reshun fault. Correlates with the probably Devonian-Permian Lun and Owir shales (Hayden, 1915; Desio, 1966; Vogeltanz, 1969; Talent et al., 1981; Pudsey, 1985).

Phyllites. Green to grey-brown-green fine grained phyllites and some meta-diamictites. Quartz, muscovite ± plagioclase ± stilpnomelane ± chlorite ± carbonate ± graphite ± clinozoisite. Strong cleavage and usually highly strained. Correlates with the probably Devonian-Permian Lun and Owir shales (Hayden, 1915; Desio, 1966; Vogeltanz, 1969; Talent et al., 1981; Pudsey, 1985).

Semi-pelites. Highly strained, isoclinally folded, dark grey-brown psammites. Quartz, plagioclase, biotite, chlorite ± garnet ± muscovite ± epidote/clinzoisite.

TIRICH MIR FAULT ZONE

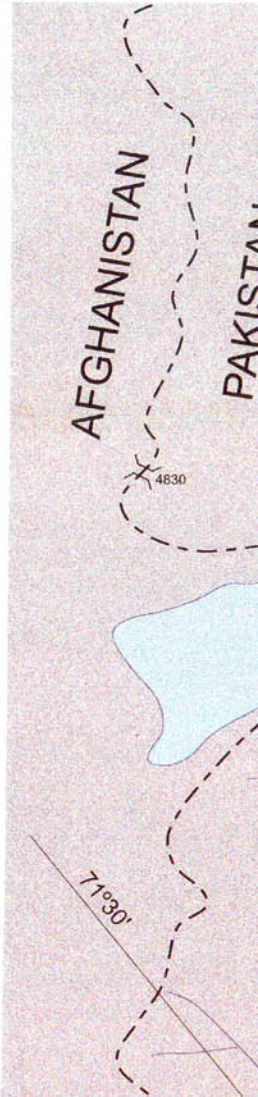

GEOLOGICAL MAP OF THE E
NORTHWEST OF CHITRAL, P

Mapped by Peter Hildebrand in the summers of 1995 and 1996, with additional information fr
Pudsey et al. (1985) and Leake et al. (1987). The location of the structural data (which is all f
extent of coverage by this study. Basemap from Calkins et al. (1981). Magnetic declination ~2

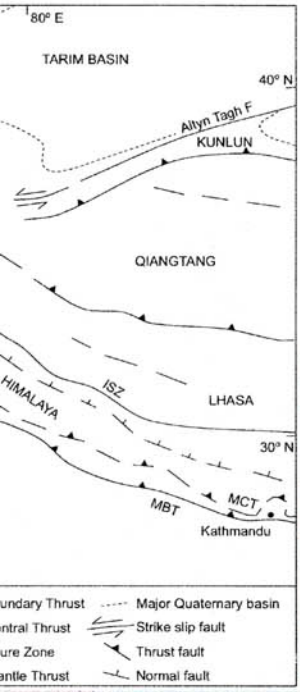

EASTERN HINDU KUSH
PAKISTAN

om Austromineral (1978), Calkins et al. (1981),
rom Hildebrand) gives an indication of the
2°.

N

10 km

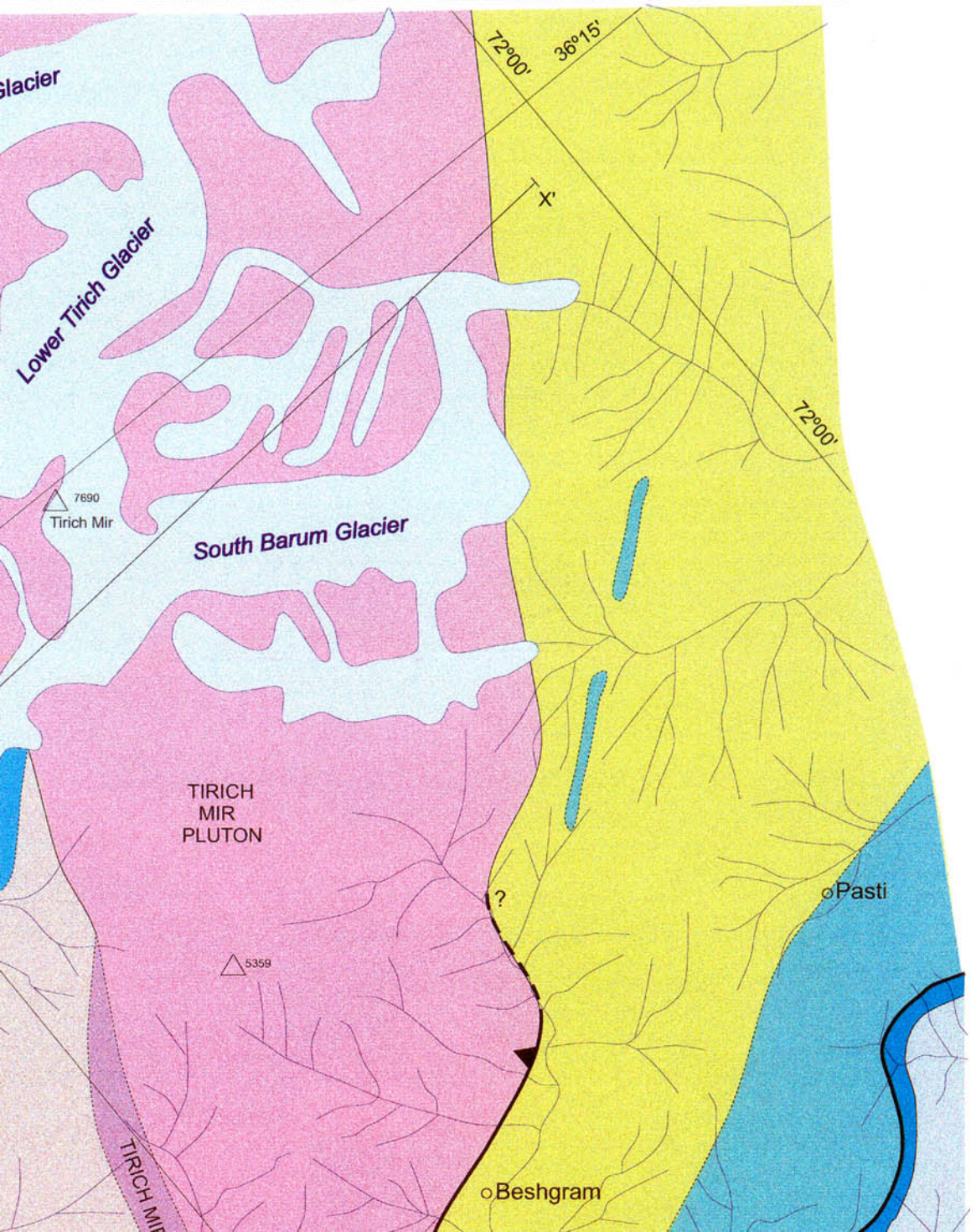

UNITS OF THE EASTERN HINDU KUSH
(according to Gaetani et al., 1996)

Amphibolites. Deformed amphibolite consisting of plagioclase, hornblende, biotite ± clinopyroxene ± orthopyroxene ± sphene ± clinozoisite. It is equigranular and is intruded by the Tirich Mir pluton. Correlate with the amphibolites and serpentinites in Rich Gol area to the northeast (Zanchi et al., 1997).

Metapelites. Variably metamorphosed graphitic pelites, consisting of quartz, plagioclase, graphite ± clay ± chloritoid ± chlorite ± muscovite ± biotite ± garnet ± staurolite ± andalusite ± tourmaline ± kyanite (very rare).Occasional quartz rich lenses, calcsilicates and amphibolites. From NE to SW, deformation and metamorphic grade generally increases. A garnet-staurolite schist from PH113 has U-Pb monazite ages of 126-135 Ma. Protoliths are probably the SW extension of the Wakhan black slates, which contain Permian and Triassic fossils (Kafarskyi and Abdullah, 1976; Buchroithner, 1980). Belemnite remains from near Besti may be Jurassic (Tipper, in Pascoe, 1924).

Sillimanite grade metapelites with quartz, plagioclase ± sillimanite ± muscovite ± biotite ± garnet ± staurolite ± andalusite ± K-feldspar ± tourmaline ± graphite. Occasional calcsilicate and amphibolite bodies. Protoliths may be SW extension of the Wakhan black slates. Abundant pegmatite and leucogranite dykes: a strongly foliated, boudinaged leucogranite dyke (PH054i) has a U-Pb monazite age of ~190 Ma; an unfoliated leucogranite dyke that cross-cuts all fabrics in the same outcrop (PH054f) has a U-Pb monazite and uraninite age of ca. 24 Ma; a syn-deformational pegmatite from the Tirich Mir Fault zone (PH130a) has U-Pb monazite and uraninite ages from 113-124 Ma.

Calcsilicates and carbonates, consisting of combinations of quartz, carbonate, diopside, garnet, epidote, scapolite, muscovite.

Gneiss with amphibolites. Gneiss consists of quartz, plagioclase, biotite and garnet; amphibolite consists of hornblende, plagioclase, biotite ± sphene ± epidote ± quartz.

INTRUSIVE ROCKS

Leucogranites consisting of quartz, K-feldspar, plagioclase, biotite ± muscovite ± tourmaline ± garnet. Includes both foliated (flg) and unfoliated (uflg) varieties. A sample of uflg (PH104) has a U-Pb monazite and xenotime age of ca. 24 Ma.

Equigranular granodiorites and phenocrystic granites. Undeformed to very weakly deformed. Consist of quartz, K-feldspar, plagioclase, biotite ± hornblende ± muscovite. Usually equigranular, but some of the granites contain abundant feldspar phenocrysts.

Porphyritic granodiorites to granites. Weakly to very strongly foliated and augen textured. Consist of quartz, K-feldspar, plagioclase, biotite ± muscovite ± sphene ± epidote/clinozoisite.

STRUCTURAL FEATURES

Contact: defined, approximate/inferred.

Antiform, with plunge.

Synform, with plunge.

Fault (thrust where marked with a triangle): solid = defined, dashed = approximate/inferred.

Foliation strike, dip and dip amount: S0 (bedding); S1 (usually penetrative cleavage/schistosity, except sometimes to the north and northeast where it is spaced); and S2 (usually spaced/fracture cleavage, but sometimes penetrative adjacent to thrusts).

Outcrop scale fold axial planes strike, dip and dip amount: D1 and D2 folds (included where not represented by S1 or S2).

Outcrop scale fold axes trend and plunge amount: D1 and D2 folds.

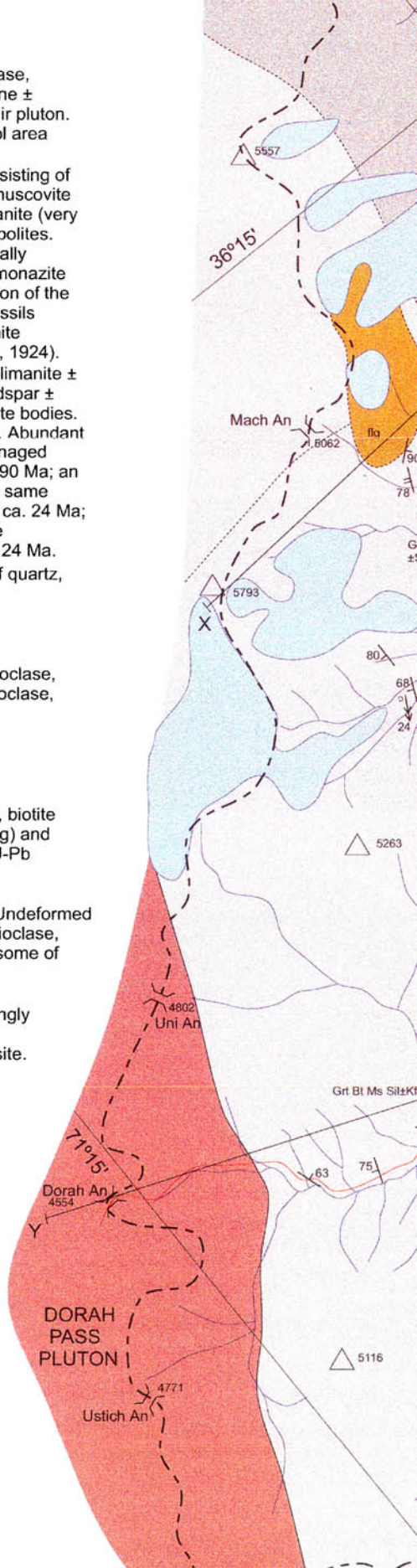

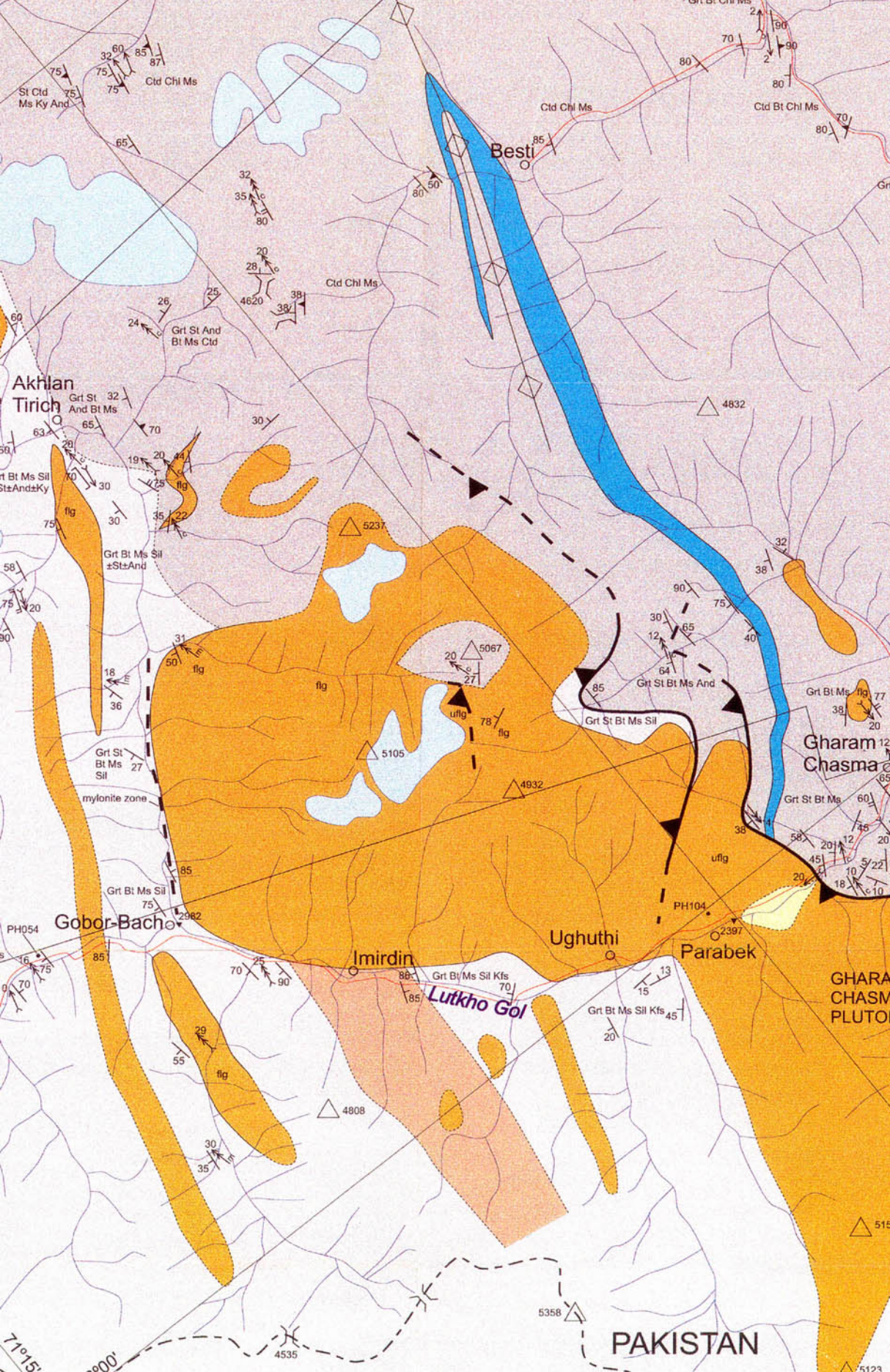
Besti
Ctd Chl Ms
Ctd Bt Chl Ms
St Ctd Ms Ky And
Grt St And Bt Ms Ctd
Akhlan Tirich
Grt St And Bt Ms
Grt Bt Ms Sil ±St±And
flg
4832
5237
5067
5105
4932
Grt St Bt Ms And
Grt St Bt Ms Sil
uflg
Gharam Chasma
Grt St Bt Ms
mylonite zone
Grt Bt Ms Sil
Gobor-Bach
2982
PH054
Imirdin
Grt Bt Ms Sil Kfs
Lutkho Gol
Ughuthi
PH104
2397
Parabek
GHARA CHASM PLUTO
4808
5358
4535
PAKISTAN

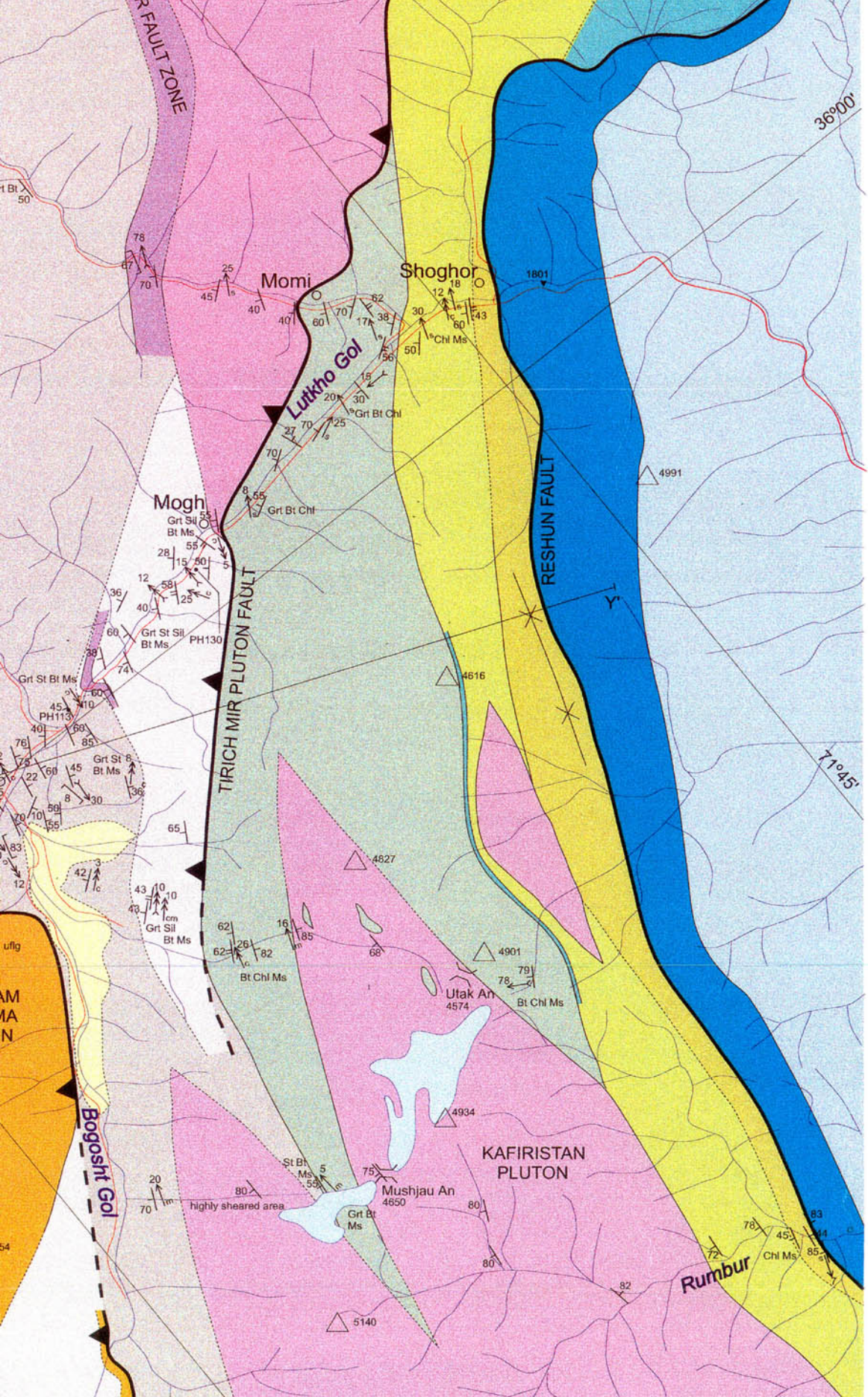
Momi
Shoghor
Lutkho Gol
Mogh
Grt Sil Bt Ms
Grt Bt Chl
Grt St Sil Bt Ms
PH130
Grt St Bt Ms
PH113
Grt St Bt Ms
TIRICH MIR PLUTON FAULT
RESHUN FAULT
Y'
4991
4616
4827
4901
Utak An
4574
Bt Chl Ms
4934
KAFIRISTAN PLUTON
Mushjau An
4650
Grt Bt Ms
highly sheared area
5140
Bogosht Gol
Rumbur
Chl Ms
1801
36°00'
71°45'

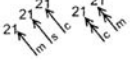

Lineations trend and plunge amount: D1 and D2; s = striation (L1-3 in text), c = crenulation, m = mineral (sillimanite in metapelites; aggregates of quartz, feldspar & biotite in the Kafiristan pluton, referred to as L1-3 in text).

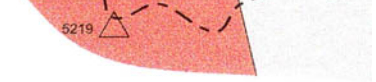

METAMORPHIC MINERALS

Grt St Ms Bt — Diagnostic metamophic mineral assemblage for metapelites: Ms = muscovite, Chl = chlorite, Ctd = chloritoid, Bt = biotite, Grt = garnet, St = staurolite, And = andalusite, Ky = kyanite, Sil = sillimanite, Kfs = K-feldspar.

OTHER FEATURES

Quaternary or Recent gravels.

Permanent snow and ice cover, including glaciers.

PH104 • — U-Pb age sample location.

△ 4900 — Mountain summit with height in metres.

2572 — Spot height in metres.

Birzin An 4593 — Pass with height in meters.

Arkario — Village.

Arkari Gol — River.

International boundary.

Road or track - usually passable in summer with 4 wheel drive.

WEST
X

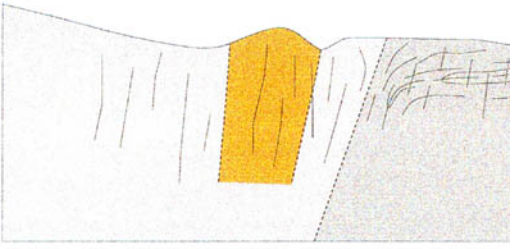

WEST
Y

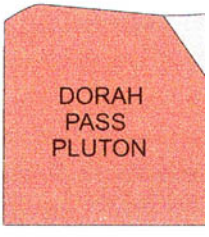

AFGHANISTAN

4859

Birzin An
4593

4900

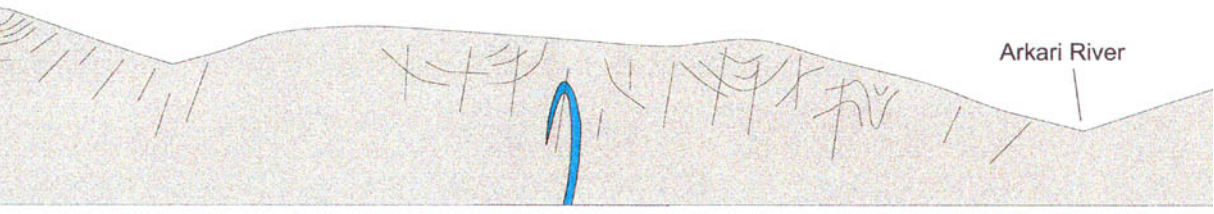

CROSS SECTIONS: HORIZONTAL SCALE = VERTICAL S

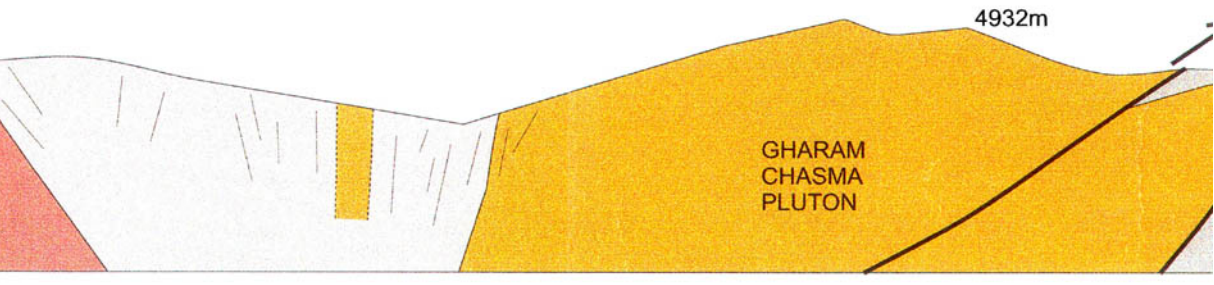

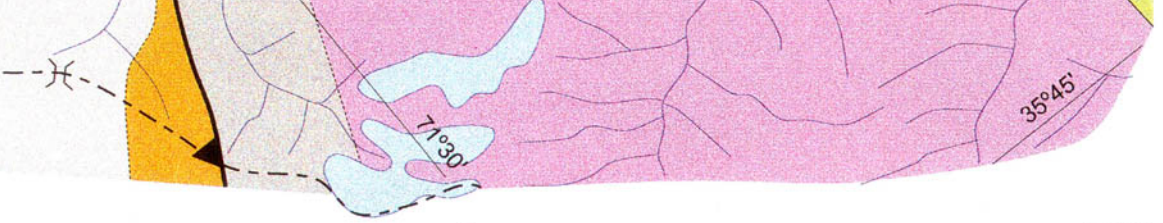
71°30'
35°45'

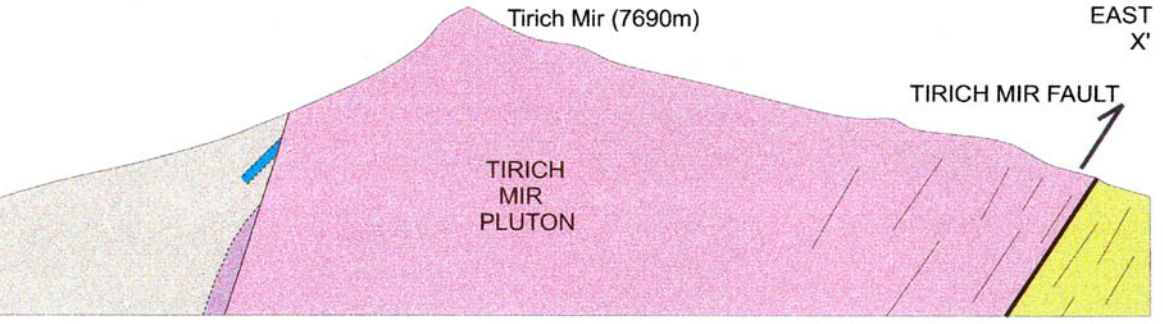
Tirich Mir (7690m)
EAST
X'
TIRICH MIR FAULT
TIRICH
MIR
PLUTON

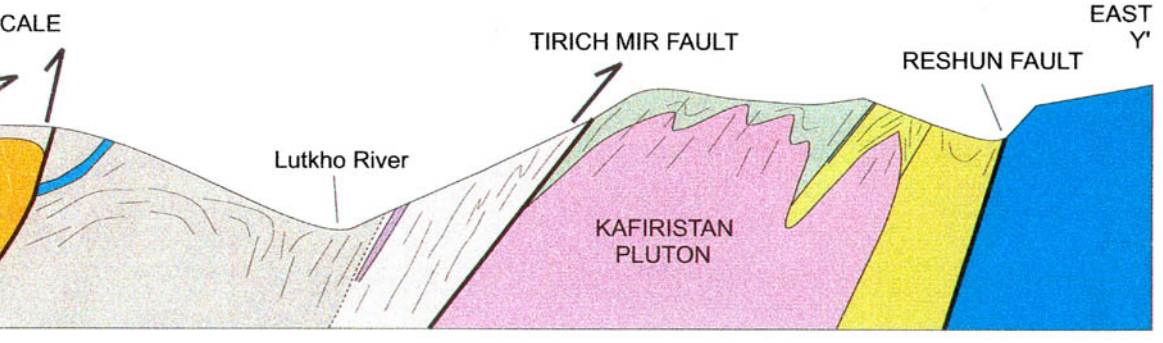
CALE
TIRICH MIR FAULT
EAST
Y'
RESHUN FAULT
Lutkho River
KAFIRISTAN
PLUTON

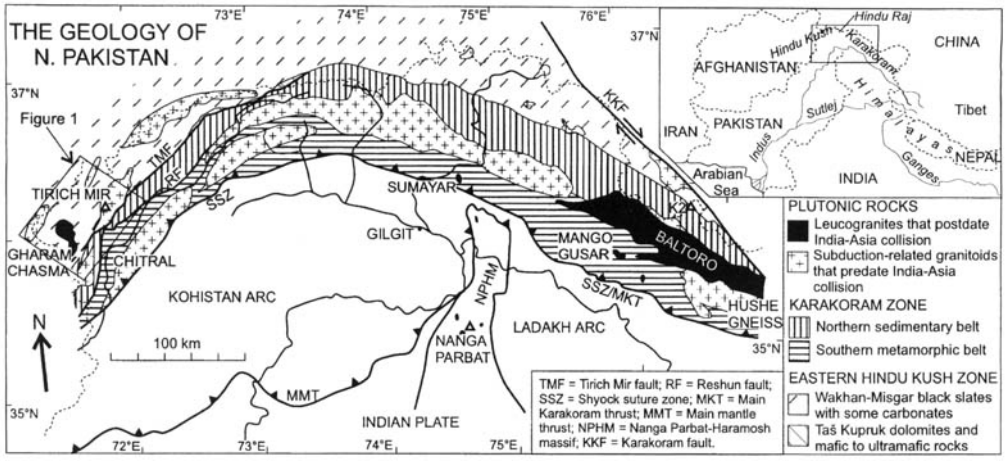

Fig. 2. Map of Northern Pakistan showing the distinction between the geological zones of the Karakoram and the eastern Hindu Kush (after Gaetani & Leven 1993; Gaetani *et al.* 1996; Searle & Khan 1996). The location of the map presented in Fig. 1 is also shown.

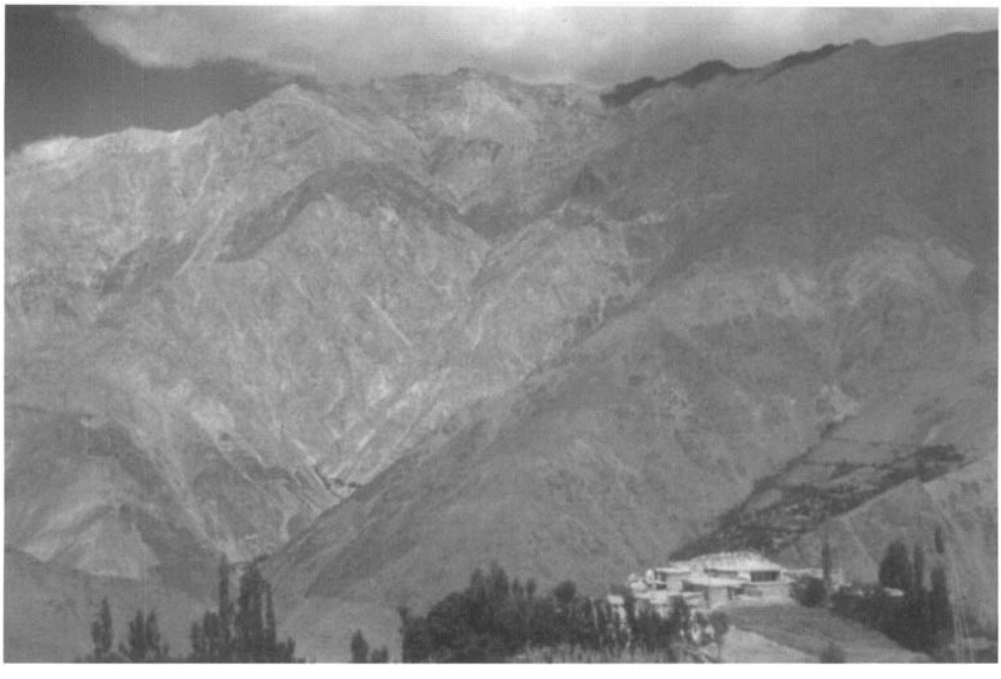

Fig. 3. Photograph taken facing northwest across the Lutkho valley, showing the part thrusted and part intrusive nature of the eastern contact of the Gharam Chasma pluton: the pale rock on the left is the leucogranite, the dark brown are the graphitic garnet–staurolite schists, which are divided by a pale band of calc-silicates.

been mapped from west of Gharam Chasma (Fig. 3) to north of Besti, a strike length of more than 20 km. As with the metapelites, they are variably deformed and metamorphosed, and consist of combinations of quartz, carbonate, diopside, garnet, epidote, scapolite and muscovite. Scheelite mineralization is sometimes associated with calc-silicate lenses (Leake *et al.* 1989).

Gneiss unit with amphibolite. In the upper Lutkho valley, quartz, plagioclase, biotite and garnet gneiss crops out within sillimanite schists and migmatites. The gneiss contains bodies of

Fig. 4. Photograph taken facing north, showing migmatites in the upper Lutkho valley, with generally unfoliated leucogranitic material parallel to and cross-cutting the S1 schistosity. Leucosomes are also sometimes folded with S1, forming D2 folds.

amphibolite that consist of hornblende, plagioclase and biotite with accessory quartz, sphene and epidote. Both these lithologies have a strong foliation, but unlike the surrounding metapelites, they show no sign of partial melting. The origin of these rocks is uncertain, but it is possible that they formed the basement to the sedimentary sequences that were the protoliths of the metapelites.

Units between the Tirich Mir Fault Zone and Reshun Fault

Phyllite units with carbonate lenses. These units are juxtaposed against the Krinj limestone (see Pudsey *et al.* 1985) by the Reshun Fault. They are highly strained green to grey-brown phyllites and semi-pelites with a well developed cleavage. The lithologies are sometimes highly graphitic, particularly adjacent to the Reshun Fault. Diamictites with quartzite and granitic clasts are common, perhaps indicating deposition beneath ice rafts in a glacial period. The minerals present in these rocks are quartz and muscovite, with varying combinations of plagioclase, stilpnomelane, chlorite, carbonate, clinozoisite and graphite. Metamorphism in these rocks is below biotite grade. Carbonate-rich lenses within these phyllites are quite common, although fossils are unlikely to be preserved due to the high strain.

These rocks were included in the Lutkho Formation of Leake *et al.* (1989), and are probably the southwestward extension of the Lun and Owir shales that are Devonian to at least Permian in age (Hayden 1915; Desio 1966; Talent *et al.* 1981; Pudsey *et al.* 1985; Gaetani & Leven 1993). The diamictites reported here are the first indication of glaciogenic sediments in this region of the southern margin of Asia.

Semi-pelitic unit. Structurally above the phyllites and beneath the Tirich Mir Fault Zone lies a monotonous sequence of highly strained, isoclinally folded, dark grey-brown semi-pelites. They contain the assemblage: quartz, plagioclase, biotite, chlorite, occasional garnet, clinozoisite/epidote and more rarely muscovite. Metamorphic conditions in this unit are higher than those in the phyllites, reaching biotite and sometimes even garnet grade. This may be due to heating from the adjacent Tirich Mir and Kafiristan plutons.

Intrusive granitoids

Three types of intrusive rocks have been identified in this area: a variety of leucogranites and

pegmatites, a suite of dominantly equigranular granodiorites to granites, and a group of porphyritic granodiorites to granites that are characterized by large feldspar megacrysts or augen.

Leucogranites and pegmatites. Within the garnet–staurolite grade metapelitic schists and migmatites are a wide variety of leucogranites and pegmatites. These range in size from small outcrop scale to the largest body, known as the Gharam Chasma pluton (Fig. 3), which covers an area of around 140 km^2. Both the leucogranites and the pegmatites range from unfoliated to strongly foliated and are sometimes augen textured. Many of the larger bodies of leucogranite are composites of unfoliated and foliated varieties, often cross-cut by late stage pegmatitic dykes. The mineralogy of the foliated and the unfoliated leucogranites, as well as the pegmatites, is broadly similar: quartz, K-feldspar and plagioclase, with varying amounts of biotite, muscovite, tourmaline and garnet, and a suite of accessory minerals that includes apatite, monazite, zircon and sometimes uraninite and xenotime. Muscovite is sometimes rare in the foliated leucogranites, and biotite is often absent in the pegmatites. Beryl can be found in the pegmatites, and aquamarine is sometimes mined by local people to the south of Gharam Chasma.

Dominantly equigranular granodiorites to granites. Two plutons fit into this category, both within the metapelitic unit: one in the north which has not been examined in any detail, and the Dorah Pass pluton in the west. These bodies are largely unfoliated and are usually equigranular, consisting of plagioclase, K-feldspar, biotite, hornblende and usually quartz, with accessories of opaques, zircon, apatite and clinozoisite. The Dorah Pass pluton is also made up of K-feldspar phenocrystic granites that often show signs of deformation and recrystallization. They do not contain hornblende and rarely contain muscovite, which is probably a product of the recrystallization. These granitoids may be related to the amphibole-bearing rocks in the northern part of the axial batholith in northern Nuristan, Afghanistan (Bordet & Boutière 1968), which have an Rb–Sr biotite age of 89–96 Ma (Desio 1964).

Porphyritic granodiorites to granites. There are two large porphyritic granodiorite to granite plutons that are characterized by large K-feldspar megacrysts. They are generally strongly foliated and augen textured, although the Tirich Mir pluton can be almost undeformed. The Kafiristan pluton is usually strongly foliated, and consists of quartz, plagioclase, K-feldspar, biotite and muscovite, with accessory minerals of apatite, sphene, zircon, opaques, clinozoisite and allanite. The Tirich Mir pluton is less foliated, more granitic in composition and has a mineralogy consisting of quartz, plagioclase, K-feldspar, biotite and muscovite, with accessories of apatite, zircon and opaques. The SE margin is a thrusted contact, while the NW one is intrusive, at least in part.

Poorly constrained and unreliable Rb–Sr whole-rock ages of about 115 Ma for the Tirich Mir pluton, and 480 Ma for the Kafiristan pluton, have been obtained by Desio (1964) and Debon *et al.* (1987) respectively.

Structure

This section deals with the deformational history of the area, as revealed by the mapping of field structures. The data are subdivided into smaller sub-areas for investigation, with a view to combining it later to determine the overall structural evolution. The subdivisions are made geographically as well as geologically, the locations of which can be seen in Fig. 1.

Categorization, relative timing and correlation of structures

Original sedimentary layering is referred to as S0. Deformational phases are distinguished on the basis of structural style and overprinting relationships observed during field mapping. Up to four phases of deformation can be recognized in any one sub-area (Fig. 5). These are referred to as D1, D2, D1–3 and D4, where D1 is the oldest and D4 the youngest. In general, two deformational phases are most clearly distinguished, which are referred to as D1 and D2, with associated foliations S1 and S2, and lineations L1 and L2. D1 is defined as being the first clearly recognizable and regionally important deformational phase that took place after sediment deposition. D2 is a later deformational phase that clearly deforms the D1-produced S1 and L1. D1 is variably developed throughout the area, and is characterized by open to isoclinal folds with axial-planar spaced cleavage to penetrative schistosity (S1). D2 is more locally developed in the different sub-areas, is characterized by open to tight folds with axial-planar spaced cleavage (S2), and is usually spatially associated with leucogranite intrusions.

Other less well constrained deformational phases include D1–3 (referred to as 1–3 because

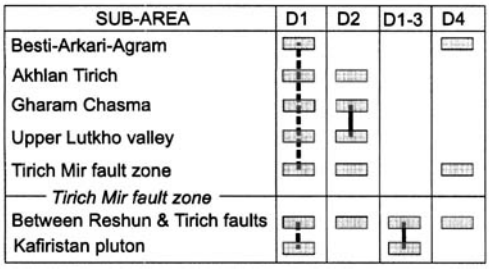

Fig. 5. Diagram showing the various sub-areas used for structural analysis shown in the left-hand column, and the extent of significant presence of the deformation phases D1, D2, D1–3 and D4 in each sub-area (marked by rectangular boxes). The thick vertical lines indicate possible correlation (dashed = tentative; solid = confident) of deformation phases between the different sub-areas, based on whether or not the structural style is both spatially and characteristically continuous. Where the boxes are not joined by vertical lines, the structural style is not continuous, either spatially or characteristically, and based on structural evidence, no correlation can be made. Note that no attempt has been made to correlate structures across the Tirich Mir pluton fault.

the timing relative to D1 and D2 is not well known), relating to the development of stretching lineations (L1–3) mainly to the east and south-east of the Tirich Mir Fault Zone, and the latest D4 brittle fractures (S4).

It is important to emphasize that these phases of deformation have been distinguished primarily on the basis of structural overprinting relationships, and where these are absent (as is often the case with spatially separated structural elements), structural style has been used. One of these phases, therefore, does not necessarily represent a single, discrete tectonic or deformation event. Furthermore, although there is consistency in the styles of the deformation fabrics that are categorized in each phase, they should not necessarily be assumed to be contemporaneous from one sub-area to another. In other words, D1 in one sub-area does not necessarily correlate with D1 in another sub-area. The same also applies for D2. Based on whether or not the structural style is both characteristically and spatially continuous from one sub-area to the next, the extent to which the different deformation phases are thought to correlate is illustrated in Fig. 5.

Structural data

The structural data are included on the geological map (Fig. 1), and a good indication of the extent of mapping coverage can be obtained from the distribution of these data. A selection of the data are plotted on the stereonets in Fig. 6. It is clear that the percentage of the map area that was covered is small, and in many cases, the mapping carried out was not very detailed. This is due to the remoteness and the difficult access to the area, as well as the size of the area covered. Consequently, the structural analysis presented here should be regarded as preliminary, as any future studies that are focused on more detailed mapping work will certainly produce refinements and improvements.

Lineation terminology

A note should be made on the lineation terminology used in this paper, which complies with that of Hobbs *et al.* (1976). There are two categories: those that are orientated parallel to contemporaneous fold axes, and those that have formed parallel to the tectonic transport direction, termed stretching lineations. The term 'crenulation' lineation refers to the axes of crenulation folds. Where a crenulation cleavage has developed, the resulting intersection lineation is parallel to the axes of the crenulation folds and therefore has the same orientation as the crenulation lineation, and consequently has not been recorded as well. A 'striation' lineation is a very fine, sub-millimetre scale, non-penetrative lineation that resembles slickensides. A 'mineral' lineation is an alignment of elongate minerals such as sillimanite (which tend to be orientated parallel to fold axes), or aggregates of minerals such as quartz, feldspar and biotite (which are stretching lineations).

The Besti–Arkari–Agram area

This area covers the data collected from around and north of Besti village, and the Arkari and Agram valleys (Fig. 1), and is characterized by the least deformed and metamorphosed metasediments in the whole area. Bedding (S0) is often difficult to distinguish with any certainty in the monotonous black slates, but is sometimes marked by more siliceous or carbonate-rich layers. A semi-penetrative foliation, parallel to the compositional layering, is typically present. No evidence of isoclinal folding with axial planes parallel to S0 was observed, and consequently this foliation is thought to have formed by simple compaction, possibly during diagenesis. However, limited mapping was carried out in this area, so this interpretation should be viewed as tentative. S0 is open to tightly folded around steeply W to WNW dipping axial planes that are marked by S1, a spaced axial planar cleavage (see

cross-section X–X′ on Fig. 1). The fold axes and associated crenulation lineations are gently to steeply NNE dipping (Fig. 6c).

The Gharam Chasma area

Most of the data for this area come from garnet–staurolite schists in the Lutkho valley around Gharam Chasma, and some from immediately north of Gharam Chasma (Fig. 1). In one outcrop, a quartzite layer preserves evidence of pre-D1 normal faulting. The compositional layering of S0 is sometimes discernible (e.g. the calc-silicate layer in Fig. 3), and is occasionally seen to define tight to isoclinal folds with variable axes orientations (Fig. 6c). Axial planar to these folds is a strongly developed, penetrative schistosity (S1), observable throughout the area. S1 has been folded about subhorizontal to gently NNE dipping fold axes, producing large open

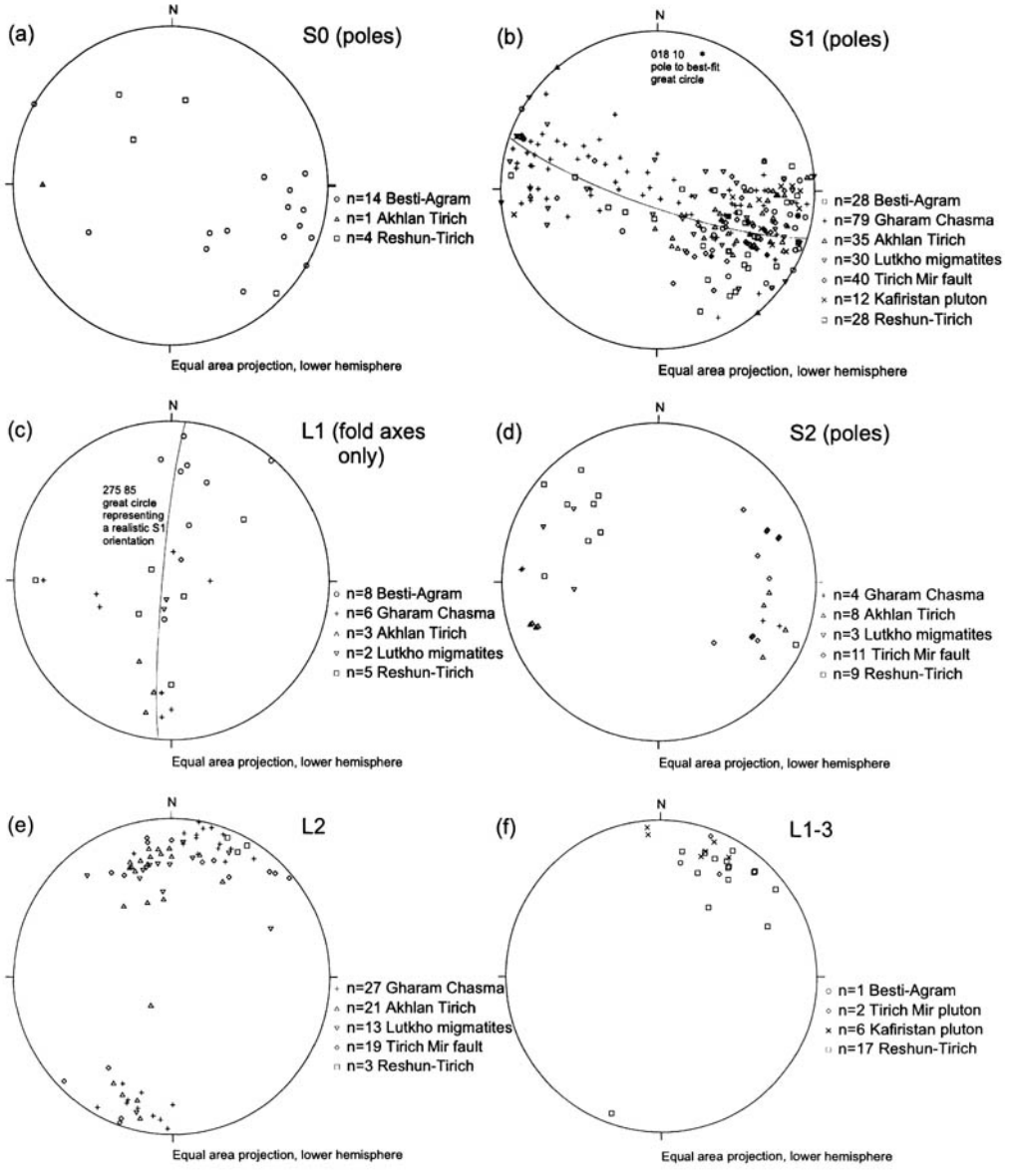

Fig. 6. Selected structural data from the various sub-areas represented on stereonets.

folds with up to kilometre-scale wavelengths (see cross-section Y–Y′ on Fig. 1). Crenulation lineations with a similar orientation are commonly developed (Fig. 6e), but axial planar S2 spaced cleavage surfaces are rare.

The eastern contact of the Gharam Chasma pluton with the garnet–staurolite schists is only well exposed in places with difficult access. Limited observations show that this unfoliated leucogranite pluton both cross-cuts and is parallel to S1. The contact is definitely tectonic in places (Fig. 7), although it is also intrusive in part (Fig. 3). Shear sense indicators are consistent with a top-to-the-east sense of movement along the west-dipping thrusts that deform S1 (Fig. 7a–d). The orientation of slickenside striations and crenulation lineations (Fig. 7a) indicate a pure dip-slip tectonic transport direction along the pre-existing S1, with no component of strike-slip at all. This is consistent with the D2 deformation as a whole, which has similarly orientated, subhorizontal NNE trending crenulation lineations (Fig. 6e). Evidence indicates that the Gharam Chasma leucogranite pluton was emplaced along thrusts during the D2 phase.

The Akhlan Tirich area

These data were collected from the garnet ± staurolite ± andalusite ± sillimanite ± kyanite schists around the Akhlan Tirich shepherd huts, to the north of the Gharam Chasma pluton (Fig. 1). Bedding (S0) is occasionally seen to define tight to isoclinal (sometimes recumbent?) folds about S1, with gently south-dipping fold axes (Figs 8a & 6c). S1 is a penetrative axial planar schistosity that is sometimes mylonitic in zones suggesting that faulting (thrusting?) may have occurred during D1 in this area. S1 has been deformed during D2 into gentle to open folds, or more rarely small-scale chevron folds (Fig. 8b), most commonly about north-dipping axes (Fig. 6e). A non-penetrative, spaced axial planar

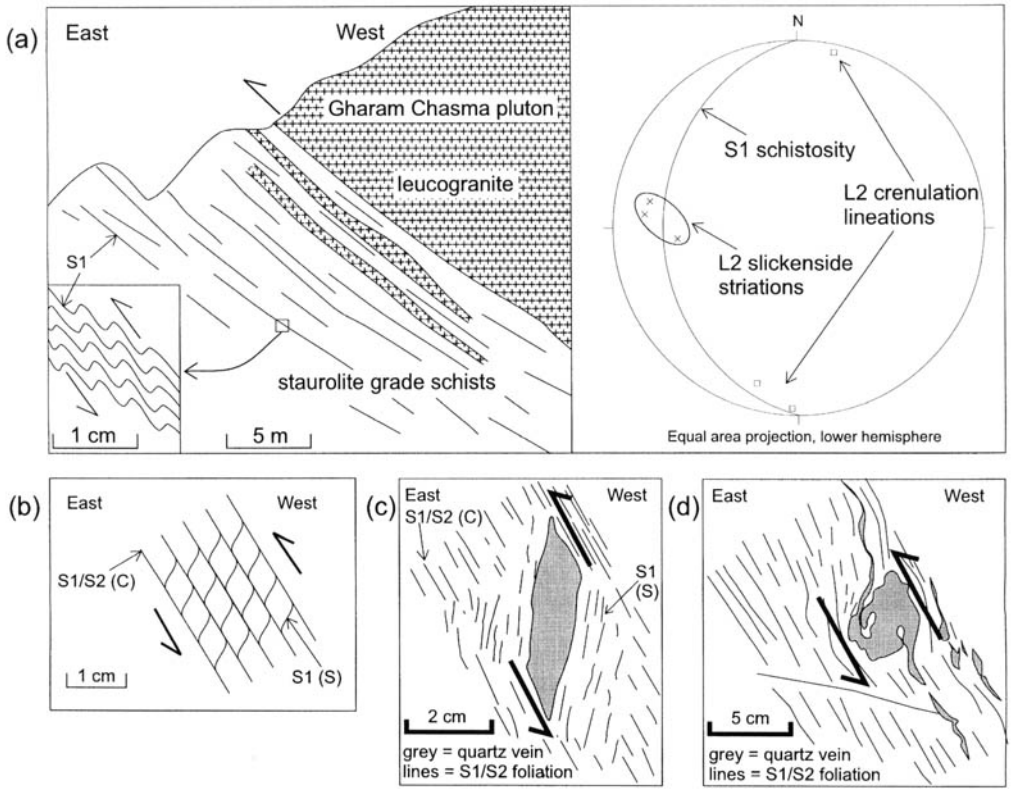

Fig. 7. Field observations on the eastern contact between the Gharam Chasma pluton and the metapelites near the Lutkho valley: (**a**) contact parallel to S1, with crenulation folds and slickenside striation lineations indicating a pure up-dip-to-the-east sense of emplacement; (**b**)–(**d**) Sketches of C–S fabrics or C-type shear bands and deformed quartz veins indicating a top-to-the-east sense of movement.

cleavage is sometimes developed (S2), which is, on average, very steeply west-dipping to vertical (Figs 6d & 8). Most of the leucogranites studied in this area have a moderate to strong foliation which is generally parallel to S1, suggesting that intrusion took place prior to or during D1.

The upper Lutkho valley migmatite area

This area covers the data collected from the sillimanite grade schists and migmatites in and around the upper Lutkho valley to the west of the Gharam Chasma pluton (Figs 1 & 4). S1 is a penetrative schistosity which has been partially annealed by migmatization, and intensely folded around gently to moderately north-dipping fold axes (Fig. 6e). A mineral lineation defined by sillimanite and orientated parallel to the D2 fold axes is also sometimes present.

Leucogranitic bodies can be deformed and foliated within S1, cross-cut S1, but be folded by D2, and cross-cut all the deformation fabrics (e.g. Fig. 4). Clearly there has been a long history of crustal melting and leucogranite emplacement, with a minimum of two stages being distinguished on the basis of field relationships: an early stage before or during D1, and a later stage during D2, which culminates with the late, cross-cutting dykes. The partial melting and associated deformation is at least partly ascribed to D2, but with the complex structural relationships, some migmatization during D1 cannot be ruled out. The eastern margin of the Dorah Pass pluton consists of deformed granodiorite that has a foliation parallel to the adjacent S1 foliation in the metapelites. The crustal melting that produced this granitoid may also have provided the heat that caused the pre- to syn-D1 leucogranite melts.

The Tirich Mir pluton fault area

This is the area bounded by the sillimanite isograd and the Tirich Mir pluton fault (Fig. 1), and has been intruded by a dense network of pegmatite and leucogranite dykes and sills. Evidence of pre-D1 deformation taking place in this area comes from the intense deformation and migmatization seen in the amphibolite unit, which does not continue into the surrounding schists. The S1 schistosity is generally moderately W to NW dipping, although locally it has been tightly folded about WSW to NW dipping axial planes with an associated spaced axial planar cleavage (Fig. 6d). The folds have subhorizontal to shallow NNW to NE plunging axes, which are consistent with the crenulation lineations and occasionally a similarly orientated mineral lineation, defined largely by sillimanite (Fig. 6e). Pegmatite and leucogranite dykes are often associated with the folding of S1. They are usually parallel to S1 and are sometimes cut by the spaced S2 cleavage and they are often folded and deformed. This indicates that D2 took place during, and perhaps outlasted, the emplacement of the pegmatites and leucogranites. The sense of vergence of the folds is top-to-the-east, and a pure dip-slip tectonic transport direction is indicated by the near horizontal fold axes and crenulation lineations (Fig. 6e).

Along the eastern margin of the Tirich Mir pluton the granite is strongly sheared and augen-textured, with a NW dipping foliation. This sheared porphyritic granite has been named the Momi gneiss by previous workers such as Buchroithner & Gamerith (1986). The continually NW dipping granite–metasediment contact along the southeast of the pluton is clearly thrusted rather than intrusive (Fig. 1). This evidence is consistent with the named Tirich Mir pluton fault being a thrust with a top-to-the-east sense of movement, placing the metapelitic rocks and the Tirich Mir pluton over the semi-pelitic and phyllitic units. However, from the available information, it is not possible to deduce whether this thrusting took place during or after intrusion of the Tirich Mir pluton.

The area between the Reshun and Tirich Mir pluton faults

This includes all the data from the semi-pelites and phyllites between the Reshun and Tirich Mir pluton faults, and the Kafiristan pluton (Fig. 1). S1 cleavage is commonly observed parallel to bedding. S1 is a penetrative cleavage with a steep to moderate NW dip that swings around to a W dip to the south (Fig. 1). Outcrop-scale D1 folds are tight to isoclinal, with the L1 fold axes having varying orientation within the S1 planes (Fig. 4c). These orientations may have been generated by a strike-slip component in the deformation. Alternatively, they could be explained by rotation within S1 of originally more upright axes during or after D1, also indicating strike-slip tectonics.

Strike-slip deformation is also indicated by the common, subhorizontal striation lineations on S1 surfaces in the phyllites, and mineral stretching lineations in the semi-pelites and the Kafiristan pluton (L1–3, Fig. 6f). The mineral stretching lineations are defined by quartz, feldspar and biotite aggregates that are interpreted to result from recrystallization by shearing parallel to the tectonic transport direction. As is the case for the development of the variably

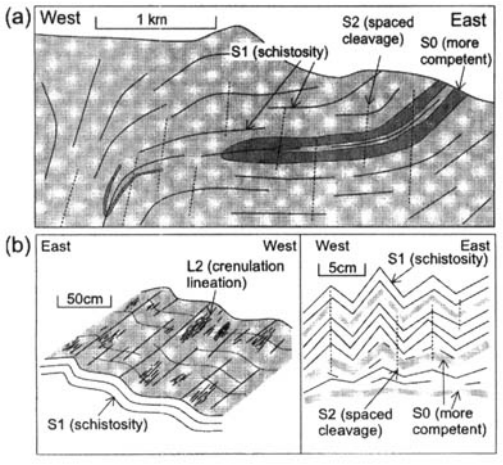

Fig. 8. Sketches showing the style of folding and the relationship between S0, S1 and S2 seen to the east of Akhlan Tirich: (**a**) a schematic section eastwards from around Akhlan Tirich; (**b**) gentle and chevron folding of S1.

orientated L1 fold axes, the timing of formation of the L1–3 lineations on S1 surfaces is ambiguous. It may have occurred during D1, or possibly after D1 when the S1 surfaces played a role in accommodating the shearing. Furthermore, the timing of L1–3 development relative to D2 is unknown. It is concluded that L1–3 lineations may have formed in response to D1, or may have formed during a separate deformation phase subsequent to D1, which may have been before or after D2. Hence the terms L1–3 during the deformational phase D1–3. The intrusive contact between the Kafiristan pluton and the semi-pelites shows signs of having been folded with an eastward sense of vergence, implying that it was emplaced pre or syn-D1, as do the phyllites to the east of the Utak Pass. This eastward vergence is consistent with the dominantly west-dipping S1 cleavage.

In summary, these observations on the D1 structures are consistent with early formation of tight to isoclinal, possibly east-verging folds, with WNW dipping axial planar S1. At some stage during D1–3, a strike-slip component in the deformation caused rotation of earlier fold axes and the development of subhorizontal striation lineations in the phyllites and mineral stretching lineations in the semi-pelites and the Kafiristan pluton. S1 is sometimes locally folded and crenulated about a locally developed, steep to moderately SW dipping spaced S2 cleavage and associated subhorizontal crenulation/intersection lineations (Fig. 6d).

Late brittle fractures

Sporadically developed in some of these areas are steeply to vertically dipping, ENE to SE striking, late, brittle fractures that sometimes have up to a few centimetres displacement on them.

Summary of the structural evolution

The main features of the structural history of the part of the eastern Hindu Kush studied are summarized in Fig. 9. Evidence for pre-D1 deformation comes primarily from the migmatized amphibolite unit. A single outcrop in the Gharam Chasma area also suggests pre-D1 normal faulting. There is considerable consistency in the nature and orientation of the structural features generated during D1, D2 and D1–3, despite the large area covered. D1 is characterized by tight to isoclinal folding of bedding and the development of S1, an axial planar cleavage that varies from spaced to a more commonly developed penetrative schistosity. In areas that are largely unaffected by D2 (the Besti–Arkari–Agram area and the majority of the area between the Reshun and Tirich Mir pluton faults), S1 is moderately to steeply W to NW dipping.

The D1 fold axes have variable orientations that largely lie within a steeply west dipping S1 plane (Fig. 6c). The few axes that do not lie within this plane are easily explained as lying within S1 planes of slightly differing orientation, or as having been re-orientated during D2 folding. The fold axis plunge variation may have resulted from rotation of originally upright folds within S1. This is interpreted to indicate a strike-slip component in a deformation phase that is referred to as D1–3, as it may have occurred during or after D1. The suggestion of strike-slip tectonics is supported by the L1–3 subhorizontal striation lineations in the phyllites and mineral stretching lineations in the Kafiristan pluton, that have been developed on S1 surfaces (Fig. 6f).

D2 resulted in gentle to open folds of S1, except in the sillimanite grade areas (the Tirich Mir pluton fault area and the upper Lutkho valley migmatites), where the folds are often tight. Fold axes and crenulation lineations are gently NNE dipping on average (Fig. 6e). S2 is a spaced axial planar cleavage that is variably developed, and except in the area between the Reshun and Tirich faults is most commonly steeply W dipping (Fig. 6d). Note the different orientation of S2 in the area between the Reshun and Tirich Mir pluton faults, which is steeply to moderately SE dipping. It is possible that the D2

in this area is unrelated to the D2 in the other areas. In addition to the folding, D2 is associated with WNW-dipping thrusts along the Tirich Mir pluton fault, and the eastern contact of the Gharam Chasma pluton. An interesting feature of the D2 deformation is that the tectonic transport direction always appears to be dip-slip, with no evidence of any strike-slip component at all.

Geological evolution and discussion

Pre-D1 geological history

Tentative evidence for basement in this area is the gneiss and amphibolite unit of unknown age that outcrops in the upper part of the Lutkho valley. The origin of the amphibolite unit is uncertain, although the intense deformation and migmatization within the unit is not present in the adjacent metapelites, and definitely predates D1, if not the deposition of the metapelitic protoliths as well. The timing of deposition of the now metamorphosed sedimentary successions is poorly constrained. The protoliths to the phyllites and carbonates between the Reshun and Tirich Mir pluton faults were probably deposited during the mid to late Palaeozoic, while those of the graphitic metapelites and calc-silicates that occur to the west of the Tirich Mir Fault Zone may range from Permian to Jurassic. Normal faulting occurred after or possibly during the deposition of the latter. These phases probably took place prior to and during the break-up of Pangea and the onset of sea floor spreading that resulted in the opening of the Tethyan ocean (Smith *et al.* 1981).

Northward-directed subduction, intrusion of granitoids and D1 deformation

Perhaps the most important aspect of trying to relate field observations to tectonic processes is to take into account the continued northward-directed subduction beneath the southern margin of Asia that was active by the Jurassic (Tapponnier *et al.* 1981), and that still continues beneath the Hindu Kush (Billington *et al.* 1977; Burtman & Molnar 1993). This subduction facilitated accretion of the eastern Hindu Kush sedimentary sequences onto the southern margin of Asia sometime during the Mesozoic. They were intruded by the Tirich Mir and Kafiristan porphyritic granitoids, and the Dorah Pass equigranular granodiorite to granite plutons, the relative timing of which is unknown. It is likely that these granitoids were emplaced above a north-dipping subduction zone after the accretion of the sedimentary sequences onto the southern margin of Asia. However, pre-accretion intrusion cannot be ruled out. These plutons form part of a vast belt of granitoid rocks that extend westwards into central Afghanistan (Debon *et al.* 1987).

The main D1 deformation phase was most likely related to the subduction and accretion that took place along the southern margin of Asia during the Mesozoic and the Cenozoic. The structures that represent this deformation may have developed over a considerable time span, and could record several discrete tectonic phases related to continued northward-directed subduction. At least part of the deformation took place after the intrusion of the foliated leucogranites and porphyritic granitoids, although it is uncertain as to whether or not D1 began before intrusion. The foliated leucogranites may be a product of crustal thickening related melting that resulted from microplate accretion along the active margin. Accretion of the Kohistan arc in the mid-Cretaceous (Pudsey 1986) and the India–Asia collision that began in the Eocene (Searle *et al.* 1987; Beck *et al.* 1995) are events that may have been important in the development of D1 structures. In addition, the northern Karakoram stratigraphy contains a record of two major episodes of tectonic deformation; one in the early to mid-Jurassic, and one during the Cretaceous, which may correspond to accretion of the Kohistan arc (Gaetani *et al.* 1993).

D2 deformation and leucogranite intrusion

D2 was probably synchronous with the emplacement of the unfoliated leucogranites. The D2 deformation phase involved thrusting-assisted leucogranite intrusion and crustal shortening that was accommodated by open to tight folding, thrusting and exhumation. U–Pb geochronology on uraninites from a syn-deformational pegmatite dyke indicate that thrusting along the Tirich Mir pluton fault took place at around 114 Ma (a similar age to the Rb–Sr whole-rock age of *c.* 115 Ma for the Tirich Mir pluton), well before intrusion of the Gharam Chasma pluton at *c.* 24 Ma (Hildebrand 1998; Hildebrand *et al.* 1998). Note that there is no structural evidence that can distinguish the relative timing of these spatially separated thrusting phases, and consequently the D2 structural category is not subdivided in this study. In the Karakoram, similar deformation styles and associated granite emplacement at 25–21 Ma, indicate the widespread importance of crustal melting along the southern margin of Asia at this time (Parrish &

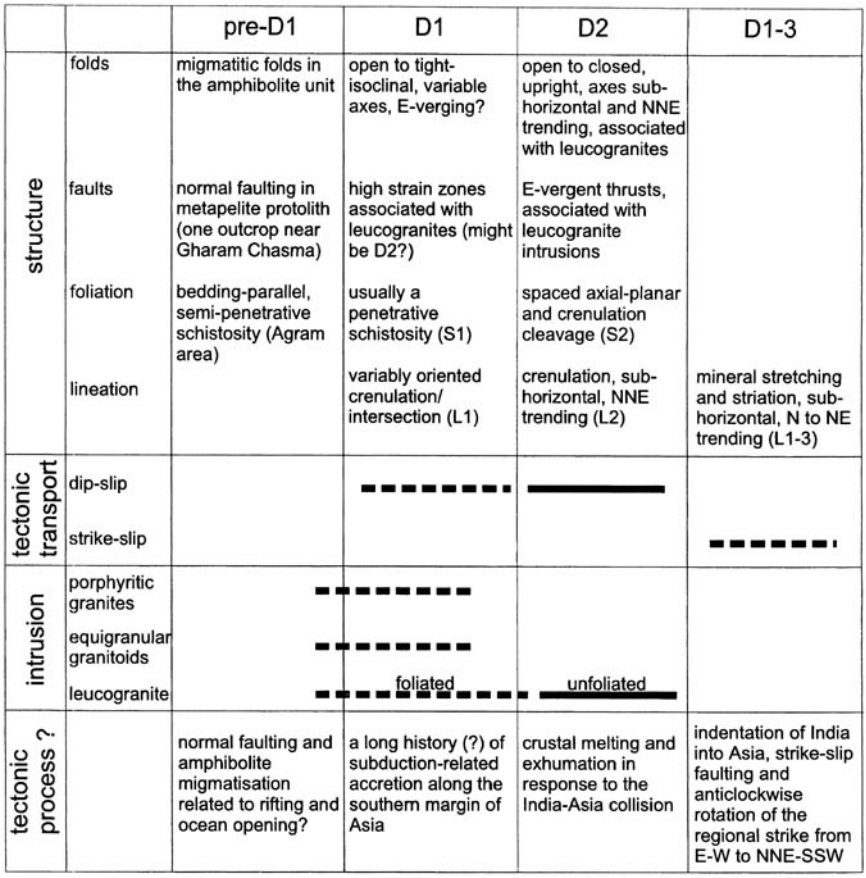

Fig. 9. Summary of the structural and magmatic history of the whole area, based only on field observations. The suggested tectonic processes are based on current knowledge about the tectonic history of the central Asian region.

Tirrul 1989; Schärer *et al.* 1990; Searle & Tirrul 1991; Searle *et al.* 1989, 1992).

Possible structural fabric rotation, D1–3 strike-slip tectonics and the indentation of India

The continued northward directed subduction from at least the Jurassic (Tapponnier *et al.* 1981), and the ongoing northward indentation of India into Asia at a rate of about 5 cm a^{-1}, which began at around 50 Ma (Molnar & Tapponnier 1975; Patriat & Achache 1984; Klootwijk *et al.* 1992), must have resulted in a long history of general N–S compression in the region. Despite this, in the eastern Hindu Kush the strike of both S1 and S2, and the trend of fold axes and crenulation lineations (L1 and L2) is generally N to NE, and not E–W as might be expected from the prevailing tectonic history and inferred regional N–S compression direction. The most obvious and simplest explanation for this observation is that the indentation of India has caused anticlockwise rotation of a previous E–W regional strike to the presently observed N to NE strike (Fig. 10). With such a model, it could be inferred that S1 and S2 would have originally been mainly north-dipping, the D1 folds generally south-verging, and D2 leucogranite emplacement south-directed along north-dipping thrusts. As there is little difference in the present-day orientations of D1 and D2 structures, it is likely that the majority of this indentation-driven rotation would have occurred after the intrusion of the D2-related leucogranites at *c.* 24 Ma.

Progressive indentation of India and anticlockwise regional strike rotation would probably have been associated with the onset of

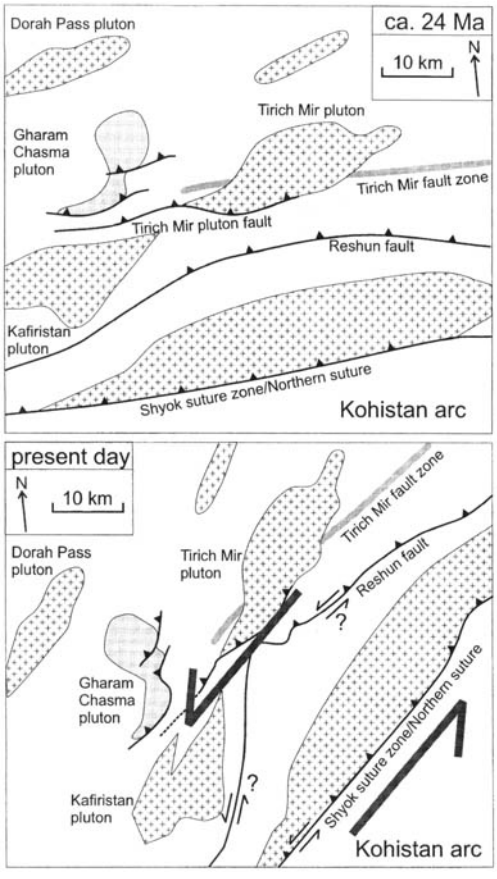

Fig. 10. Diagrams illustrating the proposed Mid-Miocene to present sinistral strike-slip deformation and anticlockwise rotation of the eastern Hindu Kush. The present day N to NE strike was probably orientated E–W and the W to NW-dipping pluton-bounding thrusts would have been N-dipping at *c.* 24 Ma.

a left-lateral transpressional tectonic environment in the eastern Hindu Kush, which could account for the subhorizontal L1–3 stretching lineations observed in this study. If this model is correct, the strike-slip deformation was probably most active after the D2 leucogranite intrusion at *c.* 24 Ma. Structures interpreted to indicate sinistral strike-slip deformation have been noted by Le Fort & Gaetani (1998) in the Hindu Raj, northeast of the area studied in this project. This deformation is thought to be related to 'bending or arc-shaping of the mountain range' in response to the India–Asia collision. In the Chitral region, strike-slip-related structures are common along the northwestern side of the Kohistan arc (Pudsey *et al.* 1985), and have also been described immediately southeast of the Reshun Fault (Talent *et al.* 1981). It appears that structures suggesting strike-slip deformation are mainly present between the Kohistan arc and the Tirich Mir Fault Zone, and apparently much less significantly developed further to the northwest.

The anomalous height of the Tirich Mir massif relative to other peaks in the Hindu Kush and the nearby Hindu Raj may be accounted for by the onset of this proposed post-24 Ma transpression and/or the resistant nature of the granite pluton relative to the surrounding phyllites and schists.

In a more regional context, the Hindu Kush strike-slip tectonics may be compared to the dextral Karakoram Fault to the east (Fig. 2), which may have been active only after the Miocene intrusion of the Baltoro and Tangtse granites of the Karakoram batholith at *c.* 17 Ma; Searle *et al.* (1998). Activity along this fault is thought to have been related to crustal shortening in the Pamir, caused by the continued indentation of India into Asia during and after the late Miocene (Searle 1996; Searle *et al.* 1998). This model is consistent with relating the strike-slip tectonics of the eastern Hindu Kush to the indentation of India, after the *c.* 24 Ma D2 leucogranite intrusion.

The significance of deep seismicity beneath the Hindu Kush

Following the discussion above, it is interesting to consider the post-India–Asia collision geological history of the Hindu Kush in a more regional context, and in the light of the present-day seismicity and seismic shear wave velocities beneath the Central Asian mountain ranges. The distribution and abundance of earthquakes and the variation in seismic shear wave velocities beneath the Hindu Kush, Karakoram and the Lhasa block of south Tibet are illustrated in Fig. 11 (van Heijst 1998). The earthquakes beneath the Hindu Kush and the Karakoram are dominantly compressional, while those beneath Tibet are extensional and only at very shallow levels. Seismicity beneath the Hindu Kush is by far the most active, occurs to the greatest depths (up to 300 km), and is thought to represent subduction of the Indian lithosphere (Roeker 1982; Hamburger *et al.* 1992; Pegler 1995). Shear wave velocities are fastest beneath the Hindu Kush and slowest beneath Tibet, possibly indicating an increase in thermal conditions from west to east, consistent with previous geophysical studies which suggest high

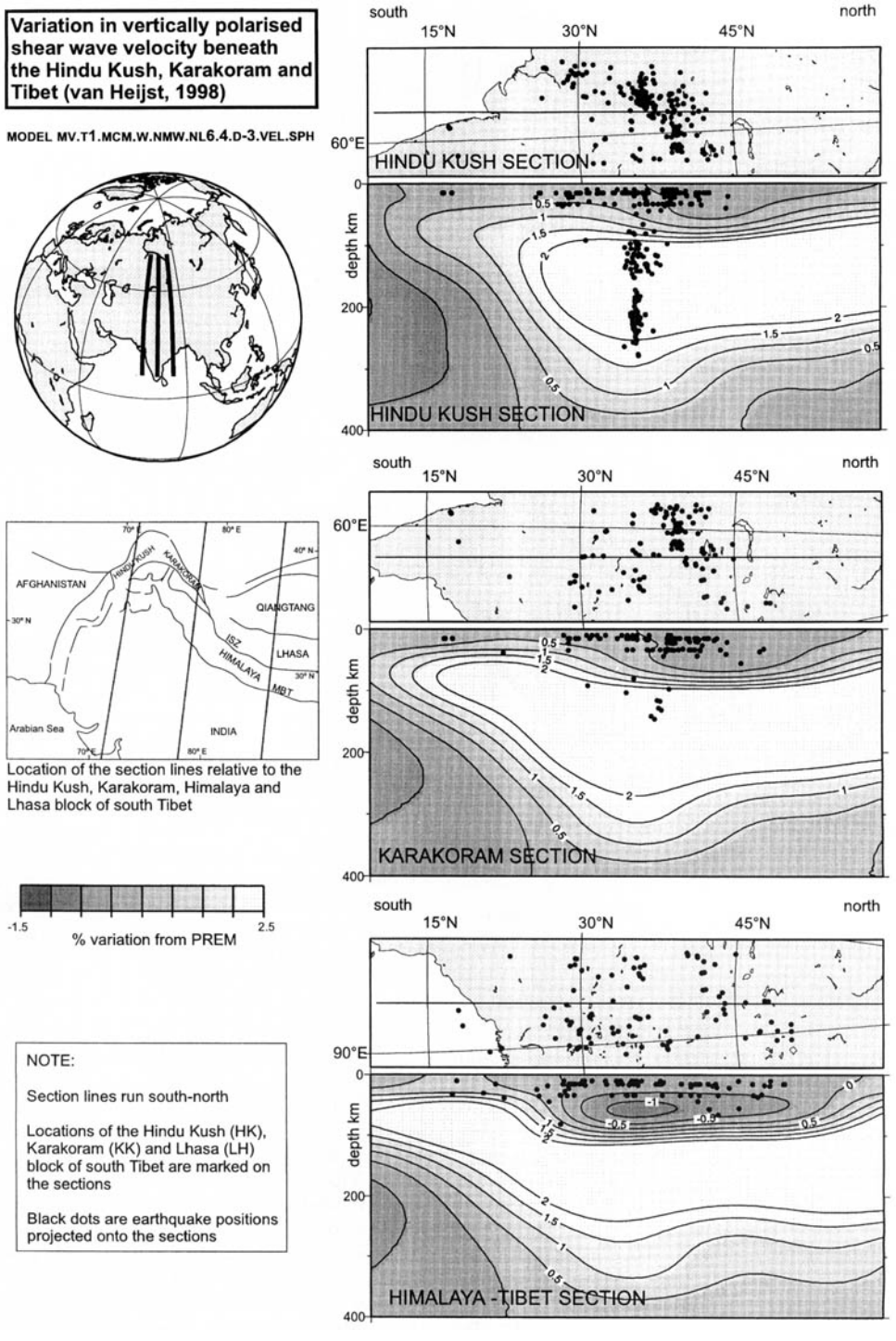

Fig. 11. South–north sections showing the variation in vertically polarized shear wave velocity beneath the Hindu Kush, Karakoram, Himalaya and Tibet (van Heijst 1998). Note that the Hindu Kush overlies the most seismically active region with exceptionally deep earthquakes. It also overlies a region with faster shear wave velocities in the upper 100 km than the regions beneath the Karakoram and the Lhasa block of south Tibet.

geotherms and possibly even crustal melts beneath south Tibet (e.g. Nelson *et al.* 1996).

U–Pb ages suggest that post-India–Asia collision crustal melting beneath the Hindu Kush is restricted to *c.* 24 Ma, whereas further east in the Karakoram, the crustal melting record is both more voluminous and more continuous, occurring from *c.* 37 to *c.* 9 Ma (Parrish & Tirrul 1989; Searle 1991). Immediately adjacent to the Karakoram in the Nanga Parbat area, there is evidence for crustal melting as young as 1 Ma (Zeitler & Chamberlain 1991; Zeitler *et al.* 1993).

These observations reflect major differences in the thermal histories of these regions. The relatively low heat flow conditions beneath the Hindu Kush are associated with restricted (both temporally and volumetrically) crustal melting, perhaps as a result of deep subduction of cooler continental lithosphere, preventing the widespread crustal melting that probably exists beneath Tibet.

Conclusions

1. Prior to the collision of first Kohistan at *c.* 85–75 Ma and finally India at 55–50 Ma, the southern margin of Asia in the eastern Hindu Kush region was dominated by biotite and K-feldspar megacrystic granites and equigranular granodiorites. These granitoids developed in an Andean-type continental margin above a north-dipping Tethyan oceanic subduction zone.
2. A phase of continental crustal melting at *c.* 24 Ma resulted in the Gharam Chasma biotite + muscovite ± garnet ± tourmaline leucogranite, which was temporally related to much more widespread crustal melting to the east in the central and eastern Karakoram (Baltoro granite). Crustal melt granites that postdate the India–Asia collision in the Hindu Kush are temporally and volumetrically restricted relative to the Karakoram. As yet, there is no evidence for crustal melting that postdates the India–Asia collision in the intervening Hindu Raj Range.
3. After the emplacement of the Gharam Chasma pluton at *c.* 24 Ma in the Hindu Kush, the regional foliation strike may have been rotated anticlockwise by up to 90°, from E–W to NE and N, in response to the continuing northward indentation of India. Left-lateral shearing, and an unquantified amount of transpressional exhumation and related surface uplift, resulted.
4. Anomalously deep and active seismicity is restricted to the Hindu Kush, and is not continuous eastward into the Karakoram and south Tibet where higher thermal gradients have resulted in widespread and ongoing crustal melting.

P. R. Hildebrand acknowledges the Rhodes Trust for funding this work and H. Tarras-Wahlberg, M. Crockett, J. L. Gurney and C. Morrison for assistance in the field. M. P. Searle acknowledges NERC grant GT5/96/13/E. We also thank Asif Khan and Qasim Jan of Peshawar University for invaluable assistance in Pakistan, and M. Gaetani and L. Ratschbacher for their helpful reviews on this manuscript.

References

AUSTROMINERAL 1978. *Mineral exploration and mine development, Chitral District*. Report for Sarhad Development Authority, Peshawar.

BECK, A., BURBANK, D. W., SERCOMBE, W. J., RILEY, G. W., BARNDT, J. K. *et al.* 1995. Stratigraphic evidence for an early collision between north-west India and Asia. *Nature*, **373**, 55–58.

BILLINGTON, S., ISACKS, B. & BARAZANGI, M. 1977. Spatial distribution and focal mechanisms of mantle earthquakes in the Hindu Kush-Pamir region: a contorted Benioff zone. *Geology*, **5**, 699–704.

BORDET, P. & BOUTIÈRE, A. 1968. Reconnaissance geologique dans l'Hindou Kouch oriental (Badakhchan, Afghanistan). *Bulletin du Societé Géologique de France*, **10**, 486–496.

BUCHROITHNER, M. F. 1980. An outline of the geology of the Afghan Pamirs: *Tectonophysics*, **62**, 13–95.

—— & GAMERITH, H. 1986. On the geology of the Tirich Mir area, central Hindu Kush (Pakistan). *Jahrbuch Geologische Bundesanst*, **128**, 367–381.

BURTMAN, V. S. & MOLNAR, P. 1993. Geological and geophysical evidence for deep subduction of continental crust beneath the Pamir. Geological Society of America Special Paper, **281**.

CALKINS, J. A., JAMIL-U-DIN, S., BHUYAN, K. & HUSSAIN, A. 1981. Geology and mineral resources of the Chitral–Partsan area, Hindu Kush Range, Northern Pakistan. *United States Geological Survey Professional Paper*, **716-G**.

DEBON, F., AFZALI, H., LE FORT, P. & SONET, J. 1987. Major intrusive stages in Afghanistan: typology, age, and geodynamic setting. *Geologische Rundschau*, **76**(1), 245–264.

DESIO, A. 1959. Cretaceous beds between Karakorum and Hindu Kush ranges. *Rivista Italiana di Paleontologia and Stratigrafia*, **55**, 221–229.

—— 1963. Review of the geologic "formations" of the western Karakorum (central Asia). *Rivista Italiana di Paleontologia e Stratigrafia*, **69**, 475–501.

—— 1964. On the geological age of some granites of the Karakorum, Hindu Kush and Badakhshan (central Asia). *In*: *Proceedings of the 22nd International Geological Congress, Delhi*, Part **11**, Section 11, 479–496.

—— 1966. The Devonian sequence in the Mastuj valley (Chitral, NW Pakistan). *Rivista Italiana di Paleontologia e Stratigrafia*, **72**, 293–320.

GAETANI, M. & LEVEN, E. 1993. Permian stratigraphy and fusulinids from Rosh Gol (Chitral, E Hindu Kush). *Rivista Italiana di Paleontologia e Stratigrafia*, **99**, 307–326.

——, LE FORT, P., TANOLI, S., ANGIOLINI, L., NICORA, A., SCIUNNACH, D. & KHAN, A. 1996. Reconnaissance geology in Upper Chitral, Baroghil and Karambar districts (northern Karakoram, Pakistan). *Geologische Rundschau*, **85**, 683–704.

——, JADOUL, F., ERBA, E. & GARZANTI, E. 1993. Jurassic and Cretaceous events in the North Karakoram: age constraints from sedimentary rocks. *In*: TRELOAR, P. J. & SEARLE, M. P. (eds) *Himalayan Tectonics*. Geological Society, London, Special Publications, **74**, 39–54.

HAMBURGER, M. W., SAREWITZ, D. R., PAVLIS, T. L. & POPANDOPULO, G. A. 1992. Structural and seismic evidence for intracontinental subduction in the Peter the First range, Central Asia. *Geological Society of America Bulletin*, **104**, 397–408.

HAYDEN, H. H. 1915. Notes on the geology of Chitral, Gilgit and the Pamir. *Records of the Geological Survey of India*, **45**, 271–326.

HILDEBRAND, P. R. 1998. *The Hindu Kush of Pakistan: mountain range evolution from active margin to continent–continent collision*. PhD thesis, Oxford University, England.

——, NOBLE, S. R., SEARLE, M. P., PARRISH, R. R. & SHAKIRULLAH 1998. Tectonic significance of 24 Ma crustal melting in the eastern Hindu Kush, Pakistan. *Geology*, **26**, 871–874.

HOBBS, B. E., MEANS, W. D. & WILLIAMS, P. F. 1976. *An outline of structural geology*. Wiley, New York.

KAFARSKYI, A. K. & ABDULLAH, J. 1976. Tectonics of the North-East Afghanistan (Badakhshan, Wakhan, Nurestan) and relationship with the adjacent territories. *Atti Convegni Lincei Roma*, **21**, 87–113.

KLOOTWIJK, C. T., GEE, J. S., PEIRCE, J. W., SMITH, G. M. & MCFADDEN, P. L. 1992. An early India–Asia contact: palaeomagnetic constraints from Ninetyeast Ridge, ODP leg 121. *Geology*, **20**, 395–398.

LEAKE, R. C., FLETCHER, C. J. N., HASLAM, H. W., KHAN, B. & SHAKIRULLAH 1989. Origin and tectonic setting of stratabound tungsten mineralisation within the Hindu Kush of Pakistan. *Journal of the Geological Society, London*, **146**, 1003–1016.

LE FORT, P. & GAETANI, M. 1998. Introduction to the Geological Map of western central Karakorum, North Pakistan Hindu Raj, Ghamubar and Darkot areas 1:250,000 scale. *Geologica* (Geoscience Laboratory Project, Islamabad, Pakistan), **3**, 1–67.

MOLNAR, P. & TAPPONNIER, P. 1975. Cenozoic Tectonics of Asia: effects of a continental collision. *Science*, **189**, 419–426.

NELSON, K. D. & 27 others 1996. Partially molten middle crust beneath southern Tibet: a synthesis of Project INDEPTH results. *Science*, **274**, 1684–1688.

PARRISH, R. R. & TIRRUL, R. 1989. U–Pb age of the Baltoro granite, northwest Himalaya, and implications for zircon inheritance and monazite U–Pb systematics. *Geology*, **17**, 1076–1079.

PASCOE, E. H. 1924. General report of the Geological Survey of India for the year 1923. *India Geological Survey Records*, **55**, part 1.

PATRIAT, P. & ACHACHE, J. 1984. India–Eurasia collision chronology has implications for crustal shortening and driving mechanisms of plates. *Nature*, **311**, 615–621.

PEGLER, G. 1995. *Studies in seismotectonics*. PhD thesis, Oxford University, England.

PUDSEY, C. J. 1986. The Northern Suture, Pakistan: margin of a Cretaceous island arc. *Geological Magazine* **123**, 405–423.

——, COWARD, M. P., LUFF, I. W., SHACKLETON, R. M., WINDLEY, B. F. & JAN, M. Q. 1985. Collision zone between the Kohistan arc and the Asian plate in NW Pakistan. *Transactions of the Royal Society of Edinburgh: Earth Sciences*, **76**, 463–479.

ROECKER, S. W. 1982. Velocity structure of the Pamir–Hindu Kush region: possible evidence of subducted crust. *Journal of Geophysical Research*, **87**, 945–959.

SCHÄRER, U., COPELAND, P., HARRISON, T. M. & SEARLE, M. P. 1990. Age, cooling history and origin of post-collisional leucogranites in the Karakoram batholith, a multi-system isotope study. *Journal of Geology*, **98**, 233–251.

SEARLE, M. P. 1991. *Geology and Tectonics of the Karakoram Mountains*. John Wiley and Sons, Chichester.

—— 1996. Geological evidence against large scale pre-Holocene offsets along the Karakoram Fault: implications for the limited extrusion of the Tibetan Plateau. *Tectonics*, **15**, 171–186.

—— & KHAN, A. 1996. *Geological map of north Pakistan* (scale 1:650,000, 1 sheet). Oxford University Department of Earth Sciences, Oxford.

—— & TIRRUL, R. 1991. Structural and thermal evolution of the Karakoram crust. *Journal of the Geological Society of London*, **148**, 65–82.

——, CRAWFORD, M. B. & REX, A. J. 1992. Field relations, geochemistry, origin and emplacement of the Baltoro granite, Central Karakoram. *Transactions of the Royal Society of Edinburgh: Earth Sciences*, **83**, 519–538.

——, REX, A. J., TIRRUL, R., REX, D. C., BARNICOAT, A. & WINDLEY, B. F. 1989. Metamorphic, magmatic and tectonic evolution of the central Karakoram in the Biafo–Baltoro–Hushe regions of northern Pakistan. Geological Society of America Special Paper, **232**, 47–74.

——, WEINBERG, R. F. & DUNLAP, W. J. 1998. Transpressional tectonics along the Karakoram fault zone, northern Ladakh: constraints on Tibetan extrusion. *In*: HOLDSWORTH, R. E., STRACHAN, R. A. & DEWEY, J. F. (eds) *Continental Transpressional and Transtensional Tectonics*.

Geological Society, London, Special Publications, **135**, 307–326.

——, WINDLEY, B. F., COWARD, M. P., COOPER, D. J. W., REX, A. J. *et al.* 1987. The closing of Tethys and the tectonics of the Himalaya. *Geological Society of America Bulletin*, **19**, 1–12.

SMITH, A. G., HURLEY, A. M. & BRIDEN, J. C. 1981. *Phanerozoic, palaeocontinental world maps*. Cambridge University Press, Cambridge.

TALENT, J. A., CONAGHAN, P. J., MAWSON, R., MOLLOY, P. D. & PICKETT, J. W. 1981. Intricacy of tectonics in Chitral (Hindu Kush): faunal evidence and some regional implications. *Himalayan Geology Seminar (1976) section IIA, Geological Survey of India Miscellaneous Publication*, **41**, 77–101.

TAPPONNIER, P., MATTAUER, M., PROUST, F. & CASSAIGNEAU, C. 1981. Mesozoic ophiolites, sutures and large scale tectonic movements in Afghanistan. *Earth and Planetary Science Letters*, **52**, 355–371.

VAN HEIJST, H. J. 1998. *New constraints on the seismic structure of the Earth from surface wave overtone phase velocity measurements*. PhD thesis, Oxford University, England.

VOGELTANZ, R. & DIEMBERGER-SIRONI, M. A. 1969. Receptaculites neptuni Defrance im Devon des Hindukusch; Receptaculities neptuni Defrance in the Devonian of Hindu Kush. *Anzeiger der Oesterreichischen Akademie der Wissenschaften, Mathematisch-Naturwissenschaftliche Klasse*, **105** (1–15), 100–101.

ZANCHI, A., GAETANI, M. & POLI, S. 1997. The Rich Gol metamorphic complex; evidence of separation between Hindu Kush and Karakorum (Pakistan). *Comptes Rendus de l'Academie des Sciences, Serie II. Sciences de la Terre et des Planetes*, **325**, 877–882.

ZEITLER, P. K. & CHAMBERLAIN, C. P. 1991. Petrogenetic and tectonic significance of young leucogranites from the northwestern Himalaya, Pakistan. *Tectonics*, **10**, 729–741.

——, —— & SMITH, H. A. 1993. Synchronous anatexis, metamorphism, and rapid denudation at Nanga Parbat (Pakistan Himalaya). *Geology*, **21**, 347–350.

This page intentionally left blank

Pre-collisional anastomosing shear zones in the Kohistan arc, NW Pakistan

L. ARBARET[1], J.-P. BURG[1], G. ZEILINGER[1], N. CHAUDHRY[2], S. HUSSAIN[3] & H. DAWOOD[3]

[1]*Geologisches Institut, ETH-Zentrum, Sonneggstrasse 5, CH-8092, Zürich, Switzerland (e-mail: arbaret@erdw.ethz.ch)*

[2]*Institute of Geology, Punjab University, Quaid-e-Azam Campus, Lahore 54590, Pakistan*

[3]*Museum of Natural History, Garden Avenue, Shakaraparian, Islamabad 44000, Pakistan*

Abstract: Ductile strain localization commonly forms a pattern of shear zones anastomosing around lenses of less deformed rock. Initiation and development of anastomosing shear zones are studied through description of the structures and deformation history of plutonic rocks that form the lower crust of the Kohistan arc. Structures and textures developed in these rocks result from primary magmatic to solid state regional strain, overprinted by anastomosing shear zones. The primary strain was mainly acquired during magmatic emplacement at 100–90 Ma. Strain localization took place continuously from magmatic emplacement to solid state deformation during cooling of the plutons and formed three successive sets of shear zones. Set 1 is composed of associated discrete Riedel and thrust shear zones developed above solidus conditions during southwestward thrusting. Continuous deformation from solidus to amphibolite facies conditions between 100 and 83 Ma formed the second set of shear zones. The lower amphibolite facies set 3 shear zones are differentiated by larger strains recorded in the thicker mylonitic zones and enlargement of the spacing between shear zones during cooling. The anastomosing pattern of shear zones described here probably represents arc-related deformation during subduction of the Tethys oceanic lithosphere below the Kohistan arc.

Ductile strain is commonly concentrated into narrow shear zones, anastomosing around lenses of lower strain, the symmetry of the anastomosing pattern reflecting that of the bulk deformation history (Gapais *et al.* 1987). Anastomosing patterns are commonly reported (e.g. Mitra 1978; Ramsay 1980; Harris & Cobbold 1984; Gapais *et al.* 1987; Lafrance *et al.* 1998), but with limited information on their geometric detail and growth history. Therefore, the way such anastomosing patterns form and evolve remains an open question. In particular, the relationships between regionally distributed strain and strain localization in shear zones is not clear.

We aim to provide preliminary answers in describing the structures and deformation history of the plutonic rocks of the lower Kohistan arc. Some of these plutonic rocks display an early fabric that defines the regional pattern, but an important part of the deformation resulted in strain localization into shear zones anastomosing around lenses of less, or undeformed rock (Treloar *et al.* 1990). We argue that the regional background strain is composite and was mainly acquired during magmatic emplacement of the various plutons. The later anastomosing shear zones result from the nucleation and growth of three successive sets of shear zones sharing similar directions. Our petrologic information does not improve previous P–T estimates, thus we will not duplicate here the geothermobarometry of these rocks. Correlation between structures and the P–T–time history provides a detailed tectonic evolution of the lower part of the Kohistan arc.

Geological setting

The Kohistan arc was an island arc within the Tethys ocean during the Late Mesozoic (Tahirkheli *et al.* 1979; Bard 1983; Coward *et al.* 1986). The tectonic history involves the 102 to 75 Ma old accretion to the Asian plate, to the north (Petterson & Windley 1985; Treloar *et al.* 1989) and closure of the Tethys ocean, to the

From: KHAN, M. A., TRELOAR, P. J., SEARLE, M. P. & JAN, M. Q. (eds) *Tectonics of the Nanga Parbat Syntaxis and the Western Himalaya*. Geological Society, London, Special Publications, **170**, 295–311. 1-86239-061-4/00/$15.00

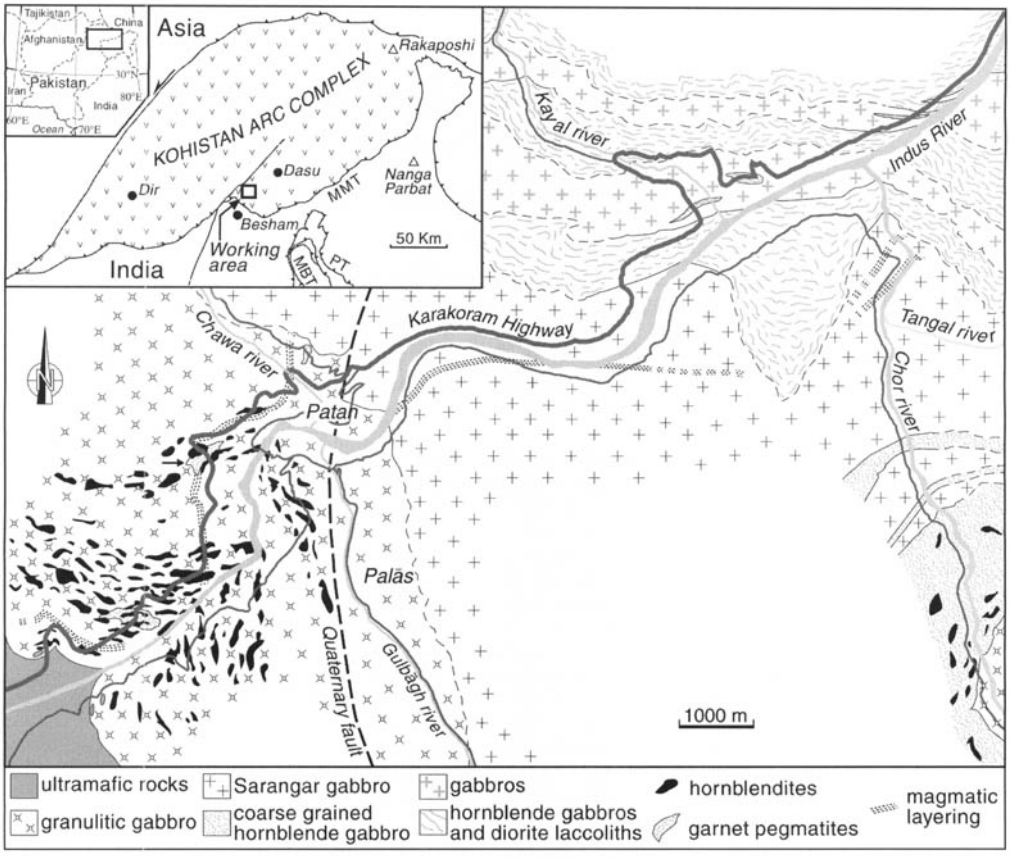

Fig. 1. Simplified geological map of the study area. Inset: localization in the Kohistan arc (modified from Bard 1983 and Burg *et al.* 1998).

south, at *c.* 55 Ma, followed by obduction of the Kohistan arc onto India (Coward *et al.* 1986). Our structural analysis was focused on the southern, i.e. lower, part of the arc sequence (Fig. 1). The study area in the southern-part of the Kamila Amphibolite Belt is comprised of metagabbros, hornblende–gabbros and diorites intruded by, and intruding, hornblendites (Treloar *et al.* 1990; Khan *et al.* 1993). The southernmost gabbro granulite facies is the upper part of the Jijal Complex (Jan & Howie 1981; Bard 1983; Yamamoto & Yoshino 1998). The structurally upper gabbro, named in this study the Sarangar gabbro, forms the lower part of the Patan Complex of Miller *et al.* (1991). The detailed petrography of these rocks has been presented by Jan & Howie (1981), Treloar *et al.* (1990), Miller *et al.* (1991), Yamamoto (1993), Yoshino *et al.* (1998) and Ringuette *et al.* (1999). All agree that they represent calc-alkaline magmas emplaced during arc activity (Khan *et al.* 1993). Ductile deformation related to the Kohistan/India fault contact, the Main Mantle Thrust (Tahirkheli *et al.* 1979), is limited to a few hundred metres above this major fault (Burg *et al.* 1998). It was therefore important to know why ductile deformation in shear zones (Treloar *et al.* 1990) was appearing several thousand metres higher in the Kohistan sequence, and to understand the kinematics involved in this deformation event. We will argue that this is an arc-related shear deformation synthetic to the subduction zone, above which the arc has grown.

Regional strain

The regional strain is defined by heterogeneously distributed foliations with associated mineral lineations. Two-dimensional mineral shape anisotropy has been measured in sections parallel to the lineation and perpendicular to the foliation (XZ planes of rocks), to estimate the orientation intensity of the mineral fabric (Fig. 2). We applied the intercept method (Rink 1976;

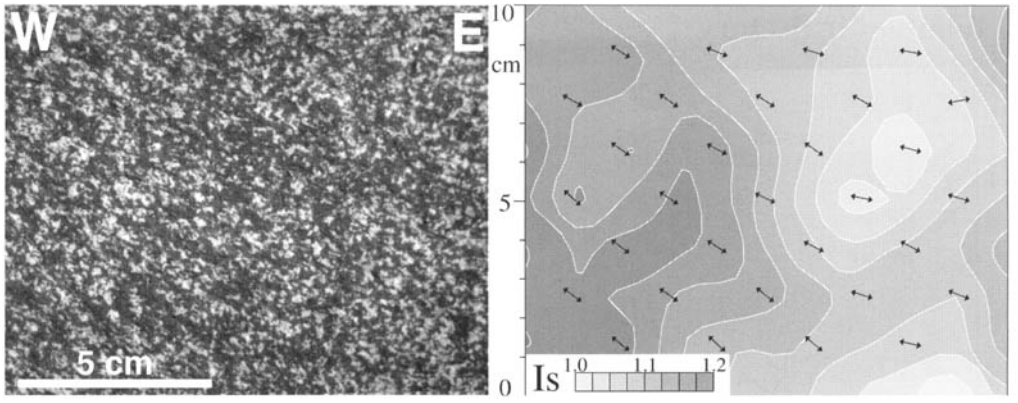

Fig. 2. Example of image analysis performed in an XZ section of the magmatic assemblage (left), showing the centimetre-scale variation of the fabric intensity Is of plagioclase between 1.05 and 1.2 (right). Note that the foliation trace (black double arrows) remains constant all over the image, independent of the fabric intensity (Sarangar gabbro; for location see Fig. 14).

Launeau *et al.* 1990; Launeau & Robin 1996) to feldspars because they are both the most common and the weakest mineral phase in all the studied rocks. Measurements close to the shear zones were not taken into consideration in order to avoid later strain effects.

Two intensity fabrics were recognized. The weak one (1.05 to 1.2, Fig. 2) is recorded in the core of the two structurally lower gabbros (Fig. 3). The weak intensity fabric corresponds to the shape-preferred orientation of the magmatic assemblages characterized by cumulate textures. The cumulate assemblage of the lowermost granulitic gabbro is composed of hypidiomorphic pyroxene, garnet, plagioclase and amphibole in textural equilibrium (Ringuette *et al.* 1999). Fabrics of this assemblage describe the *c.* 40° NW-dipping foliation and the *c.* 35° NW-plunging lineation (Figs 3 & 4). In the coarse-grained Sarangar gabbro that lies to the north of, and above, the granulitic gabbro (Fig. 1), weak intensity fabrics correspond to the coarse-grained magmatic cumulate, garnet-free assemblage of pyroxene and plagioclase (Fig. 5a). These intensity fabrics describe E–W trending vertical foliations bearing a W-plunging lineation (Figs 3 & 4).

The highest intensity fabrics (1.2 to > 1.6) were measured in three main locations. First, in the granulitic gabbro, the high intensity fabrics progressively replace the magmatic, low intensity fabrics, in particular toward the basal contact with ultramafic rocks (Fig. 3). Higher intensity fabrics mark a transition from magmatic to solid state deformation by plastic deformation of plagioclase and rigid rotation of pyroxene and other mineral phases towards the pluton boundaries. Local S–C structures and the angular relationship between the mineral fabric and magmatic layering indicate a bulk southwest-directed shear (Fig. 5b).

The second location of high intensity fabrics is the contact between the granulitic and the Sarangar gabbros. The extension of this fabric on both sides of the contact has a maximum width of about 2000 m. In the Sarangar gabbro, this high intensity fabric of orientated pyroxene and deformed plagioclase decreases and progressively gives way to a magmatic fabric towards the core of the pluton. Consistent foliation, lineation and kinematic directions and this geographical distribution suggest that the peri-plutonic high-intensity fabric represents solid state, ductile deformation at the boundary with the granulitic gabbro, during the Sarangar gabbro emplacement. In the granulitic gabbro, the high intensity fabric has overprinted the magmatic fabric (Fig. 3). These structural relationships indicate that the Sarangar gabbro is younger and has intruded the cooler-than-solidus granulitic gabbro.

Finally, strong and homogeneous orientation intensity fabrics occur throughout the hornblende–gabbro and diorite laccoliths that have intruded the Sarangar gabbro to the north (Fig. 3). Attitudes have an average 38° N-dip foliation with a NE-striking lineation (Figs 3 & 4). There is no preserved magmatic fabric in these rocks whose deformation is fundamentally solid state with rotated porphyroclasts indicating

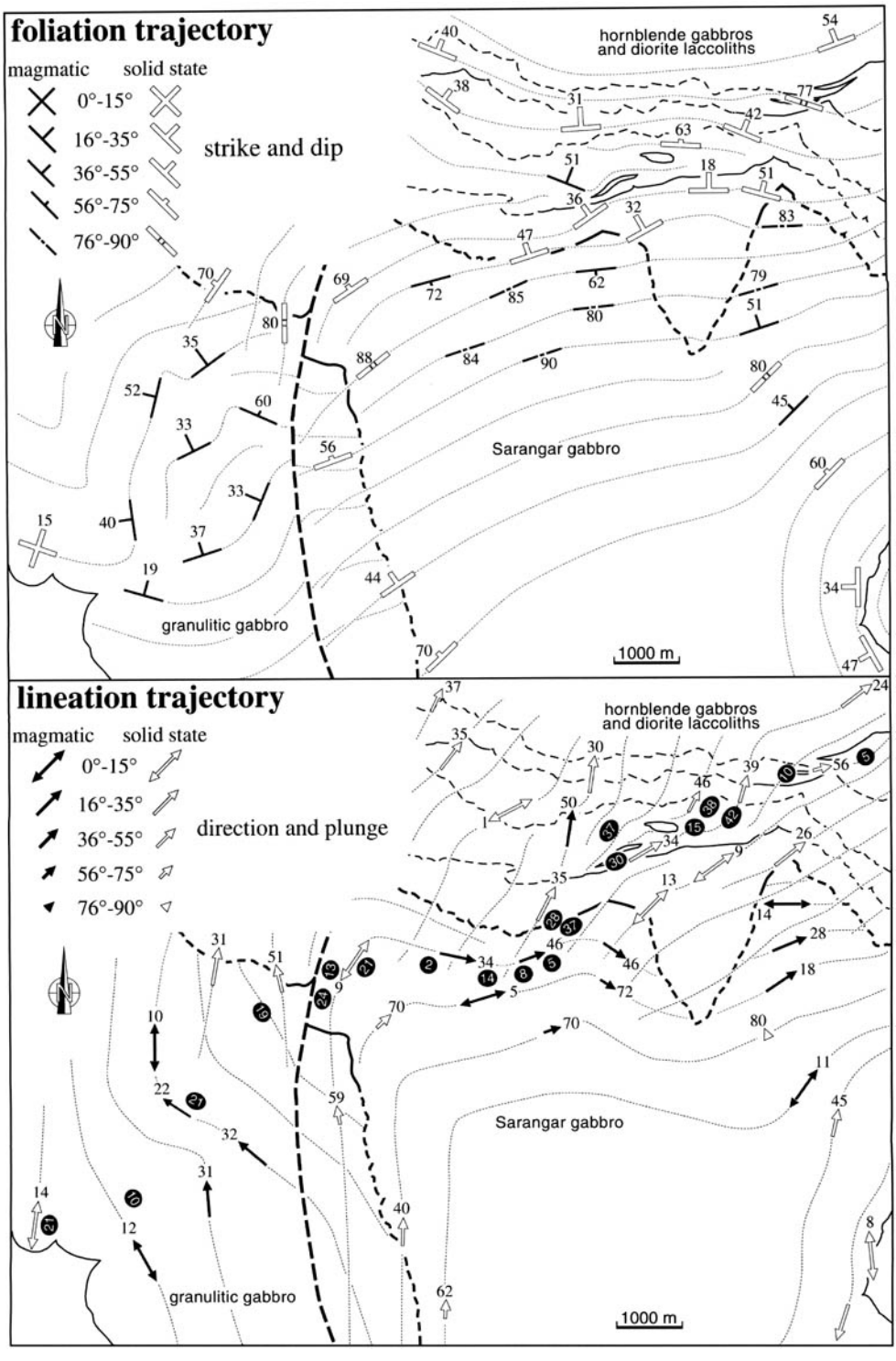

Fig. 3. Trajectories of magmatic and solid state foliations and lineations. Black ellipses indicate direction and intensity (percentage of anisotropy) of fabric measured in XZ planes.

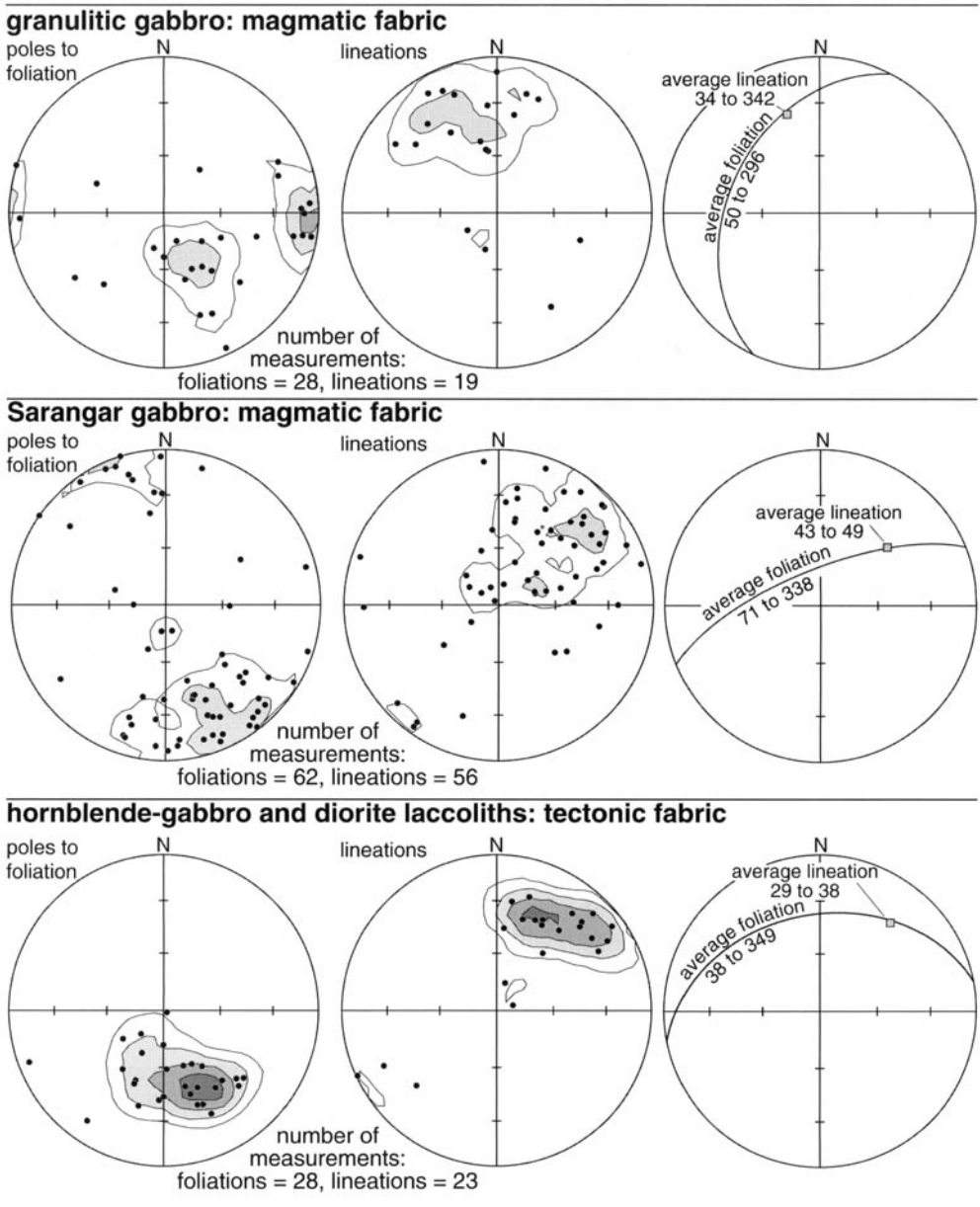

Fig. 4. Lower hemisphere equal-area projections of poles to foliations and lineations. Starkey density contours: 2, 4, 6 and 8%.

southwest-directed sense of shear, as recognized also in the northern parts of the Kamila belt (Treloar *et al.* 1990).

The metamorphic history of the granulitic gabbro includes sub-solidus isobaric cooling of the magmatic paragenesis within granulite facies conditions ($T = c.$ 750 °C and $P = c.$ 1.8 GPa, Ringuette *et al.* 1999). An Sm–Nd cooling age of 91 Ma (Yamamoto & Nakamura 1996) is slightly younger than Sm–Nd and Rb–Sr ages of 96 and 101 Ma, respectively, measured by Anczkiewicz & Vance (this volume). Preserved plagioclase–clinopyroxene assemblages indicate crystallization at 800 °C and 0.8–1.1 GPa in the Sarangar gabbro (Yoshino *et al.* 1998), whose age is not available. However, it should be bracketed by the

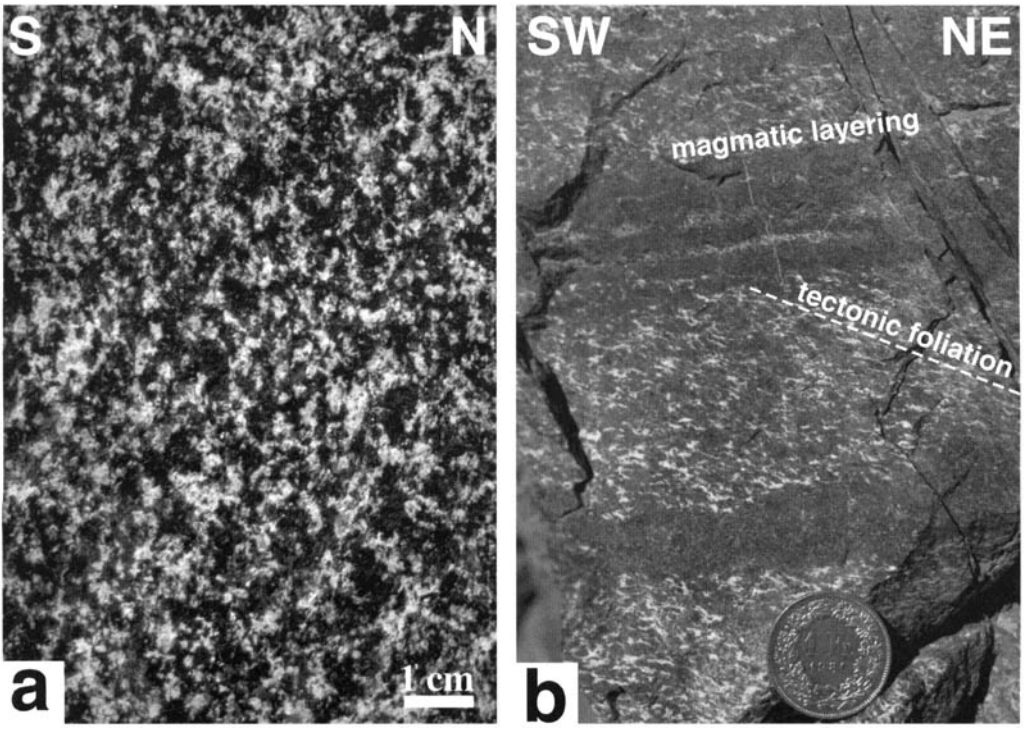

Fig. 5. (**a**) Magmatic texture in the Sarangar gabbro in an XZ section, trace of the foliation is vertical. (**b**) Cross-cutting relationships between the magmatic layering and the trace of the tectonic foliation indicating southwest-directed shear in the granulitic gabbro. Coin size is 23 mm. Locations in Fig. 14.

100–90 Ma old granulitic gabbro and the regional hydration phase at about 83 Ma (Ar–Ar age of amphibole, Treloar *et al.* 1990).

Therefore, the regional fabric fundamentally reflects magmatic emplacement of mafic, calc-alkaline magmas during the pre-collisional arc formation.

Shear strain localization

Shear strain localization is responsible for the anastomosing pattern of shear zones in the Kamila Shear Zone (Treloar *et al.* 1990) from which we have separated three successive sets.

Set 1

Set 1 is composed of shear zones less than 1 m long and a few centimetres wide (Figs 6 & 7). They bend the earlier magmatic foliation and layering, where present, without noticeable change in grain size and mineral assemblage. These shear zones apparently formed at conditions above the solidus because the magmatic paragenesis remained stable in their most deformed centres. Set 1 shear zones were found along structural and compositional discontinuities and within the bulk rock mass where they may be cut by millimetre-thick feldspar-rich magmatic joints (Fig. 7). Structural discontinuities are discrete, feldspar-rich magmatic joints, hornblendite boundaries and veins of quartz, feldspar and amphibole a few millimetres thick (Fig. 8), which supports the interpretation of the set 1 shear zones as being above solidus features.

Most of the set 1 shear zones have a normal sense in the field and are organized in two orientation populations (Fig. 9). The dominant one corresponds to shallowly S-dipping to horizontal shear zones with a SE- to SW-vergence. The second, apparently conjugate population, is formed of homogeneously NE-verging, N-dipping shear zones. These conjugate populations could indicate some subvertical flattening. However, field observation shows that many of the NE-verging shear zones are localized along upper and lower borders of hornblendite bodies that have rotated consistently with the bulk SE- to SW-vergent shear (Fig. 6). Reverse set 1 shear zones developed along more homogeneously NE-dipping planes with the same lineation direction as the normal

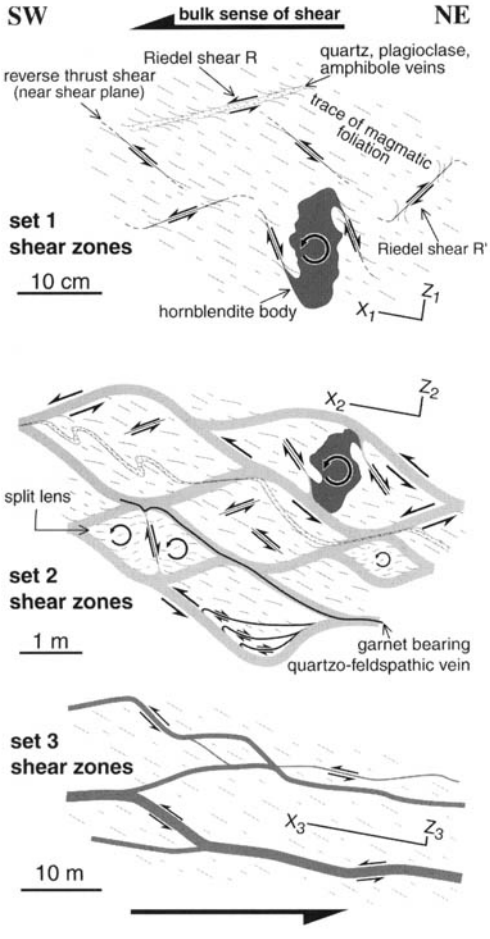

Fig. 6. Synthetic sketch of the three successive sets of shear zones. Set 1, centimetre-scale shear zones are developed along Riedel orientations consistent with a general, nearly horizontal southwest-directed shear during the late magmatic emplacement of the gabbros. Upper amphibolite facies set 2 shear zones developed later along the same orientations as set 1 shear zones. Lengthwise propagation of set 1 shear zones formed a metre-scale, anastomosing pattern in which partial melting yielded garnet-bearing quartzo-feldspathic veins. Northeast-directed normal set 2 shear zones developed essentially in response to rotation of hornblendite bodies and split lenses. The third set of shear zones, characterized by a larger spacing, developed in lower amphibolite facies conditions along and within similarly orientated set 2 shear zones.

shear zones. Thus, reverse and normal set 1 shear zones are kinematically consistent. Differences in orientation fit Riedel orientations in movement zones (Riedel 1929). The most common population of normal SW-vergent shear zones would represent Riedel shears R (Fig. 6). The reverse N-vergent shear zones have an attitude consistent with R′ Riedel shears (Fig. 6). We contend that the NE-dipping reverse shear zones were the closest to the main shear plane (primary shear bands D or, rather, thrust shears P; Tchalenko 1968). Indeed, they are nearly parallel to the regional lithological boundaries of intensely sheared rocks (the regional reference plane), which were nearly horizontal before tilting of the Kohistan arc subsequent to its obduction onto India (Tahirkheli *et al.* 1979; Coward *et al.* 1986).

All set 1 shear zones are therefore attributed to a general SW-directed shear. Set 1 shear zones have the same orientation in both the granulitic and the Sarangar gabbros, independent of the magmatic fabrics. We conclude that set 1 shear zones are a response to regional stresses. Limited grain size reduction in their centres and measurements of the passively curved foliation indicate shear strains $\gamma < 5$ (March 1932; Ramsay 1980). The geographical distribution of these shear zones is undetermined because solid state deformation in the other plutons and set 2 shear zones may have overprinted them.

Set 2

Set 2 is the most spectacular anastomosing pattern of mylonitic shear zones that wrap around lenses of less deformed rock with their long axis plunging to the northeast (Figs 6 & 10). Bordering continuous strain gradients include progressively curved rock-foliations whose fabric intensities increase to 1.9. The replacement of diopside and hypersthene by ferroan pargasitic to tshermakitic hornblendes (Treloar *et al.* 1990) is correlated with the increasing intensity of the fabric in the strain gradients. However, pyroxene porphyroclasts exist in the mylonite, which suggests that metamorphic conditions were dry enough to prevent full retrogression.

Some 66% of set 2 shear zones are N-dipping to flat-lying, SW-verging reverse shear zones bearing a *c.* 30° NE-plunging lineation (Fig. 11). They branch into horizontal to W-dipping, SW-verging normal shear zones bearing a *c.* 14° SW-plunging lineation. The change in attitude accommodates the shape of the preserved rock lenses. Some 11% of set 2 shear zones are NE-verging normal shear zones that developed, as did some of the set 1 zones, around the tips of rotated hornblendite bodies (Fig. 6). The other set 2 shear zones correspond to reactivated, similarly orientated SE-verging set 1 shear zones. The thickness of the mylonitic centre of set 2 shear zones, defined by mylonitic foliations parallel to the shear zone borders, varies along

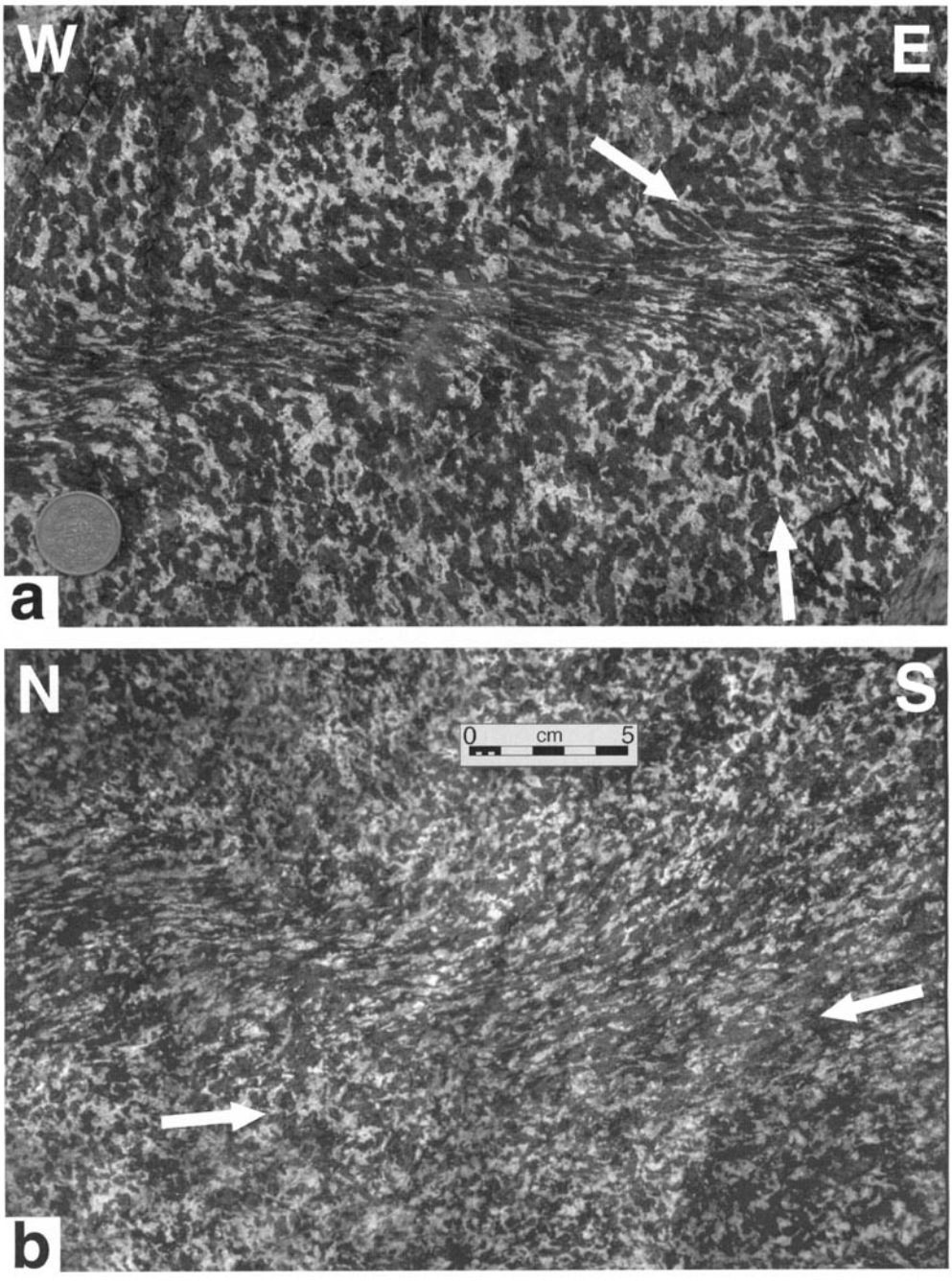

Fig. 7. Set 1 shear zones (location in Fig. 14). (**a**) Normal W-vergent Riedel shear zone cross-cut by a plagioclase-rich magmatic joint (arrows). (**b**) Lengthwise terminating set 1 shear zone. Arrow as in (a).

a single shear zone from less than 5 cm to more than 4 m (Fig. 12). Centimetre-wide splay shears may occur within lenses in response to rapid direction changes of set 2 shear zones or between rotating parts of split lenses (Figs 6 & 10b).

Long axes (**a**) and perpendicular short axes (**c**) of rock lenses were measured on 60 regularly shaped lenses of less-deformed gabbro, observed in XZ outcrops with respect to the stretching lineation and foliation of the bounding set 2 shear

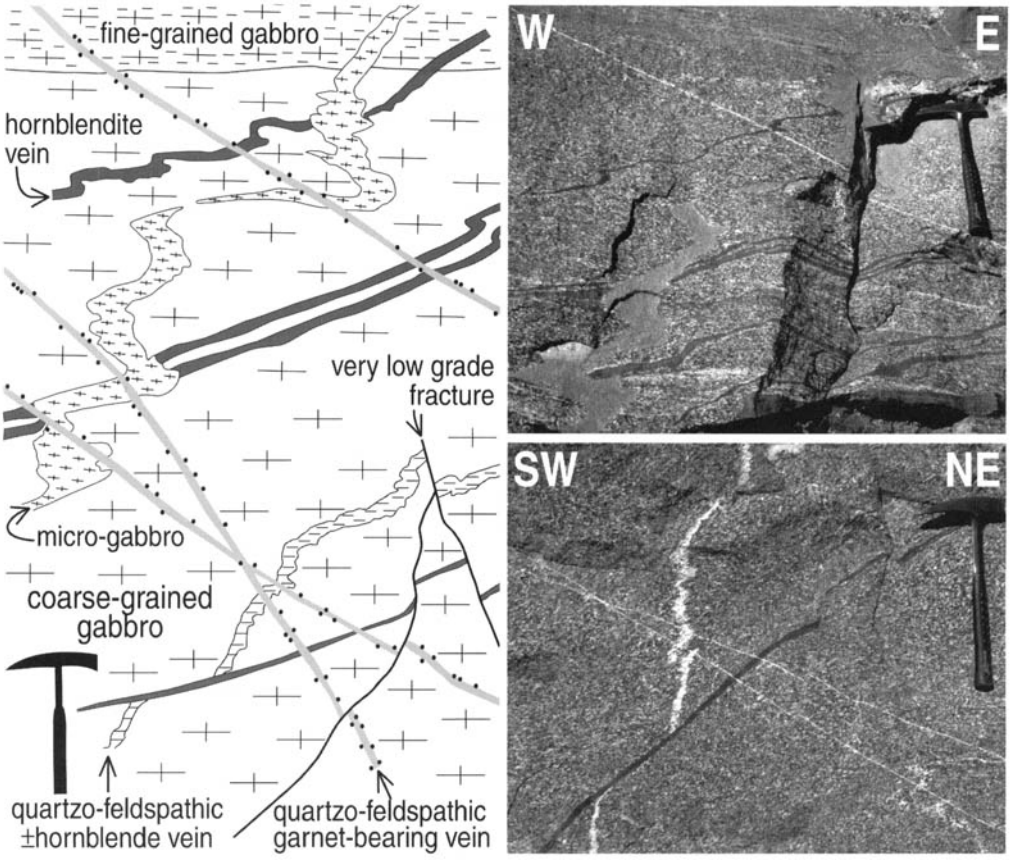

Fig. 8. Synthetic sketch of cross-cutting relationships between structural features in the Sarangar gabbro based on two successive outcrops (right).

zones. Measurements were limited for the sake of reliability to lenses less than 5 m long. Axis **a** v. axis **c** defines a linear relation at any scale (Fig. 13). Similar asymmetric lens shapes at all scales and strongly dominant SW-vergence indicate that set 2 shear zones developed during distributed non-coaxial deformation (Gapais *et al.* 1987).

Set 2 shear zones occur over the whole area (Fig. 14). In the Sarangar gabbro, they form a pervasive pattern with an average spacing of 8–10 m between shear zones. This regular spacing indicates periodicity in their distribution. The anastomosing pattern becomes dense, forming metric lenses of less deformed rock along the contact with the underlying granulitic gabbro in which the set 2 pattern has a metric distribution above the hornblendite-rich area. In the lower part of the granulitic gabbro, the spacing between set 2 shear zones increases in the hornblendite-rich area. No shear zone was found in the lowest 1000 m. In the hornblende-gabbros and diorite laccoliths, to the north, i.e. above the Sarangar gabbro, spacing between set 2 shear zones is about 50 m.

Metamorphic conditions associated with set 2 shear zones were estimated at 550–650 °C under pressures of 0.9–1.0 GPa (Bard 1983; Treloar *et al.* 1990). Partial melting in set 2 mylonites generated quartz–plagioclase–garnet-bearing segregation veins, some of which have been deformed by subsequent shearing (Fig. 10c), while others remained almost undeformed in transtensional zones between lenses (Fig. 10d). Partial melting indicates temperatures exceeding 650 °C under pressures of >0.8 GPa (Burnham 1979) for the initiation of set 2 shear zones, which is consistent with the upper amphibolite facies crystal plasticity described by Treloar *et al.* (1990).

The minimum age for set 2 shear zones is inferred from the 87 Ma amphibole–epidote–

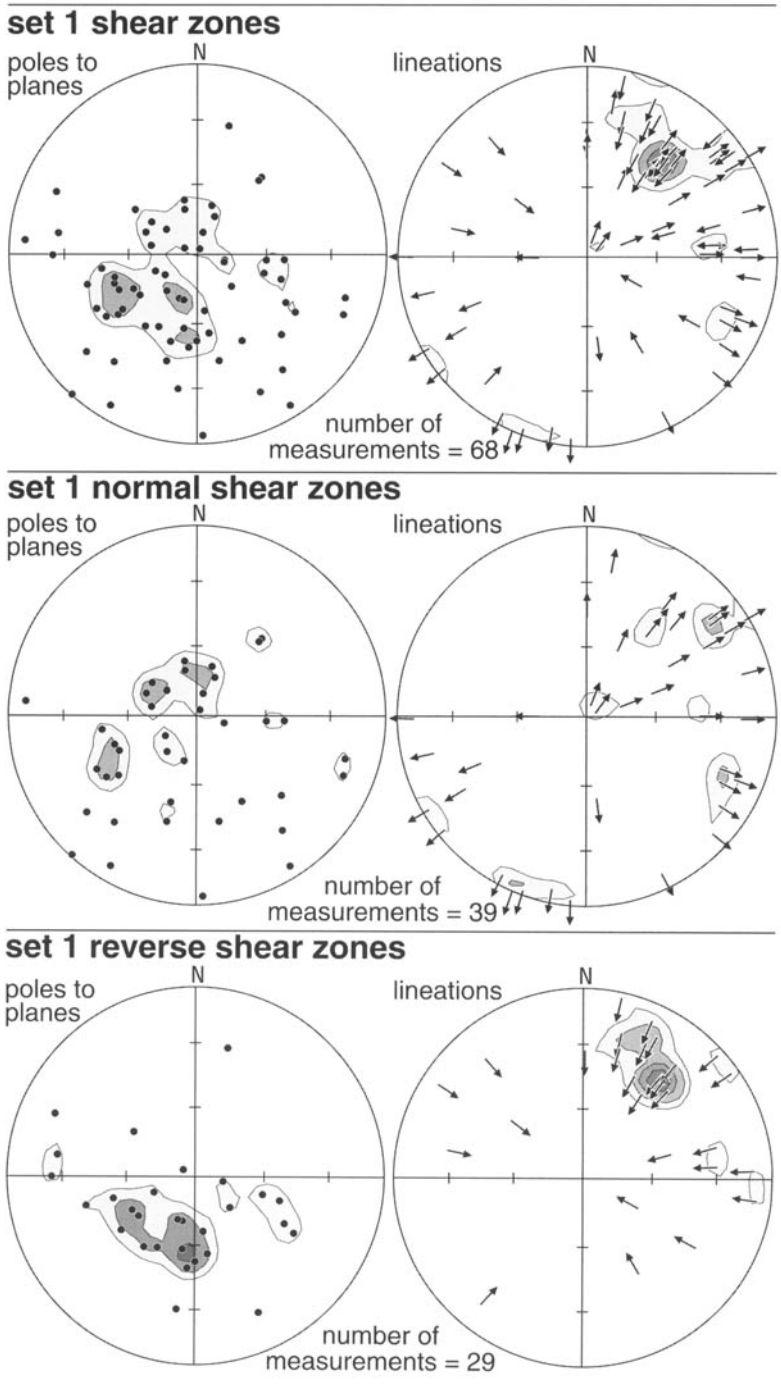

Fig. 9. Lower hemisphere equal-area projections of poles to planes and stretching lineations of set 1 shear zones, arrows pointing to the shear direction. Starkey density contours: 2, 4, 6 and 8%.

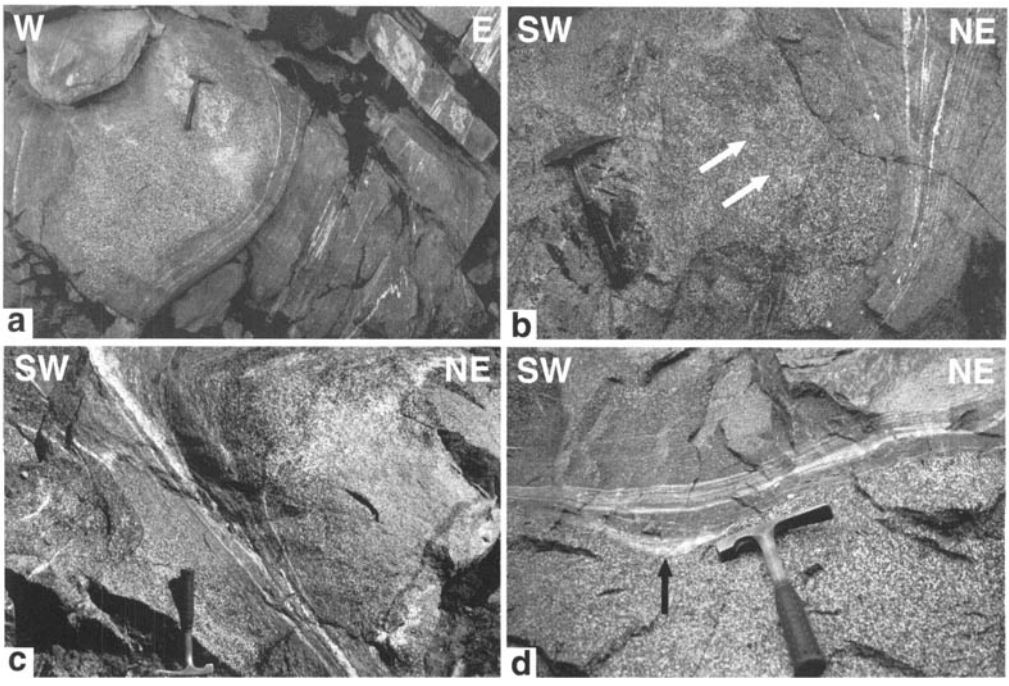

Fig. 10. Set 2 shear zones pattern (location in Fig. 14). (**a**) Shear zone wrapping around a lens of undeformed gabbro. (**b**) Rapid change in orientation of a shear zone inducing nucleation of centimetre-wide splay shears in the lens (parallel to the white arrows). (**c**), (**d**) Syn-mylonitic quartz-feldspar garnet-bearing veins in set 2 shear zones with (black arrow in d) undeformed segment of vein in a transtensional zone in a neck region of a lens of the Sarangar gabbro.

paragonite assemblage that has partially overprinted the granulite facies assemblage in the granulitic gabbro (Anczkiewicz 1998).

Set 3

Set 3 corresponds to several, tens of metres long, shallow S-dipping to 30° NE-dipping shear zones with a wavelength of over 50 m (Figs 6 & 15). Thickness distribution of the set 3 ductile mylonite zones presents a unimodal distribution (Fig. 12). Mylonitic zones display a strongly foliated and fine-grained matrix containing plagioclase with brittle deformation and relicts of amphiboles. Grain size reduction and rotated porphyroclasts of garnet and plagioclase derived from stretched pegmatite veins indicate shear strain $\gamma > 10$. Curvature of the foliation, along with the hornblendite and felsic veins within the shear zone boundaries, indicate SW-directed shearing in set 3 shear zones (Fig. 15b). Set 3 shear zones, which contain metric lenses of undeformed rock, developed along and within similarly orientated set 2 shear zones. The mylonitic assemblage is composed of quartz, plagioclase, amphibole and porphyroclastic garnet. This assemblage points to lower amphibolite facies conditions, which are not dated but are probably around the 83 Ma Ar–Ar age proposed for the end of the regional amphibolite facies metamorphism (Treloar *et al.* 1989; Wartho *et al.* 1996). Set 3 shear zone distribution is limited to the Sarangar gabbro and the hornblende–gabbro and diorite laccoliths with an average spacing of over 50 m (Fig. 14).

Discussion

The geometry of the anastomosing pattern and kinematic analysis of strain localization from regionally distributed fabrics provide a preliminary answer to the deformation history of the plutonic rocks, forming the lower part of the Kohistan arc.

The composite regional fabric, developed above solidus conditions, fundamentally reflects magmatic emplacement of mafic, calc-alkaline plutons around 100–90 Ma. The onset of shear strain localization is marked by the occurrence of set 1 shear zones whose Riedel-type attitudes were controlled by regional stresses. The continuous evolution from magmatic fabrics to solid

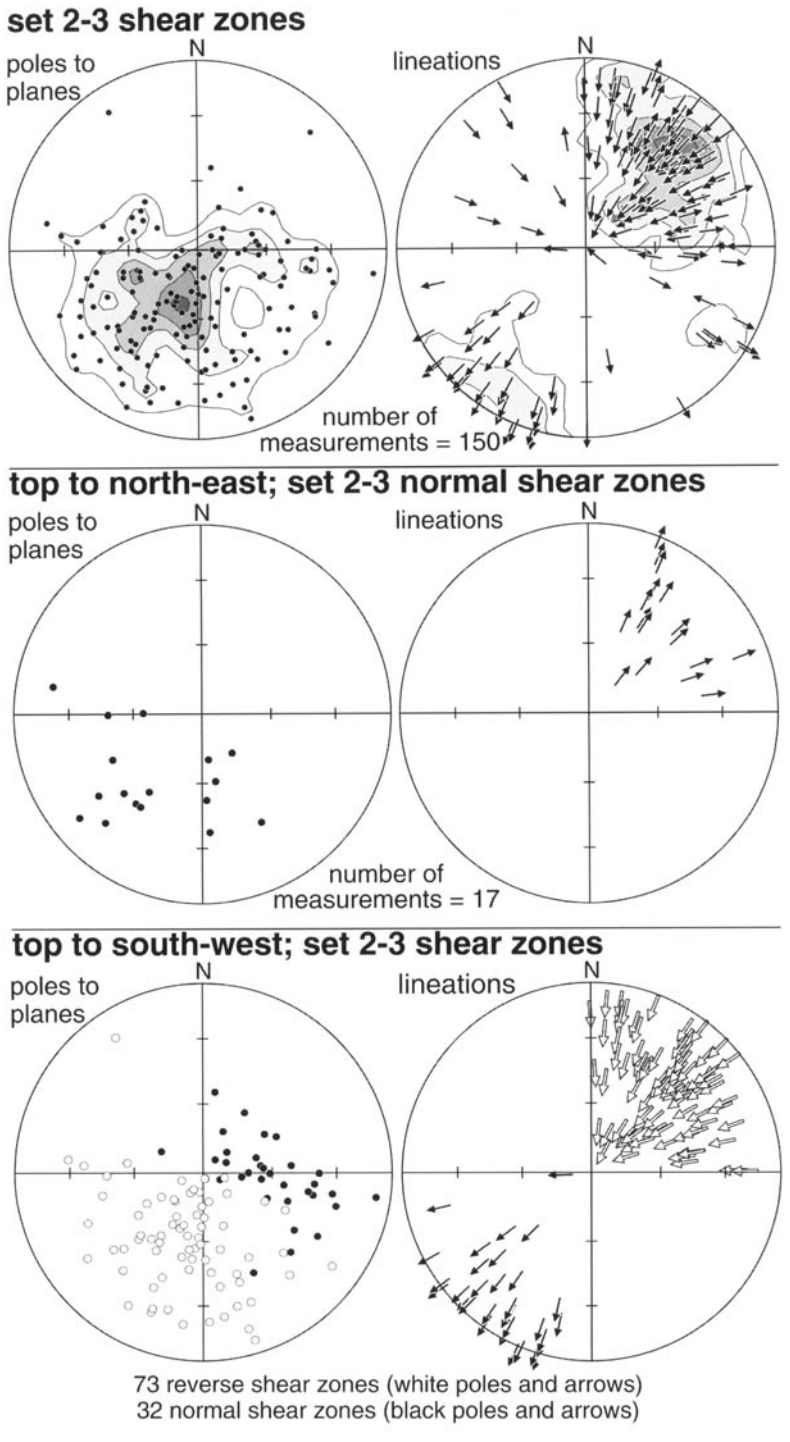

Fig. 11. Lower hemisphere equal-area projections of poles to planes and stretching lineations of set 2–3 shear zones, arrows pointing to the shear direction. Sense of shear determination is based on the curvature direction of foliations and the geometry of feldspar and garnet porphyroclasts in mylonites. Starkey density contours: 2, 4, 6, 8 and 10%.

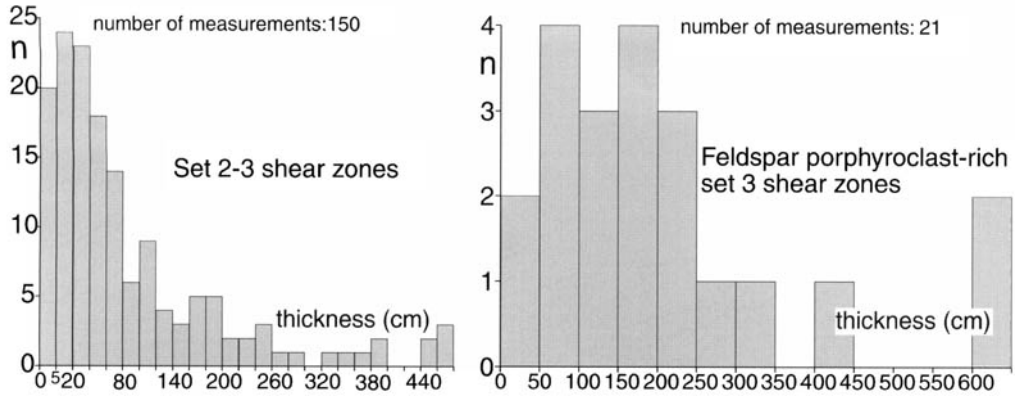

Fig. 12. Thickness distribution of mylonitic central zones of set 2 and 3 shear zones (average thickness = 1.27 m; median value = 50 cm) and feldspar porphyroclast-rich set 3 shear zones (average thickness = 2.8 m and median value = 1.9 m).

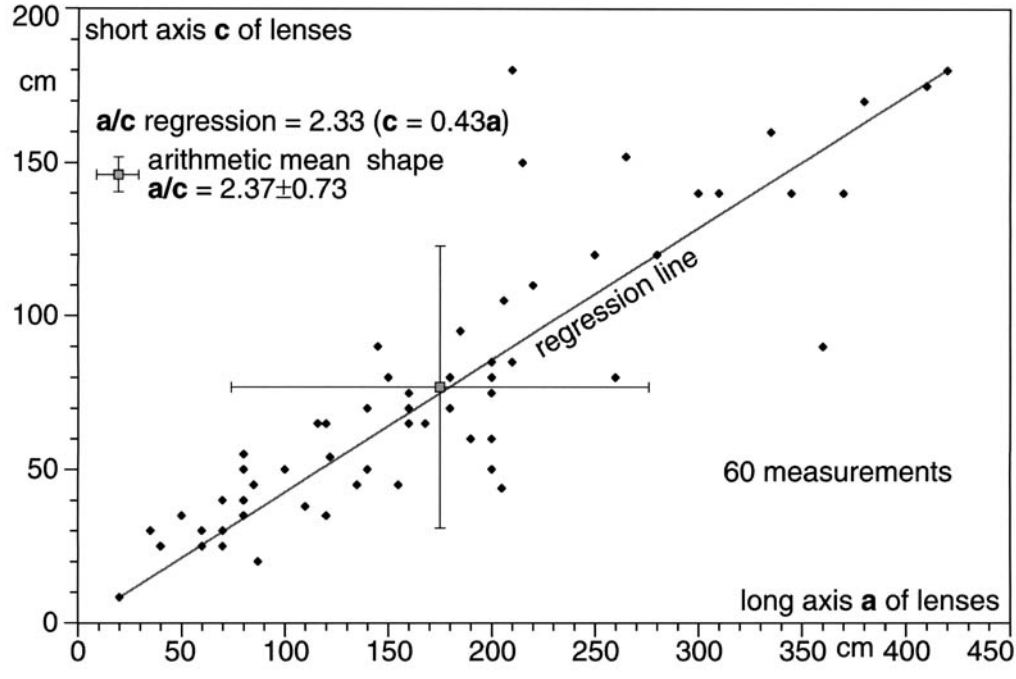

Fig. 13. Major axis **a** v. short axis **c** calculated from lenses of less-deformed gabbro observed in outcrop sections perpendicular to the foliation plane and parallel to the stretching lineation of the surrounding shear zones. Long axes of lenses vary between 35 and 420 cm and perpendicular short axes range from 8 to 180 cm.

state deformation indicates that strain localization began above or at solidus conditions of the mafic magmas. Similarity of attitudes suggests that the asymmetric anastomosing pattern of set 2 and set 3 shear zones formed by the lengthwise propagation of the set 1 shear zones. This cooling evolution is marked by a progressive increase in spacing of the array of shear zones.

Treloar *et al.* (1990) regarded shearing in the Kamila Amphibolite Belt at temperatures greater than 500 °C until 80 ± 5 Ma as the major expression of arc thickening produced by collision with Asia, to the north, between 102 and 75 Ma. Treloar *et al.* (1996) revisited this scenario and suggested that heating metamorphism and melting of the lower arc were rather

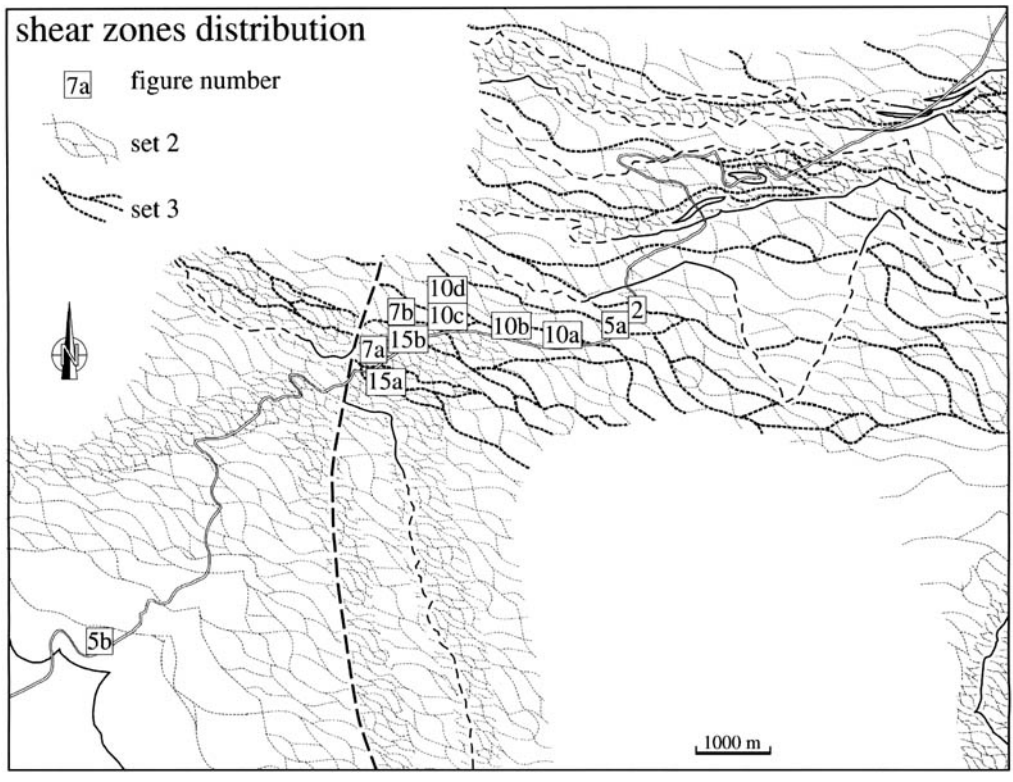

Fig. 14. Distribution and density of the set 2 and 3 shear zone patterns. Squared numbers give location of photographs.

related to magmatic underplating and intra arc-rifting (Khan *et al.* 1989, 1993).

Age constraints indicate that SW-directed thrusting responsible for the three successive sets of anastomosing shear zones was active between 100 and 80 Ma at the latest. This supports the interpretation in terms of progressive development of the anastomosing pattern during magmatic, quasi-isobaric cooling and subsequent retrogression through the hornblende blocking temperature of the calc-alkaline plutons. This time span range includes shearing in the Kamila Amphibolitic Belt between 100 and 83 Ma (Treloar *et al.* 1990), but also the extensional emplacement of the Chilas Complex (Burg *et al.* 1998) at *c.* 84 Ma (U–Pb age, Zeitler *et al.* 1981). Because of the apparent age discrepancy and the structural presence of an extensional zone between the southern Kohistan and the Northern suture, with Asia, we do not follow Treloar *et al.* (1996) in their collisional interpretation of the studied shear zones and shear fabrics. Instead, we attribute the anastomosing shear zones in the lower part of the Kohistan, to arc-related deformation during northward subduction of the Tethys lithosphere below the Kohistan arc. The sense of subduction has imparted the bulk, syn-magmatic sense of shear.

Conclusion

The calc-alkaline plutons forming the lower part of the Kohistan arc have recorded the structural dynamics during their emplacement and subsequent solid state deformation. Regionally distributed magmatic-related fabrics and set 1 shear zones developed under solidus conditions. Set 2 and 3 anastomosing shear zones were superposed onto set 1 shear zones, with increasingly localized deformation along Riedel shear directions. The anastomosing pattern has grown through lengthwise propagation of initially discrete set 1 shear zones, while thickening of the propagating shear zones remained minor. These events occurred successively between 100 and 83 Ma during the continuous SW-directed shearing, probably initiated by subduction accretion of the Tethys lithosphere below the Kohistan arc.

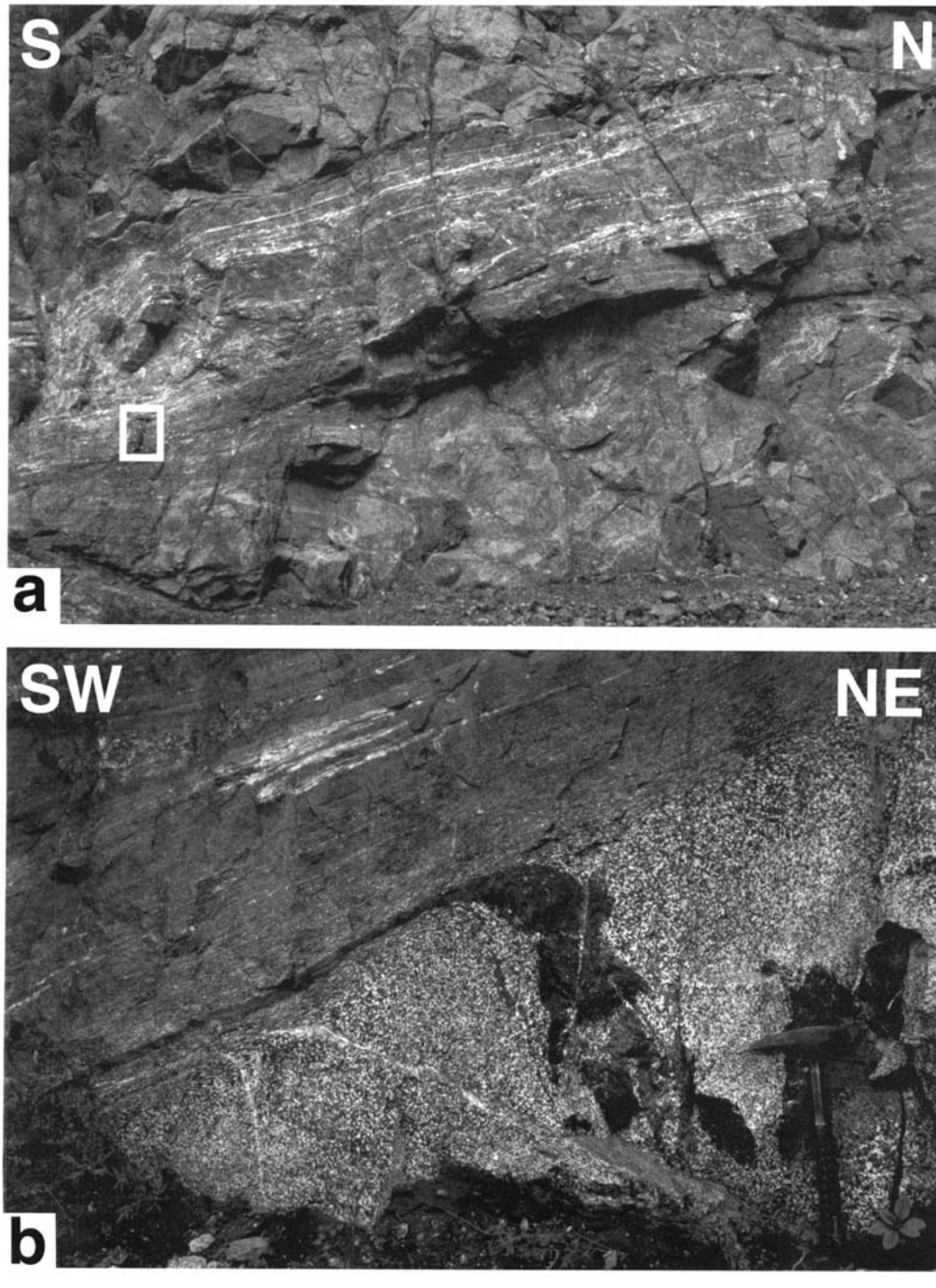

Fig. 15. Set 3 shear zones (locations in Fig. 14): (**a**) feldspar-rich normal shear zone (scale hammer is squared); (**b**) hornblendite and felsic veins curved within the lower boundary of a SW-directed normal shear zone.

Supported by the Swiss National Science Foundation (grant 20-49372.96). We thank D. Seward for her patient correction of the preliminary version of this text and P. J. Treloar and J. Grocott for detailed reviews of the manuscript. N. Chaudhry (Punjab University), S. Hussain and H. Dawood (Museum of Natural History) acknowledge the support of their institutions.

References

ANCZKIEWICZ, R. 1998. *Structural and geochronological study of the India–Kohistan arc collision, lower Swat region of Pakistan, NW Himalaya.* PhD thesis, Swiss Federal Institute of Technology, Zurich.

—— & VANCE, D. 2000. Isotopic constraints in the evolution of metamorphic conditions in the Jijal–Patan complex and the Kamila Belt of the Kohistan arc, Pakistan Himalaya. *This volume.*

BARD, J. P. 1983. Metamorphism of an obducted island arc: example of the Kohistan sequence (Pakistan) in the Himalayan collided range. *Earth and Planetary Science Letters*, **65**, 133–144.

BURG, J. P., BODINIER, J. L., CHAUDHRY, S., HUSSAIN, S. & DAWOOD, H. 1998. Infra-arc mantle–crust transition and intra-arc mantle diapirs in the Kohistan Complex (Pakistani Himalaya). petro-structural evidence. *Terra Nova*, **10**, 74–80.

BURNHAM, C. W. 1979. Magmas and hydrothermal fluids. *In*: BARNES, H. L. (ed.) *Geochemistry of hydrothermal ore deposits.* Wiley-Interscience Publication, New York, 71–136.

COWARD, M. P., WINDLEY, B. F., BROUGHTON, R. D., LUFF, I. W., PETTERSON, M. G., *et al.* 1986. Collision tectonics in the NW Himalayas. *In*: COWARD, M. P. & RIES, A. C. (eds) *Collision Tectonics.* Geological Society, London, Special Publications, **19**, 203–219.

GAPAIS, D., BALE, P., CHOUKROUNE, P., COBBOLD, P. R., MAHJOUB, Y. & MARQUER, D. 1987. Bulk cinematics from shear zone pattern: some field examples. *Journal of Structural Geology*, **9**, 635–646.

HARRIS, L. B. & COBBOLD, P. R. 1984. Development of conjugate shear bands during bulk simple shearing. *Journal of Structural Geology*, **7**, 37–44.

JAN, M. Q. & HOWIE, R. A. 1981. The mineralogy and geochemistry of the metamorphosed basic to ultrabasic rocks of the Jijal complex, Kohistan, NW Pakistan. *Journal of Petrology*, **22**, 85–126.

KHAN, M. A., JAN, M. Q., WINDLEY, B. F., TARNEY, J. & THIRLWALL, M. 1989. The Chilas mafic–ultramafic igneous complex: the root of the Kohistan island arc in the Himalaya of northern Pakistan. *In*: MALINCONICO, L. L. & LILLIE, J. (eds) *Tectonic of the Western Himalayas.* Geological Society of America, Special Papers, **232**, 75–94.

——, —— & WEAVER, B. L. 1993. Evolution of the lower arc crust in Kohistan, N. Pakistan: temporal arc magmatism through early, mature and intra-arc rift stages. *In*: TRELOAR, P. J. & SEARLE, M. P. (eds) *Himalayan Tectonics.* Geological Society, London, Special Publications, **74**, 123–138.

LAFRANCE, B., JOHN, B. E. & FROST, B. R. 1998. Ultra high-temperature and subsolidus shear zones: examples from the Poe Mountain anorthosite, Wyoming. *Journal of Structural Geology*, **20**, 945–955.

LAUNEAU, P. & ROBIN, P.-Y. F. 1996. Fabric analysis using the intercept method. *Tectonophysics*, **267**, 91–119.

——, BOUCHEZ, J. L. & BENN, K. 1990. Shape preferred orientation of object populations: automatic analysis of digitized images. *Tectonophysics*, **180**, 201–211.

MARCH, A. 1932. Mathematische Theorie der Regelung nach der Korngestalt bei affiner Deformation. *Zeitschrift Kristallographie*, **81**, 285–297.

MILLER, D. J., LOUCKS, R. R. & ASHRAF, M. 1991. Platinum group elements mineralisation in the Jijal layered mafic–ultramafic complex, Pakistani Himalayas. *Economic Geology*, **86**, 1093–1102.

MITRA, G. 1978. Ductile deformation zones and mylonites: The mechanical processes involved in the deformation of crystalline basement rocks. *American Journal of Science*, **278**, 1057–1084.

PETTERSON, M. G. & WINDLEY, B. F. 1985. Rb–Sr dating of the Kohistan arc-batholith in the Trans-Himalaya of N. Pakistan, and tectonic implications. *Earth and Planetary Science Letters*, **74**, 45–57.

RAMSAY, J. G. 1980. Shear zone geometry: a review. *Journal of Structural Geology*, **2**, 83–99.

RIEDEL, W. 1929. Zur Mechanik geologischer Brucherscheinungen. *Centralblatt Mineralogie, Abteilung B*, 354–368.

RINGUETTE, L., MARTIGNOLE, J. & WINDLEY, B. F. 1999. Magmatic crystallization, isobaric cooling, and decompression of the garnet-bearing assemblages of the Jijal sequence (Kohistan terrane, western Himalayas). *Geology*, **27**, 139–142.

RINK, M. 1976. A computerized quantitative image analysis procedure for investigating features and an adapted image process. *Journal of Microscopy*, **107**, 267–286.

TAHIRKHELI, R. A. K., MATTAUER, M., PROUST, F. & TAPPONNIER, P. 1979. The India Eurasia suture zone in northern Pakistan: synthesis and interpretation of recent data at plate scale. *In*: FARAH, A. & DEJONG, K. A. (eds) *Geodynamics of Pakistan.* Geological Survey of Pakistan, Quetta, 125–130.

TCHALENKO, J. S. 1968. The evolution of kink bands and the development of compression textures in sheared clays. *Tectonophysics*, **6**, 159–174.

TRELOAR, P. J., BRODIE, K. H., COWARD, M. P., JAN, M. Q., KHAN, M. A. *et al.* 1990. The evolution of the Kamila shear zone, Kohistan, Pakistan. *In*: SALISBURY, M. H. & FOUNTAIN, D. M. (eds) *Exposed Cross-sections of the Continental Crust.* Kluwer Academic, The Netherlands, 175–214.

——, PETTERSON, M. G., JAN, M. Q. & SULLIVAN, M. A. 1996. A re-evaluation of the stratigraphy and evolution of the Kohistan arc sequence, Pakistan Himalaya: implications for magmatic and tectonic arc-building processes. *Journal of the Geological Society, London*, **153**, 681–693.

——, REX, D. C., GUISE, P. G., COWARD, M. P., SEARLE, M. P. *et al.* 1989. K–Ar and Ar–Ar geochronology of the Himalayan collision in NW Pakistan: constraints on the timing of suturing, deformation, metamorphism and uplift. *Tectonics*, **8**, 881–909.

WARTHO, J.-A., REX, D. C. & GUISE, P. G. 1996. Excess argon in amphiboles linked to greenschist facies alteration in the Kamila amphibolite Belt, Kohistan island arc system, northern Pakistan: insights from $^{40}Ar/^{39}Ar$ step-heating and acid leaching experiments. *Geological Magazine*, **133**, 595–609.

YAMAMOTO, H. 1993. Contrasting metamorphic *P–T*–times paths of the Kohistan granulites and tectonics of the western Himalayas. *Journal of the Geological Society, London*, **150**, 843–856.

—— & NAKAMURA, E. 1996. Sm–Nd dating of garnet granulites from the Kohistan complex, northern Pakistan. *Journal of the Geological Society, London*, **153**, 965–969.

—— & YOSHINO, T. 1998. Superposition of replacements in the mafic granulites of Jijal complex of the Kohistan arc, northern Pakistan: dehydration and rehydration within deep arc crust. *Lithos*, **43**, 219–234.

YOSHINO, T., YAMAMOTO, H., OKUDAIRE, T. & TORIUMI, M. 1998. Crustal thickening of the lower crust of the Kohistan arc (N. Pakistan) deduced from Al zoning in clinopyroxene and plagioclase. *Journal of Metamorphic Geology*, **16**, 729–748.

ZEITLER, P. K., TAHIRKHELI, R. A. K., NAESSER, C., JOHNSON, N. & LYONS, J. 1981. Preliminary fission track ages from the Swat Valley, northern Pakistan. *Geological Bulletin of the University of Peshawar*, **13**, 63–65.

This page intentionally left blank

Timing of magmatic and metamorphic events in the Jijal complex of the Kohistan arc deduced from Sm–Nd dating of mafic granulites

H. YAMAMOTO[1] & E. NAKAMURA[2]

[1]*Department of Earth and Environmental Sciences, Faculty of Science, Kagoshima University, Korimoto 1-21-35, Kagoshima 890-0065, Japan (e-mail: hyam@sci.kagoshima-u.ac.jp)*

[2]*The Pheasant Memorial Laboratory for Geochemistry & Cosmochemistry, Institute for Study of the Earth's Interior, Okayama University at Misasa, Tottori-ken 682-0193, Japan*

Abstract: Mafic to ultramafic granulites in the northeastern part of the Jijal complex include two-pyroxene granulite, garnet–clinopyroxene granulite and garnet hornblendite. Field and textural relations indicate that two-pyroxene granulite is a relict left after formation of the garnet–clinopyroxene granulite and garnet hornblendite was an originally intrusive rock which dissected the protoliths of mafic granulites. Sm–Nd mineral isochron ages of 118 ± 12 Ma, 94.0 ± 4.7 Ma and 83 ± 10 Ma were determined for two-pyroxene granulite, garnet–clinopyroxene granulite and garnet hornblendite respectively. These ages, together with previously reported chronological data, led to the following tectonic implications: (1) crystallization of the granulite protoliths predates, or is coeval with, the tectonic accretion of the Kohistan arc to the Asian continent; (2) crustal thickening related to the accretion was probably responsible for the high-pressure granulite-facies metamorphism in the Jijal complex; (3) formation of the garnet hornblendite assemblage was probably after crystallization of garnet–clinopyroxene granulite.

In the western Himalaya, the Kohistan sequence is sandwiched between the Main Mantle Thrust on the south and the Shyok Suture on the north, between the Asian and Indian continental plates (e.g. Tahirkheli *et al.* 1979; Bard 1983; Coward *et al.* 1986; Pudsey 1986). The Kohistan sequence is considered to be a part of an island arc (Kohistan arc) which was accreted to the Asian continent prior to its collision with the Indian continent (Coward *et al.* 1987). In the southern part of the arc, a fault-bounded wedge, mainly composed of garnet–granulites and ultramafic rocks, covers an area of at least 150 km^2 and is called the Jijal complex (Jan & Howie 1981). The Jijal complex is regarded as a fragment of the lower crust of the arc (e.g. Coward *et al.* 1987; Yamamoto 1993).

A number of petrological studies describe a variety of granulites in the Jijal complex, although the granulite-facies metamorphism is not well integrated into the tectonic history of the Kohistan arc. A scarcity of isotopic ages is one of the major difficulties in interpreting the Jijal complex. Several mineral isochron ages of the granulites of the Jijal complex have been published (Coward *et al.* 1986; Yamamoto & Nakamura 1996; Anczkiewicz & Vance 1997) although, in most cases, isotopic ages are quoted without isotopic data and petrographic descriptions. High quality isotopic ages are prerequisites for understanding the lower crustal process. In this paper, we present three new Sm–Nd mineral isochron ages of granulites from the northern part of the Jijal complex and discuss the timing of the magmatic and metamorphic events.

Geological setting

The Jijal complex extends for more than 30 km along strike and has a maximum width of about 15 km. The northeastern part of the complex is dominated by garnet granulite whilst the southwestern part consists of peridotite and pyroxenite (Fig. 1). The northeastern and the southwestern parts are named the Patan granulite body and the Jijal ultramafic body respectively (Yamamoto & Yoshino 1998).

From: KHAN, M. A., TRELOAR, P. J., SEARLE, M. P. & JAN, M. Q. (eds) *Tectonics of the Nanga Parbat Syntaxis and the Western Himalaya*. Geological Society, London, Special Publications, **170**, 313–319. 1-86239-061-4/00/$15.00

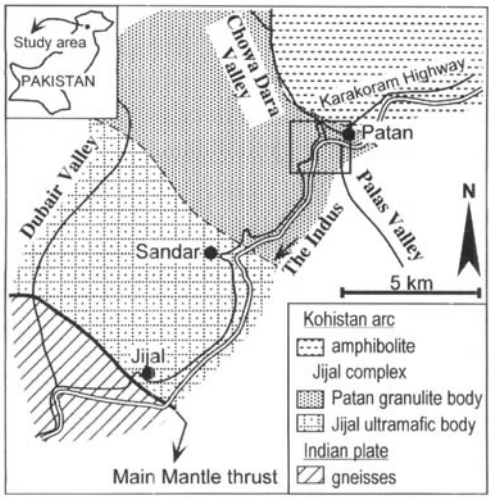

Fig. 1. Lithological map of the southern part of Indus Kohistan. Open box marks limits of the route map (Fig. 2).

The rocks of the Patan granulite body can be divided into plagioclase-rich and plagioclase-absent lithologies (Jan & Howie 1981). The plagioclase-rich rocks include garnet–clinopyroxene granulite, two-pyroxene granulite and amphibolite. The mineral assemblage of a two-pyroxene granulite is orthopyroxene + clinopyroxene ± hornblende + plagioclase ± quartz and that of the garnet–clinopyroxene granulite is garnet + clinopyroxene ± hornblende + plagioclase + quartz. Two-pyroxene granulite crops out only around Patan (Fig. 2), where the older assemblage is preserved because of incomplete replacement. The garnet–clinopyroxene granulite forms elongate patches, lenses or bands separated by narrow reaction zones from the host two-pyroxene granulite (Fig. 3a). Pressure–temperature conditions for the garnet–clinopyroxene granulite are estimated at 670–790 °C at 12–14 kbar (Jan & Howie 1981) and 697–949 °C at 11–17 kbar (Yamamoto 1993). A wider range of P–T conditions (750–1150 °C at 12–19 kbar) for this rock type is reported by Ringuette *et al.* (1998). Garnet–clinopyroxene granulite, together with two-pyroxene granulite, is locally intersected by bands of amphibolitization (from several centimetres to several metres). The attitudes of amphibolitized zones are discordant to those of garnet–clinopyroxene granulite patches or lenses (Yamamoto & Yoshino 1998).

It is argued in some papers that the garnet-bearing mineral assemblage in the gabbroic rocks of the Jijal complex was crystallized from a melt under high pressure conditions (Miller *et al.* 1991; Kausar *et al.* 1998; Ringuette *et al.* 1998). This 'magmatic garnet issue' probably arises

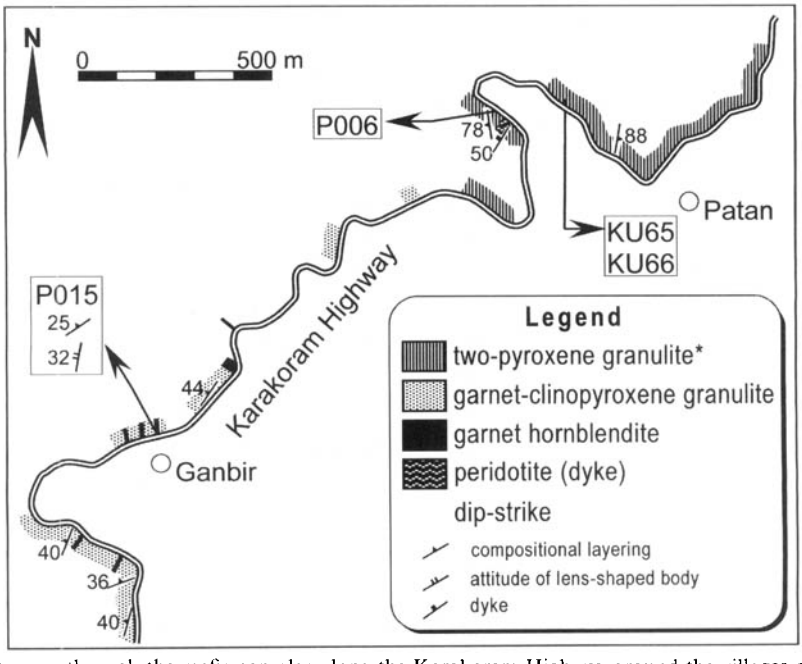

Fig. 2. Route map through the mafic complex along the Karakoram Highway around the villages of Patan and Ganbir. *, two-pyroxene granulite including bands and lenses of garnet–clinopyroxene granulite.

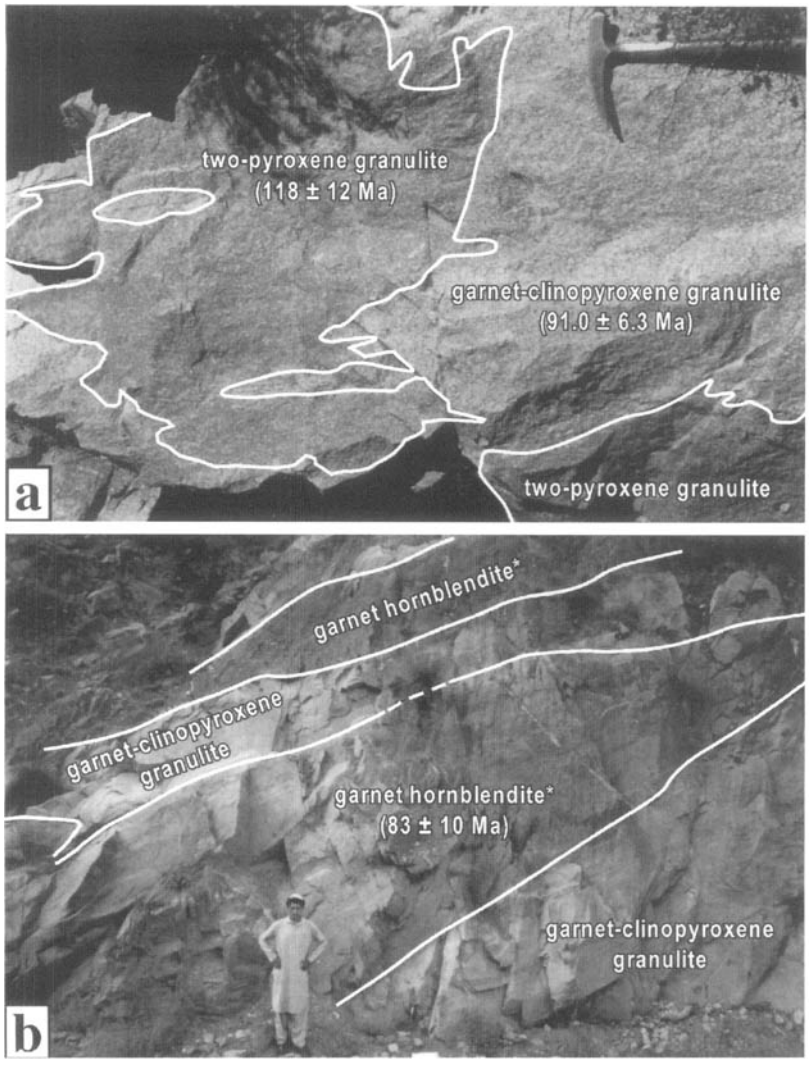

Fig. 3. Field photographs: (**a**) occurrence of two-pyroxene granulite and garnet–clinopyroxene granulite near Patan (KU65 and KU66); (**b**) lens-shaped bodies (N10° E 32° W) of garnet hornblendite set in the garnet–clinopyroxene granulite near Ganbir (P015).

from the description that 'garnet gabbro' has magmatic–sedimentary layering (Miller *et al.* 1991). The two-pyroxene granulite and the garnet–clinopyroxene granulite in this area exhibit compositional layering that is similar to the magmatic sedimentary structure reported by Miller *et al.* (1991). A pyroxene-dominated layer in the garnet-absent domains changes into a garnet-dominated layer in the garnet-bearing domains, and these layers are continuous through the irregular boundaries between the domains (Yamamoto & Yoshino 1998, fig. 4b). This strongly indicates that the layers were not formed in separate intrusive bodies, but in the same body. A possible scenario for 'magmatic garnet' involves a highly improbable process that garnet and orthopyroxene were crystallized in separate domains, then formed magmatic-sedimentary layering in the individual domains, and that layers in the adjacent domains met each other just like a single layer.

There are zones of transitional mineral assemblages up to 2 cm wide along the boundaries between garnet-bearing and garnet-absent domains. Orthopyroxene and garnet occur together only in the transitional zones and

these minerals are not in direct contact at microscopic scale. Where orthopyroxene is located close to garnet, thin films of quartz or clinopyroxene separate them. In the transitional zones, modal garnet increases and orthopyroxene–plagioclase decreases away from the two-pyroxene granulite domain toward the garnet–clinopyroxene granulite domain. The compositional layering is preserved even in the transitional zones. These lines of evidence indicate that the garnet-bearing mineral assemblage is a metamorphic replacement which overprints the previous layering.

Plagioclase-rich rocks include pod- and lens-shaped bodies of plagioclase-free rocks of garnet hornblendites (garnet + hornblende + clinopyroxene) associated with garnet clinopyroxenite, garnetite and, less commonly, hornblendite (Fig. 3b). The distribution of garnet in the garnet hornblendite is variable even within a single pod or lens. Pods and lenses of garnet hornblendite commonly have garnet-rich rims several centimetres wide and hornblende-rich cores, and in places patches and bands of garnetite and garnet clinopyroxenite. The boundaries between garnet–clinopyroxene granulite (host rock) and garnet hornblendite (replacement rock) are discordant to the compositional layering present in the host rock. The compositional layering in garnet–clinopyroxene granulite abruptly terminates at the boundary. The pods and lenses of the plagioclase-free rocks are regarded as intrusions into the protoliths of the plagioclase-rich rocks. Jan & Howie (1981) reported P–T conditions of some plagioclase-absent rocks as 640–850 °C at 12–14 kbar.

Analytical method and results

Methods of isotopic analysis, including sample preparations used in this study, follow those of Yamamoto & Nakamura (1996) derived from Makishima & Nakamura (1991) and Shibata (1992). The Nd isotopic ratios were normalized to $^{146}Nd/^{144}Nd = 0.7219$. Isotopic data were fitted to isochrons after York (1969) using the program 'ISOPLOT' (Ludwig 1994). The errors quoted for age and initial ratio were obtained by the multiplication of the 2σ error by the square root of MSWD (e.g. Kullerud 1991). The ages are calculated assuming a ^{147}Sm decay constant of 6.54×10^{-12} a^{-1} (Lugmair & Marti 1978).

Results of the Sm–Nd analyses are summarized in Table 1 and Fig. 4. Sample locations are shown in Fig. 2. Isotopic ratios of whole-rock and mineral separates of the two-pyroxene granulite (KU65) fit an isochron with MSWD of 1.1. The age and initial $^{143}Nd/^{144}Nd$ ratio are calculated as 118 ± 12 Ma and 0.512703 ± 0.000017 respectively. The isotopic ratios from the garnet–clinopyroxene granulite (P006) give an isochron age of 94.0 ± 4.7 Ma with an initial $^{143}Nd/^{144}Nd$ ratio of 0.512787 ± 0.000012 and MSWD of 1.7. The isotopic ratios from the garnet hornblendite (P015) define an errorchron with an MSWD of

Table 1. *Nd isotopic ratios and concentrations of Sm and Nd*

Sample no.		Sample wt (g)	Sm (ppm)	Nd (ppm)	$^{147}Sm/^{144}Nd$	$^{143}Nd/^{144}Nd$	$\pm 2\sigma_m$
KU65	Opx	0.034842	1.076	2.705	0.2405	0.512887	0.000018
	Cpx	0.026617	9.370	20.631	0.2747	0.512917	0.000010
	Pl	0.033771	0.2831	2.198	0.0779	0.512764	0.000012
	Wr	0.042472	1.866	5.220	0.2162	0.512853	0.000024
KU66*	Grt	0.025575	1.497	1.006	0.9003	0.513299	0.000020
	Cpx	0.025634	2.805	10.852	0.1563	0.512862	0.000011
	Pl	0.021776	0.0709	0.8942	0.0480	0.512790	0.000014
	Rt	0.008523	0.0285	0.1728	0.0999	0.512810	0.000060
	Wr	0.019462	2.058	6.074	0.2049	0.512867	0.000015
P006	Grt	0.027901	1.338	0.9319	0.8684	0.513323	0.000015
	Cpx	0.029210	3.687	10.929	0.2040	0.512904	0.000012
	Pl	0.029451	0.1221	0.956	0.0773	0.512842	0.000013
	Wr	0.048283	1.073	2.861	0.2267	0.512926	0.000013
P015	Grt	0.029619	0.7607	0.2899	1.587	0.513611	0.000024
	Cpx	0.018397	1.810	4.431	0.2470	0.512885	0.000008
	Hbl	0.029081	2.992	6.392	0.2831	0.512891	0.000008
	Wr	0.052032	2.042	4.090	0.3020	0.512941	0.000014

$\pm 2\sigma_m$: within-run error on $^{143}Nd/^{144}Nd$ ratio.
*Data from Yamamoto & Nakamura (1996).
Abbreviations: Opx, orthopyroxene; Cpx, clinopyroxene; Grt, garnet; Hbl, hornblende; Pl, plagioclase; Rt, rutile; Wr, whole rock.

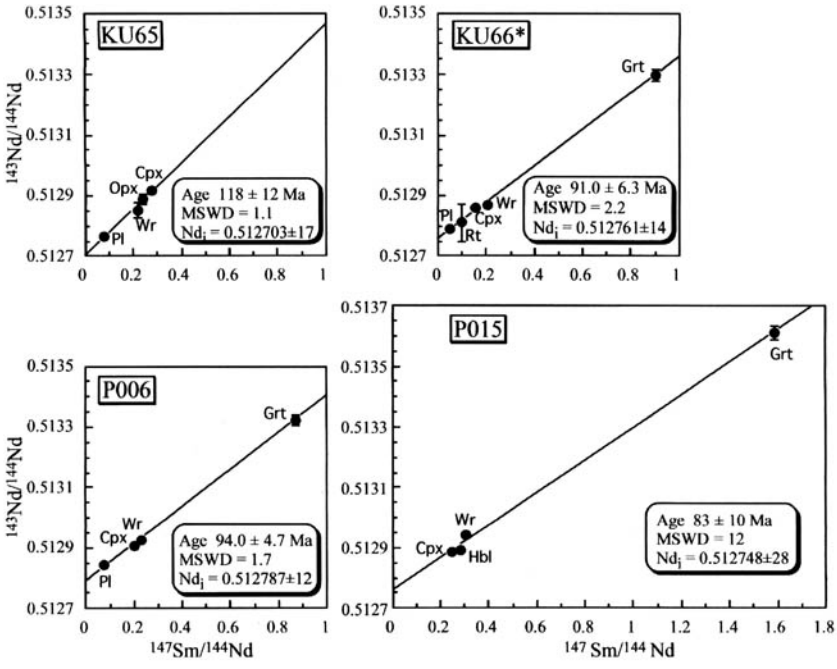

Fig. 4. Sm–Nd isochron diagrams. Abbreviations are as mentioned in Table 1. *, data from Yamamoto & Nakamura (1996).

12 and an age of 83 ± 10 Ma corresponding to an initial $^{143}Nd/^{144}Nd$ ratio of 0.512748 ± 0.000028. The large MSWD and error are probably related to textural disequilibrium indicated by uneven distribution of garnet and hornblende. The poor fit is not substantially improved even if hornblende or whole rock are excluded from the isochron calculation because of the exceedingly imbalanced $^{147}Sm/^{144}Nd$ ratios among the minerals.

Interpretation of ages

Garnet is a critical mineral in Sm–Nd dating for garnet-bearing mafic rocks because of its very high Sm/Nd ratio in comparison with most rock-forming minerals (Geyh & Schleicher 1990). The closure temperatures (T_c) for Sm–Nd diffusion in garnet from dry granulite and eclogite is estimated to be higher than 700 °C (Cohen *et al.* 1988; Jagoutz 1988; Hensen & Zhou 1995). According to Hensen and Zhou (1995), high-pressure mafic granulite, which includes garnet partially broken down to an orthopyroxene-bearing assemblage during the overprinting granulite event, retains an Sm–Nd isotopic memory of earlier high-pressure event. They inferred that T_c in garnet, with an effective diameter of 1 mm, is at least 700–750 °C from the orthopyroxene stability limit. Garnet grains of samples KU66 and P006 are generally larger than 1 mm. Assuming the minimum T_c to be 700 °C, the age of garnet–clinopyroxene granulite closely approximates the high-pressure granulite facies event in the Patan granulite body. Sm–Nd ages of garnet–clinopyroxene granulite in the previous reports are 103.9 Ma (Thirwall pers. comm. quoted in Coward *et al.* 1986), 91.0 ± 6.3 Ma (Yamamoto & Nakamura 1996) and 95.7 ± 2.7 Ma (Anczkiewicz & Vance 1997). The 103.9 Ma age is an indirect report with no indication of error. The other two and the age of P006 in this study are indistinguishable within indicated errors and those mean values cluster in the 96 to 90 Ma range. The high-pressure granulite facies metamorphism most likely took place between 96 Ma and 90 Ma.

Comparison of the results from KU65 and KU66, which represent the host rock and replacement rock respectively in the same outcrop, illustrates an important point in interpreting the ages. KU65 has a steeper regression line than that for KU66 and the ages of the two samples are consistent with field relations. Despite the overprinting granulite-facies event, which attained temperatures of > 700 °C, the orthopyroxene–clinopyroxene–plagioclase assemblage in the two-pyroxene granulite seems

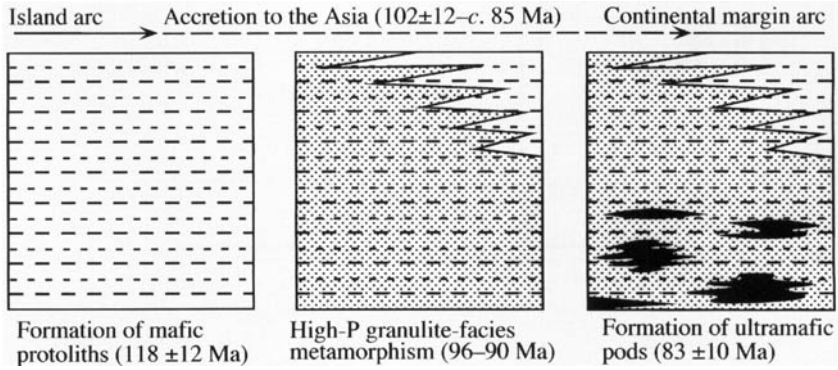

Fig. 5. Interpretation of the mutual relationships between the mafic–ultramafic rocks of the Patan granulite body and the ages of magmatic–metamorphic events.

to retain a memory of an earlier event that probably dates igneous crystallization of the parent gabbronorite. T_c in clinopyroxene is critical for dating two-pyroxene granulite, because clinopyroxene has the highest Sm and Nd content and Sm/Nd ratio among the major minerals in this rock. According to the Sm diffusion coefficients in diopside experimentally determined by Sneeringer *et al.* (1984), the T_c for Sm in 2 mm sized diopside under a cooling rate of greater than 10 °C Ma^{-1} is higher than 850 °C. The T_c for Sm is presumably applicable to Nd and this implies that the Sm–Nd system in the two-pyroxene granulite will retain an isotopic memory even if a temporary thermal overprint at 800 °C occurs.

The formation of mafic granulites can be correlated with a tectonic event that involved the Kohistan arc near this time. The date of tectonic accretion of the Kohistan arc to the Asian continent is not well constrained, but was inferred to be between 102 ± 12 and *c.* 85 Ma (Petterson & Windley 1985; Treloar *et al.* 1989). The crystallization of the gabbroic protoliths (118 ± 12 Ma) and the following high-pressure granulite-facies metamorphism (96–90 Ma) were earlier than, or coeval with, the accretion. We suggest a tectonic implication for these ages that the crust of Kohistan was thickened during the convergent motion of Kohistan–Asia and that the lower crust attained high-pressure granulite-facies P–T conditions up to the time of accretion.

As illustrated by the fact that the compositional layering in garnet–clinopyroxene granulite is cut by pods and lenses of garnet hornblendite, the formation of protoliths of the plagioclase-absent rocks postdates that of the protoliths of the plagioclase-rich rocks. This field evidence does not denote whether crystallization of the garnet hornblendite was earlier or later than that of the garnet–clinopyroxene granulite. The 83 ± 10 Ma age of P015 is indistinguishable from the ages of garnet–clinopyroxene granulite when analytical uncertainties with expanded 2σ errors are considered. Although the large error precludes a more rigorous comparison, garnet hornblendite is probably young compared with the tight cluster of the ages of garnet–clinopyroxene granulite in the 96 to 90 Ma range. It is unlikely that the emplacement of plagioclase-absent rocks predates the crystallization of garnet–clinopyroxene granulite. Our proposed chronological relationships are summarized in Fig. 5.

We acknowledge T. Shibata, M. Yoshikawa and N. Akiyoshi for technical support during the chemical separation and mass spectrometry. We also thank M. Maboko, P. J. Treloar and D. Vance for improving this paper with critical reading and suggestions. This work was carried out under the Visiting Research Program of the Institute for Study of the Earth's Interior, Okayama University at Misasa.

References

Anczkiewicz, R. & Vance, D. 1997. Chronology of subduction, collision and regional metamorphism in Kohistan, Pakistan Himalaya. *Terra Nova*, **9**, 345.

Bard, J. P. 1983. Metamorphism of an obducted island arc: example of the Kohistan sequence (Pakistan) in the Himalayan collided range. *Earth and Planetary Science Letters*, **65**, 133–144.

Cohen, A. S., O'Nions, R. K., Siegenthaler, R. & Griffin, W. L. 1988. Chronology of the pressure–temperature history recorded by a granulite terrain. *Contributions to Mineralogy and Petrology*, **98**, 303–311.

Coward, M. P., Windley, B. F., Broughton, R. D. & 5 Others. 1986. Collision tectonics in the NW Himalayas. *In*: Coward, M. P. & Ries, A. C. (eds) *Collision Tectonics*. Geological Society, London, Special Publications, **19**, 203–219.

——, BUTLER, R. W. H., KHAN, M. A. & KNIPE, R. J. 1987. The tectonic history of Kohistan and its implications for Himalayan structure. *Journal of the Geological Society, London*, **144**, 377–391.

GEYH, M. A. & SCHLEICHER, H. 1990. *Absolute Age Determination*. Springer-Verlag, Berlin Heidelberg.

HENSEN, B. J. & ZHOU, B. 1995. Retention of isotopic memory in garnets partially broken down during an overprinting granulite-facies metamorphism: Implications for the Sm–Nd closure temperature. *Geology*, **23**, 225–228.

JAGOUTZ, E. 1988. Nd and Sr systematics in an eclogite xenolith from Tanzania: Evidence for frozen mineral equilibria in the continental lithosphere. *Geochimica et Cosmochimica Acta*, **52**, 1285–1293.

JAN, M. Q. & HOWIE, R. A. 1981. The mineralogy and geochemistry of the metamorphosed basic and ultrabasic rocks of the Jijal complex, Kohistan, NW Pakistan. *Journal of Petrology*, **22**, 85–126.

KAUSAR, A. B., PICARD, C. & GUILLOT, S. 1998. Evidence for High-Temperature–Pressure crystallization during early magmatism of the Kohistan arc, Northern Pakistan. *Special Issue Geological Bulletin, University of Peshawar*, **31**, 91–92.

KULLERUD, L. 1991. On the calculation of isochrons. *Chemical Geology*, **87**, 115–124.

LUDWIG, K. R. 1994. *ISOPLOT, a plotting and regression program for radiogenic-isotope data, ver. 2.75*. United States Geological Survey, Open-File Report **91-445**.

LUGMAIR, G. W. & MARTI, K. 1978. Lunar initial $^{143}Nd/^{144}Nd$: Differential evolution of the lunar crust and mantle. *Earth and Planetary Science Letters*, **39**, 3349–3357.

MAKISHIMA, A. & NAKAMURA, E. 1991. Faraday cup efficiency in a multicollector mass spectrometer. *Chemical Geology*, **94**, 105–110.

MILLER, D. J., LOUCKS, R. R. & ASHRAF, M. 1991. Platinum-group element mineralization in the Jijal layered ultramafic–mafic complex, Pakistani Himalayas. *Economic Geology*, **86**, 1093–1102.

PETTERSON, M. G. & WINDLEY, B. F. 1985. Rb–Sr dating of the Kohistan arc-batholith in the Trans-Himalaya of N. Pakistan and tectonic implications. *Earth and Planetary Science Letters*, **74**, 54–75.

PUDSEY, C. J. 1986. The Northern Suture, Pakistan: margin of a Cretaceous island arc. *Geological Magazine*, **123**, 405–423.

RINGUETTE, L., MARTIGNOLE, J. & WINDLEY, B. F. 1998. Pressure–Temperature evolution of garnet-bearing rocks from the Jijal complex (western Himalayas, northern Pakistan): from high-pressure cooling to decompression and hydration of a magmatic arc. *Special Issue Geological Bulletin, University of Peshawar*, **31**, 167–168.

SHIBATA, T. 1992. *The lead, strontium and neodymium isotopic studies on the Quaternary volcanic rocks from northeastern Japan: implications for the slab-mantle interaction in subduction zone*. PhD thesis, Okayama University.

SNEERINGER, M., HART, S. R. & SHIMIZU, N. 1984. Strontium and samarium diffusion in diopside. *Geochimica et Cosmochimica Acta*, **48**, 1589–1608.

TAHIRKHELI, R. A. K., MATTAUER, M., PROUST, F. & TAPPONNIER, P. 1979. The India Eurasia suture zone in northern Pakistan: synthesis and interpretation of recent data at plate scale. *In*: FARAH, A. & DEJONG, K. A. (eds) *Geodynamics of Pakistan*. Geological Survey of Pakistan, Quetta, 125–130.

TRELOAR, P. J., REX, D. C., GUISE, P. G. & 6 OTHERS. 1989. K–Ar and Ar–Ar geochronology of the Himalayan collision in NW Pakistan: Constraints on the timing of suturing, deformation, metamorphism and uplift. *Tectonics*, **8**, 881–909.

YAMAMOTO, H. 1993. Contrasting metamorphic P–T–time paths of the Kohistan granulites and tectonics of the western Himalayas. *Journal of the Geological Society, London*, **150**, 843–856.

—— & NAKAMURA, E. 1996. Sm–Nd dating of garnet granulites from the Kohistan complex, northern Pakistan. *Journal of the Geological Society, London*, **153**, 965–969.

—— & YOSHINO, T. 1998. Superposition of replacements in the mafic granulites of the Jijal complex of the Kohistan arc, northern Pakistan: dehydration and rehydration within deep arc crust. *Lithos*, **43**, 219–234.

YORK, D. 1969. Least-squares fitting of a straight line with correlated errors. *Earth and Planetary Science Letters*, **5**, 320–324.

This page intentionally left blank

Isotopic constraints on the evolution of metamorphic conditions in the Jijal–Patan complex and the Kamila Belt of the Kohistan arc, Pakistan Himalaya

R. ANCZKIEWICZ[1] & D. VANCE[2]

[1]*Geologisches Institut, ETH-Zentrum, Sonneggstr.5, CH-8092, Zürich, Switzerland. Present address: Institute of Geological Sciences, Polish Academy of Sciences, Cracow Research Centre, Senacka 1, 30-001 Krakow, Poland (e-mail: ndanczki@kinga.cyf-kr.edu.pl)*

[2]*Institut für Isotopengeologie und Mineralogische Rohstoffe, ETH-Zentrum Sonneggstr.5, CH-8092, Zürich, Switzerland. Present address: Department of Geology, Royal Holloway, University of London, Egham, Surrey TW20 0EX, UK*

Abstract: Pressure–temperature data and Sm–Nd and Rb–Sr garnet ages are presented for retrogressed granulitic rocks of the Jijal–Patan complex and the Kamila Amphibolite Belt. Despite the retrogression and hydration, the two samples contain garnet and hydrous minerals that yield pressures and temperatures similar to previous estimates for pristine granulite facies rocks from the same area. The Sm–Nd and Rb–Sr garnet ages are concordant at 95–100 Ma for the two samples and for both isotopic systems. These ages are interpreted as dating cooling through 700–800 °C following magmatic crystallization and granulite facies metamorphism. In the case of the garnet amphibolites from the Kamila Belt, the garnets retain prograde major element zonation. In addition, the closure temperature for the Rb–Sr system is very close to the recorded temperature. For these reasons, the age of 100 Ma must represent a time close to that when the pressure and temperature preserved in the mineralogy and its chemistry was recorded. The isotopic equilibrium between garnet and paragonite at 90–100 Ma suggests that the regional hydration event that affected the lower crust of the Kohistan arc also occurred at this time. Cooling rates calculated from the Rb–Sr and Sm–Nd ages for the partially retrogressed granulite give a minimum of 3–6 °C Ma^{-1} and imply a different tectonic mechanism for the exhumation of the lower crust than is typical for granulites. This process may be related to early regional decompression following the collision of the Kohistan arc with Eurasia.

The Kohistan complex (Fig. 1) has been interpreted as a fossil island arc resulting from the subduction of Tethyan oceanic lithosphere during Mesozoic time (Bard 1983). Between 102 ± 12 and *c.* 85 Ma the Kohistan island arc was accreted to Asia, forming the Northern Suture of the western Himalaya (Petterson & Windley 1985; Treloar *et al.* 1989). Continued subduction led to the main India–Asia collision (65–50 Ma) and obduction of the arc onto the leading edge of India along the Main Mantle Thrust or Indus Suture (Patriat & Achache 1984; Coward *et al.* 1986; Beck *et al.* 1995). During continental collision, the arc rotated along an E–W axis exposing its lower crustal segment, today represented by the Jijal–Patan ultramafic–mafic complex and the Kamila Amphibolite Belt (Fig. 1).

Current thinking about the processes responsible for the tectonic evolution of the lower crustal segment of Kohistan is hampered by a scarcity of data on the timing of high temperature crystallization and subsequent exhumation. In addition, the high temperature nature of the processes occurring at the base of the arc makes the interpretation of the existing chronological data problematic. Recent *P–T* work (Ringuette *et al.* 1999) suggests that about 10–15 kbar of decompression occurred in the Jijal complex while the rock were above 700 °C. In this case, the tectonic significance of chronological data, even for isotopic systems and minerals that

From: KHAN, M. A., TRELOAR, P. J., SEARLE, M. P. & JAN, M. Q. (eds) *Tectonics of the Nanga Parbat Syntaxis and the Western Himalaya.* Geological Society, London, Special Publications, **170**, 321–331. 1-86239-061-4/00/$15.00

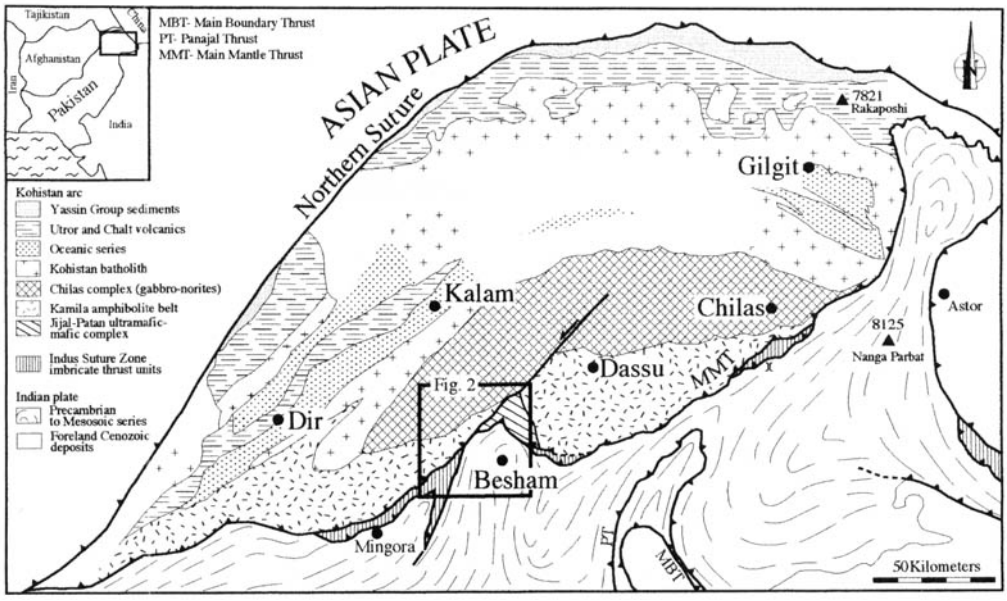

Fig. 1. Geological map of the Kohistan arc (after Bard 1983 and Burg *et al.* 1998).

record relatively high-temperature conditions such as Sm–Nd in garnet (e.g. Yamamoto & Nakamura 1996), is unclear.

In this study we present Sm–Nd and Rb–Sr ages on garnets from retrogressed garnet granulites from the Jijal complex and from garnet amphibolites in the Kamila Belt. These data place tighter constraints on the nature of the processes occurring in the base of the Kohistan crust. In addition, we show that cooling from high temperatures to those in the region of 700 °C occurred simultaneously both in the Jijal complex and in the Kamila Belt at 100–95 Ma.

Evolution of the Jijal–Patan complex and the Kamila Belt

The Jijal–Patan complex (Fig. 2) consists of ultramafic and mafic rocks representing two different modes of magmagenesis (Jan & Howie 1981; Yamamoto & Yoshino 1998) close to the mantle/crust boundary. The ultramafic unit of Jijal–Patan is dominantly composed of peridotites, pyroxenites, websterites and dunites (Jan & Howie 1981; Jan & Windley 1990) and has been interpreted as infra-arc mantle (Burg *et al.* 1998). The mafic unit represents the lowermost crust of the arc (Miller *et al.* 1991; Burg *et al.* 1998) and mainly comprises garnet granulites with volumetrically smaller amounts of two-pyroxene granulites, amphibolites, garnet hornblendites and garnetites.

There is some uncertainty over the *P–T* evolution of the garnet granulites in the Jijal complex which has led to differences in their petrogenetic interpretation. Yamamoto (1993) uses the fact that Al_2O_3 increases from core to rim in orthopyroxene, in conjunction with an increase in the grossular content of garnet, to suggest that garnet growth resulted from heating and burial of two-pyroxene granulites during crustal thickening caused by accretion of basaltic magma at mid-crustal depths. On the other hand, Ringuette *et al.* (1999) regard garnet in the garnet granulites as resulting both from magmatic processes, as well as from sub-solidus isobaric cooling of cumulates emplaced at the base of the oceanic arc-type crust. Similarly, Burg *et al.* (1998) interpreted garnet granulites as gabbroic intrusions within mantle rocks. The important point for the chronological results presented here is that all models require temperatures and pressures for garnet growth of over 850 °C at 15–20 kbar, followed by decompression of 5–10 kbar while the rocks were still above about 700 °C.

Previous Sm–Nd whole-rock mineral isochron dating of Jijal garnet granulites resulted in a 91.0 ± 6.3 Ma age, which was interpreted as dating cooling following crustal thickening due to the Asia–Kohistan arc collision (Yamamoto & Nakamura 1996).

The Kamila Amphibolite Belt also preserves relics of the early granulite stage seen in the Jijal–Patan complex. While the amphibolitization developed only locally in the Jijal garnet

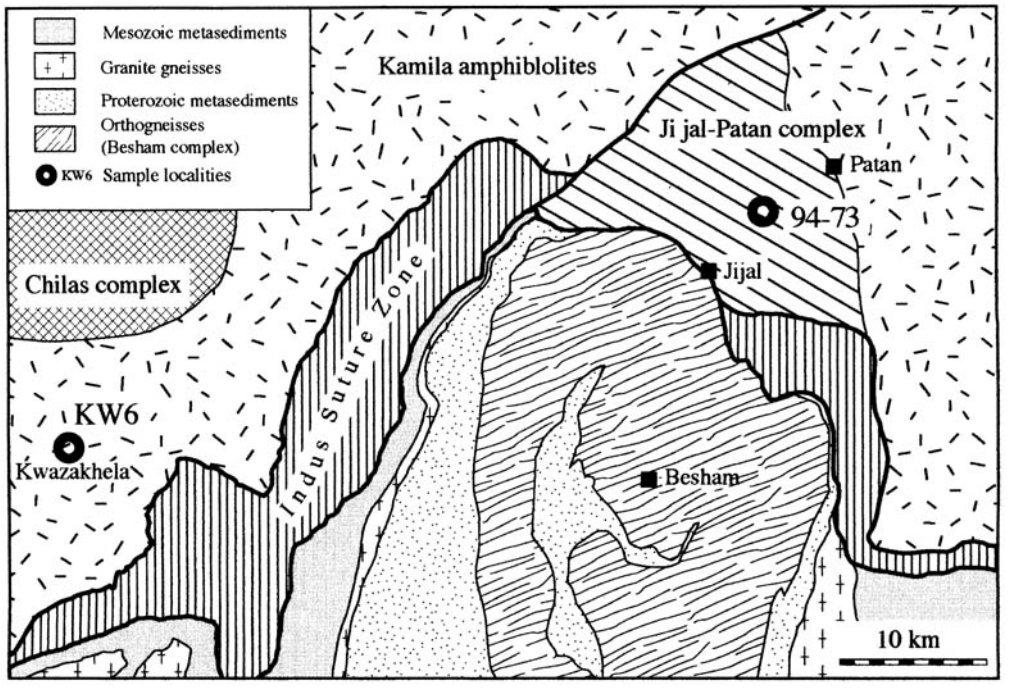

Fig. 2. Geological map of the Besham syntaxis (modified and simplified after DiPietro *et al.*, 1998).

granulites, this hydration process is widespread in the lower crustal rocks of the Kohistan arc (Figs 1 & 2) and is responsible for the formation of the Kamila amphibolites from two-pyroxene granulites (Jan 1988; Treloar *et al.* 1990; Khan *et al.* 1993).

Evolution of P–T conditions for the Kamila amphibolites has been inferred from Al zoning patterns in pyroxene and plagioclase measured on relics of the two-pyroxene granulites (Yoshino *et al.* 1998). The rocks record increasing pressure after magmatic crystallization and cooling at medium crustal levels from temperatures exceeding 1000 °C (Yoshino *et al.* 1998). The subsequent P–T increase is interpreted as being a result of crustal thickening associated with accretion of basaltic magma at mid-crustal depth. Peak pressure conditions have been determined as 8–11 kbar at about 800 °C. In common with the Jijal–Patan complex, this high-temperature stage was followed by an amphibolite and greenschist facies retrograde path.

Sample description and P–T conditions

Sample 94-73 is a retrogressed garnet granulite, collected from a few tens of metres above the ultramafic–mafic contact of the Jijal–Patan complex (Fig. 2). The main minerals are hornblende, paragonite, garnet, epidote group minerals, Fe–Ti oxides and rare scapolite (Fig. 3a). Garnet grains are sub- and anhedral, fine- to medium-grained and contain few inclusions, whereas amphibole is euhedral and subhedral and contains numerous quartz inclusions. Epidote commonly forms vermicular intergrowths with quartz while paragonite occurs as large (about 5 mm), euhedral crystals.

Garnet cores are chemically relatively homogeneous (Fig. 4), but there is pronounced zonation near the rims with the pyrope component decreasing by more than 10 mol%. There are smaller, complementary, increases in the almandine and grossular components over the same interval. Except for the small increase in Fe seen near the rim (Fig. 4a), this zonation pattern is very similar to that observed by others (Yamamoto & Yoshino 1998; Ringuette *et al.* 1999) for pristine garnet granulites. A summary of the compositions of the remaining minerals is given in Table 1. The absence of plagioclase allows only a minimum pressure, of about 15 kbar, to be established (Table 2). The rim mineral compositions, however, imply a temperature in the region of 850–950 °C for final equilibration (Table 2). Pressures >15 kbar and temperatures *c.* 900 °C overlap with the previously published range for fresh Jijal–Patan granulites (Yamamoto 1993; Ringuette *et al.* 1999).

Sample KW6 is an amphibolite collected along the road section in the vicinity of Kwazakhela in the Swat valley (Fig. 2). It is composed of hornblende, plagioclase, epidote group minerals, paragonite, garnet and Fe–Ti oxides. Garnet occurs as euhedral and

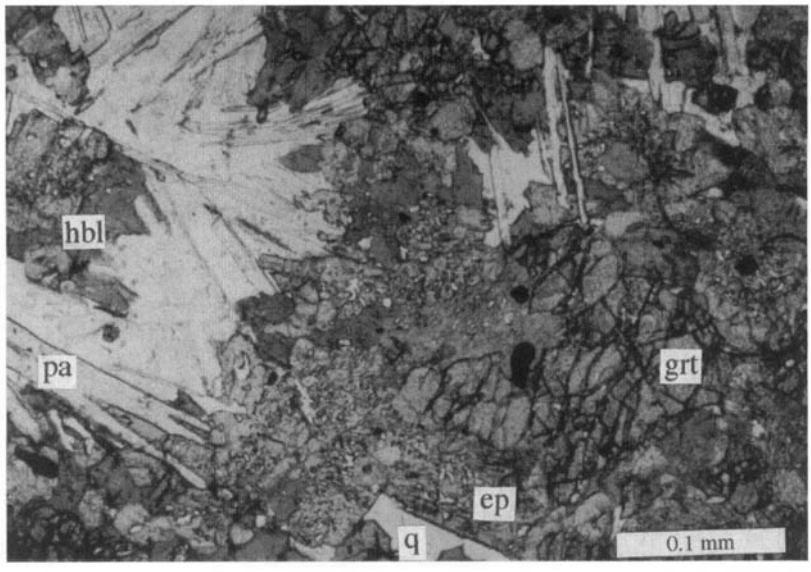

(a)

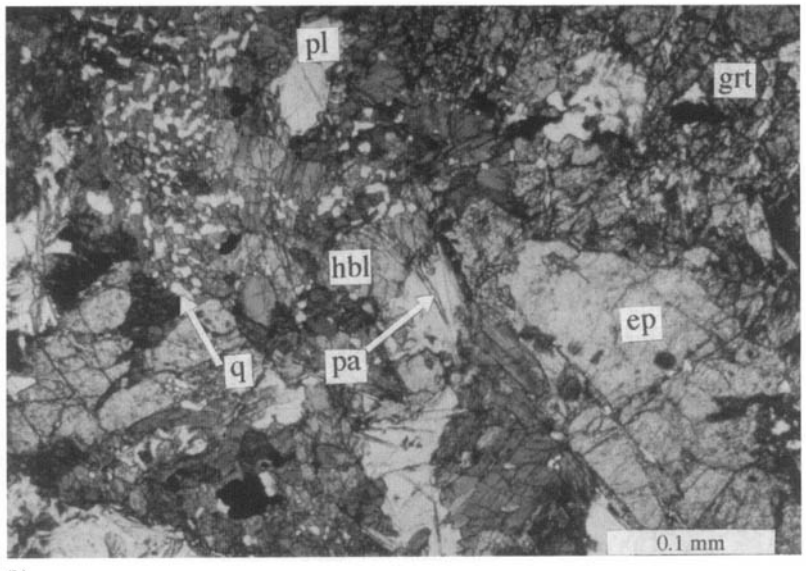

(b)

Fig. 3. Photomicrographs of the analysed samples: (**a**) 94-73 from the Jijal–Patan complex; (**b**) KW6 from the Kamila Belt. Abbreviations: q, quartz; ep, epidote; pa, paragonite; pl, plagioclase; grt, garnet; hbl, hornblende. See text for comments.

subhedral, strongly cracked grains. Garnet grains are inclusion-poor but do contain some inclusions of quartz, plagioclase and rutile. Inclusions are always connected by cracks within matrix phases and underwent all the hydration reactions observed in the matrix. Amphibole and epidote group minerals contain numerous quartz inclusions and form a 'vermicular' type texture (Fig. 3b). Tiny chlorite crystals grew in the cracks.

The major element zonation in the garnet from KW6 (Fig. 4b) does not show the increasing Fe/(Fe + Mg) ratio and decreasing pyrope content from core to rim that is seen in sample 94/73 (Fig. 4a) and that is so typical of retrograde re-equilibration. In fact, the Fe/(Fe + Mg) ratio decreases from core to rim while the pyrope content increases. In addition, the spessartine content of the core is higher than the rim (Table 2) while the grossular content decreases outward from the

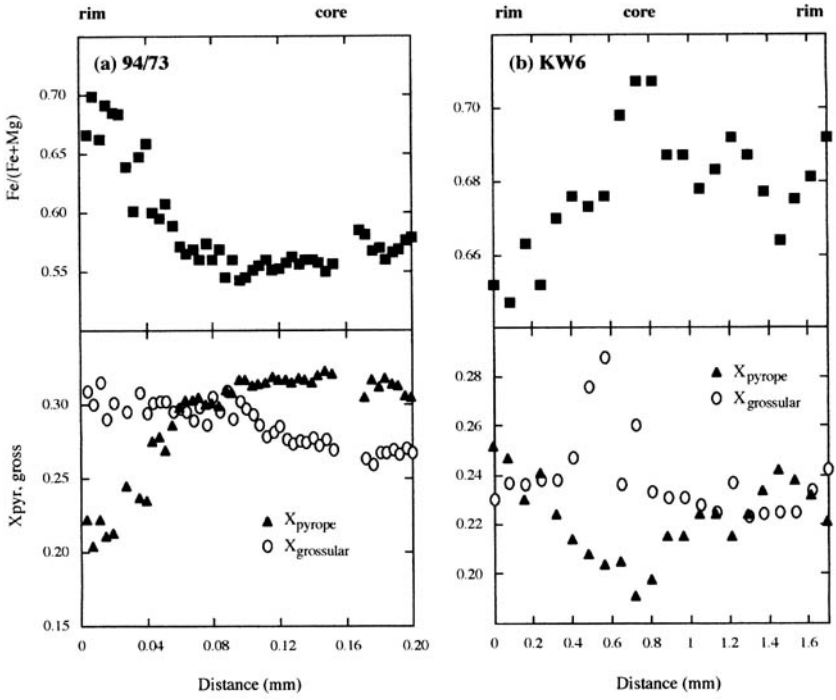

Fig. 4. Major element chemistry of garnets in sample (**a**) 94-73 and (**b**) KW6 plotted as mole fractions of the major garnet components.

core. This zonation pattern is, in fact, typical of prograde zonation profiles formed during increasing pressure and temperature (e.g. Vance & Mahar 1998) and suggests that garnet in this rock preserves remnant growth zonation that has not, at least not completely, diffusively relaxed. *P–T* calculations (Table 2) suggest final equilibration between garnet, amphibole, plagioclase, rutile and ilmenite at pressures around 8 kbar and temperatures of about 700–800 °C. These conditions are identical to those of the pressure peak recorded by relict pyroxene granulites of 8–11 kbar and 800 °C (Yoshino *et al.* 1998).

Sm–Nd and Rb–Sr isotopic results

Sm–Nd and Rb–Sr isotopic results are summarized in Table 3 and plotted as isochron diagrams in Fig. 5. Analytical techniques closely followed those of Cohen *et al.* (1988). Details of blanks and mass spectrometry are given in the footnote to Table 3.

The concentrations of Sm, Nd, Rb and Sr (0.02–1.6 ppm) in garnets are within the range typical for garnet from metabasites (e.g. Cohen *et al.* 1988; Thöni & Jagoutz 1992; Burton *et al.* 1995). Such low concentrations, in conjunction with high measured Sm/Nd ratios, demonstrate the absence of any contribution to the Sm–Nd budget from REE-rich phases. Model ages calculated for whole rock–garnet pairs are all in the range 95–100 Ma for both samples and for both isotopic systems investigated. The observed concordance among the samples and for the two isotopic systems is crucial to the interpretation, and is a strong argument in favour of the robustness of the ages. For example, problems associated with whole rock–garnet disequilibrium are highly unlikely to affect both isotopic systems and both rocks equally so that the concordance of the ages strongly suggests the complete absence of such problems.

Hornblende from sample 94-73 is not in isotopic equilibrium with the whole rock and garnet at 100 Ma (Fig. 5b). In fact, hornblende, together with whole rock and paragonite, defines an 'isochron' of 59 ± 12 Ma (MSWD = 0.46; Fig. 5b). The significance of all these ages is discussed below.

Discussion

Garnet ages and isotopic closure

The *P–T* history of the rocks and the diffusion rates of Sm, Nd, Rb and Sr in garnet are both of

Table 1. *Major element analyses of the major mineral phases in samples 94/73 and KW6*

	Garnet				Amphibole				Plagioclase	Paragonite	Epidote
	94/73 core	94/73 rim	KW6 core	KW6 rim	94/73 core	94/73 rim	KW6 core	KW6 rim	KW6 rim	94/73 rim	94/73 rim
SiO_2	38.53	39.52	37.03	37.32	44.43	46.23	41.71	41.98	60.03	47.31	38.50
TiO_2	0.10	0.05	0.02	0.00	0.51	0.28	0.81	0.95	0.01	0.28	0.08
Al_2O_3	21.32	21.27	20.50	20.76	15.23	13.65	15.09	14.89	25.26	39.39	27.64
Fe_2O_3	2.33	1.33	5.14	4.08	4.31	3.52	4.29	3.90	0.24	0.00	8.08
FeO	18.34	22.00	20.85	21.90	8.37	9.23	12.00	12.35	0.00	0.72	0.07
MnO	0.50	1.22	3.11	1.71	0.08	0.16	0.07	0.13	0.02	0.01	0.10
MgO	8.21	5.33	4.94	5.91	11.86	11.76	9.76	9.95	0.00	0.10	0.16
CaO	9.59	10.95	8.37	7.80	9.77	10.03	11.45	11.54	7.82	0.79	23.30
Na_2O	0.08	0.11	0.14	0.10	3.55	3.04	2.14	2.37	7.02	6.34	0.00
K_2O	0.01	0.01	0.04	0.00	0.12	0.08	0.19	0.24	0.05	0.21	0.00
Total	99.00	101.78	100.13	99.58	98.23	97.97	97.51	98.30	100.45	95.15	97.95
Si	2.966	3.012	2.910	2.927	6.381	6.641	6.178	6.181	2.664	3.015	2.999
Ti	0.006	0.003	0.001	0.000	0.055	0.030	0.090	0.105	0.000	0.013	0.005
Al	1.935	1.911	1.899	1.920	2.579	2.312	2.635	2.585	1.322	2.960	2.538
Fe^{3+}	0.135	0.076	0.304	0.241	0.466	0.380	0.478	0.432	0.008	0.000	0.473
Fe^{2+}	1.180	1.402	1.370	1.437	1.005	1.108	1.487	1.521	0.000	0.038	0.005
Mn	0.033	0.079	0.207	0.114	0.010	0.019	0.009	0.016	0.001	0.001	0.007
Mg	0.942	0.605	0.579	0.691	2.538	2.518	2.155	2.183	0.000	0.009	0.019
Ca	0.791	0.894	0.705	0.656	1.503	1.544	1.817	1.821	0.372	0.054	1.946
Na	0.012	0.016	0.021	0.015	0.989	0.847	0.615	0.677	0.604	0.784	0.000
K	0.001	0.001	0.004	0.000	0.022	0.015	0.036	0.045	0.003	0.017	0.000
Total	8.000	8.000	8.000	8.000	15.547	15.414	15.500	15.566	4.974	6.892	7.991
Oxygens	12	12	12	12	23	23	23	23	8	11	12.5
$X_{almandine}$	0.40	0.47	0.48	0.50					Ca/(Ca + Na)	K/(K + Na + Ca)	
X_{pyrope}	0.32	0.20	0.20	0.24							
$X_{grossular}$	0.27	0.30	0.25	0.23					=0.38	=0.92	
$X_{spessartine}$	0.01	0.03	0.07	0.04							
$Fe^{tot}/(Fe^{tot} + Mg)$	0.58	0.71	0.74	0.71	0.36	0.37	0.47	0.47			

Table 2. *Results of average P–T calculations using Thermocalc[1] for samples 94/73 and KW6*

94/73
Equilibria used[2]:
(1) 5py + 3fact = 5alm + 3tr
(2) 12cz + 2parg = py + 7gr + 2pa + 5ma + tr
(3) 12ma + 9gl = 4py + 2gr + 18pa + 3tr
(4) 2ma + gl = 2pa + ts
(5) gr + 2ep = andr + 2cz
(6) gr + fep = andr + cz
(7) 2andr + ma + q = gr + 2fep

T = 860–970 °C for P = 15–30 kbar. Pressure not precisely determined
(sigfit < 0.6, cutoff value for 95% confidence = 1.45)

KW6
Equilibria used:
(1) 2py + 4gr + 3ts + 12q = 3tr + 12an
(2) 3an + 6ilm + 3q = gr + 2alm + 6ru
(3) 3tr + 6parg + 18an = 4py + 8gr + 6ts + 3gl
(4) 3tr + 3ts + 6parg + 18ab = 4py + 8gr + 12gl

P = 7–9 kbar, T = 690–860 °C
(sigfit = 0.7, cutoff value for 95% confidence = 1.61)

[1]See Powell & Holland (1994) for details.
[2]Abbreviations for mineral end-members: py, pyrope; fact, Fe-actinolite; alm, almandine; tr, tremolite; cz, clinozoisite; parg, pargasitic hornblende; gr, grossular; pa, paragonite; ma, margarite; gl, glaucophane; ep, epidote; andr, andradite; an, anorthite; ab, albite; ru, rutile; ilm, ilmenite; q, quartz; fep, Fe-epidote; ts; tschermakitic hornblende.

relevance to the interpretation of the isotopic ages presented here and are discussed below. Early magmatic crystallization of gabbroic magma in both the Jijal–Patan complex and the Kamila Amphibolite Belt involved temperatures >1000 °C (Yamamoto 1993; Yoshino *et al.* 1998; Ringuette *et al.* 1999). The subsequent thermal evolution involved a significant period at temperatures greater than *c.* 800 °C, though there is some disagreement as to the exact P–T path. For the Jijal–Patan complex, Ringuette *et al.* (1999) envisage a relatively simple history in which magmatic crystallization is followed by a period of isobaric cooling, after which around 10 kbar of decompression occurred whilst the rocks remained above *c.* 700 °C. Yamamoto (1993), on the other hand, infers garnet to have grown during a heating and burial cycle to pressures <15 kbar and temperatures *c.* 900 °C, after magmatic crystallization and initial cooling but before decompression began. In this scenario, burial and heating were followed by decompression and cooling to amphibolite facies conditions at 700 °C and 10 kbar. Similarly, Yoshino *et al.* (1998) propose heating and burial to form granulites in the Kamila Belt, in this case to temperatures of *c.* 800 °C for the maximum pressure of 8–11 kbar.

The P–T data presented here cannot distinguish between these two scenarios and, despite being obtained on hydrous assemblages, are perfectly consistent with both. In the case of sample 94/73 from the Jijal–Patan complex, the recorded pressures of >15 kbar at temperatures of 900 °C could reflect the early part of the decompression path in both models. For sample KW6 from the Kamila amphibolites, the recorded P–T of 8–10 kbar and 800 °C is perfectly consistent with the maximum pressure conditions in the P–T path of Yoshino *et al.* (1998). Clearly, both rocks experienced temperatures in excess of 700–750 °C during and after garnet growth. Recent direct measurements of diffusion rates of Sm and Nd in garnet (Ganguly *et al.* 1998*a*) suggest a closure temperature (T_c) around 700–750°C for cooling rates between 5 and 50 °C and a grain size of around 1–2 mm and are in general agreement with earlier results (Coghlan 1990). Coghlan (1990) also measured the diffusion rate of Sr in garnet and found that T_c for the Rb–Sr system should be 50–100 °C higher than for Sm–Nd—in this case around 800 °C. If the data of Coghlan for Sr diffusion are appropriate then the isotopic ages obtained here do not date garnet growth but instead date cooling through 700–800 °C. However, the Rb–Sr age for KW6 must come close to dating the pressure peak at 10 kbar and 800 °C (Table 2; Yoshino *et al.* 1998) recorded by the mineral assemblage. The prograde major element zonation of KW6 garnets, along with the fact that the diffusion rates of Nd and Sr in garnet are similar to those of the major elements (Coghlan 1990; Ganguly *et al.* 1998*a*, *b*), supports the fact that the P–T–t recorded by this rock is close to that at which garnet grew. The concordancy of the two Sm–Nd ages also suggests that cooling through 700–750 °C occurred simultaneously in the Jijal–Patan complex and the Kamila Amphibolite Belt.

The uncertainties on the Sr ages are rather large due to rather low standard reproducibility and the small spread in Rb/Sr ratios between garnet and whole rock. It is interesting, however, that the absolute values of the ages for the Rb–Sr system are older than those for Sm–Nd in both cases. Taken at face value, and along with the diffusion data (Coghlan 1990; Ganguly *et al.* 1998*a*), these data would imply cooling rates, in the interval 800 to 700 °C, of 10–20° Ma^{-1}. However, the large errors on the Rb–Sr ages mean that the cooling rates could be as low as about 3–6 °C Ma^{-1}. These cooling rates are

Table 3. *Summary of Sm–Nd and Rb–Sr isotopic analyses*

	Wt (mg)	Sm (ppm)	Nd (ppm)	$^{147}Sm/^{144}Nd$	$^{143}Nd/^{144}Nd$	Rb (ppm)	Sr (ppm)	$^{87}Rb/^{86}Sr$	$^{87}Sr/^{86}Sr$
94-73 Jijal–Patan mafic rocks, retrograded garnet granulite									
wr	35.3	1.49	4.25	0.2123	0.512902 ± 5	0.49	225	0.00633	0.704062 ± 26
grt	28.6	1.59	1.12	0.8578	0.513306 ± 10	0.02	0.22	0.2668	0.704437 ± 28
amph	8.45					0.58	8.88	0.1907	0.704224 ± 26
parag	9.5					0.95	603	0.00457	0.704073 ± 26
KW6 Kamila Belt, amphibolite									
wr	2.51	8.70		0.1743	0.512834 ± 8	0.59	319	0.00533	0.703864 ± 22
grt	24.9	0.26	0.12	1.2678	0.513510 ± 37	0.02	0.10	0.6998	0.704843 ± 15

Errors are 2σ. $^{87}Rb/^{86}Sr$ and $^{143}Sm/^{144}Nd$ errors determined at 0.5 and 0.3% respectively. Decay constants used: $\lambda_{^{147}Sm} = 6.54 \times 10^{-12}\ a^{-1}$, $\lambda_{^{87}Rb} = 1.42 \times 10^{-11}\ a^{-1}$. $^{143}Nd/^{144}Nd$ normalized to $^{146}Nd/^{144}Nd = 0.7219$. Over the period of the analyses the La Jolla standard yielded $^{143}Nd/^{144}Nd = 0.511855 \pm 8$ (2σ standard deviations of individual runs). $^{87}Sr/^{86}Sr$ normalized to $^{86}Sr/^{88}Sr = 0.1194$. Over the period of analyses, NBS 987 gave 0.710292 ± 22 (2σ standard deviation of individual runs). Total procedural blanks were 8 pg for Nd and 30 pg for Sr.

significantly faster than those commonly inferred for granulite facies terraines (e.g. Mezger *et al.* 1991) and favour the view of Kamber *et al.* (1996). In addition, the fact that these rocks come from very different crustal levels, yet record identical Rb–Sr and Sm–Nd ages lends further support to the theory that post metamorphic cooling was fast.

In summary, these data imply magmatic crystallization, cooling, perhaps a burial cycle (Yamamoto 1993; Yoshino *et al.* 1998) and further cooling to *c.* 700–750 °C by 95 Ma in Kohistan.

Timing and conditions of hydration

The samples that have been the subject of our analysis are garnet amphibolites that preserve relicts of granulite facies assemblages. It has already been noted that the zonation pattern in the garnet from sample 94-73 is the same as that observed in garnet from unhydrated garnet granulites (Fig. 4; Yamamoto 1993; Ringuette *et al.* 1999). This implies that garnet may be a relict feature of granulite facies or magmatic conditions and might be expected to exhibit chemical and isotopic disequilibrium with the other phases in the rock. However, the *P–T* conditions for equilibration of mineral rims (Table 2) are identical to those obtained for pristine garnet granulites. The approach used here to calculate pressures and temperatures (see Powell & Holland 1994 for details) allows the identification of phases that are significantly out of equilibrium. In the case of both 94-73 and KW6, no such disequilibrium has been found between garnet and hydrous phases. This seems to imply that the hydration event occurred very close to the high temperature–high pressure conditions recorded by the garnet granulites.

The above conclusion is also supported by the isotopic data. The Sr content of the paragonite in sample 94-73 is 600 ppm and inspection of the Rb–Sr systematics in Fig. 5b demonstrates that this phase dominates the Rb–Sr budget of the rock. Given this situation, it is clear that the garnet–whole rock Rb–Sr age can essentially be viewed as a garnet–paragonite age. In this case the concordancy of the Rb–Sr and Sm–Nd garnet ages suggests only two possibilities. The first of these is that the garnet equilibrated with the whole rock and closed to Rb–Sr diffusion before hydration and that the Sr brought in by the fluid, and at least partially incorporated into the paragonite, was so similar in isotopic composition to the whole rock that there was no significant change in the Rb–Sr systematics of the whole rock. This is unlikely, however, given

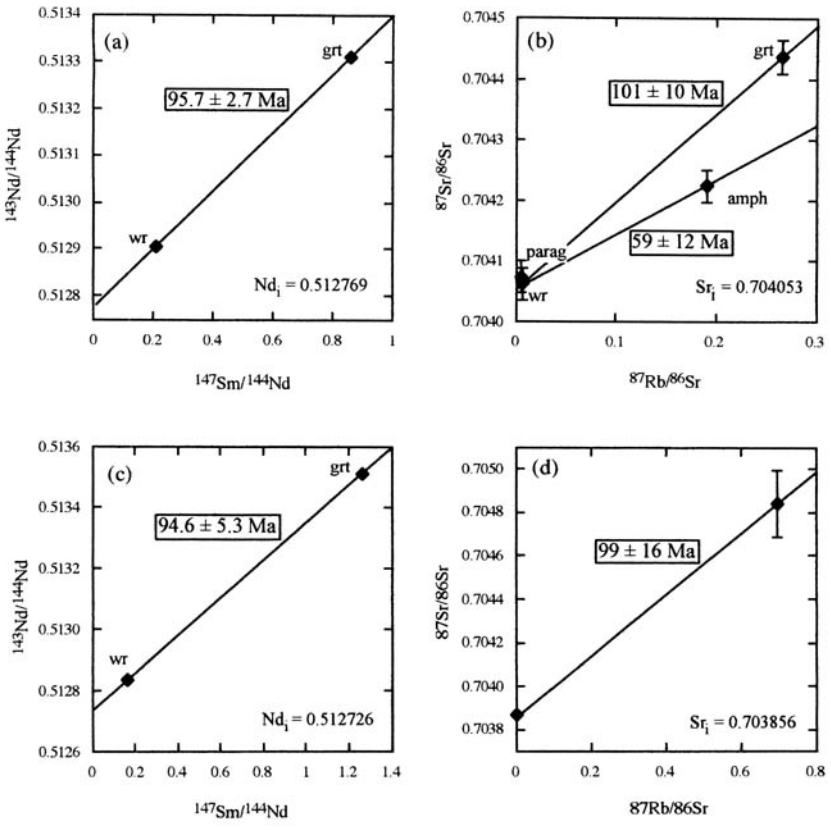

Fig. 5. Sm/Nd and Rb/Sr isochron diagrams for: (**a**,**b**) sample 94-73; (**c**,**d**) sample KW6 (errors are 2σ). Abbreviations: wr, whole rock; grt, garnet; amph, amphibole; parag, paragonite; Nd_i, Sr_i = initial Nd and Sr ratios.

the fact that the surrounding rocks, which might be expected to have the same Sr isotopic composition, are at granulite facies and are unlikely to be a source of the fluid. The second possibility is that the hydrating fluid infiltrated the rock before garnet had closed so that paragonite and garnet could equilibrate isotopically and record the same age as the Sm–Nd system. In this second case, the hydration event must have occurred before closure of the isotopic systems in garnet at 95–100 Ma.

Rb–Sr data for the amphibole, however, are not in accord with this simple scenario. Figure 5b shows that the amphibole is out of isotopic equilibrium with garnet at 95–100 Ma. The observation is enigmatic and cannot be accounted for unequivocally without further data, but there is one simple explanation that is wholly consistent with the present dataset. The Sr content of the amphibole is about 9 ppm, whereas that of the paragonite is 600 ppm. This would imply that if both mineral phases were open to Sr exchange at some time after 95–100 Ma, the effect of that opening would be much greater on the hornblende than the paragonite. In addition, the effect on the amphibole would be that it would acquire less radiogenic Sr from the paragonite and thus lower its age, as is observed. The validity of this explanation of the data depends on the relative closure temperatures for the Rb–Sr system in paragonite and hornblende. While no experiments have been done on the diffusion rate of Sr in paragonite, the T_c for muscovite is known to be around 500–550 °C (von Blanckenburg *et al.* 1989) and that for paragonite is likely to be higher given the much greater compatibility of Sr with the latter. Diffusion experiments on amphibole (Brabander & Giletti 1993) suggest a T_c around 650 °C. Thus a thermal event after 95–100 Ma that reached temperatures around 600 °C would lead to limited exchange between

paragonite and amphibole, and that exchange would have a greater effect on the latter because of the mass balance constraints. Because of the uncertainty over the degree of exchange that occurred, there is no guarantee that the Sr 'age' of the amphibole accurately dates the event concerned and the thermal pulse could actually have occurred at any time after the apparent age of the amphibole at 59 ± 12 Ma.

Conclusions

We have presented evidence for simultaneous cooling of the Jijal–Patan complex and the Kamila Amphibolite Belt through 700–800 °C at 95–100 Ma. Existing data on the *P–T* history (Yamamoto 1993; Ringuette *et al.* 1999) demonstrate that this period of cooling was also the one when major decompression began. The isotopic ages obtained here and elsewhere (Yamamoto & Nakamura 1996) also coincide with the age for the collision of the arc with Asia and the formation of the Northern Suture (Petterson & Windley 1985; Treloar *et al.* 1989) and seem to imply a genetic link between the two processes. The minimum cooling rates inferred here of 3–5 °C Ma^{-1} certainly suggest much faster unroofing than is typical for granulite facies rocks (1 °C Ma^{-1}; Mezger *et al.* 1991). Whatever the reason for the cooling and decompression at this time, the data presented here suggest that it was a major regional feature that affected rocks that are currently around 100 km apart.

We have also argued that the regional hydration event that formed the Kamila amphibolites and the partial retrogression of the Jijal–Patan garnet granulites was coeval with or occurred very shortly after the cooling and decompression recorded by the garnet ages. Burg *et al.* (1998) related the hydration process in the Jijal–Patan complex to fluids evolved from magmatic crystallization of gabbroic magma and/or fluids coming from the underlying upper mantle. This could account for the immediate amphibolitization after granulite facies metamorphism.

Special thanks to I. M. Villa for enlightening discussions. We thank F. Oberli and J.-P. Burg for discussion on the manuscript. We are also grateful to S. Hussain and H. Dawood for help in the field and to R. Orlowski for help with microprobe analysis. This project was supported by the European Union and Swiss National Science Foundation Grant No. 21-39080.93.

References

BARD, J. P. 1983. Metamorphism of an obducted island arc; example of the Kohistan Sequence (Pakistan) in the Himalayan collided range. *Earth and Planetary Science Letters*, **65**, 133–144.

BECK, R. A., BURBANK, D. W., SERCOMBE, W. J., RILEY, G. W., BARNDT, J. K. *et al.* 1995. Stratigraphic evidence for an early collision between northwest India and Asia. *Nature*, **373**, 55–58.

BLANCKENBURG, F. V., VILLA, I. M., BAUR, H., MORTEANI, G. & STEIGER, R. H. 1989. Time calibration of a *P–T* path from the western Tauern window, Eastern Alps: the problem of closure temperatures. *Contributions to Mineralogy and Petrology*, **101**, 1–11.

BRABANDER, D. J. & GILETTI, B. J. 1993. Strontium diffusion kinetics in amphibole. *EOS*, **74**, 611.

BURG, J. P., BODINIER, J. L., CHAUDHRY, S., HUSSAIN, S. & DAWOOD, H. 1998. Infra-arc mantle–crust transition and intra-arc mantle diapirs in the Kohistan Complex (Pakistani Himalaya): petrostructural evidence. *Terra Nova*, **10**, 74–80.

BURTON, K. W., KOHN, M. J., COHEN, A. S. & O'NIONS, R. K. 1995. The relative diffusion of Pb, Nd, Sr and O in garnet. *Earth and Planetary Science Letters*, **133**, 199–211.

COGHLAN, R. A. N. 1990. *Studies in diffusional transport: grain boundary transport of oxygen in feldspars, diffusion of oxygen, strontium and the REEs in garnet and thermal histories of granitic intrusions in south-central Maine using oxygen isotopes*. PhD thesis, Brown University, Providence, Rhode Island.

COHEN, A. S., O'NIONS, R. K., SIEGENTHALER, R. & GRIFFIN, W. L. 1988. Chronology of the pressure–temperature history recorded by a granulite terrain. *Contributions to Mineralogy and Petrology*, **98**, 303–311.

COWARD, M. P., WINDLEY, B. F., BROUGHTON, R. D., LUFF, I. W., PETTERSON, M. G. *et al.* 1986. Collision tectonics in the NW Himalayas. *In*: COWARD, M. P. & RIES, A. C. (eds) *Collision Tectonics*. Geological Society, London, Special Publications, **19**, 203–219.

DIPIETRO, J. A., POGUE, K. R., HUSSAIN, A. & AHMAD, I. 1999. A Geological Map of the Indus Syntaxis and surrounding area, Northwest Himalaya, Pakistan. *In*: MACFARLANE, A., SORKHABI, R. & QUADE, J. (eds) *Himalaya and Tibet: Mountain roots to mountain tops*. Geological Society of America, Special Papers, **328**, in press.

GANGULY, J., TIRONE, M. & HERVIG, R. L. 1998*a*. Diffusion kinetics of samarium and neodymium in garnet, and a method for determining cooling rates in rocks. *Science*, **281**, 805–807.

——, CHENG, W. & CHAKRABORTY, S. 1998*b*. Cation diffusion in aluminosilicate garnets: experimental determination in pyrope–almandine diffusion couples. *Contributions to Mineralogy and Petrology*, **131**, 171–180.

JAN, M. Q. 1988. Geochemistry of amphibolites from the southern part of the Kohistan arc, N. Pakistan. *Mineralogical Magazine*, **52**, 147–159.

—— & HOWIE, R. A. 1981. The mineralogy and geochemistry of the metamorphosed basic and ultrabasic rocks of the Jijal Complex, Kohistan, NW Pakistan. *Journal of Petrology*, **22**, 85–126.

—— & WINDLEY, B. F. 1990. Chromian spinel–silicate chemistry in ultramafic rocks of the Jijal Complex Northwest Pakistan. *Journal of Petrology*, **31**, 667–715.

KAMBER, B. S., BIINO, G. G., WIJBRANS, J. R., DAVIES, G. R. & VILLA, I. M. 1996. Archaean granulites of the Limpopo Belt, Zimbabwe: One slow exhumation or two rapid events? *Tectonics*, **15**, 1414–1430.

KHAN, M. A., JAN, M. Q. & WEAVER, B. L. 1993. Evolution of the lower arc crust in Kohistan, N. Pakistan: temporal arc magmatism through early, mature and intra-arc rift stages. *In*: TRELOAR, P. J. & SEARLE, M. P. (eds) *Himalayan Tectonics*, Geological Society, London, Special Publications, **74**, 123–138.

MEZGER, K., RAWNSLEY, C. M., BOHLEN, S. R. & HANSON, G. N. 1991. U–Pb garnet, sphene, monazite, and rutile ages: implications for the duration of high-grade metamorphism and cooling histories. *Journal of Geology*, **99**, 415–428.

MILLER, D. J., LOUCKS, R. R. & ASHRAF, M. 1991. Platinum-group element mineralization in the Jijal layered ultramafic–mafic complex, Pakistani Himalayas. *Economic Geology*, **86**, 1093–1102.

PATRIAT, P. & ACHACHE, J. 1984. India–Eurasia collision chronology has implications for crustal shortening and driving mechanism of plates. *Nature*, **311**, 615–621.

PETTERSON, M. G. & WINDLEY, B. F. 1985. Rb–Sr dating of the Kohistan arc-batholith in the Trans-Himalaya of North Pakistan, and tectonic implications. *Earth and Planetary Science Letters*, **74**, 45–57.

POWELL, R. & HOLLAND, T. J. B. 1994. Optimal geothermometry and geobarometry. *American Mineralogist*, **79**, 120–133.

RINGUETTE, L., MARTIGNOLE, J. & WINDLEY, B. 1999. Magmatic crystallization isobaric cooling, and decompression of the Jijal sequence (Kohistan terrane, western Himalayas). *Geology*, **27**, 139–142.

THÖNI, M. & JAGOUTZ, E. 1992. Some new aspects of dating eclogite in orogenic belts: Sm–Nd, Rb–Sr, and Pb–Pb isotopic results from the Austroalpine Saualpe and Koralpe type-locality (Carinthia/Styria, SE Austria). *Geochimica et Cosmochimica Acta*, **56**, 347–368.

TRELOAR, P. J., BRODIE, K. H., COWARD, M. P., JAN, M. Q., KHAN, M. A. *et al.* 1990. The evolution of the Kamila shear zone, Kohistan, Pakistan. *In*: SALISBURY, M. H. & FOUNTAIN, D. M. (eds) *Exposed Cross-Sections of the Continental Crusts*. Kluwer Academic Press, Amsterdam, 175–214.

——, REX, D. C., GUISE, P. G., COWARD, M. P., SEARLE, M. P., WINDLEY, B. F., PETTERSON, M. G., JAN, M. Q. & LUF, I. W. 1989. K-AR and Ar-Ar Geochronology of the Himalayan collision in NW Pakistan: constraints on the timing of auturing, deformation, metamorphism and uplift. *Tectonics*, **8**, 881–909.

VANCE, D. & MAHAR, E. 1998. Pressure–temperature paths from *P–T* pseudosections and zoned garnets: potential, pitfalls and examples from the Zanskar Himalaya, NW India. *Contributions to Mineralogy and Petrology*, **132**, 225–245.

YAMAMOTO, H. 1993. Contrasting metamorphic P–T–time paths of the Kohistan granulites and tectonics of the western Himalayas. *Journal of the Geological Society, London*, **150**, 843–856.

—— & NAKAMURA, E. 1996. Sm–Nd dating of garnet granulites from the Kohistan Complex, northern Pakistan. *Journal of the Geological Society, London*, **153**, 965–969.

—— & YOSHINO, T. 1998. Superposition of replacements in the mafic granulites of the Jijal complex of the Kohistan arc, northern Pakistan: dehydration and rehydration within deep arc crust. *Lithos*, **43**, 219–234.

YOSHINO, T., YAMAMOTO, H., OKUDAIRA, T. & TORIUMI, M. 1998. Crustal thickening of the lower crust of the Kohistan arc (N. Pakistan) deduced from the Al-zoning in clinopyroxene and plagioclase. *Journal of Metamorphic Geology*, **16**, 729–748.

This page intentionally left blank

Formation of mélanges in the Indus Suture Zone, Ladakh Himalaya by successive subduction-related, collisional and post-collisional processes during Late Mesozoic–Late Tertiary time

A. H. F. ROBERTSON

Department of Geology and Geophysics, Grant Institute, West Mains Road, Edinburgh EH9 3JW, UK

Abstract: The classic Indus Suture Zone in western Ladakh includes two zones (southern and northern) of highly dismembered rocks, that in the past were widely interpreted as ophiolitic mélanges, created mainly by subduction/accretion processes. The 'ophiolitic mélange' was reported to include chaotically distributed blocks of ophiolitic rocks (e.g. serpentinite, gabbro, basalt) and sedimentary rocks (chert, limestone) set in a matrix of deep-sea clastic sediments. This accretionary hypothesis is tested in this paper and found to be inadequate. Units formed simply by oceanic subduction–accretion (i.e. local mud-matrix mélange) are minimal (< 1% by volume). In reality, the southern and northern mélange zones are the end products of complex multi-stage tectonic processes, involving subduction (mid-Late Cretaceous to Early Tertiary), initial emplacement (latest Cretaceous), collision (Palaeocene–Eocene) and post-collisional (Late Tertiary) stages. Important components of the mélange as a whole include thrust sheets and broken formation of relatively coherent volcanic-sedimentary successions related to the North Indian passive margin (Karamba and Lamayuru complexes), also mid-Late Cretaceous oceanic arc-type volcanics and volcaniclastic sediments (Dras arc complex). Dismembered serpentinite thrust sheets, cut by swarms of (subduction influenced) diabase dykes, most likely record detached oceanic basement related to the oceanic Dras arc complex. Associated serpentinite was injected along tectonic contacts and into adjacent units during collisional and post-collisional deformation, locally forming serpentinite mélange. Post-collisional, Early–mid-Tertiary non-marine coarse clastic sediments (Indus Group) unconformably overlie various units (serpentinite, volcaniclastics, blueschists) in different locations, and were later thrusted and folded within the southern and northern mélange zones in response to regional Late Tertiary tightening of the suture. As a result, backthrusting reversed the original thrust stacking order, placing the originally most southerly units at the highest structural level. The Indus Suture Zone 'ophiolitic mélanges' in western Ladakh are, thus, mainly not ophiolitic (i.e. dismembered oceanic crust), or mélange in entirety (i.e. chaotic blocks), but are instead dominated by disrupted thrust sheets and broken formation of the Mesozoic Lamayuru–Karamba continental margin and the Upper Cretaceous oceanic Dras arc complex, with only minor preserved remnants of units formed by subduction/accretion (e.g. mud-matrix mélange; oceanic exotics).

The southern and northern mélange zones reflect the existence of several N-dipping subduction zones active in latest Cretaceous–Palaeogene times. Although only minor volumes of accreted oceanic material (oceanic lithosphere and trench-type sediments) are preserved within the Indus Suture Zone in western Ladakh, additional accreted material was bulldozed further south onto the Zanskar continental shelf and is now preserved as mélanges beneath the Spontang ophiolite. Similar mélange is also preserved in eastern Ladakh. Subduction zones evolved into a major interconnected shear zone (suture) during Early Tertiary (54–50 Ma) collisional deformation, dismembering upper (oceanic arc) and lower plate (continental margin) units to produce most of the southern and northern mélange zones. After suturing and initial deposition of non-marine coarse clastic cover sediments, inherited weakness zones within the Indus Suture Zone were exploited, increasing disruption during Late Tertiary regional backthrusting.

The methods used here in the analysis of the Indus Suture Zone mélange could well prove to be useful elsewhere in the Himalaya and in other orogenic belts. This work also emphasizes the need to distinguish between true mélange v. thrust sheets and broken formation in the field, and also cautions against use of the term ophiolitic mélange unless all the components of a dismembered ophiolite are actually present together.

From: KHAN, M. A., TRELOAR, P. J., SEARLE, M. P. & JAN, M. Q. (eds) *Tectonics of the Nanga Parbat Syntaxis and the Western Himalaya*. Geological Society, London, Special Publications, **170**, 333–374. 1-86239-061-4/00/$15.00

'Ophiolitic mélanges' are an important constituent of many collisional zones, including the Indus Suture Zone, discussed here. Such mélanges are typically described as being dominated by ophiolitic blocks, formed by fragmentation and pervasive mixing of oceanic lithosphere by mainly tectonic processes (Saleeby 1979, 1984). In 1974, Gansser published an influential paper on the origins of Tethyan 'ophiolitic mélanges' including those of the Indus Suture Zone of the Himalaya (Fig. 1). He pointed out that ophiolitic mélanges commonly form by a combination of tectonic and sedimentary processes, that they are generally overlain by large ophiolitic thrust sheets (e.g. Spontang ophiolite), and that they mark sutures recording the former existence of oceanic basins (Gansser 1980). Many authors have reported occurrences of 'ophiolitic mélanges', in different orogenic belts, including the Alpine–Mediterranean Tethys (Woodcock & Robertson 1984) and the Franciscan terrane of western USA (Blake 1984). However, it is not always appreciated that many mélanges represent the end product of a series of tectonosedimentary processes and are, thus, potentially invaluable for the interpretation of orogenic belts if they can be unravelled.

Following, Gansser's (1974) insights, Frank *et al.* (1977) mapped 'ophiolitic mélange', including blueschists in Ladakh, as two main

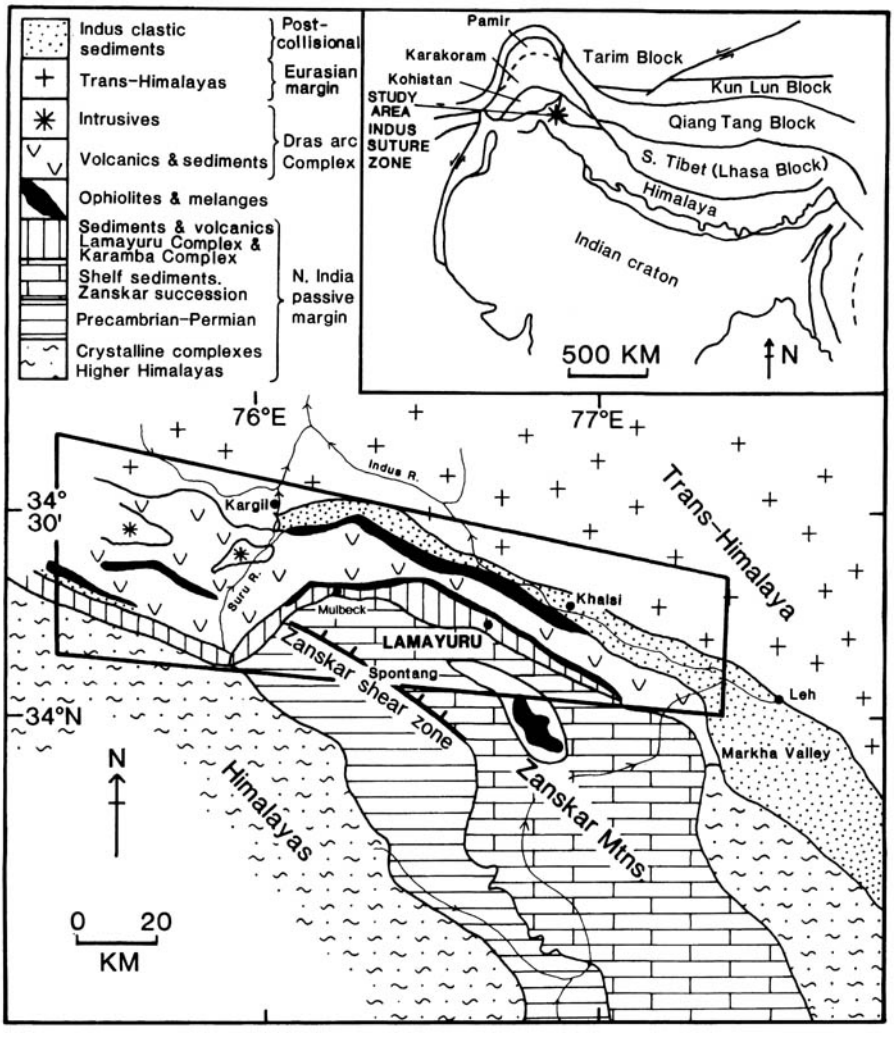

Fig. 1. Setting of the Indus Suture Zone in Ladakh. Area discussed here marked by box. Inset: regional tectonic context.

zones, N and S of the 'Dras volcanics' and, also, locally below the Zanskar Thrust, south of Lamayuru (Fig. 2). Data and interpretations of previous workers are summarized in Table 1. Key findings were as follows: The existence of blueschists in the Indus Suture Zone was confirmed by Virdi *et al.* (1977), who suggested a subduction-related origin. Fuchs (1979, 1986) mapped 'ophiolitic mélanges' (e.g. Omlung Mélange) in eastern Ladakh and argued that these reflect ocean closure and collisional processes beginning in latest Cretaceous times. Searle (1983) interpreted two zones of 'ophiolitic mélange' in Ladakh as the result of Late Cretaceous subduction–accretion, modified by the effects of Early Tertiary collisional deformation and Neogene backthrusting. An accretionary model was developed by Indian geologists (Sinha & Mishra 1992*a*, *b*, 1994, 1995; Sinha & Upadhyay 1990, 1997), who argued that 'ophiolitic mélanges' within the Indus Suture Zone represent the off-scraping of blocks of Tethyan oceanic lithosphere, including one, or several, large oceanic seamounts that were incorporated into a vast, chaotic accretionary prism with a sedimentary matrix.

Existing tectonic models for the Indus Suture Zone 'ophiolitic mélanges' are tested in this paper, using a combination of field mapping, petrographic and geochemical study, biostratigraphy and existing radiometric dating. The key to an understanding of the mélanges lies in the recognition within them of a number of discrete tectonic units, each with an identifiable origin, which can be compared with adjacent units of the Indus Suture Zone. It will be shown that the existing subduction–accretion hypothesis must be modified to take account of the additional roles of emplacement-related, collision-related and post-collisional processes, and that the mélange zones are the end products of a series of recognizable tectonic events. This paper also provides a case history for the recognition of and distinction between thrust sheets, broken formation and mélange of ophiolitic or other origins.

Definitions of terms

An **ophiolite** is a mappably coherent 'oceanic' sequence that encompasses, in ascending order, tectonized and/or layered ultramafics, layered and massive gabbros, sheeted dykes (locally absent) and extrusives. **Mélange** is here used as a purely descriptive (non-genetic) field term for a pervasively mixed unit, irrespective of whether mixing took place by sedimentary, or tectonic processes, or both. An **ophiolitic mélange**, thus, consists of a dismembered ophiolite, commonly associated with pelagic sediment (e.g. radiolarian chert). The presence of a single lithology (e.g. serpentinite), or even several lithologies (e.g. basaltic extrusives and chert) should not be taken to signify an ophiolitic mélange, since other origins could be possible (e.g. layered igneous complex, or seamount). If serpentinite dominates this would be termed **serpentinitic mélange**. A mélange maps out as a chaotic body, in contrast to a **broken formation** that preserves a disrupted, but still recognizable original stratigraphy, that is, however, more internally disrupted than within thrust sheets (see American Geological Institute 1961).

Methodology

This work is based on two field season's of study of the Indus Suture Zone mélanges, focusing on unravelling the tectonostratigraphy of representative segments of both the southern and northern mélange zones, where accessible. Fieldwork was supplemented by laboratory petrographic study, especially to identify the composition of clastic sedimentary rocks. A small number of samples of fine-grained sedimentary rocks were studied using whole-rock X-ray diffraction. Around 100 samples of basic extrusive igneous rocks were collected and analysed by X-ray fluorescence, using the methodology of Fitton & Dunlop (1985), and the results were analysed using standard tectonic discrimination plots and MORB-normalized 'spider' diagrams (Pearce *et al.* 1984).

Regional tectonic setting

'Ophiolitic mélanges' exposed in Ladakh form part of the Indus Suture Zone separating the Eurasian and Indian plates (Fig. 1). 'Ophiolitic mélanges' in Ladakh mainly crop out as two separate NW–SE trending zones, of which the southern one is a >100 km long and <10 km wide zone, whereas the northern zone is more discontinuous (Thakur 1981; Fig. 2). In this study it will be shown that, using the above definitions, much of the 'ophiolitic mélange' of the Indus Suture Zone in Ladakh is neither 'ophiolitic' in the sense of a dismembered ophiolite, nor ideal 'mélange' in the sense of comprising mappably chaotic blocks. Here, the terms **southern mélange zone** and **northern mélange zone,** respectively, are used for the two lineaments of highly disrupted rocks (Fig. 2). However, this does not imply that these units consist entirely of ideal mélange (see above definitions).

A prerequisite for understanding the tectonic setting of the mélange zones is a knowledge

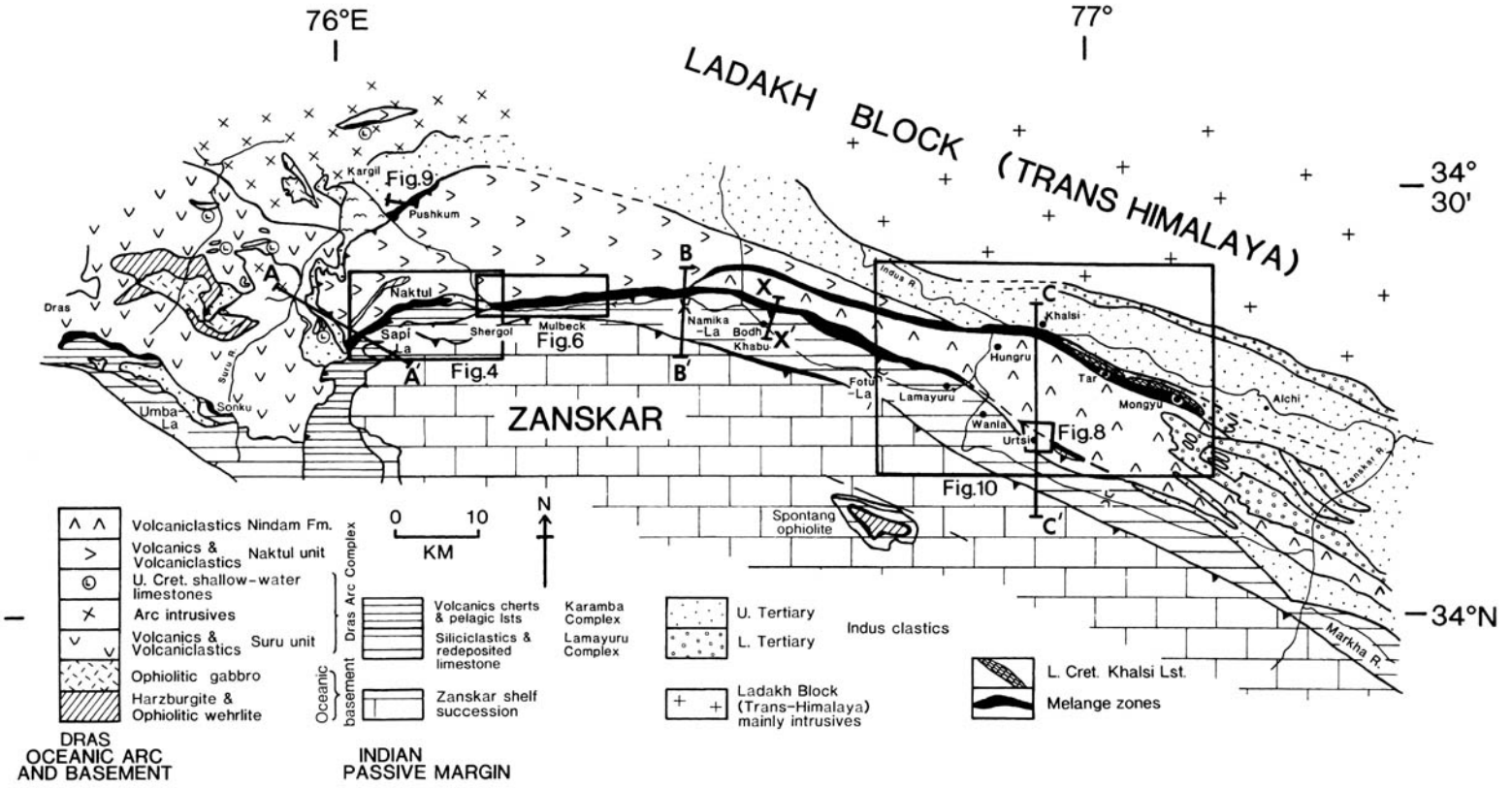

Fig. 2. Outline geological map of the Indus Suture Zone and adjacent units in Ladakh. Note the location of 'ophiolitic mélanges' as two zones north and south of the Dras arc complex (northern and southern mélange zones). Areas shown in more detailed maps are marked by boxes.

Table 1. *Summary of previous work on mélanges; see text for explanation*

Author	Main points	Comments	Present interpretation
Gannser 1974	Ophiolitic melange in Indus Suture Zone	Related to suturing of continental crust	Much of 'ophiolitic melange' is neither melange nor ophiolitic
Virdi *et al.* 1977	Recognized blueschists	Implied subduction in Ladakh	Still valid
Frank *et al.* 1977	'Ophiolitic melange'; blueschists in N	N zone affected by subduction	Mostly not melange, but part of Dras arc Complex
Fuchs 1979, 1989	'Ophiolitic melange' in E Ladakh	U Cretaceous ophiolite emplacement	Not included in this study
Thakur & Mishra 1983	'Ophiolitic melange' in N and S zones	Recognized ophiolitic melange, HP rocks & Indus molasse	Detailed model not proposed
Honegger *et al.* 1989	HP rocks, E and T-type MORB; 100 Ma K/Ar age	Mid-Cretaceous intra-oceanic subduction under arc to N	Origin as distal N-Indian margin
Searle 1983; Searle *et al.* 1987	Summary of 'ophiolitic melange'	Subduction–accretion model	Minimal subduction/accretion complex material is present
Reuber 1989	Ophiolitic basement to Dras arc	Melange zones in Suru Valley in W	Serpentinite sheets possibly Dras arc basement
Sutre 1991	Karamba unit, part of N Indian margin	Dras arc part of Andean-type margin	Oceanic arc origin of Dras arc favoured here
Sinha & Upadhyay 1990	Subduction/accretion model	Genesis by 'subduction kneading'	Sedimentary matrix and processes play little role
Sinha & Mishra 1992*a*, *b*, 1994	Accretion of giant oceanic seamount	Volcanic blocks seen as accreted seamounts	Volcanics are part of N-Indian passive margin (Karamba)
Robertson & Degnan 1993	Reconstructed Lamayuru passive margin	Channelized limestones present	'Mulbeck limestones' not accreted exotics
Sharp & Robertson 1998	Reconstructed Karamba distal passive margin	Intact thrust sheets present	Karamba Complex is not accreted ophiolitic melange

of the regional tectonostratigraphy (Figs 2, 3). Here, it is important to appreciate that the present tectonic stacking order is the reverse of that anticipated from southward thrusting onto the North Indian continental margin, following an important phase of Late Tertiary northward backthrusting, coeval with uplift of the High Himalaya (Colchen *et al.* 1985; Searle 1986; Corfield & Searle this volume).

The following main tectonic units are present from the structural top downwards:

1. The **Zanskar shelf succession**, including the overthrust Spontang ophiolite and underlying Spontang mélange (Gaetani & Garzanti 1991; Searle *et al.* 1997).
2. The **Lamayuru complex**, interpreted as the Mesozoic proximal deep-water passive margin (mainly sedimentary rocks) of the Indian plate (Bassoullet *et al.* 1981; Searle 1983; Robertson & Degnan 1993).
3. The **Karamba complex,** interpreted as the stratigraphically higher and more distal parts of the North Indian passive margin, including thick, mainly Jurassic, volcanics (Sutre 1991; Danelian & Robertson 1997; Robertson & Sharp 1998).
4. The **southern mélange zone** (Shergol Mélange of Thakur 1981), previously interpreted as

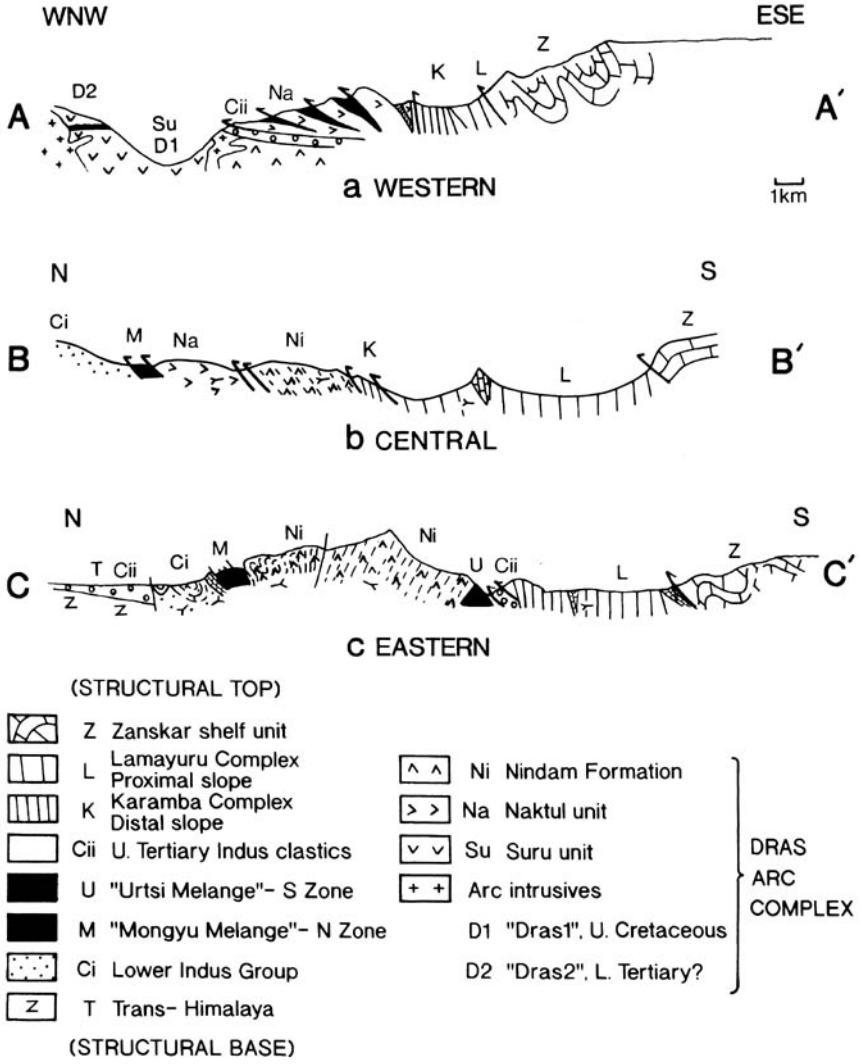

Fig. 3. Cross-sections of the Indus Suture Zone in the study area showing the setting of the northern and southern mélange zones. Lines of section shown in Fig. 2.

mainly Late Cretaceous ophiolitic mélange formed as an accretionary prism (Sinha & Mishra 1992*a*, *b*, 1994, 1995), but re-interpreted here as of composite origin (see below).

5. The mid-Late Cretaceous **Dras arc complex**, interpreted as an emplaced oceanic arc (e.g. Searle 1983; Riebel 1984; Reuber 1989; Robertson & Degnan 1994); the Dras arc complex is divisible into three main thrust sheets: the Suru unit in the west, the Naktul unit in the centre of the area, and the Nindam Formation in the east. The Suru and Naktul units include intrusive, volcanic and volcaniclastic lithologies, whereas the Nindam Formation is a coherent volcanic-sedimentary succession (Robertson & Degnan 1994).
6. The **northern mélange zone** (Frank *et al.* 1977; Thakur 1981), previously interpreted as 'ophiolitic mélange', or 'wildflysch'.
7. The **Ladakh Block** (Trans-Himalaya) (e.g. Scharer *et al.* 1984; Sharma & Choubert 1983; Fig. 2).

During Early Tertiary collision of the Indian and Eurasian plates (54–50 Ma) the Dras arc complex was thrust over the North Indian margin. The Dras arc complex, together with the Kohistan arc to the west (in Pakistan) is inferred to have sutured to the Eurasian margin (Karakoram) in latest Cretaceous time along the Shyok Suture Zone (Thakur 1981, 1990; Thakur & Mishra 1984; Coward *et al.* 1986). According to alternative interpretations, the Lamayuru–Karamba–Zanskar passive margin was first deformed in association with ophiolite obduction (Spontang ophiolite), either in latest Cretaceous (Searle 1986; Searle *et al.* 1987, 1997), or not until Eocene time (e.g. Reuber *et al.* 1987; Gaetani & Garzanti 1991). The hypothesis of Late Cretaceous emplacement is supported by recent structural work on the Spontang ophiolite and related mélanges (Searle *et al.* 1997; Corfield 1999; Corfield & Searle 2000) and biostratigraphical work on the North Indian passive margin sediments (i.e. Lamayuru and Karamba units) which indicates that deep-sea sedimentation ceased in Late Cretaceous time (Danelian & Robertson 1997; Robertson & Sharp 1998). The collision of Eurasia and India in Ladakh is equated with an inferred Early Eocene age of the youngest nummulite-rich limestones, traditionally dated as Ypresian (Garzanti & Van Haver 1988). Studies of modern collisional settings, as in the eastern Mediterranean (Robertson *et al.* 1998) show that the initial stages of collision take place at depth beneath the sea-floor, followed by emergence only when collision advances. In view of such factors, collision of India and Eurasia in Ladakh is simply referred to as Early Tertiary in this paper. Following this collision, erosion created non-marine post-lower Eocene clastic successions of the Indus Group ('Indus molasse'; Van Haver 1984; Van Haver *et al.* 1984; Garzanti & Van Haver 1988). Subsequently, both the northern and southern mélange zones and adjacent units experienced north-vergent back-thrusting, during Late Tertiary time (Colchen *et al.* 1985; Searle 1986).

'Ophiolitic mélange' is also reported from eastern Ladakh (Markha valley area; Fig. 2; i.e. Omlung Mélange; Fuchs 1979, 1986; unpublished data). This unit is similar to the mélanges underlying the Spontang ophiolite which, in turn, overlie the Zanskar shelf succession to the south of the Indus Suture Zone (Reuber *et al.* 1987; Searle *et al.* 1997; Corfield 1999; Fig. 1). These mélange units include dismembered ophiolitic rocks and large detached blocks and thrust sheets ('exotics') of Permo-Triassic shallow-water limestone. The only known counterpart of these units in western Ladakh studied here is a single detached block of Permo-Triassic shallow-water carbonate and volcanics near Lamayuru (Fig. 2). This is interpreted as a carbonate build-up developed on a volcanic seamount, oceanward of the Zanskar shelf succession (Robertson 1998). There is, thus, clearly a genetic link between the Indus Suture Zone mélanges (discussed here) and the Spontang mélanges and this must be considered in any interpretation.

Tectonostratigraphy of the southern mélange zone

Outcrops were studied in both the western (western segment) and eastern (eastern segment) areas of the southern mélange zone (Fig. 2).

Western segment

Sapi–La area (Fig. 4). An outline map is given in Fig. 4, together with sections of the structurally lower part in the west, in Fig. 5. Additional sections are given in Robertson & Sharp (1998). Previously, the southern mélange zone (Shergol Mélange of Thakur 1981) was taken to comprise a true mélange composed of basic igneous rocks, deep-sea sedimentary rocks, serpentinite and schists. This unit is structurally underlain by coherent, folded and locally thrust-imbricated lithologies of the Upper Cretaceous Naktul unit of the Dras arc complex (Robertson & Degnan 1994). These rocks are, in turn, structurally

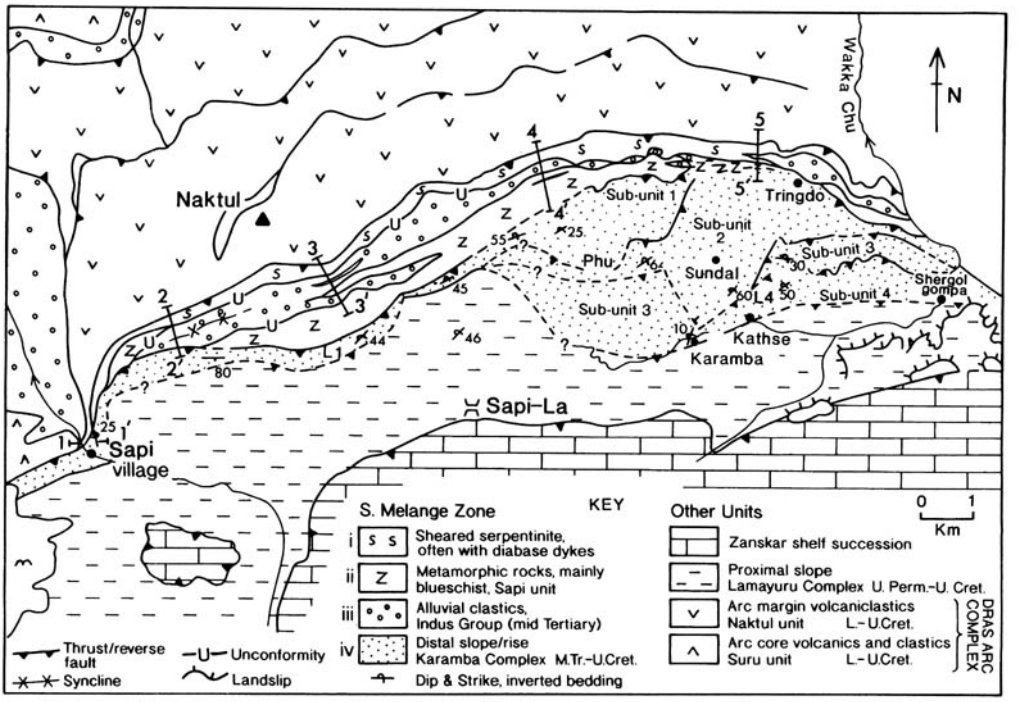

Fig. 4. Geological map of the Sapi–La area (southern mélange zone, western segment, based on mapping by Honegger (1983), Sutre (1991) and Robertson & Sharp (1998)). This area, considered as ophiolitic mélange by some workers (e.g. Sinha & Mishra 1992*a*, *b*, 1994, 1995), extends from the Dras arc complex in the north to the Lamayuru complex in the south. However, most of this is here assigned to the Karamba complex (North Indian distal passive margin unit).

overlain by Triassic clastic successions of the Lamayuru complex, mainly sandstones and shales (Bassoullet *et al.* 1981; Sutre 1991; Robertson & Sharp 1998) and finally by the Zanskar shelf succession. Reconnaissance mapping shows that the Lamayuru complex, cut by numerous sills, is well exposed further west in the Umba–La area (west of Suru valley; Fig. 2).

The following units were identified within the Sapi–La area from the structural top downwards during this study (Fig. 5).

(i) *Sheared serpentinite*, locally with inclusions of gabbro and diabase. This serpentinite maps out as a laterally continuous thrust sheet, ranging from tens to several hundreds of metres in width. In addition, highly sheared strands of serpentinite (up to tens of metres wide and hundreds of metres long) are locally found separating structurally overlying units.

(ii) *Metamorphic rocks, mainly blueschist ('Sapi unit')*. A metamorphic outcrop widens from tens of metres wide, in the east, to several kilometres in the Sapi–La area; this then wedges out to the west (towards Sapi village; Fig. 4). The metamorphic rocks comprise blueschists (including marble and quartzite), structurally underlain by greenschists, including meta-lavas, meta-carbonates and meta-chert (Honegger 1983; Honegger *et al.* 1982, 1989).

(iii) *Alluvial clastics (Indus Group–mid Tertiary)*. Coarse clastic sedimentary rocks (i.e. conglomerate, sandstone, shale) map out as anatomising strands, typically up to hundreds of metres wide and up to several kilometres long, in contact with both sheared serpentinite and metamorphic units; contacts are either unconformable or tectonic (Fig. 5).

(iv) *Karamba complex (Mid Triassic–Late Cretaceous)*. This consists of sheared and folded units (commonly inverted) of pelagic carbonate, radiolarian chert, limestone, shale and sandstone, together with basic extrusive igneous rocks. This unit was interpreted as ophiolitic mélange by Honegger *et al.* (1982) and Sinha & Mishra (1992*a*, *b*, 1994, 1995), whereas others (Sutre 1991; Robertson & Degnan 1994; Danelian & Robertson 1997; Robertson &

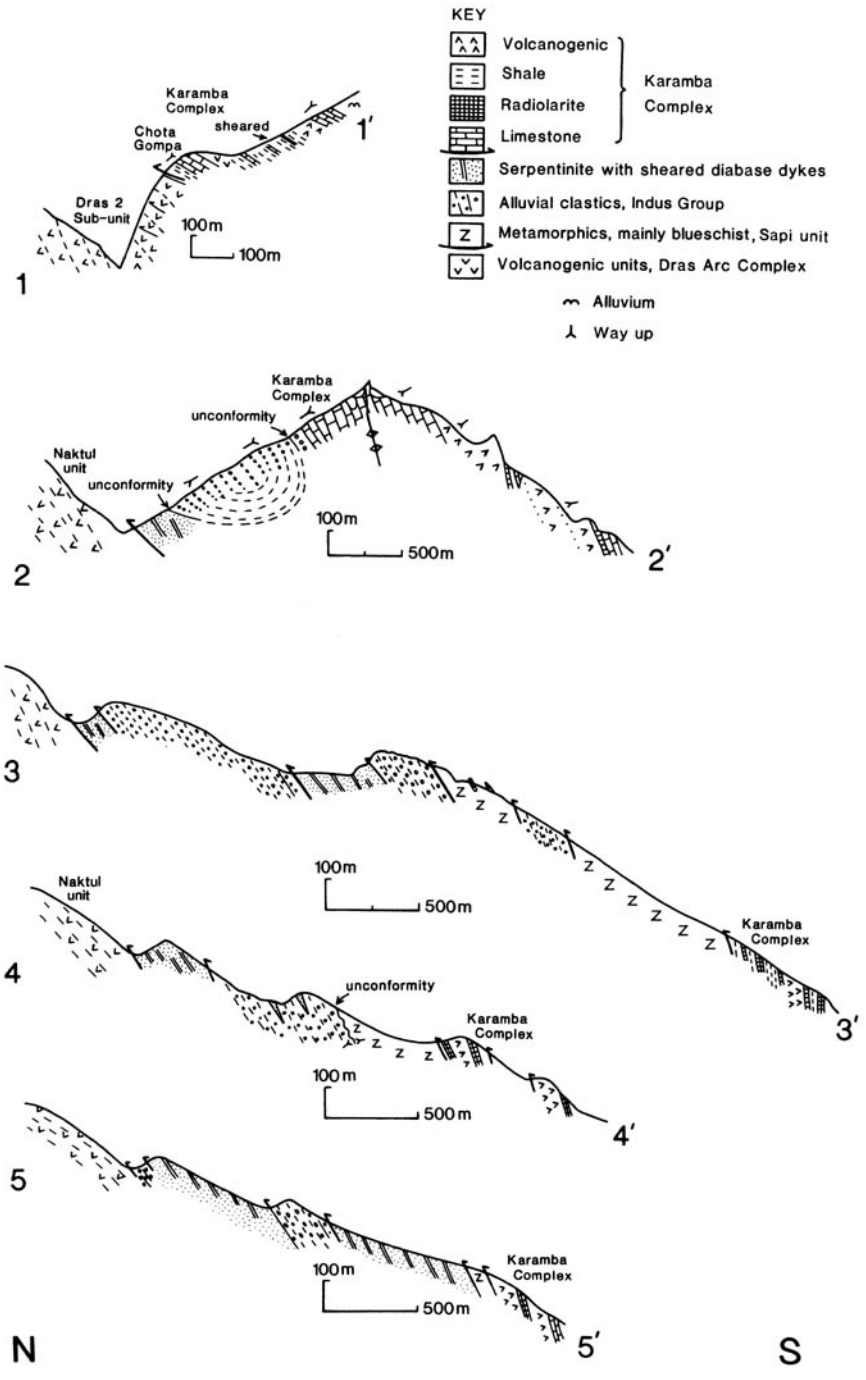

Fig. 5. Cross-sections of outcrops located between the Dras arc complex (Naktul unit) in the north and the Karamba complex (distal North Indian margin) in the south. This area includes serpentinite, blueschists and Indus Group clastics. Lines of sections are marked on Fig. 4. Additional cross-sections of the Karamba and Lamayuru complexes in the Sapi–La area are given by Robertson & Sharp (1998).

Sharp 1998) recognize the presence of a thrust deformed, but otherwise coherent Mid Triassic–Late Cretaceous succession that they interpreted as a distal part of the North Indian passive margin.

Shergol–Mulbeck area (Fig. 6a, b). This area is the eastward continuation of the Sapi–La area described above. The tectonostratigraphy is similar, but the outcrop width is reduced and the units present are more tectonically fragmented. There is no well developed metamorphic sheet between the structurally underlying Dras arc complex (Naktul unit) and the overlying Karamba complex, although small outcrops of blueschists are locally present (west of Shergol). The following units are present from the structural base upwards.

(i) *Volcanic-sedimentary unit (Karamba complex).* This is highly sheared, with only rare intact successions exposed within thrust sheets (Fig. 6a, section D–D′). Locally (west of Namika–La), there is a demonstrable upward continuity from thick-bedded Triassic? siliciclastic turbidites (similar to those of the Lamayuru complex) to basic volcanics, volcaniclastic sediments, radiolarian chert and Late Cretaceous pelagic carbonate, typical of the Karamba complex. A measured log was published in Robertson & Degnan (1993). These observations confirm that the origins of the Lamayuru and Karamba complexes are intimately related, as part of the North Indian passive margin.

(ii) *Sheared serpentinite*, locally with diabase dykes, as observed in the Sapi–La area further west (Fig. 6a; section A–A′). Anastomosing strands of sheared serpentinite are intercalated between slices of the Karamba complex in places.

(iii) *Terrigenous clastics with sills (Lamayuru complex).* This was previously correlated with 'ophiolitic mélange' as detached blocks of diabase (of assumed ophiolitic origin) in a matrix of sheared shale and sandstone, together with large blocks of shallow-water limestone (Searle 1983; Searle *et al.* 1987; Sinha & Upadhyay 1990). However, the diabase is entirely made up of disrupted diabase sills within the Lamayuru complex, which thus represents a strongly sheared, thrust imbricated, but otherwise intact stratigraphic succession of mainly Triassic sandstone turbidites and dark shales (Robertson & Degnan 1993). Structurally above additional lithologies with fewer sills are typical of the Lamayuru complex.

(iv) *Alluvial clastics (Indus Group).* This unit maps out as a lozenge-shaped thrust sheet in the north and as a laterally continuous thrust sheet in the south, bounded by sheared contacts with serpentinite by the Karamba complex and the Lamayuru complex in different areas. Bedding is locally overturned (Fig. 6a; section B–B′).

Bodh Khabu area. The importance of the Bodh Khabu area (Fig. 2) is that it establishes structural continuity between the western and eastern segments of the southern mélange zone, over a distance of >60 km. Reconnaissance mapping north of Bodh Khabu village, *c.* 20 km east of Mulbeck (Fig. 7), revealed the units outlined below, again from the structural top downwards. Of these, only (ii) and (iii) are correlated with the southern mélange zone.

(i) *Volcaniclastic Nindam Formation (Dras arc complex)*, including Upper Cretaceous volcaniclastics and pelagic carbonates of the Nindam Formation (Dras arc complex), as seen in the eastern segment (Sutre 1991; Robertson & Degnan 1994; see below).

(ii) *Sheared serpentinite.* An up to several hundred metre-wide unit is present, with inclusions of gabbro and diabase.

(iii) *Karamba complex (volcanic-sedimentary unit).* This comprises thrust-imbricated successions of massive and pillowed basaltic rocks intercalated with radiolarian cherts and minor pelagic carbonates.

(iv) *Blueschist.* A thin (<5 m), discontinuous thrust sheet of sheared blueschist was locally observed in the south in tectonic contact with overlying terrigenous sediments of the Lamayuru complex.

(v) *Shales, sandstones and diabase sills.* These represent coherent successions correlated with the Lamayuru complex.

Eastern segment

The eastern segment of the southern mélange zone extends from west of Lamayuru, eastwards to the Urtsi area, and then links with mélange units in the Markha valley further west that are outside the scope of this paper (Fig. 2). Within the eastern segment, the southern mélange zone was envisaged as simply comprising chaotic blocks of serpentinite, pillow lava, schist and clastic sediments (Thakur & Mishra 1983). However, a more organized tectonostratigraphy is revealed by this study.

Lamayuru area (Fig. 2). The main feature of the mélange zone in this area is the presence of a large (several hundred metres) detached block of Permo-Triassic limestone (Bassoullet *et al.* 1978), associated with basaltic rocks and lava breccias of chemically within-plate type (Robertson 1998). This block is separated from the Nindam Formation (Dras arc complex) to the north by a narrow (< 50 m) strand of sheared serpentinite. In adjacent areas, where the exotic block is absent, the serpentinite is structurally overlain to the south by a laterally continuous unit of coarse clastic sediments (correlated with the lower part of the Indus Group); this is, in turn, structurally overlain by Triassic sandstone turbidites and shales within the type area of the Lamayuru complex.

Urtsi area (Fig. 8). Where well exposed further east, near Urtsi village (Fig. 8), the southern mélange zone is structurally overlain by the Dras arc complex (Nindam Formation; Sutre 1991; Robertson & Degnan 1994) to the north, and is also structurally overlain by non-marine coarse clastic sediments of probable Oligocene age to the south (Skyu–Chilling Formation of Sutre 1991). The following units crop out from the structural top downwards within the southern mélange zone (Fig. 8).

(i) *Thrust sheets of mainly volcaniclastic sediments.* Redeposited volcaniclastic sediments and calciturbidites are interbedded, forming both laterally continuous and lenticular disrupted thrust sheets (Fig. 8a).
(ii) *Coarse clastics.* A thin unit of clast-supported conglomerate, correlated with the base of the Oligocene? Skyu–Chilling Formation (Indus Group) unconformably overlies the mainly volcaniclastic sedimentary rocks of unit (i) (Fig. 8; central area of map).
(iii) *Block-in-matrix mélange.* Blocks of pillow lava, lava breccia, radiolarian chert, sandstone, conglomerate and marble are set in a matrix of shale and thinly bedded redeposited limestone (Sutre 1991); blueschist facies minerals were reported by Honegger *et al.* (1989).

Tectonostratigraphy of the northern mélange zone

The northern mélange zone is well exposed in the west (Pushkum area, western segment), but further west is largely obscured by intrusive rocks (Frank *et al.* 1977; Reuber 1989). Traced eastwards, the northern zone runs into a poorly known area (inaccessible for political reasons), until it reappears as a continuous outcrop (30 km long; eastern segment) that, in turn, disappears beneath sediments of the Indus Group. In addition, the northern and southern mélange zones are connected by a narrow (< 500 m) strand of sheared serpentinite mélange, 30 km long, which separates the volcanic-sedimentary Naktul unit in the west from the volcaniclastic Nindam Formation in the east (both units of the Dras arc complex). As far as is known, this cross-cutting serpentinitic strand (Fig. 2) does not include additional exotic lithologies (Thakur 1981; Thakur & Mishra 1983).

Western segment

Pushkum area (Fig. 9). This area is complicated by numerous plutonic bodies, mainly granodiorite, interpreted as Late Cretaceous–Early Tertiary intrusions along an Andean-type margin (Sharma & Choubert 1983; Scharer *et al.* 1984). Frank *et al.* (1977) sketched sections across the northern mélange zone, near 'Pashkyum' and reported sheared lenses of serpentinite, diabase, gabbro, acidic volcanics and various metamorphic rocks, including crossite- and glaucophane-bearing schist, mica-schist and gneiss. These authors also noted a westward extension of the northern mélange zone (SW of Kargil; Fig. 2), cut by granodioritic intrusions into the Trans-Himalaya unit (Ladakh Batholith). Near Pushkum, the northern mélange zone is structurally overlain by mainly coarse volcaniclastic sediments of the Late Cretaceous Naktul unit (Dras arc complex). Related lithologies include pillow lava, pelagic limestone, radiolarian chert and Late Cretaceous shallow-water limestone of Albian–Aptian age (Honegger 1983; Sutre 1991; Robertson & Degnan 1994). In addition, the mélange zone is structurally underlain by coarse non-marine sediments of the Indus Group (Van Haver 1984).

The following units are present within the northern mélange zone from the structural top downwards.

(i) *Sheared serpentinite*, with inclusions of diabase and gabbro.
(ii) *Volcanic-sedimentary unit.* This is mapped as a thrust sheet of pillowed and massive basic lava, depositionally overlain by radiolarian and volcaniclastic sediments.
(iii) *Metamorphic rocks.* Thin thrust sheets (up to tens of metres thick) of both blueschists and greenschists (Frank *et al.* 1977).

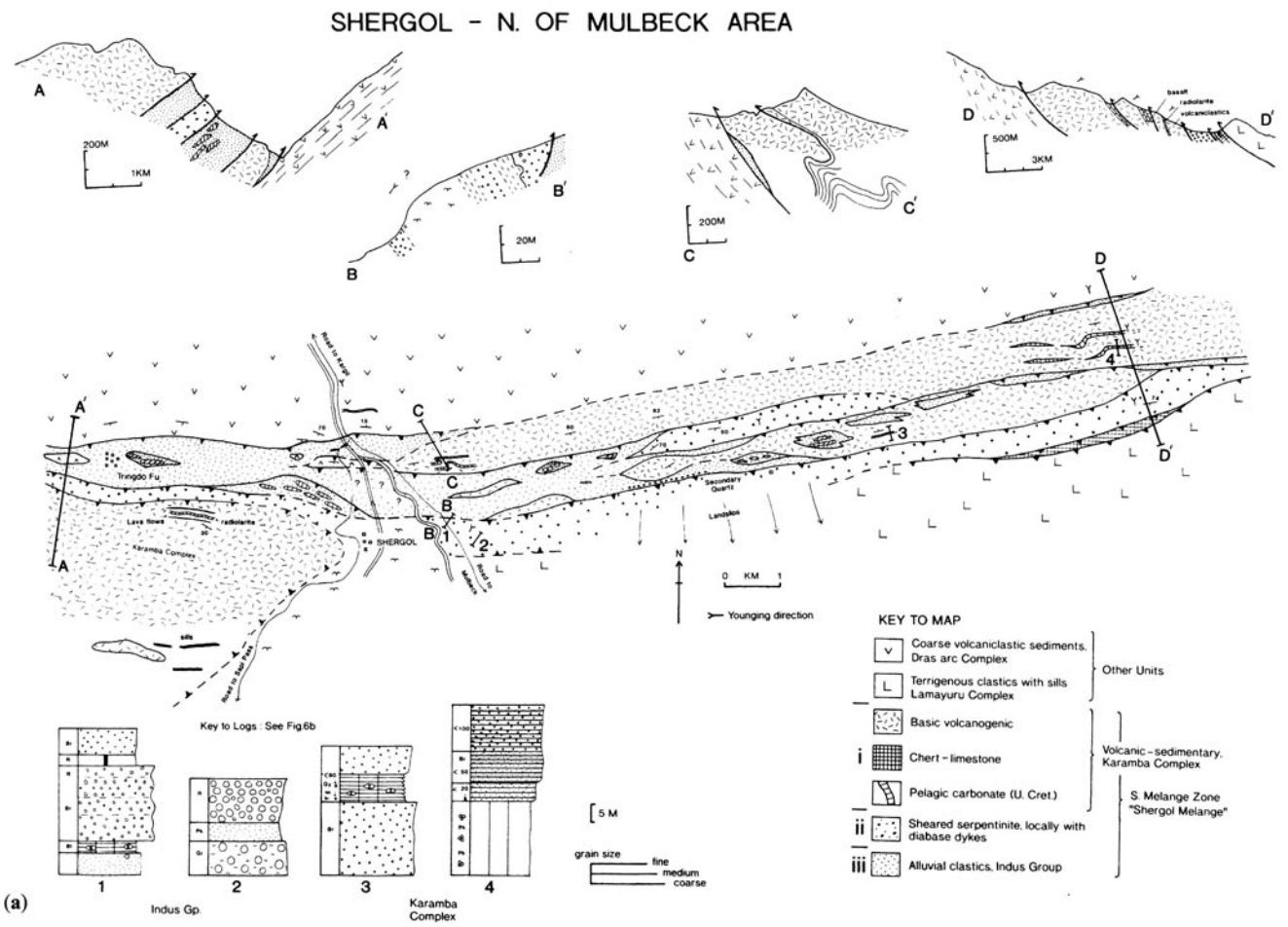

Fig. 6. (**a**) Sketch map with local sections and sedimentary logs of the southern mélange zone (western segment), west of Shergol ('Shergol mélange'). The key in (a) refers to the map and cross-sections only. Units mapped are mainly correlated with the underlying Dras arc complex, Karamba complex and Indus Group clastics. (**b**) Key to all sedimentary logs.

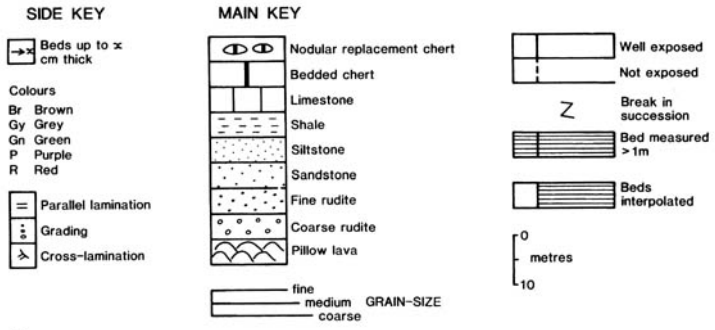

(b)

Eastern segment

Hungru–Mongyu area (Fig. 10). The northern mélange zone ('Mongyu mélange') is well exposed for 30 km, along strike from near Hungru to Mongyu (Fig. 2), especially in steep-sided valleys running southwards from the Indus River. Van Haver *et al.* (1984) recognized a 'Nappe de Tar' composed of 'wildflysch', lavas, agglomerates and hyaloclastites. In this area, the northern mélange zone is structurally overlain by volcaniclastic sediments of the Late Cretaceous Nindam Formation (Dras arc complex; Degnan & Robertson 1994; Fig. 10a, b, e) and structurally underlain by Aptian–Albian shallow-water limestones (Khalsi Limestone; Tewari *et al.* 1970; Fig. 10 a, b, e), locally passing upwards into Early Tertiary (Palaeocene) deep-water clastic sedimentary rocks (Tar Formation; Garzanti & Van Haver 1988). The Khalsi Limestone was previously interpreted as part of a subduction–accretion complex (Garzanti & Van Haver 1988), or part of an Andean-type fore-arc succession located along the southern margin of the Ladakh Block/Trans-Himalaya (Fig. 2; Sutre 1991; Robertson & Degnan 1994; Sinha & Upadhyay 1997). In this study, the Khalsi Limestone is inferred to represent a carbonate platform constructed on the Ladakh Block, part of the S Eurasian continental margin, which then evolved into a fore-arc basin of an Andean-type margin in Early Tertiary time. It is, therefore, not included within the mélange zone.

Two main units are present from the structural top downwards within the northern mélange zone outcrop, as follows.

(i) *Sheared serpentinite.* This ranges from strands only a few metres to *c.* 1 km wide, with local inclusions of diabase and gabbro.

(ii) *Shale-volcanic unit.* This is composed of disordered blocks and thrust sheets of quartzo-feldspathic and micaceous sandstones, basic-andesitic lavas and volcaniclastic sediments set in a matrix of black micaceous shale.

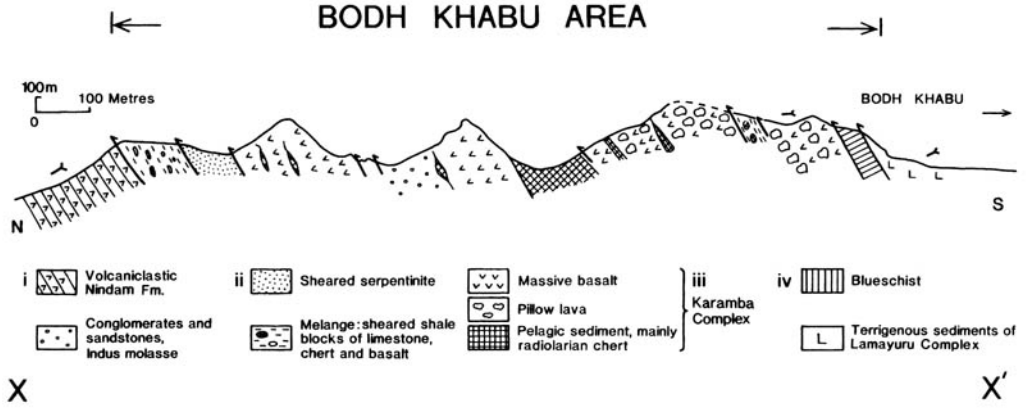

Fig. 7. Cross-section of the southern mélange zone near Bodh Khabu (see Fig. 2 for location). The volcanics and pelagic sediments (limestone and chert) are correlated with the Karamba complex in the type area further west (near Sapi–La).

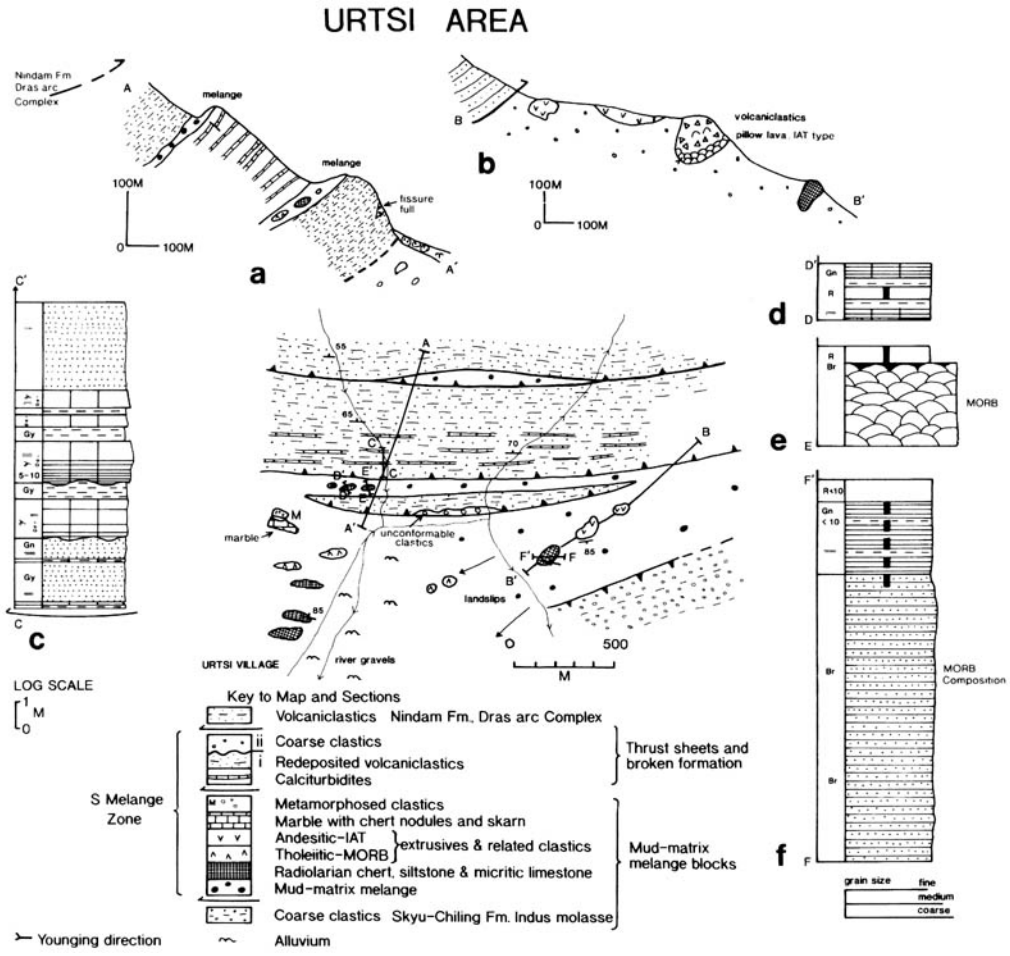

Fig. 8. Sketch map, cross-sections and logs near Urtsi (southern mélange zone, eastern segment; 'Urtsi mélange'). See Fig. 2 for location and Fig. 6b for key to sedimentary logs.

Lithology and origin of units

Based on the above tectonostratigraphic outline, a number of discrete lithotectonic units can be recognized in one, other, or both of the southern and northern mélange zones, and these will now be described and interpreted in turn.

Units associated with the Lamayuru complex

Most of the outcrop area of the Lamayuru complex is relatively stratigraphically intact, although strongly deformed (Bassoullet *et al.* 1981; Robertson & Degnan 1993; Sinha & Upadhyay 1993, 1994) and has not been included within 'ophiolitic mélange' by previous workers. However, Searle *et al.* (1987) mapped 'blocks of diabase' within a matrix of sheared shale and sandstone (between Shergol and Mulbeck; Fig. 2), as mélange. Locally, in the Mulbeck area the Lamayuru succession (mainly Triassic sandstone and shale) is highly sheared, such that the competent sills are highly disrupted (Fig. 11). By contrast, in less deformed areas further east (e.g. Bodh Khabu area) and further west (Umba–La area) identical diabase dykes are present as numerous diabase sills (locally pegmatitic) within much less deformed clastic sediments of the Lamayuru complex. The sills all exhibit excellent chilled margins with host Lamayuru sediments. Chemical analysis shows that the basic sills in the Mulbeck area are compositionally of strongly enriched (alkaline), within-plate type composition (Table 1; Fig. 14). For comparison, diabase sills were also analysed (Fig. 14) from an area where the Lamayuru clastic succession is less

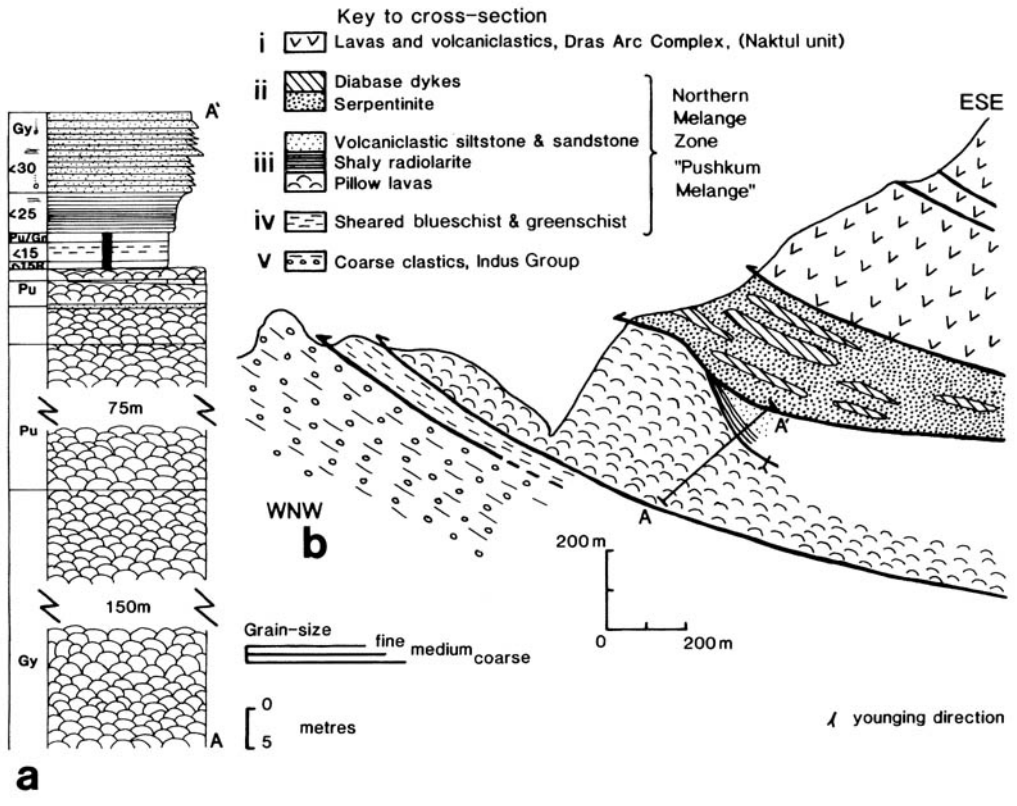

Fig. 9. Pushkum area, northern mélange zone, western segment (see Fig. 2 for location): (**a**) stratigraphic log; (**b**) structural cross-section. For key to sedimentary logs see Fig. 6b.

deformed, near Umba–La (west of Suru valley; Fig. 2). These rocks are chemically very similar to the disrupted sills in the Mulbeck area. In addition, in the Mulbeck area, Searle (1983) interpreted detached masses of Late Triassic to Mid-Jurassic shallow-water limestone (Bassoullet *et al.* 1981) as accreted exotic limestones derived from within the Tethyan ocean. However, Robertson & Degnan (1993) showed that these limestones pass depositionally upwards into debris flows related to the Lamayuru passive margin succession. These limestones were, therefore, reinterpreted as originally related to the Zanskar shelf margin and are not seen as accreted oceanic units (in contrast to, for example, the Lamayuru exotic; Robertson 1998). Furthermore, Sinha & Upadhyay (1993, 1994) reported numerous 'detached blocks' of mainly Jurassic limestone from elsewhere in the Lamayuru complex (e.g. Namika–La area; Fig. 2) and suggested that these slid in from the neighbouring Zanskar shelf. However, Robertson & Degnan (1993) showed, by detailed logging, that these limestones are entirely redeposited, channelized limestones **interbedded** with the Lamayuru complex deep-water passive margin succession, and should not be interpreted as part of the mélange.

Discussion. The Lamayuru complex is an intact succession of deep-water, relatively proximal, sedimentary rocks that accumulated on the North Indian passive continental margin and does not include any units that were accreted from within the Neotethys ocean further north. The detached masses of limestone at Mulbeck are likely to represent fragments of the deformed Zanskar shelf margin that reached their final position as a result of Neogene backthrusting. The swarms of diabase sills are interpreted as being genetically related to basic extrusives within the stratigraphically higher and more distal Karamba complex (see below). Well-lithified, channelized limestone conglomerates within shale and sandstone formed relatively competent units within the Lamayuru complex; these were exploited by multi-stage thrusting and folding to produce the illusion of numerous blocks in a matrix. Where highly tectonically

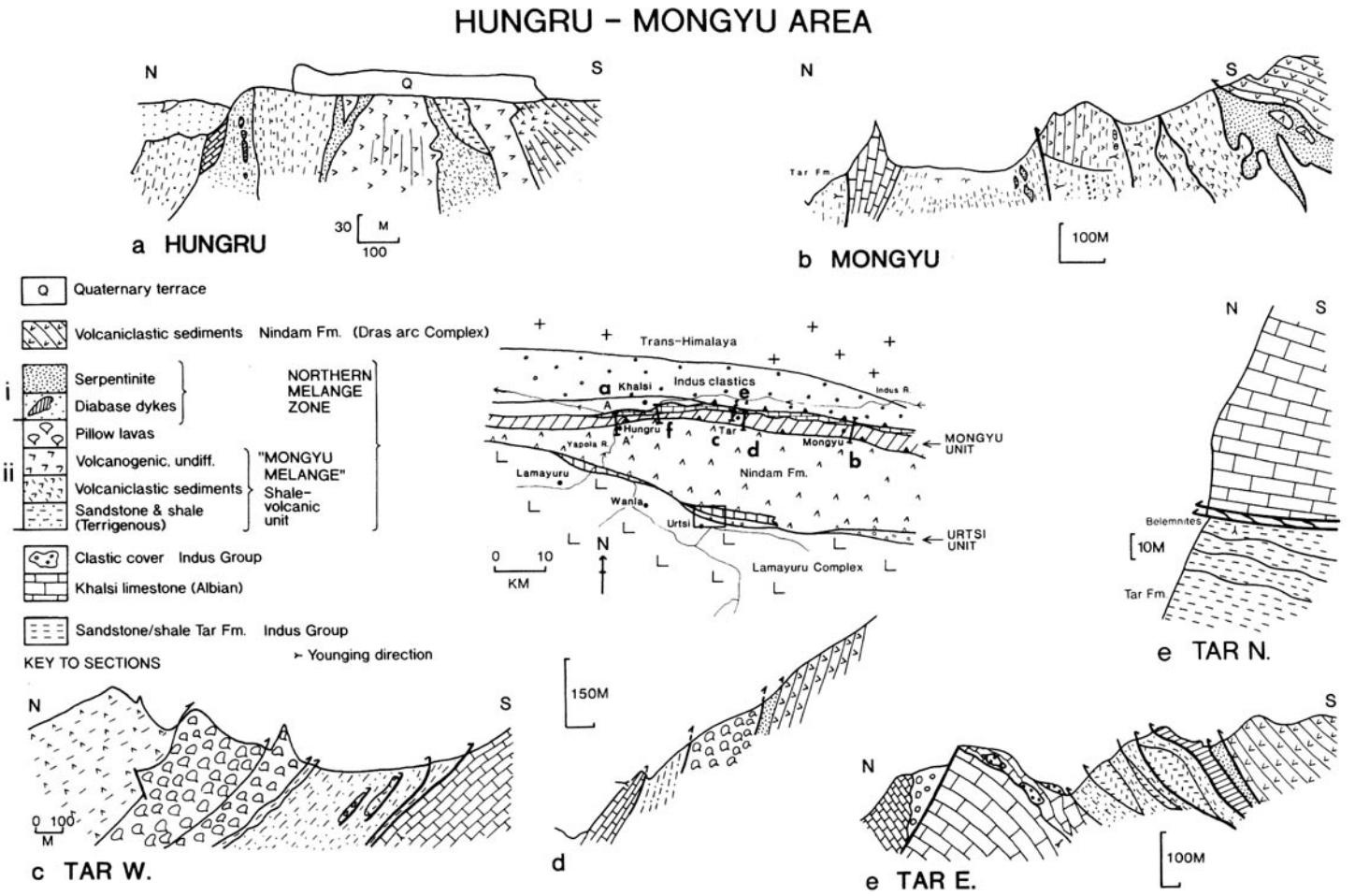

Fig. 10. Map and local sections of the Hungru–Mongyu area, northern mélange zone, eastern segment. Note the tectonic contacts with both the volcaniclastic Nindam Formation above and the Aptian/Albian Khalsi Limestone below. Map modified from Sutre (1991).

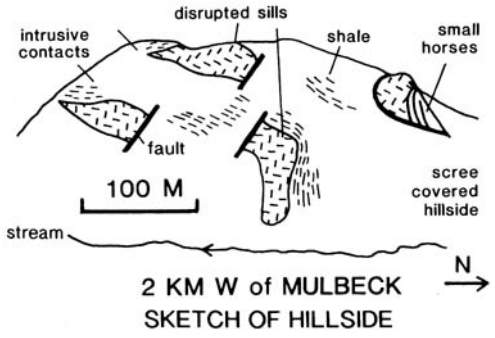

Fig. 11. Field sketch showing diabase sills intruded into sandstones and shales of the Lamayuru complex, later locally disrupted into blocks (west of Mulbeck). These are mapped as broken formation, but not as mélange.

disrupted, the Lamayuru complex should thus be mapped as a broken formation, but not as mélange, as an original structural integrity is still preserved.

Units associated with the Karamba complex

Sapi–La area. Detailed mapping and section logging has established that 'ophiolitic mélange', structurally beneath the Lamayuru complex in the Sapi–La area (western segment), represents the originally stratigraphically higher and more distal parts of the Mesozoic (Triassic–Late Cretaceous) North Indian passive continental margin, as discussed in detail elsewhere (Danelian & Robertson 1997; Robertson & Sharp 1998; Fig. 13a). Three main thrust sheets are present, each of which is mainly inverted (Fig. 12). Facies and structural analysis show that prior to tectonic emplacement, the sediments originally became thinner-bedded, finer grained and more distal towards the north. A large volcanic build-up was constructed near, or within, the inferred continent–ocean transition zone during Mid-Jurassic time, based on dating by radiolarians within siliceous sediments associated with the extrusives (Danelian & Robertson 1997). It is important to realize that the volcanics are entirely interbedded with the continental margin-type succession and thus, cannot, be considered as blocks in a mélange. However, the term, broken formation, is appropriate where the succession is strongly disrupted. The Karamba complex experienced, probably, several phases of southward-directed compression and thrusting related to emplacement, followed by Neogene northward backthrusting (Robertson & Sharp 1998). Analysis of basic extrusive rocks from the

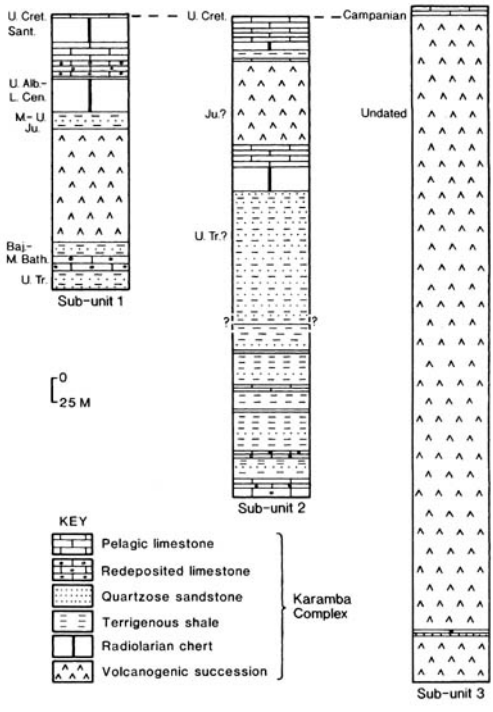

Fig. 12. Generalized logs of the three main thrust sheets (mainly inverted) exposed in the type area of the Karamba complex, interpreted as the distal part of the North Indian passive margin. Detailed bed-by-bed logs and biostratigraphical age data are given in Sutre (1991), Danelian & Robertson (1997) and Robertson & Sharp (1998). These successions are not 'ophiolitic mélange', although they could be mapped as broken formation and localized mélange.

Sapi–La area (Table 2) indicates a mainly enriched within-plate character (alkaline), whilst a few are compositionally close to mid-ocean ridge basalt (Honegger *et al.* 1982; Sinha & Mishra 1992*a*, *b*, 1994, 1995; this study; Fig. 14). The WP- and near MOR-type basalts occur together in single interbedded successions, suggesting that all the Karamba lavas belong to a single basalt–alkaline basalt fractionation series. Dating using both radiolarians within associated cherts and calcareous fossils shows that the extrusives are mainly Jurassic in age, but minor Triassic volcanics are present, and volcanism may extend into Early Cretaceous time (Danelian & Robertson 1997; Robertson & Sharp 1998). Chemical analysis also did not reveal any systematic differences in the compositions between the (minor) Triassic volcanics and the overlying Jurassic (and possibly) younger ones.

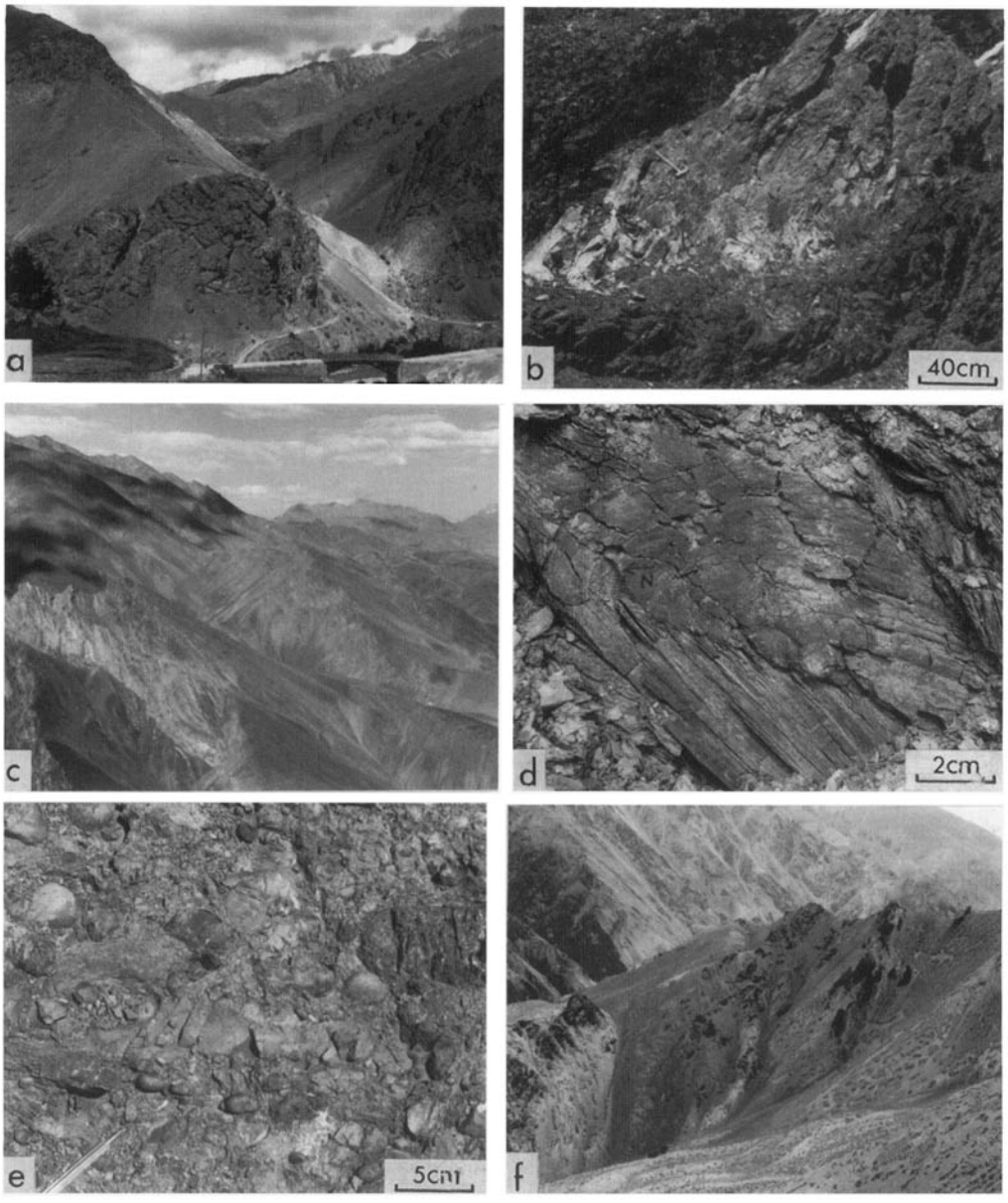

Fig. 13. Field photographs of the southern mélange zone. (**a**) View W from near Shergol bridge across volcanics and sediments of the Karamba complex to the Dras arc complex (far right). (**b**) Rodingitized, lenticular sheared diabase dyke within serpentinite (1.5 km east of Tringdo). (**c**) View east from near Shergol to the contact between the Dras arc complex (partly clouded, to left) and the southern mélange zone, dominated by thrust sheets of volcaniclastic sediment correlated with the Karamba complex. (**d**) North-verging folds in deformed clastic sediments, southern mélange zone, 2.5 km ENE of Shergol. (**e**) Debris flow with well-rounded pebbles in a shale matrix, correlated with the Indus Group, Mulbeck area (Fig. 6, log 2). (**f**) A thin strand of sheared serpentinite and clastics of the Indus Group (both dark) sandwiched between the Nindam Formation (pale, in distance to left) and the Lamayuru complex (smooth hillside to right), near Lamayuru.

Mulbeck area. A very similar volcanic-sedimentary assemblage of the Karamba Formation (not previously discussed in detail) is found east of Shergol (Fig. 13c). Tectonically disrupted, locally folded thrust sheets of basalt, volcaniclastic sandstone, siltstone and mudstone occur together with subordinate redeposited limestones, pelagic limestones and radiolarian cherts (Fig. 6A–A′ to D–D′). The lithologies are deformed by north-facing thrusts and folds (Fig. 6C–C′, D–D′). The basic volcanics are interbedded with volcanogenic sediments, mostly sandstones, in units up to tens of metres thick. Individual volcaniclastic sandstone beds, up to 1 m thick, typically exhibit turbidity current structures (e.g. grading, micro-cross lamination) and contain occasional clasts of shallow-water limestone (up to 3 cm thick). Associated volcaniclastic siltstones are interbedded with pale, to dark mudstones, muddy limestones and rare limestone beds, up to 0.4 m thick (Fig. 6a, logs 3–4; bottom left of figure). Pelagic limestones form units up to 20 m thick, and include finely laminated and burrow-mottled textures (Fig. 6C–C′). Individual burrows are filled with volcaniclastic silt, pelagic foraminifera and calcite-replaced radiolarians. The presence of planktic foraminifera, including *Globotruncana* sp., indicate a Late Cretaceous age (Shah & Sharma 1977; this study), as in the Sapi–La area further west (Fig. 12). Calciturbidites, with shallow-water-derived constituents (e.g. shell and algal fragments) are also present locally, as are rare radiolarian chert intercalations, up to 3 m thick (e.g. near Shergol bridge; Fig. 13a). Small slices of red radiolarian chert are also present near Shergol village, and become more abundant further west, in the Sapi–La area (Fig. 12).

Namika–La. Further east, near Namika–La (Fig. 2) local deformed, mainly inverted successions of basic lavas are associated with radiolarian cherts, calciturbidites, pelagic carbonates and epiclastic (volcanogenic) sediments (Robertson & Degnan 1993). Chemical analysis of basalts reveals enriched, within-plate type compositions, similar to the type area of the Karamba complex in the Sapi–La area (Table 1; Fig. 14).

Bodh Khabu area. Volcanic-sedimentary lithologies, correlated with the Karamba complex, are well exposed further east, in the Bodh Khabu area (Fig. 7), where they form a laterally continuous unit (800 m–1.5 km wide) between the intact Upper Cretaceous Dras arc complex to the north and the Lamayuru complex to the south. Reconnaissance mapping indicates that this volcanic-sedimentary unit consists of imbricate thrust sheets of basic volcanic rocks (mainly aphyric or feldspar-phyric), lava breccias and volcaniclastic sedimentary rocks, interbedded with pelagic sedimentary rocks (radiolarian chert and pelagic limestone). The lavas are locally pillowed and, where visible, are inverted. The outcrop is split by two narrow (tens of metres) strips of block-in-matrix type mélange.

Interpretation: distal Indian passive margin. The volcanic-sedimentary unit exposed at several localities for >60 km along strike (Mulbeck, Namika–La, Bodh Khabu) is correlated with the Karamba complex of the type locality (Sapi–La area) and is interpreted as the disrupted stratigraphically higher and relatively distal part of the North Indian passive margin. This contrasts with previous interpretations of the extrusives as one, or several, oceanic seamounts that were accreted into a Late Cretaceous ophiolitic mélange (Searle 1983; Searle *et al.* 1987; Sinha & Mishra 1992*a*, *b*, 1994, 1995). Thus, all of the volcanics and related sediments of the Karamba complex relate to the deep-water distal North Indian passive margin and are now preserved as thrust sheets and broken formation and cannot be interpreted simply as accreted 'ophiolitic mélange' as in some earlier studies.

Serpentinitic unit

Sheared serpentinized ophiolitic rocks mainly occur structurally beneath the Dras arc complex in both the northern and southern mélange zones.

In the Sapi–La area (southern mélange zone, western segment) serpentinite forms a laterally continuous (locally anastomosing) thrust sheet extending *c.* 20 km from near Sapi village in the west to NW of Shergol gompa in the east (Fig. 4). The serpentinite includes numerous diabase dykes mainly orientated subparallel to bounding tectonic contacts of the serpentinite sheet (Fig. 5; sections 2–5). The diabase varies from individual intact dykes to elongate detached blocks including numerous dykes, again within sheared serpentinite. Anastomosing strands of sheared serpentinite are locally intercalated with blueschists and coarse clastic sediments (Indus Group) and are also present as sheared strands within the adjacent Karamba complex.

East of Shergol (Fig. 6) anastomosing strands of sheared serpentinite (mainly chrysotile), crop out with subvertical, to moderately steeply dipping attitudes (strands up to 3 km long and 400 m wide). The protoliths are harzburgite, wehrlite, dunite and pyroxenite. Serpentinized wehrlite is cut by numerous sheared, rodingitized

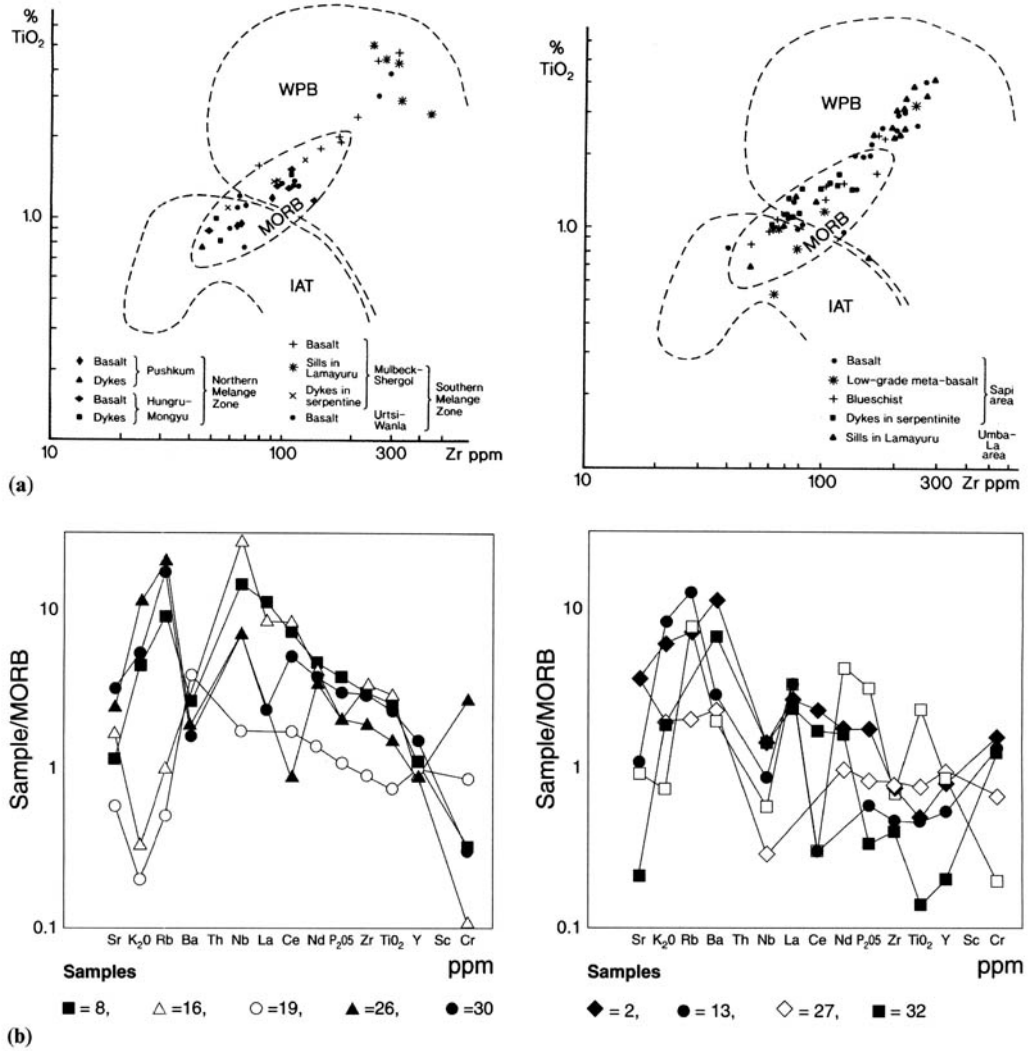

Fig. 14. Geochemical plots of basic igneous rocks from the Indus Suture Zone. (**a**) Ti/Zr plots (left) from most localities, (right) from Sapi–La and Umba–La; see Table 1 for representative complete analyses. (**b**) MORB-normalized 'spider' diagrams: (top left) within-plate type basic igneous rocks—variably altered; (top right) subduction-influenced basic igneous rocks; (bottom) MOR-like basic igneous rocks. Normalizing values as follows: TiO_2 1.5%, Nb 3.5 ppm, Zr 90 ppm, Y 30 ppm, Sr 120 ppm, Rb 2 ppm, Ni 138 ppm, Cr 250 ppm, Nd 3.5 ppm, La 3 ppm. Chemical analysis was carried out using the methodology of Fitton & Dunlop (1985). Lithologies and locations of samples are shown in Table 2.

diabase and gabbroic dykes (locally pegmatitic) (Fig. 6a; section A–A′). The serpentinitic unit in this area exhibits polyphase deformation, including early shearing, later-stage kinking and development of E–W trending slickensides. Further east within the southern mélange zone, isolated dykes are again found within serpentinite (e.g. Bodh Khabu area). Also, near Lamayuru, sheared serpentinite separates deformed basal clastics of the Indus Group to the north (within the mélange zone) from the Lamayuru complex to the south (Fig. 13f), whilst counterparts of the Karamba complex are absent.

In the Pushkum area (northern mélange zone, western segment; Fig. 9a) a serpentinite unit, 200–300 m thick, is dominated by highly sheared serpentinized ultramafic rocks, mainly wehrlite, harzburgite and minor dunite. These ultramafic rocks are cut by numerous basic dykes, again orientated subparallel to the margins of the serpentinite thrust sheet. Individual dykes, 1–4 m wide, form swarms up to 50 m wide, in which up to 80% of the outcrop locally comprise dykes. However, outcrops of 100% dykes without host rocks are not observed. Individual dykes are clearly chilled against the host serpentinite, and serpentinite is locally engulfed within diabase. Chilled margins exhibit basaltic to doleritic textures, whilst the cores of the thicker dykes are commonly gabbroic, to pegmatitic. Many dykes are extensively rodingitized.

In the Hungru–Mongyu area further east (northern mélange zone, eastern segment; Fig. 10), serpentinite forms discontinuous, anastomosing sheets, pinching and swelling over *c.* 10 km laterally, from zero to several hundred metres in outcrop width (Fig. 10a–e). The protoliths of the sheared serpentinite are mainly wehrlite, harzburgite and minor dunite. The serpentinite is again cut by numerous dolerite and/or gabbroic dykes, individually up to 2.5 m thick. The dykes are locally intensely sheared and disrupted to form lenticular blocks that are extensively rodingitized. In addition, the serpentinite locally contains inclusions of gabbroic rock, as observed opposite Hungru (near 'Lamayuru loops').

Dykes showing minimal alternation were collected for geochemical analysis. Diabase dykes from the Pushkum and Sapi–La areas are chemically depleted relative to MORB, especially in Nb (Table 2; Fig. 14). These samples plot in the island arc tholeiite field (IAT) on the Cr/Y discrimination diagram and several other standard tectonic discrimination plots (Pearce *et al.* 1984; not shown here). Several dykes from the Hungru–Mongyu area (west bank of Yapola River; Fig. 10) and from east of Shergol are compositionally closer to MORB (i.e. without relative Nb depletion).

Interpretation. The serpentinite unit could be interpreted in two different ways. The first is as the roots of a dismembered ophiolite, of which only depleted mantle (harzburgite) and layered ultramafics (wehrlite, dunite) are preserved. The dismembered ultramafic rock could, thus, be interpreted as accreted oceanic lithosphere, i.e. as fragments of oceanic lithosphere emplaced above a subduction zone. Diabase dykes are, indeed, known to be emplaced into ultramafic ophiolitic rocks, especially within inferred fracture zone settings (e.g. Arakapas transform, Cyprus; Murton & Gass 1986; Kings Kawaeh ophiolitic mélange, Western Sierra Nevada, California; Saleeby 1979, 1984). In this model, the serpentinite could be considered as exotic with respect to the associated oceanic Dras arc complex (Naktul unit and Nindam Fm.). Alternatively, the serpentinite intruded by sheared diabase dykes could represent part of the deformed oceanic basement of the adjacent Dras arc complex. Reuber (1989) showed that in the Suru valley west of the study area (Fig. 2) the Dras arc complex locally rests on an ophiolitic basement, including wehrlite, harzburgite, pyroxenite and dunite and that this ophiolite is cut by swarms of diabase dykes. A crustal sequence, including gabbro, diabase, pillow lavas and radiolarian cherts of inferred Late Jurassic age (based on dating of radiolaria) is also locally reported in this area (Honegger 1983). The ophiolitic basement there is unconformably overlain by a several kilometre thick succession of arc volcanics and volcaniclastic sediments (Suru and Naktul units; Dietrich *et al.* 1983; Riebel 1984; Reuber 1989), which include local Late Cretaceous shallow-water limestones (Mangain & Rao 1965). In this alternative, the swarms of diabase dykes could represent feeders for the overlying Dras arc extrusives. The Nb depletion observed in some diabase dykes from Pushkum and Sapi–La is suggestive of subduction-influenced magmatism. During later regional southward tectonic emplacement, the Dras arc and its inferred ophiolitic substratum were detached from underlying upper mantle rocks that were subducted. The surviving ophiolitic basement was also detached from its overlying volcanic arc succession and emplaced as highly sheared thrust sheets and broken formation, transitional to serpentinite mélange in some areas. Smaller anastomosing strands of sheared serpentinite were injected into structurally adjacent units during a multi-phase deformation history. The

Table 2. *Selected geochemical analyses*

	Diabase dykes			Basaltic extrusives								Sediments		Lamayuru complex	
	1 (47)	2 (134)	3 (87)	4 (23)	5 (25)	6 (163)	7 (68A)	8 (201)	9 (214)	10 (218)	11 (219)	12 (220)	13 (41)	14 (215)	15 (108)	16 (60)
Major elements																
SiO_2	51.38	54.13	50.60	49.85	51.48	46.66	52.50	46.78	52.49	45.09	46.72	51.60	49.80	43.47	49.79	48.40
Al_2O_3	16.59	12.58	14.81	15.93	16.32	17.31	15.84	13.10	16.42	16.42	17.00	14.91	15.41	17.96	14.14	16.45
Fe_2O_3	7.83	6.05	9.48	8.43	9.32	8.49	9.75	14.41	11.64	7.83	10.46	9.14	8.40	10.76	11.47	11.80
MgO	7.73	10.93	6.87	8.02	6.25	7.45	4.35	6.45	3.44	7.18	6.79	8.20	10.06	10.92	4.59	4.62
CaO	9.55	8.44	10.25	10.07	9.37	12.51	8.65	6.52	3.63	7.21	3.17	3.89	8.85	3.38	6.80	4.40
Na_2O	3.78	3.23	3.51	3.35	2.84	2.50	5.17	4.44	7.03	5.32	6.16	5.28	2.64	4.46	4.40	5.84
K_2O	0.24	0.90	0.34	0.21	0.24	0.04	0.15	0.66	0.62	0.17	0.07	0.10	1.22	0.70	0.02	0.05
TiO_2	0.70	0.72	1.05	0.84	1.08	0.81	1.54	3.82	1.53	0.82	1.17	1.04	0.69	1.11	2.38	4.36
MnO	0.16	0.13	0.16	0.13	0.13	0.14	0.18	0.20	0.16	0.15	0.18	0.14	0.15	0.25	0.17	0.14
P_2O_5	0.80	0.21	0.10	0.11	0.15	0.09	0.18	0.45	0.21	0.16	0.15	0.10	0.07	0.14	0.70	0.25
LOI	2.31	1.95	2.63	3.86	3.32	3.70	1.50	2.81	3.16	9.42	4.85	5.41	3.00	7.37	6.26	3.52
TOTAL	98.04	97.32	97.28	96.94	97.19	96.00	98.32	96.88	96.59	90.34	94.77	94.33	97.30	92.51	93.44	96.00
Trace elements																
Ba	21	224	790	5	17	—	24	52	16	32	13	8	57	47	76	53
V	243	177	299	216	244	253	249	416	213	175	195	196	238	181	174	317
La	6	8	—	—	4	2	1	33	—	4	—	1	10	4	20	26
Ce	8	23	7	4	17	12	15	71	13	12	10	1	3	—	51	83
Nd	—	14	1	—	6	3	5	37	3	4	—	—	—	—	23	33
Cr	55	392	170	258	94	324	251	80	233	405	527	455	325	510	12	27
Ni	53	217	51	128	47	131	103	70	48	142	167	170	109	161	7	25
Cu	11	4	68	43	39	57	55	107	35	6	83	63	9	176	5	40
Zn	53	46	67	61	69	35	81	122	109	231	124	68	66	101	87	89
Pb	6	1	1	2	2	1	1	4	4	2	2	2	3	1	3	5
Rb	7	14	7	2	5	2	2	18	1	8	2	1	25	3	1	2
Sr	718	436	718	48	383	34	311	137	145	92	78	66	129	110	124	201
Y	24	24	24	21	29	24	36	33	42	22	18	18	16	13	36	28
Zr	82	68	82	63	101	50	129	266	88	60	65	62	42	78	202	305
Nb	3	5	3	4	4	5	4	50	4	5	2	2	3	5	41	97

LOI, Loss on ignition.

Localities (1991 samples): 1, diabase dyke, Pushkum; 2, diabase dyke, Yapola R., west bank; 3, diabase dyke, 1 km east of Shergol; 4–5, pillow lava, Pushkum; 6–7, basalt, west bank Yapola R.; 8, pillow lava, 1 km north of Wanla; 9–12, pillow lava, Urtsi mélange, type area; 13, volcaniclastic sediment, Pushkum area; 14, volcaniclastic sediment on basic lava, Urtsi area; 15, basalt in Lamayuru complex, west of Namika–La; 16, dolerite sill cutting Lamayuru complex, 0.5 km NW of Mulbeck.

Table 2. *Continued*

	Karamba complex													Lamayuru		Naktul (Dras)
	Basaltic extrusives					Greenschists		Blueschists			Diabase dykes			Sills		Extrusive
	17 (159)	18 (285)	19 (286)	20 (230)	21 (240)	22 (137)	23 (154)	24 (157D)	25 (162C)	26 (196)	27 (133)	28 (247)	29 (250)	30 (38)	31 (56A)	32 (268)
Major elements																
SiO_2	41.12	57.01	46.37	48.15	46.78	48.23	46.65	49.00	45.83	44.17	49.89	50.48	50.46	48.23	48.10	87.32
Al_2O_3	12.34	15.04	14.67	14.30	16.79	15.26	14.26	7.46	12.81	13.46	14.83	13.24	15.16	12.52	13.28	3.17
Fe_2O_3	13.44	8.97	11.18	10.39	13.46	10.14	14.72	12.29	11.45	11.94	10.31	11.46	10.75	15.67	14.09	3.00
MgO	12.78	7.87	8.25	7.07	5.73	5.94	6.74	10.48	9.97	10.73	6.87	7.16	6.77	5.27	5.92	3.46
CaO	10.14	7.61	11.24	11.14	3.68	10.78	4.24	9.70	9.53	8.90	10.95	10.49	8.90	7.96	9.24	0.67
Na_2O	1.49	3.42	2.84	3.30	5.32	3.12	3.33	2.04	2.23	1.34	3.06	3.33	3.47	3.23	3.32	0.17
K_2O	0.73	2.23	0.03	0.89	0.09	0.84	0.11	0.79	0.61	1.70	0.29	0.05	0.90	0.79	0.52	0.28
TiO_2	2.50	1.35	1.12	1.63	2.54	1.17	3.47	1.42	2.40	2.29	1.14	1.52	1.57	3.46	2.93	0.21
MnO	0.21	0.17	0.20	0.16	0.31	0.17	0.27	0.22	0.17	0.16	0.18	0.21	0.18	0.23	0.20	0.03
P_2O_5	0.26	0.09	0.13	0.23	0.38	0.90	0.38	0.16	0.20	0.25	0.10	0.14	0.18	0.36	0.28	0.04
LOI	4.86	2.96	4.34	3.06	4.33	4.02	5.72	6.49	4.60	5.01	2.44	2.14	1.70	1.97	1.85	2.07
TOTAL	99.98	100.51	100.38	100.31	99.41	99.97	99.98	100.06	99.81	99.97	100.06	100.24	100.03	99.70	99.74	100.17
Trace elements																
Ba	37	75	77	446	86	95	39	90	64	38	46	119	33	32	118	132
V	208	207	253	282	8	264	453	260	227	247	319	218	294	440	358	39
La	0	—	0	15	7	0	10	2	0	0	0	0	0	7	11	7
Ce	55	9	17	33	42	7	3	23	45	9	—	17	8	51	36	17
Nd	16	8	11	19	28	10	34	7	29	28	8	22	14	30	26	13
Cr	920	403	217	203	54	494	499	1737	572	690	170	149	302	78	91	316
Ni	558	94	85	90	33	110	139	929	298	365	43	60	85	60	73	920
Cu	89	76	55	122	50	69	58	178	73.7	95	41	52	69	246	198	9
Zn	119	67	94	83	134	141	124	230	96.2	107	85	100	67	142	124	27
Pb	3	0	0	2	0	5	2	0.5	2	2	2	1	1	2	2	1
Rb	19	56	1	9	2	17	15	20	14	41	4	1	2	34	19	0
Sr	39	52	69	320	258	227	109	139	389	294	427	145	833	382	591	25
Y	27	26	30	24	35	27	26	16	30	27	29	37	26	45	37	6
Zr	174	69	81	121	207	79	62	101	179	172	73	107	80	261	197	36
Nb	24	3	6	34	23	3	2	14	24	25	1	2	2	24	19	5

Additional localities (1993 samples): 17–18, basalt, Sub-unit 1, Sapi–La area; 19–20, basalt, Bodh Khabu section; 22–23, greenschist, Sapi–La area; 24–26, blueschist, Sapi–La area; 27–29, diabase dykes in serpentinite, Sapi–La area; 30–31, diabase sills in Lamayuru complex, Umba–La; 32, clast of andesitic extrusive from the Naktul unit (Dras arc complex), adjacent to the southern mélange zone, Sapi–La area.

present structural position of the serpentinite thrust sheets above the Dras arc complex relates to Late Tertiary backthrusting.

In summary, it is probable that the serpentinite with swarms of diabase dykes represents the tectonically disrupted and remobilized original oceanic substratum of the Cretaceous oceanic Dras arc complex. It would, thus, represent part of a dismembered ophiolite cut by arc-related dykes, now preserved as thrust sheets, broken formation and, locally, as anastomosing strands of sheared serpentinite, injected into adjacent units: regarding this unit simply as 'ophiolitic mélange' would be a considerable over-simplification.

Volcanic–volcaniclastic unit

Within both the southern and northern mélange zones, pillow lavas, lava breccia and volcaniclastic sediments were previously considered to be blocks of oceanic crustal rocks within an 'accretionary ophiolitic mélange' (Searle *et al.* 1987; Sinha & Upadhyay 1990; Thakur 1990), although again this proves to be an over-simplification. The best examples of this unit are in the northern mélange zone in the Puskum area and in the southern mélange zone, near Urtsi (Fig. 2), which are now considered in turn.

Pushkum area. In the Pushkum area (Fig. 9a) a single thrust sheet of basaltic lavas (several kilometres long in outcrop; Fig. 15a) is depositionally overlain by volcaniclastic sediments. The succession begins with vesicular pillow lava, with minor interbedded sediments, up to 250 m thick. The basal zone, 20 m thick, comprises sheared lava with a shaly matrix. Stratigraphically higher, more intact pillow lavas are interbedded with thin lenses (up to tens of centimetres thick) of calcarenite, volcaniclastic sandstone and siltstone, pink pelagic carbonate, radiolarian mudstone and radiolarian chert.

In thin section, calcarenite intercalated within pillow lavas includes black devitrified glass grains, ferruginous oxide, bioclastic carbonate (including echinoderm plates) and strained shards of volcanic quartz (with resorbed margins). Micritic limestone is ferruginous, with poorly preserved microfossils set in a fine-grained volcaniclastic matrix, with angular acidic extrusive grains, volcanic quartz crystals and devitrified, black volcanic glass shards. X-ray diffraction of these carbonates revealed calcite, fluorite, ankerite and hausemanite (Mn_3O_4).

Chemical analysis of the basic extrusives shows that two samples of the pillow basalts from the coherent succession are relatively depleted (e.g. in Ti, Nb) island arc-type tholeiites, or near MORB in composition (Table 1; Fig. 14). A sample of intercalated volcaniclastic sandstone is chemically similar.

The lavas are depositionally overlain by thin-bedded, fine-to-medium-grained carbonate grainstones, then by red/purple radiolarian cherts (Fig. 9a). The grainstones include altered volcanic glass, quartz, epidote, chlorite and millimetre-thick layers of fine-grained ferruginous sediment. The cherts are recrystallized to microcrystalline quartz and/or calcite, with a fine-grained volcaniclastic matrix. Whole-rock X-ray diffraction reveals quartz, haematite, albite, chlorite and muscovite. Cherts higher in the succession are argillaceous and more thickly bedded (beds up to 15 cm thick). Above, come medium-bedded volcaniclastic siltstones, then medium-bedded, hydrothermally altered volcaniclastic siltstones and sandstones, up to 10 m thick. In thin section, the siltstones include angular quartz crystals (i.e. broken phenocrysts), polycrystalline quartz, recrystallized volcanic quartz, altered feldspar crystals (i.e. phenocrysts) and small basalt lithoclasts (with plagioclase microphenocrysts), set in a matrix of fine-grained quartz, feldspar, clay and epidote. The sandstones contain altered plagioclase, rhyolite and large volcanic quartz crystals in a matrix of fine-grained acidic tuff, chlorite and radiolarians (preserved as microcrystalline quartz) and bioclastic limestone clasts, in a matrix of microcrystalline quartz, clay and epidote.

Interpretation. The volcanic and volcaniclastic lithologies in the Puskhum area are interpreted as remnants of basaltic crust erupted in deep water above a subduction zone and can thus be correlated with the adjacent Dras arc complex (Naktul unit). Calcarenites within the pillow lavas were derived from a shallow-water carbonate setting. Disseminated iron and manganese oxides, both within the lavas and at the base of the overlying sediments, are probably of hydrothermal origin. The micritic carbonate, within and overlying, the uppermost lavas was deposited above the carbonate compensation depth (CCD). The overlying radiolarian cherts possibly record high siliceous productivity rather than deposition below the CCD. The overlying volcaniclastic sandstones are interpreted as deep-water turbidites, derived from basic, intermediate and acidic extrusives, reworked with air-fall silicic tuff. Similar volcaniclastic turbidites are present within the structurally overlying Dras arc complex (Naktul unit; Robertson & Degnan 1994). In addition, Cretaceous shallow-water carbonates are present as redeposited units

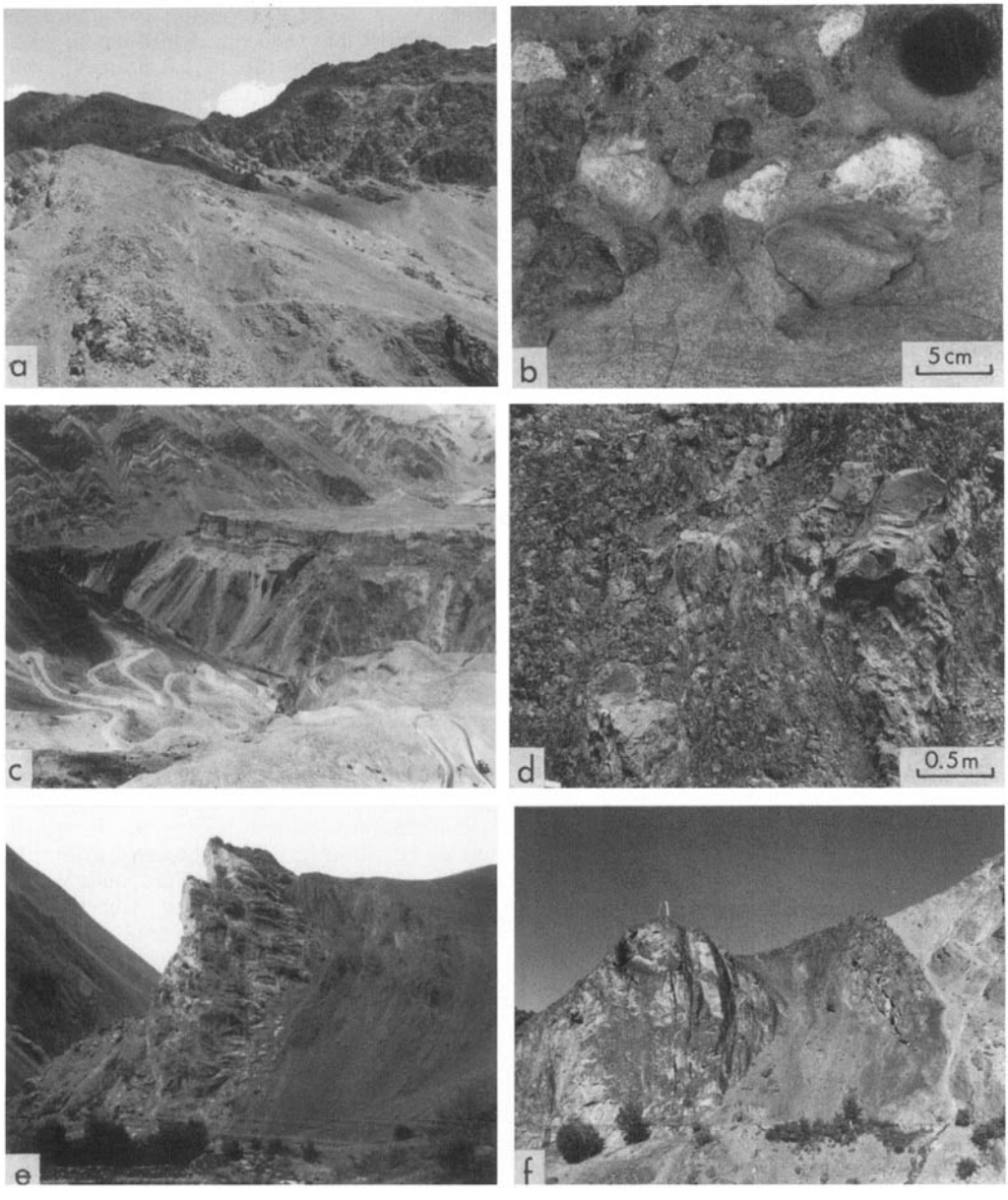

Fig. 15. Field photographs of the northern mélange zone. (**a**) Pushkum area, 2 km north of Pushkum. Basaltic pillow lavas are depositionally overlain by chert and volcaniclastic turbidites (pale), then overthrust by the Naktul unit of the Dras arc complex (dark). (**b**) Conglomerates of the Kargil Formation, Indus Group, near Pushkum. (**c**) View down the 'Lamayuru loops' (opposite Hungru) to the Hungru–Mongyu area (northern complex), beneath Quaternary terrace. Indus Group sediments to left in distance. (**d**) Sheared sandstone blocks in a sheared shaly matrix, Mongyu. (**e**) High-angle reverse fault contact between northern mélange zone (dark, to right) and Albian/Aptian Khalsi Limestone (craggy, centre). (**f**) Upper Cretaceous volcaniclastics of the Nindam Formation (pale, right), thrust over the northern mélange zone, Mongyu section (see Fig. 10).

within the Naktul and Suru units of the Dras arc complex in the area (Honegger 1983; Reuber 1989; Robertson & Degnan 1994). The volcanic–volcaniclastic unit at Pushkum is, thus, interpreted as part of the Dras arc complex (Naktul unit) that was detached and overridden during its emplacement.

Urtsi area. In the Urtsi area (Fig. 8) volcanics and related volcaniclastic sediments ('Urtsi mélange') are seen at successive structural levels, as follows. First, near the structural base several large (> 100 m long) disrupted thrust sheets, separated by shale, comprise bedded basaltic pillow breccia and subordinate pillow lavas (Fig. 8b). Individual pillowed flows are discontinuous and pass laterally into lava breccia. Chemical analysis of the extrusive clasts reveals a depleted island arc tholeiite-type composition (Table 1; Fig. 14). Second, structurally above is a lenticular slice of volcaniclastic sediments, locally including clasts of shallow-water limestone (Fig. 17e), in places unconformably overlain by coarse clastic sediment, correlated with the Indus Group (see below). Third, above this comes a more laterally continuous thrust slice composed of alternations of fine- to locally, coarse-grained volcaniclastic sandstones, interbedded with thin- to medium-bedded calciturbidites, forming *c.* 40% of the succession (Fig. 8c). In thin section, the thin-bedded limestones (calcilutite) are packed with radiolarians, *Globotruncana* sp. and benthic foraminifera (e.g. *Miliolina* sp.), in a matrix containing quartz and plagioclase. The medium-bedded calciturbidites are composed of micritic grains and scattered, volcanic quartz crystals (with resorbed margins), in a matrix of pelagic micrite, calcite-replaced radiolarians, chloritized volcanic grains, shell fragments, polycrystalline quartz, small muscovite laths and algal limestone grains (Fig. 18a). Thicker-bedded calciturbidites are dominated by poorly preserved shallow-water carbonate grains, including echinoderm plates and spines, rudist and algal fragments, rare lithoclasts of acid and basic volcanics, altered plagioclase crystals, scattered quartz grains, altered glass and chlorite. Siltstone lithoclasts contain tiny muscovite laths, volcanic glass, altered volcanic grains, silicic tuff (with recrystallized radiolarians), micrite (with calcite-replaced radiolarians), marble, plagioclase, dolostone, calcite-replaced radiolarite, siltstone and mudstone (with recrystallized planktic foraminifera) and shell fragments, in a micritic matrix (including chlorite and Fe-oxide). Finally, structurally higher, a succession within a large disrupted thrust sheet begins with shales and thin-bedded, fine-grained limestones, with turbidites exhibiting Bouma D–E division structures (Fig. 8c). Amalgamated units (up to 1.6 m thick) near the base are mainly calcilutites (5–10 cm thick), interbedded with medium- to thick-bedded grainstones (up to 0.8 m thick), with channelling and small (centimetre-sized) rip-up clasts. The succession continues with mainly fine-grained volcaniclastic sedimentary rocks (up to 250 m thick), interbedded with grainstone turbidites (< 1 m thick). In thin section, the basal lithologies are acidic tuffs, with calcite, basalt, quartz shards, rare clinopyroxene, plagioclase, sphene, radiolarians and rare carbonate allochems, set in a fine-grained chloritic matrix. These disrupted thrust sheets are, in turn, structurally overlain by intact volcanogenic successions of the Cretaceous Nindam Formation (north of area of Fig. 8; see Fig. 10, map).

Interpretation. The volcanic–volcaniclastic lithologies of the Urtsi area (shown as andesitic–IAT extrusives in Fig. 8) can generally be correlated with the Dras arc complex. However, these lithologies differ from those of the structurally overlying Nindam Formation, which is entirely sedimentary, relatively fine grained and lacks extensive calciturbidites. The source of the calciturbidites with shallow-water derived grains is unclear, but was possibly from proximal shallow-water units of the Dras arc complex that are not now preserved in the overlying Nindam Formation. The structurally overlying Nindam Formation includes minor quantities of redeposited shallow-water carbonates; these sediments are, however, more abundant within the more proximal Naktul and Suru units of the Dras arc complex further west (Robertson & Degnan 1994). In the west, the core of the Dras arc complex was apparently destroyed during subduction or thrust emplacement. Also, the base of the Nindam Formation is not preserved intact, and this may have included lithologies similar to those now within the mélange zone. In summary, fragments of proximal arc or basal fore-arc lithologies may have survived as blocks within the southern mélange zone. Most of these lithologies form thrust sheets and broken formation and are only locally sufficiently disrupted to be termed mélange (e.g. at Urtsi).

Metamorphic units

The best known metamorphic unit is located in the Sapi–La area (southern mélange zone, western segment; Fig. 4). Honegger *et al.* (1989) identified lawsonite blueschist facies metamorphism, with estimated maximum formation temperatures of 350–420 °C and pressures of

9–11 kbar. The blueschist protoliths are E-type, or T-type MORB; similar, for example, to modern Azores basalts. K/Ar dating of three samples yielded an age of *c.* 100 Ma (Honegger *et al.* 1989). During this study it was observed that the blueschists map out as alternating bands of metabasic igneous rocks (e.g. garnet mica schist) and meta-siliceous sediment (meta-chert), on a scale of tens to hundreds of metres. Metasediments exceed meta-igneous rocks by about threefold in the Sapi–La area. Individual meta-igneous bands (typically tens of metres wide) are lens shaped and can be traced up to several hundred metres along strike. Some outcrops exhibit a well developed, folded schistosity, intense layer-parallel shearing, and kink banding at a high angle to an earlier foliation. Planar shear bands up to several tens of centimetres wide commonly separate undeformed areas up to several metres wide; these bands lack penetrative cleavage and retain relict igneous features (e.g. pillows and unstrained vesicles). Secondary calcite veining is common throughout. In places, the blueschists have undergone variable degrees of retrogression to greenschist. In the west, the blueschists are separated from the unmetamorphosed volcanics and sediments of the Karamba complex (to the south) by one, or several, thrust sheets of low-grade (greenschist) meta-lavas, recrystallized limestones and meta-cherts. In this study chemical analysis showed that the blueschists range from enriched within-plate basalt type to near MORB composition (Fig. 14). The low-grade meta-lavas (greenschists) show a similar range in composition, although several samples show relative Nb depletion that could be suggestive of a subduction influence.

Blueschists and greenschists are also locally present in the Pushkum area (northern mélange zone, western segment; Fig. 9). Frank *et al.* (1977) reported the presence of crossite- and lawsonite-bearing schists. In addition, greenschists are represented there by a narrow (< 20 m wide), discontinuous outcrop of psammitic and pelitic schists. Numerous quartz veins, up to 10 cm thick, are strongly sheared. In thin section, the mica-schists exhibit a well developed crenulation cleavage, cut by a strain-slip cleavage. Late muscovite growth occurs along strain bands. Shear bands are deflected around quartzose pods. Some quartz replaces original carbonate sediment. Siltstone, with a micritic matrix, is identifiable in some schists. Small quartz porphyroblasts with sheared margins are cut by later calcite veins. Whole-rock X-ray diffraction of one schist sample revealed the presence of quartz, calcite, albite, chlorite and muscovite.

In addition, a blueschist mineralogy was reported from mud-matrix mélange at Urtsi (Honegger *et al.* 1989) and during this study an additional occurrence of blueschist was noted in the Bodh Khabu area (Fig. 7).

Interpretation. Geochemical discrimination diagrams of meta-basalts within blueschists (although potentially unreliable owing to possible alteration) indicates mainly near-MOR to enriched compositions (Honegger *et al.* 1989; this study). Blueschists, greenschists and volcanics of the Karamba complex are compositionally similar. Honegger *et al.* (1989) interpreted the blueschists in terms of mid-Cretaceous intra-oceanic subduction and accretion of oceanic crust and seamounts, coeval with genesis of an oceanic magmatic arc to the north. The layering of meta-igneous and metasedimentary protoliths within the blueschist could either represent metamorphosed volcanic-sedimentary successions similar to the adjacent Karamba complex (continental margin related), or thrust imbricated, accreted open-ocean crust (possibly seamounts) and associated siliceous pelagic sediments (meta-cherts). Similar chemical compositions of volcanics would be expected in both cases (within-plate type) and, thus, the two alternatives cannot be distinguished at present. In either scenario, these units were subducted, underplated within a Late Cretaceous? subduction zone, and later exhumed. In addition, the greenschists represent basaltic extrusives and deep-sea sediments, of either continental margin or oceanic origin; these were less deeply buried than the blueschists. In summary, the blueschists and greenschists represent thrust slices of metamorphosed volcanic rocks and deep-sea sedimentary rocks of either distal continental margin or oceanic origin and should not be simply classified as meta-ophiolitic mélange.

Mud-matrix mélange

This is best developed at Urtsi (southern mélange zone, eastern outcrop; Fig. 8) where it dominates the southern part of the outcrop, and occurs as lenses between disrupted thrust sheets of volcaniclastic sediments (described earlier) and forms the matrix of a mélange with scattered blocks. The matrix of the mud-matrix mélange is composed of cleaved black shale, with local highly sheared, thin-to-medium-bedded quartzose sandstone, siltstone, calcilutite and grainstone, mostly turbidites, up to 0.3 m thick. In thin section, a calcareous, shaly matrix comprises quartz grains, plagioclase, muscovite and calcite-replaced radiolarians and *Globotruncana* sp. The

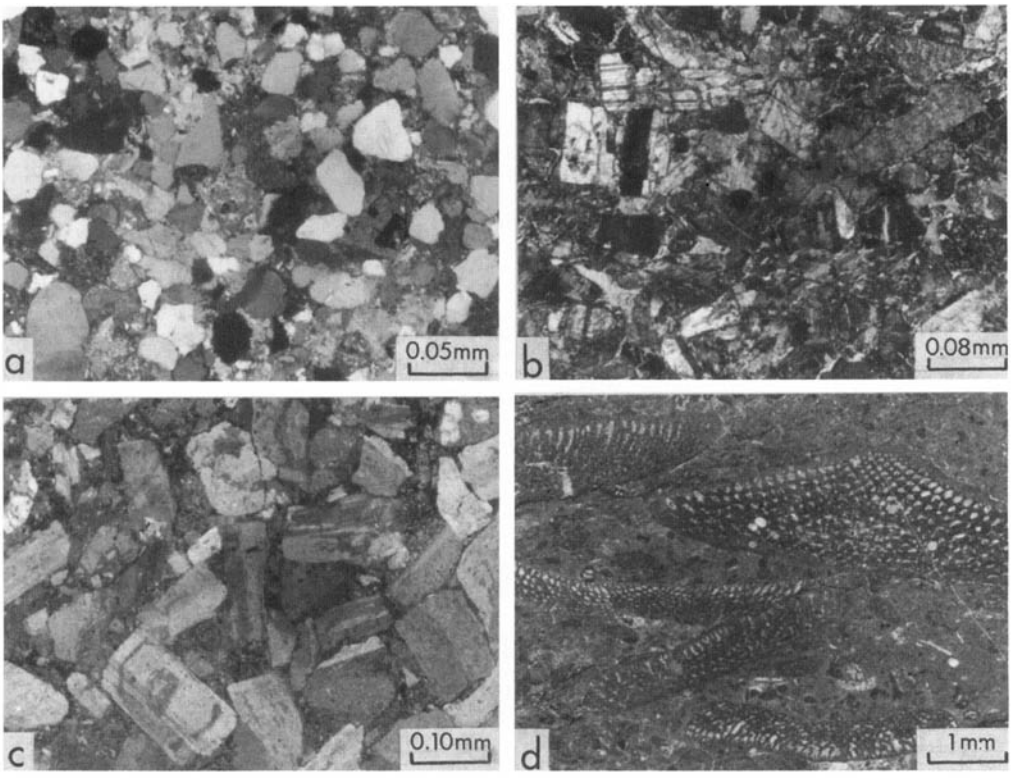

Fig. 16. Photomicrographs of northern mélange zone lithologies. (**a**) Terrigenous sandstones from the Hongru–Mongyu area, northern complex, eastern segment. Compositionally, these are similar to the Indus clastic successions (Gres vert de Tar) overlying the Trans-Himalaya active margin to the north. (**b**) Volcaniclastic sandstone turbidite; note the very immature epiclastic texture. (**c**) Crystal tuff composed mostly of zoned feldspar. (**d**) *Orbitolina* from a micritic limestone clasts in a volcanogenic debris flow. (a–d) Mongyu section; (a–c) photomicrographs; (d) positive print from a thin section; see Fig. 10.

following lithologies are present as blocks within a matrix.

Tholeiitic volcanics and related sediments. A number of dark, purple-weathering blocks (up to 6 m across) contain local successions of tholeiitic volcanics (Fig. 17b), overlain by radiolarian cherts (Fig. 8e). In one block, silicified volcaniclastic sediment penetrates down into cracks in underlying pillow lava. Another large block is entirely sedimentary massive volcaniclastic sandstone, passing stratigraphically upwards, based on way-up evidence (i.e. grading), into green, silicified calciturbidites (in beds up to 10 cm thick), then into ribbon radiolarite (Fig. 8f). Analysis of the basaltic clasts within this volcaniclastic sediment revealed a near-MORB composition (Table 1; Fig. 14). Sutre (1991) reported Late Jurassic radiolarians from these cherts (although a supporting faunal list was not provided). Metre-sized blocks of sheared pillow basalt and radiolarian chert are also scattered through the mud-matrix mélange (Fig. 8b). Honegger *et al.* (1989) reported blueschist minerals from some of these blocks. Three basalt analyses revealed MOR, enriched MORB- and WP-type compositions (Table 1; Fig. 14a). Other small blocks associated with lava blocks include thin-bedded calciturbidites, replaced by chert and greenish carbonate with pyrite, often tectonically brecciated. A large isolated block exposed further west (north of Wanla; Fig. 10) comprises massive, aphyric tholeiite, depositionally overlain by red ribbon radiolarites, 10 m thick. Three analyses of this block revealed an enriched WPB-type composition (Table 1; Fig. 14). In addition, chemical analysis of disrupted thrust sheets within the mélange exhibit a depleted IAT-type composition; these rocks probably represent fragments of the subduction-related Dras arc complex.

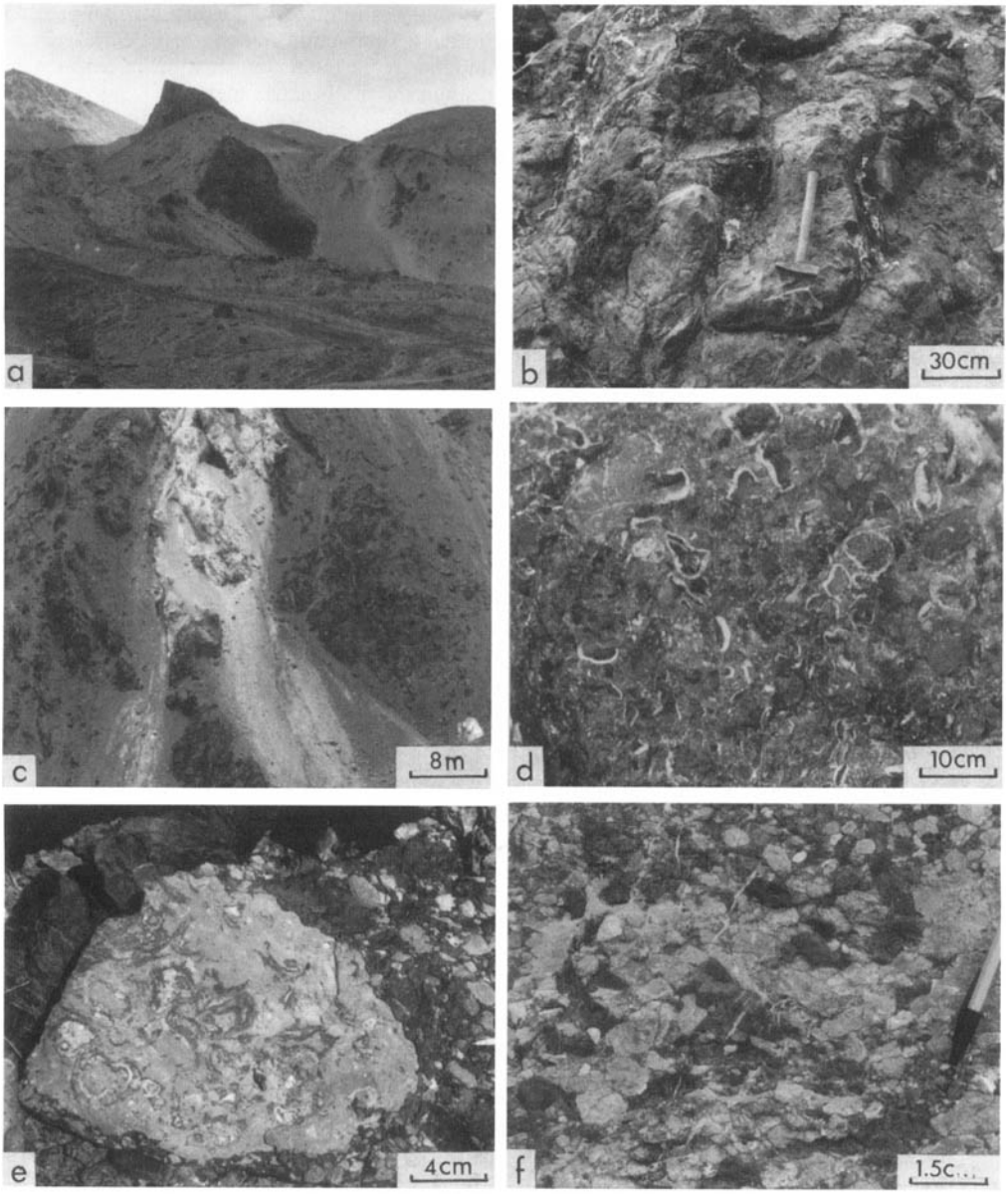

Fig. 17. Field photographs of the southern mélange zone near Urtsi village (eastern segment). (**a**) Large blocks of basalt and related sediments in mud-matrix mélange; the pointed block in the distance is IAT-type basalt; that below (centre) is MOR composition volcaniclastics with radiolarian chert. (**b**) MOR-type pillow lava block, with interstitial ferruginous sediment and hydrothermal carbonate. (**c**) Block of marble with calc-silicate (skarn) at the edges. (**d**) Small clasts of red partly recrystallized sandstone, rimmed with fibrous calcite (white). (**e**) Clast of shelly limestone within volcaniclastic sediment (lower disrupted volcaniclastic sheet). (**f**) Conglomerate of subrounded clasts, mainly volcaniclastics (dark) and limestone (pale), unconformably overlying the disrupted volcaniclastic thrust sheets (Indus Group); see Fig. 8.

Limestones and sandstones. Thin beds of impure limestone with redeposited carbonate grains are interpreted as distal calciturbidites, commonly extensively replaced by green chert. In addition, siliciclastic sandstones, of up to medium-grain size and bedding, exhibit the Bouma C and E

division structures of turbidity currents (Bouma 1962).

Marble and skarn. One large block of marble (up to 20 m long by 5 m wide, *c.* 500 m north of Urtsi village; Fig. 8, map) is composed of metamorphic, brecciated calc-silicate (skarn) at the margins, while the interior preserves traces of sedimentary features, including bedding and nodules of replacement chert (Fig. 17c). Throughout the adjacent mélange there are also numerous, metre-sized, blocks of coarsely crystalline carbonate or calc-silicate, lined with fibrous calcite, or sparry calcite (Fig. 17d).

Coarse clastics. Blocks of coarse clastic sediment, including breccia, sandstone, minor conglomerate are correlated with the Indus Group. These are described separately below.

Interpretation: multiply deformed subduction/accretion complex. The mud-matrix mélange is interpreted as a fragment of a trench-accretionary complex. The presence of both blueschists and low-grade (diagenetic/anchizone) blocks and matrix points to mixing of material from different structural levels within a subduction setting. The lava blocks within the mud-matrix mélange are interpreted as fragments of oceanic crust (MORB type) and possible seamounts (i.e. WPB-blocks). Associated volcaniclastic sandstones (MOR-composition) record submarine erosion and accumulation of the ocean floor prior to accretion. Overlying radiolarian cherts are interpreted as open-ocean pelagic sediments of Late Jurassic age according to Sutre (1991). Interbedded siliceous limestones are seen as distal calciturbidites. These limestones are compositionally similar to thicker and coarser turbidites within the Karamba and Lamayuru complexes and may thus represent distal deep-sea sediments derived from the North Indian passive margin. In addition, the matrix is terrigenous and includes sandstone turbidites, again suggesting ultimate derivation from the North Indian margin, in contrast to the volcaniclastic sediments of the Dras arc complex. The origin of the marble blocks is uncertain, but could be similar to the Albian–Aptian Khalsi Limestone (see below). These carbonates do not appear to be redeposited in contrast to scarse limestones within the structurally overlying Nindam Formation (Dras arc complex). In addition, the presence of detached blocks of coarse clastics correlated with the Early Tertiary sediments of the Indus Group (see below) shows that the mélange was tectonically reworked during, or after, collisional deformation (see below). In summary, a multi-stage history involving accretion at a subduction trench, thrust emplacement and post-collisional deformation is required to explain the mud-matrix mélange.

Volcaniclastic–terrigenous unit

In the Hungru–Mongyu area ('Mongyu mélange'), volcanic/volcaniclastic and terrigenous lithologies are observed, but these are invariably separated by thrusts, showing that two contrasting clastic successions are tectonically intercalated (Fig. 15e, f).

Volcanic/volcaniclastic component. Local facies differences are observed in each of three traverses studied: at Hungru (Yapola River; Fig. 10a) in the west, at Tar (Fig. 10c), and at Mongyu in the east (Fig. 10b). Outcrops in the west along the south bank of the Indus River and in the Yapola River, near Hungru (Fig. 15c), include pillow lava, massive lava and sheared, flow-banded vesicular feldspar-phyric andesite (with phenocrysts up to 1 cm long). In well exposed outcrops further east, in the Tar (Fig. 10c–e) and Mongyu (Fig. 10b) sections, andesitic extrusives dominate (locally epidote-rich), along with talus breccia composed of angular to subrounded, vesicular clasts (up to 2 m across), within a subordinate volcaniclastic matrix. Occasional interbeds of matrix-supported conglomerates contain andesitic clasts and rare clasts of oxidized sulphides (gossan material). Local interbeds of coarse-grained green tuff, up to 1 m thick, contain scattered, well-rounded clasts of limestone, up to 20 cm across. The sediments between the blocks and disrupted thrust slices are mainly thin- to medium-bedded volcaniclastic turbidites, shales and tuffaceous sediments. Local sandstone interbeds contain thin laminae, entirely made up of feldspar crystals, interpreted as crystal tuffs. Both the shales and sandstones are locally pyritic. There are also interbeds of muddy, fossiliferous calcilutite and limestone, with shells and rudist fragments.

In thin section, the volcaniclastic sandstones comprise altered, zoned plagioclase phenocrysts (with fluid inclusions), volcanic quartz shards, augite, biotite and large muscovite laths (with strain slip cleavage) (Fig. 16b, c). Lithoclasts include altered basalt (often chloritized), basalt-derived silt, rhyolite (flow textured), devitrified volcanic glass, mudstone (with muscovite), volcaniclastic sandstone and biomicrite. The matrix is volcanogenic, with well preserved microfossils, including radiolarians and benthic foraminifera (e.g. *Orbitolina* sp.; Fig. 16d). In some samples examined the matrix is acidic tuff, partly replaced

by calcite. Rare grainstone interbeds include echinoderm plates, rudist fragments, *Miliolina* sp., micrite with *Globotruncana* sp. and calcified radiolarians. Rare limestone boulders in volcaniclastic debris flows also contain *Orbitolina* sp., in a micritic matrix, with altered plagioclase, calcite-replaced sponge spicules, radiolarians, *Globotruncana* sp. and bryozoans. Some radiolarians are pyritized.

Three basalt samples were analysed from each of two basalt blocks exposed along the west side of Yapola River (near Hungru; Fig. 10a) and these are relatively close to MOR in composition (Table 1; Fig. 14). These lavas form part of the mélange that structurally underlies the Nindam Formation to the north of its outcrop. They are similar to the blocks of basalt analysed from the mélange to the south of the Nindam Formation oucrop (e.g. Wanla, Urtsi; see above).

Terrigenous component. Cleaved, micaceous black shale, quartzose siltstone and sandstone are well exposed, for example near Mongyu village (Fig. 10b). Individual sandstone beds, up to 2.5 m thick, are lenticular. Steep-sided channels (up to 4 m wide and 2 m deep) are cut into mainly shale sequences. Sandstones exhibit bottom structures (e.g. flutes, grooves) and internal structures (e.g. grading, convolute lamination, ripple drift cross-lamination), indicative of deposition from turbidity currents (Bouma 1962). Sandstone dykes are locally injected upwards into shale. Interbedded black shales are rich in plant material and fine pyrite, locally bioturbated, and/or contain local calcareous concretions. Whole-rock X-ray diffraction revealed quartz, minor chamosite and muscovite. Thicker-bedded turbidites are disrupted into elongate blocks ('phacoids') and show evidence of intense layer-parallel extension (Fig. 15d). The size of the blocks ranges from the thickness of individual beds (< 3 m), to packets of sandstone/shale (tens of metres thick).

In thin section, the turbiditic sandstones contain numerous angular, to subrounded (rarely well rounded) grains of plutonic and vein quartz origin, showing straight, or slightly undulose extinction (Fig. 16a). Typical plutonic quartz is subhedral, and turbid, with numerous inclusions. Other minerals are plagioclase, large muscovite laths and rare clinopyroxene. Lithoclasts are very common and include siltstone, mudstone (with tiny feldspar crystals), carbonate allochems (e.g. shells, echinoderm plates), radiolarian chert, recrystallized chert, basalt (with altered plagioclase), rhyolite, devitrified volcanic glass, granite, polycrystalline quartz, mica-schist and gneiss. The matrix is fine-grained, with opaque ore minerals, chlorite, calcite and common dolomite rhombs.

Interpretation. The disrupted thrust sheets and blocks include lavas, lava breccias and volcaniclastic sandstones, of basaltic to andesitic composition and acidic tuffs. However, terrigenous-derived sediment (quartz, muscovite) is also present as intersliced units. The presence of *Orbitolina* sp. and *Globotruncana* sp. indicates a Late Cretaceous age. The volcanogenic component is correlated with the structurally overlying Upper Cretaceous Dras arc complex (Sutre 1991; Robertson & Degnan 1994). Lithologies are similar to successions of the Suru unit of the Dras arc complex in the Suru valley west of the present study area (Fig. 2), in contrast to the finer-grained more distal facies of the locally overlying Nindam Formation (Robertson & Degnan 1994). The Suru unit is interpreted as part of the core of the Late Cretaceous oceanic Dras arc complex, in contrast to the Naktul unit and the Nindam Formation that are interpreted as proximal, to distal, fore-arc units, respectively (Robertson & Degnan 1994). The lithologies in the Hungru–Mongyu area are, likewise, interpreted as remnants of a proximal oceanic arc unit that is otherwise not preserved in this area. Large foraminifera (i.e. *Orbitolina* sp.) within volcaniclastic turbidites were derived from a shelf-depth carbonate setting. Redeposited limestones with similar large foraminifera are present within the proximal Suru and Naktul units of the Dras arc complex in the west (Reuber 1989; Sutre 1991; Robertson & Degnan 1994).

The terrigenous slices are made up of quartzose sandstone turbidites and micaceous, plant-rich black shales. The presence of marked channelling within the turbidites is suggestive of high slope gradients, while common soft-sediment instability and the rare sedimentary dykes indicate the presence of tectonically unstable conditions. Sub-seafloor conditions were reducing, judging from the abundance of pyrite and organic matter (with local chamosite). The sediments later underwent intense layer-parallel extension, producing fabrics as seen in accretionary mélange and highly extended thrust sheets (Cloos 1982).

The depositional age of the terrigenous sediments is uncertain as these are undated. The facies are dissimilar to the clastic sediments, in both the structurally underlying and overlying units. The structurally underlying Aptian–Albian Khalsi Limestone locally passes depositionally upwards into clastic successions (Gres Vert de Tar of Van Haver 1984) that accumulated along the margin of the Trans-Himalaya

(Ladakh Batholith). The succession includes thick channelized conglomerates with abundant well-rounded granitic and rhyolitic clasts (e.g. near the confluence of the Yapola and Indus rivers and near Khalsi, Fig. 10), and contrasts strongly with the finer-grained terrigenous sediments of the volcaniclastic–terrigenous unit ('Mongyu mélange'). Also, the succession in the structurally overlying Nindam Formation (Dras arc complex) is reported by Sutre (1991) to pass depositionally upwards into latest Cretaceous (Maastrichtian) volcaniclastic shales, without terrigenous sandstones, and then without a structural break into nummulitic limestones (e.g. south of Alchi, Fig. 2), although significant stratigraphic hiatuses may be present. The foraminiferal limestones are dated as Early Eocene (Ypresian; 54–50 Ma; Van Haver 1984; Garzanti & Van Haver 1988). The Nummulitic Limestones are the youngest marine sediments within the Indus Suture Zone and pass depositionally upwards into the non-marine 'Indus molasse'. Two alternative settings can be considered for the terrigenous sediments: First, they accumulated in a deep basin, or trench setting adjacent to an inferred fore-arc of an Andean-type margin to the north (Van Haver 1984), comparable, for example, with the Nankai trench (Taira *et al.* 1992). In this model the opposing volcanogenic (Dras arc-related) and terrigenous (Andean-margin related) units were sutured during Early Tertiary (Palaeocene–Eocene) when they were pervasively deformed and intersliced. Second, the terrigenous sediments instead formed close to the North Indian passive margin, possibly as a foredeep, or trench, that was imbricated and overridden by the Dras arc complex during Early Tertiary (Palaeocene–Eocene) continental collision, and then backthrust to the present position. The strongly micaceous composition of the sandstones, similar to sandstones of the Lamayuru complex, supports the latter hypothesis.

Coarse clastic unit: Indus Group

Coarse clastic sediments (Indus Group) are tectonically intercalated with both the southern and northern mélange zones. In the Sapi–La area (Fig. 4), coarse clastic sediments unconformably overlie blueschist, serpentinite, or the Karamba complex directly at different localities (Fig. 5.2, 5.4). In the west, the clastic unit unconformably overlies serpentinite and is deformed into a large north-facing syncline. Further east in the Sapi–La area (west of Tringdo; Fig. 4), coarse clastic sediments occur as numerous thrust-bounded lenses within blueschists (Fig. 5.5; too small to show on Fig. 4). These sediments are mainly composed of blueschist clasts and are interpreted as remnants of basal conglomerates and breccias. The unconformity surface is highly irregular when traced along strike for >100 m. In the west (Fig. 5.2), the base of the succession is mainly composed of volcanogenic clasts including numerous pebbles of highly fossiliferous (Upper Cretaceous) shallow-water limestones (up to 0.6 m in diameter) and rare diabase. The limestone clasts themselves are mainly composed of breccia and conglomerate, in which individual clasts exhibit sutured contacts resulting from pressure solution and are set in a ferruginous gritty matrix. Fossils include rudists, *Orbitolina* sp., Monopleurids, calcareous algae, bivalves (e.g. pectens) and echinoderms. Where present, the matrix of the limestone-breccia clasts is micritic limestone. In addition, individual (reworked) blocks of oolitic limestone (up to 0.8 m in diameter) occur very close to the unconformity surface. Rare intercalations of red shale are also seen near the base of the succession, overlain by thick-bedded conglomerates, rarely interbedded with shaly partings. In general, these basal conglomerates contain a high percentage of meta-igneous and meta-sedimentary rocks (e.g. blueschist and meta-chert). The succession fines stratigraphically upwards into grey, flaggy-bedded, planar-laminated sandstone containing scattered outsize, rounded clasts. Further east (Fig. 5.4, 5.5), basal breccias are locally composed almost entirely of very angular blueschist clasts.

East of Shergol (Mulbeck area; Fig. 6), elongate, discontinuous, mainly inverted, thrust sheets of coarse Indus clastic sediments are well exposed in the south, adjacent to the Lamayuru complex. Locally intact successions (Fig. 6a, logs 1-2) include grey matrix-supported debris flow deposits, locally passing stratigraphically upwards into lenticular clast-supported conglomerates (Fig. 13e), interbedded with coarse red sandstones and shales. The matrix-supported conglomerates include subrounded blocks and clasts of sheared serpentinite, volcaniclastic sandstone and pelagic carbonate, up to 0.4 m thick. The sandstones comprise well-rounded grains of dark grey micrite, red radiolarian chert, silicified grainstones and extrusives in a coarse sandy matrix. Interbedded grey-red shales are micaceous. In thin section, the sandstones contain angular, to subangular grains of unstrained volcanic quartz and acidic extrusives (including dacite and rhyolite), together with carbonate allochems (e.g. echinoderm plates) and rare muscovite, in a fine-grained volcaniclastic

and calcareous matrix, with much calcite replacement.

Further east, in the Bodh Khabu area (Fig. 7), disrupted thrust sheets of coarse Indus clastics are imbricated within the volcanic-sedimentary Karamba complex (see earlier). A thrust sheet of subvertical coarse clastics, *c.* 900 m thick, is also well exposed near Lamayuru. These sediments are strongly sheared and isoclinally folded with fold hinges being sheared out to produce a phacoidal fabric locally. The stratigraphically lowest part of the succession (in the north) comprises thick-bedded non-marine sandstones, reddish shales and matrix-supported debris flow deposits, with well rounded pebbles including grey micritic limestone, silicified grainstone, red chert clasts and rare extrusive and volcaniclastic rock clasts. Provenance apparently was from relatively competent units, as exposed in the adjacent Nindam Formation.

Further east, in the Urtsi area (Fig. 8, map), coarse Indus clastic sedimentary rocks locally unconformably overlie disrupted thrust slivers of volcaniclastic sediments (see above). Basal, clast-supported, polymict conglomerates there contain subangular to rounded clasts of volcaniclastic sediment, fossiliferous limestone, vesicular andesite and rare red chert (1–15 cm in size; Fig. 17f). In thin section, overlying reddish sandstones contain angular volcanic quartz shards, dacite, basalt, chloritized volcanic glass, altered volcanic grains, silicic tuff (with recrystallized radiolarians), micrite (with calcite-replaced radiolarians), marble, plagioclase, dolomite, calcite-replaced radiolarite, siltstone and mudstone (with recrystallized planktic foraminifera) and shell fragments, set in a micritic matrix, including chlorite and iron oxide. In addition, thick-bedded, relatively undeformed breccias fill fissures in the surfaces of an underlying volcaniclastic thrust sheet (Fig. 8; 300 m east of A–A′). Similar unmetamorphosed red clastics (i.e. medium-bedded sandstone, siltstone and conglomerate) are also present as metre-scale, detached blocks within the adjacent mud-matrix mélange (see above). These blocks include clasts of recrystallized radiolarite (with dolomite rhombs), pink marl, rare basalt, green volcaniclastic siltstone (with volcanic quartz), minor devitrified glass, polycrystalline quartz, shell fragments, algal micrite (coating grains) and blue chlorite, set in a coarse sparry calcite cement. In thin section, some samples are strongly recrystallized (Fig. 18c), whereas less altered lithologies include subrounded, well-sorted grains of acidic tuff and altered basic volcanics (with palagonite) and carbonate, in a fine-grained, ferruginous matrix (Fig. 18d). Quartz crystals show straight, or slightly undulose extinction. Many of these clasts are rimmed by fibrous calcite (Fig. 18c). In addition, sheared, partly recrystallized red sandstone and conglomerate is in local contact with large elongate blocks of marble (Fig. 8; *c.* 500 m north of Urtsi).

Interpretation: incorporated Indus clastics. The coarse clastic unit is correlated with the upper part of the non-marine, fluvial and lacustrine successions of the Early Tertiary Indus Group ('Indus Molasse'; Brookfield & Andrews-Speed 1984; Van Haver 1984; Garzanti & Van Haver 1988; Sutre 1991; Fig. 2). These units crop out as intact successions adjacent to the northern and southern mélange zones, where they are variously known as the Kargil Formation (possibly Late Eocene–Oligocene) in the Puskum area (Van Haver 1984; Van Haver *et al.* 1984; Fig. 15b); as the Shergol Conglomerates of the Mulbeck area (Thakur 1981; Sutre 1991), and as the Skyu–Chilling Formation (possibly also Late Eocene–Oligocene) in the Urtsi area (Van Haver 1984; Sutre 1991). At present, these local units are too poorly dated to integrate into a regional stratigraphy.

The coarse clastic unit accumulated, possibly during and certainly soon after Early Tertiary collisional deformation. Thrusting created a rugged, emergent topography, with the overlying basal breccias recording very local derivation (e.g. Sapi–La and Urtsi). The presence of basal debris flows in the Mulbeck and Lamayuru areas indicates that the non-marine clastics began to accumulate under conditions of high slope gradients, in turn suggesting that the clastics may have begun to accumulate during tectonic emplacement (e.g. as small piggy-back basins). Higher in the succession, the provenance was more varied, suggesting wider sediment dispersal by fluvial processes. At Urtsi, after deformation, volcaniclastic thrust sheets were exposed, fissured and unconformably overlain by non-marine clastics, containing a derived marine biota. Equivalent clastics further west (near Lamayuru), dominated by reddish shales, sandstones and debris flow deposits were mainly eroded from the Upper Cretaceous volcanogenic Nindam Formation. During Oligocene time the clastic sediments are envisaged as forming a semi-continuous cover over the entire suture zone (from the edge of the Zanskar shelf in the south to the Trans-Himalaya in the north, broken by exposed highs (e.g. Dras arc complex units)). There is no evidence of deep erosion into basement units at this stage and the basal coarse clastics largely reflect derivation from units that are still exposed in nearby areas. Following

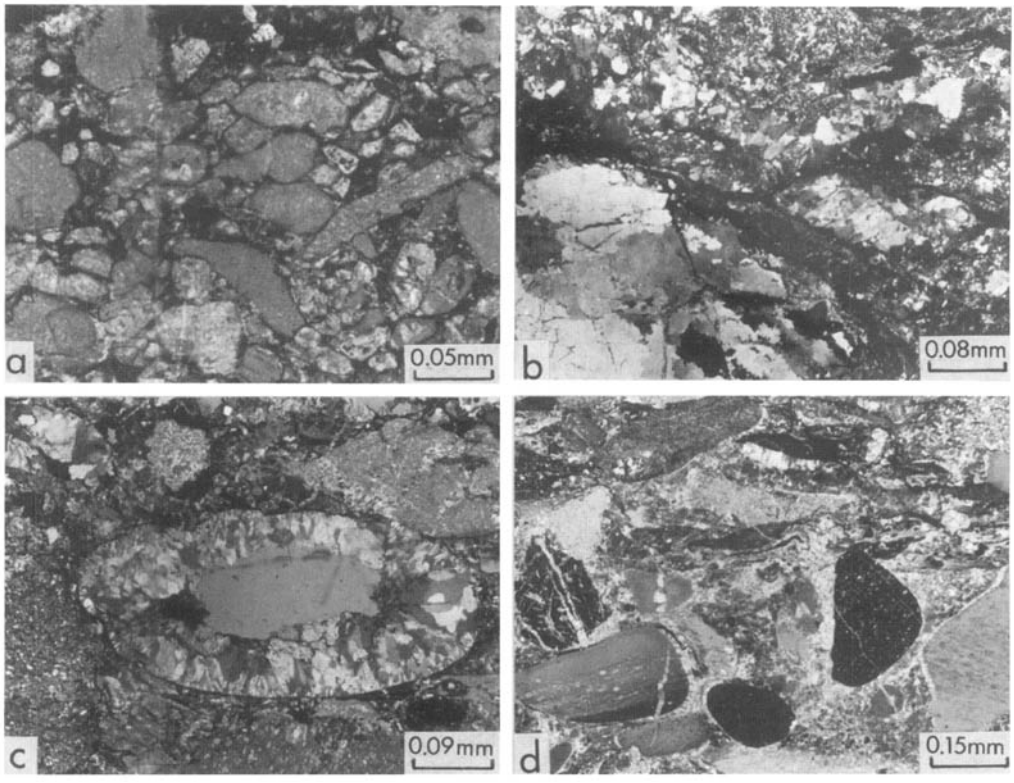

Fig. 18. Photomicrographs of the southern mélange zone near Urtsi village (eastern segment). (**a**) Calciturbidite within the (intermediate-level) volcanogenic, disrupted thrust sheet (Fig. 8a). (**b**) Partly recrystallized, red volcanogenic sandstone. (**c**) Sparry calcite filling void in sheared, partly recrystallized volcaniclastic sandstone. (**d**) Sandstone unconformably overlying Upper Cretaceous sandstones, correlated with the Indus Group. Note the well-rounded grains, including radiolarian chert (left, lower) and sparry calcite cement. (a–d) Blocks in type area at Urtsi; (a–c) photomicrographs and (d) positive print from a section.

deposition, the coarse clastic unit was thrust intercalated with other units during regional Late Tertiary backthrusting. The pre-existing suture zone then acted as a zone of weakness, lubricated by serpentinite, favouring re-imbrication and incorporation of overlying clastics within the southern and northern mélange zones.

Discussion: tectonic evolution

Two main options are:

1. the Northern and Southern mélange zones record the trace of essentially a single subduction zone that links up at depth beneath the intervening Dras arc complex, with the presence of the two lineaments being an artefact of remobilization during collisional and post-collisional tectonics;
2. the northern and southern mélange zones record the traces of two different, northward-dipping subduction zones; the southern one marks a subduction zone south of the oceanic Dras arc, whereas the northern one records a separate subduction zone located between the oceanic Dras arc and the Eurasian margin (Ladakh Batholith/Trans-Himalaya) to the north. There are some similarities between the two mélange zones: blueschists, serpentinite with diabase dykes, and units related to the Dras arc complex are present in both, whereas the Karamba–Lamayuru passive margin units are restricted to the southern mélange zone.

The second option must take account of the interpretation of the main suture between the Dras–Kohistan arc and the Eurasian margin (Karakoram) as the Shyok suture zone (northern suture) in Pakistan (Pudsey 1986); this runs eastwards into India to the north of the Ladakh Batholith/Trans-Himalaya, in the Nubra valley

area (Thakur & Mishra 1984); i.e. well north of the northern mélange zone. The northern mélange zone cannot thus simply record a suture zone between the Eurasian continental margin and an oceanic Dras arc complex to the south. A simple E–W correlation of units on both sides of the Nanga Parbat syntaxis would suggest that the host rocks of the Ladakh Batholith (Trans-Himalaya) might represent an eastward extension of the oceanic Kohistan arc. However, there is considerable evidence that the Trans-Himalaya includes Palaeozoic–Mesozoic terrigenous and magmatic units that can be correlated with the tectonostratigraphy of the Lhasa Block of Tibet (Searle *et al.* 1987; Raz & Honegger 1989; Einsele *et al.* 1994; Robertson & Degnan 1994; Sinha & Upadhyay 1997). Assuming the Dras–Kohistan arc was oceanic in origin, a suture (now represented by the northern mélange zone) necessarily lay between an oceanic Dras arc complex to the south and the Trans-Himalaya (Eurasian) margin to the north, at least in Late Cretaceous time. The oceanic Kohistan arc in Pakistan was amalgamated with the Eurasian margin by latest Cretaceous time (Coward *et al.* 1986; Petterson & Windley 1991; Khan *et al.* 1993). However, the absence of strong uplift, erosion, or coeval deformation of the Cretaceous Nindam Formation in Ladakh (east of Hongru) suggests that forceful collision was delayed there until Early Tertiary time (Robertson & Degnan 1994). During the amalgamation of the Kohistan–Dras arc with the Eurasian margin, the Nindam Formation fore-arc apparently remained further south, shielded from major deformation until collision with India in Early Tertiary time.

It is also possible that the Ladakh Batholith represents an exotic terrane that was displaced westwards along the Eurasian margin, prior to amalgamation of the Kohistan arc/Karakoram margin pre-75 Ma. If so, the northern mélange zone could effectively represent a duplication of the Shyok Suture Zone. It is still debatable whether the Dras/Kohistan arc was sited far south of the Eurasian (Karakoram) margin and was necessarily separated by an important suture zone (Khan *et al.* 1998), or alternatively if the arc was located close to (Pudsey 1986), or even straddling the Eurasian margin (Sutre 1991; Rolland *et al.* 1999). However, there is no petrographic evidence of continentally derived material within arc-type volcanics and volcaniclastics sediments of the Shyok Suture Zone that are correlated with the Kohistan arc (Robertson & Collins 1999). In addition, there is no evidence from Ladakh of continentally derived material within the Dras arc complex (Robertson & Degnan 1994), and recent chemical evidence on the composition of the volcaniclastic sediments of the Nindam Formation (including Nd isotopes) does not indicate the presence of any continental crustal influence (Clift *et al.* in press). Instead, the Dras arc complex is comparable with a number of modern oceanic volcanic arcs, notably the Mariana and Lau–Tonga arcs in the SW Pacific. The dominantly coarse debris flow deposits of the Naktul unit are similar, for example, to the Late Miocene mass-flow deposits of the oceanic Lau–Tonga Forearc Basin (Boe 1994), and similar Pliocene deposits from the Woodlark Basin related to arc rifting (Taylor *et al.* 1999). The Nindam Formation can also be closely compared with a range of modern oceanic fore-arc basins elsewhere (Clift *et al.* 1998 in press).

In summary, the southern mélange zone records the trace of a Late Cretaceous regionally northward-dipping subduction zone, reactivated by Early Tertiary collisional deformation and again by Neogene backthrusting. The northern mélange zone represents a suture zone separating the Trans-Himalaya (part of the Eurasian continental margin) from the Dras oceanic arc. It is probable that these two subduction zones operated independently during the initial Cretaceous subduction history; however, they merged as a single suture zone during the Early Tertiary collisional emplacement, with the present-day outcrop pattern owing much to the effects of Late Tertiary northward backthrusting related to uplift of the High Himalaya to the south.

When the wider regional evidence is taken into account, an overall plate tectonic working hypothesis can be suggested. Northward-dipping intra-oceanic subduction within Neotethys ocean first gave rise to the Dras–Kohistan arc (Albian–Late Cretaceous; Fig. 19a). Recent work also suggests that a separate (third) subduction zone was possibly activated closer to the North Indian passive margin in the Late Cretaceous (Corfield 1999). The Spontang mélanges were accreted above this subduction zone. The Lamayuru exotic of the southern mélange zone is compositionally very similar to the Spontang mélanges, as are the mélanges of the Markha valley, within the Indus Suture Zone, east of the main study area (unpublished data). This is important as it suggests that the southern mélange zone was the main root zone for the Spontang mélange and Spontang ophiolite during latest Cretaceous time (Corfield & Searle this volume), as shown in Fig. 19b. Alternatively, if the Dras arc had already collided with the North Indian continental margin by latest Cretaceous, only one subduction zone would be required south of the

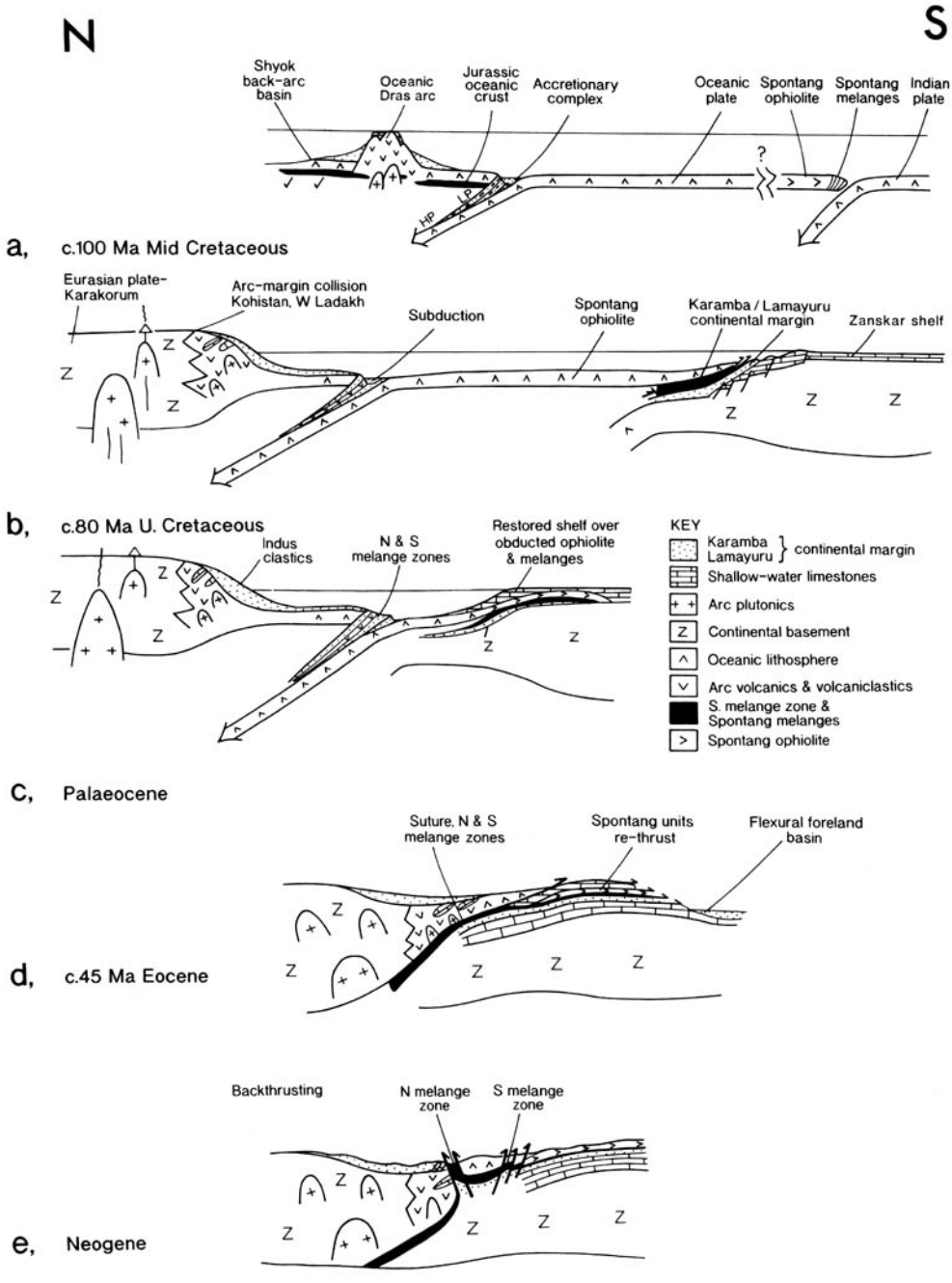

Fig. 19. Plate tectonic sketches to illustrate the formation of the southern and northern complexes in the Indus Suture Zone of Ladakh. The key events were Cretaceous northward subduction/accretion and initial partial tectonic emplacement onto the North Indian margin; Palaeocene final consumption of any remaining oceanic crust between Eurasia and India; Late Palaeocene–Eocene collision of Eurasia with India, and Late Tertiary backthrusting. Note: these two-dimensional cartoons do not take account of along strike variation. For example, the Kohistan arc in the west collided with the Eurasian (Karakoram) margin in the Late Cretaceous, whereas further east forceful collision (e.g. of the preserved oceanic Nindam fore-arc) was delayed until Early Tertiary time, possibly reflecting initial 'soft' collision, or diachronous collision.

oceanic Dras arc complex. Relatively early collision is, indeed, inferred further west in the Himalayan Suture Zone (NW India), where an Upper Palaeocene shallow-water carbonate cover is reported (Beck *et al.* 1995). In Ladakh, marine sedimentation persisted locally into the Late Palaeocene or Early Eocene (nummulitic limestones), followed by the non-marine Indus clastics.

Further north, the oceanic Kohistan arc was amalgamated with the Eurasian (Karakoram) margin in the east (Pakistan) prior to 75 Ma. However, the collision was diachronous and a narrow remnant basin apparently survived further east between the oceanic Dras arc and the Trans-Himalayan (Eurasian) continental margin, explaining the presence of continuing Early Tertiary marine sedimentation (not shown in Fig. 19). During the Early Tertiary (Palaeocene), any remaining oceanic crust between Eurasia (including the by then amalgamated Dras/Kohistan arc) and India was subducted, and passive margin conditions were probably restored on the North Indian margin following emplacement of the Spontang ophiolite and underlying Spontang mélanges (Searle *et al.* 1998; Corfield 1999; Fig. 19c). With further convergence, the Eurasian and Indian continents forcefully collided in Early Tertiary time and units previously emplaced onto the Zanskar shelf in the Late Cretaceous were reactivated and thrust further south over a related foreland basin (Corfield 1999; Corfield & Searle this volume); also, the previously amalgamated Dras arc was thrust southwards over the North Indian margin (Fig. 19d). Any previous separate subduction traces were then amalgamated as a single major suture zone, lubricated by serpentinite. By this stage, nearly all the crustal material previously located between the Eurasian margin (Dras arc complex/Trans-Himalaya) and the North Indian margin (Lamayuru/Karamba complexes) was either subducted or bulldozed onto the Zanskar shelf south of the present Indus Suture Zone, explaining the scarcity of accreted open-ocean units (e.g. seamounts). As noted earlier, previously reported accreted oceanic seamounts (Sinha & Mishra 1992*a*, *b*) are now recognized as part of the distal North Indian passive margin (Robertson & Collins 1999) and were thus not accreted from within Neotethys. During the Late Tertiary, coeval with uplift of the High Himalaya, zones of weakness within the Indus Suture Zone were reactivated by northward thrusting, reverse faulting and folding, related to regional backthrusting. The present outcrop pattern then emerged following extensive erosion.

Finally, the wider implications of this study are that, although previously generally interpreted as 'ophiolitic mélange', careful analysis has revealed a number of discrete tectonic units (e.g. passive margin, oceanic arc, true accretionary mélange), thus considerably enhancing understanding of the tectonic evolution of the Indus Suture Zone. The mélange is the end product of a long history of tectonic events, not one process (e.g. subduction/accretion). A number of other 'ophiolitic' suture zones could well benefit from similar analysis.

Conclusions

1. In this study the previous hypothesis of 'ophiolitic mélanges' of the Indus Suture Zone in Ladakh as a vast, chaotic subduction–accretion complex generated by sedimentary and tectonic processes was tested and found to be a considerable oversimplification. The previously recognized southern and northern mélange zones units in reality contain little evidence of chaotic mélange generated by dismembering oceanic lithosphere, or of a sedimentary matrix formed by subduction/accretion processes.
2. Two parallel zones (southern and northern mélange zones) in Ladakh can be subdivided into discrete tectonic units of contrasting origin. The preserved units are mainly related to the adjacent North Indian passive margin and the overlying Upper Cretaceous oceanic Dras arc complex rather than accreted oceanic lithosphere.
3. The southern mélange zone includes disrupted, alkaline diabase sills within Triassic sandstone turbidites and shales; these are related to the proximal North Indian passive margin (Lamayuru complex). In addition, stratigraphically intact thrust sheets of Triassic–Late Cretaceous volcanic-sedimentary units (including alkaline lavas) record the distal, originally stratigraphically higher parts of the North Indian passive margin (Karamba complex). These units are therefore not accreted Tethyan oceanic crust (e.g. seamounts) and not mélange, but are appropriately termed broken formation as stratal coherence is still evident.
4. Serpentinite forms substantial dismembered thrust sheets, broken formation (and local serpentinite mélange), located in the higher part of both the southern and northern mélange zones and is interpreted as ultramafic oceanic lithosphere (i.e. deep

intrusive parts of an ophiolite). Locally, serpentinite was injected into adjacent units as anastomosing sheared serpentinite mélange. The serpentinite unit is intruded by swarms of diabase dykes, previously assumed to comprise blocks of ophiolitic sheeted diabase within ophiolitic mélange. Some of these dykes exhibit subduction-influenced chemistry and most likely represent original feeders of the oceanic Dras arc complex.

5. Volcanics and volcaniclastic sediments, previously loosely interpreted as blocks of 'ophiolitic extrusives' were found to be dismembered volcanogenic thrust sheets and broken formation, including (subduction-influenced) basalts, andesites and volcaniclastic sediments. These lithologies are correlated with units of the structurally adjacent Cretaceous oceanic Dras arc complex in both the southern and northern mélange zones.
6. Blueschists indicative of high-pressure metamorphism (i.e. at Sapi–La) and subordinate associated greenschists may record either accreted oceanic seamounts and associated deep-sea sediments, or, underthrust fragments of the distal North Indian continental margin (Karamba complex), based on the mainly within-plate type basalt chemistry typical of both of these alternative settings.
7. Coarse non-marine clastic sediments correlated with the post-Lower Eocene Indus Group ('Indus molasse') locally unconformably overlie each of the above units (i.e. North Indian passive margin, Dras arc complex, blueschists) and record syn- or early post-collisional deposition. These clastics were thrust intercalated with other units of the southern and northern mélange zones during regional Late Tertiary backthrusting.
8. Late Cretaceous volcanogenic units (basalt, andesite, volcaniclastic sediments) are tectonically intercalated with undated terrigenous turbiditic successions as blocks and slices in the northern mélange zone in the east (Hungru–Mongyu area). The terrigenous sediments may have accumulated in a deep-basin, or trench, setting between the Trans-Himalayan (Eurasian) continental margin unit to the north and the oceanic Dras arc to the south. Alternatively, they could have accumulated close to the North Indian margin, followed by over-thrusting by the Dras arc during Early Tertiary collisional deformation. In both hypotheses, these terrigenous sediments were dismembered and intersliced with inferred proximal units of the Upper Cretaceous Dras arc complex during the Early Tertiary collision (54–50 Ma) and later backthrust during the Late Tertiary. This unit qualifies as mélange of tectonic origin, but is non-ophiolitic.
9. Mud-matrix mélanges in the southern mélange zone, eastern areas (Urtsi) and locally elsewhere represent fragments of a subduction–accretion complex of probable Late Cretaceous age, including oceanic-derived units (MOR basalts and radiolarian cherts). However, these are volumetrically insignificant ($<1\%$ of the southern and northern zone outcrop).
10. Deformation of units in the northern and southern mélange zones was achieved by mainly tectonic, rather than sedimentary, processes. Three stages of tectonic deformation gave rise to the present structure: (1) latest Cretaceous subduction/accretion and partial emplacement over the North Indian margin (south mélange zone only); (2) Early Tertiary collision and emplacement over the North Indian margin as a stack of thrust sheets; (3) Late Tertiary regional backthrusting. The southern subduction zone evolved into a major shear zone during collisional deformation, dismembering upper (oceanic arc) and lower plate (continental margin) units to produce much of the southern mélange zone. The northern mélange zone also reflects reactivation of a previous active margin, with shearing and disruption during Early Tertiary emplacement. Syn/post-collisional clastics (Indus Group) formed an initial unconformable cover (Eocene/Oligocene) over the suture zone, and this was later sliced into the mélange related to pervasive Late Tertiary backthrusting and folding.
11. Regional comparisons suggest that the southern mélange zone was the root of the Spontang ophiolite and underlying mélanges overlying the Zanskar shelf succession south of the Indus Suture Zone. Much of this mélange was accreted at a subduction zone and later bulldozed southwards or subducted, explaining the paucity of true subduction/accretion material within the northern and southern mélange zones actually within the Indus Suture Zone.
12. This study indicates that the classic Indus Suture Zone 'mélanges' are mainly not ophiolitic (i.e. not dismembered Tethyan oceanic lithosphere) and are also mainly not mélanges, as most units do not represent

chaotic blocks (with or without a matrix). These units cannot be considered mainly as an accretionary prism related to subduction/accretion of Tethyan oceanic lithosphere, as in some previous hypotheses. Also, sedimentary processes played little role in actual formation of the mélange zones (e.g. olistostromes are effectively absent). The southern and northern ophiolite zones, instead, formed mainly in response to multi-stage subduction–accretion, collisional and post-collisional tectonic processes. 'Ophiolitic mélanges' elsewhere could benefit from comparable analysis.

An overseas Field Research Grant of the Royal Society is gratefully acknowledged. P. Degnan and I. Sharp provided welcome assistance in the field. Thanks also go to E. Bull and D. Baty for assistance with drafting; to Y. Cooper for photography; D. James for X-Ray fluorescence and G. Angell for X-ray diffraction analysis. Helpful comments on an initial version of the manuscript were made by A. Barber and M. P. Searle. The final manuscript benefited from comments by J. DiPietro, D. Cunningham and P. Clift.

References

American Geological Institute 1961. *Dictionary of Geological Terms*. Dolphin Books, New York.

Bassoullet, J.-P., Colchen, M., Marcoux, J. & Mascle, G. 1978. Permien terminal néritique, Scythien pélagique et volcanisme sous-marin, indices de proccessus tectono-sédimentaires distensifs a la limité Permien-Trias dans un bloc exotique de la suture de l'Indus (Himalaya du Ladakh). *Comptes Rendus de l'Academie des Sciences de Paris*, **287D**, 675–678.

——, ——, —— & —— 1981. Les masses calcaires du flysch Triasico-Jurassique de Lamayuru (zone de la suture de L'Indus, Himalaya du Ladakh): klippes sédimentaires et élements de plate-forme rémanies. *Rivista Italiano di Paleontologica e Stratigraphica*, **86**, 825–844.

Beck, R. A. & 13 others. 1995. Stratigraphic evidence for an early collision between northwest India and Asia. *Nature*, **373**, 55–58.

Blake, M. C. Jr. (ed.) 1984. *Franciscan geology of Northern California*. Society of Economic Paleontologists and Mineralogists, Los Angeles.

Boe, R. 1994. Nature and record of Late Miocene mass-flow deposits from the Lau–Tonga forearc basin, Tonga Platform (Hole 840B). *In*: Hawkins, J. E. W., Parson, L. M., Allan, J. F. *et al. Proceedings of ODP, Scientific Results*, **135**, College Station, TX (Ocean Drilling Program): 87–100.

Bouma, A. H. 1962. *Sedimentology of some flysch deposits*. Elsevier, Amsterdam.

Brookfield, M. E. & Andrews-Speed, C. P. 1984. Sedimentology, petrography and tectonic significance of the shelf, flysch and molasse clastic deposits across the Indus suture zone, Ladakh, NW India. *Sedimentary Geology*, **40**, 249–286.

Clift, P. D., Degnan, P. J., Hannigan, R. & Blusztajn, J. Sedimentary and geochemical evolution of the Dras Fore-Arc basin, Indus Suture, India. *Geological Society of America Bulletin*, in press.

——, MacLeod, C. J., Tappin, D., Wright, D. & Bloomer, S. H. 1998. Tectonic controls on sedimentation in the Tonga Trench and Forearc, SW Pacific. *Geological Society of America Bulletin*, **110**, 483–496.

Cloos, M. 1982. Flow melange, numerical modelling and geological constraints on the origin of the Franciscan complex, California. *Bulletin of the Geological Society of America*, **93**, 330–345.

Colchen, M., Mascle, G. & Van Haver, T. 1985. Some aspects of collision tectonics in the Indus Suture Zone, Ladakh. *In*: Coward, M. P. & Ries, A. (eds). *Collision Tectonics*. Geological Society, London, Special Publications, **19**, 175–186.

Corfield, R. I. 1999. *Origin and emplacement of the Spontang Ophiolite and crustal shortening processes in the Ladakh–Zanskar Himalaya, NW India*. DPhil thesis, University of Oxford.

—— & Searle, M. P. 2000. Crustal shortening estimates across the north Indian margin, Ladakh, NW India. *This volume*.

Coward, M. P., Windley, B. F., Broughton, R. D., Luff, I. W., Petterson, M. G. *et al.* 1986. Collision tectonics in the NW Himalayas. *In*: Coward, M. P. & Ries, A. C. (eds) *Collision Tectonics*. Geological Society, London, Special Publications, **19**, 203–219.

Danelian, T., & Robertson, A. H. F. 1997. Radiolarian evidence for the stratigraphy and palaeooceanography of the deep-water passive margin of the Indian plate (Karamba Formation, Indus Suture Zone, Ladakh Himalaya). *Marine Micropalaeontology*, **30**, 171–195.

Deitrich, V. J., Frank, W. & Honegger, K. 1983. A Jurassic–Cretaceous island arc in the Ladakh–Himalayas. *Journal of Volcanology and Geothermal Research*, **18**, 405–433.

Einsele, G., Liu, B., Durr, S., Frisch, W. & 8 others, 1994. Xigaze forearc basin (Cretaceous, Tibet): sediments and basin evolution. *Sedimentary Geology*, **90**, 1–32.

Fitton, J. G. & Dunlop, H. M. 1985. The Cameroon line, West Africa and its bearing on the origin of oceanic and continental alkali basalt. *Earth and Planetary Science Letters*, **72**, 23–38.

Frank, W., Gansser, A. & Trommsdorf, V. 1977. Geological observations in the Ladakh Himalaya. *Schweizerische Mineralogische und Petrographisches Mitteilungen*, **57**, 89–113.

Fuchs, G. 1979. On the geology of western Ladakh. *Geologisches Jahrbuch*, **122**, 513–540.

—— 1986. The geology of the Markha–Khurnak Region in Ladakh (India). *Geologisches Jahrbuch*, **128**, 403–437.

GAETANI, M. & GARZANTI, E. 1991. Multicycle history of the Northern India continental margin (Northwestern Himalayas). *American Association of Petroleum Geologists Bulletin*, **75**, 1427–1446.

GANSSER, A. 1974. The ophiolitic mélange, a worldwide problem on Tethyan examples. *Eclogae Geologicae Helvetiae*, **67**, 459–507.

—— 1980. The significance of the Himalayan suture zone. *Tectonophysics*, **62**, 27–52.

GARZANTI, E. & VAN HAVER, T. 1988. The Indus clastics: forearc basin sedimentation in the Ladakh Himalaya (India). *Sedimentary Geology*, **59**, 237–249.

HONEGGER, K. 1983. *Strukturen and Metamorphose im Zanskar Kristallin (Ladakh, Kashmir, Indien)*. PhD thesis, ETH Zurich, Switzerland.

——, DIETRICH, V., FRANK, W., GANSSER, A., THONI, M. & TROMMSDORF, V. 1982. Magmatism and metamorphism of the Ladakh Himalayas (the Indus–Tsanpo suture zone). *Earth and Planetary Science Letters*, **60**, 253–292.

——, LE FORT, P., MASCLE, G. & ZIMMERMAN, J. L. 1989. The blueschists along the Indus suture zone in Ladakh, NW Himalaya. *Journal of Metamorphic Geology*, **7**, 57–72.

KHAN, M. A., JAN, M. Q. & WEAVER, B. L. 1993. Evolution of the lower arc crust in Kohistan, N Pakistan: temporal arc magmatism through early, mature and intra-arc rift stages. *In*: TRELOAR, P. J. & SEARLE, M. P. (eds) *Himalayan Tectonics*. Geological Society, London, Special Publications, **74**, 123–138.

——, STERN, R. J., GRIBBLE, R. F. & WINDLEY, B. F. 1998. Geochemical and isotopic constraints on subduction polarity, magma sources and palaeogeography of the Kohistan Arc, northern Pakistan. *Journal of the Geological Society, London*, **154**, 935–946.

MANGAIN, V. O. & RAO, B. R. 1965. Orbitolines from the limestone intercalations of Dras Volcanics: Jammu and Kashmir State. *Journal of the Geological Society of India*, **6**, 122–129.

MURTON, B. J. & GASS, I. G. 1986. Western Limassol Forest Complex, Cyprus: Part of an Upper Cretaceous leaky transform fault. *Geology*, **14**, 255–258.

PEARCE, J. A., LIPPARD, S. J. & ROBERT, S. 1984. Characteristics and tectonic significance of suprasubduction zone ophiolites. *In*: KOKELAAR, B. P. & HOWELLS, M. F. (eds) *Marginal Basin Geology*. Geological Society, London, Special Publications, **6**, 7–97.

PETTERSON, M. G. & WINDLEY, B. F. 1991. Changing source regions of magmas and crustal growth in the Trans-Himalaya of N Pakistan and tectonic implications. *Earth and Planetary Science Letters*, **74**, 4–75.

PUDSEY, C. J. 1986. The Northern Suture, Pakistan: margin of a Cretaceous island arc. *Geological Magazine*, **123**, 405–423.

RAZ, U. & HONEGGER, K. 1989. Magmatic and tectonic evolution of the Ladakh Block from field studies. *Tectonophysics*, **161**, 107–118.

REUBER, I. 1989. The Dras arc: two successive volcanic events on eroded oceanic crust. *Tectonophysics*, **161**, 93–106.

——, COLCHEN, M. & MEVEL, C. 1987. The geodynamic evolution of the South Tethyan margin in Zanskar, NW Himalaya, as revealed by the Spontang ophiolitic melanges. *Geodynamica Acta*, Paris, **1**, 283–296.

——, MONTIGNY, R., THUIZAT, R. & HEITZ, A. 1989. K/Ar ages of ophiolites and arc volcanics of the Indus suture zone: clues on the early evolution of Neotethys. *Eclogae Geologicae Helvetiae*, **82**, 699–715.

RIEBEL, G. 1984. *L'asociation pluto-volcanique de Dras (suture de l'Indus, Hinalaya du Ladakh): Petrologie d'un fragmente d'arc insulaire*. Thèse 3ème cycle, Université Louis Pasteur, Strasbourg.

ROBERTSON, A. H. F. 1998. Rift-related sedimentation and volcanism of the North Indian plate inferred from a Permo-Triassic exotic block at Lamayuru (Ladakh Himalaya) and regional comparisons. *Journal of Asian Earth Sciences*, **16**, 159–172.

—— & COLLINS, A. S. 1999. Significance of the Shyok Suture Zone (Northern Suture) in N Pakistan (Skardu area): Twofold division into Cretaceous Kohistan arc-margin and Eurasian (Karakorum) continental margin units. 14th Himalaya–Karakoram–Tibet Workshop, Kloster Ettal, Germany, March 24–26, 1999. *Terra Nostra*, **2**, 128–130.

—— & DEGNAN, P. J. 1993. Sedimentology and tectonic implications of the Lamayuru Complex: deep-water facies of the Indian passive margin, Indus Suture Zone, Ladakh Himalaya. *In*: SEARLE, M. P. & TRELOAR, P. J. (eds) *Himalayan Tectonics*. Geological Society, London, Special Publications, **74**, 299–321.

—— & —— 1994. The Dras arc Complex: lithofacies and reconstruction of a Late Cretaceous oceanic volcanic arc in the Indus Suture Zone, Ladakh Himalaya. *Sedimentary Geology*, **92**, 117–145.

—— & SHARP, I. 1998. Mesozoic deep-water slope/rise sedimentation and volcanism along the North Indian passive margin: evidence from the Karamba Complex, Indus suture zone (Western Ladakh Himalaya). *Journal of Asian Earth Sciences*, **16**, 195–215.

——, EMEIS, K.-C., RICHTER, C. and the Scientific Party of Leg 180. 1998. Collision related break-up of a carbonate platform (Eratosthenes Seamount) and mud volcanism on the Mediterranean Ridge: preliminary synthesis and implications of tectonic results of ODP Leg 160 in the Eastern Mediterranean Sea. *In*: CRAMP, A., MACLEOD, C. J., LEE, S. & JONES, E. J. W. (eds) *Geological Evolution of Ocean Basins: Results from the Ocean Drilling Program*. Geological Society, London, Special Publications, **131**, 243–271.

ROLLAND, Y., PICCARD, C. & PECHER, A. 1999. Rare earth and isotopic evidence of volcanics from northern Ladakh Arc and southern Karakorum Margin (NW Himalaya)-accretion history. 14th Himalaya–Karakoram-Tibet Workshop, Kloster

Ettal, Germany, March, 24–26, 1999. *Terra Nostra*, **2**, 130–131.

SALEEBY, J. 1979. Kawaeh Serpentinite Melange, Southwest Sierra Nevada foothills, California. *Geological Society of America Bulletin*, **90**, 29–46.

—— 1984. Tectonic significance of serpentinite mobility and ophiolitic mélange. *Geological Society of America Bulletin*, **198**, 153–168.

SCHARER, U., HAMET, J. U. & ALLEGRE, C. J. 1984. The Transhimalaya (Gandese) plutonism in the Ladakh region: a U–Pb and Rb–Sr study. *Earth and Planetary Science Letters*, **67**, 327–339.

SEARLE, M. P. 1983. Stratigraphy, structure and evolution of the Tibetan–Tethys zone in Zanskar and the Indus suture zone in the Ladakh Himalaya. *Royal Society of Edinburgh Transactions, Earth Sciences*, **73**, 205–219.

—— 1986. Structural evolution and sequence of thrusting in the High Himalayan Tibetan–Tethys and Indus suture zones of Zanskar and Ladakh, western Himalaya. *Journal of Structural Geology*, **8**, 923–938.

——, COOPER, D. W. J. & REX, A. J. 1988. Collision tectonics of the Ladakh–Zanskar Himalaya. *Philosophical Transactions of the Royal Society of London*, **A326**, 117–150.

——, CORFIELD, R. I., STEPHENSON, B. & MCCARRON, J. 1997. Structure of the North India continental margin in the Ladakh–Zanskar Himalayas: implications for the timing of obduction of the Spontang ophiolite, India–Asia collision and deformation events in the Himalayas. *Geological Magazine*, **134**, 297–316.

——, WINDLEY, B. F., COWARD, M. P., COOPER, D. W. J., REX, A. J. *et al.* 1987. The closing of Tethys and the tectonics of the Himalayas. *Geological Society of America Bulletin*, **98**, 678–701.

SHAH, S. K. & SHARMA, M. L. 1977. A preliminary report on the fauna in radiolarites of the ophiolitic melange zone around Mulbekh, Ladakh. *Current Science*, **46**, 817.

SHARMA, K. K. & CHOUBERT, V. M. 1983. Petrology, geochemistry and geochronology of the southern margin of the Ladakh Batholith between Upsi and Chamatang. *In*: THAKUR, V. C. & SHARMA, K. K. (eds) *Geology of Indus Suture Zone*. Wadia Institute of Himalayan Geology, Dehra Dun.

SINHA, A. K. & MISHRA, M. 1992*a*. Emplacement of ophiolitic melange along continental collision zone of Indus Suture Zone in Ladakh Himalaya, India. *Journal of Himalayan Geology*, **3**, 179–189.

—— & —— 1992*b*. Plume activity and seamounts in Neotethys: evidence supported by geological and geochronological data. *Journal of Himalayan Geology*, **3**, 91–99.

—— & —— 1994. The existence of oceanic islands in the Neotethys: Evidences from Ladakh Himalayas India. *Current Science*, **7**, 721–727.

—— & —— 1995. Fragmented oceanic island from Ophiolitic Melange of ancient convergent zone in western Ladakh Himalaya, India. *In*: SRIVASTAVA, R. & CHANDRA, R. (eds) *Magmatism in relation to Diverse Tectonic Settings*. Oxford and IBH Publishing company, New Delhi, 393–414.

—— & UPADHYAY, R. 1990. Subduction acretion and subduction kneading: a possible mechanism for the incorporation of sedimentary sequences within the ophiolitic mélange belt in the Western Ladakh Himalaya. *Journal of Himalayan Geology*, **1**, 259–264.

—— & —— 1993. Mesozoic pre-orogenic deep marine sediments along the Indus–Yarlung Suture. *Terra Nova*, **5**, 271–281.

—— & —— 1994. Tectonic setting and pre-orogenic sedimentation along the Indus-Tsangpo (Yarlung) Suture Zone of Ladakh India. *Journal of Asian Earth Sciences*, **9**, 435–450.

—— & —— 1997. Tectonics and sedimentation in the passive margin, trench, fore-arc and backarc areas of the Indus Suture Zone in Ladakh and Karakorum: a review. *Geodynamica Acta (Paris)*, **10**, 1–12.

SUTRE, E. 1991. *Les formations de la marge nord-Neotethsienne et les melanges ophiolitique de la zone de suture de l'Indus en Himalaya du Ladakh*. These Docteur de L'Universite de Poitiers, **1**.

TAIRA, A., HILL, I. & ODP Leg 131 Scientific Party. 1992. Sediment deformation and hydrogeology of the Nankai Trough accretionary prism: synthesis of shipboard results of ODP Leg 131. *Earth and Planetary Science Letters*, **109**, 431–450.

TAYLOR, B., HUCHON, P., KLAUS, A. *ET AL.* *Proceedings of the ODP, Initial Reports*, **180**. Ocean Drilling Program, Texas [CD-ROM].

TEWARI, B. S., PANDE, I. C. & KUMAR, R. 1970. Lower Cretaceous fossiliferous limestone from Khalsi, Ladakh. *Publication of the Centre of Advanced Study in Geology*, Panjab University, Chandigarh, **7**, 197–200.

THAKUR, V. C. 1981. Regional framework and geodynamic evolution of the Indus–Tsangpo suture zone in the Ladakh Himalayas. *Transactions of the Royal Society of Edinburgh, Earth Sciences*, **72**, 89–97.

—— 1990. Indus Tsangpo suture in Ladakh—its biostratigraphy and tectonics. *Proceedings of the Indian Academy of Science*, **99**, 169–185.

—— & MISHRA, D. K. 1983. Ophiolitic mélanges in the Indus Suture Zone: lithological description and structural features. *In*: THAKUR, V. C. & SHARMA, K. K. (eds) *Geology of Indus suture zone of Ladakh*. Wadia Institute of Himalayan Geology, Dehra Dun, 21–31.

—— & ——,1984. Tectonic framework of the Indus and Shyok suture zone in eastern Ladakh, northwest Himalaya. *Tectonophysics*, **101**, 207–220.

VAN HAVER, T. 1984. *Etude stratigraphique, sedimentologique et structurale d'un bassin d'avant arc: example du bassin de l'indus, Ladakh, Himalaya*. These, Docteur de troisieme cycle, Centre National de la Recherche Scientifique.

——, BASSOULLET, J.-P., BLONDEAU, A. & MASCLE, G. 1984. Les séries détritiques du bassin de L'Indus au Ladakh: nouvelles données stratigraphiques et structurales. *Rivista Italiano Paleontologicae e Stratigraphica*, **90**, 87–102.

VIRDI, N. S., THAKUR, V. C. & KUMAR, S. 1977. Blueschist facies metamorphism from the Indus Suture Zone and its significance. *Himalayan Geology*, Dhera Dun, **7**, 479–482.

WOODCOCK, N. H. & ROBERTSON, A. H. F. 1984. The structural variety in Tethyan ophiolite terrains. *In*: GASS, I. G. & SHELTON, A. W. (eds) *Ophiolites and Oceanic Lithosphere*. Geological Society, London, Special Publications, **13**, 321–332.

The Main Mantle Thrust in Pakistan: its character and extent

J. A. DIPIETRO[1], A. HUSSAIN[2], I. AHMAD[3] & M. A. KHAN[3]

[1]*Department of Geology, University of Southern Indiana, 8600 University Boulevard, Evansville, Indiana 47712, USA (e-mail: DiPietro@usi.edu)*

[2]*Geological Survey of Pakistan, 148/285, New Defence Colony, Shami Road, PO Box 1355, Peshawar, Pakistan*

[3]*National Centre of Excellence in Geology, University of Peshawar, Peshawar, Pakistan*

Abstract: The Main Mantle Thrust (MMT) represents the tectonic boundary between metamorphic shield and platform rock of the Indian plate hinterland, and dominantly mafic and ultramafic rock of the Kohistan–Ladakh arc complex in Pakistan. In some areas, this boundary is a sharp planar fault with development of mylonite; in other areas, it is a brittle–ductile imbricate zone; in still other areas, it contains large, discontinuous, slices of internally sheared and deformed ophiolitic mélange. The character of the MMT along its entire trace is discussed and it is concluded that there is no single continuous fault which marks the contact between the Indian plate and the Kohistan–Ladakh arc. On this basis, we propose a revised definition for the MMT that is consistent with both the original definition and with the usage of the term in literature. We suggest that the MMT fault contact be defined as the series of faults, of different age and tectonic history, that collectively define the northern margin of the Indian plate in Pakistan. On this basis, faults that define the MMT vary in age from Quaternary to possibly as old as Late Cretaceous. Discontinuous lenses of ophiolitic mélange that overlie the MMT fault contact, and which intervene between the Indian plate and the Kohistan–Ladakh arc, are considered to be part of an MMT zone that is equivalent with the Indus Suture Zone.

The Main Mantle Thrust (MMT) was originally defined as the tectonic boundary that separates mafic and ultramafic rock of the Kohistan arc complex from crystalline shield rock of the Indian plate (Tahirkheli 1979*a*, *b*; Tahirkheli & Jan 1979; Tahirkheli *et al.* 1979). It was described as extending eastward from Afghanistan, through Swat to Babusar, and then northward around the Nanga Parbat–Haramosh massif to Ladakh where it connected with the Indus Suture Zone (Fig. 1). The best known location of the MMT is along the Karakoram Highway in the Indus valley near Jijal. Here, the fault is a sharp, planar contact with mylonitic and brittle fabrics. Subsequent work along the length of the MMT has indicated that, in many areas, the tectonic boundary is not a single fault plane but is a series of faults of different age and tectonic history. The purpose of this paper is to define the character of the MMT along its extent and to reach a consensus regarding its location and tectonic significance.

In some areas along the MMT, a thick imbricated mélange zone of greenschist, blueschist, serpentinite and ultramafic rock intervenes between Kohistan and the Indian plate. These rocks are considered to be part of a third tectonic terrane, the Indus Suture Zone. The MMT was identified as the continuation of the Indus Suture Zone by Tahirkheli *et al.* (1979) and, although they clearly indicated that these rocks were part of the MMT fault zone, they placed the MMT fault contact variably above (Tahirkheli *et al.* 1979) or below (Tahirkheli 1979*b*; Tahirkheli & Jan 1979) rocks of the Indus Suture Zone. In all cases, they considered the Dargai mafic–ultramafic complex to be a klippe underlain by the MMT. Along its entire length, the MMT was considered to be a south-directed thrust fault that was active in the Late Cretaceous or early Cenozoic during deformation and foliation development in the underlying Indian plate.

Important contributions to the study of the Main Mantle Thrust include Kazmi *et al.* (1984, 1986) and Lawrence *et al.* (1989). Working primarily in the Swat region, these authors unambiguously equated the MMT with the Indus Suture Zone and named the rocks within the Indus Suture Zone (including the Dargai mafic–ultramafic complex) as the Indus Suture

From: KHAN, M. A., TRELOAR, P. J., SEARLE, M. P. & JAN, M. Q. (eds) *Tectonics of the Nanga Parbat Syntaxis and the Western Himalaya*. Geological Society, London, Special Publications, **170**, 375–393. 1-86239-061-4/00/$15.00

mélange group. Thus, rather than a single fault plane, the authors equated the MMT with the entire suture zone. They showed that the MMT (Indus Suture) Zone contained faults of different age and tectonic history and thus revealed the complexity of the fault zone. The basal fault of the MMT (Indus Suture) Zone, which is in direct contact with Indian plate rocks, was named the Kishora Thrust. The roof fault, which separates the MMT (Indus Suture) Zone from the Kohistan arc complex, was named the Kohistan Fault. Subsequent workers have shown the MMT either as a fault zone equivalent with the Indus Suture Zone, or as a fault plane located variably above or below the Indus mélange such that the MMT is equivalent with either the Kohistan or the Kishora Fault (Yeats & Lawrence 1984; Searle 1991; Treloar & Searle 1993; Bender & Raza 1995; Kazmi & Jan 1997). In many cases, the MMT is shown as a planar fault contact between Kohistan and the Indian plate in which the intervening mélange is not shown. Most of the tectonic interpretations of the MMT are consistent with Tahirkheli *et al.* (1979) and suggest that Kohistan was overthrust onto the Indian plate along a south-directed thrust fault in the Late Cretaceous or early Cenozoic. It will be shown that the MMT has a prolonged tectonic history that is not entirely consistent with simple south-directed overthrusting of Kohistan. The following sections describe the character of the MMT, beginning in the Nanga Parbat area and continuing westward to the Afghan border.

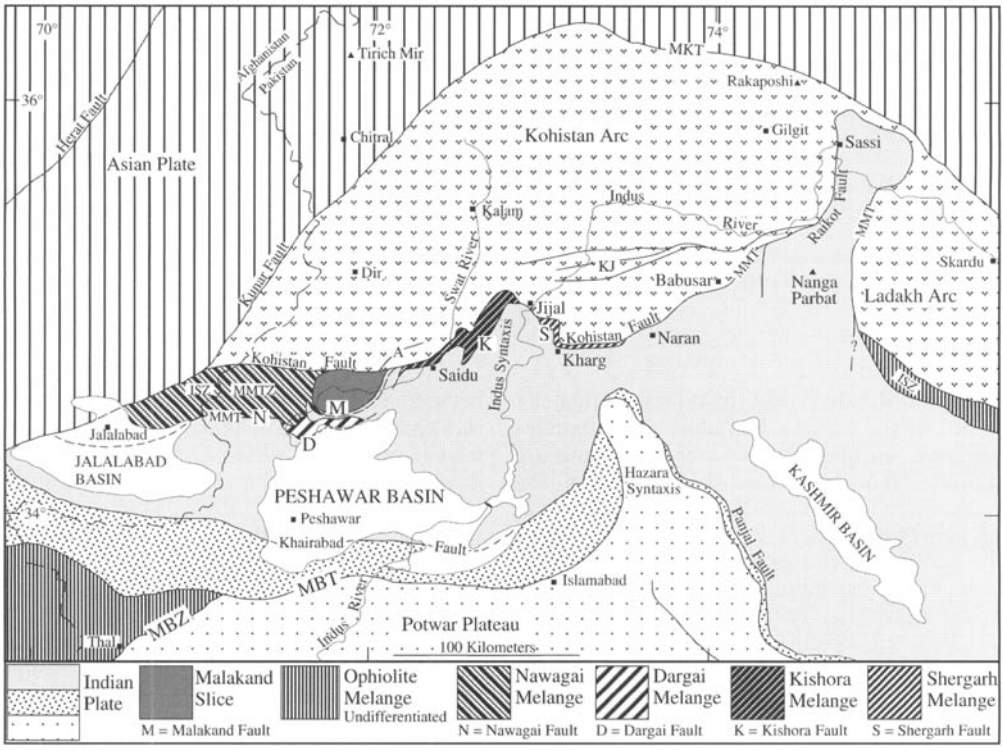

Fig. 1. Tectonic map showing major faults of the northwest Himalaya. The Main Mantle Thrust Zone (MMTZ) represents the boundary between the Indian plate and the Kohistan–Ladakh arc in Pakistan and is equivalent to the Indus Suture Zone. It includes discontinuous fault slices of mélange that lie between the Kohistan arc and the Indian plate. The fault slices are divided into the Nawagai, Dargai, Kishora and Shergarh mélange units which collectively represent the Indus Suture mélange group. West of Nanga Parbat, the MMTZ is bounded on its north side by the Kohistan–Raikot fault system and on its south side by the Nawagai–Dargai–Kishora–Shergarh fault system. The Main Mantle Thrust (MMT) is placed south of the mélange units and south of the Kohistan–Ladakh arc such that it represents the series of faults, of different age and tectonic history, that collectively define the northern boundary of the Indian plate in Pakistan. The Malakand slice is interpreted as an allochthonous slice of the Indian plate rock trapped along the MMTZ and nearly surrounded by Indus mélange. A, Ahingaro Fault Zone; KJ, Kamila–Jal Shear Zone; ISZ, Indus Suture Zone mélange; MBT, Main Boundary Thrust; MBZ, Mélange Boundary zone; MKT, Main Karakoram Thrust.

Nanga Parbat–Haramosh region

The tectonic boundary between Kohistan and the Indian plate (the MMT) in the Nanga Parbat area is marked by the active Raikot Fault Zone (Fig. 2). This is a zone of right-lateral strike-slip and reverse faults which strike roughly north and dip vertical to steeply east (Lawrence & Ghauri 1983*a*; Madin *et al.* 1989; Shroder *et al.* 1989; Treloar *et al.* 1991). The fault zone cuts across the major rock units and the metamorphic fabric in both the Kohistan arc and the Indian plate (Fig. 2). It is characterized by offset Holocene deposits, brittle and cataclastic deformation, and minor development of mylonite across a zone that is locally more than 3 km wide. The Raikot Fault is not folded and there is no report of ophiolite along its mapped trace. The amount of displacement is unknown. Butler *et al.* (1989) referred to the southern part of the Raikot Fault near Bunji as the Liachar Thrust and the northern part, near Sassi, as the Shabatot strike-slip fault. Displacement along the Raikot Fault is opposite to that normally attributed to the MMT.

Ductile mylonite fabrics are developed along the Raikot Fault at Sassi where metamorphic foliation in both the Kohistan arc and the Indian plate are parallel with the mylonite zone. Both Madin *et al.* (1989) and Treloar *et al.* (1991) interpreted the mylonite as formed during the early history of the Raikot Fault which, they suggested, has been active since the Miocene or since before 9 Ma respectively. Madin *et al.* (1989) suggested that the Raikot Fault has completely cut out any evidence for an early period of

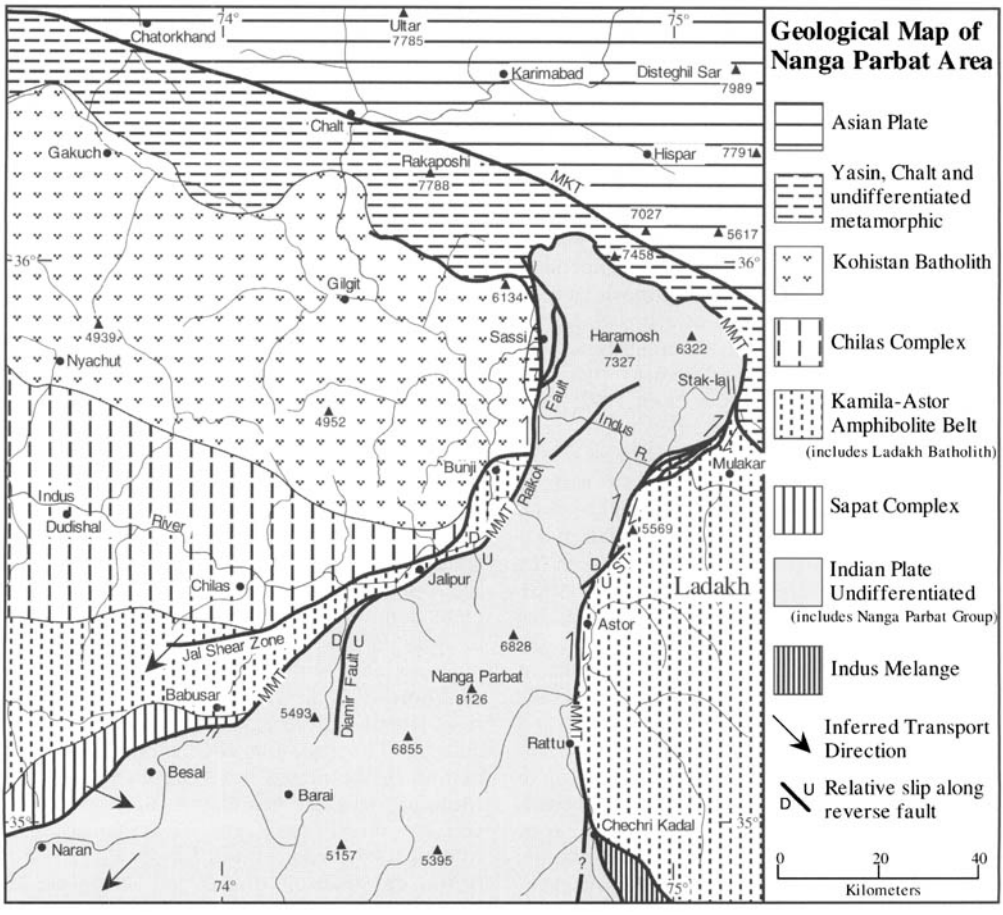

Fig. 2. Generalized geological map of the Nanga Parbat area. Based on Lawrence & Ghauri (1983*a*), Madin *et al.* (1989), Shroder *et al.* (1989), Searle (1991), Pognante *et al.* (1993), Khan *et al.* (1995), Tahirkheli (1996), Kazmi & Jan (1997), Edwards (1998), Pêcher & Le Fort (1999), T. Argles (pers. comm.) and our own observations. ST, Subsar Thrust. Half-arrows represent relative strike-slip motion.

southward thrusting along the Kohistan–Indian plate contact. Butler *et al.* (1989), on the other hand, suggested that the mylonite represents an earlier-formed southward-vergent thrust fault which was subsequently deformed and rotated to the vertical along the Raikot Fault.

South of Sassi, the Raikot Fault swings to the west and southwest and closely follows the Indus River to an area about 25 km east of Chilas. From here, the fault diverges southward, away from the Kohistan–Indian plate contact and into the Indian plate where it is a north-striking, 5 km wide, vertical to east-dipping, east-side-up, reverse, brittle–ductile shear zone referred to as the Diamir Shear Zone which is believed to be Late Miocene and younger (Fig. 2; M. A. Edwards, pers. comm.). Further west, near Babusar, the Kohistan–Indian plate (MMT) contact is represented by an older fault that is discussed in the next section. A large, open, north-trending, recumbent fold (Gashit Fold) is associated with the Diamir Shear Zone along its western margin. The fold intersects and overturns the older MMT contact from an original WNW dip to a steep ESE dip (Fig. 3).

The Raikot Fault extends north of Sassi for about 8 km where it apparently dies out (Fig. 2; Pêcher & Le Fort 1999). In this area, the tectonic contact between Kohistan and the Indian plate is an older fault that is folded around the northern flank of the Nanga Parbat–Haramosh massif. The fault has been described as a broad, north-dipping, mylonite zone with dominantly top-to-the-south or southeast displacement that was active before *c.* 8.4 Ma (Butler *et al.* 1992; Villa *et al.* 1996; Pêcher & Le Fort 1999).

The MMT was located on the northeast side of the Nanga Parbat–Haramosh massif east of Stak-la, where it was described as a right-lateral mylonitic shear zone that dips 25–40° ESE and is associated with retrograde metamorphism in the Nanga Parbat group (Pognante *et al.* 1993). Foliation in the Nanga Parbat group is parallel with the shear zone, whereas foliation in the Ladakh arc is deflected northward consistent to right-lateral displacement. From Stak-la, the MMT trends SE to the Indus gorge where it is a moderate to steeply east-dipping, ductile, right-lateral, strike-slip, imbricate mylonite zone, up to 5 km wide, that is overprinted with minor brittle, east-side-down, normal faults. The mylonite zone contains lenses of Astor (Ladakh) amphibolite; Nanga Parbat schist, paragneiss and garnet–amphibolite; and serpentinized mafic–ultramafic rock (some with retrogressed eclogite facies assemblages) and talc–carbonate schist which presumably are remnants of Indus Suture subduction mélange (Pêcher & Le Fort 1999). North of Astor, the mylonite zone is cut by a brittle, northwest-vergent thrust fault (the Subsar Thrust) which locally forms the boundary between the Indian plate and the Ladakh arc (Fig. 2, T. Argles, pers. comm.).

The MMT was traced southward into the Astor valley where, near Astor, it is a sharp, planar, ductile fault that trends N–S with vertical to moderate westward overturned dips (Edwards 1998). The imbrication that is present in the Indus gorge is absent here. The contact separates highly strained kyanite-grade schist and marble of the Nanga Parbat group from a nearly one kilometre thick zone of mylonitic Astor (Ladakh) amphibolite. Foliation in the Nanga Parbat group is roughly parallel to the mylonitic tectonic contact. The mylonitic amphibolite has been traced to Rattu where it maintains its N–S strike and near-vertical to steep east or west dip. From Rattu, the mylonite zone extends southward and either connects directly with the Indus Suture Zone or diverges from the suture zone and extends into the Indian plate in a manner similar to the Diamir–Raikot Fault Zone on the west side of Nanga Parbat. This second option is shown with a question mark in Fig. 2. Kinematic indicators are not common but suggest dominantly right-lateral strike-slip displacement along the entire trace of the mylonite zone. Lenses of ophiolitic ultramafic rock and talc–carbonate schist are present within the mylonite zone and along the contact with the Nanga Parbat group. Brittle normal and reverse faults overprint the mylonite zone but displacement appears to be minor.

In summary, the Kohistan–Indian plate contact along the western margin of the Nanga Parbat–Haramosh massif has been reactivated by the active, dominantly brittle, Raikot Fault, which shows both right-lateral and reverse (east-side-up) displacement. The Ladakh–Indian plate contact along the northern and eastern margins of the massif is marked by a ductile mylonite zone with S to SE displacement along the northern margin, and with dominantly right-lateral displacement along the eastern margin. The mylonite zone along the eastern margin of the massif has been interpreted as a Miocene or older expression of a southward-verging thrust fault that was subsequently rotated to the vertical and locally deformed by brittle deformation during late Neogene and Quaternary exhumation of Nanga Parbat (Edwards 1998). The young deformation around the entire massif has obscured the Miocene and older tectonic history of the MMT Zone in this area.

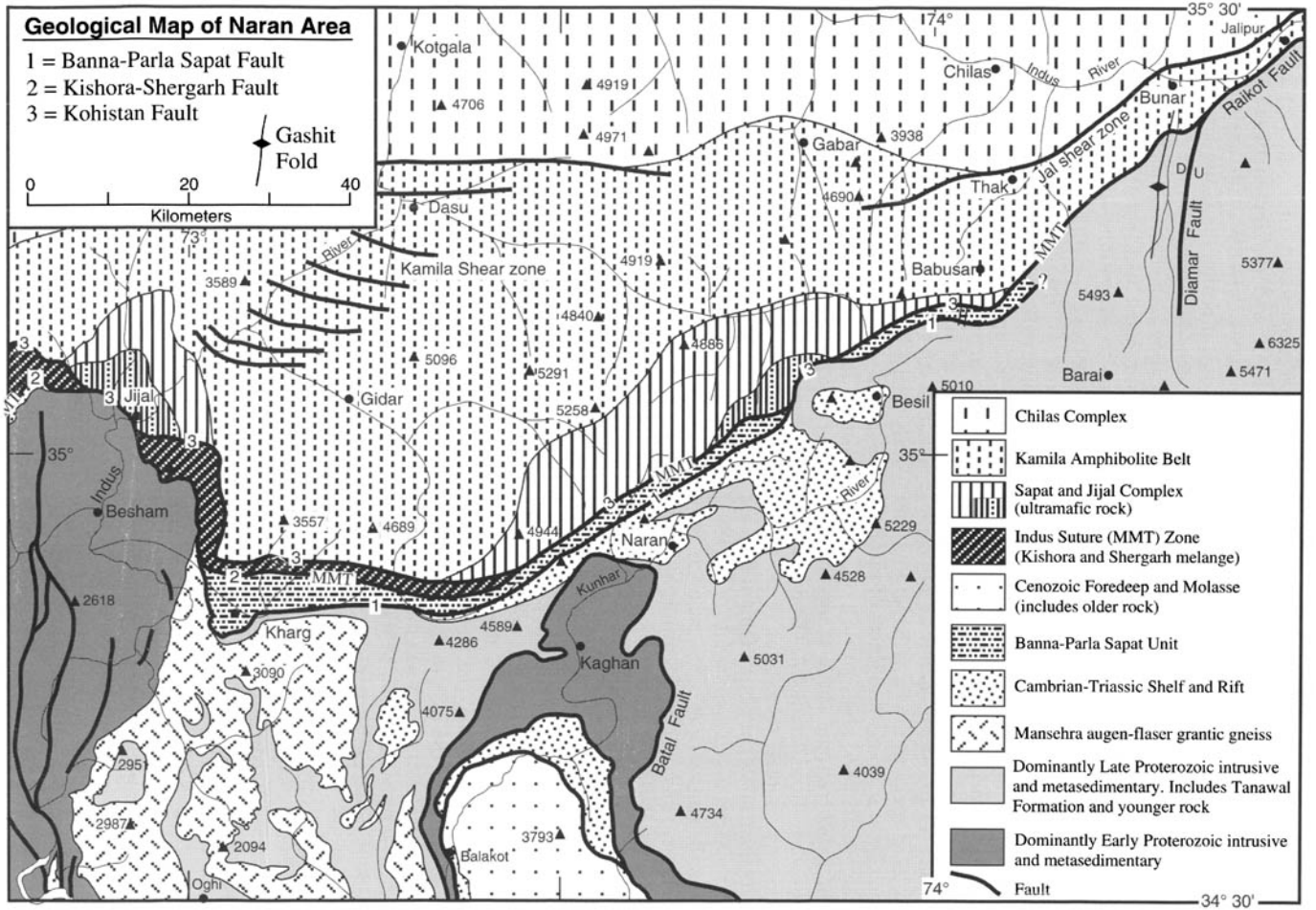

Fig. 3. Geological map of the Kharg–Naran–Babusar region. Based on Calkins *et al.* (1975), Treloar *et al.* (1990), Greco & Spencer (1993), Khan *et al.* (1995), DiPietro *et al.* (1999) and our own observations. U/D, Relative slip along reverse faults.

Babusar–Naran area

Rock in the hanging wall of the MMT in the Babusar–Naran area consists of the Sapat mafic–ultramafic complex, which is interpreted as the lower part of the Kohistan arc stratigraphically below the Kamila Amphibolite Belt (Jan *et al.* 1993; Khan *et al.* 1995). Ultramafic cumulates, at the base of the Sapat complex, are exposed along the MMT west of Besil (Fig. 3). From this area eastward, the MMT ramps upsection through gabbroic rock of the Sapat complex and into the Kamila Amphibolite Belt (Fig. 3).

Rock on the Indian plate directly below the MMT consists of graphite, garnet and/or staurolite-bearing quartz-mica schist with minor marble (Greco *et al.* 1989; Ghazanfar *et al.* 1991; Smith *et al.* 1994). Khan *et al.* (1995) mapped these rocks as the Parla Sapat unit and indicated that it contains rare lenses of serpentinite, talc–carbonate and greenstone which represent either tectonic slices of ophiolite or ophiolitic olistostromal material. The presence of these lenses prompted Ghazanfar *et al.* (1991) and Smith *et al.* (1994) to place a fault at the base of the Parla Sapat unit. Chamberlain *et al.* (1991) referred to the unit as a calc-schist mélange. Both Chamberlain *et al.* (1991) and Smith *et al.* (1994) considered the Parla Sapat unit to be part of the MMT fault zone, although Smith *et al.* (1994) placed the MMT fault contact structurally above the Parla Sapat unit at the base of the Sapat complex. Greco *et al.* (1989) and Khan *et al.* (1995) considered the Parla Sapat unit to be part of the Indian plate. Although the intervening area has not been mapped, the Parla Sapat unit appears to represent the eastern continuation of the Banna Formation, which was mapped in the Kharg area directly below the MMT by Treloar *et al.* (1989*b*) and DiPietro *et al.* (1999) who described it as a graphitic schist with grey marble. This correlation, and the rarity of ophiolitic rock, suggest that the Parla Sapat unit is part of the Indian plate and that the MMT lies structurally above this unit even if the base of the unit is faulted. The age of the Parla Sapat unit is uncertain. Khan *et al.* (1995) suggested a correlation with the Mesozoic Saidu Formation which forms the top of the Indian plate directly below the MMT in Swat. DiPietro *et al.* (1999) suggested a correlation of the Saidu Formation with the Banna Formation, implying that all three rock units are equivalent. The Parla Sapat unit is locally cut out along the MMT west of Besil. Also present, just south of Naran and trending to within 5 km of the MMT, is a mylonite zone referred to as the Batal Fault by Chaudhry *et al.* (1986). This fault also appears to truncate stratigraphy in the Indian plate (Fig. 3).

Khan *et al.* (1995) described the MMT in the Naran–Babusar area as a sharp planar thrust fault that cuts across rock units in both the Kohistan arc and the Indian plate. The fault trends roughly NE–SW with shallow NW to vertical dips. Locally, the fault plane dips south due to later folding. The MMT is marked by a mylonite zone at the base of the Sapat complex in which ultramafic rock shows retrograde metamorphism to serpentinite and other greenschist-facies assemblages. Both Greco *et al.* (1989) and Khan *et al.* (1995) indicated that the mylonitic serpentinite cuts across and truncates foliation in the Parla Sapat unit. A strong, steep, west-plunging crenulation lineation is developed in the Parla Sapat unit directly below the MMT which Khan *et al.* (1995) interpreted as indicating an ESE thrust direction. Greco *et al.* (1989) also suggested an ESE or SE thrust direction on the basis of large scale NE–SW-trending folds that they interpreted as forming during final emplacement of Kohistan (Fig. 4). The folds deform foliation on the Indian plate and developed under (retrograde) greenschist facies metamorphism. Greco *et al.* (1989) also noted a strong NE-plunging stretching lineation in Indian plate rocks which they interpreted as indicating an earlier SW-directed thrust movement. Chamberlain *et al.* (1991) suggested that the SW-directed thrusting was associated with peak amphibolite facies metamorphism and with foliation development on the Indian plate, and was followed by later SE-directed emplacement of Kohistan. On the basis of radiometric ages, they concluded that SW-directed thrusting took place before 50 or 40 Ma and that final SE-directed emplacement of Kohistan took place between 40 and 25 Ma. South of the MMT, the Batal Fault records the SW to SE rotation of vergence (Bossart *et al.* 1988; Greco & Spencer 1993).

North of the MMT, in the Kohistan arc, Treloar *et al.* (1990) identified the Kamila–Jal Shear Zone which shows SW-directed transport (Figs 1, 2, 3). They indicated that the shear zone is older than 83 Ma and, therefore, probably older than SW-directed structures on the Indian plate. However, it remains possible that some of the SW-directed structures on the Indian plate are considerably older than 50 Ma and that a connection exists with development of the Kamila–Jal Shear Zone. Regardless of this, the relationships imply that SW-directed transport was widespread in both the Indian plate and in the southern part of the Kohistan arc in the Late Cretaceous and early Paleogene.

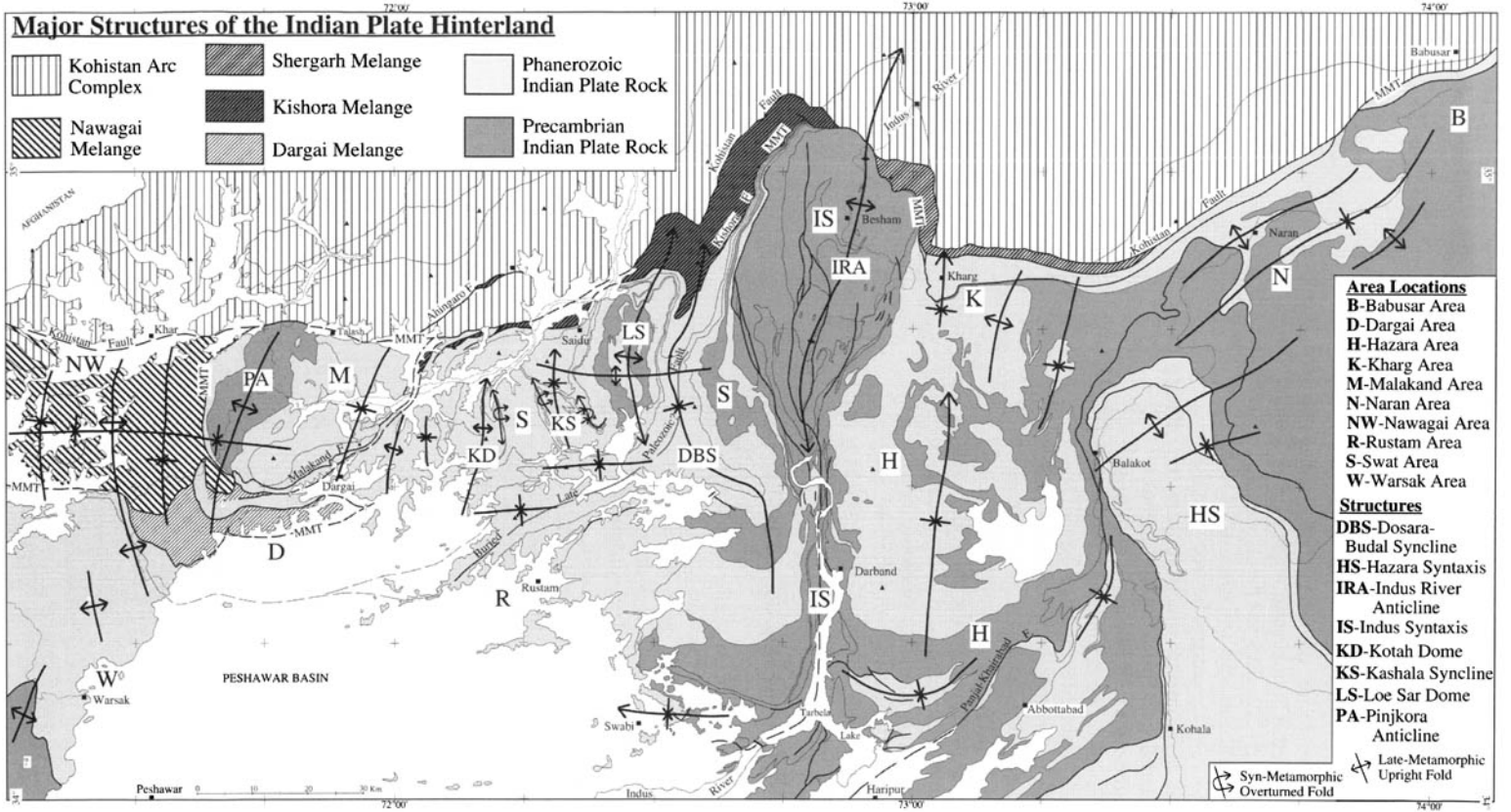

Fig. 4. Structural map that shows area locations and major folds along the MMT Zone between Nawagai and Babusar. N–S-trending folds deform the mélange units but, with the exception of the Indus River anticline, do not deform the Kohistan Fault. Based on Calkins *et al.* (1975), Greco & Spencer (1993), DiPietro *et al.* (1999) and unpublished mapping.

The age of the MMT in this area and its overall southward displacement history are consistent with the original definition of the MMT. In addition, the fault marks a sharp boundary between mafic–ultramafic rock of the Kohistan arc complex and metamorphic rock of the Indian plate. However, the displacement history appears to be longer and more complex than that originally envisioned. Chamberlain *et al.* (1991) pointed out that early SW-directed displacement, prograde metamorphism and foliation development on the Indian plate cannot be tied directly to emplacement of Kohistan which appears to have been emplaced in a southeasterly direction after peak metamorphism. It is important to note that the MMT in this area is not associated with a well-developed ophiolite mélange zone (Jan *et al.* 1993). Khan *et al.* (1995) indicated that ophiolite slivers (greenstone and talc–carbonate) in the Parla Sapat unit were incorporated prior to mylonite development along the MMT. The slivers could have been emplaced during early SW-directed thrusting of a large ophiolite body that was subsequently overridden by ESE or SE emplacement of the Kohistan arc. Greenstone lenses within the Sapat complex may represent imbricated slivers of ophiolite that were brought up along the MMT during final emplacement of Kohistan.

Burg *et al.* (1996) described shallow northerly plunging, tight to open ('cascade') folds with shallow-dipping axial planes near Naran that deform the regional foliation in both the hanging wall and footwall of the MMT. They showed that the origin of these folds is consistent with a combination of horizontal and vertical shortening and suggested that this stress regime was produced by NW-directed backsliding of the Kohistan arc (normal faulting) along the MMT. They suggested a minimum of 7 km of backsliding probably between 25 and 20 Ma during greenschist facies (retrograde) metamorphism. Khan *et al.* (1995) described similar folds, but indicated that these folds also deform the MMT. In addition, extensive backsliding may not be consistent with the lowest part of the Kohistan arc (Sapat ultramafic rock) exposed in the hanging wall block. A possible alternative to backsliding is that the northerly vergent folds are the result of NW–SE-directed compression and horizontal flattening of inclined layers after final emplacement of the Kohistan arc, and possibly during development of the Diamir Shear Zone and Gashit Fold. In this interpretation, horizontal and vertical shortening is distributed across a wide zone in both the hanging wall and footwall of the MMT without significant displacement along the MMT itself. Regardless of whether or not significant backsliding has occurred, nearly all workers agree that displacement along the MMT ended in this area by 15 Ma (Chamberlain *et al.* 1991).

Kharg area

The Kharg area is the only area east of the Indus syntaxis in which a thick zone of sheared ophiolite mélange is exposed along the MMT (Figs 3, 5, 6). The mélange is part of the Indus Suture mélange group and consists dominantly of greenstone with subordinate serpentinite, metachert, blueschist and phyllitic rock (Majid & Shah 1985). The base of the unit is a fault contact with graphitic schist and dark grey marble of the Banna Formation. This is the fault that is commonly referred to as the MMT (Treloar *et al.* 1989*a*, *b*, *c*; DiPietro *et al.* 1999). We also apply the local name of Shergarh Fault to this contact to distinguish it from the MMT at Naran. The mélange zone that is carried by the Shergarh Fault is referred to as the Shergarh mélange.

The Shergarh Fault Zone is marked by interlayers of Banna graphitic schist and greenstone with sharp contacts that are parallel to the regional foliation. Strong mylonite and lineation fabrics are absent along the fault zone suggesting that displacement was pre- or syn-metamorphic in the sense that peak metamorphism outlasted the shear deformation associated with mylonite formation and thereby annealed and destroyed most of the mylonite fabrics. This implies that the Shergarh Fault is older than the MMT at Naran. Weak stretching lineations in the Shergarh mélange plunge gently *c.* N30E, suggesting a SW transport direction. Mineral lineations in Indian plate rock below the Indus mélange plunge generally north or NE (Fernandez 1983; Williams 1989). Mapping northwest of Kharg indicates that the Shergarh Fault bends sharply northward and then northwestward where it truncates stratigraphy in the underlying Indian plate. As the Shergarh Fault is approached, NE-striking foliation in the Indian plate bends

Fig. 5. Geological map of the Kharg–Indus syntaxis–Swat–Malakand–Nawagai region. Based on unpublished mapping supplemented with Calkins *et al.* (1975), Badshah (1979), Aslam *et al.* (1982), Rafiq (1984), Hussain *et al.* (1984, 1989), Ahmad & Lawrence (1992), DiPietro & Ahmad (1995) and DiPietro *et al.* (1999). See Fig. 6 for an explanation of rock units.

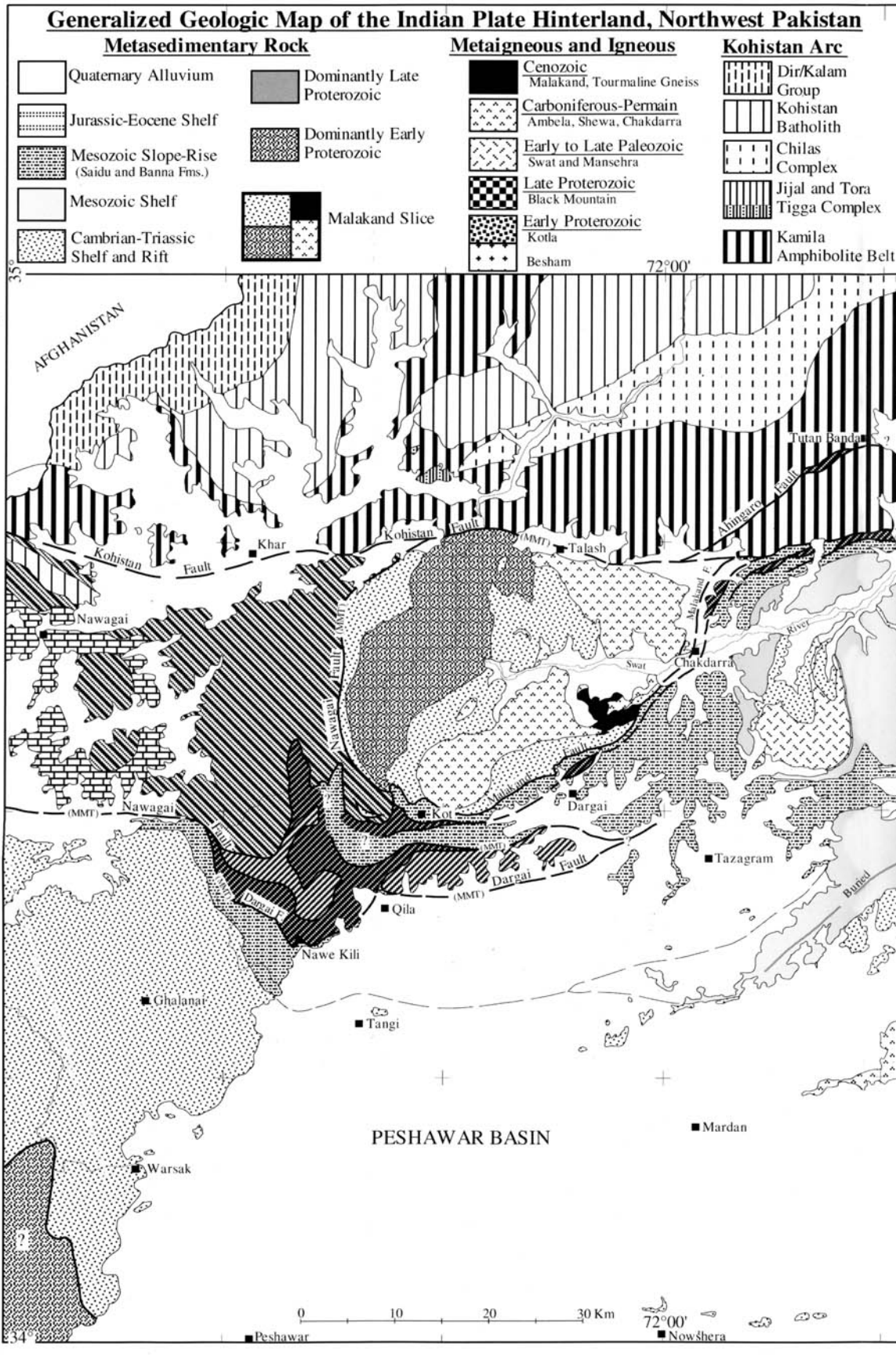
Generalized Geologic Map of the Indian Plate Hinterland, Northwest Pakistan
Metasedimentary Rock
Quaternary Alluvium
Jurassic-Eocene Shelf
Mesozoic Slope-Rise
(Saidu and Banna Fms.)
Mesozoic Shelf
Cambrian-Triassic
Shelf and Rift
Dominantly Late
Proterozoic
Dominantly Early
Proterozoic
Malakand Slice
Metaigneous and Igneous
Cenozoic
Malakand, Tourmaline Gneiss
Carboniferous-Permain
Ambela, Shewa, Chakdarra
Early to Late Paleozoic
Swat and Mansehra
Late Proterozoic
Black Mountain
Early Proterozoic
Kotla
Besham
Kohistan Arc
Dir/Kalam
Group
Kohistan
Batholith
Chilas
Complex
Jijal and Tora
Tigga Complex
Kamila
Amphibolite Belt
35°
72°00'
AFGHANISTAN
Tutan Banda
Ahmgarro Fault
Kohistan Fault
Khar
(MMT)
Talash
Nawagai
Main Mantle Thrust
Malakand F.
River
Swat
Chakdarra
Nawagai
(MMT)
Kot
Dargai
Tazagram
Dargai Fault
Qila
Nawe Kili
Ghalanai
Tangi
PESHAWAR BASIN
Mardan
Warsak
0 10 20 30 Km
34°
Peshawar
72°00'
Nowshera


Indus Suture Zone
Nawagai Melange
Nawagai Marble
Shergarh, Kishora, Dargai Melange
(Includes Ahingaro serpentinite melange)
Dargai Mafic/Ultramafic Complex
Compilation by J. A. DiPietro, 1999
73°00'
35°00'
34°
Kohistan
Puran
Indus
River
Jijal
Fault
MMT
Shergarh
Alpurai
Besham
Saidu
Kishora
Swat
River
Chakesar
Fault
Indus R.
Khar
Banna
Oghi
Daggar
Paleozoic?
Late
Rustam
Darband
Mansehra
Darband Fault
Tarbela Lake
Abbottabad
Swabi
Panjal-Khairabad Fault
Haripur
Indus
River

abruptly northward into conformity with the orientation of the fault zone. This relationship is also observed with the Kishora Fault along the NW flank of the Indus syntaxis (Fig. 5). The significance will be discussed in the next section in relation to the Kishora Fault.

The top of the Indus mélange unit is a fault contact with the Kohistan arc complex. Because this fault occupies the same structural position as the Kohistan Fault in Swat, we extend the nomenclature of Kazmi *et al.* (1984) and refer to this fault as the Kohistan Fault. The hanging wall of the Kohistan Fault consists dominantly of Kamila amphibolite and gabbro. Local lenses of ultramafic rock suggest that Sapat or Jijal-like complexes may also be present (possibly as fault slices), but geological mapping is incomplete. The Kohistan Fault is well exposed in the area north of Kharg where it dips moderately to steeply N or NE. The fault is associated with mylonitic, cataclastic and brittle deformation fabrics across a zone less than 30 m wide, but is without strong lineation development. The fault locally truncates foliation in the underlying greenstone. Fault strands associated with the Kohistan Fault cut into the Shergarh mélange, as suggested by the presence of fractured blocks of Kamila amphibolite within the mélange.

Although the transport direction along the Kohistan Fault is uncertain in this area, the field relationships imply significant late-metamorphic displacement and it is probable that this fault was active at about the same time as the MMT at Naran. Figures 1 and 3 correlate the Kohistan Fault at Kharg with the MMT at Naran and Babusar and, thus, extend the nomenclature of Kazmi *et al.* (1984) to the area east of Babusar where the Kohistan Fault merges with the active Raikot Fault. The absence of ophiolitic mélange at Naran, and in the Indus syntaxis at Jijal, indicates that the Shergarh mélange is lens-shaped and that the Shergarh Fault must truncate below the Kohistan Fault (Fig. 3).

Field relationships suggest a correlation between the Banna Formation and the Parla Sapat unit. The base of the Banna Formation is a sharp contact, parallel to regional foliation, that is not intensely sheared or lineated relative to surrounding rock. It has been interpreted as a fault (the Banna Fault of Treloar *et al.* 1989*a*, *b*, *c*) which would imply that the base of the Parla Sapat unit is also a fault. A thin layer of garnetiferous schist correlated with the Tanawal Formation underlies the Banna Formation, followed by a wide area of Cambrian Mansehra augen gneiss (Fig. 3). These rocks cannot confidently be correlated with rock units mapped at Naran, and we suspect truncation of map units along both the Banna and the Batal Faults as shown in Fig. 3. Vince & Treloar (1996) interpreted the Banna, Shergarh and Kohistan Faults as originally south-vergent thrust faults that were later reactivated as normal faults. They suggested that extension occurred under low-grade metamorphic and brittle conditions beginning sometime before 22 Ma and ending before 16 Ma. DiPietro *et al.* (1999) indicated that brittle deformation does not characterize the Banna Fault and that this fault, and possibly the Shergarh Fault, are folded by north–south-trending late-metamorphic folds (Fig. 4). As with the Naran area, we suggest an alternative to backsliding, in which the extensional deformation and north-vergent folds are distributed across the MMT Zone rather than associated with major normal faulting. We interpret the Banna and Shergarh Faults as dominantly syn-metamorphic, south-west-vergent thrust faults. Both faults appear to predate the last brittle movement along the Kohistan Fault.

Indus syntaxis–Swat region

The best known location of the MMT is in the Indus valley at Jijal (Figs 3, 5). Here, Indus mélange is absent and the MMT separates Precambrian gneiss of the Indian plate (Besham complex) from ultramafic rock of the Kohistan arc (Jijal complex). Lawrence & Ghauri (1983*b*) describe the MMT as a planar fault that strikes N38° W and dips 34° NE. The base of the Jijal complex is a fault breccia with serpentinite matrix. The breccia overlies mylonitic ortho- and paragneisses of the Besham complex which are folded into NNE-trending, ESE-vergent folds. Lawrence & Ghauri (1983*b*) interpreted these features as indicating an early period of ductile movement, followed later by dominantly brittle movement. The folds that deform the mylonitic fabric in the Besham complex suggest that late movement was SE or ESE-directed. The characteristics suggest that the fault was active at about the same time as the Kohistan Fault in the Kharg–Naran–Babusar area. The implication is that both the Shergarh and Kishora Faults are absent and that the MMT at Jijal is represented by the Kohistan Fault. From Jijal, the Kohistan Fault extends northwestward, truncating the Jijal complex, and then southwestward into the Swat valley where the Kamila Amphibolite Belt consistently forms the hanging wall block. The fault has not been studied in detail in this area and, further southwest, the fault disappears below Swat River valley alluvium.

A thick zone of sheared ophiolitic mélange appears from below the Kohistan Fault along the western flank of the Indus syntaxis and trends SSW to where it is folded by the Dosara–Budal syncline (Fig. 4). It then continues westward across the Swat region to Chakdarra where it thins and pinches out along strike within the Saidu Formation (Figs 5, 6). The mélange zone was divided into the Mingora, Charbagh and Shangla mélange units by Kazmi *et al.* (1984), who also named the basal fault of the mélange as the Kishora Fault. We refer to the entire mélange slice between the Kishora and Kohistan faults as the Kishora mélange. Both the Kishora and Kohistan faults in Swat have been referred to as the MMT.

The Kishora Fault shows many of the same characteristics as the Shergarh Fault. Whereas graphitic phyllite and marble of the Banna Formation forms a continuous belt below the Shergarh Fault, similar rock of the Mesozoic Saidu Formation forms a continuous belt below the Kishora Fault (Figs 3, 5, 6). There is, however, no evidence for a fault (equivalent to the Banna Fault) at the base of the Saidu Formation (Martin *et al.* 1962; Kazmi *et al.* 1984, 1986; Lawrence *et al.* 1989; DiPietro *et al.* 1993, 1999). As with the Shergarh mélange, greenstone forms the major rock unit in the Kishora mélange particularly north of Alpurai. However, blueschist and serpentinite are abundant west of Alpurai, along with phyllitic and meta-argillaceous rock. The Kishora Fault is well exposed and, in many areas, it is a sharp contact between Saidu phyllite and ophiolitic talc–carbonate schist, greenstone or greenish phyllite. Locally, these rocks are interlayered with Saidu phyllite across a wide (200 m) zone. Contacts between the rocks are parallel to regional foliation and do not show strong mylonite or lineation fabrics relative to surrounding rock. Fault attitude is variable due to later folding. The fault is interpreted as a syn-metamorphic fault that was later deformed by late-metamorphic, N–S-trending folds, such as the Dosara–Budal syncline (Lawrence *et al.* 1989; DiPietro & Lawrence 1991; DiPietro *et al.* 1999). Stretching lineation data from the Kishora mélange, and from granitic rock in the underlying Indian plate, are scattered, but a majority plot in either the NE or the SW quadrant (Fig. 7a, b, c). This is consistent with SW-directed emplacement of the Kishora mélange during metamorphism in the underlying Indian plate.

The relationships suggest that the Kishora Fault was active at about the same time as the Shergarh Fault and we suggest a correlation between the two. Although the two faults may correlate, the mélange units themselves are imbricated and sheared and, therefore, may have variable tectonic histories. For example, the northern part of the Kishora mélange (the Shangla mélange) may be more closely associated with the Kohistan Fault than with the Kishora Fault (Lawrence *et al.* 1989). This implies that structures in the mélange units span the geological history between emplacement of mélange along the Kishora and Shergarh faults and final emplacement of the Kohistan arc along the Kohistan Fault. Late to post-metamorphic normal faults were noted by King (1964), Kazmi *et al.* (1984, 1986), Lawrence *et al.* (1989) and DiPietro *et al.* (1999) in both the mélange and Indian plate, but the small displacement (typically less than a few metres) and lack of stratigraphic disruption indicated to them that they are regionally insignificant. Anczkiewicz *et al.* (1998), by contrast, suggested regional-scale normal faulting across the Indian plate and mélange zone.

Although the structural relationships between the Kishora and Shergarh faults are similar, the continuity is disrupted by the intervening Indus syntaxis. The northward bend of the MMT Zone in this area is the result of folding across the N–S trending Indus River anticline. This is the largest of a series of N–S-trending folds (including the Dosara–Budal syncline) that extend westward into the Swat region and eastward into the Kharg area where they deform the Kishora, Banna and probably the Shergarh faults (Fig. 4; Lawrence *et al.* 1989; DiPietro & Lawrence 1991; DiPietro *et al.* 1999). With the exception of the Indus River anticline, these folds do not deform the Kohistan Fault. The folds, therefore, were active after final movement along the Kishora, Banna and Shergarh faults, but before final emplacement of the Kohistan arc along the Kohistan Fault. The Indus River anticline was apparently active during and after final emplacement of the Kohistan arc, and thus has a longer history than folds to the east and west. The young age of the Indus River anticline and the folding of the Kohistan Fault probably results from fold amplification related to Neogene and younger displacement along N–S-trending brittle faults that cut the Indus River anticline (Fig. 5). We suggest that the truncation of Indus mélange in this area is the result of the Kohistan Fault cutting across the rock units and into the core of the developing Indus River anticline during final ESE–SE emplacement of the Kohistan arc.

The Indus syntaxis is also the only area where the Kishora and Shergarh faults cut across and truncate stratigraphy in the Indian plate. Elsewhere, the faults are consistently underlain by

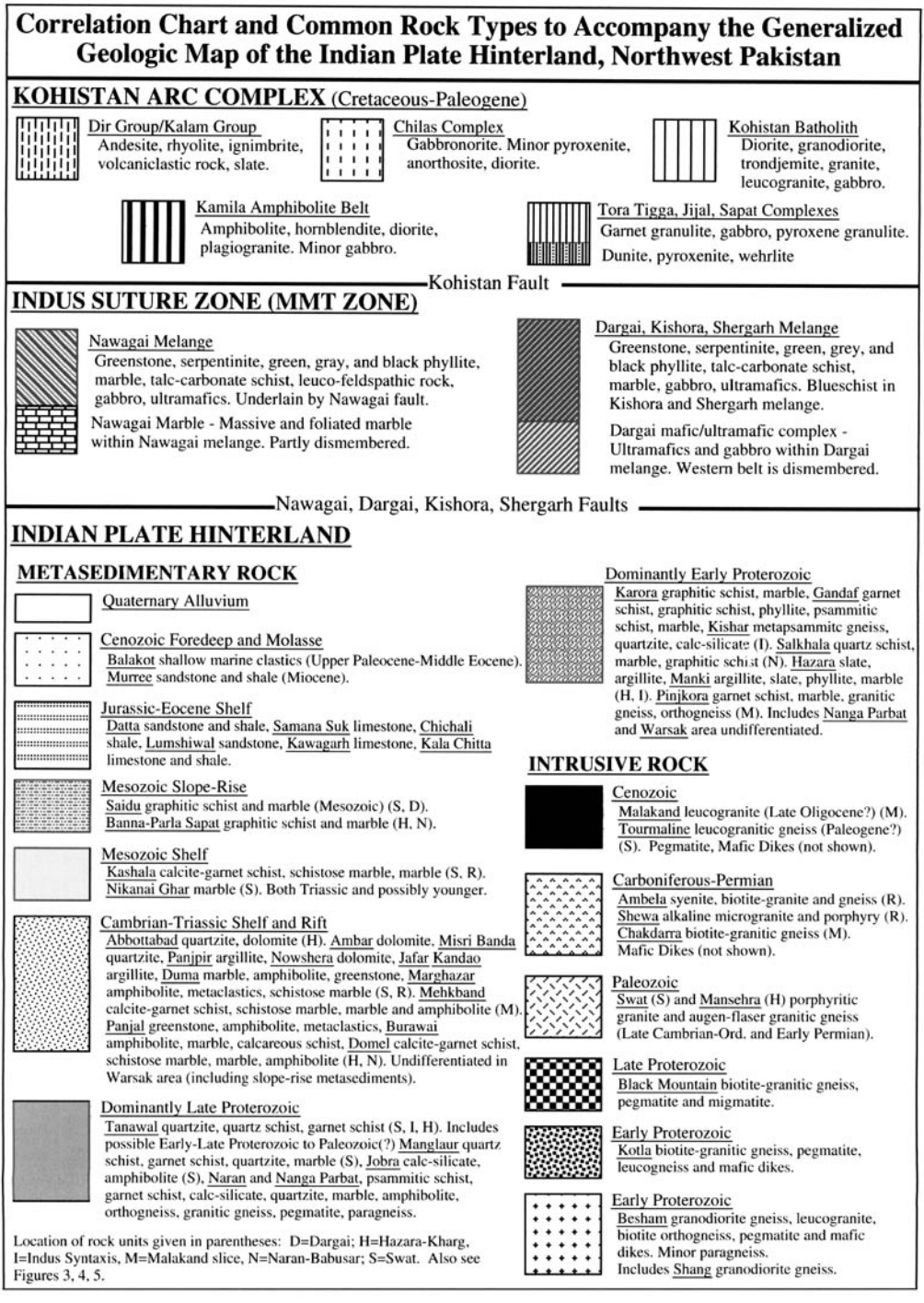

Fig. 6. Explanation of rock units to accompany Figs 3 and 5.

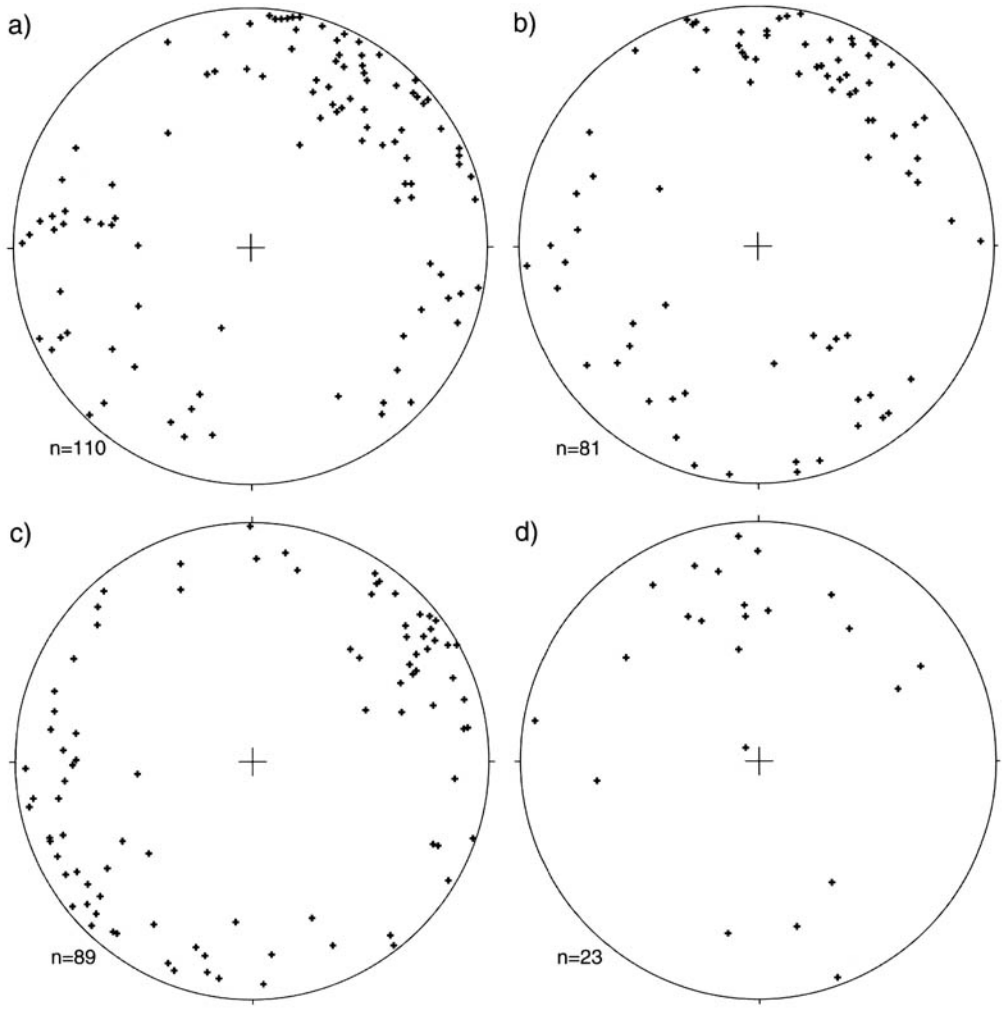

Fig. 7. Lower hemisphere equal-area projections of stretching lineation data from the Swat–Malakand–Nawagai region: (**a**) Kishora mélange (from Anczkiewicz *et al.* 1998); (**b**) Swat granitic gneiss within the Loe Sar dome (from DiPietro & Lawrence 1991); (**c**) Swat granitic gneiss within the Kotah dome (from King 1964 – see Figs 4 and 5 for location of the Loe Sar and Kotah domes); (**d**) Malakand and Nawagai slices.

the Saidu and Banna formations respectively and are parallel with regional foliation. The cross-cutting relationship was observed in the NW corner of the syntaxis northeast of Alpurai. Foliation in the Saidu Formation is severely bent into parallelism with the Kishora Fault within about 5 m of the contact, but the rocks are not strongly lineated and there is little evidence for brittle deformation. One possibility is that the Indus syntaxis area was a basement high that existed before the Himalayan orogeny. Phanerozoic stratigraphy would have been relatively thin or absent across the basement high and, during Himalayan metamorphism, the Kishora–Shergarh Fault could have overridden the area and truncated the stratigraphy. Continued recrystallization following fault activity preserved the original truncation but destroyed most of the fault zone fabrics. A second possibility is that the truncation results from reactivation associated with the younger Kohistan Fault.

Western Swat–Malakand–Nawagai region

The Kohistan Fault is well exposed from Saidu westward to the Afghan border, where it trends roughly E–W and dips vertical to steeply north.

In this area, it is an imbricate zone of mixed rock, locally more than 100 m wide, that is characterized by brittle and cataclastic deformation which locally overprints mylonite fabrics. The imbricate zone includes Kamila amphibolite, which is fractured and locally reduced to a scaly phyllitic matrix; fractured blocks of greenstone, talc–carbonate schist, and serpentinite derived presumably from the Kishora and Nawagai mélanges; and exotic blocks that include limestone and metagreywacke. The imbricate zone is clearly associated with displacement along the Kohistan Fault and is considered to be younger than, and separate from, the Kishora and Nawagai mélanges. With the exception of this narrow ophiolite-bearing imbricate zone, mélange is absent along the northern flank of the Malakand slice. It is possible that the imbricate zone is structurally equivalent with the volcanic mélange reported along the Kohistan Fault at Babusar (Chamberlain *et al.* 1991).

Significant displacement along the Kohistan Fault in this area was post-metamorphic. The fault zone truncates foliation in the Kamila Amphibolite Belt and cuts directly across rock units and foliation in both the Indian plate and the mélange units (Fig. 5). It also truncates N–S-trending late-metamorphic folds that deform the Indian plate and the mélange units (Fig. 4). Kinematic indicators are generally absent along the Kohistan Fault, but there is clear evidence for right-lateral strike-slip motion along its entire trace west of Saidu where north-striking foliation in the Indian plate, and in the mélange, is abruptly deflected to the east and truncated at the Kohistan imbricate zone. This is also evident from the map pattern in which all of the rock units are deflected to the east due to drag (Fig. 5). Right-lateral movement along the Kohistan Fault is consistent with ESE to SE-directed final emplacement inferred for the Kohistan arc in the Indus syntaxis and Naran–Babusar area. The Ahingaro Fault Zone shows dominantly brittle deformation and is interpreted as a splay off the Kohistan Fault, although its displacement history, and extension to the east, are uncertain (DiPietro & Ahmad 1995).

Several tectonic slices are present south of the Kohistan Fault including the Malakand slice and the Dargai and Nawagai mélange slices. The Malakand slice is either an allochthonous block of Indian plate rock separated from the underlying Saidu Formation by the Malakand Fault, or is part of a large overturned fold. It is shown as an allochthonous slice in Fig. 5 based on a lack of stratigraphic correlation between rock units in the Malakand slice and adjacent rock units in Swat. Details regarding the stratigraphy and structural position of the Malakand slice will await future publications.

The Malakand Fault is well exposed between Chakdarra and Kot where it dips moderately to steeply N or NW. In some areas a knife-sharp contact separates Mekhband marble, of the Malakand slice, from underlying Saidu phyllite. In other areas the rocks are interlayered across a zone more than 100 m wide. Contacts, in all areas, are parallel to regional foliation and are not intensely sheared relative to surrounding rock. Strong mylonite and lineation fabrics are absent and the contact is deformed by late-metamorphic N–S-trending folds. The relationships suggest syn-metamorphic displacement followed by continued metamorphic recrystallization. The direction of slip is unknown, but weak N- to NW-orientated stretching lineations suggest that it could have been emplaced in a S to SE direction (Fig. 7d). Southeastward transport is in contrast to the generally southwestward transport suggested for the Kishora mélange, but is consistent with final southeastward emplacement of the Kohistan arc.

The Malakand slice is flanked on its south and west sides by a large ophiolite mélange complex that extends westward into the Jalalabad Basin where it is presumably truncated by the Kunar Fault (Fig. 1). This area has not been mapped in detail; therefore, the interpretations given below are preliminary pending further investigation. On the basis of previous work (Badshah 1979; Aslam *et al.* 1982; Hussain *et al.* 1984, 1989; Rafiq 1984) and our own reconnaissance, we suggest that there are at least two mélange units; the Dargai mélange, which structurally underlies the Malakand slice, and the Nawagai mélange, which overlies the Malakand slice. Both mélange units contain abundant greenstone interlayered with serpentinite, talc–carbonate schist, ultramafic rock and variable phyllitic rock, some of which resemble the Saidu phyllite. The Dargai mélange is underlain by the Dargai Fault and includes the Dargai mafic–ultramafic complex. Figure 5 shows the complex as two separate bodies within the Dargai mélange: an eastern one that is partly surrounded by the Saidu Formation, and a western one that is dismembered within the Dargai mélange. The Nawagai mélange is underlain by the Nawagai Fault and includes the Nawagai marble (Tahirkheli 1979*a*) which is a large, partly dismembered body of massive to strongly foliated, nearly pure calcite marble that crops out primarily near the Afghan border (Fig. 5). Smaller bodies of marble are dispersed throughout the Nawagai mélange. The age of these marble bodies, and whether they represent part of the Indian plate or an exotic block, is

unknown, but they are clearly interlayered with ophiolite mélange.

The Dargai Fault is exposed at Qila where the Dargai mafic–ultramafic complex is in sharp contact with the underlying Saidu phyllite (Fig. 5). Ultramafic rock is massive away from the contact, but develops a foliation near the contact that is parallel to foliation in the Saidu Formation. A strong lineation is not developed. The Dargai Fault is also exposed at Nawe Kili, where blocks of greenstone and talc–carbonate schist appear in the upper part of the Saidu Formation and progressively become more abundant over a distance of about 100 m. Dips are generally to the N and NW but the contact is folded. The fault is interpreted as a syn-metamorphic fault although foliation in some of the ophiolite lenses is truncated by foliation in the enclosing Saidu phyllite and contacts are locally sheared or brecciated, suggesting that the mélange has been modified by later deformation. The fault at Nawe Kili may not be the same fault as at Qila, but both are shown as the Dargai Fault because both represent the basal fault of the Dargai mélange. The Dargai Fault has not been studied in detail west of Nawe Kili. The rock units between Qila and Kot form a wide imbricate zone, undoubtedly modified by folding and late brittle deformation that, in addition to typical mélange and Saidu phyllite, also contains abundant amphibolite, garnet schist and marble that correlate with rock in the Malakand slice. For this reason, it is uncertain if the Dargai Fault at Qila wraps around to the north side of the Dargai mafic–ultramafic complex or, if this is an imbricate fault that places the Saidu Formation structurally above the Dargai mélange. It is shown as a separate imbricate fault in Fig. 5.

The Nawagai Fault is exposed along the western flank of the Malakand slice where it consistently dips westward, structurally above the Malakand slice. Again, there is little evidence for lineation development along the fault. The fault can be traced southward to Kot where it occupies the higher elevations and appears to truncate the Malakand Fault, the Saidu Formation, and a layer of mélange within the Saidu Formation. Further west, the Nawagai Fault truncates the Dargai mélange around a series of folds, and then continues to the Afghan border where marble forms the hanging wall block structurally above the Saidu Formation. The fault is interpreted as a S to SE-directed, syn-metamorphic fault roughly contemporaneous with, but younger than, the Malakand Fault. It is suggested that syn- and post-emplacement imbrication and folding has significantly disrupted both the Dargai and Nawagai mélanges as well as the fault contact that separates them. It is possible that the Nawagai Fault actually represents a series of faults that collectively form the base of the Nawagai mélange.

The Kishora mélange is present west of Saidu as a thin belt that crops out just south of the Kohistan Fault. The mélange is well developed near Saidu with thick layers of greenstone, marble, talc–carbonate schist, green and grey phyllite, and an unusual, coarse-grained, pegmatite-like, talc–quartz–feldspar rock that locally grades to talc–carbonate. At the Kishora Fault, the rocks are interlayered with Saidu phyllite across a zone up to 200 m wide with contacts that are parallel with regional foliation. Between Saidu and Chakdarra, the north-dipping Kishora mélange pinches out along strike such that mélange, and the Kishora Fault, are lost within a monotonous sequence of Saidu phyllite and marble. At this point, a distinctive belt of mélange is absent and Saidu phyllite (with a few small, discontinuous lenses of mélange) is in direct contact with the Kohistan Fault Zone (Fig. 5).

Additional lenses of mélange are present in the Saidu Formation west of the pinch-out that are not continuous with the main belt of Kishora mélange (Fig. 5). The mélange lenses are arranged in a N- to NW-dipping, right-stepping, en-echelon pattern that is truncated by the Kohistan Fault. They are structurally above the pinched-out lens of Kishora mélange but structurally below the Malakand Fault. Just north of Chakdarra, the mélange lenses, and the enclosing Saidu Formation, are bent sharply southward and the two mélange lenses pinch out in the Saidu Formation. Between Chakdarra and Kot, the Saidu Formation strikes SW and W and dips steeply north such that it is consistently structurally below the Malakand slice. Thus, the Malakand slice occupies a structural position at the top of the Saidu Formation that was formerly occupied by the Kishora mélange. Several additional mélange lenses appear in the Saidu Formation between Chakdarra and Kot, including a large body south of Kot and another just north of Dargai (Fig. 5). These occur along strike of each other such that they define a possible fault zone directly below the Malakand Fault. The inferred fault is shown with a dashed line in Fig. 5. Contacts are without strong shear or lineation fabric suggesting syn-metamorphic emplacement. The location of the fault suggests that it may be an imbricate fault more closely related to the Malakand Fault than either the Kishora or Dargai faults.

Both the Dargai mélange and the Kishora mélange appear to be interlayered with and

structurally above the Saidu Formation but structurally below the Malakand slice. On the basis of similar structural position, we tentatively correlate the Dargai, Kishora and, by extension, the Shergarh mélange slices. It is possible that the Nawagai mélange was part of the same mélange sequence, but has since been imbricated and emplaced structurally above the Malakand slice.

The fate of both the Dargai and the Kishora faults is uncertain. Both could die out in the Saidu Formation. The Kishora Fault could have jumped to the top of the Saidu Formation where it is presently cut out or buried by the Malakand Fault. The Dargai Fault could wrap around to the north side of the Dargai mélange. The Kishora Fault could continue along strike through the Saidu Formation and connect directly with the Dargai Fault at the base of the Dargai mafic–ultramafic complex at Qila. Alternatively, the Kishora Fault could have been continuous with the Dargai Fault at Qila, but was subsequently overridden by imbricate faults within the Saidu Formation that are associated with emplacement of the Malakand slice. At present, we tentatively favour the last possibility. Several of these possibilities imply that part of the Saidu Formation is allochthonous and/or that part of the mélange represents sheared olistostromal blocks within the Saidu Formation.

Discussion of deformational events

Structures along the MMT Zone span the geological interval from Late Cretaceous to the present. Deformation began with Late Cretaceous, SW-directed displacement along the Kamila–Jal Shear Zone followed by syn-metamorphic, SW-directed thrusting and mélange emplacement along the Batal, Banna, Shergarh, Kishora and Dargai faults. This was followed by SSE-directed(?) syn-metamorphic emplacement of the Malakand and Nawagai slices and subsequent imbrication. SSE-directed emplacement of these slices implies that rotation from a southwestward to a southeastward transport direction occurred during metamorphism in the area west of the Indus syntaxis and could partly explain the scattered stretching lineation data (Fig. 7). All of these faults were then deformed by N–S-trending folds before about 50 or 40 Ma (DiPietro *et al.* 1999). This was followed by late to post-metamorphic (Oligocene–Early Miocene) ESE to SE emplacement of the Kohistan arc along the Kohistan Fault. This fault completely cuts out or buries the previously emplaced Indus mélange in the Malakand, Indus syntaxis and Naran–Babusar areas (Fig. 8). Final emplacement of the Kohistan arc is associated with right-lateral strike-slip faulting west of Saidu; additional folding and imbrication in the mélange zones; development of the Ahingaro Fault Zone; and development of NE–SW-trending folds in the Naran–Babusar region. Backsliding of Kohistan, if present, could have occurred immediately following final emplacement. Miocene and younger deformation included the development of N–S-trending brittle faults in the Indus syntaxis region; the continued development of the Indus River anticline; the reactivation of the Kohistan Fault as the Raikot Fault; the folding of the MMT

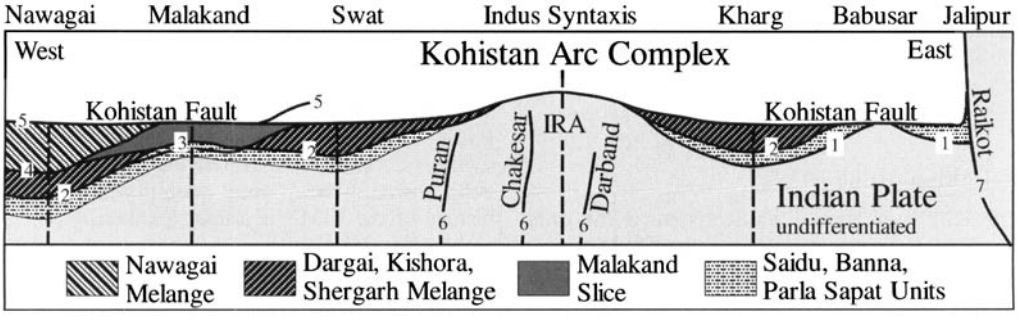

Fig. 8. Schematic west to east cross-section along the strike of the MMT. All rock units are truncated by the Kohistan Fault which merges with the active Raikot Fault in the east. Numbers indicate inferred relative order of last movement along each fault. 1, Banna–Parla Sapat Fault; 2, Dargai–Kishora–Shergarh Fault; 3, Malakand Fault; 4, Nawagai Fault; 5, Kohistan and Ahingaro Faults; 6, Puran, Chakesar and Darband faults; 7, Raikot Fault. Faults numbered 1 and 2 are closely related and presumably roughly coeval, as are faults numbered 3 and 4. The Puran, Chakesar and Darband faults may have initiated at about the same time as the Raikot Fault but are no longer active. Faults numbered 1–4 are deformed by N–S-trending folds (dashed lines) that include the Indus River anticline (IRA). The Indus River anticline is the only N–S-trending fold that clearly deforms the Kohistan Fault.

around the northern flank of the Nanga Parbat–Haramosh massif; and the rotation and local brittle reactivation of the MMT along the eastern flank of the massif. Recent deformation is largely restricted to the Nanga Parbat region.

Oligocene to Early Miocene displacement along the Kohistan Fault predates the development of the Nanga Parbat–Haramosh massif. It is possible, therefore, that the Kohistan Fault originally extended further east along the base of the Ladakh arc prior to reactivation along the Raikot Fault and uplift of the massif. Although this would suggest that some of the deformation along the northern and eastern flanks of the massif is related to the Kohistan Fault, it does not necessarily imply that the mylonite zone that is presently developed along the margins of the massif is directly related to the Kohistan Fault. The mylonite fabric could be as young as Late Miocene and therefore younger than the inferred age of the Kohistan Fault.

The brittle N–S-trending faults in the Indus syntaxis region are interpreted as developing along pre-existing Precambrian anisotropies (DiPietro *et al.* 1999; Pogue *et al.* 1999). In addition, a buried late Palaeozoic fault is believed to be present below the Mesozoic shelf west of the Indus syntaxis (Figs 5, 6; Pogue *et al.* 1992; DiPietro *et al.* 1993, 1999). These pre-existing anisotropies may, in part, be responsible for the northward deflection of the MMT and for the extreme attenuation of Indian plate rock units along the western flank of the Indus syntaxis. Note that the Puran Fault parallels the MMT in this area (Fig. 5). The Diamir–Raikot Fault may have had an origin similar to the Puran Fault, but continued to develop into a major fault. In this interpretation, the Raikot Fault follows the original trend and reactivates the Kohistan Fault, thereby extending the history of the MMT to the Holocene.

Definition of the MMT

The Kohistan–Raikot Fault system is the only through-going structure along the MMT Zone. It marks the entire southern and eastern boundaries of the Kohistan arc complex and it includes the best known location of the MMT at Jijal. It would be logical, therefore, to refer to this fault as the MMT. Restricting the definition of the MMT to the Kohistan–Raikot Fault system would, however, exclude the older Indus mélange which is part of the original definition and which is consistently referred to in the literature as part of the MMT. Indus mélange, on the other hand, is discontinuous below the Kohistan Fault and therefore, no single through-going fault could be considered to be the MMT.

We suggest that the MMT fault contact be defined, not as a single continuous fault, but as the series of faults of different age and tectonic history that collectively define the northern margin of the Indian plate in Pakistan. Used in this sense, the MMT is equivalent with the Mélange Boundary zone of Beck *et al.* (1996). In areas east of Kharg, where large ophiolite slices are absent, the MMT would be represented by the Kohistan–Raikot Fault system and by faults and mylonite zones that define the northern and eastern flanks of the Nanga Parbat–Haramosh massif (including the Subsar Fault; Fig. 2). West of Kharg, the MMT would be represented by the Shergarh Fault at Kharg, the Kohistan Fault in the Indus syntaxis, the Kishora Fault in Swat, the Kohistan Fault near Chakdarra and Talash, the Nawagai Fault along the west side of the Malakand slice, imbricate faults along the northern margin of the Dargai mélange, the Dargai Fault at Qila and Nawe Kili, and the Nawagai Fault to the Afghan border. The definition of Kazmi *et al.* (1984) could then be followed by defining an MMT 'zone' as equivalent with the Indus Suture Zone such that it represents the mélange slices and all of the faults (of any age) that separate the Indian plate from the Kohistan–Ladakh arc. West of Kharg, the MMT (Indus Suture) Zone would be bound on its north side by the Kohistan Fault, and on its south side by the Shergarh–Kishora–Dargai–Nawagai fault system.

This definition follows the original intent of the MMT and is consistent with how the term has been used in the literature. The definition allows for individual faults and tectonic slices to be named and discussed specifically, as was done in this paper, and allows for new data and for different interpretations. As more detail becomes available, individual faults, such as the Kohistan Fault, could be subdivided into smaller fault segments. The only difference between this definition and the original definition is that the history of the MMT is longer (extending to the active Raikot Fault) and more complicated. These details were not available in 1979.

This research was funded by National Science Foundation grant EAR-9316021. The people of Pakistan, particularly Sohrob, Regimen and Sher Ali, are thanked for gracious hospitality and field assistance. The manuscript was improved by the critical reviews of L. Arbaret, T. Argles, M. A. Edwards and P. J. Treloar. The authors thank T. Argles, W. S. F. Kidd, M. A. Edwards and D. A. Schneider for discussion and for information derived from maps of the Nanga Parbat area presented at the 1999 Himalayan–

Karakoram–Tibet Workshop in Kloster Ettal, Germany. We have also benefited from discussions with R. A. K. Tahirkheli, M. Q. Jan and K. R. Pogue.

References

AHMAD, I. & LAWRENCE, R. D. 1992. Structure and metamorphism of the Chakdarra area NW of Swat River, Pakistan. *Geological Bulletin, University of Peshawar*, **25**, 95–112.

ANCZKIEWICZ, R., BURG, J. P., HUSSAIN, S. S., DAWOOD, H., GHANZANFAR, M. & CHAUDHRY, M. N. 1998. Stratigraphy and structure of the Indus Suture in the Lower Swat, Pakistan, NW Himalaya. *Journal of Asian Earth Sciences*, **16**, 225–238.

ASLAM, M., KHALIL, M. A. & SADIN, M. 1982. *Geology of Gandao quadrangle, Mohmand agency, NWFP, Pakistan*. Geological Survey of Pakistan, Information Release no. **130**.

BADSHAH, M. S. 1979. Geology of Bajaur and northern part of Mohmand. *Geological Bulletin, University of Peshawar*, **11**, 163–179.

BECK, R. A., BURBANK, D. W., SERCOMBE, W. J., KHAN, A. S. & LAWRENCE, R. D. 1996. Late Cretaceous ophiolite obduction and Paleocene India-Asia collision in the westernmost Himalaya. *Geodinamica Acta*, **9**, 114–144.

BENDER, F. K. & RAZA, H. A. 1995. *Geology of Pakistan*. Beitrage zur egionalen geologie der erde, band 25, Gebruder Borntraeger, Berlin.

BOSSART, P., DIETRICH, D., GRECO, A., OTTIGER, R. & RAMSAY, J. G. 1988. The tectonic structure of the Hazara–Kashmir syntaxis, Southern Himalayas, Pakistan. *Tectonics*, **7**, 273–297.

BURG, J. P., CHAUDHRY, M. N., GHAZANFAR, M., ANCZKIEWICZ, R. & SPENCER, D. 1996. Structural evidence for back sliding of the Kohistan arc in the collisional system of northwest Pakistan. *Geology*, **24**, 739–742.

BUTLER, R. W. H., GEORGE, M., HARRIS, N. B. W., JONES, C., PRIOR, D. J., TRELOAR, P. J. & WHEELER, J. 1992. Geology of the northern part of the Nanga Parbat massif, northern Pakistan, and its implications for Himalayan tectonics. *Journal of the Geological Society, London*, **149**, 557–567.

——, PRIOR, D. J. & KNIPE, R. J. 1989. Neotectonics of the Nanga Parbat syntaxis, Pakistan, and crustal stacking in the northwest Himalayas. *Earth and Planetary Science Letters*, **94**, 329–343.

CALKINS, J. A., OFFIELD, T. W., ABDULLAH, S. K. M. & TAYYAB ALI, S. 1975. *Geology of the southern Himalaya in Hazara, Pakistan, and adjacent areas*. United States Geological Survey Professional Paper **716-C**.

CHAMBERLAIN, C. P., ZEITLER, P. K. & ERICKSON, E. 1991. Constraints on the tectonic evolution of the northwestern Himalaya from geochronologic and petrologic studies of Babusar Pass, Pakistan. *Journal of Geology*, **99**, 829–849.

CHAUDHRY, M. N., GHAZANFAR, M. & QAYYUM, M. 1986. Metamorphism at the Indo-Pak plate margin, Kaghan valley, District Mansehra, Pakistan. *Geological Bulletin, Punjab University*, **21**, 62–86.

DIPIETRO, J. A. & AHMAD, I. 1995. Tectonic setting of the Ahingaro serpentinite zone within the Kohistan arc complex, Swat, Pakistan. *Geological Bulletin, University of Peshawar*, **28**, 27–29.

—— & LAWRENCE, R. D. 1991. Himalayan structure and metamorphism south of the Main Mantle thrust, Lower Swat, Pakistan. *Journal of Metamorphic Geology*, **9**, 481–495.

——, POGUE, K. R., HUSSAIN, A. & AHMAD, I. 1999. Geologic map of the Indus Syntaxis and surrounding area, northwest Himalaya, Pakistan. *In*: MACFARLANE, A., SORKHABI, R. B. & QUADE, J. (eds) *Himalaya and Tibet: Mountain Roots to Mountain Tops*. Geological Society of America Special Paper **328**, 159–178.

——, ——, LAWRENCE, R. D., BAIG, M. S., HUSSAIN, A. & AHMAD, I. 1993. Stratigraphy south of the Main Mantle thrust, Lower Swat, Pakistan. *In*: TRELOAR, P. J. & SEARLE, M. P. (eds) *Himalayan Tectonics*. Geological Society, London, Special Publications, **74**, 207–220.

EDWARDS, M. A. 1998. *Examples of tectonic mechanisms for local contraction and exhumation of the leading edge of India; Southern Tibet and Nanga Parbat, Pakistan*. PhD thesis, State University of New York at Albany.

FERNANDEZ, A. 1983. Strain analysis of a typical granite of the Lesser Himalayan cordierite granite belt: the Mansehra pluton, northern Pakistan. *In*: SHAMS, F. A. (ed.) *Granites of the Himalayas Karakoram and Hindu Kush*. Institute of Geology, Punjab University, Lahore, 183–200.

GHAZANFAR, M., CHAUDHRY, M. N. & HUSSAIN, M. 1991. Geology and petrotectonics of southeast Kohistan, northwest Himalaya, Pakistan. *Kashmir Journal of Geology*, **8 & 9**, 67–97.

GRECO, A. & SPENCER, D. A. 1993. A section through the Indian plate, Kaghan valley, NW Himalaya, Pakistan. *In*: TRELOAR, P. J. & SEARLE, M. P. (eds) *Himalayan Tectonics*. Geological Society, London, Special Publications, **74**, 221–236.

——, MARTINOTTI, G., PAPRITZ, K., RAMSAY, J. G. & REY, R. 1989. The crystalline rocks of the Kaghan Valley (NE-Pakistan). *Eclogae Geologicae Helvetiae*, **82**, 629–653.

HUSSAIN, S. S., CHAUDHRY, M. N., DAWOOD, H. & ANWAR, J. 1989. Geology and emerald mineralization of Barang–Turghao area, Bajaur agency, Pakistan. *Kashmir Journal of Geology*, **6 & 7**, 87–102.

——, KHAN, T., DAWOOD, H. & KHAN, I. 1984. A note on the Kot–Prang Ghar mélange and associated mineral occurrences. *Geological Bulletin, University of Peshawar*, **17**, 61–68.

JAN, M. Q., KHAN, M. A. & QAZI, M. S. 1993. The Sapat mafic–ultramafic complex, Kohistan arc, north Pakistan. *In*: TRELOAR, P. J. & SEARLE, M. P. (eds) *Himalayan Tectonics*. Geological Society, London, Special Publications, **74**, 113–121.

KAZMI, A. H. & JAN, M. Q. 1997. *Geology and Tectonics of Pakistan*. Graphic publishers, Karachi, Pakistan.

——, LAWRENCE, R. D., ANWAR, J., SNEE, L. W. & HUSSAIN, S. S. 1986. Mingora emerald deposits (Pakistan): suture associated gem mineralization. *Economic Geology*, **81**, 2022–2028.

——, ——, DAWOOD, H., SNEE, L. W. & HUSSAIN, S. 1984. Geology of the Indus suture zone in the Mingora–Shangla area of Swat, N. Pakistan. *Geological Bulletin, University of Peshawar*, **17**, 127–144.

KHAN, M. A., JAN, M. Q., QAZI, M. S., KHAN, M. A., SHAH, Y. & SAJJAD, A. 1995. Geology of the drainage divide between Kohistan and Kaghan, N. Pakistan. *Geological Bulletin, University of Peshawar*, **28**, 65–77.

KING, B. H. 1964. *The structure and petrology of part of Lower Swat, West Pakistan, with special reference to the origin of the granitic gneisses*. PhD thesis, University of London.

LAWRENCE, R. D. & GHAURI, A. A. K. 1983*a*. Evidence of active faulting in Chilas district, northern Pakistan. *Geological Bulletin, University of Peshawar*, **16**, 185–186.

—— & —— 1983*b*. Observations on the structure of the Main Mantle thrust at Jijal, Kohistan, Pakistan. *Geological Bulletin, University of Peshawar*, **16**, 1–10.

——, KAZMI, A. H. & SNEE, L. W. 1989. Geological setting of the emerald deposits. *In*: KAZMI, A. H. & SNEE, L. W. (eds) *Emeralds of Pakistan: Geology, gemology & genesis*. Van Nostrand Reinhold, New York, 13–38.

MADIN, I. P., LAWRENCE, R. D. & UR-REHMAN, S. 1989. The northwestern Nanga Parbat–Haramosh massif: evidence for crustal uplift at the northwestern corner of the Indian craton. *In*: MALINCONICO, L. L. & LILLIE, R. J. (eds) *Tectonics of the western Himalayas*. Geological Society of America, Special Paper, **232**, 169–182.

MAJID, M. & SHAH, M. T. 1985. Mineralogy of the blueschist facies metagreywacke from the Shergarh Sar area, Allai Kohistan, N. Pakistan. *Geological Bulletin, University of Peshawar*, **18**, 41–52.

MARTIN, N. R., SIDDIQUI, S. F. A. & KING, B. H. 1962. A geological reconnaissance of the region between the lower Swat and Indus Rivers of Pakistan. *Geological Bulletin, Punjab University*, **2**, 1–14.

PÊCHER, A. & LE FORT, P. 1999. Late Miocene tectonic evolution of the Karakoram–Nanga Parbat contact zone (northern Pakistan). *In*: MACFARLANE, A., SORKHABI, R. B. & QUADE, J. (eds) *Himalaya and Tibet: Mountain Roots to Mountain Tops*. Geological Society of America Special Paper, **328**, 145–158.

POGNANTE, U., BENNA, P. & LE FORT, P. 1993. High pressure metamorphism in the High Himalaya Crystallines of the Stak Valley, northeastern Nanga Parbat–Haramosh massif, Pakistan Himalaya. *In*: TRELOAR, P. J. & SEARLE, M. P. (eds) *Himalayan Tectonics*. Geological Society, London, Special Publications, **74**, 161–172.

POGUE, K. R., DIPIETRO, J. A., RAHIM, S., HUGHES, S., DILLES, J. H. & LAWRENCE, R. D. 1992. Late Paleozoic rifting in northern Pakistan. *Tectonics*, **11**, 871–883.

——, HYLLAND, M. D., YEATS, R. S., KHATTAK, W. U. & HUSSAIN, A. 1999. Stratigraphic and structural framework of Himalayan foothills, northern Pakistan. *In*: MACFARLANE, A., SORKHABI, R. B. & QUADE, J. (eds) *Himalaya and Tibet: Mountain Roots to Mountain Tops*. Geological Society of America Special Paper, **328**, 257–274.

RAFIQ, M. 1984. Extension of the Skhakot–Qila ultramafic complex in the Utman Khel, Mohmand Agency, N.W.F.P., Pakistan. *Geological Bulletin, University of Peshawar*, **17**, 53–59.

SEARLE, M. P. 1991. *Geology and Tectonics of the Karakoram Mountains*. John Wiley and Sons, Chichester.

SHRODER, J. F., KHAN, M. S., LAWRENCE, R. D., MADIN, I. P. & HIGGINS, S. M. 1989. Quaternary glacial chronology and neotectonics in the Himalaya of northern Pakistan. *In*: MALINCONICO, L. L. & LILLIE, R. J. (eds) *Tectonics of the western Himalayas*. Geological Society of America, Special Paper, **232**, 275–294.

SMITH, H. A., CHAMBERLAIN, C. P. & ZEITLER, P. K. 1994. Timing and duration of Himalayan metamorphism within the Indian plate, northwest Himalaya, Pakistan. *Journal of Geology*, **102**, 493–508.

TAHIRKHELI, R. A. K. 1979*a*. Geology of Kohistan and adjoining Eurasian Indo-Pakistan continents, Pakistan. *Geological Bulletin, University of Peshawar*, **11**, 1–30.

—— 1979*b*. Geotectonic evolution of Kohistan. *Geological Bulletin, University of Peshawar*, **11**, 113–130.

—— 1996. *Tectonostratigraphic domains of northern collisional belts in Pakistan*. Geoscience Laboratory, Geological Survey of Pakistan, map.

—— & JAN, M. Q. 1979. A preliminary geological map of Kohistan and the adjoining areas, N. Pakistan. *Geological Bulletin, University of Peshawar*, **11**, fold out, scale 1:1 000 000.

——, MATTAUER, M., PROUST, F. & TAPPONIER, P. 1979. The India–Eurasia suture zone in northern Pakistan; synthesis and interpretation of recent data at plate scale. *In*: FARAH, A. & DE JONG, K. A. (eds) *Geodynamics of Pakistan*. Geological Survey of Pakistan, Quetta, 125–130.

TRELOAR, P. J. & SEARLE, M. P. (eds) 1993. *Himalayan Tectonics*. Geological Society, London, Special Publications, **74**.

——, BRODIE, K. H., COWARD, M. P., JAN, M. Q., KHAN, M. A. *et al.* 1990. The Evolution of the Kamila shear zone, Kohistan, Pakistan. *In*: SALISBURY, M. H. & FOUNTAIN, D. M. (eds) *Exposed cross-sections of the continental crust*. Kluwer Academic Publishers, Netherlands, 175–214.

——, BROUGHTON, R. D., WILLIAMS, M. P., COWARD, M. P. & WINDLEY, B. F. 1989*a*. Deformation, metamorphism and imbrication of the Indian plate, south of the Main Mantle thrust, north Pakistan. *Journal of Metamorphic Geology*, **7**, 111–125.

——, COWARD, M. P., WILLIAMS, M. P. & KHAN, M. A. 1989*b*. Basement-cover imbrication south of the Main Mantle thrust, north Pakistan. *In*: MALINCONICO, L. L. & LILLIE, R. J. (eds) *Tectonics of the western Himalayas*. Geological Society of America, Special Paper, **232,** 275–294.

——, POTTS, G. J., WHEELER, J. & REX, D. C. 1991. Structural evolution and asymmetric uplift of the Nanga Parbat syntaxis, Pakistan Himalaya. *Geologische Rundschau*, **80**, 411–428.

——, WILLIAMS, M. P. & COWARD, M. P. 1989*c*. Metamorphism and crustal stacking in the north Indian plate, north Pakistan. *Tectonophysics*, **165**, 167–184.

VILLA, I., LE FORT, P. & LEMENNICIER, Y. 1996. Late Miocene to early Pliocene tectonometamorphism and cooling in south central Karakoram and Indus–Tsangpo suture, Chomo Lungma area (NE Pakistan). *Tectonophysics*, **260**, 201–214.

VINCE, K. J. & TRELOAR, P. J. 1996. Miocene, north-vergent extensional displacements along the Main Mantle thrust, NW Himalaya, Pakistan. *Journal of the Geological Society, London*, **153**, 677–680.

WILLIAMS, M. P. 1989. The geology of the Besham area, north Pakistan: Deformation and imbrication in the footwall of the Main Mantle thrust. *Geological Bulletin, University of Peshawar*, **22**, 65–82.

YEATS, R. S. & LAWRENCE, R. D. 1984. Tectonics of the Himalayan thrust belt in northern Pakistan. *In*: HAQ, B. U. & MILLIMAN, J. D. (eds) *Marine geology and oceanography of Arabian Sea and coastal Pakistan*. Van Nostrand Reinhold, New York, 177–198.

This page intentionally left blank

Crustal shortening estimates across the north Indian continental margin, Ladakh, NW India

R. I. CORFIELD[1] & M. P. SEARLE

Department of Earth Sciences, Oxford University, Parks Road, Oxford OX1 3PR, UK (e-mail: mikes@earth.ox.ac.uk)

[1]*Present address: BP Anoco Exploration, Farburn Industrial Estate, Dyce, Aberdeen, AB21 7PB, UK*

Abstract: A structural and lithological map has been produced covering the Spontang ophiolite and the north Indian continental margin from the Indus Suture Zone in the north to the high-grade metamorphic rocks and granites of the High Himalaya in the south. Cross-section balancing techniques have been used to identify, quantify and sequentially restore three major phases of deformation (D1–3) affecting the north Indian continental margin resulting in >85 km (280%) shortening.

D1 in the late Cretaceous involved obduction of the Spontang ophiolite, associated Neo-Tethyan thrust sheets and Mesozoic continental slope deposits onto the outer passive margin. D1 was responsible for 200% shortening by internal folding and duplex formation within stratigraphic units in the outer shelf, but did not affect the innermost parts of the Indian passive margin. Restoration of later structures suggests that the allochthonous thrust sheets were emplaced a minimum of 70 km onto the continental margin.

D2 from the early Eocene to Oligocene was the main phase of deformation associated with the collision of India and Asia. Re-thrusting places the Spontang ophiolite and associated mélanges over the Maastrichtian to Lower Eocene neo-autochthonous cover which accommodated 140–160% shortening in the hanging wall. D2 progressed with the propagation of thrusting down section and towards the foreland causing crustal thickening and Barrovian metamorphism. The thick, argillaceous late Cretaceous Kangi La Formation decoupled deformation in higher and lower structural levels in outer shelf areas.

D3 backthrusting and break-backthrusting in the late Tertiary formed a pop-up structure at the northern edge of the continental margin associated with a further 190–230% shortening and inversion of structures in the Indus Suture Zone. A major anticlinal structure also initiated across the southern edge of the Indus Suture Zone. South of Spontang reactivation of D2 thrusts as late D2/D3 normal faults was associated with gravitational collapse of the High Himalaya to the south. Extensional movement on these structures was probably concomitant with shortening in the pop-up structure to the north.

A reduction in present day and restored thickness of the Tethyan Himalaya and an increase in absolute shortening from east to west probably reflects a variation in the partitioning of deformation across the whole width of the orogen. This may be associated with the indentation of India into Asia to the northwest.

One of the major tectonic questions posed by the India–Asia collision is what is the total amount of crustal shortening across the Indian plate rocks of the Himalaya south of the actual zone of continent–continent collision, the Indus Suture Zone (ISZ)? The northern margin of the Indian plate is preserved in the strongly deformed Tethyan passive margin platform and shelf sedimentary rocks of the Zanskar Range. Despite intense folding and thrusting, it is possible to estimate minimum shortening from detailed mapping and construction of balanced and restored cross-sections. It is not, however possible to constrain accurately the shortening across the High Himalayan Crystalline (HHC) zone to the south because of the high degree of ductile strain in these middle and deep crustal metamorphic and magmatic rocks. Previous attempts at estimating minimum shortening across the Indian continental margin rocks of the Himalaya were published by Searle (1986) and Searle *et al.* (1988) for Ladakh–Zanskar, Steck *et al.* (1993) for eastern Zanskar–Lahoul and Ratschbacher *et al.* (1994) for South Tibet.

From: KHAN, M. A., TRELOAR, P. J., SEARLE, M. P. & JAN, M. Q. (eds) *Tectonics of the Nanga Parbat Syntaxis and the Western Himalaya*. Geological Society, London, Special Publications, **170**, 395–410. 1-86239-061-4/00/$15.00

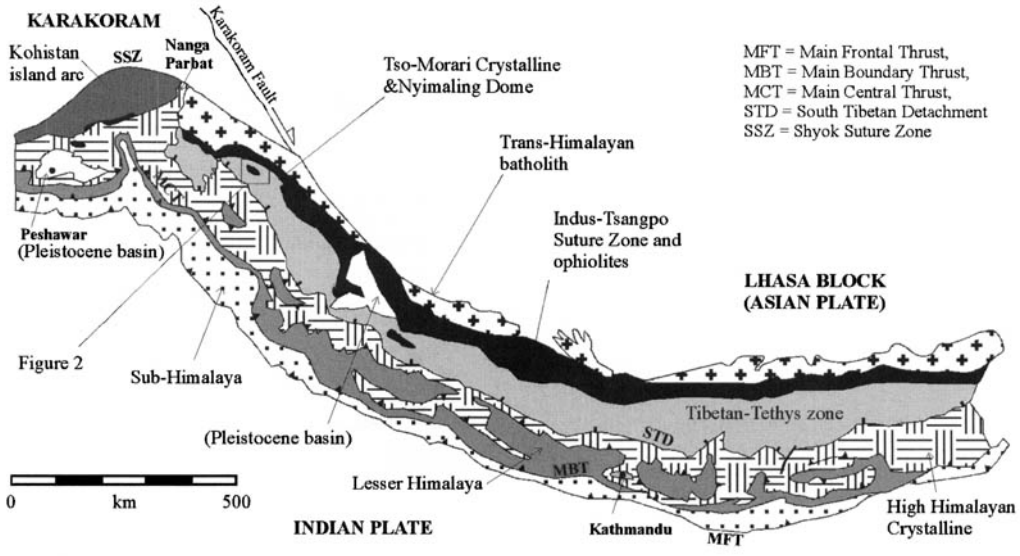

Fig. 1. Tectonic framework of the Himalaya showing the location of the main structural features of the orogen and the regional context of the study.

Attempts at restoring the Higher and Lesser Himalayan thrust sheets have been made by Schelling & Arita (1991) and Schelling (1992) in eastern Nepal and Srivastava and Mitra (1994) in the Garhwal Himalaya of India.

Preservation of the highest structural levels associated with the Spontang ophiolite combined with considerable vertical relief and excellent exposure make the Ladakh–Zanskar Himalaya an ideal region in which to study the structural evolution of the Indian continental margin (Fig. 1). We present here a geological map of the north Indian continental margin in the Ladakh–Zanskar region (Fig. 2) and balanced and restored cross-sections through the region (Fig. 3). In this paper we first describe the overall structural evolution in terms of three major deformation phases (Searle 1986; Searle *et al.* 1988, 1997) and then describe the structural evolution of the Indus Suture Zone and north Indian continental margin. We use field structural observations and balanced cross-sections to constrain the minimum amounts of crustal shortening and compare these to estimates from elsewhere along the Himalayan chain.

Geological overview

The Tethyan Himalaya (Gansser 1964) consists of Palaeozoic to early Tertiary rocks of the north Indian continental margin, Tertiary molasse deposits and Neo-Tethyan island arcs, ophiolites and ophiolitic mélange zones of the Indus–Tsangpo Suture Zone and the Andean-type intrusive rocks of the southern Asian continental margin. The Ladakh area of northwest India preserves one of the most accessible and best exposed sections through the Tethyan Himalaya. Since early reconnaissance mapping of the region (Lydekker 1883; Frank *et al.* 1977; Fuchs 1977, 1982; Keleman & Sonnenfeld 1983; Searle 1983) there has been a considerable amount of work carried out on the regional stratigraphy (Gaetani *et al.* 1980; Baud *et al.* 1984; Gaetani & Garzanti 1991; Robertson & Degnan 1993) and structure (Searle 1986; Searle *et al.* 1988, 1997; Steck *et al.* 1993). The timing of obduction of the Spontang ophiolite southwards onto the north Indian continental margin has also been the subject of controversy. Several authors proposed early Eocene obduction of the Spontang ophiolite (Fuchs 1977, 1982; Keleman & Sonnenfeld 1983; Baud *et al.* 1984; Colchen & Reuber 1986; Garzanti *et al.* 1987). However, the recognition of an earlier phase of deformation led Searle (1983, 1986) to propose a late Cretaceous ophiolite obduction event, which has been confirmed by recent work (Searle *et al.* 1997; Corfield 1998; Corfield *et al.* 1999)

Fig. 2. Geological map of the Spontang ophiolite compiled from mapping during the summers of 1995 and 1996, using SPOT satellite to correlate geology across inaccessible terrain.

Balanced and restored cross
continental Margin, Zanska

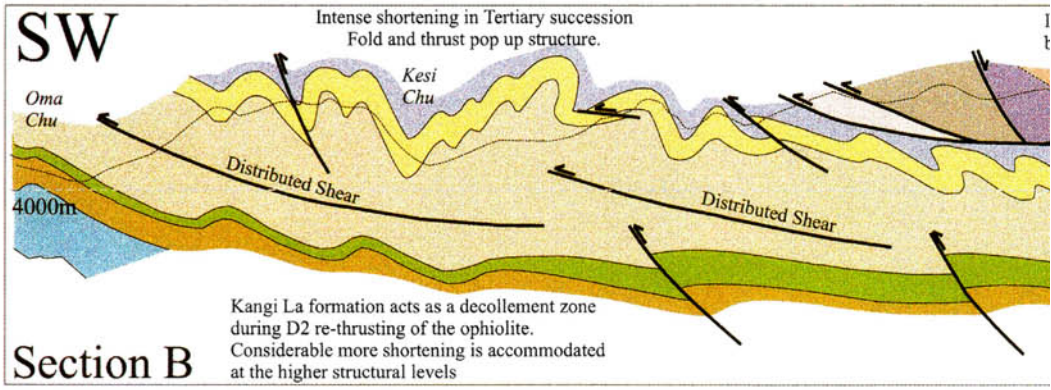

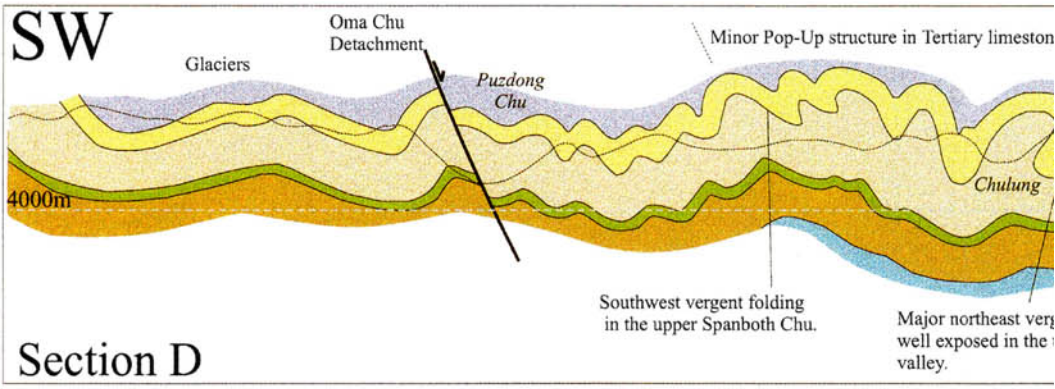

Structural evolution of the Zanskar Himalaya

The structures of the Tethyan Himalaya in the Zanskar region can be split into three separate deformation events.

D1 Late Cretaceous ~ 75-65Ma. Obduction of the Spontang ophiolite and a foreland propagating sequence of allochthonous thrust sheets onto the north Indian continental margin. The Dras-Kohistan island arc had probably collided with the southern margin of Asia by this time (Reuber 1989, Treloar *et al.* 1989, Robertson & Degnan 1994).

D2 Eocene-Oligocene - 54-25Ma - India -Asia collision, re-thrusting of the Spontang ophiolite and allochthonous thrust sheets, thrusting propagating down-sequence with the onset Himalayan metamorphism.

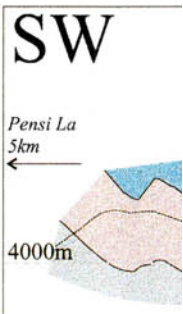

s-sections through the north In
ar Himalaya, NW India.

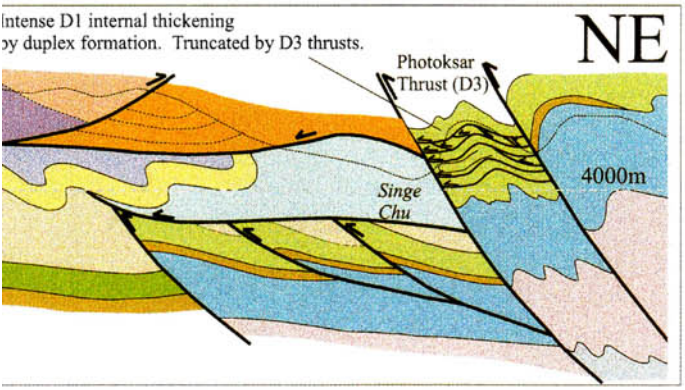

The key and the locations of Sections A
on the accompanying map.

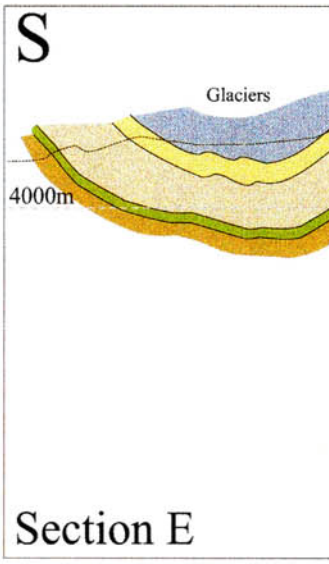

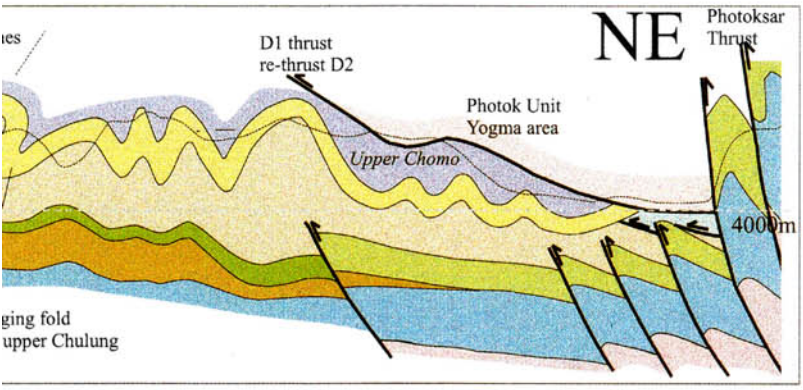

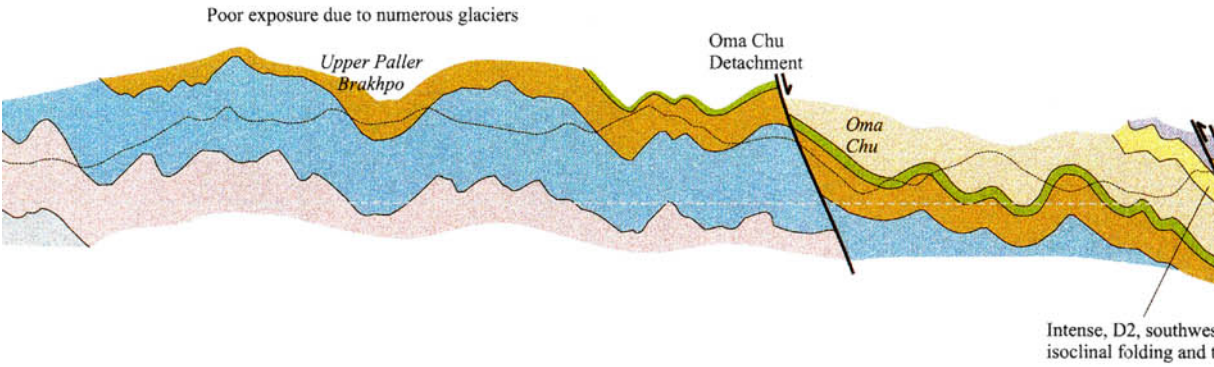

Scale

dian

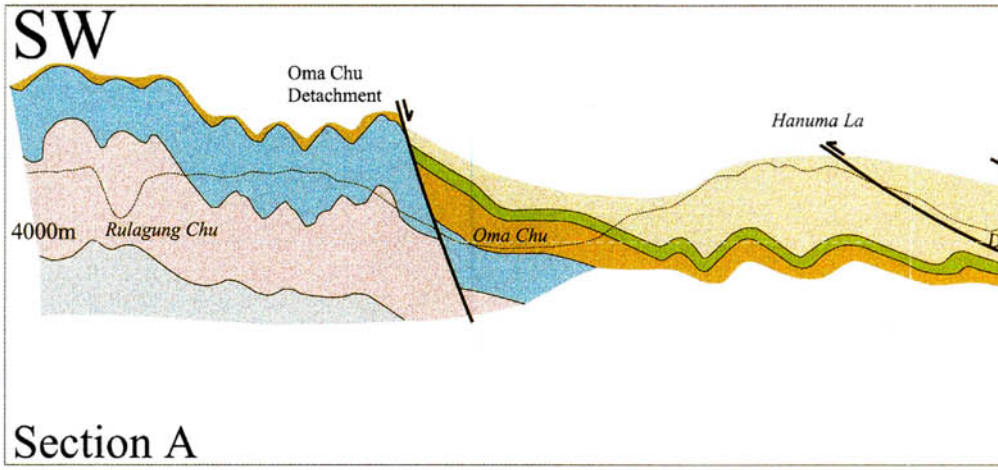

·E are shown

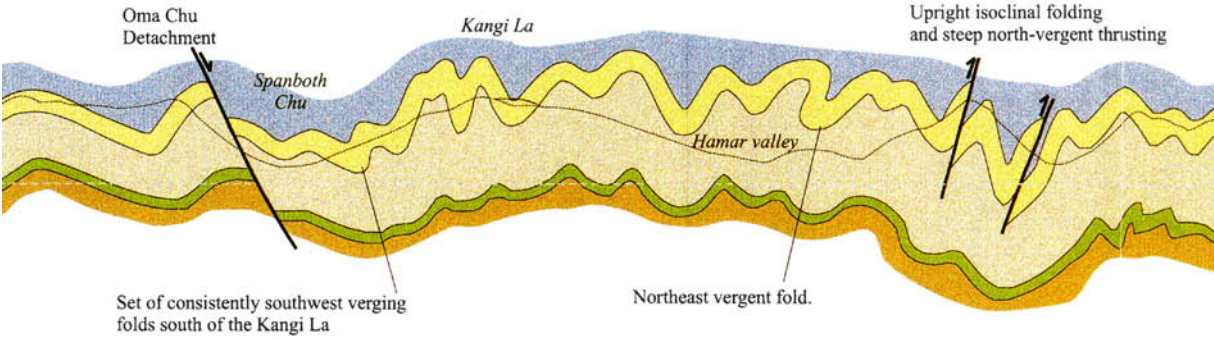

Constraints of the thickness of the Kangi La formation are poor in this section as topography is limited and the lower contact is seldom exposed.

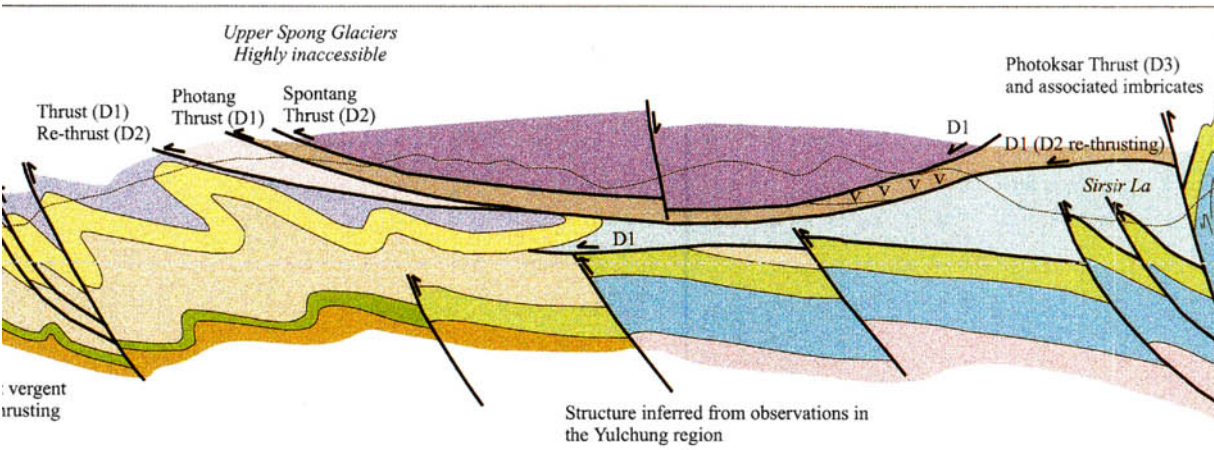

Structure inferred from observations in the Yulchung region

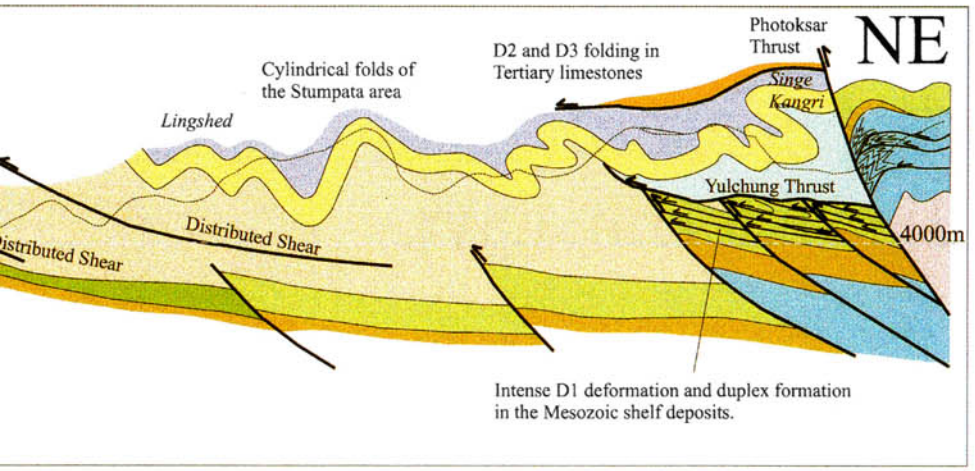
NE
Photoksar Thrust
D2 and D3 folding in Tertiary limestones
Cylindrical folds of the Stumpata area
Singe Kangri
Lingshed
Yulchung Thrust
Distributed Shear
istributed Shear
4000m
Intense D1 deformation and duplex formation in the Mesozoic shelf deposits.

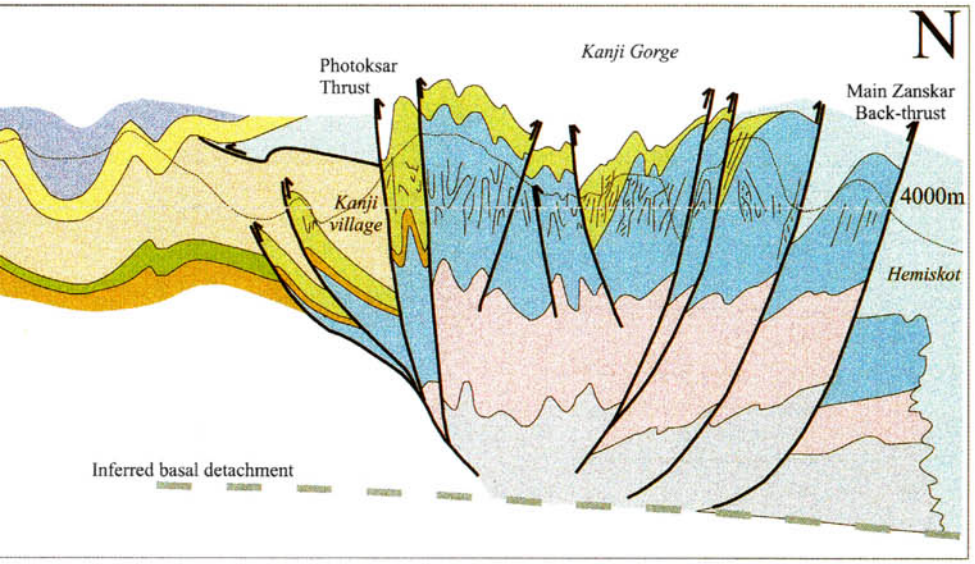
N
Kanji Gorge
Photoksar Thrust
Main Zanskar Back-thrust
Kanji village
4000m
Hemiskot
Inferred basal detachment

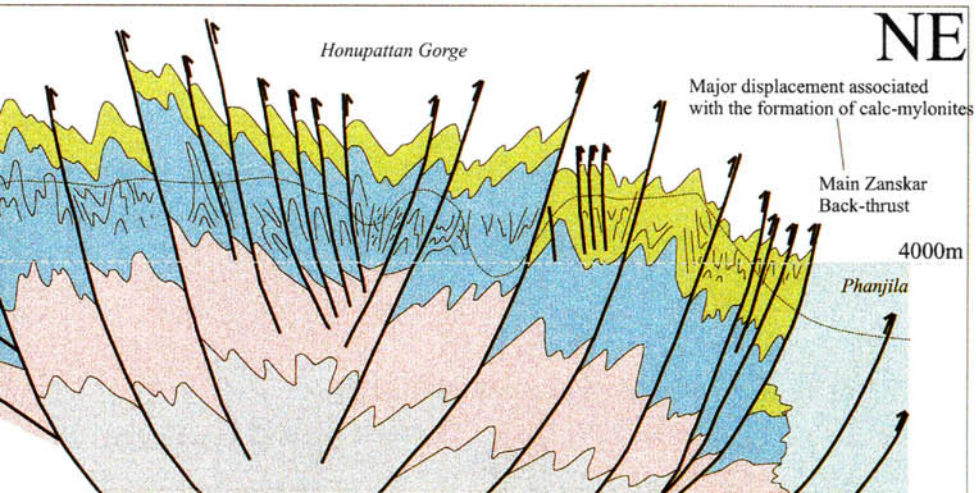
NE
Honupattan Gorge
Major displacement associated with the formation of calc-mylonites
Main Zanskar Back-thrust
4000m
Phanjila

D3 - Miocene-Recent - 25-0Ma Gravitational collapse of the High Himalaya causing normal faulting in the south of the region. Back-thrusting affects the northern parts edge of the Indian continental margin and the Indus Suture Zone.

Section

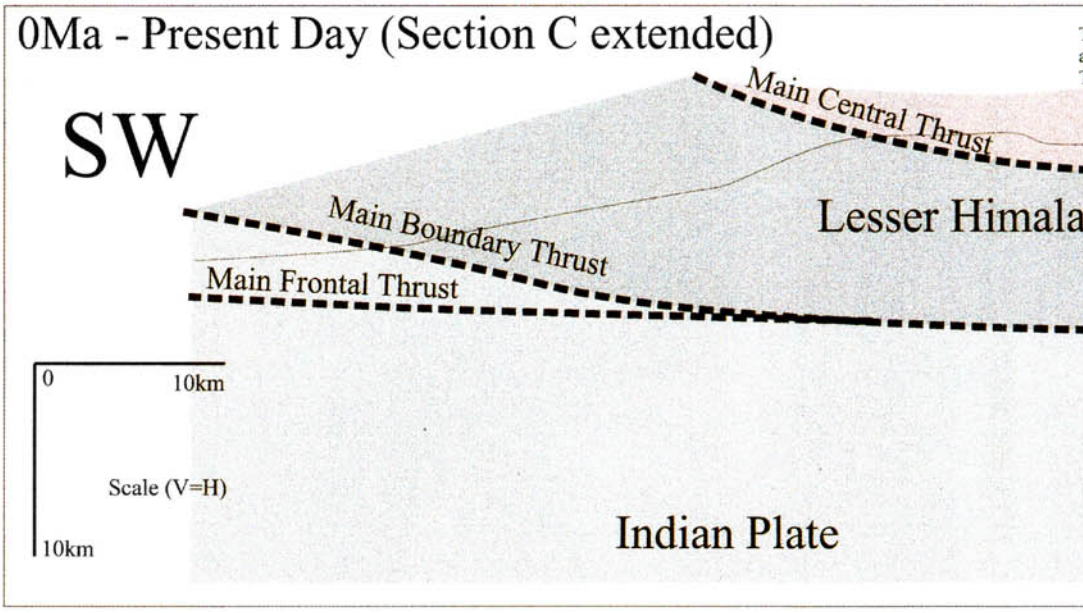

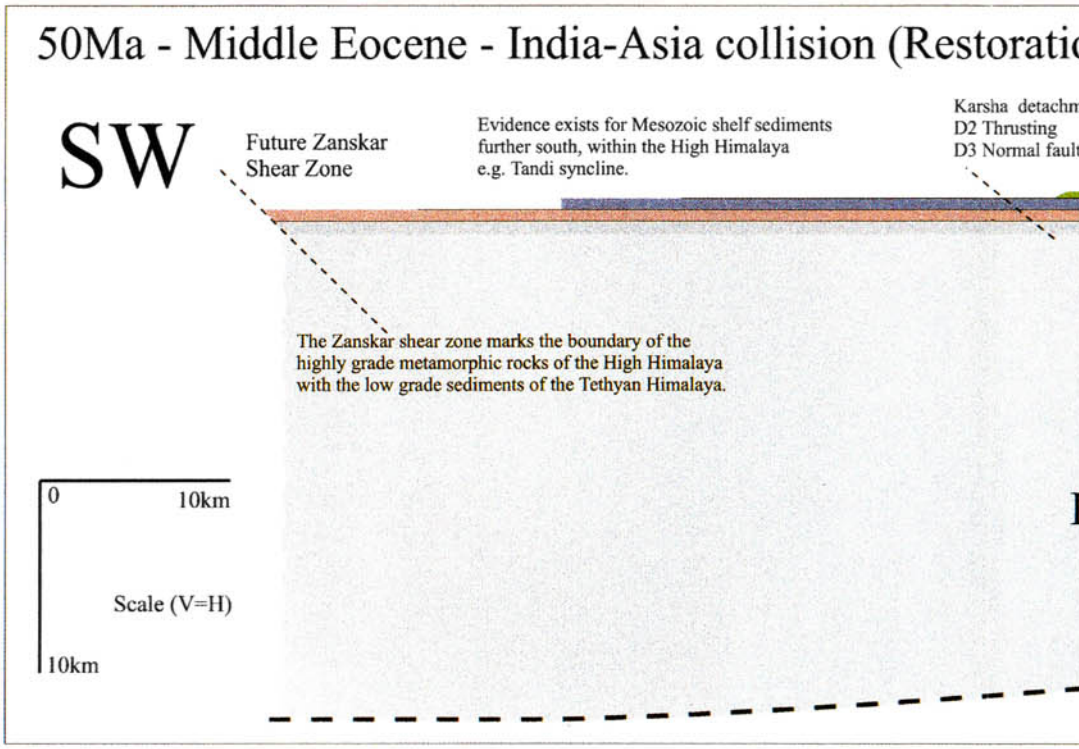

C

0 5 10km

Vertical Scale = Hor

he major Himalayan structures to the southwest of the balanced section
re illustrated (after Stephenson 1997) to place the cross-section in its regional context.
opography and the exact geometry of structures here are only intended to be approximate.

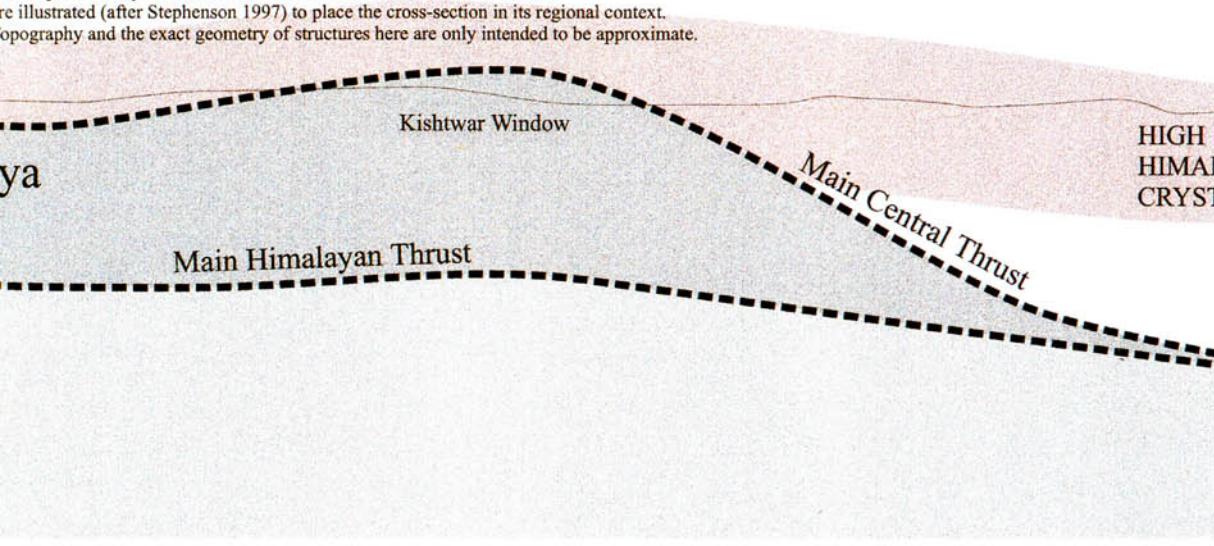

on of D2 and D3 structures for Section C)

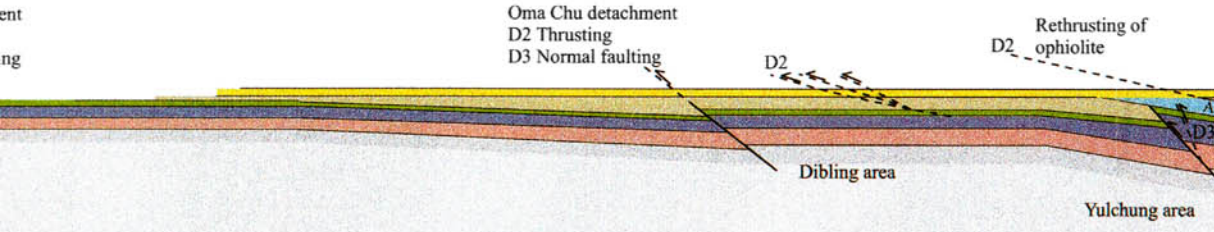

ndian Plate

Inferred basal detachment

izontal Scale

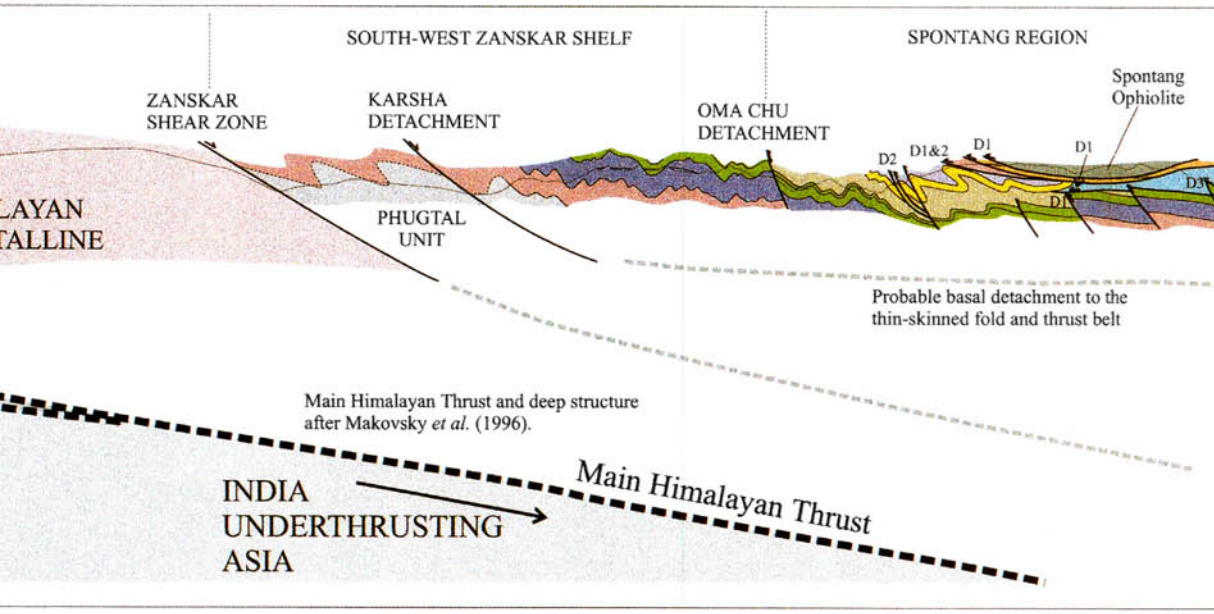

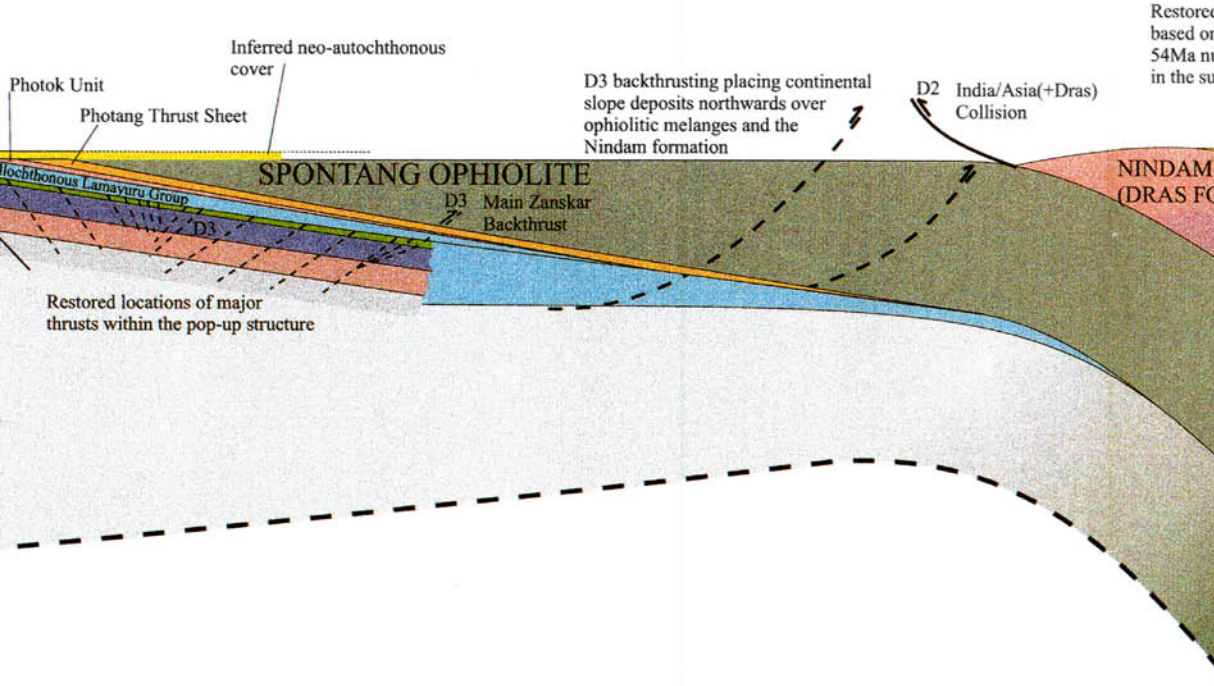

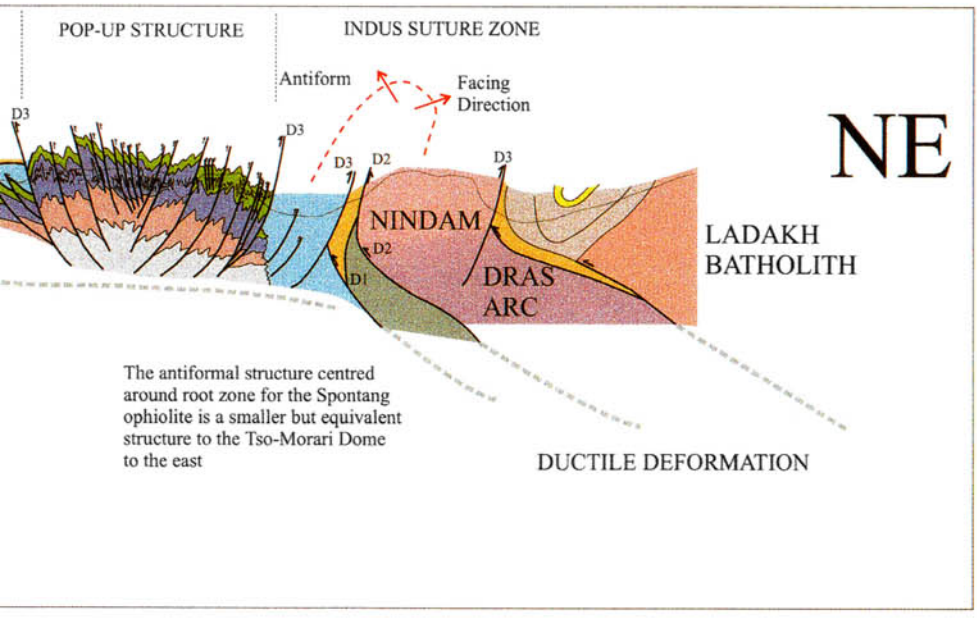

d width of the Indus basin after Searle *et al.* (1990)
n mapping of the Zanskar river section.
ummulitic limestones date final marine conditions
ture zone, thereby dating collision.

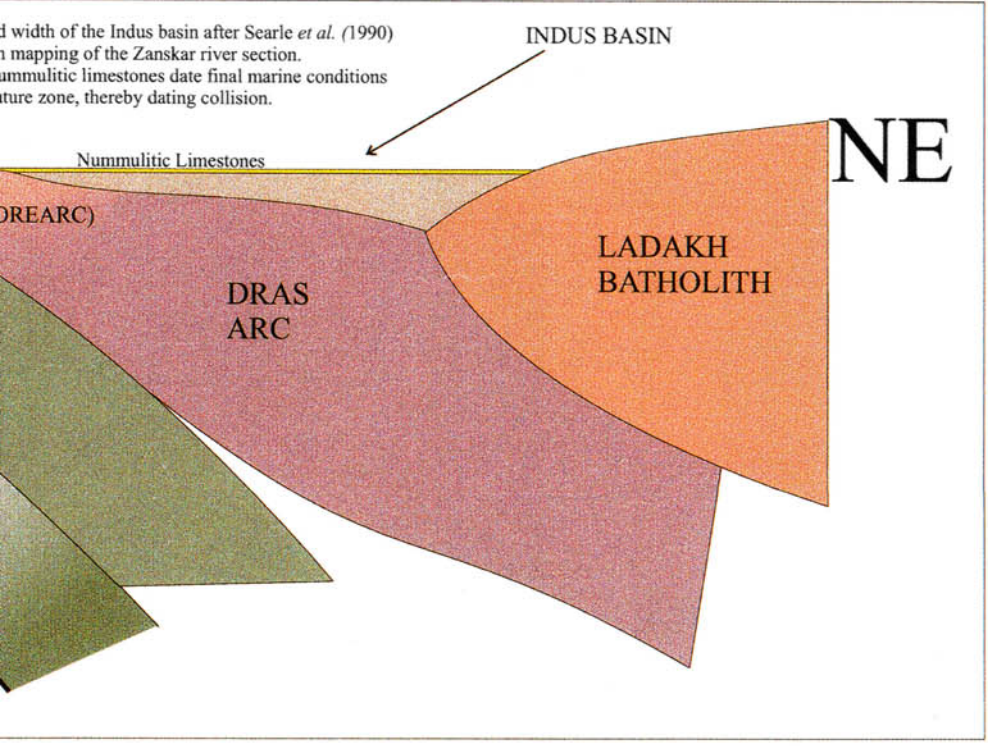

Geological map of the Spontang Opl and the north Indian continental mar Ladakh Himalaya.

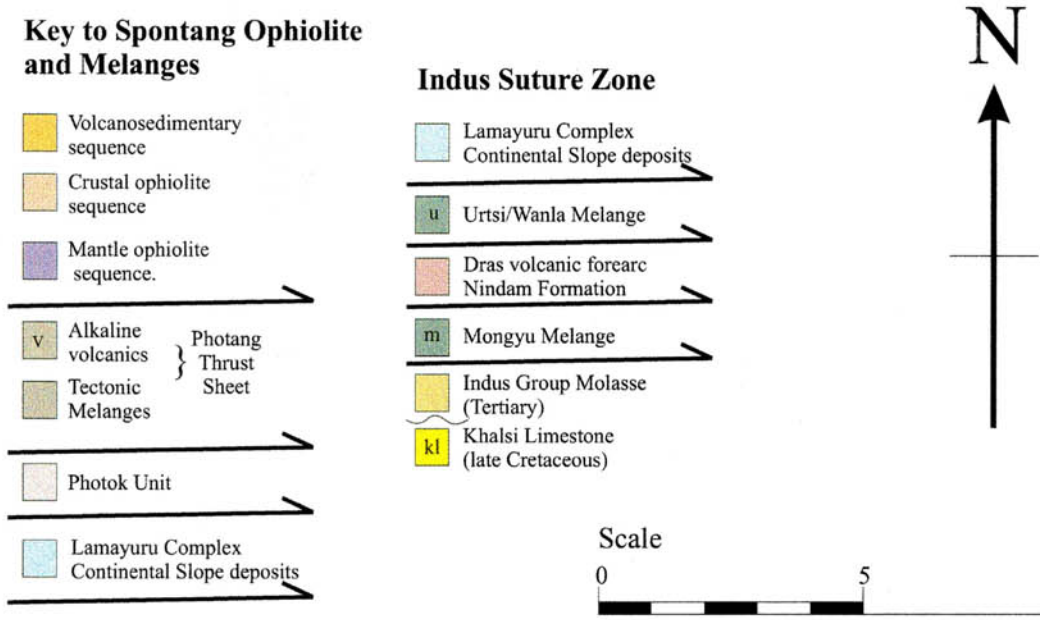

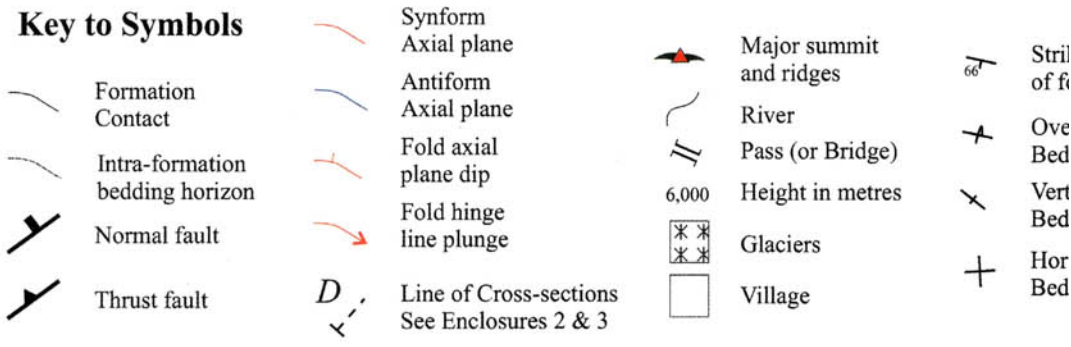

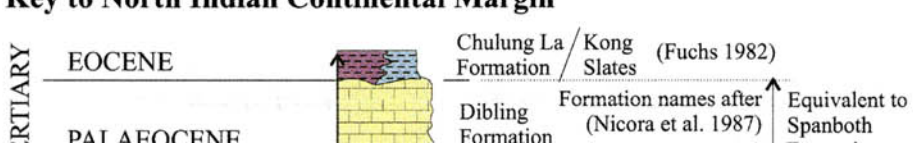

hiolite
rgin,

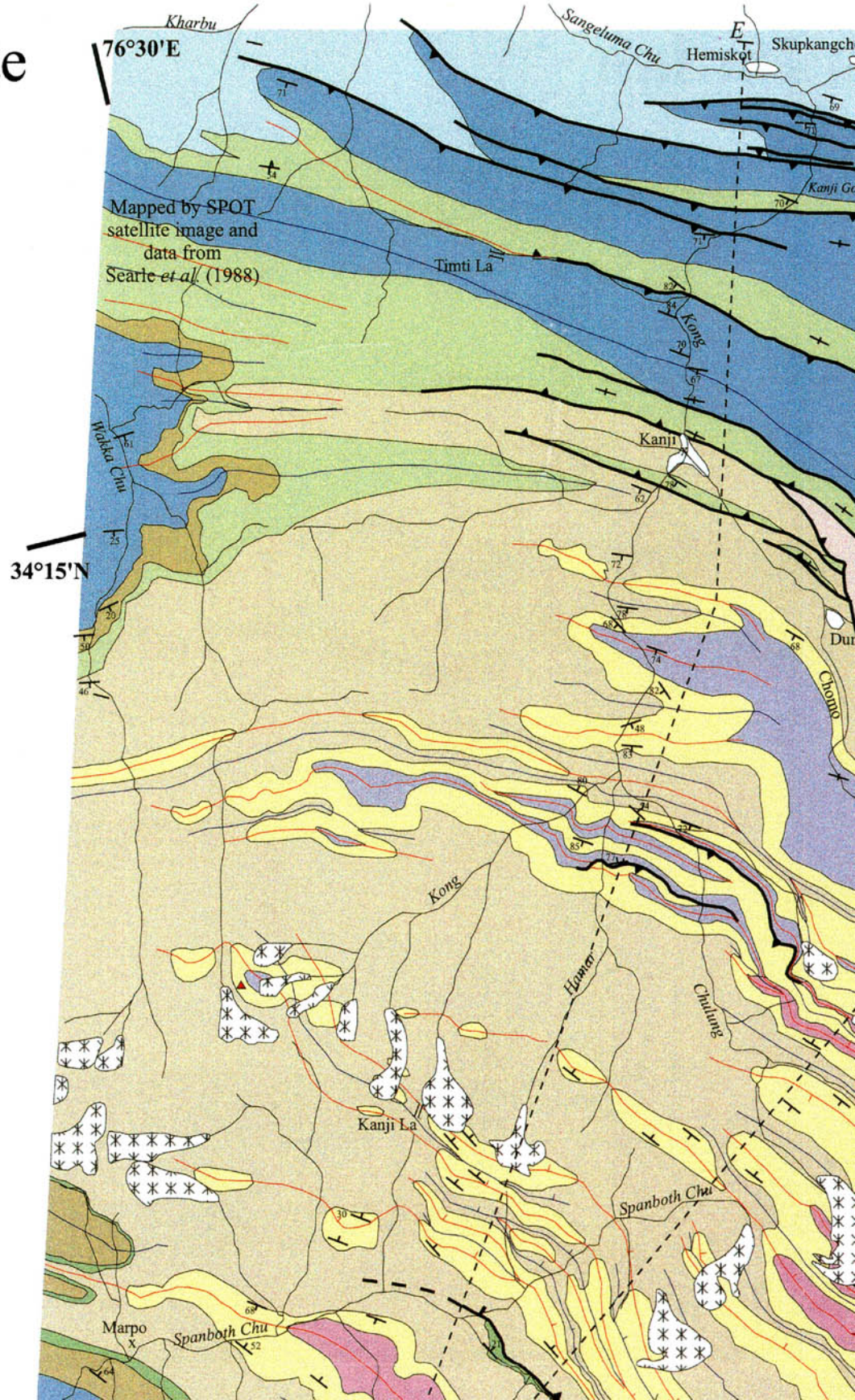


Younging
Lamayuru
Quaternary
Lake deposits
DRAS FOREARC
(NINDAM FORMATIO
Prinkiti La
MAIN ZANSKAR BACKTHRUST
Wanla
Shilla
Yapola
Phanjila
Shillakong Gorge
Honupattan
Yogma La
Yogma
Kangri
Snuzi La
5050
Shillakong West
Shillakong East
5,500
5,700
Snuzi
Kangri
5,400
PHOTANG
THRUST
4800
Sirsir La
SPONTANG
THRUST
6,000
Spong
Kangri
Spong
5,550
Photang
Photoksar
Bumiktse La
Chulung La
Photang
Kangri
6,000
Photang East
Bumiktse Chu

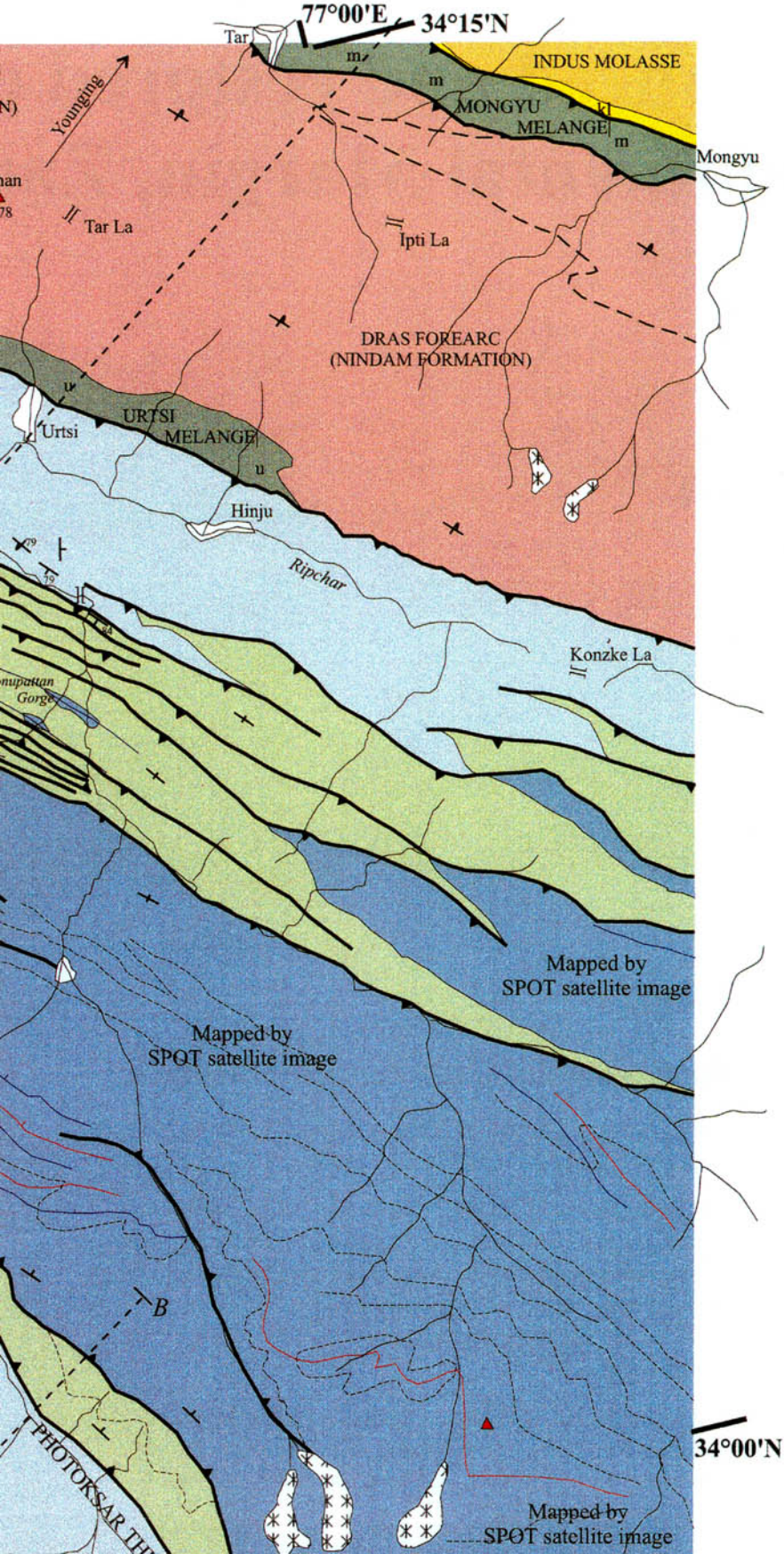
77°00'E
34°15'N
Younging
INDUS MOLASSE
MONGYU
MELANGE
Mongyu
Tar La
Ipti La
DRAS FOREARC
(NINDAM FORMATION)
URTSI
MELANGE
Urtsi
Hinju
Ripchar
Konzke La
Mapped by
SPOT satellite image
Mapped by
SPOT satellite image
B
34°00'N
Mapped by
SPOT satellite image

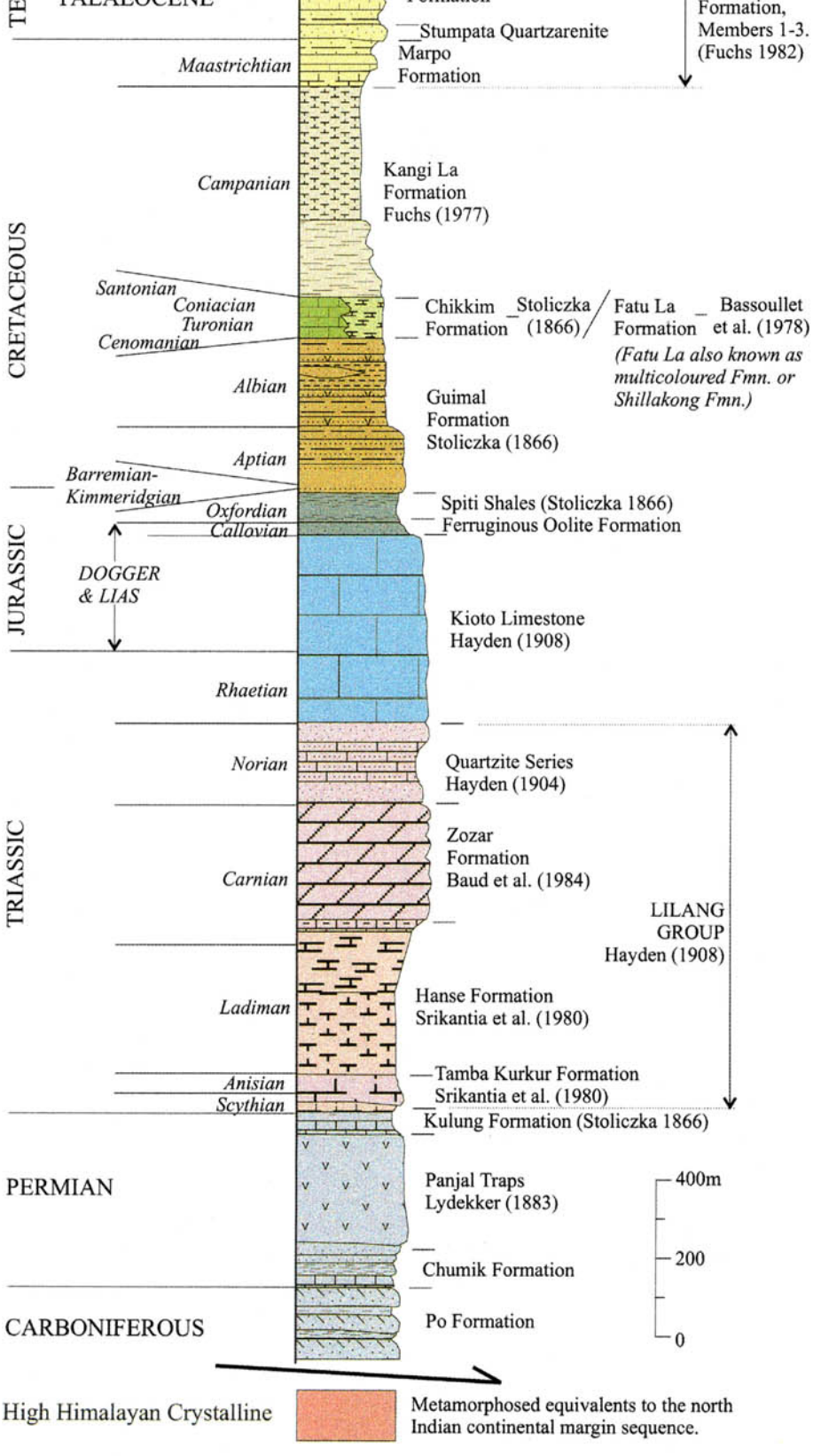
TE
PALAEOCENE
Formation,
Members 1-3.
(Fuchs 1982)
Stumpata Quartzarenite
Maastrichtian
Marpo
Formation
Campanian
Kangi La
Formation
Fuchs (1977)
CRETACEOUS
Santonian
Coniacian
Turonian
Cenomanian
Chikkim
Formation
Stoliczka
(1866)
Fatu La
Formation
Bassoullet
et al. (1978)
(Fatu La also known as
multicoloured Fmn. or
Shillakong Fmn.)
Albian
Guimal
Formation
Stoliczka (1866)
Aptian
Barremian-
Kimmeridgian
Oxfordian
Callovian
Spiti Shales (Stoliczka 1866)
Ferruginous Oolite Formation
JURASSIC
DOGGER
& LIAS
Kioto Limestone
Hayden (1908)
Rhaetian
Norian
Quartzite Series
Hayden (1904)
Zozar
Formation
Baud et al. (1984)
Carnian
LILANG
GROUP
Hayden (1908)
TRIASSIC
Ladiman
Hanse Formation
Srikantia et al. (1980)
Anisian
Scythian
Tamba Kurkur Formation
Srikantia et al. (1980)
Kulung Formation (Stoliczka 1866)
PERMIAN
Panjal Traps
Lydekker (1883)
400m
200
0
Chumik Formation
CARBONIFEROUS
Po Formation
High Himalayan Crystalline
Metamorphosed equivalents to the north
Indian continental margin sequence.

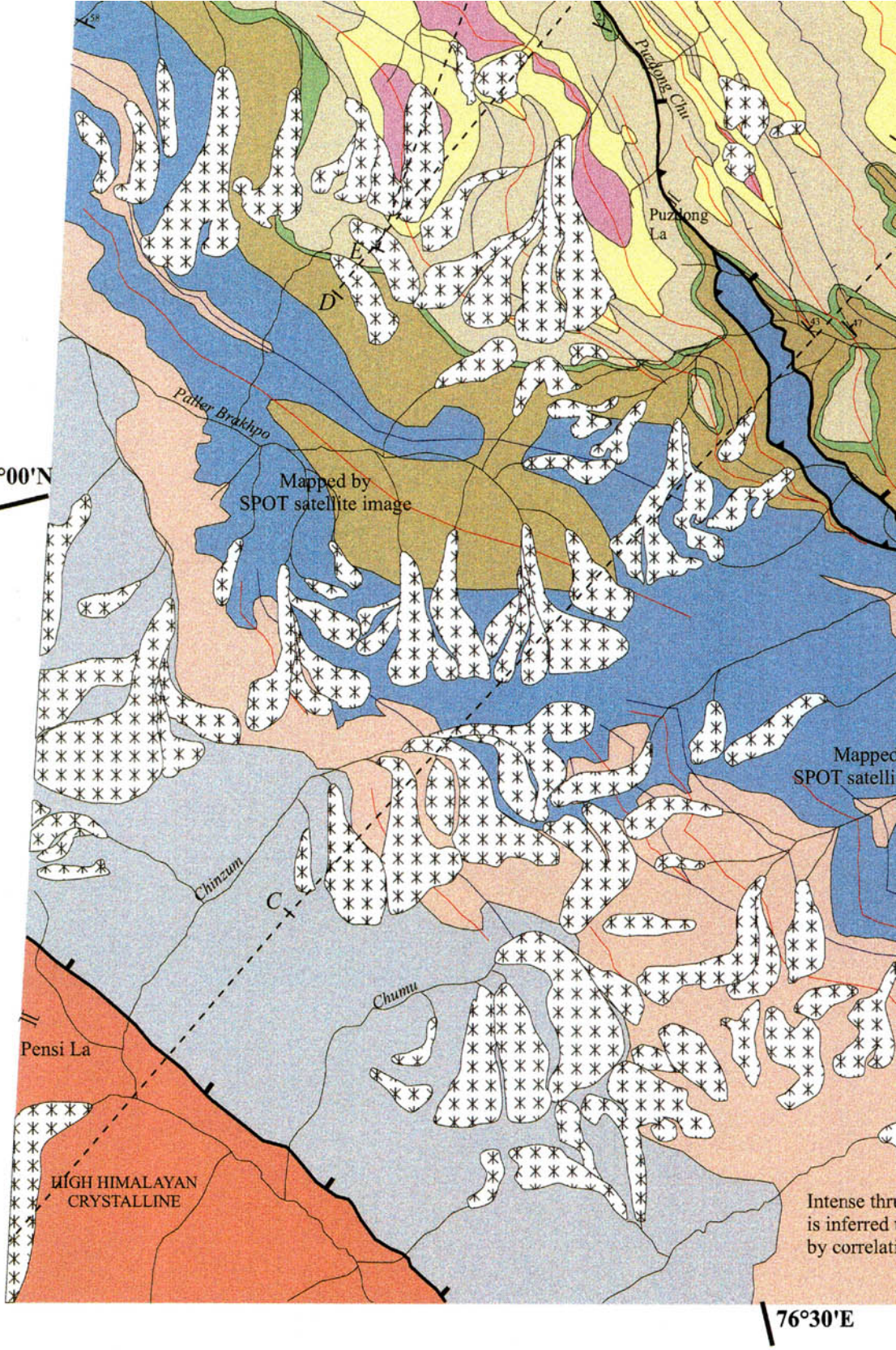
Puzilong Chu
Puzilong La
Pather Brakhpo
Mapped by SPOT satellite image
34°00'N
Chinzum
Chumu
Pensi La
HIGH HIMALAYAN CRYSTALLINE
76°30'E

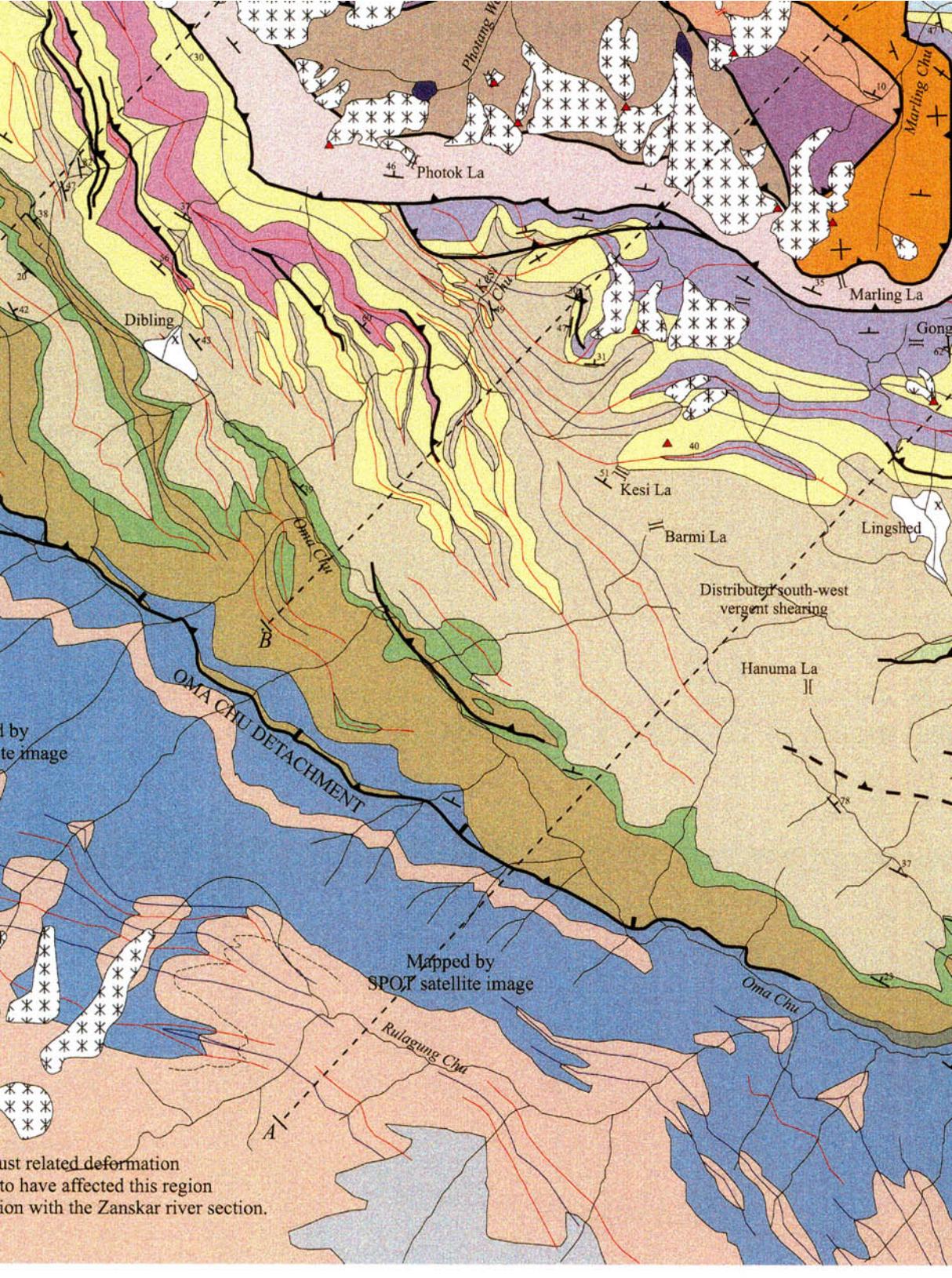

ust related deformation
to have affected this region
ion with the Zanskar river section.

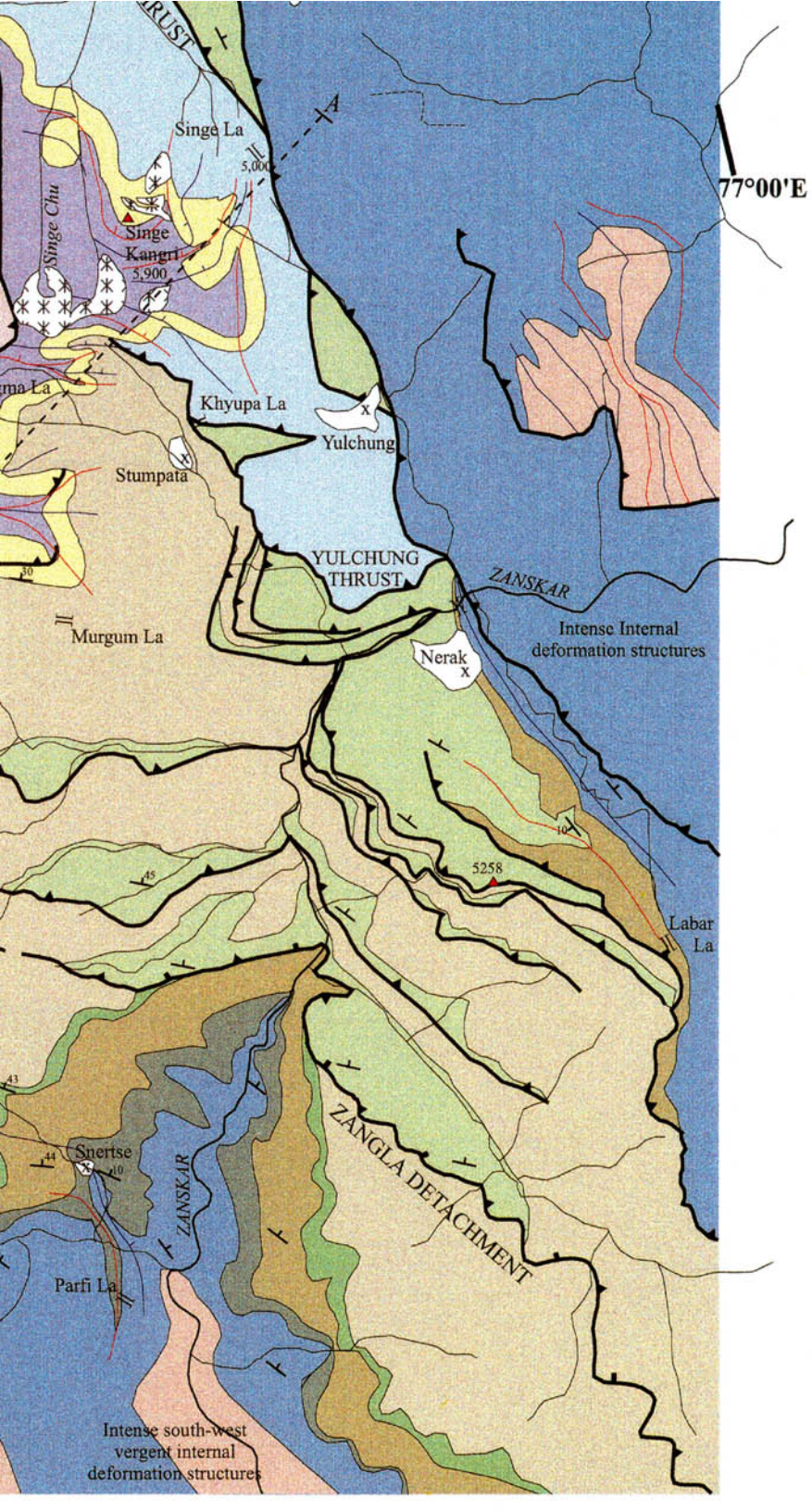
Singe La
5,000
Singe Chu
Singe Kangri
5,900
Khyupa La
Yulchung
Stumpata
YULCHUNG THRUST
ZANSKAR
Intense Internal deformation structures
Murgum La
Nerak
77°00'E
5258
Labar La
ZANGLA DETACHMENT
Snertse
ZANSKAR
Parfi La
Intense south-west vergent internal deformation structures

Table 1. *Major deformation events in the north Indian continental margin*

Deformation	Timing	Characteristics
D1	Late Cretaceous	Obduction of the Spontang ophiolite, Photang thrust sheet and Lamayuru complex continental slope deposits southwestwards onto the Zanskar passive margin. Approximately 200% shortening in the outer shelf sediments accommodated largely by internal deformation.
D2	Eocene–Oligocene	India–Asia collision (54–50 Ma) Southwestwards re-thrusting of the Spontang ophiolite and Photang thrust sheet. Southwest-verging folding and thrusting throughout the entire Mesozoic to early Tertiary Zanskar shelf sequence
D3	Miocene–Recent	Photoksar break-backthrust steps back in the thrust sequence cross-cutting D1 and D2 structures. Pop-up structure forms with north-directed backthrusting at the northern margin and south-directed break-backthrusting at the southern margin. North-directed backthrusting affects the entire ISZ. Normal faulting associated with topographic collapse of the HHC zone affects the southern Tethyan sediments.

By detailed structural mapping using the excellent regional stratigraphic framework (Gaetani & Garzanti 1991) it has been possible to balance and restore several cross-sections for each of the three major phases of deformation which have affected the north Indian continental margin. A previous attempt at balancing and restoring a cross-section from the ISZ to the HHC zone in the eastern Ladakh region was made by Steck *et al.* (1993). This transect was compiled from mapping carried out on and around the Leh–Manali road running NNW–SSE, obliquely across the NW–SE structural trend of the region. However, there is no evidence which distinguishes the earliest (late Cretaceous) phase of deformation along this section.

Overview of the structure

Table 1 summarizes the major phases of deformation which have been recognized, confirming the broad structural chronology of Searle (1983, 1986). Broadly speaking, the structural strike of the area runs from NW to SE, subparallel to the ISZ. All the major structural features can therefore be introduced with reference to the balanced and restored cross-section. From northeast to southwest, four major geographical subdivisions are recognized on the basis of their structure.

- **Indus Suture Zone**. Remnant Neo-Tethyan oceanic rocks consisting of Permian to Palaeogene marine sediments and volcanics and middle Eocene to Recent continental molasse sediments. Early deformations have been overprinted by intense north-vergent deformation associated with the D3 event.
- **Pop-up structure**. D3 structure immediately south of the ISZ involving northwest-vergent backthrusting at its NW side and southwest-vergent break-backthrusting at its SW side.
- **Spontang region**. Area southwest of the pop-up structure preserving earlier D1 and D2 structures which have not been overprinted by the later D3 deformation.
- **Southwestern Zanskar**. Area northeast of the HHC zone affected by late D2/early D3 normal faulting related to the Zanskar Shear Zone.

The regional structure is now discussed with reference to these subdivisions and restoration of the deformation events is considered in reverse chronological order.

Indus Suture Zone

A structural section through the ISZ along the Yapola River immediately north of the Spontang ophiolite has been examined in detail (Fig. 4). The section is dominated by north-vergent backthrusting and folding which characterizes the whole length of the ISZ in the Ladakh Himalaya (e.g. Searle *et al.* 1990). The

Fig. 3. Cross-sections through the map in Fig. 2. Cross-section C through the central part of the Spontang ophiolite, extending from the Indus Suture Zone in the north to the High Himalayan in the south has been palinspastically restored to 50 Ma (post-Spontang ophiolite obduction, pre-India–Asia collision).

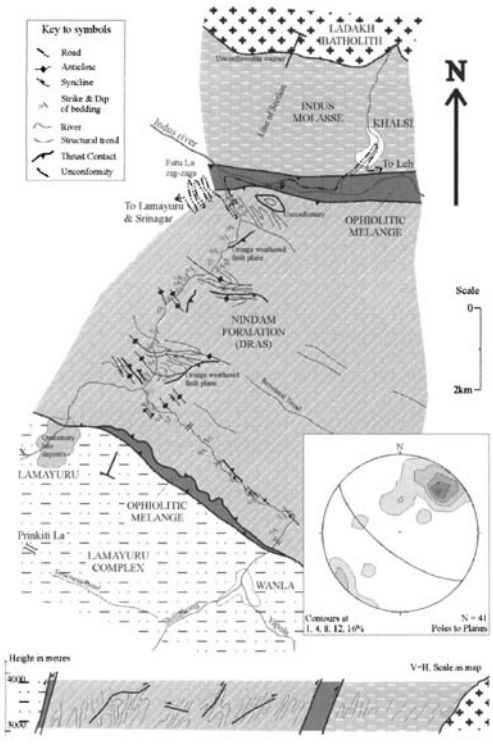

Fig. 4. Map of the Indus Suture Zone north of the Spontang ophiolite between Wanla and Khalsi. Inset: stereogram of poles to planes of bedding within the Nindam Formation (lower hemisphere, equal-area projection).

non-marine, continental molasse deposits of the Indus Group form the northern margin of the ISZ and dip steeply to the south in this section, tight to isoclinally folded about steeply southward dipping axial planes. The molasse unconformably overlies Late Cretaceous to Middle Eocene granodiorites of the Ladakh batholith to the north with an on-lapping relationship. The youngest sediments of the Indus Group are Late Miocene to Early Pliocene in age and are affected by the D3 deformation (Searle *et al.* 1997) providing a maximum age constraint on the D3 deformation. The Aptian platformal carbonates of the Khalsi limestone mark the base of the Indus Group and are in tectonic contact with the ophiolitic mélanges (Garzanti & Van Haver 1988).

The ophiolite mélange zone is approximately 500 m thick at the confluence of the Yapola and Indus rivers and correlates laterally with the Mongyu mélange 20 km to the east, which is discussed in detail by Robertson (2000). The mélange consists of tectonically juxtaposed and highly sheared sheets of serpentinized harzburgites and dunites, amphibolites, gabbro pegmatites and rodingites, in addition to sheared volcanic rocks and sediments. The mélange zone cuts across D2 folding within the units to the south, suggesting that it was emplaced into its current structural position during D3. At the southern edge of this ophiolitic mélange, remnants of the Neo-Tethyan Dras intra-oceanic island arc are preserved.

North of the Spontang ophiolite only the Nindam Formation of the Dras arc is preserved, interpreted as the distal deep-water volcaniclastic forearc apron (Robertson & Degnan 1994). Further to the east a mélange unit separates the proximal Dras forearc rocks of the Naktul unit from the Nindam Formation (Robertson & Degnan 1994). The mélange probably represents the tectonized remnants of Dras arc basement and extrusive rocks which have survived collision.

The Nindam Formation is bounded to the north and south by steeply dipping, north-vergent thrusts. Internal structures within the Nindam Formation consist of minor, largely north-verging thrusts and folds on all scales. While this folding is responsible for some thickening of the unit there is no evidence to suggest any large-scale repetition of sequence. Fining-upward sequences from sand to mud grades within the turbiditic horizons indicate a consistent younging direction to the north and that the unit as a whole is overturned. The overturning can be attributed to steepening during the early stages of shortening, followed by later north-vergent backthrusting and large-scale folding.

An ophiolitic mélange zone separates the southern edge of the Nindam Formation from the Lamayuru complex and can be followed intermittently westward along the southern margin of the Dras arc rocks to the Shergol mélange (Thakur 1981). North of Wanla the mélange is around 50 m thick, consisting of blocks ranging from less than 1 cm to several metres in size of bioclastic carbonates, basaltic lavas, serpentinites, ophicalcites and deformed cherts within a dark grey shaly matrix. A laterally equivalent unit has also been described eastward along this contact, north of Urtsi village and can be interpreted as 'relatively *in situ*' late Jurassic oceanic basement to the Dras arc (Sutre 1990), or as a thrust-bound subduction–accretionary complex (Robertson & Degnan 1994; Robertson 2000). An exotic block described from the mélange unit further to the west, immediately north of Lamayuru village (Bassoullet *et al.* 1978; Robertson 1998) is consistent with the latter explanation. This belt of mélange is all that

remains of the root zone for the Spontang ophiolite and may correlate with the accretionary complex (Photang thrust sheet) which underlies the ophiolite (Corfield *et al.* 1999).

The Lamayuru complex forms the southern edge of the Indus Suture Zone along its whole length north of the Spontang ophiolite and has been reconstructed as a relatively intact continental slope to base of slope succession (Robertson & Degnan 1993). Bedding has a reasonably uniform orientation, steeply dipping to the south with occasional way-up structures indicating a younging direction to the south. Due to the fissile nature of the shales and marls which comprise much of the Lamayuru complex exposed in this region, the deformation has occurred along broad shear zones as opposed to major brittle faults. Cleavage has formed parallel to the bedding in most outcrops studied, throughout the whole sequence. Locally, metre-scale folding and thrusting is observed within these fissile beds and occasional larger-scale folding is evident in more competent units with the majority of structures verging to the north. However, there is no evidence for the large-scale repetition of sequence (Robertson & Degnan 1993). Colchen *et al.* (1986) have reported south-vergent structures within the Lamayuru complex to the east of the Yapola River, interpreted as rare remnants of an earlier phase of deformation although detailed mapping has failed to confirm this observation.

Early tectonic evolution of the Indus Suture Zone

The Dras–Kohistan arc is widely interpreted to have collided with the southern margin of the Asian plate in the middle to late Cretaceous (Reuber 1989; Treloar *et al.* 1989; Robertson & Degnan 1994). Given this interpretation, it is possible to place constraints on the restoration of the Asian margin immediately preceding India/Asia collision. It is likely that the Indus Basin was initiated in the suture between the Dras arc and the Ladakh batholith, with Aptian–Albian carbonate platforms (Khalsi limestone) forming around the margins of the arc and the Ladakh batholith (Garzanti & Van Haver 1988). At this stage the arc edifice would have separated the newly forming Indus Basin from the Nindam forearc deposits (Fig. 3).

An oblique collision with the Asian plate is implied by the lack of early Tertiary Andean-type arc plutonics and extrusives in the eastern parts of the Dras complex, i.e. north of the Spontang ophiolite (Robertson & Degnan 1994) as compared to those present in the Suru unit of the Dras arc to the west. Only the western part of the arc would have collided forcefully at 80 Ma, while the eastern part would have remained as an inactive forearc ridge, consistent with the apparently greater width of the Indus Basin to the east. This interpretation is also consistent with the apparent lack of deformation in the Nindam Formation until the Eocene (Robertson & Degnan 1994).

Early Eocene Nummulitic limestones were deposited during the final marine incursion into the Indus Basin, marking the time of collision of the Asian plate (and the accreted Dras arc) with India (Garzanti & Van Haver 1988). Collision was followed by regional uplift and the onset of terrestrial molasse sedimentation (Indus Group). From the Zanskar River section east of the studied area, Searle *et al.* (1990) have estimated a minimum of 36 km shortening in the Eocene–late Miocene molasse, giving a minimum basin width of 60 km. Due to the erosion levels and extent of deformation of the Lamayuru complex and Nindam Formation, it was not possible to follow a single stratigraphic horizon for any significant distance. Consequently, the amount of shortening accommodated by the shaly units could not be constrained with any accuracy.

The opposite facing directions of the Lamayuru and Nindam formations suggest an anticlinal structure centred around the mélange which separates them. During the early stages of D3 deformation a major north-verging anticline appears to have initiated across the original root zone of the Spontang ophiolite. Continued shortening across this structure led to the development of north-directed backthrusts approximately parallel to the axial plane of the anticlinal structure. This feature correlates very well with the Nyimaling dome structure of eastern Ladakh (Steck *et al.* 1993), a similar north-verging anticlinal structure responsible for the uplift of the Tso–Morari crystalline complex in its core (Fig. 1).

Pop-up structure

The pop-up structure consists of northeast-vergent thrusts and northeast-facing folds in the northeast and southwest-vergent thrusts and southwest-facing folds in the southwest. Deep v-shaped gorges cut through the steeply dipping Mesozoic limestones of the pop-up structure which has also exerted significant control on drainage, rivers often following the strike of the regional structure. The geographical expression of the pop-up structure is a WNW–ESE trending belt, approximately 6 km thick in the WNW,

widening to more than 20 km along the Zanskar River in the SE. This belt is slightly folded in the horizontal plane, the dominant strike of structures changing from E–W at the western side to NW–SE at the eastern side in the Zanskar River region.

The Main Zanskar backthrust (MZB) places Mesozoic carbonates of the Zanskar passive margin northward over continental slope deposits at the northern margin of the pop-up structure. Towards the east of the area there is a stepping of the main thrust plane towards the north on a series of imbricate faults. A typical length of one of these imbricate faults is between 20 & 30 km, though the largest single fault running along the south side of the Yapola valley is nearly 40 km long. The largest displacement of *c.* 1.5 km is found along this fault between the villages of Hemiskot and Phanjila. Across the fault zone in the Yapola valley, at least four major repetitions can be recognized in the mylonitized multicoloured pelagic carbonates of the Fatu La Formation. The calc-mylonites are extensively recrystallized with 120° angled grain boundary junctions and have a well-defined foliation associated with the mylonitization. Microstructures within quartz veins also involve extensive suturing along grain boundaries and the development of ribbon quartz. Shear sense indicators in offset veins and stylolites suggest pure thrust motion. The extent of mylonitization decreases gradually, moving southward away from the MZB throughout the pop-up structure. Towards the south, deformation is associated with lower temperature, brittle structures.

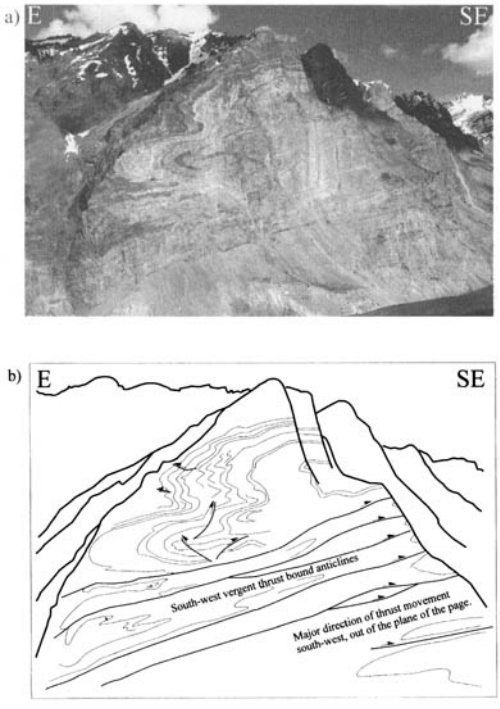

Fig. 5. (**a**) View of the hanging wall of the Photoksar break-backthrust from the Bumiktse La. (**b**) Interpretation of the structures in the hanging wall of the Photoksar break-backthrust. Intense D1 folding and thrusting is responsible for the internal thickening in the Fatu La pelagic carbonates. The D3 Photoksar thrust cuts across these structures, preserving them in the hanging wall.

The Photoksar break-backthrust (PBT) is the largest of an imbricate system of faults which marks the northern edge of the pop-up structure (Fig. 5). The fault is a major control on the regional topography, a system of low passes in the footwall connecting the major river valleys which run perpendicular to the fault. The vertical throw reaches at least 2 km between the Sirsir La and Singe La (Fig. 2) immediately north of the middle and thickest part of the Spontang ophiolite. This section of the fault plane also shows the shallowest northerly dip, approximately 60° at the Bumiktse La. Moving along the strike east or west, the throw of the PBT becomes reduced and deformation becomes partitioned into a series of smaller imbricate thrusts. The imbricate structure is most clearly exposed between the Snuzi La and Sirsir La where the subvertically bedded, highly deformed Fatu La Formation forms a series of pinnacled ridges which parallel the PBT. These ridges have eroded out where the tips of imbricate thrusts are exposed, the harder weathering carbonates forming the hanging wall of each thrust with the shales of the Lamayuru complex in the footwall (Fig. 6).

The hanging wall of the Photoksar break-backthrust consists of the highly deformed Mesozoic carbonates of the Zanskar passive margin sequence. North of the Bumiktse La cliffs in excess of 1 km in height exhibit spectacular folding and thrusting in the pelagic carbonates of the Fatu La Formation. The subhorizontal D1 & D2 thrusts and isoclinal folds in the Fatu La Formation have been cut across by the steeper D3 PBT, and are clearly exposed in the hanging wall cliffs (Fig. 5).

D3 shortening

Throughout much of the stratigraphy of the pop-up zone, there is a major sedimentary hiatus in the late Jurassic and early Cretaceous separating the shelf carbonates of the Kioto Formation from the pelagic limestones of the Fatu La

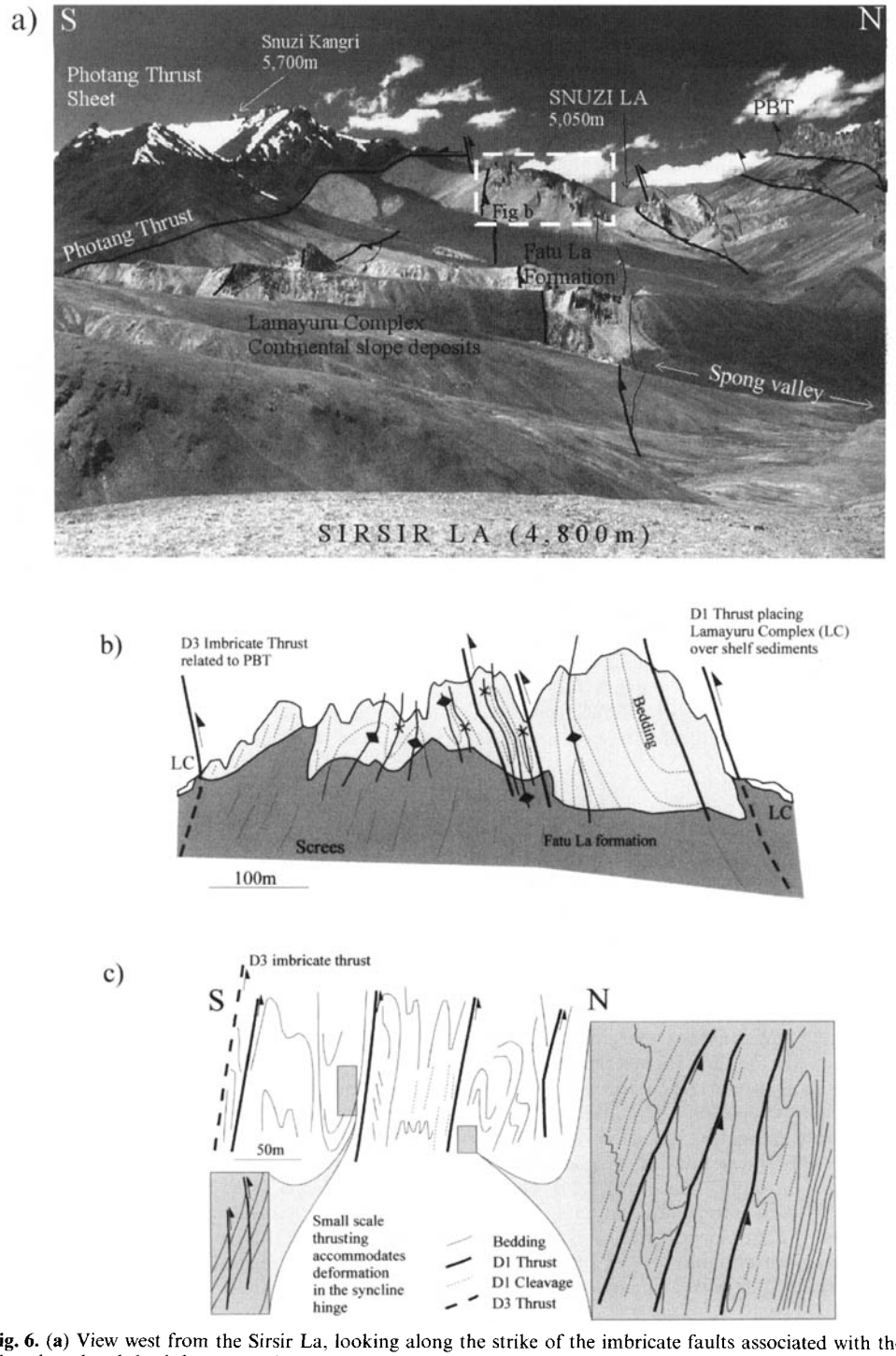

Fig. 6. (**a**) View west from the Sirsir La, looking along the strike of the imbricate faults associated with the Photoksar break-backthrust (PBT). (**b**) Detailed structure of one of the imbricate thrust slices shown in Fig. 5a. Internal structures within the imbricate slice are associated with the D1 deformation. (**c**) Detailed structure in the Fatu La Formation in the hanging wall of a D3 imbricate thrust related to the PBT, immediately south of Kanji village.

Formation (Gaetani & Garzanti 1991). The clear contrast between the dark grey, orange weathering Kioto Formation and the pastel-coloured Fatu La Formation enabled this horizon to be mapped over a wide area in the field using SPOT satellite imagery. The extent of deformation is such that the horizon itself is commonly exploited by bedding parallel thrusting, though the concordance in bedding orientation across the horizon generally distinguished these from other thrusted contacts. Compositional layering, particularly in the Fatu La Formation, allowed consistent identification of original bedding despite extensive recrystallization.

Shortening within the pop-up zone has been accommodated by two distinct mechanisms: large-scale thrusting and intra-formation folding and thrusting. D1 and D2 appear to have been largely accommodated by the latter mechanism (Fig. 7). However, D3 pop-up structures involve folding of, and thrusting across, the Kioto–Fatu La unconformity. A simple estimate of this D3 shortening has been obtained across five different transects based on line balancing of the Kioto Formation–Fatu La Formation contact, which will not reflect shortening by internal deformation mechanisms. Estimates fall within the range 190–230% for each of the transects, despite the increasing width of the pop-up zone from east to west.

D1 & D2 shortening in the outer shelf

Due to the extreme overprinting of the D3 deformation, accurate estimation of the D1 and D2 shortening across the outer margin is difficult. In particular, the mylonitization and intense internal deformation structures make estimation of the original stratigraphic thicknesses of the outer margin questionable. In the Nerak area, at the southern margin of the D3 pop-up zone, the D1 and D2 deformations are much more clearly preserved and better estimates of the original stratigraphic thicknesses can be made. Separate estimates, based on the style of deformation observed and area-balancing of cross-sections through this area, suggest a minimum of 200% shortening associated with the D1 and D2 deformation. This is also consistent with observations based only on the structural style of the northern parts of the pop-up structure.

The assumption that the D3 deformation can be line balanced and the D1 and D2 deformations can be area-balanced gives an overall minimum estimate of shortening, since it is assumed that there is no loss of cross-sectional area from out-of-sequence thrusting. Combining the shortening estimates therefore gives an overall 380–460% minimum shortening estimate. In the best constrained section the value is 420%.

The similar percentage shortening estimates obtained for each of the sections is also significant and is consistent with the uniform stratigraphic level exposed across the pop-up structure. Many of the D3 thrusts have been steepened into the vertical plane, some of which have subsequently been overturned by movement on other thrusts. This is particularly clear in the west of the area where the PBT and the associated imbricate thrusts are essentially vertical. On reaching a subvertical position, geometric constraints mean that continued motion on the thrust is a very inefficient means of accommodating shortening. Consequently, continued shortening would result in the initiation of new, lower angle thrusts. The pop-up zone would have grown in width as deformation progressed, new thrusts forming at the margins of the structure as old thrusts rotated into steeper orientations.

Spontang region

The Spontang region, immediately south of the pop-up structure, preserves the only clear evidence of the late Cretaceous deformation (Fig. 8). D1 involved the obduction of the Spontang ophiolite and a foreland propagating sequence of Neo-Tethyan thrust sheets onto the north Indian continental margin (Searle 1986; Searle *et al.* 1997; Corfield 1998). The lowest of these thrust sheets consists of Lamayuru complex continental slope deposits emplaced directly over the passive margin sediments along the Yulchung Thrust. Maastrichtian Marpo limestones deposited over the thrust tip northwest of Stumpata village (Figs 2 and 3) provide a minimum age limit for movement on the thrust (Corfield *et al.* 1999). However, the Spontang ophiolite and other Neo-Tethyan thrust sheets are now clearly structurally higher than the Maastrichtian to early Eocene limestones, which led many authors to favour Eocene obduction (Fuchs 1982; Keleman & Sonnenfeld 1983). This is a consequence of D2 re-thrusting beneath all the D1 Neo-Tethyan thrust sheets, excepting the continental slope deposits. The D2 thrust, clearly exposed in the lower Marling valley, cuts up-section through the Maastrichtian to early Eocene limestones, truncating bedding in the footwall. This contact is further evidence that the limestones were originally deposited on top of the obducted ophiolite, assuming the basic rule of thrusting that thrusts always propagate

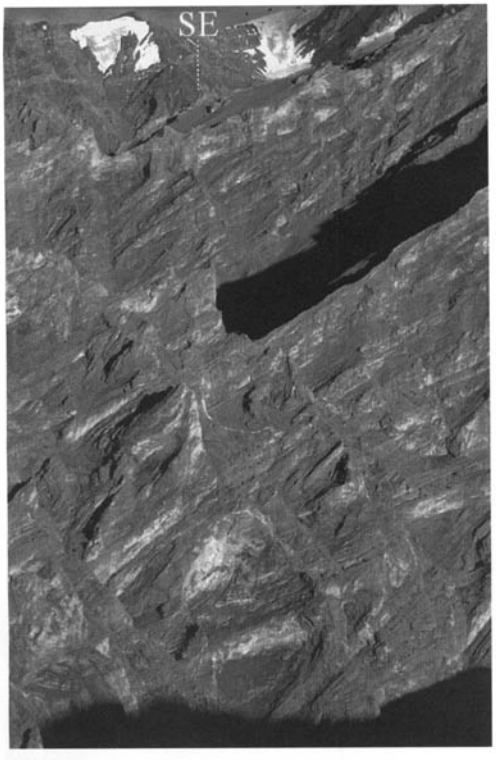

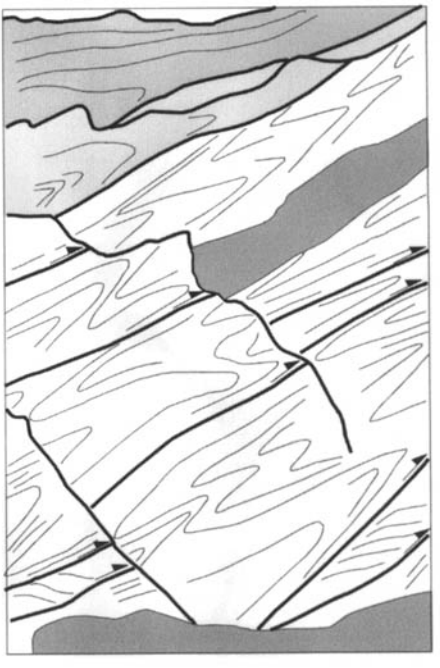

(a)

(b)

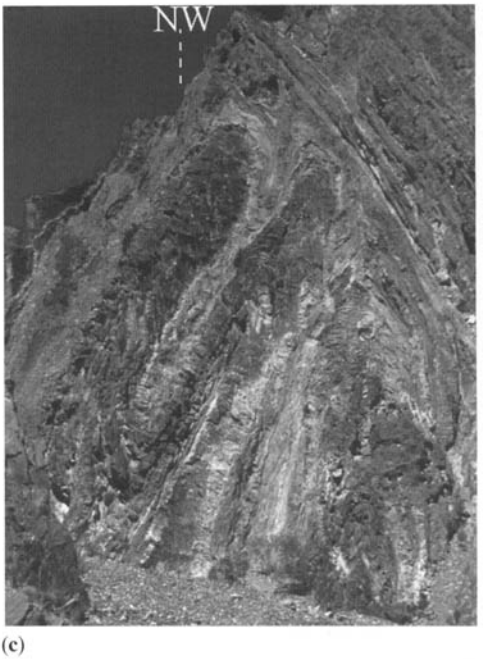

(c)

Fig. 7. Illustration of the different structures accommodating deformation within the pop-up structure. (**a**) Photo and line drawing interpretation of intense chevron folding and duplex formation in the Kioto limestones, Zanskar River gorge north of Nerak, > 1 km vertical relief. (**b**) Large-scale isoclinal folding in the Lilang group carbonates (*c.* 500 m vertical relief), Zanskar River gorge. (**c**) Ruck folding of Kioto limestones beneath a roof thrust (*c.* 10 m across), Shillakong.

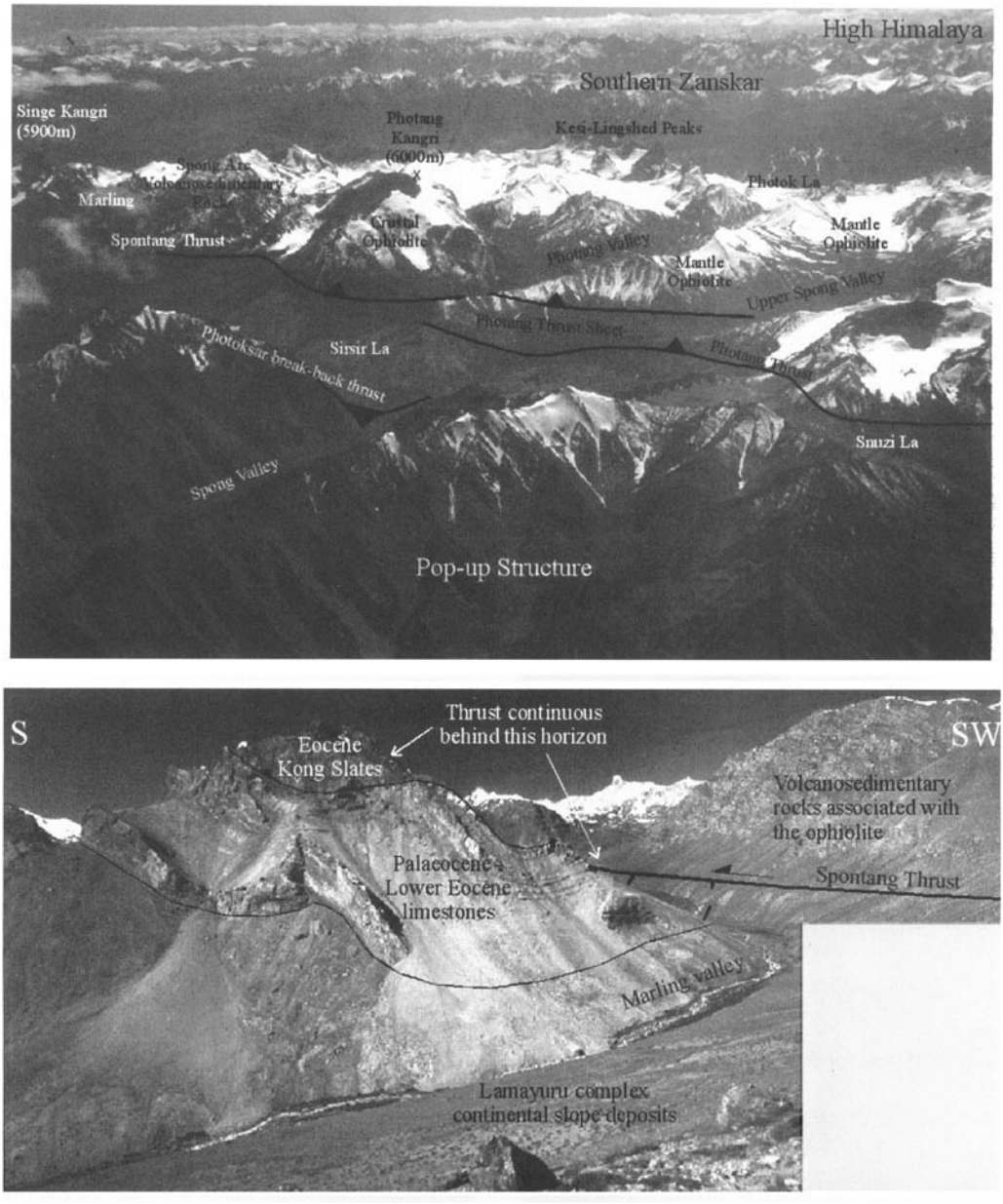

Fig. 8. (**a**) Southward aerial view over the pop-up zone to the Spontang ophiolite and associated Neo-Tethyan rocks of the Spong arc and the Photang thrust sheet. (**b**) In the lower Marling valley, the contact of ophiolitic rocks thrust over the Tertiary limestone sequence can be constrained to within 20 m. This thrust truncates bedding in the limestones and has cut up through the Tertiary sequence from below. This is strong evidence that the ophiolite was emplaced prior to deposition of the limestone sequence (D1) and was then re-thrust to its current structural position above the limestones following India–Asia collision (D2), given the assumption that thrusting always cuts up-section.

up-structural section in the direction of transport (Fig. 3, 50 Ma section). The D2 re-thrusting is also closely associated with complex uplift–subsidence patterns in the Palaeocene–Eocene stratigraphy and the formation of a piggy-back basin, in advance of the thrust sheet during the final ocean closure between India and Asia (Corfield 1998).

Implicit in these observations is that the tip of the Yulchung Thrust represents the leading edge to which the Neo-Tethyan thrust sheets were obducted in the late Cretaceous. Along cross-section D (Fig. 3) the minimum undeformed width across the pop-up structure has been estimated as 44 km. The tip of the Yulchung Thrust restores to a position approximately 10 km to the south of the PBT in section D (Fig. 3). The northeastern edge of the continental margin is poorly defined and can be placed between the MZB and the northern limit of the Lamayuru complex continental slope deposits, for which 15 km represents a conservative minimum estimate of the original width. Therefore, the Neo-Tethyan thrust sheets were emplaced a minimum of 70 km onto the north Indian continental margin in the late Cretaceous.

D2 south of the pop-up structure

The large amplitude folding of the Maastrichtian to lower Eocene shallow-water limestone sequence is one of the most distinctive features of the Spontang region. Sandwiched between the thick sandy marls of the Kangi La Formation and the equally fissile units of the Eocene Kong and Chulung La slates, the competent limestone unit exhibits disharmonic folding on a massive scale. The style of folding within the limestone layers varies from upright large wave-length cylindrical folding in the thicker, more competent units in the east to tighter southwest-vergent chevron folding near Dibling in the southwest. The only place in which the Tertiary limestones appear to be affected by D3 is in the Singe region in the footwall of the Photoksar break-backthrust. Axial planes of the D2 folds have an E–W strike with steeply to gently inclined northerly dips, indicating south-vergent deformation. D3 folding is restricted to the immediate vicinity of the PBT, characterized by open folding about upright NNW–SSE striking axial planes. This orientation approximately parallels the strike of the PBT in this region and the obvious conclusion is that the D3 folding formed contemporaneously with, and in the hanging wall to, the major break-backthrust. The spectacular peak of Singe Kangri occupies the site of one of the interference maxima of the superimposed folding events (Fig. 9), explaining its current elevation comparable to the peaks comprised of the structurally overlying ophiolite immediately to the west.

The limestones accommodate consistent D2 shortening of 140–160% across the width of their exposure despite the variety of folding styles. D1 and D2 shortening for the Mesozoic shelf sediments in the Nerak region, south of the Photoksar break-backthrust has already been estimated as a minimum of 200%. The greater shortening in the Mesozoic shelf sediments is further evidence for the D1 event prior to deposition of the Maastrichtian to early Eocene succession. The absolute shortening accommodated along the restored cross-section is 6.8 km between the base of the ophiolite and the Oma Chu Detachment.

To the northeast, deformation in the Tertiary limestones is entirely decoupled from deformation in the Mesozoic shelf sequence beneath. This is a consequence of the intervening very thick (>1 km) Kangi La Formation shales towards the distal northeastern parts of the shelf. Deformation of this shaly unit is essentially ductile and decouples the very large amplitude disharmonic folding in the limestones from the underlying units. However, towards the southwest the Kangi La Formation thins rapidly and the kilometre amplitude folds of the Tertiary sequence are not decoupled from the underlying Mesozoic units. Folding throughout the entire sequence is more open and alone accommodates less shortening than the disharmonic folding to the northeast. Shortening was also accommodated at all levels along the Oma Chu Detachment, a major D2 thrust which was later reactivated by normal faulting (see following section). At this point there is no misfit in shortening between the Tertiary and Mesozoic successions, suggesting that D1 ophiolite emplacement deformation did not affect these inner parts of the shelf.

The overall vergence patterns in the Tertiary limestones are not entirely uniform. Southwest of the ophiolite and beneath its leading edge, all the structures show a consistent southwest vergence. However, in the hanging wall of the PBT, underneath the northern, more distal parts of the ophiolite, the dominant trend is east–west-striking fold axial planes, with south-verging structures developed in the east. This pattern cannot be related to the effect of the D3 PBT which has been shown to superimpose folding on this earlier south-vergent event in the Singe region. One possible explanation for this is that in the earliest stages of India–Asia collision, the re-thrusting of the ophiolite was south-directed, giving rise to the E–W-striking structures seen immediately south of the initiation site for re-thrusting. As the collision between the irregular plate boundaries became complete and the suture evolved into the NW–SE-striking orientation seen today, the dominant direction of over-thrusting may have gradually rotated to the southwest to produce the dominant orientation of D2 and D3 structures.

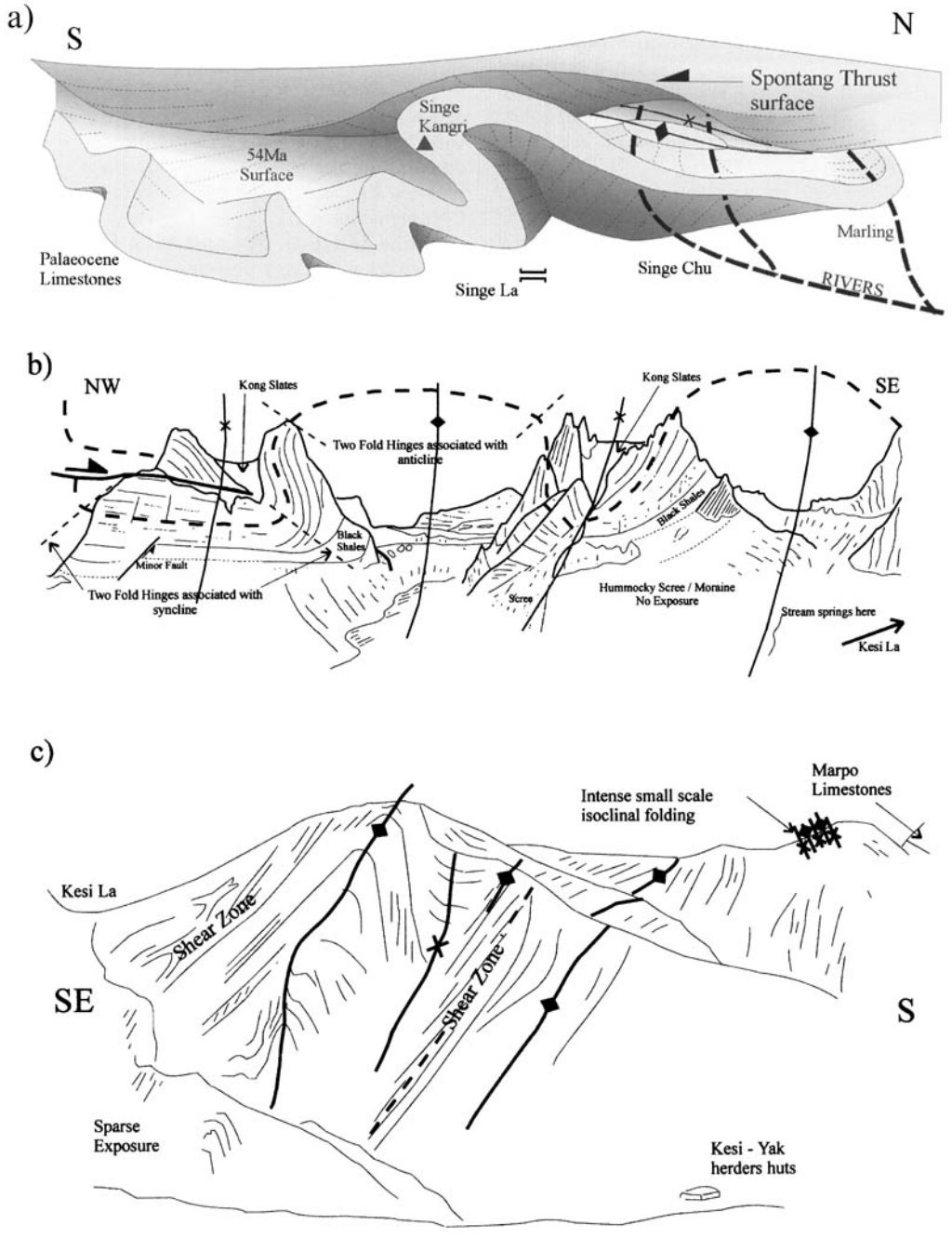

Fig. 9. (**a**) Three-dimensional representation of the structure in the Singe Kangri region. The D2 south-vergent folding event has been overprinted in this region by a later WSW-vergent folding associated with the Photoksar Thrust. (**b**). Sketch of the corries northwest of the Kesi La at the head of the Kesi valley. Progressive shortening in the Tertiary limestones has resulted in the formation of two hinge planes for each fold, followed by fracturing of the northern limb of the NW syncline. (**c**) Sketch of the style of deformation in the Kangi La Formation to the south of the Kesi La. The formation is typically cut by zones of distributed shearing (centre) and localized small-scale development of isoclinal folding (top right). The dominant control on the regional structural orientation is the folding of the thick, competent Tertiary limestone sequence. The Kangi La Formation on the large scale behaves in a ductile manner accommodated on the small scale by folding and shearing in all orientations.

Southern Zanskar

The structures preserved south of the Oma Chu valley are related to D2 deformation at depth and extend south across the entire High Himalayan slab. The D2 event was responsible for the thickening of the Indian crust and burial to high-grade metamorphic conditions. The southern parts of the Zanskar passive margin are also affected by late D2 to D3 normal faulting, extending as far north as the Oma Chu and Zangla detachments at the northern edge of the lower Zangla unit. This normal faulting has followed on from earlier southwest-vergent thrusting responsible for the thickening of the passive margin sediments. The normal faults which have developed commonly exploit planes of weakness created by earlier major thrusts and are termed detachments.

The Oma Chu Detachment runs along the southern side of the Oma Chu valley (Fig. 2), forming the southern margin of the upper Zangla unit. Garzanti & Brignoli (1989) named this fault the 'Oma Chu Thrust', noting the jump in illite crystallinity from 3.9 to 10.2 and a jump in chlorite crystallinity from 2.2 to 3.4 from south to north across the fault. A higher metamorphic grade is associated with lower values in the crystallinity index. Therefore, the hanging wall of the Oma Chu Detachment was metamorphosed at lower grades than the footwall. Garzanti & Brignoli (1989) considered the hanging wall to belong to the higher-level, upper Zangla thrust sheet. However, to give rise to the sharp change in crystallinity values, movement on the Oma Chu Detachment must have postdated the metamorphic event. Therefore, the lower grade of the hanging wall is only consistent with normal motion on the fault. Post-metamorphic thrusting would result in the opposite trend in metamorphic grade while pre/syn-metamorphic thrusting would not result in a significant change in grade across the fault.

We interpret this structure as a D2 thrust which has been reactivated along much of its length as a D3 normal fault. This is most clearly seen between Dibling and the Puzdong La (Fig. 2), where the normal fault does not exactly coincide with the earlier thrust plane. The resulting block which separates the two thrust planes is preserved as a structural high in the hanging wall of the D2 thrust and the footwall of the D3 normal fault, exposing older rocks at the same structural level. Along much of the length of the fault, Cretaceous Guimal sandstones in the hanging wall are juxtaposed with early to mid-Jurassic Kioto limestones in the footwall. The relatively steep dip of the Oma Chu Detachment (approximately 50–60° NE) resulted from the reactivation of a former thrust fault. The Oma Chu Detachment dies out to the east, the fault plane stepping north forming the similar Zangla Detachment (Searle *et al.* 1997). The units above and below the detachment have been shortened independently with fold axial planes truncated by the detachment. Once again the shaly horizons within the Zanskar shelf sequence, in particular the Spiti shales and the Kangi La Formation, have acted as décollement horizons with different fold orientations in the footwall and hanging wall. Further to the southwest, the Karsha Detachment and the Zanskar Shear Zone are similar normal faults.

Shortening in southern Zanskar

Following the southwest-vergent folding and thrusting of the Tertiary succession during the early stages of India–Asia collision, deformation propagated southwestward and down the structural section. Evidence of nappe formation at this stage is seen in the Oma Chu and Zangla detachments (prior to normal faulting), which mark major structural breaks in fold axis orientations indicative of independent shortening in the superposed units.

Line balancing of stratigraphic horizons, which can be widely correlated using SPOT satellite imagery across the region between the Karsha Detachment and the Oma Chu Detachment, gives estimates of 160–170% shortening due to folding alone. Further shortening is accommodated by considerable internal thickening of stratigraphic units and by widespread thrusting that could not be resolved on the SPOT image. However, along several sections observed in the field these structures are responsible for a minimum of a further 180% shortening. A combination of these estimates gives a minimum value of around 300% shortening across southern Zanskar. The present-day width of this section is 15 km, therefore the absolute shortening is at least 30 km across a minimum undeformed width of 45 km. South of the Karsha Detachment, no attempt has been made to estimate the shortening, or the throw along the detachment itself, due to insufficient data.

Overall shortening

Figure 3 shows a fully sequentially restored cross-section from the Zanskar Shear Zone in the south to the Indus Suture Zone in the north, incorporating the shortening estimates discussed in the text. The total minimum shortening estimated between the Main Zanskar backthrust in the north to the Karsha Detachment in the

south is 85 km across a present-day width of *c.* 45 km along section D. This value does not include any estimates of shortening in the poorly constrained units of the Indus Suture Zone. This value is in remarkable agreement with the 87 km shortening obtained by Steck *et al.* (1993) for their Nyimaling–Tsarap Nappe. This estimate was based on a model of simple shear and was independent of inferred deformation events and timings. Imbricate structures grading into a large ductile shear zone with depth characterize the northern parts of the Zanskar passive margin in eastern and western areas. There is no clear evidence for significantly different shortening mechanisms taking place along the strike of the Zanskar Tethyan Himalaya, as suggested by Steck *et al.* (1993).

Along-strike variation

It is a striking feature of the structure in the Ladakh Himalaya that the width of the Tethyan Himalaya increases dramatically from west to east, which is also mirrored in the width of the D3 pop-up structure (Fig. 2). Since the percentage shortening across each transect is fairly constant, there are two major implications for the regional tectonics: (1) the restored width of the Tethyan Himalaya increases significantly to the east; and (2) the absolute shortening across the Tethyan Himalaya is greater in the east.

The reason for the along-strike variation in the accommodation of shortening may itself reflect the original geometry of the north Indian continental margin. It is possible that the original width of the passive margin sequence thinned towards the west. However, there is no evidence from the Zanskar shelf sediments to support such a hypothesis. Part of the problem lies in the inaccessibility of the region along the India–Pakistan border, the geology of which remains poorly understood. Alternatively, the significantly reduced width of the Tethyan zone in the west may reflect higher rates of exhumation of the HHC unit due to more rapid thickening, uplift and erosion. This in turn would be directly related to the palaeo-Indian continental margin, indenting significantly into Asia around this NW corner of India (e.g. Dewey *et al.* 1989). Due to the NW Indian indentor, D2 deformation related to India–Asia collision would have been more intense the further west and closer to the front of the indentor. This is consistent with the very rapid exhumation rates in the Nanga–Parbat region (Whittington 1996), and may imply that the Tethyan Himalaya and HHC unit have been significantly structurally telescoped and eroded due to the high exhumation rates in this region.

Another explanation for the reduced width of the Tethyan zone in the west could be that subduction of the distal Indian passive margin sediments has occurred. Although subduction of the leading edge of the Indian continental margin has probably occurred with evidence of high-pressure blueschists (Sapi La glaucophane schists in west Ladakh; Searle *et al.* 1988) and the Tso Morari eclogites in east Ladakh, it is highly unlikely that the great thickness of shelf carbonate has been subducted in the western area. The preservation of slope sediments in the western ISZ near Sapi La (Robertson & Degnan 1993) is also inconsistent with this explanation. In summary, the lateral variations observed across the Tethyan Himalaya of Ladakh would appear to be best explained by the effects of peninsular northwest India indenting the Asian plate to the west of the area, with increased erosion in the NW removing the 'missing' shelf carbonate cover.

Conclusions

Detailed structural mapping around the Spontang ophiolite and across the northern Indian shelf sediments to the Indus Suture Zone in the Zanskar–Ladakh Himalaya has revealed the three-dimensional geometry of the structures. Cross-cutting relationships and balanced sections have confirmed that the overall evolution involved three major phases of crustal shortening: a pre-collisional ophiolite obduction stage (D1); a post-collisional folding and thrusting event which occurred right across the Ladakh–Zanskar Himalaya (D2); and a late Tertiary phase of SW-vergent re-thrusting and NE-vergent backthrusting across the northern margin of the Indian plate (D3). Reactivation of earlier SW-vergent thrusts as NE-directed low-angle normal faults in SW Zanskar was related to uplift and exhumation of the High Himalaya to the south and SW.

Balanced and sequentially restored cross-sections across the entire north Indian plate margin from the Indus Suture Zone to the Zanskar Shear Zone, the northern boundary of the High Himalayan slab, shows a minimum shortening of 85 km (280%). The Spontang ophiolite was obducted an absolute minimum of 70 km southwestwards onto the Mesozoic passive margin of India during the late Cretaceous, D1. The ophiolite was subsequently re-thrust during D2 deformation over Maastrichtian–Lower Eocene limestones. Major differences in magnitude and style of folding occur in the Mesozoic shelf carbonates and the Lower Tertiary limestones,

confirming a late Cretaceous phase of deformation on the north Indian plate.

Thrusts bounding the SW margin of the pop-up zone truncate earlier fold axial planes and thrusts in the footwall, showing that the late Tertiary D3 deformation, including the NE-directed backthrusting along the Indus Suture Zone, occurred after a major phase of crustal shortening and thickening following India–Asia collision at 54–50 Ma. Major low-angle normal faults across the SW part of the Zanskar shelf place younger rocks onto older and are related to uplift of the High Himalayan slab along the footwall of the Zanskar Shear Zone. These detachments separate packages of rocks which show different structural styles of folding.

Due to the preservation of the Spontang ophiolite and to the excellent exposures and deep erosion levels in Ladakh, this area probably preserves all of the deformation history along the leading edge of the Indian plate. Elsewhere, only the later stages of deformation are preserved.

This work was supported by NERC DPhil. grant GT4/95/247/E to R. Corfield and NERC grant GT5/96/13/E to M. Searle. We are grateful to A. Robertson and R. Strachan for reviews and the Tectonic Studies Group and Geological Society of London for contributing funds towards publication of the colour maps and sections. We are also grateful to Fida Hussein Mitoo and Lobsang & Namgal Tsering of Leh, Lobsang Namgal of Pishu, Rich Bisley and Owen Green for their assistance in the field.

References

BASSOULLET, J-P., COLCHEN, M., GUEX, J., LYS, M., MARCOUX, J. & MASCLE, G. 1978. Permien terminal neritique, Scythian pelagique et volcanisme sous-marin, indices de processes tectono-sedimentaires distensifs a la limite Permien–Trias dans un bloc exotique de la suture de l'Indus (Himalaya du Ladakh). *Comptes Rendus de l'Academie des Sciences*, **287**, 675–678.

BAUD, A., GAETANI, M., GARZANTI, E., FOIS, E., NICORA, A. & TINTORI, A. 1984. Geological observations in south-eastern Zanskar and adjacent Lahul area (north-western Himalaya). *Eclogae Geologicae Helvetiae*, **77**, 171–197.

COLCHEN, M. & REUBER, I. 1986. Les melanges ophiolitiques du Zanskar, Himalaya du Ladakh. *Comptes Rendus, de l'Academie des Sciences, Paris, Serie II*, **303**, 719–724.

——, MASCLE, G. & VAN HAVER, T. 1986. Some aspects of collision tectonics in the Indus suture zone, Ladakh. *In*: COWARD, M. P. & RIES, A. C. (eds) *Collision Tectonics*. Geological Society, London, Special Publications, **19**, 173–184.

CORFIELD, R. I. 1998. *Origin and emplacement of the Spontang ophiolite and crustal shortening processes in the Ladakh–Zanskar Himalaya, NW India*. DPhil. thesis, University of Oxford.

——, SEARLE, M. P. & GREEN, O. R. 1999. Photang thrust sheet: an accretionary complex structurally below the Spontang ophiolite constraining timing and tectonic environment of ophiolite obduction, Ladakh Himalaya, NW India. *Journal of the Geological Society, London*, **156**, 1031–1044.

DEWEY, J. F., CANDE, S. & PITMAN, W. C. 1989. Tectonic evolution of the India/Eurasia collision zone. *Eclogae Geologicae Helvetiae*, **82**, 717–734.

FRANK, W., THONI, M. & PERTSCHELLER, F. 1977. Geology and petrography of Kulu–South Lahul area. *Colloques Internationaux du Centre National de la Recherche Scientifique*, **268/2**, 147–172.

FUCHS, G. 1977. Traverse of Zanskar from the Indus to the Valley of Kashmir—a preliminary note. *Jahrbuch der Geologischen Bundesanstalt*, **120**, 165–217.

—— 1982. The Geology of Western Zanskar. *Jahrbuch der Geologischen Bundesanstalt*, **125**, 1–50.

GAETANI, M. & GARZANTI, E. 1991. Multicyclic history of the Northern India Continental Margin (North-western Himalaya). *American Association of Petroleum Geologists Bulletin*, **75**, 1427–1446.

——, NICORA, A. & PREMORI SILVA, I. 1980. Uppermost Cretaceous and Palaeocene in the Zanskar Range (Ladakh–Himalaya). *Rivista Italiana di Paleontologia e Stratigrafia*, **86**, 127–166.

GANSSER, A. 1964. *Geology of the Himalayas*. J. Wiley, Chichester.

GARZANTI, E. & BRIGNOLI, G. 1989. Low temperature metamorphism in the Zanskar sedimentary nappes (NW Himalaya, India). *Eclogae Geologicae Helvetiae*, **82**, 669–684.

—— & VAN HAVER, T. 1988. The Indus Clastics: forearc basin sedimentation in the Ladakh Himalaya (India). *Sedimentary Geology*, **59**, 237–249.

——, BAUD, A. & MASCLE, G. 1987. Sedimentary record of the northward flight of India and its collision with Eurasia (Ladakh Himalaya, India). *Geodynamica Acta*, **1**, 297–312.

HAYDEN, H. H. 1904. *The Geology of Spiti, with part of Bashahr and Rupshu*. Memoirs of the Geological Survey of India, **36**, 1–129.

—— 1908. *Geology and Geology of the Himalaya (Part 4)*. Geological Survey of India, Calcutta.

KELEMAN, P. B. & SONNENFELD, M. D. 1983. Stratigraphy, structure, petrology and local tectonics, Central Ladakh, NW Himalaya. *Schweizerische Mineralogische und Petrographische Mitteilungen*, **63**, 267–287.

LYDEKKER, R. 1883. The Geology of the Kashmir and Chamba territories and the British district of Khagan. *Memoirs of the Geological Survey of India*, **22**, 1–344.

NICORA, A., GARZANTI, E. & FOIS, E. 1987. Evolution of the Tethys Himalaya continental shelf during Maastrichtian to Palaeocene (Zanskar, India). *Rivista Italiana di Paleontologia e Stratigrafia*, **92**, 439–496.

RATSCHBACHER, L., FRISCH, W. & LIU, G. 1994. Distributed deformation in southern and western Tibet during and after the India–Asia collision. *Journal of Geophysical Research*, **99, B10**, 19917–19945.

REUBER, I. 1989. The Dras Arc: two successive volcanic events on eroded oceanic crust. *Tectonophysics*, **161**, 93–106.

ROBERTSON, A. H. F. 1998. Rift-related sedimentation and volcanism of the north-Indian margin inferred from a Permian–Triassic exotic block at Lamayuru, Indus Suture Zone (Ladakh Himalaya) and regional comparisons. *Journal of Asian Earth Sciences* **16, 2–3**, 159–172.

—— 2000. Formation of mélanges in the Indus Suture Zone, Ladakh Himalaya by successive subduction-related, collisional and post-collisional processes during late Mesozoic–Late Tertiary time. *This volume*.

—— & DEGNAN, P. J. 1993. Sedimentology and tectonic implications of the Lamayuru Complex: deep-water facies of the Indian passive margin, Indus Suture Zone, Ladakh Himalaya. *In*: TRELOAR, P. J. & SEARLE, M. P. (eds) *Himalayan Tectonics*. Geological Society, London, Special Publications, **74**, 299–321.

—— & —— 1994. The Dras arc Complex: lithofacies and reconstruction of a late Cretaceous oceanic volcanic arc in the Indus Suture Zone, Ladakh Himalaya. *Sedimentary Geology*, **92**, 117–145.

SCHELLING, D. 1992. The tectonostratigraphy and structure of the eastern Nepal Himalaya. *Tectonics*, **11**, 925–943.

—— & ARITA, K. 1991. Thrust tectonics, crustal shortening, and the structure of the far-eastern Nepal Himalaya. *Tectonics*, **10**, 851–862.

SEARLE, M. P. 1983. Stratigraphy, structure and evolution of the Tibetan–Tethys zone in Zanskar and the Indus suture zone in the Ladakh Himalaya. *Transactions of the Royal Society of Edinburgh: Earth Sciences*, **73**, 205–219.

—— 1986. Structural evolution and sequence of thrusting in the High Himalayan, Tibetan–Tethys and Indus Suture Zones of Zanskar and Ladakh, Western Himalaya. *Journal of Structural Geology*, **8**, 923–936.

——, COOPER, D. J. W. & REX, A. J. 1988. Collision Tectonics of the Ladakh–Zanskar Himalaya. *Philosophical Transactions of the Royal Society of London*, **A326**, 117–150.

——, CORFIELD, R. I., STEPHENSON, B. & MCCARRON, J. 1997. Structure of the North Indian continental margin in the Ladakh–Zanskar Himalayas: Implications for the timing of obduction of the Spontang ophiolite, India–Asia collision and deformation events in the Himalaya. *Geological Magazine*, **134**, 297–316.

——, PICKERING, K. T. & COOPER, D. J. W. 1990. Restoration and evolution of the intermontane Indus molasse basin, Ladakh Himalaya, India. *Tectonophysics*, **174**, 301–314.

SRIKANTIA, S. V., GANESAN, T. M., RAO, R. N., SINHA, P. K. & TIRKEY, B. 1980. Geology of the Zanskar Area, Ladakh Himalaya. *Himalayan Geology*, **8**, 1009–1033.

SRIVASTAVA, P. & MITRA, G. 1994. Thrust geometries and deep structure of the outer and lesser Himalaya, Kumaon and Garhwal (India): implications for evolution of the Himalayan fold-and-thrust belt. *Tectonics*, **13**, 89–109.

STECK, A., SPRING, L., VANNAY, J-C., MASSON, H., STUTZ, E. *et al.* 1993. Geological transect across the North-western Himalaya in eastern Ladakh and Lahoul (A model for the continental collision of India and Asia). *Eclogae Geologicae Helvetiae*, **86**, 219–263.

STOLICZKA, F. 1866. *Geological Sections across the Himalayan mountains from Wang-tu-bridge on the river Sutlej to Sungdo on the Indus; with an account of the formations in Spiti accompanied by a revision of all known fossils from that district.* Memoirs of the Geological Survey of India, **5**, 1–354.

SUTRE, E. 1990. *Les formations de la marge nord-Neotethsienne et les melanges ophiolitiques de la zone de suture de l'Indus en Himalaya du Ladakh.* Thesis, Docteur de L'Universite de Poitiers.

THAKUR, V. C. 1981. Regional framework and geodynamic evolution of the Indus–Tsangpo suture zone in the Ladakh Himalaya. *Transactions of the Royal Society of Edinburgh: Earth Sciences*, **72**, 89–97.

TRELOAR, P. J., REX, D. C., GUISE, P. G., COWARD, M. P., SEARLE, M. P. *et al.* 1989. K–Ar and Ar–Ar geochronology of the Himalayan collision in NW Pakistan; constraints on the timing of suturing, deformation, metamorphism and uplift. *Tectonics*, **8**, 881–909.

WHITTINGTON, A. G. 1996. Exhumation overrated at Nanga Parbat, northern Pakistan. *Tectonophysics*, **260**, 215–226.

Glaucophane and barroisite eclogites from the Upper Kaghan nappe: implications for the metamorphic history of the NW Himalaya

B. LOMBARDO[1], F. ROLFO[2] & R. COMPAGNONI[1,2]

[1]*C.N.R.-C.S. Geodinamica Catene Collisionali, c/o DSMP, Via Valperga Caluso 35, I-10125, Torino, Italy (e-mail: lombardo@dsmp.unito.it)*

[2]*Dipartimento di Scienze Mineralogiche e Petrologiche, Università di Torino, Via Valperga Caluso 35, I-10125, Italy*

Abstract: This paper presents the results of a petrographical and mineral chemical study of glaucophane- and barroisite-bearing eclogites from the Upper Kaghan nappe in the Higher Himalayan Crystallines of the Pakistan Himalaya, and discusses the implications of the *P–T* path recorded in such rocks for the tectonic and metamorphic history of the NW Himalaya. The eclogites described here come from a previously undescribed outcrop at Gittidas, but belong to the same suite as the garnet–omphacite–phengite–quartz–rutile eclogites previously described elsewhere in the Upper Kaghan nappe. The metamorphic peak assemblage is garnet–omphacite–rutile–quartz in glaucophane eclogite and garnet–omphacite–zoisite–rutile ± kyanite ± phengite ± ankerite in barroisite eclogite. Most samples contain a significant amount of amphibole, white mica and quartz. White mica may be present either as part of the peak assemblage (phengite) or as a retrogressive phase after kyanite (paragonite). Amphibole is later than the metamorphic peak assemblage and is barroisite in most samples, but in relatively Fe-rich eclogite it is glaucophane with significant Na in the A site, Ca in the M4 site and tetrahedral Al. Garnet displays strong prograde zoning in the barroisite eclogites, with Mg increasing and Fe decreasing from core to rim. The iron-rich core is crowded with mineral inclusions of the peak assemblage, but inclusions of earlier paragonite, green and blue-green amphibole were also found. Peak metamorphic conditions in the barroisite eclogites have been estimated at $T = 610 \pm 30\,^{\circ}C$ and $P = 24 \pm 2$ kbar from Fe/Mg partition in garnet–omphacite pairs, and from the garnet–omphacite–phengite barometer. These values are close to the equilibration conditions estimated for the eclogites of the North Himalayan Tso-Morari Dome. Strong similarities between metamorphic evolution of the Upper Kaghan nappe and metamorphic evolution of the eclogite-bearing units of the Neelum valley just to the east of the Kaghan valley indicate that the eclogite occurrences of the Kaghan–Neelum area define an eclogite-bearing terrane of regional extent, which was subjected to high pressure metamorphism in middle Eocene times. A comparison of the metamorphic evolution recorded in the eclogites of the NW Himalaya with that of the granulitized eclogites recently discovered in the E Himalaya suggests the possibility of a Himalaya-wide eclogitic metamorphism of pre-Miocene age. Therefore, the main difference between the Higher Himalayan Crystalline nappes of the NW Himalaya and those of the E Himalaya appears to lie less in the early part of their metamorphic evolution than in the different *P–T* paths they followed during exhumation.

Occurrences of medium-temperature eclogites are widely recognized as a distinctive feature of many continental collision zones (Smith 1988; Carswell 1990). Their importance for unravelling the processes operating during continental collision lies in the fact that the presence of eclogite rocks is often the only evidence that a metamorphic terrain may have passed through high pressure conditions, since country rocks to eclogites often appear devoid of high pressure mineral assemblages. This situation has led to widely different tectonic models, proposed to explain the genesis of the high pressure (HP) metamorphism and to hotly debated controversies such as that on the 'foreign' v. '*in situ*' origin for the Caledonian eclogites of western Norway.

In the Himalayan mountain belt, eclogites were first reported from the Upper Kaghan nappe in the NW Himalaya (Chaudry & Ghazanfar 1987, p. 27; Spencer *et al.* 1990; Pognante & Spencer 1991; Spencer 1993). In addition to the

From: KHAN, M. A., TRELOAR, P. J., SEARLE, M. P. & JAN, M. Q. (eds) *Tectonics of the Nanga Parbat Syntaxis and the Western Himalaya*. Geological Society, London, Special Publications, **170**, 411–430. 1-86239-061-4/00/$15.00

more frequent garnet–omphacite–quartz–rutile ± phengite eclogites described by Pognante & Spencer (1991) and dated as Eocene by Tonarini *et al.* (1993), glaucophane eclogites were found in the Upper Kaghan valley in summer 1991 by U. Pognante and P. Benna (Pognante 1992, p. 11) and subsequently also in the North Himalayan Tso Morari Dome of E Ladakh (De Sigoyer *et al.* 1997). Eclogites similar to those described by Pognante & Spencer (1991) and Spencer (1993) in the Kaghan valley have been described from the nearby Neelum valley (Fontan 1998 and references therein) and the Indus Suture Zone (Le Fort *et al.* 1997), whereas granulitized eclogites have been recently reported from the Kharta region of southern Tibet, about 35 km to the east of the Everest–Makalu massif (Lombardo *et al.* 1998).

This contribution has three aims: (1) presenting the results of a petrographical and mineral chemical study of the eclogite samples from the High Himalayan Crystallines (HHC) of the Upper Kaghan valley in which Pognante (1992) discovered the presence of glaucophane; (2) combining data from the Upper Kaghan nappe with data from the nearby Neelum valley (Fontan 1998 and references therein), to show that the eclogite occurrences of this area define an eclogite-bearing terrane of regional extent; (3) in the light of the new data from the E Himalaya, to discuss contrasting P–T–t paths along the HHC and the possibility of a Himalaya-wide eclogitic metamorphism.

Geological setting

The samples of eclogite were collected by U. Pognante and P. Benna near the summer settlement of Gittidas, in the Upper Kaghan valley 7 km SW of Babusar Pass (Fig. 1). The area is part of the Upper Kaghan nappe, which lies between the Main Central Thrust (=Batal Thrust of earlier authors) and the Main Mantle Thrust, the continuation of the Indus Suture Zone west of the Nanga Parbat massif (Spencer *et al.* 1990). The Main Central Thrust (MCT) separates an underlying Salkhala unit from an overlying Higher Himalayan Crystalline unit, the Upper Kaghan nappe. The rocks above the MCT are all in the amphibolite facies, whereas greenschist facies rocks lie beneath the MCT. Within mylonitic metapelites of the MCT Zone, kyanite and garnet are stable, as are garnet and hornblende in mylonitic amphibolites. Especially in the upper parts of the Salkhala unit, prograde metamorphism in biotite–garnet subfacies of the greenschist facies has outlasted a first pervasive deformation, whereas in the lower parts the ubiquitous paragenesis chlorite + biotite ± garnet is syntectonic (Greco *et al.* 1989).

The stratigraphy and metamorphic history of the Upper Kaghan nappe have been described by Chaudry & Ghazanfar (1987), Greco *et al.* (1989), Spencer (1993) and Greco & Spencer (1993). According to Spencer *et al.* (1990) the Upper Kaghan nappe (corresponding to the Sharda Group defined in the nearby Neelum valley by Chaudry & Ghazanfar 1987) consists of a basement (metagranites and paragneisses), a First (lower) Cover of probable Early Palaeozoic age (metagreywacke unit, corresponding to the Naran and Lulusar formations) and of a Second (upper) Cover of Late Palaeozoic–Early Mesozoic age (Burawai Formation: oligoclase- and garnet-bearing amphibolites, marbles, schists and dolomites, and Babusar Pass Garnetiferous Graphitic Gneiss/Schist).

The metagranites are two-mica, K-feldspar porphyroblastic augen gneisses having Alpine kyanite and garnet. An HP (eclogitic?) overprint in the granitic basement of the middle Kaghan valley is indicated by the growth of kyanite needles in plagioclase and by rims of garnet around magmatic biotites (Greco *et al.* 1989, fig. 8). Garnet, kyanite and rutile are found as accessory minerals in the Gittidas Granite Gneiss of the Upper Kaghan valley (Spencer 1993), some layers of which contain sillimanite, andalusite and rarely kyanite (Chaudry & Ghazanfar 1987, p. 26). These, and the xenoliths and screens of garnetiferous Al-silicate-bearing gneisses reported by Chaudry & Ghazanfar (1987), are possibly relics of a pre-Himalayan contact metamorphism of sillimanite/andalusite grade partly overprinted by the Himalayan metamorphism of kyanite grade.

Both metagreywacke of the Naran Formation (First Cover) and metapelite of the Burawai Formation (Second Cover) contain the characteristic assemblage kyanite–garnet–staurolite–biotite, which appears to have developed syn- to post-kinematic relative to the penetrative foliation and to the first folding event (Greco *et al.* 1989). Quartz veins and patches are common in the Bans metapelites of the Burawai Formation. These very often bear blue kyanite crystals, which may at places reach 10 cm in length (Chaudry & Ghazanfar 1987).

According to Treloar (1997), kyanite- and sillimanite-grade rocks on the hanging wall of the Batal Thrust were metamorphosed at *c.* 650 ± 50 °C and 9 ± 2 kbar. In the lower Kaghan valley, on the footwall, and to the south of the Batal Thrust, garnet grade rocks yield P–T estimates of 540 ± 40 °C at 10 ± 2 kbar. A P–T–t path, calculated through

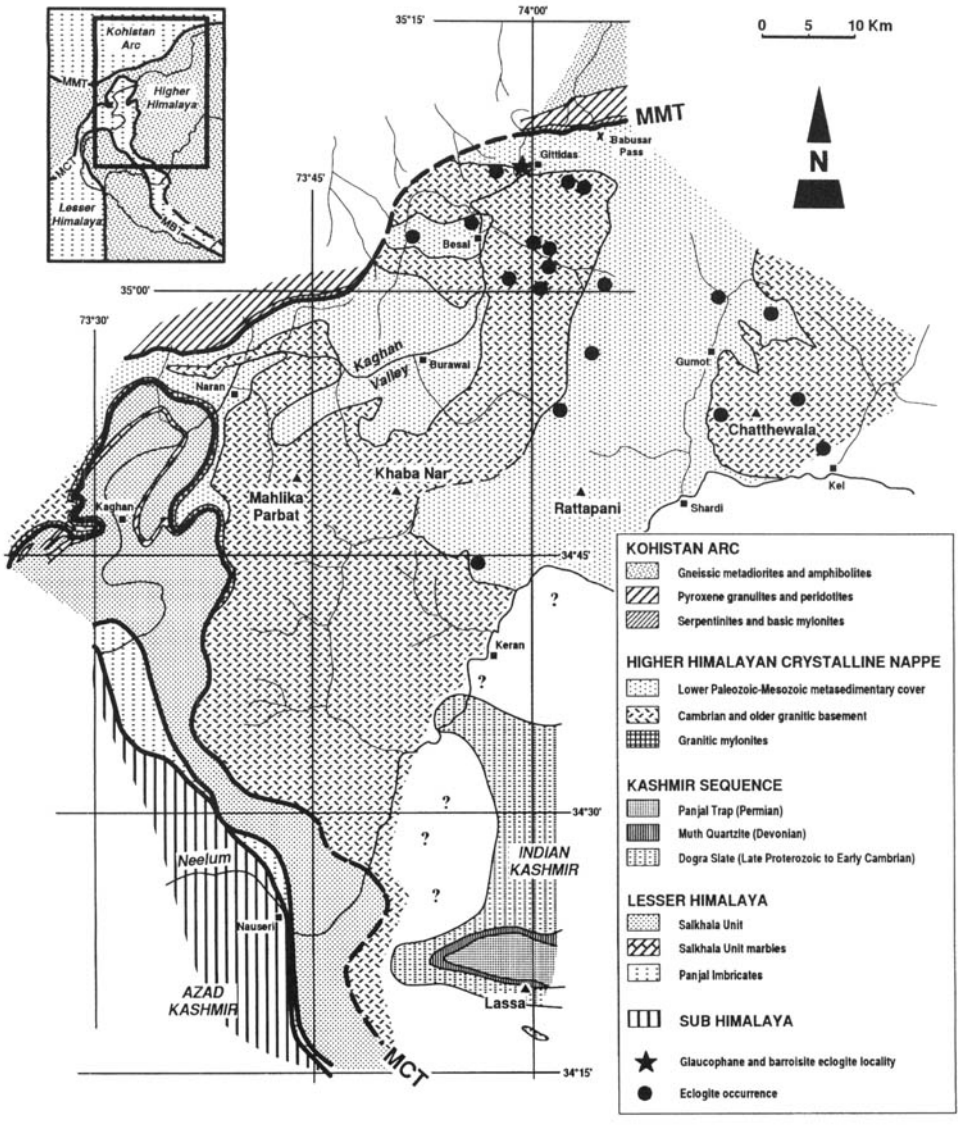

Fig. 1. Geological sketch map of the area from the Kaghan valley to the middle Neelum valley (after Wadia 1934, plate 12; Greco & Spencer 1993; Fontan 1998 and references therein), showing the extent of the eclogite-bearing terrain in the HHC of NW Himalaya. Locations of the eclogite outcrops are shown after data given by Spencer (1993) and Fontan (1998, and pers. comm.). MCT: Main Central Thrust; MMT: Main Mantle Thrust; MBT: Main Boundary Thrust.

forward modelling of garnet zonation profiles (Spear & Selverstone 1983; Spear & Peacock 1990) for a kyanite-grade rock from the upper Kaghan valley, indicates an increasing pressure trajectory, with very little evidence for a significant pressure decrease after the metamorphic peak (Treloar 1995).

Metapelites of the Lulusar Formation (First Cover) contain the characteristic assemblage kyanite–garnet–muscovite–biotite, apparently without staurolite, whereas the Babusar Pass Garnetiferous Graphitic Gneiss/Schist is characterized by garnet–muscovite–biotite assemblages with accessory sillimanite (Chaudry &

Ghazanfar 1987, p. 22). Geothermobarometrical calculations on samples from this unit (Chamberlain *et al.* 1991) record equilibration temperatures of about 550 °C at P of 8.5 kbar, with maximum temperatures up to 580 °C. P–T paths calculated using inclusion minerals in garnet show an initial increase in temperature of 50 to 100 °C, followed by a decrease in temperature of 50 °C from the temperature maximum to the temperature of final equilibration.

Discordant but deformed dolerite dykes and schistose garnet–amphibolite sheets are locally abundant in the granitic basement and in the First Cover, and appear to represent the hypabissal equivalents (feeder dykes) of the metabasaltic rocks of the Second Cover. The primary assemblages (Ca-rich plagioclase, augite, ilmenite ± olivine) are progressively transformed into amphibolite assemblages with the development of garnet, green hornblende ± diopside, oligoclase, biotite and clinozoisite (Papritz & Rey 1989).

Eclogites occur in the basement and in both cover units of the Upper Kaghan nappe east of a N–S line joining Burawai with Keran in the Neelum valley (Fig. 1). Like the amphibolites, they occur in the basement and in the First Cover as feeder dykes to the lava flows of the Second Cover. Preservation of the eclogite mineral assemblage is far better in the basement and in the First Cover than in the Second Cover (Pognante & Spencer 1991; Spencer 1993). The outcrops where the eclogite mineral assemblage (garnet–omphacite–rutile) is best preserved are at Kaar, in the Purbi Nar (Nar = valley), 25 km SE of Gittidas, and in Lohlul Nar, only 2.5 km west of Gittidas (Pognante & Spencer 1991; Spencer 1993).

Bulk geochemistry and εNd–εSr correlations suggest affinity of the eclogites with the metadolerites and amphibolites of the Higher and Lesser Himalaya, described by Papritz & Rey (1989) in the Kaghan–Neelum area, and with the unmetamorphosed Permian Panjal Traps of Kashmir and Zanskar (Spencer *et al.* 1995).

From the observations of Pognante (1992, table 1) and our study of the samples collected by him, the Gittidas eclogites appear to be associated with a metasedimentary paragneiss sequence with the high pressure assemblage garnet–white mica–plagioclase–kyanite–staurolite–zoisite–rutile. The paragneiss may be part of the First Cover or, alternatively, of the older metapelitic sequence of garnetiferous Al-silicate-bearing gneisses reported by Chaudry & Ghazanfar (1987) and Spencer (1993), which in the Gittidas area is intruded by the Gittidas Granite Gneiss.

Timing of the eclogite metamorphism

Geochronological data from a variety of sources indicate that the eclogitic metamorphism in the Upper Kaghan nappe predates 40 Ma. A garnet–omphacite Sm/Nd isochron from two eclogite samples from the Kaar outcrop in the Purbi Nar dates the growth of the eclogite paragenesis at 49 ± 6 Ma. Ages of 43 ± 1 Ma and 39–40 Ma were obtained on phengite with the Rb/Sr method and on rutile with the U/Pb method, respectively (Tonarini *et al.* 1993). This has been confirmed by U/Pb dating with the SHRIMP technique of zircons from a metamorphosed feeder dyke of gabbro in the basement. Apart from a number of clearly discordant ages, an age of 44 ± 3 Ma was found on a metamorphic rim. Oscillatory zoned domains yielded an age of about 269 Ma (Permian). One spot age of *c.* 470 Ma in a magmatic domain proves the presence of inherited zircon components of very probably Early Paleozoic age (Spencer & Gebauer 1996).

Also from the Kaghan valley, but in the Naran area, several kilometres down section from Gittidas, U/Pb dating of zircons within granite sheets that cut the main phase S1 tectonic fabrics and of zircon rims within granites, both at *c.* 47 Ma, places a minimum age on the metamorphism (Zeitler & Chamberlain 1991; Smith *et al.* 1994).

$^{40}Ar/^{39}Ar$ ages of minerals from rocks exposed along the road section between Gittidas and the MMT north of Babusar Pass are reported by Chamberlain *et al.* (1991). Hornblende (sample BBR35, 2 km east of Babusar Pass) displays a somewhat discordant but overall flat spectrum typical of metamorphic amphiboles. The best estimate for the sample's age, obtained from isotope-correlation analysis, is 42.6 ± 1.6 Ma. Muscovite (sample BBR7, collected at the Babusar Pass) yields a nearly flat age spectrum having a mean $^{40}Ar/^{39}Ar$ age of about 24.8 ± 0.6 Ma. Two biotite samples (BBR3, just north of Gittidas and BBR35, 2 km east of Babusar Pass), having flat age spectra and showing no indications of trapped Ar of unusual composition, yielded ages of 22.4 ± 0.3 and 25.2 ± 0.5 Ma, respectively. Such young ages date post-metamorphic cooling of the Upper Kaghan nappe and are corroborated by a zircon fission-track age of 17.5 ± 2.4 Ma from an outcrop just north of Gittidas (sample BBR3) and an apatite fission-track age of 6.9 ± 4.8 Ma at the Babusar Pass (sample BBR7). In view of the relatively large time span between ages in the eclogites and such mica ages, however, it is likely that the younger cooling ages are not directly

related to the eclogite event but, rather, to the Miocene-aged extensional faults which reworked the uppermost part of the High Himalayan Crystallines and the MMT Zone (Vince & Treloar 1996).

At regional scale, K/Ar and $^{40}Ar/^{39}Ar$ hornblende, muscovite and biotite cooling ages of 40 to 35 Ma, 30 to 24 and 29 to 22 Ma, respectively, from the Swat, Besham and Hazara nappes, constrain peak metamorphism also in the region SW of the Kaghan valley as predating 40 Ma and define an Oligocene to Miocene post-metamorphic cooling history (Treloar & Rex 1990).

Petrography and mineral chemistry

Eclogites

Two varieties of eclogite were found in the samples collected by U. Pognante and P. Benna, glaucophane eclogite and barroisite eclogite. The two varieties show significant differences in mineralogy and mineral chemistry (Tables 1–4) which probably reflect differences in the bulk chemical composition of the protolith, the glaucophane eclogite being relatively Fe-rich and the barroisite eclogites being relatively Mg and Al-rich. Both eclogite varieties are massive to foliated, fine- to medium-grained rocks and consist of omphacite, garnet, amphibole and white mica, with accessory rutile, ilmenite and apatite. Most samples also contain up to 15 vol.% of quartz.

Glaucophane-eclogite is characterized by the metamorphic peak assemblage: omphacite, garnet, minor quartz and accessory rutile and apatite (Fig. 2a). The metamorphic foliation was clearly stable during the eclogite-facies peak, as it is mainly defined by alignments of omphacite and aggregates of rutile + ilmenite.

Garnet commonly shows an atoll-like structure, with a large, rounded core hosting inclusions of amphibole and omphacite, and an idioblastic rim free of mineral inclusions. Mineral inclusions are mainly concentrated at the core–rim boundary and consist of abundant omphacite, glaucophane, green amphibole and accessory allanitic epidote, ilmenite, rutile and apatite. These inclusions define an S_i highly discordant to S_e. At the garnet rim, very small fluid inclusions are locally abundant. Garnet is almandine, with pyrope contents of 13–15 mol.%, minor grossular (8 mol.%) and very minor spessartine (Fig. 3a). As shown by a qualitative X-ray map of a garnet porphyroblast (Fig. 4a), garnet is

Table 1. *Representative electron microprobe analyses of garnet*

	T133			T136			T137
	58Grt63c core	58Grt64 int	58Grt65r rim	68Grt117c core	68Grt115 int	68Grt113r rim	70Grt4r rim
SiO_2	37.46	36.74	37.42	38.38	39.40	40.49	39.48
Al_2O_3	20.67	20.06	20.67	21.59	21.34	22.97	22.25
Fe_2O_3	0.81	1.48	0.73	0.60	1.24	0.05	0.80
FeO	33.74	30.78	33.81	29.82	24.49	17.52	25.07
MnO	1.11	0.22	0.78	1.17	0.52	0.00	0.50
MgO	3.38	1.95	3.69	2.75	6.48	12.22	7.70
CaO	3.06	7.53	2.72	7.97	7.71	7.18	6.17
Total	100.23	98.76	99.82	102.28	101.17	100.42	101.97
Si	3.00	2.99	3.00	2.99	3.02	3.00	2.99
Al	1.95	1.92	1.96	1.98	1.93	2.00	1.98
Fe^{3+}	0.05	0.09	0.04	0.04	0.07	0.00	0.05
Fe^{2+}	2.26	2.09	2.27	1.94	1.57	1.08	1.59
Mn	0.07	0.02	0.05	0.08	0.03	0.00	0.03
Mg	0.40	0.24	0.44	0.32	0.74	1.35	0.87
Ca	0.26	0.66	0.23	0.66	0.63	0.57	0.50
Grossular	0.06	0.17	0.06	0.20	0.18	0.19	0.14
Almandine	0.76	0.69	0.75	0.65	0.53	0.36	0.54
Pyrope	0.13	0.08	0.15	0.10	0.24	0.45	0.29
Spessartine	0.03	0.01	0.02	0.03	0.01	0.00	0.01
Andradite	0.02	0.05	0.02	0.02	0.04	0.00	0.02

T133: glaucophane eclogite; T136 and T137: barroisite eclogites. End members and Fe^{3+} were calculated with the NORM algorithm (Ulmer 1986).

Table 2. *Representative electron microprobe analyses of pyroxene*

	T133			T136	T137
	59Px71 core	59Px78 int	59Px77 rim	66Px24 int	70Px6r rim
SiO_2	55.84	55.68	56.43	56.93	57.50
TiO_2	0.17	0.12	0.30	na	0.11
Al_2O_3	10.16	10.88	9.84	10.94	12.62
FeO	9.34	8.90	9.10	2.46	2.52
MnO	na	0.18	0.18	na	0.00
MgO	5.79	5.62	5.91	9.21	8.37
CaO	9.73	10.19	10.79	13.32	11.92
Na_2O	8.94	8.78	8.49	7.21	7.65
Total	99.97	100.36	101.05	100.07	100.70
Si	1.99	1.98	2.00	2.00	2.00
Al^{IV}	0.01	0.02	0.00	0.00	0.00
ΣT	2.00	2.00	2.00	2.00	2.00
Al^{VI}	0.42	0.44	0.41	0.45	0.52
Ti	0.00	0.00	0.01	na	0.00
Fe^{3+}	0.20	0.18	0.16	0.04	0.00
Fe^{2+}	0.08	0.09	0.11	0.04	0.07
Mn	na	0.01	0.01	na	0.00
Mg	0.31	0.30	0.31	0.48	0.43
ΣM1	1.01	1.01	1.01	1.01	1.03
Ca	0.37	0.39	0.41	0.50	0.45
Na	0.62	0.61	0.59	0.49	0.52
ΣM2	0.99	0.99	0.99	0.99	0.96
Jd	41.9	42.7	42.2	45.2	51.6
Quad	38.0	38.5	41.8	50.8	48.4
Ae	20.1	18.8	16.0	4.0	0.0
Fe″/Mg	0.25	0.30	0.35	0.08	0.17

T133: glaucophane eclogite; T136 and T137: barroisite eclogites. End members and Fe^{3+} were calculated with the NORM algorithm (Ulmer 1986). na, not analysed.

compositionally zoned, with a Ca-rich shell of composition Alm_{70} Prp_8 Sps_1 Grs + Adr_{21} separating a core and outer rim nearly of the same composition (Alm_{75} Prp_{15} Sps_2 Grs + Adr_8). Especially at the core–rim boundary, retrograde brown biotite develops at the expense of garnet.

Both the matrix and inclusion *omphacite* is zoned (Fig. 3b), from Jd_{47} Acm_{12} in the core to Jd_{32} Acm_{25} in the rim. Omphacite is commonly replaced by a symplectite of albite (An_{1-2}) + clinopyroxene (Jd_{13-20}) + amphibole with grain size increasing outwards from the contact with omphacite. According to the IMA classification (Leake *et al.* 1997) the symplectite amphibole is Mg-katophorite $(Na_{0.67}\ K_{0.04})\ (Ca_{1.17}\ Na_{0.83})(Mg_{3.22}\ Fe^{2+}_{0.99}\ Mn_{0.02}\ Fe^{3+}_{0.38}\ Al_{0.33}\ Ti_{0.07})(Al_{0.71}\ Si_{7.29})O_{23}$.

Quartz mainly occurs as monomineralic granoblastic polygonal aggregates, which are elongated according to the main rock S_e foliation.

Amphibole occurs as zoned porphyroblasts with blue-violet glaucophane cores and blue-green barroisite rims (Fig. 2c). A representative composition is $(Na_{0.36}\ K_{0.06})\ (Na_{1.66}\ Ca_{0.34})\ (Mg_{2.32}\ Fe^{2+}_{1.29}\ Fe^{3+}_{0.37}\ Al_{0.99}\ Ti_{0.01})(Al_{0.16}\ Si_{7.84})O_{23}$ for glaucophane and $(Na_{0.45}\ K_{0.03})(Ca_{1.34}\ Na_{0.66})\ (Mg_{2.86}\ Fe^{2+}_{1.36}\ Fe^{3+}_{0.49}\ Al_{0.24}\ Ti_{0.06})(Al_{0.66}\ Si_{7.34})O_{23}$ for barroisite (Fig. 5). A number of features in the crystal chemical formula differentiate the Gittidas glaucophane from glaucophanes of low temperature eclogites and suggest a higher temperature of formation, as is the case of glaucophanes from eclogitic rocks of Norway, the Dora–Maira massif of the Western Alps and the Qinling–Dabie collision zone of central China (Ungaretti *et al.* 1981; Kienast *et al.* 1991; Zhang & Liou 1994). Such features are: (1) high tetrahedral Al (up to 0.2 atoms p.f.u.), (2) high Ca in the M4 site (up to 0.4 atoms p.f.u.), and (3) high Na in the A site (up to 0.4 atoms p.f.u.).

Table 3. *Representative electron microprobe analyses of amphibole from the glaucophane eclogite (T133)*

	58Anf4 core	58Anf6 rim	60Anf86 core	60Anf88/1 rim	V59Anf73 core	59Anf75 rim
SiO_2	56.02	50.67	54.99	52.40	53.28	54.98
TiO_2	0.14	0.53	0.29	1.06	0.05	0.09
Al_2O_3	6.95	5.29	6.50	3.74	10.00	9.22
Fe_2O_3	3.52	4.48	6.02	5.81	4.34	5.79
FeO	10.98	11.20	7.70	6.30	10.15	9.03
MnO	0.09	0.00	0.10	0.08	0.08	0.05
MgO	11.14	13.24	12.16	16.27	10.03	10.37
CaO	2.30	8.65	2.57	8.16	2.94	2.41
Na_2O	7.43	3.94	6.79	4.14	6.79	6.64
K_2O	0.32	0.16	0.26	0.17	0.16	0.18
Total	98.89	98.17	97.38	98.13	97.84	98.76
Si	7.84	7.34	7.77	7.44	7.54	7.66
Al^{IV}	0.16	0.66	0.23	0.56	0.46	0.34
Al^{VI}	0.99	0.24	0.85	0.06	1.21	1.17
Ti	0.01	0.06	0.03	0.11	0.01	0.01
Fe^{3+}	0.37	0.49	0.64	0.62	0.46	0.61
Fe^{2+}	1.29	1.36	0.91	0.75	1.20	1.05
Mn	0.01	0.00	0.01	0.01	0.01	0.01
Mg	2.32	2.86	2.56	3.44	2.12	2.15
Ca	0.34	1.34	0.39	1.24	0.45	0.36
Na (M4)	1.66	0.66	1.61	0.76	1.56	1.64
Na(A)	0.36	0.45	0.25	0.38	0.31	0.15
K	0.06	0.03	0.05	0.03	0.03	0.03

Structural formulae are calulated on the basis of 13 cations and 23 oxygens. Fe^{3+} has been calculated from stoichiometry with the NORM algorithm (Ulmer 1986). Crystals 58 and 60 are poikiloblasts of blue (cores) to blue-green (rims) amphibole in the matrix. Crystal 59 is an amphibole inclusion within garnet.

Two representative samples of the more abundant *barroisite-eclogites* were studied in detail. Sample T136 is characterized by the metamorphic peak assemblage: omphacite–garnet–kyanite–zoisite/clinozoisite–quartz–ankerite, with accessory rutile and apatite. Paragonite is present either as inclusions in garnet or as a retrogression phase after kyanite, whereas the amphibole develops as porphyroblasts overgrowing the peak assemblage. In sample T137 the metamorphic peak assemblage is omphacite–garnet–phengite–zoisite/clinozoisite–quartz and accessory rutile and apatite.

Garnet T136 is strongly zoned with a reddish, iron-rich core (Alm_{65} Prp_{10} Sps_3 Grs + Adr_{22}) and a perfectly idioblastic, colourless, iron-poor rim of composition Alm_{36} Prp_{45} Grs_{19} (Figs 3a and 4b). The Fe-rich cores host inclusions of zoisite, Fe-poor clinozoisite, rutile, kyanite, paragonite and yellow-green Na–Ca amphibole, whereas the Mg-rich rims are devoid of mineral inclusions (Fig. 2b). Garnet T137 is likewise zoned, from an iron-rich core (Alm_{63} Prp_{16} Grs + Adr_{21}) to an iron-poor rim (Alm_{51} Prp_{32} Grs_{17}).

Omphacite T136 is compositionally quite homogeneous (Fig. 3b), X_{Jd} ranging betweeen 0.42 and 0.45, with low contents of aegirine (X_{Acm} = 0.02–0.05). It usually contains very small rutile needles, most likely derived from exsolution of a Ti-rich phase, possibly brown hornblende. This interpretation is corroborated by the local presence of inclusions of a relict colourless amphibole in the omphacite. Omphacite T137 is slightly more jadeite-rich (X_{Jd} = 0.47–0.52), but again with low contents of aegirine (X_{Acm} = 0.04–0.06).

Rutile often occurs as skeletal crystals with prismatic shape, most likely derived from the breakdown of older ilmenite, which is still preserved as relics in the garnet core.

Phengite, which is present only in sample T137, has a paragonite content of 8–12 mol.% and is rich in the celadonite component (Si content up

Table 4. *Representative electron microprobe analyses of amphibole from the barroisite eclogites (T136 and T137)*

	67Anf133 core	67Anf134 int	67Anf135 rim	67Anf126 core	67Anf127 int	Anf128 rim	70Anf37c (T137) core
SiO_2	53.45	53.17	48.09	52.39	52.94	53.18	52.76
TiO_2	0.22	0.04	0.05	0.29	0.13	0.22	0.32
Al_2O_3	9.70	10.04	12.73	9.10	10.48	6.44	9.43
Fe_2O_3	2.49	1.72	1.93	0.80	2.59	2.38	5.11
FeO	3.21	4.54	5.04	5.36	3.78	3.57	2.09
MnO	0.13	0.00	0.00	0.13	0.23	0.00	0.00
MgO	16.75	16.03	15.74	17.03	16.33	19.42	16.37
CaO	9.10	9.14	10.63	8.47	9.10	12.58	6.94
Na_2O	3.22	3.47	3.82	4.02	3.59	1.74	4.58
K_2O	0.06	0.04	0.09	0.00	0.00	0.00	0.04
Total	98.34	98.20	98.12	97.59	99.18	99.53	97.64
Si	7.32	7.32	6.75	7.30	7.23	7.29	7.29
Al^{IV}	0.68	0.68	1.25	0.70	0.77	0.71	0.71
Al^{VI}	0.89	0.95	0.86	0.79	0.92	0.33	0.82
Ti	0.02	0.04	0.01	0.03	0.01	0.02	0.03
Fe^{3+}	0.26	0.18	0.20	0.08	0.27	0.25	0.53
Fe^{2+}	0.37	0.52	0.59	0.62	0.43	0.41	0.24
Mn	0.02	0.00	0.00	0.02	0.03	0.00	0.00
Mg	3.42	3.29	3.34	3.54	3.32	3.97	3.37
Ca	1.34	1.35	1.60	1.26	1.33	1.85	1.03
Na (M4)	0.66	0.65	0.40	0.74	0.67	0.15	0.97
Na (A)	0.20	0.28	0.65	0.34	0.28	0.46	0.26
K	0.01	0.01	0.02	0.00	0.00	0.00	0.01

Structural formulae are calculated on the basis of 13 cations and 23 oxygens. Fe^{3+} has been calculated with the programme of Holland & Blundy (1994).

to 3.49 atoms). A representative composition is: $(Na_{0.08}\ K_{0.92})(Mg_{0.49}\ Fe^{2+}_{0.07}\ Al_{1.41}\ Ti_{0.03})(Al_{0.51}\ Si_{3.49})O_{11}$. Phengite flakes included within garnet porphyroblasts show very similar compositions.

Zoisite/clinozoisite is present in the groundmass of both T136 and T137 and as inclusions in garnet and paragonite. A representative composition of zoisite is $Ca_{0.99}\ (Al_{2.92}\ Fe^{3+}_{0.08})\ Si_{3.01}O_{12.5}$ (T136). Clinozoisite has a restricted compositional range (Zo_{72-76}). A representative composition is $Ca_{0.99}\ (Al_{2.72}\ Fe^{3+}_{0.28})\ Si_{3.00}O_{12.5}$ (T136).

Amphibole is zoned, with barroisite cores and edenite rims (Fig. 5). A representative composition is $(Na_{0.20}\ K_{0.01})(Ca_{1.34}\ Na_{0.66})(Mg_{3.42}\ Fe^{2+}_{0.37}\ Fe^{3+}_{0.26}\ Al_{0.89}\ Ti_{0.02})(Al_{0.68}\ Si_{7.32})O_{23}$ for barroisite and $(Na_{0.65}\ K_{0.02})(Ca_{1.60}\ Na_{0.40})(Mg_{3.29}\ Fe^{2+}_{0.59}\ Fe^{3+}_{0.20}\ Al_{0.86}\ Ti_{0.01})(Al_{1.25}\ Si_{6.75})O_{23}$ for edenite.

In sample T137 the barroisitic amphibole shows a slightly different composition $(Na_{0.29}\ K_{0.01})(Ca_{1.04}\ Na_{0.96})(Mg_{3.42}\ Fe^{2+}_{0.47}\ Fe^{3+}_{0.31}\ Al_{0.95})(Al_{0.60}\ Si_{7.32})O_{23}$, with higher Na in sites A and M4, higher octahedral Al, and lower tetrahedral Al. Such crystal-chemical features suggest a slightly higher pressure of formation relative to barroisite in T136.

Paragonite is present only in barroisite eclogite T136. The muscovite component ranges between 5 and 8 mol.%. A representative composition is $(Na_{0.93}\ K_{0.07})\ Al_{3.00}\ Si_{3.00}O_{11}$.

During retrogression omphacite breaks down to a very fine-grained symplectite of albite (An_6) + clinopyroxene (Jd_{13-20}) + amphibole, phengite breaks down to a very fine-grained symplectite of biotite + plagioclase (An_{34}). Also barroisite is unstable and breaks down to Mg-hornblende (Table 4, an.128) which, relative to barroisite, has lower octahedral Al, higher Ca in M4, Na in A and Mg/Fe. Garnet is locally replaced by a thin corona of Fe-rich green amphibole and by yellow-brown biotite growing along cracks of the garnet host.

Country rocks to the eclogites

The Gittidas eclogites are associated with a metasedimentary sequence of paragneiss with the high-pressure assemblage: garnet, K-white mica, plagioclase, kyanite, staurolite, zoisite, epidote and accessory rutile.

Garnet porphyroblasts host inclusions of fine-grained rutile, quartz, plagioclase, graphite, zoisite, epidote and white mica, which define an old metamorphic foliation. Kyanite inclusions are only found in the garnet rim, and are partially replaced by margarite. As in the barroisite eclogites, garnet is strongly zoned, with reddish cores and colourless rims; this suggests that the metapelitic country rocks probably suffered the same metamorphic evolution as did the eclogites. Two distinctive kyanite populations are present, a small and a large one, the small kyanite crystals looking of later formation than the large kyanites. Rutile is found both inside and outside garnet porphyroblasts. Margarite is typically found, together with biotite, as fine-grained aggregates replacing kyanite during decompressive retrogression in the amphibolite facies.

Metamorphic evolution and equilibration conditions of the Kaghan eclogites

In summary, petrographic evidence of the prograde metamorphic evolution of the eclogites is given by mineral inclusions of zoisite, epidote, rutile, kyanite and amphibole hosted within garnet porphyroblasts. All these minerals are compatible with a prograde path at relatively high pressures and medium temperatures. The occurrence of zoisite/clinozoisite + kyanite instead of lawsonite constrains the prograde evolution at T higher than the lawsonite stability field. The occurrence of glaucophane inclusions in garnet, and the occurrence of amphibole relics and small rutile needles inside omphacite, suggests that a Ti-rich amphibole was first transformed to an Na-amphibole and then to an Na-pyroxene during prograde metamorphism at increasing pressures. At peak metamorphic conditions glaucophane was probably not stable, though clear evidence of its disequilibrium with omphacite and garnet is lacking. The growth of porphyroblastic glaucophane, most likely at the expense of omphacite, would thus mark the early decompression. Paragonite was also produced at the expense of kyanite during this stage. Further evidence of decompression is given by the occurrence of amphibole + albite fine-grained symplectite overgrowing omphacite and of biotite + feldspar intergrowths replacing phengite. All together, these observations suggest that the Gittidas eclogites were subjected to a decompressional evolution in the epidote–amphibolite facies without significant thermal relaxation (except perhaps in the very last stages).

To constrain better the P–T path followed by the Gittidas eclogites, equilibration conditions have been estimated by geothermobarometry (Table 5). Peak metamorphic temperatures of about 610–620 °C, at an assumed pressure of 24 kbar, have been obtained for the barroisite eclogites T136 and T137 from Fe/Mg partition in garnet–omphacite pairs using representative compositions of omphacite and garnet rims, and the experimental calibration of the garnet–clinopyroxene thermometer by Ellis & Green (1979). Equilibration temperatures about 25 °C lower result from the modified version of this calibration given by Powell (1985). Such estimates are comparable to peak metamorphic temperatures, calculated by Pognante & Spencer (1991) and Spencer (1993) using the garnet–clinopyroxene thermometer for eclogites sampled in other localities of the upper Kaghan valley (Kaar, Lohlul Nar and the Besal mountain) which, for a nominal pressure of 15 kbar, are 638 ± 31 °C, 650 ± 47 °C, 636 ± 42 °C (calibration of Ellis & Green 1979), and 581 ± 38 °C, 604 ± 53 °C, 617 ± 55 °C (calibration of Krogh 1988), respectively.

The peak metamorphic temperature, obtained for the glaucophane eclogite T133 by the garnet–clinopyroxene thermometer and the calibration of Ellis & Green (1979), is significantly lower (by about 90–100 °C) than that obtained for the barroisite eclogites. As noted by several workers (Droop *et al.* 1990, and references therein), this is commonly observed in eclogites from the Alps and elsewhere when omphacite is relatively aegirine-rich, and is probably an effect of the aegirine component in clinopyroxene, which is not taken into account by existing calibrations of the garnet–clinopyroxene thermometer.

In phengite-bearing eclogite T137, the peak metamorphic temperature has also been estimated by the garnet–phengite thermometer as experimentally calibrated by Green & Hellman (1982) for basaltic rock compositions (Table 5). As in their experiments, all Fe in phengite was assumed to be divalent; the equilibration temperature of 617 °C obtained for a nominal pressure of 24 kbar has to be taken as maximum value only. We note, however, that this temperature is encouragingly close to that derived by the garnet–clinopyroxene thermometer (611 °C).

Peak metamorphic pressures were constrained for the Gittidas eclogites by: (1) the jadeite content of omphacite co-existing with quartz in the absence of plagioclase (maximum $X_{Jd} = 0.52$), and the calibration of the reaction albite = jadeite + quartz by Holland (1980), which indicate minimum pressures in excess of 13–14 kbar (at a nominal T of 600 °C); (2) the

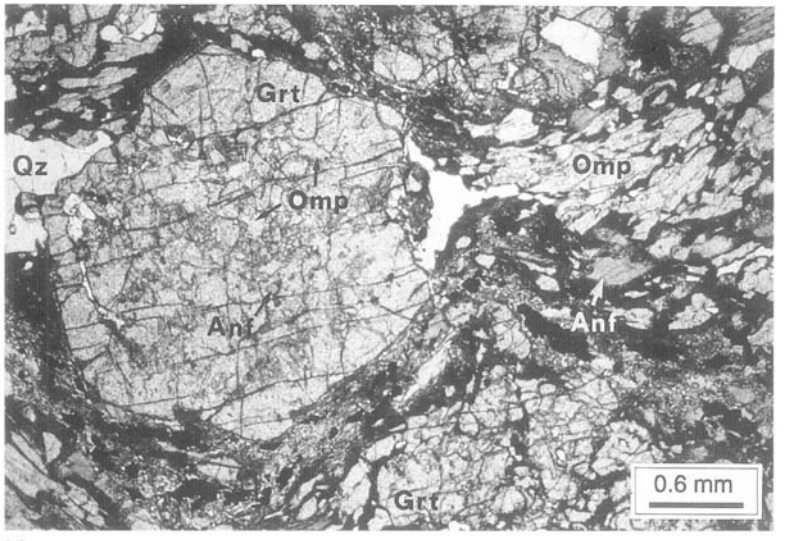

(a)

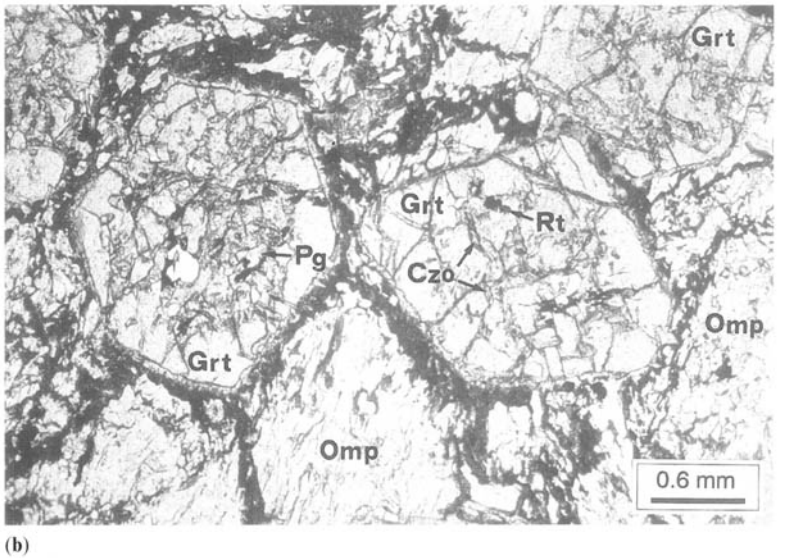

(b)

Fig. 2. (**a**) Microstructure of the glaucophane eclogite from Gittidas. The metamorphic foliation is defined by omphacite (Omp) and rutile, together with blue amphibole (Anf). Garnet porphyroblasts (Grt) have an idioblastic rim and a core crowded with inclusions of omphacite, green amphibole, quartz and rutile. Note the pressure shadows of quartz (Qz) around garnet. (**b**) Microstructure of the barroisite eclogite from Gittidas. Perfectly idioblastic porphyroblasts of garnet (Grt) occur together with large crystals of omphacite (Omp), and show inclusion-free rims and large reddish cores crowded with inclusions of zoisite and clinozoisite (Czo), rutile (Rt), kyanite, paragonite (Pg), amphibole and quartz. (**c**) A detail of the glaucophane eclogite from Gittidas. Amphibole (Anf) is zoned, from blue-violet cores to blue-green rims, whereas omphacite (Omp) is replaced by a symplectite of albite + amphibole with grain size increasing outwards from the contact with omphacite. (**d**) A detail of the barroisite eclogite from Gittidas, showing nearly colourless amphibole (Anf) and the omphacite (Omp) partly replaced by a very fine-grained symplectite of albite + amphibole.

garnet–omphacite–phengite barometer (Waters & Martin 1993), based on the KMASH-system reaction equilibrium: pyrope + 2 grossular + 3 celadonite = 6 diopside + 3 muscovite. Following the approach and assumptions of Carswell *et al.* (1997), we obtained a metamorphic pressure of about 24 kbar for the phengite-bearing eclogite T137 (Table 5); (3) the

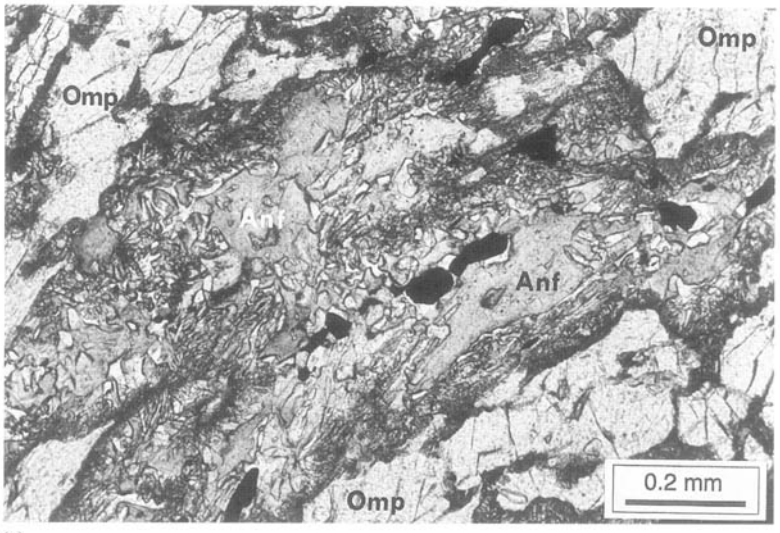

(c)

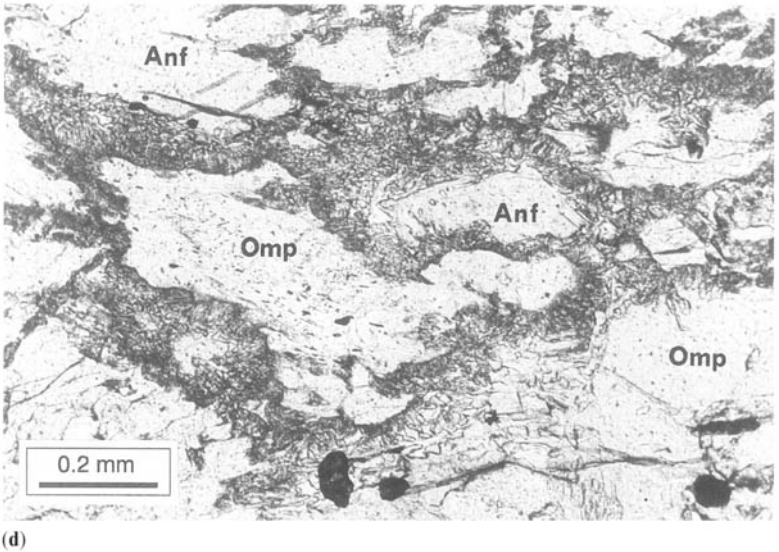

(d)

garnet + zoisite/clinozoisite + kyanite + quartz/coesite geobarometer developed by Okay (1995). This barometer is based on the reaction zoisite/clinozoisite = grossular + kyanite + quartz/coesite, resulting in progressively more grossular-rich compositions in garnet as metamorphic pressures increase. Pressures estimated from plotting garnet compositions of both barroisite eclogites in the garnet composition–pressure diagram given by Okay (1995, fig. 7) are at about 23 kbar.

Such estimates of peak metamorphic pressures are well within the jadeite stability field and quite close to the coesite stability field (Fig. 6). They are significantly higher than previous estimates of 18 kbar as the maximum P (Pognante & Spencer 1991), which were based on the assumption that jadeite is absent in metapelitic and metagranitic rocks hosting the Kaghan eclogites, but are corroborated by the recent work of O'Brien *et al.* (1999) who discovered coesite inclusions in omphacite of the Lohul Nar eclogite, 2.5 km west of Gittidas. Water activity at metamorphic peak must have been high, but less than unity, as the intersection of the garnet–omphacite–phengite barometer with the garnet–omphacite and garnet–phengite thermometers (Fig. 6) falls outside the lawsonite stability field

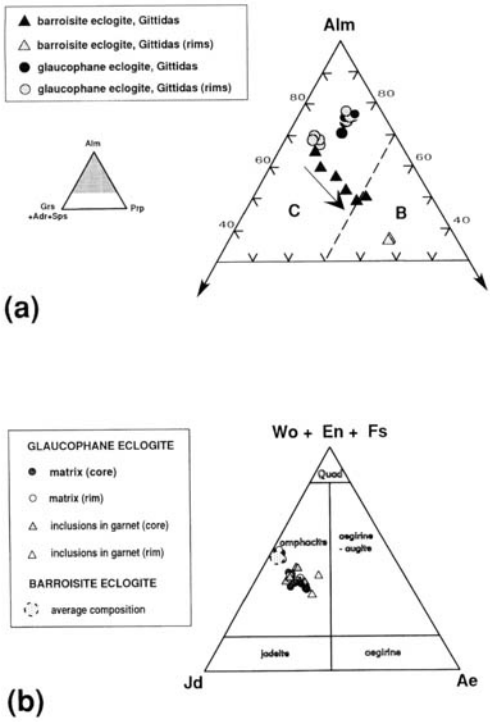

Fig. 3. (**a**) Compositions of garnet from the glaucophane and barroisite eclogites from Gittidas in the almandine–pyrope–grossular triangle. B and C are the composition fields of garnets from eclogites associated with gneisses and blueschists (Coleman *et al.* 1965), respectively. Mineral abbreviations are after Kretz (1983). (**b**) Compositions of omphacite from the glaucophane and barroisite eclogites from Gittidas in the jadeite–aegirine–wollastonite + enstatite + ferrosilite diagram of Morimoto *et al.* (1988).

only if the reaction lawsonite = zoisite + kyanite + quartz + H_2O is calculated for $aH_2O < 1.0$. Alternatively, and in our opinion, less likely, peak metamorphic T in the Gittidas eclogites have been underestimated by about 30 °C.

Metamorphic pressures of about 22 kbar for the post-eclogitic stage were derived from the reaction paragonite = kyanite + jadeite + H_2O, as suggested by O'Brien (1993) and Okay (1995), using a petrogenetic grid calculated by Castelli *et al.* (1998) with the thermodynamic approach of Connolly (1990) for the CNMASH system (Fig. 6). Equilibration temperatures slightly in excess of 600 °C have been obtained for this stage using garnet amphibole pairs from the barroisite eclogite T136 and the calibration of Graham & Powell (1984), whereas equilibration temperatures for garnet and amphibole rims from the glaucophane eclogite are much lower (436 °C). This is not surprising as the Graham & Powell empiric calibration is for hornblende and not for glaucophane or sodic-calcic amphibole, which has a different crystal chemistry. On the other hand, growth of glaucophane, which at high metamorphic pressures has a maximum thermal stability of up to about 700 °C (see discussion in Zhang & Liou 1994 and Pawley 1992, and descriptions of natural examples in Kienast *et al.* 1991 and Zhang & Liou 1994), does not necessarily imply a decrease in metamorphic temperature, and we conclude that in the Gittidas eclogites fluid infiltration at the beginning of decompression may have been isothermal, resulting in a quasi-adiabatic post-eclogite P–T path (Fig. 7).

At a regional scale, peak metamorphic temperatures similar to those recorded in the Gittidas eclogites have been calculated by De Sigoyer *et al.* (1997) using THERMOCALC (Holland & Powell 1990) for the glaucophane eclogites of the North Himalayan Tso Morari Dome ($T = 580 \pm 60$ °C); peak metamorphic pressures have been estimated at 20 ± 3 kbar. Using the garnet–clinopyroxene thermometer and the garnet–omphacite–phengite barometer, as in this paper, and the data given by De Sigoyer *et al.* (1997), peak metamorphic temperatures are 634 °C (at a nominal pressure of 24 kbar), and peak metamorphic pressures are 27 kbar respectively. For the post-eclogitic stages the estimates of De Sigoyer *et al.* (1997) are $T = 580 \pm 60$ °C, $P = 11 \pm 3$ kbar (blueschist–amphibolitic stage), and $T = 610 \pm 80$ °C, $P = 9 \pm 3$ kbar (amphibolitic stage).

Discussion: an eclogite-bearing terrain in the HHC of NW Himalaya

As noted by Chaudry & Ghazanfar (1987), the rocks of upper Kaghan are in physical continuity with those of the Shardi area, Neelum valley. Recent work in this area (Fontan 1998 and references therein) has confirmed that strong similarities exist between the metamorphic evolution of the Upper Kaghan nappe and the metamorphic evolution of the eclogite-bearing NE Kalapani and Shontar units of the Neelum valley (Fig. 1).

Five metamorphic stages have been detected in the NE Kalapani and Shontar units. The oldest stage (Mx) is a prograde metamorphism of blueschist facies preceding the eclogitic peak, with estimated $T < 550$ °C and $P > 10$ kbar. Stage Mx is recorded by trails of mineral inclusions (Mg-chloritoid, white mica, quartz) inside the cores of zoned garnets in micaschists of

Table 5. *Equilibration temperatures and pressures*

Barroisite eclogite T136	Garnet rim (68/113)	Omphacite int (66/24)	Amphibole rim (67/126)	
Calibration	Garnet–clinopyroxene (Ellis & Green 1979)			
*P*nom (kbar)	24			
T (°C)	622			
Calibration	Garnet–hornblende (Graham & Powell 1984)			
T (°C)	615			
Calibration	Hornblende–plagioclase (Holland & Blundy 1994)			
*P*nom (kbar)	15			
T (°C)	548			
Barroisite eclogite T137	**Garnet rim (70/4)**	**Omphacite rim (70/6)**	**Amphibole core (70/37)**	**Phengite rim (70/14)**
Calibration	Garnet–clinopyroxene (Ellis & Green 1979)			
*P*nom (kbar)	24			
T (°C)	611			
Calibration	Garnet–phengite (Green & Hellman 1982)			
*P*nom (kbar)	24			
T (°C)	617			
Calibration	Garnet–hornblende (Graham & Powell 1984)			
T (°C)	483			
Calibration	Garnet–omphacite–phengite (Waters & Martin 1993)			
*T*nom (°C)	610			
P (kbar)	24.3			
Glaucophane eclogite T133	**Garnet rim (58/65)**	**Omphacite rim (59/77)**	**Amphibole rim (68/6)**	
Calibration	Garnet–clinopyroxene (Ellis & Green 1979)			
*P*nom (kbar)	24			
T (°C)	523			
Calibration	Garnet–hornblende (Graham & Powell 1984)			
T (°C)	436			

T133: glaucophane eclogite; Tl36 and T137: barroisite eclogites.

the Himalayan cover. Stage M1 is eclogitic and corresponds to the metamorphic peak, with estimated $T = 600 \pm 50$ °C and $P > 13$–14 kbar. The apparent lack of jadeite + quartz assemblages in quartzo-feldspathic rocks suggests an upper P limit of 18 kbar. Stage M1 is followed by nearly isothermal decompression to 8–10 kbar (stage M2), causing the formation of albite + sodic augite symplectite after omphacite and of the main mineral assemblage biotite + muscovite + garnet + kyanite + staurolite in micaschists. The fourth stage (M3) is characterized by a further drop in pressure ($P = 4$–5 kbar), coupled with a decrease in temperature ($T = 450$–550 °C). The last stage (M4) is a greenschist facies retrogression at low pressure (3–4 kbar?) and temperature (400–450 °C).

The timing of metamorphic and deformational events in the Neelum valley is similar to the timing established for the Upper Kaghan nappe. In the Neelum valley the first phase of ductile deformation (D1) is coeval with the peak of Himalayan metamorphism (the eclogitic M1 stage), and produced a penetrative schistosity (S1) associated with isoclinal folding, which is dated as middle Eocene by $^{40}Ar/^{39}Ar$ analyses on white micas present in shear zones. A second phase of deformation (D2) produced isoclinal overturned folds associated with north-dipping shear zones and is earlier than N to S movement along the Main Central Thrust, as this thrust cross-cuts earlier mylonites as well as the metamorphic isograds. The end of the D2 phase (corresponding to the M3 stage of Fontan 1998) is placed at about 30 Ma. Petrofabric analysis and $^{40}Ar/^{39}Ar$ data indicate that the late shear movements along the MCT postdate the M3 stage, extending up to about 25 Ma (late Oligocene). Together with marked similarity in the post-eclogite P–T path, this suggests that the

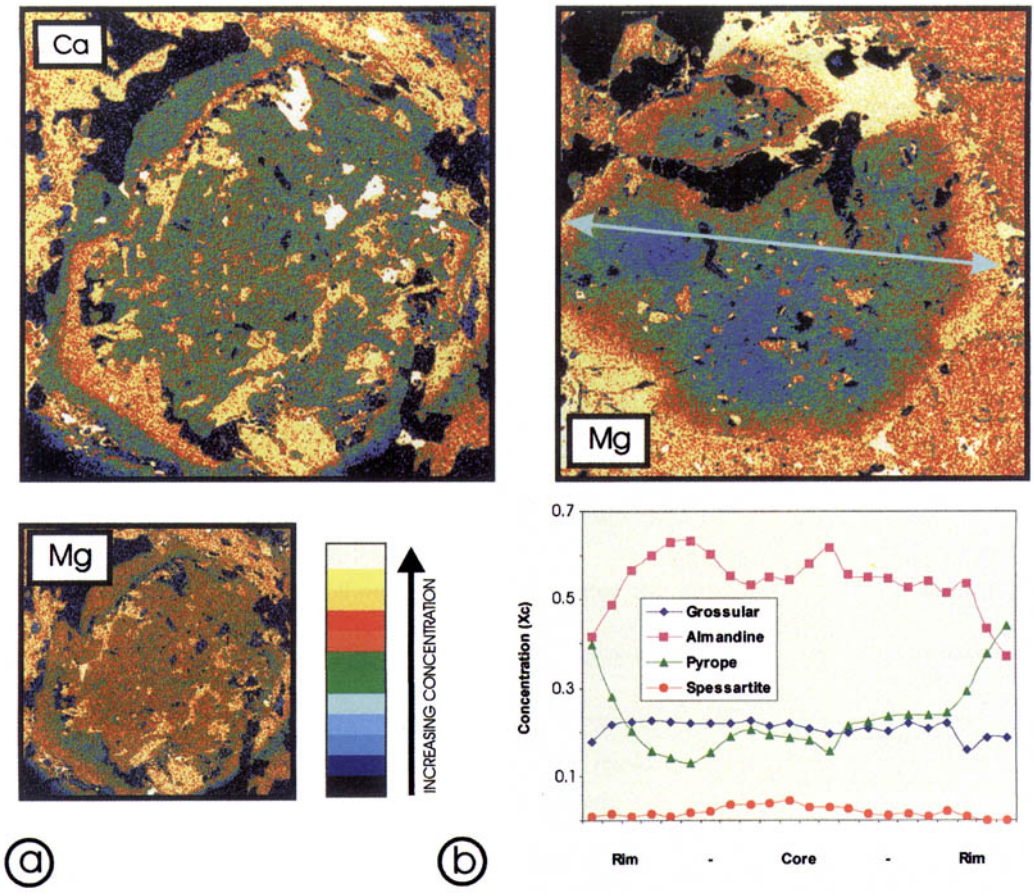

Fig. 4. (**a**) Qualitative X-ray map of a garnet porphyroblast from the glaucophane eclogite T133 of Gittidas. The image is 512 × 512 pixels. Note complex zoning, with a Ca-rich shell separating a core and outer rim nearly of the same composition. Yellow patches in the Ca map are inclusions of omphacite. (**b**) Qualitative X-ray map and compositional profile of a garnet porphyroblast from the barroisite eclogite T136 of Gittidas. Garnet is strongly zoned with an iron-rich core and perfectly idioblastic iron-poor rim. The Fe-rich core hosts inclusions of zoisite, Fe-poor clinozoisite, rutile, kyanite, paragonite and yellow-green Na–Ca amphibole, whereas the Mg-rich rim is devoid of mineral inclusions.

Upper Kaghan nappe and the eclogite-bearing units of the Neelum valley may be parts of a single eclogite-bearing terrane metamorphosed in Eocene times.

Contrasting *P–T–t* paths along the High Himalayan Crystallines

As noted by several authors the metamorphic history of the HHC in northern Pakistan is significantly different from that of the HHC in the area from Zanskar to Bhutan, because in the HHC of northern Pakistan there is no evidence for either a high grade metamorphic overprint or a widespread partial melting event followed by leucogranite emplacement (Treloar 1989; Pognante 1992). Also, cooling histories for the HHC of northern Pakistan (Treloar & Rex 1990) indicate that stacking and subsequent unroofing had proceeded to such an extent that the metamorphic pile had cooled to below 300 °C by 25 Ma. In contrast, in the E Himalaya, for example in the Everest–Makalu area, post-metamorphic cooling of the HHC to below 300 °C is significantly younger (13–16 Ma, Pognante 1992 and references therein).

The occurrence of eclogites only in the NW Himalaya and their apparent absence in the E Himalaya has also been considered a major feature differentiating the two parts of the Himalayan belt and suggesting that their different metamorphic evolutions are related to the

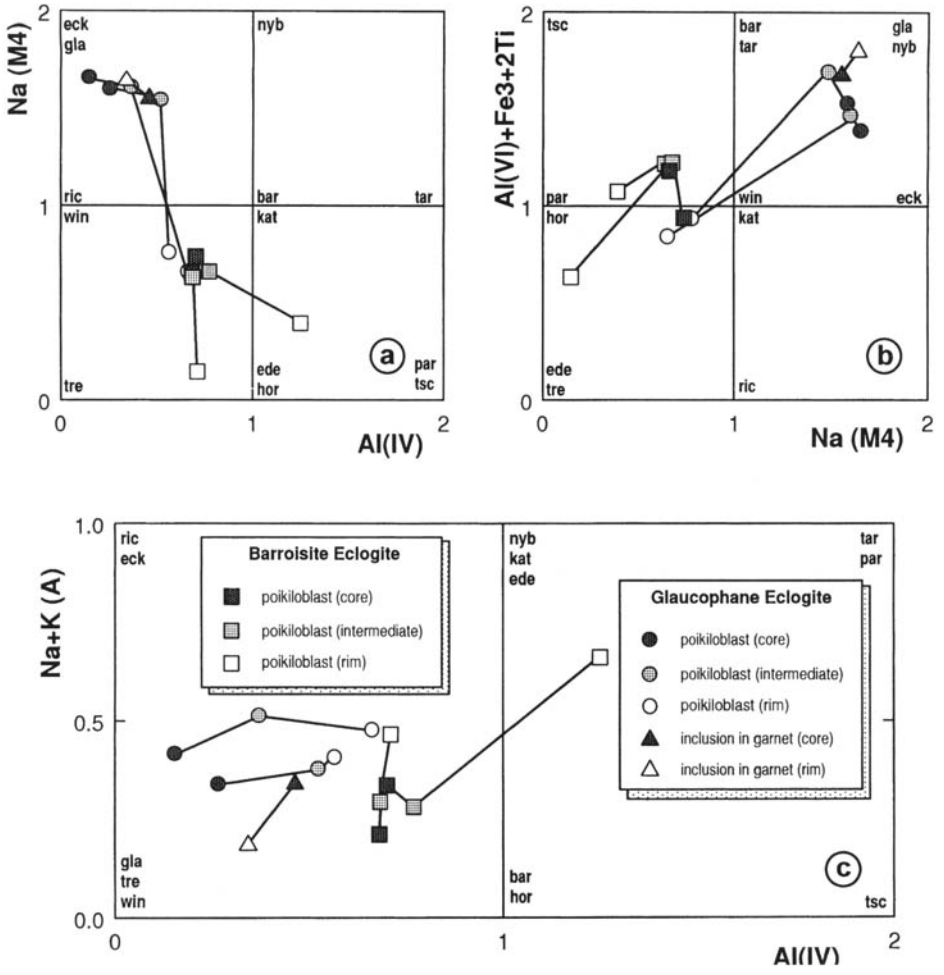

Fig. 5. Crystal chemistry of amphiboles from the Gittidas eclogites. (**a**) Plot of the Na content in the M4 site v. tetrahedral aluminium. (**b**) Plot of the sum of the high-charge octahedral cations v. the Na content in the M4 site. (**c**) Plot of the sum of the cations in the A site v. tetrahedral Al. End-member amphiboles are indicated by the first three letters of the IMA name.

diachronous collision of India with Eurasia (Guillot *et al.* 1999). The recent finding of granulite-overprinted eclogites in the E Himalaya (Lombardo *et al.* 1998), however, invalidates this view, and rather confirms earlier suspicions that the eclogite event recorded in the NW Himalaya was actually a Himalaya-wide metamorphism that shortly postdated collision and which was subsequently overprinted through much of the Himalayan belt by the later MCT-related thermal event (Treloar *et al.* 1989).

The granulite-overprinted eclogites were found in the Kharta region of southern Tibet at the top of the Main Central Thrust Zone (Lombardo *et al.* 1998). The Kharta eclogites occur as boudinaged dykes in thrust sheets of granitic orthogneiss, quartzite and mylonite marble which crop out just below the high-grade Barun Gneiss, the lowest lithological unit of the HHC in the Everest–Makalu region. In a hand specimen the eclogites are black, dense rocks, with red garnets (Alm_{41-61} Prp_{10-16} Sps_{0-3} $Grs + Adr_{25-35}$) several millimetres in size, set in a matrix of amphibole. By comparison with less recrystallized eclogites of medium T (e.g. Variscan eclogites from the Moldanubian or the French Massif Central: O'Brien 1990 and references therein) there is, however, little doubt that these rocks are strongly re-equilibrated eclogites.

Primary omphacite is not preserved in the Kharta eclogites sampled so far, but it is replaced by a distinctive recrystallized symplectite

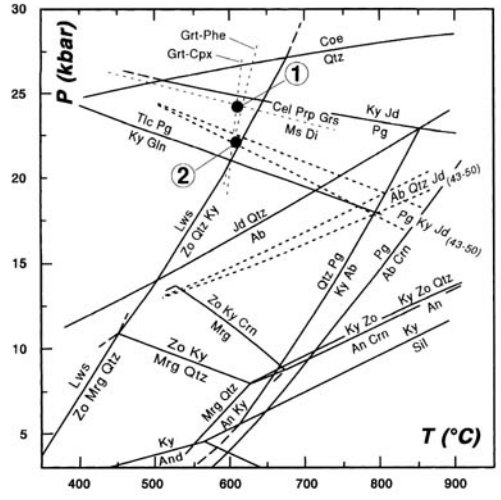

Fig. 6. Selected phase relationships in the CNMASH system calculated by Castelli *et al.* (1998) with the thermodynamic approach of Connolly (1990) and the database of Holland & Powell (1990). Phases are: Ab = albite, An = anorthite, And = andalusite, Coe = coesite, Crn = corundum, Jd = jadeite, Ky = kyanite, Lws = lawsonite, Mrg = margarite, Pg = paragonite, Qtz = quartz, Sil = sillimanite, Tlc = talc, Zo = zoisite. Dashed lines are jadeite-isopleths bracketing the stability fields of omphacite with compositions between Jd_{43} and Jd_{50} (diopside–jadeite solution model of Gasparik 1985), in equilibrium with Ab + Qtz and Pg + Ky, respectively. Light dashed lines show the KMASH-system reaction equilibrium: pyrope (Prp) + 2 grossular (Grs) + 3 ideal celadonite (Cel) = 6 diopside (Di) + 3 ideal muscovite (Ms) calculated with the expression given by Waters & Martin (1993) and the assumptions of Carswell *et al.* (1997); Fe–Mg fractionation in garnet–omphacite and garnet–phengite pairs of barroisite eclogites T136 and T137, respectively. Points 1 and 2 are the *P–T* conditions estimated for the eclogitic and post-eclogitic, high pressure stages, respectively.

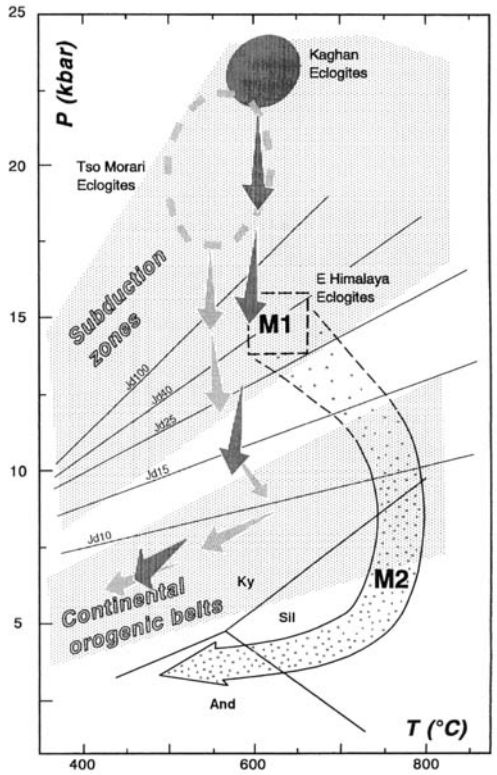

Fig. 7. Comparison of the *P–T* paths recorded in the Upper Kaghan nappe eclogites, the North Himalayan Tso Morari eclogites (after De Sigoyer *et al.* 1997) and the E Himalaya eclogites (after Lombardo *et al.* 1998). M1 and M2 are the *T* and minimum *P* conditions assumed for the eclogitic event in the E Himalaya, and the *P–T* conditions calculated for the Miocene granulite event, respectively. The dotted *P–T* path is that recorded in the Barun Gneiss, the lithotectonic unit of the highest metamorphic grade and tectonically lowest in the HHC of the Everest–Makalu region.

of plagioclase and diopside. Garnet crystals are surrounded by a corona of plagioclase (An_{40}) rimmed by orthopyroxene (En_{37-47}) where garnet abutted matrix quartz. The pale milky green patches, which are conspicuous in a few samples, appear under the microscope to consist of plagioclase–biotite intergrowths replacing a pristine phengite, no relics of which have survived. Rutile, too, has been almost completely replaced by titanite. The amphibole matrix is comprised of brown hornblende $(Na_{0.32-0.43}K_{0.15-0.20})(Na_{0.10-0.18}Ca_{1.82-1.90})(Mg_{1.51-2.17}Fe^{2+}_{2.00-2.52}Fe^{3+}_{0.06-0.33}Al_{0.43-0.46}Ti_{0.20-0.25})(Al_{1.50-1.30}Si_{6.50-6.70})O_{23}$, which replaces garnet and orthopyroxene and also grows on the diopside–plagioclase symplectite. The hornblende crystal chemistry, specifically high Ti and tetrahedral Al, and low octahedral Al, indicate this is a low-pressure, high-temperature amphibole close in composition to amphiboles formed at *P–T* conditions at the boundary between the upper amphibolite and granulite facies (e.g. Dal Piaz *et al.* 1983).

Mineral assemblages, reaction textures and geothermobarometry suggest that two superposed metamorphic events are recorded in the Kharta eclogites. The first event was eclogitic, probably with metamorphic *T* around 600–650 °C and minimum *P* between 12 and 14 kbar. The second event was granulitic, with medium *P* (5.5–6.5 kbar) and high *T* (700–750 °C). This event has strongly affected

the rocks hosting the eclogite bodies and the overlying Barun Gneiss which, however, has rare relics of HP mineral assemblages.

The timing of the eclogitic event is as yet unconstrained by radiometric ages, but must be older than the high-grade metamorphism and generation of the Miocene leucogranites, the oldest of which in this area is the Makalu pluton, whose intrusion is dated by monazite ages of 24.0 ± 0.2 and 21.9 ± 0.2 Ma (Schärer 1984). Also, the eclogitic event must be older than 25 Ma, the age estimated for the Eohimalayan metamorphism from $^{40}Ar/^{39}Ar$ data on hornblende from amphibolites occurring at the top of the HHC in the Dinggyê area, 40 km east of the Kharta region (Hodges *et al.* 1994). Assuming that the Kharta eclogites are not Precambrian in age, but Himalayan as mantained by Lombardo & Rolfo (2000), and noting that the India–Eurasia continental collision is thought to have occurred at 41–45 Ma in E Himalaya (Searle *et al.* 1988), 30–35 Ma could be a reasonable estimate, for the age of the eclogite event.

From a tectonic viewpoint, the newly found eclogite occurrence suggests that, whereas in the NW Himalaya eclogites generated shortly after continental collision were exhumed along a cooling path (Treloar 1995, 1997), and thus reached shallow crustal levels essentially unaltered, in most of the Himalayan belt thermal relaxation of the thickened continental crust almost completely erased the mineralogical record of the early stages of continental collision. Therefore, the main difference between the crystalline nappes of NW Himalaya and those of E Himalaya appears to lie less in the early part of their metamorphic evolution than in the different P–T paths they followed during their exhumation.

Conclusions

1. Petrographical and mineral chemical study of eclogite samples from Gittidas in the Upper Kaghan valley documents the occurrence of glaucophane and barroisite eclogites in the Upper Kaghan nappe. A number of crystal-chemical features differentiates the Gittidas glaucophane from glaucophanes of low-temperature eclogites and suggests a higher temperature of formation, as indicated for glaucophanes of similar composition from the Scandinavian Caledonides, the Western Alps and the Qinling–Dabie Shan collision zone of central China.
2. Peak metamorphic temperatures of about 610–620 °C have been obtained for the Gittidas barroisite eclogites by the garnet–clinopyroxene and garnet–phengite thermometers using representative compositions of omphacite, garnet and phengite. This estimate is comparable to equilibration temperatures calculated by Pognante & Spencer (1991) and Spencer (1993) for eclogites sampled in other localities of the Upper Kaghan nappe. Equilibration pressures of 23–24 kbar have been estimated by the garnet–omphacite–phengite and garnet–zoisite / clinozoisite–kyanite–quartz / coesite barometers. Such estimates of peak metamorphic pressures are quite close to the coesite stability field and significantly higher than previous estimates of 18 kbar as maximum metamorphic pressure.
3. Metamorphic pressures of about 22 kbar for the post-eclogitic stage were derived from the reaction paragonite = kyanite + jadeite + H_2O. Equilibration temperatures slightly in excess of 600 °C have been obtained for the post-eclogitic stage using barroisite and compositions of the outer garnet rims. This suggests that in the Gittidas eclogites decompression (and fluid infiltration) was not accompanied by heating, resulting in a steep, quasi-adiabatic post-eclogite P–T path.
4. Strong similarities between the metamorphic evolution of the Upper Kaghan nappe and the metamorphic evolution of the eclogite-bearing NE Kalapani and Shontar units of the nearby Neelum valley show that the eclogite occurrences of the Kaghan–Neelum area define an eclogite-bearing terrane of regional extent, which was subjected to high pressure metamorphism in middle Eocene times.
5. A comparison of the metamorphic evolution recorded in the eclogites of the NW Himalaya with that of eclogites recently discovered in the E Himalaya suggests the possibility of a Himalaya-wide eclogitic metamorphism of pre-Miocene age. Therefore, the main difference between the crystalline nappes of the NW Himalaya and those of the E Himalaya appears to lie less in the early part of their metamorphic evolution than in the different P–T paths they followed during exhumation. In particular the NW Himalaya eclogites lack the high temperature and low pressure Miocene overprinting which in most of the Himalayan belt has almost completely erased the mineralogical record of the early stages of continental collision.

This paper is dedicated to the memory of our friend and colleague Ugo Pognante (Torino, 1954—Mont

Blanc Massif, 1992). We thank Piera Benna for information about the Upper Kaghan samples, Raffaella Ruffini for help in processing the qualitative X-ray maps, Luciano Ungaretti for discussing the crystal chemistry of the Gittidas glaucophane, David Spencer for information about the Upper Kaghan geology and Aphrodite Indares for reading an earlier version of the ms and suggesting improvements. The paper benefited from stimulating reviews by P. J. O'Brien and A. Okay.

Laboratory work was financially supported by C.N.R., C.S. Geodinamica Catene Collisionali, Torino. Mineral analyses and X-ray maps of garnet were acquired in the electron microprobe laboratory of the Department of Mineralogy and Petrology, University of Torino. This laboratory is also financially supported by the C.N.R., C.S. Geodinamica Catene Collisionali. Fieldwork in the NW Himalaya by Ugo Pognante was financially supported by the National Research Council of Italy through the Everest-K2 Project and by the EEC contract No. Cl1*-CT90-0852 (Geology of the Karakorum).

References

CARSWELL, D. A. (ed.) 1990. *Eclogite facies rocks.* Blackie, Glasgow & London.

——, O'BRIEN, P. J., WILSON, R. N. & ZHAI, M. 1997. Thermobarometry of phengite-bearing eclogites in the Dabie Mountains of central China. *Journal of Metamorphic Geology*, **15**, 239–252.

CASTELLI, D., ROLFO, F., COMPAGNONI, R. & XU, S. 1998. Metamorphic veins with kyanite, zoisite and quartz in the Zhu–Jia–Chong eclogite, Dabie Shan, China. *The Island Arc*, **7**, 159–173.

CHAMBERLAIN, C. P., ZEITLER, P. K. & ERICKSON, E. 1991. Constraints on the tectonic evolution of the northwestern Himalaya from geochronologic and petrologic studies of Babusar Pass, Pakistan. *Journal of Geology*, **99**, 829–849.

CHAUDRY, M. N. & GHAZANFAR, M. 1987. Geology, structure and geomorphology of upper Kaghan valley, NW Himalaya, Pakistan. *Geological Bulletin, University of Punjab*, **22**, 13–57.

COLEMAN, R. G., BEATTY, L. B. & BRANNOCK, W. W. (1965). Eclogites and eclogites: their differences and similarities. *Geological Society of America Bulletin*, **76**, 483–508.

CONNOLLY, J. A. D. 1990. Multivariable phase diagrams: an algorithm based on generalised thermodynamics. *American Journal of Science*, **290**, 666–718.

DAL PIAZ, G. V., LOMBARDO, B. & GOSSO, G. 1983. Metamorphic evolution of the Mt. Emilius klippe, Dent Blanche nappe, Western Alps. *American Journal of Science*, **283-A**, 438–458.

DE SIGOYER, J., GUILLOT, S., LARDEAUX, J. M. & MASCLE, G. 1997. Glaucophane-bearing eclogites in the Tso Morari dome (eastern Ladakh, NW Himalaya). *European Journal of Mineralogy*, **9**, 1073–1083.

DROOP, G. T. R., LOMBARDO, B. & POGNANTE, U. 1990. Formation and distribution of eclogite facies rocks in the Alps. *In*: CARSWELL, D. A. (ed.) *Eclogite facies rocks.* Blackie, Glasgow & London, 225–259.

ELLIS, D. J. & GREEN, D. H. 1979. An experimental study of the effect of Ca upon garnet clinopyroxene Fe–Mg exchange equilibria. *Contributions to Mineralogy and Petrology*, **71**, 13–22.

FONTAN, D. 1998. *Regional geological mapping, metamorphic P–T–t paths evaluations and ore potential assessment in Neelum valley (Azad Kashmir, NE Pakistan).* PhD thesis, Université de Louvain.

GASPARIK, T. 1985. Experimentally determined compositions of diopside–jadeite pyroxene in equilibrium with albite and quartz at 1200–1350 °C and 15–34 kb. *Geochimica et Cosmochimica Acta*, **49**, 865–870.

GRAHAM, C. M. & POWELL, R. 1984. A garnet–hornblende geothermometer: calibration, testing, and application to the Pelona Schist, Southern California. *Journal of Metamorphic Geology*, **2**, 13–31.

GRECO, A. & SPENCER, D. A. 1993. A section through the Indian Plate, Kaghan Valley, NW Himalaya, Pakistan. *In*: TRELOAR, P. J. & SEARLE, M. P. (eds) *Himalayan Tectonics.* Geological Society, London, Special Publications, **74**, 221–236.

——, MARTINOTTI, G., PAPRITZ, K., RAMSAY, J. G. & REY, R. 1989. The crystalline rocks of the Kaghan Valley (NE Pakistan). *Eclogae Geologicae Helvetiae*, **82**, 629–653.

GREEN, D. H. & HELLMAN, P. L. 1982. Fe–Mg partitioning between coexisting garnet and phengite at high pressures, and comments on a garnet–phengite geothermometer. *Lithos*, **15**, 253–266.

GUILLOT, S., COSCA, M., ALLEMAND, P. & LE FORT, P. 1999. Contrasting metamorphic and geochronologic evolution along the Himalayan belt. *In*: MACFARLANE, A., SORKHABI, R. & QUADE, J. (eds) *Himalaya and Tibet: Mountain roots to mountain tops.* Geological Society of America Special Papers, **328**, 117–128.

HODGES, K. V., HAMES, W. E., OLSZEWSKI, W., BURCHFIEL, B. C., ROYDEN, L. H. & CHEN, Z. 1994. Thermobarometric and $^{40}Ar/^{39}Ar$ geochronologic constraints on Eohimalayan metamorphism in the Dinggyê area, southern Tibet. *Contributions to Mineralogy and Petrology*, **117**, 151–163.

HOLLAND, T. J. B. 1980. The reaction albite = jadeite + quartz determined experimentally in the range 600–1200 °C. *American Mineralogist*, **65**, 129–134.

—— & BLUNDY, J. D. 1994. Non-ideal interactions in calcic amphiboles and their bearing on amphibole–plagioclase thermometry. *Contributions to Mineralogy and Petrology*, **116**, 433–447.

—— & POWELL, R. 1990. An enlarged and updated internally consistent thermodynamic dataset with uncertainties and correlations: the system K_2O–Na_2O–CaO–MgO–FeO–Fe_2O_3–Al_2O_3–SiO_2–C–H_2–O_2. *Journal of Metamorphic Geology*, **8**, 89–124.

KIENAST, J. R., LOMBARDO, B., BIINO, G. & PINARDON, J. L. 1991. Petrology of very-high-pressure eclogitic rocks from the Brossasco–Isasca

Complex, Dora–Maira Massif, Italian Western Alps. *Journal of Metamorphic Geology*, **9**, 19–34.

KRETZ, R. 1983. Symbols for rock-forming minerals. *American Mineralogist*, **68**, 277–279.

KROGH, E. J. 1988. The garnet–clinopyroxene geothermometer: a reinterpretation of existing experimental data. *Contributions to Mineralogy and Petrology*, **99**, 44–48.

LEAKE, B. E., WOOLLEY, A. R., ARPS, C. E. S., BIRCH, W. D., Gilbert, M. C. *et al.* 1997. Nomenclature of amphiboles; report of the Subcommittee on Amphiboles of the International Mineralogical Association Commission on New Minerals and Mineral Names. *European Journal of Mineralogy*, **9**, 623–651.

LE FORT, P., GUILLOT, S. & PÊCHER, A. 1997. HP metamorphic belt along the Indus suture zone of NW Himalaya: new discoveries and significance. *Comptes Rendus de l'Académie des Sciences, Paris*, **325**, 773–778.

LOMBARDO, B. & ROLFO, F. 2000. Two contrasting eclogite types in the Himalayas: implications for the Himalayan orogeny. *Journal of Geodynamics*, in press.

——, PERTUSATI, P., ROLFO, F. & VISONÀ, D. 1998. First report of eclogites from the E Himalaya: Implications for the Himalayan orogeny. *Memorie di Scienze Geologiche (Padova)*, **50**, 67–68.

MORIMOTO, N., FABRIES, J., FERGUSON, A. K., GINZBURG, I. V., ROSS, M. *et al.* 1988. Nomenclature of pyroxenes. *Schweizerische mineralogische und petrographische Mitteilungen*, **68**, 95–111.

O'BRIEN, P. J. 1990. Eclogite formation and distribution in the European Variscides. *In*: CARSWELL, D. A. (ed.) *Eclogite facies rocks*. Blackie, Glasgow & London, 204–224.

—— 1993. Partially retrograded eclogites of the Munchberg Massif, Germany: records of mulyistage Variscan uplift history in the Bohemian Massif. *Journal of Metamorphic Geology*, **11**, 241–260.

——, ZOTOV, N., LAW, R., AHMED KHAN, M. & QASIM JAN, M. 1999. Coesite in eclogite from the Upper Kaghan Valley, Pakistan: A first record and implications. *Abstracts of the 14th Himalaya–Karakorum–Tibet Workshop*; *Terra Nostra*, Kloster Ettal, **99**, 109–111.

OKAY, A. I. 1995. Paragonite eclogites from Dabie Shan, China: re-equilibration during exhumation? *Journal of Metamorphic Geology*, **13**, 449–460.

PAPRITZ, K. & REY, R. 1989. Evidence for the occurrence of Permian Panjal Trap Basalts in the Lesser- and Higher-Himalayas of the Western Syntaxis Area, NE Pakistan. *Eclogae Geologicae Helvetiae*, **82**, 603–627.

PAWLEY, A. R. 1992. Experimental study of the compositions and stabilities of syntetic nyböite and nyböite-glaucophane amphiboles. *European Journal of Mineralogy*, **4**, 171–192.

POGNANTE, U. 1992. Different P–T–t paths and leucogranite occurrences along the High Himalayan Crystalline: implications for subduction and collision along the northern Indian margin. *Geodinamica Acta*, **6**, 5–17.

—— & SPENCER, D. A. 1991. First report of eclogites from the Himalayan belt, Kaghan valley (northern Pakistan). *European Journal of Mineralogy*, **3**, 613–618.

POWELL, R. 1985. Regression diagnostics and robust regression in geothermometer/geobarometer calibration: the garnet–clinopyroxene thermometer revisited. *Journal of Metamorphic Geology*, **3**, 327–342.

SCHÄRER, U. 1984. The effect of initial ^{230}Th disequilibrium on young U–Pb ages. The Makalu case, Himalaya. *Earth and Planetary Science Letters*, **67**, 191–204.

SEARLE, M. P., WINDLEY, B. F., COWARD, M. P., COOPER, D. J., REX, A. J. *et al.* 1988. The closing of Tethys and the tectonics of the Himalaya. *Geological Society of America Bulletin*, **98**, 678–701.

SMITH, D. C. (ed.) 1988. *Eclogites and Eclogite-facies Rocks*. Elsevier, Amsterdam.

SMITH, H. A., CHAMBERLAIN, C. P. & ZEITLER, P. K. 1994. Timing and duration of Himalayan Metamorphism within the Indian Plate, Northwestern Himalaya, Pakistan. *Journal of Geology*, **102**, 493–508.

SPEAR, F. S. & PEACOCK, S. M. 1990. *Metamorphic P–T–t paths: program manual and computer exercises for the calculation of metamorphic phase equilibria, pressure–temperature–time paths and thermal evolution of orogenic belts*. Geological Society of America, Short Course.

—— & SELVERSTONE, J. 1983. Quantitative P–T paths from zoned minerals: theory and tectonic applications. *Contributions to Mineralogy and Petrology*, **83**, 348–357.

SPENCER, D. A. 1993. *Tectonics of the Higher- and Tethyan Himalaya, Upper Kaghan Valley, NW Himalaya, Pakistan: Implications of an early collisional, high pressure (eclogite facies) metamorphism to the Himalayan belt*. PhD thesis, Swiss Federal Institute of Technology, Zürich, Switzerland, Dissertation no. 10194.

—— & GEBAUER, D. 1996. SHRIMP evidence for a Permian protolith age and a 44 Ma metamorphic age for the Himalayan eclogites (Upper Kaghan, Pakistan). *Abstracts of the 11th Himalaya–Karakorum–Tibet Workshop*, Flagstaff, 147–150.

——, POGNANTE, U. & TONARINI, S. 1995. Geochemical and Sr–Nd isotopic characterisation of Higher Himalayan eclogites (and associated metabasites). *European Journal of Mineralogy*, **7**, 89–102.

——, RAMSAY, J., SPENCER-CERVATO, C., POGNANTE, U., CHAUDRY, M. N. & GHAZANFAR, M. 1990. High pressure (eclogite facies) metamorphism in the Indian plate, NW Himalaya, Pakistan. *In*: *Proceedings of the Second Pakistan Geological Congress, Geological Bulletin University of Peshawar*, **23**, 87–100.

TONARINI, S., VILLA, I. M., OBERLI, F., MEIER, M., SPENCER, D. A., POGNANTE, U. & RAMSAY, J. G. 1993. Eocene age of eclogite metamorphism in Pakistan Himalaya: implications for India–Eurasia collision. *Terra Nova*, **5**, 13–20.

TRELOAR, P. J. 1989. Imbrication and unroofing of the Himalayan Thrust Stack of the North Indian Plate, North Pakistan. *Geological Bulletin, University of Peshawar*, **22**, 25–44.

—— 1995. Pressure–temperature–time paths and the relationship between collision, deformation and metamorphism in the north-west Himalaya. *Geological Journal*, **30**, 333–348.

—— 1997. Thermal controls on early-Tertiary, short-lived, rapid regional metamorphism in the NW Himalaya. *Tectonophysics*, **273**, 77–104.

—— & REX, D. C. 1990. Cooling and uplift histories of the crystalline thrust stack of the Indian Plate internal zones west of Nanga Parbat, Pakistan Himalaya. *Tectonophysics*, **180**, 323–349.

——, COWARD, M. P., WILLIAMS, M. P. & KHAN, M. A. 1989. Basement-cover imbrication south of the Main Mantle Thrust, North Pakistan. Geological Society of America, Special Paper, **232**, 137–152.

ULMER, P. 1986. *NORM—Program for cation and oxygen mineral norms*. Computer Library, Institut für Mineralogie und Petrographie, Swiss Federal Institute of Technology, Zürich, Switzerland.

UNGARETTI, L., SMITH, D. C. & ROSSI, G. 1981. Crystal-chemistry by X-ray structure refinement and electron microprobe analysis of a series of sodic-calcic to alkali amphiboles from the Nybo eclogite pod. *Bulletin de Minéralogie*, **104**, 400–412.

VINCE, K. J. & TRELOAR, P. J. 1996. Miocene, north-vergent extensional displacements along the Main Mantle Thrust, NW Himalaya. *Journal of the Geological Society, London*, **153**, 677–680.

WADIA, D. N. 1934. The Cambrian-Trias sequence of north-west Kashmir. *Geological Survey of India Records*, **68**, 121–176.

WATERS, D. J. & MARTIN, H. N. 1993. Geobarometry of phengite-bearing eclogites. *Terra Abstracts*, **5**, 410–411.

ZEITLER, P. K. & CHAMBERLAIN, C. P. 1991. Petrogenetic and tectonic significance of young leucogranites from the northwestern Himalaya, Pakistan. *Tectonics*, **10**, 729–741.

ZHANG, R. Y. & LIOU, J. G. 1994. Coesite-bearing eclogite in Henan Province, central China: detailed petrography, glaucophane stability and PT-path. *European Journal of Mineralogy*, **6**, 217–233.

Metamorphic evolution, ^{40}Ar–^{39}Ar chronology and tectonic model for the Neelum valley, Azad Kashmir, NE Pakistan

D. FONTAN[1], M. SCHOUPPE[2], C. J. HUNZIKER[3], G. MARTINOTTI[4] & J. VERKAEREN[5]

[1]*S.E.A. Environmental Service Consulting S.a.s., via Santa Chiara, 52, 10122 Torino, Italy (e-mail: geology@seaconsult.it)*

[2]*EC Commission D.G. XII, Rue de la Loi, 200, 1049 Bruxelles, Belgium*

[3]*Institut de Minéralogie et Pétrographie BFSH 2, 1015 Lausanne, Switzerland*

[4]*Dipartimento di Scienza della Terra, Via Valperga Caluso, 37, 10125 Torino, Italy*

[5]*Unitè de Géologie, Université catholique de Louvain-la-Neuve, 1348 Louvain-la-Neuve, Belgium*

Abstract: This paper describes the geology, tectonometamorphic history and geochronology of part of the northern flank of the Neelum valley in Azad Kashmir, NE Pakistan. Metamorphic crystalline rocks in this area belong to the Lesser and Higher Himalayan Crystalline complexes. Geological mapping of about 1500 km^2 confirms the presence of three main tectonic units characterized by similar lithostratigraphic sequences but with different tectonometamorphic histories. Whether these tectonic units belong to the Lesser or Higher Himalayan Crystallines depends on the, still controversial, position of the Main Central Thrust. A tectonic model, involving syn-convergent exhumation, is suggested that is consistent with new petrographic and geochronological data, and with a revised interpretation of the Main Central Thrust.

The Neelum valley (Fig. 1) is located on the Indian plate south of the Main Mantle Thrust (MMT) between the Hazara and Nanga Parbat syntaxes. Three major shear zones divide the area (Fig. 2) into discrete tectonic units. The Salkhala unit, which lies between the Main Central Thrust (MCT) and the Main Boundary Thrust (MBT), is the lowest of these. It includes rocks of both the Panjal Traps and the Salkhala Formation (Greco 1989). The Kalapani unit, which outcrops between the MCT and the Gumot Shear Zone (GSZ) is the middle unit. The GSZ (Schouppe 1995; Fontan 1998) forms a 100–200 m ductile shear zone. The Shontar unit, which includes rocks that outcrop to the northeast of the GSZ, is the highest of the three units. Due to similarities with rocks in the Kaghan valley (Greco *et al.* 1989; Spencer 1993; Lombardo *et al.* 2000), the upper two units are ascribed to the Higher Himalayan Crystalline unit (HHC). Our mapping in the Neelum valley suggests that the MCT trace is not coincident with those previously proposed by Greco (1989) and Tahirkheli (1988 1992). The MCT forms a kilometric syntaxial bend from Mohri to Luat (Fig. 2) that is expressed in the field by a 50–300 m thick mylonitic zone. In the Luat area the MCT separates greenschist facies rocks of the Salkhala unit from amphibolite facies rocks of the Kalapani unit (Ghazanfar *et al.* 1983; Ghazanfar & Chaudhry 1986). Elsewhere this metamorphic jump is not observed, with rocks of both the Salkhala and Kalapani units being at greenschist facies.

Lithostratigraphy

The lithostratigraphy (Fig. 3) of the Lesser and Higher Himalayan Crystalline rocks outcropping in the Neelum valley is made up of a Precambrian to Upper Palaeozoic basement overlain by a Permian to Lower Mesozoic cover. The Naril and Kundalshahi groups form the basement. The Naril Group is a gneissic complex directly overlain by metasediments of the Kundalshahi and Surgun groups. It is dominated by gneisses with high-grade biotite–orthoclase–sillimanite-bearing relics and strongly boudinaged amphibolite layers. The gneiss and its associated rocks are intruded by K-feldspar porphyroblastic

From: KHAN, M. A., TRELOAR, P. J., SEARLE, M. P. & JAN, M. Q. (eds) *Tectonics of the Nanga Parbat Syntaxis and the Western Himalaya.* Geological Society, London, Special Publications, **170**, 431–453. 1-86239-061-4/00/$15.00

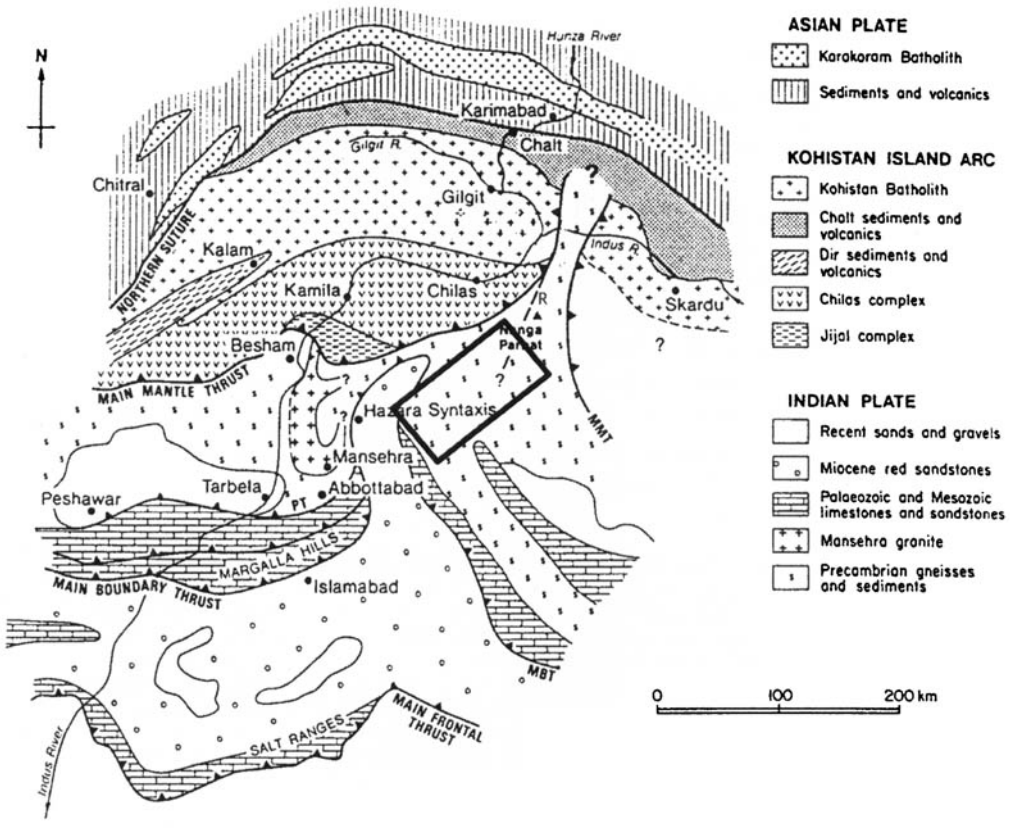

Fig. 1. Geological map of Northern Pakistan showing the location of the studied area (bold line). R, Raikot Fault; PT, Panjal Thrusts (from Treloar *et al.* 1989).

granites that probably correlate with the Cambro-Ordovician, Mansehra-type, granites dated at 516 ± 16 Ma by Le Fort *et al.* (1980). The gneisses are tentatively correlated with the 1850 Ma aged Iskere Gneiss that outcrops at Nanga Parbat (Zeitler *et al.* 1989). Mafic layers within the gneisses can be correlated with the type-A metabasites that outcrop in the Nanga Parbat region (Pognante & Lombardo 1989).

As it is also intruded by the Mansehra-type granites, the Kundalshahi Group is probably also Precambrian in age. The Kundalshahi Group is a thick metasedimentary sequence divided into two units. The Kuttar unit includes garnet-bearing schists, frequently phyllitic, that grade upward into alternations of quartz mica-schists, impure quartzites and rare marble horizons. Discontinuous, strongly deformed, metaconglomerates separate the Kuttar unit from the Kattha unit, which is mainly composed of impure quartzites and paragneisses. The metaconglomerates are tentatively correlated with the Tanakki conglomerates of the Hazara area (Baig & Lawrence 1987), which separate low grade rocks of the Hazara Formation, metamorphosed during the Pan-African or Hazaran orogeny at 600–900 Ma, from the overlying unmetamorphosed Abbottabad Group. The Kattha unit is tentatively correlated with arenaceous rocks of the Tanol Formation which form the lower part of the Abbottabad Group, and with the 'First Cover' sequence in the Kaghan valley (Spencer 1993). On the basis of lithological similarities, the Kattha unit may be the equivalent of the late Precambrian to early Cambrian Phe Formation in Zanskar (Vannay 1993).

The Mansehra-type granites form kilometric bodies intrusive into the Naril and Kundalshahi groups. They range in composition from leucoadamellite to granodiorite, often porphyritic, with a sub-alkaline and peraluminous geochemical signature (Schouppe 1995). The cover is made up of the metasedimentary Surgun Group. The Upper Palaeozoic to Mesozoic Surgun

Group is divided into three lithological units. From base upward, these are: (1) Unit A—paragneisses grading into impure quartzites; (2) Unit B—white and yellow marbles, dark calc-schists and minor quartzites; and (3) Unit C—garnet-bearing micaschists, graphite-bearing schists, impure quartzites and minor metaconglomerates. The metasediments can be considered as equivalent to the autochthonous Tibetan sediments, deposited on the passive margin of the Indian plate during the upper Palaeozoic (e.g. Fuchs 1985; Gaetani *et al.* 1985; Spencer 1993). Unit B is correlated with the Burawai Fm. (Greco *et al.* 1989) and the 'Second Cover' sequence (Spencer 1993) of the Kaghan valley where faunal evidence indicates an upper Palaeozoic to Lower Mesozoic age (Bossart *et al.* 1984; Greco & Spencer 1993). It can also be correlated with the fossiliferous Triassic limestones and unfossiliferous infra-Trias carbonates interstratified with the Panjal volcanics (Wadia 1934) and the Panjal Sequence (Greco 1989). The age of Unit A is likely to be Lower Carboniferous to Permian, Unit B is likely to be Permian to Trias while Unit C is likely to be Trias to Mesozoic. The metasedimentary sequence of the Surgun Group is comparable to the Carboniferous to Triassic Alpurai Group of the Swat area (Treloar *et al.* 1989; DiPietro *et al.* 1993). Basic rocks that are correlated with the Carboniferous–Triassic Panjal Traps (e.g. Wadia 1931; Calkins *et al.* 1975; Bossart *et al.* 1984; Greco 1989; Papritz & Rey 1989; Spencer 1993; Schouppe 1995) form dykes and sills that cut, or are subparallel to, the regional foliation of both cover and basement sequences. They also occur as concordant bodies in the cover sequences where they are interpreted as syn-sedimentary extrusive rocks. Geochemistry indicates a basaltic, Fe-rich tholeiitic composition (Schouppe 1995). Macroscopic features including pillows, amygdales and interlayered tuffaceous layers, as well as conformable alternations with crinoidal limestones, exclude an oceanic origin as suggested by Ghazanfar & Chaudhry (1984). The macroscopic features indicate a continental/marine depositional environment of alternating shallow water and subaerial episodes (Honegger *et al.* 1982; Greco 1989). The Early Carboniferous to Permian age of these volcanic rocks is documented by stratigraphic data from various parts of the Himalaya (Nakazawa & Kapoor 1973; Reynolds *et al.* 1983; Gaetani *et al.* 1990; Vannay & Spring 1993) and by geochronological data (Baig 1990; Spencer 1993). In the Neelum valley no data permit a precise age determination; although if the correlation between Unit B and the 'Second Cover' sequence of Spencer (1993) is correct, the Panjal Traps must be younger than Upper Palaeozoic to Lower Mesozoic. Therefore, the possibility exists that at least part of the marbles of Unit B could be early Permian in age.

Both the cover and basement sequences are deformed by four ductile tectonic phases, related to the Himalayan orogeny (Schouppe 1995; Fontan 1998). Meso-scale D1 structures consist mainly of isoclinal intrafolial folds that can be correlated with macro-scale overturned, tight recumbent folds. S1 foliation is preserved within microlithons in the S2 foliation or as orientated inclusion trails in garnets. In both the LHC and HHC, garnets in micaschists are characterized by the presence of S-shaped and straight inclusion trails discordant to the external foliation. Where orientated minerals, mainly micas, form these inclusion trails, they are interpreted as a relic S1 foliation.

D2 structures chiefly consist of isoclinal overturned and recumbent folds characterized by rounded hinge zones. The S2 foliation is pervasive in rocks of the HHC, especially in those of the cover sequences, but appears weaker in the LHC. The D3 phase forms hectometric open folds with axes that plunge to the NE and SW with subvertical to steeply NW dipping axial planes. This phase is associated with weakly pervasive chlorite and white mica foliations that wrap the post-kinematic minerals, mainly garnets. The D4 phase forms kilometric-scale gentle folds with axes that plunge toward the NNW and with subvertical axial planes.

Metamorphic evolution

The Lesser Himalayan Crystallines

In the Salkhala unit, Tertiary metamorphism is characterized by a prograde metamorphic evolution (M1 to M3), followed by a low-grade retrogression (M4). M1 is inferred on the basis of rare relics; M2, characterized by a syn-kinematic assemblage, was at low-temperature greenschist facies conditions. This was followed by a post-kinematic M3 phase at high-temperature greenschist facies. Late stage chlorite growth is interpreted as a retrogressive event (M4) probably at low-temperature greenschist facies conditions.

In schists of the Kuttar unit, the initial metamorphic assemblage (M1) is preserved only in inclusion-rich cores of sub-millimetric, zoned garnets, and consists of greenschist facies chlorite, white mica and quartz. These inclusions form S-shaped trails and the orientation of the white mica and chlorite suggests a D1 foliation. The

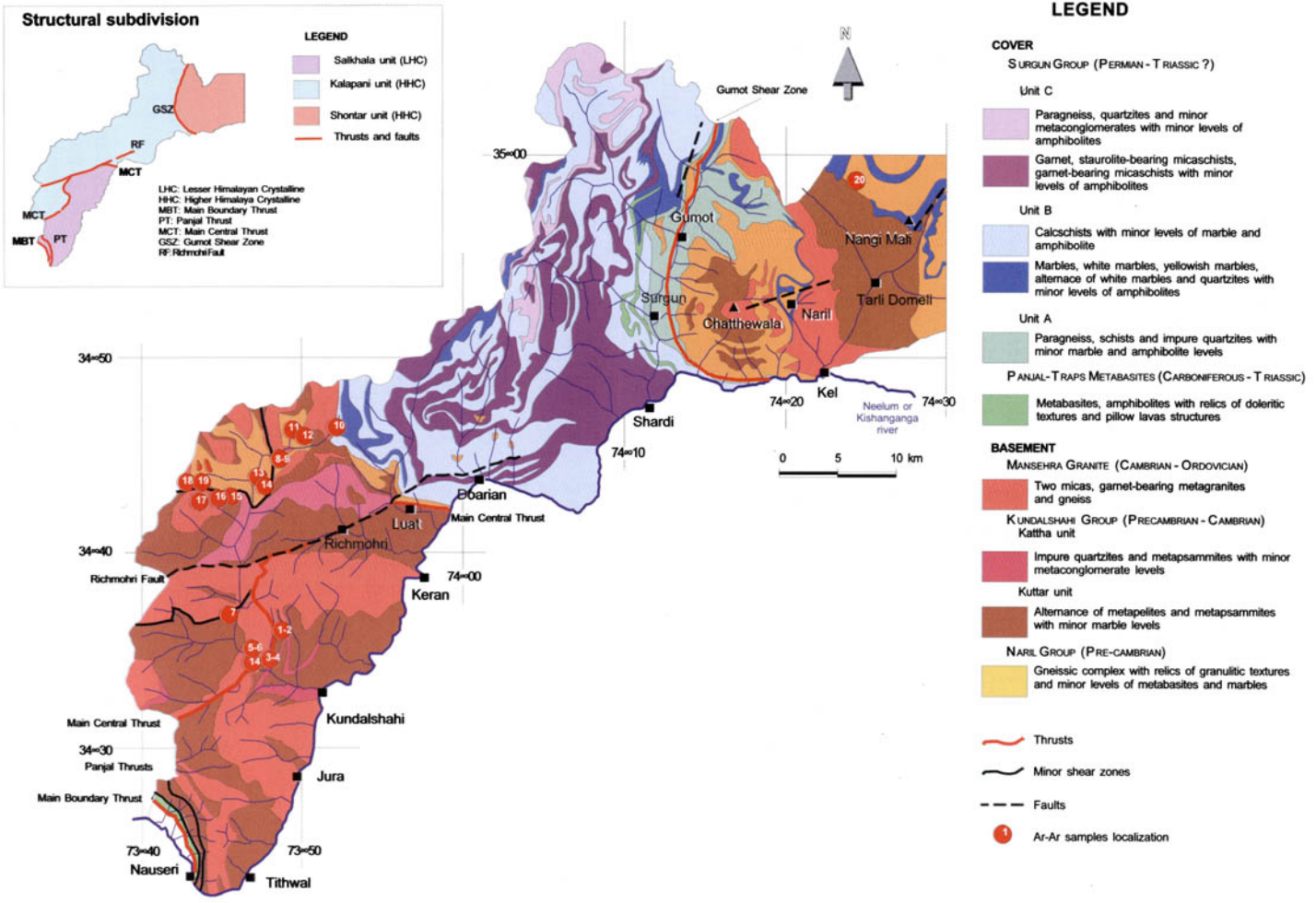

Fig. 2. Geological map of the Neelum valley (redrawn from Schouppe 1995 and Fontan 1998).

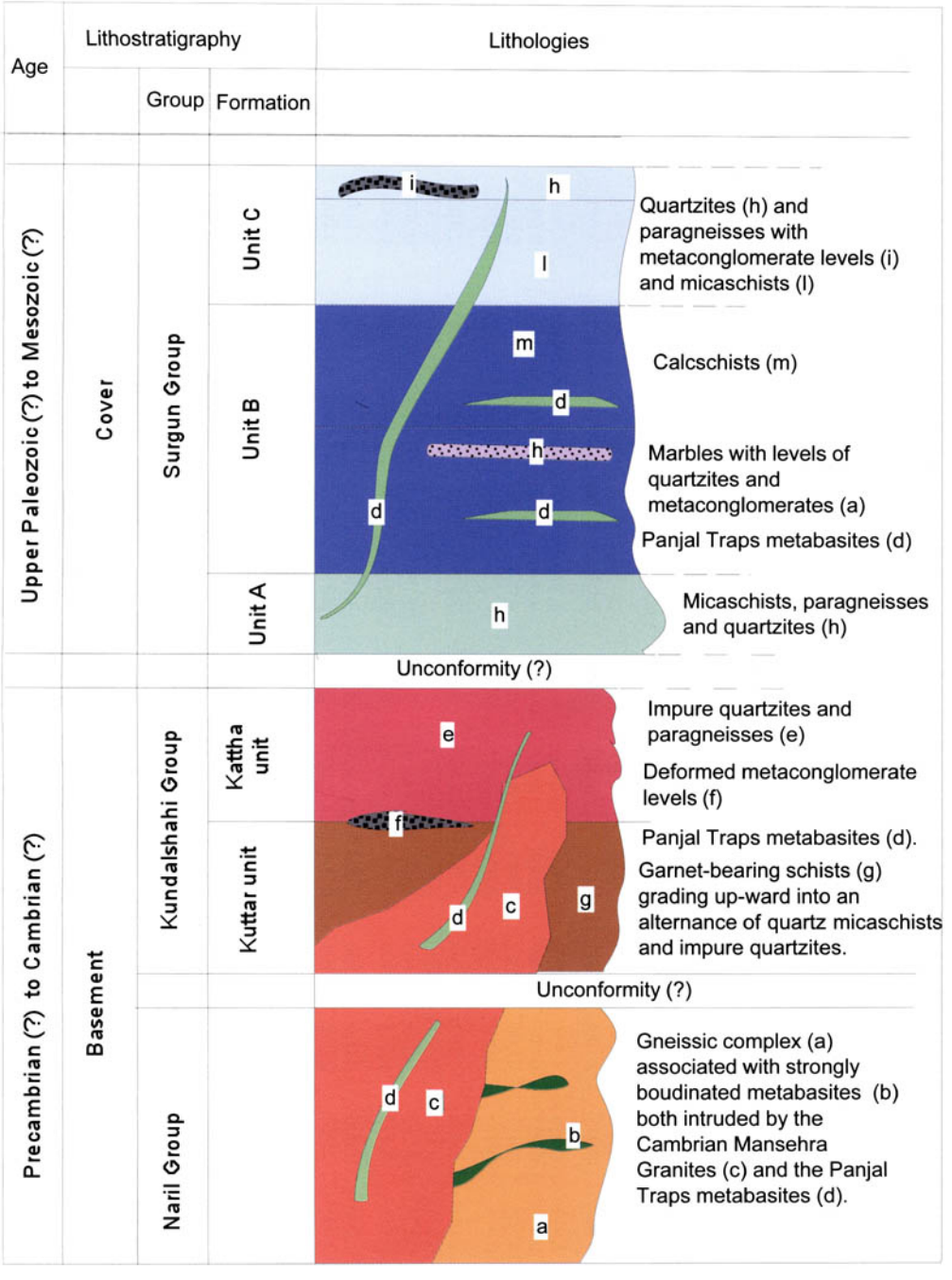

Fig. 3. Schematic lithostratigraphic column.

M2 assemblage consists of garnet (Grt I), biotite (Bt I), chlorite, quartz and white mica. White mica, biotite (Bt I) and chlorite outline a pervasive foliation formed on the M1 mineral assemblage. The garnets are characterized by S-shaped or spiralled inclusion trails that indicate nucleation and growth during progressive shortening mainly related to the D2 deformation.

Table 1. *Representative zoned garnet analysis and compositional trend across a garnet (biotite and garnet-bearing greenschist zone)*

N.	163	164	165	166	167	168	169	170	171	172	173	174	175	176	177
SiO_2	36.99	36.83	37.06	36.82	36.77	36.68	36.50	36.68	36.39	36.82	36.56	36.43	36.80	36.98	37.35
TiO_2	0.02	0.09	0.18	0.10	0.19	0.24	0.08	0.18	0.10	0.14	0.09	0.03	0.04	0.08	0.03
Al_2O_3	20.29	20.46	20.39	20.34	20.22	20.12	20.46	20.02	20.10	20.19	20.34	20.35	20.49	20.27	20.27
Cr_2O_3	0.05	0.04	0.08	0.05	0.00	0.02	0.17	0.01	0.00	0.05	0.06	0.09	0.06	0.08	0.11
FeO	33.78	33.33	31.65	28.81	24.58	24.10	24.53	26.36	30.75	33.74	33.88	34.11	32.78	32.33	32.08
MnO	0.95	1.77	2.74	7.73	11.65	12.93	14.21	9.76	5.41	1.48	1.27	1.19	1.65	1.58	1.56
MgO	2.15	1.89	2.14	1.28	0.87	0.76	0.89	1.00	1.30	1.71	1.86	2.05	2.54	2.60	2.54
CaO	5.76	5.59	5.77	4.87	5.70	5.14	3.16	6.00	5.95	5.85	5.92	5.73	5.65	6.03	6.06
Total	**99.99**	**100.00**	**100.01**	**100.00**	**99.98**	**99.99**	**100.00**	**100.01**	**100.00**	**99.98**	**99.98**	**99.98**	**100.01**	**99.95**	**100.0**
Si	2.980	2.973	2.982	2.986	2.985	2.984	2.980	2.976	2.953	2.976	2.955	2.944	2.959	2.971	2.995
Al IV	0.020	0.027	0.018	0.014	0.015	0.016	0.020	0.024	0.047	0.024	0.045	0.056	0.041	0.029	0.005
Al VI	1.907	1.919	1.916	1.931	1.919	1.913	1.948	1.891	1.876	1.899	1.892	1.883	1.901	1.890	1.911
Cr	0.003	0.003	0.005	0.003	0.000	0.001	0.011	0.001	0.000	0.003	0.004	0.006	0.004	0.005	0.007
Ti	0.001	0.005	0.011	0.006	0.012	0.015	0.005	0.011	0.006	0.009	0.005	0.002	0.002	0.005	0.002
Fe^{3+}	0.093	0.078	0.070	0.062	0.070	0.071	0.040	0.100	0.128	0.092	0.108	0.122	0.102	0.106	0.081
Fe^{2+}	2.182	2.171	2.060	1.892	1.599	1.569	1.635	1.688	1.959	2.188	2.182	2.183	2.102	2.066	2.070
Mn	0.065	0.121	0.187	0.531	0.801	0.891	0.983	0.671	0.372	0.101	0.087	0.081	0.112	0.108	0.106
Mg	0.258	0.227	0.257	0.155	0.105	0.092	0.108	0.121	0.157	0.206	0.224	0.247	0.304	0.311	0.304
Ca	0.497	0.483	0.497	0.423	0.496	0.448	0.276	0.522	0.517	0.507	0.513	0.496	0.487	0.519	0.521
Z	3.000	3.000	3.000	3.000	3.000	3.000	3.000	3.000	3.000	3.000	3.000	3.000	3.000	3.000	3.000
Y	2.004	2.005	2.002	2.002	2.001	2.000	2.004	2.003	2.010	2.004	2.009	2.013	2.009	2.006	2.001
X	3.003	3.003	3.001	3.001	3.001	3.000	3.002	3.002	3.006	3.002	3.006	3.008	3.006	3.004	3.000
alm	0.727	0.723	0.686	0.630	0.533	0.523	0.545	0.562	0.652	0.729	0.726	0.726	0.699	0.688	0.690
sps	0.022	0.040	0.062	0.177	0.267	0.297	0.327	0.223	0.124	0.034	0.029	0.027	0.037	0.036	0.035
pyr	0.086	0.076	0.086	0.052	0.035	0.031	0.036	0.040	0.052	0.069	0.075	0.082	0.101	0.104	0.101
grs	0.117	0.118	0.123	0.105	0.124	0.106	0.064	0.118	0.105	0.117	0.112	0.100	0.108	0.115	0.129
anr	0.047	0.042	0.040	0.034	0.041	0.043	0.022	0.056	0.067	0.050	0.057	0.062	0.052	0.055	0.041
uvr	0.002	0.001	0.003	0.002	0.000	0.001	0.005	0.000	0.000	0.002	0.002	0.003	0.002	0.003	0.003
Xmg	0.106	0.095	0.111	0.076	0.062	0.055	0.062	0.067	0.074	0.086	0.093	0.102	0.127	0.131	0.128
A	0.283	0.289	0.294	0.322	0.362	0.367	0.361	0.346	0.312	0.287	0.287	0.285	0.287	0.288	0.287
Fe_2O_3	1.542	1.291	1.153	1.016	1.148	1.157	0.646	1.644	2.092	1.521	1.775	2.014	1.691	1.758	1.345
FeO	32.393	32.169	30.613	27.896	23.547	23.059	23.949	24.880	28.868	32.372	32.283	32.298	31.259	30.748	30.870

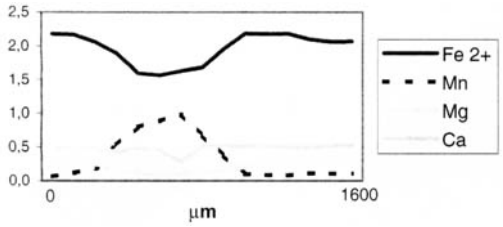

Table 1. Cont.

Core-to-rim compositional zoning patterns in garnets (Table 1) suggest prograde reactions during M1 to M3. Fe^{2+}–Mg–Mn and Fe^{2+}–Mg–Ca trends indicate a core-to-rim decrease in Ca that probably reflects the progressive growth of calcic phases such as plagioclase, amphibole and epidote during the garnet-producing reaction (Fontan 1998). Using the Grt–Bt and Grt–Phe thermometers and the Grt–Ilm barometer, sample 64/92 yields temperature ranges of 400–500 °C at 4–5 kbar (Table 2). The M3 assemblage is characterized by garnet (Grt II), biotite (Bt II), amphibole, plagioclase and epidote. The second garnet generation (Grt II) forms an inclusion-free rim around the previous garnet (Grt I) or small euhedral isolated blasts. Biotite (Bt II) partially replaces the white mica and the older biotite (Bt I). Ferro-tschermakite to tschermakite amphibole, forming random euhedral poikiloblasts sieved with rounded (Fig. 6a), fine-grained quartz inclusions, indicates high-temperature greenschist facies conditions. *P–T* conditions of 500–600 °C at 6–9 kbar are calculated for sample 139/92 using the Grt–Bt and the Grt–Hbl thermometers and the Grt–Pla–Bt–Qtz, Grt–Pla–Alsi–Qtz barometers (Table 2).

The reaction of ilmenite to sphene and the growth of late chlorite as large poikiloblasts on the foliation and as an epitaxial growth over older chlorites, amphibole, white mica and biotite, are interpreted as an M4 re-equilibration at low-temperature greenschist facies conditions. The undulose extinction of chlorite poikiloblasts (chl III) is interpreted as a consequence of D4.

The Higher Himalayan Crystallines

In the Kalapani and Shontar units, M1 assemblages are divided into three zones (Z1, Z2, Z3 of Fig. 4). High-pressure, high-temperature greenschist facies conditions are preserved in the SW part of the Kalapani unit, eclogitic facies metamorphism in the NE part of the Kalapani unit and high-pressure granulites in the SE part of the Shontar unit. The M2 assemblages can similarly be divided into three zones (Z1, Z2, Z3 of Fig. 5). High-temperature greenschist facies conditions are preserved in the SW part of the Kalapani unit, kyanite-bearing amphibolite facies conditions in the NE part of the Kalapani unit and in the Shontar unit and sillimanite-bearing amphibolite facies conditions in the Chattewala area of the Shontar unit. Over the whole of the HHC, M3 is characterized by upper greenschist facies conditions, while the growth of late chlorite blasts suggests lower grade conditions during M4.

The NE part of the Kalapani unit. In this zone, both metabasic rocks and micaschists show a retrograde metamorphic evolution. The metabasites show an incomplete retrogressive re-equilibration from M1 through to M3 and M4 (Fig. 8). M1 eclogites contain a fine- to medium-grained granoblastic omphacite (Cpx I) and garnet (Grt I) with minor rutile, ilmenite and white mica, probably phengite (Pognante & Spencer 1991) bearing assemblages (Fig. 6b). Omphacite occurs as pale green to colourless isolated corroded grains inside symplectites. The latter are composed of vermicular intergrowths of diopside (Cpx II) and albite (Pla I) and are interpreted as the product of omphacite breakdown. The newly formed pyroxene is in optical continuity with the parent omphacite grains. Euhedral or sub-euhedral garnet grains (Prp_{40}) are uniformly distributed. Rutile and ilmenite are scattered in the rocks. Ilmenite is present as anhedral grains included in garnet and omphacite blasts. Rutile forms euhedral grains mostly included in garnet blasts. Representative mineral chemistry of the garnet and pyroxene is listed in Table 3. Eclogitic facies conditions have been estimated using the Grt–Omp Mg–Fe exchange geothermometer and the calibration of Holland (1983) (samples 6*/91, 9*/91, 13*/91 and 28*/91, Table 2). Garnet (Grt I) and omphacite (Cpx I) pairs give temperatures of 600 ± 50 °C, while the jadeite content ($X_{Jd\ mean} = 0.43$) in omphacites gives a minimum pressure of 13–14 kbar (Gourirane 1993; Fontan 1998). These *P–T* conditions are similar to those proposed by Pognante & Spencer (1991) and by Lombardo *et al.* (2000) for the Kaghan valley eclogites.

The Ab–Jd–Qtz barometer (Holland 1980) applied to Na-plagioclase (Pla I) and clinopyroxene (Cpx II) symplectite pairs gives pressures of 8–10 kbar at 600 °C, indicating an isothermal pressure decrease from the M1 peak. The pressure decrease is also indicated by the presence of at least three amphiboles of different chemical composition. The first (Hbl I) forms narrow rims around the garnet blasts and ranges from pargasite, ferroan–pargasite, pargasitic–hornblende to edenitic–hornblende. The second

Table 2. *Pressure and temperature estimates for the LHC and HHC*

	LHC		HHC											
	Salkhala unit		NE Kalapani unit				SW Kalapani unit			Shontar unit				
	64/92	139/92	6*,9*,13*,28*/91	13/91	39/91, 132/91	173/93	220/92	121/92	254/92	K**/92	146/93	154/93	101/91	
Grt-Bt, Ferry & Spear (1978)*	M2 459 ± 28 °C	M3 567 ± 19 °C			M3 550 ± 25 °C		M2 530 ± 20 °C	M2 517 ± 13 °C	M2 578 ± 30 °C	M2 650 ± 70 °C		M2 806 ± 31 °C		
Grt-Phe, Hynes & Forest (1988)	M2 427 °C			M2 654 ± 37 °C										
Grt-Hbl, Graham & Powell (1982)	at 450 °C M2 4.25 kbar	M3 519 ± 27 °C								M2 670 ± 70 °C				
Grt-Hbl, Perchuk *et al.* (1985)		M3 514 ± 29 °C								M2 670 ± 70 °C	M1 666 ± 58 °C	M2 545 °C		
Grt-Tur, Colopietro & Friberg (1987)									M3 359 ± 28 °C					
Grt-Cpx, Powell (1985)			M1 611 ± 20 °C										M2 748 ± 8 °C	
Grt-Cpx, Ellis & Green (1979)			M1 633 ± 20 °C										M2 760 ± 8 °C	
Grt-Cpx, Pattison & Newton (1989)			M1 633 ± 20 °C											
Hbl-Pl, Holland & Blundy (1994)						M1 700 ± 50 °C						M2 756 ± 35 °C		
Jd content in cpx, Holland (1980)			at 600 °C M1 13–14 kbar											
Ab-Jd-Qtz, Holland (1980)			at 600 °C M2 10.3 ± 0.9 kbar			at 650 °C M1 9 ± 0.5 kbar								
Grt-Ilm (GRAIL), Bohlen *et al.* (1983)				at 600 °C M2 9.9 ± 0.2 kbar	at 550 °C M3 4.4 ± 0.6 kbar			at 500 °C M2 4.9 ± 0.5 kbar	at 500 °C M2 5.2 kbar					
Grt-Pl-Bt-Qtz, Hoisch (1990)		at 550 °C M3 8.1 kbar												
Grt-Pl-Alsi-Qtz, Newton & Haselton (1981)		at 550 °C M3 7.4 kbar									at 650 °C M1 12.5 ± 0.5 kbar			
Grt-Pl-Alsi-Qtz, Hodges & Spear (1982)		at 550 °C M3 7.5 kbar												
Grt-Pl-Alsi-Qtz, Ganguly & Saxena (1984)		at 550 °C M3 8.3 kbar												
Grt-Bt-Ms-Alsi, Hodges & Crowley (1985)		at 550 °C M3 8.4 kbar												
Grt-Pl-Alsi-Qtz, Koziol (1989)		at 550 °C M3 7.9 kbar												
Grt-Bt-Ms-Alsi, Holdaway *et al.* (1988)					at 550 °C M3 4.3 kbar									

Rock-types: 13/91 schist (Surgun Group), 29/91 schist (Surgun Group), 39/91 schist (Surgun Group), 132/91 mylonitic granite, 6*, 7*, 9*, 13*, 28*/91 retrogressed eclogites (Panjal Traps), 101/91 metaquartzite (Kundalshahi Group), 64/92 schist (Kundalshahi Group), 121/92 schist (Kundalshahi Group), 139/92 schist (Kundalshahi Group), 220/92 schist (Kundalshahi Group), 254/92 metagranite (Mansehra-type), 146/93 metabasite (Panjal Traps), 154/93 basic granulite (Panjal Traps) and 173/93 metabasite (Panjal Traps). Pressures and temperatures have been estimated using the programmes of Spear *et al.* (1991).

*: with Berman (1990) Garnet solution model.

**: samples utilized by Kervyn (1993).

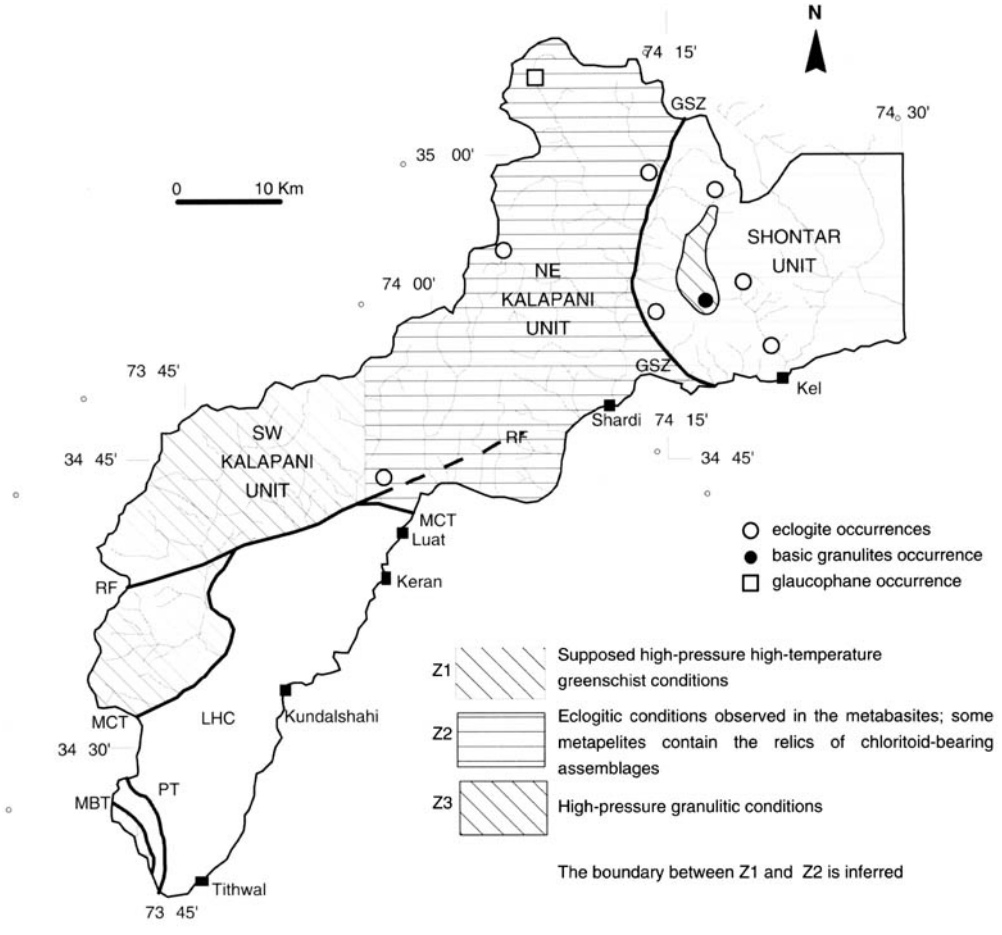

Fig. 4. Metamorphic zonation generated by the M1 phase in the HHC (Kalapani and Shontar units). In the LHC (Salkhala unit), M1 is inferred. (LHC and HHC: respectively Higher and Lesser Himalayan Crystalline units; MBT: Main Boundary Thrust; PT: Panjal Thrust; MCT: Main Central Thrust; GSZ: Gumot Shear Zone; RF: Richmohri Fault; C: Chattewala area.)

amphibole (Hbl II) forms an epitaxial growth on Hbl I and is of tschermakite and tschermakitic–hornblende composition. The third is a magnesium–hornblende (Hbl III) that forms large (1–2 mm) random pleochroic blasts sieved by small albite and rounded quartz inclusions, and which grows on both the cpx–pla symplectite and garnet (Fig. 6c). Oligoclase poikiloblasts (Pla II) are in apparent equilibrium with euhedral epidote blasts, mainly clinozoisite and pistacite. Biotite (Bt II) forms large blasts which grow on the symplectite, and small epitaxial crystals on Hbl I and II. A thin biotite rim also develops along the border between symplectite and ilmenite. Hbl II and Hbl III, oligoclase (Pla II), epidote and biotite (Bt II) are all part of the M2 assemblage.

The transition towards garnet–epidote amphibolites is gradual and is characterized by the disappearance of omphacite and the replacement of vermicular symplectite by microgranoblastic aggregates, made of oligoclase (Pla I), sodic augite (Cpx III) (Fig. 7a) and rare epidote grains. In these aggregates, amphibole (Hbl II) and orientated biotite (Bt II) define a pervasive foliation that includes the early garnet blasts (mainly Grt I and II). There is a reduction in garnet size and the formation of new small euhedral garnets (Grt III, Fig. 7c) in the foliation. With further re-equilibration and deformation under greenschist facies conditions, the amphiboles, garnets and biotites react to chlorite and sphene to rutile (assemblage M3–M4). The rock is characterized by a strong foliation made of

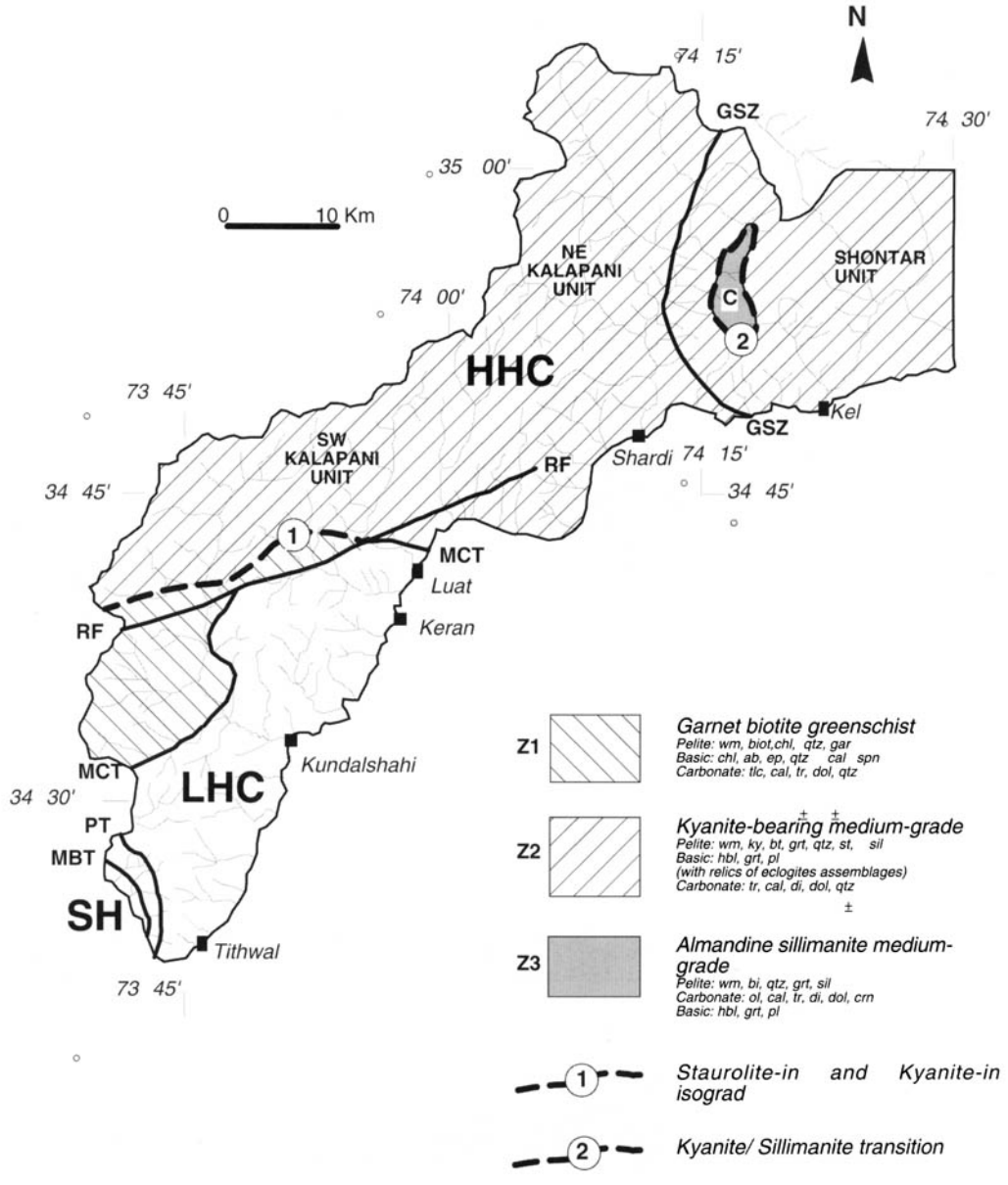

Fig. 5. Metamorphic zonation (Z1, Z2 and Z3) related to the medium-grade M2 phase in the HHC. (MBT: Main Boundary Thrust; PT: Panjal Thrust; MCT: Main Central Thrust; GSZ: Gumot Shear Zone; RF: Richmohri Fault; C: Chattewala area.)

nematoblastic aggregates of greenish amphibole (Hbl IV) associated with euhedral pistacite. Na-rich plagioclase (albite to oligoclase) constitutes small grains between amphibole blasts and 'eyes', sieved with small clinozoisite grains.

In the micaschists, the mineral assemblage consists of quartz and white mica with chlorite, biotite, garnet, kyanite, staurolite, tourmaline, epidote, plagioclase, sphene, rutile, opaque phases and graphite and is a function of medium-grade metamorphism. The presence of early garnets (Grt I) with S-shaped and straight inclusions trails, formed by relics of chloritoid, rutile, ilmenite, quartz and white mica,

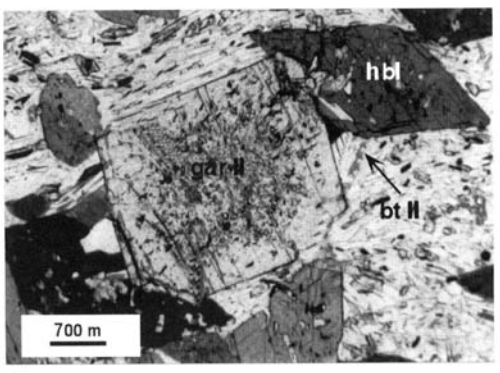

(a)

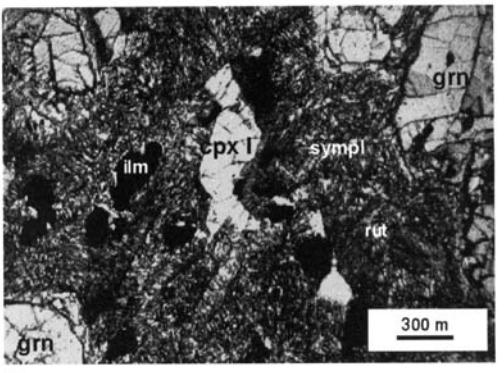

(b)

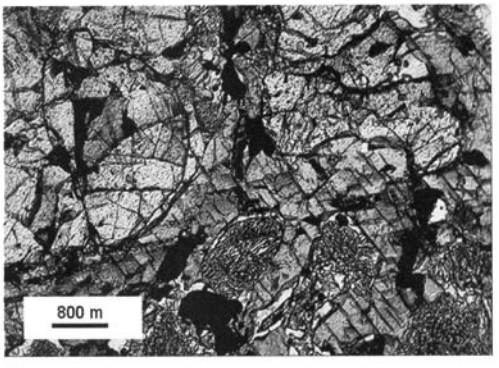

(c)

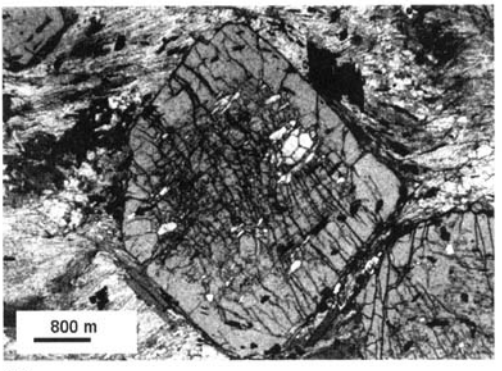

(d)

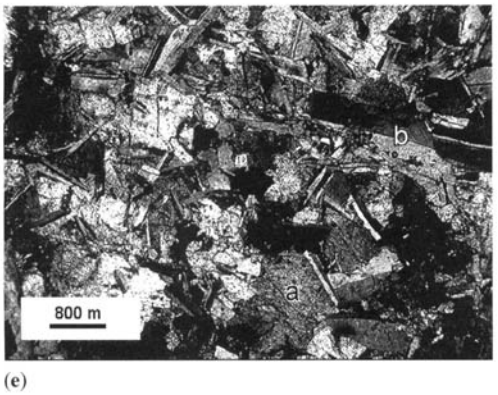

(e)

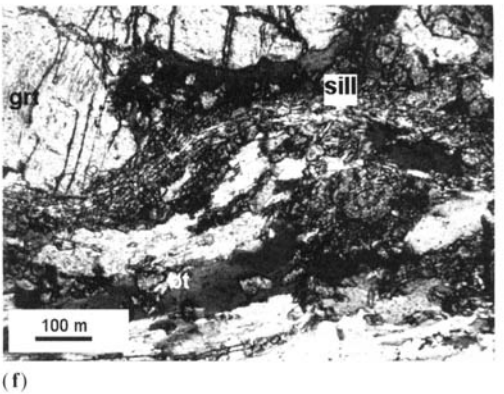

(f)

Fig. 6. (**a**) M3 assemblage in the Kutton schists (Kundalshahi Group). The paragenesis includes white mica, quartz and epidote (matrix) with large zoned garnet (gar II), green amphibole (hbl) and smaller biotite (bt II). (**b**) Typical aspect of the retrogressed eclogites. In the fine-grained vermicular, symplectites (simpl) is still visibly a relic of omphacite (cpx I). Note the euhedral garnet blasts (grn) and the larger ilmenite (ilm) blasts. Small rutile blasts are present in the symplectites. (**c**) The amphibole III grows on the garnet (grt1) and the symplectite (Sympl). Note the increase of grain size of the symplectitic products (plagioclase, pl1 and clinopyroxene). (**d**) Micaschist with garnet porphyroblasts (Unic C, Surgun Group). The straight inclusion (S1) trails are made of white mica, ilmenite quartz and rare chloritoid. (**e**) Preserved magmatic intergranular texture in SW Kalapani tectonic unit (a: clinopyroxene, b: plagioclase). (**f**) M2 assemblage garnet (grt), sillimanite (sill) and biotite (bt) related to the M2 metamorphic stage (Shontar unit, Chattewala area).

Table 3. *Representative analyses of some minerals forming the eclogites: clinopyroxene of the symplectites, omphacites and garnets (sample 6*/91)*

	cpx in the symplectites			omphacites				garnets			
N.	12	14	15	21	22	23	N.	56	57	58	59
SiO_2	53.12	52.22	52.60	54.89	54.81	54.89	SiO_2	39.16	39.26	39.05	38.99
TiO_2	0.26	0.19	0.12	0.12	0.15	0.07	TiO_2	0.04	0.04	0.04	0.00
Al_2O_3	5.85	6.60	5.61	11.21	10.94	11.10	Al_2O_3	21.52	21.85	21.42	21.87
Cr_2O_3	0.04	0.03	0.00	0.00	0.00	0.02	Cr_2O_3	0.00	0.02	0.00	0.00
FeO	5.65	5.63	5.80	4.76	4.67	4.79	FeO	24.60	23.93	24.76	24.69
MnO	0.10	0.09	0.08	0.00	0.09	0.01	MnO	0.37	0.36	0.37	0.45
MgO	12.34	12.05	12.52	8.37	8.35	8.36	MgO	7.71	7.56	7.40	7.57
CaO	19.16	19.34	19.61	13.07	12.95	12.78	CaO	7.06	7.16	6.85	6.64
Na_2O	3.03	2.91	2.66	6.87	7.10	6.91	**Total**	**100.46**	**100.18**	**99.89**	**100.21**
K_2O	0.02	0.01	0.01	0.00	0.01	0.00					
Total	**99.57**	**99.07**	**99.01**	**99.29**	**99.07**	**98.93**	Si	2.998	3.008	3.009	2.994
							Al IV	0.002	0.000	0.000	0.006
Si	1.934	1.911	1.929	1.961	1.959	1.967					
Al IV	0.066	0.089	0.071	0.039	0.041	0.033	Al VI	1.940	1.973	1.945	1.974
Fe^{3+}	0.000	0.000	0.000	0.000	0.000	0.000	Cr	0.000	0.001	0.000	0.000
Cr IV	0.000	0.000	0.000	0.000	0.000	0.000	Ti	0.002	0.002	0.002	0.000
Al VI	0.185	0.196	0.172	0.433	0.420	0.436	Fe^{3+}	0.058	0.022	0.050	0.027
Ti	0.007	0.005	0.003	0.003	0.004	0.002					
Cr VI	0.001	0.001	0.000	0.000	0.000	0.001	Fe^{2+}	1.517	1.512	1.545	1.558
Fe^{3+}	0.081	0.088	0.082	0.076	0.105	0.072	Mn	0.024	0.023	0.024	0.029
Fe^{2+}	0.087	0.080	0.091	0.063	0.034	0.067	Mg	0.880	0.863	0.850	0.867
Mn	0.003	0.003	0.002	0.000	0.003	0.000	Ca	0.579	0.588	0.565	0.546
Mg	0.637	0.627	0.650	0.425	0.434	0.422					
							Z	3.000	3.008	3.009	3.000
Fe^{2+}	0.005	0.004	0.005	0.003	0.001	0.004	Y	2.000	1.998	1.998	2.001
Mn	0.000	0.000	0.000	0.000	0.000	0.000	X	3.000	2.986	2.985	3.001
Mg	0.033	0.031	0.035	0.021	0.011	0.025					
Ca	0.747	0.758	0.771	0.500	0.496	0.491	alm	0.506	0.506	0.518	0.519
Na	0.214	0.206	0.189	0.476	0.492	0.480	sps	0.008	0.008	0.008	0.010
K	0.001	0.000	0.000	0.000	0.000	0.000	pyr	0.293	0.289	0.285	0.289
							grs	0.163	0.184	0.163	0.168
T	2.000	2.000	2.000	2.000	2.000	2.000	anr	0.030	0.012	0.026	0.014
M(1)	1.000	1.000	1.000	1.000	1.000	1.000	uvr	0.000	0.001	0.000	0.000
M(2)	1.000	1.000	1.000	1.000	1.000	1.000					
							Xmg	0.367	0.364	0.355	0.357
jd	0.133	0.118	0.107	0.400	0.387	0.407	A	0.288	0.293	0.289	0.290
ac	0.081	0.088	0.082	0.076	0.105	0.072					
ur	0.001	0.001	0.000	0.000	0.000	0.001	Fe_2O_3	1.007	0.374	0.869	0.473
Ti ts	0.007	0.005	0.003	0.003	0.004	0.002	FeO	23.694	23.593	23.978	24.264
Ca ts	0.052	0.078	0.064	0.033	0.033	0.029					
pm	0.002	0.001	0.001	0.000	0.001	0.000					
fs	0.046	0.042	0.048	0.033	0.017	0.036					
en	0.335	0.329	0.342	0.223	0.222	0.223					
wo	0.344	0.337	0.351	0.232	0.230	0.230					

discordant to the external foliation, is tentatively related to the high-pressure M1 metamorphism (Fig. 6d). M2 is marked by a second garnet generation (Grt II) that forms inclusion-free rims around Grt I or, rarely, small and isolated subeuhedral blasts in apparent equilibrium with random, undeformed euhedral porphyroblasts of kyanite, staurolite and tourmaline that grow on a muscovite-rich foliation. Using the Grt–Phe geothermometer and the Grt–Ilm geobarometer M2 P–T conditions are estimated at 600–700 °C at 10 kbar (Table 2, sample 13/91).

The M3 metamorphism is documented by the growth and/or re-crystallization of biotite and garnet. In micaschists (sample 39/91) and deformed granites (sample 132/91), the Grt–Bt geothermometer and the Grt–Ilm, and Grt–Bt–Ms–Ky geobarometers indicate P–T conditions of 450–550 °C at 4–5 Kbar (Table 2). The presence of late chlorite blasts on amphibole

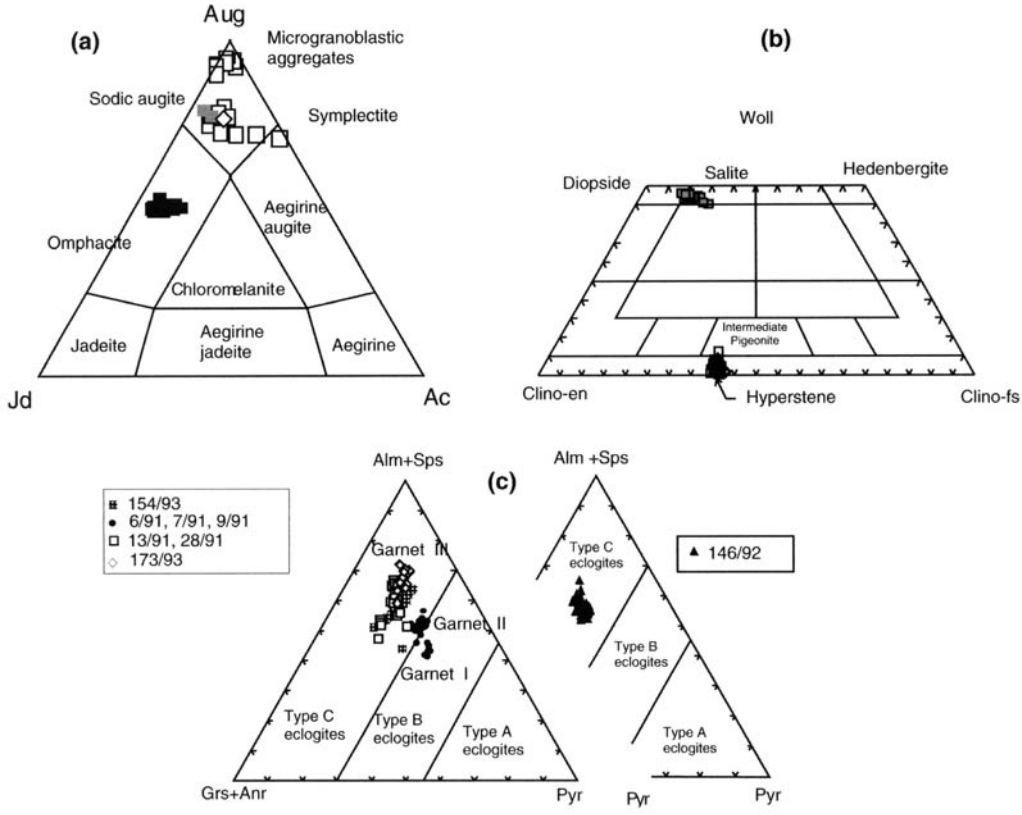

Fig. 7. (**a**) Nomenclature of the metamorphic pyroxene on the augite–jadeite–acmite triangular plot (Essene & Fyfe 1967). Filled and open squares correspond respectively to omphacite relics, symplectic intergrowths and to granoblastic aggregates in the eclogite-derived samples 6/91*, 7/91*, 9/91*, 13/91* and 28/91*. Grey filled squares represent the two metamorphic clinopyroxenes found in sample 154/93. Open diamond corresponds to the pyroxene found in sample 173/93. (**b**) Nomenclature of magmatic ortho- and clinopyroxenes. Grey squares: metabasites (sample 154/92 collected in high-grade area). Open diamond: metabasites collected in medium-grade area (sample 173/93). (**c**) Triangular plot pyrope–almandine + spessartine–grossularite + andradite of Coleman *et al.* (1965). The garnets of the eclogites (samples 6/91*, 7/91*, 9/91*, 146/92 and 154/62) and the garnets of sample 173/93 are plotted. These metabasites are associated with the basement (Kundalshahi and Naril groups) fall at the boundary of fields C (eclogites into metamorphic rocks of the alpine-type orogenic zones—associated with blueschists) and B (eclogites associated with migmatitic gneissic terrains). Garnets of the retrogressed eclogitic rocks (samples 13/91* and 28/91*) associated with the cover (Surgun Group) fall in field C (eclogites into metamorphic rocks of the alpine-type orogenic zones, associated with blueschists).

and biotite and the reaction of ilmenite to sphene document M4 re-equilibration under greenschist facies conditions.

The *P–T* evolution of the NE Kalapani unit is shown in Fig. 8. The retrograde path is characterized by an isothermal decompressive trend from eclogitic facies (M1 phase) through the upper amphibolite facies (M2 phase) to greenschist facies conditions (M3 phase).

The SW part of the Kalapani unit. The lack of eclogitic assemblages in the metabasic rocks is interpreted here as a primary feature rather than a consequence of pervasive retrogressive reactions. The metabasic rocks usually consist of garnet-poor amphibolites in which relics of magmatic intergranular texture are frequently visible (Fig. 6e). In sample 173/93, the magmatic minerals (mainly orthopyroxenes, clinopyroxenes and plagioclase phenocrysts with minor skeletal ilmenites) are replaced by amphibole–garnet–biotite–chlorite-bearing assemblages. Magmatic pyroxenes, diopside to salite in composition (Fig. 7b), are almost completely altered to fine-grained aggregates of randomly orientated green Al-rich tschermakitic amphiboles and rare sodic augites (Fig. 7a). Magmatic plagioclases show a normal concentric zonation

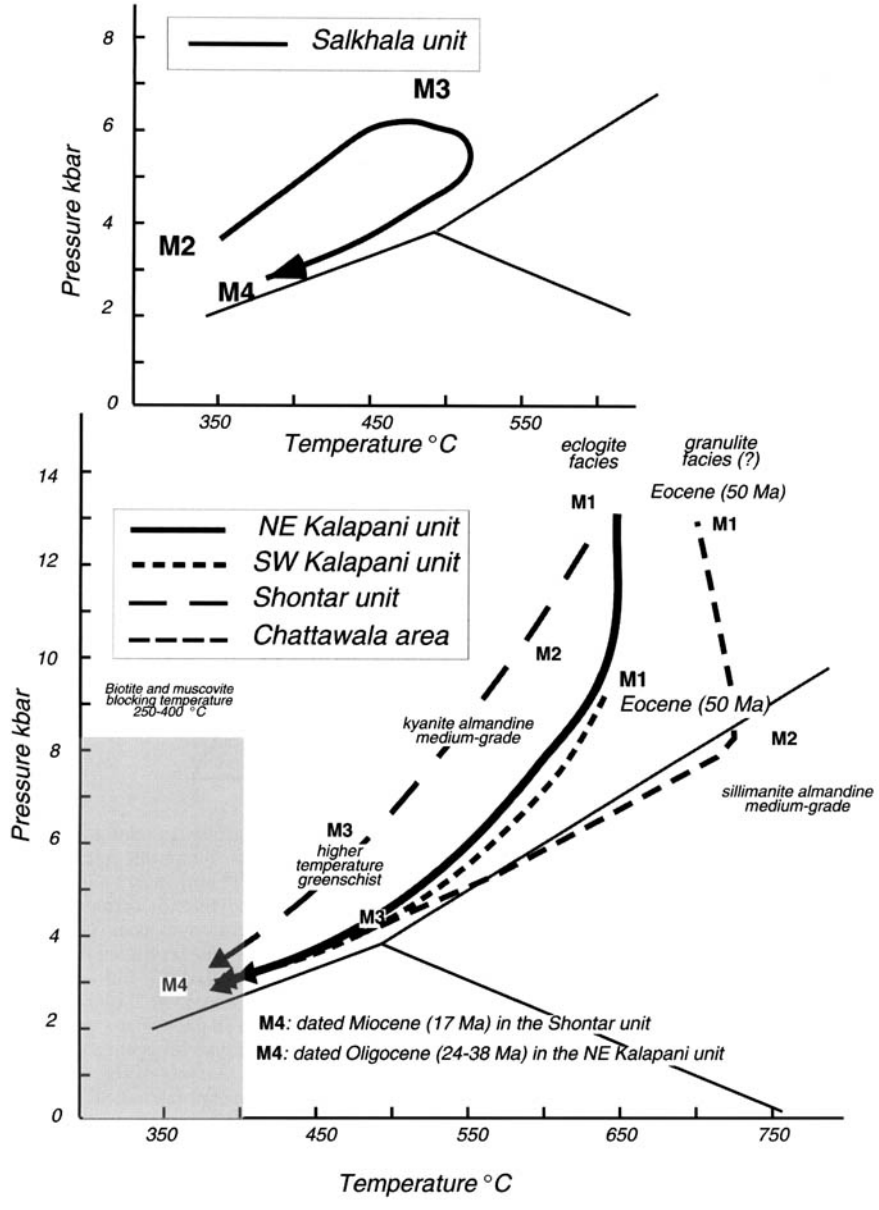

Fig. 8. Proposed *P–T–t* paths for the Salkhala and NE and SW part of the Shontar and Kalapani units.

with labradorite cores and oligoclase rims and contain very fine-grained zoisite/clinozoisite crystals. Garnet forms skeletal porphyroblasts growing on the hornblende tschermakite aggregates. Small mimetic biotites grow on the amphibole. The tschermakitic amphibole and clinopyroxene are both related to the M1 high-pressure phase. The hornblende tschermakite–garnet–biotite-bearing assemblage is an M2 one. In the deformed rocks the pervasive foliation is made of nematoblastic amphibole aggregates and biotite. Albite forms small interstitial crystals, in apparent equilibrium with small euhedral zoisite and clinozoisite crystals. Random chlorite needles grow on amphiboles and garnets. The albite, amphibole, sphene and epidote-bearing paragenesis dates from retrogression to lower grade conditions during M3 or

M4. The metamorphic peak that corresponds to the M1 phase was determined for the metabasic rocks (sample 173/93) at 650–750 °C and 8–9 kbar using the Pl–Hbl thermometer and the Ab–Jd–Qtz barometer (Table 2).

The micaschists consist of millimetric quartz- and mica-rich layers. Orientated white mica, biotite and chlorite in the mica-rich layers are part of an equilibrium M2 assemblage that includes quartz, garnet, amphibole, plagioclase, epidote, opaque phases and graphite. Two garnet generations are observed. The older forms an inclusion-rich core and the second an inclusion-free rim. Large amphibole poikiloblasts are occasionally present. Chlorite forms small, randomly orientated, poikiloblasts. Epidote, plagioclase (albite/oligoclase) and opaque phases, mainly ilmenites, are scattered through the rocks. Three foliations have been observed; the pervasive syn-kinematic foliation (S2) is related to the second deformation phase (D2). The presence of microlithons in the S2 foliation and of inclusion trails in garnet blasts are interpreted as an earlier S1 foliation (D1). The weakly pervasive chlorite and white mica-bearing foliation (S3), that wraps the post-kinematic garnet (Grt II), is related to M3 during D3. The M2 P–T conditions were derived using the Grt–Bt and Grt–Phe thermometers. Temperature ranges from 500 to 650 °C. The presence of kyanite in the assemblage indicates $P > 4$ kbar (Table 2, samples 220/92, 121/92 and 254/92).

The Shontar unit. The Shontar unit is also characterized by the presence of widespread garnet, biotite, white mica, staurolite and kyanite. These form an M2 amphibolite-facies assemblage. Effects of M1 are poorly preserved due to the pervasive nature of M2. In the metabasic rocks, eclogite relicts similar to those in the NE part of the Kalapani unit are preserved.

In the garnet–white mica–biotite–staurolite–kyanite-bearing micaschists, P–T conditions have been derived using the Grt–Bt thermometer and the Grt–Pla–Bt–Qtz and the Grt–Pla–Bt–Ms barometers. The derived M2 P–T conditions are 575–600 °C at 8–12 kbar (Table 2). P–T conditions for M3 at 440 °C and 5.5 kbar have been derived from fluid inclusion thermometry using corundum from Nangi Mali mine (Loprete 1995; Fontan 1998). The presence of late chlorite blasts on amphibole and biotite and the reaction of ilmenite to sphene document M4 re-equilibration at greenschist facies conditions.

In the Chattewala area in the SW part of the Shontar unit, garnet–sillimanite–biotite–muscovite–quartz-bearing assemblages form the M2 assemblage. The foliation is composed of discontinuous biotite flakes separating millimetric quartz-rich layers (Fig. 6f). Characteristic right-angled blasts, totally replaced by a random overgrowth of fine-grained prismatic sillimanite, are interpreted as older kyanite blasts and document a retrograde path.

In metabasic rocks, garnet–plagioclase–amphibole–biotite-bearing assemblages (sample 146/93) are interpreted as high-pressure granulites formed during M1. P–T conditions derived using the Grt–Pla–Bt–Qtz thermometer and the Grt–Hbl barometer are at 650–750 °C and 10–15 kbar (Table 2). M2 was at sillimanite-bearing medium-grade conditions. The P–T conditions are calculated using garnet–pyroxene–amphibole-bearing metabasic rock (sample 154/93) and plagioclase–pyroxene-bearing metapsammites (sample 101/91). Temperatures of 710 ± 50 °C are calculated using the Pla–Hbl, and Grt–Bt thermometers on sample 154/93 and the Grt–Cpx thermometer on sample 101/91 (Table 2). In these samples the derived pressure values are geologically inconsistent; therefore, the presence of fibrolitic sillimanite and the absence of potassic feldspar and cordierite constrains pressure to 5–10 kbar (Fig. 8).

^{40}Ar–^{39}Ar geochronology

Twenty ^{40}Ar–^{39}Ar radiometric age determinations on muscovite, biotite, phlogopite and amphibole were performed in the Isotope Laboratory at the University of Lausanne. Muscovites, biotite, amphiboles and phlogopites were analysed from the LHC (Salkhala unit) and the HHC (Kalapani and Shontar units), as well as from mylonites of the MCT and the Jamgarh Shear Zone (JSZ). All the analysed minerals were fresh: biotites and muscovites show no signs of retrogression to chlorite, and amphiboles do not show epitaxial growth of biotite and chlorite. The data permit the determination of geological ages which, coupled with the geothermobarometric results and with bibliographic data, allow the definition of P–T–t paths for the Neelum valley tectonic units. The ^{40}Ar–^{39}Ar data are presented in Fig. 9a, b.

The ^{40}Ar–^{39}Ar ages obtained on the muscovites, biotites and phlogopites can be interpreted as cooling ages and date the retrograde M3, greenschist facies metamorphic event in the Kalapani and Shontar units. Only the hornblende age from sample 297 can be interpreted as a metamorphic age which dates the prograde M3 greenschist facies metamorphism in the Salkhala unit.

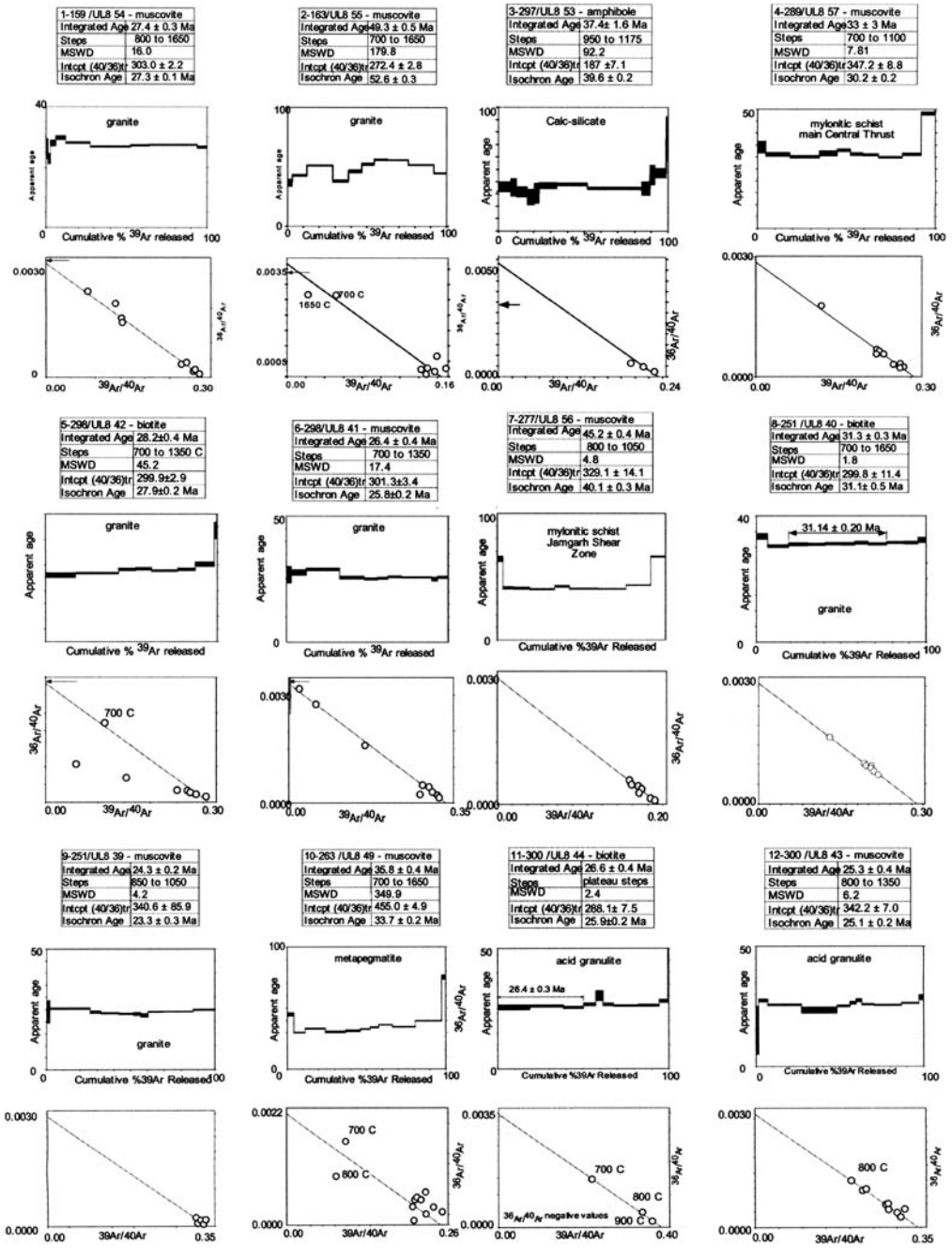
1-159 /UL8 54 - muscovite
Integrated Age 27.4 ± 0.3 Ma
Steps 800 to 1650
MSWD 16.0
Intcpt (40/36)tr 303.0 ± 2.2
Isochron Age 27.3 ± 0.1 Ma
granite
Cumulative % 39Ar released
2-163/UL8 55 - muscovite
Integrated Age 49.3 ± 0.5 Ma
Steps 700 to 1650
MSWD 179.8
Intcpt (40/36)tr 272.4 ± 2.8
Isochron Age 52.6 ± 0.3
granite
700 C
1650 C
3-297/UL8 53 - amphibole
Integrated Age 37.4± 1.6 Ma
Steps 950 to 1175
MSWD 92.2
Intcpt (40/36)tr 187 ±7.1
Isochron Age 39.6 ± 0.2
Calc-silicate
4-289/UL8 57 - muscovite
Integrated Age 33 ± 3 Ma
Steps 700 to 1100
MSWD 7.81
Intcpt (40/36)tr 347.2 ± 8.8
Isochron Age 30.2 ± 0.2
mylonitic schist
main Central Thrust
6-296/UL8 42 - biotite
Integrated Age 28.2±0.4 Ma
Steps 700 to 1350 C
MSWD 45.2
Intcpt (40/36)tr 299.9±2.9
Isochron Age 27.9±0.2 Ma
granite
700 C
6-298/UL8 41 - muscovite
Integrated Age 26.4 ± 0.4 Ma
Steps 700 to 1350
MSWD 17.4
Intcpt (40/36)tr 301.3±3.4
Isochron Age 25.8±0.2 Ma
granite
7-277/UL8 56 - muscovite
Integrated Age 45.2 ± 0.4 Ma
Steps 800 to 1050
MSWD 4.8
Intcpt (40/36)tr 329.1 ± 14.1
Isochron Age 40.1 ± 0.3 Ma
mylonitic schist
Jamgarh Shear
Zone
8-251 /UL8 40 - biotite
Integrated Age 31.3 ± 0.3 Ma
Steps 700 to 1650
MSWD 1.8
Intcpt (40/36)tr 299.8 ± 11.4
Isochron Age 31.1± 0.5 Ma
31.14 ± 0.20 Ma
granite
9-251/UL8 39 - muscovite
Integrated Age 24.3 ± 0.2 Ma
Steps 850 to 1050
MSWD 4.2
Intcpt (40/36)tr 340.6 ± 85.9
Isochron Age 23.3 ± 0.3 Ma
granite
10-263 /UL8 49 - muscovite
Integrated Age 35.8 ± 0.4 Ma
Steps 700 to 1650
MSWD 349.9
Intcpt (40/36)tr 455.0 ± 4.9
Isochron Age 33.7 ± 0.2 Ma
metapegmatite
700 C
800 C
11-300 /UL8 44 - biotite
Integrated Age 26.6 ± 0.4 Ma
Steps plateau steps
MSWD 2.4
Intcpt (40/36)tr 288.1± 7.5
Isochron Age 25.9±0.2 Ma
acid granulite
26.4 ± 0.3 Ma
700 C
800 C
900 C
36Ar/40Ar negative values
12-300 /UL8 43 - muscovite
Integrated Age 25.3 ± 0.4 Ma
Steps 800 to 1350
MSWD 6.2
Intcpt (40/36)tr 342.2 ± 7.0
Isochron Age 25.1 ± 0.2 Ma
acid granulite
800 C
Apparent age
Cumulative %39Ar Released
39Ar/40Ar
36Ar/40Ar

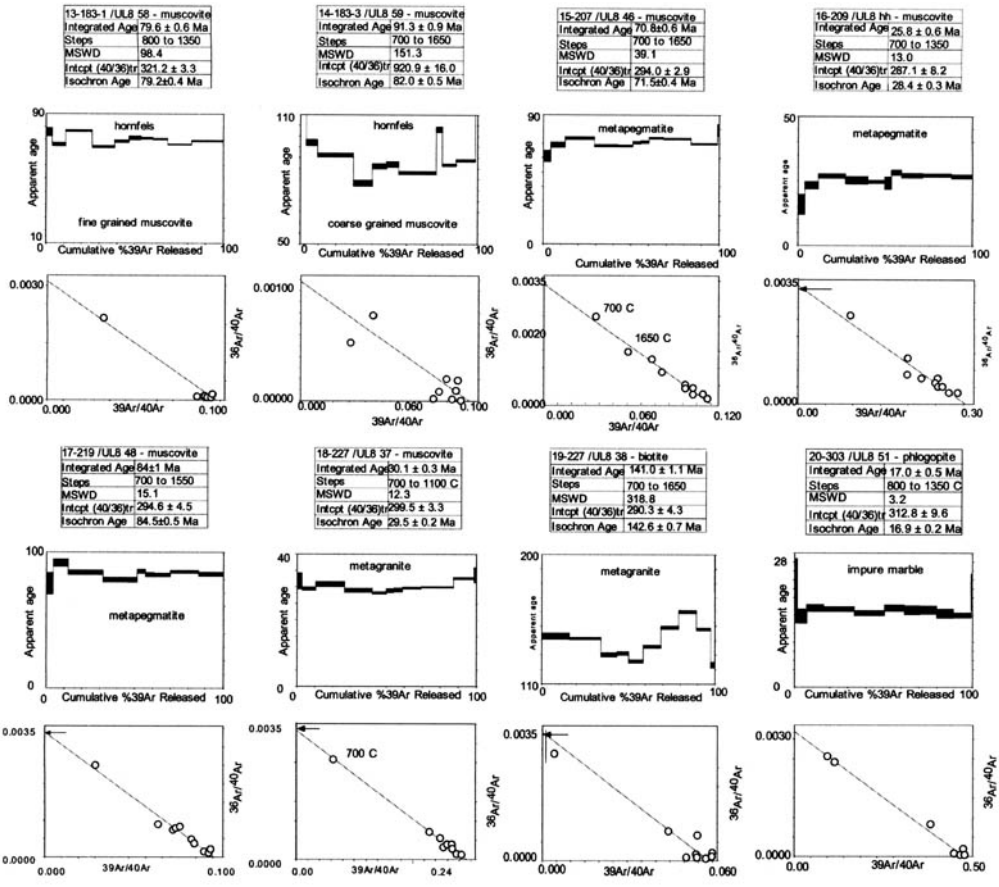

Fig. 9. (b) Ar–Ar diagrams (13–20).

Apparent Upper Cretaceous ages

Large magmatic muscovites in meta-pegmatites (207, 219), and metamorphic muscovites in a hornfels (183) from the SW Kalapani unit give early to upper Cretaceous ages (84–70 Ma). In Pakistan, upper Cretaceous ages have previously been recorded from Indian plate rocks of the HHC (Treloar & Rex 1990a; Tonarini *et al.* 1993). In the Kaghan valley, Tonarini *et al.* (1993) considered Cretaceous K/Ar and Ar–Ar ages to be '... statistically acceptable but geologically meaningless ...' and rejected them as they were probably indicative of excess argon. However, these ages could also be interpreted as dating metamorphism related to subduction processes that occurred prior to the high-pressure eclogite facies metamorphism (Smith *et al.* 1994) or to a thermal event, probably caused by crustal shortening, that occurred prior to collision. All of the muscovites analysed here with Cretaceous ages have irregular spectra which we interpret as being the result of excess Ar. Hence, in accord with Tonarini *et al.* (1993), we favour the interpretation that the upper Cretaceous ages are probably the result of argon loss or excess argon phenomena and hence are geologically meaningless.

Eocene ages

Muscovites from the Mansehra Granite, where it outcrops in the Salkhala unit (sample 163), yield an age of *c.* 52 Ma, although the spectrum has a clear saddle shape indicative of excess Ar and this age must therefore be ignored. Late Eocene ages of *c.* 40 Ma are reported here for an amphibole from a calc-silicate rock (sample 297; 39.6 ± 0.2 Ma) from the MCT Zone and for muscovites from a mylonitic schist (sample 277: 40.1 ± 0.3). The muscovite has a very broad U-shaped spectrum, which may be indicative of excess Ar, and hence this age must be treated with caution. The amphibole age is similar to

those described by Treloar & Rex (1990*a*, *b*) from the Hazara region. As maximum temperatures for the MCT Zone during the M3 metamorphic peak were at 500–600 °C, which is close to the closure temperature for hornblende, the amphibole age of 40 Ma either closely dates the peak metamorphism or an early stage of post-metamorphic cooling. Eocene ages which date the peak metamorphism for the HHC have been documented from eclogites (Tonarini *et al.* 1993) and granites (Smith *et al.* 1994) from the Kaghan valley. Tonarini *et al.* (1993) and Spencer *et al.* (1995) used a variety of techniques that yielded consistent age data: 49 ± 6 Ma on garnet–clinopyroxene Sm/Nd, 43 ± 1 Ma phengite Rb/Sr, and 39–40 Ma rutile U/Pb. Similar ages were documented by Smith *et al.* (1994): 47 ± 3 zircon U/Pb and *c.* 41 Ma hornblende Ar/Ar; and by Spencer & Gebauer (1996): 44 Ma, SHRIMP on zircons. These ages probably date eclogite facies metamorphism. No Ar–Ar age determinations are available for the Neelum valley HHC eclogites, although it is likely that their metamorphism was synchronous with the high-pressure metamorphism in the Kaghan valley (Fontan 1998; Lombardo *et al.* 2000).

Oligocene ages

Oligocene ages of 25–38 Ma are interpreted as cooling ages. They are characteristic of the Salkhala unit, where they date the retrograde M4 event, and Shontar and Kalapani units where they date the M3 Tertiary metamorphic phase. Oligocene ages are common in the surrounding regions as reported in the bibliography, and are generally related to post-metamorphic cooling through medium- to low-grade metamorphic conditions (Zeitler 1985; Treloar *et al.* 1989; Zeitler *et al.* 1989; Treloar & Rex 1990*a*, *b*; Chamberlain *et al.* 1991; Spring *et al.* 1993; Tonarini *et al.* 1993).

In the Neelum valley, amphiboles (sample 297/93) and muscovites (sample 289/93) from the MCT Zone give ages of 40 Ma and 29–32 Ma respectively. These ages are interpreted as dating cooling after the metamorphic peak. A number of muscovites (samples 209, 227, 251, 289, 298 and 300) give ages of between 23 and 30 Ma. Biotite ages, although similar, are often older than muscovites from the same sample, and this is taken to indicate that the biotite ages are affected by excess argon.

Miocene ages

Phlogopite from a marble in the Shontar unit (sample 303) gives a mid-Miocene age (about 17 Ma) that is interpreted as dating the Tertiary M3 metamorphic phase. Even if there is some argon loss, as in other biotites, this age may be significant as it is younger than those from other tectonic units.

Pressure–temperature–time paths

The metamorphic history outlined above, coupled with the Ar–Ar age data, allow the identification of two regions with different *P–T–t* histories (Fig. 8). The metamorphic evolution of the LHC (Salkhala unit) shows prograde phases during M1 to M3, followed by re-equilibration during M4 at lower grade conditions. The amphibole age from sample 297 probably dates the peak metamorphism. This is earlier than the peak metamorphism in the HHC. In the NE part of the Kalapani unit, blueschist relics in the metapelites and eclogite relics in the metabasic rocks both date from the high pressure period dated as mid-Eocene by Tonarini *et al.* (1993) and Spencer & Gebauer (1996). In the Kalapani and Shontar units of the HHC, retrogression was along a path of isothermal decompression from M1 eclogite facies conditions, through high-pressure amphibolite facies conditions during M2 to M3 and M4 greenschist facies conditions. The muscovite data date cooling of rocks of the Kalapani unit exposed between the MCT and the Gumot Shear Zone during M3 and M4 through *c.* 350 °C during the Oligocene.

Tectonic model and conclusion

Any tectonic model for the Neelum valley should account for: (1) the contemporaneity of the retrograde metamorphic paths in the HHC and the prograde metamorphism in the LHC; (2) thrust planes becoming younger towards the SW and that metamorphic grade of the shear surfaces decrease towards the SW; (3) metamorphic grade increases towards the NE from anchizone to sillimanite and kyanite, almandine amphibolite facies from the lowermost to the uppermost tectonic unit.

The tectonic models of Chemenda *et al.* (1995) and Malaveille (1997) can be adapted to account for the metamorphic and structural development of the Neelum valley (Fig. 10). Subduction of the Tethyan oceanic crust ultimately led to collision between the Indian and Asian continental plates. Along the Asian margin, subduction resulted in the formation of the Kohistan–Ladakh island arc. The Kohistan Sequence developed in two main stages separated by suturing to the Asian plate along the Shyok Suture in the mid-Cretaceous (Coward *et al.* 1986). The first, from

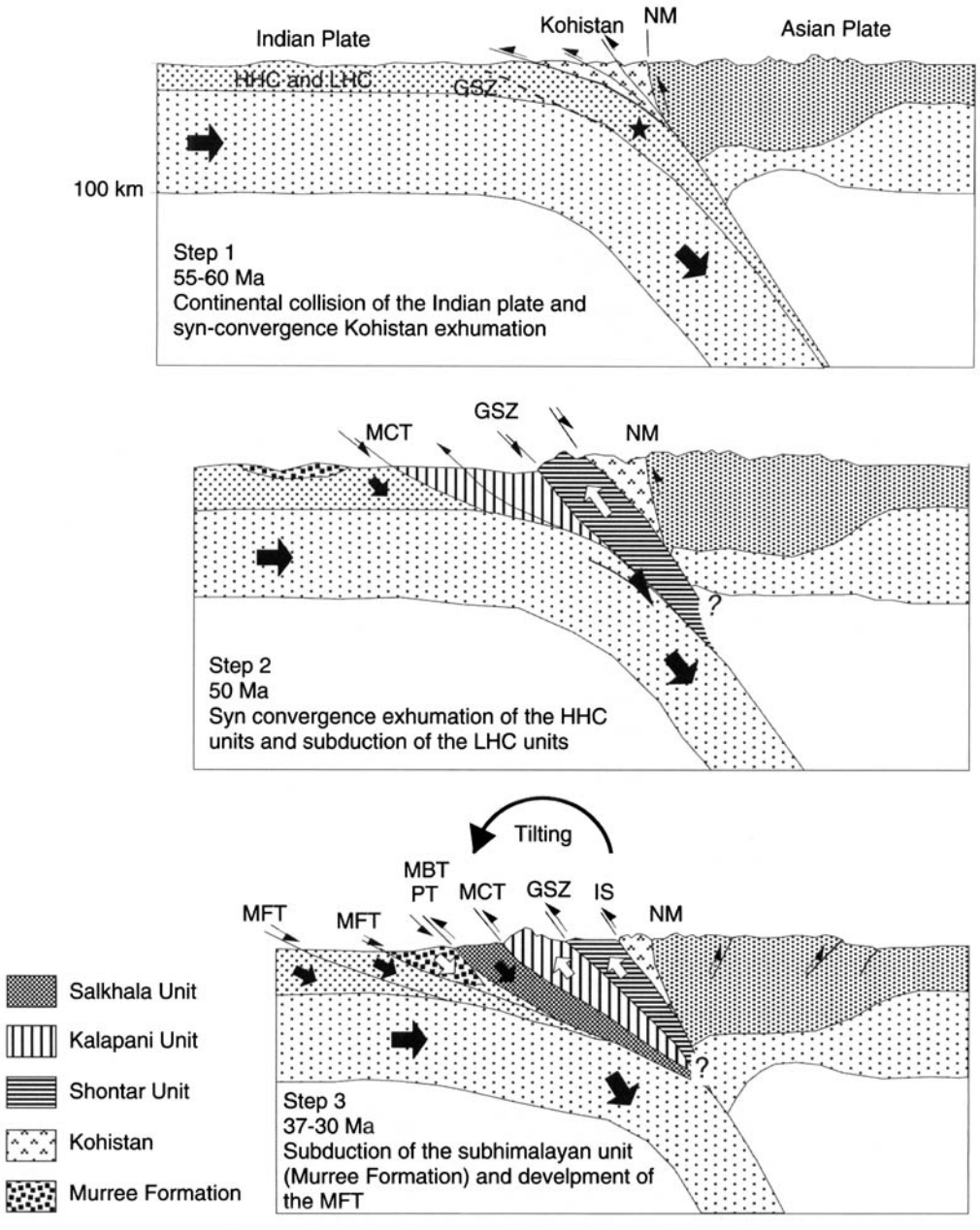

Fig. 10. Schematic tectonic evolution of the mapped area. (**a**) 55–60 Ma: start of the continental collision of the Indian plate and syn-convergence exhumation of the Kohistan arc (overthrusting). (**b**) 50 Ma: metamorphic peak in the Shontar and Kalapani units (Higher Himalayan Crystallines) and starting of the syn-convergence exhumation testified by retrograde *P–T* paths. In the Lesser Himalayan Crystallines a new syn-convergent subduction zone develops along the future Main Central Thrust (MCT). (**c**) At about 36–37 Ma: metamorphic prograde peak of the Salkhala unit (LHC) and start of the exhumation in the Lesser Himalayan Crystallines. In the southern part the subduction of the Subhimalaya element (intra-continental evolution) starts along the Main Boundary Thrust (MBT) and Panjal Thrusts (PT). NM: Northern Megashear; IS: Indus Suture Zone; GSZ: Gumot Shear Zone; MCT: Main Central Thrust; PT: Panjal Thrusts; MBT: Main Central Thrust; MFT: Main Frontal Thrust.

late Jurassic to mid-Cretaceous, was as an intra-oceanic island arc. The second, from late Cretaceous to Eocene, was as an Andean-type volcanic arc. As a result of early Tertiary collision, the arc was thrust south along the Main Mantle Thrust (MMT), onto the north margin of the Indian continent (Maluski & Matte 1984; Searle 1986) (Fig. 10, step 2). This thrusting occurred after blueschist facies metamorphism in the subduction zone (Desio & Shams 1980; Maluski & Schaeffer 1982; Maluski & Matte 1984; Honegger *et al.* 1989). Timing of collision is best dated using the depositional age of the Murree Formation, which contains large clastic wedges deposited in collisional basins formed during early stages of the orogeny (Bossart & Ottiger 1989; Garzanti *et al.* 1996). In the Neelum valley, the Palaeocene to mid-Eocene ages of the Murree Fm. (Ottiger 1986) indicate that collision probably started in the early Palaeocene. Eclogite facies metamorphism in the HHC occurred between 50 and 45 (Tonarini *et al.* 1993; Spencer & Gebauer 1996) during subduction of continental India beneath Kohistan. Rapid syn-convergent exhumation of the high pressure rocks, probably largely a function of buoyancy (Malaveille 1997), caused uplift of the subducted continental crust coupled with a flattening of shear zone dips (Fig. 10, step 2).

The GSZ and MCT were probably initiated after high-pressure metamorphism when syn-convergent exhumation of the Shontar and Kalapani units commenced. Metamorphism of the HHC commenced during underthrusting along the MCT. Peak metamorphism in the MCT Zone and the LHC at *c.* 40 Ma was after that of the HHC. The GSZ and MCT thrusts probably divide the continental slab into different units with different uplift rates. The HHC, with a higher pressure and earlier metamorphic peak, probably had a higher uplift rate during the Eocene and early Oligocene than the LHC. Initial movements along these thrusts can be inferred as being post-mid Eocene for the GSZ and Eocene/Oligocene for the MCT. The last movements along these thrusts must be later than the medium-grade metamorphic event and are probably Oligo-Miocene in age. They cut the isograds and divide the HHC and the LHC units of different metamorphic grades. Although mylonitic surfaces cut the D2 structures they are deformed by D3 crenulation cleavages.

Continuing subduction of the lithosphere (intra-continental evolution—Fig. 10, step 3) induced a third continental subduction zone within the Indian continental margin. According to Greco (1989) these movements may have taken place after the early to middle Miocene. This event probably initiated underthrusting of the Subhimalayan unit (Murree Formation) along the Panjal Thrust and then the Main Boundary Thrust. This thrusting would have further accommodated exhumation of the crystalline sequences.

This work was carried out under EC Contract no. CI1–0571–M (GDF). Thanks are due to Bruno Lombardo for useful discussions on Himalayan geology and to Peter Treloar for critical review. Thanks are due also to Azad Kashmir Mineral and Industrial Development Corporation, and especially to its director, Hussein Malik, and his team for logistic support and continuous encouragement.

References

BAIG, M. S. 1990. *Structure and geochronology of pre-himalayan and himalayan orogenic events in the northwest Himalaya, Pakistan, with special reference to the Besham area.* PhD thesis, Oregon State University.

—— & LAWRENCE, R. D. 1987. Precambrian to early Paleozoic orogenesis in the Himalaya. *Kashmir Journal of Geology*, **5**, 1–22.

BERMANN, R. G. 1990. Mixing properties of Ca-Mg-Fe-Mn garnets. *American Mineralogist*, **75**, 328–344.

BOHLEN, S. T., WALL, W. T. & BOETTCHER, A. L. 1983. Experimental investigation and geological application of equilibria in the system FeO–TiO_2–Al_2O_3–SiO_2–H_2O. *American Mineralogist*, **68**, 1049–1058.

BOSSART, P., & OTTIGER, R. 1989. Rocks of the Murree formation: indicators of a descending foreland basin of late Paleocene to middle Eocene age? *Eclogae Geologicae Helvetiae*, **82**, 133–165.

——, DIETRICH, D., GRECO, A., OTTIGER, R. & RAMSAY, J. G. 1984. A new structural interpretation of the Hazara-Kashmir Syntaxis, Southern Himalaya, Pakistan. *Kashmir Journal of Geology*, **2**, 19–36.

CALKINS, J. A., OFFIELD, T. W., ABDULLAH, S. K. M. & TAYYAB ALI, S. 1975. *Geology of the Southern Himalaya in Hazara, Pakistan, and adjacent areas.* USGS Prof. Paper, **716C**.

CHAMBERLAIN, C. P., JAN, M. Q. & ERIKSON, E. 1991. Constraints of the tectonic evolution of the northwestern Himalaya from geochronologic and petrologic studies of Babusar Pass, Pakistan. *Journal of Geology*, **99**, 829–849.

CHEMENDA, A. I., MATTAUER, M., MALAVIEILLE, J. & BOKUN, A. N. 1995. Evolution of Geologic structures in Micro- to Macro-Scales. *Earth and Planetary Science Letters*, **132**, 225–232.

COLEMANN, R. G., LEE, D. E., BEATTY, L. B. & BRANNOCK, W. W. 1965. Eclogites and eclogites: their differences and similarities. *Geological Society of America Bulletin*, **76**, 438–508.

COLOPIETRO, M. R. & FRIBERG, L. M. 1987. Tourmaline–biotite as a potential geothermometer for metapelites, Black Hills, South Dakota. *Geological*

Society of America, Abstract with Programs, **19**, 624.

COWARD, M. P., WINDLEY, B. F., BROUGHTON, R. D., LUFF, I. W., PETTERSON, M. G. *et al.* 1986. Collision Tectonics in the NW Himalayas. *In*: COWARD, M. P. & RIES, A. C. (eds) *Collision Tectonics*. Geological Society, London, Special Publications, **19**, 203–219.

DESIO, A. & SHAMS, F. A. 1980. The age of the blueschists and the Indus–Kohistan suture Line, NW Pakistan. *Rendiconti Accadademia Nazionale dei Lincei*, **68**, 74–79.

DIPIETRO, J. A., POGUE, K. R., LAWRENCE, R. D., BAIG, M. S., HUSSAIN, A. & AHMAD, I. 1993. Stratigraphy south of the Main Mantle Thrust, lower Swat, Pakistan. *In*: TRELOAR, P. J. & SEARLE, M. (eds) *Himalayan Tectonics*. Geological Society, London, Special Publications, **74**, 207–220.

ELLIS, D. J. & GREEN, D. H. 1979. An experimental study of the effect of Ca upon garnet–clinopyroxene Fe–Mg exchange equilibria. *Contributions to Mineralogy and Petrology*, **71**, 13–22.

ESSENE, E. J. & FYFE, W. S. 1967. Omphacite in Californian Metamorphic Rocks. *Contributions to Mineralogy and Petrology*, **15**, 1–23.

FERRY, J. M. & SPEAR, F. S. 1978. Experimental calibration of the partitioning of Fe and Mg between biotite and garnet. *Contributions to Mineralogy and Petrology*, **66**, 113–117.

FONTAN, D. 1998. *Regional geological mapping, metamorphic P–T–t paths evaluation and ore potential assessment in Neelum Valley (Azad Kashmir, NE Pakistan)*. PhD thesis, Université Catholique de Louvain-La-Neuve, Belgium.

FUCHS, G. 1985. The Tibetan (Tethys) Zone—is it Allochthonous? *In*: GUPTA, V. J. (ed.) *Contribution to Himalayan Geology*, **3**, 67–77.

GAETANI, M., CASNEDI, R., FOIS, E., GARZANTI, E., JADOUL, F., NICORA, A. & TINTORI, A. 1985. Stratigraphy on the Tethys Himalaya in Zanskar, Ladakh. Initial report. *Rivista italiana di Paleontologia Stratigrafica*, **91**, 443–478.

——, GARZANTI, E. & TINTORI, A. 1990. Permo-Carboniferous stratigraphy in SE Zanskar and NW Lahul (NW Himalaya, India). *Eclogae Geologicae Helvetiae*, **83**, 143–161.

GANGULY, J. & SAXENA, S. K. 1984. Mixing properties of alumosilicates garnets: constraint from natural and experimental data, and application to geothermobarometry. *Journal of Metamorphic Geology*, **69**, 710–714.

GARZANTI, E., CRITELLI, S. & INGERSOLL, R. V. 1996. Paleogeographic and paleotectonic evolution of the Himalayan Range as reflected by detrital modes of Tertiary sandstones and modern sands (Indus transect, India and Pakistan). *Geological Society of America Bulletin*, **108**, 631–642.

GHAZANFAR, M. & CHAUDHRY, M. N. 1984. A Palaeozoic ophiolite and island arc sequence of Hazara-Kashmir Syntaxis, District Manshera. *Kashmir Journal of Geology*, **2**, 37–38.

—— & —— 1986. Reporting M.C.T. in Northwest Himalaya. *Geological Bulletin of the University of Punjab*, **21**, 10–18.

——, BAIG, M. S., CHAUDHRY, M. N. 1983. Geology of Tithwal Kel area Neelum Valley, Azad Jammu and Kashmir. *Kashmir Journal of Geology*, **1**, 1–10.

GOURIRANE, A. 1993. *Etude petrologique et geothermobarometrique des eclogites de la haute-valleé du Neelum (Himalaya, Pakistan)*. Faculté des Science, Laboratoire de Géologie et minéralogie, UCL, Louvan-La-Neuve (Belgium).

GRAHAM, C. M. & POWELL, R. 1984. A garnet–hornblende geothermometer: calibration, testing, and application to the Pelona Schist, Southern California. *Journal of Metamorphic Geology*, **2**, 13–21.

GRECO, A. 1989. *Tectonics and Metamorphism in the Western Himalaya Syntaxis area (Azad Kashmir, NE Pakistan)*, Dissertation ETH-Zürich, Nr. 8779.

—— & SPENCER, D. A. 1993. A section through the Indian Plate, Kaghan Valley, NW Himalaya, Pakistan. *In:* TRELOAR, P. J. & SEARLE, M. P. (eds) *Himalayan Tectonics*. Geological Society, London, Special Publications, **74**, 221–236.

——, MARTINOTTI, G., PAPRITZ, K., RAMSAY, J. G. & REY, R. 1989. The crystalline rocks of the Kaghan Valley (NE-Pakistan). *Eclogae Geologicae Helvetiae*, **82**, 629–653.

HODGES, K. V. & CROWLEY, P. 1985. Error estimation and empirical geothermobarometry for pelitic systems. *American Mineralogist*, **70**, 702–709.

—— & SPEAR, F. S. 1982. Geothermometry, geobarometry and the Al_2SiO_4 triple point at Mt. Moosilauke, New Hampshire. *American Mineralogist*, **67**, 1118–1134.

HOISH, T. D. 1990. Empirical calibration of six geobarometers for the mineral assemblage quartz + muscovite + biotite + plagioclase + garnet. *Contributions to Mineralogy and Petrology*, **104**, 225–234.

HOLDAWAY, M. J., DUTROW, B. L. & HINTON, R. W. 1988. Devonian and Carboniferous metamorphism in west-central Maine: The muscovite–almandine geobarometer and the staurolite problem revisited. *American Mineralogist*, **73**, 20–47.

HOLLAND, T. J. B. 1980. The reaction albite = jadeite + quartz determined experimentally in the range 600–1200 °C. *American Mineralogist*, **65**, 129–134.

—— 1983. The experimental determination of activities in disordered and short-range ordered jadeitic pyroxenes. *Contributions to Mineralogy and Petrology*, **82**, 214–220.

—— & BLUNDY, J. 1994. Non-ideal interactions in calcic amphiboles and their bearing on amphibole-plagioclase thermometry. *Contributions to Mineralogy and Petrology*, **116**, 433–447.

HONEGGER, K., DIETRICH, V., FRANK, W., GANSSER, A., THÖNI, M., TROMMSDORFF, V. 1982. Magmatism and metamorphism in the Ladakh Himalayas (The Indus—Tsangpo Suture Zone). *Earth and Planetary Science Letters*, **60**, 253–292.

——, LE FORT, P., MASCLE, G., ZIMMERMAN, J. L. 1989. The blueschists along the Indus Suture

Zone in Ladakh, NW Himalaya. *Journal of Metamorphic Geology*, **7**, 57–72.

HYNES, A. & FORREST, R. C. 1988. Empirical garnet–muscovite geothermometry in low-grade metapelites (Selwyn Range Canadian Rockies). *Journal of Metamorphic Geology*, **6**, 297–309.

KERVYN, F. 1993. *Etude du contexte tecto-métamorphique d'une mine de rubis situé dans le Muzaffarabad District en Azad kashmir*. MSc thesis, Faculté des Science, Laboratoire de Géologie et Minéralogie, UCL, Louvain-La-Neuve, Belgium.

KOZIOL, A. M. 1989. Recalibration of garnet–plagioclase–Al_2SiO_5–quartz (GASP) geobarometer and application to natural parageneses. *EOS*, **70**, 493.

LE FORT, P., DEBON, F. & SONET, J. 1980. The 'Lesser Himalayan' Cordierite Granite Belt. Typology and Age of the Pluton of Mansehra (Pakistan). *Geological Bulletin, University of Peshawar* (Special Issue), **3**, 51–61.

LOMBARDO, B., ROLFO, F. & COMPAGNONI, R. 2000. Glaucophane and barroisite eclogites from the Upper Kaghan nappe: implications for the metamorphic history of NW Himalaya. *This volume*.

LOPRETE, E. 1995. *Studio geochimico e microtermometrico delle inclusioni fluide, in marmi e rubini del Surgun Group (Himalaya, Pakistan nord-orientale)*. MS Thesis Dipartimento di mineralogia e petrografia, Facoltà di Scienze M.F.N., Torino.

MALAVIEILLE, J. 1997. Normal faulting and exhumation of metamorphic rocks in mountain belts. *In*: SENGUPTA, S. (ed.) *Evolution of geological structures in Micro to Macro Scales*. Special volume in honour of Prs Subir Kumar Ghosh and Ksitin Naha. Chapman & Hall, London.

—— & CHEMENDA, A. I. 1997. Impact of initial geodynamic setting on structure, ophiolite emplacement and tectonic evolution of collisional belts. *Ofioliti*, **22**, 3–13.

MALUSKI, J. & MATTE, P. 1984. Ages of alpine tectonometamorphic events in the northwestern Himalaya (northern Pakistan) by ^{39}Ar–^{40}Ar method. *Tectonics*, **3**, 1–18.

—— & SCHAEFFER, O. 1982. A ^{39}Ar–^{40}Ar laser probe dating of terrestrial rocks. *Earth and Planetary Science Letters*, **59**, 21–27.

NAKAZAWA, K. & KAPOOR, H. M. 1973. Spilitic pillow lava in Panjal Traps of Kashmir. *Memoir of the Faculty of Science, Kyoto University Series on Geology & Mineralogy*, **9**, 83–98.

NEWTON, R. C. & HESELTON, H. T. 1981. Thermodynamics of the garnet–plagioclase–Al_2SiO_5–quartz geobarometer. *In*: NEWTON, R. C., NAVROSKY, A. & WOOD, B. J. (eds) *Thermodynamics of Minerals and Melts*. Springer-Verlag, Berlin, 125–142.

OTTIGER, R. 1986. *Einge Aspekte der Geologie der Hazara–Kashmir Syntaxis (Pakistan)*. Diss. ETH Nr. 8083, Zürich.

PAPRITZ, K. & REY, R. 1989. Evidence for the occurrence of Panjal Trap Basalts in the Lesser- and Higher Himalaya of the Western Syntaxis area, NE Pakistan. *Eclogae Geologicae Helvetiae*, **82**, 603–627.

PATTINSON, D. R. M. & NEWTON, R. C. 1989. Reversed experimental calibration of the garnet-clinopyroxene Fe-Mg exchange thermometer. *Contribution to Mineralogy and Petrology*, **101**, 87–103.

PERCHUK, L. L., ARANOVICH, L. Y., PODLESKII, K. K., LAVRANT'EVA, I. V., GERASIMOV, V. Y. *et al.* 1985. Precambrian granulites of the Aldan sheld, eastern Siberia, URSS. *Journal of Metamorphic Geology*, **3**, 262–310.

POGNANTE, U. & LOMBARDO, B. 1989. Metamorphic evolution of the High Himalaya Crystallines in SE Zanskar, India. *Journal of Metamorphic Geology*, **7**, 9–17.

—— & SPENCER, D. A. 1991. First report of eclogites from the Himalaya belt, Kagan valley (northern Pakistan). *European Journal of Mineralogy*, **3**, 613–618.

POWELL, R. 1985. Regression diagnostics and robust regression in geothermometry and geobarometry: the garnet–clinopyroxene geothermometer revisited. *Journal of Metamorphic Geology*, **3**, 231–243.

REYNOLDS, P. H., BROOKFIELD, M. E. & MCNUTT, R. H. 1983. The age and nature of Mesozoic–Tertiary magmatism across the Indus Suture Zone in Kashmir and Ladakh (NW India and Pakistan). *Geologische Randschau*, **72**, 981–1004.

SCHOUPPE, M. 1995. *Geologié de la Valleé de la Neelum Azad Kashmir NO—Himalaya: cartographie geologique de terrain assisteé par la telédetection; lithostratigraphie et etude des roches orthoderivées; tectonique et modellisation de la deformation himalayenne*. PhD thesis, Faculté des Sciences, Laboratoire de Géologie et Minéralogie, UCL, Louvain-La-Neuve.

SEARLE, M. P. 1986. Structural evolution and sequence of thrusting in the High Himalayan, Tibetan—Tethys and Indus Suture zones of Zanskar and Ladakh, Western Himalaya. *Journal of Structural Geology*, **8**, 923–936.

SMITH, H. A., CHAMBERLAIN, C. P. & ZEITLER, P. K. 1994. Timing and duration of Himalaya metamorphism within the Indian Plate, Northwest Himalaya, Pakistan. *Journal of Geology*, **102**, 493–508.

SPEAR, F. S., PEACOCK, S. M., HOHN, M. J., FLORENCE, F. P. & MENARD, T. 1991. Computer programs for petrologic P–T–t path calculations. *American Mineralogist*, **76**, 2009–2012.

SPENCER, D. A. 1993. *Tectonics of the Higher- and Tethyan Himalaya, Upper Kaghan Valley, NW Himalaya, Pakistan: implication of an early collisional, high pressure (eclogite facies) metamorphism to the Himalaya belt*. PhD thesis, Swiss Federal Institute of Technology, Zurich.

—— & GEBAUER, D. 1996. *SHRIMP evidence for Permian protholit age and a 44 Ma metamorphic age from the Himalaya eclogites (Upper Kaghan, Pakistan): Implications for the subduction of Tethys and the subdivision terminology of the NW Himalaya*. Himalaya–Karakoram–Tibet Workshop Flagstaff, Arizona, USA, 147–150.

——, TONARINI, S. & POGNANTE, U. 1995. Geochemical and Sr–Nd isotopic characterisation of

Higher Himalaya eclogites and associated metabasites. *European Journal of Mineralogy*, **7**, 89–102.

SPRING, L., BUSSY, F., VANNAY, J. C., HUNON, S. & COSCA, M. A. 1993. Early Permian granitic dykes of alkaline affinity in the Indian High Himalaya of upper Lahul and SE Zanskar; geochemical characterization and geotectonic implications. *In*: TRELOAR, P. & SEARLE, M. P. (eds) *Himalayan Tectonics*. Geological Society, London, Special Publications, **74**, 251–264.

TAHIRKHELI, R. A. K. 1988. Presence of the Main Central Thrust in the tectonic domain of northwestern Himalaya in Pakistan. *Geological Bulletin, University of Peshawar*, **21**, 131–140.

—— 1992. Shontargali Thrust: the Main Central Thrust (MCT) of northwestern Himalaya, Pakistan. *In*: SINHA, A. K. (ed.) *Himalaya Orogen and Global Tectonics*, 107–120.

TONARINI, S., VILLA, I., OBERLI, F., MEYER, M., SPENCER, D. A., POGNANTE, U. & RAMSAY, J. G. 1993. Eocenic age of eclogite metamorphism in Pakistan Himalaya: implications for India–Eurasian collision. *Terra Nova*, **5**, 13–20.

TRELOAR, P. J. & REX, D. C. 1990*a*. Cooling, uplift and exhumation rates in the crystalline thrust stack of the North Indian Plate, west of the Nanga Parbat syntaxis. *Tectonophysics*, **180**, 323–349.

—— & —— 1990*b*. Cooling history of the crystalline thrust stack of the internal zones of the Pakistan Himalaya. *Journal of the Geological Society, London*, **147**, 735–738.

——, ——, GUISE, P. G., COWARD, M. P., SEARLE, M. P., WINDLEY, B. F. *et al.* 1989. K–Ar and Ar–Ar geochronology of the Himalaya collision in NW Pakistan: constraints on the timing of suturing, deformation and uplift. *Tectonics*, **8**, 881–909.

VANNAY, J. C. 1993. *Géologie des châines du haut-Himalaya et du Pir Panjal au Haut-Lahul (NW-Himalaya, Inde)*. Mémoires de Geologie (Lausanne), **16**.

—— & SPRING, L. 1993. Geochemistry of the continental basalts within the Tethyan Himalaya of Lahul-Spiti and SE Zanskar, Northwest India. *In:* TRELOAR, P. J. & SEARLE, M. P. (eds) *Himalayan Tectonics*. Geological Society, London, Special Publications, **74**, 237–249.

WADIA, D. N. 1931. The syntaxis of the North-West Himalaya: Its rocks, tectonics and orogeny. *Records Geological Survey of India*, **65**, 189–220.

—— 1934. The Cambrian–Trias sequence of North-Western Kashmir (parts of Muzaffarabad and Bramula District). *Records Geological Survey of India*, **68**, 121–176.

ZEITLER, P. K. 1985. Cooling history of the NW Himalaya, Pakistan. *Tectonics*, **4**, 127–151.

——, SUTTER, J. F., WILLIAMS, I. S., ZARTMAN, R. & TAHIRKHELI, R. A. K. 1989. Geochronology and temperature history of the Nanga Parbat–Haramosh Massif, Pakistan. *In:* MALINCONICO, L. L. & LILLIE, R. J. (eds) *Tectonics of the western Himalayas*. Geological Society of America, Special Paper, **232**, 1–22.

This page intentionally left blank

Exotic conglomerates of the Neogene Siwalik succession and their implications for the tectonic and topographic evolution of the Western Himalaya

I. A. ABBASI[1] & P. F. FRIEND[2]

[1]*Department of Geology, University of Peshawar, N.W.F.P. Pakistan*

[2]*Department of Earth Sciences, University of Cambridge, Downing St, Cambridge CB2 3EQ, UK (e-mail: pff1000@esc.cam.ac.uk)*

Abstract: Published information on the Siwalik Group (Neogene) conglomerates in the Sub-Himalayan belt of Himachal Pradesh, India, and the Potwar Plateau, Pakistan, is used as the basis of a model that recognizes two types of conglomerates with different relationships to the linear Himalayan mountain front. The two types are: (1) foothills-fed conglomerates, widespread along the mountain front, that mark the appearance in the basinal succession of sediments derived from within the Sub-Himalayan fold-and-thrust belt or the neighbouring Lower Himalaya; these Upper Siwalik conglomerates provide information about relatively young frontal fault activity and the growth of local river systems that transferred the sediment generated; and (2) high-mountain-fed conglomerates, with restricted lateral extent along the front, that mark the presence of large trunk rivers, draining the Lower and Higher zones of the Himalaya; these Middle and Upper Siwalik conglomerates provide information about the extent of older incision in the high mountains, and the position in the basin of the major drainage paths.

Our work on the Janak (formerly Indus) Conglomerate Formation, outcropping near the present Indus River, shows that it is a high-mountain-fed conglomerate, and was deposited by a large braided system (channels up to 15 m deep) that drained southwards from the High Himalaya of northernmost Pakistan. The conglomerate was deposited between 9 and 1 Ma, and is preserved as a formation 1.5 km thick and 25 km wide, perpendicular to flow. This conglomerate marks the position of the Palaeo-Indus in this part of the foreland basin. The syntaxial position of the present Indus in the mountain front, and the remarkable route of the upper Indus, have resulted from drainage evolution during the later stages of transpressive indentation of the western margin of the Indian block. Our interpretation of the Janak Conglomerate implies that this special role of the Indus must have already started by 9 Ma.

The name Siwalik Group has been given to the sediments that fill much of the Neogene basin that extends for more than 2000 km from Northern Pakistan across northern India, Nepal and into Burma. It was realized by geologists as early as Cautley (1840) that erosion of the ancestral Himalaya had provided much of the fill of this basin, which is now regarded as one of the classic examples of a 'peripheral basin' (Dickinson 1974), a foreland basin that formed as a result of tectonic and sedimentary loading along the front of a mountain belt. Work on the Siwalik Group has yielded Neogene terrestrial faunas of major palaeontological importance, an outstandingly clear palaeomagnetic reversal stratigraphy (synthesized by Burbank *et al.* 1996), and important understanding of fluvial sedimentology and palaeosols. Yet it has proved difficult to relate features visible in this remarkable basinal succession to specific features of the evolution of the geology and topography of the Greater Himalayan Mountain belt.

In this paper we draw attention to the significance of major conglomerates that are a general feature of the upper parts of the sedimentary successions that make up the Siwalik Group. We focus our attention on conglomerates that are exotic in the sense that their clasts are not intraformational (derived from the erosion of contemporaneous basinal sands or muds) but have come from outcrops marginal to, or outside, the basin. These exotic conglomerates

From: KHAN, M. A., TRELOAR, P. J., SEARLE, M. P. & JAN, M. Q. (eds) *Tectonics of the Nanga Parbat Syntaxis and the Western Himalaya*. Geological Society, London, Special Publications, **170**, 455–466. 1-86239-061-4/00/$15.00

provide distinctive markers in otherwise rather uniform successions of sandstone and mudstone.

Some early discussions of Siwalik basin evolution recognized that conglomerates were a special feature of the linear mountain-front outcrop zone of the group, although palaeocurrent and detailed provenance data were not then available. In the absence of such data, some early workers suggested incorrectly that a single major 'Indo-Brahm' or 'Siwalik' river (Pascoe 1919; Pilgrim 1919) had flowed westward along the line of the present Sub-Himalayan mountain front, depositing the gravels that became the conglomerates. Subsequent detailed study has shown that most of the sediment was transported southward from the mountains to the basin, and we begin by reviewing some of this detail. This work provides the basis of a model that relates the conglomerates to a tectonic and geomorphological pattern similar to that active along the mountain front today. After developing this model, we then briefly describe, for the first time, a conglomerate formation that has special interest, because it was deposited by the palaeo-Indus, and has implications for the evolution of the western Himalayan syntaxis.

Conglomerates of the Siwalik Group

The tectonic setting and general stratigraphy of the Siwalik Group has been reviewed recently by Burbank *et al.* (1996). We select two areas for our discussion of conglomerates in the sections that follow. Our discussion of the geology of the Himalayan belt uses the terminology of lithotectonic zones, first proposed by Gansser (1964), and summarized for the purposes of this discussion in Table 1, along with terminology of the bounding structures.

Himachal Pradesh Re-entrant (76–77° E), India

This section of the Sub-Himalayan belt contains the widest outcrop areas of the Siwalik Group in India (Areas 4 and 5 on Fig. 1). Raiverman *et al.* (1975*a*, *b*) distinguished three different conglomerate formations in a section measured in the Sarkaghat anticline (S, Fig. 1), placing the lowest of them in the Middle Siwalik, and the middle and upper ones in the Upper Siwalik. All contain clasts of Lower and Higher Himalayan provenance, with an increase in the proportion of Higher Himalayan material in the upper conglomerate. They concluded that the early conglomerate was the mature deposit of a well-defined river system, probably the palaeo-Beas, the ancestor of the present Beas River (Fig. 1), which is the main trunk river now draining the Himachal Pradesh Re-entrant. In contrast, the later conglomerates were immature deposits, transported by local river systems and influenced by active fold and thrust tectonics. A similar succession was reported by Meigs *et al.* (1995) from the Jawalmukhi area (J, Fig. 1) about 40 km from Raiverman's locality. They also recognized a distinctive Middle Siwalik conglomerate which they were able to date, on the basis of palaeomagnetic data, as forming between 8.7 and 7.2 Ma ago. They emphasized tectonic controls in interpreting this conglomerate as derived from the hanging wall of the Main Boundary Thrust (MBT), and deposited in a depression formed in the basin margin by thrust loading in the source area.

Kumar & Tandon (1985) provided a detailed sedimentological account of the classic Upper Siwalik succession exposed in the area of the Ghaggar River (area 5, G, on Fig. 1), 120 km south of the Sarkaghat anticline. Detailed logs,

Table 1. *Himalayan zones, arranged from south to north*

Terminology of Gansser (1964)	Description (bounding structures in brackets)
	{Salt Range, Himalayan Frontal or Main Frontal Thrust}
Sub Himalaya	Tertiary sediments, mainly clastic rocks (Siwaliks) in foreland basins, locally older Cenozoic and older formations along the range front.
	{Main Boundary Thrust, MBT}
Lower Himalaya	Precambrian metasediments; Palaeozoic and Mesozoic sediments (carbonates, arenaceous & argillaceous); granitic intrusions; volcanics
	{Main Central Thrust, MCT}
Higher Himalaya	granitic intrusions; volcanics, gneisses, complex schists, Palaeozoic and Mesozoic metasediments (Himalayan Detachment Zone)
Tibetan or Tethys Himalaya	Palaeozoic and Mesozoic shelf sediments, with volcanics
	{Northern, Main Himalayan, Indus or Tsangpo Suture, Main Mantle Thrust, MMT}

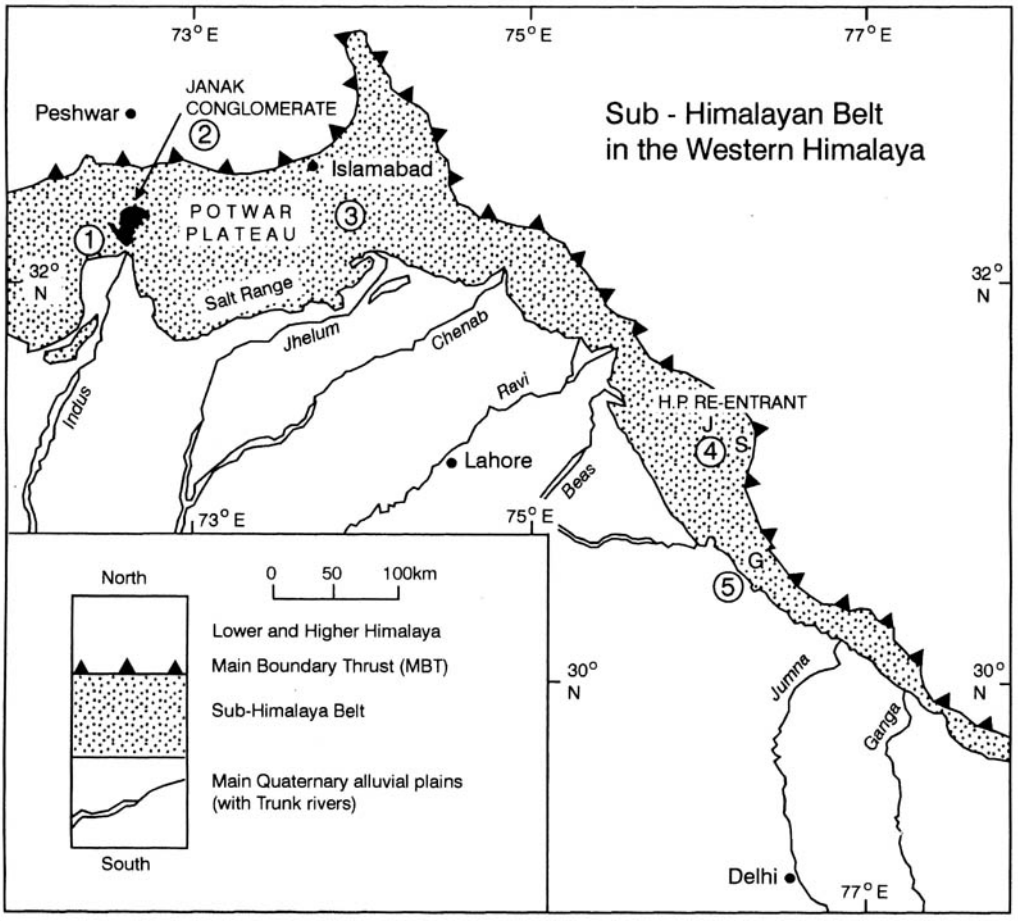

Fig. 1. Outline geological map of the Sub-Himalayan belt in the W Himalaya. The outcrops of the belt consist of Cenozoic strata including the Neogene Siwalik Group, with earlier strata in the Salt Range and further west. The circled numbers refer to columns on Fig. 2; at (4), H.P. Re-entrant refers to the Himachal Pradesh Re-entrant, and J and S mark the locations of Jawalmukhi and Sarkaghat, and at (5), G marks the Ghaggar River (see text). The outcrop of the Janak Conglomerate is shown.

lithofacies, cycle and sediment vector (palaeocurrent) data were interpreted in terms of anastomosing rivers, with very variable flow trends, followed by southerly prograding alluvial fans, forming the main conglomerate. Details of the provenance of the conglomerate clasts are not available.

Potwar Plateau (72.5–74.5° E), Pakistan

A sustained programme of structural, stratigraphical and palaeomagnetic work on the Siwalik Group of the Potwar Plateau, Pakistan, and nearby areas, has yielded a wealth of detailed information (reviewed by Burbank *et al.* 1996, but also see: Burbank & Raynolds 1984, 1988; Raynolds & Johnson, 1985; Johnson *et al.* 1986; Burbank *et al.* 1988). In the Jhelum River area of the Potwar (Figs 1, 2), the dating of the onset of Upper Siwalik conglomerate deposition was used to track the southerly build-out of a gravel bajada over a distance of more than 40 km over 2 Ma along the axis of a depression thought to have been created by tectonic loading. The gravel was taken to have been derived from the scarps of the MBT some 60 km upstream from the northernmost preserved conglomerate. In most Upper Siwalik conglomerates, the clasts match rock types available in the hanging walls of faults that were likely to have been active within, or bounding, the Sub-Himalayan fold-and-thrust belt and the appearance of conglomerates has

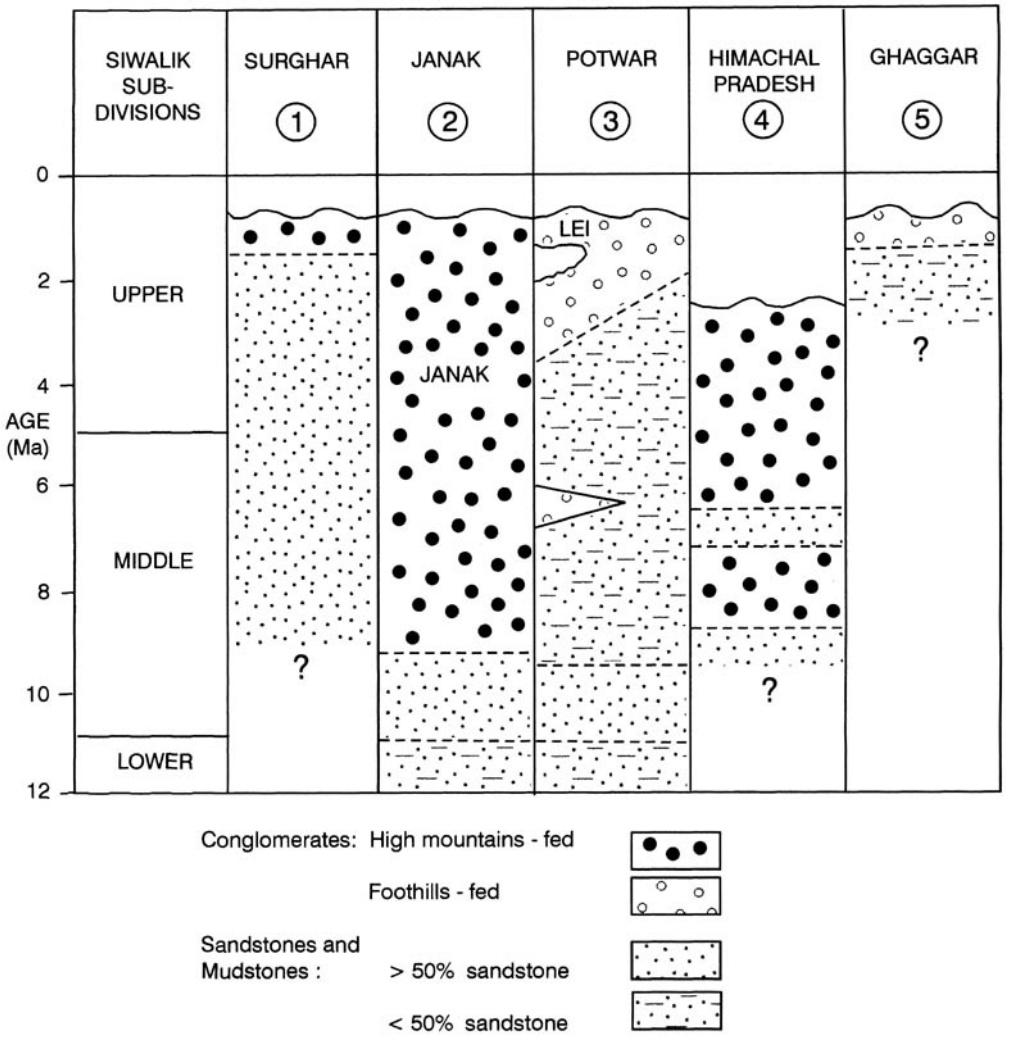

Fig. 2. Chronological distribution of some of the conglomerates in the Siwalik Group discussed in the text. Column numbers refer to locations marked on Fig. 1.

been attributed to southward movement into the basin of this outer zone of the orogen. Some studies have shown evidence for out-of-sequence patterns and very varied geometries. A large-scale example of this is the fault emergence of the Salt Range (Figs 1, 2), about 6.5 Ma (Burbank *et al.* 1996) which sent a wedge of locally derived conglomerate northwards into the northern Potwar Plateau.

Near the northeastern edge of the Potwar Plateau, the Lei Conglomerate (*c.* 1.8–1.6 Ma, Fig. 2) rests with perpendicular unconformity on a 6 km thick succession terminating with conglomerates dated at 2.1 Ma (Burbank *et al.* 1996). Vertical folding and large amounts of erosion, probably fault related, are remarkably closely constrained between two distinct episodes of conglomerate accumulation.

Model of conglomerate patterns along the Himalayan front

Having briefly outlined selected published information on occurrences of conglomerate in the Siwalik Group, we now suggest a general model (Fig. 3) that explains some of the varied features noted in terms of present-day drainage patterns, specifically those of the Indo-Gangetic plains (Sinha & Friend 1994), and the Himalayan mountains (Friend 1998). Our model

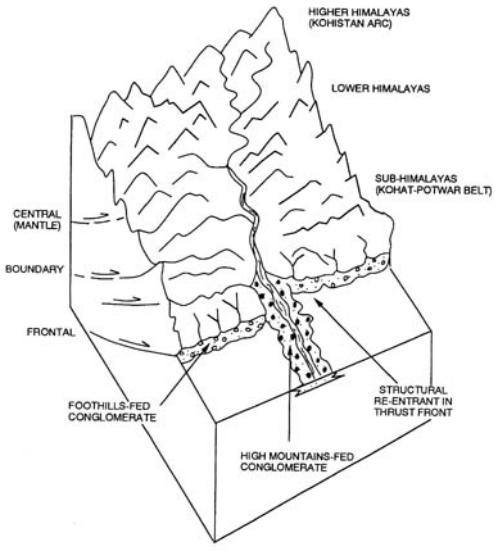

Fig. 3. Model displaying the difference in setting between conglomerates of the high-mountains-fed and foothills-fed types. Main lithotectonic subdivisions of bounding thrusts in the Himalaya are labelled using the scheme of Gansser (1964). Nomenclature commonly used in Northern Pakistan is shown in brackets.

distinguishes two distinct geomorphological and tectonic settings (Fig. 3) of the major conglomerates of the Siwalik Group.

Foothills-fed conglomerates

The Siwalik conglomerates of this type occur generally in the Upper Siwalik, and appear to have formed as prograding bajada deposited by relatively small rivers that were consequent in that they flowed directly from contemporaneous uplift features, often fault scarps, within the Lower Himalaya or Sub-Himalaya. In general tectonic terms, many of these controlling structures can be regarded as components of the hanging wall of the MBT. The conglomerates discussed above that outcrop in the northeastern Potwar and Pakistani Kashmir form good examples of this type, but so also are many of the Upper Siwalik conglomerates that form a stratigraphic feature at the top of the Siwalik succession along most of the Sub-Himalayan belt of Pakistan, India and Nepal.

This type of conglomerate appears to have been deposited by river systems equivalent to the present-day foothills-fed rivers (Sinha & Friend, 1994). The present-day rivers are consequent, i.e. a direct river flow response, to the uplift of the foothills or Sub-Himalaya, and their catchments lie within these hills.

High-mountains-fed conglomerates

The Siwalik conglomerates of this type are most distinctive where they occur in the Middle Siwalik. They were formed by very large gravel-bearing river systems, deriving material from the full range of Himalayan litho-tectonic zones, and having catchments, therefore, that penetrated across most of the orogen. They generally form distinct, thick successions limited laterally to extents of 10–20 km transverse to the general river direction. These high-mountains-fed conglomerates clearly mark the entry points into the alluvial basin of major rivers that were draining much of the width of their own sector of the complex mountain belt. In the case of the Himachal Pradesh early conglomerates, this distinctive deposit appears likely to have been formed by a trunk or main-arc river (Friend 1998), that can usefully be regarded as the ancestral or palaeo-Beas. This type of conglomerate appears to have been deposited by rivers similar to the present-day, mountain-fed rivers, distinguished by Sinha and Friend (1994) in eastern India. These rivers derive their water and sediment from most of the litho-tectonic zones of the high mountain-belt.

Janak Conglomerate Formation

General aspects of the formation

We now describe the Janak Conglomerate Formation which was earlier named the Indus Conglomerate Formation by Abbasi & Friend (1989). We propose this new name because of the possibility of confusion with stratigraphic terms used in the Indus Suture Zone of Ladakh, India, where the terms Indus Group, Indus Formation, Indus Molasse and Indus Flysch have all been used in recent years (e.g. Srivastava *et al.* 1979; Searle *et al.* 1990; Searle 1996). The name of Janak belongs to a village located on the northwestern edge of the outcrop area of the formation, at 71°38′30″E, and 33°14′30″N (Figs 1 & 4).

The study by Gill (1952) of the Siwalik Group of the Potwar area (Figs 1 & 2) was the first in which it was recognized that the mainly sandstone-dominated successions of the central Potwar are the lateral equivalents of major conglomerates further west, near the Indus River. Outcropping on both the western and eastern sides (Fig. 4) of the Indus River, these form the Janak Conglomerate. They crop out over a total area of about 400 km^2, and have a maximum preserved thickness of 1.5 km. Much of the outcrop area is dissected by steep-sided,

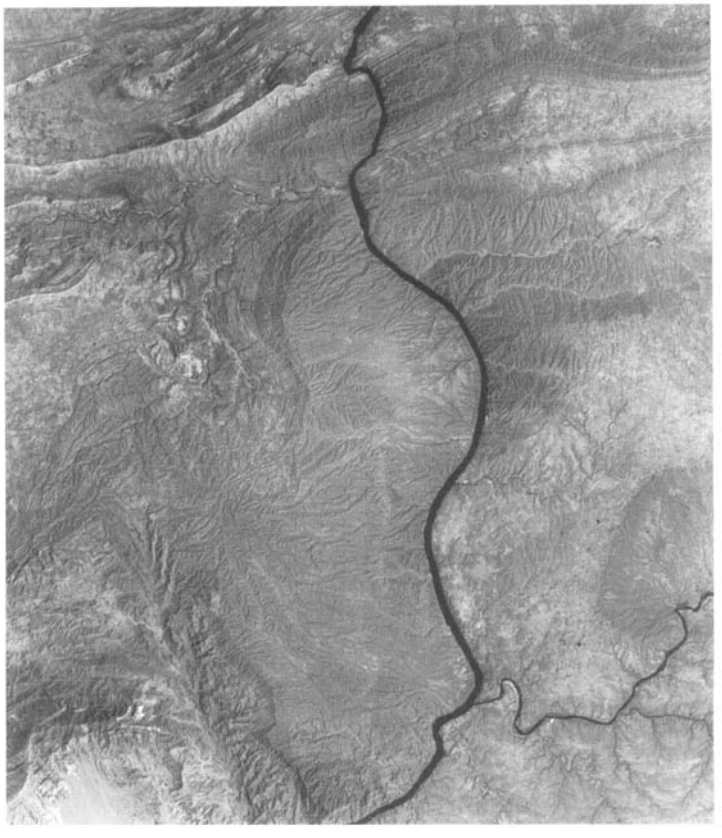

(a)

Fig. 4. Side-by-side comparison of (**a**) part of an Edge-enhanced Landsat-TM image (151-37; 03.09.89) and (**b**) line-drawing of the Janak Conglomerate Formation outcrop area, with geological interpretation. Edge-enhanced processing technique applied using ER Mapper software.

50–100 m deep valleys, producing a distinctive pattern on satellite imagery (Fig. 4a). These valleys are floored by spreads of gravel composed of rounded clasts reworked from the conglomeratic outcrops of the valley walls (Fig. 5).

Although most of the Janak Formation consists of the conglomerates that will be described below, it also contains varying proportions of sandstone. On average, the succession coarsens upwards, but this is due to the increasing ratio of conglomerate to sandstone rather than to any noticeable change in the clast-size of individual conglomerate beds. For typical exposures with successions between 30 and 50 m thick, the conglomerate/sandstone ratio is about 1 : 1 in the lower part of the formation, and about 4 : 1 in the middle and upper parts of the formation. Overbank, mud-grade sediments are absent except for occasional beds in the lower part. A general estimate of clast composition is as follows: mafic volcanic rocks, 32%; quartzite, 27%; gneiss, 21%; limestone, 7%; sandstone, 6%; granites, 3%; other rock types, 4%. The petrology of the clasts can be matched with that of rocks exposed in the Himalaya to the north (Abbasi & Friend 1989), and the mafic volcanic clasts particularly have clearly been derived from the Kohistan arc terrane, just to the north of the northwest corner of the area covered on Fig. 1.

Conglomerate lithofacies

Lateral variation is apparent in most of the conglomerate outcrops of the Janak Formation, but we have found it helpful (Fig. 5) to generalize in terms of lithofacies of the conglomerates and associated sandstones, using a modified version

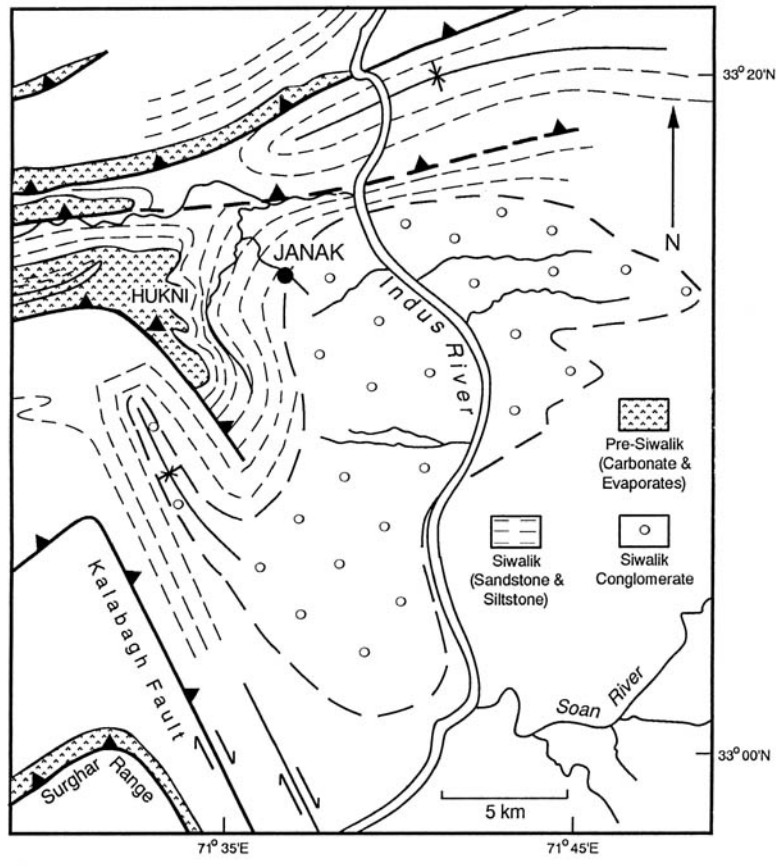

(b)

of the coded classification suggested by Miall (1978), as follows:

- conglomerates: Gh, horizontally-bedded conglomerates; Gp, cross-stratified conglomerates; Gm, unstratified (massive) conglomerates;
- sandstones: Sh, horizontally stratified sandstone; Sp, cross-stratified sandstones; St, trough cross-stratified sandstones.

Figure 5 provides examples of gravel and sand-grade facies patterns in outcrops of the Janak Conglomerate, using the above lithofacies classification.

We first describe the commonest conglomerate lithofacies (Gh) which is defined by its horizontal stratification, developed with strata some tens of centimetres thick in conglomerate sheets that are normally metres thick. The strata vary in their distinctiveness (Fig. 5a). Some strata are defined by grading of clast size, usually 'normal', or fining-upwards, but most simply involve differences in clast-size or form. Where the strata are reasonably distinct, they give a multistoried appearance to the conglomerate sheets.

Sorting and rounding of the clasts are generally high, and the average clast diameter is between 5 and 10 cm. The fabric is generally clast-supported, although it may locally be matrix-supported with the matrix being usually medium-grained sandstone. Imbrication of the clasts is moderately clear at most localities, and always indicates flow directions towards the south, with individual measurements ranging between SSW and SSE.

The dominance of this facies (Gh) is typical of the gravel deposits of proximal braided rivers deposited from relatively shallow, but high velocity flow over longitudinal bars and in the shallow intervening channels (Ore 1964; Hein & Walker 1977; Rust 1978, 1984). This facies forms most typically in the cores of river-bars.

The second conglomerate lithofacies (Gp) makes up about 20% of the conglomerate beds,

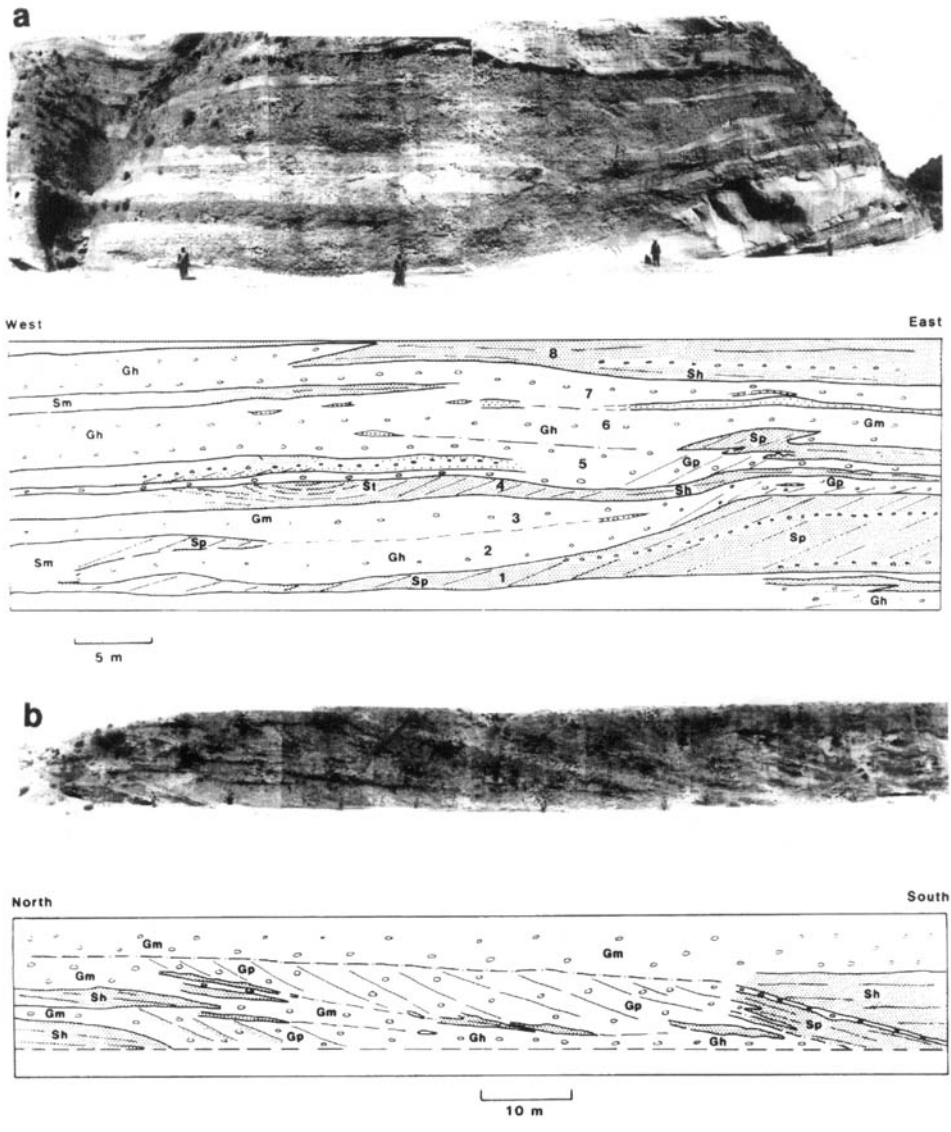

Fig. 5. Photomosaics of outcrops of the Janak Conglomerate Formation. The line drawings have been constructed correcting for tectonic and topographic effects. (**a**) Location 71°41′, 33°8′55″N; channelized conglomerates with sandstone sheets at top, numbers indicate the succession of bars. (**b**) Location 71°40′30″E, 33°9′40″N; large-scale planar cross-bedded conglomerate of facies Gp. The facies Gp is over 7 m thick and passes about 70 m downstream into finer-grained facies Sp and Sh.

and is characterized by the presence of cross-stratification. This cross-stratification varies greatly in set thickness, which is rarely less than 1 m, and ranges up to 7 m (Fig. 5b). The conglomerate fabric is generally clast-supported, and the common matrix is a medium-grained sandstone. The dips of the cross-stratification do not exceed 30°.

The outcrop shown in Fig. 5b is dominated by a compound structure, some 11 m thick, in which two large sets of cross-stratified conglomerate, Gp, dip parallel to each other, and appear to represent two episodes of southward aggradation and downstream progradation of a major bar. More than 70 m of progradation took place before the prograding bar-face was covered by a

distinctive fill of horizontally stratified sand. The bar evolution appears to have been punctuated by episodes of local sand deposition (Sp and Sh), and the later episodes preserved can be interpreted in terms of the change from bar-head aggradation to downstream bar progradation and then sand-deposition on the bar tail. The supposed bar tail of the downstream end of the outcrop, shown in Fig 5b, provides an example of gravel-grade material in the upper parts of the large cross-set interfingering with sand-grade material in the lower parts, apparently implying periodic avalanching of coarse clasts down slope into levels that otherwise received winnowed sand from suspension (Rust 1975).

In general, we consider that lithofacies Gp was deposited during the migration of the downstream margins of longitudinal or transverse bars (Hein & Walker 1977; Rust 1978, 1984). In places where migration did not take place over many metres or tens of metres, the cross-strata appear to have formed when channel-form features were filled by accretion of their sloping margins. These channels were sometimes large enough to scale with the largest cross-sets and the bars in which they formed, but were sometimes considerably smaller, and presumably formed in minor, perhaps bar-top or low-water channels.

The great thickness of some of the cross-stratification sets implies river depths, at times of flood that were significantly greater than the cross-set thicknesses, and we suggest depths of at least 15 m as a reasonable estimate for the bar feature of 11 m thickness. Any laterally persistent cross-set implies some persistence of the flood flow, which would be unlikely to have been very short-lived (Middleton & Trujillo 1984). However, it is difficult to be precise about this, and a recent account of catastrophic flood transport of gravel bars (Carling 1996) has described gravel bars of comparable size to some of those implied by the Janak Conglomerate structures.

The third conglomerate lithofacies is characterized by a lack of stratification, so may be termed massive (Gm), and commonly lacks imbrication of the clasts as well. The conglomerates of this type represent rapid deposition under high energy flow conditions (Bull 1977), or stream flows with particularly high concentrations of bed-load sediment (Morrison & Hein 1987). The lack of stratification appears to reflect a lack of regular periodic accumulation events, and this may be typical of the first, high energy, growth of a bar core, or the first development of a new channel bed as a flood starts to pass. Both of these settings for lithofacies Gm are implied by the architectural geometries of the outcrops studied.

River morphology and scale

The local architecture and the sandstone and conglomerate lithologies of this formation (Fig. 5) are highly diagnostic of a mixed gravel and sand braidplain, and it is clear that the proportion of gravel to sand increased significantly during its accumulation history. Major bars were generally, but not always, made of gravel, and the intervening and secondary channels tended to be plugged with sand, although the plugging sometimes also involved gravel accumulations (particularly forming lithofacies Gm).

There is little doubt that this formation was deposited by a braided river system. The scale of the cross-stratification in some of the conglomerates shows that channel and bar depths and heights ranged up as far as 11 or 12 m, implying flood water depths of 15 m at least, similar to those that occur in the major rivers that presently drain the Himalaya. Clast imbrication suggests that this large river system drained towards the south.

Stratigraphic relationships of the formation

Area of the Janak Conglomerate (Fig. 1). The Siwalik Group consists of some 4 km of sediment, and shows an overall coarsening upwards (Abbasi 1994):

	Max. thickness (m)	Age (Ma)
(3) Janak Conglomerate Formation	1500	8 to Quaternary
(2) Shakadarra Formation	1800	10–8
(1) Chinji Formation	700	14–10

The Chinji Formation consists predominantly of bright red mudstones along with grey or brown channel-body sandstones, and extends with similar lithology both eastwards across the whole of the Potwar Plateau, and southwestwards along the rest of the Siwalik Group outcrop belt. Palaeomagnetic dating of the Chinji Formation in the Potwar Plateau area (Johnson *et al.* 1985; Burbank *et al.* 1996) suggests an age range of 14 to 11 Ma, and this range appears to vary little along the outcrop.

The Shakadarra Formation consists mainly of sandstone, although it contains siltstone in its lower part, and increasing amounts of fine conglomerate in its upper part. In the Potwar Plateau to the east, the lithologically similar Nagri Formation also contains minor siltstones and some pebble beds. Palaeomagnetic work on the Nagri Formation in the Potwar (Johnson *et al.* 1985; Burbank *et al.* 1996) has suggested an age of 11 to 9.5 Ma. Unpublished palaeomagnetic

work on the Shakardarra Formation has suggested a similar age (R. A. Beck, pers. comm.). On these grounds we conclude that the onset of deposition of the Janak Conglomerate Formation occurred about 9 Ma, and that it continued until Quaternary times, when uplift and folding terminated sedimentation in its type area (McDougal 1989).

Lateral relationship. Gill (1952) drew attention to the limited lateral extent of the conglomerates that we now call the Janak Conglomerate Formation. They are stratigraphically equivalent to predominantly siltstone/sandstone formations to the east and southwest, along the regional trend of the Siwalik outcrops. The only detailed studies of their lateral equivalents have been carried out in the Surghar Range area to the southwest (Fig. 1, area 1). Palaeomagnetic dating has shown that during the time interval when the Janak Conglomerate was accumulating in the northeast, a 3.5 km thick, predominantly sandstone, succession was forming where the Surghar Range is now located (Khan 1984; Khan & Opdyke 1993; Pivnik & Khan 1996). Petrological work on this very thick sandstone formation (Abid *et al.* 1983), generally called the Nagri Formation, has shown that its provenance was similar to that of the Janak Conglomerate (Abbasi & Friend 1989; Abbasi & Khan 1990), and we conclude that it was deposited downstream in the same major river system.

We do not have systematic information on the detailed nature of the transitions from the Janak Conglomerate into the laterally equivalent finer-grained sediments. Did the Janak Conglomerates form by aggradation of coarse material in some large lobate depositional feature, perhaps like one of the mega-fans of the present-day eastern India (Sinha & Friend 1994)? We feel that this thick (1500 m) gravel body is unlikely to have formed entirely as a positive feature on the alluvial surface, and must have been constrained laterally between erosional terracing at least periodically. This is how we have portrayed this type of conglomerate body in our model (Fig. 3).

Wider conclusions on the evolution of Himalayan drainage

The present-day drainage system of the Himalaya consists of (1) a relatively regularly-spaced series of main-arc (or trunk) rivers, flowing south into the foreland basin; and (2) the two major syntaxial rivers, the Indus and Tsangpo–Brahmaputra, that cross the two dramatic syntaxial bends to the west and east of the Himalayan arc respectively (Friend 1998). Our detailed study of the Janak Conglomerate has provided evidence that a river large enough to have been the palaeo-Indus syntaxial river was in existence at 9 Ma. The full history of the geomorphological evolution of the remarkable drainage pattern of the Middle and Upper Indus River must reflect a complex sequence of events that occurred as the western margin of the Indian indenter moved transpressively into the main mass of Asia. More detailed work on the structural evolution of the mountains and the depositional history of the foreland will be required before this drainage history can be analysed fully.

I. A. Abbasi acknowledges support from a UK Commonwealth Staff Fellowship and a US Fulbright Fellowship. Detailed comments by R. A. Beck, I. Jarvis, Y. Najman, H. G. Reading and P. J. Treloar have greatly improved early drafts of this paper.

References

ABBASI, I. A. 1994. Fluvial architecture and depositional system of the Miocene molasse sediments, Shakardarra Formation, southeastern Kohat, Pakistan. *Geological Bulletin, University of Peshawar*, **27**, 81–98.

—— & FRIEND, P. F. 1989. Uplift and evolution of the Himalayan orogenic belts, as recorded in the foredeep sediments. *In*: DERBYSHIRE, E. & OWEN, L. A. (eds) *The Neogene of the Karakoram and Himalayas*. Zeitschrift fur Geomorphologie, Special Publication, **76**, 75–88.

—— & KHAN, M. A. 1990. Heavy mineral analysis of the molasse sediments, Trans Indus Ranges, Kohat, Pakistan. *Geological Bulletin, University Peshawar*, **23**, 215–229.

ABID, I. A., ABBASI, I. A., KHAN, M. A. & SHAH, M. T. 1983. Petrography and geochemistry of the Siwalik sandstone and its relationship to the Himalayan orogeny. *Geological Bulletin, University of Peshawar*, **16**, 65–83.

BULL, W. B. 1977. The alluvial fan environments. *Progress in Physical Geography*, **1**, 222–270.

BURBANK, D. W. & RAYNOLDS, R. G. H. 1984. Sequential late Cenozoic structural disruption of the northern Himalayan foredeep. *Nature*, **311**, 114–118.

—— & —— 1988. Stratigraphic keys to the timing of thrusting in terrestrial foreland basins: Applications to the northwestern Himalayan. *In*: KLEINSPEHN, K. L. & PAOLA, C (eds) *New perspectives in basin analysis*. Springer Verlag, New York, 331–351.

——, BECK, R. A. & MULDER, T., 1996. The Himalayan foreland basin. *In*: YIN, A. & HARRISON, T. M. (eds) *The Tectonic Evolution of Asia*. Cambridge University Press, 149–188.

——, ——, RAYNOLDS, R. G. H., HOBBS, R. & TAHIRKHELI, R. A. K. 1988. Thrust and gravel progradation in foreland basins: A test of post-

thrusting gravel dispersal. *Geology*, **16**, 1143–1146.

——, RAYNOLDS, R. G. H. & JOHNSON, G. D. 1986. Late Cenozoic tectonics and sedimentation in the north-western Himalayan foredeep: II. Eastern limb of the northwest syntaxis and regional synthesis. *In*: ALLEN, P. A. & HOMEWOOD, P. (eds) *Foreland Basins*. International Association of Sedimentologists Special Publication, **8**, 293–306.

CARLING, P. A. 1996. Morphology, sedimentology and paleohydraulic significance of large gravel dunes, Altai Mountains, Siberia. *Sedimentology*, **43**, 647–664.

CAUTLEY, P. T. 1840. On the structure of the Sevalik Hills, and the organic remains found in them. *Transactions of the Geological Society of London*. Second series, **5** (2), 267–278, with separate Pl.19.

DICKINSON, W. R. 1974. Plate tectonics and sedimentation. *In*: DICKINSON, W. R. (ed.) *Tectonics & sedimentation*. Society of Economic Paleontologists and Mineralogists Special Publication, **22**, 1–27.

FRIEND, P. F. 1998. General form and age of the denudation system of the Himalaya. *GFF*, **120**, 231–236.

GANSSER, A. 1964. *Geology of the Himalayas*. Interscience Publication Company, London.

GILL, W. D. 1952. Stratigraphy of the Siwalik Series northern Potwar, Punjab, Pakistan. *Quarterly Journal of the Geological Society of London*, **107**, 375–394.

HEIN, F. J. & WALKER, R. G. 1977. Bar evolution and development of stratification in the gravely, braided Kicking Horse River, B.C. *Canadian Journal of Earth Sciences*, **14**, 562–570.

JOHNSON, G. D., RAYNOLDS, R. G. H. & BURBANK, D. W. 1986. Late Cenozoic tectonics and sedimentation in the northwestern Himalayan foredeep, I: Thrust ramping and associated deformation in the Potwar region. *In*: ALLEN, P. A. & HOMEWOOD, P. (eds) *Foreland Basins*. International Association of Sedimentologists Special Publication, **8**, 273–291.

JOHNSON, N. M., STIX, J., TAUXE, L., CERVENY, P. F. & TAHIRKHELI, R. A. K. 1985. Paleomagnetic chronology, fluvial processes and tectonic implications of the Siwalik deposits near Chinji village, Pakistan. *Journal of Geology*, **93**, 27–40.

KHAN, M. J. 1984. Brief results of the paleomagnetic studies of the Siwalik Group of the Trans Indus Ranges, Pakistan. *Geological Bulletin, University of Peshawar*, **17**, 176–179.

—— & OPDYKE, N. D. 1993. Position of the PaleoIndus as revealed by the magnetic stratigraphy of the Shinghar and Surghar Ranges, Pakistan. *In*: SHRODER, J. F. (ed.) *Himalaya to the Sea, geology, geomorphology and the quaternary*. Routledge, London and New York, 198–212.

KUMAR, R. & TANDON, S. K. 1985. Sedimentology of Plio-Pleistocene late orogenic deposits associated with interplate subduction—The Upper Siwalik subgroup of a part of the Punjab Sub-Himalaya, India. *Sedimentary Geology*, **42**, 105–158.

MCDOUGAL, J. W. 1989. Tectonically-induced diversion of the Indus River, west of Salt Range, Pakistan. *Paleogeography, Paleoclimatology, Paleoecology*, **71**, 301–307.

MEIGS, A. J., BURBANK, D. W. & BECK, R. A. 1995. Middle-late Miocene (>10 Ma) formation of the Main Boundary thrust in the western Himalaya. *Geology*, **23**, 423–426.

MIALL, A. D. 1978. Lithofacies types and vertical profile models in braided river deposits: a summary. *In*: MIALL, A. D. (ed.) *Fluvial Sedimentology*. Canadian Society of Petroleum Geology, Memoir, **5**, 597–604.

MIDDLETON, L. T. & TRUJILLO, A. 1984. Sedimentology and depositional setting of the Upper Proterozoic Scanlan Conglomerate, Central Arizona. *In*: KOSTER, E. H. & STEEL, R. J. (eds) *Sedimentology of Gravels and Conglomerates*. Canadian Society of Petroleum Geologists, Memoir, **10**, 189–201.

MORRISON, S. R. & HEIN, F. J. 1987. Sedimentology of the White Channel Gravels, Klondike area, Yukon Territory: Fluvial deposits of a confined valley. *In*: ETHRIDGE, F. G., FLORES, F. M. & HARVEY, M. D. (eds) *Recent Developments in Fluvial Sedimentology*. Special Publications of Society of Economic Paleontologists and Mineralogists, **39**, 205–216.

ORE, H. T. 1964. Some criteria for recognition of braided streams deposits. *University of Wyoming Contributions to Geology*, **3**, 1–14.

PASCOE, E. H. 1919. The early history of the Indus, Brahmaputra and Ganga. *Quarterly Journal of the Geological Society of London*, **75**, 138–157.

PILGRIM, G. E. 1919. Suggestions concerning the history of northern India, arising out of a study of the Siwalik Boulder Conglomerate. *Journal of the Asiatic Society of Bengal*, **15**, 81–99.

PIVNIK, D. A. & KHAN, M. J. 1996. Transition from foreland- to piggyback-basin deposition, Plio-Pleistocene Upper Siwalik Group, Shinghar Range, NW Pakistan. *Sedimentology*, **43**, 631–646.

RAIVERMAN, V. 1975*a*. Classification and origin of Siwalik conglomerates. *In*: *Proceedings IX International Congress Sedimentology*, **10**, 111–116.

—— 1975*b*. Beas valley gravels: A study towards reconstruction of a physical model of deposition of Siwalik Conglomerates. *In*: *Proceedings IX International Congress Sedimentology*, **10**, 117–121.

RAYNOLDS, R. G. H. & JOHNSON, G. D. 1985. Rates of Neogene depositional and deformational processes, northwestern Himalayan foredeep margin, Pakistan. *In*: SNELLING, N. J. (ed.) *The chronology of the geological records*. Geological Society, London, Memoir, **10**, 297–311.

RUST, B. R. 1975. Fabric and structure in glaciofluvial gravels. *In*: JOPLING, A. V. & MCDONALD, B. C. (eds) *Glaciofluvial and Glaciolacustrine Sedimentation*. Society of Economic Paleontologists and Mineralogists, Special Publication, **23**, 238–248.

—— 1978. Depositional models for braided alluvium. *In*: *Canadian Society Petroleum Geologists, Memoirs*, **5**, 605–625.

—— 1984. Proximal braidplain deposits in the middle Devonian Malbaie Formation of eastern Gaspe, Quebec, Canada. *Sedimentology*, **31**, 675–696.

SEARLE, M. P. 1996. Geological evidence against large-scale pre-Holocene offset along the Karakoram fault: Implications for the limited extrusion of the Tibetan Plateau. *Tectonics*, **15**, 171–186.

——, PICKERING, K. T. & COOPER, D. J. W. 1990. Restoration and evolution of the intermontane Indus-molasse basin, Ladakh Himalaya, India. *Tectonophysics*, **174**, 301–314.

SINHA, R. & FRIEND, P. F. 1994. River systems and their sediment flux, Indo-Gangetic Plains, northern Bihar, India. *Sedimentology*, **41**, 825–845.

SRIVASTAVA, R., PAL, D. & MATHUR, N. S. 1979. Sedimentological studies of Indus Formation, Ladakh. *Himalayan Geology*, **9**, 668–700.

Stratigraphic and tectonic evolution of the northwestern Indian plate and Kabul Block

M. S. BADSHAH[1], E. GNOS[2], M. Q. JAN[3] & M. I. AFRIDI[1]

[1]*Federally Administered Tribal Areas Development Corporation (FATADC), Peshawar, Pakistan*

[2]*Mineralogisch-Petrographisches Institut, Universität Bern, Baltzerstrasse 1, 3012 Bern, Switzerland*

[3]*National Centre of Excellence in Geology, University of Peshawar, Pakistan*

Abstract: A 1:500 000 scale geological map covering large parts of the northwest Pakistan–southeast Afghanistan border region between 31–34° N and 69–71° E has been compiled. The map covers the tribal areas of Kurram and of North and South Waziristan in Pakistan, where the map is based on unpublished data of the Federally Administered Tribal Areas Development Corporation. The map area comprises Precambrian crystalline rocks of the Indian and Kabul blocks, Permian to Quaternary sedimentary rocks, and the Late Cretaceous–Palaeocene Kabul–Altimur and Zhob–Waziristan–Khost ophiolite complexes. The Himalayan collision resulted in extrusion of the Kabul Block along the Chaman Fault system and formation of the Katawaz Basin which was filled with clastic deposits of the 'Early-Indus' fan. Ongoing contractional tectonics led to southward thrusting of the Spinghar Indian crystalline basement over the Miocene Murree Formation. New names and type sections are proposed for six units in the Spinghar and South Waziristan. These units are the Daradar Dolomite, Spinghar Quartzite, Sikaram Series, Makai Limestone, Wana Schist and Kaniguram Slates.

The map at 1:500 000 scale presented here (Fig. 1) is a compilation of largely unpublished mapping work by the Federally Administered Tribal Areas Development Agency (Badshah 1972, 1973, 1974, 1977*a*, *b*, *c*, 1983*a*, *b*, 1984, 1985; Khan 1978; Khan & Khan 1985; Khan & Inamullah 1987; Afridi & Tariq 1988; Allaudin 1988; Khan *et al.* 1988, and others), by the USGS (Hemphill & Kidwai 1973; Meissner *et al.* 1974, 1975), by the Pakistan Mineral Development Corporation (Afridi *et al.* 1969), and by the Geological Survey of Pakistan (Khan *et al.* 1982). The Afghanistan part is based on Kaever (1967*a*, *b*), Mennessier (1968, 1969, 1977), Ganss (1970), Wittekindt (1973), Wittekindt & Weippert (1973), Bosum *et al.* (1974), Meissner (1977), Cassaigneau (1979), Mennessier & Beun (1981, 1985) and GEOCART (1983). The map covers Kurram, North and South Waziristan and parts of the Orakzai and Khyber Agencies, as well as parts of the Kohat, Bannu and Dera Ismail Khan Divisions in the Frontal Regions of Pakistan, and parts of Logar, Paktia, Paktika, Kabul and Nangarhar Provinces in Afghanistan (Fig. 2). An E–W cross-section through the area was published by Tapponnier *et al.* (1981). The coverage of the tribal area part of Pakistan is based on geological mapping at 1:50 000 scale. Field based data were also preferred for the rest of the compilation. The map complements those published by Jones (1960), Bannert *et al.* (1992) and Bender & Raza (1995), and with them provides a clear overview of the geology of much of the Pakistan–Afghanistan border from Khyber south to the Karachi area. Tectonostratigraphically, the map area is divided into: (1) Spinghar (Kohe Sofaid), (2) Waziristan–Khost and western Kurram, (3) Kohe Sulaiman, Dera Ismail Khan and Bannu, (4) South Waziristan, (5) Katawaz Basin and (6) Kabul Block and the Altimur Range. A brief description of these follows. Detailed descriptions of type localities are only given for the newly named units.

Spinghar (= Kohe Sofaid = white mountain)

Forming a natural barrier between Afghanistan and Pakistan, the Spinghar consists of Indian basement crystalline, metamorphosed Palaeozoic and relatively unmetamorphosed Mesozoic rocks

From: KHAN, M. A., TRELOAR, P. J., SEARLE, M. P. & JAN, M. Q. (eds) *Tectonics of the Nanga Parbat Syntaxis and the Western Himalaya*. Geological Society, London, Special Publications, **170**, 467–475. 1-86239-061-4/00/$15.00

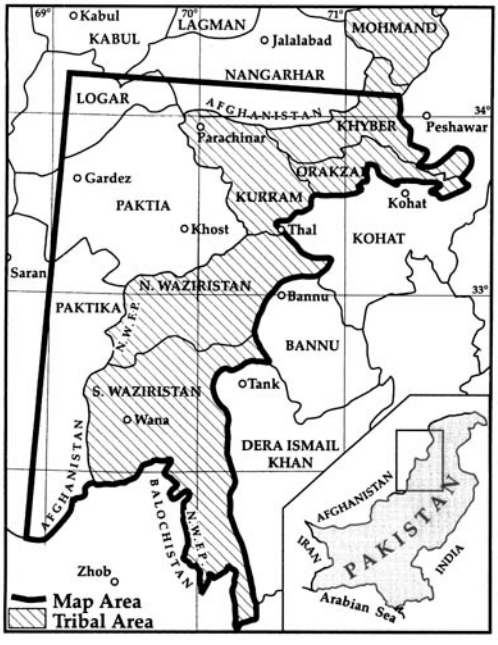

Fig. 2. Overview map of the NW Pakistan–SE Afghanistan border area. Province names used in the description are indicated. The bold, irregularly-shaped frame indicates the area covered by the map.

thrust southward as a nappe over Indian shelf sediments as young as Miocene. It is likely that mica K–Ar cooling ages for the undated Spinghar Crystalline rocks would be similar to the 20–40 Ma range obtained for the Jalalabad area located to the northwest (Wittekindt 1973). Because of a thrust contact the rock units exposed north of the Murree Formation are different to lithologies south of it.

North of the Murree Formation

Rocks of the Spinghar Crystalline unit (Pcc) occupy the eastern crest region of the Spinghar and extend into Afghanistan where they have been grouped into the Precambrian (Wittekindt & Weippert 1973). The rocks are part of the Indian plate Crystalline basement and include granites, augen gneisses and migmatites intruded by granite, aplite and doleritic sheets. Amphibolite and serpentinite lenses are common, and metamorphosed carbonates occur locally. The Spinghar crystalline unit forms the core of the Spinghar nappe which is thrust southward over the Daradar Dolomite, Sikaram Series, Spinghar Quartzite and the Makai Limestone. With the exception of Sikaram mountain, the majority of the Spinghar Peaks are made up of this crystalline basement.

The Daradar Dolomite (Sd) is a siliceous, white to greyish-white and hard dolomite containing up to 19 wt% MgO. Dolerite intrusions are common. Soapstones (talc) exist at many places along fracture zones and at the contacts with the mafic intrusions. The dolomite contains silver-rich lead–copper mineralization in the western part of Spinghar at Neemtota (34°00′30″ N/60°55′00″ E). The dolomite is highly deformed and generally dips steeply northward, forming south-facing cliffs. The dolomite overlies the Spinghar Crystalline unit and is correlated with similar rocks of Silurian to Devonian age in the Khyber Agency (Khan *et al.* 1970). The upper contact with the Spinghar Quartzite is probably disconformable.

The Spinghar Quartzite (Os) consists of white to grey-white, bedded quartzite with grit and conglomerate at the base. In the eastern Spinghar, the quartzite is imbricated and occurs in two horizons with graphitic phyllites of the Sikaram Series in between. The Quartzite is correlated with the Siluro-Devonian Spinrag Quartzite at Jamrud in the Khyber Agency (Khan *et al.* 1970). Contacts with the underlying Daradar Dolomite and the overlying Sikaram Series are believed to be tectonic. The contact with the Makai limestone appears unconformable.

The Sikaram Series (PCs) is dominantly exposed along the western Spinghar, and forms the summit of the 4755 m Sikaram Sar. It consists of claystones and carbonaceous shale in its lower part, and slate and graphitic schist in the upper part. At Hussain Mela, boudins of quartz–mica schist contain 2–8 cm sized garnet porphyroblasts in their cores. The Sikaram Series is several thousand metres thick in the west, thins to a few metres in central Spinghar and gradually increases in thickness eastward where it becomes more graphitic. The series has a thrust contact with the Daradar Dolomite and the Spinghar Crystalline unit. Griesbach (1892) reported Triassic Lithodendroid fossils from eastern Spinghar. In the northern Khyber Agency the lithologically similar Landikotal Slate was dated as Ordovician–Silurian by Stauffer (1968) and Khan *et al.* (1970). Based on its stratigraphic position above the Siluro-Devonian Daradar

Fig. 1. Geological map of Spinghar, Kurram, Waziristan and Kohe Suleiman (Pakistan) and parts of Nahgarhar Khost, Paktia and Paktika (Afghanistan).

GEOLOGICAL MAP O
KOHE SULEIMAN (PA
KHOST, PAKTIA AND

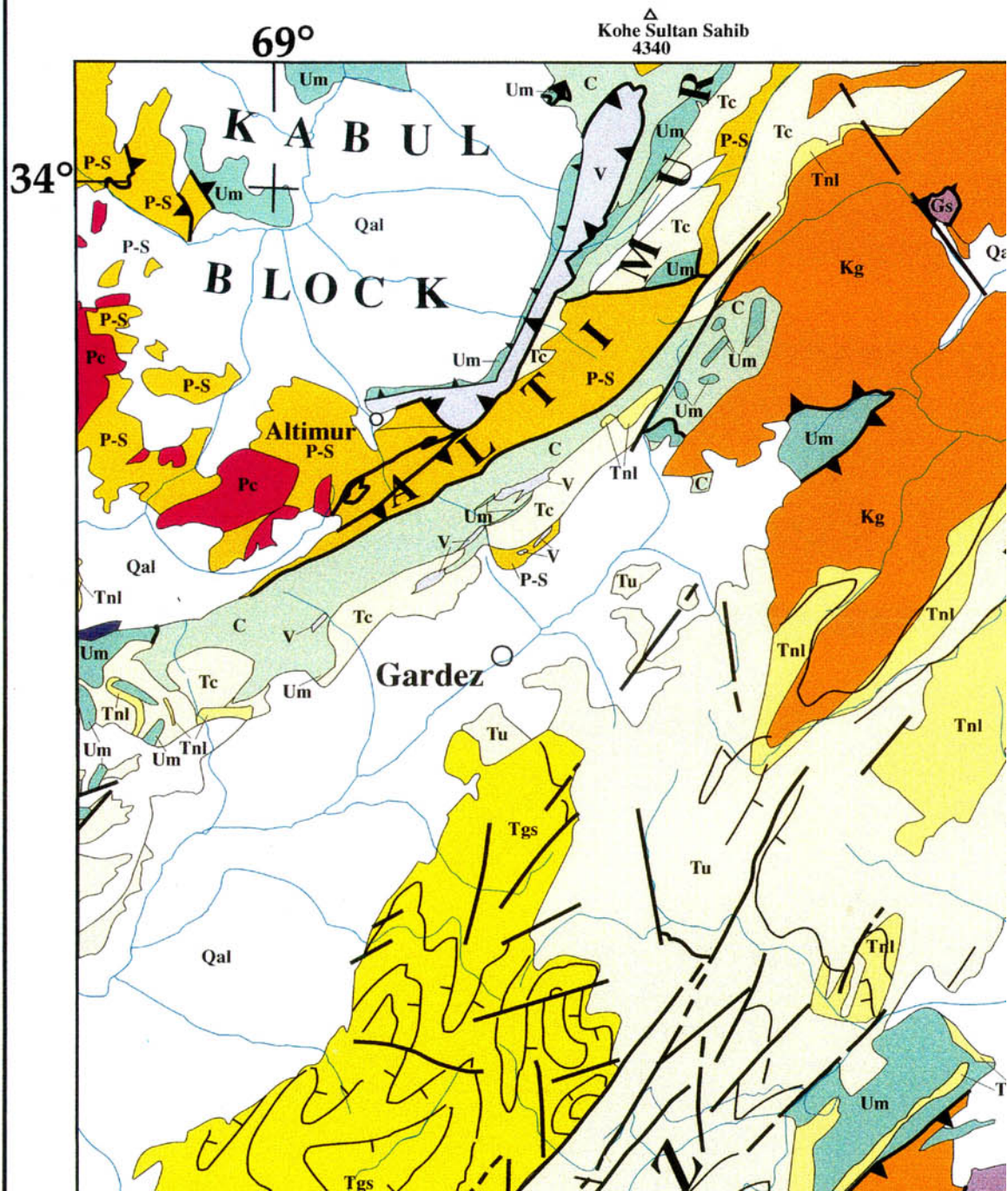

OF SPINGHAR, KURRAM,
AKISTAN) AND PARTS OF
PAKTIKA (AFGHANISTA

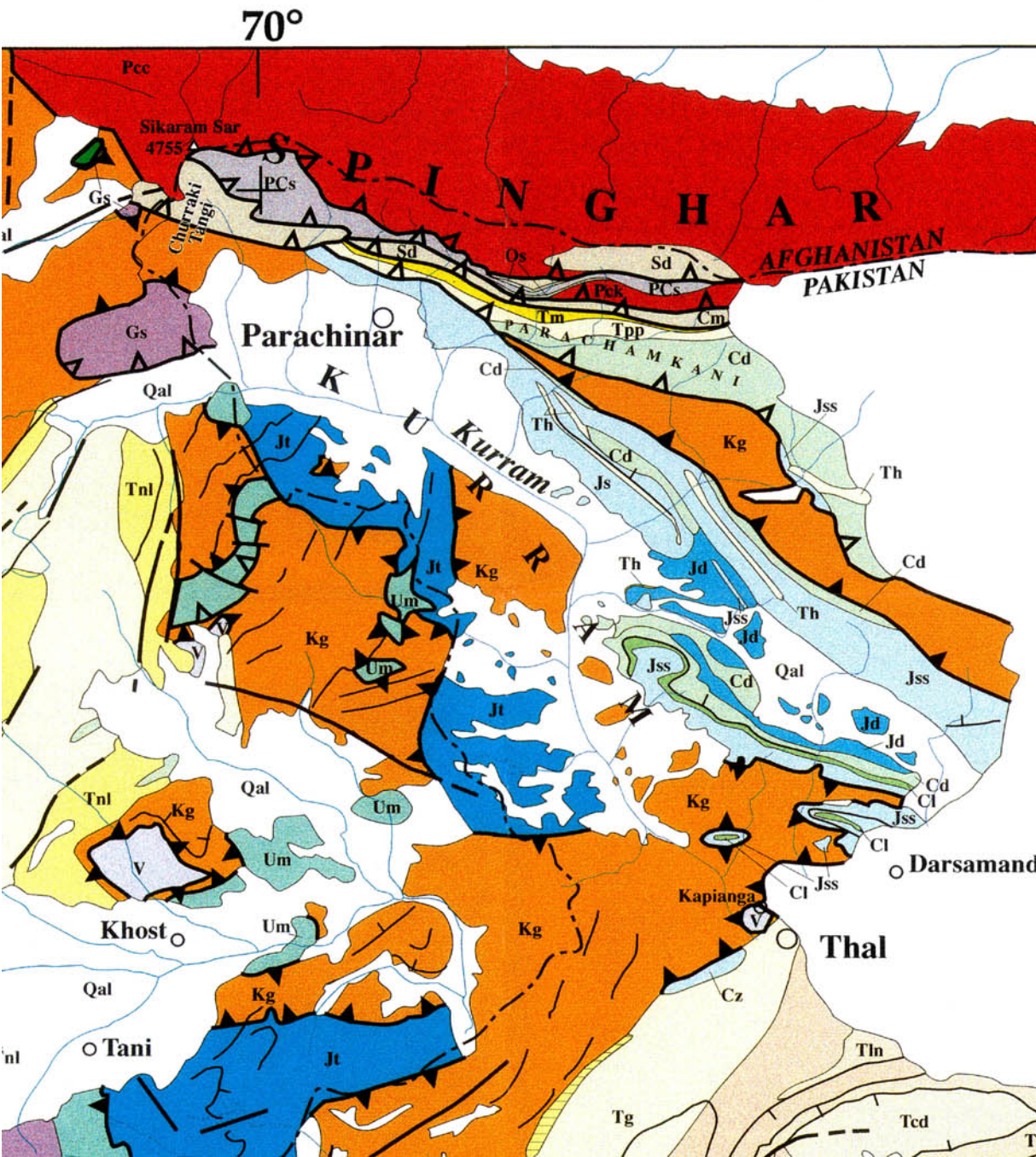

, WAZIRISTAN AND
F NANGARHAR,
AN)

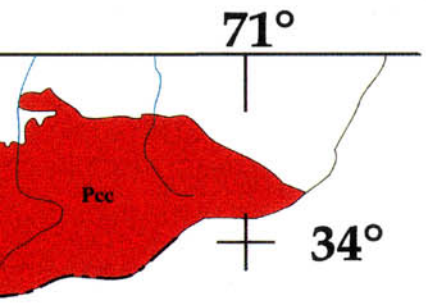

SPINGHAR (KOHE SOFAID)

Qal	Alluvium
Tm	Murree Formation
Tpp	Patala and Panoba Formations
Th	Hangu Formation
Cd	Darsamand Limestone
Cl	Lumshiwal Formation
Cm	Makai Limestone
Jss	Samana Suk Formation
Jd	Datta Formation
PCs	Sikaram Series
Os	Spinghar Quartzite
Sd	Daradar Dolomite

KOHE SULEIMAN

Qal	Alluvium
Tcd	Chaudawan, Dhok Patan and Malaghan Formations
Tln	Litra and Nagri Formations
Tvc	Vihowa and Chinji Formations
Tck	Chitarwata and Kamlial Formations
Tdr	Drazinda Shale
Tpk	Pir Koh Limestone
Tdo	Domanda Shale
Thr	Habib Rahi Limestone
Tbz	Zam Burj Shale Member
Tbb	Baska Shale Member
Tgk	Ghazij (Karghal Shale Member)

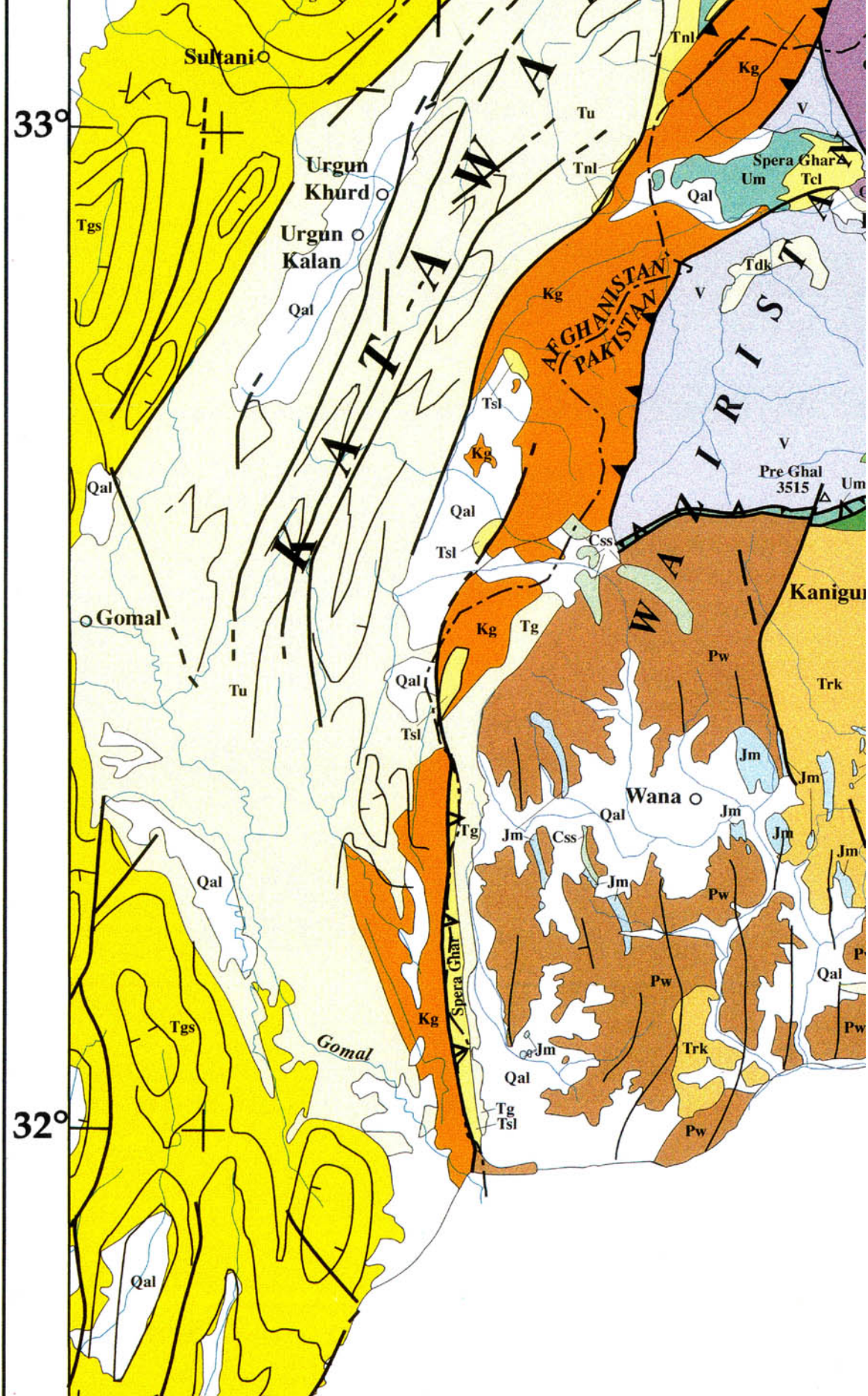
Sultani
33°
Urgun Khurd
Urgun Kalan
Tgs
Qal
KATAWAZ
Tu
Tnl
Kg
V
Spera Ghar
Um
Tcl
Qal
Tdk
AFGHANISTAN
PAKISTAN
WAZIRISTAN
Tsl
Kg
Pre Ghal 3515
Um
Qal
Tsl
Css
Gomal
Kg
Tg
Qal
Tsl
Tu
Kanigur
Pw
Trk
Jm
Wana
Qal
Jm
Tg
Jm
Css
Jm
Jm
Jm
Qal
Tgs
Gomal
Kg
Spera Ghar
Jm
Qal
Tg
Tsl
Trk
Pw
Qal
Pw
32°
Qal

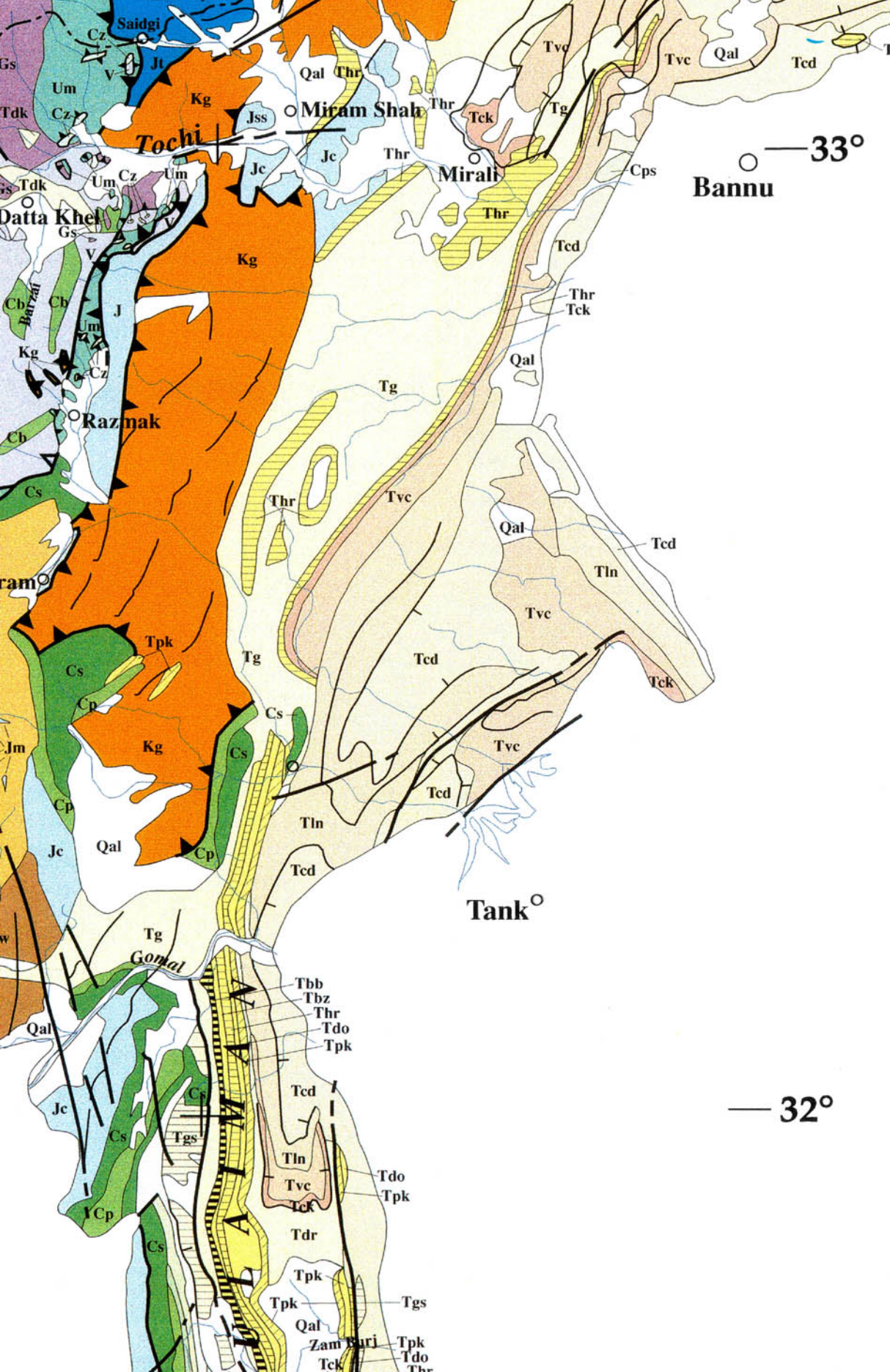
Saidgi
Cz
Jt
V
Gs
Um
Tdk
Kg
Jss
Miram Shah
Tochi
Jc
Qal
Thr
Tvc
Tcd
Tg
Tck
Mirali
Bannu
33°
Cps
Datta Khel
Barzai
Cb
J
Razmak
Cs
Tpk
Cp
Jm
Tln
Gomal
Tbb
Tbz
Tdo
Tgs
Tdr
Zam
Buri
Tck
Thr
Qal
Tg
Tvc
Tcd
Tln
Tck
Tank
32°

Thr

Pcc Spinghar Crystalline

KHOST AND NORTH AND SOUTH WAZIRISTAN AREAS

Qal Alluvium

Tcl Spera Ghar Conglomerate and Limestone

Tg Ghazij Formation

Tdk Datta Khel Clastics

Kg Kurram Group

Gs Gabbro and Sheeted Dike Complex

Um Ultramafic rocks and metamorphic sole

Cz Zhizha Olistostrom

Cb Barzai Chert

V Pillow Lavas and Sheet Flows

Cs Sembar Formation

Jc Chiltan Limestone

Jss Samana Suk Limestone

Jt Tani Formation

SOUTH WAZIRISTAN

Qal Alluvium

Tsl Spera Ghar Limestone

Tg Ghazij Formation

Kg Kurram Group

Css Metamorphosed Sandstone

Tgs Ghazij (Shinsang Shale Member)

Td Dungan Formation

Cps Pab Sandstone

Cmk Mughal Kot Formation

Cp Parh Limestone

Cs Sembar Formation

Jc Chiltan Limestone

KATAWAZ BASIN

Qal Alluvium

Tgs Gomal, Sultani and Saraudza Formations

Tnl Nummulitic Limestone

Tu Urgun Formation

Tc Basal Conglomerate

KABUL BLOCK, ALTIMUR RANGE

Qal Alluvium

Tnl Nummulitic Limestone

Tc Basal Conglomerate, Azrao Flysch, Zin-Tiza Formation

C Late Cretaceous

Um Kabul and Altimur Ophiolite Ultramafics

V Kabul and Altimur Lavas

P-S Permian to Senonian

Pc Kabul Crystalline

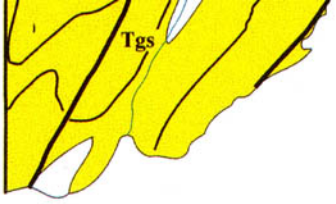

Zhob

0

31°

69°

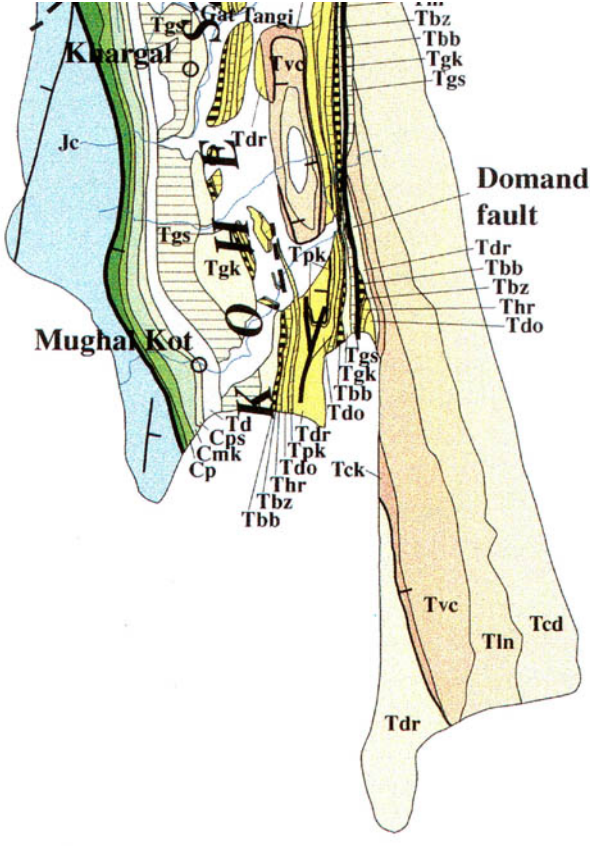

50 km

70°

Compilation by M. S. Badshah, 1

Sources: Kaever, 1967; Afridi *et a*
1973; Wittekindt & Weippert, 19
1975; Badshah, 1977a, b, c; Meis
1983a, b, 1984, 1985; Khan & Kh
Khan, 1988; Pervez, 1988; Afridi
Mazhar, 1989; Tariq, 1990, 1991;

Drawing by E. Gnos, M. A. Z. Af

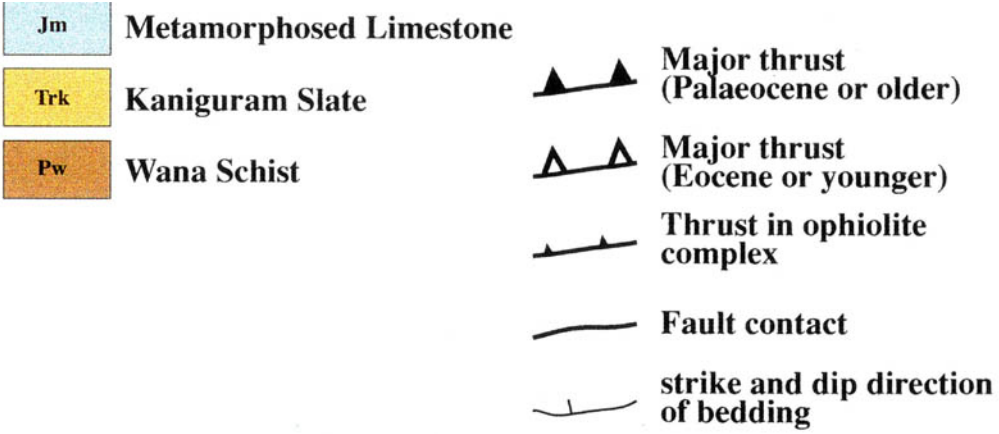

1997

al., 1969; Ganss,1970; Badshah, 1972, 1973; Hemphill & Kidwai, 1973; Wittekindt,
)73; Badshah, 1974; Khan, 1974, 1975; Bosum *et al.*, 1974; Meissner *et al.*, 1974,
ssner, 1977; Khan, 1978; Cassaigneau, 1979; Mennessier & Beun, 1981; Badshah,
han, 1985; Mennessier & Beun, 1985; Khan & Inamullah, 1987; Allaudin, 1988;
i & Tariq, 1988; Tariq & Shafa, 1988; Khan *et al.*, 1988; Afridi, 1989; Khan &
; Badshah, 1994.

fridi & M. I. Afridi

Dolomite, we consider the Sikaram Series to be between Siluro-Devonian and Triassic in age.

The Makai Limestone (Cm) comprises several hundred metres of thick, greenish-grey to dark grey, thinly bedded, siliceous limestones. It is strongly folded and unconformably overlies the Sikaram Series, Spinghar Quartzite, Daradar Dolomite and the Spinghar Crystalline unit. It contains conglomerate and grit at the base, indicating a transgressive unconformity. The unit is tentatively assigned a Cretaceous age. The stratigraphically higher part of the overturned unit is strongly deformed into calcareous schists (probably mylonites) showing a sheared contact with the Miocene Murree Formation. This zone is interpreted as the basal thrust of the Spinghar nappe which has crystalline rocks at its core.

South of the Murree Formation

The formations found south of the Murrees continue into the Hangu–Aurakzai area. The rocks have been described by Latif (1970), Fatmi (1972), Fatmi & Cheema (1972), Meissner *et al.* (1974, 1975), Shah (1977) and Rabbani (1978). The formations cover a range from Jurassic to Tertiary, and include the Datta Formation (Jd), Shinawari Formation (Jsh), Samanasuk Limestone (Jss), Chichali Formation (Cc), Lumshiwal Formation (Cl), Darsamand Limestone (Cd), Kawagarh Formation (Ck), Hangu Formation (Th), Lockhart Limestone (Tl), Patala and Panoba Formations (Tpp), and the Murree Formation (Tm).

The Middle Jurassic Samanasuk Limestone thins westward and pinches out in central Spinghar, north of Parachinar. The Chichali and Kawagarh formations are present as thin units in the Spinghar area but are not shown separately on the map. The Lockhart Limestone, however, has not been identified in Spinghar (Rabbani 1978). Because the Patala and Panoba formations could not be conclusively distinguished, the two formations are shown as one unit on the map. Khan & Khan (1985) identified the Miocene Fatejang Member as marking the basal part of the Murree Formation in the Spinghar. Because the Murree Formation is overthrust by the older Makai limestone this yields an important age constraint for Miocene southward thrusting of the Spinghar nappe.

Waziristan–Khost and western Kurram

This area is tectonically complex and consists of para-autochthonous sedimentary rocks of the Indian plate (Tani Formation (Jt); Kaever 1967*a*), overthrust by an ophiolite complex composed of two tectonic units, the Kurram Group nappe, and a post-nappe sedimentary cover. Outcrops of the ophiolite occur in South and North Waziristan, Kurram and Bannu in Pakistan, and Paktia in Afghanistan (Fig. 2), and outside the map area near Zhob in northern Baluchistan. The ophiolite complex is strongly folded with steep N- to NE-trending axial planes and locally SE-vergent folds. The western part of the Waziristan ophiolite complex has not been studied in detail, although lavas dominate over peridotites.

Within the ophiolite complex two tectonic units are recognized. The lower unit contains Pillow Lavas and Sheet Flows (V), the overlying Albian to Senonian (Cassaigneau 1979; Beck 1995) Barzai Chert (Cb), and the Campanian Zhizha Olistostrom (Cz). These three rock units are in stratigraphic continuity. Cyprus-type massive sulphide deposits are reported from the pillow lavas (Badshah 1983*b*, 1985, 1986). The upper unit of the ophiolite complex consists of a metamorphic sole and ultramafic rocks (Um), which include amphibolite to blueschist facies metamorphic sole rocks and a serpentinized, harzburgitic mantle sequence carrying sporadic chromite deposits (Jones 1960; Jan *et al.* 1985). The crustal sequence consists of the Gabbro and Sheeted Dyke Complex (Gs). A large gabbro massif occurs west of Kurram in Afghanistan (Cassaigneau 1979). Outcrops of the Sheeted Dyke Complex are present near Datta Khel and along the Manzarkhel–Saidgi line in North Waziristan. A detailed description of the Zhob–Waziristan–Khost ophiolite complex and the tectonostratigraphic evolution of the area is given by Gnos *et al.* (in press).

The Kurram Group is an extensive sedimentary nappe overlying the ophiolite complex and the Indian shelf sediments. It is stratigraphically poorly known. The Jurassic–Cretaceous 'Khorram Formation' of Kaever (1967*a*), the undifferentiated Jurassic–Cretaceous of Hemphill & Kidwai (1973), and the Triassic to Jurassic 'Série de Khost' and 'Série d'Ahmadhkhel' of Cassaigneau (1979) are tentatively included here in this group. However, we exclude the Chale Talao Kurram Formation of Meissner *et al.* (1975), which was correctly shown as Kirthar limestone and Ghazij shale by Hemphill & Kidwai (1973). Pillow lavas with red interpillow sediments are present at several localities within the Kurram Group. We consider the Kurram Group to be Triassic to Late Cretaceous in age, containing reworked Late Permian and Triassic material (Cassaigneau 1979).

Both the ophiolite complex and the Kurram Group are covered by latest Maastrichtian and younger sedimentary rocks. These include the Datta Khel Clastics (Tdk), the Ghazij Formation (Tg) and the Speraghar Conglomerate, and the Habib Rahi Limestone (Tcl). The Datta Khel Clastics contain material derived locally from the ophiolite complex and the Kurram nappe. The unit unconformably overlies the ophiolite complex and the Kurram Group and is itself unconformably overlain by the Ghazij Formation or the Spera Ghar Conglomerate. This relationship suggests a latest Maastrichtian to Palaeocene age for post-ophiolite sedimentation. The full outcrop extent of the Ghazij Formation is unknown. On the map the known small outcrops are included with the Speraghar Limestone/Speraghar Conglomerate. Nummulites date the limestone at Speraghar as Early Eocene (Adams, pers. comm. 1986).

Kohe Sulaiman, FR Dhera Ismail Khan and FR Bannu

Jurassic to sub-Recent formations are found in the southeastern part of the map area and include, from base upward, the Chiltan Limestone (Jc), Sembar Formation (Cs), Parh Limestone (Cp), Mughal Kot Formation (Cmk), Pab Sandstone (Cps), Dungan Formation (Td), Ghazij Formation (Tg), Baska Formation (Tb), Kirthar Formation, Chitarwata and Kamlial formations (Tck), Siwalik Group and Gat Tang Formation. The stratigraphy of this area is well known and detailed descriptions were given by Williams (1959), Jones (1960), Hemphill & Kidwai (1973) and Badshah (1977*c*).

The Goru Formation that separates Sembar and Parh in parts of Baluchistan (Jones 1960) does not crop out in the map area. Badshah (1977*c*) subdivided the Ghazij Formation into a lower Shinsang Shale Member, an upper Karghal Shale Member, and the Baska Formation (Tb) into a lower Baska Shale Member (Tbb) and an upper Zamburj Shale Member (Tbz). This subdivision is used on the map. Hemphill & Kidwai (1973) divided the Kirthar Formation into the Habib Rahi Limestone (Thr), the Domanda Shale (Tdo), the Pir Koh Limestone (Tpk), and the Drazinda Shale (Tdr) Members. The Kirthar Formation should have a Group status for possible further subdivision. Rocks similar to the Kirthar Formation are widespread in the Katawaz Basin to the west of Waziristan ophiolite complex. The Kamlial Formation is lithologically similar to the Chitarwata Formation and hence is not distinguished on the map.

The Siwaliks in Dera Ismail Khan include, from base upward, the Vihowa, Litra and the Chaudhwan formations (Hemphill & Kidwai 1973). In Bannu, the Siwaliks include the Chinji, Nagri and Dhok Pathan–Malaghan formations (Pilgrim 1913; Morris 1938). Because of their continuity in both areas, these are treated as Vihowa/Chinji, Litra/Nagri and Chaudhwan/Dhok Pathan–Malaghan formations on the map. The Gat Tang Formation, defined by Badshah (1977*c*), seems to have a transitional contact to sub-Recent and Recent deposits. It is probably an equivalent to the Late Pleistocene to sub-Recent Bostan Formation of Jones (1960). The formation is not shown on the map.

South Waziristan

Rock units structurally underlying the Zhob–Waziristan–Khost ophiolite complex in South Waziristan show a low-grade metamorphic overprint (e.g. Beck 1995). We consider the Metamorphosed Limestone (Jm) to be the metamorphosed equivalent of the Chiltan limestone, exposed in the Kohe Sulaiman to the southeast, and that the Metamorphosed Sandstone (Css) represents the metamorphosed Pab Sandstone as no other massive sandstone is known in the region. The Kurram Group (Kg), Ghazij Formation (Tg) and Speraghar Limestone (Tsl), structurally overlying the ophiolite complex, are not metamorphosed. Quaternary Lake deposits similar to those of the Zhob area in Baluchistan (Jones 1960) are present at the southern border to Baluchistan. The following two units are newly defined here.

The Wana Schist (Pw) consists of medium to thin bedded, greenish-grey and dark schists and phyllites covering a large area, and are part of an open N-trending anticline flanked by Mesozoic sedimentary rocks. The schists are intensely folded with well developed box and chevron folds. Kink bands, crenulation cleavages and intrafolial quartz veins are characteristic. Low greenschist facies metamorphism is considered to be due to the southward thrusting of the Zhob–Waziristan–Kost ophiolite complex and Kurram Group onto the Indian margin. The Wana Schist could be Palaeozoic in age.

The Kaniguram Slate (Trk) consists of greenish-grey and black, fine-grained, intensely fractured, splintery, thin to thick bedded slates that occupy the northeastern areas near the southern ophiolite contact and a narrow strip along the western margin of the ophiolite. They could be

equivalent to the Tani Formation of the Waziristan–Khost–Kurram region.

Katawaz Basin

This relatively young structure developed after thrusting of the Zhob–Waziristan–Khost ophiolite complex and the Kurram Group nappe. The basin formation started during Late Cretaceous/Palaeocene (Jones 1960; Kaever 1967*b*; Ganss 1970; Cassaigneau 1979) with the main development during the Late Palaeocene–Miocene when more than 10 000 m of sedimentary rocks were deposited. Syntectonic internal discordances, slumps (olistostroms), syn-sedimentary faults and folds are frequent. The tectonic environment was transtensional in its initial stage and transpressional since the middle Miocene when the Chaman Fault developed (Cassaigneau 1979). Miocene to Recent calc-alkaline and alkaline volcanic rocks and quartz–microdioritic intrusions are associated with the Chaman Fault system along the western rim of the basin (Bordet 1975). After deposition of a basal conglomerate (Dab Series) marine deposition started with Late Palaeocene to Late Eocene platform limestones along the rims, and pelagic sediments (Urgun Formation) in the centre of the basin (Kaever 1967*b*; Mennessier 1977; Cassaigneau 1979). The younger sediments are dominated by sandstone. Rocks older than Oligocene/Miocene show vertical schistosity. The Katawaz Basin deposits are interpreted as the more proximal fan part of a palaeo-Indus delta that continuously extended into the more distal Makran Flysch part.

On the map the Basal Conglomerate (Tc), Nummulitic Limestone (Tnl) and Urgun Formation (Tu) are shown separately, whereas the Gomal, Sultani and Saraudza formations (Tgs) are shown as one unit. Descriptions of the different units found in the Katawaz Basin are given in Cassaigneau (1979), Mennessier & Beun (1985), Treloar & Izatt (1993), Jadoon & Kurshid (1996), Quayyum *et al.* (1996, 1997) and Haq & Davies (1997).

Kabul Block and the Altimur Range

The Kabul Block consists of a Late Proterozoic crystalline basement covered by Permian to Senonian shelf sediments (Kingil Series) which, in turn, is overthrust by the Kabul–Altimur ophiolite complex. The ophiolite is unconformably covered by the Santonian–Campanian Ali-Pai-Bel Limestone. The Altimur Range is lithologically similar but with more internal thrusting and faulting. The descriptions below are mainly based on the compilation by Mennessier & Beun (1985).

The Kabul Crystalline rocks (Pc) consist of quartz–garnet–muscovite–biotite ± kyanite schist with intercalated hornblende–plagioclase layers and marbles, and intrusions of diorite, anorthosite and diabase. The crystalline basement has an autochthonous, greenschist facies sedimentary cover (Kingil Series and Altimur Unit (P–S)). Fossils allow the units to be dated as Late Permian to Senonian (Mennessier & Beun 1985). The autochthonous sedimentary rocks were overthrust by the Kabul–Altimur ophiolite complex which includes the Kabul ophiolitic complex, Kotagae Series, Akhundkhel Series and Rokian Series of Mennessier & Beun (1985). Only the Ultramafic rocks (Um) and Lavas (V) are distinguished on the map. The ophiolite complex consists of serpentinized harzburgite, lherzolite and dunite, and gabbroic rocks outside the map area. Dolerite dykes are frequent in the peridotite. Radiolarian cherts yield Aptian to Turonian ages. The ophiolite complex is also overprinted by greenschist facies metamorphism.

Non, or only weakly, metamorphosed sedimentary rocks cover the Kabul–Altimur ophiolite complex. These include Late Cretaceous (C), Palaeocene to Early Eocene Couches Rouges–Azrao Flysch–Varigated Conglomerate–Zin–Tiza Formation (Tc), and Early to Middle Eocene Nummulitic limestone (Tnl). The Tertiary deposits are in continuation with units in Western Pakistan, described above and thus correlable (Fig. 3). For a detailed description of the units in Afghanistan, the reader is referred to Mennesier & Beun (1985).

Stratigraphic correlations

Previous to this work, working stratigraphies had been developed separately for each of the different sub-areas covered by the map. As a result, individual units and formations have been given different names in different subareas. Figure 3 represents an attempt to develop a stratigraphic overview for the whole region. Existing names have been used where possible.

Tectonic evolution

After a Late Permian incursion of the Tethyan sea from the north over metamorphosed basement (E Afghanistan, Kaever 1967*b*) or Palaeozoic sediments (Spinghar), break-up of Gondwana started in the Triassic with marine sedimentation occurring as far south as the central Indus basin. Shallow to open marine

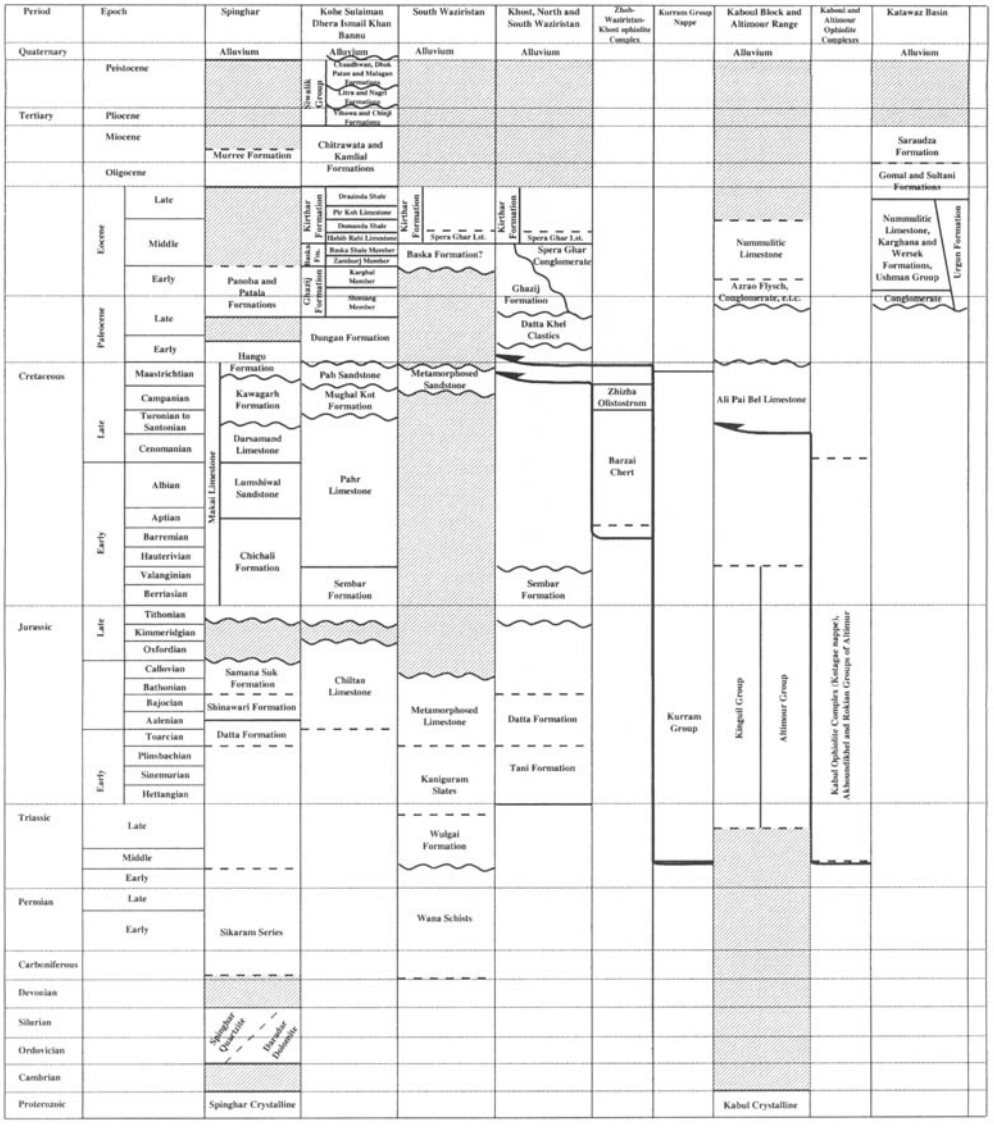

Fig. 3. Correlation table showing formation names and corresponding age ranges used on the map and in the text. Hatched areas are stratigraphic gaps. A wavy line indicates an unconformable contact, and a dashed line an approximate limit.

conditions, deepening to the east, with high energy carbonates dominant along the western side of Greater India, are recorded through the Triassic to Middle Jurassic (Jones 1960). Plant relics are common in the Lower Jurassic (Stuart 1922; Kaever 1967*a*; Beck *et al.* 1996) and ammonites in the Upper Jurassic (Kaever 1967*a*; Hemphill & Kidway 1973; Beck *et al.* 1996). E–W sedimentation differences became strongly accentuated with the separation of East and West Gondwana in the Late Jurassic (e.g. Cochran 1988). This is marked in the map area by erosion of Middle to Late Jurassic strata along the whole length of the western Indian margin, and transgression of the Lower Cretaceous Sembar Formation with common development of a transgressive conglomerate at its base.

The closure rate of Neo-Tethys increased with increasing separation of India–Seychelles from Madagascar between *c.* 100 and 84 Ma, initiating

the Zhob–Waziristan–Khost subduction zone (Gnos *et al.* in press). Common limonitic beds, as in the Aptian to lower Cenomanian Lumishiwal sandstone of the Indian shelf, indicate a regressive deltaic facies and subaereal exposure. In Southern Pakistan the stratigraphic record over this time period is continuous. This late Cretaceous unconformity was followed by the transgressive Coniacian–Campanian Kawagarh Formation and the Mughal Khot Formation (Beck *et al.* 1996; Burris 1996). The latter contains large olistoliths of Jurassic shallow-water limestones which are probably correlated with a similar olistolithic layer of Jurassic shallow-water limestones that form the youngest (Campanian) beds in the lower ophiolitic unit. We interpret this as a result of the collision of the Indian passive margin with the Zhob–Waziristan–Khost trench, resulting in crustal flexure and a depositional break. Final ophiolite obduction thus occurred in Campanian or Maastrichtian time.

Late ophiolite emplacement or nappe thrusting in the Kabul–Altimur and Zhob–Waziristan–Khost areas was toward the SE. However, this direction may not indicate the original direction of obduction because the folds may have been rotated in a counter-clockwise sense during the southwestward extrusion of the Afghanistan continental block and formation of the Katawaz Basin (Cassaigneau 1979; Tapponnier *et al.* 1981; Beck *et al.* 1996).

During the late Maastrichtian to Palaeocene the Zhob–Waziristan–Khost ophiolite was thrust beneath a nappe of deep-marine to pelagic sediments (Kurram Group). The thrust stack was then folded and thrust further cratonward and exposed to subaerial weathering (Cassaigneau 1979; Beck *et al.* 1995). During rapid Palaeocene subsidence of the Kurram region, lower to middle Palaeocene strata (up to P3) became tilted. Whether this was caused by collision of the India–Kabul margin with Asia or with an intraoceanic trench is still unclear. Two scenarios are possible. Cassaigneau (1979), Tapponnier *et al.* (1981) and Treloar & Izatt (1993) interpreted the Kabul Block as a fragment of Gondwana that collided with India–Seychelles at the end of the Cretaceous. They inferred that the Kabul–Altimur ophiolite obduction was Palaeocene in age. Critical to this model is that obduction of the Kabul–Altimur ophiolites occurred in the Palaeocene and thus postdates the Campanian–Maastrichtian age of obduction for the Zhob–Waziristan–Khost ophiolite. The biostratigraphic data constrain the age of obduction to the Maastrichtian–Palaeocene interval. Alternatively, Beck *et al.* (1996) interpreted the Kabul Block as representing the leading part of the Indian plate that was sheared off and pushed to the southwest during early India–Asia collision. We suggest that the Kabul–Altimur ophiolite complex may be the deformed and metamorphosed equivalent of the Zhob–Waziristan–Khost ophiolite complex, and that the allochthonous Kurram Group represents a nappe rooting on the Eurasian plate (Meissner *et al.* 1975). Radiometric data from the Kabul–Altimur ophiolite and palaeomagnetic data from the Late Cretaceous/early Tertiary sedimentary rocks of the Kabul Block are needed to solve the problem. Ongoing collison resulted in the extrusion of the Kabul Block, formation of the Chaman Fault system, and formation of the Katawaz Basin that was filled up with the fan deposits of an early 'Indus river' (Cassaigneau 1979; Treloar & Izatt 1993; Quayyam *et al.* 1996, 1997).

Subduction of the India Plate margin during Himalayan collision resulted in the Miocene-aged southward thrusting of the Spinghar Crystalline unit and cover rocks over the Murree Formation. Greenschist facies metamorphism in the northern parts of the Kabul Block, along the southern border of the Waziristan ophiolite complex and beneath the Spinghar Thrust, seems to have developed locally as a result of southward thrusting of northern units over southern units.

Many angular unconformities, well documented in eastern Kurram and Waziristan, record a series of stratigraphically discrete episodes of late Palaeocene, early Eocene and Neogene deformation during Himalayan contractional tectonism (Beck *et al.* 1995). Present earthquakes are frequent on thrust planes and on strike-slip or normal faults in the map area (e.g. Lawrence *et al.* 1992).

References

AFRIDI, M. I. & TARIQ, M. 1988. *Geological map of Wana subdivision, South Waziristan, 1:200000, with report.* Federally Administered Tribal Areas Development Corporation, unpublished.

——, MAMON, A. S. & YELDEZ, O. 1969. *Geological map of Parachinar, 1:50000, with report.* PMDC (Pakistan Mineral Development Corporation), unpublished.

ALLAUDIN 1988. *Geological map of Jandola area, 1:50000, with report.* Federally Administered Tribal Areas Development Corporation, unpublished.

BADSHAH, M. S. 1972. *Waziristan, a metallogenetic province; important occurrences of copper, chromite and manganese in parts of North and South*

Waziristan Agencies. FATADC unpublished report file 35 G, vol. 1, 1–19.

—— 1973. *Geological map between Daradar Tangi and Peiwar Tangi (Upper Kurram Agency), 1:50 000 with report*. FATADC, unpublished.

—— 1974. *Geology of Shalozan Weir site, Kurram Agency*. FATADC unpublished report, 1–10.

—— 1977*a*. *Detailed investigation and exploration of prospective areas in FATA*. FATADC project report and PCII proforma, 1–65.

—— 1977*b*. *Exploitation of soapstone in Daradar valley, Kurram Agency*. FATADC project report and PCII proforma, 1–49.

—— 1977*c*. Geology and mineral potential of Shirani area, F.R.D.I. Khan. *Records of the Federally Administered Tribal Areas Development Corporation, Peshawar*, **1**, 1–44.

—— 1983*a*. *Geological map between Dradar Tangai and Peiwar Tangai (Upper Kurram Agency), 1:50 000, with report*. Federally Administered Tribal Areas Development Corporation, unpublished.

—— 1983*b*. Geology and breccia pipe primary and secondary copper mineralization in Waziristan. *2nd national seminar on Development of Mineral Resources, Peshawar, 21–24 May 1983*, 1–16.

—— 1984. *Probe core drilling for copper in North Waziristan*. FATADC project report and PCII proforma, 1–17.

—— 1985. Development potential of Waziristan copper. *Records of the Federally Administered Tribal Areas Development Corporation, Peshawar, Pakistan*, **3**, 1–35.

—— 1986. *Evaluation of Shinkai copper in North Waziristan Agency*. FATADC project report and PCII proforma, 1–23.

—— 1994. Information for October 1994 Round Table Conference on Minerals, Islamabad, 1–19.

BANNERT, D., CHEEMA, A., AHMED, A. & SCHÄFER, U. 1992. The structural development of the western fold belt, Pakistan. *Geologisches Jahrbuch Reihe B*, **80**, 3–60.

BECK, R. A. 1995. *Late Cretaceous ophiolite obduction and Paleocene India–Asia collision in the westernmost Himalaya*. PhD thesis, University of Southern California, Los Angeles.

——, BURBANK, D. W., SERCOMBE, W. J., RILEY, G. W., BARNDT, J. K. *et al.* 1995. Stratigraphic evidence for an early collision between northwest India and Asia. *Nature*, **373**, 55–58.

——, BURBANK, D. W., SERCOMBE, W. J., KHAN, M. A. & LAWRENCE, R. D. 1996. Late Cretaceous ophiolite obduction and Paleocene India–Asia collision in the westernmost Himalaya. *Geodinamica Acta*, **9**, 114–144.

BENDER, F. K. & RAZA, H. A. 1995. *Geology of Pakistan*. Gebrüder Bornträger, Berlin.

BORDET, P. 1975. Les volcans recents du Dacht-E-Nawar (Afghanistan Central). *Annales Scientifiques de l'Université de Cleremont*, **53**, 1–86.

BOSUM, W., HOMILIUS, J. & WITTEKIND, H. 1974. Beiträge geophysikalischer Untersuchungen zur Geologie des Gebietes von Khost und Yaqubi/SE-Afghanistan. *Geologisches Jahrbuch, Reihe E*, **2**, 1–22.

BURRIS, J. H. 1996. *Late Cretaceous collapse of the NW Indo-Pakistani continental margin*. Senior Thesis, Miami University, Oxford, OH.

CASSAIGNEAU, C. 1979. *Contribution à l'étude des structures Inde–Eurasie. La zone de suture de Khost dans le Sud-Est de l'Afghanistan, l'obduction Paléocène et la tectonique Tertiaire*. PhD thesis, Université des Sciences et Techniques du Languedoc, Montpellier, France.

COCHRAN, J. R. 1988. Somali Basin, Chain Ridge, and origin of the northern Somali Basin gravity and geoid low. *Journal of Geophysical Research*, **93**, 11985–12008.

FATMI, A. N. 1972. Stratigraphy of the Jurassic and Lower Cretaceous rocks and Jurassic ammonites from northern areas of West Pakistan. *British Museum of Natural History Bulletin (Geology)*, **20**, 299–380.

—— & CHEEMA, M. R. 1972. Early Jurassic cephalopods from Kisor–Marwat Ranges (Sheikh Budin Hills), Dera Ismail Khan District, N.W.F.P., Pakistan. *Pakistan Geological Survey Records*, **21**, 1–9.

GANSS, O. 1970. Zur Geologie von Südost–Afghanistan. *Geologisches Jahrbuch Beihefte*, **84**, 1–203.

GEOCART ORGANIZATION FOR SURVEYING AND CARTOGRAPHY 1983. *National atlas of the Democratic Republic of Afghanistan*, 1–36.

GNOS, E., BADSHAH, M. S., AFRIDI, M. I., BECK, R. A., MCWILLIAMS, M. O. *et al.* in press. The Zhob–Waziristan–Khost ophiolite complex: a key to understanding the pre-Himalayan evolution of the Indian margin.

GRIESBACH, C. L. 1892. The Geology of the Safed Koh. *Records of the Geological Survey of India*, **25**, 59–109.

HAQ, S. S. B. & DAVIES, D. M. 1997. Oblique convergence and lobate mountain belts of western Pakistan. *Geology*, **25**, 23–26.

HEMPHILL, W. R. & KIDWAI, A. H. 1973. *Stratigraphy of the Bannu and Dera Ismail Khan areas, Pakistan*. United States Geological Survey Professional Paper, **716-B**.

JADOON, I. A. K. & KURSHID, A. 1996. Gravity and tectonic model across the Suleiman fold belt and the Chaman fault zone in western Pakistan and eastern Afghanistan. *Tectonophysics*, **254**, 89–109.

JAN, M. Q., WINDLEY, B. F. & KHAN, A. 1985. The Waziristan Ophiolite, Pakistan: general geology and chemistry of chromite and associated phases. *Economic Geology*, **80**, 294–306.

JONES, A. G. 1960. *Reconnaissance geology of part of western Pakistan: A Colombo Plan Co-operative Project Report*. Government of Canada.

KAEVER, M. 1967*a*. Zur Geologie des Gebietes von Khost und Yakubi-SE Afghanistan. *Neues Jahrbuch Geologische und Paläontologische Monatshefte*, **6**, 361–383.

—— 1967*b*. Untersuchungen zur Schichtfolge im Gebiet Quasim-Khel-Ali-Khel, E-Afghanistan. *Neues Jahrbuch Geologische und Paläontologische Monatshefte*, **5**, 284–304.

KHAN, A., REHMAN, F., AHMAD, M. & KHAN, M. Y. 1988. *Geological map of Hangu Quadrangle, Aurakzai Agency, 1:50000, with report.* Federally Administered Tribal Areas Development Corporation, unpublished.

——, SHAH, Z. H., SAHIBZADE & NAEEM, M. 1970. Geology of Gundai Sar and vicinity, Jamrud, Khyber Agency. *Geological Bulletin, Peshawar University*, **5**, 115–130.

——, WAHABUDDIN & SHAH, M. R. 1982. Preliminary report on the ophiolite occurrences in part of Waziristan, N.W.F.P., Pakistan. *Pakistan Geological Survey Information Release*, **129**, 1–23.

KHAN, A. K. 1974. Prospection and mining of soapstone in Kurram Agency. *FATADC project report and PCII proforma*, 1–21.

—— 1975. Investigation and large scale mapping in FATA. *FATADC PCII proforma*, 1–11.

KHAN, J. 1978. *Geological map of Haibat Khel area, South Waziristan Agency, 1:50000, with report.* Federally Administered Tribal Areas Development Corporation, unpublished.

—— & KHAN, M. A. 1985. *Geological map of Parachamkani and Masuzai areas, Kurram Agency, 1:50000, with report.* Federally Administered Tribal Areas Development Corporation, unpublished.

KHAN, L. M. 1988. *Geological map of Gomal area, South Waziristan Agency, 1:50000, with report.* Federally Administered Tribal Areas Development Corporation, unpublished.

—— & INAMULLAH 1987. *Geology and stratigraphy of Frontier Region Bannu, 1:50000, with report.* Federally Administered Tribal Areas Development Corporation, unpublished.

LAFIF, M. A. 1970. Micropaleontology of the Chanali Limestones, Upper Cretaceous of Hazara, West Pakistan. *Weinheim Jahrbuch Geologie, B, A Sonderband*, **15**, 25–61.

LAWRENCE, R. D., KHAN, S. & NAKATA, T. 1992. Chaman fault, Pakistan–Afghanistan. *Annales Tectonicae, special issue supplement to volume 6*, 196–223.

MEISSNER, C. R., HUSSAIN, M., RASHID, M. A. & SETHI, U. B. 1975. *Geology of the Parachinar Quadrangle, Pakistan.* United States Geological Survey Professional Paper, **716-F**.

——, MASTER, J. M., RASHID, M. A. & HUSSAIN, M. 1974. *Stratigraphy of the Kohat Quadrangle, Pakistan.* United States Geological Survey Professional Paper, **716-D**.

MEISSNER, G. 1977. *Carte géologique de la chaîne d'Altimour, 1:100000.* Service Géologique d'Afghanistan; mission géologique du CNRS en Afghanistan, Université de Picardie (France).

MENNESSIER, G. 1968. Etude tectonique des montagnes de la région de Kaboul. *Notes at Mémoire Moyen Orient*, **4**, 1–185.

—— 1969. Sur les formations paléogènes de la partie centrale de la chaîne d'Altimour. *Compte Rendue Sommaire de la Société Geologique de France*, **8**, 314–316.

—— 1977. Stratigraphie, tectonique et évolution du fossé de Kaboul (Afghanistan). *Mémoir hors série Societé géologique de France*, **8**, 153–168.

—— & BEUN, N. 1981. *Carte géologique du Fossé de Kaboul et de ses prolongements méeridionaux 1:250000.* Service Géologique d'Afghanistan; mission MP1 du C.N.R.S. Université de Picardie, Amiens, France.

—— & —— 1985. *Atlas de cartes géologiques de l'Afghanistan entre Gol-Bahar et l'Ab-E-Istada (fossé de Kaboul et prolongement méridionaux).* Département de Géologie, Amiens, France.

MORRIS, T. O. 1938. The Bain Boulder bed; a glacial episode in the Siwalik Series of the Marwat Kundi Range and Sheikh Budin, North-West Frontier Province, India. *Quarterly Journal of the Geological Society of London*, **94**, 385–421.

PERVEZ, J. 1988. *Geological map of Sarkand area, South Waziristan Agency, 1:50000, with report.* Federally Administered Tribal Areas Development Corporation, unpublished.

PILGRIM, E. S. 1913. The correlation of the Siwaliks with mammal horizons of Europe. *India Geological Survey Records*, **43**, 264–326.

QUAYYUM, M., LAWRENCE, R. D. & NIEM, A. R. 1997. Discovery of the palaeo-Indus delta-fan complex. *Journal of the Geological Society, London*, **154**, 753–756.

——, NIEM, A. R. & LAWRENCE, R. D. 1996. Newly discovered Palaeogene deltaic sequence in Katawaz Basin, Pakistan, and its tectonic implications. *Geology*, **24**, 835–838.

RABBANI, M. A. 1978. Geology of Aurakzai Agency. *Federally Administered Tribal Areas Development Corporation Records*, **2**, 1–47.

SHAH, S. M. I. 1977. *Stratigraphy of Pakistan.* Geological Survey of Pakistan.

STAUFFER, K. W. 1968. Siluro-Devonian reef complex near Nowshera, West Pakistan. *Bulletin of the Geological Society of America*, **79**, 1331–1350.

STUART, M. 1922. The geology of the Takki Zam Valley, and the Kaniguram–Makin area, Waziristan. *Records of the Geological Survey of India*, **54**, 87–102.

TAPPONNIER, P., MATTAUER, M., PROUST, F. & CASSAIGNEAU, C. 1981. Mesozoic ophiolites, sutures, and large-scale tectonic movements in Afghanistan. *Earth and Planetary Science Letters*, **52**, 355–371.

TARIQ, M. 1990. *Geological map of western part of Kurram Agency, 1:50000, with report.* Federally Administered Tribal Areas Development Corporation, unpublished.

—— 1991. *Geological map of parts of Frontier Region and lower Kurram Agency, 1:50000, with report.* Federally Administered Tribal Areas Development Corporation, unpublished.

—— & SHAFA, M. 1988. *Geological map of Miran Shah and Mir Ali sub-division, North Waziristan Agency, 1:50000, with report.* Federally Administered Tribal Areas Development Corporation, unpublished.

TRELOAR, P. J. & IZATT, C. N. 1993. Tectonics of the Himalayan collision between the Indian Plate and

the Afghan Block: a synthesis. *In*: TRELOAR, P. J. & SEARLE, M. P. (eds) *Himalayan Tectonics*. Geological Society, London, Special Publications, **74**, 69–87.

WILLIAMS, M. D. 1959. Stratigraphy of the lower Indus basin, West Pakistan. *World Petroleum Congress, 5th Proceedings, New York, section 1, paper 19*, 377–390.

WITTEKINDT, H. 1973. *Erläuterungen zur geologischen Karte von Zentral- und Südafghanistan, 1:500 000*. Federal Institute for Geoscience and Natural Resources, Hannover.

—— & WEIPPERT, D. 1973. *Geologische Karte von Zentral und Südafghanistan, 1:500 000*. Federal Institute for Geoscience and Natural Resources, Hannover.

Index

Page numbers in italic, e.g. *432*, signify references to figures. Page numbers in bold, e.g. **185**, denote references to tables.